

# **Design and synthesis of peptide and small molecule Protein-RNA Interaction Inhibitors**

Dissertation

Zur Erlangung des Doktors der Naturwissenschaften der Naturwissenschaftlich-  
Technischen Fakultät der Universität des Saarlandes

von

**Ben Georges Edouard Zoller**

Saarbrücken, 2024

**Tag des Kolloquiums: 18.09.2024**

**Dekan: Prof. Dr.-Ing. Michael Vielhaber**

**Berichterstatter: Prof. Dr. Martin Empting  
Prof. Dr. Christian Ducho**

**Akad. Mitglied: Dr. Angelika Ullrich**

**Vorsitz: Prof. Dr. Andriy Luzhetskyy**



Die vorliegende Arbeit wurde von Oktober 2019 bis März 2024 unter Anleitung von Prof. Dr. Martin Empting in der Fachrichtung Pharmazeutische und Medizinische Chemie der Naturwissenschaftlich-Technischen Fakultät der Universität des Saarlandes sowie am Helmholtz-Institut für Pharmazeutische Forschung Saarland (HIPS) in der Abteilung Antiviral and Antivirulence Drugs (AVID) angefertigt.

# Acknowledgements

First of all, I want to thank Prof. Dr. Martin Empting, for the opportunity of conducting my Ph.D thesis under his supervision at HIPS. His clear vision for the project, guidance on necessary experiments, and unlimited support were instrumental throughout my journey. I deeply appreciate the trust and freedom he granted me. Moreover, I want to thank the additional members of my thesis committee, my second supervisor Prof. Dr. Christian Ducho as well as Dr. Angelika Ulrich for the constructive and helpful discussions during our thesis committee meetings.

Many thanks go to Dr. Yingwen Wu, who conducted the biophysical assay which cost her a lot of time and energy, for the fruitful science we conducted together. Additionally, I want to thank Kyana Mazlom for her investment in the biological lab after Yingwen left and her effort to get the assays running. A big thank goes to my colleagues from the AVID group Erik Kosche, Konrad Wagner and Aylin Berwanger who were always willing to help and created an aggregable and collegial working atmosphere.

I am thankful for the enriching discussions with my former office mates Dr. Christian Schütz and Dr. Vlad Hapko. Gratitude also extends to my colleagues from the DDOP and the CBCH-group with whom I shared lab space.

A big thank you goes to my long-term friends Sebastian Palm and Tom Schmit, with whom I had the chance to spend many time during my studies in Saarbrücken and who were always there for me.

Next, I want to thank all my family members who supported me a lot during my studies with emotional as well as financial support. At most I want to thank my parents, without their help I could never have reached my goals. I am truly grateful for the support in all kind of ways they delivered throughout my life and especially during my Ph.D thesis.

A final but profound thank goes to my girlfriend, Samira Speicher. Even in dark and frustrating times, her never ending support and love gave me the strength to keep going.

“He who learns without thinking will be bewildered;  
he who thinks without learning will be in danger”

Confucius

# Summary

Two omnipresent and increasing health threats in our society are antimicrobial resistance and cancer. Despite the existence of powerful treatments for microbial infections, the widespread (mis)use of antibiotics and a lack of innovation and economical interest in antimicrobial research have resulted in the propagation of multi-drug resistant pathogen strains. These strains pose a serious risk to public health, a threat that is expected to intensify in the future.

The second major health threat is cancer, while cancer research does receive significant public and economic attention, it remains the second leading cause of death globally. With numerous types of cancer and phenotypes showing resistance to conventional therapies such as chemotherapy and radiotherapy, there is a pressing need for innovative treatment options.

Two different RNA binding proteins are investigated in this doctoral thesis. The first one being, the “carbon storage regulator A” (CsrA), a posttranscriptional regulator, which is wide-spread and conserved in most Gram-negative pathogens but absent in eukaryotes, rendering it a promising anti-virulence target.

The second protein under investigation is the “Insulin-like growth factor 2 mRNA binding protein 2” (IMP2), a posttranscriptional regulator, found in mammals, which is crucial for foetal development. The upregulation of IMP2 in many mammalian cancer cell lines as well as the confirmed promotion of cancer cell proliferation make IMP2 a promising target for anti-cancer therapies.

The aim of this thesis was to uncover novel inhibitors targeting CsrA and IMP2 *in vitro*, crucial for validating the envisioned proof-of-concept demonstrating that inhibiting CsrA and IMP2 will yield the desired *in vivo* effects in forthcoming studies, thereby validating these proteins as viable targets for antimicrobial and anticancer interventions. The thesis reasons the rationale behind selecting those proteins as potential new targets, explains how *in vitro* hit identification was performed and concludes with the medicinal chemistry-driven optimisation of these compounds.

# Zusammenfassung

Zwei allgegenwärtige und zunehmende Gesundheitsbedrohungen in unserer Gesellschaft sind antimikrobielle Resistenz und Krebs. Trotz der Existenz effizienter Behandlungen gegen mikrobielle Infektionen hat der weit verbreitete Missbrauch von Antibiotika und ein Mangel an Innovation und wirtschaftlichem Interesse an antimikrobieller Forschung zur Verbreitung von multiresistenten Pathogenstämmen geführt. Diese Stämme stellen eine ernsthafte Gefahr für die öffentliche Gesundheit dar, eine Bedrohung, die in Zukunft voraussichtlich zunehmen wird.

Die zweite Gefahr für die öffentliche Gesundheit, stellt Krebs dar. Obwohl die Krebsforschung erhebliche öffentliche und wirtschaftliche Aufmerksamkeit erhält, bleibt Krebs weltweit die zweithäufigste Todesursache. Mit zahlreichen Krebsarten und Unterarten, die gegen konventionelle Therapien wie Chemotherapie und Strahlentherapie resistent sind, besteht ein dringender Bedarf an innovativen Behandlungsoptionen.

In dieser Doktorarbeit werden zwei verschiedene RNA-bindende Proteine untersucht. Das erste davon ist der "Carbon Storage Regulator A" (CsrA), ein posttranskriptionaler Regulator, welcher in den meisten gramnegativen Bakterien sehr verbreitet und in seiner Struktur stark konserviert ist, aber in Eukaryoten fehlt, was ihn zu einem vielversprechenden Ziel für Antivirulenz-Wirkstoffe macht. Das zweite untersuchte Protein ist das "Insulin-like Growth Factor 2 mRNA Binding Protein 2" (IMP2), ein posttranskriptionaler Regulator, der in Säugetieren vorkommt und für die fötale Entwicklung entscheidend ist. IMP2 ist in zahlreichen Säugetierkrebszelllinien hochreguliert und wurde mit der Begünstigung der Zellproliferation bei Krebs in Verbindung gebracht, was es zu einem vielversprechenden Ziel für eine Therapie gegen Krebs macht.

Das Ziel dieser Arbeit war es, neue Inhibitoren zu identifizieren, die CsrA und IMP2 *in vitro* inhibieren können. Dies ist ein entscheidender Schritt um in einem späteren Stadium zeigen zu können, dass die Hemmung von CsrA und IMP2 die gewünschten *in vivo*-Effekte erzielen kann und damit die anvisierten Proteine als valide Antivirulenz bzw. Anti-Krebs Targets zu bestätigen. Die Arbeit begründet die Auswahl dieser Proteine als potenzielle neue Ziele, erläutert, wie die Identifizierung von Hits *in vitro* durchgeführt wurde, und schließt mit der medizinisch-chemischen Optimierung dieser Verbindungen ab.

## Publications included in this Thesis

**Publication 1:** V. Jakob\*, B. G. E. Zoller\*, J. Rinkes, Y. Wu, A. F. Kiefer, M. Hust, S. Polten, A. M. White, P. J. Harvey, T. Durek, D. J. Craik, A. Siebert, U. Kazmaier, M. Empting, *Phage display-based discovery of cyclic peptides against the broad spectrum bacterial anti-virulence target CsrA*, *Eur. J. Med. Chem.* 2022

<https://doi.org/10.1016/j.ejmech.2022.114148>

\* These authors contributed equally

**Publication 2:** Y. Wu, B. G.E. Zoller, M. A. M. Kamal, S.-K. Hotop, C.-M. Lehr, M. Brönstrup, P. Dersch, M. Empting, *Establishment of an In Bacterio assay for the Assessment of Carbon Storage Regulator A (CsrA) inhibitors*, *ChembioChem* 2023

<https://doi.org/10.1002/cbic.202300369>

**Publication 3:** C. Dahlem\*, A. Abuhaliema\*, S. M. Kessler\*, T. Kröhler, B. G. E. Zoller, S. Chanda, Y. Wu, S. Both, F. Müller, K. Lepikhov, S. H. Kirsch, S. Laggai, R. Müller, M. Empting, A. K. Kiemer, *First Small-Molecule Inhibitors Targeting the RNA-Binding Protein IGF2BP2/IMP2 for Cancer Therapy*, *ACS Chem. Biol.* 2022

<https://doi.org/10.1021/acscchembio.1c00833>

\* These authors contributed equally.



# Abbreviations

Boc: tert-Butyloxycarbonyl

BPO: Benzoyl peroxide

DCC: Dicyclohexylcarbodiimide

DCM: Dichloromethane

DIC: Diisopropylcarbodiimide

Dipea: Diisopropylethylamine

DNA: Deoxyribonucleic acid

E. coli: Escherichia coli

EtOAc: Ethylacetate

FDA: food and drug administration

FluPo: Fluorescence polarisation

Fmoc: Fluorenylmethoxycarbonyl

LC-MS: Liquid chromatography-mass spectrometry

mRNA: messenger ribonucleic acid

NBS: N-Bromosuccinimide

Pbf: 2,2,4,6,7-pentamethyl-2,3-dihydrobenzofuran-5-sulfonyl

PD: pharmacodynamic

PK: pharmacokinetic

RNA: ribonucleic acid

SELEX: Selective Evolution of Ligands by Exponential enrichment

SPR: Surface Plasmon Resonance

STD-NMR: saturation-transfer difference nuclear magnetic resonance spectroscopy

STEC: Shiga toxin producing Escherichia coli

TBAI: Tetrabutyl ammonium iodide

tBu: tert-Butyl

Trt: Trityl

WHO: world health organization

# Table of contents

1. Introduction .....	1
2. State of the art.....	4
2.1 Target Proteins .....	4
2.1.1 Carbon storage regulator A (CsrA) .....	4
2.1.2 IMP2.....	5
2.2. Previously identified inhibitors .....	7
2.2.1 CsrA .....	7
2.2.1 IMP2.....	7
2.3 Phage display .....	9
2.4 Solid Phase Peptide Synthesis (SPPS).....	10
2.5 Biophysical assays.....	14
2.5.1 Surface plasmon resonance (SPR) spectroscopy.....	14
2.5.2 Fluorescence polarisation spectroscopy .....	16
3. Workflow .....	18
3.1 CsrA.....	18
3.2 IMP2 .....	19
4. Results and Discussion .....	21
4.1 Peptides inhibiting the CsrA-RNA interaction .....	21
4.2 Establishment of a Luciferase assay for the assessment of CsrA inhibitors .....	35
4.3 Small molecules inhibiting the CsrA-RNA interaction .....	44
4.4 Small molecules inhibiting the IMP2-RNA interaction .....	57
5. Conclusion .....	74
5.1 Peptides inhibiting the CsrA-RNA interaction .....	74
5.2 Establishment of an <i>in-bacterio</i> luciferase assay for the assessment of CsrA inhibitors .....	76
5.3 Small molecules inhibiting the CsrA-RNA interaction .....	77
5.4 Small molecules inhibiting the IMP2-RNA interaction.....	79
6. Outlook.....	82
7. References.....	83
8. Supporting Information .....	88
8.1 Peptides Inhibiting the CsrA-RNA interaction .....	88
8.2 Establishment of a luciferase assay for the assessment of CsrA inhibitors.....	155
8.3 Small molecules inhibiting the CsrA-RNA interaction .....	162

8.4 Small molecules inhibiting the IMP2-RNA interaction.....	381
--	-----

# 1. Introduction

RNA-binding proteins (RBP), belong to a vast and underexplored class of post-transcriptional regulators.<sup>[1]</sup> By binding to specific RNA targets, they can either stabilize or destabilize them, thereby influencing RNA translation. RBP's play a crucial role in metabolic regulation and the proper functioning of both eukaryotic and prokaryotic organisms. Targeted inhibition of RBP's holds the potential to significantly alter metabolic function, offering a promising avenue for addressing two significant health challenges: antimicrobial resistance and cancer.<sup>[2,3]</sup>

Since decades, many researchers have warned about an incoming crisis of antimicrobial resistance (AMR).<sup>[4]</sup> The relentless proliferation of multi-drug resistant bacterial pathogens, especially among Gram-negative species, presents a significant and pressing threat to modern healthcare systems, with increasing cases of mortality.<sup>[5]</sup> Notably, multidrug-resistant ESKAPE pathogens, namely *Enterococcus faecium*, *Staphylococcus aureus*, *Klebsiella pneumoniae*, *Acinetobacter baumannii*, *Pseudomonas aeruginosa*, and *Enterobacteriaceae* occupy the top spots on the WHO's global priority pathogens list, as published in 2017. Consequently, there is an imperative to discover innovative anti-infective candidates with novel modes of action (MoA).

All FDA approved drugs rely on one of six MoA's, most of them were discovered ages ago. Unfortunately, finding new targets for antibiotics is a slow and challenging process.<sup>[6]</sup> Thus most pathogens were able to adapt over time and new strains of (multi)-drug resistant bacteria emerged, driven by spontaneous mutations and natural selection.<sup>[7]</sup> Even though there are efforts towards the discovery of new MoA's, such as the development of Zosurabalpin, a new form of macrocycle which relies on the inhibition of Liposaccharide transporters,<sup>[8]</sup> the discovery of new targets is sluggish and resistance will develop over time.

Another overlooked, yet substantial challenge, whose significance has become evident in recent years, is polymicrobial infections.<sup>[9]</sup> The human microbiome, when in a healthy state, comprises a diverse array of microbes that coexist harmoniously and symbiotically. These microorganisms defend against harmful pathogens by producing their own antimicrobial compounds. In contrast, harmful microbial communities are less diverse but possess the capability to amplify each other's virulence through collaborative competition (microbial interference), mutual nutrient exchange, or immune system oversight.<sup>[10,11]</sup> Combatting these pathogenic microbial communities is more complex than addressing individual microbes, and finding a solution is hindered by the difficulty of eradicating them without negatively impacting the beneficial commensal flora.<sup>[9-12]</sup>

A recent innovation in the field is the introduction of antivirulence drugs. These agents target specific virulence factors in bacteria, disarming them without affecting bacterial growth or survival. This unique approach helps to circumvent bacterial resistance.<sup>[13]</sup> Another major advantage of these drugs is the targeted action against one or multiple bacteria. In contrast to conventional antibiotics they have a minimal impact on the beneficial commensal flora, which is advantageous for patients.<sup>[13]</sup>

Mainly acute and chronic infections of the respiratory and gastrointestinal tract, where polymicrobial infections play a major role, are ideal candidates for the potential use of

antivirulence drugs.<sup>[11]</sup> The antivirulence agents could modulate complex communities in order to reestablish and protect the commensal balance.<sup>[12]</sup>

For the treatment of a clinically relevant strain, only one FDA approved antivirulence drug is currently on the market, namely Bezlotoxumab for the treatment of *Clostridium difficile*. A major contribution to the virulence of *C. difficile* are the endotoxins TcdA as well as TcdB, they are able to selectively glycosylate host GTPases of the RHO family, inside epithelial cells, leading to a hindrance in their normal function.<sup>[13]</sup> As RHO GTPases regulate multiple processes, such as organisation of the actin cytoskeleton as well as the regulation of immune cell signalling and motility, their perturbation leads to a reduced immune response and cytoskeletal destabilisation.<sup>[14]</sup> Merck developed two monoclonal antibodies (mAbs) targeting TcdA and TcdB, respectively and could show in a phase 3 clinical trial, that Bezlotoxumab, targeting TcdB in conjugation with standard of care antibiotics led to a significantly lowered recurrence rate than the control group, leading to the FDA approval in 2016.<sup>[15]</sup> Even though relevant resistance formation was not observed yet, the incidence and intensity of *C. difficile* infections is increasing and Bezlotoxumab might emerge as a powerful tool for the combat against *C. difficile* infections in the future.

However there are several candidates in clinical and preclinical trials.<sup>[13]</sup> For example the well-established macrolide antibiotic Azithromycin, shows some promising inhibition of quorum sensing in *Pseudomonas aeruginosa* when administered in low doses that do not inhibit cell growth.<sup>[16]</sup> The monoclonal antibody Shigamab, developed by Bellus Health, inhibits Shiga Toxin of the dangerous *E. coli* strain STEC.<sup>[17]</sup> The monoclonal Antibody MEDI4893 inhibits  $\alpha$ -toxin of *Staphylococcus Aureus* an important virulence factor<sup>[18]</sup> and savarin addresses AgrA a major transcriptional regulator in *Staphylococcus Aureus*.<sup>[19]</sup> Moreover there is a plethora of possible concepts, which did not yet make it to clinical studies, such as the inhibition of PqsR<sup>[20]</sup> or LasB<sup>[21]</sup> for the treatment of an *Pseudomonas aeruginosa* infections.

The RBP, carbon storage regulator A (CsrA), also known as the regulator of secondary metabolites (RsmA) in some species,<sup>[22]</sup> is a compelling yet relatively unexplored target for modulating virulence.<sup>[23]</sup> CsrA is prevalent among Gram-negative pathogens, characterized by high sequence and functional conservation.<sup>[24,25]</sup> Knock-out studies conducted in *Pseudomonas aeruginosa*, *Yersinia pseudotuberculosis*, and *Helicobacter Pylori* have underscored its pivotal role in bacterial virulence, accentuating its potential as a therapeutic target.<sup>[26,27]</sup> Functioning as a post-transcriptional regulator, the CsrA/RsmA protein binds to and regulates mRNA translation, thereby exerting pleiotropic effects on the bacterial transcriptome.<sup>[28,29]</sup> Utilizing CsrA-RNA inhibitors as antivirulence agents represents a novel and promising strategy in combating polymicrobial infections and multidrug resistance.

The second significant health concern addressed in this thesis receives more widespread attention by BIG pharma than the first one. However, cancer remains a substantial burden on global health.<sup>[30]</sup> Ferlay et al. conducted a thorough analysis of the GLOBOCAN database, which contains data from 185 countries and provides information on 38 different cancer sites, sourced from the International Agency for Research on Cancer.<sup>[31]</sup> Their findings revealed that 19 million new cases of cancer were reported in 2020, resulting in nearly 10 million fatalities. These statistics underscore a 25% likelihood for individuals to develop cancer before the age of 75, with a 10% risk of the disease being fatal.<sup>[31]</sup>

Although the World Health Organization (WHO) suggests that adopting a healthy lifestyle, including reducing tobacco and alcohol consumption, engaging in regular exercise, maintaining a normal body weight, and following a nutritious diet, could potentially decrease global cancer cases by up to 50%, it's important to recognize that not all cancer cases can be prevented through these preventive measures.<sup>[31]</sup> Furthermore, many individuals struggle to adhere to these healthy lifestyle practices, and there is a widening disparity between social levels, with underprivileged populations often facing greater challenges in adopting such measures.<sup>[32]</sup>

Even though cancer ranks as the second leading cause of death in most countries, falling behind cardiovascular diseases, there appears to be promising avenues for addressing the latter in the future, while there remains an urgent need for innovative cancer treatment options. Furthermore, the risk of developing cancer significantly escalates with age, and with society aging progressively, this issue is prone to amplify in the future. Ultimately, it is evident that cancer persists as the primary health menace in our present era.<sup>[30]</sup>

Two of the most lethal cancer types are liver carcinoma, responsible for 830,000 deaths in 2020, ranking third, and colorectal cancer with 916,000 annual fatalities, ranking second.<sup>[31]</sup> Despite treatment options such as chemotherapy, radiotherapy, or surgical removal, half of these cancers remain incurable.<sup>[33,34]</sup> Emerging prospects like targeted immune-boosting therapies, non-coding RNA-based treatments, and probiotics offer new hope.<sup>[33]</sup> However, these potential remedies are still in development, emphasizing the immediate need for novel strategies to combat these cancers.

The insulin-like growth factor 2 mRNA binding protein (IMP2 or IGF2BP2), is a posttranscriptional mRNA binding protein. Like many other RNA binding proteins, it plays a crucial role in RNA maturation, stability, localization, and translation.<sup>[1]</sup> Notably, it has been identified as a significant driver of cancer progression at the post-transcriptional level, contributing to heightened expression of oncogenes and reduced expression of tumor suppressor genes.<sup>[1]</sup>

The analysis of colorectal cancer (CRC) tissue compared to normal colorectal tissue revealed a significant upregulation of IMP2 in the cancerous tissue, with only 10% of the examined CRC samples showing normal levels of IMP2 expression.<sup>[35]</sup> Furthermore, several associations between IMP2 and cancer cell proliferation were identified. Among others, IMP2 was found to bind to the mRNA of the oncogenic protein kinase RAF1 at its 3'UTR, preventing its degradation by microRNA (miR-195). Consequently, the overexpression of IMP2 results in elevated levels of RAF1 in CRC tissue, promoting cancer cell proliferation.<sup>[36]</sup>

In the realm of hepatocellular carcinoma, analogous findings have been noted. There is a pronounced overexpression of IMP2 in hepatocellular cancer tissues, with significant implications for its involvement in cancer cell proliferation. This includes the activation of glucose transporters and the reactivation of dormant pathways, offering meaningful insights into its role.<sup>[37,38]</sup>

## 2. State of the art

### 2.1 Target Proteins

#### 2.1.1 Carbon storage regulator A (CsrA)

Over the past three decades, our comprehension of the important role played by the carbon storage regulator A (CsrA) in microbial virulence, particularly in *Escherichia coli*, has significantly advanced, thanks to the dedicated efforts of numerous scientists, with T. Romeo's group making notable contributions through multiple publications. Initially, they successfully elucidated the structure of CsrA, revealing two homodimers with identical RNA binding sites. Additionally, through SELEX experiments, they pinpointed ACA and GGA motifs as the predominant RNA targets of CsrA.<sup>[39]</sup> It became evident that the regulation of CsrA is very complex, involving autoregulation and the participation of additional enzymes, specifically CsrB and CsrC.<sup>[40]</sup> The CsrA system was also found in *Clostridium acetobutylicum* and *Yersinia pseudotuberculosis*, where it has similar functions as in *E. coli*.<sup>[41]</sup>

CsrA was found to suppress the translation of the “suppressor of cell division inhibition A” (sdiA) by binding to the Shine-Dalgarno sequence and prevent ribosomal binding.<sup>[42]</sup> Since sdiA encodes the quorum sensing receptor for N-acyl-L-homoserine, a crucial component in *E. coli*'s quorum sensing system, and is involved in the transcription of CsrB, a known antagonist of CsrA, it is evident that CsrA exerts a significant influence on quorum sensing. Inhibiting CsrA is expected to yield beneficial effects on bacterial virulence.<sup>[42]</sup>

Furthermore, CsrA has been identified as an activator of flhDC expression, the master operon of flagella production, essential for bacterial motility which contributes significantly to the bacterial virulence.<sup>[43]</sup>

Most bacteria grow in static, matrix-enclosed communities, called biofilms. Within these communities, they are protected against antibiotics as well as the immune system. Perturbation of the biofilm could lead to a drastic reduction in virulence. Knock out studies conducted by T. Romeo's group demonstrated that CsrA is a repressor of biofilm formation as well as an activator of biofilm dispersal.<sup>[44]</sup> Inhibiting CsrA results in increased biofilm growth, primarily attributed to the repression of intracellular glycogen biosynthesis and catabolism. They excluded the role of extracellular, surface or regulatory factors, usually involved in biofilm production, by employing strains defective of those factors. The increased biofilm growth leads to the formation of a distinctly complex multicellular biofilm structure, which differs from the usual biofilm design. If such an alteration of the biofilm structure is beneficial or unfavourable for bacterial virulence is not known yet. Additionally, the inhibition of CsrA shows a direct reduction of biofilm dispersal, which is crucial for bacteria to colonize new regions. It is likely, that reduced biofilm dispersal hinders the well-functioning of bacteria and negatively influences their virulence.<sup>[44]</sup>

Romeo's group was able to show, that CsrA regulates the translation of the carbon starvation gene *cstA* in *E. coli*, by blocking the access to its transcript.<sup>[45]</sup> The carbon starvation gene *cstA* was previously shown to play a major role in carbon starvation and to encode for a peptide transporter, which is important for peptide transport and helps the cell to avoid starvation.<sup>[46]</sup>

Consequently, inhibiting CsrA is anticipated to result in the reduced uptake of over 30 peptides, in the targeted organisms.

The groups of P. Dersch and M. Brönstrup, analysed the metabolome and transcriptome of CsrA deficient strains in *E. coli* by RNA-sequencing and extensive GC-MS as well as LC-MS analysis.<sup>[47]</sup> The comparison between wildtype and knockout strains revealed notable disparities in their metabolism. Knockout strains exhibited heightened levels of products from the glycogen synthesis pathway and fructose-6-phosphate, while metabolites associated with the citrate cycle and aromatic amino acids were downregulated. Nucleobases and nucleosides exhibited increased levels, whereas nucleotides displayed reduced levels. Colonic acid levels were significantly elevated, accompanied by observable changes in cell morphology under electron microscopy.<sup>[47]</sup>

These findings underscore the significance of CsrA in metabolic processes; a disrupted metabolism not only hinders the proper functioning of the pathogen but also adversely affects its virulence.

### **2.1.2 IMP2**

IMP2, short for Insulin-like growth factor 2 (IGF2) mRNA binding protein and also called IGF2BP2, is a member of the newly discovered IMP family, consisting of IMP1, IMP2 and IMP3, and belongs to the m6A reader gene family.<sup>[3]</sup> Through its K-homology (KH) domains, it can identify and bind to m6A sites located on the 3'UTR or stop codon of target mRNA, consequently modulating gene expression by enlisting mRNA stabilizers.<sup>[48]</sup> KH-domains consist of a highly conserved, nucleic acid-binding peptide sequence containing approximately 70 amino acids and are present in many RBP's, their name is derived from the first protein where they were observed, the heterogeneous nuclear Ribonucleoprotein K. N(6)-Methyladenosine (m6A) is a common modification for mRNA, which enables the dynamic regulation of gene expression.

The IMP family members share consistent functional domains: two RNA recognition motif (RRM) domains situated on the N-terminal, and four KH domains situated on the C-terminal, all of which engage with mRNA. The consensus binding sequence on the target mRNA for this family is GG(m6A)C.<sup>[49]</sup>

Although IMP1-3 expression is typically high during foetal development, it generally decreases in most tissues after birth.<sup>[50]</sup> However, in certain cancers such as colon cancer or pancreatic ductal adenocarcinoma (PDAC), IMP levels tend to be elevated, with IMP2 showing the most pronounced increase compared to IMP1 and IMP3.<sup>[51,52]</sup>

Several studies have investigated the role of IMP2 in cancer progression in more detail. Huan et. al. investigated the role of IMP2 in PDAC and concluded that IMP2 contributes to PDAC cell proliferation, by upregulation of the glucose transporter Glut1, through stabilization of its mRNA.<sup>[53]</sup>

Janiszweka et. al. reported IMP2's important impact on oxidative phosphorylation in glioblastoma sphere cultures.<sup>[54]</sup> This mechanism has demonstrated significance in cancer cell energy generation and its viability. While binding to respiratory chain subunits encoding mRNA, IMP2 ensures a well-functioning oxidative phosphorylation process in these cells and thus contributes to cancer cell proliferation.



The overexpression of IMP2 seems most problematic in liver cancer. Kessler et. al.<sup>[37]</sup> recently described the ability of IMP2 to promote hepatocarcinogenesis by amplification of inflammation inducing a more aggressive phenotype of Hepatocellular carcinoma.

Xing and coworkers, found that IMP2 is elevated in human hepatocellular carcinoma (HHC) and contributes to enhanced cell migration and proliferation by activating the Wnt/ $\beta$ -catenin pathway.<sup>[38]</sup> The pathway is named after the Wnt (wingless Int1) protein, it is crucial for embryonic development and is typically inactive in adult cells but is reactivated in various tumor cells. Wnt activation leads to the release of unbound  $\beta$ -catenin, which then binds to multiple transcription factors, thus promoting cell proliferation.

Dai et. al. conducted studies utilizing IMP2 knockout mice, revealing that despite being smaller and thinner overall, these mice remained healthy.<sup>[55]</sup> Their research unveiled that IMP2 binds to mRNA encoding for UCP1 (uncoupling protein 1), a membrane protein known for facilitating thermogenesis in mammals, and inhibits its translation. Consequently, the absence of IMP2 resulted in increased UCP1 expression and improved metabolic activity. Overexpression of IMP2 on the other hand, as proven by E.Tybl et. al., often induced steatosis and amplified hepatocarcinogenesis.<sup>[56]</sup> In summary, these studies demonstrate IMP2's capacity to modulate mouse metabolism by regulating the translation of its target mRNA.

This overexpression of IMP2 often correlates with more aggressive cancer phenotypes and poorer responses to chemotherapy.<sup>[57]</sup> In essence, IMP2 exerts control over the expression and translation of oncogenes both directly and indirectly, thereby promoting cell proliferation, accelerating cell growth rates, enhancing cell invasion and migration, and influencing cell metabolism. Inhibiting IMP2 presents a promising avenue for controlling the growth of cancer cells overexpressing IMP2, offering hope for the treatment of otherwise fatal cancer diseases (see **Figure 1**).<sup>[3]</sup>

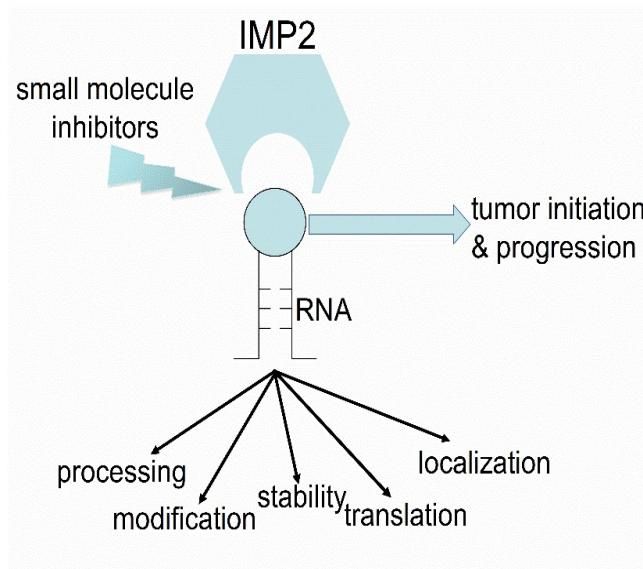


**Figure 1:** Post translation role played by IMP2<sup>[3]</sup>

## 2.2. Previously identified inhibitors

### 2.2.1 CsrA

In a prior investigation, conducted by C. Maurer, R. Hartmann, M. Empting and their colleagues, it was demonstrated that RNA could be displaced by small molecules.<sup>[26]</sup> This pivotal study forms the foundation of the present thesis, revealing seven structurally diverse molecules (**Figure 2**) capable of interrupting the interaction between CsrA from *Yersinia pseudotuberculosis* and a short RNA fragment featuring the crucial core binding motif GGA. The development of an SPR and FluPo test system as well as the RNA fragment, marked significant milestones for future research.<sup>[26,58]</sup>

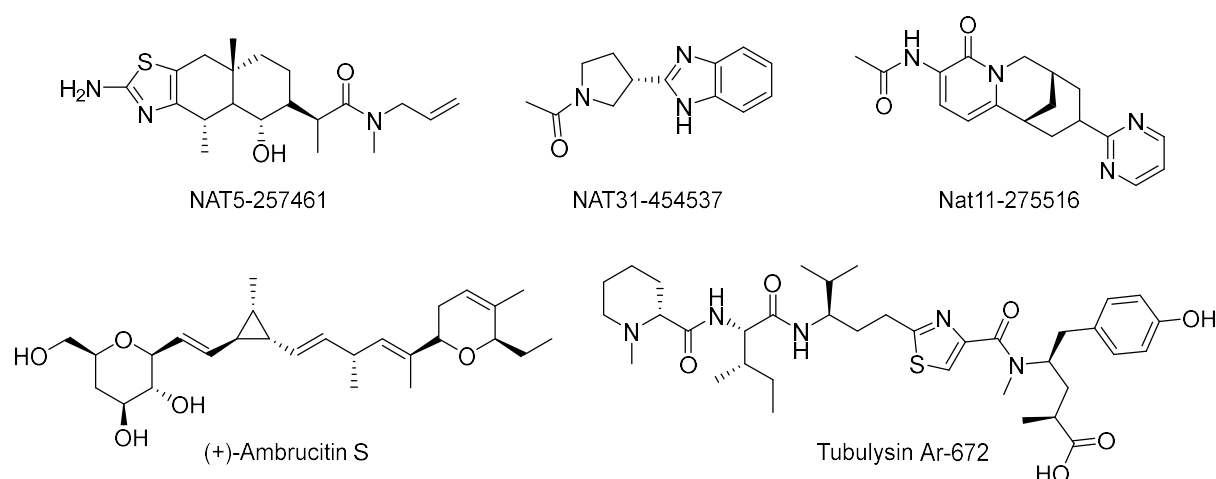


**Figure 2:** Potential CsrA binders identified by Maurer et. al. in a fluorescence polarisation screening of database.

The group of Wang was able to identify the primary binding mode of these molecules via molecular docking, molecular dynamics and binding free energy calculations.<sup>[58]</sup> If the inhibitors have the appropriate size (**NAT5-257461**, **NAT31-454537**, **Nat11-275516**), they are able to specifically bind the G11(RNA) binding site of RNA and build a stable complex with it. Whereas bigger molecules (**(+)-Ambrucitin S**, **Tubulyisin Ar-672**), bind to the whole CsrA interface in a more loose manner, without losing much activity. The calculated and experimentally determined free binding energy are in good accordance.<sup>[58]</sup>

Regrettably, the molecules identified in this study exhibited only moderate activity. Furthermore, they were all derived from natural products, resulting in a high structural complexity that posed challenges for derivatization through a conventional Medicinal Chemistry (MedChem) approach.<sup>[26]</sup>

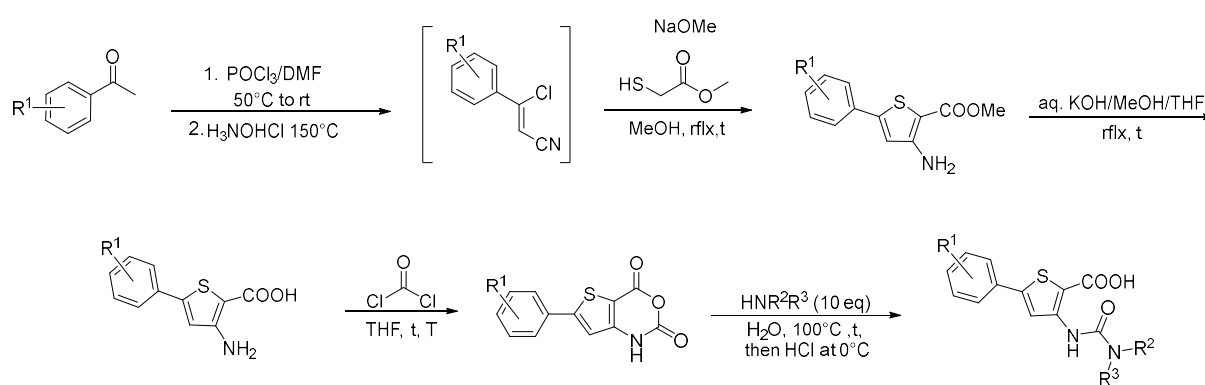
### 2.2.1 IMP2

In the search of potential IMP2 binders, a Fluorescence Polarisation (FluPo) screening employing *E.coli*-IMP2 was engaged, showing eighteen primary actives from two different classes. Further assays, such as a thermal shift assay and STD-NMR, confirmed ten hits, of which three compounds were used for *in vivo* assays.<sup>[3]</sup>

The identified hits belong to two well-known classes of molecules, the Ureidothiophenene as well as the Benamidobenzoic acid. Molecules belonging to these classes were identified as inhibitors of the RNA Polymerase during a previously conducted pharmacophore-based virtual screening at the Helmholtz Institute for Pharmaceutical Research Saarland (HIPS).<sup>[57] [58]</sup>

These compounds are able to hinder the synthesis of RNA from a DNA template, a well-know MoA for antibiotics.<sup>[59,60]</sup> However, the mechanism of transcription inhibition by these molecules differs from conventional antibiotics like Rifampicin.<sup>[60]</sup> While Rifampicin targets the beta subunit of RNA polymerase, these novel compounds bind to the switch region, akin to Myxopyronin A and B<sup>[61]</sup> and Coralopyronin A,<sup>[62]</sup> suggesting that they may not exhibit cross-resistance with Rifampicin.<sup>[63,64]</sup>

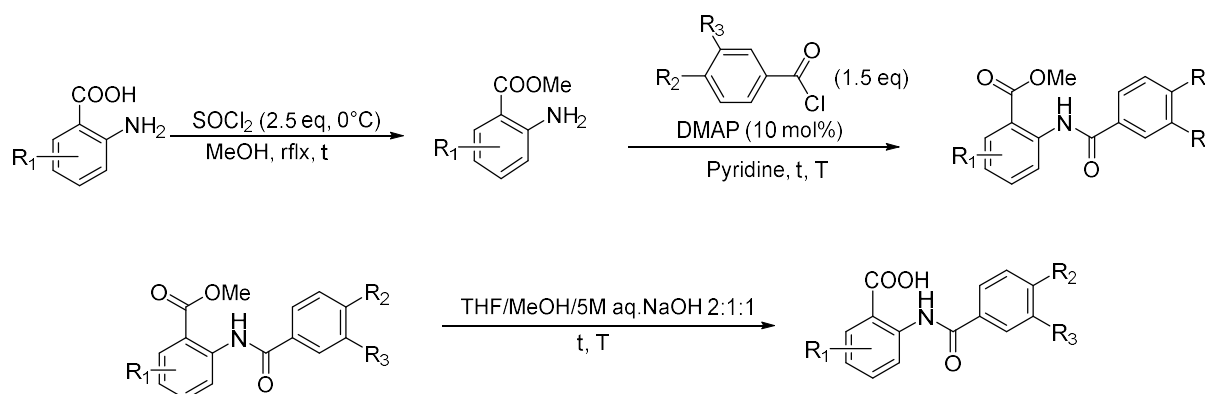
In the publication from Sahner et. Al. the synthesis of the first class, the so called Ureidothiophenes is described for a wide range of derivatives (**Scheme 1**).<sup>[60]</sup>



**Scheme 1:** Proposed Synthesis of Ureidothiophenes by Sahner et. al.<sup>[60]</sup>

Whereas a second publication from Hinsberger et. al. describes the synthesis of molecules belonging to the second set of molecules, the so called Benamidobenzoic acids (**Scheme 2**).<sup>[59]</sup>

While the RNA Polymerase and its inhibition is not of relevance for this thesis, the synthesis of those two classes of inhibitors is of utmost importance for the design and synthesis of the first small molecular inhibitors of the protein IGF2BP2/IMP2.<sup>[3]</sup>



**Scheme 2:** Proposed synthesis of Benamidobenzoic acids by Hinsberger et. al.<sup>[59]</sup>

## 2.3 Phage display

In recent times, there has been a growing interest in the use of small macrocyclic peptides as pharmaceutical agents.<sup>[65]</sup> Their increasing popularity results from the enhanced rigidity and connected stability,<sup>[66]</sup> which contributes to an improved pharmacokinetic/pharmacodynamic (PK/PD) profile,<sup>[67]</sup> rendering them superior to their linear counterparts. Moderate size as well as easy synthetic access makes them perfect for addressing complicated targets, such as peptide-RNA interaction, where the interaction interface is rather large.<sup>[68,69]</sup>

However, it's worth noting that when the cyclic peptide size surpasses ten amino acids, maintaining oral bioavailability becomes challenging.<sup>[70]</sup> Therefore, aiming for a medium peptide size within the range of 5-7 amino acids appears optimal. This allows us to profit from the benefits while remaining within the borderline Lipinski-range also called the “extended” range, to which typical natural products usually belong.<sup>[70]</sup>

One highly effective method for generating a library of randomized peptides is through the use of phage display.<sup>[68]</sup> This technique, pioneered by Smith in 1985<sup>[71]</sup> and subsequently adopted by others,<sup>[72]</sup> involves screening random peptides displayed on bacteriophages for their binding affinity to specific targets.<sup>[73]</sup> Bacteriophages, due to their ability to carry a diverse range of amino acid sequences on their outer surface, serve as excellent carriers for this purpose.<sup>[68]</sup>

By cloning a customized, randomized DNA oligo into the appropriate phagemid, the structure of the displayed peptides on the phage surface can be tailored.<sup>[68,69]</sup> Through a process of phage panning and subsequent screening of phage clones, optimal binding peptides for specific targets can be identified. For a schematic representation of the various steps involved in phage display, refer to the illustrative figure created by Jaroszewicz et al. (**Figure 3**).<sup>[68]</sup>

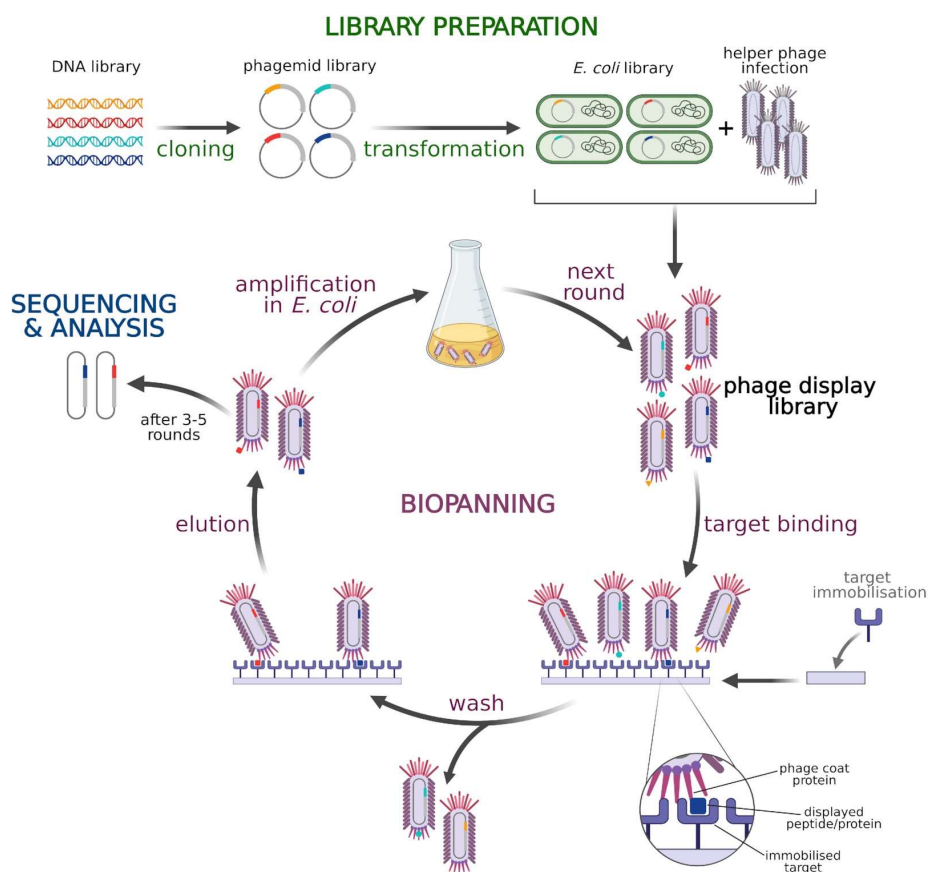


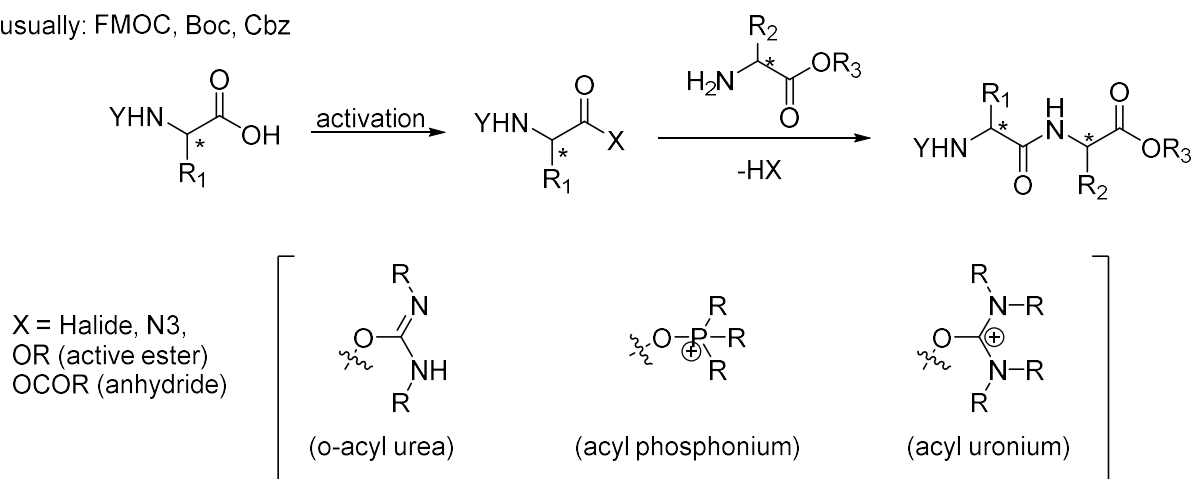
**Figure 3:** Graphical explanation of the function of the Phage display technology, illustrated by Jaroscewicz et. al.<sup>[68]</sup>

However, a persistent challenge has been the utilization of very short DNA oligos for cloning into the appropriate phagemid.<sup>[69]</sup> While there were existing methods to address this issue, they proved to be time-consuming and yielded only minimal outputs.<sup>[74]</sup> V. Jakob et. al. successfully developed a protocol, using the previously introduced hot fusion technique to integrate an oligo sequence of approximately 60 base pairs, with the library comprising 21 base pairs.<sup>[69,75]</sup> This library enables the expression of heptameric peptides, with five random amino acids and two fixed cysteine positions for subsequent oxidation to the corresponding disulfide bridged peptide.<sup>[69]</sup>

## 2.4 Solid Phase Peptide Synthesis (SPPS)

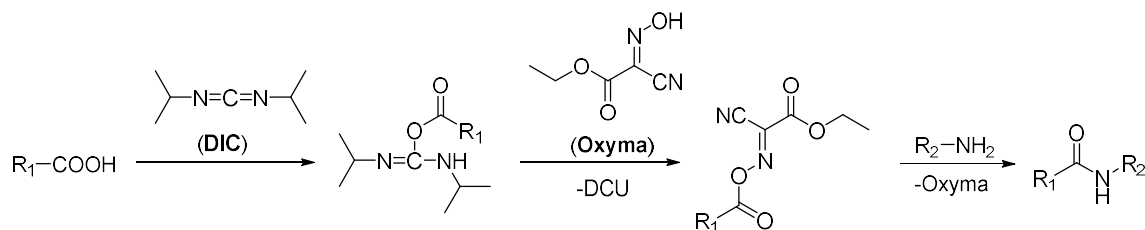
Amide coupling reactions are widely utilized in organic synthesis and are essential in various medicinal chemistry approaches. The fundamental concept involves activating carboxylic acids to render the carbonyl carbon electrophilic enough to undergo attack by a deprotonated amine. This procedure leads to the creation of an amide bond along with a protonated leaving group, as depicted in (Scheme 3).

Y usually: Fmoc, Boc, Cbz



**Scheme 3:** General principle of amide coupling reagents.<sup>[76]</sup>

In recent decades, significant advancements have occurred in the development of coupling reagents. Traditional methods using acid halides or anhydrides have been associated with racemization and the formation of inherent side products such as N-carboxyanhydrides and diketopiperazines. While newer coupling reagents address these issues, they bring along their own challenges, such as N-acylurea formation with carbodiimides like DCC or guanidinium formation with uronium salts.<sup>[76]</sup> The synergistic use of carbodiimides and benzotriazoles has proven highly effective, leading to the development of combined reagents like uronium salts (e.g., HATU, HBTU) and phosphonium salts (e.g., Bop, PyBop), which surpass previously introduced reagents in terms of selectivity and racemisation suppression. However, HATU presents concerns regarding potential explosiveness and cost, prompting continued exploration for optimal coupling reagents. The introduction of Oxyma by El-Faham and Albericio in 2009, revolutionized the field, providing a safe, cost-effective additive for carbodiimide couplings that even outperformed HATU in terms of efficiency, particularly for sterically demanding peptide couplings.<sup>[76,77]</sup> Thus, the combination of DIC and Oxyma (**Figure 6**) was used in this thesis for most peptide couplings on solid support.



**Scheme 4:** Specific coupling conditions, frequently used throughout this thesis.<sup>[76]</sup>

Traditional in-solution peptide synthesis proves efficient for single peptide couplings. However, when multiple couplings are required for protein assembly, the process becomes laborious, as each coupling step necessitates a workup and sometimes a purification step.

In 1963 Robert Bruce Merrifield introduced a groundbreaking concept: performing peptide synthesis on a polymer support surface.<sup>[78]</sup> This innovation allowed coupling and deprotection reagents to be washed away, while the growing peptide fragment remained tethered to the polymer support until final cleavage, vastly simplifying multi-step peptide coupling.

Merryfield's approach is depicted in (**figure 4**). It utilizes nitrated, chloromethylated polystyrene as the solid support, later called resin. Employing the benzyloxycarbonyl (Cbz) protecting group for the amine and HBr/HOAc as the deprotection agent, he employed DCC as the coupling reagent. Final cleavage from the resin occurred with a sodium hydroxide solution or concentrated HBr/HOAc.<sup>[78]</sup> Despite the drawback of prolonged use of HBr/HOAc for peptide cleavage, Merryfield succeeded in synthesizing H-Leu-Ala-Gly-Val-OH, the first tetrapeptide on solid support, laying the groundwork for this field. While the nowadays used resins, reagents and protecting groups for solid phase peptide synthesis (SPPS) are different from Merryfield design, the underlying principle remains unchanged. He even came up with the name of the strategy and was rewarded with the nobel prize in chemistry in 1984 for his innovative work.<sup>[79]</sup>

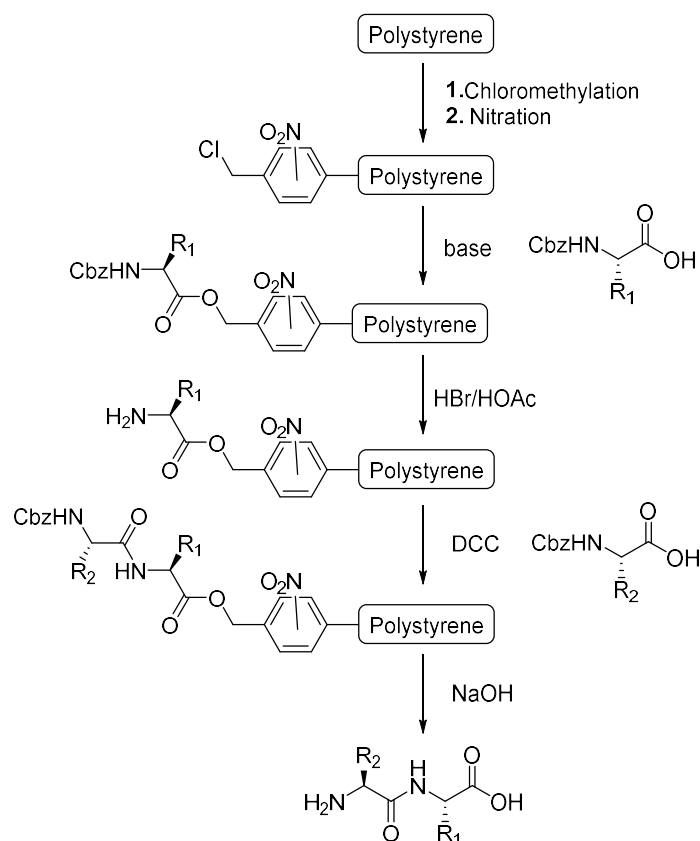


**Figure 4:** Illustration of Merryfield's first attempts to synthesize peptides on resin.<sup>[78]</sup>

During the early stages of SPPS, the BOC-strategy predominated, utilizing BOC-protected amino acids cleaved under relatively gentle acidic conditions, often paired with acid-stable side chain protecting groups like benzyl. The major problem was the cleavage from the resin, where HF needs to be applied, which is an extremely dangerous reagent that requires special lab ware and safety precautions.

In the last decades, the Fmoc-strategy emerged as being superior. In this approach, Fmoc-protected amino acids are used, the Fmoc-group can be removed using secondary amines like piperidine. The side chain protecting groups (such as tBu, Boc, Pbf, Trt) are sensitive to acid and can be cleaved together with the peptide from the resin, providing a reliable and robust method for peptide synthesis. **Figure 5** illustrates the principle of SPPS in a comprehensive manner.<sup>[80]</sup>

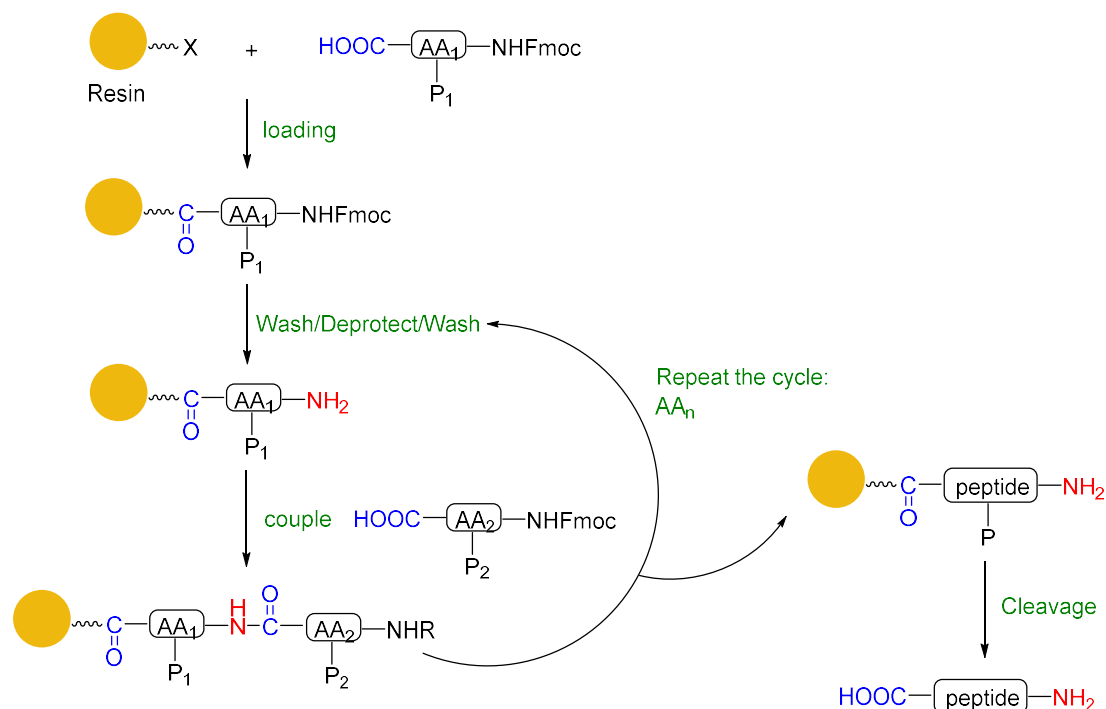


**Figure 5:** Function of modern SPPS, inspired by Palomo's illustration.<sup>[80]</sup>

As coupling reagents evolved, so did the solid supports used. Among the most commonly utilized resins are those facilitating the release of peptides as either amides or acids. Additionally, there exist more specialized resins capable of yielding peptides as esters, alcohols, hydrazides, or thioesters, after cleavage although these are infrequently employed. Prominent examples of resins for producing free acids include Wang resin, HMPB resin, and 2-Chlorotrityl resin. Wang resin necessitates strong acidic conditions for cleavage (95% TFA for 2 hours), while HMPB and Chlorotrityl resins require only mild acidic conditions (1% TFA for 1-5 minutes), enabling the cleavage of fully protected peptides. For amides, the Rink amide resin demands strong acidic conditions, whereas the Pal amide and Sieber amide resins require only mild acidic conditions (see **Figure 6**).



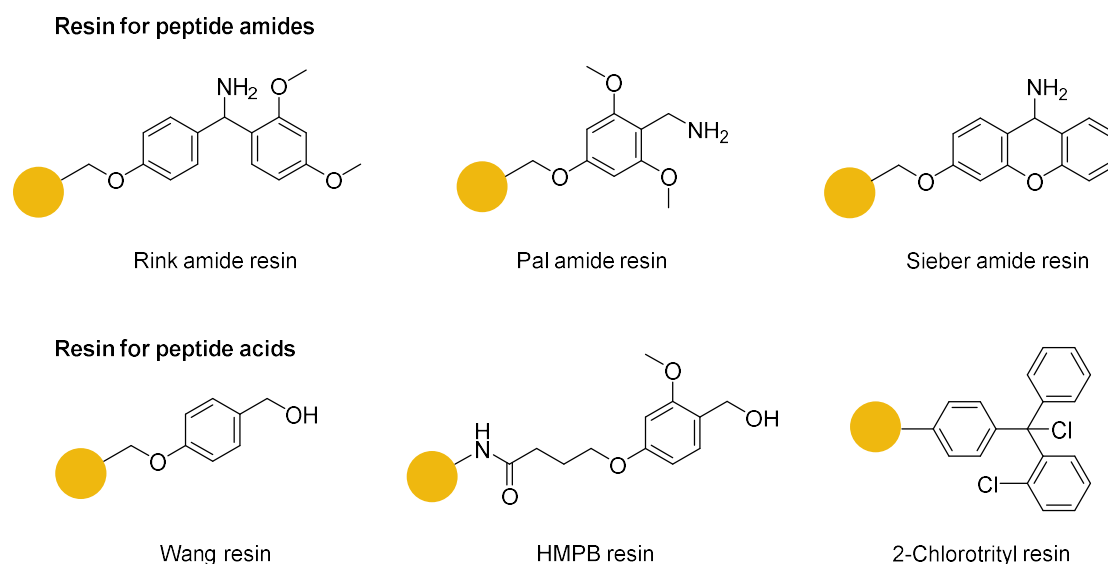


**Figure 6:** Example of different resins used in SPPS.<sup>[80] [79]</sup>

## 2.5 Biophysical assays

In medicinal chemistry, a primary objective is to discover molecules that efficiently and selectively bind to specific targets, typically proteins. Accurate quantification of this binding is crucial for optimizing compounds and facilitating comparisons between them. In most cases the first parameter of interest is either the  $IC_{50}$  or the  $K_d$ -value, measured in *in vitro* experiments.

The half maximal inhibitory concentration ( $IC_{50}$ ) indicates the amount of a substance required to inhibit a biological process by 50%. On the other hand, the dissociation constant ( $K_d$ ) represents the concentration of an inhibitor at which half of the target biomolecules are inhibited.  $K_d$  quantifies the equilibrium of direct binding and is typically more accurate than the  $IC_{50}$  value when comparing inhibitory effects.<sup>[81]</sup>

Various methods exist for determining  $IC_{50}$  and  $K_d$ -values. In our study, we employed either surface plasmon resonance spectroscopy (SPR) or fluorescence polarization spectroscopy for screening and evaluating these compounds ( $K_d$ -values were measured for SPR- spectroscopy and  $IC_{50}$ -values in the case of fluorescence polarization spectroscopy).

### 2.5.1 Surface plasmon resonance (SPR) spectroscopy

When light transitions from a denser medium (higher refractive index) to a less dense medium (lower refractive index), it undergoes refraction. At a critical angle, total internal reflection occurs, this causes the light to be rather reflected at the surface, than being refracted.<sup>[82]</sup> If one of the two mediums is a metal surface, such as a gold film, the incoming light can be absorbed by the electrons within the gold surface, causing them to resonate. These resonating electrons are termed surface plasmons, and the angle at which surface plasmon generation occurs is referred to as the resonance angle. At this angle, a decrease in the intensity of the emitted beam can be observed. The resonance angle is highly dependent on surface properties such as molecular mass.<sup>[82]</sup>

In the SPR spectroscopy, the gold surface is usually coated with a lipophilic dextran matrix and can be immobilized with a molecule of interest in our case a protein. The protein of interest can either be immobilized directly to the gold surface via standard chemical protocols or in an indirect manner in which case another molecule in general an antibody or a protein such as streptavidin are immobilised on the gold surface and the protein of interest will bind this protein in a strong but non-covalent manner, for example via biotin-tag.<sup>[83,84,85]</sup> Usually SPR spectrometers feature the so called Kretschmann configuration (shown in **Figure 7**).

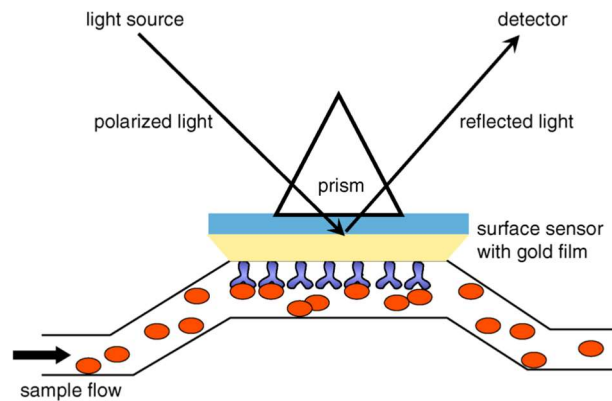


**Figure 7:** Kretschmann configuration of an SPR-experiment setup.<sup>[82]</sup>

The detection signal in SPR-spectroscopy is the shift of the intensity drop, which occurs at the resonance angle. The resonance angle is directly related to the refractive index near the surface. This refractive index, in turn, is influenced by the molecular weight of the gold surface. When an analyte binds to the protein of interest, there is a change in molecular weight, which leads to a shift in the resonance angle. In SPR spectroscopy, the measured signal is the alteration of the resonance angle over time. Typically, 1000 response units (RU) correspond to an angle change of  $0.1^\circ$ .<sup>[82]</sup> A comprehensive figure of the evaluation of the signal over time and its biophysical meaning is shown in (**Figure 8**).

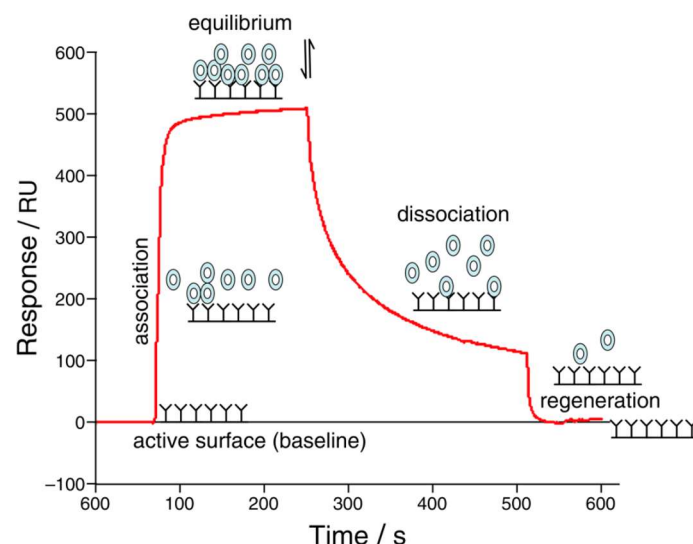


**Figure 8:** Response/signal curve of an SPR-experiment with added explanation of the biophysical processes at each step, illustration from Bakhitar et. al.<sup>[82]</sup>

## 2.5.2 Fluorescence polarisation spectroscopy

Ordinary light exhibits an infinite array of spatial orientations. However, when employing a polarization filter, it selectively permits only light waves aligned in a vertical orientation to pass through. Upon encountering a fluorophore, this vertically oriented light wave triggers its excitation, enabling the emission of a similarly oriented light wave.<sup>[82]</sup>

In most Fluorescence polarisation assays, those fluorophores are bound to biomolecules, such as RNA, in our case. These molecules are able to freely rotate in solution, thus emitting light waves with varying orientations. The orientation of the emitted light is defined by the spatial orientation of the biomolecule itself, the duration for which light is emitted in a defined orientation depends on the rotational speed which itself is correlated to the size and weight of the biomolecule. A secondary polarisation filter is utilized to isolate the lightwaves with the same orientation as the initially polarized light wave. The intensity of the light passing the second filter is used as a signal in the assay.<sup>[86]</sup> (see **Figure 9**).

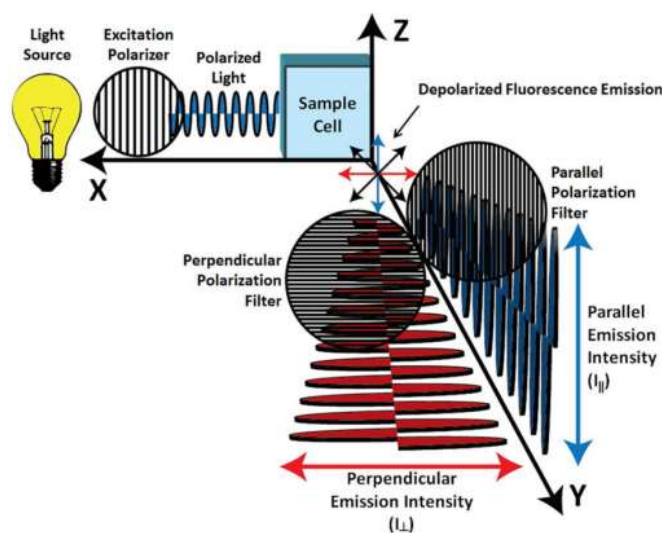


**Figure 9:** Experimental setup of an Fluorescence Polarisation experiment.<sup>[86]</sup>

Fluorescence Polarization assays employ diverse setups, all aimed at monitoring the changes in polarized light intensity over time. When a fluorophore binds to a large and heavy molecule either covalently or non-covalently, its rotation in solution slows down, preserving the proper orientation for light to pass through the filter for a longer duration, resulting in a stronger signal. Conversely, smaller molecules rotate more rapidly, leading to a weaker signal.<sup>[86]</sup> In our study, we utilize a fluorescence labelled RNA sequence, which is designed to bind to CsrA. The resulting RNA-protein complex, rotates slowly, thereby generating a strong signal. However, when a potent inhibitor binds strongly to CsrA, it displaces the labelled RNA, causing free fluorescein-labelled RNA to be released into the solution. This results in a decrease in signal intensity. Monitoring this intensity drop over time allows for the determination of  $IC_{50}$  values for inhibitors (see **Figure 10**).

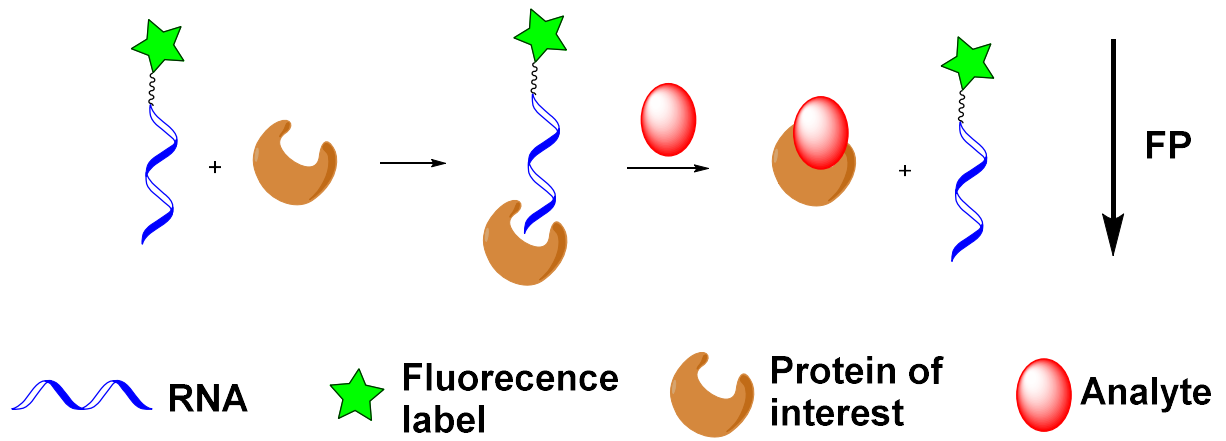
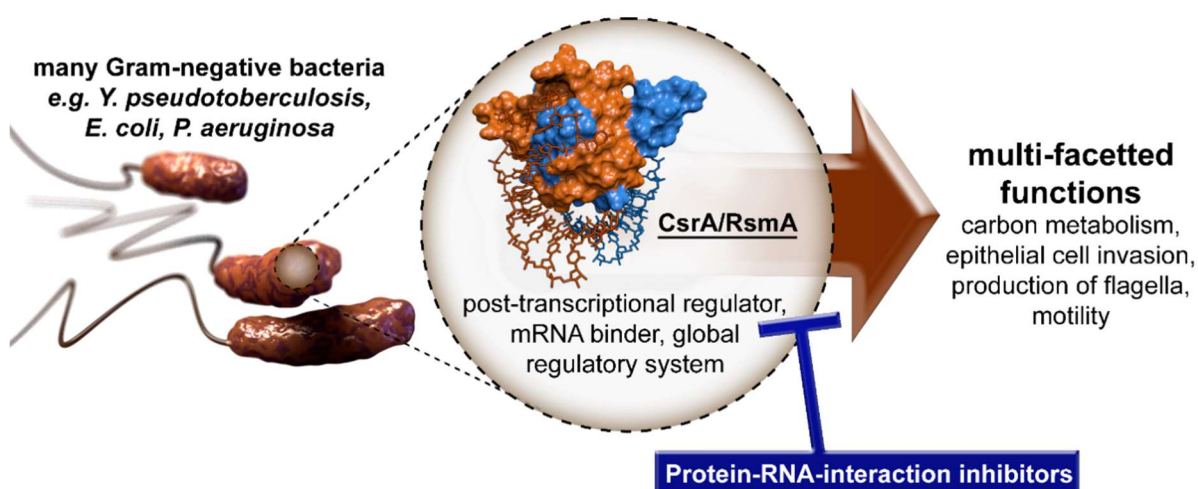


Figure 10: Illustration of the function of FluPo for the assessment of RNA-protein interaction inhibitors.<sup>[87]</sup>

## 3. Workflow

### 3.1 CsrA

Previous investigations suggest that CsrA plays a key role in the regulation of multiple processes in several pathogenic bacteria. Thus, its inhibition should strongly dysregulate the bacteria and have a major impact on bacterial virulence (**Figure 11**). The main goal of this thesis was to find additional molecules that inhibit the CsrA-RNA interaction *in vitro* and ultimately to find molecules which were able to do so *in vivo*. The documentation of the effects of *in vivo* CsrA-inhibition could deliver the proof of concept that CsrA is a druggable antivirulence target, which would be a major milestone in antivirulence drug discovery.



**Figure 11:** Diverse functions exerted by CsrA, rendering it a promising antivirulence target.

Consequently, we faced the challenge of designing molecules that were sufficiently large and structurally complex to disrupt the CsrA-RNA interaction, yet still feasible to synthesize. This led to the use of the previously mentioned self-constructed phage-library by V. Jakob in a phage display-based screening approach. The phage display and careful biophysical evaluation of hits, led to the discovery of a small macrocyclic peptide which was able to inhibit the CsrA-RNA interaction *in vitro*.<sup>[69,2,88]</sup>

The first part of this thesis consists of derivatisation and optimisation of the initial screening hit peptide via SPPS, an easy way to synthesize complex peptides in short time. This work culminated in the discovery of a redox-stabilized triazole-bridged heptapeptide with good activity against CsrA from *E. coli* and *Y. pseudotuberculosis* as well as moderate activity against RsmA from *Pseudomonas aeruginosa* and the publication of this work in the European Journal of Medicinal Chemistry.<sup>[2]</sup>

While the initial design of CsrA inhibitors demonstrated on-target activity, they fell short in demonstrating in-cell activity, primary attributed to poor membrane permeability. This limitation became evident in permeability assays using caco-2 cells. Attempts to enhance permeability through peptide derivatization, including the conjugation of cell-penetrating peptides and other

N or C-terminal modifications, proved unsuccessful, as even slight modifications led to a significant decrease in activity.

We therefore decided to switch back to small molecules. We choose a commercial Enamine library containing 11.000 structurally diverse compounds for screening (Discovery Diversity Set-10, Enamine). Following *in-silico* preselection and SPR-screening, we identified five compounds from four different classes as primary actives. Upon resynthesis, two compounds from distinct classes demonstrated activity against CsrA from *E. coli*.

Since we were aware of the problems attributed to cell wall barriers of Gram-negative bacteria, where on-target activity alone does not guarantee an impact on bacterial function, we wanted to assess in-cell activity. Consequently, we shifted from a purely biophysical screening approach to an “*in-bacterio*” assay for hit optimization. We successfully developed a luciferase-based reporter gene assay, measuring the increase in luminescence relative to CesT as a signal for in-cell activity.<sup>[12]</sup>

The subsequent phase of the CsrA-RNA interaction inhibitor discovery process involves synthesizing and optimizing more than fifty compounds from the two classes that demonstrated activity in the biophysical screening.

### 3.2 IMP2

A Fluorescence Polarisation-based screening of several in-house libraries was conducted by the group of A. at Saarland University to identify potential IMP2 binders. After exclusion of 16 original hits, due to fluorescence quenching and fourteen more due to unspecific binding, eighteen molecules belonging to two different classes were identified as IMP2 binders capable of replacing the protein-bound RNA.<sup>[3]</sup>

As those molecules belong to the Benzamidobenzoic acid class, as well as the Uredothiophene class, the synthesis of these compound classes was well known in literature, as described by Sahrer et. al.<sup>[60]</sup> and Hinsberger et. al.<sup>[59]</sup> previously.

My role in this publication, was the development of an improved route for the synthesis of these compounds. Mostly optimizing reaction temperature and time, amounts and the nature of reagents and solvents, as well as procedures for work-up and purification. I focused on five compounds shown in (**Figure 11**), which were used in excessive amounts for *in vivo* studies using zebrafish xenograft models.

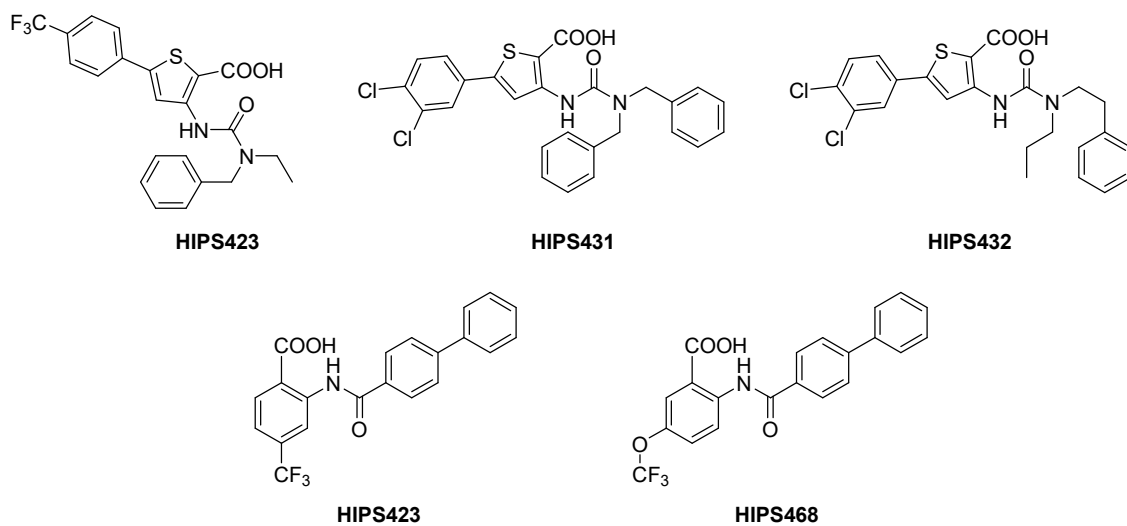


**Figure 12:** Molecules synthesized as IMP2 inhibitors for in vivo experiments.<sup>[3]</sup>

## 4. Results and Discussion

### 4.1 Peptides inhibiting the CsrA-RNA interaction

Phage display-based discovery of cyclic peptides against the broad spectrum bacterial anti-virulence target CsrA

Authors:

Valentin Jakob\*, Ben G. E. Zoller\*, Julia Rinkes, Yingwen Wu, Alexander F. Kiefer, Michael Hust, Saskia Polten, Andrew M. White, Peta J. Harvey, Thomas Durek, David J. Craik, Andreas Siebert, Uli Kazmaier and Martin Empting

\* These authors contributed equally.

Bibliographic Data:

*Eur. J. Med. Chem.* **2022** <https://doi.org/10.1016/j.ejmech.2022.114148>

Author Contributions: Valentin Jakob wrote the manuscript, has done CsrA expression, performed the assays and was involved in peptide synthesis and analytics. Ben G. E. Zoller performed extensive automated and manual peptide synthesis, generating over 100 heptameric peptide derivatives contributing to the optimisation of the initial hit compound by Alanine scan and SAR studies. Moreover, he developed macrocyclization procedures for the disulfide and triazole compounds and was engaged in disulfide bridge displacement studies, leading to the development of the redox-stable 1,4 triazole compound. Additionally, Ben G. E. Zoller contributed to compound characterisation by measuring and analysing LC-MS, HRMS and NMR data of all synthesized peptides and wrote parts of the manuscript and the SI. Julia Rinkes was involved in peptide synthesis and analytics and wrote some parts of the SI. Dr. Yingwen Wu was involved in CsrA expression and in some assays, especially E. coli CsrA. Dr. Alexander F. Kiefer contributed to peptide synthesis, data evaluation and processing and wrote parts of the manuscript. Prof. Dr. Michael Hust and Saskia Polten provided access to their Phage Display technology and supported the conduction of phage panning and isolation. Dr. Andrew M. White synthesized compounds 6a, 6b and 6c, made parts of the analytics of these and wrote some parts of the SI. Dr. Peta J. Harvey generated and deposited the NMR structures. Dr. Thomas Durek and Prof. David J. Craik were involved in planning and wrote parts of the manuscript. Andreas Siebert supported automated peptide synthesis and was always a great help during the experiments with it. The group of Prof. Dr. Uli Kazmaier provided the peptide synthesizer. Prof. Dr. Martin Empting conceived the concept of the study, interpreted the data of the presented idea and wrote parts of the manuscript.





## Contents lists

## European Journal of Medicinal Chemistry



## Phage display-based discovery of cyclic peptides against the broad spectrum bacterial anti-virulence target CsrA

Valentin Jakob <sup>a, b, 1</sup>, Ben G.E. Zoller <sup>a, b, 1</sup>, Julia Rinkes <sup>a, b</sup>, Yingwen Wu <sup>a, b</sup>,  
 Alexander F. Kiefer <sup>a, b</sup>, Michael Hust <sup>c</sup>, Saskia Polten <sup>c</sup>, Andrew M. White <sup>d</sup>,  
 Peta J. Harvey <sup>d</sup>, Thomas Durek <sup>d</sup>, David J. Craik <sup>d</sup>, Andreas Siebert <sup>e</sup>, Uli Kazmaier <sup>e</sup>, Martin  
 Empting <sup>a, b, \*</sup>

<sup>a</sup> Department of Drug Design and Optimization (DDOP), Helmholtz-Institute for Pharmaceutical Research Saarland (HIPS) - Helmholtz Centre for Infection Research (HZI), Campus E8.1, 66123, Saarbrücken, Germany <sup>b</sup> Department of Pharmacy, Saarland University, Campus E8.1, 66123, Saarbrücken, Germany <sup>c</sup> Technische Universität Braunschweig, Institut für Biochemie, Biotechnologie und Bioinformatik, Spielmannstr. 7, 38106, Braunschweig, Germany <sup>d</sup> ARC Centre of Excellence for Innovations in Peptide and Protein Science, Institute for Molecular Bioscience, The University of Queensland, Brisbane, QLD, 4072, Australia <sup>e</sup> Institut für Organische Chemie Saarland University Campus C4.2, 66123, Saarbrücken, Germany

artic  
le in  
fo

Disulfide bridges  
 Disulfide mimetics  
 Peptides  
 Phage display  
 Triazole bridge

abstract

### Article history:

Received 26 November  
 2021  
 Received in revised  
 form  
 18 January 2022  
 Accepted 18 January  
 2022 Available online  
 24 January 2022

### Keywords:

Competitive CsrA  
 inhibition

Small macrocyclic peptides are promising candidates for new anti-infective drugs. To date, such peptides have been poorly studied in the context of anti-virulence targets. Using phage display and a self-designed peptide library, we identified a cyclic heptapeptide that can bind the carbon storage regulator A (CsrA) from *Yersinia pseudotuberculosis* and displace bound RNA. This disulfide-bridged peptide, showed an IC50 value in the low micromolar range. Upon further characterization, cyclisation was found to be essential for its activity. To increase metabolic stability, a series of disulfide mimetics were designed and a redox-stable 1,4-disubstituted 1,2,3-triazole analogue displayed activity in the double-digit micromolar range. Further experiments revealed that this triazole peptidomimetic is also active against CsrA from *Escherichia coli* and RsmA from *Pseudomonas aeruginosa*. This study provides an ideal starting point for medicinal chemistry optimization of this macrocyclic peptide and might pave the way towards broadacting virulence modulators.

## 1. Introduction

For many years, researchers have warned about the antimicrobial resistance (AMR) crisis [1-3]. The rampant spread of multidrug resistant bacterial pathogens combined with the lack of novel treatment options, especially against Gram-negative species, poses a great threat for our modern healthcare systems [4]. For this reason, the discovery of

new anti-infective candidates with novel and innovative mechanisms-of-action are needed. We consider the carbon storage regulator A (CsrA; in some species

also called the regulator of secondary metabolites, RsmA) [5] as an attractive, yet underexplored, virulence-modulating target

[6,7]. It is widespread in Gram-negative pathogens [8] where its sequence and function is highly conserved [9]. Knock-out studies in *Pseudomonas aeruginosa*, *Yersinia pseudotuberculosis* and *Helicobacter pylori* [10] have demonstrated its critical role in bacterial virulence and highlighted its potential as a therapeutic target [11]. The CsrA/RsmA protein is a post-transcriptional regulator [12], that binds and regulates translation of mRNA and, thus exerts pleiotropic effects on the bacterial transcriptome (Fig. 1) [13,14].

Through its mRNA binding activity it is involved in the regulation of quorum sensing [15], motility [16], carbon metabolism [17], peptide uptake via *cstA* [18-20] and biofilm development [21]. To disrupt the function of CsrA/RsmA at the molecular level, protein-RNA interaction inhibitors need to be devised. CsrA usually occurs as a homodimer, with two identical RNA-binding sites [22].

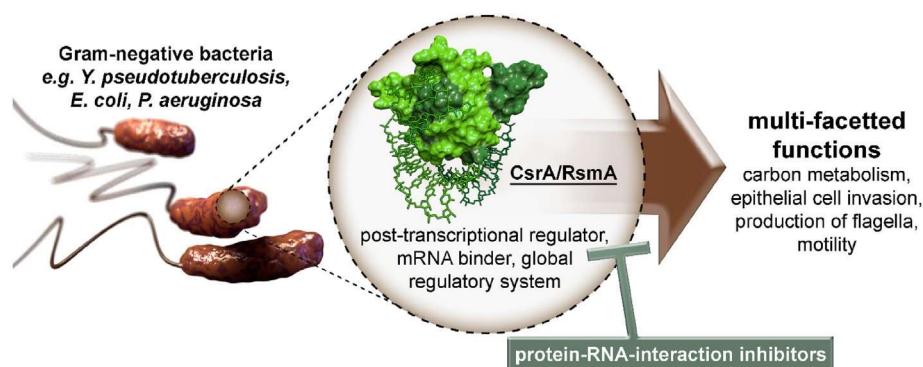


Fig. 1. CsrA/RsmA as a promising drug target for multi-pathogen virulence modulation by disruption of an essential protein-RNA interaction.

In a previous study using *Yersinia* CsrA and a short piece of RNA that contained the important core binding motif GGA, it was shown that this RNA can be displaced by small molecules [10,23]. In the present work, we sought to find novel lead molecules within the extended Lipinski space (MW between 500 and 1000 Da) [24-26]. These molecules should provide a suitable basis for disrupting macromolecule-macromolecule interactions while still retaining the potential for membrane permeability and oral bioavailability [26,27].

## 2. Materials and methods

### 2.1. Phage display

A detailed description of the experimental procedures used for oligomer design, cloning, library packaging and phage display was previously published as a protocol [28]. In brief, an oligomer was designed, which encodes for a very small peptide library,

which has the structure XCXXXCX. There are two fixed cysteine positions in it and X encodes for any amino acid except cysteine. The oligomer was synthesized by Ella Biotech GmbH. This library was cloned into the phagemid pHAL30 [29] where it displays  $2.48 \times 10^6$  different peptides. The library was packed into M13K07 phages, which are able to present the peptides on their surface to a protein target.

Under oxidative conditions, the cysteines are forming a macrocycle over the disulfide bond. For selection of potential CsrA binders, phage display was established. For this process, CsrA\_biot\_His<sub>6</sub> was bound to a streptavidin-coated ELISA plate well. After blocking with BSA/milk powder, the pre-selected library, where BSA and streptavidin binders were excluded, was added. Unspecific binders were eliminated with a plate washer (Tecan Hydroflex), where PBS pH 7.4 containing Tween-20 was used. After the third panning

round the clones were separated on agar plates. 32 clones were sequenced and checked for plausibility. Criteria for selection were an intact sequence with low tryptophane content and one glutamic acid, while carboxyl groups are beneficial for binding to positively charged surfaces on CsrA. We identified two interesting sequences containing a glutamate residue within the macrocycle. Peptide 1 (Ac-V-[CSELC]<sub>cyclic</sub>-W-NH<sub>2</sub>) could be successfully synthesized. Synthesis and macrocyclization of the alternative sequence Ac-H-[CQEVC]<sub>cyclic</sub>-P-NH<sub>2</sub> yielded only dimerized product (data not shown). Nevertheless, this finding underscores the potential ionic interaction between the glutamate side chain and basic residues on the protein surface.

CsrA coating amount of the wells, detergent amount in PBS buffer as well as washing stringency with the plate washer were optimized. Before each panning round, the wells were coated with either 4 µg or 40 µg CsrA<sub>biot</sub>-His<sub>6</sub>. The better results were obtained with 4 µg. 0 µg CsrA was used as negative control. Before phage elution with trypsin, PBS containing different amounts of Tween-20 (0.05%, 0.1% or 0.2%) was tried to rinse the wells with the plate washer. Since the variation effect was not significant, 0.1% Tween-20 was chosen as the detergent amount. The number of washing cycles, however, had a significant impact on the results. Tested were 2/4/6, 4/8/10 and 10/10/10 washing cycles. The first number corresponds to the number of washing cycles after the first panning round, the second after the second and the third after the third round. The more washing rounds were used, the more sequences containing frame shifts or predominantly hydrophobic amino acids (i.e., more than one tryptophan residues) were found. This was the case for the 4/8/10 and 10/10/10 variant. If, on the other hand, fewer washing cycles were used (2/4/6), a large proportion of pHAL30 origin empty vector containing no peptide encoding sequence was found, but also a few desired peptide

sequences as potential binders. Peptide 1 was one of those useful sequences.

## 2.2. Fluorescence polarization assay

The fluorescence polarization assay has been established by Maurer et al. [10]. Fluorescence polarization was recorded using a CLARIOstar microplate reader (BMG LABTECH, Ortenberg, Germany) with an extinction filter at 485 nm and emission filter at 520 nm. Gain adjustment was performed before starting each measurement to achieve maximum sensitivity. The FP values were measured in millipolarization units (mP). The assay was performed two times in duplicates and the IC<sub>50</sub> value was calculated using sigmoidal logistic fit in Origin. Fluorescein-labeled RNA (for *Yersinia* CsrA: 5'-UUCACGGAGAA[flc]; for *E. coli* CsrA: 5'-AGACAAGGAUGU [flc]) was obtained from Sigma Aldrich in HPLC purity. The results of the dose-dependent measurement are shown in [Figure S3 and S4](#).

A 20 mM peptide in DMSO stock solution was diluted with assay buffer (10 mM HEPES, 150 mM NaCl, 0.005% (v/v) Tween-20, ad DEPC-treated H<sub>2</sub>O (RNase free water), pH 7.4) in a way that 3 mM peptide in 15% DMSO was achieved (21 µL 20 mM peptide in DMSO + 119 mL assay buffer). Afterwards, a 1:2 dilution series containing 12 steps was utilized by diluting 70 µL of assay buffer containing 15% DMSO with 70 µL of the peptide in assay buffer with 15% DMSO from this solution ([figure S2](#)), starting from 3 mM ended in 1,46 µM. Using a 12-channel pipette, 10 µL of each concentration were transferred to a 384 well microtiter plate (black, flat bottom, Greiner Bio-One) in two replicates and another 10 µL of 1.2 µM (2.4 µM for *E. coli* CsrA) of the corresponding CsrA-biot-His<sub>6</sub> protein (in assay buffer) were added to each well and quickly centrifuged to be preincubated for 1 h on a Duomax 1030 shaker under light exclusion. 10 µM

fluorescein-labeled RNA (RNA<sub>flc</sub>) was diluted with assay buffer to a concentration of 45 nM obtaining an end concentration of 15 nM in the assay. After short centrifugation the plate was incubated for 1.5 h on the shaker under light exclusion. The final concentrations in the assay were 400 nM (800 nM for *E. coli* CsrA) CsrA-biot-His<sub>6</sub> (monomer concentration), 5% DMSO, 15 nM RNA<sub>flc</sub> and 1000 μM-0.49 μM peptide.

Furthermore, a high control was prepared to check for the homogeneity of fluorescence for the complex between protein and RNA<sub>flc</sub>, a low control to verify the homogeneity of fluorescence for the free RNA<sub>flc</sub> as well as a blank to exclude any deviation due to the matrix of the assay. For the high control components were 10 μL of 15% DMSO in assay buffer, 10 μL of protein and 10 μL of RNA<sub>flc</sub>, for the low control corresponding 10 μL of 15% DMSO in assay buffer, 10 μL of assay buffer and 10 μL of RNA<sub>flc</sub> and the blank consisted of 10 μL of 15% DMSO in assay buffer and two times 10 μL of assay buffer. These three controls were measured in 24-lets.

Moreover, a fluorescence control was performed for the peptides measured to check for the possibility of fluorescence quenching. Therefore, the first component was 10 μL of the dilution series of the corresponding peptide, second component was 10 μL of assay buffer and third component was 10 μL of RNA<sub>flc</sub>.

Thereby, fluorescence intensity was calculated by determination of the sum of blank corrected based on raw data parallel and perpendicular for the highest concentration on the one hand and for the lowest concentration on the other hand. Afterwards, the average of these two values was determined and the deviation from fluorescence intensity to the average value should be under 20% for no fluorescence quenching. This was the reason why the 1000

μM and 500 μM value was not included in the assay for **3d** and **5a**.

### 2.3. Microscale thermophoresis assay (MST)

The MST assay was performed according to the protocol of the Monolith NT™ His-Tag labelling Kit RED-tris-NTA and was used for Peptide **1** only. The *Yersinia* CsrA-biot-His<sub>6</sub> monomer concentration was adjusted with assay buffer (10 mM HEPES, 150 mM NaCl, 0.005% (v/v) Tween-20, ad DEPC-treated H<sub>2</sub>O (RNase free water), pH 7.4) to 200 nM in a volume of 100 μL, mixed with 100 μL 100 nM dye (Nano RED) and incubated for 30 min in the dark at room temperature. The sample was centrifuged for 10 min at 4 C and 15000 g. This was the ready-labeled protein. A 20 mM peptide DMSO stock solution was diluted with assay buffer to 2 mM, that the highest end concentration in the assay was 1000 μM with 5% DMSO. 20 μL of the 2 mM peptide was transferred into a first PCR tube and 10 μL of assay buffer containing 10% DMSO was transferred into each next PCR tube 2-16. For the serial dilution series of the peptide, 10 μL of the ligand from tube 1 were transferred to tube 2 with a pipette and mixed by pipetting up-and-down several times. The procedure was repeated for tube 3-16 and 10 μL from tube 16 were discarded. Finally, 10 μL of the labeled protein were added to each PCR tube, mixed with a pipette and incubated in the dark for 45 min. All 16 dilutions were loaded into Monolith NT™ Standard Capillaries and measured in the Monolith NT.115™ device with 60% excitation power and 40% MST power. The protein concentration in the assay was 50 nM. The assay was performed three times in duplicates and the K<sub>d</sub> value of 10.5 ± 1.4 μM was calculated using sigmoidal logistic fit in Origin. The results from the MST assay for peptide 1 can found in [figure S5](#).

## 2.4. Peptide synthesis and macrocyclization

### 2.4.1. General information

All resins were purchased from Rapp Polymere. The azide/ alkyne building blocks Fmoc-L-azidoalanine (Fmoc-Aza-OH), Fmoc-L-propargylglycine (Fmoc-Pra-OH) and Fmoc-L-homoazidoalanine (Fmoc-Aha-OH) were purchased from Carl Roth VG. Fmoc-Val-OH, Fmoc-Ala-OH, Fmoc-Glu(OtBu)-OH, Fmoc-Leu-OH and FmocCys(Trt)-OH were purchased from Novabiochem. Fmoc-Ser(tBu)OH was purchased from TCI.

### 2.4.2. General Fmoc-SPPS procedure

Most peptides were synthesized manually via solid phase peptide synthesis (SPPS) using Fmoc chemistry. The resin was swollen for 30 min in DMF. For Fmoc deprotection piperidine/DMF (1:4, v:v) was added and shaken for 5 min, twice. It was then washed five times with DMF followed by the second round of adding piperidine/DMF (1:4) with incubating 5 min on a shaker. It was washed five times with DMF, five times with DCM and again one time with DMF. We used double coupling for each amino acid. The amino acid (4.0 eq.) was solved in DMF together with 3.9 eq 3-[Bis(dimethylamino)methyl]imidazolium hexafluorophosphate (HBTU) followed by adding 8.0 eq. N-Ethyl-N-(propan-2-yl)propan-2-amine (DIPEA). This solution was pre-activated for 5 min on a shaker. The activated solution was added to the resin and incubated for 1 h on a shaker. After washing five times with DMF, it was added an activated amino acid/HBTU/DIPEA/DMF solution again and incubated 1 h on a shaker. The resin was washed five times with DMF and five times with DCM. This was followed by two deprotection cycles and two coupling cycles of the next amino acid.

### 2.4.3. General acetylation procedure

For Acetylation, DMF/DIPEA/Ac<sub>2</sub>O (12:8:5, v:v:v) was added to the resin and shaken for

0.5 h. Then it was washed five times with DMF, five times with DCM and again one time with DMF.

### 2.4.4. General cleavage procedure

For protein cleavage from the solid support and removal of the side chain protecting groups a cleavage cocktail containing trifluoroacetic acid (TFA)/triisopropylsilane (TIS)/H<sub>2</sub>O/anisole (95:2:2:1, v:v:v) with a spatula tip of dithiothreitol (DTT) was added to the resin and incubated 2.5-3.0 h on a shaker. The liquid was collected and TFA was removed under reduced pressure, followed by precipitation with cold (-20 °C) methyl tert-butyl ether (MTBE). The crude peptide was gained by centrifugation (4600 rpm, 4 °C, 10 min) followed by MTBE washing (3x) and repeated centrifugation.

### 2.4.5. General cyclisation procedure

For disulfide cyclisation the crude lyophilized peptide was dissolved in H<sub>2</sub>O/ACN (1:1, v:v) with a concentration of 1 mg peptide per 1 mL solvent and 1-3% DMSO was added. The pH was adjusted to 7.7 using 1 M aq. ammonium carbonate solution. The solution was stirred for 1-4 days. The reaction was monitored by LC-MS.

### 2.4.6. General preparative HPLC procedure

The purification was done with a DIONEX UltiMate 3000 UHPLC<sub>p</sub> focused (Thermo Scientific), containing pump, diode array detector, and automated fraction collector. We used a VP 250/10 NUCLEODUR C18 Gravity, 5 μM (Macherey-Nagel) column with a gradient from 10 to 50% solvent B over 25 min (solvent A: H<sub>2</sub>O (0.05% formic acid), solvent B: ACN (0.05% formic acid)) and a 5 mL/ min flowrate. Pure fractions were checked by LC-MS, combined and lyophilized.

## 3. Results and discussion

### 3.1. Phage display

We devised a strategy to screen a library of disulfideconstrained heptapeptides covering a mass range between 548 and 1193 Da via phage display (Scheme 1) [28]. The use of phageencoded libraries displaying millions of compound variants [30] has proven to be an excellent method for finding novel binders for several targets [31]. An important example is the search for small antibody fragments, so called single-chain variable fragments (scFvs) for any desired target [32,33]. Phage display can also be transferred to libraries encoding for short peptides [31,34]. This method allows screening of whole peptide libraries to find potential binders for a given target [35]. Our self-designed phage library encodes for a peptide library with the general structure XCXXXCX ( $2.48 \times 10^6$  variants) [28]. It contains two cysteine residues at fixed positions, which form a disulfide bond under oxidative conditions; X encodes for any amino acid except cysteine. This design provides the means to identify very small peptides with a mass range of around 550-1200 Da that are rigidified by a well-defined macrocyclization motif. We screened this library against immobilized *Yersinia* CsrA (biotinylated and His-tagged CsrA construct CsrA\_biot\_His<sub>6</sub>; more details on phage display and CsrA expression can be seen in Supporting Information and a published protocol) bound to a streptavidin-coated ELISA well. After three rounds of panning, phage binding with high affinity were separated on agar plates. After sequencing of 32 clones, we identified one sequence as a potential CsrA binder. The criteria for selection were intact sequences and avoidance of a high tryptophan content (more than two Trp), which usually leads to unspecific binding [36]. Notably, the selected sequence contained a glutamic acid residue - a feature we deemed plausible as anionic carboxyl groups should be of benefit for binding the positively charged surface of CsrA

possessing a high content of basic amino acids.

### 3.2. First evaluation of peptidic hit

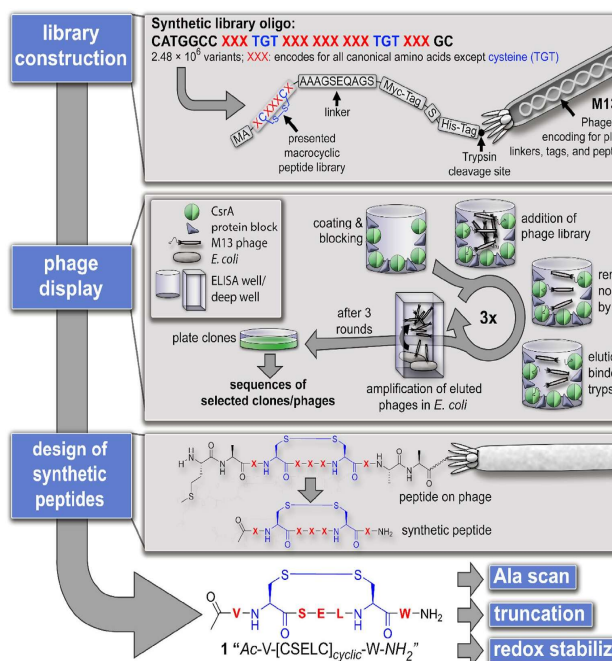
This peptidic hit (**1**) was synthesized by solid phase peptide synthesis (SPPS) in disulfide-cyclized, N-terminally acetylated and C-terminally amidated form. These modifications were chosen because the sequence is presented within a peptide backbone extending beyond its N- and C-termini on the phage during the panning experiment. The peptide was characterized by LC-MS, HRMS and NMR (Supporting Information). Using an established fluorescence polarization assay [10] (2.4), peptide **1** was tested for its ability to displace mRNA from CsrA. In this assay a fluorescein (flc)-labeled RNA (5'-UUCACGGAGAA[flc]) and CsrA\_biot\_His<sub>6</sub> were used to probe the protein-RNA interaction. The labeled RNA was successfully displaced by peptide **1** with an IC<sub>50</sub> value in the micromolar range ( $6.9 \pm 1.3 \mu\text{M}$ , Fig. 2). This peptide amongst the most potent compounds discovered against CsrA to date and is readily synthetically accessible. Previously identified natural products such as MM14 and tubulylin Ar-672, have shown similar potency ( $4 \pm 1 \mu\text{M}$  and  $11 \pm 1 \mu\text{M}$ , respectively) [10], but are much more challenging to synthesize.

When the assay was conducted in the presence of 5 mM DTT, peptide **1** lost its activity almost completely. Under these conditions the disulfide bond is reduced and the macrocycle linearized. Thus, we concluded that the conformational constraint induced by the disulfide bond is essential for activity. This observation also supports a conformation-specific (structure-dependent) interaction between the peptide and CsrA. Additionally, a microscale thermophoresis (MST) assay was performed with peptide **1** and CsrA\_biot\_His<sub>6</sub> yielding a  $K_d$  of  $10.5 \pm 1.4 \mu\text{M}$  (2.5). This assay further supports a direct specific interaction between the peptide and CsrA.

### 3.3. Alanine scan and truncation

To gain further insights into the underlying structure-activity relationship (SAR) of peptide **1** we synthesized an array of derivatives by Fmoc-SPPS, oxidized them with DMSO and tested for inhibitory activity in the fluorescence polarization assay. The resulting IC<sub>50</sub> values are listed in Table 1.

To investigate the importance of the N-terminal acetylation as well as the C-terminal amide, peptides 2a and 2b were synthesized, respectively. We observed slightly increased IC<sub>50</sub> values ( $27.6 \pm 4.0 \mu\text{M}$  and  $17.4 \pm 2.0 \mu\text{M}$ , respectively) indicating that both modifications contribute to the overall affinity of peptide **1**. To identify possible interaction hotspots, an alanine scan of peptide **1** was performed.



**Scheme 1.** Phage display-based selection process from library design to peptide hit identification. Library construction: An oligomer was constructed to code for the subsequent peptide library. After cloning and packaging in M13 phage, genotype and phenotype are coupled by presenting the encoded peptide including tags and linkers simultaneously. Phage display: The peptide phage library was used in the panning process, in which the enrichment of potential CsrA binders is achieved. Sequences of the bound peptides were identified by sequencing the coding phage gene. Design of synthetic peptides: Representation of a phage from panning to which a general library peptide including peptide backbone is linked, compared to the synthesized peptides. Here, N-terminal acetylation and C-terminal amidation simulate the peptide backbone. Furthermore: A representation of the selected peptide **1** is given, which was characterized in more detail as a "hit" in the context of this paper.

As expected, activity was abolished when both cysteine residues were replaced by alanine (3a) corroborating our earlier findings when using DTT to linearize peptide 1 (Fig. 1). Similarly, when Ser3 (3c) or Trp7 (3f) were changed to alanine, dramatic losses of activity were observed.

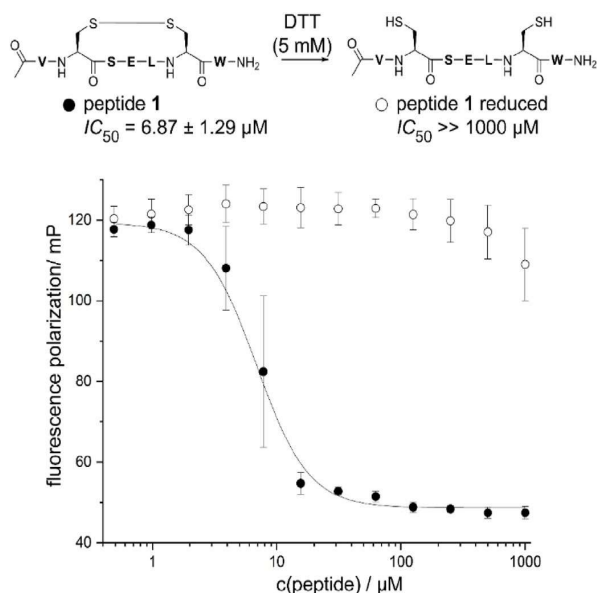


**Fig. 2.** Displacement of RNA<sub>flc</sub> from CsrA<sub>biot\_His6</sub> with peptide 1 and its reduced derivative measured via fluorescence polarization. Data shown are from two independent experiments measured in duplicate and were fitted to a sigmoidal logistic, Levenberg Marquardt inhibition model (solid line). The results of peptide 1 (filled circles) as well as peptide 1 in the presence of 5 mM DTT in the assay are shown (open circles).

**Table 1**  
Peptides 1e4b with corresponding IC<sub>50</sub> values obtained from the fluorescence polarization assay and their activity relative to peptide 1.

Entry	Sequence <sup>a</sup>	IC <sub>50</sub> /mM <sub>b</sub> Y. pseudotuberculosis	Relative activity <sup>c</sup>
1	Ac-V-[CSELC] <sub>cys</sub> -W-NH <sub>2</sub>	6.9 ± 1.3	1
2a	HeV-[CSELC] <sub>cys</sub> -W-NH <sub>2</sub>	27.6 ± 4.0	0.25
2b	Ac-V-[CSELC] <sub>cys</sub> -W-OH	17.4 ± 2.0	0.4
3a	Ac-VASELAW-NH <sub>2</sub>	[1000]	e
3b	Ac-A-[CSELC] <sub>cys</sub> -W-NH <sub>2</sub>	114 ± 8	0.06
3c	Ac-V-[CAELC] <sub>cys</sub> -W-NH <sub>2</sub>	>1000	e
3d	Ac-V-[CSALC] <sub>cys</sub> -W-NH <sub>2</sub>	22.8 ± 0.7	0.3
3e	Ac-V-[CSEAC] <sub>cys</sub> -W-NH <sub>2</sub>	57.9 ± 2.1	0.12
3f	Ac-V-[CSELC] <sub>cys</sub> -A-NH <sub>2</sub>	>500	e
4a	Ac-e-[CSELC] <sub>cys</sub> -W-NH <sub>2</sub>	128 ± 4	0.05
4b	Ac-V-[CSELC] <sub>cys</sub> -e-NH <sub>2</sub>	[1000]	e

<sup>a</sup> Differences relative to peptide 1 are shown in bold or as “e” for deletions. Each

peptide is disulfide-cyclized (except 3a) over the cysteines.

<sup>b</sup> Standard error of the sigmoidal curve fit is given (two independent experiments,

measured in duplicates).

<sup>c</sup>

Relative activity for a peptide x is given as the ratio IC<sub>50</sub>(peptide 1)/IC<sub>50</sub>(peptide x).

Therefore, the interactions mediated by the serine and tryptophan sidechains are essential hotspots for high affinity. Furthermore, the Ala-scan allowed us to conclude that substitution of residues Val1 (3b), Glu4 (3d) or Leu5 (3e) has a less pronounced effect on activity, showing IC<sub>50</sub> values of 114 ± 8 μM, 22.8 ± 0.7 μM, and 57.9 ± 2.1 μM, respectively. In the case of the Glu4Ala mutation, this result was surprising. CsrA is an RNA-binding protein possessing a positively charged surface area due to an abundance of lysine and arginine residues. Hence, the presence of the carboxylic acid function in peptide 1 hinted at a potential salt bridge as an important contribution to affinity. If the proposed ionic interaction between Glu4 and the basic amino acid sidechains of CsrA was optimally positioned, a dramatic loss of affinity would have been expected for compound 3d. As this was not the case, this position should be investigated in more detail in future optimization efforts.

Two truncated versions were tested for inhibitory activity to check whether further reduction in size is possible. A version without Val1 (4a) had an IC<sub>50</sub> of 128 ± 4 μM, which is comparable to the value obtained for the Val1Ala mutant, 3b (114 ± 8 μM). If tryptophan is omitted (4b), the activity in the measured concentration range is completely lost and in line with our findings with the Trp7Ala mutant (3f). Hence, we conclude that the complete seven amino acid sequence is required for high activity.

### 3.4. Disulfide replacement by triazole bridge

In a final step, we sought to protect peptide 1 from reductive linearization, which we consider essential for achieving intracellular activity. To this end, we made use of the “triazole bridge” approach [37] and replaced the cysteine residues with non-natural amino



acids bearing alkyne and azide functions in their sidechain for facile click chemistry-based macrocyclization [38-40]. Notably, this strategy provides selective access to either a 1,4-disubstituted or 1,5-disubstituted bridging motif depending on whether copper(I)- or ruthenium(II)-catalyzed azide-alkyne cycloaddition is applied (abbreviated CuAAC or RuAAC, respectively). This method had recently been used, with great success, by the groups of Tomassi et al. [41], Tala et al. [42] and Pacifico et al. [43] to generate redox stable derivatives of disulfide bridge containing peptides. By this means, several different triazole-bridged peptides were generated (Table 2). The linear precursor peptides were synthesized using commercially available building blocks Fmoc-protected propargylglycine (Fmoc-Pra-OH) and Fmoc-protected azidoalanine (Fmoc-Aza-OH) or Fmoc-protected azidohomoalanine (Fmoc-AhaOH). In-solution CuAAC macrocyclization of the unprotected peptides in separate reactions delivered three 1,4-disubstituted 1,2,3-triazole variants (**5a-5c**), which were characterized by LC-MS, HRMS and NMR (Supporting Information) and tested in the fluorescence polarization assay (Table 2). **5a**, originating from an azidoalanine-bearing precursor, showed an  $IC_{50}$  of  $35.3 \pm 0.6 \mu\text{M}$ , which correlates to a moderate 5-fold reduction in potency compared to the disulfide counterpart **1**. Installing an elongated macrocyclization motif by using azidohomoalanine instead (**5c**) leads to a further reduction of activity ( $76.0 \pm 3.3 \mu\text{M}$ ). Changing the orientation of the triazole ring by switching positions of the propargylglycine and azidoalanine residues (**5b**) resulted in an  $IC_{50}$  of  $92.8 \pm 4.0 \mu\text{M}$ .

Previous work on a 14-amino acid, backbone cyclic protease inhibitor peptide SFTI-1, demonstrated the utility of 1,5-disubstituted bridging motifs, which are installed via RuAAC in solution or on resin [37,44]. In the case of our current CsrA-RNA interaction inhibitor **1**, this strategy was surprisingly not

beneficial. Macrocyclic peptide **6a** achieved only an  $IC_{50}$  of  $178 \pm 12 \mu\text{M}$ . If the azidoalanine in position 2 was replaced by azidohomoalanine (**6b**), the  $IC_{50}$  value increased even further to  $337 \pm 34 \mu\text{M}$ . Finally, exchanging the positions of Aha and Pra (**6c**) did not show any significant difference in comparison to **6b** ( $IC_{50} = 309 \pm 15 \mu\text{M}$ ).

To demonstrate the potential for a broader anti-Gram-negative activity we tested peptide **1** and our triazole-stabilized derivatives against the *E. coli* and the *Pseudomonas aeruginosa* homologs of CsrA (RsmA, Table 2). Surprisingly, disulfide-cyclized inhibitor **1** showed a reduced activity ( $IC_{50}$  (*E. coli*) =  $182 \pm 67 \mu\text{M}$ ,  $IC_{50}$  (*P. aeruginosa*) =  $272 \pm 68 \mu\text{M}$ ), while the 1,4-disubstituted triazoles **5a**, **5b** and **5c** now outperformed the parent peptide ( $IC_{50}$  (*E. coli*) =  $4.9 \pm 0.9 \mu\text{M}$ ,  $6.8 \pm 1.5 \mu\text{M}$ , and  $3.4 \pm 0.6 \mu\text{M}$ ,  $IC_{50}$  (*P. aeruginosa*) =  $20 \pm 5.4 \mu\text{M}$ ,  $22.8 \pm 5.0 \mu\text{M}$ , and  $30.2 \pm 3.2 \mu\text{M}$ ). The 1,5-disubstituted congeners again showed reduced activity compared to their 1,4-counterparts, albeit still being more active than the disulfide compound **1**. Considering the high sequence identity between CsrA from *Yersinia* and *E. coli* (95%) [45], it is fair to assume that this finding provides evidence for the potential site of interaction of the macrocyclization motif for our inhibitor scaffold. The only differences in amino acid sequence between the *Y. pseudotuberculosis* and *E. coli* proteins are at distinct residues of the C-terminus, including Pro58Gln, Thr59Ser, and Thr60Ser, respectively (see sections regarding protein expression in the Supporting Information). This region is also close to the protein-RNA interaction interface (Fig. 3). Hence, we hypothesize that the inhibitor scaffold covers an area encompassing interactions to both sites (C-terminus and RNA-binding site). Unfortunately, attempts to co-crystallize the peptide with CsrA have not been successful to date. To gain access to structural information, we solved the structure of

peptide 1 by NMR (PDB ID 7M7X, BMRB ID 30895, Fig. 3a and Supporting Information). With this ligand structure ensemble in hand we performed a docking experiment based on a *Y. pseudotuberculosis* CsrA homology model derived from a protein-RNA complex determined by NMR [46]. The result of the docking experiment is shown in Fig. 3b (see also Supporting Information). The binding pose of peptide 1 is in line with the SAR derived via the Ala-scan and truncation experiments. For example, the side chains of “hot spot” residues Ser3 and Trp7 form key contacts with Lys38 and Val40, while the other residues are primarily involved in backbone-based interactions (Fig. 3c). Although this pose will need further validation in future studies, it provides a basis for explaining the observed differences between *Y. pseudotuberculosis* and *E. coli* CsrA. We hypothesize that the differences in activities seen for compounds in Table 2 are potentially resulting from the Pro58Gln mutation changing the C-terminal interaction site from a rather hydrophobic environment to a more polar one, which might favor the hydrogen acceptor functions of the triazole. Implementation of a 1,5-motif (6a - 6c), however, could result in steric clashes between the ligand and the protein target rendering them less effective in this scenario.

Along similar lines, the decreased sequence identity between CsrA (*Y. pseudotuberculosis*, *E. coli*) and RsmA (*P. aeruginosa*) of 85% (*E. coli* - *P. aeruginosa*) or 86% (*Y. pseudotuberculosis* - *P. aeruginosa*) arising again mainly at the C-terminal end might explain the different SAR observation made (Table 2, Supporting Information).

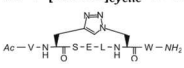
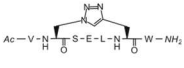
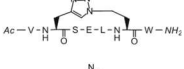
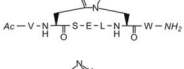
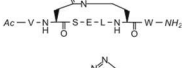
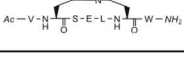
#### 4. Conclusion

In summary, we have shown that the 1,4-disubstituted triazole bridging motif established in 5a is a suitable disulfide replacement that is active against *Y. pseudotuberculosis*, *E. coli* and *P.*

*aeruginosa* CsrA. In combination with our phage display-based screening methodology, we have provided a generic approach towards the identification, initial qualification, and subsequent redox-protection of short macrocyclic peptides as protein-RNA-interaction inhibitors. The phage display methodology proved to be a rapid approach towards identification of the first macrocyclic peptide able to disrupt the CsrA-RNA interaction. The starting scaffold peptide 1 was thoroughly characterized by fluorescence polarization-based functional activity tests as well as MST-based protein binding assay. Exchanging the disulfide bond with a redox stable 1,2,3-triazole bridge gave us active non-natural derivatives suitable for future cell-based assays. Contrary to previous studies, we have observed that in the current system the synthetically easier accessible 1,4-disubstituted 1,2,3-triazole was the superior disulfide mimic showing an IC<sub>50</sub> value in the 2-digit micromolar range. Based on NMR-based solution structure determination of the native peptide sequence and docking experiments structure-guided optimization can now be attempted. This novel scaffold serves as a suitable starting point for the generation of high potency CsrA inhibitors, also because it is applicable against CsrA from further bacterial species with high medical need (*P. aeruginosa*).

**Table 2**

Peptide 1 and triazole-bridged variants 5a-6c with corresponding IC<sub>50</sub> values obtained for *Yersinia* and *E. coli* CsrA and RsmA from *P. aeruginosa* from a fluorescence polarization assay.

Entry	Sequence	IC <sub>50</sub> /μM <sup>a</sup> <i>Yersinia</i>	IC <sub>50</sub> /μM <sup>a</sup> <i>E. Coli</i>	IC <sub>50</sub> /μM <sup>a</sup> <i>P. aeruginosa</i>
<b>1</b>	Ac-V-[CSEL <sub>C</sub> ]-W-NH <sub>2</sub>	6.9 ± 1.3	182 ± 67	272 ± 68
<b>5a</b>		35.3 ± 0.6	4.9 ± 0.9	20 ± 5.4
<b>5b</b>		92.8 ± 4.0	6.8 ± 1.5	22.8 ± 5.0
<b>5c</b>		76.0 ± 3.3	3.4 ± 0.6	30.2 ± 3.2
<b>6a</b>		178 ± 12	48.1 ± 16	50 ± 15
<b>6b</b>		337 ± 34	51.6 ± 27.1	44.4 ± 9.7
<b>6c</b>		309 ± 15	83.4 ± 47.1	37 ± 17

<sup>a</sup> Standard error of the sigmoidal curve fit is given (two independent experiments, measured in duplicate).

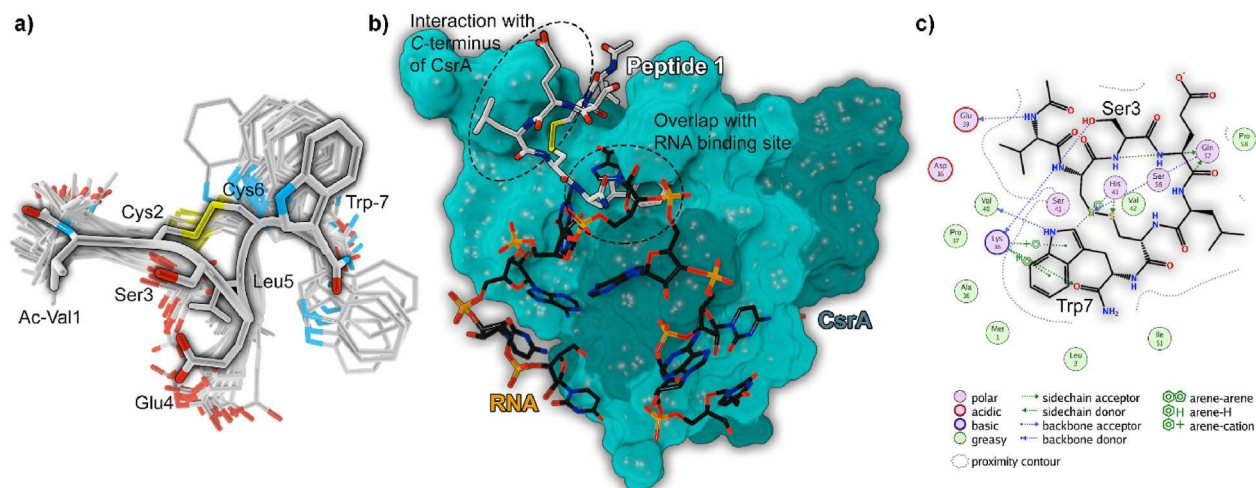


**Fig. 3.** In silico analysis of the peptide-CsrA interaction. a) Overlay of 20 NMR-derived solution structures of peptide 1 (PDB ID 7M7X, BMRB ID 30895) showing the peptide backbone as a tube and highlighting conformer 1 (entry 1 in pdb) for clarity. b) Depiction of docking-derived interaction hypothesis highlighting key interaction sites. Carbons of peptide 1 are shown in white and RNA carbons in black. Surface of the two CsrA chains shown in light cyan and dark cyan. c) 2D interaction profile of binding hypothesis for peptide 1. “Hot spot” residues identified via Ala-scan (Ser3 and Trp7) are indicated.

## Author contribution

The author contributions can be found in the supporting information.

## Declaration of competing interest

The authors declare that they have no known competing financial interests or personal relationships that could have appeared to influence the work reported in this paper.

## Acknowledgments

This work is supported by the Deutsche Forschungsgemeinschaft (DFG) through “RESIST - Resolving Infection Susceptibility” cluster of excellence (EXC 2155). Work in DJCs lab on cyclic peptides is supported by the Australian Research Council (CE200100012). We thank Prof. Dr. Tony Romeo for sending us the plasmid for *E. coli* CsrA expression.

## Appendix A. Supplementary data

Supplementary data to this article can be found online at <https://doi.org/10.1016/j.ejmech.2022.114148>.

## References

- [1] M. Jemal, T. Deress, T. Belachew, Y. Adem, Antimicrobial resistance patterns of bacterial isolates from blood culture among HIV/AIDS patients at felege hiwot referral hospital, northwest Ethiopia, *Internet J. Microbiol.* 2020 (2020) 8893266, <https://doi.org/10.1155/2020/8893266>.
- [2] H. Inoue, R. Minghui, Antimicrobial resistance: translating political commitment into national action, *Bull. World Health Organ.* 95 (2017) 242, <https://doi.org/10.2471/BLT.17.191890>.
- [3] Z. Kmiotowicz, Few novel antibiotics in the pipeline, WHO warns, *BMJ* 358 (2017) j4339, <https://doi.org/10.1136/bmj.j4339>.
- [4] S. Vasoo, J.N. Barreto, P.K. Tosh, Emerging issues in Gram-negative bacterial resistance: an update for the practicing clinician, *Mayo Clin. Proc.* 90 (2015) 395e403, <https://doi.org/10.1016/j.mayocp.2014.12.002>.
- [5] Y. Irie, M. Starkey, A.N. Edwards, D.J. Wozniak, T. Romeo, M.R. Parsek, *Pseudomonas aeruginosa* biofilm matrix polysaccharide Psl is regulated transcriptionally by RpoS and post-transcriptionally by RsmA, *Mol. Microbiol.* 78 (2010) 158e172, <https://doi.org/10.1111/j.1365-2958.2010.07320.x>.
- [6] A.M. Nuss, A.K. Heroven, P. Dersch, RNA regulators: formidable modulators of *Yersinia* virulence, *Trends Microbiol.* 25 (2017) 19e34, <https://doi.org/10.1016/j.tim.2016.08.006>.
- [7] F.M. Barnard, M.F. Loughlin, H.P. Fainberg, M.P. Messenger, D.W. Ussery, P. Williams, P.J. Jenks, Global regulation of virulence and the stress response by CsrA in the highly adapted human gastric pathogen *Helicobacter pylori*, *Mol. Microbiol.* 51 (2004) 15e32, <https://doi.org/10.1046/j.13652958.2003.03788.x>.
- [8] A.H. Potts, C.A. Vakulskas, A. Pannuri, H. Yakhnin, P. Babitzke, T. Romeo, Global role of the bacterial post-transcriptional regulator CsrA revealed by integrated transcriptomics, *Nat. Commun.* 8 (2017) 1596, <https://doi.org/10.1038/s41467-017-01613-1>.
- [9] E.R. Morris, G. Hall, C. Li, S. Heeb, R.V. Kulkarni, L. Lovelock, H. Sillistre, M. Messina, M. Camara, J. Emsley, P. Williams, M.S. Searle, Structural rearrangement in an RsmA/CsrA ortholog of *Pseudomonas aeruginosa* creates a dimeric RNA-binding protein, RsmN, *Structure* 21 (2013) 1659e1671, <https://doi.org/10.1016/j.str.2013.07.007>.
- [10] C.K. Maurer, M. Fruth, M. Empting, O. Avrutina, J. Hoßmann, S. Nadmid, J. Gorges, J. Herrmann, U. Kazmaier, P. Dersch, R. Müller, R.W. Hartmann, Discovery of the first small-molecule CsrA-RNA interaction inhibitors using biophysical screening technologies, *Future Med. Chem.* 8 (2016) 931e947, <https://doi.org/10.4155/fmc-2016-0033>.
- [11] G. Sharma, S. Sharma, P. Sharma, D. Chandola, S. Dang, S. Gupta, R. Gabrani, *Escherichia coli* biofilm: development and therapeutic strategies, *J. Appl. Microbiol.* 121 (2016) 309e319, <https://doi.org/10.1111/jam.13078>.
- [12] J. Timmermans, L. van Melderen, Post-transcriptional global regulation by CsrA in bacteria, *Cell, Mol. Life Sci.* 67 (2010) 2897e2908, <https://doi.org/10.1007/s00018-010-0381-z>.
- [13] E. van Assche, S. van Puyvelde, J. Vanderleyden, H.P. Steenackers, RNA-binding proteins involved in post-transcriptional regulation in bacteria, *Front. Microbiol.* 6 (2015) 141, <https://doi.org/10.3389/fmicb.2015.00141>.
- [14] N.A. Sabnis, H. Yang, T. Romeo, Pleiotropic regulation of central carbohydrate metabolism in *Escherichia coli* via the gene *csrA*, *J. Biol. Chem.* 270 (1995) 29096e29104, <https://doi.org/10.1074/jbc.270.49.29096>.
- [15] H. Yakhnin, C.S. Baker, I. Berezin, M.A. Evangelista, A. Rassini, T. Romeo, P. Babitzke, CsrA represses translation of *sdiA*, which encodes the N-acylhomoserine-L-lactone receptor of *Escherichia coli*, by binding exclusively within the coding region of *sdiA* mRNA, *J. Bacteriol.* 193 (2011) 6162e6170, <https://doi.org/10.1128/JB.05975-11>.
- [16] B.L. Wei, A.M. Brun-Zinkernagel, J.W. Simecka, B.M. Prüss, P. Babitzke, T. Romeo, Positive regulation of motility and *flhDC* expression by the RNA-binding protein CsrA of *Escherichia coli*, *Mol. Microbiol.* 40 (2001) 245e256, <https://doi.org/10.1046/j.1365-2958.2001.02380.x>.
- [17] M.Y. Liu, G. Gui, B. Wei, J.F. Preston, L. Oakford, U. Yüksel, D.P. Giedroc, T. Romeo, The RNA molecule CsrB binds to the global regulatory protein CsrA and antagonizes its activity in *Escherichia coli*, *J. Biol. Chem.* 272 (1997) 17502e17510, <https://doi.org/10.1074/jbc.272.28.17502>.
- [18] Y. Tan, Z.-Y. Liu, Z. Liu, H.-J. Zheng, F.-L. Li, Comparative transcriptome analysis between *csrA*-disruption *Clostridium acetobutylicum* and its parent strain, *Mol. Biosyst.* 11 (2015) 1434e1442, <https://doi.org/10.1039/c4mb00600c>.
- [19] J.E. Schultz, A. Matin, Molecular and functional characterization of a carbon starvation gene of *Escherichia coli*, *J. Mol. Biol.* 218 (1991) 129e140, [https://doi.org/10.1016/0022-2836\(91\)90879-B](https://doi.org/10.1016/0022-2836(91)90879-B).
- [20] A.K. Dubey, C.S. Baker, K. Suzuki, A.D. Jones, P. Pandit, T. Romeo, P. Babitzke, CsrA regulates translation of the *Escherichia coli* carbon starvation gene, *cstA*, by blocking ribosome access to the *cstA* transcript, *J. Bacteriol.* 185 (2003) 4450e4460, <https://doi.org/10.1128/jb.185.15.4450-4460.2003>.
- [21] D.W. Jackson, K. Suzuki, L. Oakford, J.W. Simecka, M.E. Hart, T. Romeo, Biofilm formation and dispersal under the influence of the global regulator CsrA of *Escherichia coli*, *J. Bacteriol.* 184 (2002) 290e301, <https://doi.org/10.1128/jb.184.1.290-301.2002>.

- [22] A.K. Dubey, C.S. Baker, T. Romeo, P. Babitzke, RNA sequence and secondary structure participate in high-affinity CsrA-RNA interaction, *RNA* 11 (2005) 1579e1587, <https://doi.org/10.1261/rna.2990205>.
- [23] X. Ren, R. Zeng, M. Tortorella, J. Wang, C. Wang, Structural insight into inhibition of CsrA-RNA interaction revealed by docking, molecular dynamics and free energy calculations, *Sci. Rep.* 7 (2017) 14934, <https://doi.org/10.1038/s41598-017-14916-6>.
- [24] G.B. Santos, A. Ganesan, F.S. Emery, Oral administration of peptide-based drugs: beyond lipinski's rule, *ChemMedChem* 11 (2016) 2245e2251, <https://doi.org/10.1002/cmdc.201600288>.
- [25] C.A. Lipinski, Rule of five in 2015 and beyond: target and ligand structural limitations, ligand chemistry structure and drug discovery project decisions, *Adv. Drug Deliv. Rev.* 101 (2016) 34e41, <https://doi.org/10.1016/j.addr.2016.04.029>.
- [26] B.C. Doak, B. Over, F. Giordanetto, J. Kihlberg, Oral druggable space beyond the rule of 5: insights from drugs and clinical candidates, *Chem. Biol.* 21 (2014) 1115e1142, <https://doi.org/10.1016/j.chembiol.2014.08.013>.
- [27] A. Capecci, M. Awale, D. Probst, J.-L. Reymond, PubChem and ChEMBL beyond Lipinski, *Mol. Inform.* 38 (2019), e1900016, <https://doi.org/10.1002/minf.201900016>.
- [28] V. Jakob, S. Helmsing, M. Hust, M. Empting, Restriction-free construction of a phage-presented very short macrocyclic peptide library, *Methods Mol. Biol.* 2070 (2020) 95e113, [https://doi.org/10.1007/978-1-4939-9853-1\\_6](https://doi.org/10.1007/978-1-4939-9853-1_6).
- [29] J. Kügler, S. Wilke, D. Meier, F. Tomczak, A. Frenzel, T. Schirrmann, S. Dübel, H. Garritsen, B. Hock, L. Toleikis, M. Schütte, M. Hust, Generation and analysis of the improved human HAL9/10 antibody phage display libraries, *BMC Biotechnol.* 15 (2015) 10, <https://doi.org/10.1186/s12896-015-0125-0>.
- [30] S. Dübel, *Handbook of Therapeutic Antibodies*, secondnd ed., John Wiley & Sons Incorporated, Weinheim, 2014.
- [31] C.G. Ullman, L. Frigotto, R.N. Cooley, In vitro methods for peptide display and their applications, *Brief. Funct. Genomics* 10 (2011) 125e134, <https://doi.org/10.1093/bfpg/ehr010>.
- [32] A. Frenzel, T. Schirrmann, M. Hust, Phage display-derived human antibodies in clinical development and therapy, *mAbs* 8 (2016) 1177e1194, <https://doi.org/10.1080/19420862.2016.1212149>.
- [33] S. Dübel, O. Stoevesandt, M.J. Taussig, M. Hust, Generating recombinant antibodies to the complete human proteome, *Trends Biotechnol.* 28 (2010) 333e339, <https://doi.org/10.1016/j.tibtech.2010.05.001>.
- [34] J. Kügler, J. Zantow, T. Meyer, M. Hust, Oligopeptide m13 phage display in pathogen research, *Viruses* 5 (2013) 2531e2545, <https://doi.org/10.3390/v5102531>.
- [35] V. Baeriswyl, C. Heinis, Phage selection of cyclic peptide antagonists with increased stability toward intestinal proteases, *Protein Eng. Des. Sel.* 26 (2013) 81e89, <https://doi.org/10.1093/protein/gzs085>.
- [36] N.B. Adey, A.H. Mataragnon, J.E. Rider, J.M. Carter, B.K. Kay, Characterization of phage that bind plastic from phage-displayed random peptide libraries, *Gene* 156 (1995) 27e31, [https://doi.org/10.1016/0378-1119\(95\)00058-E](https://doi.org/10.1016/0378-1119(95)00058-E).
- [37] M. Empting, O. Avrutina, R. Meusinger, S. Fabritz, M. Reinwarth, M. Biesalski, S. Voigt, G. Buntkowsky, H. Kolmar, Triazole bridge": disulfide-bond replacement by ruthenium-catalyzed formation of 1,5-disubstituted 1,2,3triazoles, *Angew. Chem. Int. Ed. Engl.* 50 (2011) 5207e5211, <https://doi.org/10.1002/anie.201008142>.
- [38] X. Jiang, X. Hao, L. Jing, G. Wu, D. Kang, X. Liu, P. Zhan, Recent applications of click chemistry in drug discovery, *Expet Opin. Drug Discov.* 14 (2019) 779e789, <https://doi.org/10.1080/17460441.2019.1614910>.
- [39] M. Roice, I. Johannsen, M. Meldal, High capacity poly(ethylene glycol) based amino polymers for peptide and organic synthesis, *QSAR Comb. Sci.* 23 (2004) 662e673, <https://doi.org/10.1002/qsar.200420021>.
- [40] G. Appendino, S. Bacchiaga, A. Minassi, M.G. Cascio, L. De Petrocellis, V. Di Marzo, The 1,2,3-triazole ring as a peptido- and olefinomimetic element: discovery of click vanilloids and cannabinoids, *Angew. Chem.* 119 (2007) 9472e9475, <https://doi.org/10.1002/ange.200703590>.
- [41] S. Tomassi, A.M. Trotta, C. Ierano, F. Merlino, A. Messere, G. Rea, F. Santoro, D. Brancaccio, A. Carotenuto, V.M. D'Amore, F.S. Di Leva, E. Novellino, S. Cosconati, L. Marinelli, S. Scala, S. Di Maro, Disulfide bond replacement with 1,4- and 1,5-disubstituted 1,2,3-triazole on C-X-C chemokine receptor type 4 (CXCR4) peptide ligands: small changes that make big differences, *Chemistry* 26 (2020) 10113e10125, <https://doi.org/10.1002/chem.202002468>.
- [42] S.R. Tala, A. Singh, C.J. Lensing, S.M. Schnell, K.T. Freeman, J.R. Rocca, C. Haskell-Luevano, 1,2,3-Triazole rings as a disulfide bond mimetic in chimeric AGRP-melanocortin peptides: design, synthesis, and functional characterization, *ACS Chem. Neurosci.* 9 (2018) 1001e1013, <https://doi.org/10.1021/acscchemneuro.7b00422>.
- [43] S. Pacifico, A. Kerckhoffs, A.J. Fallow, R.E. Foreman, R. Guerrini, J. McDonald, D.G. Lambert, A.G. Jamieson, Urotensin-II peptidomimetic incorporating a non-reducible 1,5-triazole disulfide bond reveals a pseudo-irreversible covalent binding mechanism to the urotensin G-protein coupled receptor, *Org. Biomol. Chem.* 15 (2017) 4704e4710, <https://doi.org/10.1039/C7OB00959C>.
- [44] A.M. White, S.J. de Veer, G. Wu, P.J. Harvey, K. Yap, G.J. King, J.E. Swedberg, C.K. Wang, R.H.P. Law, T. Durek, D.J. Craik, Application and structural analysis of triazole-bridged disulfide mimetics in cyclic peptides, *Angew. Chem. Int. Ed. Engl.* 59 (2020) 11273e11277, <https://doi.org/10.1002/anie.202003435>.
- [45] A.K. Heroven, K. Bohme, P. Dersch, The Csr/Rsm system of Yersinia and related€ pathogens: a post-transcriptional strategy for managing virulence, *RNA Biol.* 9 (2012) 379e391, <https://doi.org/10.4161/rna.19333>.
- [46] O. Duss, E. Michel, N. Diarra dit Konte, M. Schubert, F.H.-T. Allain, Molecular basis for the wide range of affinity found in Csr/Rsm protein-RNA recognition, *Nucleic Acids Res.* 42 (2014) 5332e5346, <https://doi.org/10.1093/nar/gku141>.

## 4.2 Establishment of a Luciferase assay for the assessment of CsrA inhibitors

Establishment of an *In Bacterio* assay for the Assessment of Carbon Storage Regulator A (CsrA) inhibitors

Authors:

Yingwen Wu, Ben G.E. Zoller, Mohamed Ashraf Mostafa Kamal, Sven-Kevin Hotop, Claus-Michael Lehr, Mark Brönstrup, Petra Dersch and Martin Empting.

Bibliographic Data:

*ChemBioChem*. **2023** <https://doi.org/10.1002/cbic.202300369>.

Author Contributions: Dr. Yingwen Wu wrote the original draft of the manuscript, has done CsrA expressions and assay development. Ben G. E. Zoller, optimized peptide synthesis on solid support and thiol macrocyclization by using an ammonium carbonate buffer system at PH=8 for macrocyclization, leading to cleaner and faster reactions. He upscaled peptide synthesis, for the disulfide and triazole peptides tested in the assays, leading to peptide amounts exceeding 50 mg. Moreover, he wrote parts of the SI and was involved in the reviewing and editing process of the manuscript. Mohamed Ashraf Mostafa Kamal wrote parts of the SI and was engaged in the development of the assay. Sven-Kevin Hotop and Prof. Dr. Claus-Michael Lehr were involved in method development and investigations regarding permeability. Prof. Dr. Mark Brönstrup helped in the editing and reviewing process and was involved in methodology development. Prof. Dr. Petra Dersch initiated and directed the study and assisted in the reviewing and editing process of the manuscript. Prof. Dr. Martin Empting initiated and directed the study, wrote parts of the manuscript and assisted in the reviewing and editing process.

## Establishment of an *In Bacterio* Assay for the Assessment of Carbon Storage Regulator A (CsrA) Inhibitors

Yingwen Wu,<sup>[a, f]</sup> Ben G. E. Zoller,<sup>[a]</sup> Mohamed Ashraf Mostafa Kamal,<sup>[b, c]</sup> Sven-Kevin Hotop,<sup>[d]</sup> Claus-Michael Lehr,<sup>[b, c]</sup> Mark Brönstrup,<sup>[d]</sup> Petra Dersch,<sup>[e]</sup> and Martin Empting\*<sup>[a, c, f]</sup>

Polymicrobial infections involving various combinations of to establish an *in bacterio* assay capable of probing and microorganisms, such as *Escherichia*, *Pseudomonas*, or *Yersinia*, quantifying the impact on CsrA-regulated cellular mechanisms. can lead to acute and chronic diseases in for example the We have successfully developed an assay based on a luciferase gastrointestinal and respiratory tracts. Our aim is to modulate reporter gene assay, which in combination with a qPCR microbial communities by targeting the posttranscriptional expression gene assay, allows for the monitoring of expression regulator system called carbon storage regulator A (CsrA) (or levels of different downstream targets of CsrA. The chaperone also repressor of secondary metabolites (RsmA)). In previous protein CesT was used as a suitable positive control for the studies, we identified easily accessible CsrA binding scaffolds assay, and in time-dependent experiments, we observed a and macrocyclic CsrA binding peptides through biophysical CesT-mediated increase in bioluminescence over time. By this screening and phage display technology. However, due to the means, the cellular on-target effects of non-bactericidal/nonlack of an appropriate *in bacterio* assay to evaluate the cellular bacteriostatic virulence modulating compounds targeting CsrA/ effects of these inhibitor hits, the focus of the present study is RsmA can be evaluated

## Introduction

Antimicrobial resistance (AMR) is a concerning worldwide health issue and inappropriate infection prevention and control is one factor for the steadily increasing occurrence of resistant microbes.<sup>[1]</sup> Without any counteractions, the spread of AMR will assumedly result in the deaths of 10 million people per year globally by 2050.<sup>[1]</sup>

Addressing and combatting AMR is very challenging, especially considering Gram-negative multi-drug-resistant (MDR) pathogens. Along these lines, carbapenem-resistant *Acinetobacter baumannii*, *Pseudomonas aeruginosa*, and *Enterobacteriaceae* are the top three on the WHO global priority pathogens list published in 2017.<sup>[2]</sup> Antibiotics or anti-infectives with alternative modes-of-action against these bacteria are therefore urgently needed.

In general, a healthy human microbiome contains diverse communities of microbes, which are stable and provide protection against colonization by pathogenic species. To suppress the growth of pathogens, commensal bacteria produce their own antimicrobial compounds such as peptides.<sup>[3]</sup> Dysbiotic communities, on the contrary, are typically less diverse and more dominated by few pathogenic species. These interactions lead to polymicrobial infections and in case these microbes are pathogenic, this can enhance the virulence of each of them. There are several examples of this effect including inhibition of competing microbes (so-called microbial interference), the mutual supply of nutrients in particular carbon sources, or subversion of immunity.<sup>[3-5]</sup>

Many acute and chronic diseases are associated with infections of the respiratory and gastrointestinal tract, where polymicrobial interactions are paramount.<sup>[4]</sup> Impacting and modulating these complex communities in order to reestablish or protect the commensal balance by small molecular entities might provide an attractive new approach for the discovery of anti-infectives. In this context, the CsrA (RsmA) protein could be considered a

promising drug target. The Csr (carbon storage regulator) or Rsm (regulator of secondary metabolites) system is a post-transcriptional regulatory system, which affects mRNA translation and/or stability, thereby regulating a multitude of cellular processes in response to environmental cues.<sup>[6-9]</sup> CsrA (RsmA) is a homodimer with two identical RNA-binding surfaces, which recognizes and binds to the GGA motifs in mRNAs. This highly conserved RNA-binding protein is widespread among Gram-negative pathogens.<sup>[6-10]</sup> For example the homology between CsrA from *Y. pseudotuberculosis* and CsrA from *E. coli* is 95%.<sup>[6]</sup> CsrA homologs can also be found in a variety of bacterial animal and plant pathogens.<sup>[6]</sup>

Early evidence showed that CsrA is not only essential for fundamental physiological properties and metabolism, but also for regulation of virulence factors required for host infection.<sup>[6]</sup> This was confirmed in previous studies by weakened virulence in murine models of e.g. *Y. pseudotuberculosis* using CsrA knock-out strains.<sup>[6,7]</sup> CsrA's activity includes for example modulation of carbon metabolism, motility, biofilm development, and quorum sensing.<sup>[7-11]</sup>

## Regulation of Csr system

The complex regulation circuits of the Csr system of *E. coli* have been described in detail in reviews.<sup>[9,10]</sup> To illustrate the composition and function of the system, a simplified version is shown in Figure 1 including the essential steps relevant for the present study. In the following, the innate antagonists of CsrA will be described more in detail.

The activity of CsrA is controlled by the sequestration of the inhibitory sRNAs CsrB and CsrC (~350 nt long). Furthermore, the amount of CsrB and CsrC determines the level of free, functional CsrA, which is available for binding target mRNAs. The reason for the considered high affinity towards CsrB is for example the existence of 22 potential binding sites, which are able to sequester ~9 CsrA dimers (Figure 2). The binding element for CsrA is suggested to be

the hairpin loop motif 5'CAGGAUG-3'.<sup>[9,10,12]</sup> Experiments with  $\sim$ *csrB/C* *E. coli* strains and *csrB/C* overexpressing strains showed that its absence or increased abundance caused pleiotropic effects on bacterial physiology. Furthermore, expression of downstream targets regulated by CsrA such as *glgC* (responsible for glycogen biosynthesis) gene, and *flhDC* (operon for biosynthesis of flagella) is similarly affected. For example, glycogen accumulation and non-motile appearance of *Yersinia csrA* mutant strain have been observed.<sup>[6]</sup> Overall the regulatory RNAs allow the bacteria to fine-tune CsrA.<sup>[9,10,12]</sup>

in virulence and metabolic gene expression.<sup>[9,10,13]</sup>

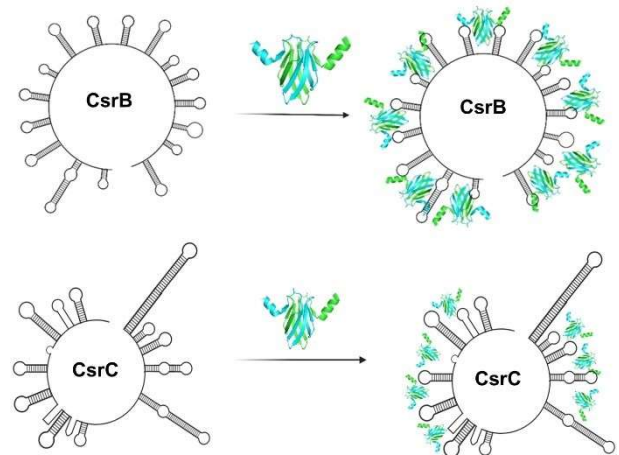


**Figure 2.** sRNA antagonists CsrB and CsrC of CsrA (PDB: 1vpz): The affinity of CsrA for CsrB is  $\sim$ 10 fold higher than for CsrC (reported  $K_{d[12]} = 8.7 \pm 0.6$  nM for CsrC) in *E. coli*, because of the large amount of the binding sites and the co-operative interaction between CsrA and CsrC transcript. Nevertheless, these two sRNAs share a similar mechanism for antagonizing the activity of CsrA. Furthermore, both CsrB and CsrC have a short half-life ( $\sim$ 2 min) which indicates that CsrA is able to respond rapidly to changes in CsrB/CsrC levels.<sup>[12]</sup>

Apart from the sRNA-mediated antagonism present in most CsrA/RsmA systems, there are some organisms that use innate proteins to modulate the activity of CsrA. For example, in Enteropathogenic *E. coli* (EPEC) a recently identified chaperone protein called CesT (Figure 3) binds to CsrA leading to alterations

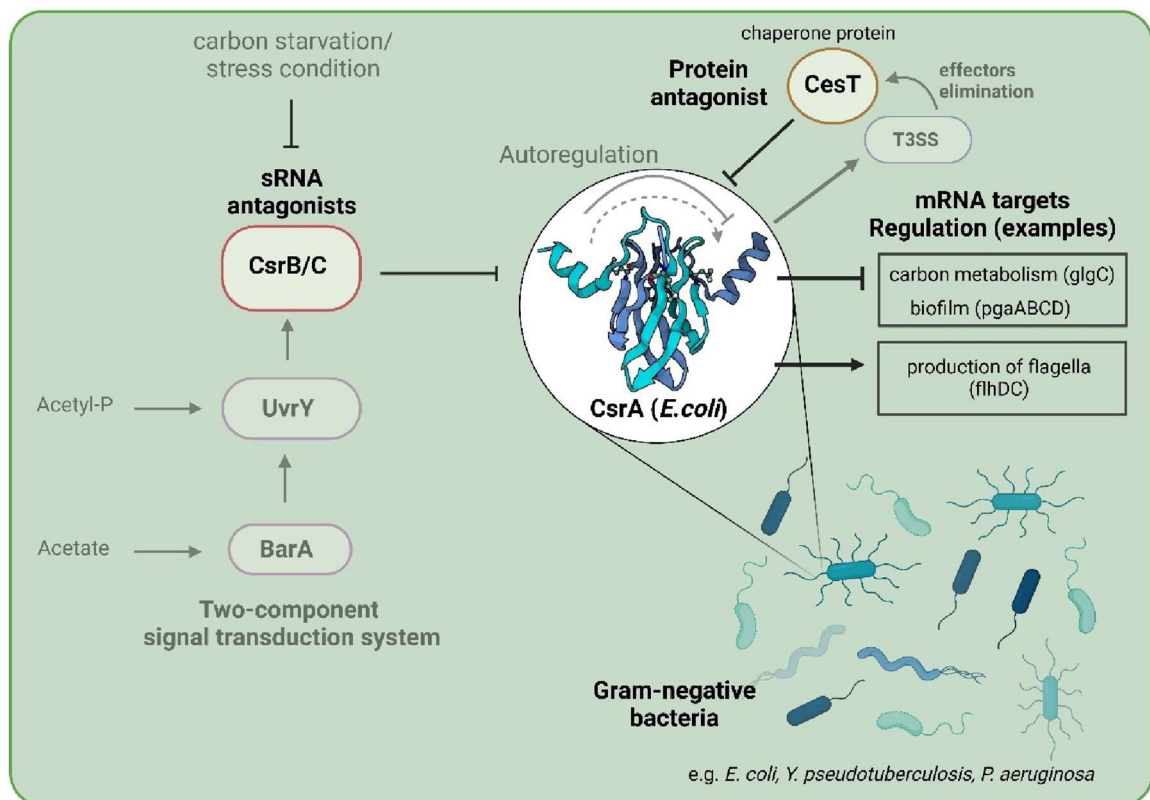


**Figure 1.** Simplified regulation circuit of CsrA in *E. coli*: CsrA is antagonized by sRNAs CsrB/C and chaperone protein CesT. The antagonists are controlled by other feedback cycles and regulatory circuits.<sup>[9,10]</sup> CsrA itself regulates e.g. the carbon metabolism and biofilm development by repressing the *glgC* (responsible for glycogen biosynthesis) gene and *pgaABCD* (operon for biosynthesis and secretion of biofilm polysaccharide adhesin) genes. Furthermore, CsrA activates the expression of *flhDC* (master operon for flagellum biosynthesis) genes to facilitate the production of flagella.



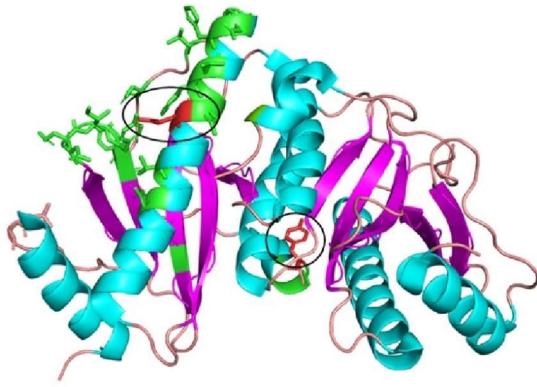


**Figure 3.** Structure of CesT with CsrA binding sites (PDB: 5Z38). CesT is a dimeric protein and one monomer consists of 5  $\beta$ -sheets (magenta); 3  $\alpha$ helices (cyan) and loops are shown in salmon. CsrA binding regions are highlighted in green and located mainly at the C-terminal region. Tyr152 and Glu121 are the important binding residues highlighted in red and encircled.<sup>[13,14]</sup>

The function of CesT is to stabilize and translocate virulence factors (effectors) that are secreted by the type three secretion system (T3SS) and are required for pathogenicity and survival in the host environment.<sup>[9,13,14]</sup> Furthermore, previous studies showed that during a T3SS-mediated bacterial infection, free CesT (not bound to T3SS effector proteins) binds to the CsrA regulator after injecting the effectors into the host cells. This results in the repression of CsrA-dependent T3SS proteins, which leads to a decrease in T3SS activity and an accumulation of the effectors that sequester CesT. These findings suggest that CsrA and T3SS activities regulate each other indirectly in a negative-feedback loop (Figure 1), while inhibition of CsrA by exogenic substances should lead to a reduction of T3SS activity.<sup>[13,14]</sup>

## Development of an *in bacterio* assay for assessing CsrA inhibition

The aim of previous studies was to find novel inhibitors of CsrA, which are capable to disrupt the CsrA-RNA interaction.<sup>[7,8]</sup> Until now, some interesting CsrA inhibitor scaffolds have been identified using different biophysical

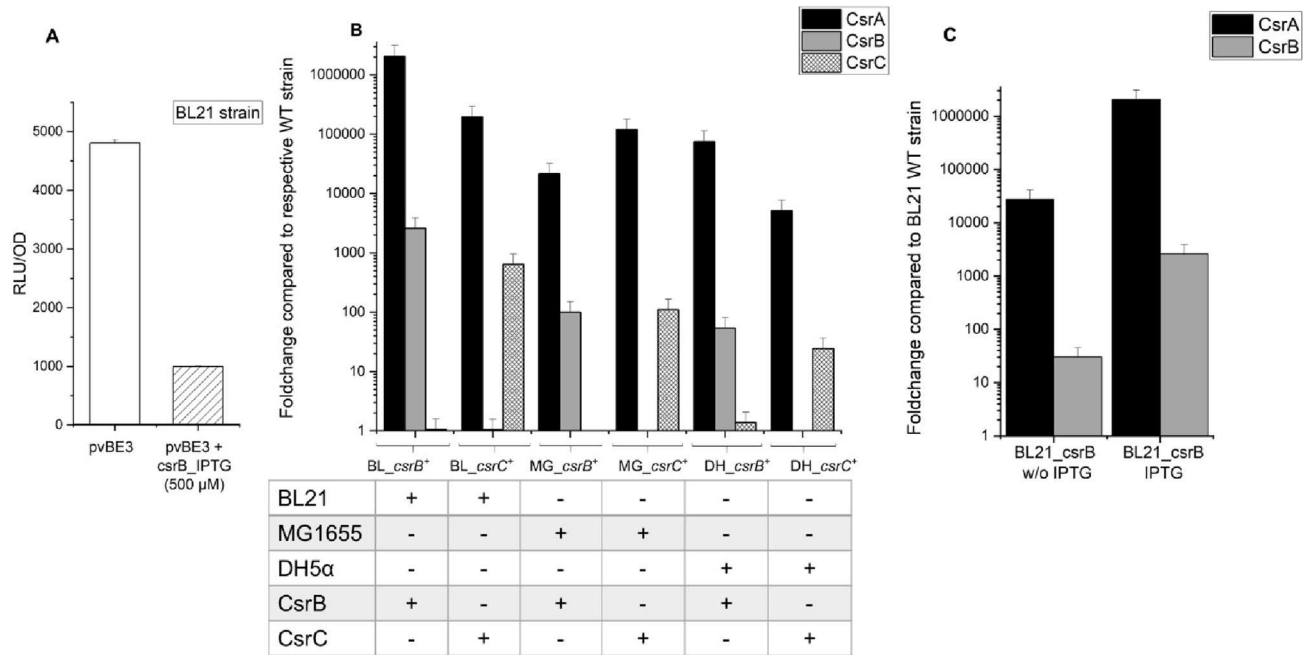
screening methods as well as phage display. The discovered hit structures have been tested in a fluorescence polarization (FP) assay for their ability to replace the RNA from CsrA.<sup>[8]</sup> One of the most active synthetic compounds, which is a triazole peptide, showed an  $IC_{50}$  value in a single-digit micromolar range.<sup>[8]</sup>

However, the biophysical assay reflects the impact on the protein-RNA interaction in a cell-free setup. Since CsrA is a target for pathoblocker compounds, which ideally lack any bactericidal or bacteriostatic effects, typical antibacterial assays like minimum inhibitory concentration (MIC) assays are not suitable. Finding an appropriate *in bacterio* assay, which enables to probe and quantify the impact on CsrA-regulated cellular mechanisms, is challenging. To this end, we employed a (combination of qPCR and) luminescence-based assay setup towards the establishment of an *in bacterio* CsrA inhibition assay.

## Results and Discussion

To study inhibitory effects on target protein levels in real-time, the bioluminescence of bacterial luciferases can be exploited. These enzymes emit light in the presence of the substrate luciferin (reduced riboflavin phosphate), which is oxidized to a long-chain aldehyde.<sup>[15]</sup> Expression of the bacterial-derived *luxCDABE* operon leads to cells emitting detectable light at 490 nm. This operon encodes the luciferase (LuxAB) and the substrate-producing enzymes (LuxCDE).<sup>[15]</sup> For our assay we used a vector (pvBE3) containing the *glgC-luxCDEAB* reporter fusion harboring the entire promoter region of *glgC* (which is negatively regulated by CsrA). As a consequence, in the presence of functional CsrA inhibitors, the bioluminescence signal is expected to increase due to the upregulation of target gene (*glgC*) expression.

In order to evaluate a *glgC-lux*-based assay results, we explored the suitability of the innate antagonists as shown in Figure 1 as



control. Since CsrB is the main sRNA antagonist of CsrA in *E. coli*, it was the first positive control that we considered. Using a lactose-inducible *csrB* expression plasmid, we induced overexpression of CsrB by IPTG (500 μM) treatment. However, unlike what we expected, the bioluminescence decreased after 4 h incubation time (Figure 4A). To gain a better understanding of this outcome, we compared the transcript levels of the individual Csr components by a qPCR gene expression assay after overexpression of CsrB or CsrC (Figure 4B).

We investigated the level of expression of both sRNAs in different strains 4 h after IPTG induction. We could confirm the successful increase of sRNA levels (in a range between 100 to 3000 fold). However, also CsrA-encoding transcripts were drastically increased (in a range between 5000 to 20.000.000 fold), indicating that CsrB and CsrC overexpression was overcompensated by a 100- to 1000-fold higher *csrA* expression. We further found that strains harboring the *csrB* overexpression plasmid have a significantly higher *csrA* transcript level than in the wild type strain even without IPTG-mediated induction (Figure 4C p=0.0128,

calculated using the t-test over the data from BL21 strain harboring *csrB* without IPTG compared to BL21 strain harboring *csrB* with IPTG). Ultimately, these qPCR results explained the observation we had from the reporter gene assay.

The results implicated that the induction of sRNA expression triggered an unknown autoregulatory control circuit of the Csr system. Autoregulation of the Csr components has been described, but these studies only report the successful inhibition of the CsrA activity by CsrB/C shown as a *csrA* knock-out phenotype and changes in glucose consumption and free fatty acids production.<sup>[16,17]</sup> Due to the observed interdependency of the Csr components, using CsrB/C as positive controls proved to be difficult.

Therefore, we decided to examine the protein antagonist CesT. This chaperone is reported to inhibit CsrA's activity and should not have an impact on the *csrA* transcript level.<sup>[13,14]</sup> To ensure that the induction of CesT does not increase CsrA expression, the qPCR gene expression assay described above was applied (Figure 5B). A first observation was, that IPTG addition did not increase *cesT*

expression over the basal (uninduced) levels. Importantly, in comparison to the results for CsrB/C, CsrA levels were less, but still affected compared to the wild type in the presence of IPTG (~10-fold), whereas no influence was observed in the absence of IPTG. This effect of the thio-sugar derivative IPTG on *csrA* expression might be linked to the involvement of CsrA in the post-transcriptional control of sugar metabolism.<sup>[9,10,17]</sup>

The promising results for the *cesT*-harboring plasmidbearing strain in the absence of IPTG, encouraged us to rely on basal (uninduced) expression in follow-up experiments. We performed the reporter gene assay using the same condition and could observe a convincing increase in bioluminescence, indicating a derepression of the *glgC-lux* fusion in the presence of the *cesT*<sup>+</sup> plasmid (Figure 5A). This suggested that the assay setup might be suitable for the identification and investigation of CsrA inhibitors. As a next step, we performed time-resolved experiments to gain insights into the kinetics of CesT-driven inactivation of CsrA in order to identify the most suitable incubation time for yielding marked effects enabling facile detection of inhibitory activities (Figure 7). Data in Figure 7A showed a consistent increase of RLU in the *cesT*<sup>+</sup> strain BL21 pvEB3, pNS6236 over the course of 5 h, while values of the reference strain BL21 pvBE3 remained essentially unchanged. At the end of our five-hour experiment, we determined the most significant effect, where the RLU of the *cesT*<sup>+</sup> strain was ~3-fold higher than the RLU of the control strain. In parallel, we also performed qPCR to monitor the expression levels of *cesT* and *csrA* over the time course of the experiment. The results can be found in the supplementary (S2) and showed that the expression level of *csrA* did increase (2-40-fold) within 2-5 h. However, the transcript level of *cesT* was about 10,000-fold higher, and no impact on *glgC-lux* expression has been observed. In order to have enough samples for both assays, we started with a volume of 100 mL culture. However, for

efficient compound testing, this large amount of culture is not suitable, because consequently high amounts of potential inhibitors are required. For this reason, we decreased the starting volume from 100 mL to 10 mL (Figure 7B). Results were reproducible. Furthermore, the expression patterns looked more defined and the induction of the reporter was more pronounced over time. Based on the data we decided to use 10 mL cultures for the testing of previously reported compounds regarding their capability of disrupting the CsrA-RNA interaction in the cell-free environment.<sup>[7]</sup>

We used disulfide- and triazole-macrocyclized peptidic CsrA inhibitors identified in our previous study as these were among the most active compounds showing IC<sub>50</sub> value in a single-digit micromolar range in a fluorescence polarization assay.<sup>[7]</sup> Figure 9 showed that in contrast to the CesT-expressing positive control, the addition of the inhibitory peptides did not lead to a significant increase in RLU values, and thus *glgC-lux* expression after 5 hours. This indicated that the peptides in the culture media are not able to inhibit CsrA in this cell-based assay. Most likely, this is due to the difficulty of the peptides to penetrate the Gram-negative cell wall and enter the cytoplasm to reach the target protein. Via subcellular quantification in the frame of uptake experiments in *E. coli* (supporting information),<sup>[16,17]</sup> we could show that, unfortunately, the peptidic scaffold indeed is not able to overcome the *E. coli* cell envelope barrier. Triazole-based peptide **1** reached only picomolar levels in the cytoplasm despite the used micromolar concentration (28 μM) in the permeability assay (Figure S4), which are insufficient in order to disrupt the CsrA-RNA interaction efficiently at reasonable concentrations. Nevertheless, we consider the general reporter gene assay concept now fit-for-purpose to facilitate phenotypic screening with the aim to identify novel inhibitors with cellular efficacy.

## Conclusion

In summary, we could establish an *in bacterio* assay, which directly measures the inhibition of CsrA based on a luciferase reporter gene assay. We could show that the expression of the chaperone protein CesT can be used as a suitable positive control for the assay because it acts as a natural intracellularly expressed antagonist of CsrA, which does not cause compensatory feedback effects. We could monitor a CesT-mediated increase of the bioluminescence over time with the most convincing effect being detectable after 5 hours of incubation.

Another interesting finding from our study is the enhancement of *csrA* transcript levels in sRNAs overexpression strains. Even without IPTG-mediated induction of *csrB* and *csrC* expression, we found a higher level of *csrA*-encoding transcripts. We suggest that a yet unknown autoregulatory control circuit of the Csr system causes this feedback mechanism. However, previous studies by other research groups showed the successful inhibition of CsrA's activity by the sRNAs through phenotypical results and changes in downstream targets of CsrA.<sup>[16,17]</sup> Hence, the interdependency of the Csr components observed in the frame of this study deserves further investigation.

One of the advantages of the established *glgC-lux* luciferase reporter assay setup is for instance the direct readout of potential CsrA inhibition. Even though the regulation of the Csr system is complex

and contains multiple feedback mechanisms, this *in bacterio* assay has a well-detectable and stable read-out in the presence of the natural antagonist CesT. That means once CsrA is less active (due to inhibition), we can directly monitor its consequence and impact through this assay. Thus, it is sensitive towards the activity of potential pathoblockers. In addition, quantitative evaluation of the cellular effect (determination of EC<sub>50</sub> values) of promising new inhibitors should be possible via concentration-dependent experiments as well as potentially gaining insights into the regulatory kinetics with the time-dependent measurement setup. Moreover, in combination with a qPCR expression gene assay, we can even observe the expression levels of different downstream targets of CsrA.

Downscaling of the required culture volume to 96-well format was successful enabling high throughput testing of potential inhibitors. Using this reporter gene assay set up for phenotypic screening from commercial synthetic or natural product libraries is highly favorable and is one of the next major steps towards tackling this challenging virulence-modulating target. The previously reported disruption of CsrA/RsmA-RNA interactions *in vitro* using the target protein from multiple species holds promise for the identification of anti-infectives/ virulence modulators with broader anti-Gram-negative activity.<sup>[8]</sup>

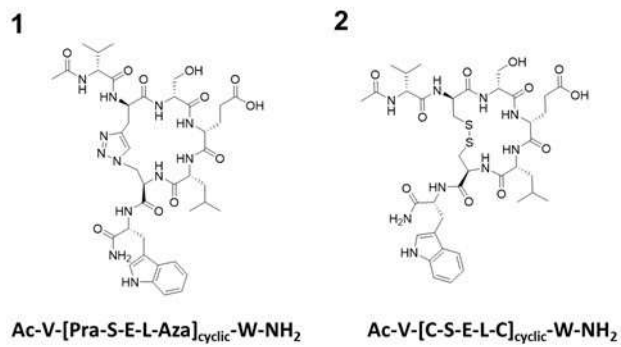
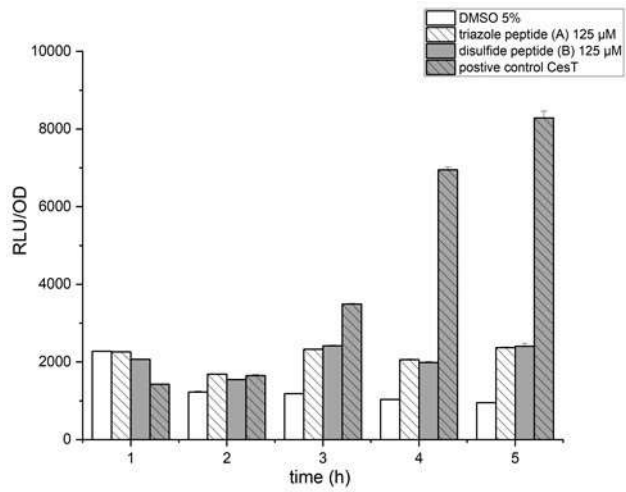


**Figure 7.** Influence of peptidic CsrA inhibitors on the expression of the CsrA dependent *glgC-lux* fusion: *E. coli* strain BL21 pvBE3 in the presence of 5% DMSO, 125 μM triazole peptide **1**, 125 μM disulfide peptide **2** or the plasmid pNS6236 (*cesT*) were grown at 37 C for 5 hours and the relative light units (RLU) were determined each hour. Error bars represent the standard deviation of four replicates

# Experimental Section

## Bacterial strains and culture conditions

All strains and plasmids used in this study are described in the supplementary Table S2. Unless otherwise indicated, bacterial strains were routinely grown in LB medium at 37 °C containing the following antibiotics with respective final concentrations: ampicillin (100 µg/mL) and kanamycin (50 µg/mL).

## Luciferase reporter gene assay

*E. coli* (BL21, DH5alpha, MG1655) pvBE3 with respective plasmids of inducible genes was grown in different vessels ranging from 10 mL (in falcon tubes) to 100 mL (in shaking flasks) at 37 °C to exponential phase ( $OD_{600} = 0.6$ ). Subsequently, IPTG (500 µM) was added to induce the expression of CsrB, CsrC, or CesT. After 4 hours the cultures were added into the wells of a microtiter plate (200 µL per well) and luminescence (relative light units – RLU) was measured in triplicate. In addition to that, optical density (OD) at 600 nm was measured in 1:10 dilution.

## Time-dependent measurement

Flask and falcon tube format: *E. coli* BL21 pvBE3 and *E. coli* BL21 pvBE3 with an additional plasmid carrying the *cesT* gene were grown at 37 °C to exponential phase ( $OD_{600} = 0.6$ ). Subsequently, compound (500 µM; 250 µM; 125 µM, final concentrations) and DMSO (5%) were added each to *E. coli* BL21 pvBE3. After 5 min the first measurement was performed (time point 5 min). The culture was added to the measuring plates (200 µL per well) and luminescence (relative light units – RLU) was determined in triplicate. Afterwards, measurements were done every hour via the same procedure. In addition to that, optical density (OD) at 600 nm was measured in 1:10 dilution.

Microtiterplate format: *E. coli* strains BL21 pvBE3 with or without\* the plasmid pNS6236 (*cesT*+) were grown at 37 °C until  $OD_{600} = 0.6$  is reached. Afterwards, cultures were diluted in LB medium to  $OD_{600} = 0.06$ . 100 µL of diluted cultures were transferred into the 96-well plates preloaded with 100 µL LB and 5% DMSO per well. (200 µL per well in total). The relative light units (RLU) and  $OD_{600}$  were determined directly from one plate every hour.

## Isolation of total RNA

The total amount of the cellular RNA from each culture was isolated using the RNeasy Mini Kit (Qiagen, Hilden, Germany) according to the manufacturer's protocol. To avoid DNA contaminations, DNA digestions were conducted with DNase (Qiagen, Hilden, Germany) for 15 min. RNA was quantified by its absorbance at 260 nm and 280 nm using NanoDrop™. RNA samples were stored at 20 °C for only one-time usage.

## Reverse transcription PCR (RT-PCR)

Reverse transcription was conducted using Applied Biosystems™ High-Capacity cDNA Reverse Transcription Kit (Applied Biosystems, USA). The reaction mixture (20 µL) contained 100 ng of RNA and 1 µL master mix with reverse transcriptase. The conditions for the RT-PCR were: 25 °C–10 min, 37 °C–120 min, 85 °C–5 min. cDNA products were either used directly for qPCR or stored at -20 °C.

## Quantitative PCR (qPCR)

The qPCR was performed using SYBR Green master mix (Thermofisher Scientific, Germany) and respective primers listed in the supplementary information (Table S3). The samples consisted of 10 µL master mix, 0.5 µL cDNA product, 7.5 µL H<sub>2</sub>O and 2 µL primers. Reactions for each sample were performed with StepOnePlus™ Real-Time PCR system (Thermofisher Scientific, Germany)

The conditions for the qPCR were: 50 °C–2 min, 90 °C–2 min (holding stage), 95 °C–15 sec, 60 °C–1 min (40 cycles in the cycling stage), 95 °C–15 sec, 60 °C–1 min, 95 °C–15 sec (melt curve stage). The difference in cycle threshold (-CT) between control samples (wildtype MG1655, BL21 and DH5alpha strains) and treated samples (strains with plasmids

containing inducible *csrB*, *csrC*, and *cesT* genes) was calculated using the Comparative Ct (~Ct) Quantification method. Expression of individual genes was normalized against the *rpoD* and *opgD* genes. All the results were calculated and analyzed using Excel (Microsoft). The resulting values represent the mean expression level of duplicates from one qPCR assay.

## Supporting Information

The authors have cited additional references within the Supporting Information.<sup>[18–19]</sup>

### Acknowledgements

This work is supported by the Deutsche Forschungsgemeinschaft (DFG) through “RESIST - Resolving Infection Susceptibility” cluster of excellence (EXC 2155). We thank Prof. Dr. Ilan Rosenshine for sending us the *cesT* plasmid pNS6236. We also thank Philipp Alexander Gansen and Dominik Kolling for their help and support. Open Access funding enabled and organized by Projekt DEAL.

### Conflict of Interests

The authors declare no conflict of interest.

### Data Availability Statement

The data that support the findings of this study are available in the supplementary material of this article.

- [1] S. A Strathdee, S. C Davies, J. R Marcelin, *Lancet* **2020**, 1050–1052.
- [2] E. Tacconelli, E. Carrara, A. Savoldi, S. Harbarth, M. Mendelson, D. L. Monnet, C. Pulcini, G. Kahlmeter, J. Kluytmans, Y. Carmeli, M. Ouellette, K. Outterson, J. Patel, M. Cavalieri, E. M. Cox, C. R. Houchens, M. L. Grayson, P. Hansen, N. Singh, U. Theuretzbacher, N. Magrini, A. O. Aboderin, S. S. Al-Abri, N. Awang Jalil, N. Benzonana, S. Bhattacharya, A. J. Brink, F. R. Burkert, O. Cars, G. Cornaglia, O. J. Dyar, A. W. Friedrich, A. C. Gales, S. Gandra, C. G. Giske, D. A. Goff, H. Goossens, T. Gottlieb, M. Guzman Blanco, W. Hryniewicz, D. Kattula, T. Jinks, S. S. Kanj, L. Kerr, M.-P. Kieny, Y. S. Kim, R. S. Kozlov, J. Labarca, R. Laxminarayan, K. Leder, L. Leibovici, G. Levy-Hara, J. Littman, S. Malhotra-Kumar, V. Manchanda, L. Moja, B. Ndoye, A. Pan, D. L. Paterson, M. Paul, H. Qiu, P. Ramon-Pardo, J. Rodríguez-Baño, M. Sanguinetti, S. Sengupta, M. Sharland, M. SiMehand, L. L. Silver, W. Song, M. Steinbakk, J. Thomsen, G. E. Thwaites van der Meer, Jos WMM, N. van Kinh, S. Vega, M. V. Villegas, A. Wechsler-Fördös, H. F. Wertheim, E. Wesangula, N. Woodford, F. O. Yilmaz, A. Zorzet, *The Lancet Infect. Dis.* **2018**, *18*, 318–327.
- [3] A. L. Welp, J. M. Bomberger, *Front. Cell. Infect. Microbiol.* **2020**, *10*, 213.
- [4] K. A. Brogden, J. M. Guthmiller, C. E. Taylor, *The Lancet* **2005**, *365*, 253–255.
- [5] E. M. Selleck, M. S. Gilmore, *mBio* **2016**, *7*, 1–3.
- [6] A. K. Heroven, K. Böhme, P. Dersch, *RNA Biol.* **2012**, *9*, 379–391.
- [7] C. K. Maurer, M. Fruth, M. Empting, O. Avrutina, J. Hoßmann, S. Nadmid, J. Gorges, J. Herrmann, U. Kazmaier, P. Dersch, R. Müller, R. W. Hartmann, *Future Med. Chem.* **2016**, *8*, 931–947.
- [8] V. Jakob, B. G. Zoller, J. Rinkes, Y. Wu, A. F. Kiefer, M. Hust, S. Polten, A. M. White, P. J. Harvey, T. Durek, D. J. Craik, A. Siebert, U. Kazmaier, M. Empting, *Eur. J. Med. Chem.* **2022**, *231*, 114148.
- [9] T. Romeo, P. Babitzke, *Microbiol. Spectrum* **2018**, *6*, 1–13
- [10] C. A. Vakulskas, A. H. Potts, P. Babitzke, B. M. Ahmer, T. Romeo, *Microbiol. Mol. Biol. Rev.* **2015**, *79*, 193–224.
- [11] V. Berndt, M. Beckstette, M. Volk, P. Dersch, M. Broenstrup, *Sci. Rep.* **2019**, *9*, 1–15.
- [12] T. Weillbacher, K. Suzuki, A. K. Dubey, X. Wang, S. Gudapaty, I. Morozov, C. S. Baker, D. Georgellis, P. Babitzke, T. Romeo, *Mol. Microbiol.* **2003**, *48*, 657–670.
- [13] N. Katsowich, N. Elbaz, R. R. Pal, E. Mills, S. Kobi, T. Kahan, I. Rosenshine, *Science* **2017**, *355*, 735–739.
- [14] M. Yadav, M. Srinivasan, N. K. Tulsian, Y. X. Liu, Q. Lin, I. Rosenshine, J. Sivaraman, *Protein Sci.* **2021**, *30*, 2433–2444.
- [15] F. Uliczka, F. Pisano, A. Kochut, W. Opitz, K. Herbst, T. Stolz, P. Dersch, *PLoS One* **2011**, *6*, 1–12.
- [16] Tony Romeo, *Mol. Microbiol.* **1998**, *29*, 1320–1330.
- [17] A. E. McKee, B. J. Rutherford, D. C. Chivian, E. K. Baidoo, D. Juminaga, D. Kuo, P. I. Benke, J. A. Dietrich, S. M. Ma, A. P. Arkin, C. J. Petzold, P. D. Adams, J. D. Keasling, S. R. Chhabra, *Microb. Cell Fact.* **2012**, *11*, 1–12.
- [18] H. Prochnow, V. Fetz, S.-K. Hotop, M. A. García-Rivera, A. Heumann, M. Brönstrup, *Anal. Chem.* **2019**, *91*, 1863–1872.
- [19] V. R. Matias, A. Al-Amoudi, J. Dubochet, T. J. Beveridge, *J. Bacteriol.* **2003**, *185*, 6112–6118.

Manuscript received: May 17, 2023

Revised manuscript received: July 12, 2023

Accepted manuscript online: July 12, 2023

Version of record online: July 25, 2023

## 4.3 Small molecules inhibiting the CsrA-RNA interaction

### 4.3.1 Introduction

In previous investigations, we have successfully identified natural product CsrA binding scaffolds and macrocyclic CsrA binding peptides using a combination of biophysical screening techniques and phage display technology (see **section 4.1**)

However, we faced limitations in achieving cellular activity, probably due to the poor means of our designed peptides to pass the bacterial cell membranes. In order to demonstrate *in bacterio* efficacy, we established a luciferase reporter gene assay (see **section 4.2**), enabling us to quantify cellular effects and expand our portfolio of screening methodologies. We decided to switch from peptides back to small molecules, to ensure better bioavailability and an enhanced PK/PD profile. Employing a commercial screening library, of 11.000 structurally diverse compounds, we conducted three consecutive steps and orthogonal filters, incorporating *in silico* preselection, fluorescence polarisation-based on-target screening, and subsequent resynthesis and reevaluation of promising hits *in bacterio*. From these efforts, we identified two distinct classes of CsrA modulators, the Aminopyrazine class as well as the Hydantoin class of compounds. Subsequently, we synthesized over fifty derivatives of both classes, intending to evaluate their cellular activity using our recently developed assay in forthcoming experiments.

### 4.3.2 Results and discussion

Our comprehensive strategy for uncovering CsrA inhibitors with activity inside bacterial cells is illustrated in **Figure 13**. We initiated the process by employing a structurally diverse compound library (Discovery Diversity Set - 10, DDS-10, Enamine), encompassing around 10.000 compounds, in an *in silico* preselection step, which was based on a pharmacophore-guided docking, biasing binding poses towards an interaction hotspot of the mRNA-binding interface of CsrA from *E.coli*.

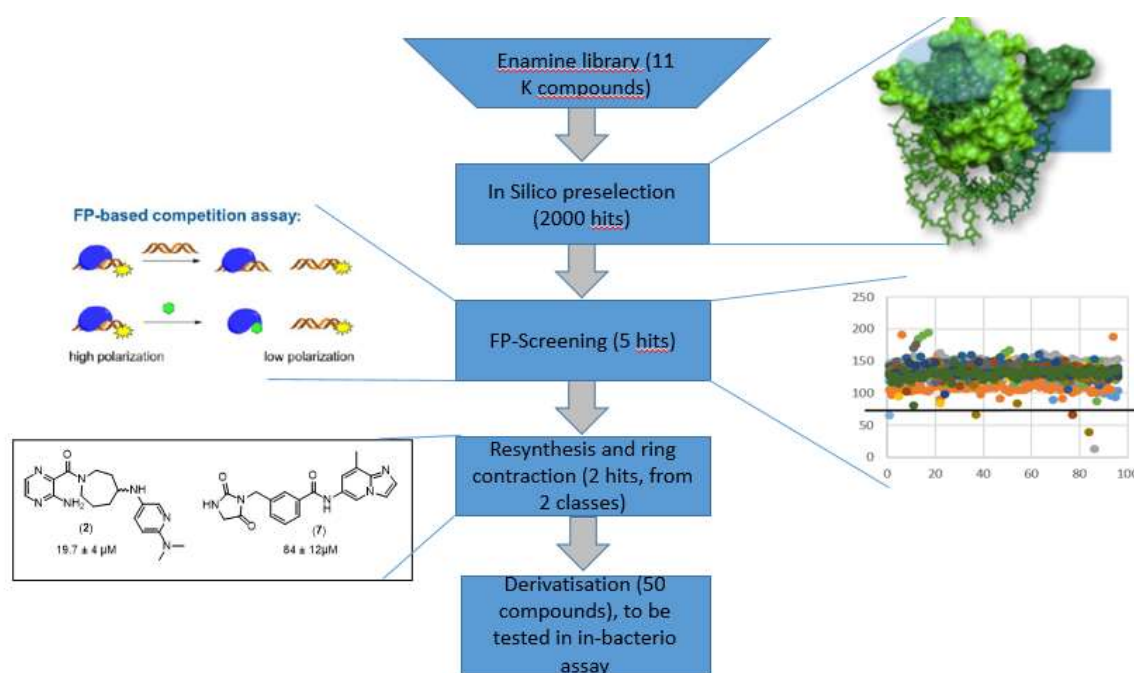
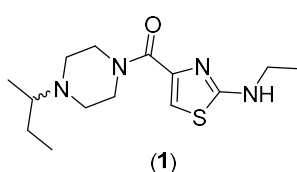


**Figure 13:** screening strategy



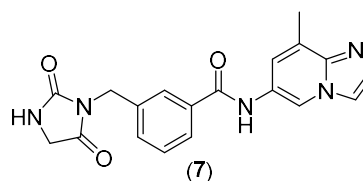
The next step of compound optimization was the resynthesis of these hits from the screening (**synthesis section**) and reevaluation of these compounds by means of FluPo assays. It was revealed that compounds from two of those classes (piperazine class and imidazo[1,5-a]pyrimidine class) were not active anymore after resynthesis (Compounds **(1)**, **(3)**, **(4)** and **(5)** (enantiomer of **3**, see SI)). Compounds from the Aminopyrazine class, to which compounds **(2)** and **(6)** belong, as well as compound **(7)** from the Hydantoin class, still showed activity but a bit significantly lower than the original value. In **(Figure 14)**, five screening hits, from four classes and their activity before and after resynthesis are shown as well as compound **(6)**, the ring contracted version of **(2)**. This was the most promising compound, yet.

**Class I: Piperazine class**



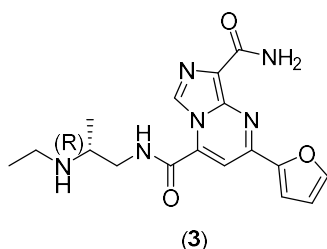
Library: IC<sub>50</sub> = 35 μM  
Resynthesis: IC<sub>50</sub> = 629 μM

**Class II: Hydantoin class**

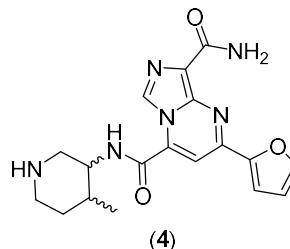


Library: IC<sub>50</sub> = 84 μM  
Resynthesis: IC<sub>50</sub> = 374 μM

**Class III: imidazo[1,5-a]pyrimidine class**

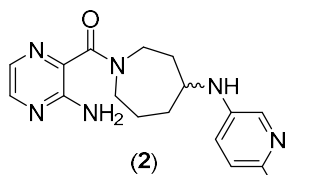


Library: IC<sub>50</sub> = 52 μM  
Resynthesis: IC<sub>50</sub> > max. conc. used

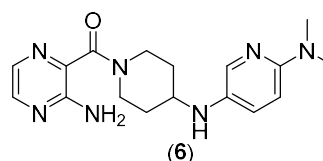


Library: IC<sub>50</sub> = 132 μM  
Resynthesis: IC<sub>50</sub> > max. conc. used

**Class IV: Aminopyrazine class**



Library: IC<sub>50</sub> = 45 μM  
Resynthesis: IC<sub>50</sub> = 19.7 μM



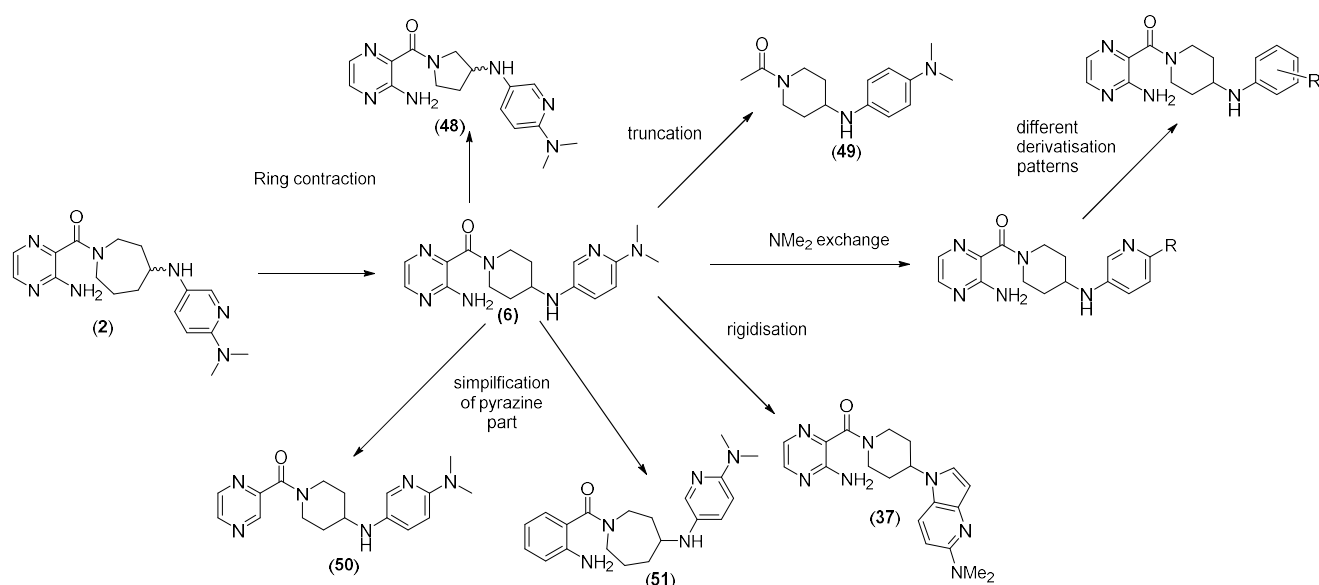
Resynthesis: IC<sub>50</sub> = 12.8 μM

**Figure 14:** Hits from the FluPo screening and their activity.

Continuing our investigation, we proceeded to synthesize and assess derivatives from the two most promising compound classes (class II and class IV with compounds **(6)** and **(7)**). Of particular interest was the aminopyrazine class. As these compounds showed the best inhibition, we synthesized a small library of 30 derivatives (**Scheme 5**).

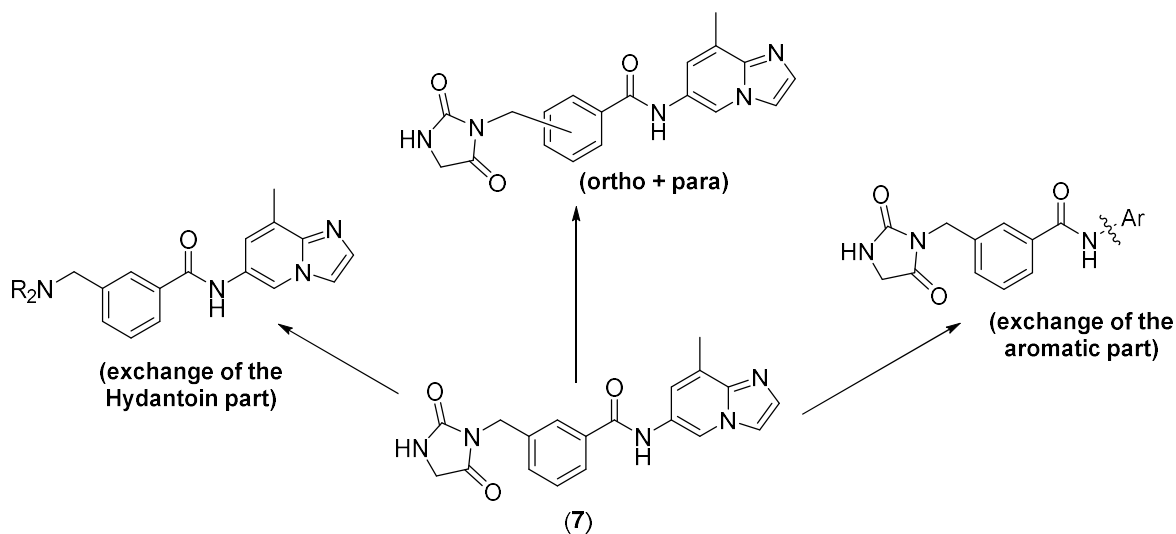
In our initial round of optimization, we transitioned from a seven-membered ring system (**2**) to a six-membered ring structure (**6**). Remarkably, this transition maintained the same level of activity while simplifying the synthetic process. It also addressed challenges related to racemic mixtures and the necessity for enantiopure compounds, as we eliminated the stereocenter.

Crucially, the left part of the molecule, consisting of the pyrazine segment, was found to be essential for activity. Consequently, we shifted our focus to derivatives of the right part of the molecule, specifically the pyridine segment, which ultimately emerged as the most potent compounds in our study.



**Scheme 5:** derivatisation scheme for the aminopyrazine class.

Additionally, from the Hydantoin-class (class II), roughly twenty different molecules were synthesized. The derivatisation pattern (**Scheme 6**), was quite straight forward. The aromatic part as well as the Hydantoin part were replaced by different moieties and the ortho as well as the para-analogue of compound (**7**) were synthesized.



**Scheme 6:** derivatisation scheme for the Hydantoin class.

We have previously identified compounds that inhibit CsrA, including peptides and small molecules, demonstrating on-target activity. [2,26] However, these compounds lacked activity within cells. Our goal now is to discover compounds with both on-target and *in-cellular* activity.

Additionally, we encountered challenges with the stability and expression of CsrA protein from *E. coli*, leading to rapid degradation and issues with reproducibility. While the FluPo assay effectively demonstrated activity in general, it proved insufficient for comparing these compounds.

To address these limitations, Wu et al. have established a luciferase-based reporter gene assay to screen for the most promising derivatives from classes **II** and **IV**.<sup>[12]</sup> This assay directly assesses in-cell effects using whole bacteria, bypassing the need for isolated *E. coli*-CsrA. While these experiments are ongoing, we cannot yet present reliable data. All synthesized compounds, intended for evaluation in the luciferase assay, are depicted in **Figure 15** and **Figure 16**.

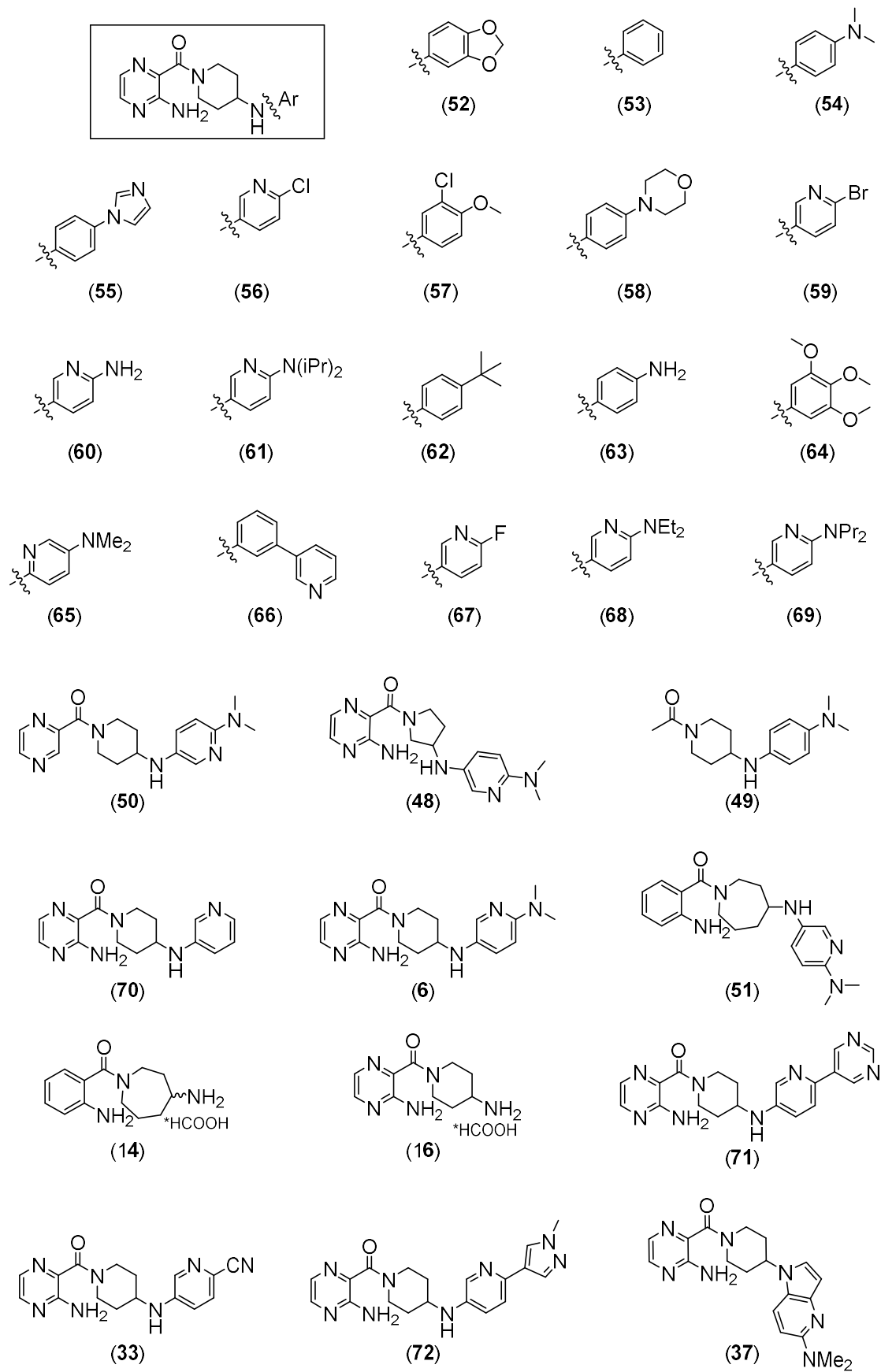


Figure 15: All compounds from class IV.

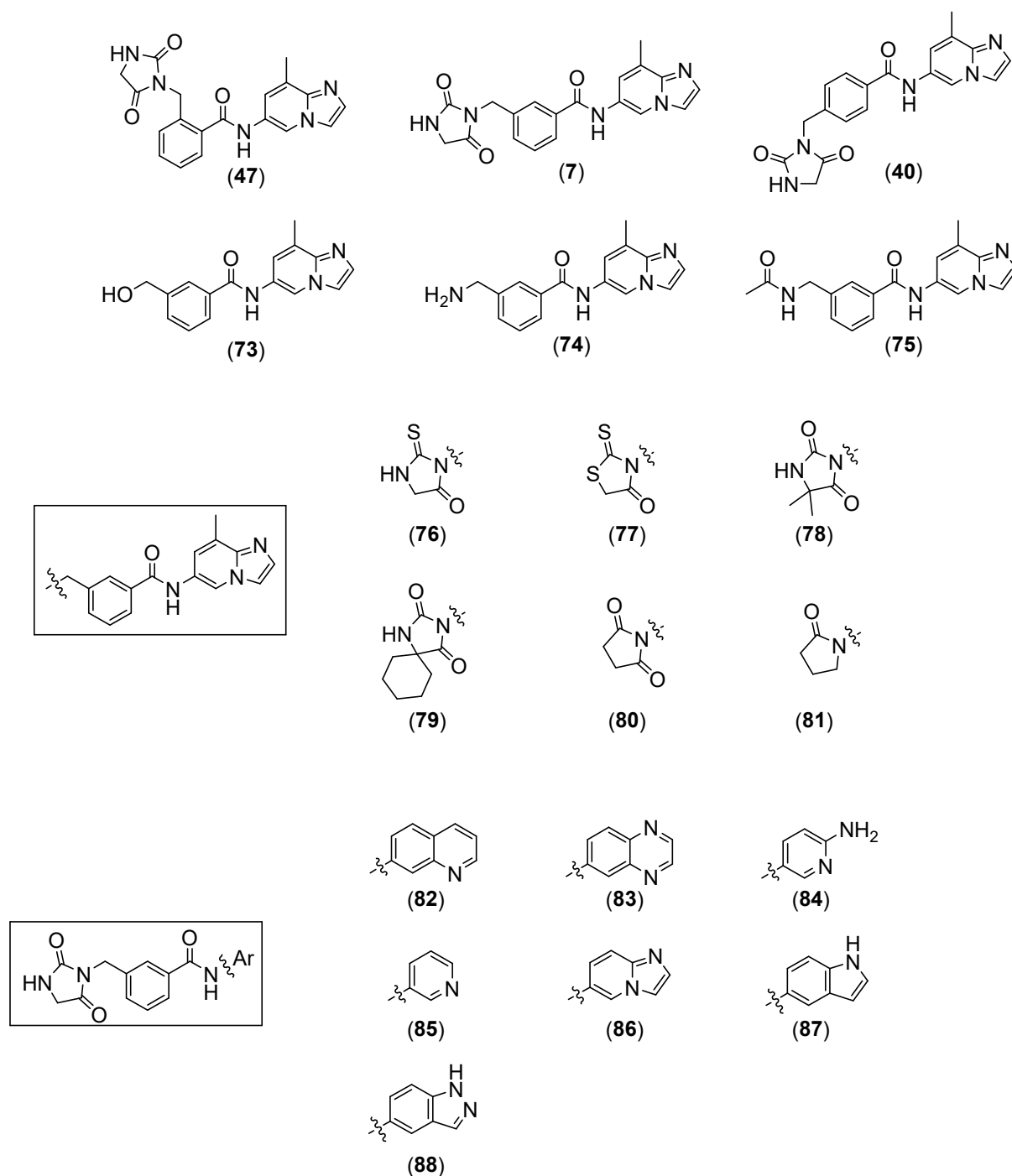


Figure 16: All compounds from class II.

### 4.3.3 Methods

#### Expression of *E. coli* CsrA-His<sub>6</sub>

The amino acid sequence for the *E. coli* CsrA-His<sub>6</sub> construct is MLILTRRVGE TLMIGDEVTV TVLGVKGNQV RIGVNPKEV SVHREEIYQR IQAEKSQQSSY HHHHH. The molecular weight of the CsrA-His<sub>6</sub> monomer is 7.68 kDa. The construct is present in pET21a+ with an ampicillin resistance and transformed into *E. coli* Lemo21. The expression protocol of *E. coli* CsrA-His<sub>6</sub> is based on protocols from Y. Lai et al.<sup>[89]</sup> and Jakob et. al.<sup>[2]</sup> with small variations.

TB medium, containing 100 µg/mL ampicillin, were inoculated with an overnight preculture. This main culture was grown at 37 °C and 180 rpm until an O.D. 600 of 0.6 was reached. Then, 1 mL of 1 M IPTG (1 mM end concentration) per liter of culture was added. The culture was grown again at 18 °C, 180 rpm overnight. Cells were harvested by centrifugation (4 °C, 6200 rpm, 20 min). The pellets were resuspended in 4.5 mL/g wet cells lysis buffer (50 mM Tris-HCl, 300 mM NaCl, 20 mM, pH 8.0) containing cComplete™ (EDTA-free protease inhibitor cocktail, Roche). Afterwards the cells were disrupted by French press. After centrifugation of the homogenisate (4 °C, 19000 rpm, 30 min), the supernatant was sterile-filtered through 0.22 µm membrane filter. For purification an ÄKTExpress™ device with a 1 mL HisTrap™ HP column was used, which was equilibrated with 20 mL lysis buffer (1 mL/min flowrate). The clear lysate was loaded on the column with 1 mL/min. This was followed by three washing steps, first washing buffer 1 (50 mM Tris-HCl, 300 mM NaCl, 20 mM imidazole, 10% glycerol, pH 8.0), second two times washing buffer 2 (50 mM Tris-HCl, 300 mM NaCl, 50 mM imidazole, 10% glycerol, pH 8.0). The elution was done with the same washing buffer except for increasing the imidazole concentration to 250 mM. Afterwards, buffer was exchanged to storage buffer (10 mM Tris-HCl, 100 mM KCl, 10 mM MgCl<sub>2</sub>, 25% glycerol, pH 8.0) with a PD10 desalting column. The CsrA-containing fractions were concentrated via Vivaspin® 20 spin filters (5 kDa MWCO, Sartorius™) and the final concentration was determined by UV spectroscopy with NanoDrop™ ( $\epsilon_{280} = 2980 \text{ M}^{-1}\text{cm}^{-1}$ , monomer). Pooled fractions were divided into aliquots, flash frozen in liquid nitrogen and stored at -80 °C.

### Fluorescence Polarization Screening Assay

The fluorescence polarization assay has been established by Maurer et al.<sup>[26]</sup> and the procedure used in current manuscript is based on Jakob et al.<sup>[2]</sup> with small changes. These changes will be described in the following section.

Instead of 1:2 dilution series containing 12 steps, the screening assay only measures one. All 1151 of pre-selected compound stock solutions (10 mM) from *in silico* screening were diluted in 100 % DMSO and then in assay buffer (10 mM HEPES, 150 mM NaCl, 0.005 % (v/v) Tween-20, ad DEPC-treated H<sub>2</sub>O (RNase free water), pH 7.4) to obtain the concentration of 300 µM. 10 µL of each compound were transferred to a 384 well microtiter plate (black, flat bottom, Greiner Bio-One) in two replicates and another 10 µL of 2.4 µM of *E. coli* CsrA-His<sub>6</sub> protein (in assay buffer) were added to each well and quickly centrifuged to be preincubated for 1 h on a Duomax 1030 shaker under light exclusion.<sup>[2]</sup> 10 µM fluorescein-labelled RNA (RNAflc) was diluted with assay buffer to a concentration of 45 nM obtaining a final concentration of 15 nM in the assay. After short centrifugation the plate was incubated for 1.5 h on the shaker under light exclusion. The final concentrations in the assay were 800 nM *E. coli* CsrA, 5 % DMSO, 15 nM RNAflc and 100 µM compounds. Using our plate layout, it is possible to screen 144 compounds in one 384 well microtiter plate.

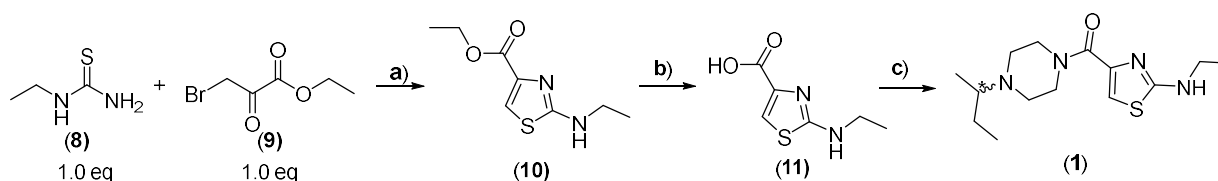
The positive control in the screening assay is a triazole-based peptide inhibitor reported earlier (see **section 4.1**) and small molecules with inhibition  $\geq 30$  % without solubility and fluorescence interference issues were defined as 'primary' hits. For hit confirmation, compounds were tested in dose–response binding experiments at concentrations of 100, 50 and 10 µM.

## Luciferase screening assay

The procedure is based on the assay protocol from Wu et al., which has been reported earlier.<sup>[12]</sup> In brief, *E. coli* strains BL21 pvBE3 with or without the plasmid pNS6236 (cesT+) were grown at 37°C until OD = 0,6 is reached.<sup>[12]</sup> Afterwards, cultures were diluted in LB medium to OD = 0.06. 100 µL of diluted culture were transferred into the 96-well plates preloaded with 100 µL LB and respective wells with compounds (duplicates, 500 µM and 250 µM end concentrations) or positive control (cesT+ and 5% DMSO) or vehicle (only 5% DMSO). The total volume per well is 200 µL. The relative light units (RLU) and OD600 were determined directly from one plate after 6-7 hours.<sup>[12]</sup>

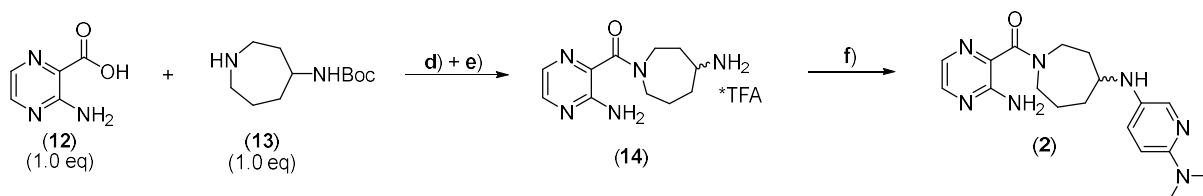
## Synthesis

The synthesis of compound (**1**) was straightforward and is shown in **Scheme 7**. The first step, the condensation of the thiourea (**8**) and the bromopyruvate (**9**) was described in literature.<sup>[90]</sup> The subsequent saponification of (**10**), using a standard procedure for ester hydrolysis (NaOH in EtOH/H<sub>2</sub>O) yielded the corresponding acid (**11**) in a moderate yield due to purification issues. The coupling of (**11**) with 1-(sec-butyl)piperazine using a T<sub>3</sub>P/Dipea system yielded the desired product (**1**) in a high yield and purity.

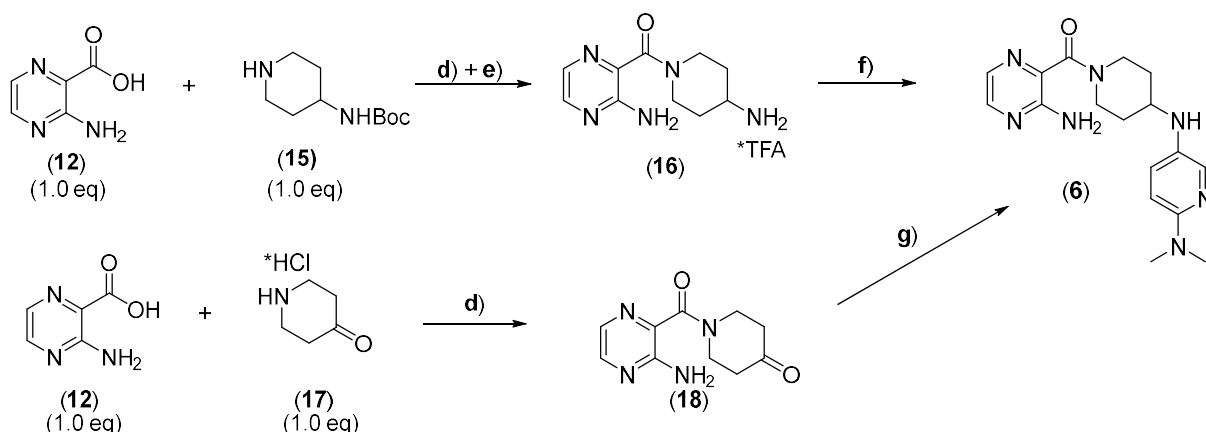


**Scheme 7:** Synthesis of compound (**1**). **a**) 1,4-dioxane, o.n, reflux; **b**) NaOH (6.0 eq), EtOH/H<sub>2</sub>O (3:2), 16h, rt; **c**) 1-(sec-butyl)piperazine (1.5 eq), T<sub>3</sub>P (4.0 eq), Dipea (6.0 eq), DCM, 16h, rt.

The synthesis of (**2**) and (**6**) is shown in **Scheme 8** and **Scheme 9**. The hits (**2**) and (**6**) can be synthesized either by a Buchwald-Hartwig reaction using the amines (**13**) and (**15**), or by a reductive amination, using the respective ketone (**17**), which was only used for (**6**). The amines and ketones were synthesized from 3-aminopyrazine-2-carboxylic acid (**12**) in one step, using peptide coupling conditions. Reductive amination is the superior route, as shown in the example of (**6**), as the Buchwald-Hartwig reaction is slow and delivers many side products.

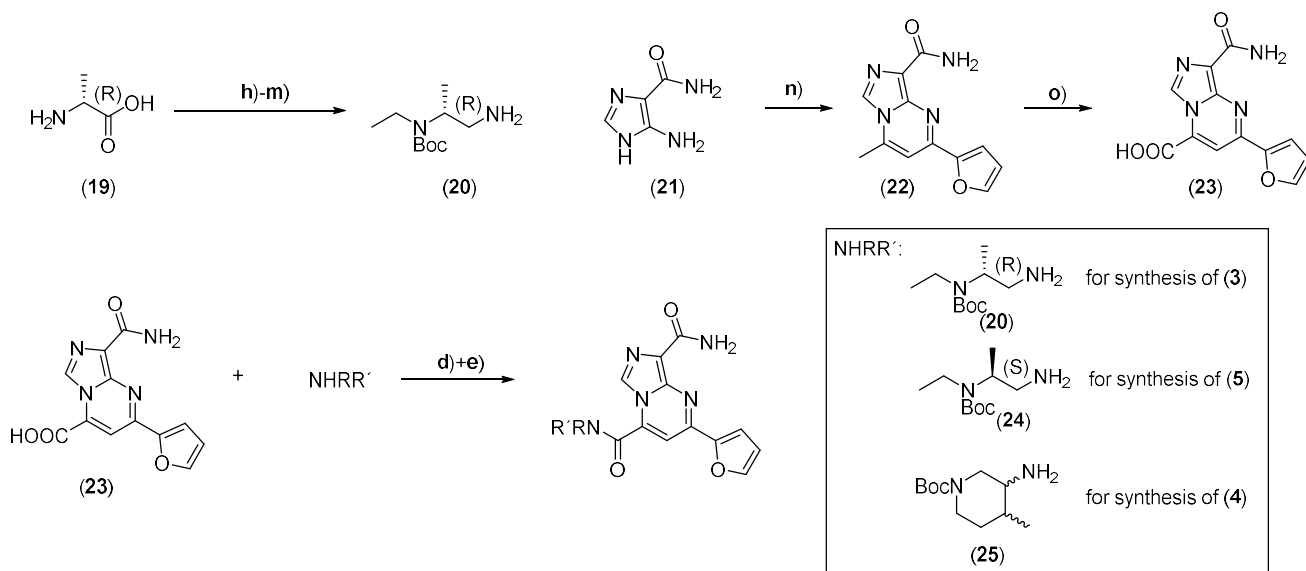


**Scheme 8:** Synthesis of compound (**2**). **d**) T<sub>3</sub>P (4.0 eq), Dipea (6.0 eq), DCM, o.n, rt; **e**) TFA/DCM 1:1, 30 min, rt; **f**) 5-bromo-N,N-dimethylpyridin-2-amine (1.0 eq), NaOtBu (4.0 eq), tBUXPhosPdG3 (0.15 eq), 1,4-dioxane, MW, 2h, 130°C.



**Scheme 9:** Synthesis of compound (6): **g)** AcOH (1.1 eq), BH(OAc)<sub>3</sub> (1.5 eq), DCM, 19h, 45°C.

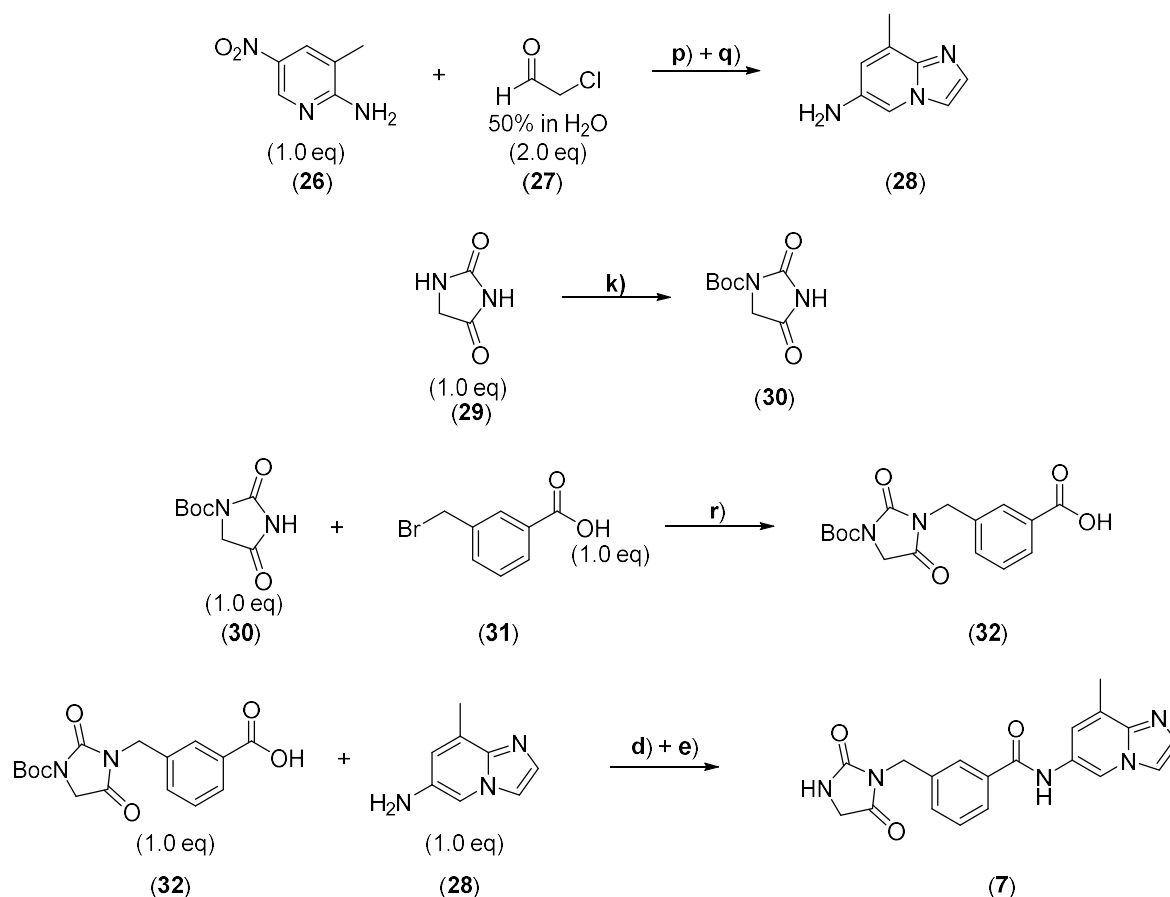
For the synthesis of the hits (3), (4) and (5) (depicted in **Scheme 10**), an amine and a carboxylic acid part were synthesized separately and then combined via amide coupling using T<sub>3</sub>P/DIPEA in DCM at rt. The synthesis of the amine parts, namely tert-butyl (R)-(1-aminopropan-2-yl)(ethyl)carbamate (20) and tert-butyl (S)-(1-aminopropan-2-yl)(ethyl)carbamate (24) from (D)-alanine (19) and (L)-alanine was well described in literature and tert-butyl 3-amino-4-methylpiperidine-1-carboxylate (25) was commercially available.<sup>[91]</sup> The synthesis of the carboxylic acid (23) took place in two steps. First the condensation of an amino-pyrazine with a diketone as described by et al. to gain (22) and then the oxidation of (22) to (23) with SeO<sub>2</sub> in Pyridine was performed.<sup>[92]</sup> The rather low yields in this step are mostly due to insufficient solubility of (23).



**Scheme 10:** Synthesis of compounds (4), (5), (6). **h)** TMSCl (4.0 eq), EtOH [0.2M], 4h, rflux; **i)** AcCl (1.0 eq), NEt<sub>3</sub> (2.0 eq), DCM, 2h, rt; **j)** LAH [2.15 eq], THF, 3h, rflux; **k)** Boc<sub>2</sub>O (1.1 eq), Dipea (2.6 eq), THF, 3h, rt; **l)** Phth (1.5 eq), PPh<sub>3</sub> (1.5 eq), DtBAD (1.5 eq), THF, 2h, rt; **m)** MeNH<sub>2</sub> (33%, aq.), EtOH, o.n, rt; **n)** 1-(furan-2-yl)butane-1,3-dione (1.0 eq), AcOH, 4h, 80°C; **o)** SeO<sub>2</sub> (4.0 eq), Py [0.1 M], 2h, 120°C.



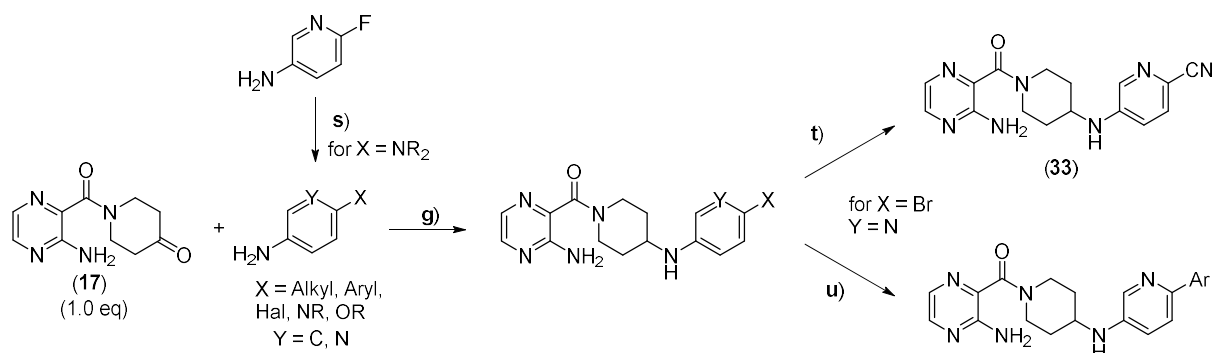
As in previous approaches, the amide (**7**), was synthesized from an acid part (**32**) and an amine part (**28**), which were then combined via amide coupling (see **Scheme 11**). The acid part could be synthesized via a nucleophilic substitution reaction, with catalytic amounts of TBAI, to allow iodine-bromine exchange in equilibrium enabling a faster reaction. The amine part, was synthesized in two steps, first the installation of the heterocyclic moiety via a condensation reaction and subsequent hydrogenation of the nitro group to the corresponding amine (**28**).



**Scheme 11:** synthesis of compound (**7**) **p)** EtOH, rflux, 2h; **q)** 1 atm H<sub>2</sub>, Pd/C (5 mol%), 5 h, rt; **r)** NaH (2.0 eq), TBAI (0.1 eq), THF, rflux, o.n.

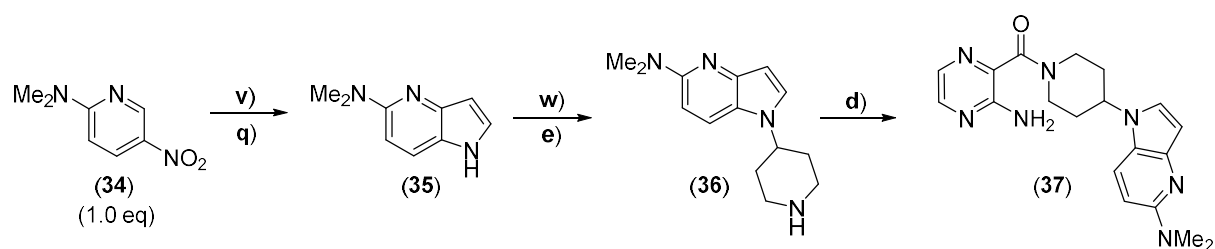
## Derivatisation

The primary derivatisation route, for molecules adhering to class II, as illustrated in **Scheme 12**, commences with a reductive amination step. This step proved to be a remarkably clean reaction, exhibiting compatibility with a broad spectrum of substrates. For certain derivatives, the desired amine for the reductive amination step was commercially available, in other cases it needed to be synthesized from the corresponding fluorine in a nucleophilic aromatic substitution reaction. More complex aromatic systems, needed to be synthesized from the corresponding bromide via a Suzuki cross coupling reaction.



**Scheme 12:** derivatisation of compound from **classII s** LiNR<sub>2</sub> [1M] in THF/Hex (4.0 eq), 70°C, 2h; **t**) K<sub>4</sub>[Fe(CN)<sub>6</sub>]\*3H<sub>2</sub>O (0.2 eq), N-Me-ImH (2.0 eq), CuI (0.2 eq), dry.Tol [0.1M], 160°C, 16h; **u**) Pd(PPh<sub>3</sub>)<sub>4</sub> (0.1 eq), 10% aq. Na<sub>2</sub>CO<sub>3</sub> solution (2.0 eq)/toluene 2:3, 130°C, o.n.

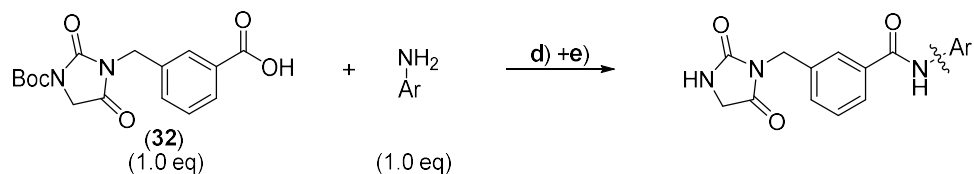
As rigidisation might increase activity, the aniline moiety was replaced by an indole moiety, as cyclisation limits the degree of free rotation. The synthesis was completed within five steps. First the Indole part (**35**) was synthesized according to literature.<sup>[93]</sup> Next, the piperidine ring was introduced via nucleophilic substitution. In the final step, amide formation with 3-aminopyrazine-2-carboxylic acid delivered the desired product. This approach is shown in **Scheme 13**.



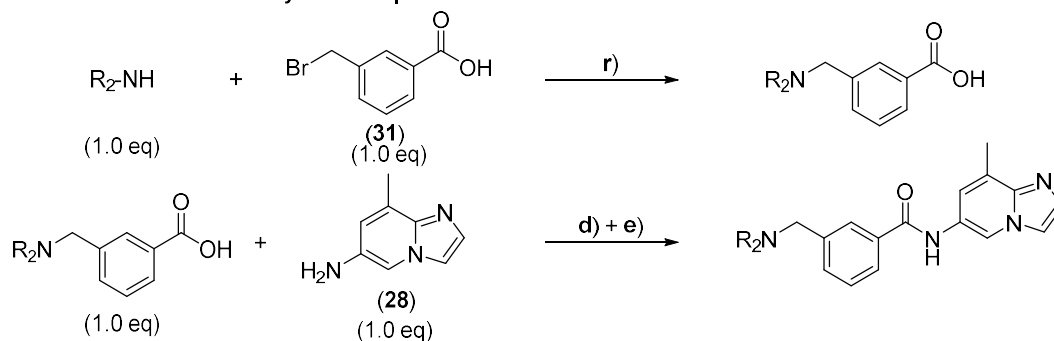
**Scheme 13:** rigidisation approach **v**) 2-(4-chlorophenoxy)acetonitrile (1.1 eq), KOtBu (2.2 eq), DMF, -10°C, 1h then 5% aq. HCl; **w**) tert-butyl 4-((methylsulfonyl)oxy)piperidine-1-carboxylate (1.2 eq), NaH (2.1 eq), DMF, 80°C, 6h.

The preparation of analogues from the class **IV** was straightforward, either the aromatic part of the molecule was changed or the Hydantoin part. The acid (**32**) was used in amide coupling reactions to get to derivatives of the aromatic part in one amide coupling step. For the synthesis of hydantoin analogues, a two-step process was necessary, where the corresponding acid for amide coupling needs to be synthesized first via nucleophilic substitution of the corresponding amine with the benzyl bromide (**31**) (**Scheme 14**).

Derivatisation of the aromatic part

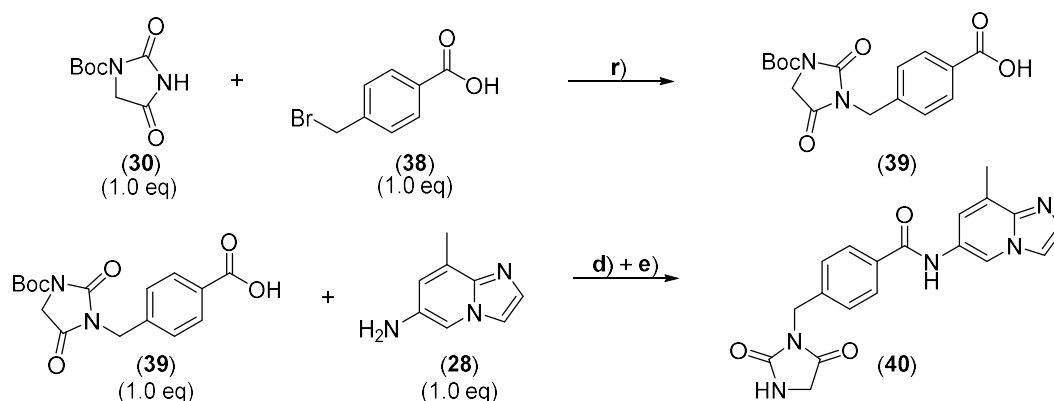


Derivatisation of the Hydantoin part



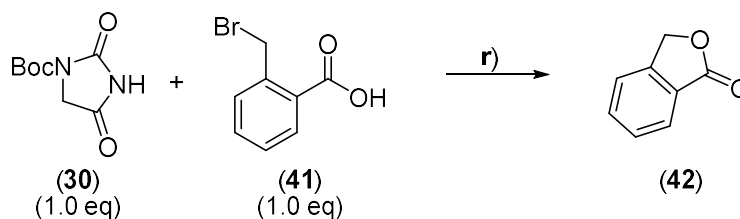
**Scheme 14:** Derivatisation reactions for molecules belonging to **classIV**.

For the synthesis of compound (40), a process analogue to the one use for the synthesis of compound (7) was used (**Scheme 15**), with the only difference being the use of *para*-substituted benzylbromide (38) instead of *meta*-substituted benzylbromide (31).



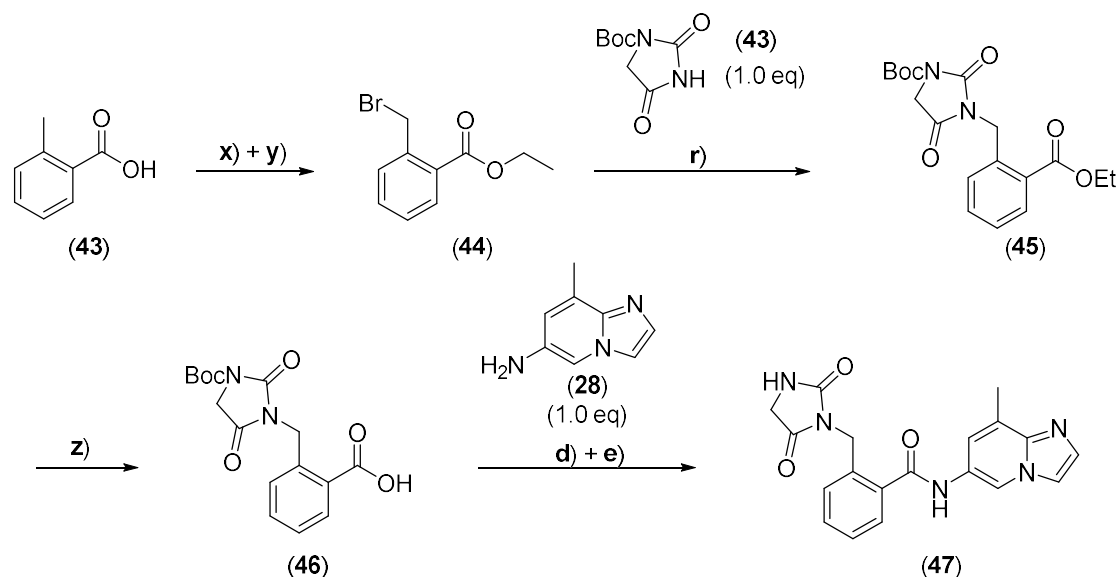
**Scheme 15:** Synthesis of *para* substituted molecule (40).

The synthesis of the *ortho*-substituted product (47), in an analogy to the synthesis of (7) and (40), via  $\text{S}_{\text{N}}2$  reaction between (30) and (41) failed, as an intramolecular cyclisation of compound (41) to the lactone (42) was favored (**Scheme 16**).



**Scheme 16:** Failed attempts to synthesis *ortho*-substituted product (47).

As the direct nucleophilic substitution is not suitable for this substrate, a modified route needed to be employed. A protection strategy of the acid is needed since the free acid group is causing troubles during this reaction. First, 2-methylbenzoic acid is protected as its ethyl ester, then a Wohl-Ziegler reaction delivered the benzylbromid (**44**), which was used in the nucleophilic substitution to deliver the desired molecule (**46**) after saponification. The acid was then coupled with amine (**28**) to deliver the desired product (**47**), as shown in (**Scheme 17**).



**Scheme 17:** Synthesis route for ortho analogue (**47**), **x**) EtOH/H<sub>2</sub>SO<sub>4</sub> 20:1, reflux, 6 h; **y**) NBS (1.1 eq), BPO (0.03 eq), MeCN, reflux, 4 h.

#### 4.3.4 Conclusion

Utilizing SPR-screening and hit validation via fluorescence polarization assays, we uncovered two novel classes of small molecular CsrA inhibitors. Additionally, we developed synthetic procedures facilitating the convenient production of four classes of molecules (refer to **Figure 14**). These modular methods enable the straightforward and efficient synthesis of a diverse array of analogues derived from the initial hits.

In total, over fifty analogues were prepared from classes **II** and **IV**. Once our reporter gene luciferase assay achieves reliable functionality, these compounds will undergo assessment for *in-bacterio* activity. The most promising hits will undergo optimization, followed by extensive SAR-studies. These compounds and their synthetic routes are promising starting points for the development of selective inhibitors of the CsrA-RNA interaction.

After optimisation of these compounds towards *in-vitro* (*IC*<sub>50</sub>-values) and *in-vivo* (% increase of luminescence) activity as well as optimisation of PK/PD values, they might be able to deliver the proof of concept, that CsrA is an antivirulence target by correlating ontarget activity to effect *in-bacterio*. The synthesis and optimisation of these compounds will rely on the previously introduced procedures.

## 4.4 Small molecules inhibiting the IMP2-RNA interaction

First Small-Molecule Inhibitors Targeting the RNA-Binding Protein IGF2BP2/IMP2 for Cancer Therapy

Authors:

Charlotte Dahlem\*, Ali Abuhaliema\*, Sonja M. Kessler\*, Tarek Kröhler, Ben G. E. Zoller, Shilpee Chanda, Yingwen Wu, Simon Both, Fabian Müller, Konstantin Lepikhov, Susanne H. Kirsch, Stephan Laggai, Rolf Müller, Martin Empting and Alexandra K. Kiemer

\* These authors contributed equally.

Bibliographic Data:

*ACS Chemical Biology* **2022** <https://doi.org/10.1021/acscchembio.1c00833>

Author Contributions: Dr. Charlotte Dahlem was involved in formal analysis and visualization as well as conceptualization. She performed some assays and contributed to the writing of the original draft. Ali Abuhaliem was responsible for formal analysis, performed some assays and was involved in the writing of the manuscript. Prof. Dr. Sonja M. Kessler worked on the conceptualisation and supervision of the project and wrote parts of the manuscript. Tarek Kröhler, worked on assay development and took part in the editing and reviewing process. Ben G. E. Zoller optimized the synthetic routes to the compounds belonging to the ureidothiophene class as well as the benzamidobenzoic acid class. The ureidothiophenes were synthesized in 5 steps, the route started with a 2 step thiophene synthesis, transforming the respective ketone, in a modified Vilsmeier-Haack reaction to the respective Chloro-propenenitriles, which could be converted to the thiophenes employing Methyl thioglycolate. Saponification of the ester followed by formation of an isatoic anhydride with phosgene and subsequent urea formation by treatment of the anhydride with the corresponding amine gave the desired ureidothiophenes in yields of 10 - 20% over five steps in amounts of 0.1 - 1 g. The benzamidobenzoic acids were synthesized in three steps with yields of 25 - 40% in amounts around 100 mg per compound. The synthesis involved acid protection, amide bond formation and acid deprotection. Ben G. E. Zoller was also involved in the editing and reviewing process of the manuscript. Shilpee Chanda, Dr. Yingwen Wu, and Simon Both performed parts of the assays in this study. Fabian Müller provided some of the visual material used in the manuscript and performed some assays. Dr. Konstantin Lepikhov helped with resources. Dr. Susanne H. Kirsch provided resources and helped in reviewing and editing the manuscript. Stephen Laggai helped in supervision and was involved in the reviewing and editing process. Prof. Dr. Rolf Müller provided resources and was involved in the review and editing process. Prof. Dr. Martin Empting worked on the conceptualization, helped supervising and wrote parts of the manuscript. Prof. Dr. Alexandra K. Kiemer initiated and directed the study, worked on the conceptualization of the investigation, was responsible for funding acquisition, wrote parts of the manuscript and assisted in the supervision of the project.

# First Small-Molecule Inhibitors Targeting the RNA-Binding Protein IGF2BP2/IMP2 for Cancer Therapy

Charlotte Dahlem, Ali Abuhaliema, Sonja M. Kessler, Tarek Kröhler, Ben G. E. Zoller, Shilpee Chanda,

Yingwen Wu, Simon Both, Fabian Müller, Konstantin Lepikhov, Susanne H. Kirsch, Stephan Laggai, Rolf Müller, Martin Empting, and Alexandra K. Kiemer\*

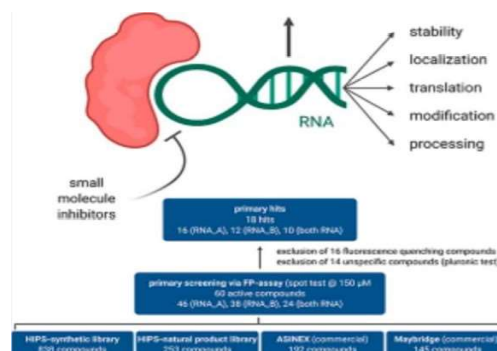
ACCESS |

Metrics &amp; More

Article Recommendations

Supporting Information

**ABSTRACT:** The RNA-binding protein IGF2BP2/IMP2/VICKZ2/p62 is overexpressed in several tumor entities, promotes tumorigenesis and tumor progression, and has been suggested to worsen the disease outcome. The aim of this study is to (I) validate IMP 2 as a potential target for colorectal cancer, (II) set up a screening assay for small-molecule inhibitors of IMP2, and (III) test the biological activity of the obtained hit compounds. Analyses of colorectal and liver cancer gene expression data showed reduced survival in patients with a high IMP2 expression and in patients with a higher IMP2 expression in advanced tumors. In vitro target validation in 2D and 3D cell cultures demonstrated a reduction in cell viability, migration, and proliferation in IMP2 knockout cells. Also, xenotransplant tumor cell growth in vivo was significantly reduced in IMP2 knockouts. Different compound libraries were screened for IMP2 inhibitors using a fluorescence polarization assay, and the results were confirmed by the thermal shift assay and saturationtransfer difference NMR. Ten compounds, which belong to two classes, that is, benzamidobenzoic acid class and ureidothiophene class, were validated in vitro and showed a biological target specificity. The three most active compounds were also tested in vivo and exhibited reduced tumor xenograft growth in zebrafish embryos. In conclusion, our findings support that IMP2 represents a druggable target to reduce tumor cell proliferation.



## INTRODUCTION

RNA-binding proteins (RBPs) play an important role in diverse physiological functions. They are involved in mRNA maturation, stability, localization, and translation of mRNA targets.<sup>[1]</sup> Insulin-like growth factor 2 (IGF2) mRNA binding proteins (IGF2BPs/IMPs/VICKZs) are highly expressed during fetal development and maturation in different tissues. Their expression decreases in most tissues after birth.<sup>[2]</sup> IMPs share structure and function similarities: they comprise two RNA recognition motifs (RRM1-2) in the N-terminal region and four KH homology domains (KH1-4) in their C-terminal region.<sup>[3]</sup> Several RNA recognition elements have been described to be recognized by IMP family members. <sup>[4-7]</sup> IMP2 plays a distinct role in cancer progression and responsiveness to chemotherapy. In different cancers, IMP2 has been shown to be more frequently amplified, and its expression is higher than those of IMP1 and IMP3.<sup>[8,10]</sup> While IMP1 and IMP2 are generally regarded as having a clear oncofetal

expression pattern, data on IMP2 are somewhat conflicting.<sup>[2,3]</sup>

The expression and translation of different oncogenes are controlled directly or indirectly by IMP2. As a consequence, IMP2 increases cell proliferation, growth rate, migration, and invasion, promotes epithelial mesenchymal transition, and affects cell metabolism.<sup>[9,11-14]</sup> IMP2 knockout mice show a reduction in size, total weight, and linear growth compared to wild types but are generally healthy. <sup>[15]</sup> Their metabolic activity and energy expenditure are improved, and the development of fatty liver disease and malignancy is reduced. Vice versa, hepatocyte-specific overexpression of p62, a shortened splice variant of IMP 2 containing its identical RNA binding domains, induces steatosis <sup>[16]</sup> and amplifies steatohepatitis and hepatocarcinogenesis. In addition to hepatocellular carcinoma, IMP2 was suggested to play a role in another gastrointestinal tumor, which in fact represents the most frequent malignancy in the gastrointestinal system, that is, colon cancer. <sup>[20,21]</sup>

Due to the important role of IMP2 in carcinogenesis and tumor progression, we hypothesized that the inhibition of the activity of IMP2 might be a novel and attractive therapeutic approach for cancer therapy. We therefore (I) undertook *in vitro* and *in vivo* approaches for target validation, (II) set up a fluorescence polarization (FP) screening assay to identify hits

from several compound libraries, and (III) validated potential inhibitors *in vitro* and *in vivo*.

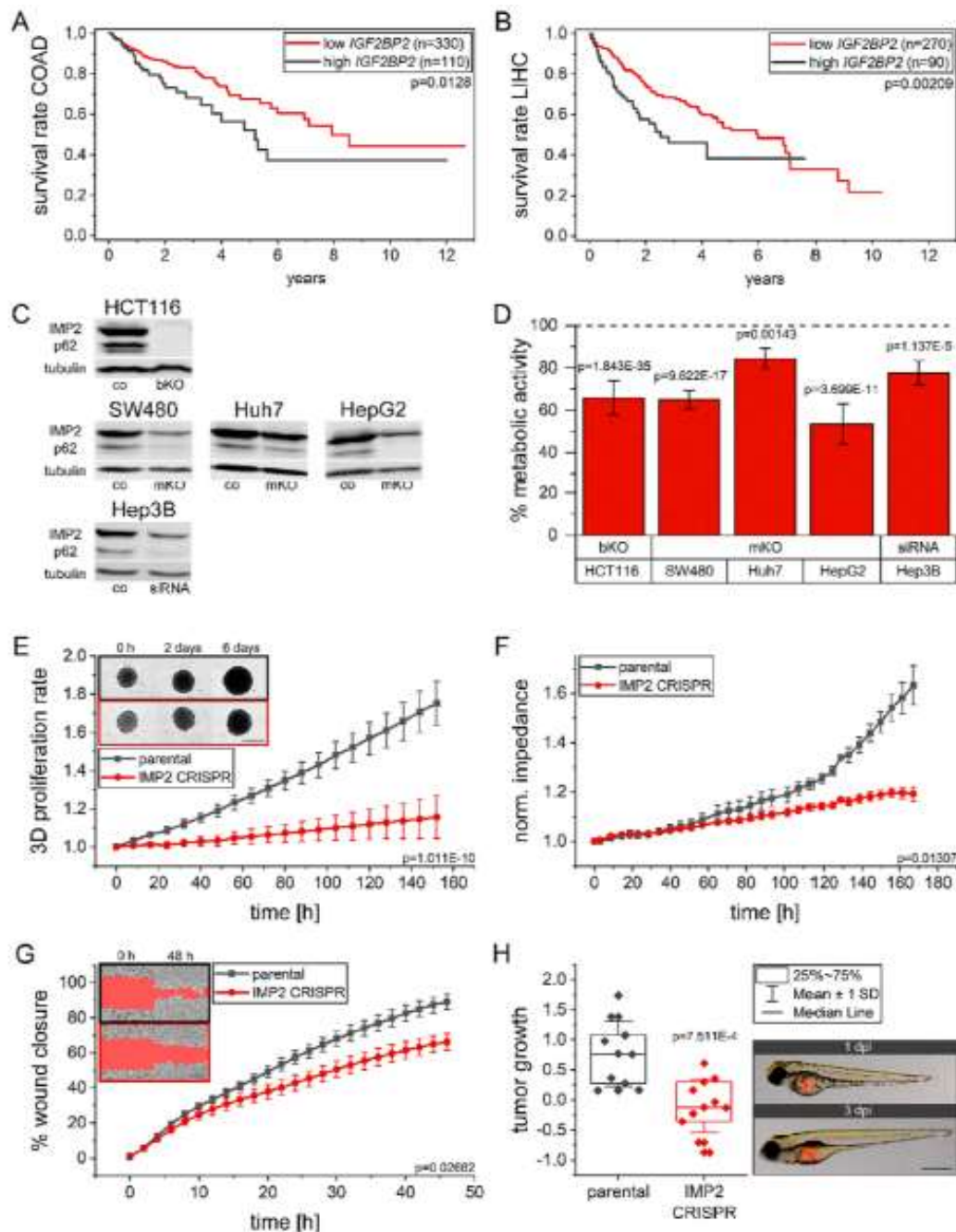


**Figure 1.** Clinical prognosis and target validation *in vitro* and *in vivo*. (A, B) Patient survival based on IMP2/IGF2BP2 mRNA expression in the TCGA datasets [COAD colon adenocarcinoma] and LIHC liver hepatocellular carcinoma]. The upper quartile is defined as a high expression. (C—H) IMP2 knockout/knockdown performed by CRISPR/Cas9 in HCT116, SW480, and Huh7 cells and by siRNA transfection in Hep3B cells. (C)

Western blots for IMP2 and its splice variant p62 in complete, biallelic (bKO) knockout HCT116 cells, partial, monoallelic (mKO) knockout SW480, Huh7, and HepG2 cells, and siRNA-knockdown Hep3B cells. Parental cells or random siRNA-transfected cells were used as controls (co). The quantification is presented in **Supporting Information Figure S3**. (D) Metabolic activity of IMP2 knockout/knockdown cells measured by the MTT assay 96 h after seeding. Data were normalized to their respective controls (dashed line),  $n = 4$  (triplicates). (E) After HCT116 spheroid formation for 3 days, the spheroid

areas were monitored by an IncuCyte system. The area was normalized to 3 day old spheroids (0 h). Representative pictures show spheroids at the starting point (0 h), 2, and 6 days after initiation of measurements; scale bar = 500 pm; n = 2 (quadruplicates). (F) Impact of IMP2 knockout on HCT116 cell impedance; n = 2 (triplicates). (G) Migratory activity of IMP2 knockout HCT116 cells analyzed in an IncuCyte system. Representative pictures demonstrate the wound area in red at the starting point (0 h) and 48 h after wounding; scale bar = 400  $\mu$ m; n = 3 (quadruplicates). (E–G) p-values were calculated for the respective last time points acquired. (H) Zebrafish embryo xenograft of HCT116 IMP2 knockout cells. Individual values of tumor growth quantification are presented in a box blot. Representative images of one parental xenotransplanted embryo at 1 dpi and 3 dpi are shown; scale bar = 1 mm.

## ■ RESULTS AND DISCUSSION

Clinical Prognosis and Target Validation in Vitro and in Vivo. Overexpression of IMP2 in colorectal cancer versus healthy colon tissue has been reported in the past. [20,22] However, to the best of our knowledge, its potential implication in clinical prognosis has only been reported in a small dataset of 19 patients. [23] Thus, we analyzed the connection between IGF2BP2 and prognosis in colon cancer in a large TCGA (The Cancer Genome Atlas) dataset. In colon adenocarcinoma patients, survival was significantly reduced in individuals with a high IGF2BP2 expression (Figure 1A). Also, analyses of the hepatocellular carcinoma TCGA dataset confirmed previous findings of a poor prognosis of patients with a high IGF2BP2 expression [9,13] (Figure 1B). Advanced colon tumor stages were associated with a significantly increased IGF2BP2 expression (Supporting Information Figure S2). Due to the smaller availability of tumor classification data in the liver dataset, analyses on individual stages were not performed.

Comparing the gene expression levels of IMP2 with those of IMP1 and IMP3 at different developmental stages in murine and human tissues revealed a similar predominant fetal expression pattern (Supporting Information Figure S1).

Two different CRISPR/Cas9 approaches as well as an siRNA-facilitated knockdown were used to reduce the expression of IMP2 and its splice variant p62 in colorectal and hepatocellular carcinoma cell lines. [10,14] Sanger sequencing (Supporting Information Figure S3 A–C) and Western blots (Figure 1C, quantification in Supporting Information Figure S3D) confirmed a complete knockout in HCT116 cells upon CRISPR/Cas9, while the knockout was only partial in SW480, Huh7, and HepG2 cells. Clonal selection resulted in single-cell clones; their genetic editing is summarized in Supporting Information Figure S3C. Multiple trials of CRISPR/Cas9 knockout did not lead to a biallelic deletion in SW480, Huh7, and HepG2 cells, supporting that IMP2 is essential for cell proliferation. In Hep3B cells, IMP2 levels were knocked down by siRNA (Figure 1C). Metabolic activity in MTT assays, which typically correlates with cell numbers, was significantly reduced upon IMP2 knockout/knockdown in all tested cell lines (Figure 1D).

Since IMP2 has been suggested to act only partially on proliferation in 2D cultures [14] and CRISPR phenotypes in 3D in vitro cultures recapitulate more accurately those of in vivo tumors, [24] we assessed the proliferation of parental and IMP2 knockout HCT116 cells in 3D spheroids. Live-cell analysis revealed a strongly reduced proliferation of IMP2 knockout spheroids (Figure 1E). To exclude possible

clonal artifacts, 3D proliferation was assessed for multiple HCT116 IMP2 knockout clones harboring different gene edits obtained from different knockout approaches (Supporting Information Figure S3C). They all showed comparable proliferation, which was significantly lower than the proliferation of parental cells (Supporting Information Figure S4).

Target specificity of IMP2 knockout in HCT116 cells was further validated by rescue experiments, demonstrating a restored metabolic and proliferative activity of knockout cells, in which IMP2/p62 was overexpressed (Supporting Information Figure S5A–D). The knockout cells displayed a reduced expression of the tumor-promoting drivers MYC and the long noncoding RNA DANCR as described targets of IMP2 [10,25,26] (Supporting Information Figure S5E,F). Their expression was partially restored when IMP2/p62 was overexpressed in knockout cells (Supporting Information Figure S5G,H). Since IMP2 facilitates its action on potentially thousands of mRNA targets via different actions, for example, regulating their stability, translation, or localization, [27,28] one would not expect that one single target is responsible for all IMP2 actions.

The major action of IMP2 on 3D growth has been suggested to be linked to its action on cell adhesion in hepatocellular carcinoma cells. [14] Electrical cell–substrate impedance sensing (ECIS) allows estimating cell adhesion in real time. [29] When this method was employed to assess cell responses toward CRISPR-facilitated IMP2 knockout, we found that the results were very similar to 3D growth (Figure 1F).

Furthermore, cell migration was significantly reduced in the absence of IMP2, as determined in a scratch wound assay (Figure 1G).

HCT116 parental and IMP2 knockout cells were then characterized for in vivo tumor growth in a zebrafish embryo xenograft model. Zebrafish embryo xenografts represent an excellent tool to perform in vivo experiments adhering to 3R rules to reduce animal experiments. Their usefulness for pharmacological studies has been extensively characterized, especially for studies on colorectal cancer. [30] In this model, tumor growth was significantly lower in IMP2 knockout cells compared to the parental control cells (Figure 1H).

IMP2 promotes tumorigenesis and tumor progression and is the most frequently amplified and the most highly expressed IMP in most cancer entities. [10] Our in vitro and in vivo data, together with published data on IMP2 in liver cancer [9,13,17], validated IMP2 as an interesting target for the treatment of gastrointestinal tumors. In vitro and in vivo inhibition of proliferation by CRISPR-mediated knockout confirmed data from the literature using shRNA knockdown



in colon cancer cells. [31,32] Xu et al. had reported similar encouraging results prompted us to screen for small-molecules in a pancreatic tumor xenograft model.[33] These molecule inhibitors of IMP2

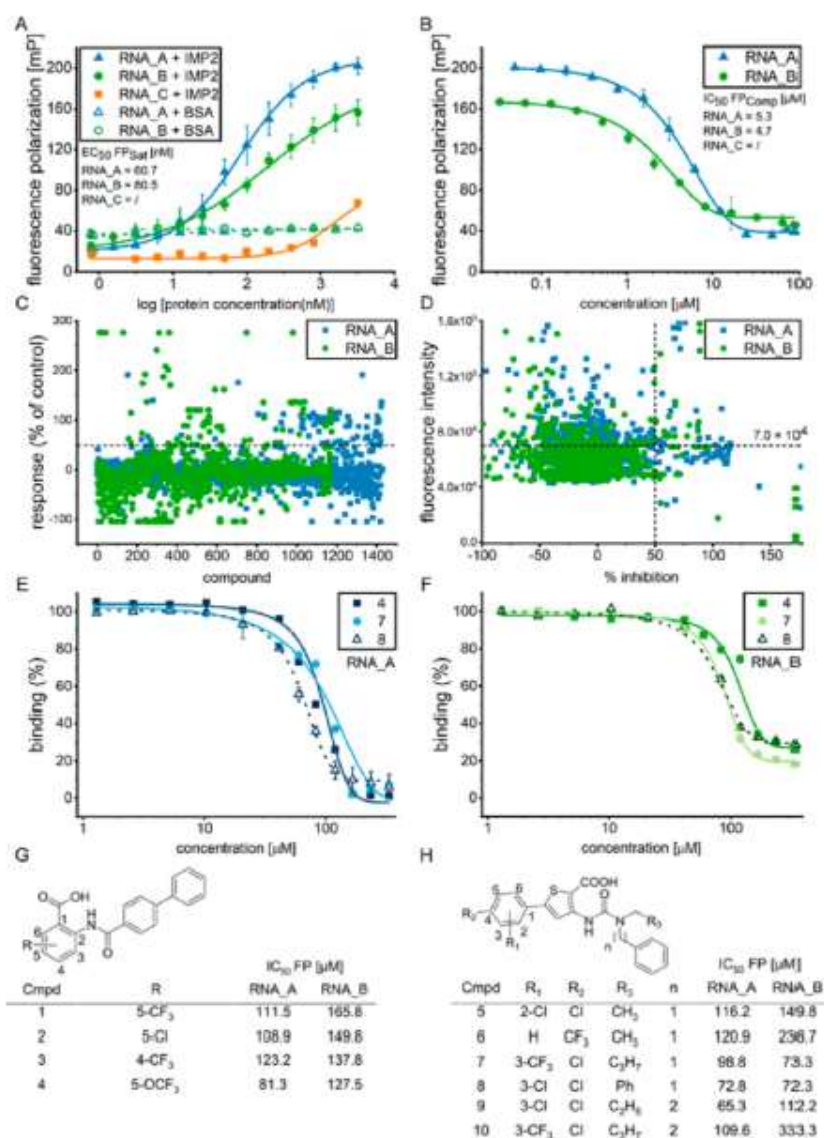


**Figure 2.** FP assay establishment and compound library screening. (A) FLC-labeled target RNA sequences (RNA A/B) and the control sequence (RNA C) were used in saturation experiments by titrating 1 nM RNA with a serial dilution of IMP2 protein or the unrelated protein BSA. (B) Competition experiments were conducted using fixed concentrations of 1 nM labeled RNA A/B, 200 nM IMP2 and varying concentrations of the respective nonlabeled RNA as a competitor. Half-maximal effective concentrations in saturation assays [EC<sub>50</sub> FP<sup>sat</sup>, and half-maximal inhibitory concentrations in competition assays (IC<sub>50</sub> FP comp) were calculated using nonlinear regression analysis. Data are represented as means of FP values ± standard deviation (SD), n = 2 (duplicates). (C) 1428 compounds for RNA A and 1175 compounds for RNA B were screened in an FP assay at a final compound concentration of 150 v/v. The scatter plot represents FP mean values of responses normalized to the response of nonlabeled RNAs used as the positive control. The dashed line indicates 50% inhibition of IMP2. (D) Mean fluorescence intensities of screened compounds were plotted against % inhibition. The dashed lines indicate the hit threshold. (E, F) Dose-response studies were performed with three representative hit compounds (compounds 4, 7, and 8) against (E) RNA A and (F) RNA B in the FP-based competition assay. Competition assays were conducted using fixed concentrations of RNA A/B (1 nM) and IMP2 (200 nM) and varying concentrations of hit compounds. Data are represented as means of FP values ± SD, n = 2 (duplicates). (G, H) Chemical structures and IC<sub>50</sub> values of hit compounds from class A and class B. Descriptive compound data are summarized in **Supporting Information Tables S1 and S2**. IC<sub>50</sub> values were calculated based on the competition assay; n = 2 (duplicates)

### Establishment of an FP Assay and Compound Screening.

We established an FP screening assay to detect potential hits capable of inhibiting IMP2/RNA interactions using several published potential binding motifs. [27,34-36] The purity, size, and integrity of IMP2 protein were confirmed by sodium dodecyl sulfate-polyacrylamide gel electrophoresis (SDS-PAGE) and Western blot analysis (Supporting Information Figure S6A,B). Since the established FP assay is based on the use of small, labeled RNA sequences, we assured the absence of any RNase activity in the protein preparation under assay conditions (Supporting Information Figure S6C). Circular dichroism spectrometry (CDS) confirmed the pronounced presence of  $\alpha$ -helical and  $\beta$ -sheet secondary structure elements indicating the correct folding of IMP2 (Supporting Information Figure S6D).

Serial dilutions of IMP2 were titrated against 1 nM of three different RNA sequences, that is, two sequences based on published binding motifs of IMP2 (RNA A and RNA B) [27,34-36] and one unspecific control sequence (RNA<sup>-</sup> C). IMP2 showed high affinity to RNA A and RNA B with EC<sub>50</sub> values of 60.7 and 80.5 nM, respectively (Figure 2A). No affine binding interactions occurred with control RNA C, and no binding was detected with bovine serum albumin (BSA), which was used as a negative control protein and titrated against RNA A/B. Non labeled RNA A and RNA B oligos were used to test the displacement of labeled RNAs in a competitive FP assay. The IC<sub>50</sub> values for RNA A and RNA B were 5.3 and 4.7  $\mu$ M, respectively (Figure 2B).

For further experimental setup for library screening, dimethyl sulfoxide (DMSO) tolerance was tested using 1 nM RNA A or RNA B with IMP2 at DMSO concentrations between 0 and 10% v/v since all library compounds were dissolved in DMSO. The FP signal was stable in DMSO concentrations up to 10% (Supporting Information Figure S7A,B). A final concentration of 5% DMSO was selected for screening experiments. FP signals were measured at different time points: the FP signals were stable between 1.5 and 4 h of incubation at room temperature. Thus, the 1.5 h time point of incubation was considered appropriate for further screening experiments (Supporting Information Figure S7C,D). The Z' value was 0.9 for both RNAs and confirmed that the FP assay was robust and appropriate for further competitive screening (Supporting Information Figure S8A—C).

We used the established FP assay to screen compounds from four libraries. In total, 1428 compounds were screened for RNA A and 1175 compounds for RNA B (Figure 2C). Fortysix compounds achieved more than 50% inhibition of IMP2 with RNA A, while 38 compounds showed activity against RNA B (Figure 2D). Twenty-four hits obtained from screenings against RNA A and 16 from RNA B were excluded due to quenching of the fluorescence intensity (FI) or due to their autofluorescent nature (Figure 2D). The addition of Pluronic (concentration 0.013%) was used to identify false positives due to aggregation of compounds on IMP2. A total of 13 compounds were excluded by this means (Supporting Information Figure S8D). Finally, 16 compounds for RNA A and 12 compounds for RNA B were considered as confirmed hits. Ten of these compounds were able to inhibit binding of both RNAs to IMP2. These 10

most promising hits belonged either to the benzamidobenzoic acid class (class A) or the ureidothiophene class (class B) (Figure 2G,H).

The compounds' IC<sub>50</sub> values were based on binding inhibition, measured by FP assay, and were found to be in the range between 65.3 and 120.9  $\mu$ M for RNA A and between 72.3 and 333.3 for RNA B (Figure 2E-H).

**Interaction of Inhibitors and IMP2.** To validate protein binding by hit compounds, a thermal shift assay (TSA, also referred to as differential scanning fluorimetry) was used. The melting temperature (T<sub>m</sub>) of IMP2 was 43 °C, and the change in T<sub>m</sub> after the addition of hit compounds was calculated. All hit compounds showed shifts in T<sub>m</sub> by —4.6 to —1.7 °C (Figure 3A,B). Tested against another RBP, that is, CsrA, [37] hit compounds 4, 6, and 9 demonstrated only marginal effects on

CsrA/RNA interaction at very high concentrations, suggesting a specificity of the compounds (Supporting Information Figure 9).

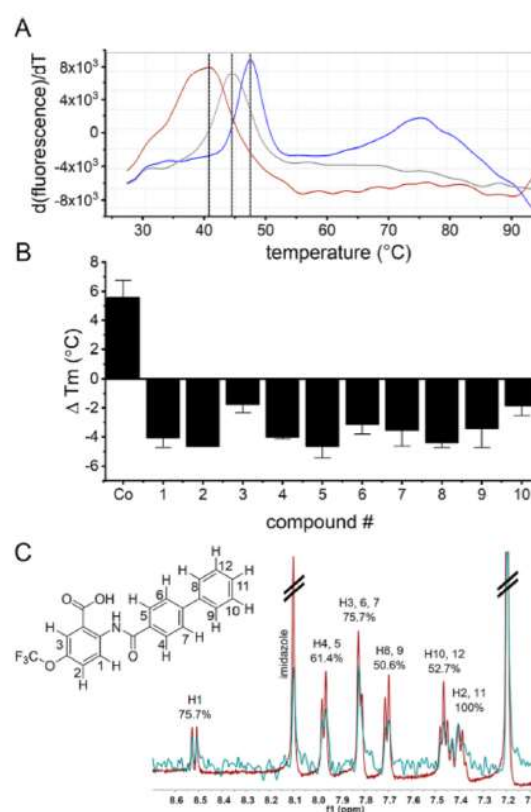


**Figure 3.** Hit compound confirmation via TSA and STD-NMR. (A) TSAs were performed at fixed concentrations of IMP2 (4.5  $\mu$ M), nonlabeled RNA (100  $\mu$ M), or hit compounds (100  $\mu$ M), measuring the fluorescence of SYPRO orange. Representative melting curves demonstrate a shift in the IMP2 melting temperature (T<sub>m</sub>) resulting from the binding to either RNA (blue) or hit compound 8 (red) compared to the control (gray). (B) Melting temperature shifts ( $\Delta$ T<sub>m</sub>) resulting from compound interactions were

quantified and compared to the nonlabeled RNA control. Data are presented as means  $\pm$  SD,  $n = 2$  (one replicate). (C) STD-NMR was performed at fixed concentrations of IMP2 (5  $\mu$ M) and compound **4** (500  $\mu$ M). The reference spectrum without protein is shown in red, and the STD difference spectrum of the IMP2/compound **4** complex is shown in green. Overlaid STD off-resonance and STD effect spectra were normalized to the signal of H2 and H11.

IMP2 has many flexible loops rendering the crystallization of full-length IMP2 a huge challenge. As an alternative, we applied saturation-transfer difference (STD)-NMR to gain coarse-grained insight into the binding mode. This enabled not only to confirm ligand/protein interactions by a nonfluorescence-dependent (orthogonal) method but also to gather information on the binding orientation of a ligand. [38–40] The proximity of ligand protons to the bound protein influences the degree of saturation transfer: the nearest protons are most prominently saturated, while the more distant protons have the weakest signals in the STD spectra. [41] Typically, the proton with the strongest STD effect is used to normalize the signals of the other protons, resulting in values between 0 and 100%.

STD-NMR was successfully performed with compounds **1–6** as well as **13** and **14** (Figure 3C; Supporting Information Figure S10). Among this set of STD-NMR-investigated compounds were four compounds belonging to class A (**1–4**) and four compounds belonging to class B (**5**, **6** and **13**, **14**).

For the latter two compounds (**13**, **14**), which inhibit only RNA A, the overall STD effect was not very prominent and did not allow for a conclusive interpretation. Importantly, hit **4** was characterized by the strongest on-target effect in the FP assay. Hence, we used its STD-NMR results in order to inform subsequent docking experiments to gain insight into the mode of inhibition. A first observation was that protons H-1, H-2, and H-3 of the benzoic acid ring interact strongly with the protein (H-1 75.796, H-2 100% observed together with H-11, H-3 75.7% observed together with H-6/7; Figure 3C). Second, within the middle ring, chemically equivalent protons H-6 and H-7 (75.7%; observed together with proton H-3) are in closer proximity to IMP2 than H-4 and H-5 (61.4%). Finally, the terminal phenyl moiety seems to interact less strongly overall (H-8/9 50.6%, H-10/12 52.7%, H-11 100% observed together with proton H-2).

With the aim to derive a plausible binding pose for class A compounds (representative **4**), we performed docking experiments with the available structure of the KH34 domain as well as a homology model of the RRMI domain considering the STD-NMR observations. In order to do this, we first generated the homology model of the IMP2 RRMI domain in complex with the ACAC RNA binding motif [34] using the homologous IMP3 RRMI2 structure (Supporting Information Figure S11 A,B). Based on the assumption that our IMP2/RNA interaction inhibitors act in an RNA-competitive manner, we docked compound **4** to the RNA-binding sites of both domains (RRMI and KH34). The highest-ranked docking poses reflected some key observations from the STD-NMR experiment and is shown in Supporting Information Figure S11C–F. In both

hypothetical ligand–target complexes, the benzoic acid head group interacts strongly with the protein. In the case of the RRMI docking pose, the carbonyl function is involved in a salt bridge with the nearby Arg90 sidechain, with H-3 being the most solvent-exposed (less interacting) proton in this ring. Protons H-4 to H-7 showed a mixed solvent exposure profile, which is in agreement with the observed STD effect. A similar outcome can be observed for the docking pose of compound **4** to the KH34 domain. Here, the carboxylic function forms a salt bridge to Arg576 and Lys583. Furthermore, the mixed solvent-exposure profile is also evident for protons H-4 to H-7. In both the docking poses, the terminal phenyl ring is a part of the molecule, which is mostly exposed to the solvent. In conclusion, these docking poses suggest that for future optimization efforts, enlargement of the identified hit scaffold (class A) should be possible at the terminal phenyl ring in order to improve efficacy. As the STD-NMR data for class B were not as conclusive as for class A, we did not put up a docking-based binding hypothesis. For that, more experimental information is needed to enable confidence-driven docking pose identification. We would like to stress that both the docking poses are hypothetical and that the current data do not allow to judge their validity beyond their agreement to the STD-NMR results. Ideally, X-ray crystallography will facilitate structure-guided optimization in the future.

**Biological Activity of Hit Compounds.** Different cancer cell lines were used to analyze the biological activity of the hit compounds. Colorectal (HCT116 and SW480) and hepatocellular (HepG2, Huh7, and Hep3B) carcinoma cells express a high amount of IMP2, whereas MCF7 cells do not express IMP2 and were therefore used as a control cell line (Cancer Cell Line Encyclopedia, [42] Western blot not shown). The lowest biological activity was noticed in MCF7 cells, supporting the specificity of the hits for IMP2 (Figure 4, Supporting Information Table S3).

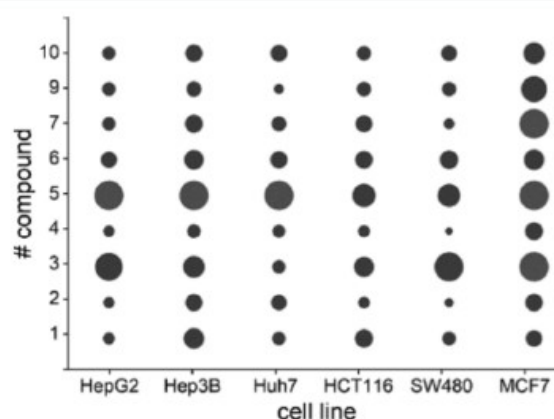


**Figure 4.** Biological activity ( $IC_{50}$  values) of final screening hits. The biological activity of screening hits was assessed via MTT assay in cancer cell lines expressing high IMP2 levels or lacking IMP2 (MCF7). Dots represent  $IC_{50}$  values (largest circle 280  $\mu$ M, smallest circle 18.2  $\mu$ M).  $n = 2–5$  (triplicates). Specific values are listed in Supporting Information Table S3. Compound **4** from class A and compound **9** from class B showed the highest potency on cells expressing IMP2, which was in concordance with the

FP assay dose—response studies. Compound 3 from class A and compound 5 from class B showed the lowest potency.

Colorectal HCT116 and hepatocellular HepG2 cancer cells were selected to compare the potency of hit compounds on parental and IMP2 knockout cells. After 96 h treatment, parental cells demonstrated a significantly higher sensitivity toward hit compounds compared to CRISPR R-modified cells (**Figure 5A,B**). Also, on measuring cell impedance, which proved to be a sensitive readout parameter for IMP2-facilitated actions, the hit compounds showed significantly

stronger effects in the parental cells (**Figure 5C,D**; **Supporting Information Figure S12**). None of these compounds were optimized for target affinity, yet this selectivity is astonishing. In addition to effects on cell metabolism and adhesion, compound treatment of HCT116 and SW480 cells resulted in a reduced expression of the IMP2 targets DANCR, MYC, and HMGAI in 2D and 3D cell cultures, as also observed for IMP2 knockout cells (**Figure 6**), further supporting the inhibitory action of the compounds on IMP2.

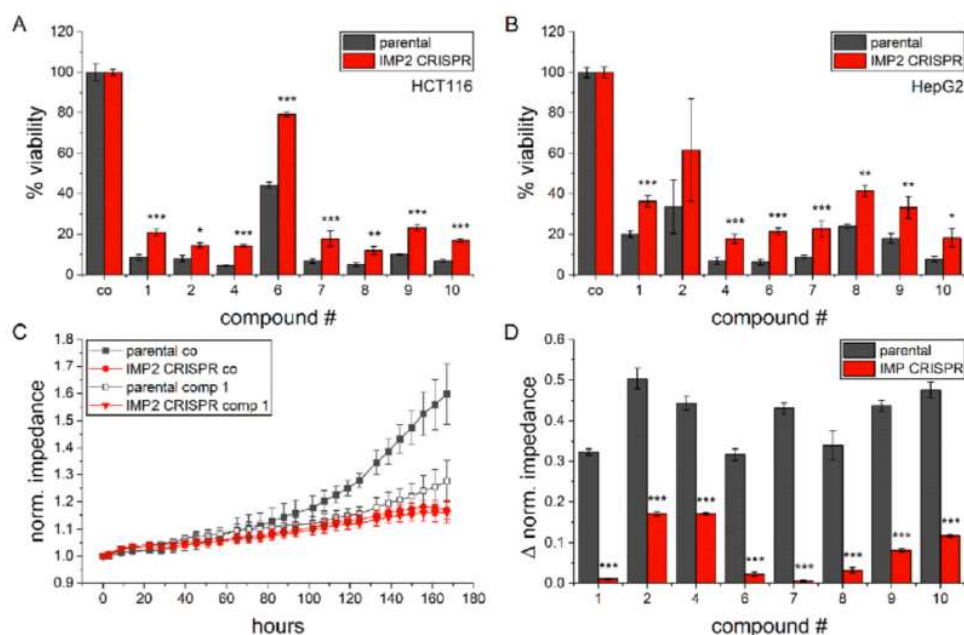


**Figure 5.** Target specificity of hit compounds. (A, B) Parental, biallelic HCT116, and monoallelic HepG2 IMP2 knockout cells were treated with 80 PM compounds or the respective DMSO solvent control. Metabolic activity was assessed 96 h after treatment via MTT assay and normalized to the respective controls;  $n = 2-5$  (triplicates). (C) Cell impedance was assessed as a readout parameter for cell density and adhesion. One representative graph for compound 1 is shown. (D) Bars indicate impedance differences between compound and control treatment for parental and knockout cells, calculated for the last acquired timepoint;  $n = 2$  (triplicates).

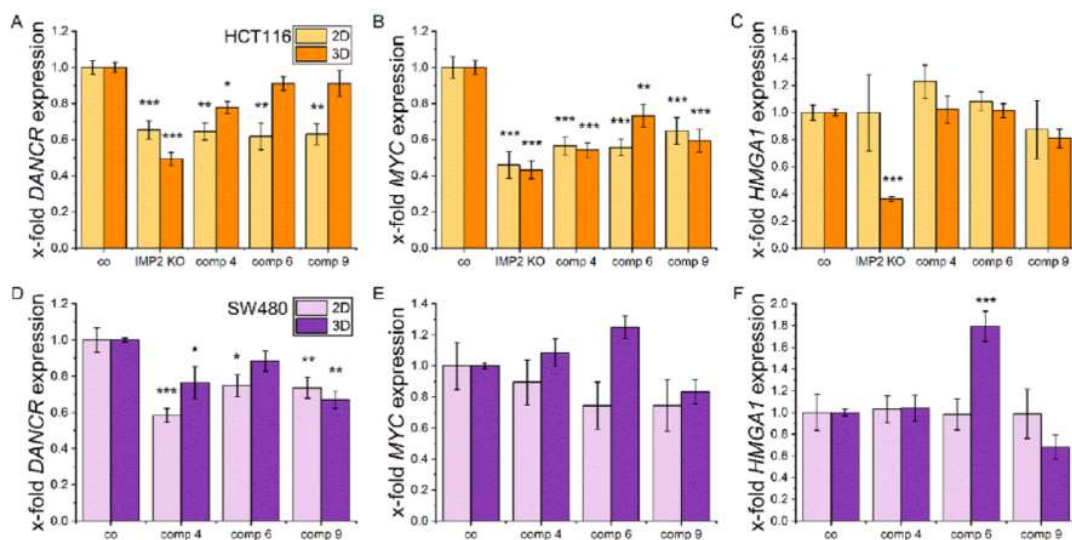


**Figure 6.** Expression of tumor-promoting DANCER, MYC, and HMGAI upon compound treatment. (A, D) DANCER, (B, E) MYC, and (C, F) HMGAI gene expression of HCT116 (A—C) and SW480 (D—F) cells after treatment with compound 4 (40 gM), 6 (50 AM), or 9 (50 AM) for 24 h, as determined by qPCR. Cells were cultured in 2D or 3D spheroid cultures. Values were normalized to the housekeeping gene RNA18S. Data are represented as means  $\pm$  SEM; n = 3 (triplicates).

The antiproliferative properties of the IMP2 knockout were observed in 3D models. Therefore, it is not surprising that the gene expression of the knockout cells also shows primarily differences between 2D and 3D cultures, as seen for HMGAI. The fact that these three target mRNAs of IMP2 are regulated also by other pathways might explain the cellular differences between HCT116 and SW480 cells, as well as the increase of HMGAI upon compound 6 treatment in SW480 cells, which might also represent a secondary effect. Compound exposure resulted in no significant changes of IMP2 gene expression in HCT 116 and SW480 cells (**Supporting Information Figure S13A**). The same was observed on protein level, except for compound 4, which reduced IMP2 in SW480 cells (**Supporting Information Figure S13B**). The attenuated expression of the tumor-promoting IMP2 targets DANCER, MYC, and HMGAI, as well as the selective effects in IMP2 expressing versus knockout cells strongly support an on-target mode-of-action. Compound treatment further inhibited tumor cell proliferation of HCT116, SW480, and Huh7 cells in 2D (**Supporting Information Figure S14**) and 3D cultures (**Supporting Information Figure S15**). Only high compound concentrations induced cell death, as indicated by membrane permeability staining. Parallel measurements of apoptosis suggested that the observed cell death was induced via a caspase-3-dependent pathway (**Supporting Information Figure S16**).

**Hit Compound Activity on Differentiated Huh7 Cells.** Long-term cultivation of Huh7 cells in human serum (HS) has been described to induce cell differentiation, leading to a change in morphology and metabolic activity toward a more normal healthy state. We therefore wanted to test whether the hit compounds affected the viability of these cells modeling normal cells. The cells' differentiation was confirmed according to their cobble-stone morphology typical for hepatocytes (**Supporting Information Figure S17A**) and an altered metabolism as shown by the increased albumin (ALB) expression (**Supporting Information Figure S17B**). [43]

In this model, compounds 6, 7, 8, 9, and 10 affected the viability of Huh7 but not of differentiated Huh7 cells. Compound 4 significantly reduced the viability of both differentiated and nondifferentiated Huh7 cells compared to the controls. Only compound 3 showed a higher effect on differentiated Huh7 cells (**Figure 7**). These results suggest a preferred compound activity against proliferating, undifferentiated cells. The identified hit scaffolds were initially synthesized as antibacterial agents, and both compound classes were designed as inhibitors of bacterial RNA polymerase (RNAP) [44,45]

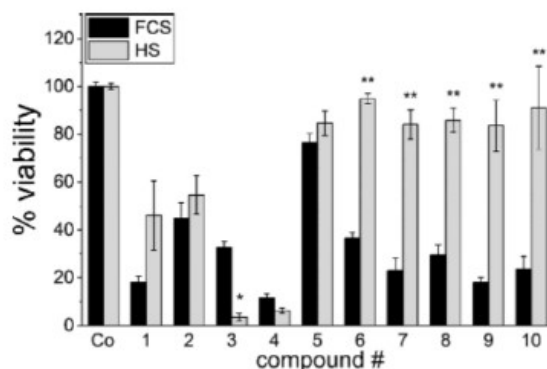


**Figure 7.** Hit compound activity on differentiated Huh7 cells. Huh7 cells were either cultured under standard FCS conditions or differentiated in HS. Cells were treated for 96 h with 50  $\mu$ M hit compounds or DMSO solvent control. Cell metabolic activity was determined by MTT; n = 2 (triplicates). \*p < 0.05 and \*\*p < 0.01 compared to values of standard FCS conditions.

Hence, they were envisioned as potential broad-spectrum antibiotics as RNAP is highly conserved among bacteria. [46] The amino acid sequences and the architecture of bacterial RNAP differ fundamentally from the eukaryotic RNAP, so that an undesired inhibition of eukaryotic RNAP is unlikely. No amino acid sequence similarities were found between either RNAP or IMP2. In fact, none of our compounds of class B impaired the viability of differentiated cells, and only one of class A congeners showed a higher effect in differentiated versus nondifferentiated cells.

**In Vivo Action of Hit Compounds.** In order to assess whether the selected hit compounds affect tumor growth in vivo, compounds 4, 6, and 9 were administered in a zebrafish embryo xenograft model. In this model, compounds 4 and 6 significantly inhibited tumor growth (**Figure 8A**). Embryos showed no compound-induced toxicity after 3 days of treatment. Tumor-bearing and 50 AM compound-injected embryos showed normal development, but compound 4 caused a somewhat hunched body axis in 22.7% of the embryos at 3 dpi (**Figure 8B**).

## ■ CONCLUSIONS

In conclusion, we validated the RBP IMP2 as a druggable anticancer target using different *in vitro* and *in vivo* approaches. By establishing an FP-based screening platform to identify inhibitors of IMP2/ RNA interactions, we found 10 hit compounds against IMP2. Our hits from two different chemical classes serve as a suitable starting point for further optimization steps with the aim to generate more potent and specific compounds. Furthermore, we laid out a clear methodological path for the screening of additional libraries in order to identify structure-divergent compound series. Moreover, the described methodology will allow to include other RNA motifs, offering a valuable resource for the discovery of new compounds targeting RBPs. The molecular mechanisms of action, that is, which pathways are specifically addressed by IMP 2 inhibition/knockout, are the subject of ongoing studies. IMP2 has been suggested to bind to thousands of targets, which is why we expect that there are multiple layers of action.

## ■ METHODS

**Materials.** Kanamycin sulfate, cOmplete protease inhibitor cocktail tablets (#04693124001, Roche), diethylpyrocarbonate (DEPC), isopropyl-P-D-thiogalactoside (IPTG), Pluronic, lysozyme, BSA, and salts were purchased from Merck (Darmstadt, Germany). Water was treated with 0.1% v/v DEPC in all experiments handling with RNA.  
**cell Lines.** The IMP2 expressing cell lines SW480, HCT116, Hep3B, HepG2, and Huh7 and nonexpressing MCF7 cells (Cancer Cell Line Encyclopedia; Ghandi et al., 2019) were used in cell-based experiments. SW480, HCT116, and MCF7 cells were maintained in Dulbecco's modified Eagle's medium (DMEM), and HepG2, Hep3B, and Huh7 cells were maintained in RPMI 1640 medium. Media were supplemented with 10% fetal calf serum (FCS), 1 mM glutamine, 100 U/mL penicillin, and 100 µg/mL streptomycin. Cells were cultured at 37 °C and 5% CO<sub>2</sub>. Cell line authentication for hepatocellular cell lines was conducted by DSMZ (Deutsche Sammlung von Mikroorganismen und Zellkulturen GmbH) and for HCT116 by STR/DNA profiling. Mycoplasma testing was performed regularly via PCR. **Zebrafish Studies.** AB wild-type zebrafish embryos were used for xenograft models. Zebrafish husbandry was conducted as described previously. [47] Zebrafish husbandry and all experiments were performed in accordance with the European Union Directive on the protection of animals used for scientific purpose (Directive 2010/63/EU) and the German Animal Welfare Act 611 Abs. 1 TierSchG). Embryos were euthanized not later than 5 days post fertilization (dpf). **IMP2 siRNA Knockdown.** A pool of four different HPLC-purified double-stranded RNA oligonucleotides was used for IGF2BP2 knockdown in Hep3B cells (Flexitube Gene Solution, Qiagen, Hilden, Germany). Random siRNA was used as the control (Qiagen, Hilden, Germany). RNA oligo sequences are shown in **Supporting Information Table S4**. IGF2BP2 knockdown was performed in 96-well plates by forward transfection (12,750 cells/well) employing INTERFERin Polyplus (Illkirch, France), as recommended by the manufacturer. Knockdown was confirmed by Western blot, and cell viability was measured using MTT assay 3 days after transfection.

**IMP2 CRISPR-Mediated Knockout.** The CRISPR/Cas9 technique was adapted to disrupt the gene of human IGF2BP2 in two human colorectal (HCT116, SW480) and two hepatocellular carcinoma (Huh7, HepG2) cell lines by ribonucleoprotein delivery. A validated single guide RNA (TrueGuide synthetic guide RNA, Thermo Fisher Scientific, Munich, Germany) targeting IMP2 (5'-ATGGACTTTTGGCTCAATA-3') and a recombinant cas9 protein (TrueCutCas9 Protein v2, #A36496, Thermo Fisher Scientific, Munich, Germany) were delivered into the cells using Lipofectamine CRISPRMAX cas9 transfection reagent (#CMAX00001, Thermo Fisher Scientific, Munich, Germany) according to the manufacturer's instructions. 80,000 cells were seeded in RPMI or DMEM media as described above, without antibiotics into a 12-well plate, incubated overnight, and transfected the next morning at a confluency of 30–70%. After 48 h of incubation time, the cells were detached, counted, and seeded into 96-well plates at a concentration of 0.8 cells/well for limiting dilution cloning. The remaining cells were used for gDNA extraction and verification of editing efficiency via the T7E1 mismatch assay.

Clones were cultured for downstream experiments until knockout of IGF2BP2, or at least reduced expression (monoallelic editing of the target region as assessed by Sanger sequencing) could be confirmed by Western blot. Clones that showed reduced IMP2 expression in Western blots underwent the whole procedure again until knockout was achieved. At least two rounds of CRISPR/Cas9 editing did not induce a biallelic knockout in SW480, Huh7, and HepG2 cells.

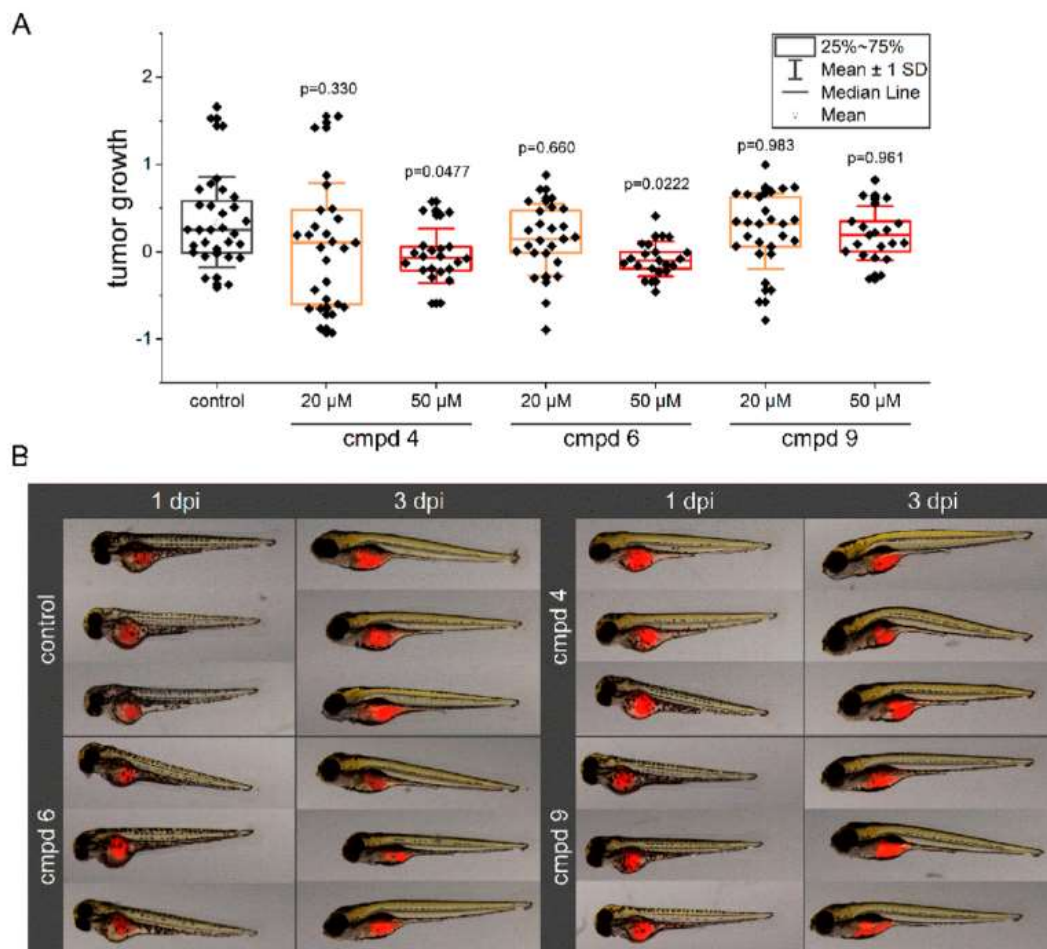


Figure 8. In vivo actions of compounds in a xenograft zebrafish embryo model. Fluorescence-labeled HCT116 cells suspended in compounds (cmpds) 4, 6, and 9 (20 and 50  $\mu$ M) containing PBS were injected into the yolk sac 2 days post fertilization (dpi) zebrafish embryos. Embryos were imaged at 1 and 3 dpi, and the tumor growth was calculated based on the tumor area changes. (A) Individual values of tumor growth quantification are presented in a box blot. (B) Representative pictures of embryos are shown.

Table 1. Sequences of the Components for the Assembly of pegRNAs

pegRNA	abbreviation	spacer sequence	3' extension	PBS length (nt)	RT template length (nt)
pegRNA1_GGtoT_11ntRT	pegRNA1_11	GACCACCTCTTCCCGGGAGCA	GCGTGGATTGCTCCCGGAAGAG	13	11
pegRNA1_GGtoT_15ntRT	pegRNA1_15	GACCACCTCTTCCCGGGAGCA	AGGGGCGTGGATTGCTCCCGGAAGAGT	13	15
pegRNA4_GG_10ntRT	pegRNA4_10	AGAGCCATGGAGAAGCTAAG	TGATGCGCTTAGCTTCTCCATGG	13	10
pegRNA4_GG_16ntRT	pegRNA4_16	AGAGCCATGGAGAAGCTAAG	TCAAACCTGATGCGCTTAGCTTCTCCATGG	13	16
pegRNA6_TA_10ntRT	pegRNA6_10	ATGCCCGCTTAGCTTCTCCA	AGCCTAATGGAGAAGCTAAGCGG	13	10
pegRNA6_TA_16ntRT	pegRNA6_16	ATGCCCGCTTAGCTTCTCCA	TTCAGAGCCTAATGGAGAAGCTAAGCGG	13	16

<sup>a</sup>These are composed of a spacer linked to the scaffold and 3' extension. All sequences are displayed in 5' to 3' direction. PBS: primer binding site.

**Prime Editing.** Design of Prime Editor System 2. The prime editor 2 system was used to achieve IGF2BP2 knockout in HCT116 cells. pCMV-PE2-P2A-GFP (Addgene plasmid #132776) and pU6pegRNA-GG-acceptor (Addgene plasmid #132777) were a gift from David Liu. [48] Vectors were chosen to deliver the prime editor and pegRNA component of system 2. Golden Gate cloning was used to insert designed pegRNAs into the latter construct. Three different spacers targeting different loci of exon 6 served as a basis for the pegRNA assembly. Desired mutations were planned to disrupt the protospacer adjacent motif of the spacer sequences. As recommended, the length of the primer binding site was kept equal with 13 nt, but the size of the reverse transcriptase (RT) template varied between 10 and 16 nt (compare Table 1). The sequence 5'-AGAGCTAGAAATAGCAAGTTAAAATAAGGCTAGTCCGTTATCAACTTGAAAAAGTGGCACCGAGTCG-3' was used as a scaffold for all pegRNAs.

**Cell Line Development.** 100,000 cells/well were seeded into 24-well plates overnight and transfected the next morning (after 16–24 h) at a confluency of approximately 60% with an equimolar ratio of the two vectors (2 pg total DNA content), employing 2  $\mu$ L of lipofectamine 3000 (#L3000008, Thermo Fisher Scientific) according to the manufacturer's instructions. 48–72 h post transfection, the cells were washed with IX PBS, detached with trypsin (#T3924, Merck), and resuspended to obtain a single cell suspension. Single GFP-positive cells were picked manually with a microneedle under a microscope and transferred into collagen-coated 60 mm dishes (collagen from rat tail, #C766160, Merck) into the squares of a grid (0.5 cm distance of the lines to each other) that had been drawn on the bottom of the dishes in advance. Periodically, colony formation of the single clones was surveyed until stable colonies were established that did not get in touch with each other and could be transferred into 96-well plates for further expansion and downstream analysis.

**Kaplan—Meier Analyses.** For survival analyses, TCGA patient survival data and IGF2BP2 mRNA expression values were obtained from OncoLnc (<http://www.oncolnc.org>). Patients were grouped into low and high (upper quartile) IGF2BP2 expressers. Kaplan—Meier analyses were performed using OriginPro 19 b (OriginLab Corporation, Northampton, MA, USA), and the log rank test was conducted to test equality over groups.

**Western Blot.** Western blots were performed as previously reported.<sup>9</sup> Antibodies used were specific for IMP2/p62 [49] and tubulin (#T9026, Merck). IRDye680-conjugated anti-rabbit IgG (#92668071, LI-COR Bioscience, Bad Homburg, Germany) and IRDye800-conjugated anti-mouse IgG (#926-32210, LI-COR Biosciences, Bad Homburg, Germany) were used as secondary antibodies. Signal intensities for IMP2 and its splice variant p62 were determined by using the Odyssey near-infrared imaging system from LI-COR Bioscience (Bad Homburg, Germany). Western blot signal intensities were quantified by Studio lite software (LI-COR Bioscience, Bad Homburg, Germany).

**qPCR.** Total RNA was isolated using the High Pure RNA Isolation Kit (#11828665001, Roche). For the analysis of 3D cultures, five spheroids were pooled. Concentration of isolated RNA was quantified by NanoDrop (Thermo Fisher Scientific), and RNA with an A260/A280 ratio higher than 1.8 was used for further experiments. RNA was transcribed using the High-Capacity cDNA Reverse Transcription Kit (#4368813, Thermo Fisher Scientific) in the presence of an RNase inhibitor (#10777-019, Invitrogen) according to the manufacturer's instructions. cDNA was analyzed using 5X HotFirePol EvaGreen qPCR Mix (#08-24-00020, Solis BioDyne, Tartu, Estonia) and the following primers: RNA18S for 5'-AGGTCTGTGATGCCCTTAGA-3', RNA18S rev 5'-GAATGGGGTTCAACGGGTTA-3', DANCER for 5'-GCTCCAGGAGTTCGTCTCTTAC-3', DANCER rev 5'TGCGCTAAGAAGACTGAGGCAG-3', MYC for 5'-AGCCACAGCATACATCCTGTCC-3', MYC rev 5'-CTCGTCGTTCCGCAACAAGTC-3', HMGAI for 5'-CTAATTGGGACTCCGAGCCG-3', HMGAI rev 5'-GTAGCAAATGCGGATGCCTT-3', ALB for 5'CACGCCTTTGGACAATGAA-3', ALB rev 5'-ATCTCGACGAAACACACCCC-3'.

**FP-Based Screening Assay. Protein Purification.** Histidinetagged IMP2 was expressed using a pET-28a(+) plasmid (Addgene plasmid #166997) in BL-21 Escherichia coli at 18 °C; the expression was induced with 0.4 mM IPTG. Bacteria were lysed, and the protein was isolated on a HisTrap HP nickel—sepharose column (#17524801, cytiva, Marlborough, MA, USA) followed by an imidazole buffer elution. Cells were harvested by centrifugation at 6733g and resuspended in binding buffer (20 mM Tris—HCl, pH 7.4, 2 mM MgCl<sub>2</sub>, 150 mM NaCl, 10% v/v glycerol, 2 mM mercaptoethanol, 40 mM imidazole). Ethylenediamine tetraacetic acid -free protease inhibitor cocktail (cOmplete) was added fresh to the binding buffer. Cells were lysed using a French press homogenizer (two passages), and cell debris was removed by centrifugation at 42,858g at 4 °C for 1 h. The supernatant was applied to a 5 mL HisTrap HP nickel—sepharose column at 0.75 mL/min on an ÄKTApurify system. The column was equilibrated with binding buffer in a 10 X column volume or until the UV signal was stable. The column was washed later with 15 X column volume with binding buffer and with 15 X column volumes of high salt at 3 mL/min (Tris—HCl, pH 7.4, 2 mM MgCl<sub>2</sub>, 1 M NaCl, 2.5% glycerol v/v, 2 mM mercaptoethanol, 40 mM imidazole). Subsequently, the column was washed with 15 X column volumes of binding buffer containing 100 mM imidazole. Then, a gradient washing was done with a linear gradient to 100% of 500 mM imidazole buffer (Tris—HCl, pH 7.4, 2 mM MgCl<sub>2</sub>, 150 mM NaCl, 2.5% glycerol v/v, 2 mM mercaptoethanol, 500 mM imidazole) in 10 X column volumes at 3 mL/min. The protein was eluted in 0.7–1 M imidazole buffer (Tris—HCl, pH 7.4, 2 mM MgCl<sub>2</sub>, 150 mM NaCl, 2.5% glycerol v/v, 2 mM mercaptoethanol, 700–1000 mM imidazole). Protein purity and identity were assessed by SDS-PAGE, Western blot, and CDS. The eluted IMP2 fractions were concentrated via centrifugal filtration using Vivaspins (30,000 MWCO, Sartorius). Buffer exchange into storage buffer (Tris—HCl, pH 7.4, 2 mM MgCl<sub>2</sub>, 150 mM NaCl, 2 mM dithiothreitol (DTT), 10% glycerol v/v, in DEPC-treated 1-120) was performed using multistep dilution inside Vivaspins. Protein concentrations were measured by both UV spectroscopy ( $\epsilon = 280$  nm) and Pierce assay (according to the manufacturer's instructions). Protein aliquots were stored at –80 °C. The absence of potential RNase contamination in the protein preparations was assessed by mixing 15  $\mu$ L of human RNA (470 ng/gL) isolated from MCF7 cells with either 15  $\mu$ L of storage buffer or 15  $\mu$ L of IMP2 protein (22.1  $\mu$ M) and incubated on ice or at room temperature for 1.5 h, and then the samples were subjected to agarose gel electrophoresis.

**Probe Design.** Based on published IMP2 target sequences, two different RNA oligonucleotides were designed as IMP2 binding partners. The sequence of RNA A was based on the published 4–5 bp motifs CAUC, [27] ACAC, [34] CCCC, [35] and ACACA, [36] and contained a 3' nucleotide extension after the fluorescein (FLC) label: FLCAUGCAUCCCCGAGCUACACACACAACA RNA B was designed based on the binding motif UUCACGUUCAC and contained a 7-nucleotide extension in front of the tandem repeat sequence CCCCCUUCACGUUCACUCUGUCU-FLC originally described in Nielsen et al., 1999. A third RNA C sequence (FLCGAAAAAAGAUUUUUUUUUAAGA)



was reported to bind to AU rich element binding proteins and was used to detect the specificity of the fluorescent probe binding to the target. [35] FLC-labeled or nonlabeled HPLC-purified single-stranded RNA oligomers were purchased from Merck.

**FP Assay.** Lyophilized RNA oligomers were dissolved in the FP assay buffer (Tris—HCl, pH 7.4, 2 mM MgCl<sub>2</sub>, 10 mM NaCl, 10% glycerol, 2 mM DTT, 10% glycerol v/v, in DEPC treated H<sub>2</sub>O) to have 100 PM stock solutions of RNAs, further diluted into 100 nM aliquots, and stored at —80 °C. Saturation experiments were performed to detect direct binding of different RNA oligomers to either IMP2 or BSA. Thereby, a constant concentration (1 nM final) of each FLC-labeled RNA with a constant concentration (1 nM) was titrated with serial dilutions in the range of 0.15 nM to 3 μM final concentration in the FP assay buffer. In the competitive FP experiments, IMP2 was used in excess (2—3 folds above the EC<sub>50</sub> values). Based on the saturation experiments, a final IMP2 concentration of 200 nM was selected to be used in subsequent competition assays with RNA A and RNA B. All competitive experiments included 1 h incubation of IMP2 with nonlabeled RNA oligo or compounds in 384-well black microplates before the addition of the labeled RNAs. Competition experiments were done at constant concentrations of RNA A and RNA B (1 nM) and a fixed IMP2 concentration (200 nM) by titration against serial dilutions of unlabeled RNAs (0.32 nM to 100 μM final). DMSO tolerance was evaluated by incubating different DMSO concentrations (0—10% v/v) and RNA\_A or RNA\_B at 1 nM, either with or without IMP2. The stability of FP values was assessed over time by measuring the FP at different time points (every 30 min until 4 h). FP and FI were measured using a CLARIOstar Plus microplate reader (BMG LABTECH, Ortenberg, Germany) with an excitation at 485—495 nm and an emission at 520—530 nm. In general, the focal height and gain adjustments were done before starting each measurement to reach the maximum sensitivity. [50] The FI values of any compound deviating more than ±20% from the values of the controls were excluded from further procedure. [37] Each sample was tested in duplicate, and the FP values are reported in millipolarization units (mp). The assay robustness was verified by assaying low controls (LCS) in 192 samples with RNA A or RNA B (1 nM final concentration) in 5% DMSO in the FP assay buffer and a high control (LC) plate containing 192 samples in the same plate in addition to 100 nM IMP2. Z' value was calculated according to the formula  $Z' = 1 - [(3SD \times HC) + (3SD \times )]/(HC_{mean} - LC_{mean})$ . [51]

**Screening Library.** Compounds from four different libraries were screened: 838 compounds were from a synthetic in-house library from the Helmholtz Institute for Pharmaceutical Research Saarland (HIPS), 253 compounds were from the in-house natural products library at HIPS, 192 compounds were from a commercial library provided by ASINEX (Winston-Salem, NC, USA; <https://www.asinex.com/>), and 145 compounds were from the commercial Maybridge library (small molecular weight chemical fragments, Thermo Fischer Scientific): [https://www.maybridge.com/portal/alias\\_Rainbow/lang\\_en/ tabID177/DesktopDefault.aspx](https://www.maybridge.com/portal/alias_Rainbow/lang_en/ tabID177/DesktopDefault.aspx). Compounds were dissolved in DMSO to a stock concentration of 5 or 10 mM depending on their solubility.

**FP-Based Screening.** Compounds were diluted in the FP assay buffer to concentrations of 450 PM. A total of 10 AL in duplicates (15% DMSO) from each compound was added into 384-well microtiter plates using an electronic Eppendorf Xplorer 12-channel pipette (Eppendorf, Hamburg, Germany). In addition, 10 μL of 600 nM IMP2 in FP assay buffer was added into the same plate, and the samples were incubated for 1 h by shaking at room temperature. Afterward, 10 μL of 3 nM RNA A/B solution in the FP assay buffer was added to the mixture and incubated for an additional 1.5 h at room temperature in the dark. Accordingly, the final assay concentrations were 1 nM RNA A/B, 200 nM IMP2, and 150 μM compounds in 5% DMSO. Any compound that enhanced or quenched the total FI more than 20% of the FI of the controls was excluded. The percentage of binding inhibition was calculated as % inhibition mean of HC — read compound value/ (mean of HCs — mean of LC) X 100%. In addition, Pluronic was added to the FP buffer to a final concentration of 0.0137% in the competitive assay to rule out any false-positive results from aggregation.

**FP-Based Dose—Response Measurement.** Two-fold serial dilutions of a 333 μM starting concentration of hit compounds were prepared in FP buffer in 5% DMSO and titrated in the presence or absence of IMP2. The experiments were performed twice independently using duplicates. Competition binding assays using CsrA from *Yersinia pseudotuberculosis* were performed as previously described. [37]

**TSA.** The shift of the melting point of IMP2 in the presence or absence of hit compounds was recorded in 96-well plates using an Applied Biosystems StepOnePlus Real-Time PCR System from Thermo Fisher Scientific. Thermal shift experiments were performed at fixed concentrations of IMP2 (4.5 PM) and 100 μM hit compound. SYPRO orange (Merck) was used in 2.5-fold concentration (stock 5000-fold) in a total volume of 20 AL. The heating gradient started at 25 °C, and the temperature was increased by 0.5 °C/min until 95 °C, detecting the fluorescence of SYPRO orange. Melting curve plots of fluorescence versus temperature were converted into melting peaks, and melting temperatures were calculated subsequently by Protein Thermal Shift Software v1.3—Thermo Fisher Scientific.

**STD-NMR.** <sup>1</sup>H-STD-NMR experiments were conducted using a Bruker Fourier spectrometer (500 MHz) (MA, USA), and the probe temperature was kept at 283 K. The final compound concentration was 500 μM based on the solubility limit in 10% DMSO-d<sub>6</sub>. A volume of 25 μL from each compound solution was diluted with 25 μL of Tris buffer pH 7.4, 150 mM NaCl in D<sub>2</sub>O. IMP2 protein/ligand was used in a 1 : 100 ratio with a final concentration of 5 μM. A control spectrum was recorded under the same conditions without a protein to test for artifacts. The STD-NMR experiments were carried out with a carrier set at —1 ppm for the on-resonance and —40 ppm for the off-resonance irradiation. Selective IMP2 protein presaturation was carried out at 0.5 s by using a train of 50 ms Gauss-shaped pulses. The STD effect resulting from the difference in signal intensity after saturation transfer was quantified using the formula STD (10 — Isat)/I<sub>o</sub>. This provides insights into the relative

proximity of the respective protons to the protein surface. 10 represents the intensity of one signal in the off-resonance or reference NMR spectrum, and Isat represents the intensity of a signal in the on-resonance NMR spectrum. The STD-NMR spectrum of the IMP2/ligand sample was subtracted from the respective STD spectrum of the ligand alone using the same NMR conditions to eliminate any artefacts arising from the ligand. Protons of the residual imidazole contamination from the elution step appear at 7.2 and 8.1 ppm.

**In Silico Studies.** The homology modeling and molecular docking experiments were performed with MOE 2019.01 (Molecular Operating Environment). A homology model for IMP2 RRMI was generated using a reported X-ray structure of IMP 3 in complex with RNA (IMP3 RRM12, pdb ID: 6GX6). [35] The sequence of IMP2 RRMI as well as 6GX6 pdb atom coordinates were loaded into MOE, and the homology model was generated using the built-in homology model function with standard parameters, AMBER10:EHT force field, and the RNA atoms of 6GX6 as the environment. In the case of docking to the KH34 domain, we used the reported NMR structure (PDB ID: 6ROL). [7] Before docking, a QuickPrep step was applied to the respective protein structure, including the RNA (ACAC) ligand in the case of the RRMI homology model. Docking was done for the promising hit compound 4, where conclusive STD-NMR data were available in order to evaluate the plausibility of the docking poses. For the RRMI homology model, the docking site was defined by the selection of protein residues in 4.5 Å proximity to RNA atoms, while for the KH34 domain, reported residues interacting with RNA were employed to define the docking site. The built-in docking feature of MOE was used with standard parameters, induced-fit refinement, and AMBER10:EHT force field. The highest ranked docking pose was further refined by applying a QuickPrep step (standard parameters, AMBER10:EHT force field), and the resulting ligand–protein complex was analyzed using the ligand interaction tool of MOE.

**Testing Hits for Inhibition of Cell Viability.** MTT. Cells were seeded into 96-well plates at a density of 2500–10,000 cells/well based on the cell type (ability to reach 95–100% confluency in the control treatment at the time of measurement). Cell metabolic activity was measured using MTT 96 h after treatment of hit compounds (1–80 PM). For each compound, the inhibition of cell activity was calculated for each concentration normalized to its respective DMSO control or nontreated control (if DMSO in the respective concentration showed viability above 90%). The dot plot was generated with Python 3.8.1 software.

**Kinetic Apoptosis/Necrosis Measurements.** For the time-dependent analysis of cell death, the cells were analyzed in an IncuCyte S3 System (Sartorius). The day after seeding, supernatants were replaced by the respective media containing the IncuCyte Cytotox Red (#4632, Sartorius) and Caspase-3/7 Green (#4440, Sartorius) reagents according to the manufacturer's instructions. Cells were treated with different concentrations of the respective compounds or DMSO vehicle control, and cell confluency as well as apoptotic and necrotic events were monitored for 3 days. Fluorescent signals from apoptotic (caspase 3/7 active) and necrotic (permeable membrane) cells were normalized to cell confluency and the time point of treatment (0 h).

**ECIS Assay.** ECIS represents a powerful tool to assess cell proliferation in real time, but cell impedance is also responsive toward changes in cell adhesion, [29] which has been shown to be affected by IMP2. [14] HCT116 parental and IMP2 CRISPR knockout cells were seeded (7000 cells/well) into 96 (96W10E+)-well plates coated with rat tail collagen (#C766160, Merck, 30 µg/mL in 0.2% acetic acid). The cells were seeded directly after the compounds were added into the plate to reduce cell stress. Cells were treated with 25 µM of hit compounds in triplicate. Effects of hit compounds on proliferation were evaluated relative to (0.25%) DMSO controls. Cell impedance was assessed in an ECIS ZO (theta) instrument (Applied BioPhysics Inc., NY, USA). Measurements were started immediately after cell seeding and were taken every 450–900 s for each well.

### **IncuCyte 2D and 3D Proliferation and Migration.**

**Proliferation.** For the 2D kinetic proliferation analysis, 5000 cells were seeded per well into 96-well plates. The next day, cells were treated with the respective compounds, and cell confluency was monitored in an IncuCyte S3 system. Cell confluency was analyzed using IncuCyte basic analyzer software, and confluency was normalized to the starting point.

For the 3D proliferation analysis, 3000 cells were seeded per well into low-attachment U-bottom 96-well plates. After spheroid formation for 3 days, spheroids were treated with the respective compounds, and monitoring in an IncuCyte S3 system was started, if not indicated otherwise. The spheroid area was analyzed using spheroid IncuCyte software, and the area was normalized to the first measuring time point after treatment (0 h).

**Migration.** Cell migration was measured using an IncuCyte S3 system. 100,000 cells per well were seeded into ImageLock 96-well plates. The next day, scratches were performed by the Woundmaker tool (IncuCyte Migration Kit). Cells were washed twice with 2% fetal bovine serum (FBS)-containing media, which was also used for further cultivation. Cells were treated with the respective compounds, and the migration was monitored for 48 h. The cell-covered wound area was analyzed and quantified using IncuCyte migration software.

**Differentiation of Huh7 Cells.** Huh7 cells were seeded into 96-well plates (3000 cells/well) in full RPMI growth medium containing 10% FBS. After 24 h, the medium was aspirated and changed to RPMI medium containing 2% HS in order to induce cell differentiation as described. [43,52] Fresh medium was added twice a week for 21 days. Differentiated cells were treated with hit compounds, and the cell viability was assessed via MTT assay 96 h after treatment.

**Zebrafish Xenograft Model and in Vivo Proliferation Measurement.** Parental and IMP2 knockout HCT116 cells were used for proliferation studies in a zebrafish embryo xenograft model.  $2 \times 10^6$  cells were suspended in 1  $\mu$ L of 0.1% BSA/PBS. At 2 days post fertilization (dpf), 2 nL of cell suspension was injected into the yolk sac by a FemtoJet microinjector (Eppendorf). Before injection, the tumor cells were stained with the cell tracker orange dye (#C34551, Thermo Fisher Scientific) according to the manufacturer's protocol. For the analysis of compound-induced effects on tumor growth, the tumor cells were suspended in 0.1% BSA/PBS containing the compounds in the indicated concentrations just before injection. Single embryos were placed into 96-well plates and imaged the next day with a Leica M205 FCA fluorescence stereomicroscope (1 day post injection, dpi). Tumor growth was determined at 3 dpi by analysis of the fluorescent tumor area and quantification by ImageJ. The growth rate was calculated as follows: (tumor area 3 dpi — tumor area 1 dpi)/tumor area 1 dpi. The effects of compound injection on the zebrafish embryo development and viability were assessed by microscopic observation of the eye, heart, and body axis formation, heartbeat, and pigmentation.

**Statistical Analysis.** Data analysis was done by Microsoft Excel, and statistics were performed using OriginPro. IC<sub>50</sub> and EC<sub>50</sub> values were calculated using nonlinear regression analysis with Origin pro version 19 software. Data are represented as means  $\pm$  SEM if not indicated otherwise. Shapiro—Wilk test was performed to analyze the data distribution. Depending on whether the data were normally distributed and on the group size, statistical differences were calculated using one-way ANOVA, Student's t-test, Mann—VWhitney U test, or Kolmogorov—Smirnov test. \**p* < 0.05; \* \**p* < 0.01 • \*\*\**p* < 0.001.

## ■ ASSOCIATED CONTENT

### Supporting Information

The Supporting Information is available free of charge at <https://pubs.acs.org/doi/10.1021/acscchembio.1c00833>.

Additional data related to the clinical prognosis of the oncofetal protein IMP 2; IMP2-knockout clones and target validation; additional data related to the FP assay screening development and validation; additional data related to hit compound activity and specificity; differentiation process of Huh7 cells in HS; descriptive data of compounds; IC<sub>50</sub> values of hit compounds; and sequences of siRNA oligonucleotides used in IMP2 knockdown (PDF)

### Author Contributions

C.D., AA, and S.M.K. have provided equal contribution. Initiation and direction of the study: A.K.K.; conceptualization: S.M.K., M.E., and A.K.K.; formal analysis: C.D. and A.A.; funding acquisition: A.K.K.; investigation: C.D., A.A., T.K., B.G.E.Z., Y.W., SB., and F.M.; resources: KL., S.H.K, and RM.; supervision: S.M.K., S.L., M.E., and A.K.K.; visualization: C.D., AA, and F.M.; writing—original draft: S.M.K., C.D., AA, M.E., and A.K.K.; writing—review & editing: T.K., B.G.E.Z., S.H.K. S.L., and RM.

### Notes

The authors declare no competing financial interest.

## ■ ACKNOWLEDGMENTS

The study was funded, in part, by the DFG (Deutsche Forschungsgemeinschaft, #KI 702) and by the Wilhelm Sander-Stiftung (#2021.068.1). The authors would like to thank R. W. Hartmann for giving access to the HIPS compound library. Also, the authors would like to thank C. Maurer, G.

Besher, M. Hamed, J. V. Valbuena-Perez, and J. Zapp for discussions and advice. The graphical abstract was created with BioRender.com.

## ■ REFERENCES

- (1) Mohibi, S.; Chen, X.; Zhang, J. Cancer the "RBP"eutics-RNAbinding proteins as therapeutic targets for cancer. *Pharmacol. Ther.* 2019, 203, 107390.
- (2) Czepukoje, B.; Abuhaliema, A.; Barghash, A.; Tierling, S.; Naß, N.; Simon, Y.; Körbel, C.; Cadenas, C.; van Hul, N.; Sachinidis, A.; et al. IGF2 mRNA Binding Protein 2 Transgenic Mice Are More Prone to Develop a Ductular Reaction and to Progress toward Cirrhosis. *Front. Med.* 2019, 6, 179.
- (3) Bell, J. L.; Wächter, K.; Mühleck, B.; Pazaitis, N.; Köhn, M.; Lederer, M.; Hüttelmaier, S. Insulin-like Growth Factor 2 mRNABinding Proteins (IGF2BPs): Post-Transcriptional Drivers of Cancer Progression? *Cell. Mol. Life Sci.* 2013, 70, 2657—2675.
- (4) Chao, J. A.; Patskovsky, Y.; Patel, V.; Levy, M.; Almo, S. C.; Singer, R. H. ZBP 1 recognition of<sup>l</sup>-actin zipcode induces RNA looping. *Genes Dev.* 2010, 24, 148—158.
- (5) Patel, V. L.; Mitra, S.; Harris, R.; Buxbaum, A. R.; Lionnet, T.; Brenowitz, M.; Girvin, M.; Levy, M.; Almo, S. C.; Singer, R. H.; et al. Spatial Arrangement of an RNA Zipcode Identifies mRNAs under PostTranscriptional Control. *Genes Dev.* 2012, 26, 43—53.
- (6) Schneider, T.; Hung, L.-H.; Aziz, M.; Wilmen, A.; Thaum, S.; Wagner, J.; Janowski, R.; Müller, S.; Schreiner, S.; Friedhoff, P.; et al. Combinatorial Recognition of Clustered RNA Elements by the Multidomain RNA-Binding Protein IMP3. *Nat. Commun.* 2019, 10, 2266.

- (7) Biswas, J.; Patel, V. L.; Bhaskar, V.; Chao, J. A.; Singer, H.; Eliscovich, C. The Structural Basis for RNA Selectivity by the IMP Family of RNA-Binding Proteins. *Nat. Commun.* 2019, 10, 4440.
- (8) Kessler, S. M.; Lederer, E.; Laggai, S.; Golob-Schwarzl, N.; Hosseini, K.; Petzold, J.; Schweiger, C.; Reihls, R.; Keil, M.; Hoffmann, J.; et al. IMP2/IGF2BP2 Expression, but Not IMP1 and IMP3, Predicts Poor Outcome in Patients and High Tumor Growth Rate in Xenograft Models of Gallbladder Cancer. *Oncotarget* 2017, 8, 89736—89745.
- (9) Kessler, S. M.; Pokorny, J.; Zimmer, V.; Laggai, S.; Lammert, F.; Bohle, M.; Kiemer, A. IGF2 mRNA Binding Protein p62/IMP2-2 in Hepatocellular Carcinoma: Antiapoptotic Action Is Independent of IGF2/P13K Signaling. *Am. J. Physiol.: Gastrointest. Liver Physiol* 2013, 304, G328-G336.
- (10) Dai, N.; Ji, F.; Wright, J.; Minichiello, L.; Sadreyev, R.; Avruch, J. IGF2 mRNA Binding Protein-2 Is a Tumor Promoter That Drives Cancer Proliferation through Its Client mRNAs IGF2 and HMGAI. *Elife* 2017, 6, No. 07155.
- (11) Huang, S.; Wu, Z.; Y.; Wei, W.; Hao, L. Insulin-like Growth Factor 2 mRNA Binding Protein 2 Promotes Aerobic Glycolysis and Cell Proliferation in Pancreatic Ductal Adenocarcinoma via Stabilizing GLUT1 mRNA. *Acta Biochim. Biophys. Sin.* 2019, 51, 743—752.
- (12) Janiszewska, M.; Suvä, M. L.; Riggi, N.; Houtkooper, R. H.; Auwerx, J.; Clément-Schatlo, V.; Radovanovic, I.; Rheinbay, E.; Provero, P.; Stamenkovic, I. Imp2 controls oxidative phosphorylation and is crucial for preserving glioblastoma cancer stem cells. *Genes Dev.* 2012, 26, 1926—1944.
- (13) Kessler, S. M.; Laggai, S.; Barghash, A.; Schultheiss, C. S.; Lederer, E.; Arlt, M.; Helms, V.; Haybaeck, J.; Kiemer, A. K. IMP2/p62 Induces Genomic Instability and an Aggressive Hepatocellular Carcinoma Phenotype. *Cell Death Dis.* 2015, 6, No. e1894.
- (14) Xing, M.; Li, P.; Wang, X.; Li, J.; Shi, J.; Qin, J.; Zhang, X.; Ma, Y.; Francia, G.; Zhang, J.-Y. Overexpression of p62/IMP2 can Promote Cell Migration in Hepatocellular Carcinoma via Activation of the Wnt/  $\beta$ -Catenin Pathway. *Cancers* 2019, 12, 7—16.
- (15) Dai, N.; Zhao, L.; Wrighting, D.; Krämer, D.; Majithia, A.; Wang, Y.; Cracan, V.; Borges-Rivera, D.; Mootha, V. K.; Nahrendorf, M.; et al. IGF2BP2/IMP2-Deficient Mice Resist Obesity through Enhanced Translation of Ucp1 mRNA and Other mRNAs Encoding Mitochondrial Proteins. *Cell Metab.* 2015, 21, 609—621.
- (16) Tybl, E.; Shi, F.-D.; Kessler, S. M.; Tierlinsky, S.; Walter, J.; Bohle, R. M.; Wieland, S.; Zhang, J.; Tan, E. M.; Kiemer, A. K. Overexpression of the IGF2-mRNA binding protein p62 in transgenic mice induces a steatotic phenotype. *J. Hepatol.* 2011, 54, 994—1001.
- (17) Simon, Y.; Kessler, S. M.; Bohle, R. M.; Haybaeck, J.; Kiemer, A. K. The Insulin-like Growth Factor 2 (IGF2) mRNA-Binding Protein p62/IGF2BP2-2 as a Promoter of NAFLD and HCC? *Gut* 2014, 63, 861—863.
- (18) Laggai, S.; Kessler, S. M.; Boettcher, S.; Lebrun, V.; Gemperlein, K.; Lederer, E.; Leclercq, I. A.; Mueller, R.; Hartmann, R. W.; Haybaeck, J.; Kiemer, A. K. The IGF2 mRNA Binding Protein p62/IGF2BP2-2 Induces Fatty Acid Elongation as a Critical Feature of Steatosis. *J. Lipid Res.* 2014, 55, 1087—1097.
- (19) Kessler, S.; Simon, Y.; Gemperlein, K.; Gianmoena, K.; Cadenas, C.; Zimmer, V.; Pokorny, J.; Barghash, A.; Helms, V.; Van Rooijen, N.; et al. Fatty Acid Elongation in Non-Alcoholic Steatohepatitis and Hepatocellular Carcinoma. *Int. J. Mol. Sci.* 2014, 15, 5762—5773.
- (20) Ye, S.; Sony, W.; Xu, K.; Zhao, X.; L. IGF2BP2 promotes colorectal cancer cell proliferation and survival through interfering with RAF-1 degradation by miR-195. *FEBS Lett.* 2016, 590, 1641—1650.
- (21) Li, T.; Flu, P.-s.; Zuo, Z.; Lin, J.-F.; M, X.; Wu, Q.-N.; Chen, Z.H.; Zeng, Z.-L.; Wang, F.; J.; et al. METTL3 Facilitates Tumor Progression via an M6A-IGF2BP2-Dependent Mechanism in Colorectal Carcinoma. *Mol. Cancer* 2019, 18, 112.
- (22) Liu, W.; Li, Z.; Xu, W.; Wang, Q.; Yang, S. Humoral Autoimmune Response to IGF2 mRNA-Binding Protein (IMP2/p62) and Its Tissue-Specific Expression in Colon Cancer. *Scand. J. Immunol.* 2013, 77, 255—260.
- (23) Bigagli, E.; De Filippo, C.; Castagnini, C.; Toti, S.; Acquadro, F.; Giudici, F.; Fazi, M.; Dolara, P.; Messerini, L.; Tonelli, F.; et al. DNA Copy Number Alterations, Gene Expression Changes and Disease-Free Survival in Patients with Colorectal Cancer: A 10 Year Follow-Up. *Cell. Oncol.* 2016, 39, 545-558.
- (24) Han, K.; Pierce, S. E.; Li, A.; Spees, K.; Anderson, G. R.; Seoane, J. A.; Lo, Y.-H.; Dubreuil, M.; Olivas, M.; Kamber, A.; Wainbery, M.; et al. CRISPR Screens in Cancer Spheroids Identify 3D Growth-Specific Vulnerabilities. *Nature* 2020, 580, 136—141.
- (25) Hu, X.; Peng, W.-X.; Zhou, H.; Jiang, J.; Zhou, X.; D.; MO, Y.-Y.; L. IGF2BP2 Regulates DANCR by Serving as an N6Methyladenosine Reader. *Cell Death Differ.* 2020, 27, 1782—1794.
- (26) Wang, Y.; Lu, J.-H.; Wu, Q.-N.; Jin, Y.; Wang, D.-s.; Chen, Y.-x.; Liu, J.; Luo, X.-J.; Q; Pu, H.-Y.; et al. LncRNA LINRIS Stabilizes IGF2BP2 and Promotes the Aerobic Glycolysis in Colorectal Cancer. *Mol. Cancer* 2019, 18, 174.
- (27) Hafner, M.; Landthaler, M.; Burger, L.; Khorshid, M.; Hausser, J.; Berninger, P.; Rothballer, A.; Ascano, M.; Jungkamp, A.-C.; Munschauer, M.; et al. Transcriptome-Wide Identification of RNA-Binding Protein and MicroRNA Target Sites by PAR-CLIP. *Cell* 2010, 141, 129—141.
- (28) Cao, J.; Mu, Q.; Huang, H. The Roles of Insulin-like Growth Factor 2 mRNA-Binding Protein 2 in Cancer and Cancer Stem Cells. *Stem cells Int* 2018, 2018, 4217259.
- (29) Stolwijk, J. A.; Wegener, J. Impedance-Based Assays along the Life Span of Adherent Mammalian Cells in Vitro: From Initial Adhesion to Cell Death. *Bioanal. Rev.* 2019, 2, 1—75.
- (30) Fior, R.; P6voa, V.; Mendes, R. V.; Carvalho, T.; Gomes, A.; Figueiredo, N.; Ferreira, M. G. Single-Cell Functional and Chemosensitive Profiling of Combinatorial Colorectal Therapy in Zebrafish Xenografts. *Proc. Natl Acad. Sci. U. S. A* 2017, 114, E8234-E8243.
- (31) Ye, Y.; Saburi, W.; Odaka, R.; Kato, K.; Sakurai, N.; Komoda, K.; Nishimoto, M.; Kitaoka, M.; Mori, H.; Yao, M. Structural Insights into the Difference in Substrate Recognition of Two Mannoside Phosphorylases from Two GH130 Subfamilies. *FEBS Lett.* 2016, 590, 828—837.
- (32) Lu, S.; Han, L.; Hu, X.; Sun, T.; Xu, D.; Li, Y.; Chen, Q.; Yao, W.; He, N.; Wang, Z.; Wu, H.; Wei, M. N6-Methyladenosine Reader IMP2 Stabilizes the ZFAS1/OLA1 Axis and Activates the Warburg Effect: Implication in Colorectal Cancer. *Journal of Hematology & Oncology* 2021, 14 (1), 123.

- (33) Xu, X.; Yu, Y.; Zong, K.; Lv, P.; Gu, Y. Up-Regulation of IGF2BP2 by Multiple Mechanisms in Pancreatic Cancer Promotes Cancer Proliferation by Activating the P13K/Akt Signaling Pathway. *J. Exp. Clin. Cancer Res.* 2019, 38, 497.
- (34) Conway, A. E.; Van Nostrand, E. L.; Pratt, G. A.; Aigner, S.; Wilbert, M. L.; Sundararaman, B.; Freese, P.; Lambert, N. J.; Sathe, S.; Liang, T. Y.; et al. Enhanced CLIP Uncovers IMP Protein-RNA Targets in Human Pluripotent Stem Cells Important for Cell Adhesion and Survival. *Cell Rep.* 2016, 15, 666–679.
- (35) Jia, M.; Gut, H.; Chao, J. A Structural Basis of IMP3 RRM12 Recognition of RNA. *RNA* 2018, 24, 1659–1666.
- (36) van Nostrand, E. L.; Freese, P.; Pratt, G. A.; Wang, X.; Wei, X.; Xiao, R.; Blue, S. M.; Chen, J.-Y.; Cody, N. A. L.; Dominguez, D.; et al. A Large-Scale Binding and Functional Map of Human RNA-Binding Proteins. *Nature* 2020, 583, 711–719.
- (37) Maurer, C. K.; Fruth, M.; Empting, M.; Avrutina, O.; Hoßmann, J.; Nadmid, S.; Gorges, J.; Herrmann, J.; Kazmaier, U.; Dersch, P.; et al. Discovery of the first small-molecule CsrA-RNA interaction inhibitors using biophysical screening technologies. *Future Med. Chem.* 2016, 8, 931.
- (38) Viegas, A.; Manso, J.; Nobrega, F. L.; Cabrita, E. J. Saturation Transfer Difference (STD) NMR: A Simple and Fast Method for Ligand Screening and Characterization of Protein Binding. *J. Chem. Educ.* 2011, 88, 990–994.
- (39) Becker, W.; Bhattiprolu, K. C.; Gubensäk, N.; Zangger, K. Investigating Protein-Ligand Interactions by Solution Nuclear Magnetic Resonance Spectroscopy. *ChemPhysChem* 2018, 19, 895–906.
- (40) Kirsch, P.; Jakob, V.; Oberhausen, K.; Stein, S. C.; Cucarro, I.; Schulz, T. F.; Empting, M. Fragment-Based Discovery of a Qualified Hit Targeting the Latency-Associated Nuclear Antigen of the Oncogenic Kaposi's Sarcoma-Associated Herpesvirus/Human Herpesvirus 8. *J. Med. Chem.* 2019, 62, 3924–3939.
- (41) Mayer, M.; Meyer, B. Characterization of Ligand Binding by Saturation Transfer Difference NMR Spectroscopy. *Angew. Chem., Int. Ed. Engl.* 1999, 38, 1784–1788.
- (42) Ghandi, M.; Huang, F. W.; Jané-Va1buena, J.; Kryukov, G. V.; Lo, C. C.; McDonald, E. R.; Barretina, J.; Gelfand, E. T.; Bielski, C. M.; Li, H.; et al. Next-Generation Characterization of the Cancer Cell Line Encyclopedia. *Nature* 2019, 569, 503.
- (43) El-Shamy, A.; Eng, F. J.; Doyle, E. H.; Klepper, A. L.; Sun, X.; Sangiovanni, A.; Iavarone, M.; Colombo, M.; Schwartz, R. E.; Hoshida, Y.; et al. A Cell Culture System for Distinguishing Hepatitis C Viruses with and without Liver Cancer-Related Mutations in the Viral Core Gene. *J. Hepatol.* 2015, 63, 1323–1333.
- (44) Hinsberger, S.; Hüsecken, K.; Groh, M.; Negri, M.; Hauptenthal, J.; Hartmann, R. W. Discovery of Novel Bacterial RNA Polymerase Inhibitors: Pharmacophore-Based Virtual Screening and Hit Optimization. *J. Med. Chem.* 2013, 56, 8332–8338.
- (45) Sahner, J. H.; Groh, M.; Negri, M.; Hauptenthal, J.; Hartmann, R. W. Novel small molecule inhibitors targeting the "switch region" of bacterial RNAP: Structure-based optimization of a virtual screening hit. *Eur. J. Med. Chem.* 2013, 65, 223–231.
- (46) Murakami, K. Structural Biology of Bacterial RNA Polymerase. *Biomolecules* 2015, 5, 848–864.
- (47) Dahlem, C.; Siow, W. X.; Lopatniuk, M.; Tse, W. K. F.; Kessler, S. M.; Kirsch, S. H.; Hoppstädter, J.; Vollmar, A. M.; Müller, R.; Luzhetskyy, A.; et al. Thioholgamide A, a New Anti-Proliferative Anti-Tumor Agent, Modulates Macrophage Polarization and Metabolism. *Cancers* 2020, 12, 1288.
- (48) Anzalone, A. V.; Randolph, P. B.; Davis, J. R.; Sousa, A. A.; Koblan, L. W.; Levy, J. M.; Chen, P. J.; Wilson, C.; Newby, G. A.; Raguram, A.; et al. Search-and-Replace Genome Editing without Double-Strand Breaks or Donor DNA. *Nature* 2019, 576, 149–157.
- (49) Lu, M.; Nakamura, R. M.; Dent, E. D.; Zhang, J.-Y.; Nielsen, F. C.; Christiansen, J.; Chan, E. K. L.; Tan, E. M. Aberrant Expression of Fetal RNA-Binding Protein p62 in Liver Cancer and Liver Cirrhosis. *Am. J. Pathol.* 2001, 159, 945–953.
- (50) Rossi, A. M.; Taylor, C. W. Analysis of Protein-Ligand Interactions by Fluorescence Polarization. *Nat. Protoc.* 2011, 6, 365–387.
- (51) Zhany, J.-H.; Chuny, T. D. Y.; Oldenburg, K. R. A Simple Statistical Parameter for Use in Evaluation and Validation of High Throughput Screening Assays. *J. Biomol. Screening* 1999, 4, 67–73.
- (52) Steenbergen, R.; Oti, M.; ter Horst, R.; Tat, W.; Neufeldt, C.; Belovodskiy, A.; Chua, T. T.; Cho, W. J.; Joyce, M.; Dutilh, B. E.; Tyrrell, D. L. Establishing Normal Metabolism and Differentiation in Hepatocellular Carcinoma Cells by Culturing in Adult Human Serum. *Sci. Rep.* 2018, 8, 11685.

## 5. Conclusion

As previously discussed, RNA-binding proteins (RBPs) play pivotal roles in both eukaryotic and prokaryotic organisms. There are many essential RBP's, which might function as potential drug targets, the validation of these targets is a superbe challenge. Through rigorous study and comprehension of these processes, scientists have identified two specific RBP's, namely CsrA and IMP2, which are of utmost significance for the proper functioning of their respective organisms. The primary objective of this thesis was to identify specific inhibitors targeting these proteins, thereby validating them as potential drug targets.

The first protein under investigation is the carbon storage regulator A (CsrA), a post-transcriptional regulator that is widely distributed and highly conserved among numerous Gram-negative bacteria. Substantial research has underscored its indispensable role in bacterial virulence. **Sections 4.1-4.3** cover the identification of small molecule and peptidic inhibitors targeting CsrA, alongside the establishment of a luciferase reporter gene assay for evaluating the in-cell activity of CsrA inhibitors.

The second protein of interest is the insulin-like growth factor 2 mRNA-binding protein 2 (IMP2). It has been discovered to be significantly overexpressed in various colorectal cancer lines, hepatocellular cancers, and other cancer cell lines. Moreover, it has been demonstrated to promote tumor progression, facilitate tumorigenesis, and worsen disease outcomes. Consequently, inhibiting IMP2 represents a promising avenue for anti-cancer drug discovery. **Sections 4.4** and **4.5** detail the identification and synthesis of potential IMP2 inhibitors and illustrate their direct *in vivo* effects on tumor growth.

For clarity, the compounds and figures presented in the subsequent sections will maintain consistent codes and numbers as those in their respective sections under Results and Discussion (e.g., **sections 4.1** and **5.1** utilize the same codes).

### 5.1 Peptides inhibiting the CsrA-RNA interaction

Understanding and targeting this macromolecule-macromolecule interaction presented a formidable challenge. Unlike typical binding pockets with defined sizes and interaction patterns, this site offered a broad interaction area, making specific interactions elusive. Furthermore, all previously identified inhibitors were derived from natural products, being large and complex compounds.<sup>[26]</sup> This suggests that small molecules may not be the most effective option for disrupting our target interaction. Hence, employing small macrocyclic peptides beyond the Lipinsky space emerged as an optimal strategy for inhibition. Several decades ago, Linpinsky introduced the rule of five, which correlates oral bioavailability with properties such as molecular weight or polarity.<sup>[70]</sup> While this rule of thumb serves as a powerful tool for the rapid assessment of screening hits, it tends to overlook potential inhibitors. Certain natural products exhibit oral bioavailability far exceeding the Lipinsky space due to factors like intramolecular hydrogen bonds or active carriers. Moreover, small molecules can also demonstrate this behavior through macrocyclization, appropriate dosage, or formulation. Molecules falling within this extended Lipinsky Ro5 space represent potential inhibitors of hard-to-target interactions while still maintaining oral bioavailability.<sup>[94]</sup>

Given the limitations and high cost associated with small peptidic databases, they were not a viable option for biophysical screening. Fortunately, our pre-established phage display-library

system (as detailed in **section 2.3**) proved to be an ideal tool for identifying peptides capable of inhibiting the CsrA interaction.<sup>[69]</sup> This library encompassed 2.48 million distinct disulfide-bridged heptapeptides with the general structure X[CXXXC]X, where X represents any canonical amino acid except Cysteine and C represents two disulfide-bridged cysteine residues. The encoded peptides, span a molecular weight range from 548 to 1193 Daltons.<sup>[69]</sup>

We used biotinylated CsrA from *Y. pseudotuberculosis*, as our target of interest. After phage panning and clone isolation, we systematically excluded peptide sequences rich in tryptophan, known for their propensity for nonspecific binding. Among the remaining sequences we identified our initial hit amino acid sequence. Synthesis of the N-acylated, C-amide variation (simulating the peptide backbone) by SPPS delivered our hit peptide (**1**). Fluorescence polarisation assays confirmed the activity of (**1**) regarding inhibition of CsrA from *Y. pseudotuberculosis*, *E. coli* as well as RsmA from *P. aeruginosa*.

The subsequent steps involved synthesizing a series of analogues to pinpoint interaction hotspots via SPPS. Rink amide Tentagel resins were utilized, with coupling carried out in DMF using DIC/Oxyma and Fmoc-protected amino acids featuring acid-labile side chain protecting groups. Furthermore alanine-scan and truncation attempts were conducted.

Replacing amino acids valine, tryptophan, or leucine with alanine, or removing valine, resulted in a decrease in activity, albeit some activity persisted (peptides **3b**, **3d**, **3e**, **4a**). Substituting the acetamide with the free amine, or replacing the carboxamide with the carboxylic acid, caused a minor drop in activity (see peptides **2a** and **2b**). However, eliminating serine, tryptophan, or the disulfide bridge itself (peptides **3a**, **3c**, **3f**, **4b**) led to a complete loss of activity, underscoring the critical role of these features in the interaction with the target.

As the reduction of disulfide bridges into free thiols in the intracellular environment is well known, we needed to replace the disulfide bridge, with a redox stable derivative to maintain intracellular activity. The use of intramolecular CuAAC delivered the desired 1,4 triazoles in good yields. To our delight the activity could be retained for *Yersinia* CsrA and even greatly improved for *E. coli* and *P. aeruginosa*. We could synthesise both isomers of the triazole bridged peptide (**5a** and **5b**), as well as the chain elongated peptide (**5c**) by use of homoazidoalanine. RuAAC facilitated the production of the 1,5 bridged triazoles (**6a** and **6b**), along with the elongated version (**6c**). Across all three pathogens, the 1,4 triazoles outperformed the 1,5-congeners, particularly those with the azide closer to the C-terminus (**5a**, **6a**). Our most promising compound, **5a**, exhibited an  $IC_{50}$  of 4.9 +/- 0.9  $\mu$ M against CsrA from *E. coli*. **Figure 17** illustrates the strategy employed in this publication.

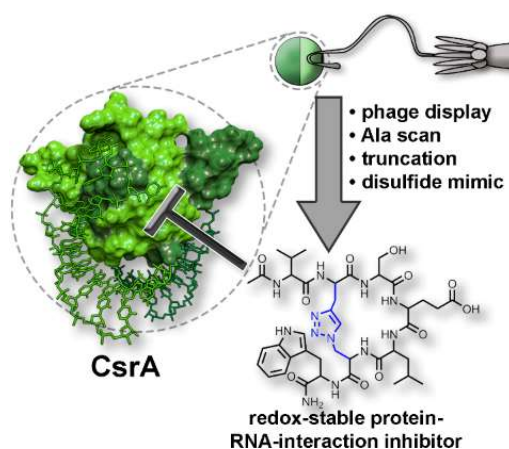


**Figure 17:** Strategy used for Hit identification.

Moreover, our collaboration partners could derive an in-solution structure of our disulfide peptide (**1**) from NMR-measurements. By using this structure as a docking pose we could derive an interaction hypothesis which was in accordance with our findings from the Ala-scan.

Overall, we were able to find a potent redox-stable CsrA inhibitor by using phage display for hit identification.

## Unpublished results and Outlook

Regrettably, our efforts to demonstrate efficacy in cell-based models using these molecules proved unsuccessful. We could however show that this is due to the very poor cell permeability of these compounds.<sup>[12]</sup> So far, we were not able to overcome this issue by modifying the peptide structure. Conjugation of cell-penetrating peptides, as well as the addition of several charged amino acids (such as Arginine) did not lead to success, yet. Even small changes in structure lead to a loss of activity. The most promising perspective we have at the moment is the encapsulation of our peptides in nanoparticles (like e.g. biodynamers, cooperation with S. Lee, UdS) to facilitate permeability over the Gram-negative cell wall without modifying the peptide structure. These experiments are currently ongoing.

## 5.2 Establishment of an *in-bacterio* luciferase assay for the assessment of CsrA inhibitors

Given that CsrA serves as an antivirulence target, its inhibition does not result in bactericidal or bacteriostatic effects. Since selective CsrA inhibitors are not supposed to directly affect the survival of bacteria, traditional assays like minimum inhibitory concentration assays (MIC) are unsuitable for our needs.

Nevertheless, we require a reliable assay capable of quantifying CsrA inhibition within bacterial hosts. This is essential for comparing compounds, ranking them, and optimizing them for *in-vivo* activity. While on-target activity provides a useful starting point for hit identification, it often fails to directly translate to *in-vivo* efficacy due to permeability issues and metabolic challenges. Identifying compounds capable of inhibiting CsrA in living bacteria, along with a tool to measure and quantify this inhibition, represents a crucial step in demonstrating the viability and druggability of CsrA as an antivirulence target.

The concept behind our reporter gene bioluminescence assay was to use the promoter region of *glgC*, a gene that is naturally suppressed by CsrA. Our objective was to identify compounds capable of inhibiting CsrA, thereby reducing the downregulation of *glgC*. This inhibition would lead to an upregulation of *glgC-lux*, consequently resulting in an overall enhancement of bioluminescence, which could then be quantified. To facilitate this, we engineered our own vector, pvBE3, housing the fusion construct *glgC- $\beta$*  along with the promoter region of *glgC*, which is of utmost interest for our aims.<sup>[95]</sup>

In order to ensure the functionality of the assay, a positive control was needed, a substance with a documented inhibitory effect on CsrA, resulting in heightened bioluminescence within the assay.<sup>[95]</sup> Furthermore, this control would serve as a benchmark for comparing hit compounds. The assay output was processed to give the percentage increase in bioluminescence relative to the positive control. Initially, our selection for this role leaned towards intracellularly expressed regulators CsrB or CsrC, known for their ability to inhibit CsrA.

Unfortunately, the use of CsrB or CsrC led to a decrease of luminescence in contradiction to our predicted results. qPCR analysis could confirm that an overexpression of CsrB, leads to an unexpected increase of CsrA encoding transcripts, leading to an upregulation of CsrA protein, which overcompensates CsrB/C inhibition and, thus explains the decrease of



bioluminescence. These findings were unexpected and not in accordance with our expectations from literature. The regulation of CsrA is very complex (see **Figure 18**) and thus hard to predict. Plausible explanations of these effects have been stated elsewhere and will not be discussed here.<sup>[95]</sup>

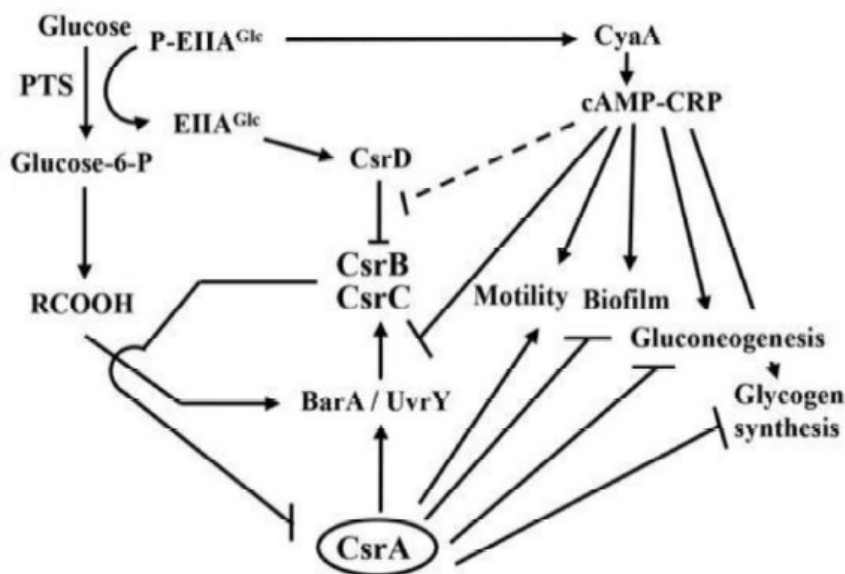


**Figure 18:** simplified regulation circuit for CsrA from *E. coli*, originated from Pannuri et. al.<sup>[96]</sup>

Since CsrB and C proved to be inappropriate positive controls, we shifted our interest to CesT, a chaperone protein, which is also known to inhibit CsrA.<sup>[97,98]</sup> Indeed, the experiments could confirm a reliable increase in luminescence employing CesT as a positive control.

With this assay in our hand, we were able to assess the activity of our peptidic hits from the **section 4.1**. Unfortunately, these peptides (**1** and **2**), did not show any increase in luminescence in the assay. Subcellular quantification of compound uptake in *E. coli* confirmed a sub-nanomolar concentration inside the cell, while in the extracellular space micromolar concentrations could be measured. This is a reasonable explanation for the absence of luminescence increase and underscores the intrinsic problems of our peptidic hits to show effects *in-bacterio*. Thus, an important next step is to find compounds which are able to penetrate the cell-membrane, and to confirm their cellular activity with this newly developed assay.

### 5.3 Small molecules inhibiting the CsrA-RNA interaction

Equipped with our newly developed assay (refer to **sections 4.2** and **5.2**), we possessed an ideal tool for evaluating the *in-bacterio* inhibition of CsrA by potential inhibitors. However, the CsrA inhibitors we had discovered thus far proved ineffective in our assay. We urgently required molecules capable of demonstrating on-target activity while also penetrating the cell membrane of Gram-negative bacteria, a task fraught with challenges. Consequently, we opted to refocus our efforts on small molecules, recognizing their enhanced likelihood of cellular uptake.

To this end, we selected a library from Enamine, comprising over 10,000 structurally diverse compounds, for SPR screening using *E. coli* CsrA. Initial *in-silico* preselection aided in excluding over 8,000 compounds, significantly simplifying the screening process. Following the screening, we identified five distinct compounds from two different classes. These molecules underwent resynthesis (details of synthetic routes provided in **section 4.3**) and were

subsequently evaluated for *in vitro* activity against *E. coli* CsrA using a fluorescence polarization assay.

Unfortunately, three molecules from two different classes didn't show any activity after resynthesis (compounds **(1)**, **(3)** and **(4)**), suggesting that the initially observed activity may have been attributed to library artifacts.

Although molecule **(7)** from the Hydantoin class exhibited decreased activity, we resolved to refine this compound further by synthesizing a series of analogues. Retrosynthetically, we divided the molecule into three parts: a left (hydantoin), middle (aromatic ring), and right (aromatic amines) segment. By employing different aromatic amines or molecules derived from hydantoin during synthesis, we successfully generated several derivatives within each analogue class.

Synthesizing the ortho-substituted compound posed a slightly greater challenge. The conventional strategy was rendered unfeasible due to the formation of a five-membered lactone. In this scenario, we had to employ an ester protecting group strategy to overcome this obstacle.

Compound **(2)**, however, exhibited outstanding activity in the FluPo assay. To our satisfaction, we discovered that a ring contraction to a six-membered ring, rather than a seven-membered ring, resulting in a symmetric compound **(6)**, not only enhanced the activity but also simplified the molecule and consequently the synthetic pathway to derivatives. Subsequently, we devised and synthesized a series of analogues, primarily derived from compound **(6)**.

These analogues underwent truncation, further ring contraction, and modification of the pyrazine ring, although most retained the original pyrazine ring of compound **(6)**, with only alterations made to the aromatic amine on the right side of the molecule. To achieve this, we developed two distinct routes: the Buchwald-Hartwig route utilizing amine **(16)** and the reductive amination route utilizing ketone **(18)**. The reductive amination route proved vastly superior, yielding cleaner products with higher efficiency.

In total, we successfully synthesized fifty distinct molecules, each representing a potential inhibitor of CsrA. Regrettably, we currently face challenges with the expression of *E. coli* CsrA, hindering our ability to test these compounds in biophysical assays for their on-target binding. Additionally, our previously established assay requires further optimization to yield reliable data. While initial findings are promising, indicating the activity of these compounds, the considerable standard deviation and fluctuating results necessitate further refinement of the assay for enhanced robustness. Moving forward, continued adjustments to the assay protocol will contribute to its reliability and stability.

## Outlook

In the future those compounds need to be tested *in-vitro* as well as *in-bacterio*, to rank them and to find the most potent inhibitors, at this point a first publication of these results is planned. Then a dedicated hit to-lead optimisation process can be initiated. Furthermore, these compounds should undergo extensive ADMET assays to optimize not only their activity but also their pharmacokinetic/pharmacodynamic (PK/PD) profile. Additionally, utilizing STD-NMR could serve to confirm their binding to the target and provide valuable insights for structural modifications. A phenotypic screening of a different library, employing our luciferase assay, could also be a formidable option to directly find molecules with good in-cell activity without the need of Biophysical screening. Potential derivatives of the classes **II** and **IV** are shown in **Figure 19** and **Figure 20**.

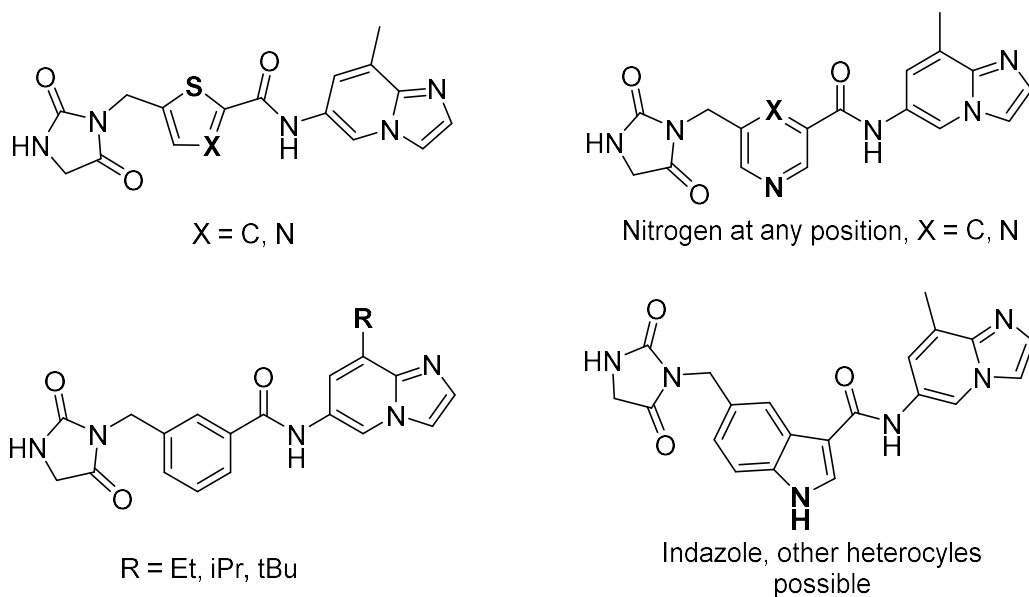


**Figure 19:** Possible derivatisation of class II compounds.

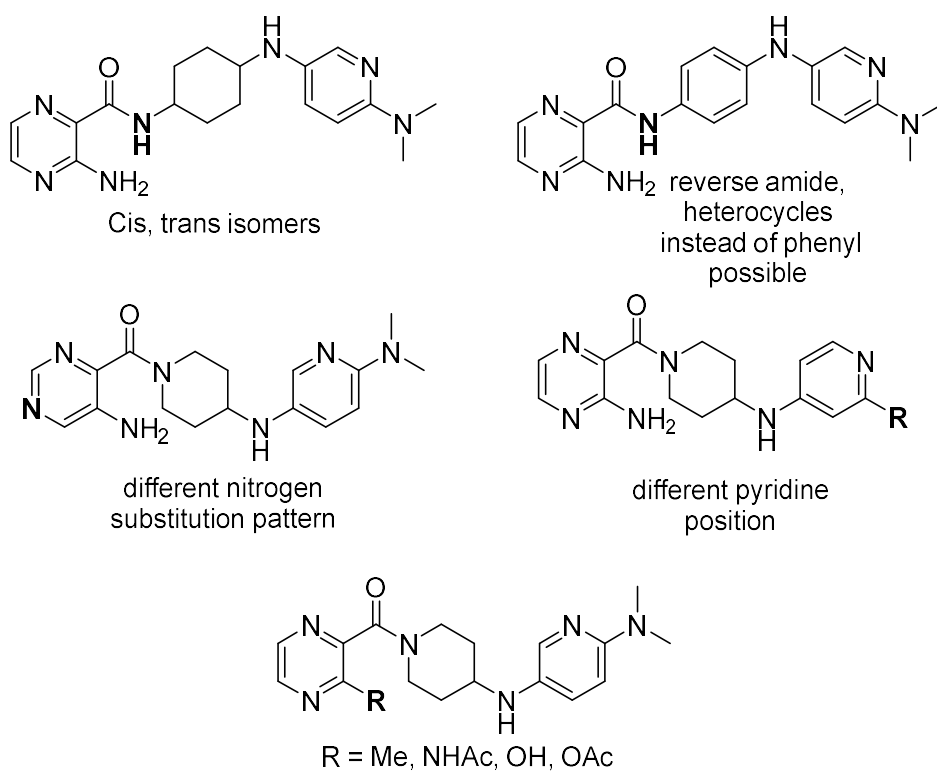


**Figure 20:** Possible derivatisation of class IV compounds.

## 5.4 Small molecules inhibiting the IMP2-RNA interaction

The aim of this study was to find small molecular inhibitors of IMP2 by development of a fluorescence polarization assay. In a second step, these confirmed IMP2-binders were assessed for in-vivo activity in Xenograft models in zebrafish larvae to confirm the tumor inhibition properties of IMP2-inhibitors and to confirm IMP2 as a potential anti-cancer target.

The first challenge was to identify an RNA sequence, which exhibits specific binding to IMP2, as this was not assessed beforehand, as it was the case for our CsrA project. From previously published IMP2 binding motifs, two potential IMP2-binding RNA sequences were deduced. RNAA as well as RNAB (sequence in **Figure 21**). While RNAA showed a higher binding affinity, both sequences proved viable for IMP2 binding and their fluorescence labelled versions were used in the FluPo-screening.

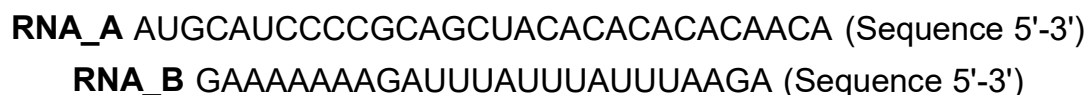


**Figure 21:** RNAA and RNAB sequences.

The screening identified 18 primary actives, from two different classes, namely the ureidothiophene class as well as the benzamidobenzoic acid class, to be potential RNA-IMP2 inhibitors. After additional experiments, such as STD-NMR as well as thermal shift assays (TSA), 10 compounds remained interesting, and three of them (compounds **4**, **6** and **9**) were selected for being the most potent inhibitors. Sahner et. al previously published, excessive information on the synthetical access to the compounds of the ureidothiophene class.<sup>[60]</sup> In **Figure 22**, the optimized method used for the synthesis of these compounds is depicted. A careful optimisation of reaction conditions was conducted.

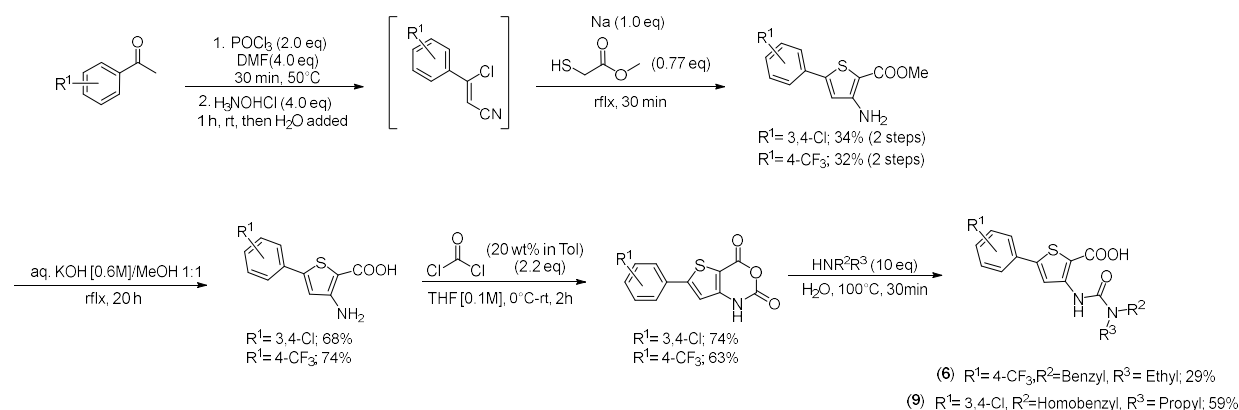


**Figure 22:** Modified conditions for the synthesis of the compounds **6** and **9** from the ureidothiophene class.

The same held true for compounds of the benzamidobenzoic acid class, previously published by Hinsberger et. al.<sup>[59]</sup> Optimized reaction conditions are shown in **Figure 23**.

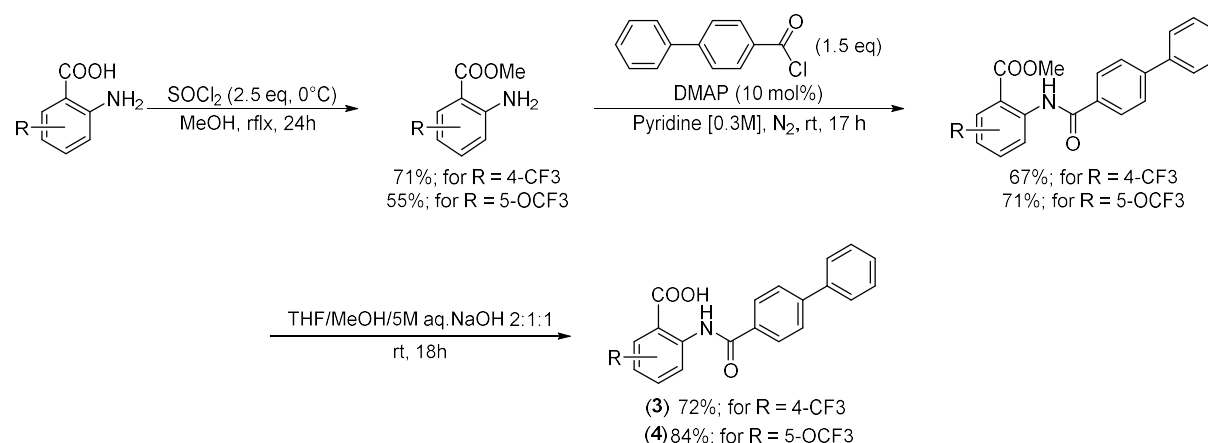


**Figure 23:** Optimized reaction conditions for the synthesis of compounds **3** and **4** from the benzamidobenzoic acid class.

Compounds **4** and **6** were able to show a significant inhibition in tumor growth in xenograft models with zebrafish embryos. These results underline the drugability of IMP2 and confirm its role as a potential anti-cancer target.

### **Outlook**

Although these compounds demonstrate efficient activity both *in vitro* and *in vivo*, their promiscuity is undeniable, particularly considering their potential inhibition of both RNAP and IMP2. Therefore, further optimization towards selectivity is imperative. Nonetheless, these findings serve as a crucial starting point for identifying more potent and selective IMP2 inhibitors. The RNA sequences uncovered are vital for subsequent hit identification. In the future, utilizing specific KH34 domains, renowned for their RNA binding specificity, in the assay instead of full-length proteins will simplify assay preparation. Ongoing library screenings for potential IMP2 inhibitors reveal promising primary active compounds that do not fall within the ureidothiophene or benzamidobenzoic acid classes. Once, selective inhibitors are found, the concept of Proteolysis targeting chimera (PROTAC) could be employed, degrading the target, by selective ubiquitination of the target protein, instead of inhibiting the protein-RNA interaction. Selective inhibition of IMP1 or IMP3 could also prove advantageous in tumors overexpressing IMP1 or -3.

## 6. Outlook

The overall challenge to discover, synthesize and optimize CsrA-RNA inhibitors was successful. Potent peptidic CsrA-RNA interaction inhibitors were discovered via phage-display technology and optimized towards activity *in-vitro*. Regrettably, these peptides faced a barrier in penetrating the cell wall of gram-negative bacteria. However, despite this setback, these compounds present avenues for further enhancement, such as conjugation to biomolecules, chemical modification, or formulation in nanoparticles. They serve as a promising scaffold for future efforts in designing and synthesizing antivirulence drugs targeting CsrA.

The establishment of the luciferase reporter gene assay marked a significant achievement. While further optimization is required to enhance its robustness, the assay demonstrates the desired effect: a measurable increase in luminescence upon inhibition of CsrA. This assay holds promise as a prototype for the development of additional phenotypic assays in the future. Given the rising significance of antivirulence targets and drugs, there will be an increasing demand for new assays that do not solely measure bactericidal effects.

Challenges arose due to technical issues regarding the reliability of the newly developed luciferase reporter gene assay and complications in purifying CsrA from *E. coli*. These hurdles hindered further optimization of the small molecules identified as potential CsrA inhibitors via SPR-screening. Nonetheless, we successfully pinpointed two classes of potential inhibitors: the hydantoin class **II** and the aminopyrazine class **IV**, synthesizing over fifty compounds within these categories. Quantification of their activity through both *in-vitro* (fluorescence polarization assay) and *in-vivo* (luciferase reporter gene assay) evaluations will enable the identification of the most promising starting point for synthesizing a potent small molecular CsrA-RNA interaction inhibitor. Armed with the synthetic methods and necessary assays, we anticipate the emergence of potent inhibitors in the near future.

Significant advancements have been made in the IMP2 field concerning assay development and compound optimization. I refined the reaction conditions for synthesizing these compounds, facilitating efficient access to them. Presently, there are plans to design PROTACS within the benzamidobenzoic class, leveraging the methods outlined in this thesis for their development. However, the issue of limited selectivity persists with these compounds. Despite demonstrating *in-vivo* effects, there is a need to optimize them for selectivity. This could potentially be achieved through chemical modification, although conducting additional screening to identify new compounds may prove to be a more successful approach.

## 7. References

- [1] S. Mohibi, X. Chen, J. Zhang, *Pharmacology & therapeutics* **2019**, *203*, 107390.
- [2] V. Jakob, B. G. E. Zoller, J. Rinkes, Y. Wu, A. F. Kiefer, M. Hust, S. Polten, A. M. White, P. J. Harvey, T. Durek et al., *European journal of medicinal chemistry* **2022**, *231*, 114148.
- [3] C. Dahlem, A. Abuhaliema, S. M. Kessler, T. Kröhler, B. G. E. Zoller, S. Chanda, Y. Wu, S. Both, F. Müller, K. Lepikhov et al., *ACS chemical biology* **2022**, *17*, 361.
- [4] Z. Kmietowicz, *BMJ (Clinical research ed.)* **2017**, *358*, j4339.
- [5] A. Cassini, L. D. Högberg, D. Plachouras, A. Quattrocchi, A. Hoxha, G. S. Simonsen, M. Colomb-Cotinat, M. E. Kretzschmar, B. Devleeschauwer, M. Cecchini et al., *The Lancet. Infectious diseases* **2019**, *19*, 56.
- [6] a) L. L. Silver, *Clinical microbiology reviews* **2011**, *24*, 71; b) M. I. Hutchings, A. W. Truman, B. Wilkinson, *Current opinion in microbiology* **2019**, *51*, 72; c) *Microorganisms for Sustainable Environment and Health*, Elsevier, **2020**; d) N. Upmanyu, V. N. Malviya in *Microorganisms for Sustainable Environment and Health*, Elsevier, **2020**, pp. 367–382.
- [7] G. Kapoor, S. Saigal, A. Elongavan, *Journal of anaesthesiology, clinical pharmacology* **2017**, *33*, 300.
- [8] a) C. Zampaloni, P. Mattei, K. Bleicher, L. Winther, C. Thäte, C. Bucher, J.-M. Adam, A. Alanine, K. E. Amrein, V. Baidin et al., *Nature* **2024**, *625*, 566; b) K. S. Pahl, M. S. A. Gilman, V. Baidin, T. Clairfeuille, P. Mattei, C. Bieniossek, F. Dey, D. Muri, R. Baettig, M. Lobritz et al., *Nature* **2024**, *625*, 572.
- [9] A. L. Welp, J. M. Bomberger, *Frontiers in cellular and infection microbiology* **2020**, *10*, 213.
- [10] E. M. Selleck, M. S. Gilmore, *mBio* **2016**, *7*.
- [11] K. A. Brogden, J. M. Guthmiller, C. E. Taylor, *Lancet (London, England)* **2005**, *365*, 253.
- [12] Y. Wu, B. G. E. Zoller, M. A. M. Kamal, S.-K. Hotop, C.-M. Lehr, M. Brönstrup, P. Dersch, M. Empting, *ChemBiochem : a European journal of chemical biology* **2023**, *24*, e202300369.
- [13] S. W. Dickey, G. Y. C. Cheung, M. Otto, *Nature reviews. Drug discovery* **2017**, *16*, 457.
- [14] G. P. Carter, J. I. Rood, D. Lyras, *Trends in microbiology* **2012**, *20*, 21.
- [15] I. Lowy, D. C. Molrine, B. A. Leav, B. M. Blair, R. Baxter, D. N. Gerding, G. Nichol, W. D. Thomas, M. Leney, S. Sloan et al., *The New England journal of medicine* **2010**, *362*, 197.
- [16] T. Köhler, G. G. Perron, A. Buckling, C. van Delden, *PLoS pathogens* **2010**, *6*, e1000883.
- [17] I. d. M. Henrique, F. Sacerdoti, R. L. Ferreira, C. Henrique, M. M. Amaral, R. M. F. Piazza, D. Luz, *Frontiers in cellular and infection microbiology* **2022**, *12*, 825856.
- [18] V. Oganessian, L. Peng, M. M. Damschroder, L. Cheng, A. Sadowska, C. Tkaczyk, B. R. Sellman, H. Wu, W. F. Dall'Acqua, *The Journal of biological chemistry* **2014**, *289*, 29874.
- [19] E. K. Sully, N. Malachowa, B. O. Elmore, S. M. Alexander, J. K. Femling, B. M. Gray, F. R. DeLeo, M. Otto, A. L. Cheung, B. S. Edwards et al., *PLoS pathogens* **2014**, *10*, e1004174.
- [20] C. Schütz, A. Hodzic, M. Hamed, A. S. Abdelsamie, A. M. Kany, M. Bauer, T. Röhrig, S. Schmelz, A. Scrima, W. Blankenfeldt et al., *European journal of medicinal chemistry* **2021**, *226*, 113797.
- [21] J. Konstantinović, A. M. Kany, A. Alhayek, A. S. Abdelsamie, A. Sikandar, K. Voos, Y. Yao, A. Andreas, R. Shafiei, B. Loretz et al., *ACS central science* **2023**, *9*, 2205.

- [22] Y. Irie, M. Starkey, A. N. Edwards, D. J. Wozniak, T. Romeo, M. R. Parsek, *Molecular microbiology* **2010**, *78*, 158.
- [23] A. K. Heroven, K. Böhme, P. Dersch, *RNA biology* **2012**, *9*, 379.
- [24] A. H. Potts, C. A. Vakulskas, A. Pannuri, H. Yakhnin, P. Babitzke, T. Romeo, *Nature communications* **2017**, *8*, 1596.
- [25] E. R. Morris, G. Hall, C. Li, S. Heeb, R. V. Kulkarni, L. Lovelock, H. Silistre, M. Messina, M. Cámara, J. Emsley et al., *Structure (London, England : 1993)* **2013**, *21*, 1659.
- [26] C. K. Maurer, M. Fruth, M. Empting, O. Avrutina, J. Hoßmann, S. Nadmid, J. Gorges, J. Herrmann, U. Kazmaier, P. Dersch et al., *Future medicinal chemistry* **2016**, *8*, 931.
- [27] G. Sharma, S. Sharma, P. Sharma, D. Chandola, S. Dang, S. Gupta, R. Gabrani, *Journal of applied microbiology* **2016**, *121*, 309.
- [28] J. Timmermans, L. van Melderen, *Cellular and molecular life sciences : CMLS* **2010**, *67*, 2897.
- [29] E. van Assche, S. van Puyvelde, J. Vanderleyden, H. P. Steenackers, *Frontiers in microbiology* **2015**, *6*, 141.
- [30] X. Ma, H. Yu, *The Yale journal of biology and medicine* **2006**, *79*, 85.
- [31] J. Ferlay, M. Colombet, I. Soerjomataram, D. M. Parkin, M. Piñeros, A. Znaor, F. Bray, *International journal of cancer* **2021**.
- [32] T. Z. Minas, M. Kiely, A. Ajao, S. Ambis, *Carcinogenesis* **2021**, *42*, 2.
- [33] A. Kumar, V. Gautam, A. Sandhu, K. Rawat, A. Sharma, L. Saha, *World journal of gastrointestinal surgery* **2023**, *15*, 495.
- [34] A. Raza, G. K. Sood, *World journal of gastroenterology* **2014**, *20*, 4115.
- [35] W. Liu, Z. Li, W. Xu, Q. Wang, S. Yang, *Scandinavian journal of immunology* **2013**, *77*, 255.
- [36] S. Ye, W. Song, X. Xu, X. Zhao, L. Yang, *FEBS letters* **2016**, *590*, 1641.
- [37] S. M. Kessler, S. Laggai, A. Barghash, C. S. Schultheiss, E. Lederer, M. Artl, V. Helms, J. Haybaeck, A. K. Kiemer, *Cell death & disease* **2015**, *6*, e1894.
- [38] M. Xing, P. Li, X. Wang, J. Li, J. Shi, J. Qin, X. Zhang, Y. Ma, G. Francia, J.-Y. Zhang, *Cancers* **2019**, *12*.
- [39] A. K. Dubey, C. S. Baker, T. Romeo, P. Babitzke, *RNA (New York, N.Y.)* **2005**, *11*, 1579.
- [40] M. Y. Liu, G. Gui, B. Wei, J. F. Preston, L. Oakford, U. Yüksel, D. P. Giedroc, T. Romeo, *The Journal of biological chemistry* **1997**, *272*, 17502.
- [41] Y. Tan, Z.-Y. Liu, Z. Liu, H.-J. Zheng, F.-L. Li, *Molecular bioSystems* **2015**, *11*, 1434.
- [42] H. Yakhnin, C. S. Baker, I. Berezin, M. A. Evangelista, A. Rassin, T. Romeo, P. Babitzke, *Journal of bacteriology* **2011**, *193*, 6162.
- [43] B. L. Wei, A. M. Brun-Zinkernagel, J. W. Simecka, B. M. Prüss, P. Babitzke, T. Romeo, *Molecular microbiology* **2001**, *40*, 245.
- [44] D. W. Jackson, K. Suzuki, L. Oakford, J. W. Simecka, M. E. Hart, T. Romeo, *Journal of bacteriology* **2002**, *184*, 290.
- [45] A. K. Dubey, C. S. Baker, K. Suzuki, A. D. Jones, P. Pandit, T. Romeo, P. Babitzke, *Journal of bacteriology* **2003**, *185*, 4450.
- [46] J. E. Schultz, A. Matin, *Journal of molecular biology* **1991**, *218*, 129.



- [47] V. Berndt, M. Beckstette, M. Volk, P. Dersch, M. Brönstrup, *Scientific reports* **2019**, *9*, 138.
- [48] J. L. Bell, K. Wächter, B. Mühleck, N. Pazaitis, M. Köhn, M. Lederer, S. Hüttelmaier, *Cellular and molecular life sciences : CMLS* **2013**, *70*, 2657.
- [49] H. Huang, H. Weng, W. Sun, X. Qin, H. Shi, H. Wu, B. S. Zhao, A. Mesquita, C. Liu, C. L. Yuan et al., *Nature cell biology* **2018**, *20*, 285.
- [50] B. Czepukojc, A. Abuhaliema, A. Barghash, S. Tierling, N. Naß, Y. Simon, C. Körbel, C. Cadenas, N. van Hul, A. Sachinidis et al., *Frontiers in medicine* **2019**, *6*, 179.
- [51] N. Dai, F. Ji, J. Wright, L. Minichiello, R. Sadreyev, J. Avruch, *eLife* **2017**, *6*.
- [52] S. M. Kessler, J. Pokorny, V. Zimmer, S. Laggai, F. Lammert, R. M. Bohle, A. K. Kiemer, *American journal of physiology. Gastrointestinal and liver physiology* **2013**, *304*, G328–36.
- [53] S. Huang, Z. Wu, Y. Cheng, W. Wei, L. Hao, *Acta biochimica et biophysica Sinica* **2019**, *51*, 743.
- [54] M. Janiszewska, M. L. Suvà, N. Riggi, R. H. Houtkooper, J. Auwerx, V. Clément-Schatlo, I. Radovanovic, E. Rheinbay, P. Provero, I. Stamenkovic, *Genes & development* **2012**, *26*, 1926.
- [55] N. Dai, L. Zhao, D. Wrighting, D. Krämer, A. Majithia, Y. Wang, V. Cracan, D. Borges-Rivera, V. K. Mootha, M. Nahrendorf et al., *Cell metabolism* **2015**, *21*, 609.
- [56] E. Tybl, F.-D. Shi, S. M. Kessler, S. Tierling, J. Walter, R. M. Bohle, S. Wieland, J. Zhang, E. M. Tan, A. K. Kiemer, *Journal of hepatology* **2011**, *54*, 994.
- [57] S. M. Kessler, E. Lederer, S. Laggai, N. Golob-Schwarzl, K. Hosseini, J. Petzold, C. Schweiger, R. Reihls, M. Keil, J. Hoffmann et al., *Oncotarget* **2017**, *8*, 89736.
- [58] X. Ren, R. Zeng, M. Tortorella, J. Wang, C. Wang, *Scientific reports* **2017**, *7*, 14934.
- [59] S. Hinsberger, K. Hüsecken, M. Groh, M. Negri, J. Hauptenthal, R. W. Hartmann, *Journal of medicinal chemistry* **2013**, *56*, 8332.
- [60] J. H. Sahner, M. Groh, M. Negri, J. Hauptenthal, R. W. Hartmann, *European journal of medicinal chemistry* **2013**, *65*, 223.
- [61] G. A. Belogurov, M. N. Vassilyeva, A. Sevostyanova, J. R. Appleman, A. X. Xiang, R. Lira, S. E. Webber, S. Klyuyev, E. Nudler, I. Artsimovitch et al., *Nature* **2009**, *457*, 332.
- [62] A. K. Krome, T. Becker, S. Kehraus, A. Schiefer, M. Gütschow, L. Chaverra-Muñoz, S. Hüttel, R. Jansen, M. Stadler, A. Ehrens et al., *Natural product reports* **2022**, *39*, 1705.
- [63] I. Chopra, *Current opinion in investigational drugs (London, England : 2000)* **2007**, *8*, 600.
- [64] J. Mukhopadhyay, K. Das, S. Ismail, D. Koppstein, M. Jang, B. Hudson, S. Sarafianos, S. Tuske, J. Patel, R. Jansen et al., *Cell* **2008**, *135*, 295.
- [65] D. J. Craik, M.-H. Lee, F. B. H. Rehm, B. Tombling, B. Doffek, H. Peacock, *Bioorganic & medicinal chemistry* **2018**, *26*, 2727.
- [66] S. J. Bogdanowich-Knipp, S. Chakrabarti, T. D. Williams, R. K. Dillman, T. J. Siahhaan, *The journal of peptide research : official journal of the American Peptide Society* **1999**, *53*, 530.
- [67] L. Diao, B. Meibohm, *Clinical pharmacokinetics* **2013**, *52*, 855.
- [68] W. Jaroszewicz, J. Morcinek-Orłowska, K. Pierzynowska, L. Gaffke, G. Węgrzyn, *FEMS microbiology reviews* **2022**, *46*.
- [69] V. Jakob, S. Helmsing, M. Hust, M. Empting, *Methods in molecular biology (Clifton, N.J.)* **2020**, *2070*, 95.
- [70] C. A. Lipinski, *Drug discovery today. Technologies* **2004**, *1*, 337.

- [71] G. P. Smith, *Science (New York, N.Y.)* **1985**, *228*, 1315.
- [72] S. S. Sidhu, H. B. Lowman, B. C. Cunningham, J. A. Wells, *Methods in enzymology* **2000**, *328*, 333.
- [73] K. Sakamoto, S. Sogabe, Y. Kamada, N. Sakai, K. Asano, M. Yoshimatsu, K. Ida, Y. Imaeda, J.-I. Sakamoto, *Biochemical and biophysical research communications* **2017**, *482*, 310.
- [74] M. Hust, T. Meyer, B. Voedisch, T. Rülker, H. Thie, A. El-Ghezal, M. I. Kirsch, M. Schütte, S. Helmsing, D. Meier et al., *Journal of biotechnology* **2011**, *152*, 159.
- [75] V. Jakob, S. Helmsing, M. Hust, M. Empting, *Methods in molecular biology (Clifton, N.J.)* **2020**, *2070*, 95.
- [76] A. El-Faham, F. Albericio, *Chemical reviews* **2011**, *111*, 6557.
- [77] A. El-Faham, F. Albericio, *Eur J Org Chem* **2009**, *2009*, 1499.
- [78] R. B. Merrifield, *J. Am. Chem. Soc.* **1963**, *85*, 2149.
- [79] M. Amblard, J.-A. Fehrentz, J. Martinez, G. Subra, *Molecular biotechnology* **2006**, *33*, 239.
- [80] J. M. Palomo, *RSC Adv* **2014**, *4*, 32658.
- [81] J. Barbet, S. Huclier-Markai, *Pharmaceutical statistics* **2019**, *18*, 513.
- [82] R. Bakhtiar, *J. Chem. Educ.* **2013**, *90*, 203.
- [83] J. P. Rast (Ed.) *SpringerLink Bücher, Vol. 748*, Humana Press, Totowa, NJ, **2011**.
- [84] Y. Liu, W. D. Wilson, *Methods in molecular biology (Clifton, N.J.)* **2010**, *613*, 1.
- [85] P. Schuck, *Annual review of biophysics and biomolecular structure* **1997**, *26*, 541.
- [86] M. D. Hall, A. Yasgar, T. Peryea, J. C. Braisted, A. Jadhav, A. Simeonov, N. P. Coussens, *Methods and applications in fluorescence* **2016**, *4*, 22001.
- [87] O. D. Hendrickson, N. A. Taranova, A. V. Zherdev, B. B. Dzantiev, S. A. Eremin, *Sensors (Basel, Switzerland)* **2020**, *20*.
- [88] J. Kügler, S. Wilke, D. Meier, F. Tomszak, A. Frenzel, T. Schirrmann, S. Dübel, H. Garritsen, B. Hock, L. Toleikis et al., *BMC biotechnology* **2015**, *15*, 10.
- [89] Y.-J. Lai, H. Yakhnin, A. Pannuri, C. Pourciau, P. Babitzke, T. Romeo, *Molecular microbiology* **2022**, *117*, 32.
- [90] F. McPhee, J. A. Campbell, W. Li, S. Andrea, Z. B. Zheng, A. C. Good, D. J. Carini, B. L. Johnson, P. M. Scola.
- [91] a) D. Quiroga, L. D. Becerra, E. Coy-Barrera, *ACS omega* **2019**, *4*, 13710; b) C. L. Gibson, A. R. Kennedy, R. R. Morthala, J. A. Parkinson, C. J. Suckling, *Tetrahedron* **2008**, *64*, 7619; c) A. Karim, A. Mortreux, F. Petit, G. Buono, G. Peiffer, C. Siv, *Journal of Organometallic Chemistry* **1986**, *317*, 93; d) D. Riether, M. Ferrara, N. Heine, U. Lessel, J. R. Nicholson, A. Pekcec, S. Scheuerer, WO 2017/178341, **2017**.
- [92] R. Skerlj, E. M. Bourque, P. Lansbury, W. J. Greenlee, A. C. Good.
- [93] J. E. Macor, *Pfizer Inc.* EP379314.
- [94] B. C. Doak, B. Over, F. Giordanetto, J. Kihlberg, *Chemistry & biology* **2014**, *21*, 1115.
- [95] Yingwen Wu, *Dissertation*, Universität des Saarlandes, Saarbrücken, **2023**
- [96] A. Pannuri, C. A. Vakulskas, T. Zere, L. C. McGibbon, A. N. Edwards, D. Georgellis, P. Babitzke, T. Romeo, *Journal of bacteriology* **2016**, *198*, 3000.

[97] M. Yadav, M. Srinivasan, N. K. Tulsian, Y. X. Liu, Q. Lin, I. Rosenshine, J. Sivaraman, *Protein science : a publication of the Protein Society* **2021**, *30*, 2433.

[98] N. Katsowich, N. Elbaz, R. R. Pal, E. Mills, S. Kobi, T. Kahan, I. Rosenshine, *Science (New York, N.Y.)* **2017**, *355*, 735.

## **Additional help**

- Chemdraw 19.1 and Microsoft Powerpoint were used, for the preparation of several schemes.
- MestreNova was used for the analysis of most NMR spectra.
- Chromeleon was used for analysis of LC-MS spectra.
- ChatGPT3.5 was used for writing purposes.

## 8. Supporting Information

### 8.1 Peptides Inhibiting the CsrA-RNA interaction

#### Phage Display-based Discovery of Cyclic Peptides against the Broad Spectrum Bacterial Anti-Virulence Target CsrA.

Valentin Jakob,<sup>1,2,+</sup> Ben G. E. Zoller,<sup>1,2,+</sup> Julia Rinkes,<sup>1,2</sup> Yingwen Wu,<sup>1,2</sup> Alexander F. Kiefer,<sup>1,2</sup> Michael Hust,<sup>3</sup> Saskia Polten,<sup>3</sup> Andrew M. White,<sup>4</sup> Peta J. Harvey,<sup>4</sup> Thomas Durek,<sup>4</sup> David J. Craik,<sup>4</sup> Andreas Siebert,<sup>5</sup> Uli Kazmaier,<sup>5</sup> and Martin Empting<sup>1,2,\*</sup>

<sup>1</sup>Department of Drug Design and Optimization (DDOP), Helmholtz-Institute for Pharmaceutical Research Saarland (HIPS) - Helmholtz Centre for Infection Research (HZI), Campus E8.1, 66123 Saarbrücken, Germany.

<sup>2</sup>Department of Pharmacy, Saarland University, Campus E8.1, 66123 Saarbrücken, Germany.

<sup>3</sup>Technische Universität Braunschweig, Institut für Biochemie, Biotechnologie und Bioinformatik, Spielmannstr. 7, 38106 Braunschweig, Germany

<sup>4</sup>ARC Centre of Excellence for Innovations in Peptide and Protein Science, Institute for Molecular Bioscience, The University of Queensland, Brisbane, QLD, 4072, Australia

<sup>5</sup>Institut für Organische Chemie Saarland University Campus C4.2, 66123 Saarbrücken, Germany

[†] These authors contributed equally to this work

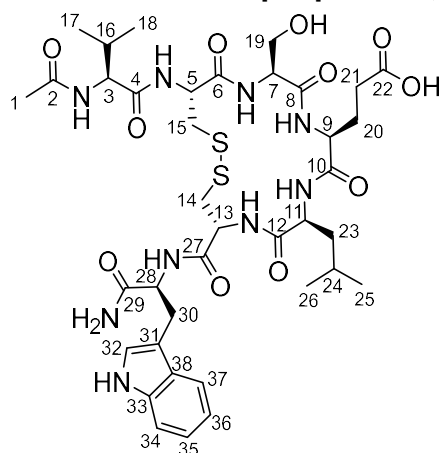
## Table of Contents

Table of Contents.....	89
Peptide Synthesis and Macrocyclization .....	90
Expression of <i>Y. pseudotuberculosis</i> CsrA-biot-His <sub>6</sub> .....	99
Expression of <i>E. coli</i> CsrA-His <sub>6</sub> .....	99
Expression of <i>P. Aeruginosa</i> RsmA-His <sub>6</sub> .....	100
Sequence Identities (BLAST).....	100
Phage Display.....	101
Fluorescence Polarization Assay .....	102
Microscale Thermophoresis Assay (MST).....	107
Calculation of the Error Bars in Fluorescence Polarization and MST Assay .....	107
NMR analysis and structure calculations.....	107
<i>In silico</i> Investigations .....	109
Analytical LC-MS .....	110
<sup>1</sup> H-NMR and <sup>13</sup> C-NMR Spectra .....	127
2D NMR Spectra.....	134
FTIR Spectra.....	136
HRMS .....	136
Author Contributions .....	154

## Peptide Synthesis and Macrocyclization

### **Ac-V-[CSELC]<sub>cyclic</sub>-W-NH<sub>2</sub> (1); 3-((4R,7S,10S,13S,16R)-16-(((S)-2-acetamido-3-methylbutanamido)-4-(((S)-1-amino-3-(1H-indol-3-yl)-1-oxopropan-2-yl)carbamoyl)-13-(hydroxymethyl)-7-isobutyl-6,9,12,15-tetraoxo-1,2-dithia-5,8,11,14-tetraazacycloheptadecan-10-yl)propanoic acid.**

The linear precursor peptide was synthesized on a Fmoc Trp(Boc) TentaGel® S RAM resin (load: 0.2 mmol/g) in a 0.2 mmol scale manually using Fmoc strategy with two coupling cycles and two deprotection cycles as described in the “general Fmoc-SPPS procedure”. The cleavage of the peptide from the resin was performed by the “general cleavage procedure” protocol, where 7 mL cleavage cocktail was used with an incubation of 3 h on a shaker. After lyophilization, 45.7 mg of crude linear product was achieved, which was used for the “general cyclisation procedure” for disulfide cyclisation of the cysteines for 2 days. For purification, the “general preparative HPLC procedure” has been performed. A yield of 2.68 mg pure (≥ 98 %) cyclized peptide (3.05 μmol, 1.53 % according to initial load of the resin) was obtained and characterized by LC-MS, <sup>1</sup>H-NMR, <sup>13</sup>C-NMR and HRMS. LC-MS: Column: Phenomenex Luna C18(2), gradient: MeCN/H<sub>2</sub>O + 0.05 % HCOOH, 5 % MeCN increase to 50% MeCN in 5.1 min, flow rate: 0.6 mL/min, t<sub>R</sub> = 3.75 min, m/z = 878.3 ([M+H]<sup>+</sup>). HRMS (ESI<sup>+</sup>) m/z calculated for C<sub>38</sub>H<sub>55</sub>N<sub>9</sub>O<sub>11</sub>S<sub>2</sub> [M+H]<sup>+</sup> 878.3530; found: 878.3528.



**<sup>1</sup>H-NMR** (500 MHz, dms<sub>o</sub>-d<sub>6</sub>, δ in ppm): 10.82 (bs, 1 H, Indole NH), 8.41 (bs, 1 H, NH), 8.30 (d, <sup>3</sup>J = 7.80 Hz, 1 H, NH), 8.15 (d, <sup>3</sup>J = 8.2 Hz, 1 H, NH), 8.06 (d, <sup>3</sup>J = 6.8 Hz, 1 H, NH), 7.99 (d, <sup>3</sup>J = 6.6 Hz, 1 H, NH), 7.97–7.92 (m, 2 H, NH), 7.56 (d, <sup>3</sup>J<sub>37,36</sub> = 7.9 Hz 1 H, H37), 7.30 (d, <sup>3</sup>J<sub>34,45</sub> = 7.9 Hz, 2 H, H34, NH), 7.12 (m, 2 H, NH, 32H), 7.03 (t, <sup>3</sup>J<sub>35,36/34</sub> = 7.3 Hz, 1 H, H35), 6.95 (t, <sup>3</sup>J<sub>36,35/37</sub> = 7.4 Hz, 1 H, H36), 4.62–4.56 (m, 1 H, H5), 4.55–4.49 (m, 1H, 13-H), 4.43–4.37 (m, 1H, 28H), 4.28–4.24 (m, 1H, 7H), 4.19 (dd, <sup>3</sup>J = 8.8, 6.7 Hz, 1H, 3-H), 4.17–4.09 (m, 2H, 9H, 11H), 3.76–3.62 (m, 2H, 19H), 3.25 (dd, <sup>2</sup>J<sub>15a,15b</sub> = 13.4, <sup>3</sup>J<sub>15a,5</sub> = 4.2 Hz, 1H, H15<sub>a</sub>), 3.13 (dd, <sup>2</sup>J<sub>30a,30b</sub> = 13.4, <sup>3</sup>J<sub>30a,28</sub> = 5.1 Hz, 1H, H30<sub>a</sub>), 3.06–2.93 (m, 4H, H14, H15<sub>b</sub>, H30<sub>b</sub>), 2.23 (t, <sup>3</sup>J<sub>21,20</sub> = 7.9 Hz, 2H, 21H), 2.00–1.90 (m, 3H, 20H, 16H), 1.88 (s, 3H, 1H), 1.60–1.53 (m, 1H, 24H), 1.52–1.47 (m, 2H, 23H), 0.87 (d, <sup>3</sup>J<sub>25,24</sub>, 3H, 25H), 0.85–0.80 (m, 9H, 17H, 18H, 26H).

**<sup>13</sup>C-NMR** (126 MHz, dms<sub>o</sub>-d<sub>6</sub>, δ in ppm): 173.1 (C22), 172.2 (C29), 171.6 (C4), 171.5 (C10), 170.2 (C6, C8 or C12), 169.8 (C6, C8 or C12), 169.5 (C-2), 169.1 (C6, C8 or C12), 136.1 (C33), 127.4 (C38), 123.6 (C32), 120.9 (C35), 118.5 (C37), 118.3 (C36), 111.3 (C34), 110.1 (C31), 61.2 (C19), 57.6 (C3), 55.9 (C7), 54.0 (C9), 53.6 (C28), 52.8 (C13), 52.5 (C5), 52.0 (C-11), 41.9 (C15), 40.7 (C14), 40.1 (C23), 30.6 (C21), 27.7 (C30), 26.9 (C20), 24.3 (C24), 23.1 (C25), 22.6 (C1), 21.6 (C26), 19.3 (C17 or C18), 18.2 (C17 or C18).

### **H-V-[CSELC]<sub>cyclic</sub>-W-NH<sub>2</sub> (2a); 3-((4R,7S,10S,13S,16R)-4-(((S)-1-amino-3-(1H-indol-3-yl)-1-oxopropan-2-yl)carbamoyl)-16-(((S)-2-amino-3-methylbutanamido)-13-(hydroxymethyl)-7-isobutyl-6,9,12,15-tetraoxo-1,2-dithia-5,8,11,14-tetraazacycloheptadecan-10-yl)propanoic acid.**

The linear precursor peptide was synthesized on a Fmoc Trp(Boc) TentaGel® S RAM resin (load: 0.2 mmol/g) in a 0.1 mmol scale manually using Fmoc strategy with two coupling cycles and two deprotection cycles as described in the “general Fmoc-SPPS procedure”. The cleavage of the peptide from the resin was done following the “general cleavage procedure” protocol, where 7 mL cleavage cocktail was used with an incubation of 2.5 h on a shaker. After lyophilization, 87.4 mg of crude linear product was achieved, which was used for the “general cyclisation procedure” for disulfide cyclisation of the cysteines for 2 days. For purification, the “general preparative HPLC procedure” has been performed. A yield of 1.03 mg pure (≥ 93 %) cyclized peptide (1.23 μmol, 1.23 % according to initial load of the resin) was obtained. LC-MS: Column: Phenomenex Luna C18(2), gradient: MeCN/H<sub>2</sub>O + 0.05 % HCOOH, 5 % MeCN increase to 50 % MeCN in 5.1 min, flow rate: 0.6 mL/min, t<sub>R</sub> = 3.15 min, m/z = 834.4 ([M-H]<sup>-</sup>). HRMS (ESI<sup>+</sup>) m/z calculated for C<sub>36</sub>H<sub>53</sub>N<sub>9</sub>O<sub>10</sub>S<sub>2</sub> [M-H]<sup>-</sup> 834.3279; found: 834.3311.

**Ac-V-[CSELC]<sub>cyclic</sub>-W-OH (2b); ((4R,7S,10S,13S,16R)-16-((S)-2-acetamido-3-methylbutanamido)-10-(2-carboxyethyl)-13-(hydroxymethyl)-7-isobutyl-6,9,12,15-tetraoxo-1,2-dithia-5,8,11,14-tetraazacycloheptadecane-4-carbonyl)-L-tryptophan.**

The linear precursor peptide was synthesized on a Fmoc Trp(Boc) TentaGel® S AC resin (load: 0.2 mmol/g) in a 0.05 mmol scale with a microwave-assisted peptide synthesizer (CEM Liberty Lite) using Fmoc strategy with two coupling cycles and two deprotection cycles, including acetylation of the *N*-terminus. The used coupling reagents were Oxyma (0.5 M) and DIC (0.25 M) in DMF. The cleavage of the peptide from the resin was done following the “general cleavage procedure” protocol, where 7 mL cleavage cocktail was used with an incubation of 2.5 h on a shaker. After lyophilization, 14.4 mg of crude uncyclized product was achieved, which was used for the “general cyclisation procedure” for disulfide cyclisation of the cysteines for 3 days. For purification, the “general preparative HPLC procedure” has been performed. A yield of 1.09 mg pure (≥ 98 %) cyclized peptide (1.24 μmol, 2.47 % according to initial load of the resin) was obtained. LC-MS: Column: Phenomenex Luna C18(2), gradient: MeCN/H<sub>2</sub>O + 0.05 % HCOOH, 5 % MeCN increase to 50 % MeCN in 5.1 min, flow rate: 0.6 mL/min, *t*<sub>R</sub> = 3.88 min, *m/z* = 879.3 ([M+H]<sup>+</sup>). HRMS (ESI+) *m/z* calculated for C<sub>38</sub>H<sub>54</sub>N<sub>8</sub>O<sub>12</sub>S<sub>2</sub> [M-H]<sup>-</sup> 877.3224; found: 877.3251.

**Ac-VASELAW-NH<sub>2</sub> (3a); (4S,7S,10S,13S)-13-(((S)-1-(((S)-1-(((S)-1-amino-3-(1H-indol-3-yl)-1-oxopropan-2-yl)amino)-1-oxopropan-2-yl)amino)-4-methyl-1-oxopentan-2-yl)carbonyl)-10-(hydroxymethyl)-4-isopropyl-7-methyl-2,5,8,11-tetraoxo-3,6,9,12-tetraazahexadecan-16-oic acid.**

This linear peptide was synthesized on a Fmoc Trp(Boc) TentaGel® S RAM resin (load: 0.2 mmol/g) in a 0.1 mmol scale manually using Fmoc strategy with two coupling cycles and two deprotection cycles as described in the “General Fmoc-SPPS procedure” followed by the “general acetylation procedure”. The cleavage of the peptide from the resin was done following the “general cleavage procedure” protocol, where 7 mL cleavage cocktail was used with an incubation of 2.5 h on a shaker. For purification, the “general preparative HPLC procedure” has been performed. A yield of 3.24 mg pure (≥ 98 %) peptide (3.97 μmol, 3.97 % according to initial load of the resin) was obtained. LC-MS: Column: Phenomenex Luna C18(2), gradient: MeCN/H<sub>2</sub>O + 0.05 % HCOOH, 5 % MeCN increase to 50 % MeCN in 5.1 min, flow rate: 0.6 mL/min, *t*<sub>R</sub> = 3.57 min, *m/z* = 816.5 ([M+H]<sup>+</sup>). HRMS (ESI+) *m/z* calculated for C<sub>38</sub>H<sub>57</sub>N<sub>9</sub>O<sub>11</sub> [M-H]<sup>-</sup> 814.4099; found: 814.4125.

**Ac-A-[CSELC]<sub>cyclic</sub>-W-NH<sub>2</sub> (3b); 3-((4R,7S,10S,13S,16R)-16-((S)-2-acetamidopropanamido)-4-(((S)-1-amino-3-(1H-indol-3-yl)-1-oxopropan-2-yl)carbonyl)-13-(hydroxymethyl)-7-isobutyl-6,9,12,15-tetraoxo-1,2-dithia-5,8,11,14-tetraazacycloheptadecan-10-yl)propanoic acid.**

The linear precursor peptide was synthesized on a Fmoc Trp(Boc) TentaGel® S RAM resin (load: 0.2 mmol/g) in a 0.2 mmol scale manually using Fmoc strategy with two coupling cycles and two deprotection cycles as described in the “general Fmoc-SPPS procedure” followed by the “general acetylation procedure”. The cleavage of the peptide from the resin was done following the “general cleavage procedure” protocol (in this case TFA/TIS/H<sub>2</sub>O/Anisole 95:2:2:1 as cleavage cocktail), where 3 mL cleavage cocktail was used with an incubation of 3 h on a shaker. After lyophilization, the crude uncyclized product was used for the “general cyclisation procedure” for disulfide cyclisation of the cysteines for 3 days. For purification, the “general preparative HPLC procedure” has been performed. A yield of 1.07 mg pure (≥ 92 %) cyclized peptide (1.26 μmol, 0.63 % according to initial load of the resin) was obtained. LC-MS: Column: Phenomenex Luna C18(2), gradient: MeCN/H<sub>2</sub>O + 0.05 % HCOOH, 5 % MeCN increase to 50 % MeCN in 5.1 min, flow rate: 0.6 mL/min, *t*<sub>R</sub> = 3.38 min, *m/z* = 850.4 ([M+H]<sup>+</sup>). HRMS (ESI+) *m/z* calculated for C<sub>36</sub>H<sub>51</sub>N<sub>9</sub>O<sub>11</sub>S<sub>2</sub> [M-H]<sup>-</sup> 848.3071; found: 848.3097.

**Ac-V-[CAELC]<sub>cyclic</sub>-W-NH<sub>2</sub> (3c); 3-((4R,7S,10S,13S,16R)-16-((S)-2-acetamido-3-methylbutanamido)-4-(((S)-1-amino-3-(1H-indol-3-yl)-1-oxopropan-2-yl)carbonyl)-7-isobutyl-13-methyl-6,9,12,15-tetraoxo-1,2-dithia-5,8,11,14-tetraazacycloheptadecan-10-yl)propanoic acid.**

The linear precursor peptide was synthesized on a Fmoc Trp(Boc) TentaGel® S RAM resin (load: 0.2 mmol/g) in a 0.05 mmol scale with a microwave-assisted peptide synthesizer (CEM Liberty Lite) using Fmoc strategy with two coupling cycles and two deprotection cycles as described in the “general Fmoc-SPPS procedure”, including acetylation of the *N*-terminus. The used coupling reagents were Oxyma (0.5 M) and DIC (0.25 M) in DMF. The cleavage of the peptide from the resin was done following the “general cleavage procedure” protocol, where 7 mL cleavage cocktail was used with an incubation of 2.5 h on a shaker. After lyophilization, the crude uncyclized product was used for the “general cyclisation procedure” for disulfide cyclisation of the cysteines for 7 days. For purification, the “general preparative HPLC procedure” has been performed. A yield of 3.44 mg pure (≥ 98 %) cyclized peptide (3.99 μmol, 7.98 % according to initial load of the resin) was obtained. LC-MS: Column: Phenomenex Luna C18(2), gradient: MeCN/H<sub>2</sub>O + 0.05 % HCOOH, 5 % MeCN increase to 50 % MeCN in 5.1 min, flow rate: 0.6 mL/min, *t*<sub>R</sub> = 3.80 min, *m/z* = 862.4 ([M+H]<sup>+</sup>). HRMS (ESI+) *m/z* calculated for C<sub>38</sub>H<sub>55</sub>N<sub>9</sub>O<sub>10</sub>S<sub>2</sub> [M-H]<sup>-</sup> 860.3435; found: 860.3463.

**Ac-V-[CSALC]<sub>cyclic</sub>-W-NH<sub>2</sub> (3d); (4R,7S,10S,13S,16R)-16-((S)-2-acetamido-3-methylbutanamido)-N-((S)-1-amino-3-(1H-indol-3-yl)-1-oxopropan-2-yl)-13-(hydroxymethyl)-7-isobutyl-10-methyl-6,9,12,15-tetraoxo-1,2-dithia-5,8,11,14-tetraazacycloheptadecane-4-carboxamide.**

The linear precursor peptide was synthesized on a Fmoc Trp(Boc) TentaGel® S RAM resin (load: 0.2 mmol/g) in a 0.2 mmol scale manually using Fmoc strategy with two coupling cycles and two deprotection cycles as described in the “general Fmoc-SPPS procedure” followed by the “general acetylation procedure”. The cleavage of the peptide from the resin was done following the “general cleavage procedure” protocol (in this case TFA/TIS/H<sub>2</sub>O/Anisole 95:2:2:1 as

cleavage cocktail), where 7 mL cleavage cocktail was used with an incubation of 4.5 h on a shaker. After lyophilization, 45 mg of crude uncyclized product was achieved, which was used for the “general cyclisation procedure” for disulfide cyclisation of the cysteines for 10 days. For purification, the “general preparative HPLC procedure” has been performed. A yield of 0.8 mg cyclized peptide (Purity:  $\geq 71\%$ ; 0.98  $\mu\text{mol}$ , 0.49 % according to initial load of the resin) was obtained. LC-MS: Column: Phenomenex Luna C18(2), gradient: MeCN/H<sub>2</sub>O + 0.05 % HCOOH, 5 % MeCN increase to 50 % MeCN in 5.1 min, flow rate: 0.6 mL/min,  $t_R = 3.82$  min,  $m/z = 820.3$  ([M+H]<sup>+</sup>). HRMS (ESI+)  $m/z$  calculated for C<sub>36</sub>H<sub>53</sub>N<sub>9</sub>O<sub>9</sub>S<sub>2</sub> [M-H]<sup>-</sup> 818.3329; found: 818.3356.

**Ac-V-[CSEAC]<sub>cyclic</sub>-W-NH<sub>2</sub> (3e); 3-((4R,7S,10S,13S,16R)-16-((S)-2-acetamido-3-methylbutanamido)-4-(((S)-1-amino-3-(1H-indol-3-yl)-1-oxopropan-2-yl)carbamoyl)-13-(hydroxymethyl)-7-methyl-6,9,12,15-tetraoxo-1,2-dithia-5,8,11,14-tetraazacycloheptadecan-10-yl)propanoic acid.**

The linear precursor peptide was synthesized on a Fmoc Trp(Boc) TentaGel® S RAM resin (load: 0.2 mmol/g) in a 0.1 mmol scale manually using Fmoc strategy with two coupling cycles and two deprotection cycles as described in the “general Fmoc-SPPS procedure” followed by the “general acetylation procedure”. The cleavage of the peptide from the resin was done following the “general cleavage procedure” protocol, where 5 mL cleavage cocktail was used with an incubation of 2 h on a shaker. After lyophilization, 44 mg of crude uncyclized product was achieved, which was used for the “general cyclisation procedure” for disulfide cyclisation of the cysteines for 3 days. For purification, the “general preparative HPLC procedure” has been performed. A yield of 1.21 mg pure ( $\geq 98\%$ ) cyclized peptide (1.45  $\mu\text{mol}$ , 1.45 % according to initial load of the resin) was obtained. LC-MS: Column: Phenomenex Luna C18(2), gradient: MeCN/H<sub>2</sub>O + 0.05 % HCOOH, 5 % MeCN increase to 50 % MeCN in 5.1 min, flow rate: 0.6 mL/min,  $t_R = 3.10$  min,  $m/z = 834.3$  ([M-H]<sup>-</sup>). HRMS (ESI+)  $m/z$  calculated for C<sub>35</sub>H<sub>49</sub>N<sub>9</sub>O<sub>11</sub>S<sub>2</sub> [M-H]<sup>-</sup> 834.2915; found: 834.2944.

**Ac-V-[CSELC]<sub>cyclic</sub>-A-NH<sub>2</sub> (3f); 3-((4R,7S,10S,13S,16R)-16-((S)-2-acetamido-3-methylbutanamido)-4-(((S)-1-amino-1-oxopropan-2-yl)carbamoyl)-13-(hydroxymethyl)-7-isobutyl-6,9,12,15-tetraoxo-1,2-dithia-5,8,11,14-tetraazacycloheptadecan-10-yl)propanoic acid.**

The linear precursor peptide was synthesized on a Fmoc Ala TentaGel® S RAM resin (load: 0.2 mmol/g) in a 0.1 mmol scale manually using Fmoc strategy with two coupling cycles and two deprotection cycles as described in the “general Fmoc-SPPS procedure” followed by the “general acetylation procedure”. The cleavage of the peptide from the resin was done following the “general cleavage procedure” protocol, where 5 mL cleavage cocktail was used with an incubation of 2.5 h on a shaker. After lyophilization, 63 mg of crude uncyclized product was achieved, which was used for the “general cyclisation procedure” for disulfide cyclisation of the cysteines for 3 days. For purification, the “general preparative HPLC procedure” has been performed. A yield of 6 mg pure ( $\geq 98\%$ ) cyclized peptide (7.86  $\mu\text{mol}$ , 7.86 % according to initial load of the resin) was obtained. LC-MS: Column: Phenomenex Luna C18(2), gradient: MeCN/H<sub>2</sub>O + 0.05 % HCOOH, 5 % MeCN increase to 50 % MeCN in 5.1 min, flow rate: 0.6 mL/min,  $t_R = 2.99$  min,  $m/z = 761.3$  ([M-H]<sup>-</sup>). HRMS (ESI+)  $m/z$  calculated for C<sub>30</sub>H<sub>50</sub>N<sub>8</sub>O<sub>11</sub>S<sub>2</sub> [M-H]<sup>-</sup> 761.2985; found: 761.2985.

**Ac- -[CSELC]<sub>cyclic</sub>-W-NH<sub>2</sub> (4a); ((4R,7S,10S,13S,16R)-16-acetamido-10-(2-carboxyethyl)-13-(hydroxymethyl)-7-isobutyl-6,9,12,15-tetraoxo-1,2-dithia-5,8,11,14-tetraazacycloheptadecane-4-carbonyl)-L-tryptophan.**

The linear precursor peptide was synthesized on a Fmoc Trp(Boc) TentaGel® S RAM resin (load: 0.2 mmol/g) in a 0.1 mmol scale manually using Fmoc strategy with two coupling cycles and two deprotection cycles as described in the “general Fmoc-SPPS procedure” followed by the “general acetylation procedure”. The cleavage of the peptide from the resin was done following the “general cleavage procedure” protocol, where 5 mL cleavage cocktail was used with an incubation of 2.75 h on a shaker. The solution was suspended in 1.5 mL DCM. At -20 °C TFA (300  $\mu\text{L}$ , 40 eq.) was added and incubated overnight. After lyophilization, 24 mg of crude uncyclized product was achieved, which was used for the “general cyclisation procedure” for disulfide cyclisation of the cysteines for 2 days. For purification, the “general preparative HPLC procedure” has been performed. A yield of 0.77 mg pure ( $\geq 98\%$ ) cyclized peptide (0.99  $\mu\text{mol}$ , 0.99 % according to initial load of the resin) was obtained. LC-MS: Column: Phenomenex Luna C18(2), gradient: MeCN/H<sub>2</sub>O + 0.05 % HCOOH, 5 % MeCN increase to 50 % MeCN in 5.1 min, flow rate: 0.6 mL/min,  $t_R = 3.39$  min,  $m/z = 777.3$  ([M-H]<sup>-</sup>). HRMS (ESI+)  $m/z$  calculated for C<sub>33</sub>H<sub>46</sub>N<sub>8</sub>O<sub>10</sub>S<sub>2</sub> [M-H]<sup>-</sup> 877.2700; found: 877.2720.

**Ac-V-[CSELC]<sub>cyclic</sub> -NH<sub>2</sub> (4b); (4R,7S,10S,13S,16R)-16-((S)-2-acetamido-3-methylbutanamido)-10-(2-carboxyethyl)-13-(hydroxymethyl)-7-isobutyl-6,9,12,15-tetraoxo-1,2-dithia-5,8,11,14-tetraazacycloheptadecane-4-carboxylic acid.**

The linear precursor peptide was synthesized on a Fmoc Cys(Trt) TentaGel® S RAM resin (load: 0.2 mmol/g) in a 0.1 mmol scale manually using Fmoc strategy with two coupling cycles and two deprotection cycles as described in the “general Fmoc-SPPS procedure” followed by the “general acetylation procedure”. The cleavage of the peptide from the resin was done following the “general cleavage procedure” protocol, where 7 mL cleavage cocktail was used with an incubation of 2.5 h on a shaker. After lyophilization, 55.9 mg of crude uncyclized product was achieved, which was used for the “general cyclisation procedure” for disulfide cyclisation of the cysteines for 3 days. For purification, the “general preparative HPLC procedure” has been performed. A yield of 0.27 mg pure ( $\geq 89\%$ ) cyclized peptide (0.39  $\mu\text{mol}$ , 0.39 % according to initial load of the resin) was obtained. LC-MS: Column: Phenomenex Luna C18(2), gradient: MeCN/H<sub>2</sub>O + 0.05 % HCOOH, 5 % MeCN increase to 50 % MeCN in 5.1 min, flow rate: 0.6 mL/min,  $t_R = 2.99$  min,  $m/z = 690.3$  ([M-H]<sup>-</sup>). HRMS (ESI+)  $m/z$  calculated for C<sub>27</sub>H<sub>45</sub>N<sub>7</sub>O<sub>10</sub>S<sub>2</sub> [M-H]<sup>-</sup> 690.2591; found: 690.2608.



### General Fmoc-SPPS procedure for triazole-bridged peptides 5a, 5b, 5c.

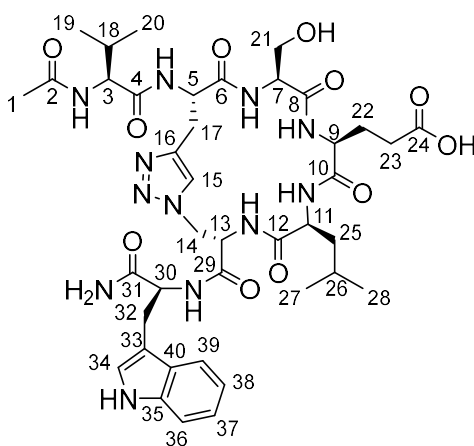
The amino acids were coupled *via* two coupling cycles. For proteinogenic amino acids a solution of the Fmoc protected amino acid (4.0 eq), HBTU (3.9 eq) and DIPEA (8.0 eq) was used. For non-proteinogenic amino acids a solution of the amino acid (3.5 eq), HATU (3.9 eq) and DIPEA (8.0 eq) was used. The resin was shaken 1 h at room temperature before every coupling step was followed by washing steps with DMF (5 x 6 mL) and DCM (5 x 6 mL). Fmoc deprotection was achieved by a reaction with 20 % piperidine in DMF for 5 min at room temperature, followed by a second deprotection step under same conditions. A solution of DMF/DIPEA/Ac<sub>2</sub>O (5:3:2) was given on the resin and shook 30 min at room temperature for the Acetylation of the peptide. The cleavage of the peptide from the resin and removal of the side chain protecting groups was done with a cleavage cocktail of TFA/H<sub>2</sub>O/anisole/TES (47:1:1:1). The mixture was shaken at room temperature for 3 h. After precipitation, the obtained solid was washed with MTBE (4 x 2 mL) and dried by freeze-drying.

### Copper-catalyzed azide-alkyne cycloaddition (CuAAC).

The linear peptide (1.0 eq) was dissolved in argon-flushed H<sub>2</sub>O (1 mL/mg). CuSO<sub>4</sub>·5H<sub>2</sub>O (2.0 eq), Na-ascorbate (4.0 eq) and DIPEA (8.0 eq) were added and the reaction mixture stirred under argon at room temperature overnight. The solvent was removed by freeze-drying and the macrocyclic peptide was purified by preparative HPLC.

### Ac-V-[Pra-SEL-Aza]<sub>cyclic</sub>-W-NH<sub>2</sub> (1,4-triazole) (5a); 3-((3S,6S,9S,12S,15S,Z)-15-((S)-2-acetamido-3-methylbutanamido)-3-(((S)-1-amino-3-(1H-indol-3-yl)-1-oxopropan-2-yl)carbamoyl)-12-(hydroxymethyl)-6-isobutyl-5,8,11,14-tetraoxo-11H-4,7,10,13-tetraaza-1(1,4)-triazolacyclohexadecaphane-9-yl)propanoic acid.

The linear precursor peptide **Ac-V-Pra-SEL-Aza-W-NH<sub>2</sub>** was synthesized manually on a Fmoc Trp(Boc) Tenta Gel S RAM resin (0.20 mmol/g) at 0.10 mmol scale. According to the general Fmoc-SPPS procedure for triazole-bridged peptides, the following amino acids and building blocks were used: Fmoc-L-Aza-OH (0.35 mmol, 3.5 eq), Fmoc-Leu-OH (0.4 mmol, 4.0 eq), Fmoc-Glu(OtBu)-OH (0.4 mmol, 4.0 eq), Fmoc-Ser(tBu)-OH (0.4 mmol, 4.0 eq), Fmoc-Pra-OH (0.35 mmol, 3.5 eq) and Fmoc-Val-OH (0.4 mmol, 4.0 eq). Fmoc-L-Aza-OH and Fmoc-Pra-OH were used together with HATU (0.39 mmol, 3.9 eq) and DIPEA (0.8 mmol, 8.0 eq), while all other amino acids were used together with HBTU (0.39 mmol, 3.9 eq) and DIPEA (0.8 mmol, 8.0 eq). The product was received as a white solid (32.6 mg, 37.0 μmol, 37 % according to the initial load of the resin). According to "Copper-catalyzed azide-alkyne cycloaddition" the macrocyclic peptide was prepared by a reaction of 27.0 mg (30.6 μmol, 1.0 eq) linear precursor peptide, 15.4 mg CuSO<sub>4</sub>·5H<sub>2</sub>O (61.2 μmol, 2.0 eq), 24.4 mg Na-ascorbate (122 μmol, 4.0 eq) and 41.5 μL DIPEA (245 μmol, 8.0 eq). The solvent was removed by freeze-drying. The macrocyclic peptide was purified by preparative HPLC (H<sub>2</sub>O:ACN 9:1→1:1) and was received as a pure (≥ 98 %) white solid (5.10 mg, 5.79 μmol, 19 %). The characterization was done by LC-MS, IR, <sup>1</sup>H-NMR, <sup>13</sup>C-NMR, 2 D NMR and HRMS (m/z). LC-MS: Column: Phenomenex Luna C18(2), gradient: MeCN/H<sub>2</sub>O + 0.05 % HCOOH, 5 % MeCN increase to 50 % MeCN in 5.1 min, flow rate: 0.6 mL/min, t<sub>R</sub> = 3.49 min, m/z = 879.5 ([M-H]<sup>-</sup>). HRMS (ESI<sup>+</sup>) m/z calculated for C<sub>40</sub>H<sub>56</sub>N<sub>12</sub>O<sub>11</sub> [M+H]<sup>+</sup> 881.4270; found: 881.4236.

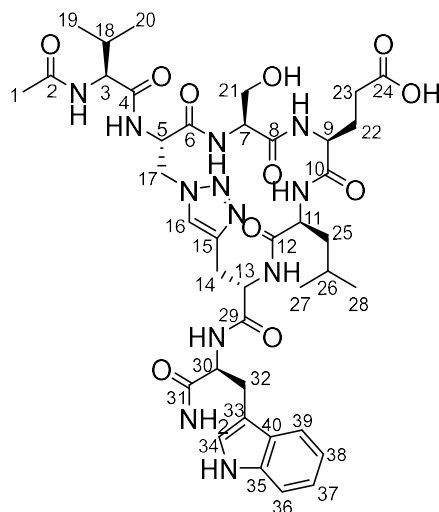


**<sup>1</sup>H-NMR** (500 MHz, CD<sub>3</sub>OD, δ in ppm): 10.0 (bs, 1 H, Indole NH), 8.46-8.55 (m, 1 H, NH), 8.27-8.35 (bs, 1 H, NH), 8.08 (d, <sup>3</sup>J<sub>NH,5</sub> = 8.24 Hz, 1 H, NH), 7.76 – 7.81 (m, 1 H, NH), 7.65 (s, 1 H, H15), 7.60 (d, <sup>3</sup>J<sub>39,38</sub> = 7.78 Hz 1 H, H39), 7.54 (d, <sup>3</sup>J<sub>NH,7</sub> = 8.24 Hz, 1 H, NH), 7.34 (d, <sup>3</sup>J<sub>36,37</sub> = 8.09 Hz, 1 H, H36), 7.09 (dd, <sup>3</sup>J<sub>37,36/38</sub> = 7.68 Hz, 1 H, H37), 7.01-7.04 (m, 1 H, H38), 7.01 (s, 1 H, H34), 4.94-5.01 (m, 1 H, H13), 4.73-4.82 (m, 3 H, H5/H14/H30), 4.59 (bs, 1 H, NH), 4.49 (d, <sup>3</sup>J<sub>14,13</sub> = 3.74 Hz, 1 H, H14), 4.30-4.34 (m, 2 H, H7/H9), 4.26-4.30 (m, 1 H, H3), 3.97-4.08 (m, 2 H, H11/H21), 3.76 (dd, <sup>2</sup>J<sub>21a,21b</sub> = 3.74 Hz, <sup>3</sup>J<sub>21,7</sub> = 11.4 Hz, 1 H, H21), 3.60-3.65 (m, 2 H, H23), 3.38 (dd, <sup>3</sup>J<sub>17a,17b</sub> = 3.74 Hz, <sup>3</sup>J<sub>17,5</sub> = 11.4 Hz, 1 H, H17), 3.19-3.26 (m, 1 H, H17), 3.16 (dd, <sup>3</sup>J<sub>32a,30</sub> = 3.66 Hz, <sup>3</sup>J<sub>32b,30</sub> = 4.88 Hz, 2 H, H32), 2.02-2.19 (m, 2 H, H18/OH), 2.00 (s, 3 H, H1), 1.77-1.94 (m, 2 H, H22), 1.52-1.68 (m, 3 H, H25/H26), 0.97 (dd, <sup>3</sup>J<sub>19/20,18</sub> = 6.48 Hz, 6 H, H19/H20), 0.92 (d, <sup>3</sup>J<sub>27,26</sub> = 6.10 Hz, 3 H, H27), 0.87 (d, <sup>3</sup>J<sub>28,26</sub> = 6.10 Hz, 3 H, H28).

**<sup>13</sup>C-NMR** (126 MHz, CD<sub>3</sub>OD, δ in ppm): 176.9 (C24), 175.3 (C31), 174.6 (C29), 173.8 (C2), 173.7 (C4), 173.1 (C12), 172.7 (C10), 171.1 (C6/C8), 138.2 (C16/C35), 128.9 (C40), 126.2 (C15), 125.0 (C34), 122.7 (C37), 120.1 (C39), 119.6 (C38), 112.4 (C36), 111.3 (C33), 63.5 (C21), 60.4 (C3), 57.0 (C7/C9), 55.9 (C30), 55.3 (C5), 54.3 (C11), 53.7 (C13), 51.3 (C14), 39.9 (C25), 32.1 (C18), 29.2 (C23), 28.6 (C32), 26.7 (C17/C22), 26.2 (C26), 23.5 (C27), 22.6 (C1), 21.6 (C28), 19.9 (C20), 18.8 (C19).

**Ac-V-[Aza-SEL-Pra]<sub>cyclic</sub>-W-NH<sub>2</sub>** (1,4-triazole) (5b); 3-((3*S*,6*S*,9*S*,12*S*,15*S*,*Z*)-15-((*S*)-2-acetamido-3-methylbutanamido)-3-(((*S*)-1-amino-3-(1*H*-indol-3-yl)-1-oxopropan-2-yl)carbamoyl)-12-(hydroxymethyl)-6-isobutyl-5,8,11,14-tetraoxo-11*H*-4,7,10,13-tetraaza-1(4,1)-triazolacyclohexadecaphane-9-yl)propanoic acid.

The linear precursor peptide **Ac-V-Aza-SEL-Pra-W-NH<sub>2</sub>** was synthesized on a microwave-assisted peptide synthesizer (Liberty Lite) using Fmoc Trp(Boc) Tenta Gel S RAM resin (0.20 mmol/g) at 0.05 mmol scale. The engaged amino acids were used in concentrations of 0.2 M in DMF. The used coupling reagents were Oxyma (0.5 M) and DIC (0.25 M) in DMF. The product was received as a white solid (32.0 mg, 36.3 μmol, 73 % according to the initial load of the resin). According to "Copper-catalyzed azide-alkyne cycloaddition" the macrocyclic peptide was prepared by a reaction of 32.0 mg (36.3 μmol, 1.0 eq) linear precursor peptide, 18.6 mg CuSO<sub>4</sub>·5H<sub>2</sub>O (74.5 μmol, 2.05 eq), 28.2 mg Na-ascorbate (142 μmol, 3.92 eq) and 55 μL DIPEA (317 μmol, 8.7 eq). The solvent was removed by freeze-drying. The macrocyclic peptide was purified by preparative HPLC (H<sub>2</sub>O:ACN 9:1→1:1) and was received as a white solid (6.42 mg, 7.29 μmol, 15 %). The characterization was done by LC-MS, <sup>1</sup>H-NMR, <sup>13</sup>C-NMR and HRMS (m/z). LC-MS: Column: Phenomenex Luna C18(2), gradient: MeCN/H<sub>2</sub>O + 0.05 % HCOOH, 5 % MeCN increase to 50 % MeCN in 5.1 min, flow rate: 0.6 mL/min, t<sub>R</sub> = 3.52 min, m/z = 879.4 ([M-H]<sup>-</sup>). HRMS (ESI<sup>+</sup>) m/z calculated for C<sub>40</sub>H<sub>56</sub>N<sub>12</sub>O<sub>11</sub> [M+H]<sup>+</sup> 881.4270; found: 881.4253.

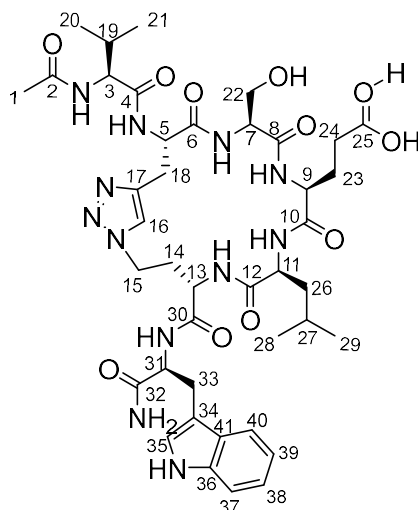


**<sup>1</sup>H-NMR** (500 MHz, CD<sub>3</sub>OD, δ in ppm): 7.64 (d, <sup>3</sup>J<sub>39,38</sub> = 7.9 Hz, 1 H, H39), 7.58 (s, 1 H, H16), 7.34 (d, <sup>3</sup>J<sub>36,37</sub> = 8.1 Hz, 1 H, H36), 7.15 (s, 1 H, H34), 7.09 (t, <sup>3</sup>J<sub>37,36/38</sub> = 7.3 Hz, 1 H, H37), 7.02 (t, <sup>3</sup>J<sub>38,37/39</sub> = 7.4 Hz, 1 H, H38), 5.13-5.09 (m, 1 H, H5), 4.75-4.66 (m, 3 H, H13/H17<sub>a</sub>/H30), 4.62-4.55 (m, 2 H, H9, H11), 4.36 (t, <sup>3</sup>J<sub>17,5</sub> = 3.5 Hz, 1 H, H17<sub>b</sub>), 4.21 (d, <sup>3</sup>J = 7.3 Hz, 1 H, H3), 4.11 (dd, <sup>2</sup>J<sub>21a,21b</sub> = 11.5 Hz, <sup>3</sup>J<sub>21a,7</sub> = 4.2 Hz, 1H, H21<sub>a</sub>), 4.03 (dd, <sup>2</sup>J<sub>32a,32b</sub> = 9.5 Hz, <sup>3</sup>J<sub>32a,30</sub> = 5.6 Hz, 1H, H32<sub>a</sub>), 3.81-3.77 (m, 1H, H32<sub>b</sub>), 3.74 (dd, <sup>2</sup>J<sub>21a,21b</sub> = 11.5, <sup>3</sup>J<sub>21b,7</sub> = 3.0, 1 H, H21<sub>b</sub>), 3.43 (dd, <sup>2</sup>J<sub>14a,14b</sub> = 15.2 Hz, <sup>3</sup>J<sub>14a,13</sub> = 3.9 Hz, 1 H, H14<sub>a</sub>), 3.25-3.18 (m, 1 H, H14<sub>b</sub>), 2.97-2.90 (m, 1H, H23<sub>a</sub>), 2.85-2.78 (m, 1H, H23<sub>b</sub>), 2.31 (br.s, 2 H, H18/OH), 2.12-2.03 (m, 2H, H22), 2.01 (s, 3 H, H1), 1.69-1.61 (m, 1H, 26H), 1.58-1.54 (m, 2 H, 25H), 0.97 (dd, <sup>3</sup>J<sub>19/20,18</sub> = 6.8 Hz, 6 H, H19/H20), 0.92 (d, <sup>3</sup>J<sub>27,26</sub> = 6.5 Hz, 3 H, H27), 0.87 (d, <sup>3</sup>J<sub>28,26</sub> = 6.4 Hz, 3 H, H28).

**<sup>13</sup>C-NMR** (126 MHz, CD<sub>3</sub>OD, δ in ppm): 177.1 (C24), 175.6 (C31), 174.6 (C29), 174.0 (C2), 173.9 (C4), 173.9 (C12), 173.6 (C10), 172.3 (C8), 171.1 (C6), 138.1 (C35), 138.1 (C15), 129.0 (C40), 125.0 (C34), 124.8 (C16), 122.6 (C37), 120.1 (C39), 119.7 (C38), 112.4 (C36), 111.7 (C33), 63.5 (C21), 60.7 (C3), 57.1 (C7/C9), 56.1 (C30), 55.9 (C13), 55.4 (C5), 54.8 (C11), 51.5 (C17), 41.1 (C25), 31.9 (C18), 28.8 (C23), 28.6 (C32), 28.1 (C14/C22), 26.2 (C26), 23.5 (C27), 22.5 (C1), 21.5 (C28), 19.8 (C20), 18.9 (C19).

**Ac-V-[Pra-SEL-Aha]<sub>cyclic</sub>-W-NH<sub>2</sub>** (1,4-triazole) (5c); 3-((3*S*,6*S*,9*S*,12*S*,15*S*,*Z*)-3-(((*S*)-2-acetamido-3-methylbutanamido)-15-(((*S*)-1-amino-3-(1*H*-indol-3-yl)-1-oxopropan-2-yl)carbamoyl)-6-(hydroxymethyl)-12-isobutyl-4,7,10,13-tetraoxo-11*H*-5,8,11,14-tetraaza-1(1,4)-triazolacycloheptadecaphane-9-yl)propanoic acid.

The linear precursor peptide **Ac-V-Pra-SEL-Aha-W-NH<sub>2</sub>** was synthesized on a microwave-assisted peptide synthesizer (Liberty Lite) using Fmoc Trp(Boc) Tenta Gel S RAM resin (0.20 mmol/g) at 0.05 mmol scale. The engaged amino acids were used in concentrations of 0.2 M in DMF. The used coupling reagents were Oxyma (0.5 M) and DIC (0.25 M) in DMF. The product was received as a white solid (35.5 mg, 39.7 μmol, 79 % according to the initial load of the resin). According to "Copper-catalyzed azide-alkyne cycloaddition" the macrocyclic peptide was prepared by a reaction of 35.5 mg (39.7 μmol, 1.0 eq) linear precursor peptide, 20.4 mg CuSO<sub>4</sub>·5H<sub>2</sub>O (81.7 μmol, 2.06 eq), 33.2 mg Na-ascorbate (168 μmol, 4.2 eq) and 55 μL DIPEA (317 μmol, 8.0 eq). The solvent was removed by freeze-drying. The macrocyclic peptide was purified by preparative HPLC (H<sub>2</sub>O:ACN 9:1→1:1) and was received as a pure (≥ 98 %) white solid (8.45 mg, 9.4 μmol, 19 %). The characterization was done by LC-MS, <sup>1</sup>H-NMR, <sup>13</sup>C-NMR and HRMS (m/z). LC-MS: Column: Phenomenex Luna C18(2), gradient: MeCN/H<sub>2</sub>O + 0.05 % HCOOH, 5 % MeCN increase to 50 % MeCN in 5.1 min, flow rate: 0.6 mL/min, t<sub>R</sub> = 3.48 min, m/z = 895.4 ([M+H]<sup>+</sup>). HRMS (ESI<sup>+</sup>) m/z calculated for C<sub>40</sub>H<sub>56</sub>N<sub>12</sub>O<sub>11</sub> [M+H]<sup>+</sup> 895.4426; found: 895.4406.



**<sup>1</sup>H-NMR** (500 MHz, CD<sub>3</sub>OD, δ in ppm): 7.66 (d, <sup>3</sup>J<sub>40,39</sub> = 7.8 Hz, 1 H, H40), 7.39 (s, 1 H, H16), 7.32 (s, 1 H, H35), 7.05 (d, <sup>3</sup>J<sub>37,38</sub> = 8.0 Hz, 1 H, H37), 7.00 (t, <sup>3</sup>J<sub>39,38/40</sub> = 7.3 Hz, 1 H, H39), 6.94 (t, <sup>3</sup>J<sub>38,37/39</sub> = 7.4 Hz, 1 H, H38), 4.85-4.81 (m, 1H, H5), 4.44-4.37 (m, 2H, H9, H31), 4.25-4.18 (m, 2H, H9, H31), 4.13 (d, <sup>3</sup>J<sub>13,14</sub> = 6.1 Hz, 1H, H13), 4.08 (dd, <sup>3</sup>J<sub>11,26</sub> = 4.1 Hz, 1H, H11), 3.89 (dd, <sup>2</sup>J<sub>22a,22b</sub> = 10.3 Hz, <sup>3</sup>J<sub>22a,7</sub> = 5.2 Hz, 1H, H22<sub>a</sub>), 3.54-3.33 (m, 3H, H22<sub>b</sub>, H15), 3.19-3.06 (m, 4H, H18, H33), 2.58 (br.s, 1H, H24), 2.49-2.40 (m, 1H, H14<sub>a</sub>), 2.23 (br.s, 1H, H23), 2.06-2.00 (m, 1H, H19), 1.99 (s, 3H, H1), 1.89-1.81 (m, 1H, H14<sub>b</sub>), 1.66-1.52 (m, 3H, H26, H27), 0.94 (dd, <sup>3</sup>J<sub>20,19/21,19</sub> = 6.6 Hz, 4.6 Hz, 6H, H20, H21), 0.91 (d, <sup>3</sup>J<sub>29,27</sub> = 5.8 Hz, 3H, H29), 0.87 (d, <sup>3</sup>J<sub>28,27</sub> = 6.0 Hz, 3H, H28).

**<sup>13</sup>C-NMR** (126 MHz, CD<sub>3</sub>OD, δ in ppm): 176.9 (C25), 176.0 (C32), 174.8 (C4 or C8 or C30), 174.7 (C4 or C8 or C30), 173.5 (C2 or C6 or C10), 173.4 (C2 or C6 or C10), 173.3 (C2 or C6 or C10), 172.2 (C12, C4 or C8 or C30), 138.0 (C36), 128.5 (C17, C41), 125.3 (C16, C35), 122.5 (C39), 120.0 (C38), 119.6 (C40), 112.3 (C37), 111.4 (C34), 62.4 (C22), 60.0 (C3), 57.2 (C7), 56.6 (C31), 54.9 (C5 or C9 or C11), 54.8 (C5 or C9 or C11), 53.6 (C13), 45.7 (C15), 39.7 (C26), 32.0 (C19), 31.2 (C14), 28.9 (C23, C24), 28.4 (C33), 26.1 (C27), 23.4 (C29), 22.4 (C1), 19.7 (C20 or C21), 18.7 (C20 or C21).

**Ac-V-[Pra-SEL-Aza]<sub>cyclic</sub>-W-NH<sub>2</sub>** (6a); (4S,7S,10S,13S)-13-(((S)-1-(((S)-1-(((S)-1-amino-3-(1H-indol-3-yl)-1-oxopropan-2-yl)amino)-3-(5-methyl-1H-1,2,3-triazol-1-yl)-1-oxopropan-2-yl)amino)-4-methyl-1-oxopentan-2-yl)carbamoyl)-10-(hydroxymethyl)-4-isopropyl-7-methyl-2,5,8,11-tetraoxo-3,6,9,12-tetraazahexadecan-16-oic acid, **Ac-V-[Pra-SEL-Aha]<sub>cyclic</sub>-W-NH<sub>2</sub>** (6b); (4S,7S,10S,13S)-13-(((S)-1-(((S)-1-(((S)-1-amino-3-(1H-indol-3-yl)-1-oxopropan-2-yl)amino)-4-(5-methyl-1H-1,2,3-triazol-1-yl)-1-oxobutan-2-yl)amino)-4-methyl-1-oxopentan-2-yl)carbamoyl)-10-(hydroxymethyl)-4-isopropyl-7-methyl-2,5,8,11-tetraoxo-3,6,9,12-tetraazahexadecan-16-oic acid and **Ac-V[Aha-SEL-Pra]<sub>cyclic</sub>-W-NH<sub>2</sub>** (6c); 3-(((S)-1-amino-3-(1H-indol-3-yl)-1-oxopropan-2-yl)carbamoyl)-12-(hydroxymethyl)-6-isobutyl-5,8,11,14-tetraoxo-11H-4,7,10,13-tetraaza-1(4,1)-triazolacycloheptadecaphane-9-yl)propanoic acid.

Each peptide was manually synthesized by Fmoc-SPPS using Rink amide-MBHA resin (0.8 mmol loading, 100-200 mesh, Chempep Inc). Fmoc-protected amino acids (Fmoc-Trp(Boc)-OH, Fmoc-Leu-OH, Fmoc-Glu(OtBu)-OH, Fmoc-Ser(tBu)-OH, Fmoc-Val-OH) were purchased from either Mimotopes or CSBio, and the azide and alkyne precursors (Fmoc-Aza-OH, Fmoc-Aha-OH and Fmoc-Pra-OH) were purchased from Chem-Impex International Inc. The peptides were synthesized on a 0.25 mmol scale and the resins were first swelled in DMF for 30 min prior to Fmoc deprotection (standard condition used throughout assembly: 20 % piperidine, 5 mL, 15 min). Each amino acid was coupled using 4.0 eq. of amino acid, 4.0 eq. of benzotriazol-1-yl-oxytripyrrolidinophosphonium hexafluorophosphate (PyBOP) and 8.0 eq. of *N,N*-

diisopropylethylamine (DIPEA) in 3 mL of DMF, shaken for 45 min. The resin was washed with DMF (3 x 5 mL) and DCM (3 x 5 mL) between each deprotection and coupling step. Following assembly of the sequences, the *N*-terminus was acetylated using acetic anhydride/DMF (1:4, 6 mL) and 2 eq. of DIPEA, shaken for 45 min. The resin was then washed thoroughly in DMF (5 x 5 mL) and DCM (5 x 5 mL), dried under a stream of N<sub>2</sub> and stored in a desiccator overnight.

The crude peptide-bound resin was next subject to ruthenium-catalyzed azide-alkyne cycloaddition (RuAAC) to install the 1,5-disubstituted 1,2,3-triazole bridge. For each analogue, 75 μmol of resin-bound peptide (**6a**: 160 mg; **6b**: 170 mg; and **6c**: 170 mg; based on initial resin loading) was loaded into a glass vessel and suspended in 2 mL of anhydrous DMF. The mixture was sparged with argon for 30 min prior to the addition of 50 mol% of chloro(pentamethylcyclopentadienyl)(cyclooctadiene)ruthenium(II) (14.2 mg, 37.5 μmol). The reaction was heated to 80 °C for 18 h under an atmosphere of argon. The resin was thoroughly washed with DMF (3 x 5 mL), 0.5 % sodium diethyldithiocarbamate trihydrate in DMF (w/v, 3 x 5 mL), MeOH (3 x 5 mL), and DCM (5 x 5 mL) and dried under N<sub>2</sub>. The peptides were next cleaved from the resin by suspending the resin in 5 mL of TFA/TIS/H<sub>2</sub>O (95:2.5:2.5, v/v/v) for 2 h, followed by precipitation with cold Et<sub>2</sub>O before being redissolved in 50 % MeCN and lyophilized. The peptide was next purified to >95 % purity by preparative RP-HPLC on a Shimadzu Prominence system with a Phenomenex Gemini C-18 column (5 μm, 250 x 10 mm) using a gradient of 20-50 % Solvent B (Solvent A: H<sub>2</sub>O with 0.05 % trifluoroacetic acid; Solvent B: 95 % acetonitrile with 0.05 % trifluoroacetic acid) at 3 mL/min. The lyophilized peptides were obtained as a white solid (**6a**: purity: ≥ 95 %\*, 0.67 mg, 0.76 μmol, 1.0 % overall yield based on the initial resin loading; **6b**: purity: ≥ 98 %, 1.72 mg, 1.92 μmol, 2.6 %; and **6c**: purity: ≥ 98 %, 1.40 mg, 1.56 μmol, 2.1 %) and further characterized by LC-MS, <sup>1</sup>H-NMR and HRMS.

**6a**: HRMS (ESI+) *m/z* calculated for C<sub>40</sub>H<sub>56</sub>N<sub>12</sub>O<sub>11</sub> [M+H]<sup>+</sup> 881.4270; found: 881.4280.

**6b**: LC-MS: Column: Phenomenex Luna C18(2), gradient: MeCN/H<sub>2</sub>O + 0.05 % HCOOH, 5 % MeCN increase to 50 % MeCN in 5.1 min, flow rate: 0.6 mL/min, *t<sub>R</sub>* = 3.52 min, *m/z* = 895.4 ([M+H]<sup>+</sup>). HRMS (ESI+) *m/z* calculated for C<sub>41</sub>H<sub>58</sub>N<sub>12</sub>O<sub>11</sub> [M+H]<sup>+</sup> 895.4426; found: 895.4428.

**6c**: LC-MS: Column: Phenomenex Luna C18(2), gradient: MeCN/H<sub>2</sub>O + 0.05 % HCOOH, 5 % MeCN increase to 50 % MeCN in 5.1 min, flow rate: 0.6 mL/min, *t<sub>R</sub>* = 3.52 min, *m/z* = 895.4 ([M+H]<sup>+</sup>). HRMS (ESI+) *m/z* calculated for C<sub>41</sub>H<sub>58</sub>N<sub>12</sub>O<sub>11</sub> [M+H]<sup>+</sup> 895.4426; found: 895.4402.

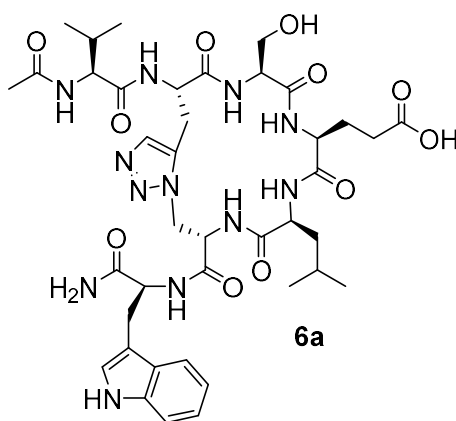


**Table S1.** NMR chemical shifts of **6a**.

Residue	H	N	H $\alpha$	H $\beta$	Others
1 Val	8.08	114.1	4.04	1.97	0.88 H $\gamma$ 1; 0.87 H $\gamma$ 2; 59.8 C $\alpha$ ; 30.0 C $\beta$ ; 17.7 C $\gamma$ 1; 18.3 C $\gamma$ 2; Ac: 1.97 3H, 21.7 CH <sub>3</sub>
2 Pra	8.73	123.5	4.73	3.02, 3.16	7.63 H $\delta$ ; 25.5 C $\beta$ ; 133.3 C $\delta$
3 Ser	7.87	118.1	4.20	3.75, 3.85	56.1 C $\alpha$ ; 60.3 C $\beta$
4 Glu	8.40	120.9	3.86	1.91 (2H)	2.16 H $\gamma$ (2H); 56.1 C $\alpha$ ; 26.4 C $\beta$ ; 33.3 C $\gamma$
5 Leu	7.73	118.6	4.09	1.25 (2H)	1.39 H $\gamma$ ; 0.74 H $\delta$ 1; 0.77 H $\delta$ 2; 52.5 C $\alpha$ ; 39.5 C $\beta$ ; 24.3 C $\gamma$ ; 20.6 C $\delta$ 1; 22.2 C $\delta$ 2
6 Aza	8.08	125.5	5.04	4.39 (2H)	52.2 C $\alpha$ ; 47.3 C $\beta$
7 Trp	7.93	123.5	4.74	3.14, 3.32	128.9 N $\epsilon$ 1; 7.13 H $\delta$ 1; 9.98 H $\epsilon$ 1; 7.58 H $\epsilon$ 3; 7.41 H $\zeta$ 2; 7.06 H $\zeta$ 3; 7.16 H $\eta$ 2; 27.0 C $\beta$ ; 124.6 C $\delta$ 1; 118.4 C $\epsilon$ 3; 112.0 C $\zeta$ 2; 119.4 C $\zeta$ 3; 122.03 C $\eta$ 2; NH <sub>2</sub> : 7.09 H1, 7.43 H2, 108.0 N

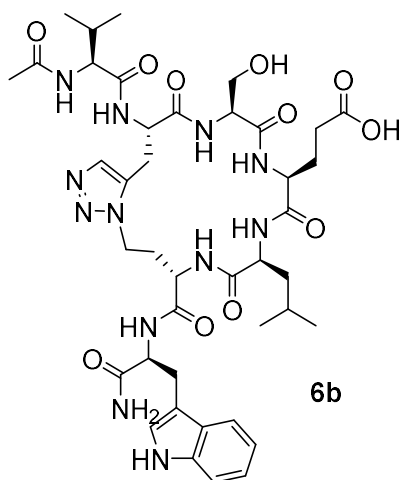


**Table S2.** NMR chemical shifts of **6b**.

Residue	H	N	H $\alpha$	H $\beta$	Others
1 Val	8.07	125.6	3.94	1.91	0.81 H $\gamma$ 1; 0.83 H $\gamma$ 2; 60.0 C $\alpha$ ; 29.8 C $\beta$ ; 18.3 C $\gamma$ 1; 17.9 C $\gamma$ 2; Ac: 1.95 3H, 21.6 CH $_3$
2 Pra	8.78	123.5	4.77	3.38, 3.11	7.54 H $\delta$ ; 25.6 C $\beta$ ; 131.7 C $\delta$
3 Ser	8.59	118.2	4.26	3.89, 3.81	57.1 C $\alpha$ ; 60.7 C $\beta$
4 Glu	7.87	119.3	4.37	2.07, 1.85	2.29 H $\gamma$ (2H); 52.2 C $\alpha$ ; 27.2 C $\beta$ ; 30.5 C $\gamma$
5 Leu	7.95	119.8	3.98	1.45, 1.35	1.41 H $\gamma$ ; 0.73 H $\delta$ 1; 0.79 H $\delta$ 2; 53.9 C $\alpha$ ; 39.2 C $\beta$ ; 24.3 C $\gamma$ ; 21.4 C $\delta$ 1; 21.7 C $\delta$ 2
6 Aha	8.33	121.8	4.40	2.24, 1.82	4.16 H $\gamma$ 1; 4.25 H $\gamma$ 2; 50.7 C $\alpha$ ; 31.7 C $\beta$ ; 44.1 C $\gamma$
7 Trp	7.99	121.4	4.62	3.27, 3.13	129.1 N $\epsilon$ 1; 7.14 H $\delta$ 1; 10.01 H $\epsilon$ 1; 7.55 H $\epsilon$ 3; 7.34 H $\zeta$ 2; 7.02 H $\zeta$ 3; 7.09 H $\eta$ 2; 27.2 C $\beta$ ; 124.6 C $\delta$ 1; 118.3 C $\epsilon$ 3; 112.0 C $\zeta$ 2; 119.3 C $\zeta$ 3; 122.0 C $\eta$ 2; NH $_2$ : 7.02 H1, 7.46 H2, 108.2 N

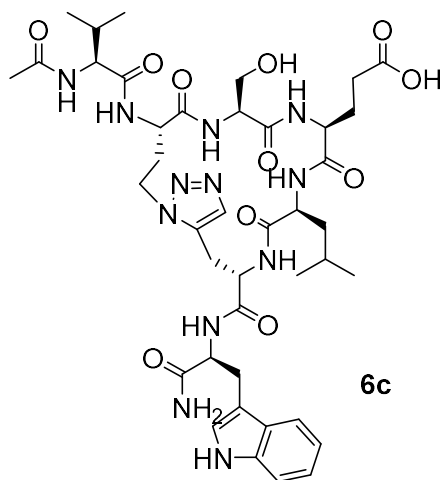


**Table S3.** NMR chemical shifts of **6c**.

Residue	H	N	H $\alpha$	H $\beta$	Others
1 Val	8.02	124.5	4.07	2.02	0.87 H $\gamma$ 1; 0.86 H $\gamma$ 2; 62.2 C $\alpha$ ; 32.6 C $\beta$ ; 21.2 C $\gamma$ 1; 20.1 C $\gamma$ 2; Ac 1.96 3H, 24.4 CH $_3$
2 Aha	8.70	124.4	4.08	2.27, 2.61	3.71 H $\gamma$ (2H); 46.1 C $\alpha$ ; 32.3 C $\beta$ ; 54.8 C $\gamma$
3 Ser	8.18	117.7	4.23	3.96, 3.79	59.5 C $\alpha$ ; 63.2 C $\beta$
4 Glu	7.88	118.5	4.15	2.00 (2H)	2.36 H $\gamma$ 2 (2H); 57.6 C $\alpha$ ; 28.7 C $\beta$ ; 33.3 C $\gamma$
5 Leu	7.58	118.1	4.11	1.02, 1.24	1.43 H $\gamma$ ; 0.69 H $\delta$ 1; 0.72 H $\delta$ 2; 56.2 C $\alpha$ ; 42.9 C $\beta$ ; 26.8 C $\gamma$ ; 24.8 C $\delta$ 1; 23.0 C $\delta$ 2
6 Pra	7.98	117.0	4.62	2.89 (2H)	7.43 H $\delta$ ; 26.84 C $\beta$ ; 134.7 C $\delta$
7 Trp	7.68	121.1	4.62	3.16, 3.31	128.8 N $\epsilon$ 1; 7.14 H $\delta$ 1; 10.0 H $\epsilon$ 1; 7.5 H $\epsilon$ 3; 7.41 H $\zeta$ 2; 7.06 H $\zeta$ 3; 7.16 H $\eta$ ; 29.8 C $\beta$ ; 127.3 C $\delta$ 1; 121.1 C $\epsilon$ 3; 114.6 C $\zeta$ 2; 122.1 C $\zeta$ 3; 124.6 C $\eta$ 2; NH $_2$ : 7.03 H1, 7.33 H2, 107.7 N

**Table S4.** Key facts about the synthesis of the individual peptides. Starting from the used resin over cleavage cocktail and cyclization and yield.

Peptide	Resin	Approach	Manually/ synthesizer	Cleavage cocktail	Crude linear peptide yield	Cyclisation	Yield after prep HPLC	Purity <sup>[a]</sup>
<b>1</b>	Fmoc Trp(Boc) TentaGel® S RAM	0.2 mmol	Manually	TFA/TIS/H $_2$ O (37:1:1) + DTT, 7 mL, 3 h	45.7 mg	ACN/H $_2$ O (1:1) 1 mg/mL, 2 % DMSO, 2 days	2.68 mg	≥98%
<b>2a</b>	Fmoc Trp(Boc) TentaGel® S RAM	0.1 mmol	Manually	TFA/TIS/H $_2$ O (37:1:1) + DTT, 7 mL, 2.5 h	87.4 mg	ACN/H $_2$ O (1:1) 1 mg/mL, 2 % DMSO, 2 days	1.03 mg	≥98%
<b>2b</b>	Fmoc Trp(Boc) TentaGel® S AC	0.05 mmol	Synthesizer	TFA/TIS/H $_2$ O (37:1:1) + DTT, 7 mL, 2.5 h	14.4 mg	ACN/H $_2$ O (1:1) 1 mg/mL, 2 % DMSO, 3 days	1.09 mg	≥98%
<b>3a</b>	Fmoc Trp(Boc) TentaGel® S RAM	0.1 mmol	Manually	TFA/TIS/H $_2$ O (37:1:1) + DTT, 7 mL, 2.5 h	n.d.	--	3.24 mg	≥98%
<b>3b</b>	Fmoc Trp(Boc) TentaGel® S RAM	0.2 mmol	Manually	TFA/TIS/H $_2$ O/Anisole (95:2:2:1), 3 mL, 3 h	n.d.	ACN/H $_2$ O (1:1) 1 mg/mL, 2 % DMSO, 3 days	1.07 mg	≥95%
<b>3c</b>	Fmoc Trp(Boc) TentaGel® S RAM	0.05 mmol	Synthesizer	TFA/TIS/H $_2$ O (37:1:1) + DTT, 7 mL, 2.5 h	n.d.	ACN/H $_2$ O (1:1) 1 mg/mL, 3 % DMSO, 7 days	3.44 mg	≥98%
<b>3d</b>	Fmoc Trp(Boc) TentaGel® S RAM	0.2 mmol	Manually	TFA/TIS/H $_2$ O/Anisole (95:2:2:1) + DTT, 7 mL, 4.5 h	45 mg	ACN/H $_2$ O (2:1) 0.17 mg/mL, 1 % DMSO, 10 days	0.8 mg	≥91% <sup>[b]</sup>
<b>3e</b>	Fmoc Trp(Boc) TentaGel® S RAM	0.1 mmol	Manually	TFA/TIS/H $_2$ O (37:1:1) + DTT, 5 mL, 2 h	44 mg	ACN/H $_2$ O (1:1) 1 mg/mL, 2 % DMSO, 3 days	1.21 mg	≥98%
<b>3f</b>	Fmoc Ala TentaGel® S RAM resin	0.1 mmol	Manually	TFA/TIS/H $_2$ O (37:1:1) + DTT, 5 mL, 2.5 h	63 mg	ACN/H $_2$ O (1:1) 1 mg/mL, 2 % DMSO, 3 days	6 mg	≥98%
<b>4a</b>	Fmoc Trp(Boc) TentaGel® S RAM	0.1 mmol	Manually	TFA/TIS/H $_2$ O (37:1:1) + DTT, 5 mL, 2.75 h	24 mg	ACN/H $_2$ O (1:1) 1 mg/mL, 2 % DMSO, 2 days	0.77 mg	≥98%
<b>4b</b>	Fmoc Cys(Trt) TentaGel® S RAM resin	0.1 mmol	Manually	TFA/TIS/H $_2$ O (37:1:1) + DTT, 7 mL, 2.5 h	55.9 mg	ACN/H $_2$ O (1:1) 1 mg/mL, 2 % DMSO, 3 days	0.27 mg	≥92%
<b>5a</b>	Fmoc Trp(Boc) TentaGel® S RAM	0.1 mmol	Manually	TFA/H $_2$ O/anisole/TE S (47:1:1:1), 3 h	32.6 mg	CuAAC	5.1 mg	≥98%
<b>5b</b>	Fmoc Trp(Boc) TentaGel® S RAM	0.05 mmol	Synthesizer	TFA/H $_2$ O/anisole/TE S (47:1:1:1), 3 h	32 mg	CuAAC	6.42 mg	≥98%

<b>5c</b>	Fmoc Trp(Boc) TentaGel® S RAM	0.05 mmol	Synthesizer	TFA/H <sub>2</sub> O/anisole/TE S (47:1:1:1), 3 h	35.5 mg	CuAAC	8.45 mg	≥98%
<b>6a/6b/6c</b>	Rink amide- MBHA resin	0.25 mmol	Manually	TFA/TIS/H <sub>2</sub> O (95:2.5:2.5, v/v/v), 2 h	160 mg / 170 mg / 170 mg	RuAAC	0.67 mg / 1.72 mg / 1.4 mg	≥95% / ≥98% / ≥98%

[a] Determined by LC-MS. [b] This peptide was very poorly soluble, therefore the cyclization reaction had to be diluted and carried out with a higher ACN amount. This also prolonged the cyclization time significantly. In addition, many side products were formed, which could not be separated easily, which explains the lower purity of ≥ 91 %.

## Expression of *Y. pseudotuberculosis* CsrA-biot-His<sub>6</sub>

The expression protocol of *Yersinia pseudotuberculosis* CsrA-biot-His<sub>6</sub> has already been published by Christine Maurer *et al.*[1] Two plasmids were transformed into electro competent *E. coli* BL21 by performing a double transformation. On the one hand pET28a with pAKH172\_biotag insert for overexpression of His- and biotin-tagged CsrA and on the other hand pBirAcm for overexpression of biotin ligase for *in vivo* biotinylation at the lysine residue of the biotintag. pET28a has a kanamycin resistance, pBirAcm a chloramphenicol resistance. The amino acid sequence for the CsrA-biot-His<sub>6</sub> construct is MLILTRRVGE TLMIGDEVTV TVLGVKGNQV RIGVNAPKEV SVHREEIYQR IQAESQPTT YLEGLNDIFE AQKIEWHELE HHHHHH. Biotin tag and His tag are underlined. The molecular weight of the CsrA-biot-His<sub>6</sub> monomer is 10.2 kDa.

4 L of LB medium, containing 50 µg/mL kanamycin and 17 µg/mL chloramphenicol, were inoculated with an overnight preculture. This main culture was grown at 37 °C and 180 rpm until an O.D. 600 of 0.6 was reached. Then, 10 mL 5 mM biotin (50 µM end concentration), 3 mL 3 M MgCl<sub>2</sub> (10 mM end concentration) and 1.19 mL 0.84 M IPTG (1 mM end concentration) per liter of culture was added. The culture was grown again at 37 °C, 180 rpm overnight. Cells were harvested by centrifugation (4 °C, 6200 rpm, 20 min). The pellets were resuspended in 4.5 mL/g wet cells lysis buffer (50 mM dipotassium hydrogen phosphate trihydrate, 300 mM sodium chloride, 10 mM imidazole, pH 8.0) containing cOplete™ (EDTA-free protease inhibitor cocktail, Roche). Afterwards the cells were disrupted by one passage through a microfluidizer. After centrifugation of the homogenisate (4 °C, 19000 rpm, 1 h), the supernatant was sterile-filtered through 0.22 µm membrane filter. For purification an ÄKTExpress™ device with a 1 mL HisTrap™ HP column was used, which was equilibrated with 20 mL lysis buffer (4 mL/min flowrate). The clear lysate was loaded on the column with 1 mL/min. This was followed by two washing steps, first 15 mL of high salt buffer (50 mM dipotassium hydrogen phosphate trihydrate, 1 M sodium chloride, 10 mM imidazole, pH 8.0), second 20 mL of binding buffer (50 mM dipotassium hydrogen phosphate trihydrate, 300 mM sodium chloride, 30 mM imidazole, pH 8.0). Next, a linear gradient from 0 to 70 % elution buffer (25 mM dipotassium hydrogen phosphate trihydrate, 150 mM sodium chloride, 125 mM imidazole, pH 8.0) within 56 min was chosen. For the final elution step, it was switched to 100 % elution buffer and the fractions were collected. The CsrA-containing fractions were concentrated via Vivaspin® 20 spin filters (3 kDa MWCO, Sartorius™), before the buffer was exchanged to storage buffer (50 mM dipotassium hydrogen phosphate trihydrate, 300 mM sodium chloride, ad DEPC-treated water (RNase-free), pH 8.0) with a PD10 desalting column. The concentration was determined by UV spectroscopy with NanoDrop™ ( $\epsilon_{280} = 8480 \text{ M}^{-1}\text{cm}^{-1}$ , monomer). If required, the united fractions were concentrated again with Vivaspin® 20 spin filters (3 kDa MWCO, Sartorius™) to adjust a monomer concentration of about 200 µM. Glycerol (10 % end concentration) was added to the protein and divided into aliquots, flash frozen in liquid nitrogen and stored at -80 °C. About 2 mg protein per liter of main culture were yielded.

## Expression of *E. coli* CsrA-His<sub>6</sub>

The amino acid sequence for the *Escherichia coli* CsrA-His<sub>6</sub> construct is MLILTRRVGE TLMIGDEVTV TVLGVKGNQV RIGVNAPKEV SVHREEIYQR IQAESQSSY HHHHH. The molecular weight of the CsrA-His<sub>6</sub> monomer is 7.68 kDa. The construct is present in pET21a+ with an ampicillin resistance. The expression protocol of *E. coli* CsrA-His<sub>6</sub> is based on Dubey *et al.*[2]

TB medium, containing 100 µg/mL ampicillin, were inoculated with an overnight preculture. This main culture was grown at 37 °C and 180 rpm until an O.D. 600 of 0.6 was reached. Then, 1.19 mL 0.84 M IPTG (1 mM end concentration) per liter of culture was added. The culture was grown again at 37 °C, 180 rpm overnight. Cells were harvested by centrifugation (4 °C, 6200 rpm, 20 min). The pellets were resuspended in 4.5 mL/g wet cells lysis buffer (50 mM potassium dihydrogen phosphate, 300 mM sodium chloride, 10 mM imidazole, 10 % glycerol, pH 8.0) containing cOplete™ (EDTA-free protease inhibitor cocktail, Roche). Afterwards the cells were disrupted by ultra-sonification (current = 50 %, every 30 sec and 5 cycles, break between every 5 cycles). After centrifugation of the homogenisate (4 °C, 19000 rpm, 1 h), the supernatant was sterile-filtered through 0.22 µm membrane filter. For purification an ÄKTExpress™ device with a 1 mL HisTrap™ HP column was used, which was equilibrated with 20 mL lysis buffer (4 mL/min flowrate). The clear lysate was loaded on the column with 1 mL/min. This was followed by three washing steps, first washing buffer 1 (50 mM potassium

dihydrogen phosphate, 300 mM sodium chloride, 20 mM imidazole, 10 % glycerol, pH 8.0), second two times washing buffer 2 (50 mM potassium dihydrogen phosphate, 300 mM sodium chloride, 50 mM imidazole, 10 % glycerol, pH 8.0). The elution was done with elution buffer (50 mM potassium dihydrogen phosphate, 300 mM sodium chloride, 250 mM imidazole, 10 % glycerol, pH 8.0) and the fractions were collected. The CsrA-containing fractions were concentrated via Vivaspin® 20 spin filters (3 kDa MWCO, Sartorius™), before the buffer was exchanged to storage buffer (50 mM dipotassium hydrogen phosphate trihydrate, 300 mM sodium chloride, ad DEPC-treated water (RNase-free), pH 8.0) with a PD10 desalting column. The concentration was determined by UV spectroscopy with NanoDrop™ ( $\epsilon_{280} = 2980 \text{ M}^{-1}\text{cm}^{-1}$ , monomer). If required, the united fractions were concentrated again with Vivaspin® 20 spin filters (3 kDa MWCO, Sartorius™) to adjust a monomer concentration of about 200  $\mu\text{M}$ . Glycerol (10 % end concentration) was added to the protein and divided into aliquots, flash frozen in liquid nitrogen and stored at -80 °C.

## Expression of *P. aeruginosa* RsmA-His<sub>6</sub>

The amino acid sequence for the *Pseudomonas aeruginosa* RsmA-His<sub>6</sub> construct is MLILTRRVGE TLMVGDDVTV TVLGVKGNQV RIGVNAPKEV AVHREEIYQRI QKEKDQEPNHKLE HHHHHH. The molecular weight of the RsmA-His<sub>6</sub> monomer is 8.1 kDa. The construct is present in pET28a with an kanamycin resistance. The expression protocol of *P. aeruginosa* RsmA-His<sub>6</sub> is based on Jean-Pierre *et al.* but with variations. [3]

TSB medium, containing 50  $\mu\text{g}/\text{mL}$  kanamycin, were inoculated with an overnight preculture. This main culture was grown at 37 °C and 180 rpm until an O.D. 600 of 0.7 was reached. Then, 2 mL 0.5 M IPTG (1 mM end concentration) per liter of culture was added. The culture was grown again at 37 °C, 180 rpm for 4 h. Cells were harvested by centrifugation (4 °C, 6200 rpm, 30 min). The pellets were resuspended in 4.5 mL/g wet cells lysis buffer (20 mM potassium dihydrogen phosphate, 500 mM sodium chloride and 20 mM Tris/HCL, pH 7.65). Afterwards the cells were disrupted by ultrasonification (current = 50 %, every 30 sec and 5 cycles, break between every 5 cycles). After centrifugation of the homogenisate (4 °C, 15 0000 g, 45 min), the supernatant was sterile-filtered through 0.22  $\mu\text{m}$  membrane filter. For purification an ÄKTAexpress™ device with a 1 mL HisTrap™ HP column was used, which was equilibrated with 20 mL lysis buffer (1 mL/min flowrate). The clear lysate was loaded on the column with 1 mL/min. This was followed by three washing steps, first washing buffer 1 (50 mM potassium dihydrogen phosphate, 300 mM sodium chloride, 20 mM imidazole, 10 % glycerol, pH 8.0), second two times washing buffer 2 (50 mM potassium dihydrogen phosphate, 300 mM sodium chloride, 50 mM imidazole, 10 % glycerol, pH 8.0). The elution was done with elution buffer (50 mM potassium dihydrogen phosphate, 300 mM sodium chloride, 250 mM imidazole, 10 % glycerol, pH 8.0) and the fractions were collected. The RsmA-containing fractions were concentrated via Vivaspin® 20 spin filters (5 kDa MWCO, Sartorius™), before the buffer was exchanged to storage buffer (10 mM Tris/HCl, 33% glycerol, pH 7.65) with a PD10 desalting column. The concentration was determined by UV spectroscopy with NanoDrop™ ( $\epsilon_{280} = 2980 \text{ M}^{-1}\text{cm}^{-1}$ , monomer). The protein was divided into aliquots, flash frozen in liquid nitrogen and stored at -80 °C.

## Sequence Identities (BLAST).

### Sequence identity RsmA(*P.aeruginosa*) – CsrA(*E.coli*) = 85%

Method:Compositional matrix adjust.,

Identities:52/61(85%), Positives:58/61(95%), Gaps:0/61(0%)

```
Query 1 MLILTRRVGETLMVGDDVTVTVLGVKGNQVRIGVNAPKEVAVHREEIYQRIQKEKDQEPN 60
      MLILTRRVGETLM+GD+VTVTVLGVKGNQVRIGVNAPKEV+VHREEIYQRIQ EK Q+ +
Sbjct 1 MLILTRRVGETLMIGDEVTVTVLGVKGNQVRIGVNAPKEVSVHREEIYQRIQAEKSQQSS 60

Query 61 H 61
      +
Sbjct 61 Y 61
```

### Sequence identity CsrA(*Y. pseudotuberculosis*) – RsmA(*P.aeruginosa*) = 86%

Method:Compositional matrix adjust.,

Identities:55/64(86%), Positives:58/64(90%), Gaps:1/64(1%)

```
Query 1 MLILTRRVGETLMIGDEVTVTVLGVKGNQVRIGVNAPKEVSVHREEIYQRIQAEKSQ-PT 59
      MLILTRRVGETLM+GD+VTVTVLGVKGNQVRIGVNAPKEV+VHREEIYQRIQ EK Q P
Sbjct 1 MLILTRRVGETLMVGDDVTVTVLGVKGNQVRIGVNAPKEVAVHREEIYQRIQKEKDQEPN 60

Query 60 TYLE 63
      LE
Sbjct 61 HKLE 64
```



### Sequence identity CsrA(*Y. pseudotuberculosis*) – CsrA(*E.coli*) = 95%

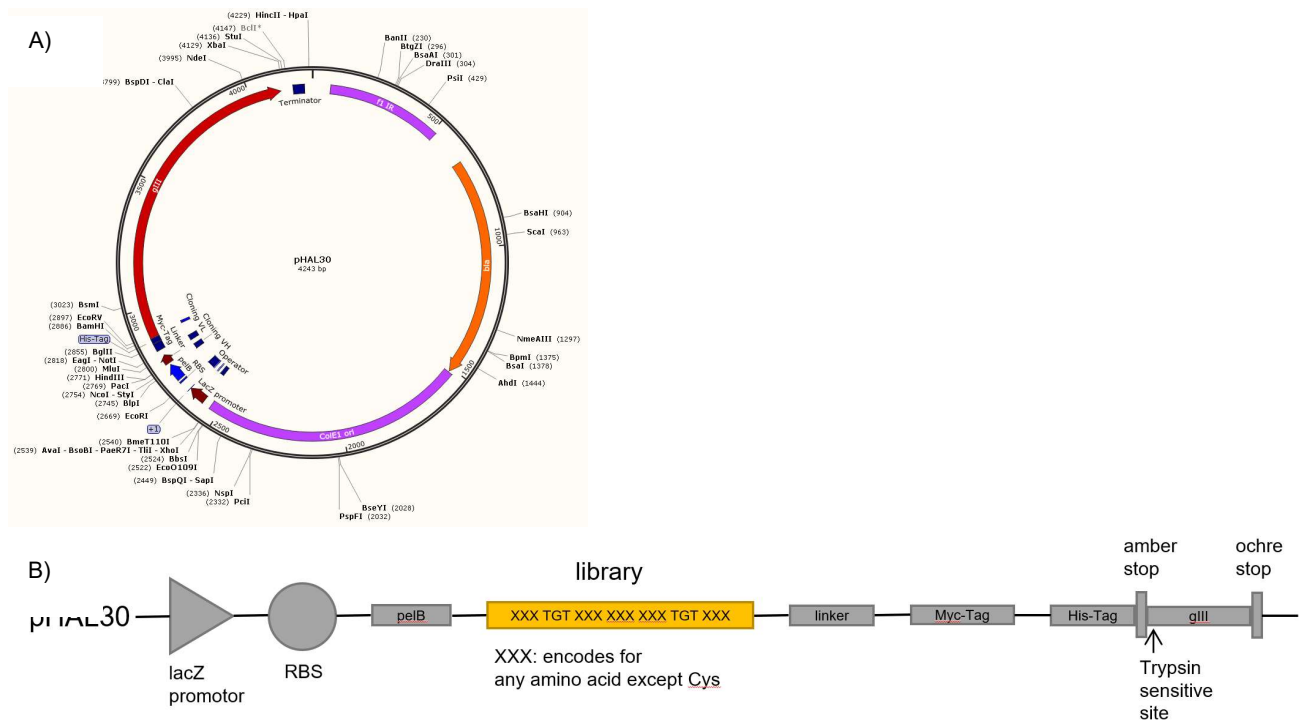
Method: Compositional matrix adjust.,

Identities: 58/61 (95%), Positives: 60/61 (98%), Gaps: 0/61 (0%)

```
Query 1 MLILTRRVGETLMIGDEVTVTVLGVKGNQVRIGVNPAPKEVSVHREEIYQRIQAEKSQPTT 60
        MLILTRRVGETLMIGDEVTVTVLGVKGNQVRIGVNPAPKEVSVHREEIYQRIQAEKSQ  ++
Sbjct 1 MLILTRRVGETLMIGDEVTVTVLGVKGNQVRIGVNPAPKEVSVHREEIYQRIQAEKSQSS 60

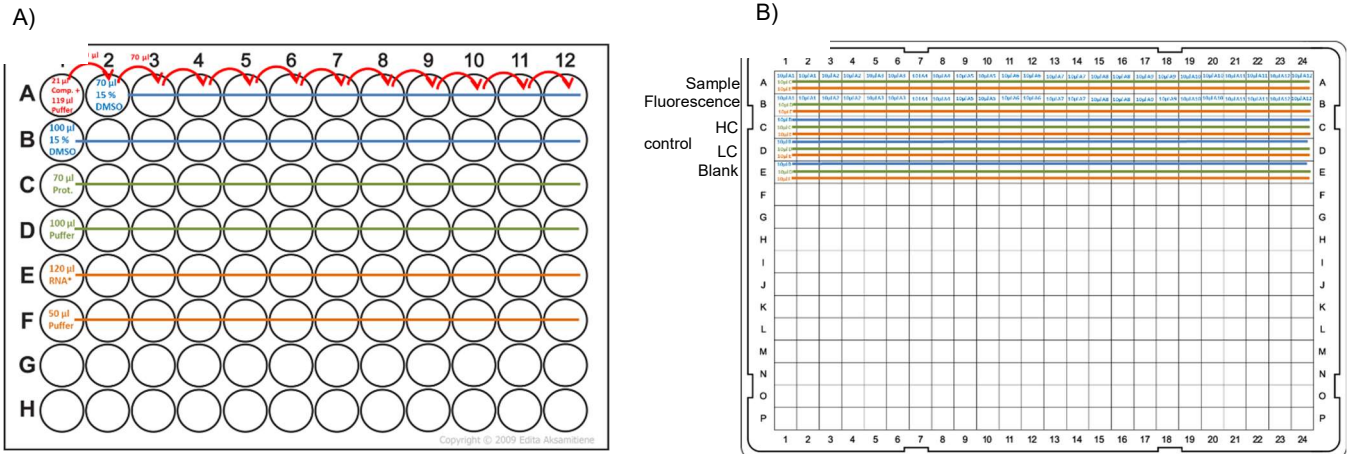
Query 61 Y 61
        Y
Sbjct 61 Y 61
```

### Phage Display



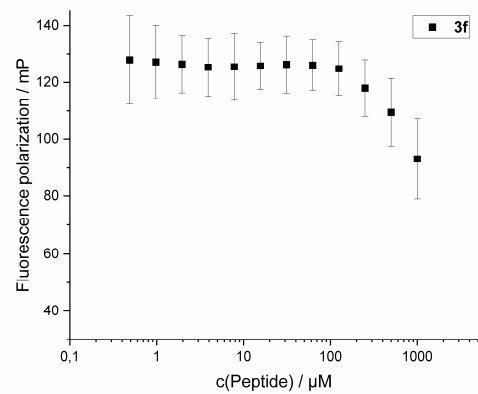
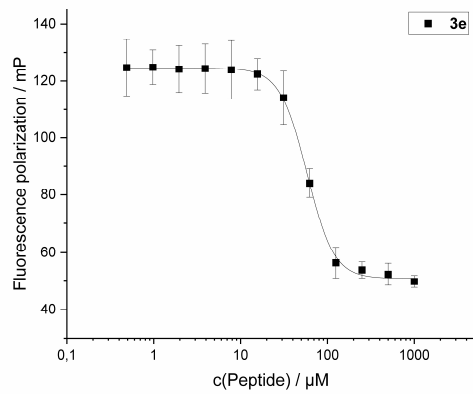
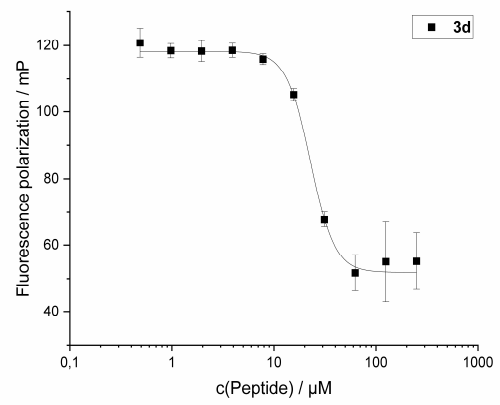
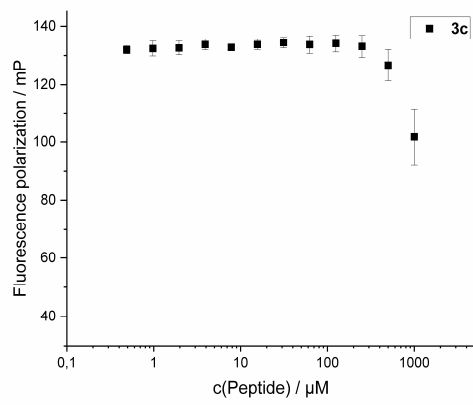
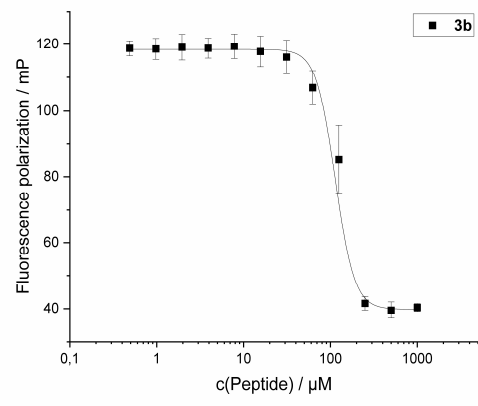
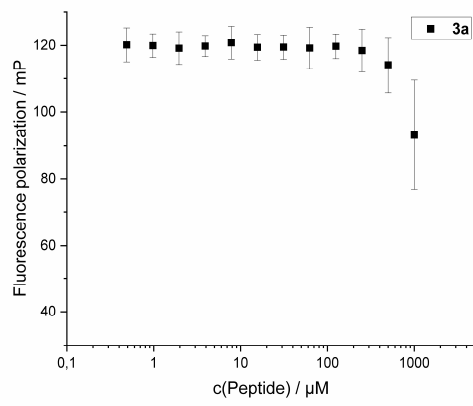
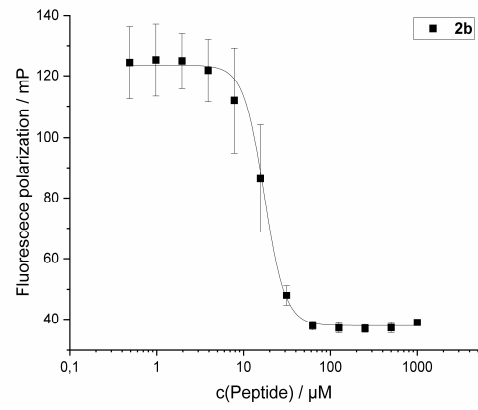
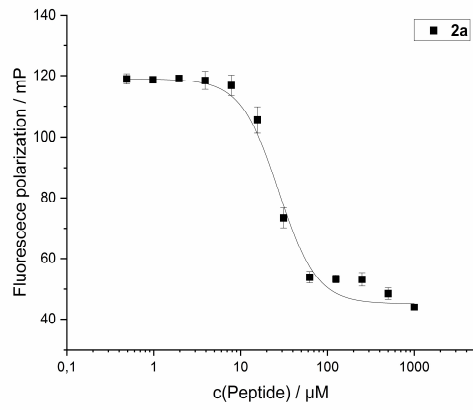
**Figure S1.** A) Vector map of pHAL30, B) Schematic drawing of pHAL30 with cloned peptide library. lacZ promoter: promoter of the bacterial lac operon; RBS: ribosome binding site; pelB: signal peptide sequence of bacterial pectate lyase *Erwinia caratovora*, mediating secretion into the periplasmic space; gIII: gene encoding for the phage protein III.[4]

## Fluorescence Polarization Assay

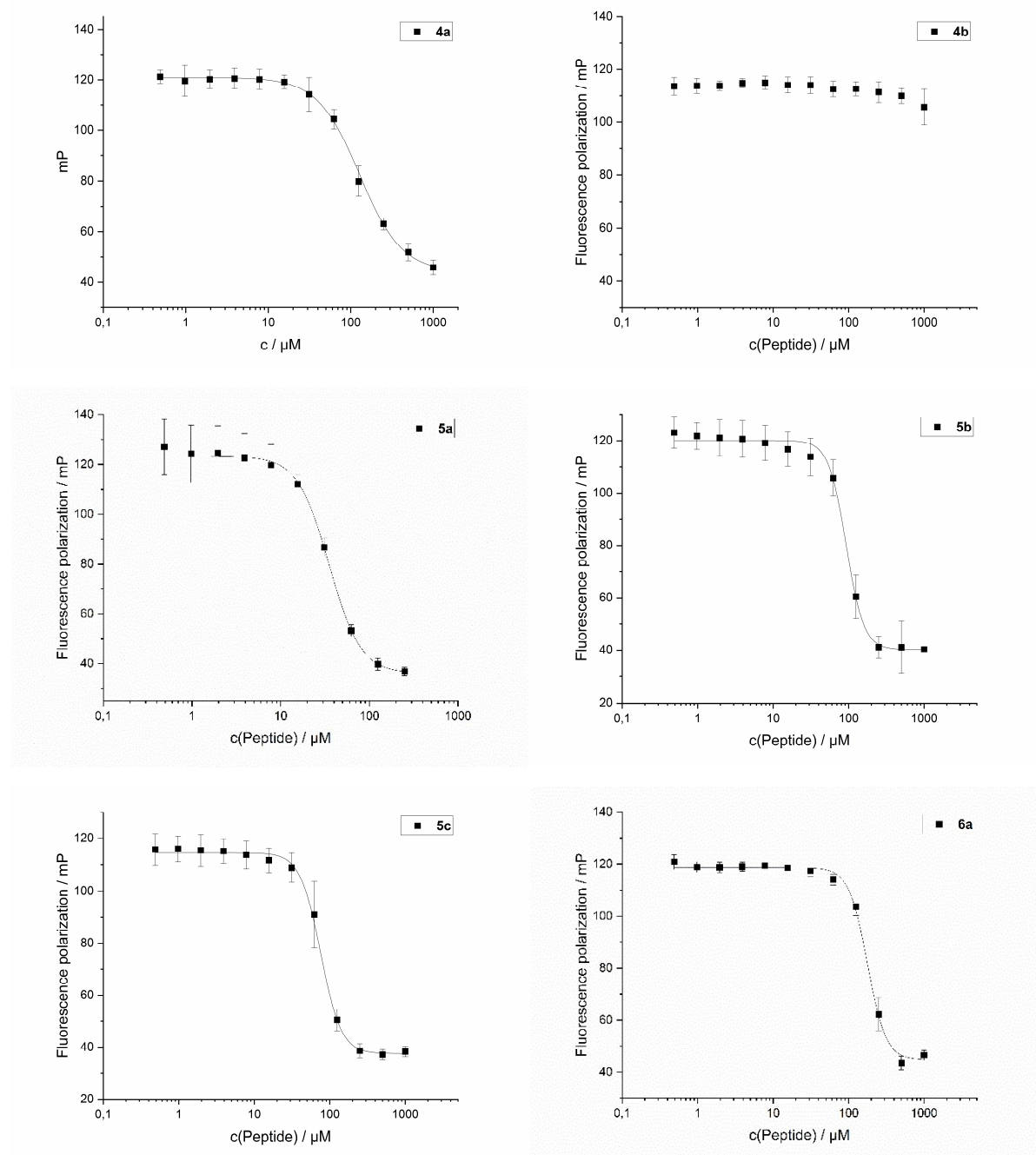


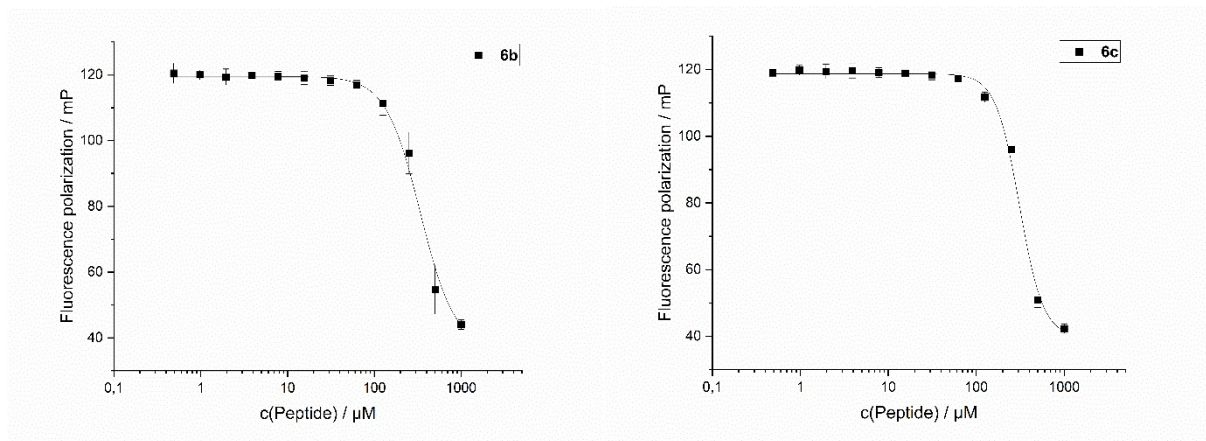
**Figure S2.** A) Preparation plate (96-well plate, clear, v-bottom, non-binding) scheme and B) measuring plate (Greiner 386 well, black, flat bottom). Transferring in duplicates with 12-channel pipette from preparation plate to measuring plate

The results from the fluorescence polarization assay for the peptides 2a-6c can be found in figure S3 for CsrA from *Y. pseudotuberculosis* and in figure S4 for CsrA from *E. Coli*.

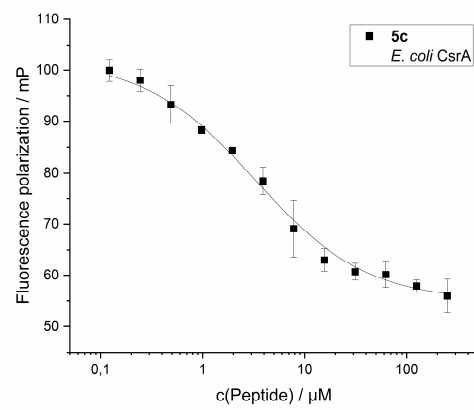
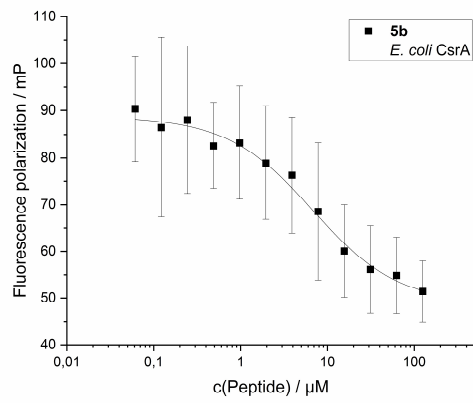
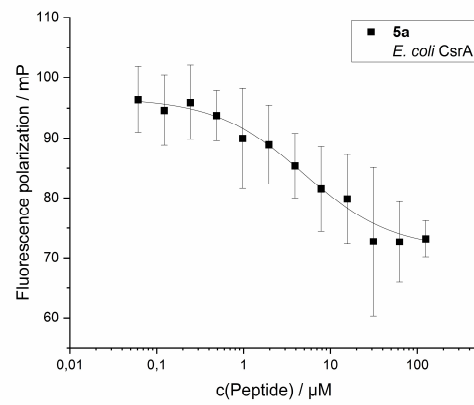
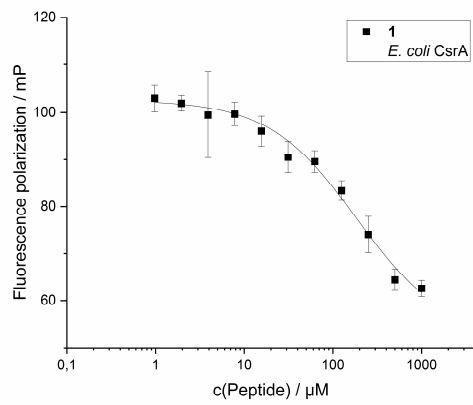


**Figure S3 (part 1).** Results of the dose-dependent fluorescence polarization assay with competition inhibition curves used to determine the half maximal inhibitory concentration (IC<sub>50</sub>) for **peptides 2a-3f** with *Yersinia* CsrA\_biot\_His<sub>6</sub>. The assay has been performed two times in duplicates





**Figure S3 (part 2).** Results of the dose-dependent fluorescence polarization assay with competition inhibition curves used to determine the half maximal inhibitory concentration ( $\text{IC}_{50}$ ) for **peptides 4a-6c** with *Yersinia* CsrA<sub>biot\_His6</sub>. The assay has been performed two times in duplicates.



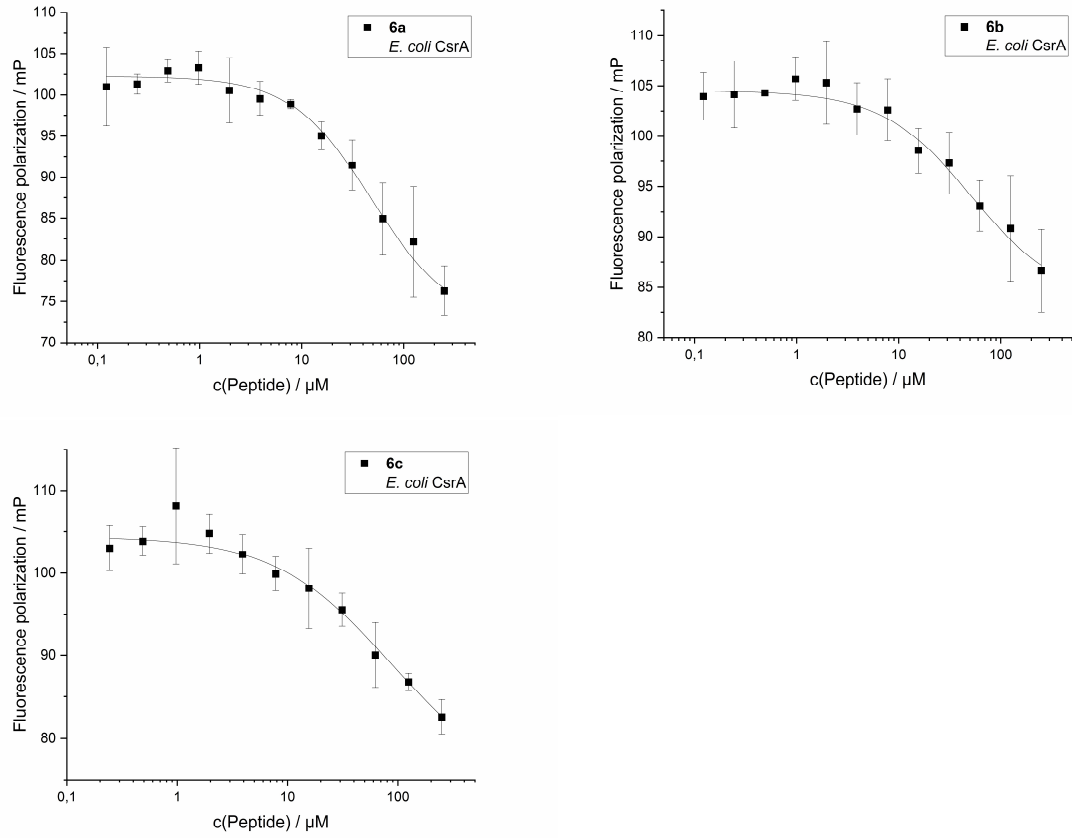


**Figure S4.** Result of the dose-dependent fluorescence polarization assay with competition inhibition curve used to determine the half maximal inhibitory concentration for peptide **5a** and **5b** with *E. coli* CsrA<sub>His6</sub> as target. The assay has been performed two times in duplicates.

## Microscale Thermophoresis Assay (MST)

Results from the MST-assay can be found in figure S5

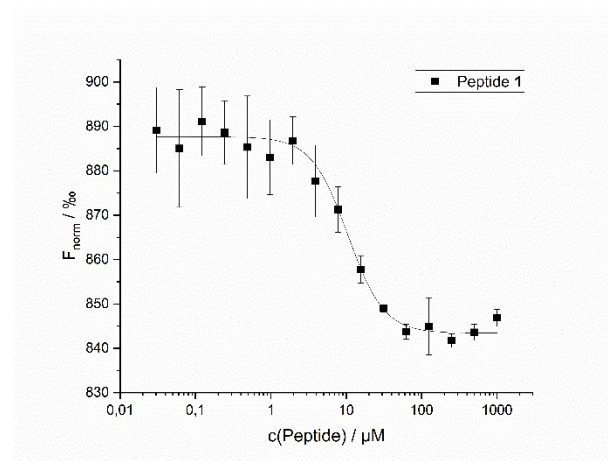


**Figure S5.** Dose-dependent MST interaction curve of peptide 1 with *Yersinia* CsrA\_biot\_His<sub>6</sub> used to determine the dissociation constant ( $K_d$ ).

## Calculation of the Error Bars in Fluorescence Polarization and MST Assay

Error bars are calculated with TINV function of Microsoft Excel, which returns the two-tailed inverse of the Student's t-distribution multiplied with the standard deviation of the mean of the measurements:

$\text{TINV}(\text{probability}, \text{deg\_freedom}) \cdot (\text{STDEV of the mean})$

The argument probability is set to 95 % and the degree of freedom to 4.

## NMR analysis and structure calculations

NMR analysis of peptide 1 was performed with a 2 mM solution in 50 % H<sub>2</sub>O/50 % d<sub>3</sub>-acetonitrile (298 K, pH 3.4) on a Bruker Avance III 600 MHz spectrometer. 2D Spectra included TOCSY, ROESY, and natural abundance heteronuclear correlation spectroscopy (<sup>15</sup>N- and <sup>13</sup>C-HSQC). TOCSY spectra were also recorded at variable temperatures (283 – 303 K) to determine amide proton temperature coefficients. Spectra were referenced to residual acetonitrile at 1.94 ppm. All spectra were processed using TopSpin v3.6 and assigned using CcpNMR Analysis.

Preliminary structures were calculated in CYANA based upon ROESY-derived distance restraints. Several dihedral angle restraints were also added as predicted by TALOS-N[5] along with a single hydrogen bond pair after consideration of preliminary structures and amide proton temperature coefficients. A final ensemble of 20 structures were generated within CNS[6] using torsion angle dynamics and refinement and energy minimization in explicit water solvent. MolProbity[7] was used to assess stereochemical quality (summarised in Table S5).

**Table S5.** Statistical analysis of peptide 1 structures<sup>[a]</sup>

Experimental restraints	
total no. distance restraints	45
intraresidue	22
sequential	23
medium range, $i-j < 5$	2
hydrogen bond restraints	2

dihedral angle restraints	
phi	5
psi	1
Deviations from idealized geometry	
bond lengths (Å)	0.012 ± 0.001
bond angles (deg)	1.161 ± 0.107
impropers (deg)	1.14 ± 0.15
NOE (Å)	0.033 ± 0.005
cDih (deg)	0.032 ± 0.104
Mean energies (kcal/mol)	
overall	-194 ± 13
bonds	3.9 ± 0.4
angles	9.0 ± 1.8
improper	3.3 ± 0.7
van Der Waals	-14.5 ± 2.2
NOE	0.05 ± 0.02
cDih	0.01 ± 0.03
electrostatic	-977 ± 33
Violations	
NOE violations exceeding 0.2 Å	0
Dihedral violations exceeding 2.0 Å	0
Rms deviation from mean structure, Å	
backbone atoms	0.79 ± 0.37
all heavy atoms	1.81 ± 0.70
Stereochemical quality <sup>[b]</sup>	
Residues in most favoured Ramachandran region, %	80.0 ± 11.0
Ramachandran outliers, %	0 ± 0
Unfavourable sidechain rotamers, %	0.0 ± 0.0
Clashscore, all atoms	0.0 ± 0.0
Overall MolProbity score	1.2 ± 0.3

[a] All statistics are given as mean ± SD.

[b] According to MolProbity [7]



## In silico Investigations

**General.** All *in silico* experiments were performed with Molecular Operating Environment (MOE) by Chemical Computing Group (CCG) release 2020.09 employing the Amber10:EHT force field.[8]

### Homology Model Building.

Homology model of *Yersinia pseudotuberculosis* CsrA in complex with RNA was built using the first entry of NMR-solution structure 2MFH from *Pseudomonas fluorescens* in complex with RNA-oligo ucaggacau.[9] The template structure 2MFH was chosen from the available structures in the PDB based on the following requirements: resolved C-terminal residues and complex with short RNA oligo.

The sequence of the template structure (*P. fluorescens*, Sec1) and the target sequence (*Y. pseudotuberculosis*, Sec2) share an identity of 71% and homology of 89% as shown by following blast result:

Score	Expect	Method	Identities	Positives	Gaps
91.7 bits(226)	3e-32	Compositional matrix adjust.	41/58(71%)	52/58(89%)	0/58(0%)
Sec2		MLILTRRVGETLMIGDEVTVTVLGVKGNQVRIGVNAPKEVSVHREEIYQRIQAEKSQP			58
		MLILTR+VGE++ IGD++T+T+LGV G QVRIG+NAPK+V+VHREEIYQRIQA + P			
Sec1		MLILTRKVGESINIGDDITITILGVSGQQVRIGINAPKDVAVHREEIYQRIQAGLTAP			58

The built-in “homology model” function of MOE was used with standard parameters, while RNA atoms were used as environment to successfully yield a model in complex with RNA.

### Docking.

Docking was performed using the built-in “Docking” function of MOE. NMR structures of peptide **1** (all 20 entries of PDB ID 7M7X, BMRB ID 30895) were used as “ligand” structures and the above-mentioned homology model as “receptor”. The docking site was defined by involving protein residues in 4.5 Å proximity to the RNA atoms as well as the C-terminal residues of one of the two identical RNA-interaction sites. The resulting selection was as follows:

```
>CsrAYP_1|Chain A|Translational repressor|Y.pseudotuberculosis HomologyModel
MLILTRR--E-----
>CsrAYP_1|Chain B|Translational repressor|Y.pseudotuberculosis HomologyModel
-----T-L--K--Q-R----APK-VSVHR-EIYQRIQAEKSQPT
```

Placement algorithm was “Triangle Matcher” with “London dG” as Scoring function generating 10 initial poses for every peptide **1** conformer (entry). Refinement method was “Induced Fit” with “GBVI/WSA dG” as Scoring function and 5 keeper poses.

The resulting 100 docking poses (5 poses × 20 entries) were sorted according to the refinement/binding score. The 10 best-scoring poses were sorted according to the “rmsd\_refine” parameter indicating binding hypothesis with minimal deviation from the initial (experimental) solution geometry. By this means, we selected the optimal pose scoring in number 8 of 100 regarding refinement/binding score and 3 of 100 regarding the “rmsd\_refine” parameter.

### Analysis and Visualisation.

The pose derived by the docking procedure described above was analysed using the “Ligand Interactions” function of MOE for generating a 2D depiction of the interaction profile (see Figure 3c from the main text). Graphic processing for manuscript figures was done using YASARA structure (YASARA Biosciences GmbH)[10] and POV-Ray 3.7.0.

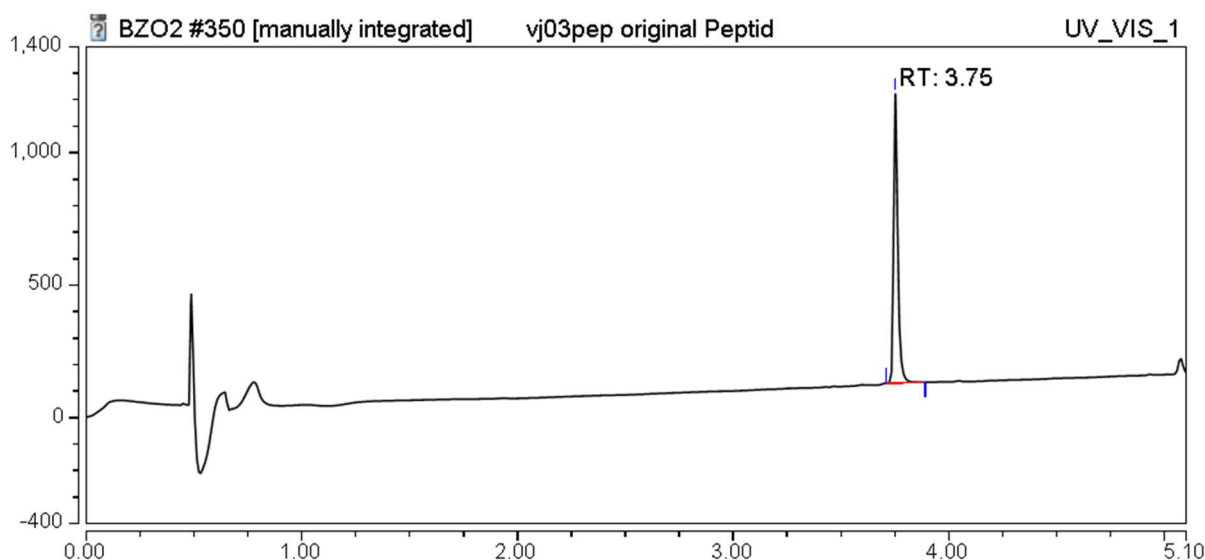
## Analytical LC-MS

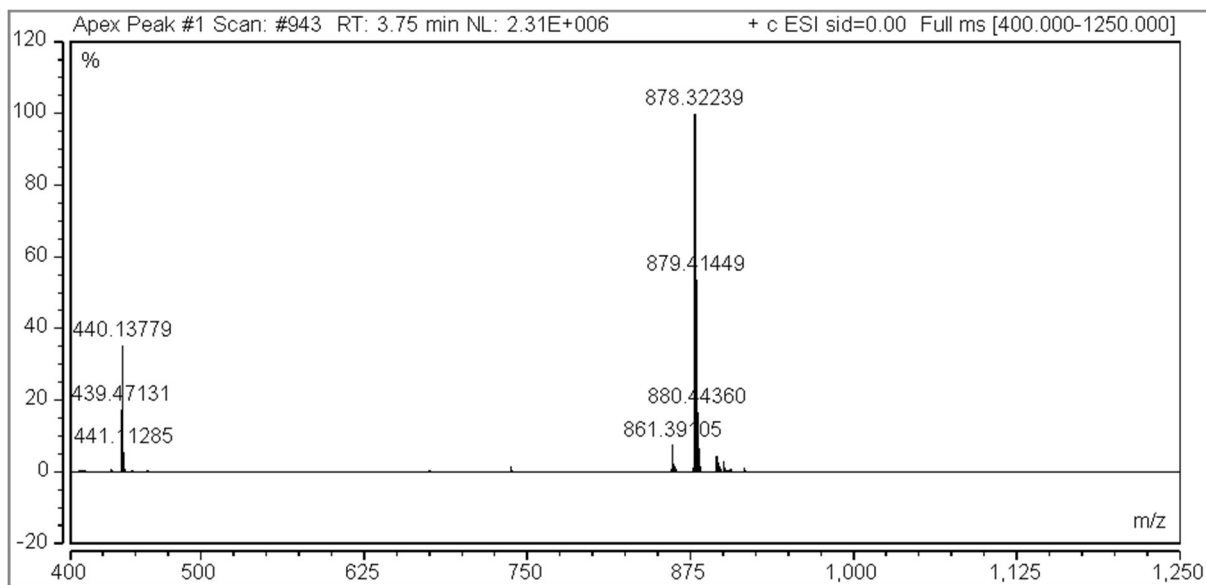
For analytical LC-MS, all samples were solved in Methanol. The measurements of compounds **1-5c** and **6b**, **6c** were done with a DIONEX UltiMate 3000 UHPLC<sup>+</sup> focused (Thermo Scientific), containing RS Pump, RS Autosampler, Diode Array Detector, Column Compartment (heated to 40 °C) and ISQ EC Mass Spectrometer. We used a HYPERSIL GOLD 1.9UM 100 x 2.1MM COLUMN (Thermo Scientific). The gradient was 5-50 % solvent B over 4.2 min (solvent A: H<sub>2</sub>O containing 0.05 % formic acid, solvent B: ACN containing 0.05 % formic acid followed by 50 % solvent B for 0.8 min all with a flowrate of 0.6 mL/min.

The graphs show the HPLC chromatogram measured at 220 nm and the total ion count in the mass track. The chromatogram was used to determine the purity of the respective peptide. The mass spectrum from the main peak of the mass track is also shown.

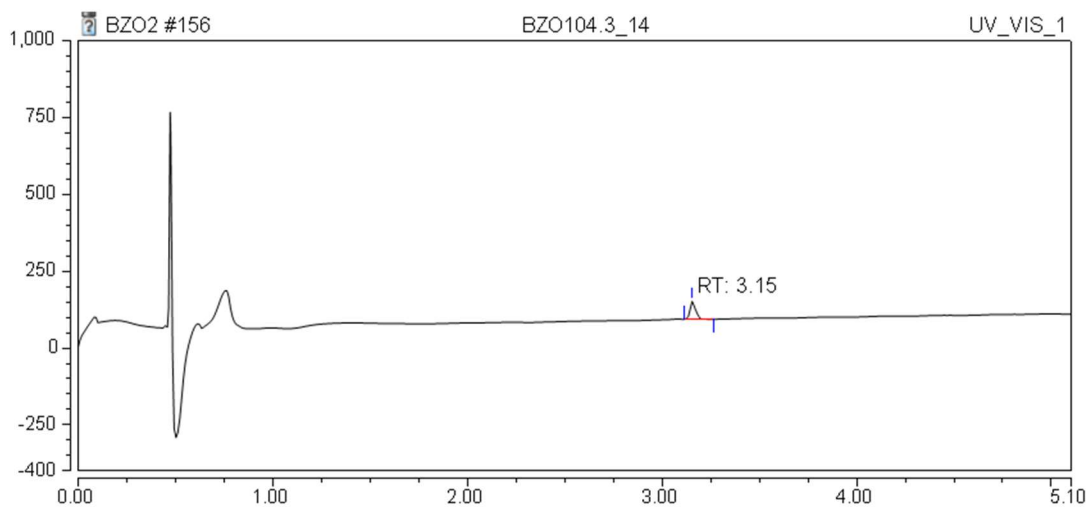
Compounds **6b** and **6c** were additionally analysed and **6a** was only analysed on a Shimadzu Prominence LC-MS system using an Agilent Zorbax 300SB-C18 column (5 µm, 150 x 2.1 mm) with a flow rate of 0.6 mL/min. The samples were analysed using a linear gradient of 0-60 % solvent B in 30 min (Solvent A: H<sub>2</sub>O with 0.05 % formic acid; Solvent B: 95 % acetonitrile with 0.05 % formic acid) and the elutants were monitored by absorbance at 214 nm and 280 nm and low resolution ESI-MS.

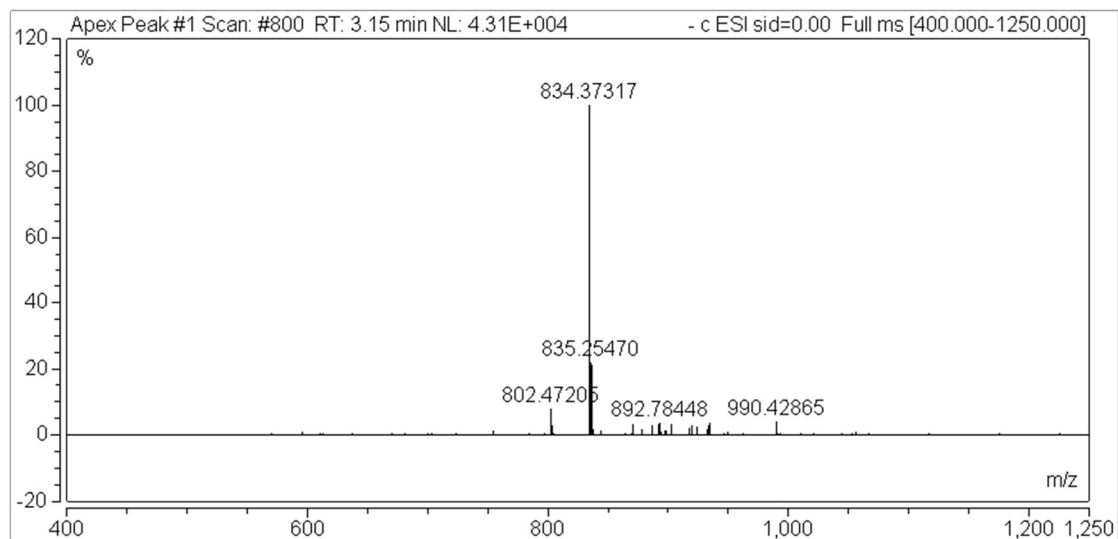
Ac-V-[CSELC]<sub>cyclic</sub>-W-NH<sub>2</sub> (1)



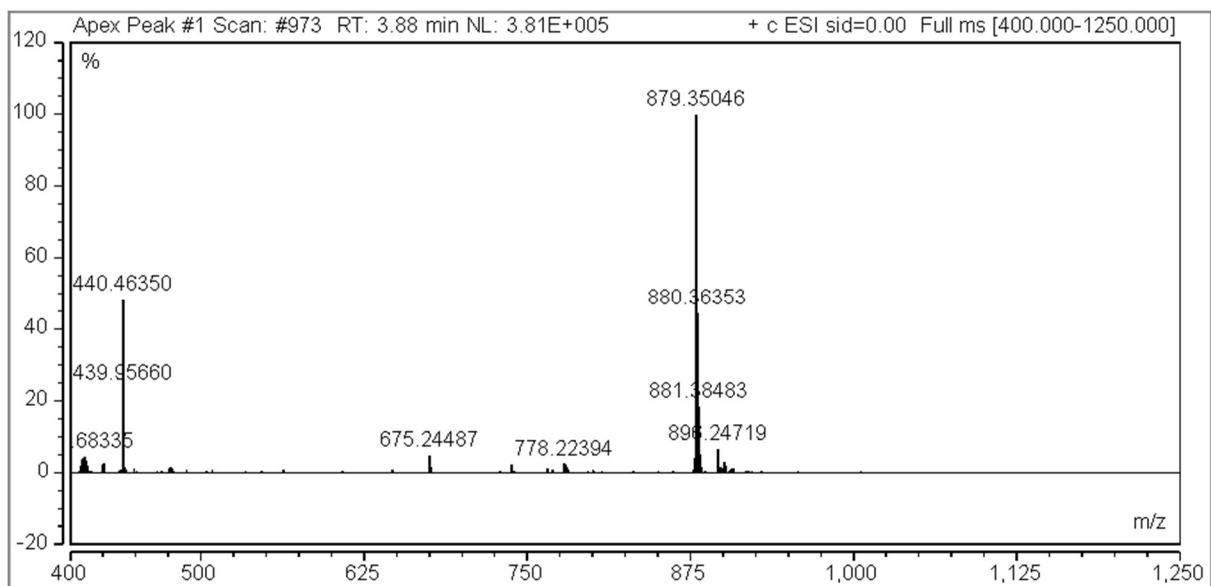
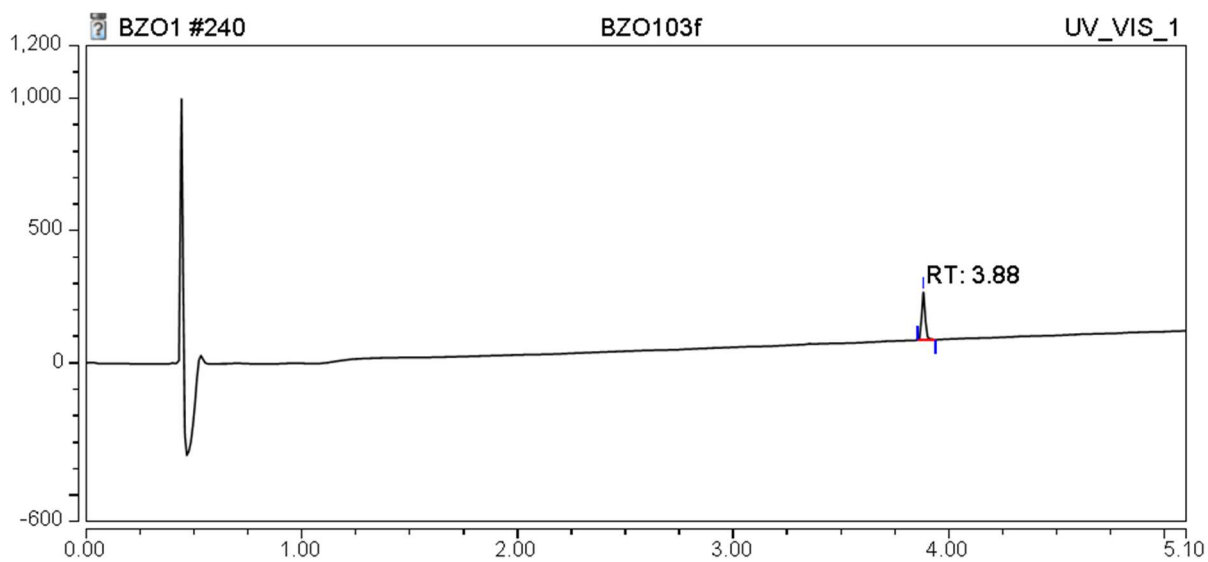


**H-V-[CSELC]<sub>cyclic</sub>-W-NH<sub>2</sub> (2a)**

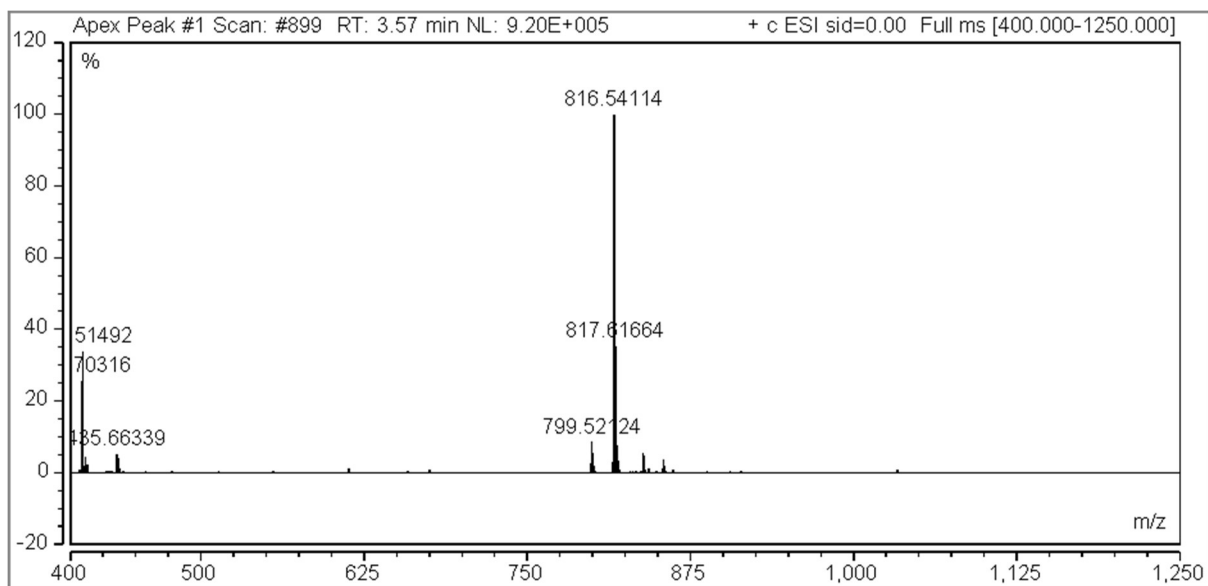
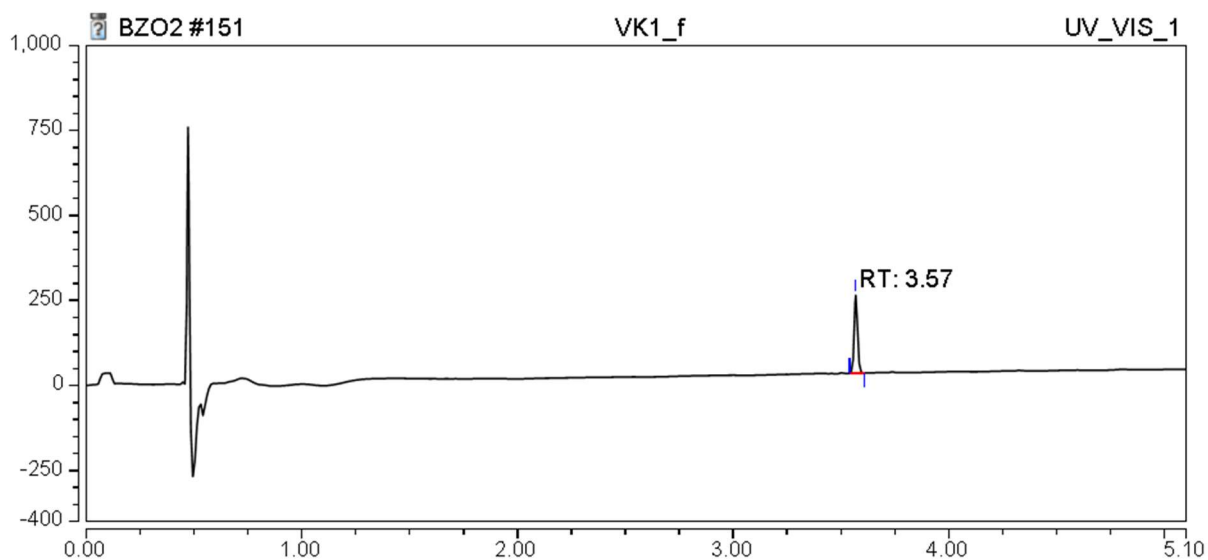




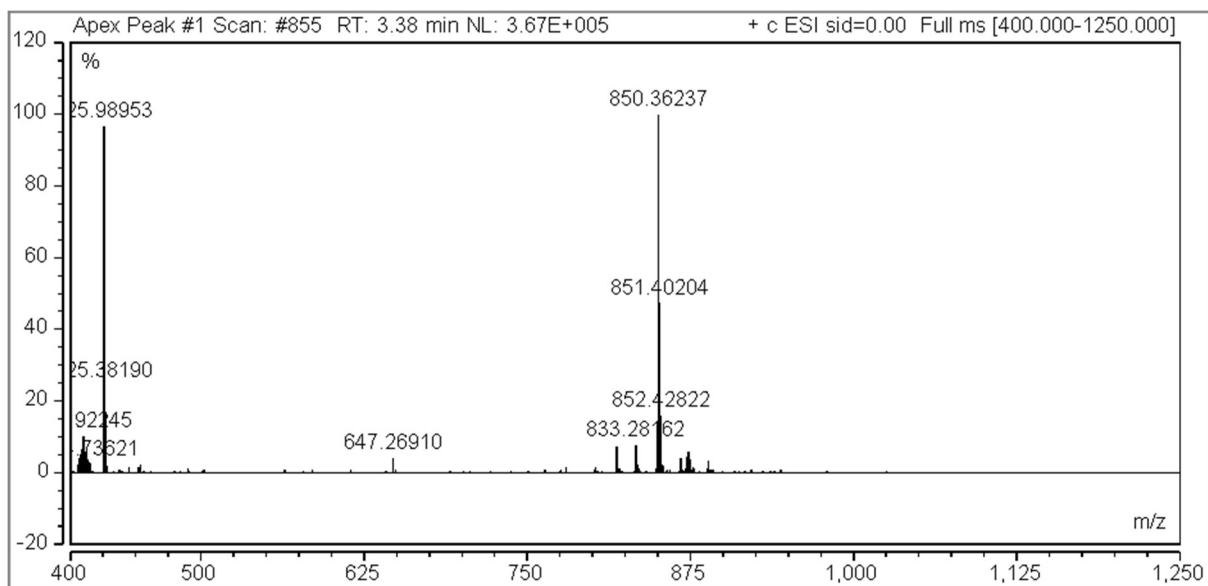
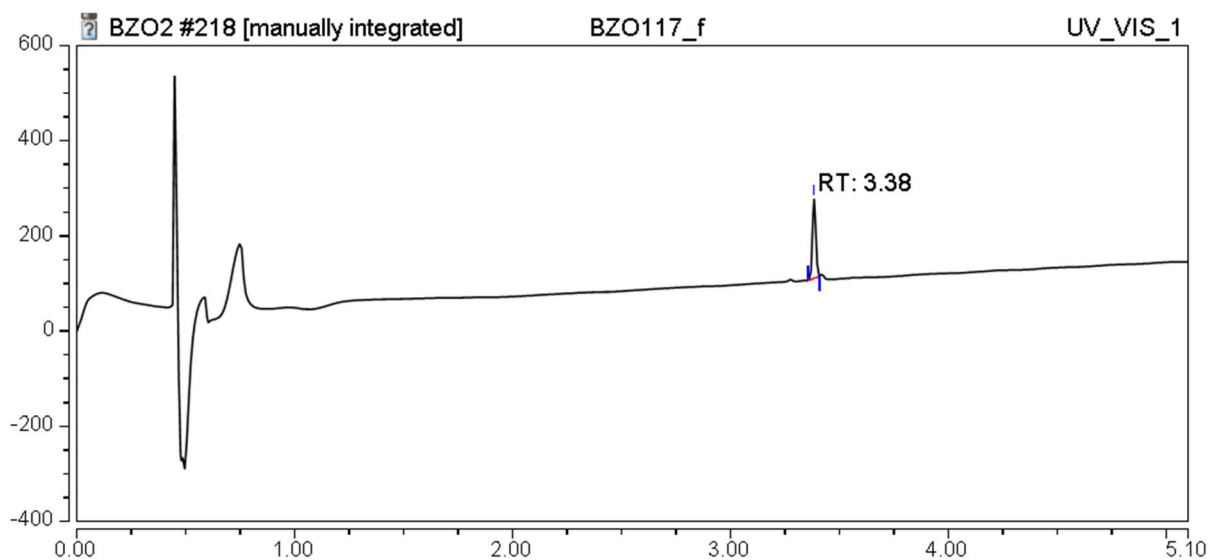
Ac-V-[CSEL<sub>C</sub>]<sub>cyclic</sub>-W-OH (2b)



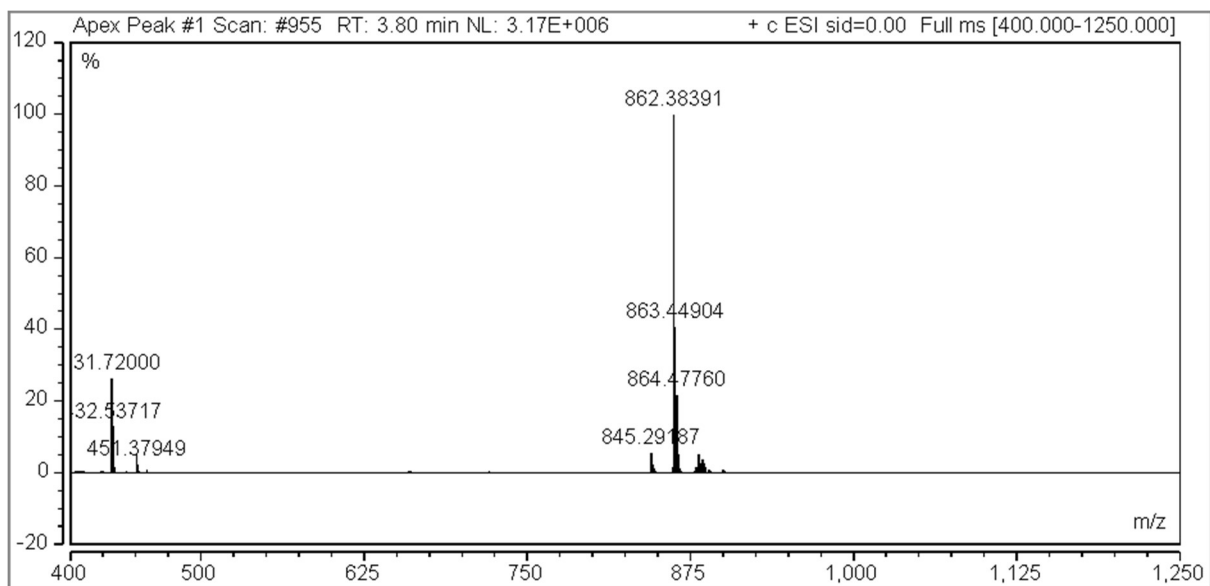
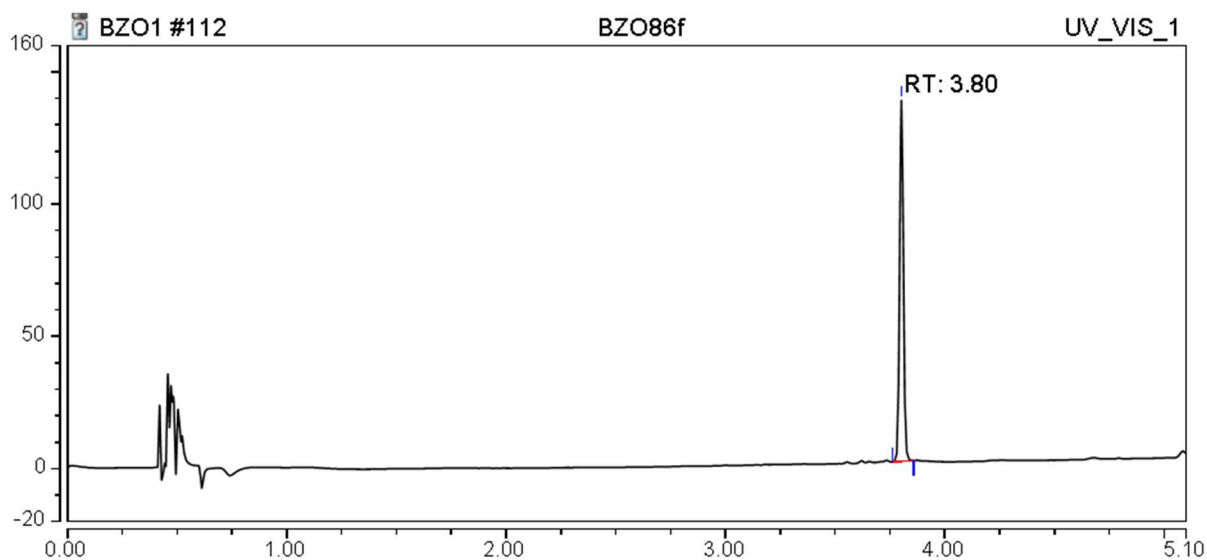
Ac-VASELAW-NH<sub>2</sub> (3a)



Ac-A-[CSELC]<sub>cyclic</sub>-W-NH<sub>2</sub> (3b)

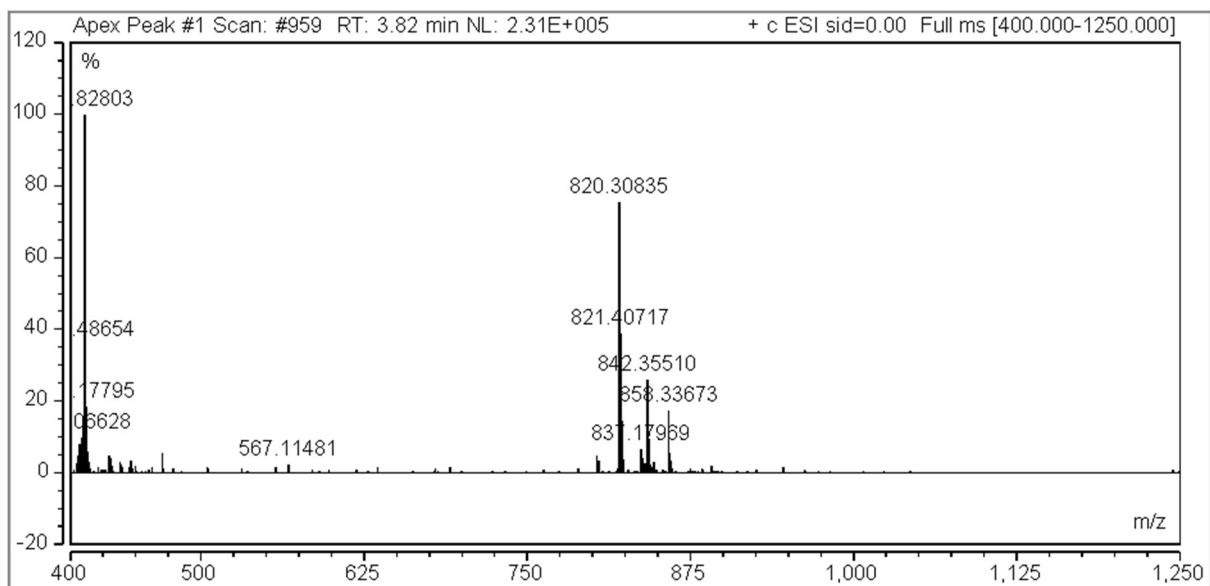
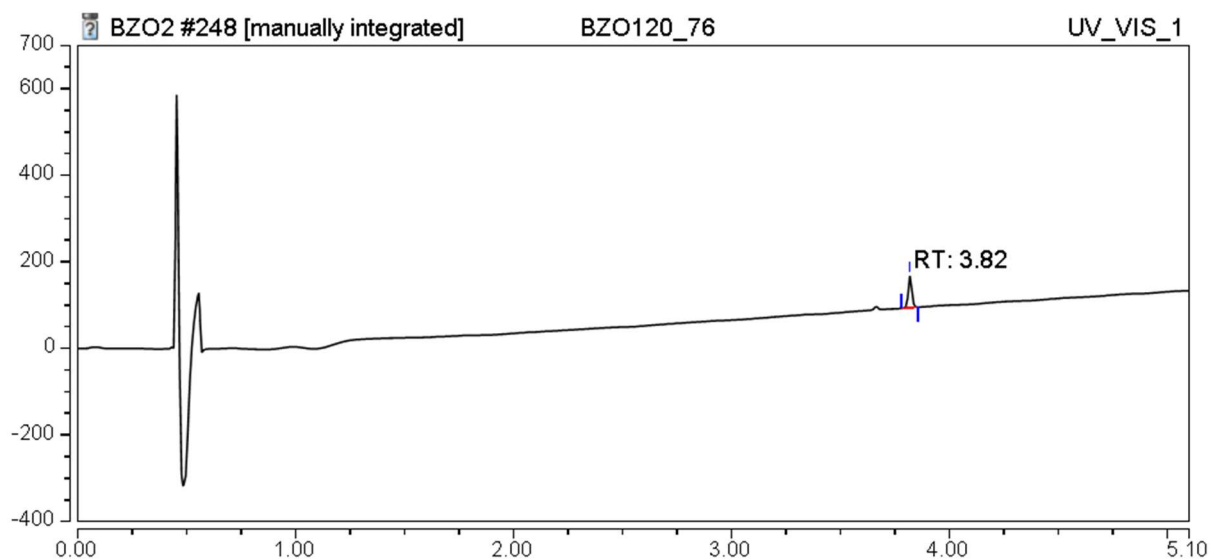


Ac-V-[CAELC]<sub>cyclic</sub>-W-NH<sub>2</sub> (3c)

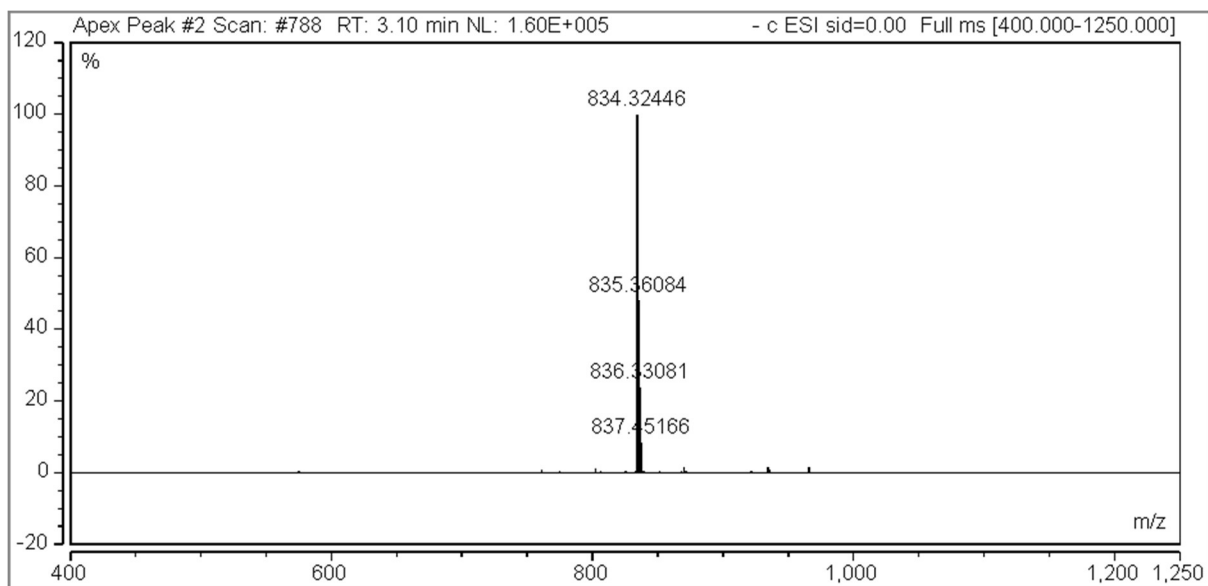
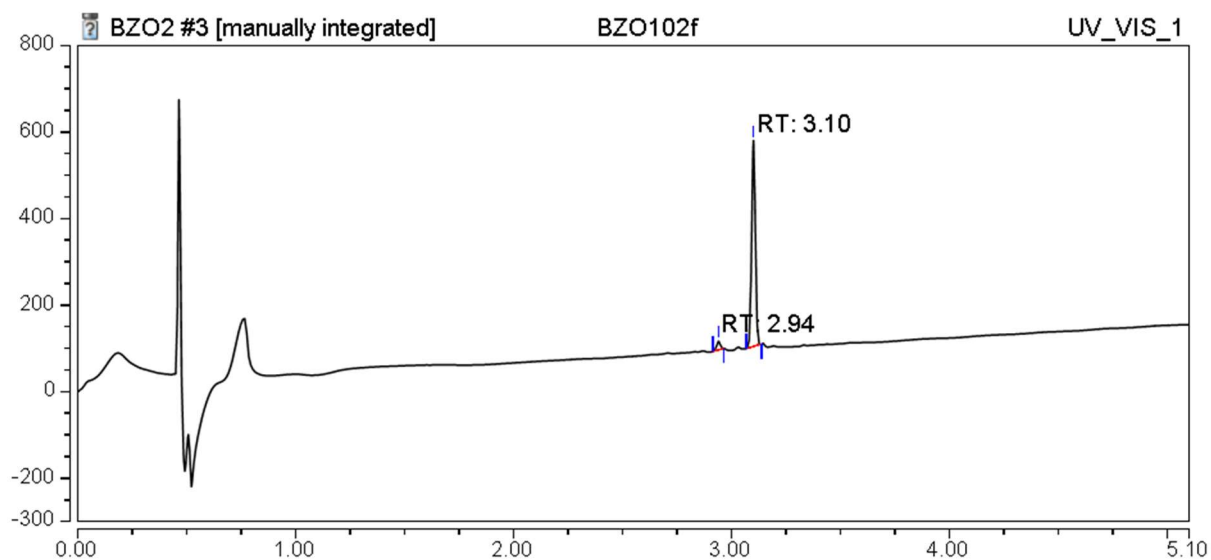




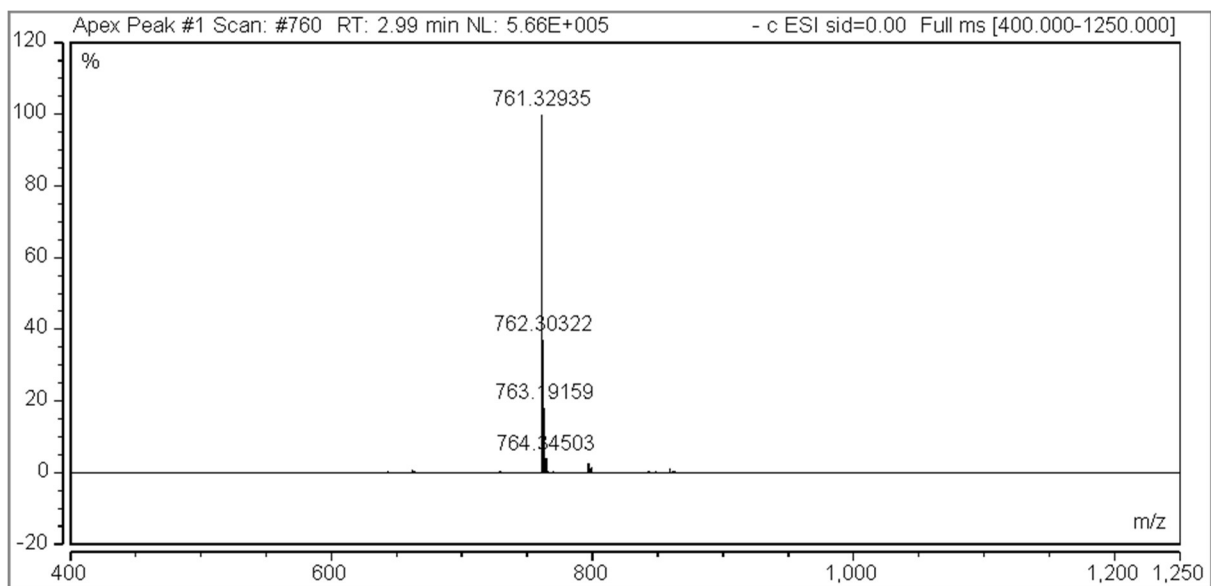
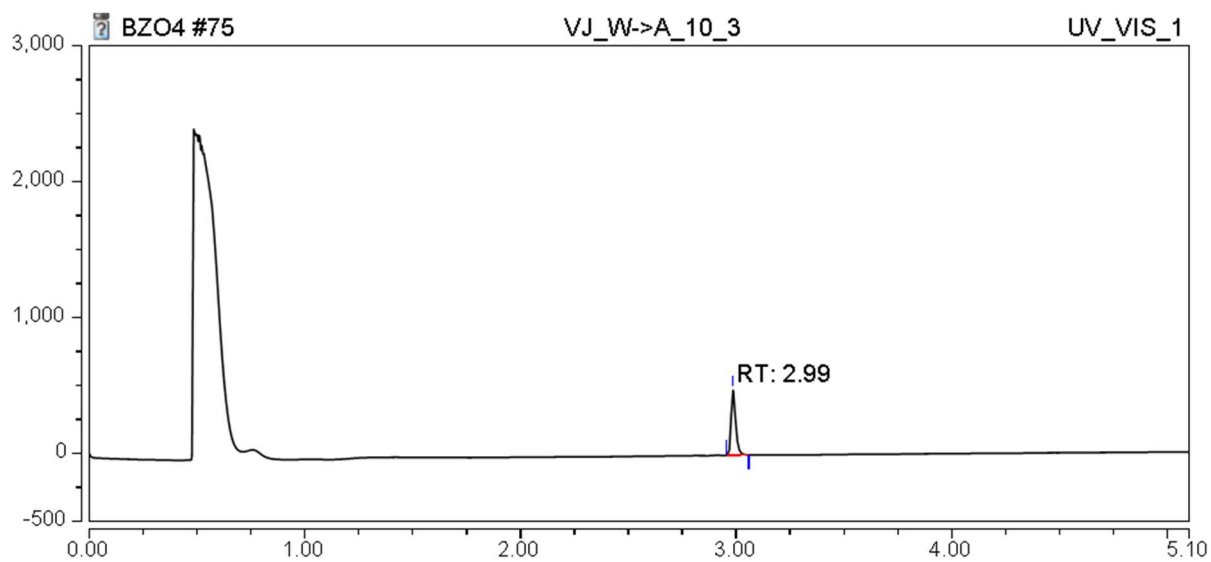
Ac-V-[CSALC]<sub>cyclic</sub>-W-NH<sub>2</sub> (3d)



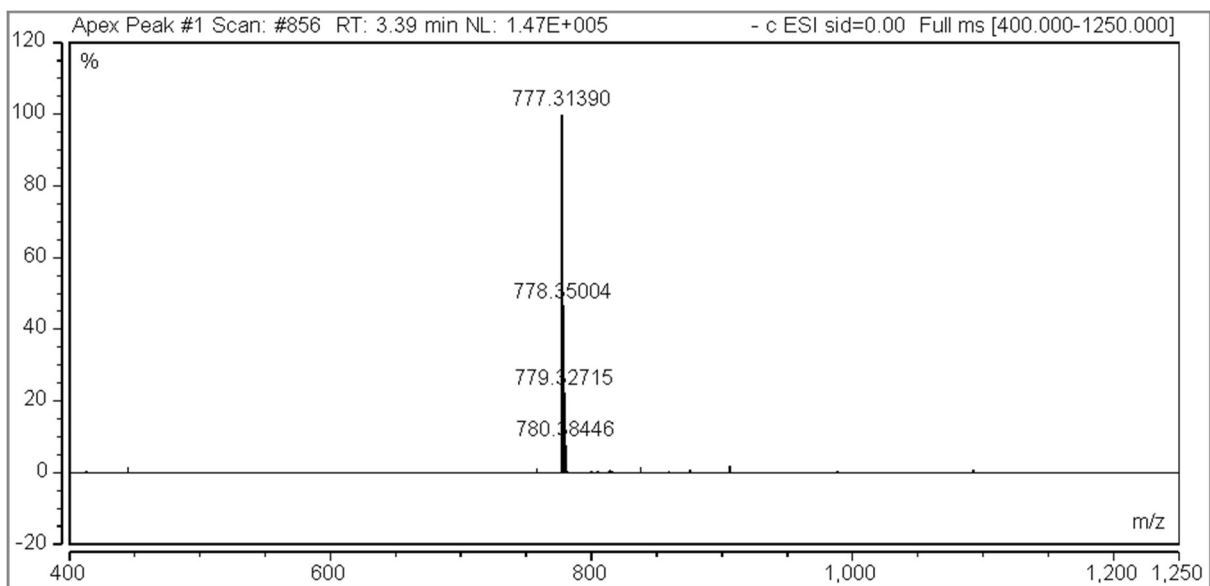
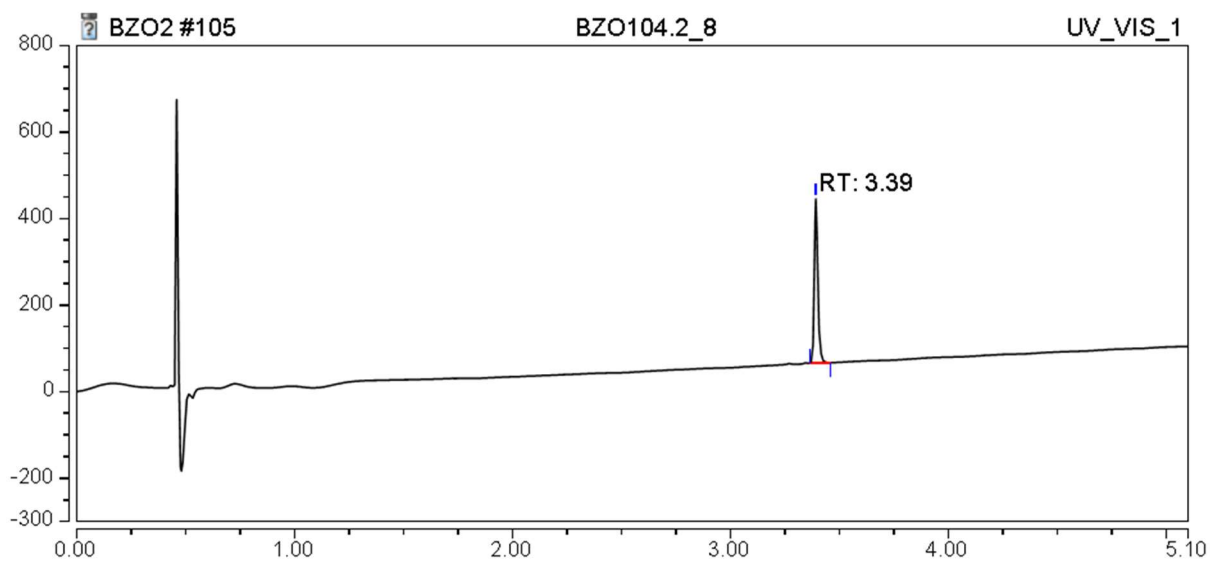
Ac-V-[CSEAC]<sub>cyclic</sub>-W-NH<sub>2</sub> (3e)



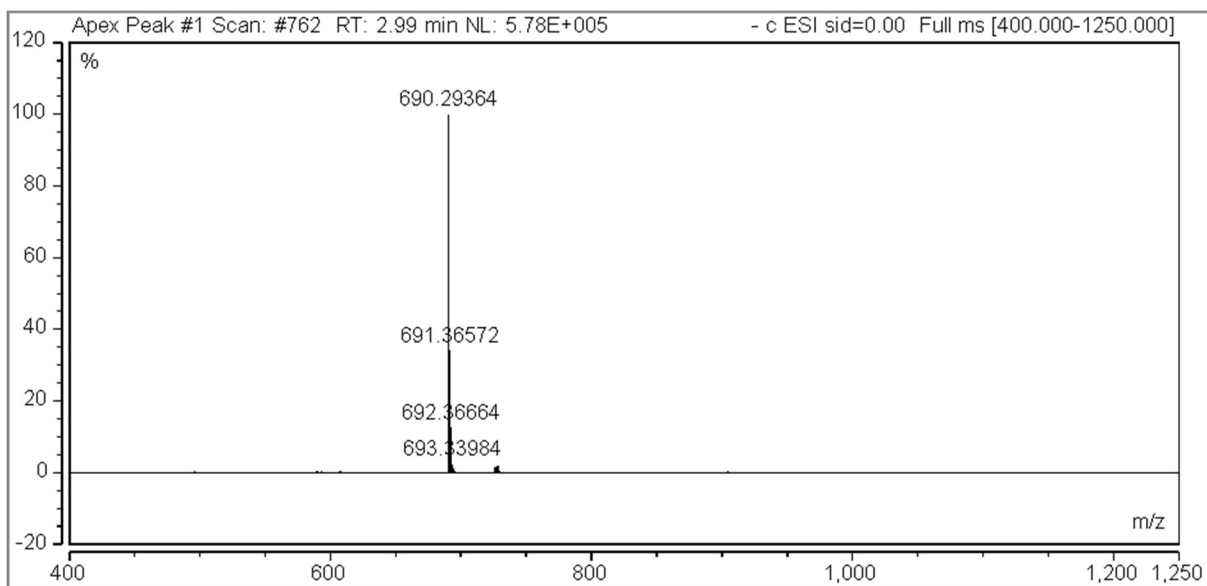
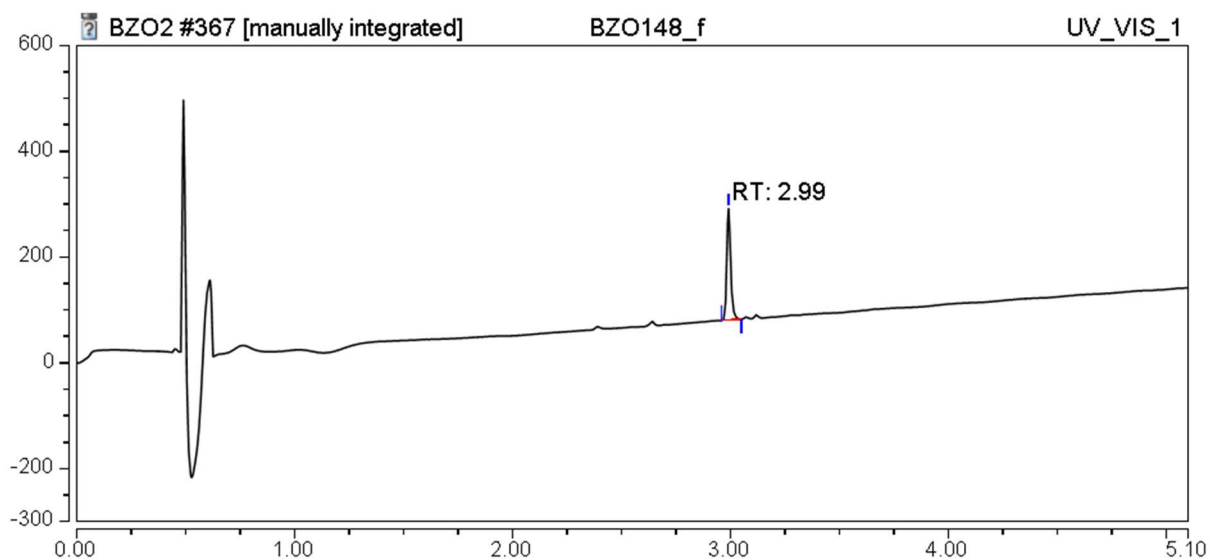
Ac-V-[CSELC]<sub>cyclic</sub>-A-NH<sub>2</sub> (3f)



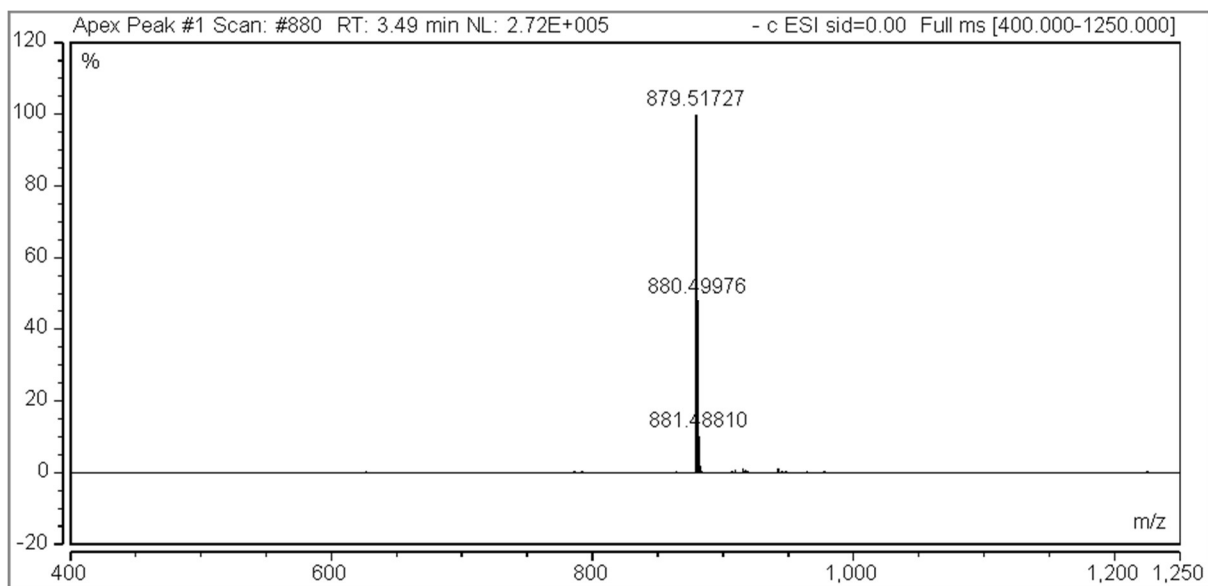
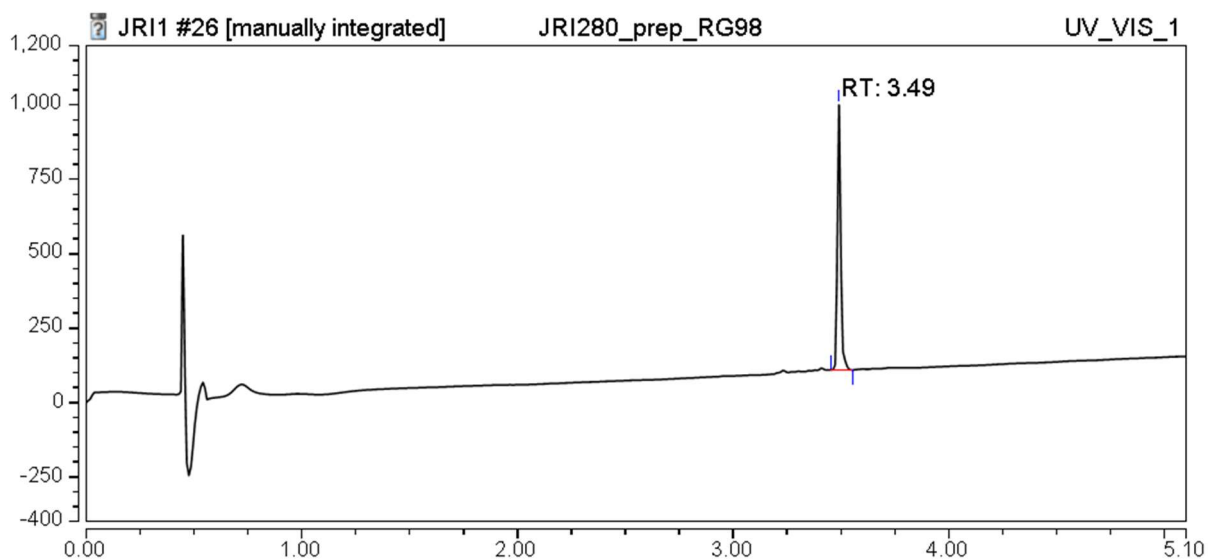
Ac- -- [CSELC]<sub>cyclic</sub>-W-NH<sub>2</sub> (4a)



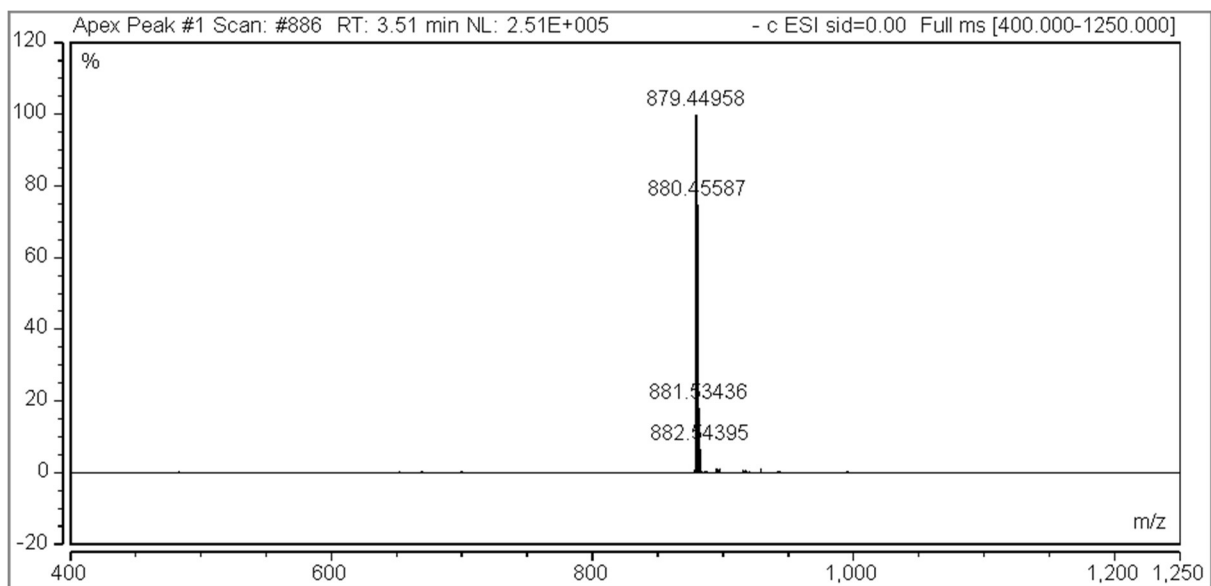
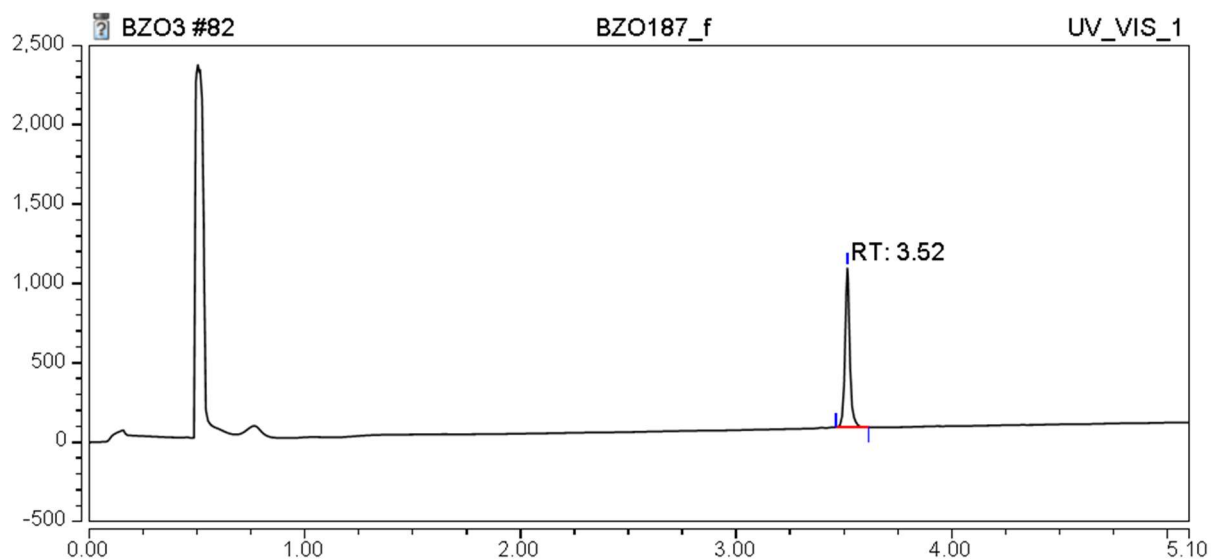
Ac-V-[CSELC]<sub>cyclic</sub> --NH<sub>2</sub> (4b)



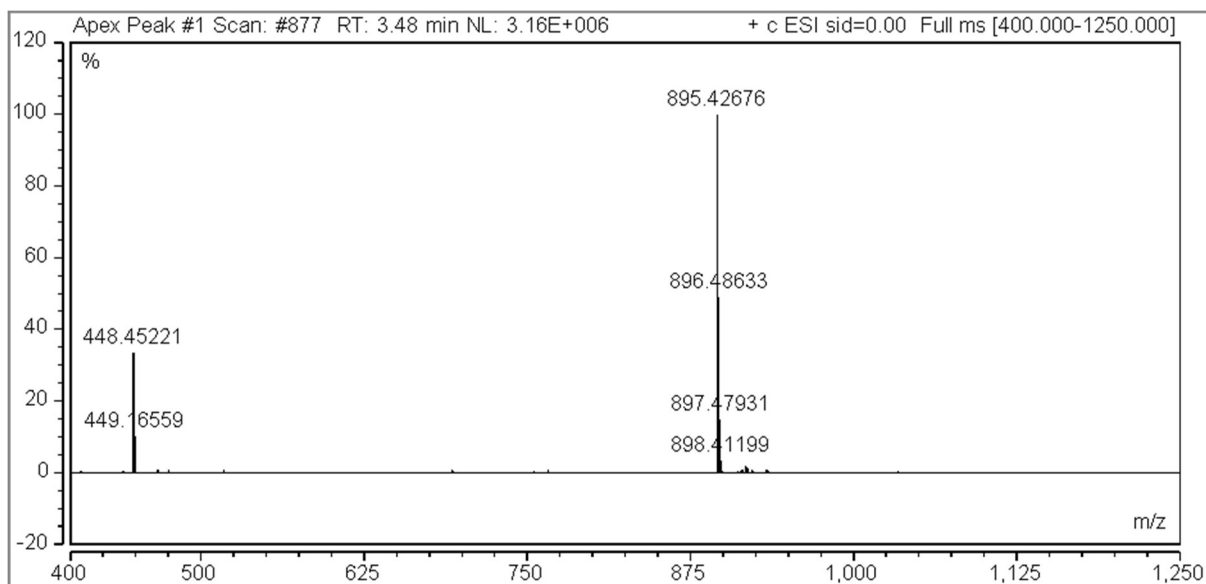
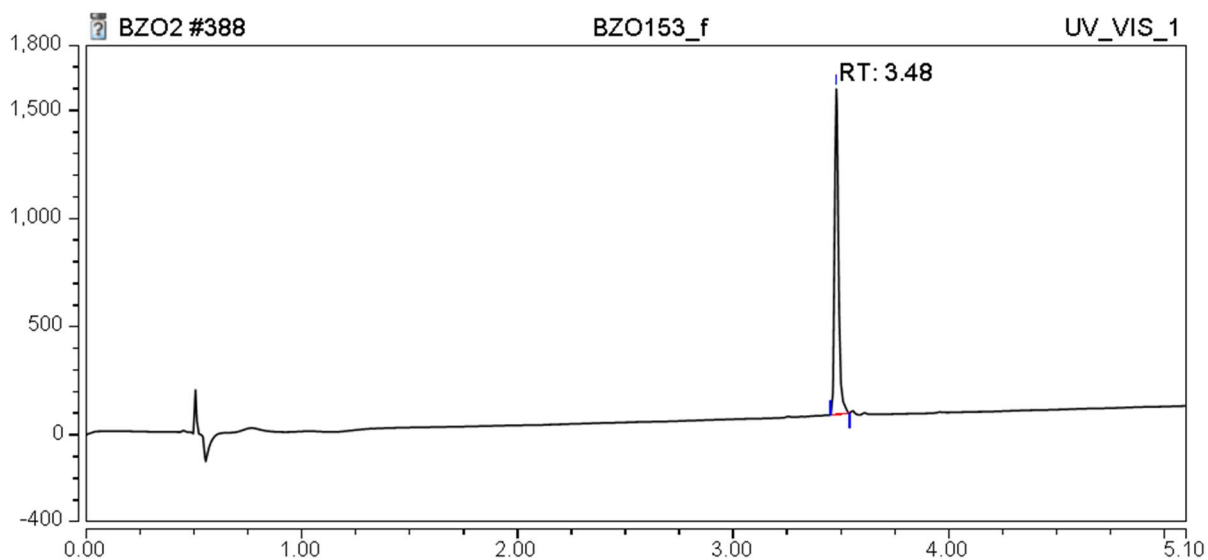
Ac-V-[Pra-SEL-Aza]<sub>cyclic</sub>-W-NH<sub>2</sub> (1,4-triazole) (5a)



Ac-V-[Aza-SEL-Pra]<sub>cyclic</sub>-W-NH<sub>2</sub> (1,4-triazole) (5b)

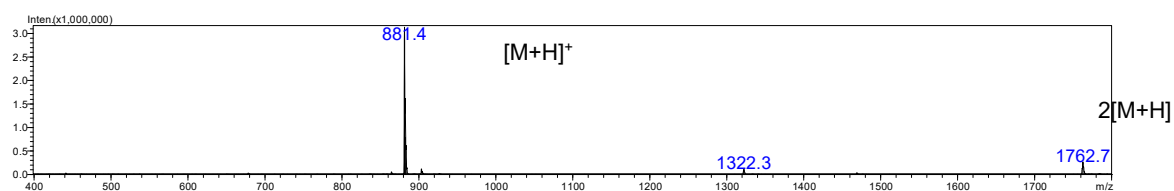
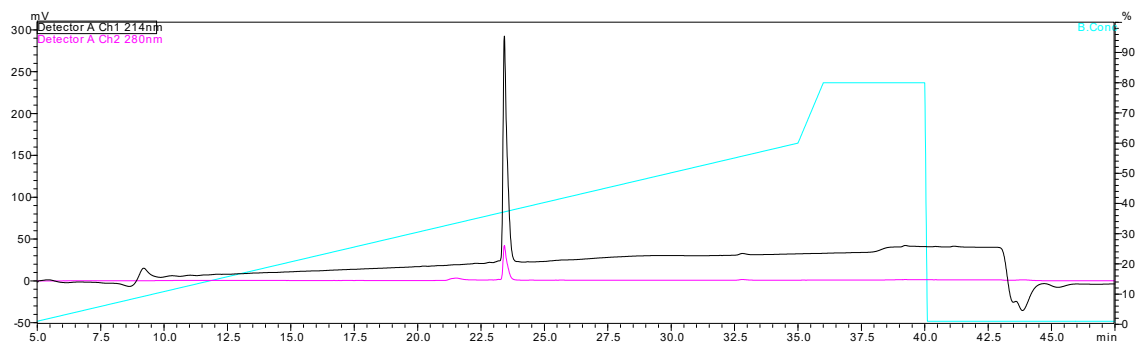


Ac-V-[Pra-SEL-Aha]<sub>cyclic</sub>-W-NH<sub>2</sub> (1,4-triazole) (5c)

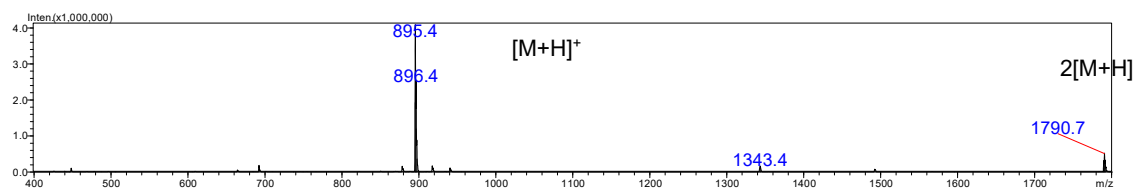
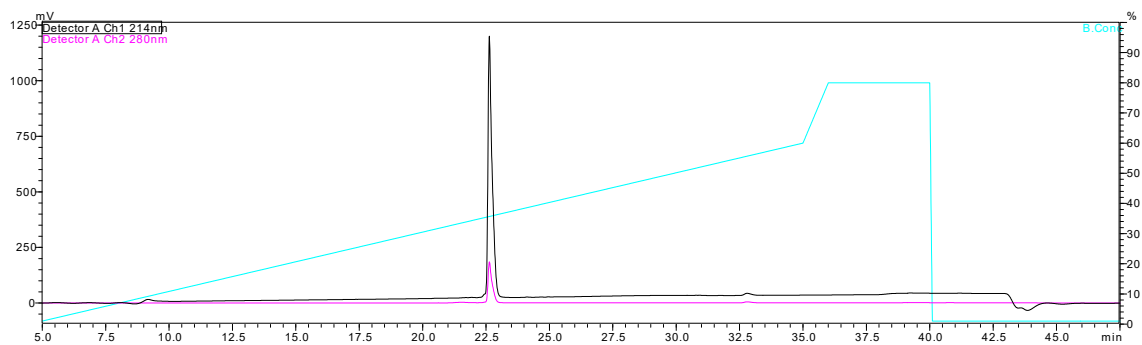




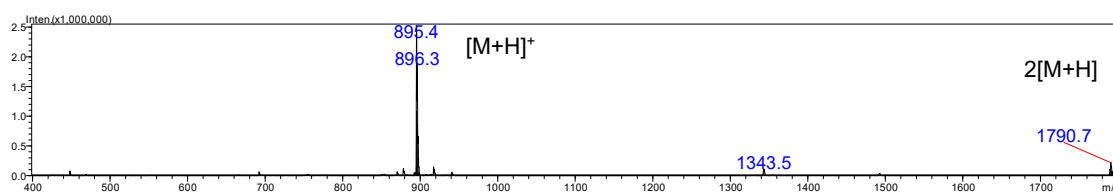
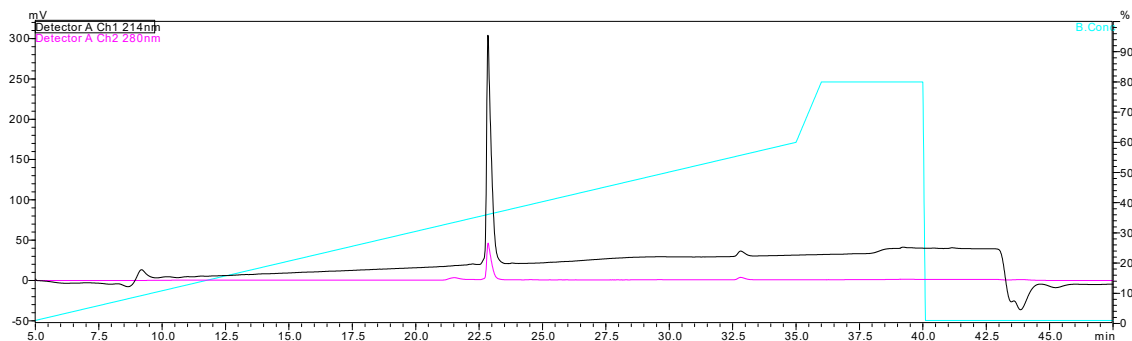
Ac-V-[Pra-SEL-Aza]<sub>cyclic</sub>-W-NH<sub>2</sub> (1,5-triazole) (6a)



Ac-V-[Pra-SEL-Aha]<sub>cyclic</sub>-W-NH<sub>2</sub> (1,5-triazole) (6b)



Ac-V-[Aha-SEL-Pra]<sub>cyclic</sub>-W-NH<sub>2</sub> (1,5-triazole) (6c)



Purity

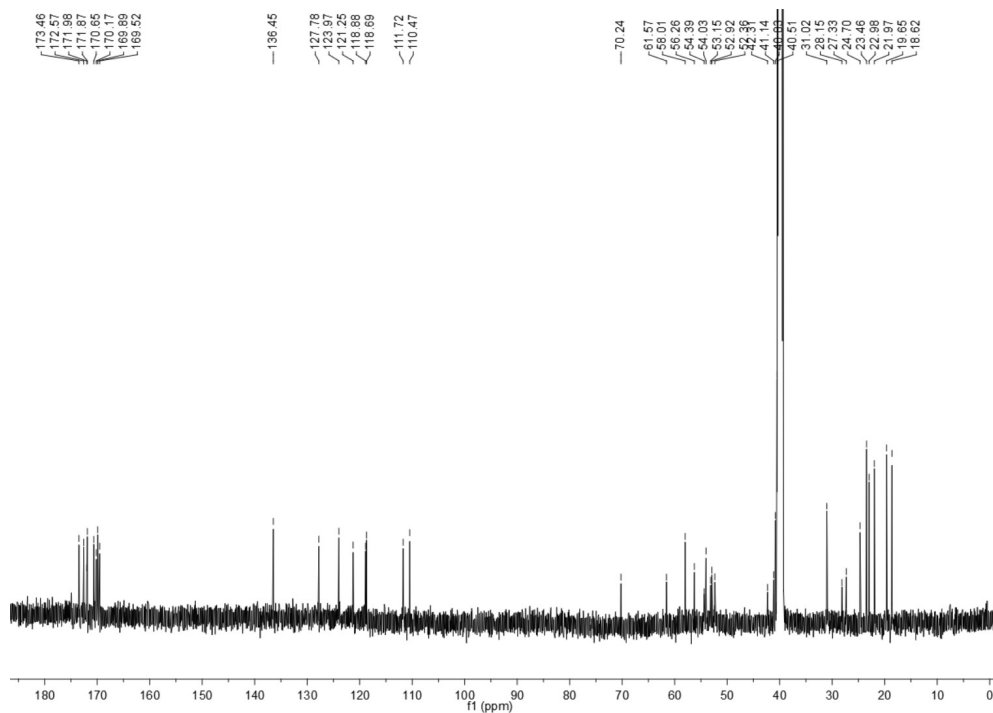
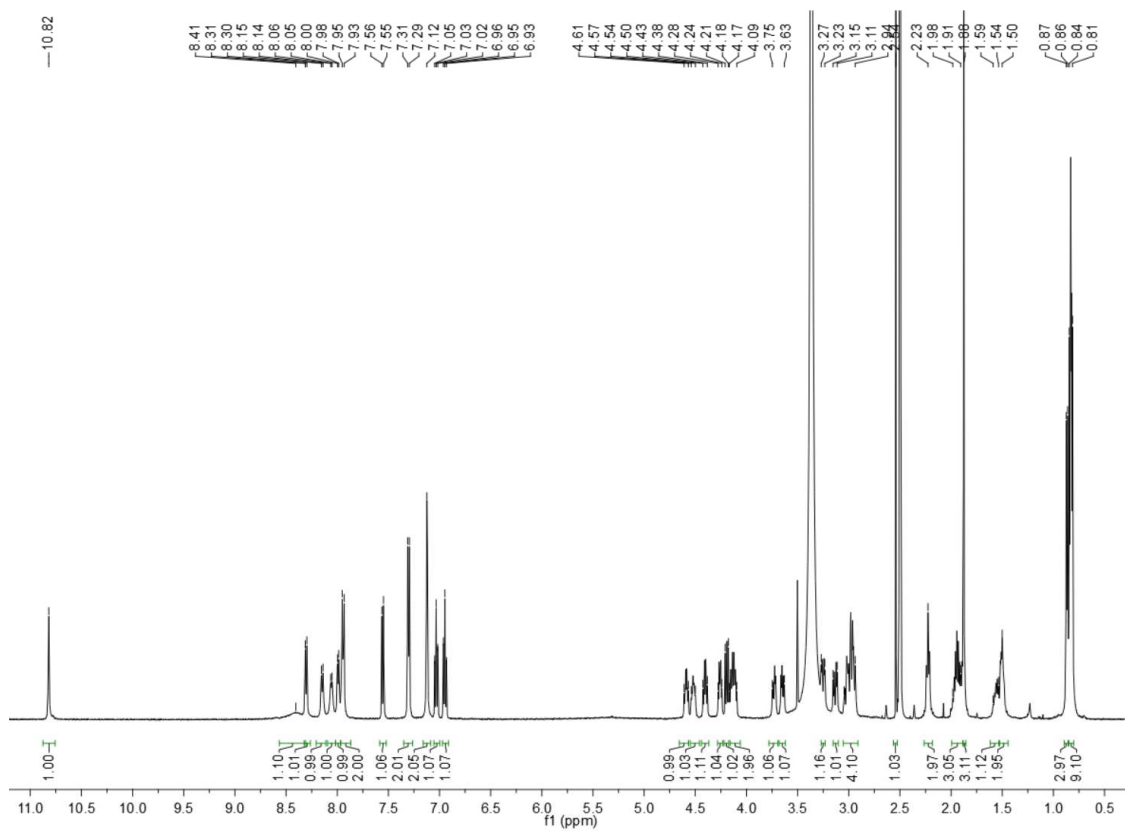
No.	Purity / %
1	100
2a	100
2b	100
3a	100
3b	95
3c	100
3d	91
3e	98
3f	100
4a	100
4b	92
5a	100
5b	100
5c	100
6a	100
6b	100
6c	100

## **<sup>1</sup>H-NMR and <sup>13</sup>C-NMR Spectra**

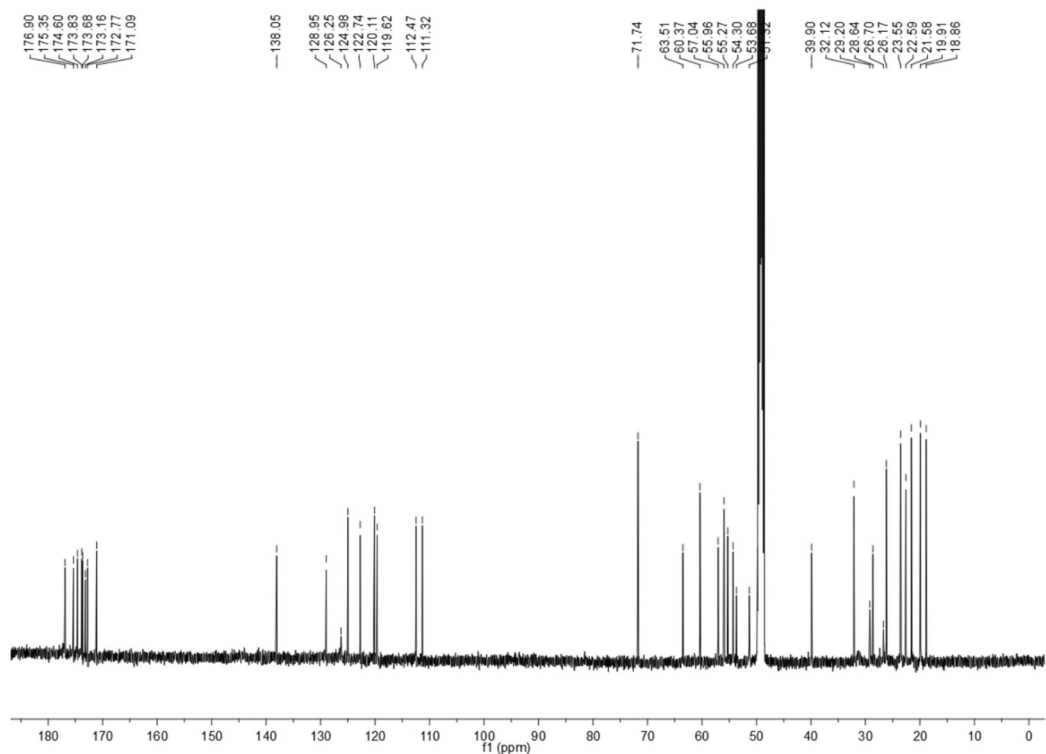
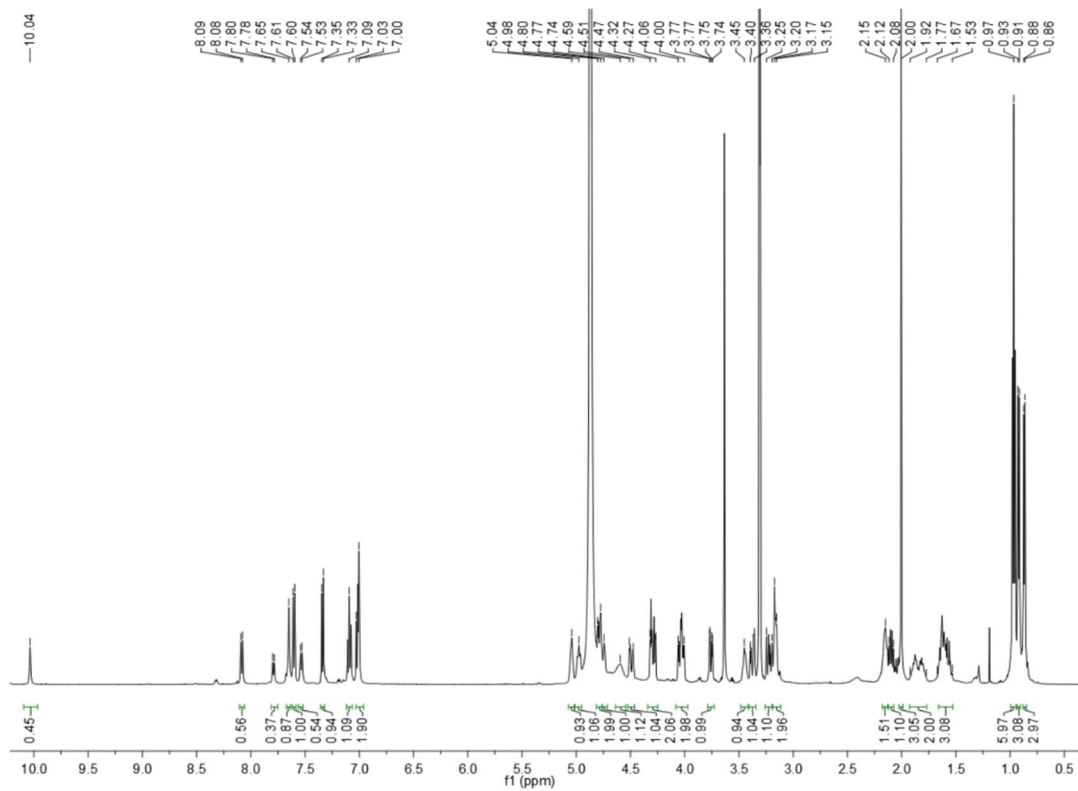
Compounds **1**, **5a-5c** were dissolved in 0.5 mL DMSO-d<sub>6</sub> and measured with Bruker Fourier spectrometer model Ultrashield Plus 500 (500 MHz for <sup>1</sup>H-NMR and 126 MHz for <sup>13</sup>C-NMR). Chemical shifts are given in parts per million (ppm) and referenced against the residual proton or carbon resonances of the >99% deuterated solvents as internal standard. Coupling constants (*J*) are given in Hertz (Hz). Data are reported as follows: chemical shift, multiplicity (s = singlet, d = doublet, t = triplet, q = quartet, m = multiplet, dd = doublet of doublets, dt = doublet of triplets, br = broad and combinations of these) coupling constants, and integration. NMR spectra were evaluated using MestReNova.

The 1,5-triazole analogues **6a**, **6b**, and **6c** were analyzed on a Bruker AVANCE III 600 MHz spectrometer equipped with a cryogenically cooled probe. The samples were prepared in 500 μL of H<sub>2</sub>O/D<sub>2</sub>O (9:1 v/v, ~2 mM, pH 3.4) and <sup>1</sup>H and <sup>13</sup>C experiments were acquired at 298 K (referencing to H<sub>2</sub>O at 4.70 ppm). The spectra were manually assigned using CCPNMR analysis 2.4.2.

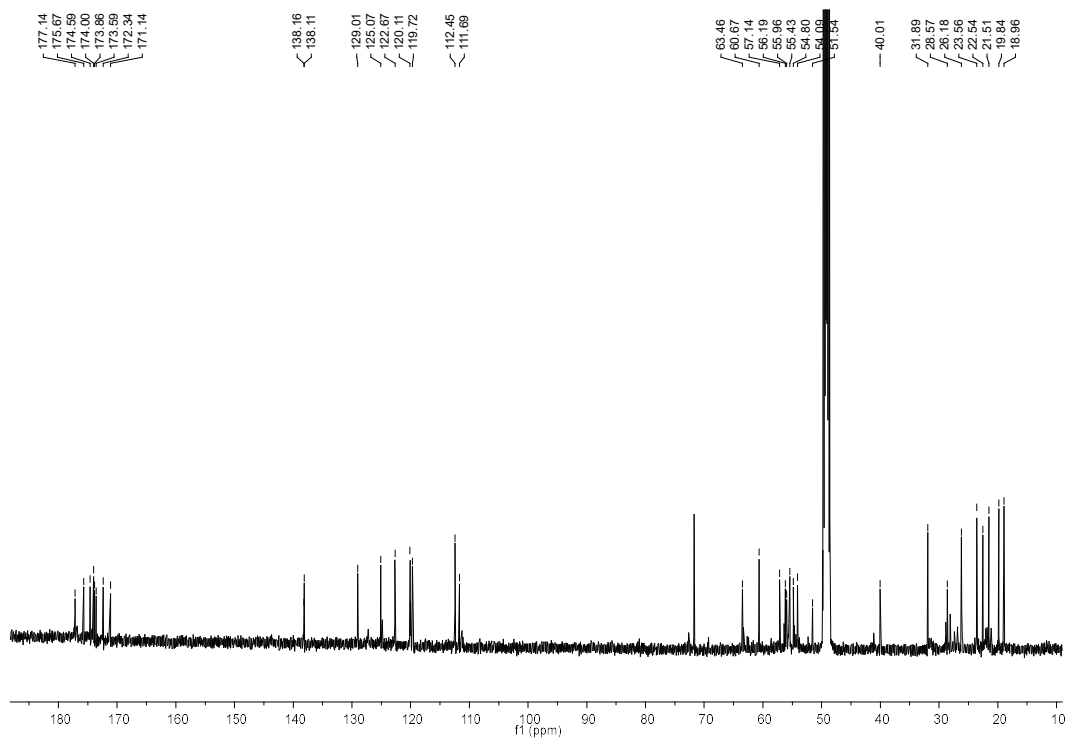
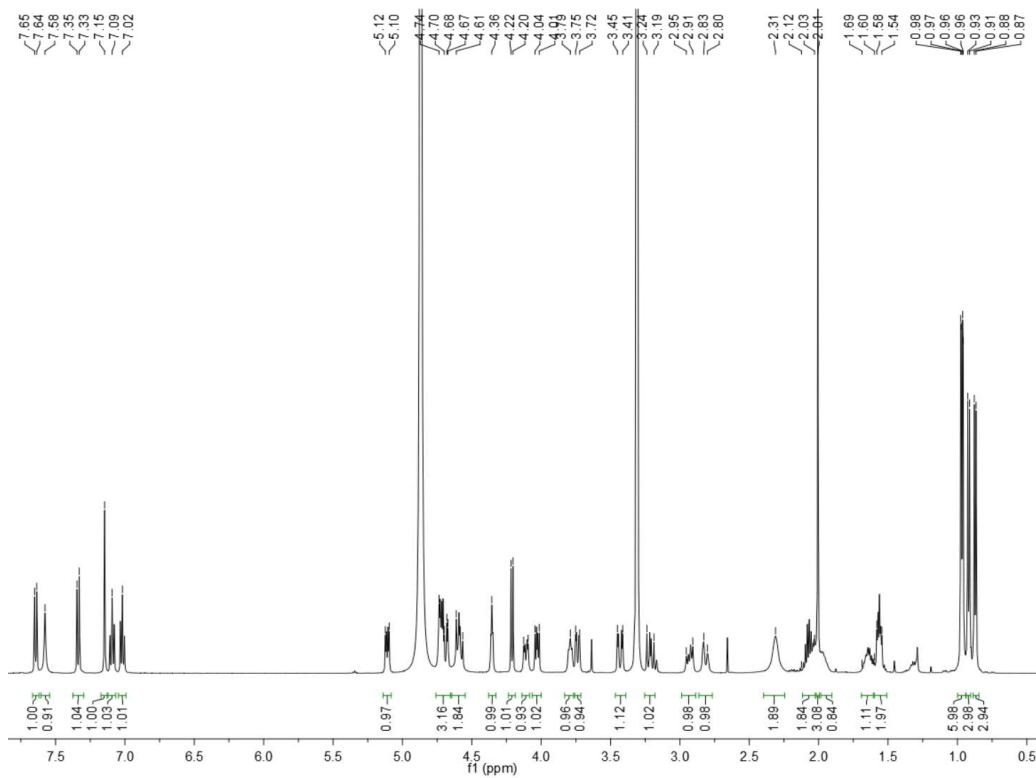
Ac-V-[CSELC]<sub>cyclic</sub>-W-NH<sub>2</sub> (1)



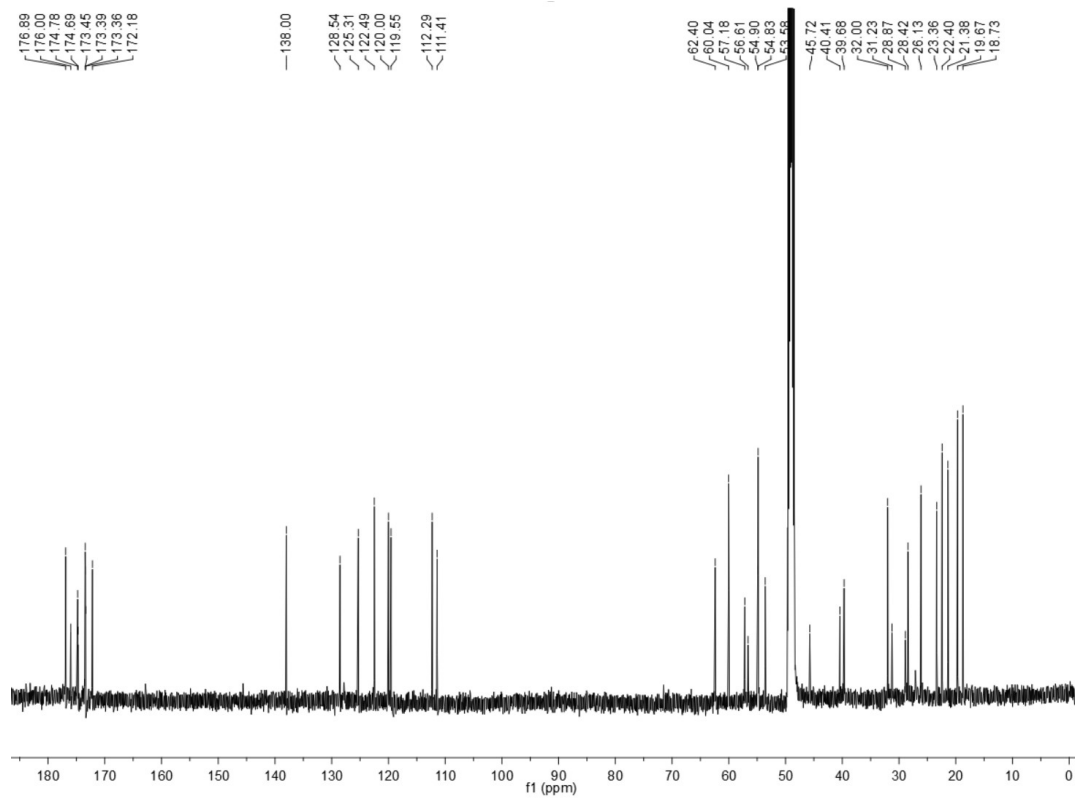
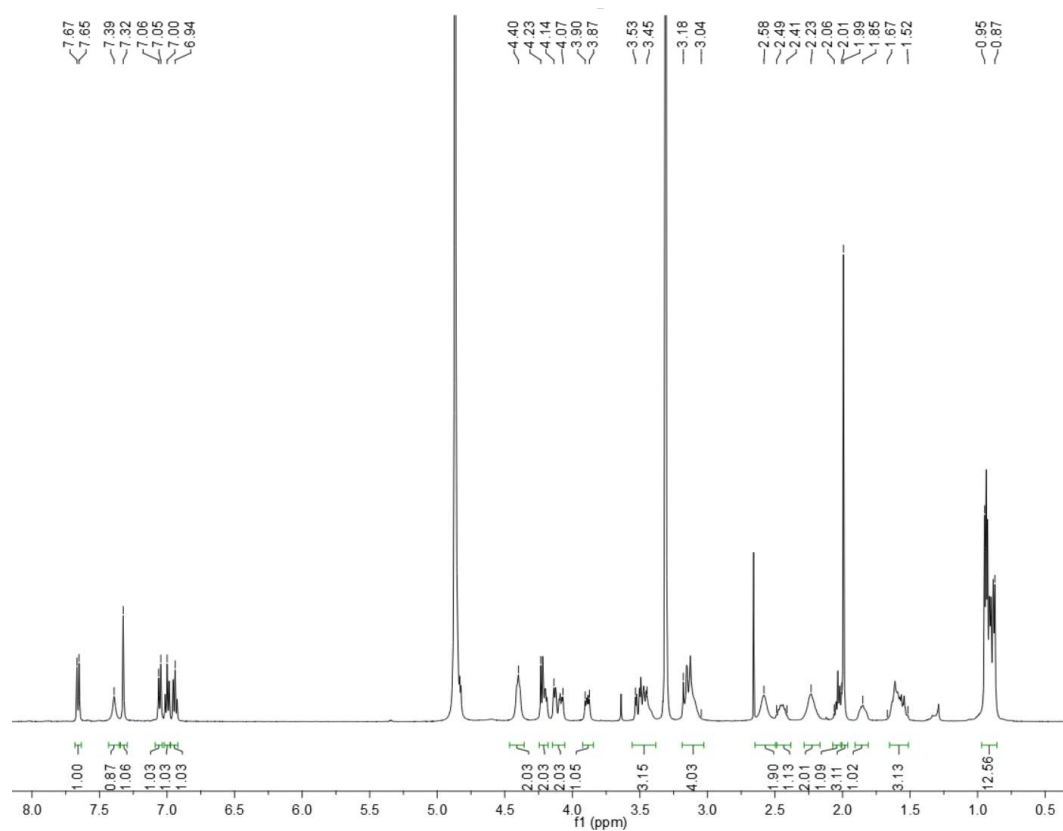
Ac-V-[Pra-SEL-Aza]<sub>cyclic</sub>-W-NH<sub>2</sub> (1,4-triazole) (5a)



Ac-V-[Aza-SEL-Pra]<sub>cyclic</sub>-W-NH<sub>2</sub> (1,4-triazole) (5b)

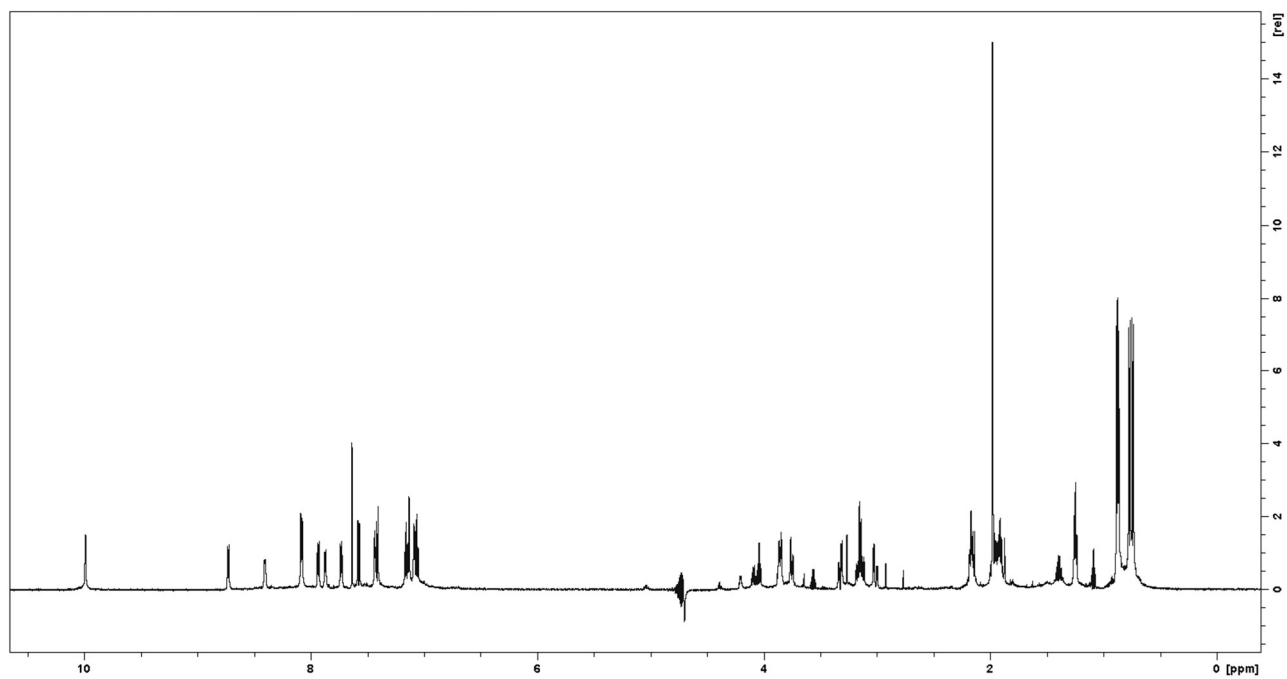


Ac-V-[Pra-SEL-Aha]<sub>cyclic</sub>-W-NH<sub>2</sub> (1,4-triazole) (5c)



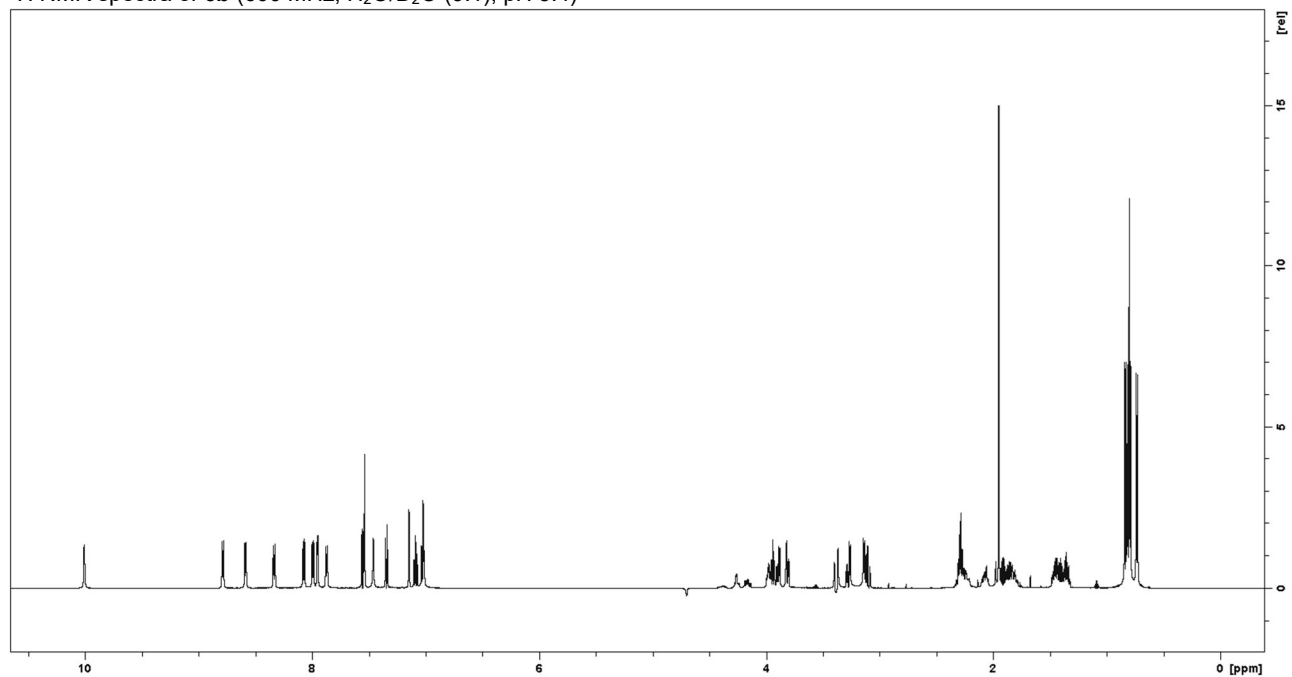
Ac-V-[**Pra-SEL-Aza**]<sub>cyclic</sub>-W-NH<sub>2</sub> (1,5-triazole) (**6a**)

<sup>1</sup>H NMR spectra of **6a** (600 MHz, H<sub>2</sub>O/D<sub>2</sub>O (9:1), pH 3.4)



Ac-V-[**Pra-SEL-**]<sub>cyclic</sub>-W-NH<sub>2</sub> (1,5-triazole) (**6b**)

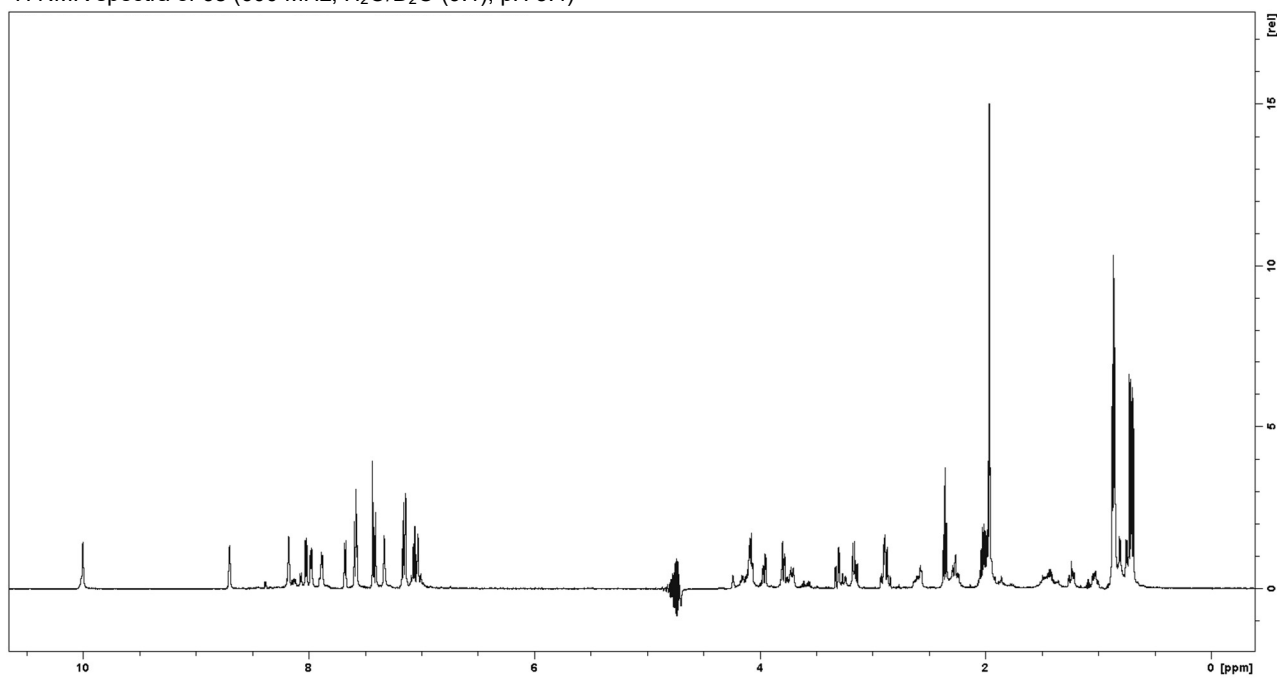
<sup>1</sup>H NMR spectra of **6b** (600 MHz, H<sub>2</sub>O/D<sub>2</sub>O (9:1), pH 3.4)





Ac-V-[Aha-SEL-Pra]<sub>cyclic</sub>-W-NH<sub>2</sub> (1,5-triazole) (**6c**)

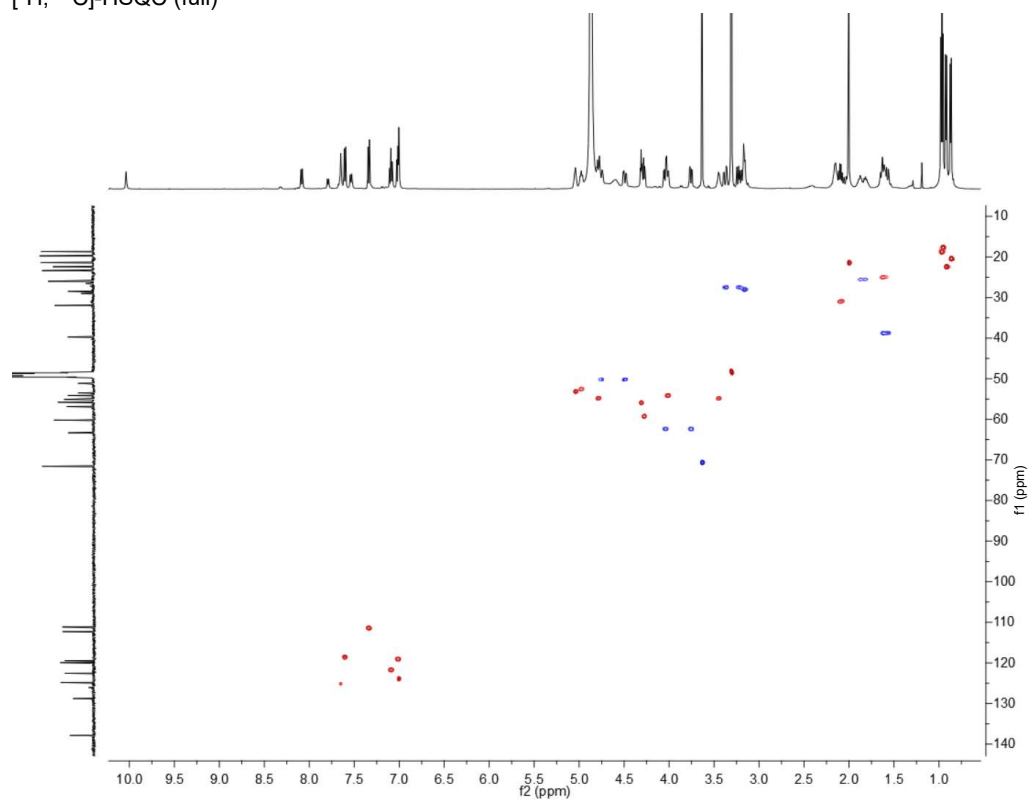
<sup>1</sup>H NMR spectra of **6c** (600 MHz, H<sub>2</sub>O/D<sub>2</sub>O (9:1), pH 3.4)



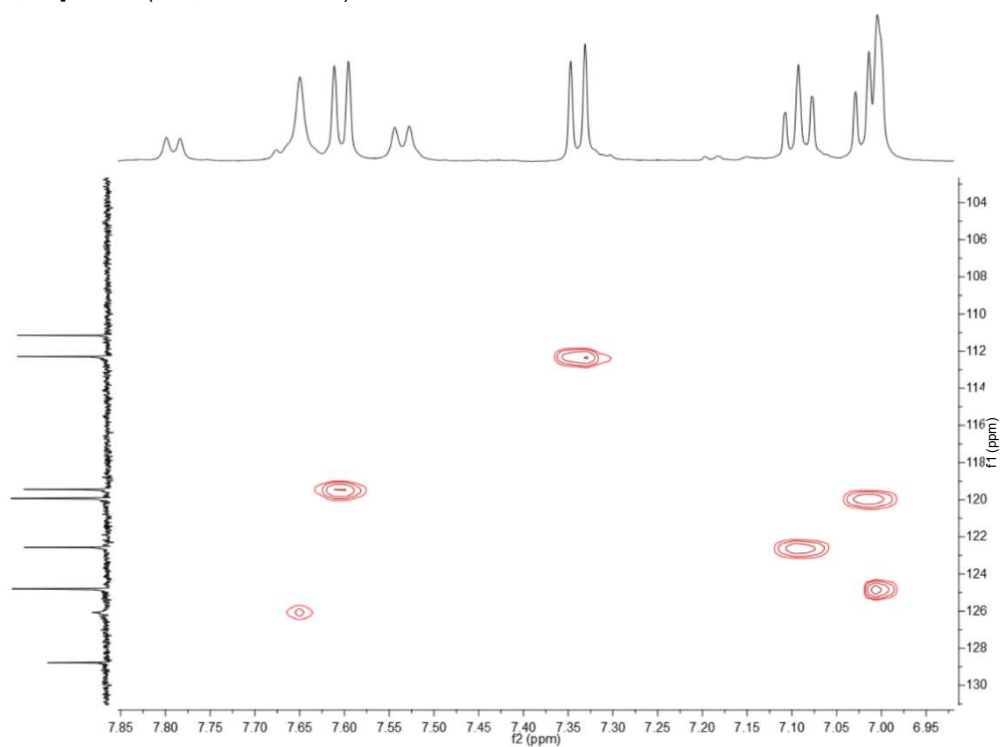
## 2D NMR Spectra

Ac-V-[Pra-SEL-Aza]<sub>cyclic</sub>-W-NH<sub>2</sub> (1,4-triazole) (**5a**)

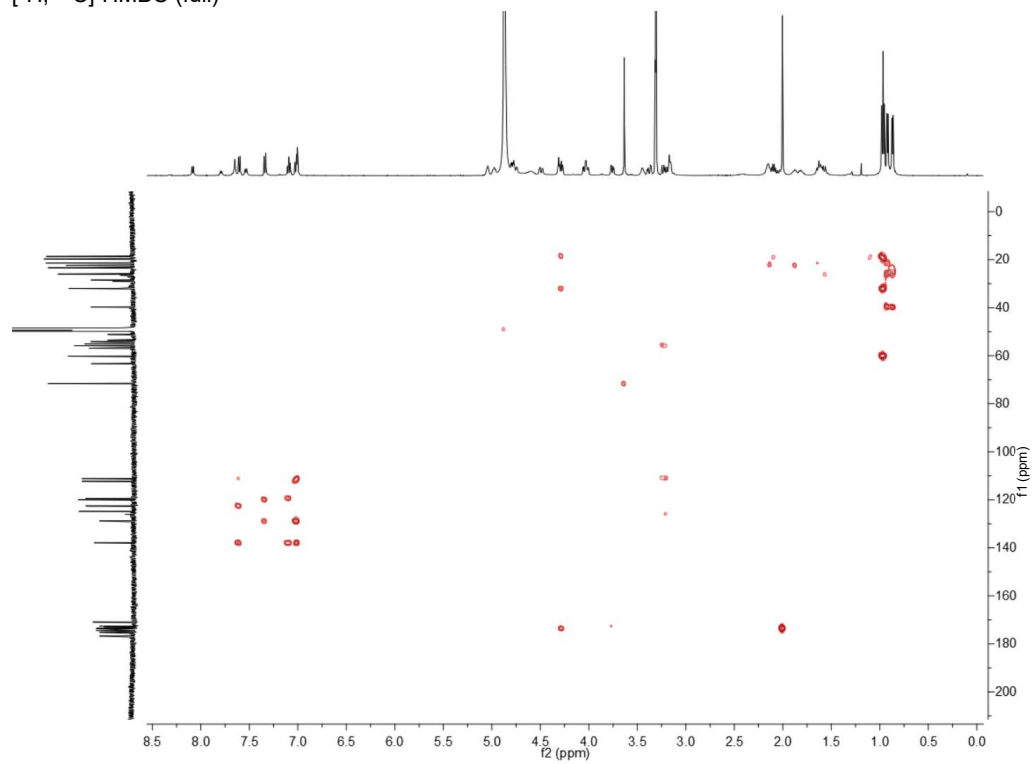
[<sup>1</sup>H, <sup>13</sup>C]-HSQC (full)



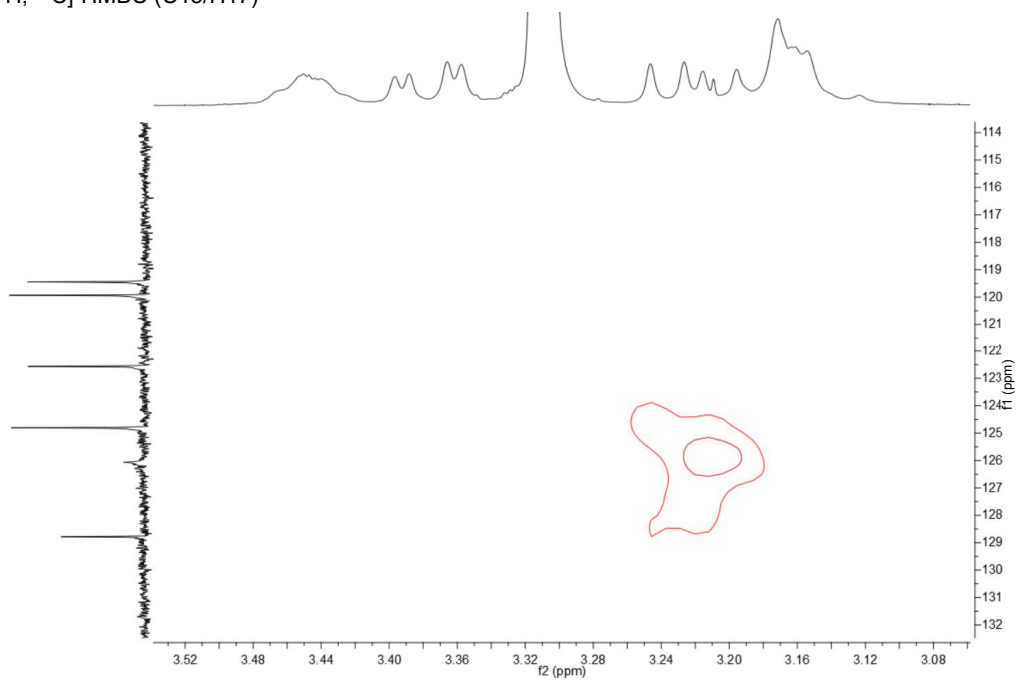
[<sup>1</sup>H, <sup>13</sup>C]-HSQC (7.65, 126.2 C/H 15) Triazole



[<sup>1</sup>H, <sup>13</sup>C]-HMBC (full)



[<sup>1</sup>H, <sup>13</sup>C]-HMBC (C15/H17)

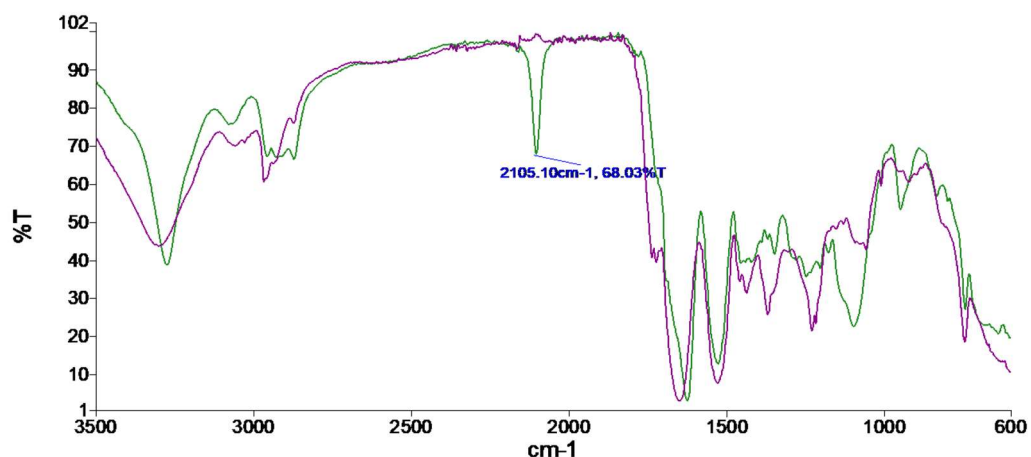


## FTIR Spectra

IR spectra were measured on a PerkinElmer Spectrum 100 FT-IR Spectrometer. The samples were measured as solid.

Ac-V-[Pra-SEL-Aza]<sub>cyclic</sub>-W-NH<sub>2</sub> (1,4-triazole) (**5a**)

### Spectrum



Green curve: before CuAAC

Purple curve: after CuAAC

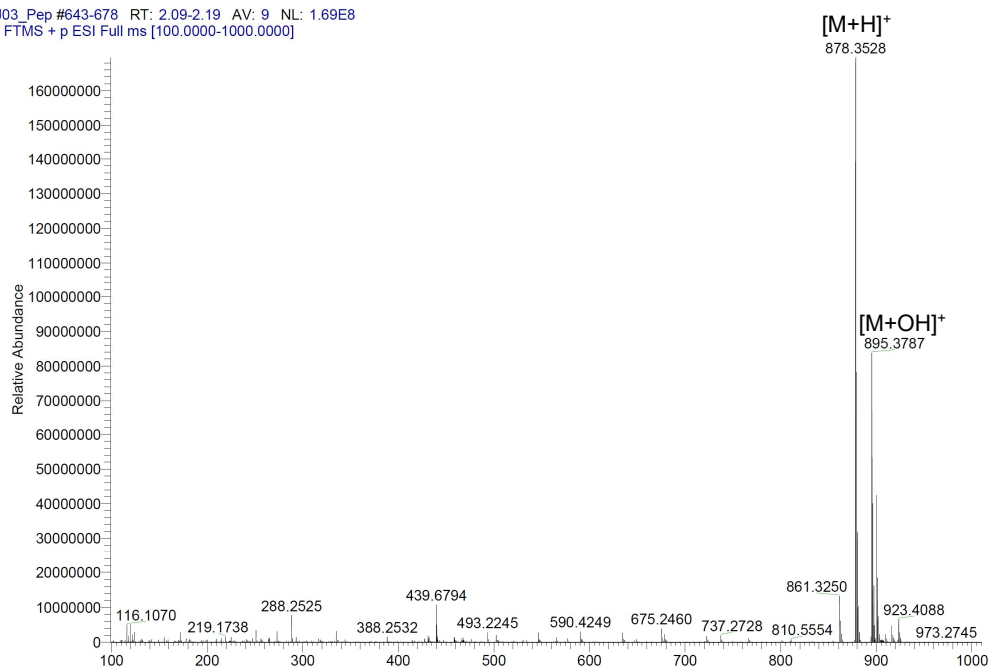
## HRMS

Compounds **1** and **5a-5c** were solved in H<sub>2</sub>O/ACN (1:1) (v/v). HRMS was done with a DIONEX UltiMate 3000 UHPLC<sup>+</sup> focused (Thermo Scientific), containing pump, autosampler, column compartment heated to 30 °C, diode array detector, and Q exactive focus. We used an EC 150/2 NUCLEODUR C18 Pyramid, 3 μm (Macherey-Nagel) column with a gradient from 90-5 % solvent B over 9 min and 1.5 min constant 5 % solvent B (solvent A: H<sub>2</sub>O (0.05 % formic acid), solvent B: ACN (0.05 % formic acid)) and a 0.5 mL/min flowrate.

Compounds **6a**, **6b** and **6c** were analyzed by HRMS on a Shimadzu interfaced UPLC coupled to an AB Sciex 5600 TripleTOF MS using time-of-flight-MS (TOF-MS) scanning. The samples were run over a linear gradient of 20-40% acetonitrile in H<sub>2</sub>O (v/v) on an Agilent Zorbax C18 column (100 x 2.1 mm, 1.8 μm) at 40 °C and a flow rate of 0.2 mL/min. The electrospray voltage was 5500 V with a source temperature of 500 °C. The data was processed using Analyst v1.6.3 software by AB Sciex.

Ac-V-[CSELC]<sub>cyclic</sub>-W-NH<sub>2</sub> (1)

VJ03\_Pep #643-678 RT: 2.09-2.19 AV: 9 NL: 1.69E8  
T: FTMS + p ESI Full ms [100.0000-1000.0000]

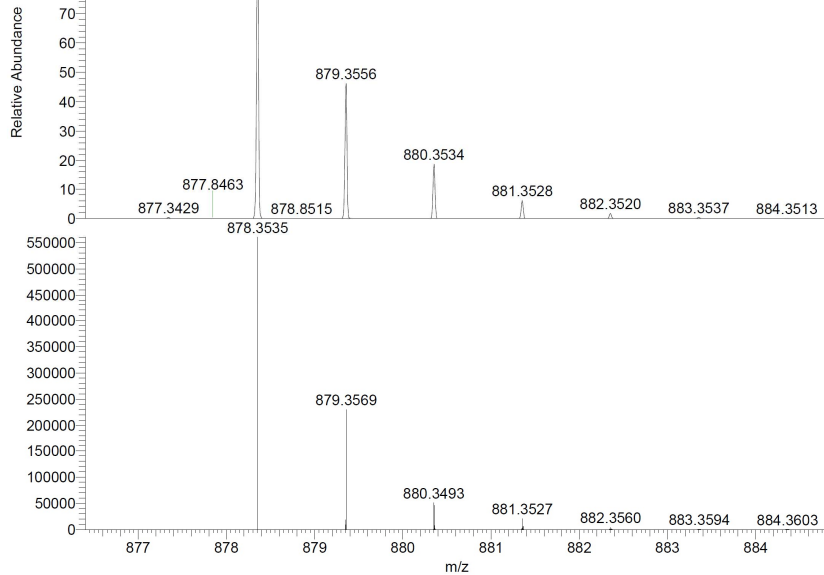


Relative Abundance

100  
90  
80  
70  
60  
50  
40  
30  
20  
10  
0

877.3429 877.8463 878.3528 878.3535 878.8515 879.3556 880.3534 881.3528 882.3520 883.3537 884.3513

NL:  
1.69E8  
VJ03\_Pep#643-678 RT:  
2.09-2.19 AV: 9 T:  
FTMS + p ESI Full ms  
[100.0000-1000.0000]



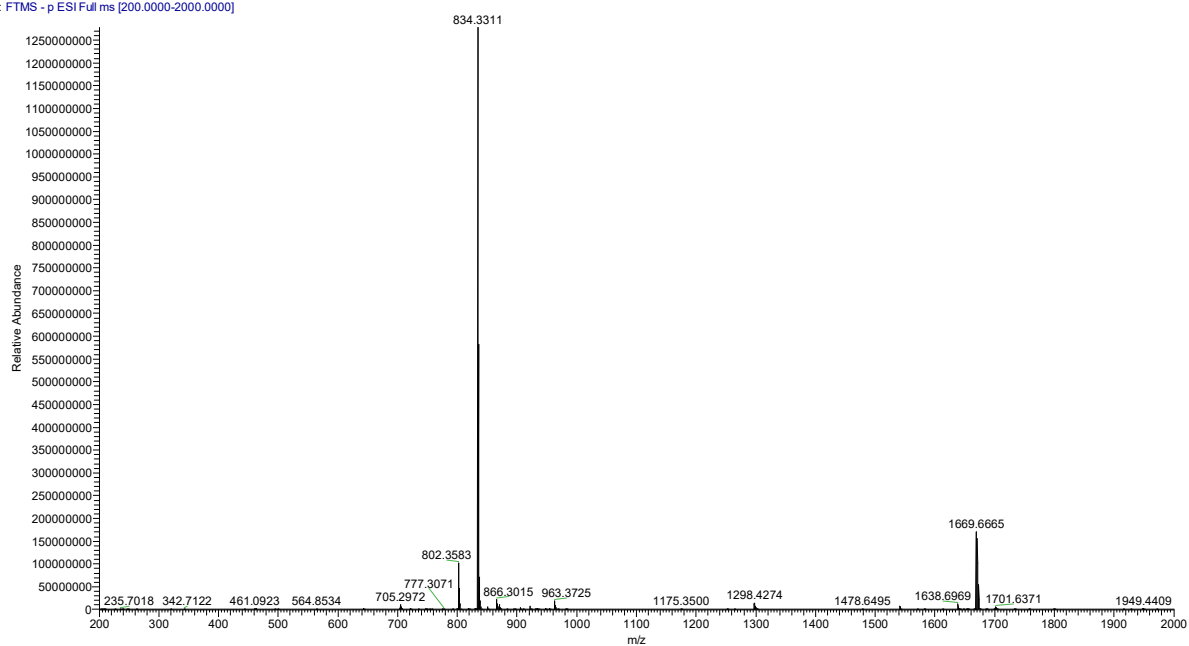
[M+H]<sup>+</sup>

NL:  
5.60E5  
C<sub>38</sub>H<sub>55</sub>N<sub>9</sub>O<sub>11</sub>S<sub>2</sub>+H:  
C<sub>38</sub>H<sub>56</sub>N<sub>9</sub>O<sub>11</sub>S<sub>2</sub>  
pa Chrg 1

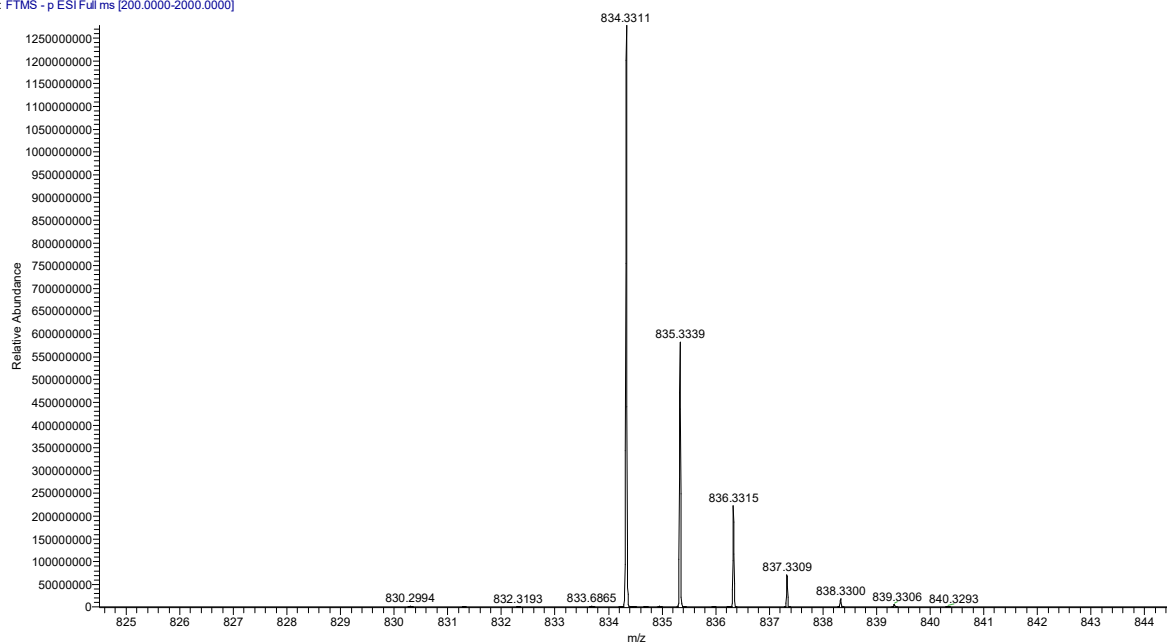
[M+H]<sup>+</sup>

**H-V-[CSELC]<sub>cyclic</sub>-W-NH<sub>2</sub> (2a)**

BZO\_peptide2a #382 RT: 3.97 AV: 1 NL: 1.28E9  
T: FTMS - p ESI Full ms [200.0000-2000.0000]

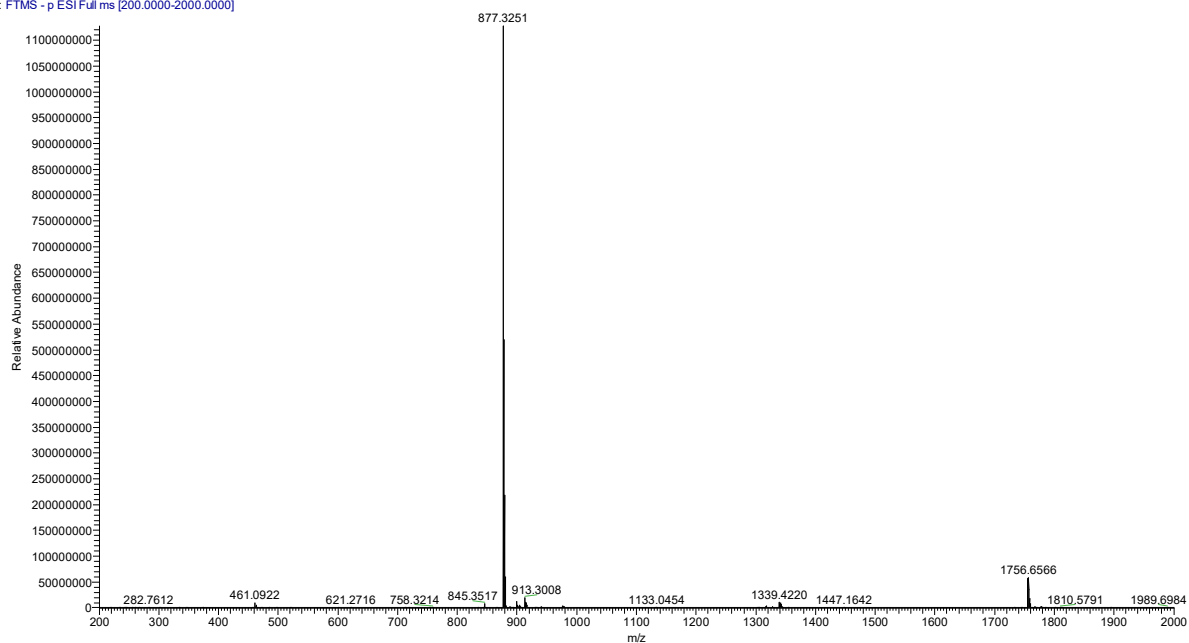


BZO\_peptide2a #382 RT: 3.97 AV: 1 NL: 1.28E9  
T: FTMS - p ESI Full ms [200.0000-2000.0000]

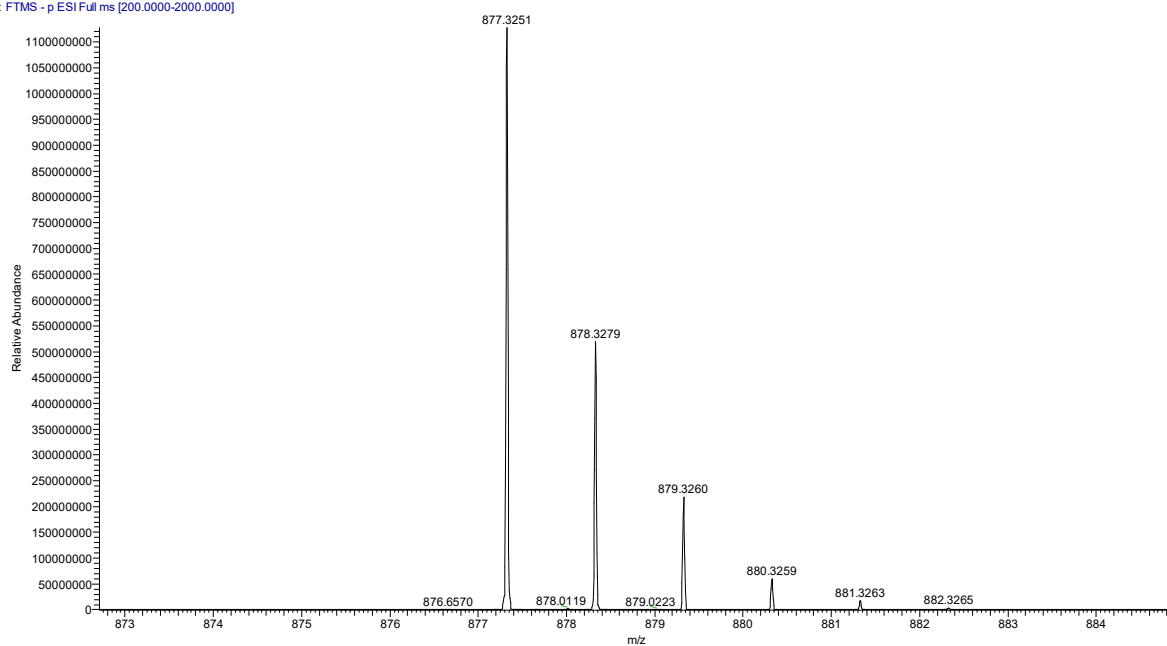


Ac-V-[CSELC]<sub>cyclic</sub>-W-OH (2b)

BZO\_peptide2b #444 RT: 4.73 AV: 1 NL: 1.13E9  
T: FTMS - p ESI Full ms [200.0000-2000.0000]

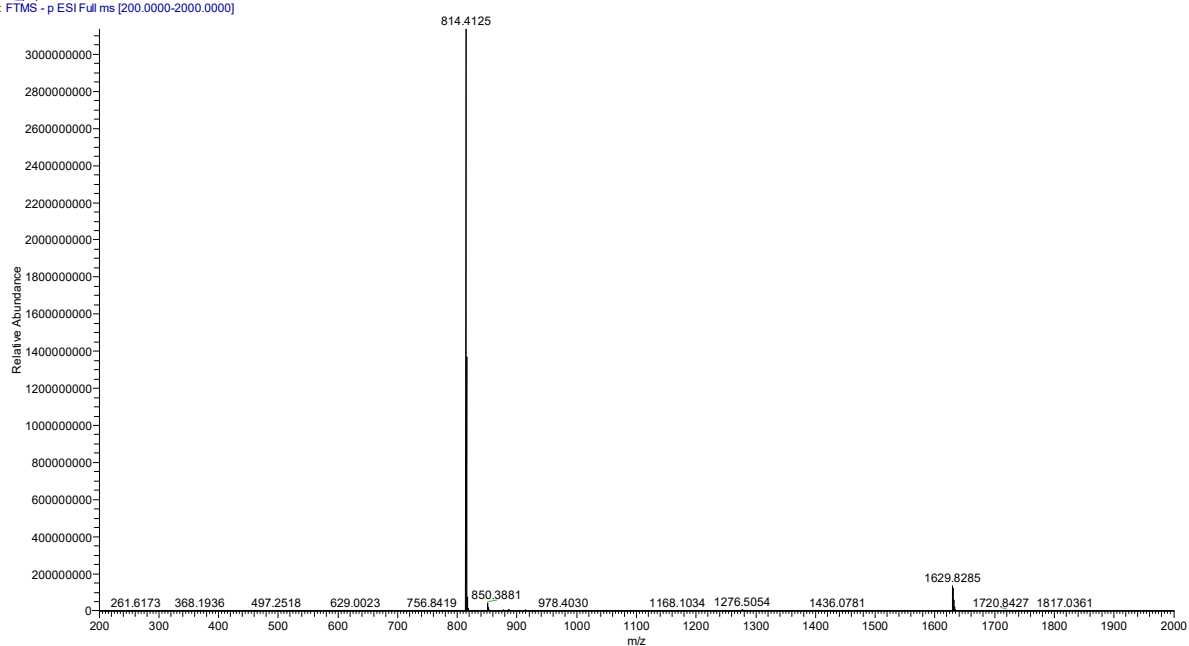


BZO\_peptide2b #444 RT: 4.73 AV: 1 NL: 1.13E9  
T: FTMS - p ESI Full ms [200.0000-2000.0000]

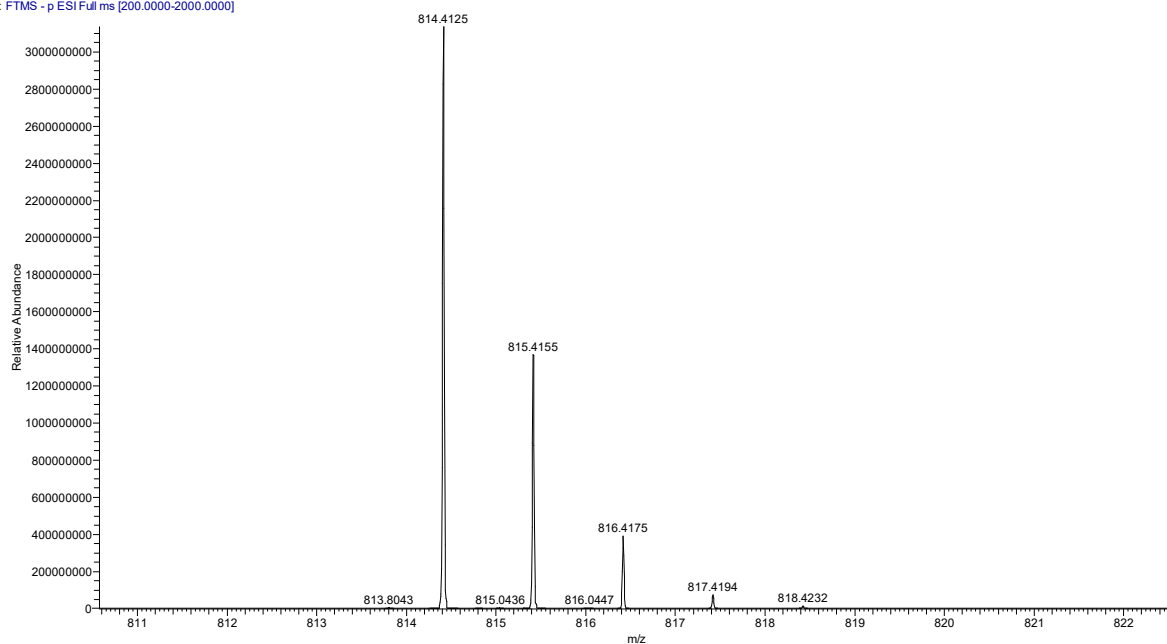


Ac-VASELAW-NH<sub>2</sub> (3a)

BZO\_peptide3a #424 RT: 4.52 AV: 1 NL: 3.13E9  
T: FTMS - p ESI Full ms [200.0000-2000.0000]



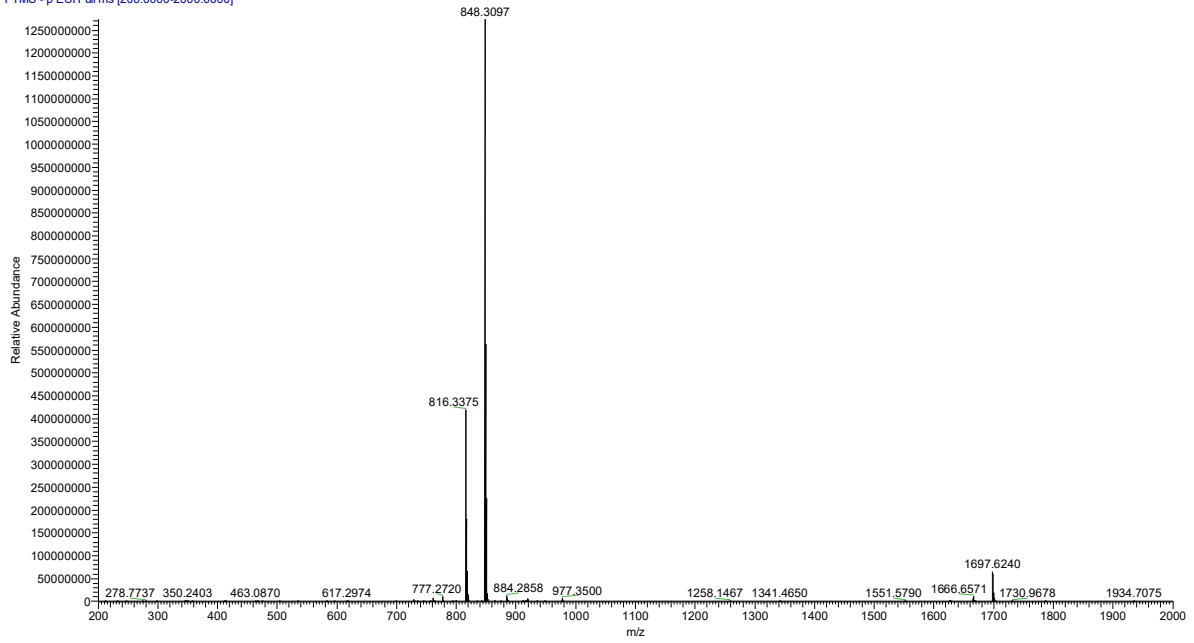
BZO\_peptide3a #424 RT: 4.52 AV: 1 NL: 3.13E9  
T: FTMS - p ESI Full ms [200.0000-2000.0000]



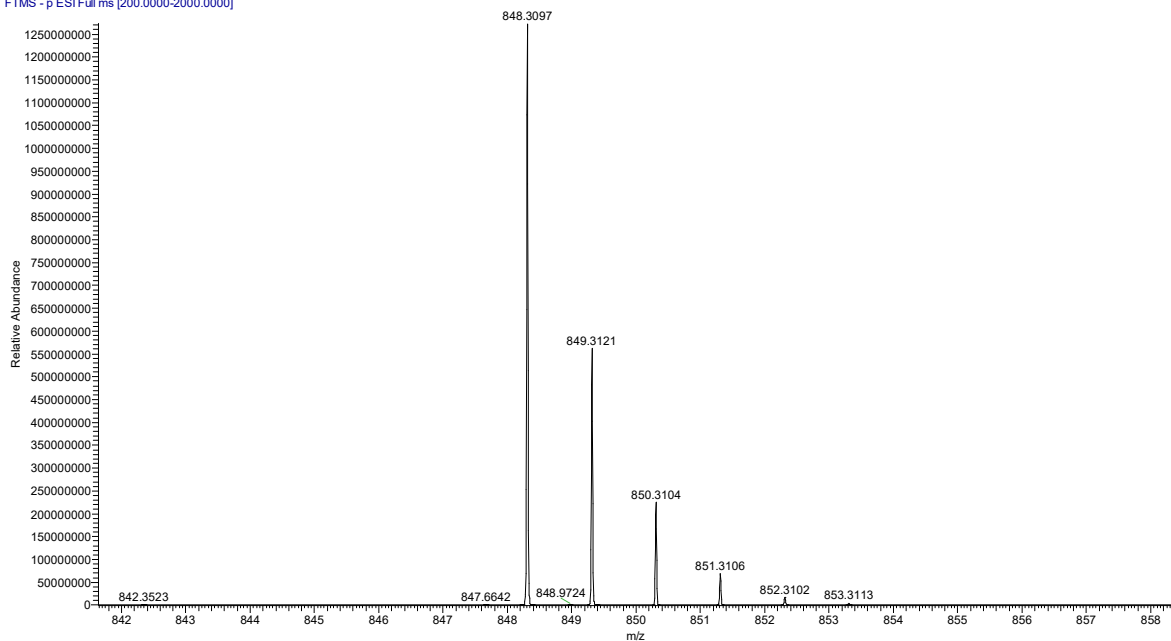


Ac-A-[CSELC]<sub>cyclic</sub>-W-NH<sub>2</sub> (3b)

BZO peptide3b #420 RT: 4.47 AV: 1 NL: 1.27E9  
T: FTMS - p ESI Full ms [200.0000-2000.0000]

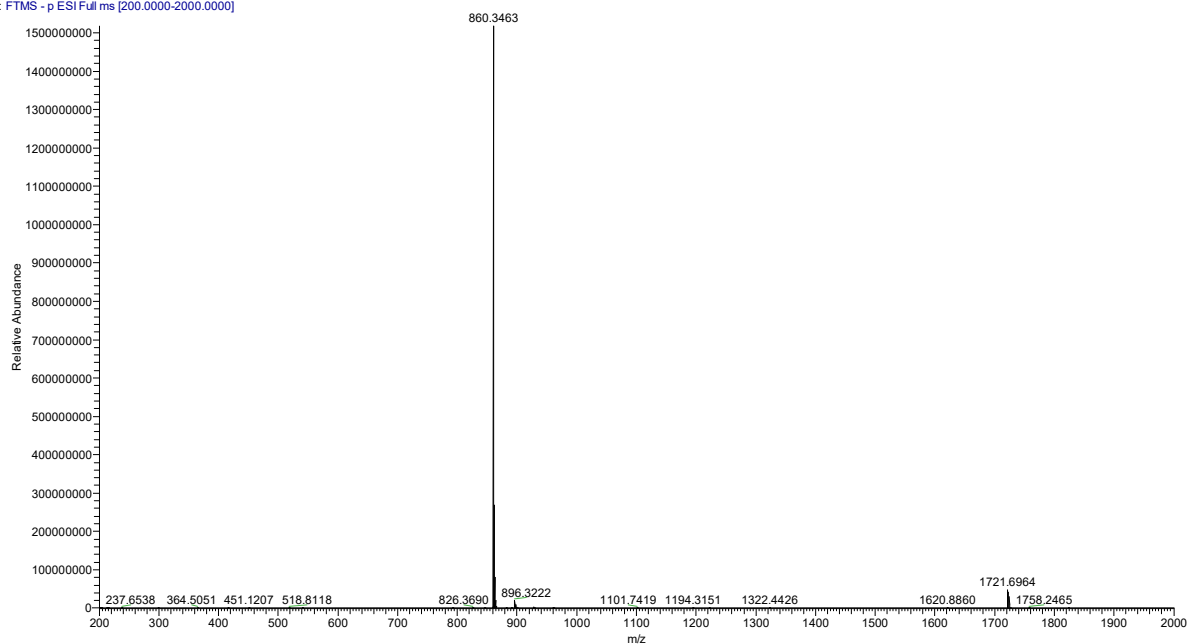


BZO peptide3b #420 RT: 4.47 AV: 1 NL: 1.27E9  
T: FTMS - p ESI Full ms [200.0000-2000.0000]

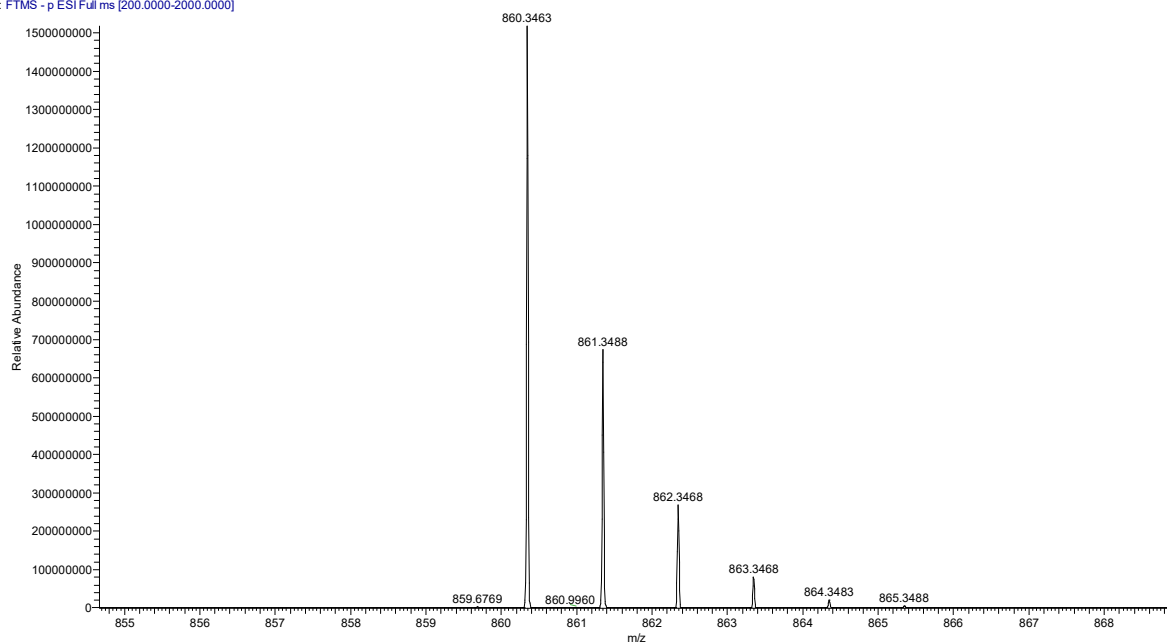


Ac-V-[CAELC]<sub>cyclic</sub>-W-NH<sub>2</sub> (3c)

BZO\_peptide3c #432 RT: 4.69 AV: 1 NL: 1.52E9  
T: FTMS - p ESI Full ms [200.0000-2000.0000]

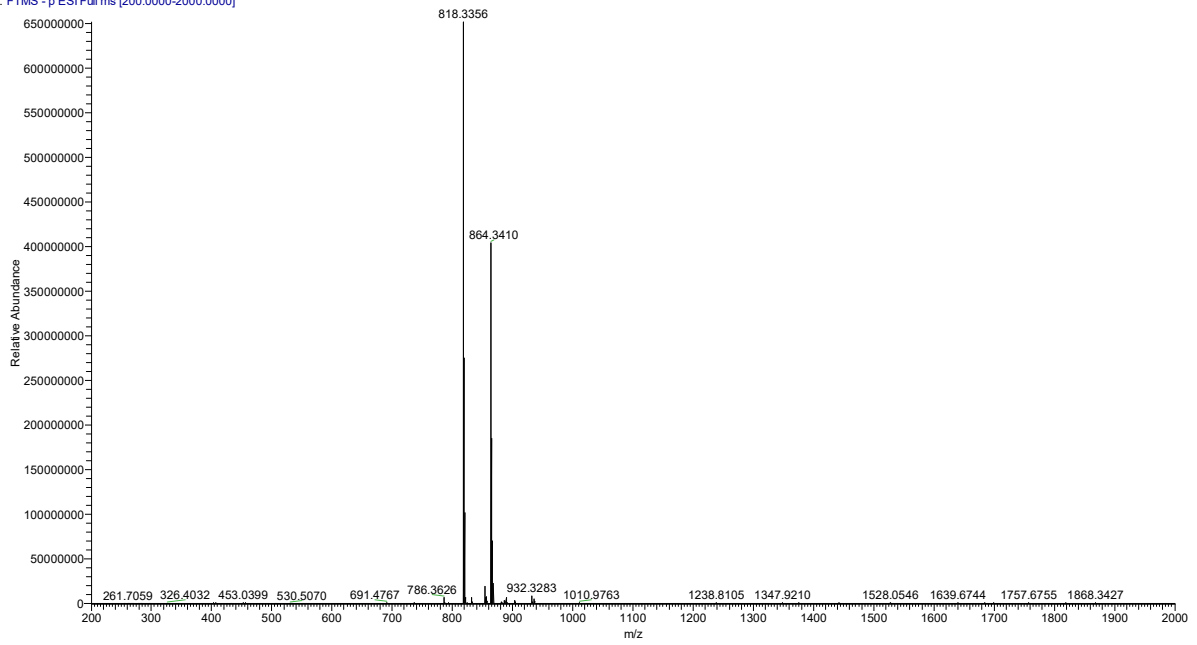


BZO\_peptide3c #432 RT: 4.69 AV: 1 NL: 1.52E9  
T: FTMS - p ESI Full ms [200.0000-2000.0000]

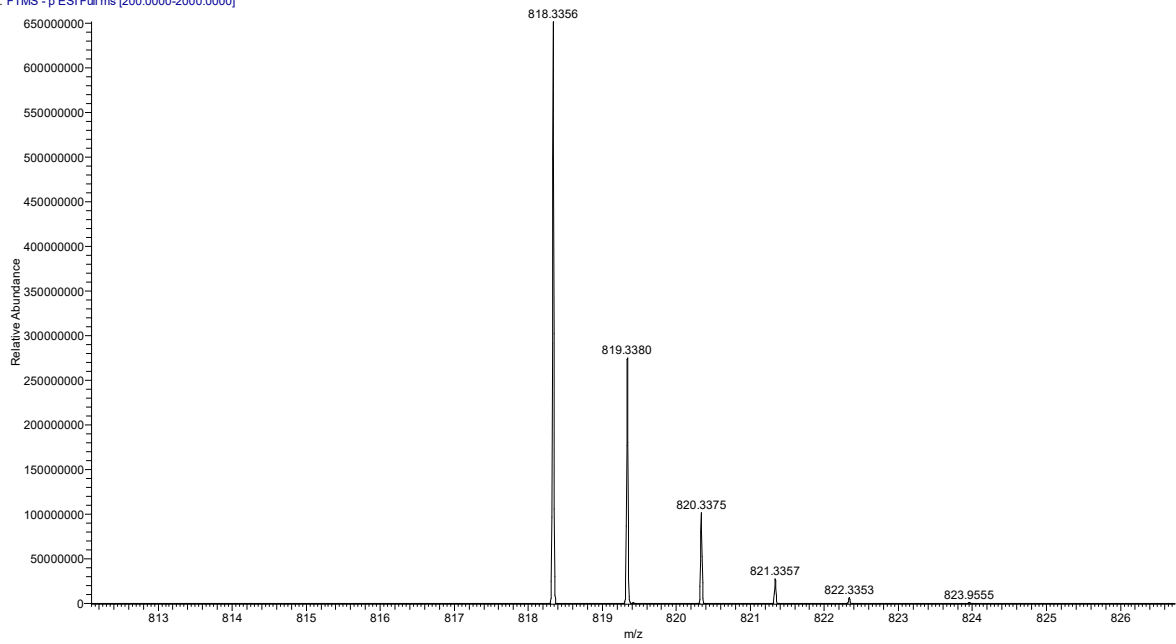


Ac-V-[CSALC]<sub>cyclic</sub>-W-NH<sub>2</sub> (3d)

BZO\_peptide3d #438 RT: 4.73 AV: 1 NL: 6.51E8  
T: FTMS - p ESI Full ms [200.0000-2000.0000]

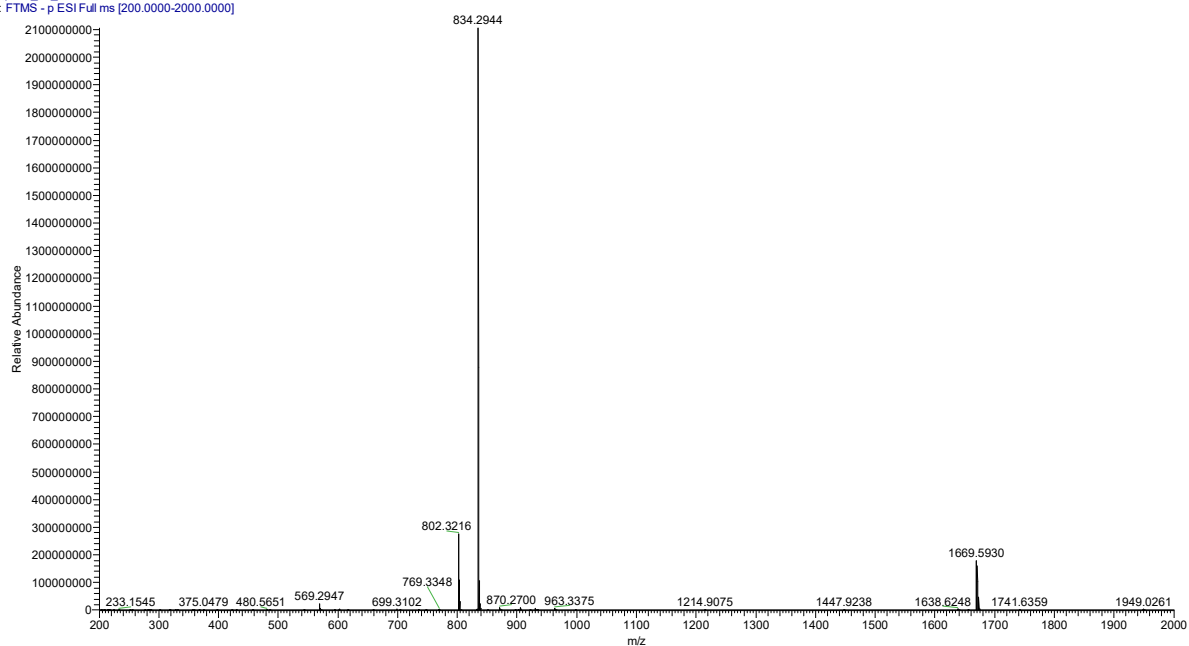


BZO\_peptide3d #438 RT: 4.73 AV: 1 NL: 6.51E8  
T: FTMS - p ESI Full ms [200.0000-2000.0000]

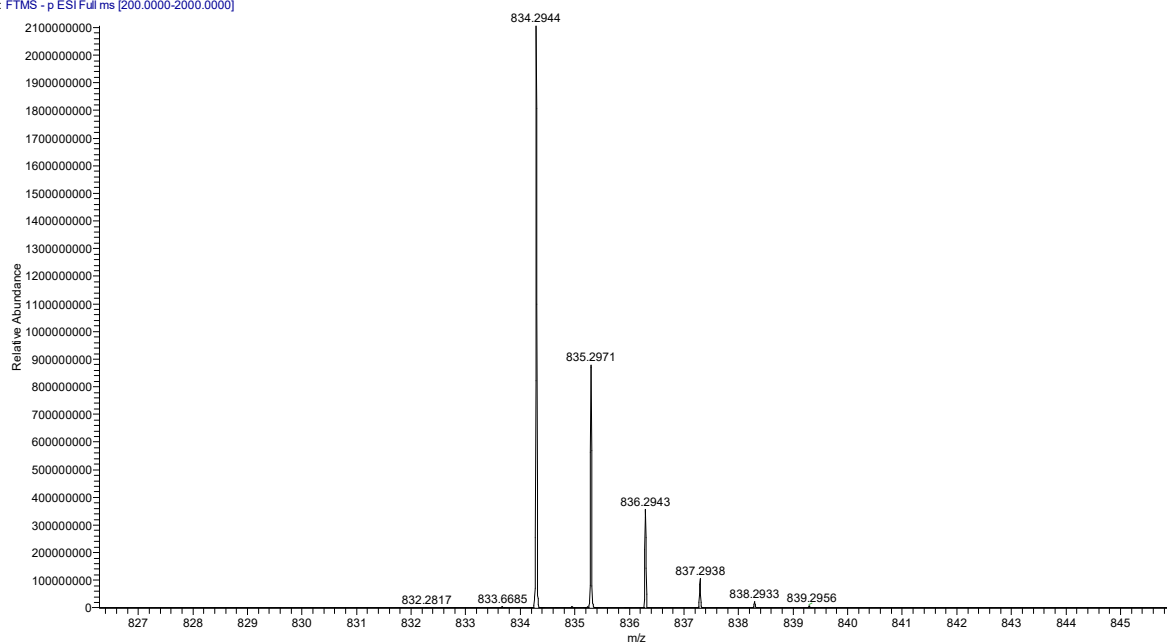


Ac-V-[CSEAC]<sub>cyclic</sub>-W-NH<sub>2</sub> (3e)

peptide\_3e\_2 #416 RT: 4.34 AV: 1 NL: 2.10E9  
T: FTMS - p ESI Full ms [200.0000-2000.0000]

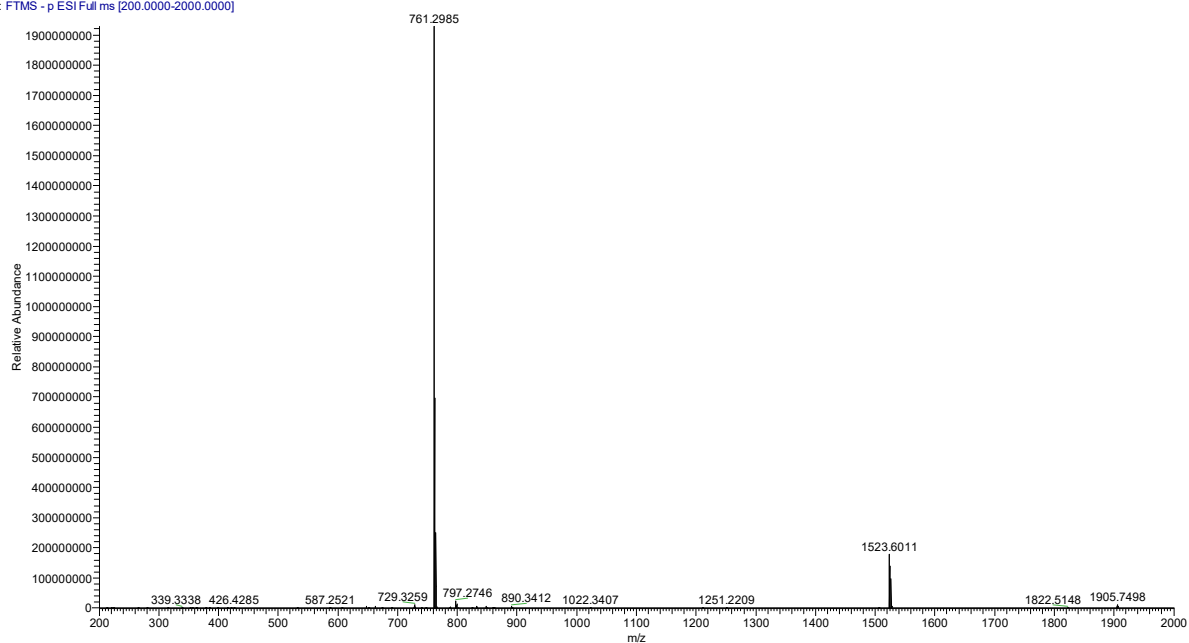


peptide\_3e\_2 #416 RT: 4.34 AV: 1 NL: 2.10E9  
T: FTMS - p ESI Full ms [200.0000-2000.0000]

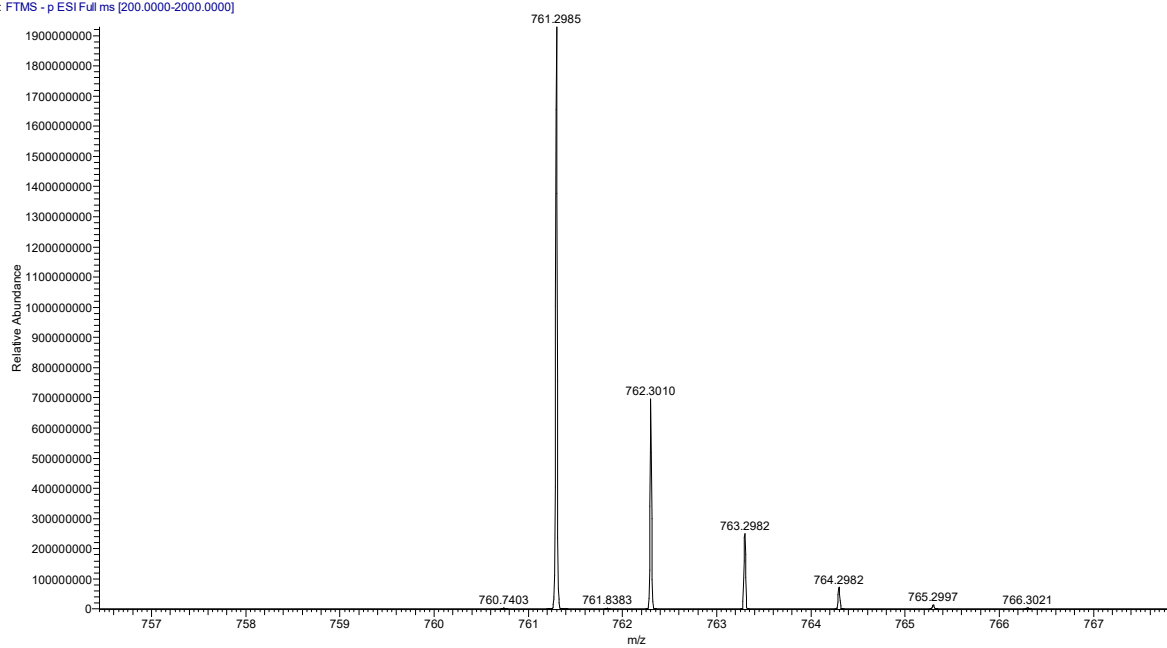


Ac-V-[CSELC]<sub>cyclic</sub>-A-NH<sub>2</sub> (3f)

BZO\_peptide3f #388 RT: 4.20 AV: 1 NL: 1.93E9  
T: FTMS - p ESI Full ms [200.0000-2000.0000]

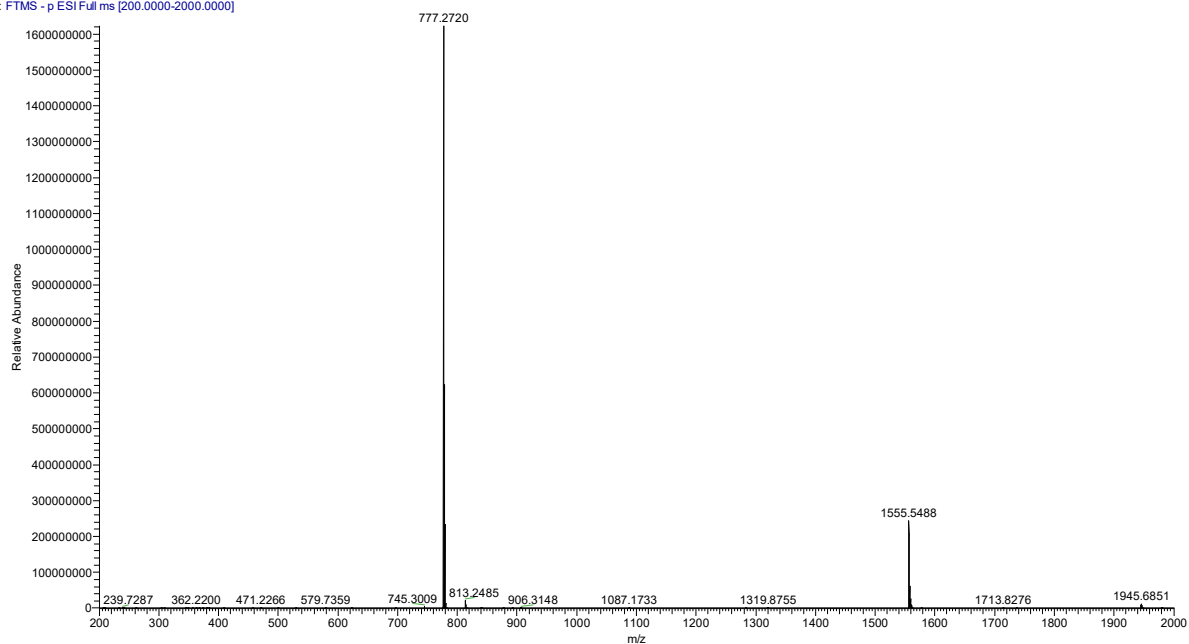


BZO\_peptide3f #388 RT: 4.20 AV: 1 NL: 1.93E9  
T: FTMS - p ESI Full ms [200.0000-2000.0000]

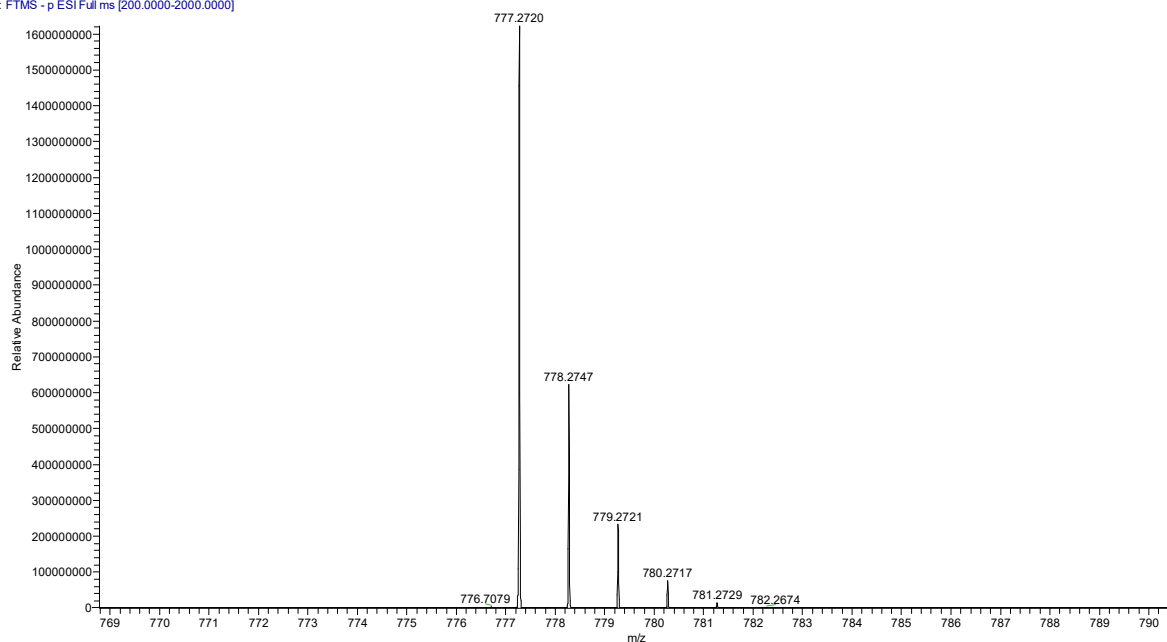


Ac- -[CSELC]<sub>cyclic</sub>-W-NH<sub>2</sub> (4a)

BZO\_peptide4a #414 RT: 4.47 AV: 1 NL: 1.62E9  
T: FTMS -p ESI Full ms [200.0000-2000.0000]

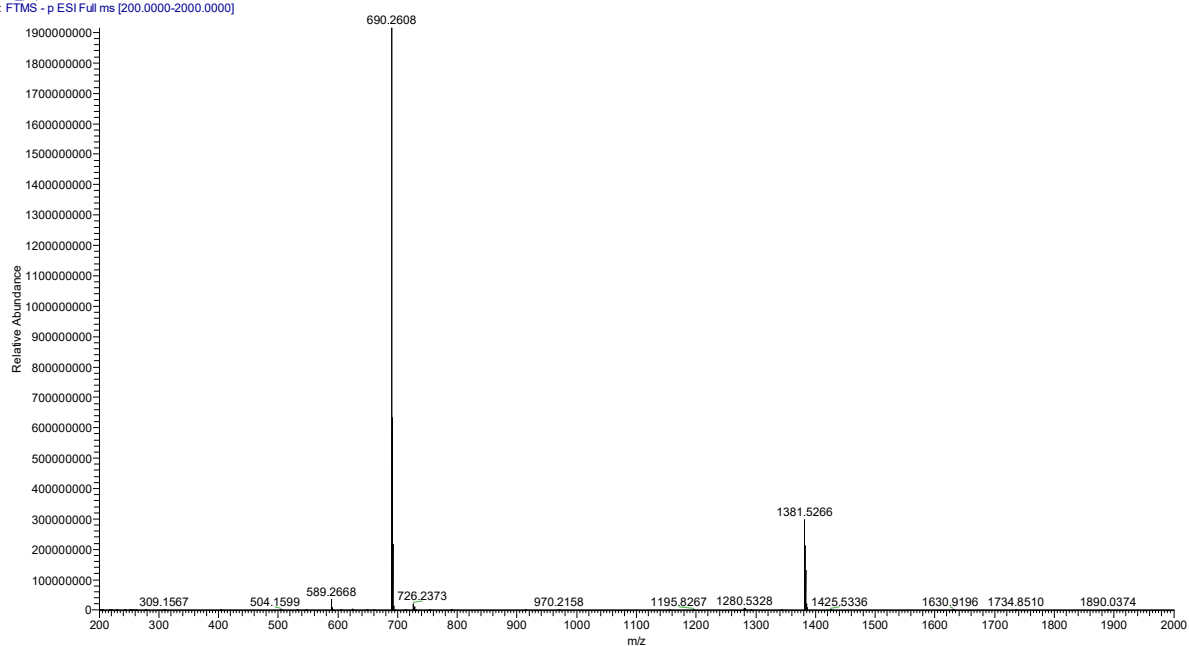


BZO\_peptide4a #414 RT: 4.47 AV: 1 NL: 1.62E9  
T: FTMS -p ESI Full ms [200.0000-2000.0000]

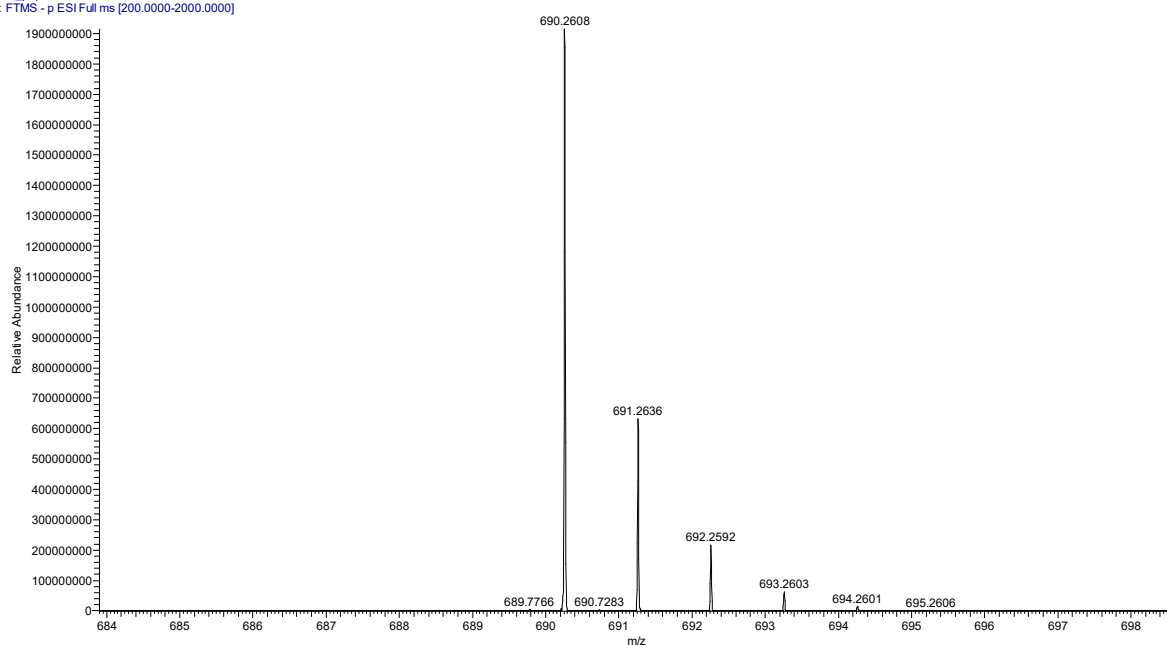


Ac-V-[CSELC]<sub>cyclic</sub> - -NH<sub>2</sub> (4b)

BZO\_peptide4b #398 RT: 4.25 AV: 1 NL: 1.91E9  
T: FTMS - p ESI Full ms [200.0000-2000.0000]

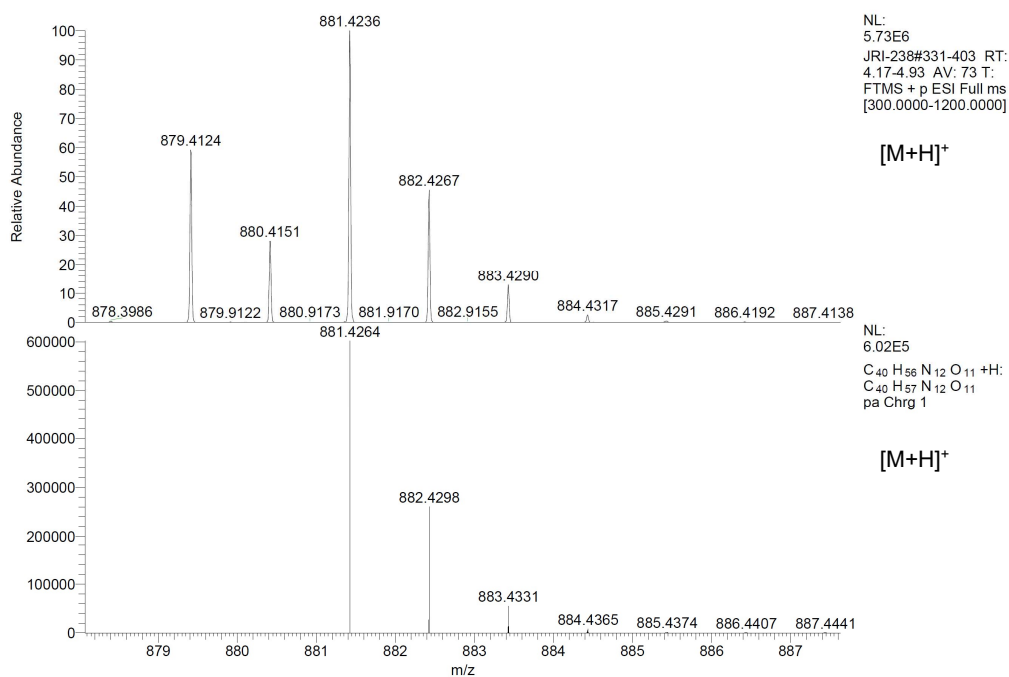
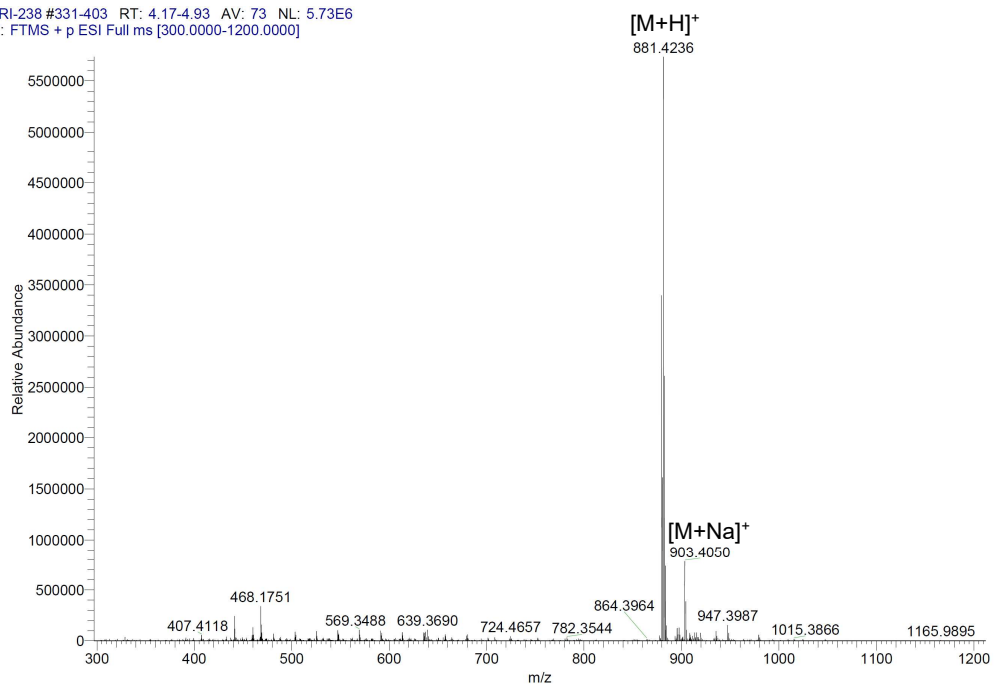


BZO\_peptide4b #398 RT: 4.25 AV: 1 NL: 1.91E9  
T: FTMS - p ESI Full ms [200.0000-2000.0000]



Ac-V-[Pra-SEL-Aza]<sub>cyclic</sub>-W-NH<sub>2</sub> (1,4-triazole) (5a)

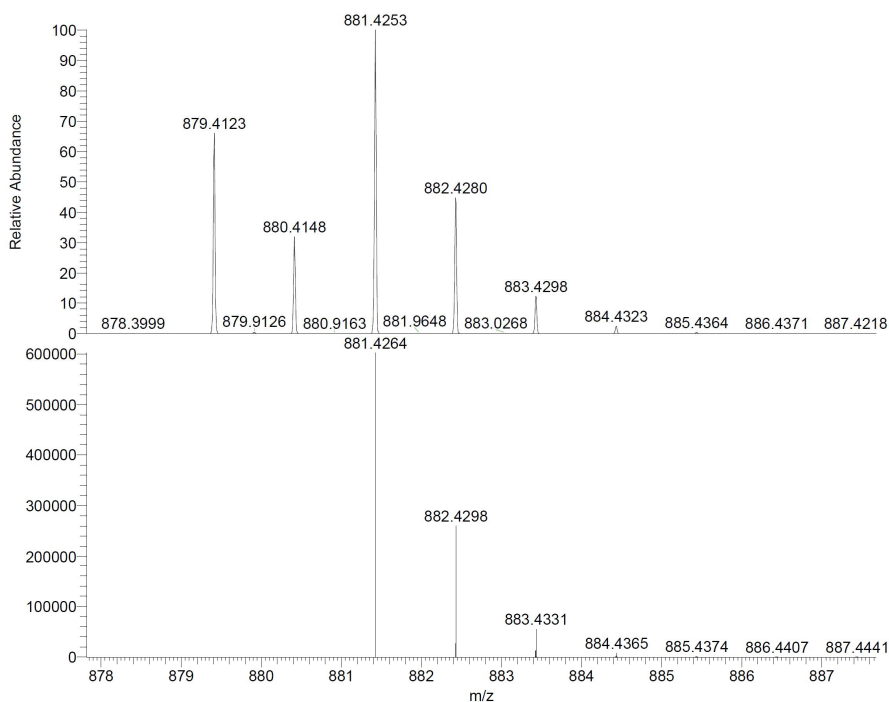
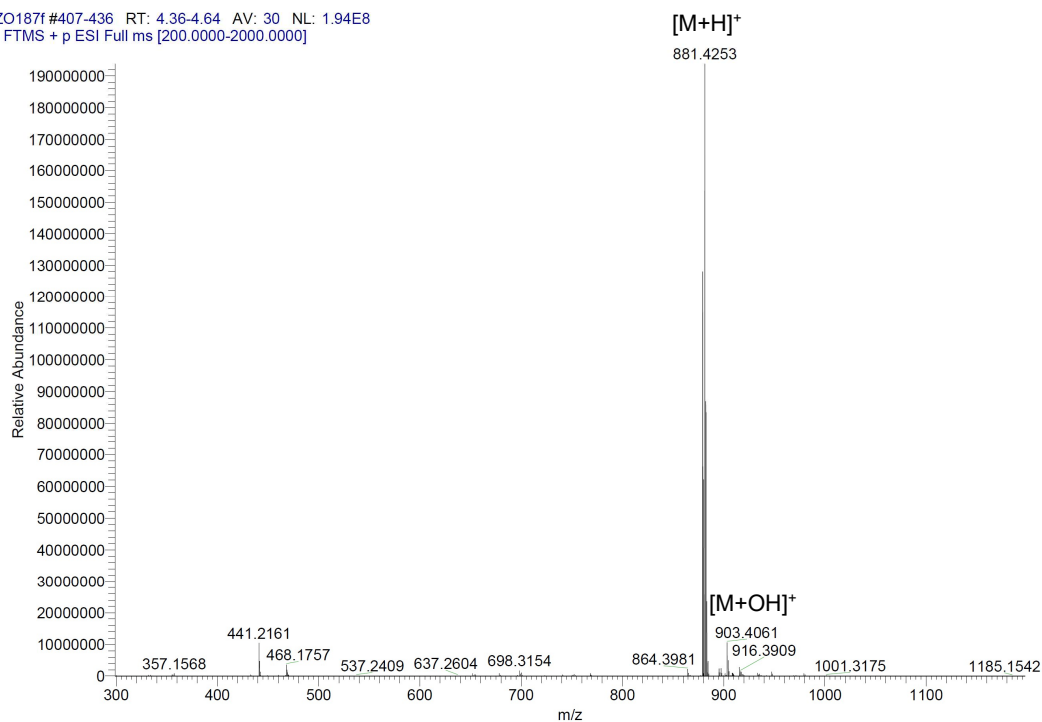
JRI-238 #331-403 RT: 4.17-4.93 AV: 73 NL: 5.73E6  
T: FTMS + p ESI Full ms [300.0000-1200.0000]





Ac-V-[Aza-SEL-Pra]<sub>cyclic</sub>-W-NH<sub>2</sub> (1,4-triazole) (5b)

BZO187f #407-436 RT: 4.36-4.64 AV: 30 NL: 1.94E8  
T: FTMS + p ESI Full ms [200.0000-2000.0000]



NL:  
1.94E8  
BZO187f#407-436  
RT: 4.36-4.64 AV: 30  
T: FTMS + p ESI Full  
ms  
[200.0000-2000.0000]

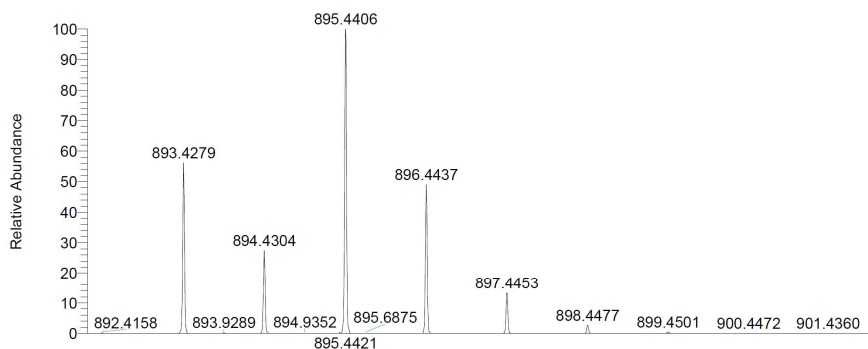
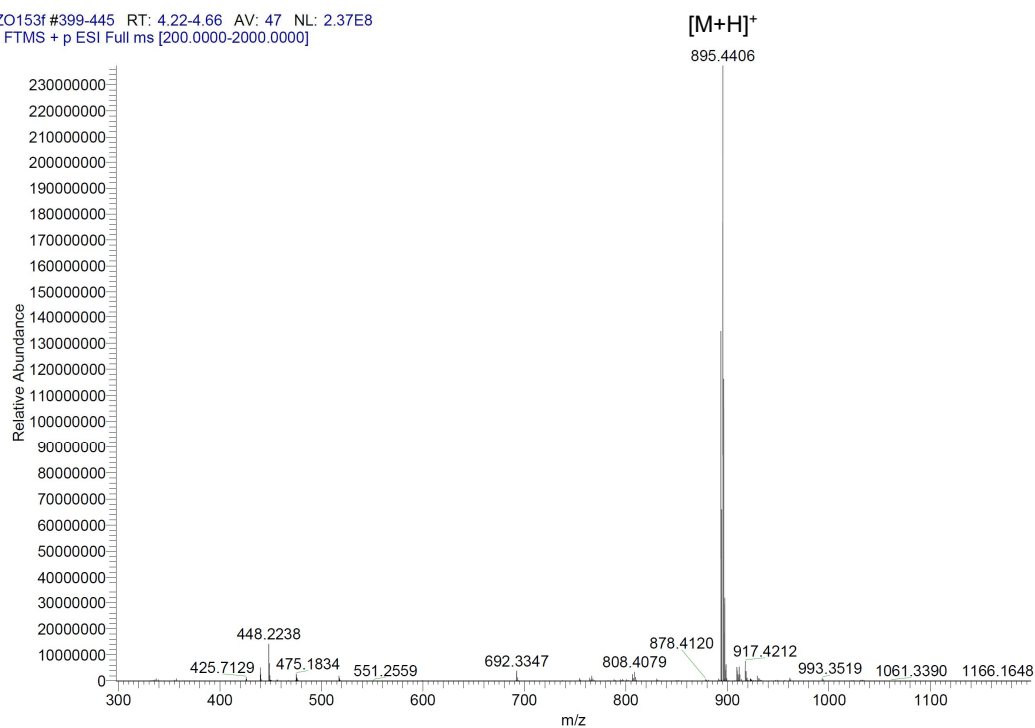
[M+H]<sup>+</sup>

NL:  
6.02E5  
C<sub>40</sub>H<sub>56</sub>N<sub>12</sub>O<sub>11</sub>+H:  
C<sub>40</sub>H<sub>57</sub>N<sub>12</sub>O<sub>11</sub>  
pa Chrg 1

[M+H]<sup>+</sup>

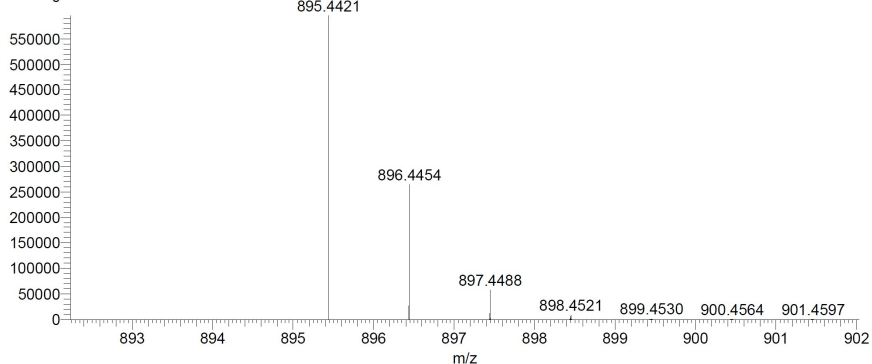
Ac-V-[Pra-SEL-Aha]<sub>cyclic</sub>-W-NH<sub>2</sub> (1,4-triazole) (5c)

BZO153f #399-445 RT: 4.22-4.66 AV: 47 NL: 2.37E8  
T: FTMS + p ESI Full ms [200.0000-2000.0000]



NL:  
4.75E8  
BZO153f#413-435  
RT: 4.35-4.57 AV: 23  
T: FTMS + p ESI Full  
ms  
[200.0000-2000.0000]

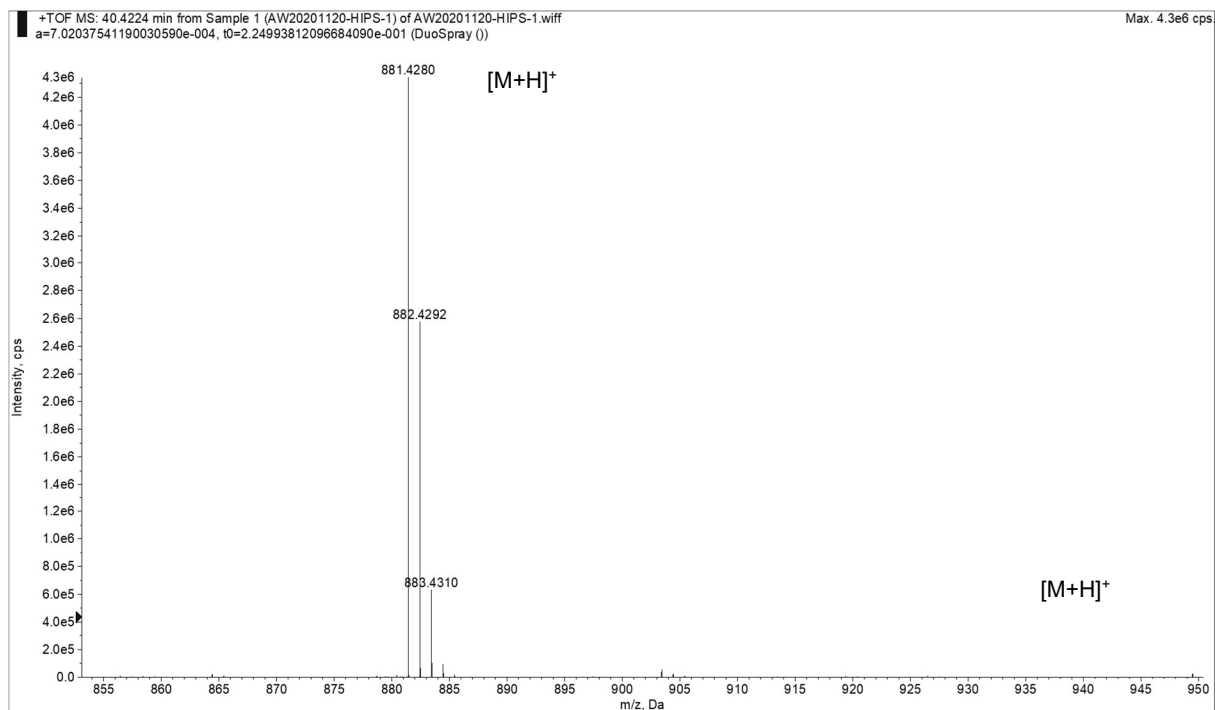
[M+H]<sup>+</sup>



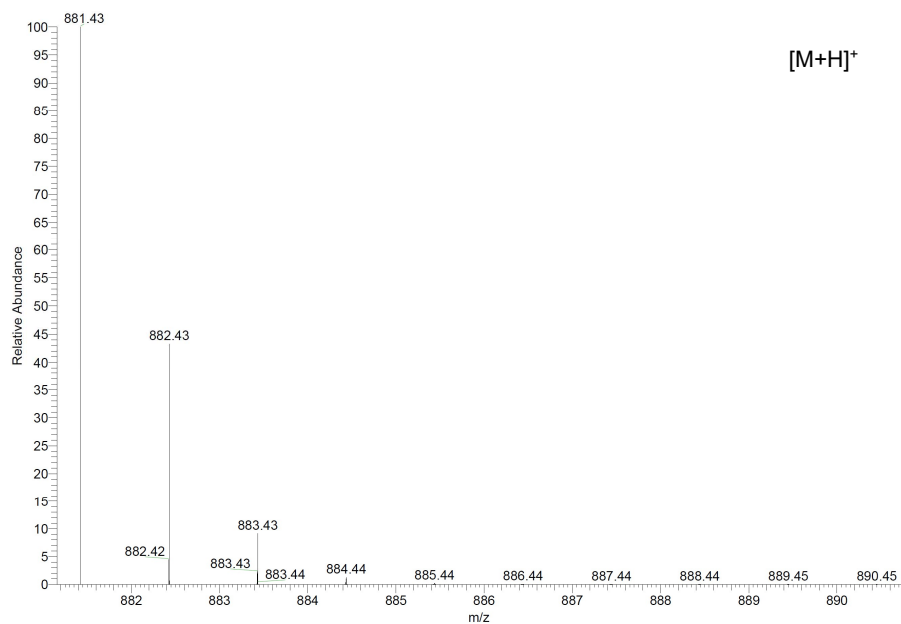
NL:  
5.95E5  
C<sub>41</sub>H<sub>58</sub>N<sub>12</sub>O<sub>11</sub>+H:  
C<sub>41</sub>H<sub>59</sub>N<sub>12</sub>O<sub>11</sub>  
pa Chrg 1

[M+H]<sup>+</sup>

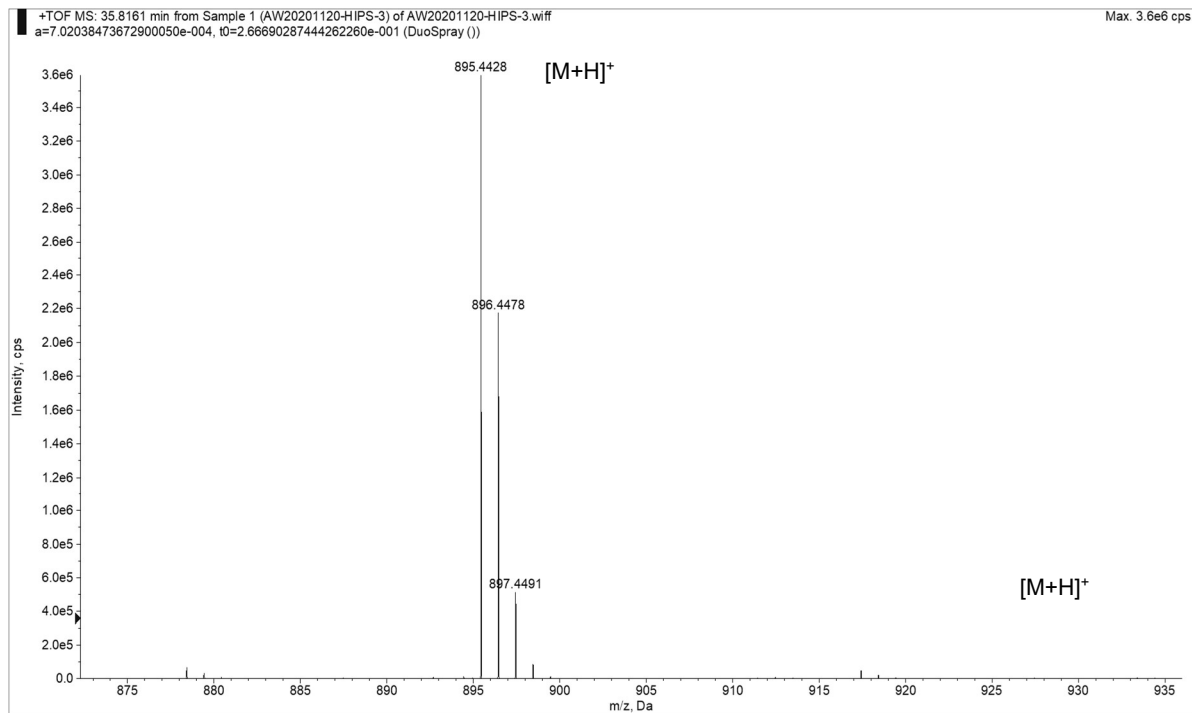
Ac-V-[Pra-SEL-Aza]<sub>cyclic</sub>-W-NH<sub>2</sub> (1,5-triazole) (6a)



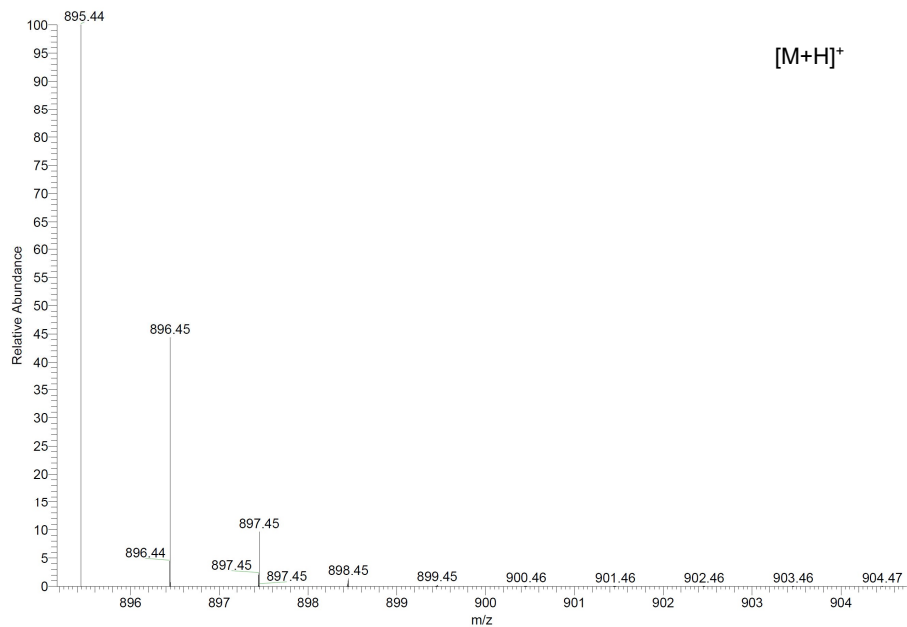
c40h56n12o11 +H: C40 H57 N12 O11 pa Chrg 1



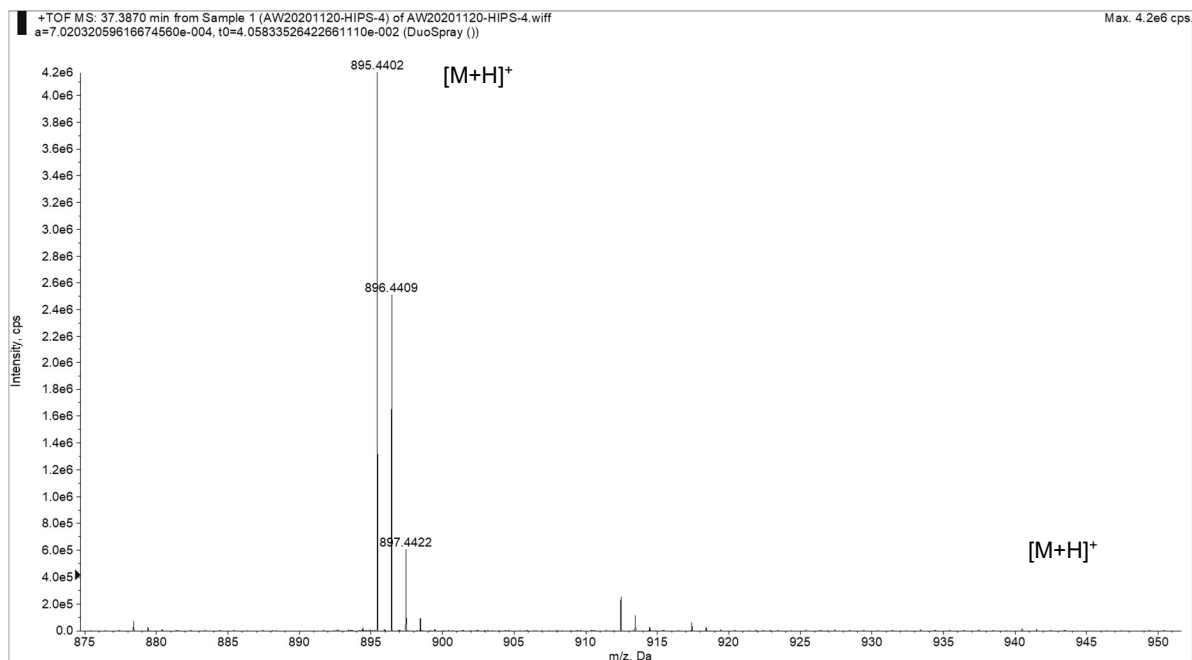
Ac-V-[Pra-SEL-Aha]<sub>cyclic</sub>-W-NH<sub>2</sub> (1,5-triazole) (6b)



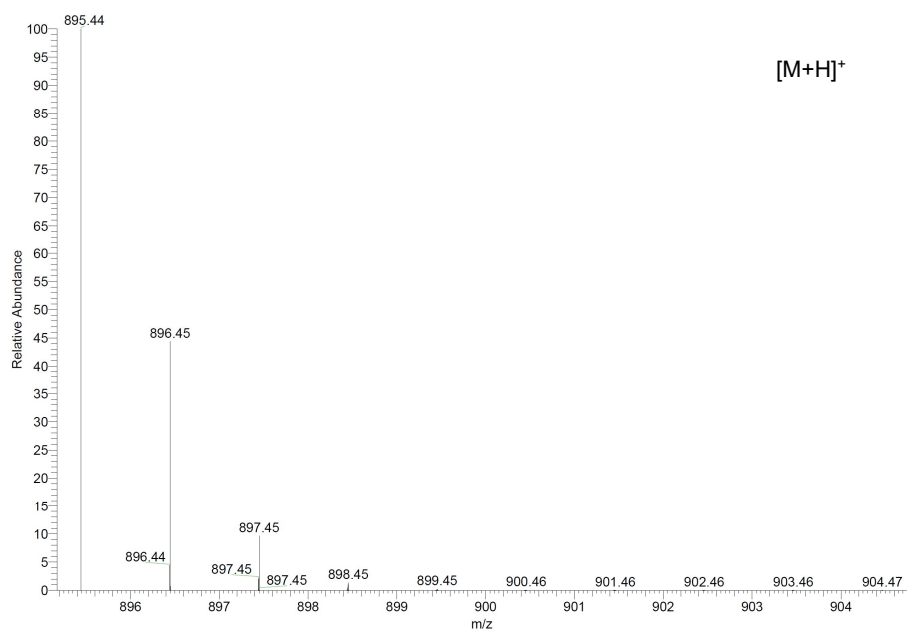
c41h58n12o11 +H: C41 H59 N12 O11 pa Chrg 1



Ac-V-[Aha-SEL-Pra]<sub>cyclic</sub>-W-NH<sub>2</sub> (1,5-triazole) (6c)



c41h58n12o11 +H: C41 H59 N12 O11 pa Chrg 1



## Author Contributions

Dr. Martin Empting conceived the concept of the study, interpreted the data of the presented idea and wrote parts of the manuscript.

Valentin Jakob wrote the manuscript, has done CsrA expression, performed the assays and involved in peptide synthesis and analytics.

Ben G. E. Zoller synthesized the peptides, performed the analytics and wrote parts of the manuscript.

Julia Rinkes involved in peptide synthesis and analytics and wrote some parts of the SI.

Yingwen Wu was involved in CsrA expression and in some assays, especially *E. coli* CsrA.

Dr. Alexander F. Kiefer contributed to peptide synthesis, data evaluation and processing and wrote parts of the manuscript.

Prof. Dr. Michael Hust and Saskia Helmsing taught us how to perform Phage Display and gave continuous support.

Andreas Siebert gave us an introduction how to handle the peptide synthesizer and was always a great help during the experiments with it.

The group of Prof. Dr. Uli Kazmaier provided the peptide synthesizer.

Dr. Andrew M. White synthesized compounds 6a, 6b and 6c, made parts of the analytics of these and wrote some parts of the SI.

Dr. Thomas Durek and Prof. David J. Craik were involved in planning and wrote parts of the manuscript.

Dr. Peta J. Harvey generated and deposited the NMR structures.

## **8.2 Establishment of a luciferase assay for the assessment of CsrA inhibitors**

# ChemBioChem

Supporting Information

## **Establishment of an In Bacterio Assay for the Assessment of Carbon Storage Regulator A (CsrA) Inhibitors**

Yingwen Wu, Ben G. E. Zoller, Mohamed Ashraf Mostafa Kamal, Sven-Kevin Hotop, ClausMichael Lehr, Mark Brönstrup, Petra Dersch, and Martin Empting\*

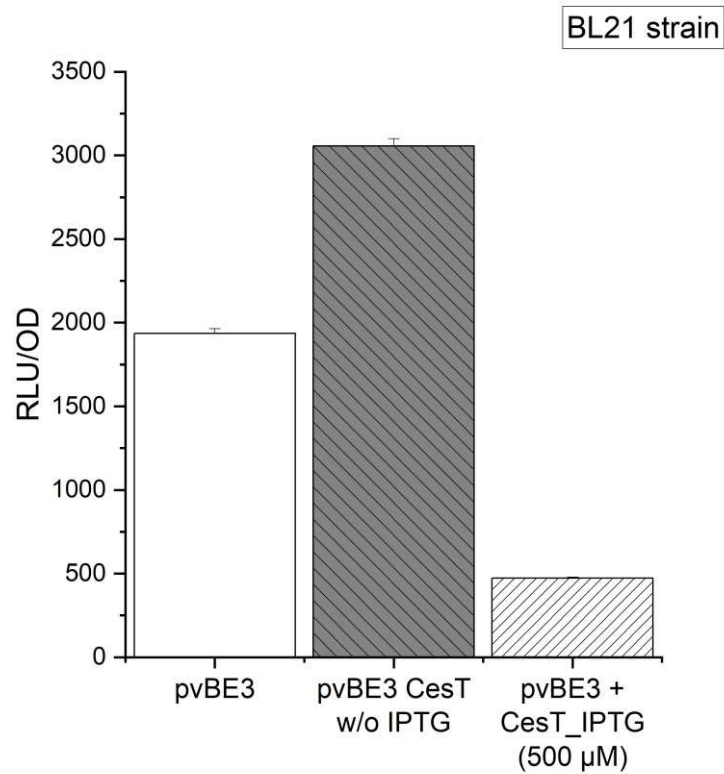


**Figure S1.** Analysis of *glgC-lux* expression in the presence and absence of CesT: *E. coli* strains BL21 pvBE3 with or without the plasmid pNS6236 (*cesT*<sup>+</sup>) were grown at 37°C until the exponential phase was reached (OD = 0.6) with or without IPTG and the relative light units (RLU) were determined. A strong reduction in bioluminescence was observed with BL21 pvBE3 overexpressing *cesT*. This confirmed the results of the qPCR analysis which showed an increased *csrA* transcript level. Error bars represent the standard deviation of four replicates

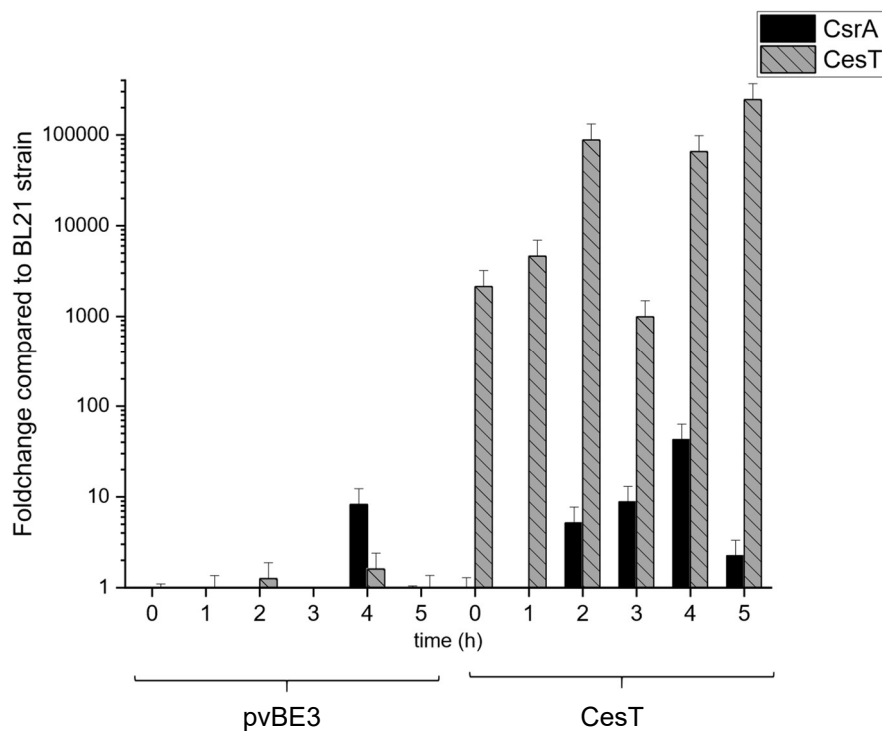




**Figure S2.** Monitoring the transcript levels of CsrA and CesT over 5 hours via qPCR: *E. coli* strains BL21 pvBE3 with or without the plasmid pNS6236 (*cesT*<sup>+</sup>) were grown at 37°C for 5 hours with or without IPTG and the relative light units (RLU) were determined each hour. The expression level of *csrA* was increased after 2-5 h of 2-40-fold *cesT* transcript levels were much higher (~1000-fold). Error bars represent the standard deviation of four replicates

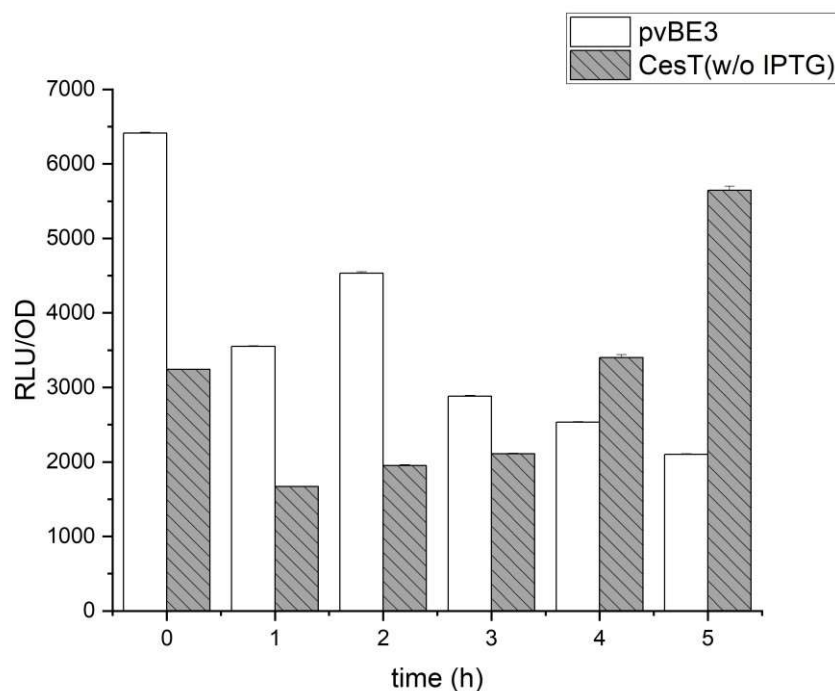


**Figure S3.** Time-dependent *glgC-lux* expression in the presence and absence of CesT. *E. coli* strains BL21 pvBE3 with or without the plasmid pNS6236 (*cesT*<sup>+</sup>) were grown at 37°C for 5 hours without IPTG and the relative light units (RLU) were determined. This depicts the same data as Figure 6A in the main text, but RLU values were normalized with OD<sub>600</sub>. RLU values of the control strain (BL21 pvBE3) were reduced, whereas the RLU values of BL21 pvBE3 harboring plasmid pNS6236 (*cesT*<sup>+</sup>) increased with time. Error bars represent the standard deviation of four replicates.

#### Cellular uptake experiments:

*E. coli* strain DSM1116 ATCC9637 was grown in Mueller Hinton Broth. The procedure of the subcellular fractionation was done according to the literature (15). The applied concentration of the compounds was 28 μM. For LC-MS analysis, protein precipitation was performed in deep 96 well plates. 80 μl of the sample was mixed with 80 μl of 1% formic acid, 120 μl acetonitrile and 120 μl methanol. Then the plate was centrifuged for 60 min at 2250 g at 4 °C. 320 μl of the supernatant were transferred, dried, and resuspended in 40 μl with caffeine as internal standard. The samples were analyzed using Agilent AdvanceBio Peptide Map 2.1 x 100 mm 2.7-Micron + AdvanceBio Peptide Map Guard 2.1x5 mm 2.7 Micron columns on Agilent 1290 UHPLC (Agilent

Technologies, Santa Clara, CA, USA) coupled with AB Sciex QTrap 6500 triple quadrupole mass spectrometer (AB Sciex Germany GmbH, Darmstadt, Germany).

**Table S1:** Triple quadrupole MS-MS parameters

	Q1 (mass) [g/mol]	Q3 (mass) [g/mol]	Declustering potential [V]	Collision energy [V]	Collision cell exit potential [V]
<b>Caffeine (IS)</b>					
quantifier	195.116	138.1	81	27	10
qualifier	195.116	110.1	81	31	6
<b>BZO153</b>					
quantifier	895.409	692.3	196	41	44
qualifier	895.409	878.4	196	29	18
<b>BZO164</b>					
quantifier	881.384	864.2	201	25	18
qualifier	881.384	678.2	201	37	48

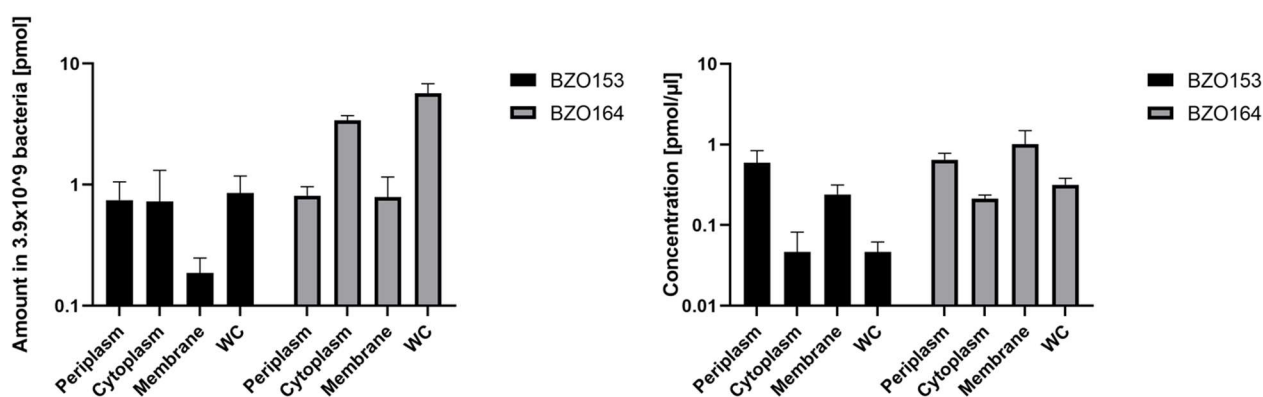


**Figure S4:** Subcellular quantification of the triazole peptides BZO153 and BZO164 in *E. coli*. Whole cell extracts (WC) were prepared and fractionated into a periplasm, cytoplasm, and membrane fraction, followed by peptide concentration measurements using LC/MS/MS. The graphs show (a) the amount (log scale) of the compounds in different bacterial compartments and (b) the concentration (log scale) of the compounds in different bacterial compartments normalized to the volumes as published.<sup>[18,19]</sup> The concentration of BZO153 in cytoplasm is  $0.047 \pm 0.035 \mu\text{M}$  and for BZO164 the

concentration was  $0.21 \pm 0.023 \mu\text{M}$ . Error bars represent the standard deviation of three replicates.

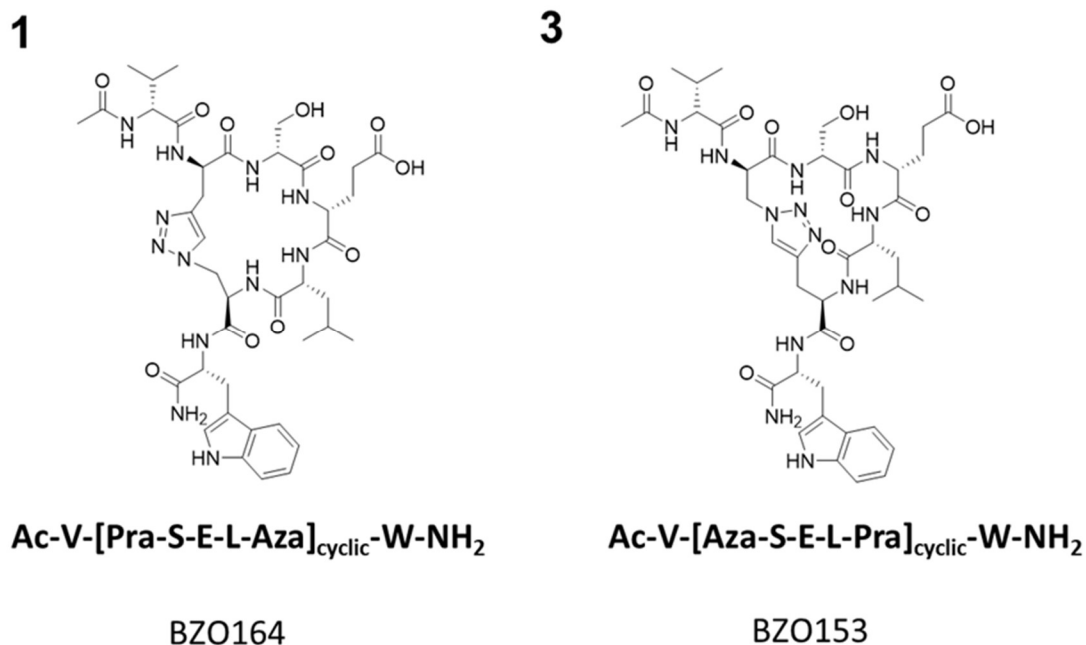


**Figure S5:** Chemical structures of the triazole peptides BZO164 **1** and BZO153 **3**.

**Table S2. Bacterial strains**

Strain	Abbreviation	Description	Notes [Reference from the main text]
BL21		F <sup>-</sup> <i>ompT hsdS<sub>B</sub></i> (r <sub>B</sub> <sup>-</sup> , m <sub>B</sub> <sup>-</sup> ) <i>gal dcm</i> (DE3)	
DH5α		F <sup>-</sup> φ80/ <i>lacZ</i> ΔM15 Δ( <i>lacZYA-argF</i> )U169 <i>recA1 endA1 hsdR17</i> (r <sub>K</sub> <sup>-</sup> , m <sub>K</sub> <sup>+</sup> ) <i>phoA supE44 λ-thi-1 gyrA96 relA1</i>	
MG1655 Δ <i>csrB</i> Δ <i>csrC</i>		MG1655 with unmarked <i>csrB/C</i> deletion	[12]
MG1655pvBE3- <i>csrB</i>	MG_CsrB	pvBE3 and pET28a(+) <sub>csrB</sub> transformed into MG1655	This study
MG1655pvBE3- <i>csrC</i>	MG_CsrC	pvBE3 and pET28a(+) <sub>csrC</sub> transformed into MG1655	This study

BL21-pvBE3	BL_p	pvBE3 transformed into BL21	This study
BL21-pvBE3 <i>csrB</i>	BL_CsrB	pvBE3 and pET28a(+)_ <i>csrB</i> transformed into BL21	This study
BL21-pvBE3 <i>csrC</i>	BL_CsrC	pvBE3 and pET28a(+)_ <i>csrC</i> transformed into BL21	This study
BL21-pvBE3 <i>cesT</i>	BL_CesT	pvBE3 and pNS6236 transformed into BL21	This study
DH5 $\alpha$ pvBE3- <i>csrB</i>	DH_CsrB	pvBE3 and pET28a(+)_ <i>csrB</i> transformed into DH5 $\alpha$	This study
DH5 $\alpha$ pvBE3- <i>csrC</i>	DH_CsrC	pvBE3 and pET28a(+)_ <i>csrC</i> transformed into DH5 $\alpha$	This study
DSM1116 ATCC9637			DSMZ

**Table S3. Plasmids and primers**

Plasmid Name	Description/Sequence	Notes [Reference from the main text]
pvBE3	pFU53 + <i>glgC</i> (upstream region including putative CsrA-binding sites; template from <i>E. coli</i> K-12 CC16) – Amp <sup>r</sup>	[15], Volker Berndt (HZI group CBIO)
pET28a(+)_ <i>csrB</i>	<i>csrB</i> gene cloned into the <i>NcoI</i> - <i>XhoI</i> sites of pET28a(+) – Kan <sup>r</sup>	BioCat GmbH
pET28a(+)_ <i>csrC</i>	<i>csrC</i> gene cloned into the <i>NcoI</i> - <i>XhoI</i> sites of pET28a(+) – Kan <sup>r</sup>	BioCat GmbH
pNS6236	CesT expression plasmid under control of the P <sub>tac</sub> promoter – Kan <sup>r</sup>	[13,14]
CsrA_forward CsrA_reverse	TAGGGGAATTGTGAGCGGAT AGCCGGATCTCAGTGGTGGT	
CsrB_forward CsrB_reverse	GATTCGGTGGGTCAGGAAGG GTTCGTTTCGCAGCATTCCA	

CsrC_forward CsrC_reverse	CAGGAGGCGAAGACAGAGGA ACGGGTCTTACAATCCTTGC	
CesT_forward CesT_reverse	CTGTCAGACCAAGTTTACTC ACTCTTCCTTTTTCAATATTATTGAAG	

## 8.3 Small molecules inhibiting the CsrA-RNA interaction

### Supporting information

#### Chemistry

Solvents and chemicals were used from Zentrales Chemikalienlager der Universität des Saarlandes or specified vendors (Carbolution, Acros Organics, Sigma Aldrich, Fluorochem, TCI, abcr, Alfa Aesar, VWR). For thin-layer chromatography, Merck Silica 60 F254 plates were used. Visualization was accomplished with UV-light ( $\lambda = 254$  nm),  $\text{KMnO}_4$  or Anisaldehyde staining. For automated flash chromatography, either a Teledyne ISCO CombiFlash Rf+ 150 or a Teledyne ISCO CombiFlash NEXTGEN 300+ equipped with RediSepRf silica columns were used. NMR spectra were recorded on a Bruker UltraShield Plus 500 MHz device. Chemical shifts ( $\delta$ ) were given in parts per million (ppm) and referenced against the residual solvent peak. Coupling constants ( $J$ ) were given in Hertz (Hz). Multiplicities were described using the abbreviations s (singlet), bs (broad singlet), d (doublet), dd (doublet of a doublet), ddd (doublet of a doublet of a doublet), t (triplet), dt (doublet of a triplet), q (quartet), hept (heptet) and m (multiplet). Liquid chromatography-mass spectrometry (LC-MS) spectra were measured on a Thermo Scientific DIONEX UltiMate3000 consisting of a diode array detector, column compartment, autosampler and pump. High resolution mass (HRMS) was determined by LC-MS/MS using Thermo Scientific Q Exactive Focus Orbitrap LC-MS/MS system. Compounds tested in biological assays generally showed (if not mentioned otherwise) >95% purity as determined by LC-MS analysis.

#### General procedures

##### 1. Amide coupling using $\text{T}_3\text{P}$ /Dipea

The carboxylic acid (1.0 eq) and the amine (1.1 eq) were solved in dry. DCM [0.1M] in a corresponding single neck flask. Then Dipea (6.0 eq) was added, and the mixture was cooled to  $0^\circ\text{C}$  with an ice bath. At  $0^\circ\text{C}$ , Propanephosphonic acid anhydride ( $\text{T}_3\text{P}$ , 50% in EtOAc, 1.2-4.0 eq) was added dropwise. The reaction was stirred overnight at rt, until LC-MS confirmed full conversion.

After completion of the reaction, a 2% aq.  $\text{Na}_2\text{CO}_3$ -solution was added to stop the reaction, stirring continued for 30 min at rt. Then the phases were separated, the aqueous phase dried over  $\text{MgSO}_4$  and the solvents were removed under reduced pressure.

##### 2. Boc deprotection

The Boc-protected product was solved in analytical grade DCM and extra pure TFA in a ratio of 5:1 and stirred at rt until LC-MS confirmed full conversion (0.5-2h). Then the crude mixture was extracted with an aq. NaOH solution [2M] and an iPrOH/ $\text{CHCl}_3$  1:3 mixture to gain the free amine after evaporation of the solvents and drying under vacuum.

### 3. Reductive amination

The ketone (1.0 eq) and the amine (1.0 eq) were solved in dry. DCM (5.0 mL, [0.1M]) in a corresponding single neck flask. Then acetic acid (30  $\mu$ L, 0.55 mmol, 1.1 eq) was added and the solution was stirred at rt. After 30 min,  $\text{BH}(\text{OAc})_3$  (1.5 eq) was slowly added and the reaction mixture was heated to reflux (45°C) overnight.

When an LC-MS after micro-workup confirmed full conversion, DCM was removed under reduced pressure and the residue was diluted with EtOAc and NaOH ([2M] aq. solution). After phase separation, the organic phase was dried over  $\text{Na}_2\text{SO}_4$  and the solvent was removed under reduced pressure (40°C, 20 mbar, 10 min) to yield the crude product.

### 4. Buchwald-Hartwig

The bromide (1.0 eq), the amine (1.2 eq) and NaOtBu (3.0 eq) were placed in an oven dried small microwave vial under argon. Then degassed dry. 1,4-dioxane (2mL, [0.1M]) was added and the mixture was stirred for five minutes before adding tBuXPhosPdG3 (0.15 eq) under argon in one portion. After argon bubbling, the sealed vial was placed in the microwave. After 1-2h at 100-130°C (LC-MS) a complete conversion could be observed.

The mixture was subsequently filtered through a thick pad of Celite to yield brown oily solids as the crude.

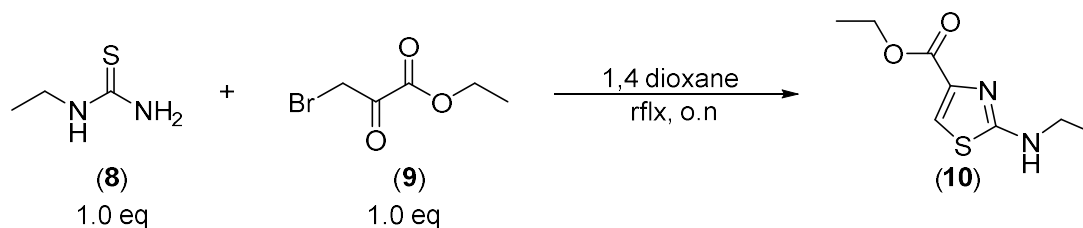
### 5. Boc protection

The corresponding amine or amide (1.0 eq) and DMAP (1.0 eq) were solved in MeCN [0.5M] in a single neck flask. Then Boc anhydride ( $\text{Boc}_2\text{O}$ , 1.2 eq) was added in one portion and the mixture was stirred at room temperature overnight. After the protection was complete,  $\text{H}_2\text{O}$  was added to stop the reaction and MeCN was removed under reduced pressure. The remaining aq. phase was extracted with EtOAc (3x). The combined organic layers were washed with brine and dried over  $\text{Na}_2\text{SO}_4$  to gain the crude product after evaporation of the solvent under reduced pressure.

### 6. Nucleophilic substitution

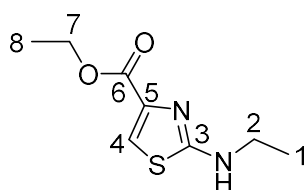
In a dried 2-neckflask, equipped with a reflux condenser, the nucleophile (1.0 eq) and TBAI (0.1 eq) were solved in dry. THF under  $\text{N}_2$ . Subsequently, NaH (60% in mineral oil, 2.0 eq) and the acid (1.0 eq) were added and the reaction mixture was heated to reflux overnight. Then, the reaction mixture was transferred to a 100 mL single neck flask and THF was removed under reduced pressure. Then a 1M aq. HCl solution was added and the product was extracted with EtOAc (3x), to gain the crude product after drying with  $\text{Na}_2\text{SO}_4$  and removal of the EtOAc under reduced pressure.

## Synthesis of ethyl 2-(ethylamino)thiazole-4-carboxylate (10)



N-Ethyl-Thiourea ((8), 522.3 mg, 5 mmol, 1.0 eq) was solved in 1,4-dioxane (25 mL, [0.2M]) in a 100 mL single neck flask equipped with a reflux condenser. Ethyl-Bromopyruvate ((9), 90%pure, 700 $\mu$ L, 5 mmol, 1.0 eq) was added in one portion. The reaction mixture was heated to 100°C and stirred for 2h. Then the mixture was cooled to rt and the solvents were removed on the rotational evaporator (40°C, 20mbar, 30 min) to obtain a off-white solid (998 mg, 5mmol, quantitative).

**LC-MS:** Column: Phenomenex Luna C18(2), gradient: MeCN/H<sub>2</sub>O + 0.05 % HCOOH, 5 % MeCN increase to 100% MeCN in 7 min, flow rate: 0.6 mL/min,  $t_R$  = 2.80.

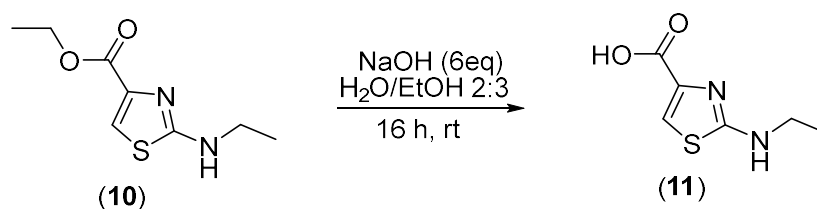


**<sup>1</sup>H-NMR** (500 MHz, dms<sub>o</sub>-d<sub>6</sub>,  $\delta$  in ppm): 8.41 (br.s, 1H, NH), 7.58 (s, 1H, H-4), 4.24 (q,  $^3J_{7,8}$  = 7.1 Hz, 2H, H-7), 3.31 (q,  $^3J_{2,1}$  = 7.2 Hz, 2H, H-2) 1.27 (t,  $^3J_{8,7}$  = 7.1 Hz, 3H, H-8) 1.16 (q,  $^3J_{1,2}$  = 7.2 Hz, 3H, H-1).

**<sup>13</sup>C-NMR** (126 MHz, dms<sub>o</sub>-d<sub>6</sub>,  $\delta$  in ppm): 168.3 (C-6), 159.8 (C-3), 138.6 (C-5), 116.8 (C-4), 60.8 (C-7), 39.9 (C-2), 14.2 (C-1 or C-8), 14.0 (C-1 or C-8).



### 2-(ethylamino)thiazole-4-carboxylic acid (**11**)

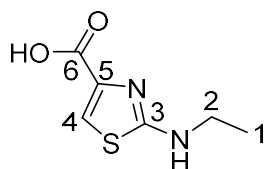


Ethyl 2-(ethylamino)thiazole-4-carboxylate (**10**, 5mmol) was dissolved in a mixture of EtOH (9mL) and water (6 mL) in a 100 mL single neck flask.

Then NaOH (1200 mg, 30 mmol, 6.0eq) was added and the mixture was sonicated until a clear solution was obtained then the mixture was stirred for 3h at rt until LC-MS confirmed full conversion.

The mixture was cooled to 0°C and aq. Conc. HCl-solution was added to PH<1. EtOH was removed and the aqueous residue was extracted with DCM (3x). The org. phase containing 15 mg of a yellow oily side product were discarded. To the aqueous phase NaOH-solution (aq., 1M) was added to reach a PH of 3, at which a white solid precipitated. The precipitate was filtrated off and dried in HV to obtain 306 mg (1.78 mmol, 36%) of the product as a white solid.

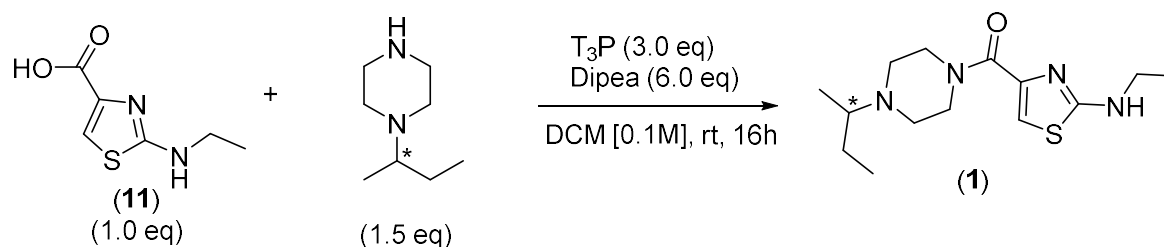
**LC-MS:** Column: Phenomenex Luna C18(2), gradient: MeCN/H<sub>2</sub>O + 0.05 % HCOOH, 5 % MeCN increase to 100% MeCN in 5.1 min, flow rate: 0.6 mL/min, t<sub>R</sub> = 1.09, m/z = 173.1 ([M+H]<sup>+</sup>)



**<sup>1</sup>H-NMR** (500 MHz, dms<sub>o</sub>-d<sub>6</sub>, δ in ppm): 7.79 (s, 1H, NH), 7.43 (s, 1H, H-4), 3.24 (q, <sup>3</sup>J<sub>2,1</sub> = 7.2 Hz, 2H, H-2), 1.14 (t, <sup>3</sup>J<sub>1,2</sub> = 7.2 Hz, 3H, H-1).

**<sup>13</sup>C-NMR** (126 MHz, dms<sub>o</sub>-d<sub>6</sub>, δ in ppm): 168.0 (C-6), 162.3 (C-3), 143.1 (C-5), 116.0 (C-4), 39.5 (C-2), 14.3 (C-1).

### Synthesis of (4-(sec-butyl)piperazin-1-yl)(2-(ethylamino)thiazol-4-yl)methanone (**1**)

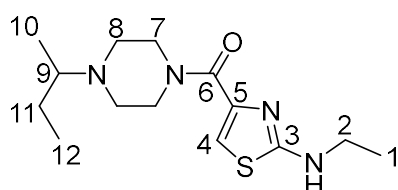


According to **standard procedure 1**, 2-(ethylamino)thiazole-4-carboxylic acid (**(11)**), 88.0 mg, 0.5 mmol, 1.0 eq) and 1-(sec-butyl)piperazine (107 mg, 0.75 mmol, 1.5 eq), dry. DCM (5 mL, [0.1M]), Dipea (520  $\mu$ L, 3.0 mmol, 6.0 eq) and T<sub>3</sub>P ( 50% in EtOAc, 950  $\mu$ L, 1.5 mmol, 3 eq) were used to gain (129.5 mg, 0.44 mmol, 90% pure) of a yellow oil after workup.

The crude oil was solved in MeCN/H<sub>2</sub>O (1:1, 3mL) and purified via prep. HPLC in one run (gradient: 5-20% MeCN in H<sub>2</sub>O in 20 min, elution after 7 min). The fractions 2-6 contained only product (>98%). The product fractions were combined and the solvents were removed under reduced pressure to obtain the product as a pale yellow oil (75.4 mg, 0.22 mmol, 44%)

**LC-MS:** Column: Phenomenex Luna C18(2), gradient: MeCN/H<sub>2</sub>O + 0.05 % HCOOH, 5 % MeCN increase to 100% MeCN in 5.1 min, flow rate: 0.6 mL/min, t<sub>R</sub> = 1.82, m/z = 297.3 ([M+H]<sup>+</sup>)

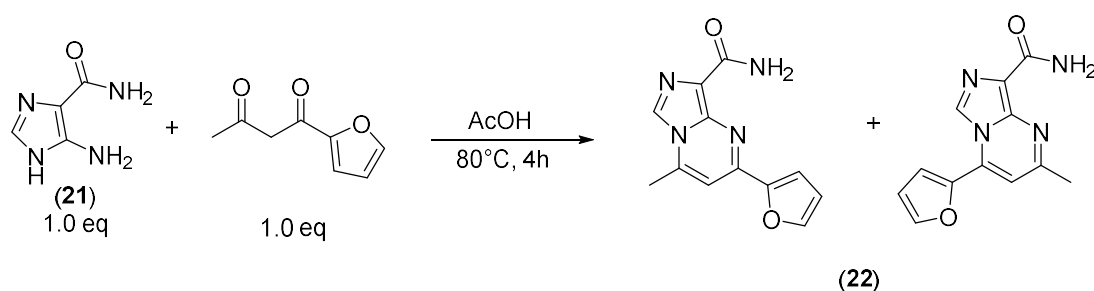
**HRMS:** m/z ([M+H]<sup>+</sup>), calculated: 297.1749 , found: 297.1731



**<sup>1</sup>H-NMR** (500 MHz, dms<sub>o</sub>-d<sub>6</sub>,  $\delta$  in ppm): 8.14 (HCOOH), 7.69 (t, 1H, NH), 6.98 (s, 1H, H-4), 3.78-3.51 (m, 4H, H-7), 3.24-3.19 (m, 3H, H-9, H-2), 2.48-2.35 (m, 4H, H-8), 1.52-1.44 (m, 1H, H-11a), 1.30-1.21 (m, 1H, H-11b), 1.15 (t, <sup>3</sup>J<sub>1,2</sub> = 7.2 Hz, 3H, H-1), 0.90 (d, <sup>3</sup>J<sub>10,9</sub> = 6.5 Hz, 3H, H-10), 0.85 (t, <sup>3</sup>J<sub>12,11</sub> = 7.4 Hz, 3H, H-12).

**<sup>13</sup>C-NMR** (126 MHz, dms<sub>o</sub>-d<sub>6</sub>,  $\delta$  in ppm): 167.8 (C-6), 163.1(C-3), 146.0 (C-5), 110.0 (C-4), 60.0 (C-9), 48.4 (C-7 or C-8), 47.7 (C-7 or C-8), 39.5 (C-2), 25.6 (C-11), 14.3 (C-1), 13.6 (C-10), 11.1 (C-12).

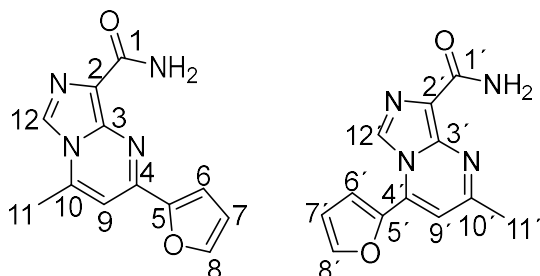
### Synthesis of 2-(furan-2-yl)-4-methylimidazo[1,5-a]pyrimidine-8-carboxamide (**(22)**)



5-amino-1H-imidazole-4-carboxamide (314.4 mg, 2.5 mmol, 1.0 eq) and 1-(furan-2-yl)butane-1,3-dione (380.9 mg, 2.5 mmol, 1.0 eq) were placed in a 100 mL single neck flask and solved in ACOH (10 mL). The mixture was heated to 90°C for 5h.

After cooling to rt, the solvents were removed under reduced pressure (60°C, 20 mbar, 1h). Then the oily residue was dried in HV for 5h. Finally, the crude product was solved in H<sub>2</sub>O/MeCN and lyophilized over night to obtain 548 mg (2.26 mmol, 90%) of the product as an deep yellow solid. NMR indicated that both possible isomers were formed, which are not distinguishable via LC-MS. The ratio of the desired to the undesired regioisomer is 6:4

**LC-MS:** Column: Phenomenex Luna C18(2), gradient: MeCN/H<sub>2</sub>O + 0.05 % HCOOH, 5 % MeCN increase to 100% MeCN in 5.1 min, flow rate: 0.6 mL/min, t<sub>R</sub> = 2.21, m/z = 243.2 ([M+H]<sup>+</sup>)

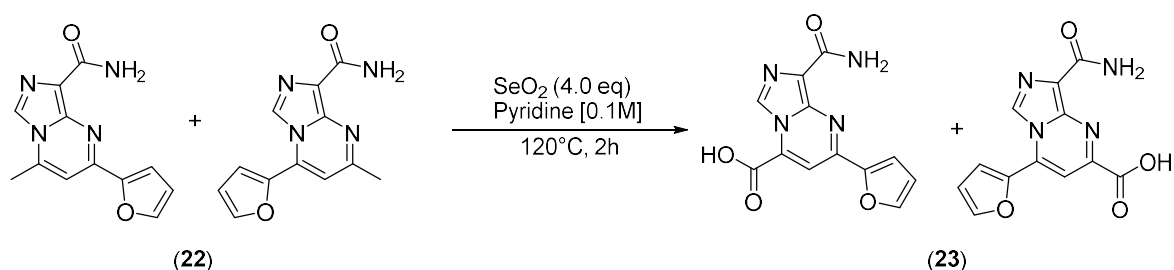


NMR spectra of mixture, NMR-data for individual compounds.

**<sup>1</sup>H-NMR** (500 MHz, dms<sub>o</sub>-d<sub>6</sub>, δ in ppm): 8.81 (s, 1H, H-9), 8.19 (d, <sup>3</sup>J<sub>8,7</sub> = 1.5 Hz, 1H, H-8), 7.83 (d, <sup>3</sup>J<sub>6,7</sub> = 3.7 Hz, 1H, H-6), 7.73 (br.s, 2H, NH<sub>2</sub>), 7.37 (s, 1H, H-12), 6.93 (dd, <sup>3</sup>J<sub>7,6</sub> = 3.6 Hz, <sup>3</sup>J<sub>7,8</sub> = 1.6 Hz, 1H, H-7), 2.61 (s, 3H, H-11).

8.43 (s, 1H, H-9'), 8.03 (d, <sup>3</sup>J<sub>8,7</sub> = 1.5 Hz, 1H, H-8'), 7.68 (br.s, 2H, NH<sub>2</sub>'), 7.54 (d, <sup>3</sup>J<sub>6,7</sub> = 3.5 Hz, 1H, H-6'), 7.34 (s, 1H, H-12'), 6.78 (dd, <sup>3</sup>J<sub>7,6</sub> = 3.4 Hz, <sup>3</sup>J<sub>7,8</sub> = 1.6 Hz, 1H, H-7'), 2.74 (s, 3H, H-11').

### Synthesis of 8-carbamoyl-2-(furan-2-yl)imidazo[1,5-a]pyrimidine-4-carboxylic acid (**23**)

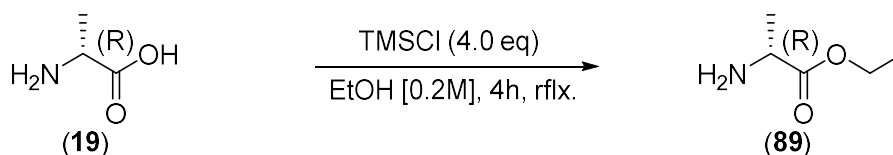


2-(furan-2-yl)-4-methylimidazo[1,5-a]pyrimidine-8-carboxamide (**22**), 419.4 mg, 1.75 mmol, 1.0 eq and SeO<sub>2</sub> (771 mg, 7.0 mmol, 1.0 eq) were placed in a 25 mL single neck flask, solved in dry.Pyridine (5.0 mL) and heated to 140°C for 30 min, after which time all the reactant was gone. A polar by-product (0.44 min at the LC-MS) was formed in excess; the desired product (2.22 min) was formed aswell (10%). After cooling down to rt, the mixture was diluted with Pyridine and filtered through 3 big syringe filters. After removal of the Pyridine under reduced pressure, 561.5 mg of a dark orange oil were obtained.

The crude was solved in MeCN/H<sub>2</sub>O/DMSO + HCOOH (3 drops) and the product was purified via prep. HPLC (5-100% MeCN in 30 min) to receive 26.3 mg (0.097 mmol, 5.5%) of the desired product as an orange solid.

**LC-MS:** Column: Phenomenex Luna C18(2), gradient: MeCN/H<sub>2</sub>O + 0.05 % HCOOH, 5 % MeCN increase to 100% MeCN in 5.1 min, flow rate: 0.6 mL/min, t<sub>R</sub> = 1.85, m/z = 273.1 ([M+H]<sup>+</sup>).

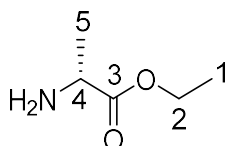
### Synthesis of ethyl D-alaninate (**89**)



(D)-Alanine 1782 mg ((**19**), 20 mmol, 1.0 eq) was placed in a 250 mL single neck flask and solved in EtOH.

Then 10 mL (80mmol, 4.0eq) TMSCl were added and the mixture was heated to reflux for 4h at 80°C.

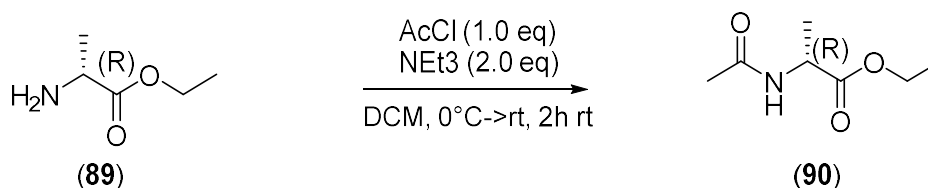
After removal of the solvent, the product was received as a colorless oil. The yield was determined over 2 steps.



**<sup>1</sup>H-NMR** (DMSO-d<sub>6</sub>, 500 MHz,  $\delta$  in ppm): 8.59 (s, 3H, NH<sub>3</sub>), 4.24-4.15 (m, 2H, H-2), 4.07-3.99 (m, 1H, H-4), 1.41 (d, <sup>3</sup>J<sub>5,4</sub> = 7.2Hz, 3H, H-5), 1.23 (t, <sup>3</sup>J<sub>1,2</sub> = 7.1 Hz, 3H, H-1).

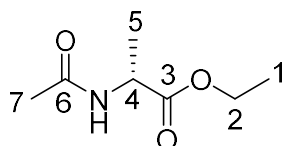
NMR contains EtOH

### Synthesis of ethyl acetyl-D-alaninate (**90**)



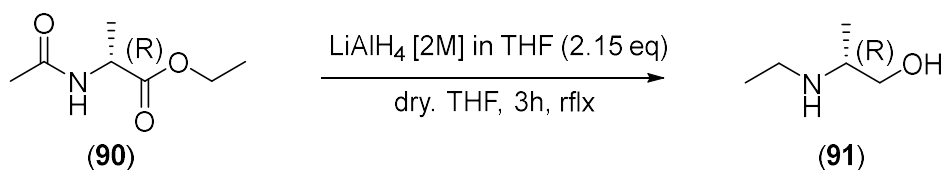
Ethyl D-alaninate ((**89**), 20mmol) was solved in DCM (90mL) in a 250 mL single neck flask and cooled to 0°C. First NEt<sub>3</sub> (5.6 mL, 40 mmol, 2.0 eq) was added at 0° and then AcCl (1.5 mL, 20 mmol, 1.0eq) solved in DCM (30 mL) was added slowly at 0°C.

After 2h reaction time, the reaction was ended by the addition of brine. The phases were separated and the organic phase was dried over NaSO<sub>4</sub>. After evaporation of the solvents under reduced pressure (product volatile!, 40°C, 100 mbar, 5min) 2609.7 mg (16.4 mmol, 82% over 2 steps) of a colorless oil were obtained.



**<sup>1</sup>H-NMR** (CDCl<sub>3</sub>, 500 MHz,  $\delta$  in ppm): 6.08 (s, 1H, amide-H), 4.57 (p, J = 7.2 Hz, 1H, H-4), 4.20 Hz(q, J = 7.1 HZ, 2H, H-2), 2.01 (s, 3H, H-7), 1.39 (d, <sup>3</sup>J<sub>5,4</sub> = 7.2Hz, 3H, H-5), 1.28 (t, <sup>3</sup>J<sub>1,2</sub> = 7.1 Hz, 3H, H-1).

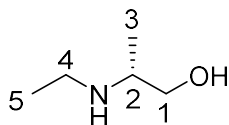
### Synthesis of (R)-2-(ethylamino)propan-1-ol (**91**)



Ethyl acetyl-D-alaninate (**90**), 2000mg, 12.5 mmol) was placed in a dry 250 mL 2-neck flask under N<sub>2</sub> and solved in dry THF (100 mL). Then LiAlH<sub>4</sub> ([2M] in THF, 13.5 mL, 27 mmol, 2.15 eq) was added slowly. The mixture was heated to reflux for 3h, then 1h at rt.

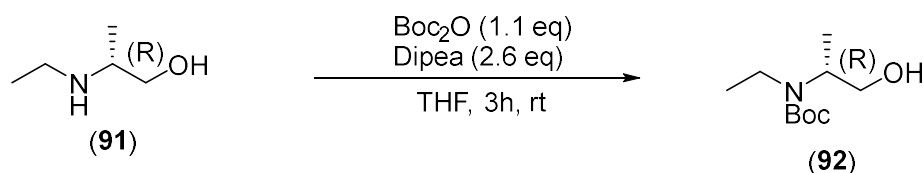
The reaction was ended by the addition of KOH-solution (aq. 30%). The mixture was filtrated, the solid washed with THF/Et<sub>2</sub>O 1:1 and then discarded. The organic phase was dried over MgSO<sub>4</sub> and the solvents were removed under reduced pressure (product volatile!, 40°C, 100 mbar, 5min).

1246 mg (12.08 mmol, 97%) of a pale yellow oil were obtained.



**<sup>1</sup>H-NMR** (DMSO-d<sub>6</sub>, 500 MHz,  $\delta$  in ppm): 4.46 (s, 1H, NH), 3.25-3.17 (m, 2H, H-1), 2.61-2.54 (m, 2H, H-4), 2.49-2.44 (m, 1H, H-2) 1.40 (s, 1H, OH), 0.99 (t, <sup>3</sup>J<sub>5,4</sub> = 6.3 Hz, 3H, H-5), 0.88 (d, <sup>3</sup>J<sub>3,2</sub> = 7.1Hz, 3H, H-3).

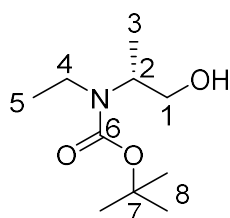
### Synthesis of tert-butyl (R)-ethyl(1-hydroxypropan-2-yl)carbamate (**92**)



(R)-2-(ethylamino)propan-1-ol (**91**), 12.1 mmol) was solved in THF (50 mL) in a 250 mL single neck flask. Then Dipea (5.35 mL, 31.5 mmol, 1.1 eq) and Boc<sub>2</sub>O (2960 mg, 13.5 mmol, 1.1 eq) were added.

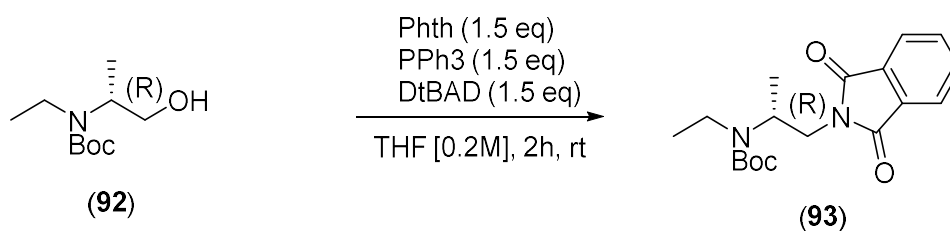
After 3h at rt, the solvent was removed under reduced pressure and DCM and H<sub>2</sub>O were added. After phase separation, the org. phase was washed with NaOH (aq., [1M]). Then Imidazole (900 mg, 13.2 mmol, 1.1 eq) was added and stirred for 1h, after which the reaction mixture was washed with HCl (aq., [0.25M], 3x) and brine. After drying over Na<sub>2</sub>SO<sub>4</sub> and solvent evaporation, 1506 mg (7.4 mmol, 61%) of a pale yellow oil were obtained.

**LC-MS:** Column: Phenomenex Luna C18(2), gradient: MeCN/H<sub>2</sub>O + 0.05 % HCOOH, 5 % MeCN increase to 100% MeCN in 5.1 min, flow rate: 0.6 mL/min at 220 nm t<sub>R</sub> = 2.86, m/z = 204.0 ([M+H]<sup>+</sup>), 104.2 ([M-Boc+H]<sup>+</sup>)



**<sup>1</sup>H-NMR** (CDCl<sub>3</sub>, 500 MHz, δ in ppm): 3.98-3.92 (m, 1H, H-2), 3.66-3.59 (m, 2H, H-4), 3.25-3.11 (m, 2H, H-1), 2.07 (s, 1H, OH), 1.47 (s, 9H, H-8), 1.18 (d, <sup>3</sup>J<sub>3,2</sub> = 7.2Hz, 3H, H-3), 1.13 (t, <sup>3</sup>J<sub>5,4</sub> = 7.1 Hz, 3H, H-5).

#### Synthesis of tert-butyl (R)-(1-(1,3-dioxoisindolin-2-yl)propan-2-yl)(ethyl)carbamate (93)

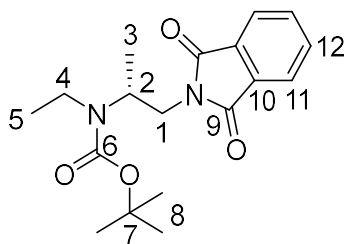


Tert-butyl (R)-ethyl(1-hydroxypropan-2-yl)carbamate ((92), 614.6 mg, 3mmol), Phthalimide (665.5 mg, 4.5 mmol, 1.5 eq) and PPh<sub>3</sub> (1183.5 mg, 4.5 mmol, 1.5 eq) were placed in a 100 mL single neck flask and solved in dry. THF (15 mL). The reaction mixture was cooled to 0°C, then Di-tert-butyl Azodicarboxylate (1042 mg, 4.5 mmol, 1.5 eq) was added slowly. The reaction was stirred for 2h at rt, after which LC-MS control confirmed full conversion.

Subsequently THF was removed under reduced pressure. EtOAc and H<sub>2</sub>O were added to the residue and the phases were separated. The organic phase was dried over Na<sub>2</sub>SO<sub>4</sub> and the solvent was removed to afford 3186.7 mg of an orange oil.

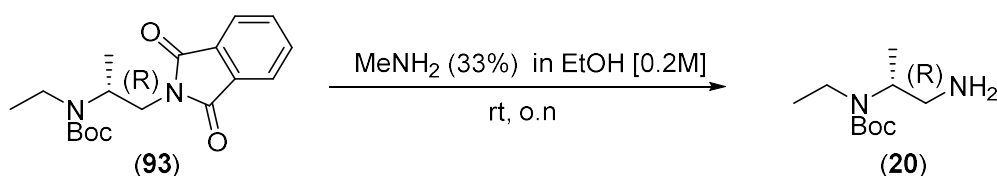
For purification, the residue was solved in MeCN/H<sub>2</sub>O/DMSO (4.5:4.5:1, 10 mL) and prep. HPLC was applied (20-100% MeCN in H<sub>2</sub>O in 30 min, elution after 22 min, 2 runs) to obtain 567.4 mg (1.71 mmol, 57%) of a pale yellow oil.

**LC-MS:** Column: Phenomenex Luna C18(2), gradient: MeCN/H<sub>2</sub>O + 0.05 % HCOOH, 5 % MeCN increase to 100% MeCN in 5.1 min, flow rate: 0.6 mL/min, t<sub>R</sub> = 3.69, m/z = 233.1([M+H]<sup>+</sup>).



**<sup>1</sup>H-NMR** (CDCl<sub>3</sub>, 500 MHz, δ in ppm): 7.93-7.75 (m, 4H, H-11, H-12), 4.43-4.17 (m, 1H, H-2), 3.80-3.64 (m, 1H, H-1<sub>a</sub>), 3.50-3.39 (m, 1H, H-1<sub>b</sub>), 3.18-2.93 (m, 2H, H-4), 1.22-1.15 (m, 3H, H-3), 1.07-0.96 (m, 12H, H-8, H-5).

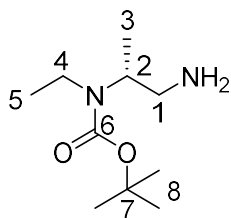
### Synthesis of tert-butyl (R)-((1-aminopropan-2-yl)(ethyl)carbamate) (**20**)



Tert-butyl (R)-((1-(1,3-dioxisoindolin-2-yl)propan-2-yl)(ethyl)carbamate) (**93**), 567mg, 1.7 mmol) was placed in a 50 mL single neck flask and dissolved in a 33% MeNH<sub>2</sub> solution in Ethanol (10 mL, 107 mmol, 63 eq). The mixture was stirred for 4 h at rt, full conversion was confirmed with LC-MS (product not UV-active).

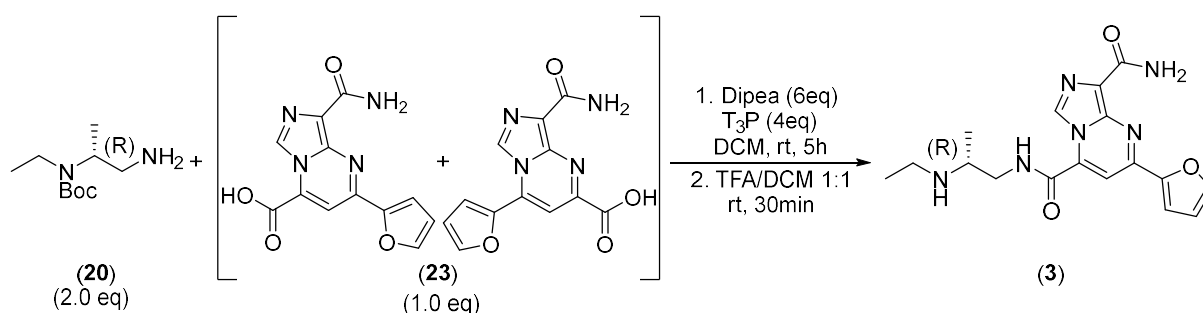
The reaction was cooled to 0°C and the formed precipitate was filtered off (no washing). Subsequently the Ethanol was removed under reduced pressure and the residue was diluted with EtOAc and a 10% aq. citric acid solution. The org. phase was discarded and the aqueous phase was basified with NH<sub>4</sub>OH solution and extracted with EtOAc (2x). Drying over Na<sub>2</sub>SO<sub>4</sub> and evaporation of the solvent yielded 213 mg (1.06 mmol, 62%) of the product as a colorless oil. The product was pure enough to use in the next step without further purification.

**LC-MS:** Column: Phenomenex Luna C18(2), gradient: MeCN/H<sub>2</sub>O + 0.05 % HCOOH, 5 % MeCN increase to 100% MeCN in 5.1 min, flow rate: 0.6 mL/min, t<sub>R</sub> = 1.85, m/z = 203.2 ([M+H]<sup>+</sup>), 103.1 ([M-Boc+H]<sup>+</sup>). Only mass signal, no UV at any wavelength.



**<sup>1</sup>H-NMR** (DMSO-d<sub>6</sub>, 500 MHz, δ in ppm): 3.42-3.20 (m, 2H, H-2, H-4<sub>a</sub>), 3.14-2.91 (m, 2H, H-4<sub>b</sub>, H-1<sub>a</sub>), 2.63-2.52 (m, 1H, H-1<sub>b</sub>), 1.39 (s, 9H, H-8), 1.10-0.95 (m, 6H, H-3, H-5).

### Synthesis of (R)-N4-(2-(ethylamino)propyl)-2-(furan-2-yl)imidazo[1,5-a]pyrimidine-4,8-dicarboxamide (**3**)



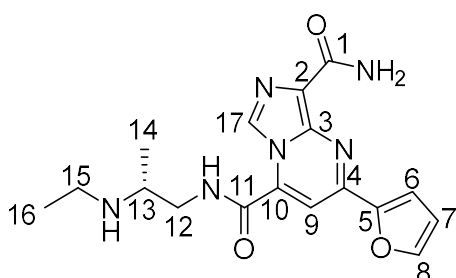
According to **general procedure 1**, 8-carbamoyl-2-(furan-2-yl)imidazo[1,5-a]pyrimidine-4-carboxylic acid ((**23**) 10.9 mg, 0.04 mmol, 1.0 eq), tert-butyl (R)-(1-aminopropan-2-yl)(ethyl)carbamate ((**20**) 16.7 mg, 0.08 mmol, 2.0 eq), dry. DCM (2.0 mL), Dipea (40  $\mu$ L, 0.24 mmol, 6.0 eq) and T<sub>3</sub>P (50% in EtOAc, 100  $\mu$ L, 0.16 mmol, 4.0 eq) were used to gain 24.5 mg of a yellow oil as crude after workup.

The crude oil was solved in MeCN/H<sub>2</sub>O (1:1, 3mL) and purified via prep. HPLC in one run (gradient: 5-100% MeCN in H<sub>2</sub>O in 30 min) to obtain 3.1 mg (0.007 mmol, 18%) of the Boc protected product as a yellow solid. It was possible to separate both isomers at this stage of the synthesis.

The crude was solved in analytical grade DCM (3.0 mL) and extra pure TFA (3.0 mL) and stirred 1h at rt until LC-MS confirmed full conversion. Then the solvents were removed under reduced pressure and the crude was dried under HV, solved in MeCN/H<sub>2</sub>O and lyophilized overnight (2x) to obtain 3.60 mg (0.07 mmol, 18%) of the product-TFA salt as an deep yellow solid.

**LC-MS:** Column: Phenomenex Luna C18(2), gradient: MeCN/H<sub>2</sub>O + 0.05 % HCOOH, 5 % MeCN increase to 100% MeCN in 5.1 min, flow rate: 0.6 mL/min, t<sub>R</sub> = 1.79, m/z = 357.2 ([M+H]<sup>+</sup>)

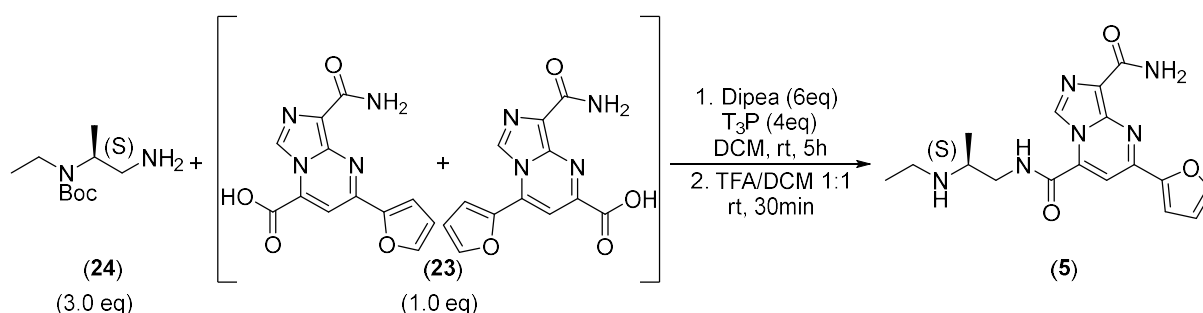
**HRMS:** m/z ([M+H]<sup>+</sup>), calculated: 357.1675, found: 357.1655



**<sup>1</sup>H-NMR** (500 MHz, dms<sub>o</sub>-d<sub>6</sub>,  $\delta$  in ppm): 9.05 (s, 1H, H-9), 8.68 (br.s, 2H, amide-NH<sub>2</sub>), 8.24 (s, 1H, H-8), 7.98 (d, <sup>3</sup>J<sub>6,7</sub> = 3.3 Hz, 1H, H-6), 7.80 (s, 1H, NH), 7.76 (s, 1H, NH), 7.52 (s, 1H, H-17), 6.98-6.95 (m, 1H, H-7), 3.70-3.62 (m, 1H, H12-a), 3.60-3.53 (m, 2H, H12-b, H-13), 3.21-3.06 (m, 2H, H-15), 1.31 (d, <sup>3</sup>J<sub>14,13</sub> = 5.6 Hz, 3H, H-14), 1.24 (t, <sup>3</sup>J<sub>16,15</sub> = 6.6 Hz, 3H, H-16).



**Synthesis of (S)-N4-(2-(ethylamino)propyl)-2-(furan-2-yl)imidazo[1,5-a]pyrimidine-4,8-dicarboxamide (5)**



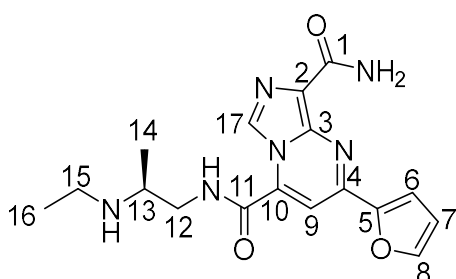
According to **general procedure 1**, 8-carbamoyl-2-(furan-2-yl)imidazo[1,5-a]pyrimidine-4-carboxylic acid ((**23**), 9.4 mg, 0.035 mmol, 1.0 eq), tert-butyl (S)-(1-aminopropan-2-yl)(ethyl)carbamate ((**24**), 22.1 mg, 0.105 mmol, 3.0 eq, synthesis analogues to (**20**), starting from (S)-alanine), dry. DCM (2.0 mL), Dipea (40  $\mu$ L, 0.24 mmol, 6.0 eq) and T<sub>3</sub>P were used to gain 56.3 mg of a yellow oil after workup.

The crude oil was solved in MeCN/H<sub>2</sub>O (1:1, 3mL) and purified via prep. HPLC in one run (gradient: 5-100% MeCN in H<sub>2</sub>O in 30 min) to obtain the Boc protected product as a yellow solid. It was possible to separate both isomers at this stage of the synthesis.

The Boc-protected product was solved in analytical grade DCM (3.0 mL) and extra pure TFA (3.0 mL) and stirred 1h at rt until LC-MS confirmed full conversion. Then the solvents were removed under reduced pressure and the crude was dried under HV, solved in MeCN/H<sub>2</sub>O and lyophilized overnight (2x) to obtain 2.73 mg (0.058 mmol, 16%) of the product-TFA salt as an deep yellow solid.

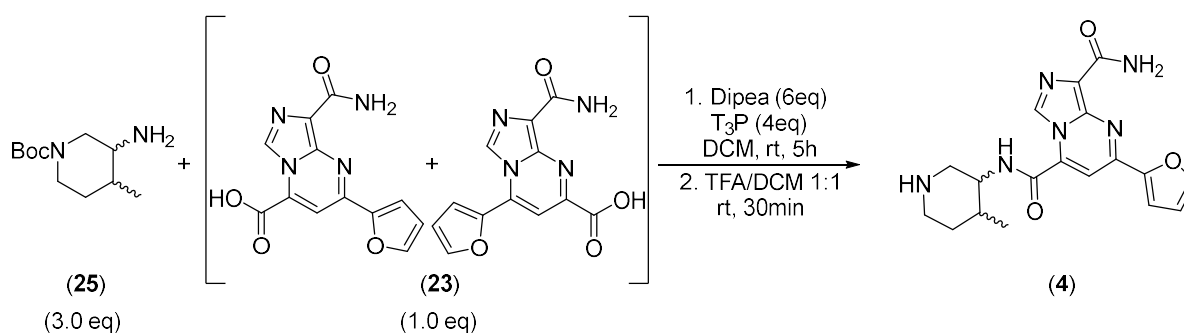
**LC-MS:** Column: Phenomenex Luna C18(2), gradient: MeCN/H<sub>2</sub>O + 0.05 % HCOOH, 5 % MeCN increase to 100% MeCN in 5.1 min, flow rate: 0.6 mL/min, t<sub>R</sub> = 1.79, m/z = 357.2 ([M+H]<sup>+</sup>)

**HRMS:** m/z ([M+H]<sup>+</sup>), calculated: 357.1675, found: 357.1655



**<sup>1</sup>H-NMR** (500 MHz, dms<sub>o</sub>-d<sub>6</sub>,  $\delta$  in ppm): 9.36 (CF<sub>3</sub>COOH), 9.05 (s, 1H, H-9), 8.68 (br.s, 2H, amide-NH<sub>2</sub>), 8.24 (s, 1H, H-8), 7.98 (d, <sup>3</sup>J<sub>6,7</sub> = 3.3 Hz, 1H, H-6), 7.80 (s, 1H, NH), 7.76 (s, 1H, NH), 7.52 (s, 1H, H-17), 6.98-6.95 (m, 1H, H-7), 3.70-3.62 (m, 1H, H12-a), 3.60-3.53 (m, 2H, H12-b, H-13), 3.21-3.06 (m, 2H, H-15), 1.31 (d, <sup>3</sup>J<sub>14,13</sub> = 5.6 Hz, 3H, H-14), 1.24 (t, <sup>3</sup>J<sub>16,15</sub> = 6.6 Hz, 3H, H-16).

**Synthesis of (S)-N4-(2-(ethylamino)propyl)-2-(furan-2-yl)imidazo[1,5-a]pyrimidine-4,8-dicarboxamide (4)**



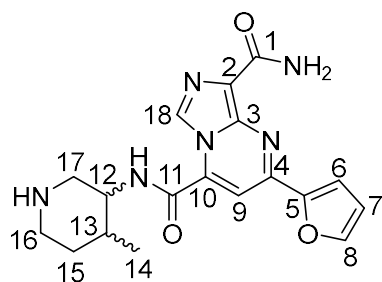
According to **standard procedure 1**, 8-carbamoyl-2-(furan-2-yl)imidazo[1,5-a]pyrimidine-4-carboxylic acid ((**23**), 8.2 mg, 0.03 mmol, 1.0 eq), tert-butyl 3-amino-4-methylpiperidine-1-carboxylate ((**25**) 19.4 mg, 0.09 mmol, 3.0 eq), dry. DCM (2.0 mL), Dipea (30  $\mu$ L, 0.18 mmol, 6.0 eq) and T<sub>3</sub>P (50% in EtOAc, 75  $\mu$ L, 0.12 mmol, 4.0 eq) were used to gain 24.5 mg of a yellow oil as crude after workup.

The crude oil was solved in MeCN/H<sub>2</sub>O (1:1, 3mL) and purified via prep. HPLC in one run (gradient: 5-100% MeCN in H<sub>2</sub>O in 30 min) to obtain the Boc protected product as a yellow solid. It was possible to separate both isomers at this stage of the synthesis.

The Boc-protected product was solved in analytical grade DCM (3.0 mL) and extra pure TFA (3.0 mL) and stirred 1h at rt until LC-MS confirmed full conversion. Then the solvents were removed under reduced pressure and the crude was dried under HV, solved in MeCN/H<sub>2</sub>O and lyophilized overnight (2x) to obtain 4.98 mg (0.0855 mmol, 28%) of the product-TFA salt as an deep yellow solid.

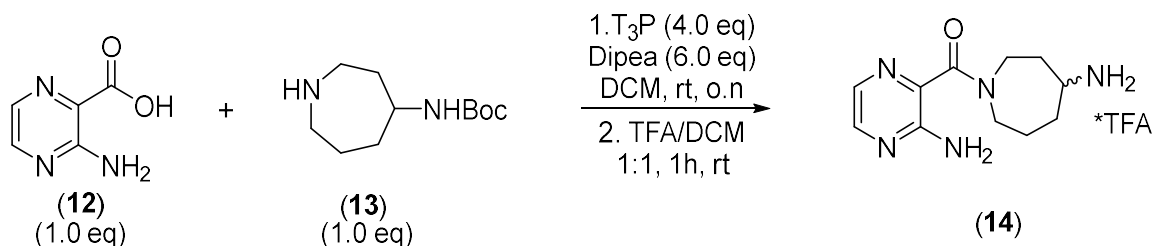
**LC-MS:** Column: Phenomenex Luna C18(2), gradient: MeCN/H<sub>2</sub>O + 0.05 % HCOOH, 5 % MeCN increase to 100% MeCN in 5.1 min, flow rate: 0.6 mL/min, t<sub>R</sub> = 1.99, m/z = 369.2 ([M+H]<sup>+</sup>)

**HRMS:** m/z ([M+H]<sup>+</sup>), calculated: 369.1675, found: 369.1655



**<sup>1</sup>H-NMR** (500 MHz, dms<sub>o</sub>-d<sub>6</sub>,  $\delta$  in ppm): 9.03 (s, 1H, H-9), 8.64 (br.s, 1H, amide NH), 8.22 (s, 1H, H-8), 7.97 (d, <sup>3</sup>J<sub>6,7</sub> = 3.5 Hz, 1H, H-6), 7.81 (br.s, 1H, amide-NH), 7.71 (s, 1H, H-18), 7.65 (br.s, 1H, amide-NH), 6.96 (dd, <sup>3</sup>J<sub>7,6</sub> = 3.6 Hz, <sup>3</sup>J<sub>7,8</sub> = 1.6 Hz, 1H, H-7), 4.40 (s, 1H, H-12), 3.52-3.38 (m, 1H, H-17a), 3.30-3.20 (m, 2H, H-17b, H-16a), 3.10-3.01 (m, 1H, H-16b), 2.23-2.15 (m, 1H, H-13), 1.85-1.68 (m, 2H, H-15), 0.98 (d, <sup>3</sup>J<sub>14,13</sub> = 6.8 Hz, 3H, H-14).

(4-aminoazepan-1-yl)(3-aminopyrazin-2-yl)methanone (14)

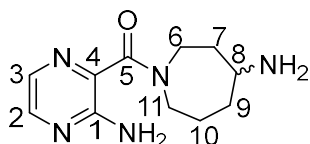


According to **standard procedure 1**, 3-aminopyrazine-2-carboxylic acid ((**12**), 139.6 mg, 1.0 mmol, 1.0 eq), tert-butyl azepan-4-ylcarbamate hydrochloride ((**13**), 251.7 mg, 1.0 mmol, 1.0 eq), dry. DCM (10mL, [0.1M]), Dipea (1 mL, 6.0 eq) and T<sub>3</sub>P (50% in EtOAc, 2.6 mL, 4.0 eq) were used to gain 319.5 mg of a yellow oil after workup which took place after 5 h reaction time.

According to **standard procedure 2**, the crude was deprotected in 1h using TFA/DCM 1:5.

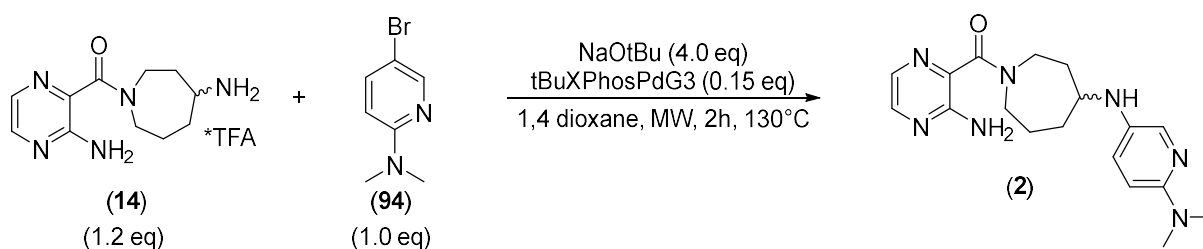
The crude oil was solved in MeCN/H<sub>2</sub>O (1:1, 4mL) and purified via prep. HPLC in three runs (1% MeCN in H<sub>2</sub>O for 5 min, then 1-20% MeCN in H<sub>2</sub>O in 20 min) to obtain 103.0 mg (0.29 mmol, 29%) of the product trifluoroacetic acid salt as a pale yellow solid.

**LC-MS:** Column: Phenomenex Luna C18(2), gradient: MeCN/H<sub>2</sub>O + 0.05 % HCOOH, 5 % MeCN increase to 100% MeCN in 5.1 min, flow rate: 0.6 mL/min, t<sub>R</sub> = 0.74, m/z = 236.3 ([M+H]<sup>+</sup>).



<sup>1</sup>H-NMR (500 MHz, dmsO-d<sub>6</sub>, δ in ppm): 8.06-8.01 (m, 1H, H-2), 7.84 (br.s, 2H, Ar-NH<sub>2</sub>), 7.77-7.73 (m, 1H, H-3), 3.60-3.11 (m, 5H, H-8, H-6, H-11), 1.95-1.22 (m, 6H, H-7, H-9, H-10).

(3-aminopyrazin-2-yl)(4-((6-(dimethylamino)pyridin-3-yl)amino)azepan-1-yl)methanone (2)



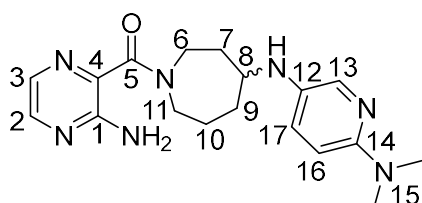
According to **standard procedure 4**, (4-aminoazepan-1-yl)(3-aminopyrazin-2-yl)methanone ((**14**), 57.6 mg, 0.2 mmol, 1.2 eq), 5-bromo-N,N-dimethylpyridin-2-amine ((**94**), 35.2 mg, 0.17 mmol, 1.0 eq), NaOtBu (63.5 mg, 0.68 mmol, 4.0 eq), dry. 1,4-dioxane (2mL, [0.1M]) and

tBuXPhosPdG3 (21.3 mg, 0.0255 mmol, 0.15 eq) were heated to 160°C for 3h in the microwave to achieve full conversion and get 54.9 mg of a yellow solid after workup.

The crude oil was solved in MeCN/H<sub>2</sub>O (1:1, 4mL) and purified via prep. HPLC in four runs (5-50% MeCN in 30 min) to obtain 2.37 mg (0.007 mmol, 4%) of the pure product as a pale yellow solid, due to a complicated separation.

**LC-MS:** Column: Phenomenex Luna C18(2), gradient: MeCN/H<sub>2</sub>O + 0.05 % HCOOH, 5 % MeCN increase to 100% MeCN in 5.1 min, flow rate: 0.6 mL/min, t<sub>R</sub>=1.89, m/z = 356.1 ([M+H]<sup>+</sup>).

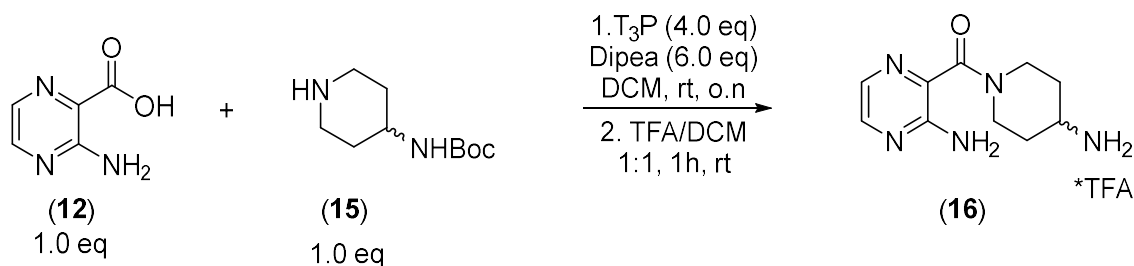
**HRMS:** m/z ([M+H]<sup>+</sup>), calculated: 356.2199, found: 356.2181



**<sup>1</sup>H-NMR** (500 MHz, dms<sub>o</sub>-d<sub>6</sub>, δ in ppm): 9.04 (s, 1H, H-2), 8.22 (d, <sup>3</sup>J<sub>3,2</sub> = 1.3 Hz, 1H, H-3), 7.97 (d, <sup>3</sup>J<sub>17,16</sub> = 3.6 Hz, 1H, H-17), 7.84 (s, 1H, NH), 7.76-7.71 (m, 1H, H-13), 7.64 (s, 1H, NH), 6.96 (dd, J = 3.6 Hz, 1.6 Hz, 1H, H-16), 4.44-4.36 (m, 1H, H-8), 3.42 (s, 3H, H-15), 3.31-3.21 (m, 4H, H-6, H-11), 3.11-3.01 (s, 1H, H-10a), 2.23-2.13 (s, 1H, H-10b), 1.85-1.66 (m, 2H, H7a, H9a), 1.31, 1.19 (m, 2H, H-7b, H-9b).

**<sup>13</sup>C-NMR** (126 MHz, dms<sub>o</sub>-d<sub>6</sub>, δ in ppm): 162.88 (C-5), 148.09 (C-1), 147.98 (C-3), 143.64 (C-14), 133.1 (C-12), 126.63 (C-2), 124.32 (C-4), 117.39 (C-17), 113.76 (C-16), 101.75 (C-13), 46.56 (C-8), 45.08 (C-6 or C-11), 41.72 (C-6 or C-11), 39.52 (C-15), 30.23 (C-7, C-9), 25.79 (C-10).

#### (4-aminopiperidin-1-yl)(3-aminopyrazin-2-yl)methanone (16)

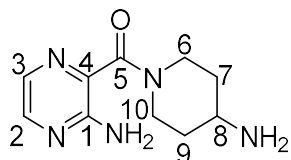


According to **standard procedure 1**, 3-aminopyrazine-2-carboxylic acid ((**12**), 69.0 mg, 0.5 mmol, 1.0 eq), tert-butyl piperidin-4-ylcarbamate ((**15**), 100.7 mg, 0.5 mmol, 1.0 eq), dry. DCM (5.0 mL, [0.1M]), DIPEA (520 μL, 6.0 eq) and T<sub>3</sub>P (50% in EtOAc, 950 μL, 4.0 eq) were used to gain 195 mg of a yellow oil after workup after 1h reaction time.

The Boc-protected product was solved in analytical grade DCM (10.0 mL) and extra pure TFA 2.0 mL) and stirred 1h at rt until LC-MS confirmed full conversion. Then the solvents were removed under reduced pressure and the crude was dried under vacuum.

The crude oil was solved in MeCN/H<sub>2</sub>O (1:1, 4 mL) and purified via prep. HPLC in three runs (1% MeCN in H<sub>2</sub>O for 5 min, then 1-20% MeCN in H<sub>2</sub>O in 20 min) to obtain 77.2 mg (0.23 mmol, 46%) of the product trifluoroacetic acid salt as a pale yellow solid.

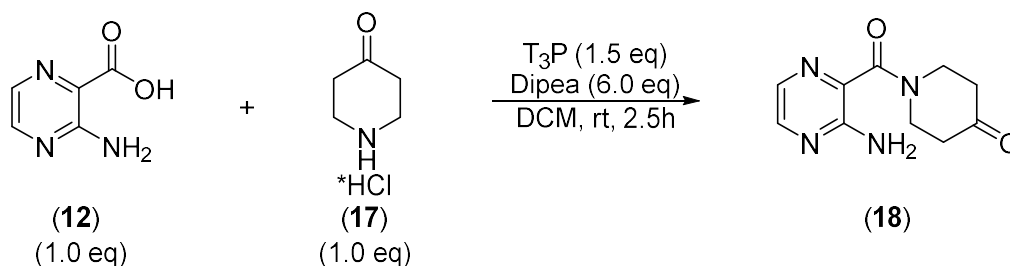
**LC-MS:** Column: Phenomenex Luna C18(2), gradient: MeCN/H<sub>2</sub>O + 0.05 % HCOOH, 5 % MeCN increase to 100% MeCN in 5.1 min, flow rate: 0.6 mL/min, t<sub>R</sub> = 0.50, m/z = 222.2 ([M+H]<sup>+</sup>).



**<sup>1</sup>H-NMR** (500 MHz, MeOH-d<sub>4</sub>, δ in ppm): 8.52 (s, 1H, NH), 8.05 (d, <sup>3</sup>J<sub>2,3</sub> = 2.5 Hz, 1H, H-2), 7.81 (d, <sup>3</sup>J<sub>3,2</sub> = 2.5 Hz, 1H, H-3), 4.73 (d, <sup>2</sup>J = 12.5 Hz, 1H, H-6a), 4.01 (d, <sup>2</sup>J = 12.0 Hz, 1H, H-10a), 3.45-3.36 (m, 1H, H-8), 3.20 (t, <sup>2</sup>J = 12.7 Hz, 1H, H-10b), 2.95 (t, <sup>2</sup>J = 12.2 Hz, 1H, H-6b), 2.19-1.94 (m, 2H, H-7a, H-9a), 1.74-1.56 (m, 2H, H-7b, H-9b).

**<sup>13</sup>C-NMR** (126 MHz, MeOH-d<sub>4</sub>, δ in ppm): 167.62 (C-5), 155.42 (C-1), 145.27 (C-2), 133.63 (C-4), 132.32 (C-3), 46.37 (C-6 or C-10), 41.58 (C-6 or C-10), 40.42 (C-8), 31.81 (C-7 or C-9), 30.99 (C-7 or C-9).

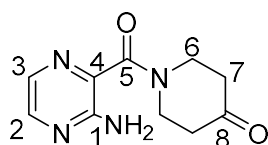
#### 1-(3-aminopyrazine-2-carbonyl)piperidin-4-one (18)



According to **standard procedure 1**, 3-aminopyrazine-2-carboxylic acid ((**12**), 695.8 mg, 5.0 mmol, 1.0 eq) and piperidin-4-one hydrochloride ((**17**), 675.6 mg, 5.0 mmol, 1.0 eq), dry. DCM (50.0 mL, [0.1M]). (5.2 mL, 6.0 eq) and T<sub>3</sub>P (50% in EtOAc, 4.8 mL, 1.5 eq) were used to obtain after workup 870.9 mg of a brown solid after 2.5 h reaction time.

The crude oil was solved in MeCN/H<sub>2</sub>O (1:1, 4mL) and purified via flash. prep. HPLC in three runs (5-40% MCN in H<sub>2</sub>O in 20 min) to obtain 553.4 mg (2.51 mmol, 50%) of the product as a pale yellow solid.

**LC-MS:** Column: Phenomenex Luna C18(2), gradient: MeCN/H<sub>2</sub>O + 0.05 % HCOOH, 5 % MeCN increase to 100% MeCN in 7 min, flow rate: 0.6 mL/min, t<sub>R</sub> = 1.11, m/z = 221.1 ([M+H]<sup>+</sup>).

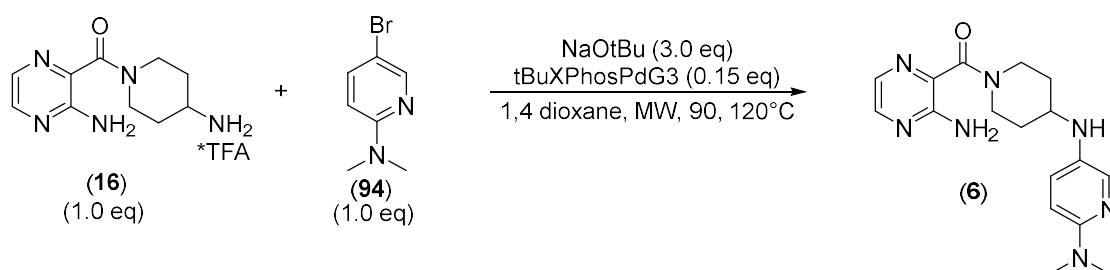


**<sup>1</sup>H-NMR** (500 MHz, dms<sub>o</sub>-d<sub>6</sub>, δ in ppm): 8.06 (d, <sup>3</sup>J<sub>2,3</sub> = 2.5 Hz, 1H, H-2), 7.78 (d, <sup>3</sup>J<sub>3,2</sub> = 2.5 Hz, 1H, H-3), 6.58 (br.s, 2H, NH<sub>2</sub>), 3.90 (t, <sup>3</sup>J = 6.3 Hz, 2H, H-6a), 3.68 (t, <sup>3</sup>J = 6.2 Hz, 2H, H-6b), 2.53 (t, <sup>3</sup>J = 6.3 Hz, 2H, H-7a), 2.41 (t, <sup>3</sup>J = 6.1 Hz, 2H, H-7b).

**<sup>13</sup>C-NMR** (126 MHz, dms<sub>o</sub>-d<sub>6</sub>, δ in ppm): 207.20 (C-8), 165.65 (C-5), 153.45 (C-1), 143.79 (C-2), 132.55 (C-4), 130.64 (C-3), 44.5 (C-6), 40.94 (C-7).

**(3-aminopyrazin-2-yl)(4-((6-(dimethylamino)pyridin-3-yl)amino)piperidin-1-yl)methanone (6)**

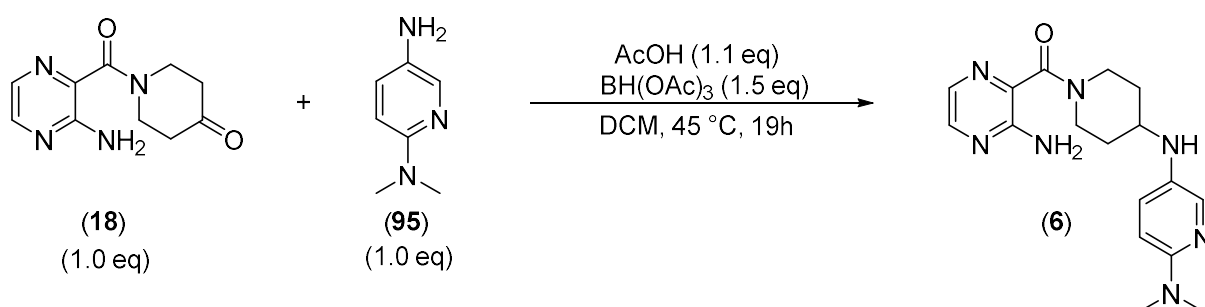
**BZO595 (Buchwald Hartwig route)**



According to **standard procedure 4**, (4-aminopiperidin-1-yl)(3-aminopyrazin-2-yl)methanone ((**16**), 39.0 mg, 0.15 mmol, 1.0 eq), 5-bromo-N,N-dimethylpyridin-2-amine ((**94**), 31.2 mg, 0.15 mmol, 1.0 eq), NaOtBu (46.3 mg, 0.45 mmol, 3.0 eq), dry. 1,4-dioxane (2mL, [0.1M]) and tBuXPhosPdG3 (17.3 mg, 0.0225 mmol, 0.15 eq) were used to gain after 90 min at 120°C in the microwave and subsequent filtration 54.9 mg of an orange oil as crude product.

The crude oil was solved in MeCN/H<sub>2</sub>O (1:1, 4mL) and purified via prep. HPLC in four runs (5-50% MeCN in 30 min) to obtain 2.16 mg (0.006 mmol, 4%) of the pure product, due to a complicated separation.

**BZO656 (reductive amination)**

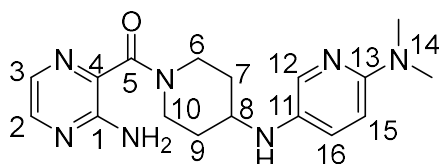


According to **standard procedure 3**, 1-(3-aminopyrazine-2-carbonyl)piperidin-4-one ((**18**), 109.5 mg, 0.5 mmol, 1.0 eq), N<sub>2</sub>,N<sub>2</sub>-dimethylpyridine-2,5-diamine ((**95**), 68.6 mg, 0.5 mmol, 1.0 eq), dry. DCM (5.0 mL, [0.1M]), (30 μL, 0.55 mmol, 1.1 eq) and BH(OAc)<sub>3</sub> (156.2 mg, 0.75 mmol, 1.5 eq) were reacted for 19 h to obtain 112.3 mg of a deep purple oil as the crude product after workup.

The crude oil was solved in MeCN/H<sub>2</sub>O (1:1, 4mL) and purified via prep. HPLC in two runs (5-20% MeCN in 30 min) to obtain 32.8 mg (0.1 mmol, 20%) of the pure product as a purple solid.

**LC-MS:** Column: Phenomenex Luna C18(2), gradient: MeCN/H<sub>2</sub>O + 0.05 % HCOOH, 5 % MeCN increase to 100% MeCN in 5.1 min, flow rate: 0.6 mL/min, t<sub>R</sub> = 1.60, m/z = 342.3 ([M+H]<sup>+</sup>).

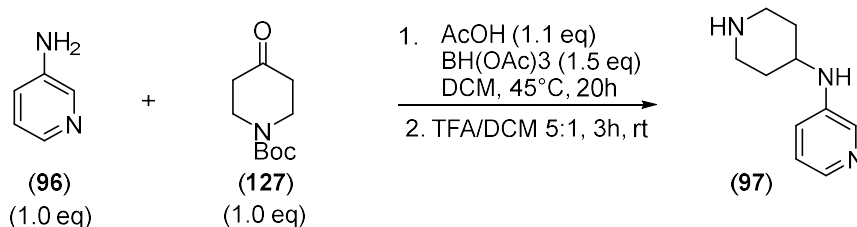
**HRMS:** m/z ([M+H]<sup>+</sup>), calculated: 342.2042, found: 342.2026



**<sup>1</sup>H-NMR** (500 MHz, dms<sub>o</sub>-d<sub>6</sub>, δ in ppm): 8.02 (d, <sup>3</sup>J<sub>2,3</sub> = 2.5 Hz, 1H, H-2), 7.75 (d, <sup>3</sup>J<sub>3,2</sub> = 2.5 Hz, 1H, H-3), 7.57 (s, 1H, H-12), 7.09 (d, <sup>3</sup>J<sub>16,15</sub> = 7.7 Hz, 1H, H-16), 6.63 (d, <sup>3</sup>J<sub>15,16</sub> = 7.9 Hz, 1H, H-15), 6.43 (br.s, 2H, Ar-NH<sub>2</sub>), 4.34 (d, <sup>2</sup>J = 12.7 Hz, 1H, H-6a), 3.63 (d, <sup>2</sup>J = 13.1 Hz, 1H, H-10a), 3.48-3.35 (m, 1H, H-8), 3.15 (t, <sup>2</sup>J = 11.3 Hz, 1H, H-10b), 3.05 (t, <sup>2</sup>J = 11.0 Hz, 1H, H-6b), 2.91 (s, 6H, H-14), 2.54 (s, 1H, NH), 1.98 (d, <sup>2</sup>J = 11.0 Hz, 1H, H-7a), 1.85 (d, <sup>2</sup>J = 11.3 Hz, 1H, H-9a), 1.41-1.27 (m, 2H, H-7b, H-9b).

**<sup>13</sup>C-NMR** (126 MHz, dms<sub>o</sub>-d<sub>6</sub>, δ in ppm): 164.98 (C-5), 153.25 (C-1), 152.14 (C-13), 143.31 (C-2), 135.01 (C-11), 133.45 (C-12), 130.67 (C-3), 126.08 (C-16), 107.82 (C-15), 49.79 (C-8), 45.05 (C-10), 40.43 (C-6), 38.7 (C-14), 32.18 (C-7), 31.23 (C-9).

### N-(piperidin-4-yl)pyridine-3-amine (97)

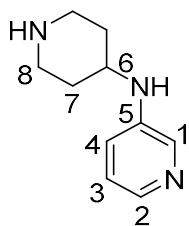


According to **standard procedure 3**, 3-Aminopyridin ((**96**), 313.6 mg, 2.3 mmol mmol, 1.1 eq), tert-butyl 4-oxopiperidine-1-carboxylate ((**127**), 601.3 mg, 3.0 mmol, 1.0 eq), dry. DCM (6.0 mL, [0.5M]), acetic acid (190 μL, 3.3 mmol, 1.1 eq) and BH(OAc)<sub>3</sub> (958 mg, 4.5 mmol, 1.5 eq) were used to gain 708.1 mg of a brown oil after workup.

Column: Phenomenex Luna C18(2), gradient: MeCN/H<sub>2</sub>O + 0.05 % HCOOH, 5 % MeCN increase to 100% MeCN in 5.1 min, flow rate: 0.6 mL/min, t<sub>R</sub> = 2.68, m/z = 278.1 ([M+H]<sup>+</sup>).

Then the Boc group was cleaved according to **standard procedure 2** to gain 353.3 mg (1.99 mmol, 66%) of the free amine as a brown solid which was used in the next reaction without further purification.

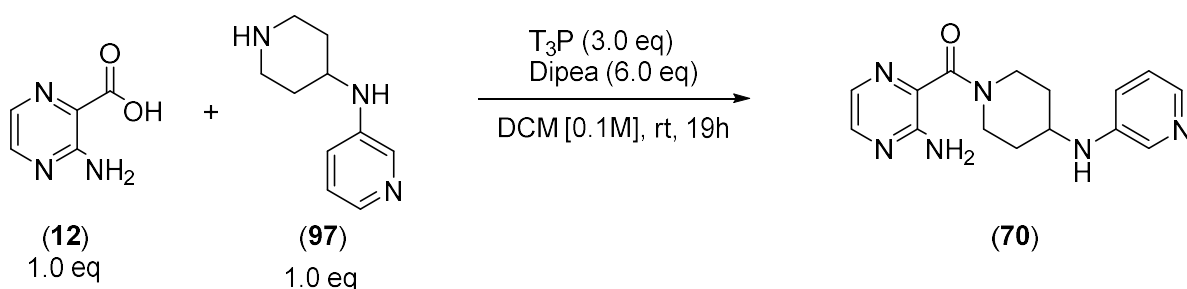
Column: Phenomenex Luna C18(2), gradient: MeCN/H<sub>2</sub>O + 0.05 % HCOOH, 5 % MeCN increase to 100% MeCN in 5.1 min, flow rate: 0.6 mL/min, t<sub>R</sub> = 0.43, m/z = 178.2 ([M+H]<sup>+</sup>).



**<sup>1</sup>H-NMR** (500 MHz, dms<sub>o</sub>-d<sub>6</sub>, δ in ppm): 7.95 (d, <sup>4</sup>J<sub>1,4</sub> = 2.8 Hz, 1H, H-1), 7.71 (dd, <sup>3</sup>J<sub>2,3</sub> = 4.5 Hz, <sup>4</sup>J<sub>2,4</sub> = 0.9 Hz), 7.04 (dd, <sup>3</sup>J<sub>3,4</sub> = 8.3 Hz, <sup>3</sup>J<sub>3,2</sub> = 4.6 Hz, 1H, H-3), 6.89 (ddd, <sup>3</sup>J<sub>4,3</sub> = 8.4 Hz, <sup>4</sup>J<sub>4,1</sub> = 2.7 Hz, <sup>4</sup>J<sub>4,2</sub> = 1.2 Hz, 1H, H-4), 5.68 (d, J = 8.1 Hz, ArNH), 3.29-3.21 (m, 1H, H-6), 2.97-2.89 (m, 2H, H<sub>8a</sub>), 2.56-2.51 (m, 2H, H<sub>8b</sub>), 1.87-1.80 (m, 2H, H<sub>7a</sub>), 1.26-1.16 (m, 2H, H<sub>7b</sub>).

**<sup>13</sup>C-NMR** (126 MHz, dms<sub>o</sub>-d<sub>6</sub>, δ in ppm): 143.89 (C-5), 136.34 (C-2), 135.65 (C-1), 123.62 (C-3), 117.54 (C-4), 62.01 (C-6), 49.22 (C-8<sub>a</sub> or C-8<sub>b</sub>), 44.97 (C-8<sub>a</sub> or C-8<sub>b</sub>), 33.08 (C-7<sub>a</sub> or C-7<sub>b</sub>), 25.5 (C-7<sub>a</sub> or C-7<sub>b</sub>).

### (3-aminopyrazin-2-yl)(4-(pyridin-3-yl)amino)piperidin-1-ylmethanone (**70**)

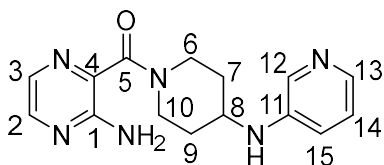


According to **standard procedure 1**, 3-aminopyrazine-2-carboxylic acid ((**12**), 278 mg, 2 mmol, 1.0 eq), N-(piperidin-4-yl)pyridine-3-amine ((**97**), 353.3 mg, 1.99 mmol, 2.0 eq), dry. DCM (20.0 mL, [0.1M]), Dipea (2.1 mL, 6.0 eq) and T<sub>3</sub>P (50% in EtOAc, 3.8 mL, 3.0 eq) were used to gain 472.2 mg of a brown oil after workup, which contained 60% of the desired product and several side products.

The crude oil was solved in MeCN/H<sub>2</sub>O/DMSO (1:1:1, 5mL) and purified via flash prep. HPLC in one run (5-100% MeCN in 30 min) to obtain 178.2 mg (0.52 mmol, 26%) of the formic acid salt as a pale yellow solid after lyophilisation.

**LC-MS:** Column: Phenomenex Luna C18(2), gradient: MeCN/H<sub>2</sub>O + 0.05 % HCOOH, 5 % MeCN increase to 100% MeCN in 5.1 min, flow rate: 0.6 mL/min, t<sub>R</sub> = 1.40, m/z = 299.3 ([M+H]<sup>+</sup>).

**HRMS:** m/z ([M+H]<sup>+</sup>), calculated: 299.1620, found: 299.1606



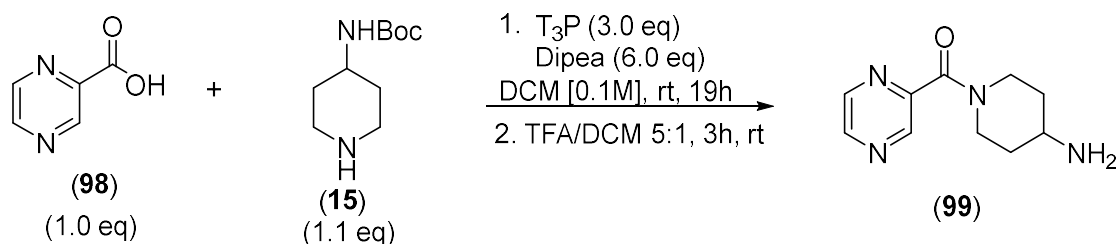
**<sup>1</sup>H-NMR** (500 MHz, dms<sub>o</sub>-d<sub>6</sub>, δ in ppm): 8.02 (d, <sup>3</sup>J<sub>2,3</sub> = 2.6 Hz, 1H, H-2), 7.99 (d, <sup>4</sup>J<sub>12,13</sub> = 2.2 Hz, 1H, H-12), 7.76 (d, <sup>3</sup>J<sub>3,2</sub> = 2.6 Hz, 1H, H-3), 7.74 (d, <sup>2</sup>J<sub>15,14</sub> = 4.4 Hz, 1H, H-15), 7.06 (dd, <sup>3</sup>J<sub>14,15</sub> = 4.4 Hz, <sup>3</sup>J<sub>14,13</sub> = 8.3 Hz, 1H, H-14), 6.96 (dd, <sup>3</sup>J<sub>13,14</sub> = 8.3 Hz, <sup>3</sup>J<sub>13,12</sub> = 2.0 Hz, 1H, H-13), 6.45 (br.s, 2H, Ar-NH<sub>2</sub>), 5.81 (s, 1H, NH), 4.36 (d, <sup>2</sup>J = 13.1 Hz, 1H, H-6a), 3.64 (d, <sup>2</sup>J = 13.5 Hz, 1H, H-10a), 3.60-3.51 (m, 1H, H-8), 3.19 (t, <sup>2</sup>J = 11.2 Hz, 1H, H-10b), 3.07 (t, <sup>2</sup>J = 11.0 Hz,



1H, H6b), 2.01 (d,  $^2J = 11.6$  Hz, 1H, H-7a), 1.88 (d,  $^2J = 11.2$  Hz, 1H, H-9a), 1.45-1.30 (m, 2H, H-7b, H-9b).

$^{13}\text{C-NMR}$  (126 MHz, dms $\text{-d}_6$ ,  $\delta$  in ppm): 165.01 (C-5), 163.12 (HCOOH), 153.27 (C-1), 143.80 (C-4), 143.35 (C-2), 136.68 (C-13), 135.60 (C-11), 133.45 (C-12), 130.68 (C-3), 123.73 (C-15), 117.93 (C-14), 48.23 (C-8), 45.08 (C-10), 40.21 (C-6), 32.03 (C-7), 31.08 (C-9).

#### (4-aminopiperidin-1-yl)(pyrazin-2-yl)methanone (**99**)

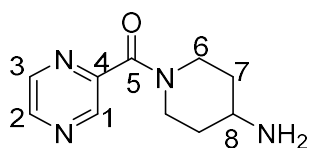


According to **standard procedure 1**, pyrazine-2-carboxylic acid (**98**), 64.4 mg, 0.5 mmol, 1.0 eq), tert-butyl piperidin-4-yl-carbamate (**15**), 108.7 mg, 0.55 mmol, 1.1 eq), dry. DCM (5 mL, [0.1M]), Dipea (0.52 mL, 6.0 eq) and T<sub>3</sub>P (50% in EtOAc, 0.95 mL, 3.0 eq) were used to gain a brown oil after workup.

Then the Boc group was cleaved according to **standard procedure 2** to gain the free amine which was solved in MeCN/H<sub>2</sub>O/DMSO (1:1:1, 5mL) and purified via flash prep. HPLC in one run (0-20% MeCN in H<sub>2</sub>O in 30 min, elution after 3 min) to obtain 27 mg (0.13 mmol, 26%) of a yellow oil.

**LC-MS:** Column: Phenomenex Luna C18(2), gradient: MeCN/H<sub>2</sub>O + 0.05 % HCOOH, 5 % MeCN increase to 100% MeCN in 5.1 min, flow rate: 0.6 mL/min,  $t_R = 52$ ,  $m/z = 207.2$  ([M+H]<sup>+</sup>).

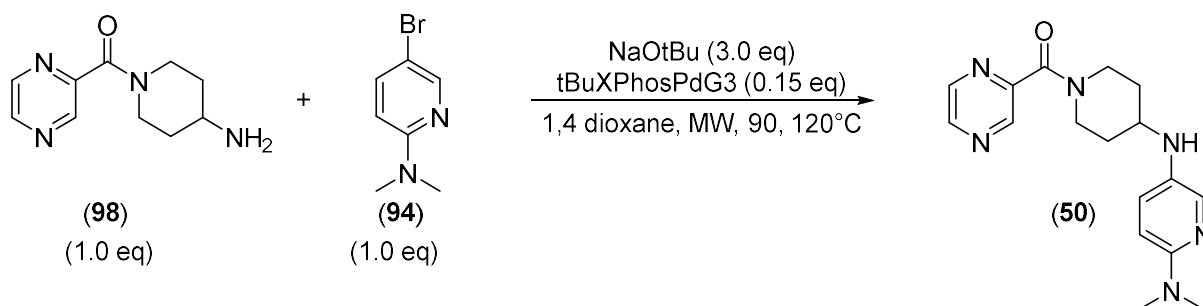
**HRMS:**  $m/z$  ([M+H]<sup>+</sup>), calculated: 207.1246, found: 207.1234



$^1\text{H-NMR}$  (500 MHz, dms $\text{-d}_6$ ,  $\delta$  in ppm): 8.82 (s, 1H, H-1), 8.75 (d,  $^3J = 2.4$  Hz, 1H, H-2), 8.67 (s, 1H, H-3), 4.45 (d,  $^2J = 13.1$  Hz, 1H, H-6a), 3.70 (d,  $^2J = 13.5$  Hz, 1H, H-10a), 3.34-3.14 (m, 1H, H-8), 3.13 (t,  $^2J = 12.2$  Hz, 1H, H-10b), 2.94 (t,  $^2J = 11.8$  Hz, 1H, H6b), 1.99 (d,  $^2J = 11.5$  Hz, 1H, H-7a), 1.84 (d,  $^2J = 11.5$  Hz, 1H, H-9a), 1.55-1.38 (m, 2H, H-7b, H-9b).

$^{13}\text{C-NMR}$  (126 MHz, dms $\text{-d}_6$ ,  $\delta$  in ppm): 164.71 (C-5), 149.47 (C-4), 145.50 (C-2), 144.20 (C-1), 143.28 (C-3), 47.05 (C-8), 44.85 (C-10), 40.02 (C-6), 31.48 (C-7), 30.69 (C-9).

**(4-((6-(dimethylamino)pyridin-3-yl)amino)piperidin-1-yl)(pyrazin-2-yl)methanone (50)**

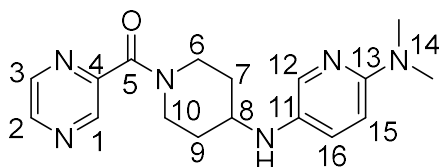


According to **standard procedure 4**, (4-aminopiperidin-1-yl)(pyrazin-2-yl)methanone ((**98**), 27mg, 0.13 mmol, 1.1 eq), 5-bromo-N,N-dimethylpyridin-2-amine ((**94**), 23.7 mg, 0.12 mmol, 1.0 eq), NaOtBu (34 mg, 0.35mmol, 3.0 eq), dry. 1,4-dioxane (1.2mL, [0.1M]) and tBuXPhosPdG3 (14.3 mg, 0.018 mmol, 0.15 eq) were used in the microwave (120°C, 1.5 h) to gain 27.0 mg of a dark residue after workup.

The crude oil was solved in MeCN/H<sub>2</sub>O/DMSO (1:1:1, 5mL) and purified via prep. HPLC in two runs (5-50% MeCN in 30 min) to obtain 4.12 mg (0.52 mmol, 26%) of the product as a yellow solid.

**LC-MS:** Column: Phenomenex Luna C18(2), gradient: MeCN/H<sub>2</sub>O + 0.05 % HCOOH, 5 % MeCN increase to 100% MeCN in 5.1 min, flow rate: 0.6 mL/min, t<sub>R</sub> = 1.65, m/z = 327.5 ([M+H]<sup>+</sup>).

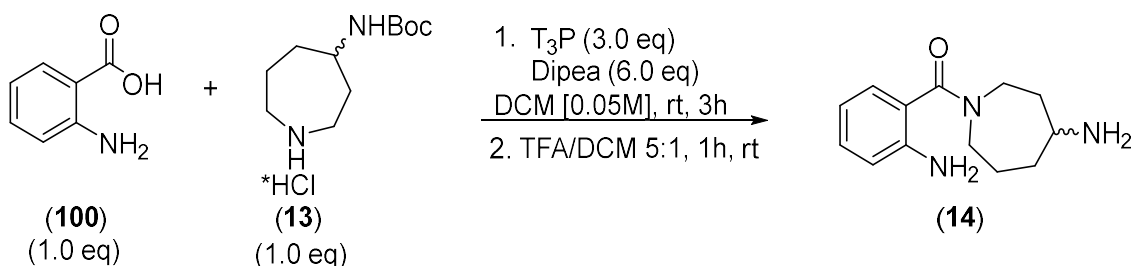
**HRMS:** m/z ([M+H]<sup>+</sup>), calculated: 327.1933, found: 327.1917



**<sup>1</sup>H-NMR** (500 MHz, dms<sub>o</sub>-d<sub>6</sub>, δ in ppm): 8.82 (d, <sup>4</sup>J<sub>1,2</sub> = 1.4 Hz, 1H, H-1), 8.74 (d, <sup>3</sup>J<sub>3,2</sub> = 2.5 Hz, 1H, H-3), 8.67 (dd, <sup>3</sup>J<sub>2,3</sub> = 2.4 Hz, <sup>4</sup>J<sub>2,1</sub> = 1.5 Hz, 1H, H-2), 7.63 (d, <sup>4</sup>J<sub>12,16</sub> = 2.5 Hz, H-12), 7.00 (d, <sup>3</sup>J<sub>16,15</sub> = 8.9 Hz, <sup>4</sup>J<sub>16,12</sub> = 2.6 Hz, 1H, H-16), 6.55 (d, <sup>3</sup>J<sub>15,16</sub> = 8.9 Hz, 1H, H-15), 4.35 (d, <sup>2</sup>J = 13.3 Hz, 1H, H-6a), 3.65 (d, <sup>2</sup>J = 13.8 Hz, 1H, H-10a), 3.48-3.39 (m, 1H, H-8), 3.19 (t, <sup>2</sup>J = 12.4 Hz, 1H, H-10b), 3.08 (t, <sup>2</sup>J = 12.2k Hz, 1H, H6b), 2.87 (s, 6H, H-14), 2.00 (d, <sup>2</sup>J = 9.9 Hz, 1H, H-7a), 1.85 (d, <sup>2</sup>J = 11.4 Hz, 1H, H-9a), 1.39-1.29 (m, 2H, H-7b, H-9b).

**<sup>13</sup>C-NMR** (126 MHz, dms<sub>o</sub>-d<sub>6</sub>, δ in ppm): 164.65 (C-5), 150.77 (C-13), 145.38 (C-3), 144.07 (C-2 or C-1), 143.32 (C-2 or C-1), 135.21 (C-11), 107.03 (C-15), 49.61 (C-8), 45.37 (C-10), 40.50 (C-6), 38.63 (C-14), 32.21 (C-7), 31.45 (C-9).

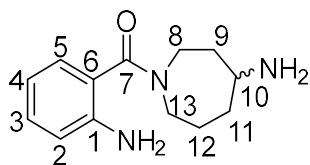
### (4-aminoazepam-1-yl)(2-aminophenyl)methanone (**14**)



According to **standard procedure 1**, 2-aminobenzoic acid ((**100**), 28.1 mg, 0.2 mmol, 1.0 eq), tert-butyl azepam-4-yl-carbamate ((**13**), 53.1 mg, 0.2 mmol, 1.0 eq), dry. DCM (5 mL, [0.1M]), Dipea (0.21 mL, 6.0 eq) and T<sub>3</sub>P (50% in EtOAc, 0.38 mL, 3.0 eq) were used to gain a brown oil after workup.

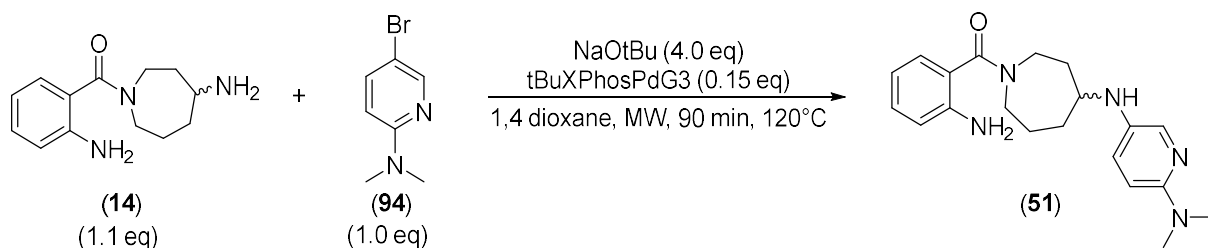
Then the Boc group was cleaved according to **standard procedure 2** to gain the free amine which was solved in MeCN/H<sub>2</sub>O/DMSO (1:1:1, 5mL) and purified via flash prep. HPLC in one run (5-30% MeCN in H<sub>2</sub>O in 30 min) to obtain 21.5 mg (0.092 mmol, 46%) of a colorless solid.

**LC-MS**: Column: Phenomenex Luna C18(2), gradient: MeCN/H<sub>2</sub>O + 0.05 % HCOOH, 5 % MeCN increase to 100% MeCN in 5.1 min, flow rate: 0.6 mL/min, t<sub>R</sub> = 1.30, m/z = 234.2 ([M+H]<sup>+</sup>).



**<sup>1</sup>H-NMR** (500 MHz, MeOH-d<sub>4</sub>, δ in ppm): 7.19-7.17 (m, 1H, H-3), 7.06 (d, <sup>3</sup>J<sub>5,4</sub> = 7.4 Hz, 1H, H-5), 6.81 (d, <sup>3</sup>J<sub>2,3</sub> = 8.1 Hz, 1H, H-2), 6.72 (t, <sup>3</sup>J<sub>4,5</sub> = <sup>3</sup>J<sub>4,3</sub> = 7.5 Hz), 4.07-3.25 (m, 5H, H-8, H-10, H-13), 2.33-1.64 (m, 6H, H-9, H-11, H-12).

### (2-aminophenyl)(4-((6-(dimethylamino)pyridine)pyridine-3-yl)amino)azepam-1-yl)methanone (**51**)

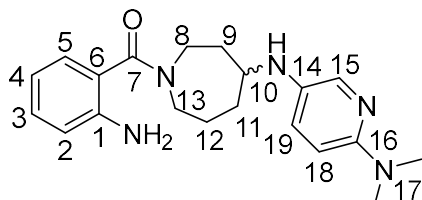


According to **standard procedure 4**, (4-aminoazepam-1-yl)(2-aminophenyl)methanone ((**14**), 19.7 mg, 0.085 mmol, 1.1 eq), 5-bromo-N,N-dimethylpyridin-2-amine ((**94**), 15.8 mg, 0.077 mmol, 1.0 eq), NaOtBu (23.2 mg, 0.23mmol, 3.0 eq), dry. 1,4-dioxane (0.8 mL, [0.1M]) and tBuXPhosPdG3 (10.1 mg, 0.0155 mmol, 0.15 eq) were used in the microwave (120°C, 1.5 h) to gain 27.7 mg of a dark residue after workup.

The crude oil was solved in MeCN/H<sub>2</sub>O/DMSO (1:1:1, 5mL) and purified via prep. HPLC in one run (0-50% MeCN in 30 min) to obtain 2.38 mg (0.52 mmol, 26%) of the product as a yellow oil.

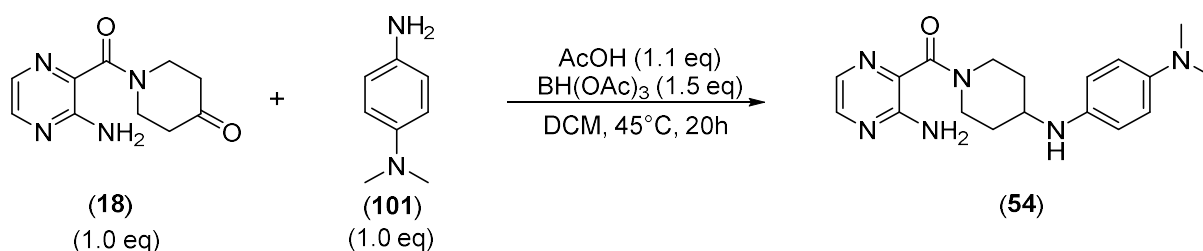
**LC-MS:** Column: Phenomenex Luna C18(2), gradient: MeCN/H<sub>2</sub>O + 0.05 % HCOOH, 5 % MeCN increase to 100% MeCN in 5.1 min, flow rate: 0.6 mL/min, t<sub>R</sub> = 2.06, m/z = 354.0 ([M+H]<sup>+</sup>).

**HRMS:** m/z ([M+H]<sup>+</sup>), calculated: 354.2294, found: 354.2280



**<sup>1</sup>H-NMR** (500 MHz, dms<sub>o</sub>-d<sub>6</sub>, δ in ppm): 7.60-7.48 (m, 1H, H-13), 7.09-7.03 (m, 1H, H-3), 6.97 (d, <sup>3</sup>J<sub>5,4</sub> = 7.4 Hz, 1H, H-5), 6.95-6.88 (m, 1H, H-19), 6.70 (d, <sup>3</sup>J<sub>2,3</sub> = 8.1 Hz, 1H, H-2), 6.56 (t, <sup>3</sup>J<sub>4,5</sub> = <sup>3</sup>J<sub>4,3</sub> = 7.5 Hz), 6.54-6.49 (m, 1H, H-18), 5.03 (br.s, 2H, NH<sub>2</sub>), 3.85-3.36i (m, 11H, H-8, H-10, H-13, H-17, ), 1.93-1.34 (m, 6H, H-9, H-11, H-12).

**(3-aminopyrazin-2-yl)(4-((4-dimethylamino)phenyl)amino)piperidin-1-ylmethanone (54)**

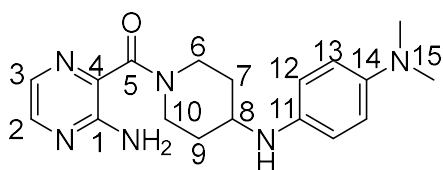


According to **standard procedure 3**, 1-(3-aminopyrazine-2-carbonyl)piperidin-4-one ((**18**), 22.0 mg, 0.1 mmol, 1.0 eq) and N1,N1-dimethylbenzene-1,4-diamine ((**101**), 14.9 mg, 0.11 mmol, 1.1 eq), dry. DCM (5.0 mL, [0.02M]), acetic acid (6 μL, 0.11 mmol, 1.1 eq) and BH(OAc)<sub>3</sub> (31.8 mg, 1.5 mmol, 1.5 eq) were used to gain a yellow oil after workup.

The crude oil was solved in MeCN/H<sub>2</sub>O/DMSO (1:1:1, 2 mL) and purified via prep. HPLC in two run (5-50% MeCN in 30 min) to obtain 4.45 mg (0.013 mmol, 13%) of the product as an off-white solid.

**LC-MS:** Column: Phenomenex Luna C18(2), gradient: MeCN/H<sub>2</sub>O + 0.05 % HCOOH, 5 % MeCN increase to 100% MeCN in 5.1 min, flow rate: 0.6 mL/min, t<sub>R</sub> = 1.63, m/z = 341.3 ([M+H]<sup>+</sup>).

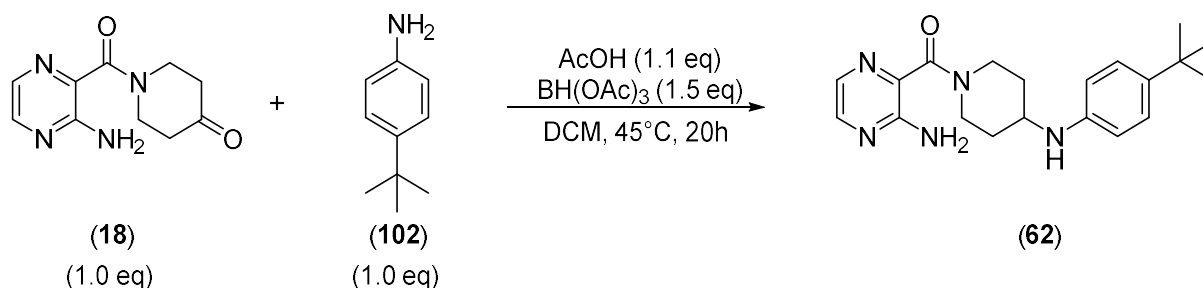
**HRMS:** m/z ([M+H]<sup>+</sup>), calculated: 341.2090, found: 341.2071



**<sup>1</sup>H-NMR** (500 MHz, dms<sub>o</sub>-d<sub>6</sub>, δ in ppm): 8.02 (d, <sup>3</sup>J<sub>2,3</sub> = 2.6 Hz, 1H, H-2), 7.76 (d, <sup>3</sup>J<sub>3,2</sub> = 2.6 Hz, 1H, H-3), 6.81-6.44 (m, 4H, H12, H-13), 6.43 (br.s, 2H, Ar-NH<sub>2</sub>), 4.34-4.23 (m, 1H, H-6a),

3.72-3.58 (m, 1H, H-10a), 3.56-3.46j (m, 1H, H-8), 3.15 (t,  $^2J = 11.2$  Hz, 1H, H-10b), 3.05 (t,  $^2J = 11.0$  Hz, 1H, H6b), 2.70 (br.s, 6H, H-15), 2.05-1.94 (m, 1H, H-7a), 1.90-1.79 (m, 1H, H-9a), 1.41-1.25 (m, 2H, H-7b, H-9b).

**(3-aminopyrazin-2-yl)(4-((4-tert-butyl)phenyl)amino)piperidin-1-yl)methanone (62)**

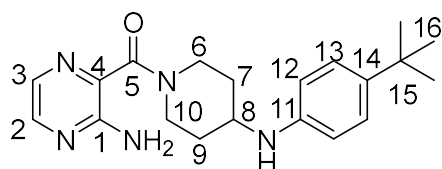


According to **standard procedure 3**, 1-(3-aminopyrazine-2-carbonyl)piperidin-4-one ((**18**), 23.7 mg, 0.108 mmol, 1.0 eq) and 4-(tert-butyl)aniline ((**102**), 17.5 L, 0.11 mmol, 1.02 eq), dry. DCM (5.0 mL, [0.02M]), acetic acid (6  $\mu$ L, 0.11 mmol, 1.1 eq) and BH(OAc)<sub>3</sub> (31.8 mg, 1.5 mmol, 1.5 eq) were used to gain a yellow oil after workup.

The crude oil was solved in MeCN/H<sub>2</sub>O/DMSO (1:1:1, 2 mL) and purified via prep. HPLC in one run (10-100% MeCN in 60 min) to obtain 9.59 mg (0.027 mmol, 27%) of the product as an off-white solid.

**LC-MS:** Column: Phenomenex Luna C18(2), gradient: MeCN/H<sub>2</sub>O + 0.05 % HCOOH, 5 % MeCN increase to 100% MeCN in 5.1 min, flow rate: 0.6 mL/min,  $t_R = 2.87$ ,  $m/z = 354.3$  ([M+H]<sup>+</sup>).

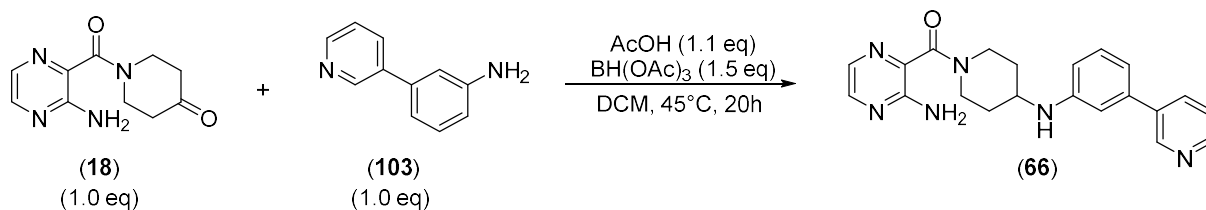
**HRMS:**  $m/z$  ([M+H]<sup>+</sup>), calculated: 357.2294, found: 354.2277



**<sup>1</sup>H-NMR** (500 MHz, dms<sub>o</sub>-d<sub>6</sub>,  $\delta$  in ppm): 8.03 (d,  $^3J_{2,3} = 2.6$  Hz, 1H, H-2), 7.76 (d,  $^3J_{3,2} = 2.6$  Hz, 1H, H-3), 7.09 (d,  $^3J_{13,12} = 8.6$  Hz, 1H, H-13), 6.54 (d,  $^3J_{12,13} = 8.6$  Hz, 1H, H-12), 6.44 (br.s, 2H, Ar-NH<sub>2</sub>), 5.31 (d,  $J = 7.2$  Hz, 1H, NH), 4.34 (d,  $^2J = 13.1$  Hz, 1H, H-6a), 3.64 (d,  $^2J = 13.5$  Hz, 1H, H-10a), 3.55-3.44 (m, 1H, H-8), 3.18 (t,  $^2J = 11.1$  Hz, 1H, H-10b), 3.08 (t,  $^2J = 11.0$  Hz, 1H, H6b), 2.01 (d,  $^2J = 10.5$  Hz, 1H, H-7a), 1.87 (d,  $^2J = 10.8$  Hz, 1H, H-9a), 1.45-1.30 (m, 2H, H-7b, H-9b), 1.21 (s, 9H, H-16).

**<sup>13</sup>C-NMR** (126 MHz, dms<sub>o</sub>-d<sub>6</sub>,  $\delta$  in ppm): 164.95 (C-5), 153.25 (C-1), 145.26 (C-11), 143.29 (C-2), 137.79 (C-14), 133.48 (C-4), 130.65 (C-3), 125.51 (C-13), 112.30 (C-12), 48.70 (C-8), 45.10 (C-10), 40.24 (C-6), 32.30 (C-7), 31.48 (C-16), 31.33 (C-9).

**(3-aminopyrazin-2-yl)(4-((3-(pyridine-3-yl)phenyl)amino)piperidin-1-yl)methanone (66)**

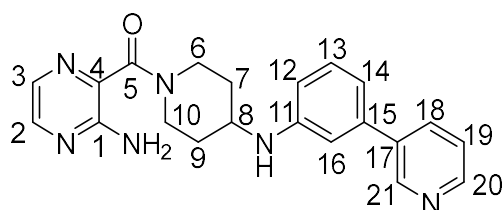


According to **standard procedure 3**, 1-(3-aminopyrazine-2-carbonyl)piperidin-4-one ((**18**), 22.4 mg, 0.10 mmol, 1.0 eq) and 3-(pyridine-3-yl)aniline ((**103**), 18.7 mg, 0.11 mmol, 1.1 eq), dry. DCM (5.0 mL, [0.02M]), acetic acid (6  $\mu$ L, 0.11 mmol, 1.1 eq) and BH(OAc)<sub>3</sub> (31.8 mg, 1.5 mmol, 1.5 eq) were used to gain a yellow oil after workup.

The crude oil was solved in MeCN/H<sub>2</sub>O/DMSO (1:1:1, 2 mL) and purified via prep. HPLC in one run (5-50% MeCN in 30 min) to obtain 4.09 mg (0.011 mmol, 11%) of the product as an off-white solid.

**LC-MS:** Column: Phenomenex Luna C18(2), gradient: MeCN/H<sub>2</sub>O + 0.05 % HCOOH, 5 % MeCN increase to 100% MeCN in 5.1 min, flow rate: 0.6 mL/min, t<sub>R</sub> = 1.97, m/z = 375.3 ([M+H]<sup>+</sup>).

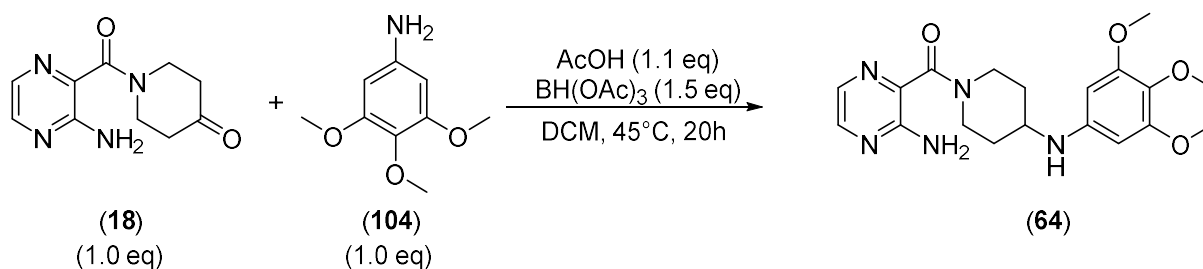
**HRMS:** m/z ([M+H]<sup>+</sup>), calculated: 375.1933, found: 375.1920



**<sup>1</sup>H-NMR** (500 MHz, dms<sup>o</sup>-d<sub>6</sub>,  $\delta$  in ppm): 8.81 (s, 1H, H-21), 8.54 (s, 1H, H-20), 8.02 (d, <sup>3</sup>J<sub>2,3</sub> = 2.5 Hz, 1H, H-2), 7.97 (d, <sup>3</sup>J<sub>18,19</sub> = 7.9 Hz, 1H, H-18), 7.76 (d, <sup>3</sup>J<sub>3,2</sub> = 2.6 Hz, 1H, H-3), 7.45 (dd, J = 7.8 = 4.8 Hz, 1H, H-19), 7.19 (t, <sup>3</sup>J<sub>13,12</sub> = <sup>3</sup>J<sub>13,12</sub> = 7.8 Hz, 1H, H-13), 6.89 (s, 1H, H-16), 6.82 (d, <sup>3</sup>J = 7.6 Hz, 1H, H-12 or H-14), 6.67 (dd, <sup>3</sup>J = 8.1 Hz, <sup>4</sup>J = 1.8 Hz, 1H, H-12 or H-14), 6.45 (br.s, 2H, Ar-NH<sub>2</sub>), 5.31 (d, J = 8.2 Hz, 1H, NH), 4.37 (d, <sup>2</sup>J = 13.1 Hz, 1H, H-6a), 3.72-3.60 (m, 2H, H-10a, H-8), 3.21 (t, <sup>2</sup>J = 11.2 Hz, 1H, H-10b), 3.10 (t, <sup>2</sup>J = 11.0 Hz, 1H, H-6b), 2.06 (d, <sup>2</sup>J = 11.0 Hz, 1H, H-7a), 1.92 (d, <sup>2</sup>J = 11.6 Hz, 1H, H-9a), 1.49-1.33 (m, 2H, H-7b, H-9b).

**<sup>13</sup>C-NMR** (126 MHz, dms<sup>o</sup>-d<sub>6</sub>,  $\delta$  in ppm): 164.96 (C-5), 153.26 (C-1), 148.32 (C-11 or C-20 or C-21), 148.21 (C-11 or C-20 or C-21), 147.59 (C-11 or C-20 or C-21), 143.31 (C-2), 138.00 (C-15), 136.52 (C-17), 134.00 (C-18), 133.47 (C-4), 130.65 (C-3), 129.76 (C-13), 123.77 (C-19), 114.31 (C-14), 112.50 (C-12), 110.50 (C-16), 48.39 (C-8), 45.16 (C-10), 40.28 (C-6), 32.25 (C-7), 31.31 (C-9).

**(3-aminopyrazin-2-yl)(4-((3,4,5-trimethoxyphenyl)amino)piperidin-1-yl)methanone (64)**

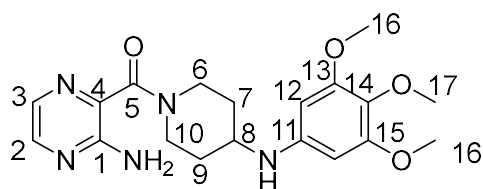


According to **standard procedure 3**, 1-(3-aminopyrazine-2-carbonyl)piperidin-4-one ((**18**), 22.5 mg, 0.10 mmol, 1.0 eq) and 3,4,5- trimethoxyaniline ((**104**), 21.9 mg L, 0.12 mmol, 1.2 eq), dry. DCM (5.0 mL, [0.02M]), acetic acid (6  $\mu$ L, 0.11 mmol, 1.1 eq) and BH(OAc)<sub>3</sub> (31.6 mg, 1.5 mmol, 1.5 eq) were used to gain a yellow oil after workup.

The crude oil was solved in MeCN/H<sub>2</sub>O/DMSO (1:1:1, 2 mL) and purified via prep. HPLC in one run (10-100% MeCN in 60 min) to obtain 10.85 mg (0.028 mmol, 28%) of the product as an off-white solid.

**LC-MS:** Column: Phenomenex Luna C18(2), gradient: MeCN/H<sub>2</sub>O + 0.05 % HCOOH, 5 % MeCN increase to 100% MeCN in 5.1 min, flow rate: 0.6 mL/min, t<sub>R</sub> = 2.11, m/z = 388.2([M+H]<sup>+</sup>).

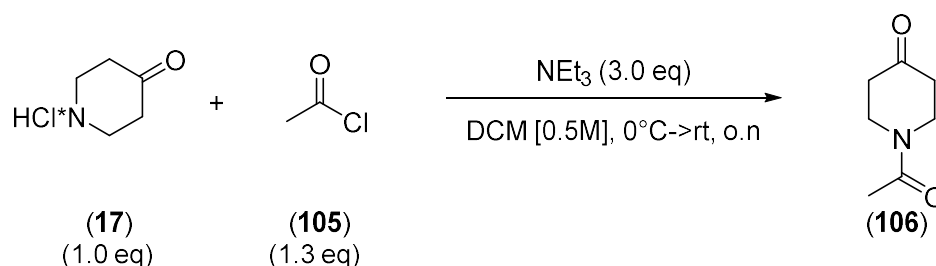
**HRMS:** m/z ([M+H]<sup>+</sup>), calculated: 388.1985, found: 388.1967



**<sup>1</sup>H-NMR** (500 MHz, dms<sub>o</sub>-d<sub>6</sub>,  $\delta$  in ppm): 8.03 (d, <sup>3</sup>J<sub>2,3</sub> = 2.6 Hz, 1H, H-2), 7.77 (d, <sup>3</sup>J<sub>3,2</sub> = 2.6 Hz, 1H, H-3), 6.45 (br.s, 2H, Ar-NH<sub>2</sub>), 5.90 (s, 2H, H-12), 5.35 (d, J = 8.3 Hz, 1H, NH), 4.32 (d, <sup>2</sup>J = 13.1 Hz, 1H, H-6a), 3.70 (s, 6H, H-16), 3.64 (d, <sup>2</sup>J = 13.6z Hz, 1H, H-10a), 3.57-3.47 (m, 4H, H-8, H-17), 3.20 (t, <sup>2</sup>J = 11.2 Hz, 1H, H-10b), 3.11 (t, <sup>2</sup>J = 11.0 Hz, 1H, H6b), 2.01 (d, <sup>2</sup>J = 10.5 Hz, 1H, H-7a), 1.87 (d, <sup>2</sup>J = 10.7 Hz, 1H, H-9a), 1.44-1.29 (m, 2H, H-7b, H-9b).

**<sup>13</sup>C-NMR** (126 MHz, dms<sub>o</sub>-d<sub>6</sub>,  $\delta$  in ppm): 165.41 (C-5), 153.96 (C15 or C-1), 153.73 (C-15 or C-1), 144.82 (C-13), 143.77 (C-2), 133.91 (C-4), 131.11 (C-3), 128.96 (C-14), 90.85 (C-12), 60.62 (C-17), 56.02 (C-16), 49.16 (C-8), 45.33 (C-10), 40.66 (C-6), 32.81 (C-7), 31.87 (C-9).

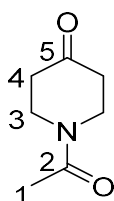
**1-acetylpiperidin-4-one (106)**



Piperidin-4-one (**17**), 676.5 mg, 5.0 mmol, 1.0 eq) was suspended in dry. DCM (10 mL, [0.5M]) in a 50 mL single neck flask and cooled to 0°C. Then NEt<sub>3</sub> (2.1 mL, 15.0 mmol, 3.0 eq) and Acetylchloride (**105**), 0.46 mL, 6.5 mmol, 1.3 eq) were added at 0°C. The reaction mixture was stirred for 2h at rt.

As TLC confirmed full conversion after 2h, a 2% aq. Na<sub>2</sub>CO<sub>3</sub>-solution was added to stop the reaction. Then the phases were separated, the aqueous phase was dried over Na<sub>2</sub>SO<sub>4</sub> and the solvents were removed under reduced pressure to obtain 563.6 mg of a yellow oil

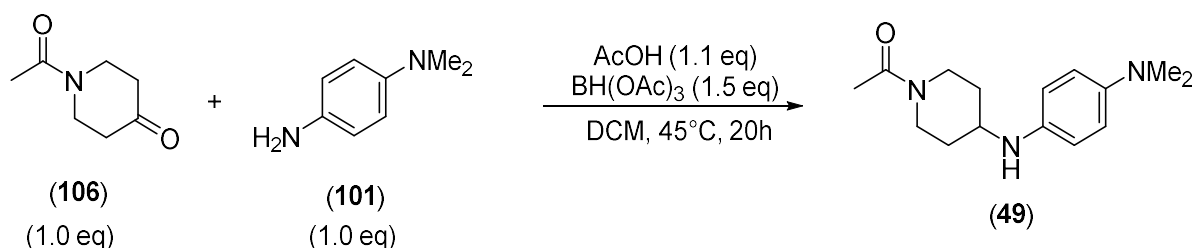
The crude oil was solved in CH<sub>2</sub>Cl<sub>2</sub>, absorbed on Isolute and purified via combi flash (24g silica column, 0-100% EtOAc in Petroleum benzene in 20 min, hold at 70% EtOAc for 5 min) to get 325.8 mg (2.31 mmol, 46%) of the desired product as a pale yellow oil.



<sup>1</sup>H-NMR (500 MHz, CDCl<sub>3</sub>, δ in ppm): 3.97-3.68 (m, 4H, H-3), 2.55-2.42 (m, 4H, H-4), 2.19 (s, 3H, H-1).

<sup>13</sup>C-NMR (126 MHz, CDCl<sub>3</sub>, δ in ppm): 206.77 (C-5), 169.47 (C-2), 45.05 (C-3), 41.30/40.92 (C-4), 21.48 (C-1).

#### 1-(4-((4-(dimethylamino)phenyl)amino)piperidin-1-yl)ethan-1-one (**49**)



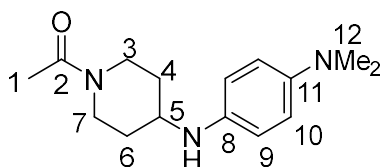
According to **standard procedure 3**, 1-acetylpiperidin-4-one (**106**), 70.8 mg, 0.5 mmol, 1.0 eq) and N<sup>1</sup>,N<sup>1</sup>-dimethylbenzene-1,4-diamine (**101**), 68.1 mg, 0.5 mmol, 1.0 eq), dry. DCM (5.0 mL, [0.1M]), acetic acid (30 μL, 0.55 mmol, 1.1 eq) and BH(OAc)<sub>3</sub> (161.7 mg, 0.75 mmol, 1.5 eq) were used to gain 117.8 mg of a dark oil after workup.

The crude oil was solved in MeCN/H<sub>2</sub>O (1:1, 2 mL) and purified via prep. HPLC in three runs (1% MeCN in H<sub>2</sub>O for 3 min, then 1-40% MeCN in 20 min) to obtain 9.80 mg (0.037 mmol, 8%) of the product as a yellow solid.

**LC-MS**: Column: Phenomenex Luna C18(2), gradient: MeCN/H<sub>2</sub>O + 0.05 % HCOOH, 5 % MeCN increase to 100% MeCN in 5.1 min, flow rate: 0.6 mL/min, t<sub>R</sub>= 1.59, m/z = 262.3 ([M+H]<sup>+</sup>).

**HRMS**: m/z ([M+H]<sup>+</sup>), calculated: 262.1919, found: 262.1907

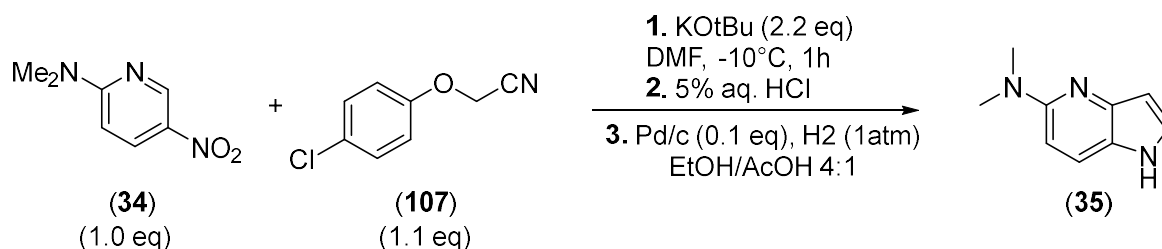




**<sup>1</sup>H-NMR** (500 MHz, CDCl<sub>3</sub>, δ in ppm): 7.29-5.64 (m, 4H, H-9, H-10), 4.32-4.09 (m, 1H, H-3a), 3.89-3.66 (m, 1H, H-7a), 3.14 (t, <sup>2</sup>J=11.2 Hz, 1H, H-7b), 2.77 (t, <sup>2</sup>J = 11.0 Hz, 1H, H-3b), 2.00 (s, 3H, H-1), 1.97-1.77 (m, 2H, H-4a, H-6a), 1.38-1.04 (m, 2H, H-4b, H-6b).

**<sup>13</sup>C-NMR** (126 MHz, CDCl<sub>3</sub>, δ in ppm): 168.37 (C-2), 140.30 (C-11), 139.90 (C-8), 115.89 (C-9), 114.66 (C-10), 55.38 (C-5), 45.04 (C-7), 41.00 (C-3), 31.69 (C-4), 31.56 (C-6), 21.17 (C-1).

### *N,N*-dimethyl-1H-pyrrolo[3,2-*b*]pyridin-5-amine (**35**)



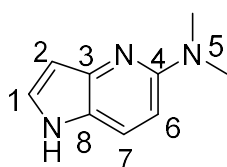
KOtBu (3773 mg, 33.6 mmol, 2.24 eq) was placed in a 100 mL 3-neck flask under N<sub>2</sub> and solved in dry. DMF (40 mL). Then *N,N*-dimethyl-5-nitropyridin-2-amine (**34**), 2504 mg, 15 mmol, 1.0 eq and 2-(4-chlorophenoxy)acetonitrile (**107**), 2781 mg, 16.6 mmol, 1.11 eq were solved in dry. DMF (20 mL) and added dropwise to the KOtBu solution at -10°C (dry. Ice/isopropanol bath) and stirred for 70 min at -10°C.

Subsequently the solution was heated to 0°C (ice bath) and a 5% aq.HCl-solution (26 mL) was added. The precipitated solid was filtered off and washed with cold water to gain 1194.7 mg (5.79 mmol, 39%) of 2-(6-(dimethylamino)-3-nitropyridin-2-yl)acetonitrile as a yellow solid.

2-(6-(dimethylamino)-3-nitropyridin-2-yl)acetonitrile (1094 mg, 5.31 mmol, 1.0 eq) was placed in 100 mL single neck flask with a septum and solved in EtOH (20 mL) and AcOH (5.0 mL) and degased by Ar bubbling (10 min). Then an 1 atm H<sub>2</sub> atmosphere (balloon) was applied and the solution was stirred for 6 h.

The mixture was diluted with EtOH, filtered over a thick pad of Celite and washed with EtOH. After evaporatrion of the solvent 1663.7 mg of a brown oil was achieved.

The crude oil was solved in MeCN/H<sub>2</sub>O/DMSO (1:1:1) and purified via prep.HPLC (1-30% MeCN in H<sub>2</sub>O) in 12 runs to obtain 147.3 mg (0.91 mmol, 18%) of a brown oil/solid as the product.

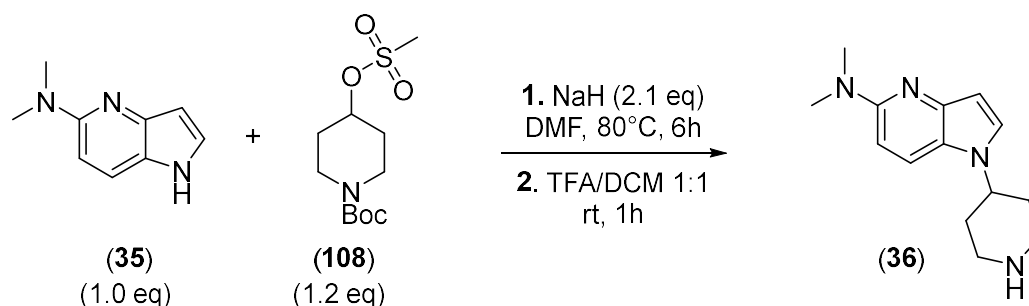


**LC-MS:** Column: Phenomenex Luna C18(2), gradient: MeCN/H<sub>2</sub>O + 0.05 % HCOOH, 5 % MeCN increase to 100% MeCN in 5.1 min, flow rate: 0.6 mL/min,  $t_R = 1.40$ ,  $m/z = 162.2$  ( $[M+H]^+$ ).

**<sup>1</sup>H-NMR** (500 MHz, dms<sub>o</sub>-d<sub>6</sub>,  $\delta$  in ppm): 10.86 (br.s, 1H, NH), 7.58 (d,  $^3J_{7,6} = 8.8$  Hz, 1H, H-7), 7.35 (s, 1H, H-1), 6.55 (d,  $^3J_{6,7} = 8.8$  Hz, 1H, H-6), 6.26 (s, 1H, H-2), 3.00 (s, 6H, H-5).

**<sup>13</sup>C-NMR** (126 MHz, dms<sub>o</sub>-d<sub>6</sub>,  $\delta$  in ppm): 155.35 (C-4), 143.54 (C-3), 127.14 (C-1), 122.28 (C-8), 121.00 (C-7), 101.88 (c-6), 100.12 (C-2), 38.87 (C-5).

***N,N*-dimethyl-1-(piperidin-4-yl)-1*H*-pyrrolo[3,2-*b*]pyridin-5-amine (36)**



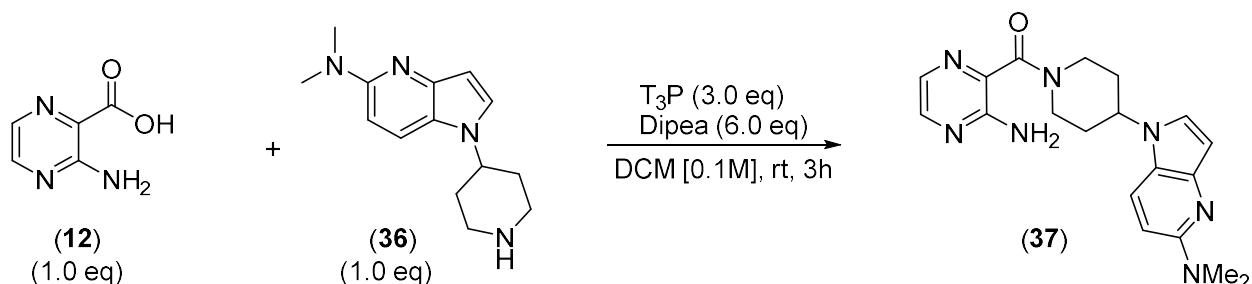
*N,N*-dimethyl-1*H*-pyrrolo[3,2-*b*]pyridin-5-amine (**(35)**, 97.3 mg, 0.60 mmol, 1.0 eq), was placed in a 25 mL 2-neck flask under N<sub>2</sub> and solved in dry. DMF (3.0 mL, [0.2M]). The solution was cooled to 0°C and NaH (60% in mineral oil, 50.7 mg, 1.26 mmol, 1.1 eq) was added to the mixture which was stirred for 10 min at rt. Subsequently *tert*-butyl-4-((methylsulfonyl)oxy)piperidine-1-carboxylate (**(108)**, 202 mg, 0.72 mmol, 1.2 eq) was added to mixture, which was heated to 80°C and stirred for 5h until full conversion by LC-MS was observed.

The reaction mixture was diluted with Et<sub>2</sub>O and washed with water (3x) and brine and dried over Na<sub>2</sub>SO<sub>4</sub>. After evaporation of the solvent 176.1 mg of a yellow solid was obtained. The crude was solved in DCM, absorbed on SiO<sub>2</sub> and purified via combi flash (0-100% EtOAc+1%TEA in Cylohexane, elution at 50%) to obtain 49.6 mg of the Boc-protected amine.

The Boc protected product was solved in DCM/TFA (1:1, 10 mL) and stirred for 1h at rt, after which the solvents were removed under reduced pressure. The crude was solved in MeCN/H<sub>2</sub>O and lyophilized over night to obtain 70.0 mg (0.195 mmol, 33%) of the desired product as the TFA salt.

**LC-MS:** Column: Phenomenex Luna C18(2), gradient: MeCN/H<sub>2</sub>O + 0.05 % HCOOH, 5 % MeCN increase to 100% MeCN in 5.1 min, flow rate: 0.6 mL/min,  $t_R = 0.89$ ,  $m/z = 245.3$  ( $[M+H]^+$ ).

**(3-aminopyrazin-2-yl)(4-(5-(dimethylamino)-1*H*-pyrrolo[3,2-*b*]pyridin-1-yl)piperidin-1-yl)methanone (37)**

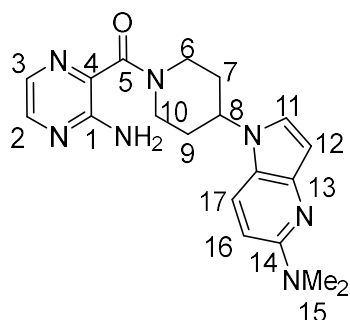


According to **standard procedure 1**, 3-aminopyrazine-2-carboxylic acid ((**12**), 28.1 mg, 0.2 mmol, 1.0 eq), *N,N*-dimethyl-1-(piperidin-4-yl)-1*H*-pyrrolo[3,2-*b*]pyridin-5-amine ((**36**), 53.1 mg, 0.2 mmol, 1.0 eq), dry. DCM (5 mL, [0.4M]), Dipea (0.21 mL, 6.0 eq) and T<sub>3</sub>P (50% in EtOAc, 0.38 mL, 3.0 eq) were used to gain 64.6 mg (90% pure) of a brown oil after workup.

The crude oil was solved in MeCN/H<sub>2</sub>O/DMSO (1:1:1, 3 mL) and purified via prep. HPLC in three runs (5-50% MeCN in 60 min) to obtain 10.55 mg (0.028 mmol, 28%) of the product as an off-white solid.

**LC-MS:** Column: Phenomenex Luna C18(2), gradient: MeCN/H<sub>2</sub>O + 0.05 % HCOOH, 5 % MeCN increase to 100% MeCN in 5.1 min, flow rate: 0.6 mL/min, t<sub>R</sub> = 1.81, m/z = 366.2 ([M+H]<sup>+</sup>).

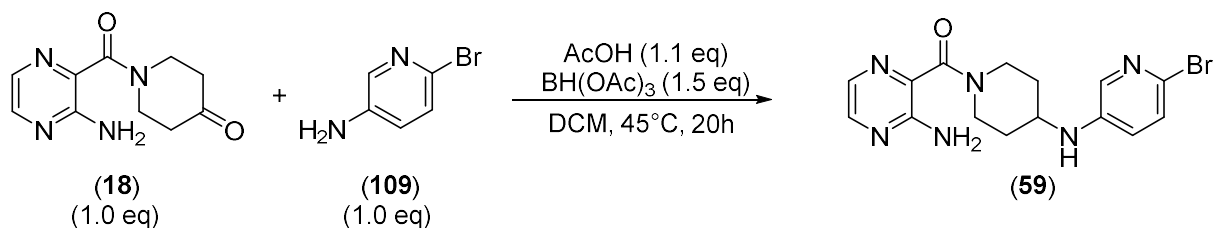
**HRMS:** m/z ([M+H]<sup>+</sup>), calculated: 366.2042, found: 366.2030



**<sup>1</sup>H-NMR** (500 MHz, dms<sub>o</sub>-d<sub>6</sub>, δ in ppm): 8.03 (d, <sup>3</sup>J<sub>2,3</sub> = 2.5 Hz, 1H, H-2), 7.81 (d, <sup>3</sup>J<sub>17,16</sub> = 9.1 Hz, 1H, H-17), 7.77 (d, <sup>3</sup>J<sub>3,2</sub> = 2.5 Hz, 1H, H-3), 7.50 (d, <sup>3</sup>J<sub>11,12</sub> = 9.1 Hz, 1H, H-11), 6.59 (d, <sup>3</sup>J<sub>16,17</sub> = 9.1 Hz, 1H, H-16), 6.53 (s, 2H, NH<sub>2</sub>), 6.26 (d, <sup>3</sup>J<sub>12,11</sub> = 3.1 Hz, 1H, H-12), 4.68 (d, <sup>2</sup>J = 12.8 Hz, 1H, H-6a), 4.64-4.53 (m, 1H, H-8), 3.78 (d, <sup>2</sup>J = 13.3 Hz, 1H, H-10a), 3.28 (t, <sup>2</sup>J = 11.0 Hz, 1H, H-10b), 3.04-2.95 (m, 7H, H-15, H6b), 2.10-2.00 (m, 2H, H-7a, H-9a), 1.95-1.81 (m, 2H, H-7b, H-9b).

**<sup>13</sup>C-NMR** (126 MHz, dms<sub>o</sub>-d<sub>6</sub>, δ in ppm): 165.11(C-5), 155.65 (C-14), 153.20 (C-1), 143.83 (C-13), 143.40 (C-2), 133.39 (C-12), 130.67 (C-3), 126.68 (C-11), 122.28 (C-18), 119.62 (C-17), 101.66 (C-16), 100.14 (C-12), 52.58(C-8), 45.67 (C-10), 40.82 (C-6), 38.83 (C-15), 32.80 (C-7), 31.48 (C-9).

**(3-aminopyrazin-2-yl)(4-((6-(bromo)pyridin-3-yl)amino)piperidin-1-yl)methanone (59)**

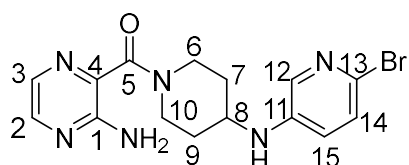


According to **standard procedure 3**, 1-(3-aminopyrazine-2-carbonyl)piperidin-4-one (**(18)**, 2490 mg, 11.35 mmol, 1.0 eq) and 2-Bromo-5-Amino-pyridine (**(109)**, 2140 mg, 12.49 mmol, 1.1 eq), dry. DCM (100.0 mL, [0.1M]), acetic acid (675  $\mu$ L, 12.5 mmol, 1.1 eq) and BH(OAc)<sub>3</sub> (3550 mg, 17.03 mmol, 1.50 eq) were used to gain a brown solid after workup.

The crude was solved in MeCN/H<sub>2</sub>O/DMSO (1:1:1, 2 mL) and purified via flash. prep. HPLC in 5 runs (10-100% MeCN in 60 min) to obtain 1734.3 mg (4.60 mmol, 46%) of the product as a beige solid.

**LC-MS:** Column: Phenomenex Luna C18(2), gradient: MeCN/H<sub>2</sub>O + 0.05 % HCOOH, 5 % MeCN increase to 100% MeCN in 5.1 min, flow rate: 0.6 mL/min,  $t_R$  = 2.53,  $m/z$  = 377.1, 379.2 ([M+H]<sup>+</sup>).

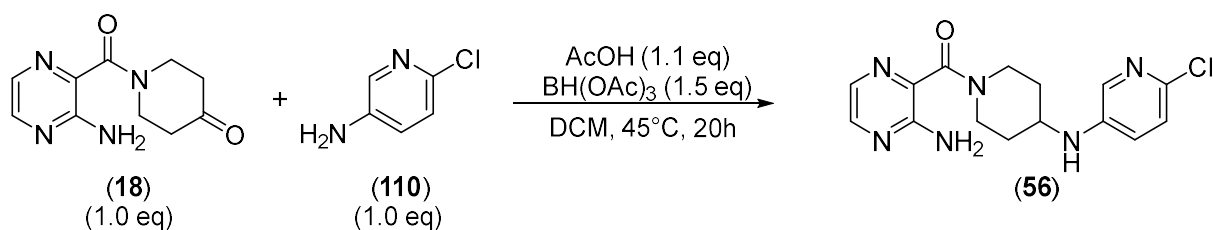
**HRMS:**  $m/z$  ([M+H]<sup>+</sup>), calculated: 377.0727, 379.0705, found: 377.013, 379.0691



**<sup>1</sup>H-NMR** (500 MHz, dms<sub>o</sub>-d<sub>6</sub>,  $\delta$  in ppm): 8.02 (d, <sup>3</sup>J<sub>2,3</sub> = 2.5 Hz, 1H, H-2), 7.77 (d, <sup>4</sup>J<sub>12,15</sub> = 3.0 Hz, 1H, H-12), 7.75 (d, <sup>3</sup>J<sub>3,2</sub> = 2.5 Hz, 1H, H-3), 7.25 (d, <sup>3</sup>J<sub>14,15</sub> = 8.6 Hz, 1H, H-14), 6.97 (dd, <sup>3</sup>J<sub>15,14</sub> = 8.7 Hz, <sup>4</sup>J<sub>15,12</sub> = 3.0 Hz, 1H, H-15), 6.45 (br.s, 2H, Ar-NH<sub>2</sub>), 6.06 (d, <sup>3</sup>J<sub>NH,8</sub> = 8.0 Hz, 1H, NH), 4.35 (d, <sup>2</sup>J = 13.2 Hz, 1H, H-6a), 3.63 (d, <sup>2</sup>J = 13.5 Hz, 1H, H-10a), 3.58-3.48 (m, 1H, H-8), 3.18 (t, <sup>2</sup>J = 11.3 Hz, 1H, H-10b), 3.05 (t, <sup>2</sup>J = 10.9 Hz, 1H, H6b), 2.00 (d, <sup>2</sup>J = 10.9 Hz, 1H, H-7a), 1.87 (d, <sup>2</sup>J = 11.2 Hz, 1H, H-9a), 1.46-1.29 (m, 2H, H-7b, H-9b).

**<sup>13</sup>C-NMR** (126 MHz, dms<sub>o</sub>-d<sub>6</sub>,  $\delta$  in ppm): 164.99 (C-5), 153.25 (C-1), 143.68 (C-13), 143.34 (C-2), 134.97 (C-11), 133.40 (C-12), 130.66 (C-3), 127.49 (C-4), 125.56 (C-14), 122.22 (C-15), 48.32(C-8), 44.99(C-10), 40.12 (C-6), 31.83(C-7), 30.88 (C-9).

**(3-aminopyrazin-2-yl)(4-((6-(Chloro)pyridin-3-yl)amino)piperidin-1-yl)methanone (56)**

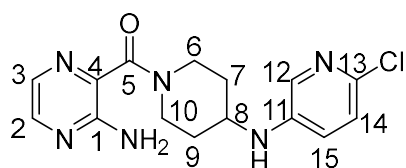


According to **standard procedure 3**, 1-(3-aminopyrazine-2-carbonyl)piperidin-4-one ((**18**), 44.2 mg, 0.2 mmol, 1.0 eq) and 2-Chloro-5-Amino-pyridine ((**110**), 25.8 mg, 0.2 mmol, 1.0 eq), dry. DCM (2.0 mL, [0.1M]), acetic acid (13  $\mu$ L, 0.22 mmol, 1.1 eq) and BH(OAc)<sub>3</sub> (65.5 mg, 0.3 mmol, 1.50 eq) were used to gain 54.1 mg a brown solid after workup.

The crude was solved in MeCN/H<sub>2</sub>O/DMSO (1:1:1, 2 mL) and purified via prep. HPLC in 2 runs (10-100% MeCN in 60 min) to obtain 5.92 mg (0.018 mmol, 9%) of the product as a beige solid.

**LC-MS:** Column: Phenomenex Luna C18(2), gradient: MeCN/H<sub>2</sub>O + 0.05 % HCOOH, 5 % MeCN increase to 100% MeCN in 5.1 min, flow rate: 0.6 mL/min, t<sub>R</sub> = 2.45, m/z = 333.2, 335.2([M+H]<sup>+</sup>).

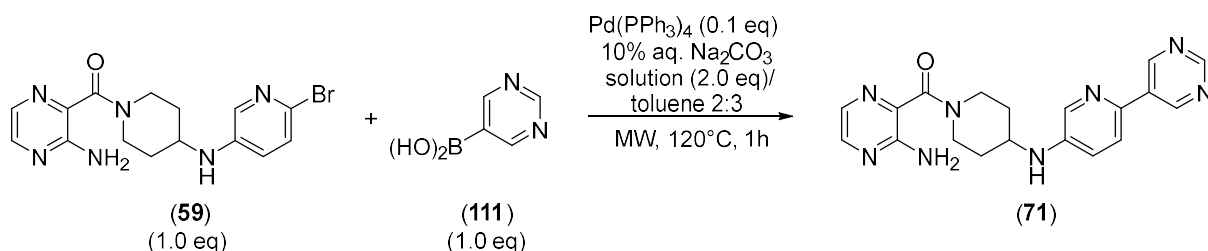
**HRMS:** m/z ([M+H]<sup>+</sup>), calculated: 333.1231, found: 333.1219



**<sup>1</sup>H-NMR** (500 MHz, dms<sub>o</sub>-d<sub>6</sub>,  $\delta$  in ppm): 8.02 (d, <sup>3</sup>J<sub>2,3</sub> = 2.6 Hz, 1H, H-2), 7.76 (d, <sup>4</sup>J<sub>12,15</sub> = 3.1 Hz, 1H, H-12), 7.75 (d, <sup>3</sup>J<sub>3,2</sub> = 2.6 Hz, 1H, H-3), 7.14 (d, <sup>3</sup>J<sub>14,15</sub> = 8.7 Hz, 1H, H-14), 7.05 (dd, <sup>3</sup>J<sub>15,14</sub> = 8.7 Hz, <sup>4</sup>J<sub>15,12</sub> = 3.0 Hz, 1H, H-15), 6.45 (br.s, 2H, Ar-NH<sub>2</sub>), 6.04 (d, <sup>3</sup>J<sub>NH,8</sub> = 8.0 Hz, 1H, NH), 4.35 (d, <sup>2</sup>J = 13.1 Hz, 1H, H-6a), 3.63 (d, <sup>2</sup>J = 13.5 Hz, 1H, H-10a), 3.59-3.50 (m, 1H, H-8), 3.18 (t, <sup>2</sup>J = 11.2 Hz, 1H, H-10b), 3.06 (t, <sup>2</sup>J = 11.0 Hz, 1H, H-6b), 2.00 (d, <sup>2</sup>J = 11.3 Hz, 1H, H-7a), 1.87 (d, <sup>2</sup>J = 11.3 Hz, 1H, H-9a), 1.45-1.30 (m, 2H, H-7b, H-9b).

**<sup>13</sup>C-NMR** (126 MHz, dms<sub>o</sub>-d<sub>6</sub>,  $\delta$  in ppm): 165.01 (C-5), 153.26 (C-1), 143.36 (C-2), 135.96 (C-11), 134.13 (C-12), 133.42 (C-13), 130.69 (C-3), 123.93 (C-14), 122.23 (C-15), 48.32 (C-8), 44.99 (C-10), 40.12 (C-6), 31.83 (C-7), 30.88 (C-9).

**(3-aminopyrazin-2-yl)(4-((6-(pyrimidin-5-yl)pyridin-3-yl)amino)piperidin-1-yl)methanone(**71**)**



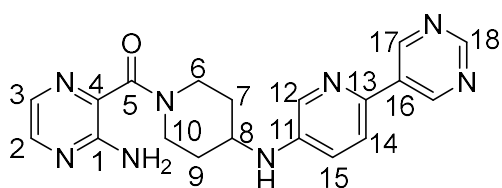
(3-aminopyrazin-2-yl)(4-((6-(bromo)pyridin-3-yl)amino)piperidin-1-yl)methanone ((**59**), 22.6 mg, 0.06 mmol, 1.0eq), Pyrimidine-5-boronic acid ((**111**), 7.4 mg, 0.06 mmol, 1.0 eq), 10% aq. Na<sub>2</sub>CO<sub>3</sub> solution (12.7 mg in 1mL H<sub>2</sub>O, 0.12 mmol, 2.0 eq) and Toluene (1.5 mL) were placed in a small microwave vial. The solvents were degased by Ar bubbling (10 min), then Pd(PPh<sub>3</sub>)<sub>4</sub> (6.9 mg, 0.006 mmol, 0.1 eq) was added, the vial was sealed, purged with argon and heated to 120°C for 1 h in the microwave.

Solvents were removed, diluted with DCM and extracted with aq. HCl-solution [0.5M]. The organic phase was discarded, the aq. Phase was basified by the addition of 2M aq. NaOH solution, extracted with EtOAc (3x) and dried over Na<sub>2</sub>SO<sub>4</sub> to obtain the crude as a brown oil.

The crude oil was solved in MeCN/H<sub>2</sub>O/DMSO (1:1:1, 3 mL) and purified via prep. HPLC in two runs (5-50% MeCN in 60 min) to obtain 3.45 mg (0.009 mmol, 15%) of the product as an off-white solid.

**LC-MS:** Column: Phenomenex Luna C18(2), gradient: MeCN/H<sub>2</sub>O + 0.05 % HCOOH, 5 % MeCN increase to 100% MeCN in 5.1 min, flow rate: 0.6 mL/min, t<sub>R</sub> = 1.96, m/z = 377.2 ([M+H]<sup>+</sup>).

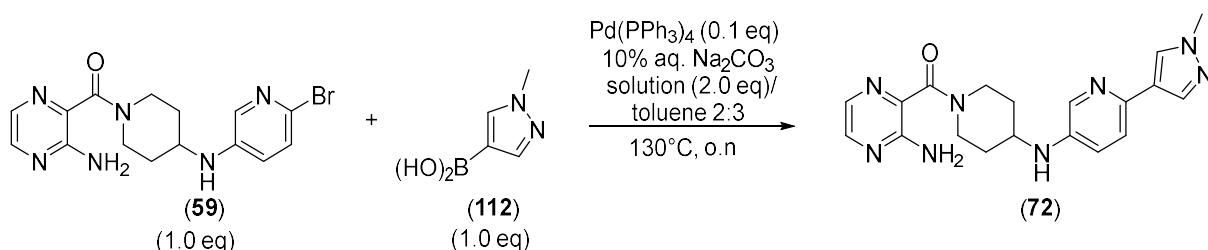
**HRMS:** m/z ([M+H]<sup>+</sup>), calculated: 366.1838, found: 377.1820



**<sup>1</sup>H-NMR** (500 MHz, dms<sub>o</sub>-d<sub>6</sub>, δ in ppm): 9.29 (s, 2H, H-17), 9.08 (s, 1H, H-18), 8.16 (d, <sup>4</sup>J<sub>12,15</sub> = 2.7 Hz, 1H, H-12), 8.03 (d, <sup>3</sup>J<sub>2,3</sub> = 2.5 Hz, 1H, H-2), 7.86 (d, <sup>3</sup>J<sub>14,15</sub> = 8.7 Hz, 1H, H-14), 7.76 (d, <sup>3</sup>J<sub>3,2</sub> = 2.5 Hz, 1H, H-3), 7.11 (dd, <sup>3</sup>J<sub>15,14</sub> = 8.7 Hz, <sup>4</sup>J<sub>15,12</sub> = 2.7 Hz, 1H, H-15), 6.46 (br.s, 2H, Ar-NH<sub>2</sub>), 6.31 (d, <sup>3</sup>J<sub>N,8</sub> = 8.0 Hz, 1H, NH), 4.38 (d, <sup>2</sup>J = 13.2 Hz, 1H, H-6a), 3.74-3.59 (m, 2H, H10<sub>a</sub>, H-8), 3.22 (t, <sup>2</sup>J = 11.3 Hz, 1H, H-10<sub>b</sub>), 3.10 (t, <sup>2</sup>J = 11.0 Hz, 1H, H6<sub>b</sub>), 2.05 (d, <sup>2</sup>J = 11.3 Hz, 1H, H-7a), 1.92 (d, <sup>2</sup>J = 11.1 Hz, 1H, H-9a), 1.49-1.35 (m, 2H, H-7b, H-9b).

**<sup>13</sup>C-NMR** (126 MHz, dms<sub>o</sub>-d<sub>6</sub>, δ in ppm): 165.01 (C-5), 156.59 (C-18), 153.25 (C-1), 153.10 (C-17), 144.07 (C-11), 143.37 (C-2), 137.77 (C-12), 136.00 (C-16), 133.44 (C-4), 132.20 (C-3), 130.67 (C-15), 121.21 (C-13), 118.28 (C-14), 48.20 (C-8), 45.02 (C-10), 40.16 (C-6), 31.93 (C-7), 31.00 (C-9).

**(3-aminopyrazin-2-yl)(4-((6-(1-methyl-1H-pyrazol-4-yl)pyridin-3-yl)amino)piperidin-1-yl)methanone (72)**



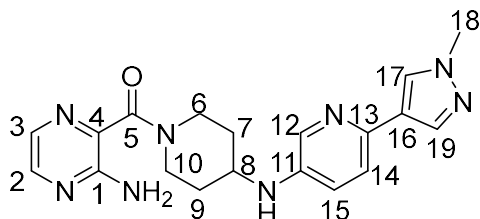
(3-aminopyrazin-2-yl)(4-((6-(bromo)pyridin-3-yl)amino)piperidin-1-yl)methanone ((**59**), 37.5 mg, 0.1 mmol, 1.0 eq), Pyrimidine-5-boronic acid ((**112**), 16.2 mg, 0.1 mmol, 1.0 eq), 10% aq. Na<sub>2</sub>CO<sub>3</sub> solution (21.2 mg in 1mL H<sub>2</sub>O, 0.2 mmol, 2.0 eq) and Toluene (1.5 mL) were placed in a small microwave vial. The solvents were degassed by Ar bubbling (10 min), then Pd(PPh<sub>3</sub>)<sub>4</sub> (11.6 mg, 0.01 mmol, 0.1 eq) was added, the vial was sealed, purged with argon and heated to 120°C for 1 h in the microwave.

The reaction mixture was diluted with DCM, extracted with a 2% aq. Na<sub>2</sub>CO<sub>3</sub> solution and dried over Na<sub>2</sub>SO<sub>4</sub> to obtain a brown oil as crude.

The crude oil was solved in MeCN/H<sub>2</sub>O/DMSO (1:1:1, 3 mL) and purified via prep. HPLC in two runs (5-50% MeCN in 60 min) to obtain 3.40 mg (0.009 mmol, 9%) of the product as a yellow solid.

**LC-MS:** Column: Phenomenex Luna C18(2), gradient: MeCN/H<sub>2</sub>O + 0.05 % HCOOH, 5 % MeCN increase to 100% MeCN in 5.1 min, flow rate: 0.6 mL/min, t<sub>R</sub> = 1.73, m/z = 379.3 ([M+H]<sup>+</sup>).

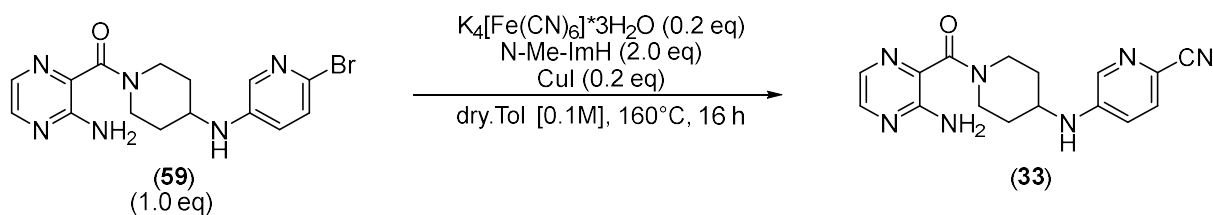
**HRMS:** m/z ([M+H]<sup>+</sup>), calculated: 379.1995, found: 379.1983



**<sup>1</sup>H-NMR** (500 MHz, dms<sub>o</sub>-d<sub>6</sub>, δ in ppm): 8.03 (d, <sup>3</sup>J<sub>2,3</sub> = 2.5 Hz, 1H, H-2), 8.01 (s, 1H, H-19), 7.96 (d, <sup>4</sup>J<sub>12,15</sub> = 2.7 Hz, 1H, H-12), 7.78 (s, 1H, C-17), 7.77 (d, <sup>3</sup>J<sub>3,2</sub> = 2.5 Hz, 1H, H-3), 7.34 (d, <sup>3</sup>J<sub>14,15</sub> = 8.5 Hz, 1H, H-14), 6.99 (dd, <sup>3</sup>J<sub>15,14</sub> = 8.6 Hz, <sup>4</sup>J<sub>15,12</sub> = 2.8 Hz, 1H, H-15), 6.46 (br.s, 2H, Ar-NH<sub>2</sub>), 5.76 (d, <sup>3</sup>J<sub>N,8</sub> = 8.1 Hz, 1H, NH), 4.37 (d, <sup>2</sup>J = 13.1 Hz, 1H, H-6<sub>a</sub>), 3.84 (s, 3H, H-18), 3.65 (d, <sup>2</sup>J = 13.5 Hz, 1H, H10<sub>a</sub>), 3.61-3.53 (m, 1H, H-8), 3.20 (t, <sup>2</sup>J = 11.2 Hz, 1H, H-10<sub>b</sub>), 3.09 (t, <sup>2</sup>J = 11.0 Hz, 1H, H6<sub>b</sub>), 2.04 (d, <sup>2</sup>J = 10.9 Hz, 1H, H-7<sub>a</sub>), 1.90 (d, <sup>2</sup>J = 11.1 Hz, 1H, H-9<sub>a</sub>), 1.47-1.32 (m, 2H, H-7<sub>b</sub>, H-9<sub>b</sub>).

**<sup>13</sup>C-NMR** (126 MHz, dms<sub>o</sub>-d<sub>6</sub>, δ in ppm): 164.99 (C-5), 153.25 (C-1), 143.33 (C-2), 141.81 (C-11), 139.69 (C-12), 135.81 (C-19), 135.05 (C-3), 133.45 (C-4), 130.67 (C-15), 127.49 (C17), 123.45 (C-13), 119.55 (C-16), 119.11 (C-14), 48.41 (C-8), 45.05 (C-10), 40.19 (C-6), 38.57 (C-18), 32.08 (C-7), 31.14 (C-9).

### (3-aminopyrazin-2-yl)(4-((6-(Cyano)pyridin-3-yl)amino)piperidin-1-yl)methanone (33)



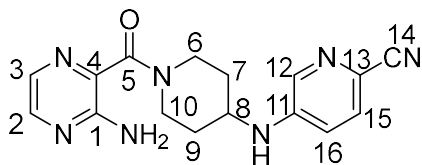
Potassium ferrocyanide trihydrate (8.7 mg, 0.02 mmol, 0.2 eq) was placed in a small crimp vial and dried for 8h at 85°C under high vacuum. Then N-Methyl Imidazole (16.5 mg, 0.2 mmol, 2.0 eq), CuI (3.8 mg, 0.02 mmol, 0.2 eq), (3-aminopyrazin-2-yl)(4-((6-(bromo)pyridin-3-yl)amino)piperidin-1-yl)methanone ((59), 38.2 mg, 0.1 mmol, 1.0 eq) and dry. Toluene (1 mL, [0.1M]) were added to the crimp vial under Argon. The vial was sealed, purged with Argon and the mixture was stirred at 160°C for 16 h after which LC-MS confirmed a clean conversion of 50%, as further heating for 5 h did not improve the conversion, the mixture was worked up at this stage.

DCM and water were added, the phases were separated. After drying of the organic phase with Na<sub>2</sub>SO<sub>4</sub>, 36.7 mg of the reactant/product 1:1 mixture were obtained as a yellow oil.

The crude oil was solved in MeCN/H<sub>2</sub>O/DMSO (1:1:1, 2 mL) and purified via prep. HPLC in two runs (5-100% MeCN in H<sub>2</sub>O in 50 min, elution after 19 min) to obtain 4.23 mg (0.013 mmol, 13%) of the product as a yellow solid.

**LC-MS:** Column: Phenomenex Luna C18(2), gradient: MeCN/H<sub>2</sub>O + 0.05 % HCOOH, 5 % MeCN increase to 100% MeCN in 5.1 min, flow rate: 0.6 mL/min, t<sub>R</sub> = 2.24, m/z = 324.2([M+H]<sup>+</sup>).

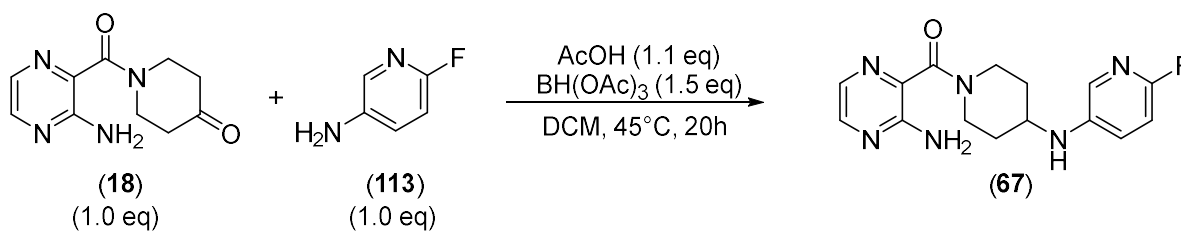
**HRMS:** m/z ([M+H]<sup>+</sup>), calculated: 324.1573, found: 324.1555



**<sup>1</sup>H-NMR** (500 MHz, dms<sub>o</sub>-d<sub>6</sub>, δ in ppm): 8.08 (d, <sup>4</sup>J<sub>12,16</sub> = 2.7 Hz, 1H, H- 12) 8.02 (d, <sup>3</sup>J<sub>2,3</sub> = 2.5 Hz, 1H, H-2), 7.76 (d, <sup>3</sup>J<sub>3,2</sub> = 2.5 Hz, 1H, H-3), 7.63 (d, <sup>3</sup>J<sub>15,16</sub> = 8.7 Hz, 1H, H-15), 7.03 (dd, <sup>3</sup>J<sub>16,15</sub> = 8.7 Hz, <sup>4</sup>J<sub>16,12</sub> = 2.8 Hz, 1H, H-16), 6.97 (d, <sup>3</sup>J<sub>N,8</sub> = 7.8 Hz, 1H, NH), 6.46 (br.s, 2H, Ar-NH<sub>2</sub>), 4.38 (d, <sup>2</sup>J = 13.1 Hz, 1H, H-6a), 3.74-3.59 (m, 2H, H<sub>10a</sub>, H-8), 3.19 (t, <sup>2</sup>J = 11.3 Hz, 1H, H-10<sub>b</sub>), 3.07 (t, <sup>2</sup>J = 11.1 Hz, 1H, H<sub>6b</sub>), 2.01 (d, <sup>2</sup>J = 11.0 Hz, 1H, H-7a), 1.88 (d, <sup>2</sup>J = 11.5 Hz, 1H, H-9a), 1.48-1.33 (m, 2H, H-7b, H-9b).

**<sup>13</sup>C-NMR** (126 MHz, dms<sub>o</sub>-d<sub>6</sub>, δ in ppm): 165.01 (C-5), 153.25 (C-1), 146.36 (C-11), 143.37 (C-2), 137.25 (C-12), 133.35 (C-4), 130.66 (C-3), 129.85 (C-15), 119.14 (C-13), 117.22 (C-16), 116.09 (C-14), 48.06(C-8), 44.92(C-10), 40.06 (C-6), 31.63 (C-7), 30.69 (C-9).

**(3-aminopyrazin-2-yl)(4-((6-(fluoro)pyridin-3-yl)amino)piperidin-1-yl)methanone (67)**



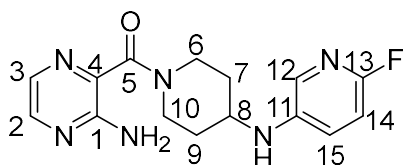
According to **standard procedure 3**, 1-(3-aminopyrazine-2-carbonyl)piperidin-4-one ((**18**), 221.4 mg, 1.0 mmol, 1.0 eq) and 2-Fluoro-5-Amino-pyridine ((**113**), 111.8 mg, 1.0 mmol, 1.0 eq), dry. DCM (7.0 mL), acetic acid (60 μL, 1.10 mmol, 1.1 eq) and BH(OAc)<sub>3</sub> (320.0 mg, 1.50 mmol, 1.50 eq) were used to gain 257.3 mg of a brown solid after workup.

The crude was solved in MeCN/H<sub>2</sub>O/DMSO (1:1:1, 5 mL) and purified via flash. prep. HPLC in one run (10-100% MeCN in 30 min) to obtain 143.7 mg (0.454, 45%) of the product as a pale yellow solid.

**LC-MS:** Column: Phenomenex Luna C18(2), gradient: MeCN/H<sub>2</sub>O + 0.05 % HCOOH, 5 % MeCN increase to 100% MeCN in 5.1 min, flow rate: 0.6 mL/min, t<sub>R</sub> = 2.22, m/z = 317.2([M+H]<sup>+</sup>).

**HRMS:** m/z ([M+H]<sup>+</sup>), calculated: 317.1526, found: 317.1509

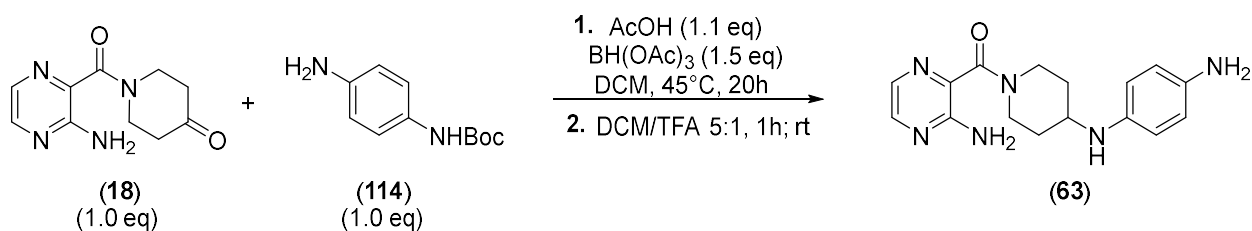




**<sup>1</sup>H-NMR** (500 MHz, dms<sub>o</sub>-d<sub>6</sub>, δ in ppm): 8.02 (d, <sup>3</sup>J<sub>2,3</sub> = 2.4 Hz, 1H, H-2), 7.76 (d, <sup>3</sup>J<sub>3,2</sub> = 2.4 Hz, 1H, H-3), 7.52 (s, 1H, H-12), 7.23-7.14 (m, 1H, H-15), 6.88 (d, <sup>3</sup>J<sub>14,15</sub> = 8.7 Hz, <sup>4</sup>J = 3.0 Hz, 1H, H-14), 6.45 (br.s, 2H, Ar-NH<sub>2</sub>), 5.76 (d, <sup>3</sup>J<sub>N,8</sub> = 8.2 Hz, 1H, NH), 4.35 (d, <sup>2</sup>J = 13.1 Hz, 1H, H-6a), 3.63 (d, <sup>2</sup>J = 13.5 Hz, 1H, H-10a), 3.58-3.47 (m, 1H, H-8), 3.17 (t, <sup>2</sup>J = 11.4 Hz, 1H, H-10b), 3.06 (t, <sup>2</sup>J = 11.2 Hz, 1H, H6b), 2.01 (d, <sup>2</sup>J = 11.8 Hz, 1H, H-7a), 1.88 (d, <sup>2</sup>J = 11.5 Hz, 1H, H-9a), 1.44-1.29 (m, 2H, H-7b, H-9b).

**<sup>13</sup>C-NMR** (126 MHz, dms<sub>o</sub>-d<sub>6</sub>, δ in ppm): 164.98 (C-5), 153.25 (C-1), 152.14 (C-13), 143.31 (C-2), 135.01 (C-11), 133.35 (C-4), 133.45 (C-12), 130.67 (C-3), 126.08 (C-16), 107.82 (C-15), 49.79 (C-8), 45.05 (C-10), 40.43 (C-6), 38.7 (C-14), 32.18 (C-7), 31.23 (C-9).

#### (4-((4-aminophenyl)amino)piperidin-1-yl)(3-aminopyrazin-2-yl)methanone (**63**)



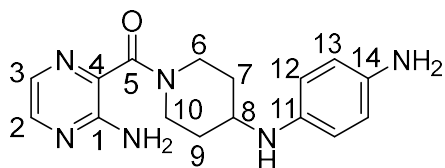
According to **standard procedure 3**, 1-(3-aminopyrazine-2-carbonyl)piperidin-4-one ((**18**), 44.5 mg, 0.2 mmol, 1.0 eq), tert-butyl (4-aminophenyl)carbamate ((**114**), 46.0 mg, 0.2 mmol, 1.0 eq), dry. DCM (5.0 mL, [0.04M]), acetic acid (12 μL, 0.22 mmol, 1.1 eq) and BH(OAc)<sub>3</sub> (64.2mg, 1.50 mmol, 1.50 eq) were used to gain a brown oil after workup.

Then the Boc group was cleaved according to standard procedure 2 to gain the free amine as a brown oil which was purified via prep. HPLC.

The crude oil was solved in MeCN/H<sub>2</sub>O/DMSO (1:1:1, 3 mL) and purified via prep. HPLC in two runs (2-30% MeCN in 30 min) to obtain 8.52 mg (0.027 mmol, 14%) of the product as a yellow solid.

**LC-MS:** Column: Phenomenex Luna C18(2), gradient: MeCN/H<sub>2</sub>O + 0.05 % HCOOH, 5 % MeCN increase to 100% MeCN in 5.1 min, flow rate: 0.6 mL/min, t<sub>R</sub> = 1.22, m/z = 313.2 ([M+H]<sup>+</sup>).

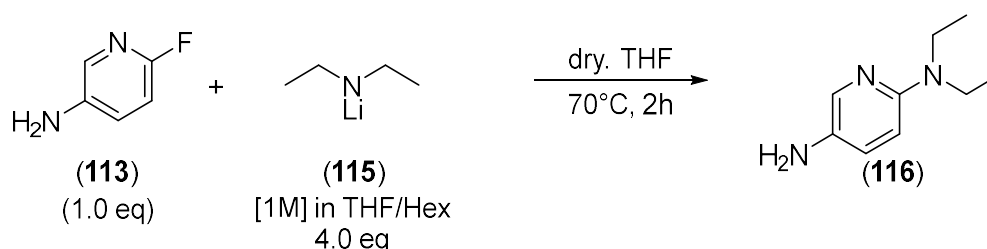
**HRMS:** m/z ([M+H]<sup>+</sup>), calculated: 377.1777, found: 377.1764



**<sup>1</sup>H-NMR** (500 MHz, dms<sub>o</sub>-d<sub>6</sub>, δ in ppm): 9.55 (br.s, 2H, Py-NH<sub>2</sub>), 8.03 (d, <sup>3</sup>J<sub>2,3</sub> = 2.6 Hz, 1H, H-2), 7.76 (d, <sup>3</sup>J<sub>3,2</sub> = 2.6 Hz, 1H, H-3), 7.09-6.91 (m, 2H, 12-H), 6.79-6.66 (m, 2H, 13-H), 6.45 (br.s, 2H, Ar-NH<sub>2</sub>), 4.39 (d, <sup>2</sup>J = 12.7 Hz, 1H, H-6a), 3.66 (d, <sup>2</sup>J = 13.3 Hz, 1H, H-10a), 3.59-3.47 (m, 1H, H-8), 3.16 (t, <sup>2</sup>J = 11.8 Hz, 1H, H-10b), 3.02 (t, <sup>2</sup>J = 11.4 Hz, 1H, H-6b), 2.00 (d, <sup>2</sup>J = 11.5 Hz, 1H, H-7a), 1.86 (d, <sup>2</sup>J = 11.3 Hz, 1H, H-9a), 1.50-1.31 (m, 2H, H-7b, H-9b).

**<sup>13</sup>C-NMR** (126 MHz, dms<sub>o</sub>-d<sub>6</sub>, δ in ppm): 165.01 (C-5), 153.28 (C-1), 143.38 (C-2), 133.31 (C-4), 130.66 (C-3), 45.02 (C-10), 40.15 (C-6), 31.60 (C-7), 30.70 (C-9).

### N<sup>2</sup>,N<sup>2</sup>-diethylpyridine-2,5-diamine (**116**)



In a 10 mL Schlenk tube, HNEt<sub>2</sub> (0.414 mL, 4.0 mmol, 4.0 eq) was solved in dry. THF (2.0 mL) under N<sub>2</sub> and cooled to 0°C. Then nBuLi ([1.6M] in hexane, 2.6 mL, 4.16 mmol, 4.16 eq) was added dropwise at 0°C and subsequently stirred at rt for 1h.

In a second 10 mL Schlenk tube, 2-Fluoro-5-Amino-pyridine ((**113**), 112.5 mg, 1.0 mmol, 1.0 eq) was solved in dry. THF (2 mL) under N<sub>2</sub> and cooled to 0°C. At 0°C the freshly prepared Lithium diethylamine solution (**115**) from the first Schlenk tube was added dropwise. Then the resulting mixture was heated to 70°C for 2h.

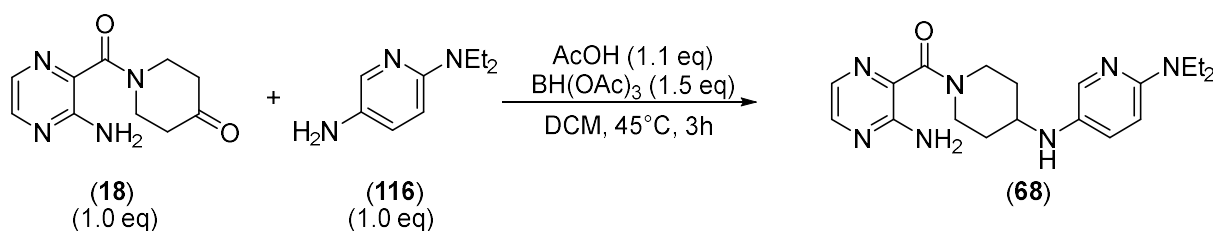
Water was added to the reaction mixture which was extracted with a 1:1 Et<sub>2</sub>O/THF mixture. The organic phase was dried over Na<sub>2</sub>SO<sub>4</sub>, after evaporation of the solvents 153.4 mg of a brown oil were obtained.

The crude oil was solved in H<sub>2</sub>O/MeCN 1:1 and purified via flash prep. HPLC (1% MeCN in H<sub>2</sub>O for 5 then 1-20% MeCN for 20 min) to obtain 83.4 mg (0.5 mmol, 50%) of a brown oil as the desired product.

Column: Phenomenex Luna C18(2), gradient: MeCN/H<sub>2</sub>O + 0.05 % HCOOH, 5 % MeCN increase to 100% MeCN in 7 min, flow rate: 0.6 mL/min, t<sub>R</sub> = 1.04, m/z = 166.2 ([M+H]<sup>+</sup>).

### (3-aminopyrazin-2-yl)(4-((6-(diethylamino)pyridin-3-yl)amino)piperidin-1-yl)methanone

(**68**)

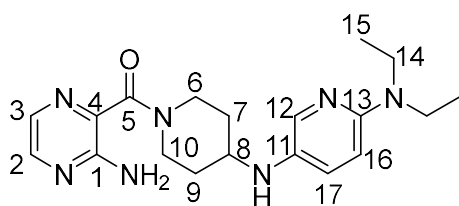


According to **standard procedure 3**, 1-(3-aminopyrazine-2-carbonyl)piperidin-4-one (**(18)**), 39.5 mg, 0.10 mmol, 1.0 eq) and  $N^2,N^2$ -diethylpyridine-2,5-diamine (**(116)**), 21.9 mg, 0.12 mmol, 1.2 eq), dry. DCM (5.0 mL, [0.01M]), acetic acid (15  $\mu$ L, 0.26 mmol, 1.1 eq) and  $BH(OAc)_3$  (76.3 mg, 1.5 mmol, 1.5 eq) were used to gain 78.2 mg of a yellow oil after workup.

The crude oil was solved in MeCN/H<sub>2</sub>O/DMSO (1:1:1, 2 mL) and purified via prep. HPLC in three runs (10-100% MeCN in 60 min) to obtain 7.13 mg (0.019 mmol, 8%) of the product as a yellow solid.

**LC-MS:** Column: Phenomenex Luna C18(2), gradient: MeCN/H<sub>2</sub>O + 0.05 % HCOOH, 5 % MeCN increase to 100% MeCN in 5.1 min, flow rate: 0.6 mL/min,  $t_R$  = 1.94,  $m/z$  = 370.3 ( $[M+H]^+$ ).

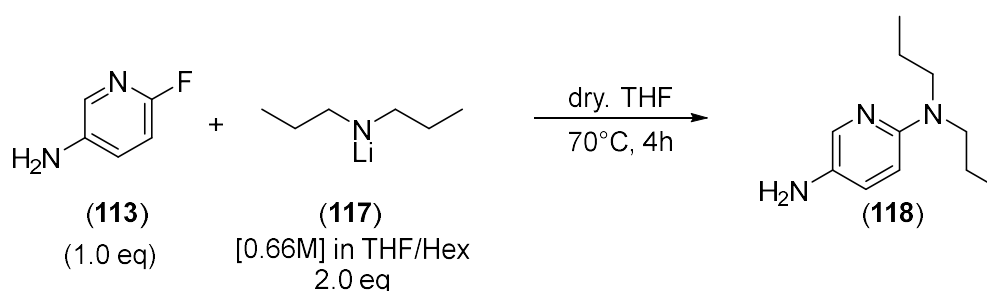
**HRMS:**  $m/z$  ( $[M+H]^+$ ), calculated: 370.2355, found: 370.2342



**<sup>1</sup>H-NMR** (500 MHz, dms<sub>o</sub>-d<sub>6</sub>,  $\delta$  in ppm): 8.02 (d,  $^3J_{2,3}$  = 2.5 Hz, 1H, H-2), 7.75 (d,  $^3J_{3,2}$  = 2.5 Hz, 1H, H-3), 7.60 (d,  $^3J_{12,17}$  = 2.5 Hz, 1H, H-12), 6.96 (dd,  $^3J_{17,16}$  = 8.9 Hz,  $^4J_{17,12}$  = 2.6 Hz, 1H, H-17), 6.50-6.35 (m, 3H, Ar-NH<sub>2</sub>, H-16) 4.33 (d,  $^2J$  = 13.1 Hz, 1H, H-6a), 3.63 (d,  $^2J$  = 13.4 Hz, 1H, H-10a), 3.36 (q,  $^3J_{14,15}$  = 6.7 Hz, 5H, H-14, H-8), 3.14 (t,  $^2J$  = 11.4 Hz, 1H, H-10b), 3.04 (t,  $^2J$  = 11.2 Hz, 1H, H6b), 1.98 (d,  $^2J$  = 11.0 Hz, 1H, H-7a), 1.85 (d,  $^2J$  = 11.7 Hz, 1H, H-9a), 1.40-1.26 (m, 2H, H-7b, H-9b), 1.04 (t,  $^3J_{15,14}$  = 6.9 Hz, 6H, H-15).

**<sup>13</sup>C-NMR** (126 MHz, dms<sub>o</sub>-d<sub>6</sub>,  $\delta$  in ppm): 164.95 (C-5), 153.24 (C-1), 150.71 (C-13), 143.28 (C-2), 134.41 (C-11), 133.54 (C-12), 133.51 (C-4), 130.65 (C-3), 125.12 (C-17), 106.16 (C-16), 50.00 (C-8), 45.11 (C-10), 41.80 (C-14), 40.25 (C-6), 32.42 (C-7), 31.47 (C-9), 12.99 (C-15).

### $N^2,N^2$ -dipropylpyridine-2,5-diamine (**(118)**)



In a 10 mL Schlenk tube,  $HNPr_2$  (1.38 mL, 10 mmol) was solved in dry. THF (8.75 mL) under  $N_2$  and cooled to 0°C. Then  $nBuLi$  ([1.6M] in hexane, 6.25 mL, 10.0 mmol) was added dropwise at 0°C and subsequently stirred at rt for 2h.

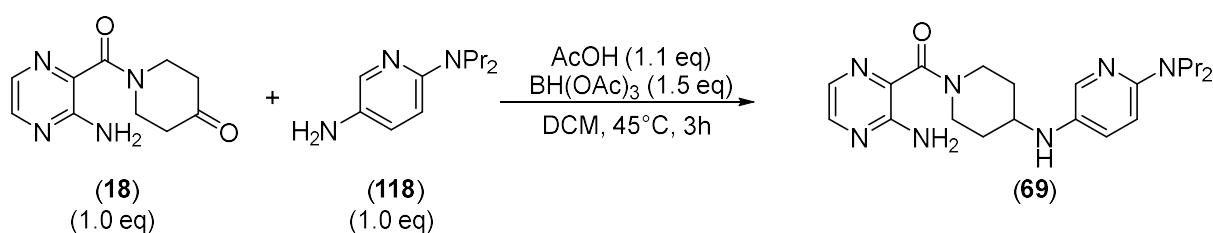
In a second 10 mL Schlenk tube, 2-Fluoro-5-Amino-pyridine (**(113)**), 112.3 mg, 1.0 mmol, 1.0 eq) was solved in dry. THF (3 mL) under  $N_2$  and cooled to 0°C. At 0°C the freshly prepared Lithium dipropylamine solution (**(117)**), 3.0 mL, 2mmol, 2.0 eq) from the first Schlenk tube was added dropwise. Then the resulting mixture was heated to 70°C for 4h.

Water was added to the reaction mixture which was extracted with a 1:1 Et<sub>2</sub>O/THF mixture. The organic phase was dried over Na<sub>2</sub>SO<sub>4</sub>, after evaporation of the solvents 137.8 mg of a reddish oil were obtained. The crude mixture contained 20% of the reactant ((**113**), 2-Fluoro-5-Amino-pyridine).

The crude oil was solved in H<sub>2</sub>O/MeCN 1:1 and purified via flash prep. HPLC (1% MeCN in H<sub>2</sub>O for 5-100% MeCN for 30 min) to obtain 48.8 mg (0.25 mmol, 25%) of a black solid as the desired product (contained 18% of (**113**) which could not be separated).

Column: Phenomenex Luna C18(2), gradient: MeCN/H<sub>2</sub>O + 0.05 % HCOOH, 5 % MeCN increase to 100% MeCN in 7 min, flow rate: 0.6 mL/min, t<sub>R</sub> = 2.29, m/z = 194.2 ([M+H]<sup>+</sup>).

**(3-aminopyrazin-2-yl)(4-((6-(dipropylamino)pyridin-3-yl)amino)piperidin-1-yl)methanone (**69**)**

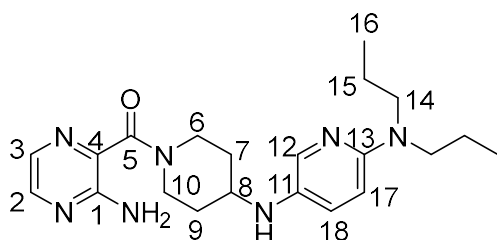


According to **standard procedure 3**, 1-(3-aminopyrazine-2-carbonyl)piperidin-4-one ((**18**), 48.8 mg, 0.25 mmol, 1.0 eq) and N<sup>2</sup>,N<sup>2</sup>-dipropylpyridine-2,5-diamine ((**118**), 55.6 mg, 0.25 mmol, 1.0 eq), dry. DCM (5.0 mL, [0.05M]), acetic acid (16 μL, 0.275 mmol, 1.1 eq) and BH(OAc)<sub>3</sub> (80.7 mg, 0.38 mmol, 1.52 eq) were used to gain 84.8 mg of a brown oil after workup, which contained (**67**) and the desired product in a ratio of 1:3.

The crude oil was solved in MeCN/H<sub>2</sub>O/DMSO (1:1:1, 2 mL) and purified via prep. HPLC in four runs (5-50% MeCN in 60 min) to obtain 6.56 mg (0.024 mmol, 7%) of the product as a yellow solid after a complicated separation.

**LC-MS:** Column: Phenomenex Luna C18(2), gradient: MeCN/H<sub>2</sub>O + 0.05 % HCOOH, 5 % MeCN increase to 100% MeCN in 5.1 min, flow rate: 0.6 mL/min, t<sub>R</sub> = 2.34, m/z = 398.3 ([M+H]<sup>+</sup>).

**HRMS:** m/z ([M+H]<sup>+</sup>), calculated: 398.2668, found: 398.2653

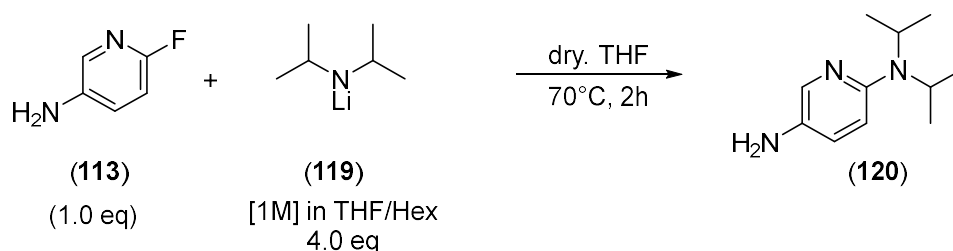


**<sup>1</sup>H-NMR** (500 MHz, dms<sub>o</sub>-d<sub>6</sub>, δ in ppm): 8.01 (d, <sup>3</sup>J<sub>2,3</sub> = 2.5 Hz, 1H, H-2), 7.75 (d, <sup>3</sup>J<sub>3,2</sub> = 2.5 Hz, 1H, H-3), 7.60 (d, <sup>3</sup>J<sub>12,17</sub> = 2.8 Hz, 1H, H-12), 6.95 (dd, <sup>3</sup>J<sub>17,16</sub> = 8.9 Hz, <sup>4</sup>J<sub>17,12</sub> = 2.8 Hz, 1H, H-18), 6.48-6.36 (m, 3H, H-17, Ar-NH<sub>2</sub>), 4.33 (d, <sup>2</sup>J = 13.2 Hz, 1H, H-6a), 3.62 (d, <sup>2</sup>J = 13.5 Hz, 1H, H-10a), 3.41-3.53 (m, 1H, H-8), 3.29-3.21 (m, 4H, H-14), 3.13 (t, <sup>2</sup>J = 11.2 Hz, 1H, H-10b), 3.03 (t, <sup>2</sup>J = 10.9 Hz, 1H, H6b), 1.98 (d, <sup>2</sup>J = 10.5 Hz, 1H, H-7a), 1.84 (d, <sup>2</sup>J = 11.2 Hz,

<sup>1</sup>H, H-9a), 1.56-1.43 (m, 4H, H-15), 1.39-1.29 (m, 2H, H-7b, H-9b), 0.84 (t, <sup>3</sup>J<sub>16,15</sub> = 7.4 Hz, 6H, H-16).

<sup>13</sup>C-NMR (126 MHz, dms<sub>o</sub>-d<sub>6</sub>, δ in ppm): 164.96 (C-5), 153.24 (C-1), 151.14 (C-13), 143.28 (C-2), 134.29 (C-11), 133.52 (C-12), 133.35 (C-4), 130.66 (C-3), 125.15 (C-18), 106.07 (C-17), 50.16 (C-14), 49.99 (C-8), 45.11 (C-10), 40.26 (C-6), 32.42 (C-7), 31.47 (C-9), 20.56 (C-15), 11.36 (C-16).

### N<sup>2</sup>,N<sup>2</sup>-diisopropylpyridine-2,5-diamine (120)



In a 10 mL Schlenk tube, HN(*i*Pr)<sub>2</sub> (0.565 mL, 4.0 mmol, 4.0 eq) was solved in dry. THF (1.4 mL) under N<sub>2</sub> and cooled to 0°C. Then *n*BuLi ([1.6M] in hexane, 2.6 mL, 4.16 mmol, 4.16 eq) was added dropwise at 0°C and subsequently stirred at rt for 1h.

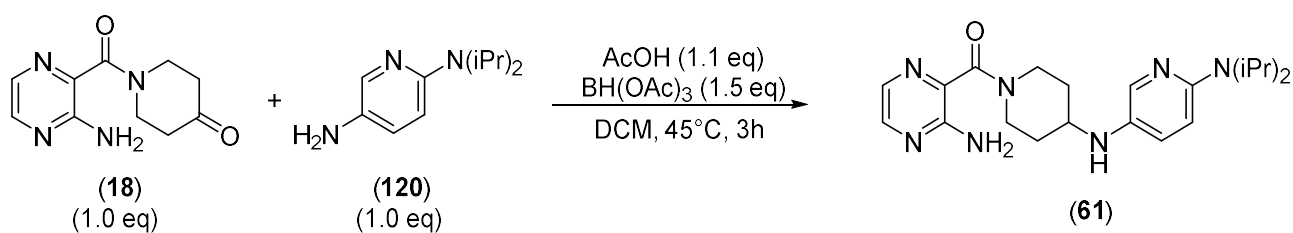
In a second 10 mL Schlenk tube, 2-Fluoro-5-Amino-pyridine ((113), 112.1 mg, 1.0 mmol, 1.0 eq) was solved in dry. THF (2 mL) under N<sub>2</sub> and cooled to 0°C. At 0°C the freshly prepared Lithium diethylamine solution (119) from the first Schlenk tube was added dropwise. Then the resulting mixture was heated to 70°C for 3h.

Water was added to the reaction mixture which was extracted with a 1:1 Et<sub>2</sub>O/THF mixture. The organic phase was dried over Na<sub>2</sub>SO<sub>4</sub>, after evaporation of the solvents 140.9 mg of a brown oil were obtained.

The crude oil was solved in H<sub>2</sub>O/MeCN 1:1 and purified via flash prep. HPLC (1% MeCN in H<sub>2</sub>O for 5 min, then 1-20% MeCN for 20 min) to obtain 25.3 mg (0.13 mmol, 13%) of a brown solid as the desired product (>98%).

Column: Phenomenex Luna C18(2), gradient: MeCN/H<sub>2</sub>O + 0.05 % HCOOH, 5 % MeCN increase to 100% MeCN in 7 min, flow rate: 0.6 mL/min, t<sub>R</sub> = 1.78, m/z = 194.2 ([M+H]<sup>+</sup>).

### (3-aminopyrazin-2-yl)(4-((6-(diisopropylamino)pyridin-3-yl)amino)piperidin-1-yl)methanone (61)

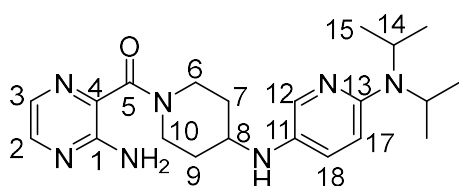


According to **standard procedure 3**, 1-(3-aminopyrazine-2-carbonyl)piperidin-4-one ((**18**), 28.7 mg, 0.13 mmol, 1.0 eq) and N<sup>2</sup>,N<sup>2</sup>-diisopropylpyridine-2,5-diamine ((**120**), 25.3 mg, 0.13 mmol, 1.0 eq), dry. DCM (3.0 mL, [0.05M]), acetic acid (8  $\mu$ L, 0.14 mmol, 1.1 eq) and BH(OAc)<sub>3</sub> (41.7 mg, 0.195 mmol, 1.52 eq) were used to gain 37.6 mg of a brown oil after workup.

The crude oil was solved in MeCN/H<sub>2</sub>O/DMSO (1:1:1, 2 mL) and purified via prep. HPLC in two (5-50% MeCN in 60 min) to obtain 5.63 mg (0.014 mmol, 11%) of the product as a yellow solid as the formic acid salt.

**LC-MS:** Column: Phenomenex Luna C18(2), gradient: MeCN/H<sub>2</sub>O + 0.05 % HCOOH, 5 % MeCN increase to 100% MeCN in 5.1 min, flow rate: 0.6 mL/min, t<sub>R</sub> = 2.21, m/z = 398.3 ([M+H]<sup>+</sup>).

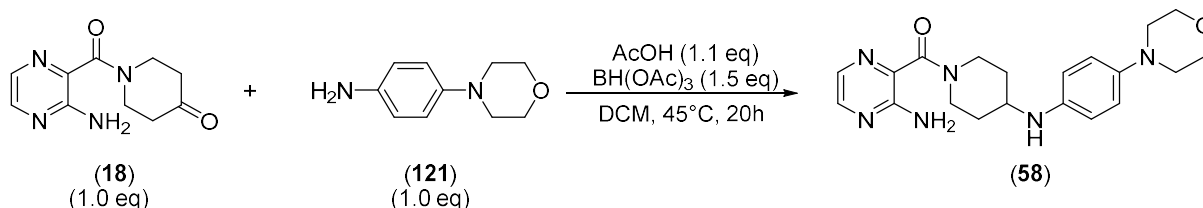
**HRMS:** m/z ([M+H]<sup>+</sup>), calculated: 398.2668, found: 398.2655



**<sup>1</sup>H-NMR** (500 MHz, dms<sub>o</sub>-d<sub>6</sub>,  $\delta$  in ppm): 81.9 (s, 1H, HCOOH), 8.02 (d, <sup>3</sup>J<sub>2,3</sub> = 2.5 Hz, 1H, H-2), 7.75 (d, <sup>3</sup>J<sub>3,2</sub> = 2.5 Hz, 1H, H-3), 7.61 (d, <sup>3</sup>J<sub>12,17</sub> = 2.9 Hz, 1H, H-12), 6.91 (dd, <sup>3</sup>J<sub>17,16</sub> = 9.0 Hz, <sup>4</sup>J<sub>17,12</sub> = 2.9 Hz, 1H, H-17), 6.48 (d, <sup>3</sup>J<sub>16,17</sub> = 9.0 Hz, 1H, H-16), 6.48 (s, 2H, Ar-NH<sub>2</sub>), 4.34 (d, <sup>2</sup>J = 13.1 Hz, 1H, H-6a), 4.03-3.93 (m, 2H, H-14), 3.63 (d, <sup>2</sup>J = 13.4 Hz, 1H, H-10a), 3.42-3.33 (m, 1H, H-8), 3.14 (t, <sup>2</sup>J = 11.4 Hz, 1H, H-10b), 3.04 (t, <sup>2</sup>J = 10.9 Hz, 1H, H-6b), 1.98 (d, <sup>2</sup>J = 10.6 Hz, 1H, H-7a), 1.85 (d, <sup>2</sup>J = 11.8 Hz, 1H, H-9a), 1.40-1.26 (m, 2H, H-7b, H-9b), 1.18 (d, 12H, H-15).

**<sup>13</sup>C-NMR** (126 MHz, dms<sub>o</sub>-d<sub>6</sub>,  $\delta$  in ppm): 164.95 (C-5), 163.48 (HCOOH), 153.24 (C-1), 150.71 (C-13), 143.28 (C-2), 134.81 (C-11), 133.51 (C-12), 133.03 (C-4), 130.65 (C-3), 124.01 (C-17), 109.94 (C-16), 49.82 (C-8), 45.19 (C-14), 45.12 (C-10), 40.26 (C-6), 32.43 (C-7), 31.48 (C-9), 20.96 (C-15).

### (3-aminopyrazin-2-yl)(4-((4-morpholinophenyl)amino)piperidin-1-yl)methanone (**58**)

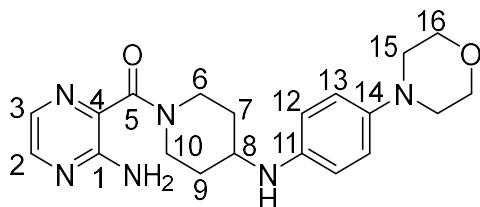


According to **standard procedure 3**, 3-aminopyrazin-2-carboxylic acid ((**18**), 23 mg, 0.1 mmol, 1.0 eq) and 4-morpholinoaniline ((**121**) 20.0 mg, 0.11 mmol, 1.1 eq), dry. DCM (5.0 mL, [0.02M]), acetic acid (6  $\mu$ L, 0.11 mmol, 1.1 eq) and BH(OAc)<sub>3</sub> (31.6 mg, 0.15 mmol, 1.5 eq) were used to gain the crude as a dark oil after workup.

The crude oil was solved in MeCN/H<sub>2</sub>O (1:1, 2 mL) and purified via prep. HPLC in two runs (5-50% MeCN in 30 min) to obtain 4.45 mg (0.013 mmol, 13%) of the product as a yellow solid.

**LC-MS:** Column: Phenomenex Luna C18(2), gradient: MeCN/H<sub>2</sub>O + 0.05 % HCOOH, 5 % MeCN increase to 100% MeCN in 5.1 min, flow rate: 0.6 mL/min, t<sub>R</sub> = 1.78, m/z = 383.3([M+H]<sup>+</sup>).

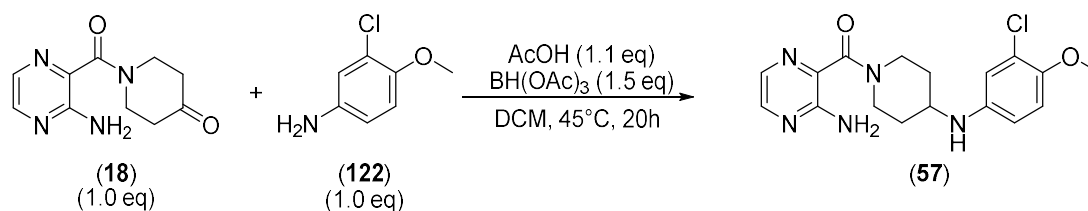
**HRMS:** m/z ([M+H]<sup>+</sup>), calculated: 383.2195, found: 383.2180



**<sup>1</sup>H-NMR** (500 MHz, dms<sub>o</sub>-d<sub>6</sub>, δ in ppm): 8.02 (d, <sup>3</sup>J<sub>2,3</sub> = 2.6 Hz, 1H, H-2), 7.76 (d, <sup>3</sup>J<sub>3,2</sub> = 2.6 Hz, 1H, H-3), 7.08-6.08 (m, 6H, H-12, H-13, Ar-NH<sub>2</sub>), 5.43 (br.s, 1H, NH), 4.56-4.16 (m, 1H, H-6a), 3.94-3.45 (m, 6H, H-10a, H-8, H-16), 3.16 (t, <sup>2</sup>J = 11.4 Hz, 1H, H-10<sub>b</sub>), 3.05 (t, <sup>2</sup>J = 11.2 Hz, 1H, H-6<sub>b</sub>), 3.01-2.62 (m, 4H, H-15), 2.13-1.74 (m, 2H, H-7<sub>a</sub>, H-9<sub>a</sub>), 1.53-1.17 (m, 2H, H-7<sub>b</sub>, H-9<sub>b</sub>).

**<sup>13</sup>C-NMR** (126 MHz, dms<sub>o</sub>-d<sub>6</sub>, δ in ppm): 164.98 (C-5), 153.25 (C-1), 143.32 (C-2), 142.49 (C-14), 141.32 (C-13), 133.45 (C-4), 130.67 (C-3), 117.63 (C-13), 113.86 (C-12), 66.23 (C-16), 50.51 (C-15), 49.43 (C-8), 45.17 (C-10), 40.31 (C-6), 32.27 (C-7), 31.46 (C-9).

**(3-aminopyrazin-2-yl)(4-((3-chloro-4-methoxyphenyl)amino)piperidin-1-yl)methanone**  
**(57)**

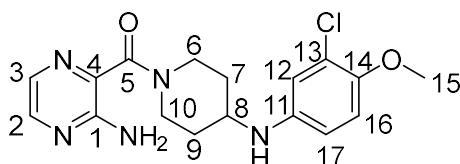


According to **standard procedure 3**, 3-aminopyrazin-2-carboxylic acid ((**18**), 22.5 mg, 0.1 mmol, 1.0 eq) and 3-chloro-4-methoxyaniline ((**122**), 18.8 mg, 0.12 mmol, 1.2 eq), dry. DCM (5.0 mL, [0.02M]), acetic acid (6 μL, 0.11 mmol, 1.1 eq) and BH(OAc)<sub>3</sub> (32.3 mg, 0.15 mmol, 1.5 eq) were used to gain the crude as a brown residue after workup.

The crude oil was solved in MeCN/H<sub>2</sub>O (1:1, 2 mL) and purified via prep. HPLC in one run (10-100% MeCN in 50 min) to obtain 4.79 mg (0.013 mmol, 13%) of the product as a pale yellow solid.

**LC-MS:** Column: Phenomenex Luna C18(2), gradient: MeCN/H<sub>2</sub>O + 0.05 % HCOOH, 5 % MeCN increase to 100% MeCN in 5.1 min, flow rate: 0.6 mL/min, t<sub>R</sub> = 2.46, m/z = 362.4, 364.2 ([M+H]<sup>+</sup>).

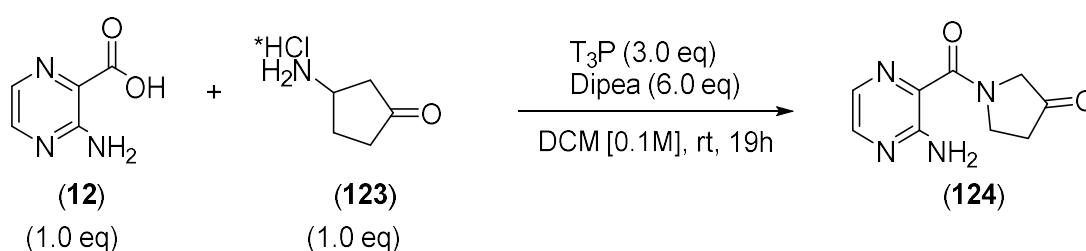
**HRMS:** m/z ([M+H]<sup>+</sup>), calculated: 362.1384, found: 362.1373



**<sup>1</sup>H-NMR** (500 MHz, dms<sub>o</sub>-d<sub>6</sub>, δ in ppm): 8.02 (d, <sup>3</sup>J<sub>2,3</sub> = 2.5 Hz, 1H, H-2), 7.75 (d, <sup>3</sup>J<sub>3,2</sub> = 2.5 Hz, 1H, H-3), 6.90 (d, <sup>3</sup>J<sub>16,17</sub> = 8.9 Hz, 1H, H-16), 6.69 (d, <sup>4</sup>J<sub>12,17</sub> = 2.6 Hz, 1H, H-12), 6.55 (dd, <sup>3</sup>J<sub>17,16</sub> = 8.8 Hz, <sup>4</sup>J<sub>17,12</sub> = 2.6 Hz, 1H, H-17), 6.44 (br.s, 2H, Ar-NH<sub>2</sub>), 5.37 (d, <sup>3</sup>J<sub>NH,8</sub> = 8.0 Hz, 1H, NH), 4.34 (d, <sup>2</sup>J = 13.1 Hz, 1H, H-6a), 3.70 (s, 3H, H-15), 3.63 (d, <sup>2</sup>J = 13.5 Hz, 1H, H-10a), 3.54-3.42 (m, 1H, H-8), 3.17 (t, <sup>2</sup>J = 11.3 Hz, 1H, H-10b), 3.06 (t, <sup>2</sup>J = 11.0 Hz, 1H, H6b), 1.99 (d, <sup>2</sup>J = 11.0 Hz, 1H, H-7a), 1.85 (d, <sup>2</sup>J = 11.2 Hz, 1H, H-9a), 1.40-1.27 (m, 2H, H-7b, H-9b).

**<sup>13</sup>C-NMR** (126 MHz, dms<sub>o</sub>-d<sub>6</sub>, δ in ppm): 165.42(C-5), 153.72 (C-1), 146.01 (C-14), 143.77 (C-2), 143.24 (C-11), 133.91 (C-13), 131.11 (C-3), 122.37(C-4), 115-24 (C-16), 114.39 (C-12), 112.50 (C-17), 57.07 (C-15) 49.47 (C-8), 45.57(C-10), 40.70 (C-6), 32.69 (C-7), 31.74(C-9).

### 1-(3-aminopyrazine-2-carbonyl)pyrrolidin-3-one (**124**)



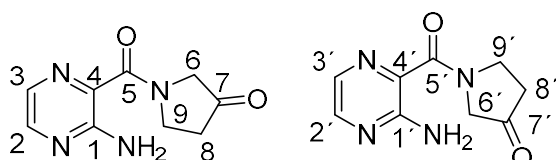
According to **standard procedure 1**, 3-aminopyrazine-2-carboxylic acid (**12**), 142.3 mg, 1.0 mmol, 1.0 eq), 3-aminocyclopentan-1-one hydrochloride (**123**), 137 mg, 1.1 mmol, 1.1 eq), dry. DCM (10 mL, [0.1M]), Dipea (1.0 mL, 6.0 mmol, 6.0 eq) and T<sub>3</sub>P (50% in EtOAc, 0.95 mL, 1.5 eq) were used to gain 279.6 mg (90% pure) of a brown oil/ after workup.

The crude oil was solved in DCM, absorbed on Isolute and purified via combi flash (24 g SiO<sub>2</sub> prepacked column, 0-5% MeOH in DCM in 15 min) to obtain 69.4 mg (0.34 mmol, 34%) of a beige solid as pure product.

**LC-MS**: Column: Phenomenex Luna C18(2), gradient: MeCN/H<sub>2</sub>O + 0.05 % HCOOH, 5 % MeCN increase to 100% MeCN in 5.1 min, flow rate: 0.6 mL/min, t<sub>R</sub> = 1.52, m/z = 207.2 ([M+H]<sup>+</sup>).

**HRMS**: m/z ([M+H]<sup>+</sup>), calculated: 207.0882, found: 207.0871

In NMR, two distinct rotamers in a ratio of 3:2 could be detected which appear on LC-MS as one species. The signals could not be assigned to the respective rotamers. For clarity we assigned the signals of the major rotamer to the first structure but it could be vice versa.

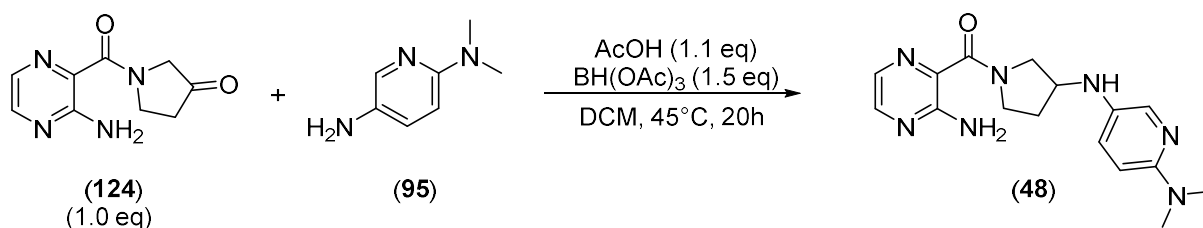


**<sup>1</sup>H-NMR** (500 MHz, CDCl<sub>3</sub>, δ in ppm): 8.10 (d, <sup>3</sup>J<sub>2,3</sub> = 2.4 Hz, 1H, H-2), 7.82 (dd, <sup>3</sup>J<sub>3,2</sub> = 2.3 Hz, J = 5.4 Hz, 1H, H-3), 7.08 (s, 1.2 H, Ar-NH), 6.88 (s, 0.8 H, Ar-NH'), 4.20 (s, 1.2 H, H-6), 4.05 (t, J = 7.7, 0.8 H, H-6'), 3.99-3.90 (m, 2H, H-9), 2.65-2.53 (m, 2H, H-8).



<sup>13</sup>C-NMR (126 MHz, dms<sub>o</sub>-d<sub>6</sub>, δ in ppm): 211.9 (C-7), 210.61 (C-7'), 165.55 (C-5'), 165.38 (C-5), 154.84 (C-1), 154.35 (C-1'), 144.92 (C-2), 144.52 (C-2'), 130.36 (C-3'), 130.42 (C-3), 129.04 (C-4, C-4'), 55.38 (C-6), 52.47 (C-6'), 45.63 (C-9'), 43.06 (C-9), 37.29 (C-8'), 34.74 (C-8).

**(3-aminopyrazin-2-yl)(3-((6-(dimethylamino)pyridin-3-yl)amino)pyrrolidin-1-yl)methanone (48)**

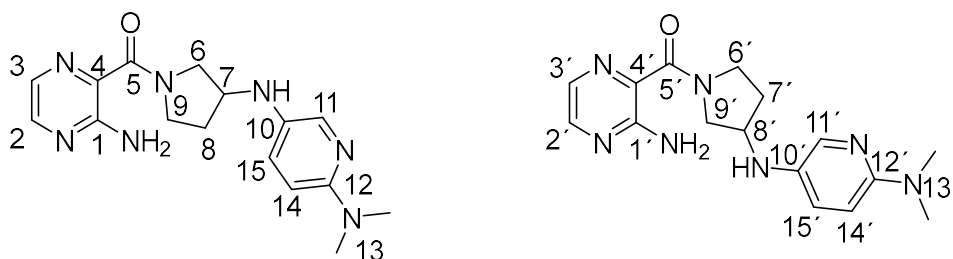


According to **standard procedure 3**, 1-(3-aminopyrazin-2-carbonyl)pyrrolidin-3-one (**(124)**, 58.1 mg, 0.28 mmol, 1.0 eq) and N,N-dimethylbenzene-1,4-diamine (**(95)**, 40.1 mg, 0.28 mmol, 1.0 eq), dry. DCM (7.0 mL, [0.05M]), acetic acid (18 μL, 0.31 mmol, 1.1 eq) and BH(OAc)<sub>3</sub> (89.1 mg, 0.42 mmol, 1.5 eq) were used to gain 48.1 mg of a dark oil after workup. The crude contained some side products and was hard to purify.

The crude oil was solved in MeCN/H<sub>2</sub>O (1:1, 2 mL) and purified via prep. HPLC in three runs (5- 50% MeCN in H<sub>2</sub>O in 30 min) to obtain 4.28 mg (0.013 mmol, 5%) of the product as a red solid after lyophilization over night.

**LC-MS:** Column: Phenomenex Luna C18(2), gradient: MeCN/H<sub>2</sub>O + 0.05 % HCOOH, 5 % MeCN increase to 100% MeCN in 5.1 min, flow rate: 0.6 mL/min, t<sub>R</sub> = 1.65, m/z = 328.3 ([M+H]<sup>+</sup>).

**HRMS:** m/z ([M+H]<sup>+</sup>), calculated: 328.1886, found: 328.1873

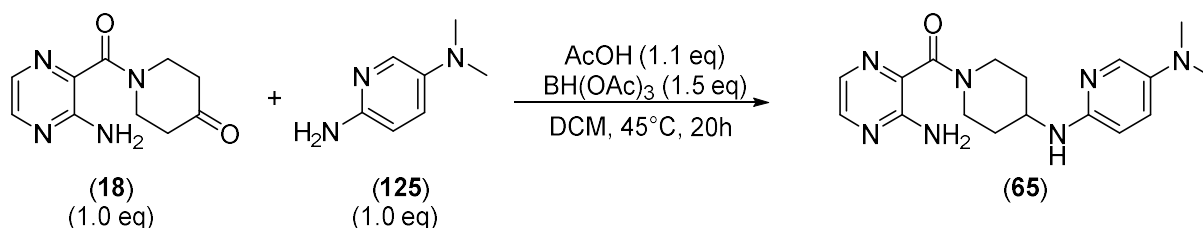


<sup>1</sup>H-NMR (500 MHz, CDCl<sub>3</sub>, δ in ppm): 8.09 (m, 0.6H, H-2), 8.05 (d, <sup>3</sup>J<sub>2',3'} = 2.4 Hz, 0.4H, H-2'), 7.80 (d, <sup>3</sup>J<sub>3,2} = 2.4 Hz, 0.6H, H-3), 7.78 (d, <sup>3</sup>J<sub>3',2'} = 2.4 Hz, 0.4H, H-3'), 7.64 (d, <sup>4</sup>J<sub>11',15'} = 2.8 Hz, 0.4H, H-11'), 7.57 (d, <sup>4</sup>J<sub>11,15} = 2.8 Hz, 0.6 H, H-11), 7.09-6.89 (m, 3H, H-15, H-15', Ar-NH2, Ar-NH2'), 6.56 (d, <sup>3</sup>J<sub>14',15'} = 8.9 Hz, 0.4 H, H-14'), 6.54 (d, <sup>3</sup>J<sub>14,15} = 8.9 Hz, 0.6 H, H-14), 3.98-3.89 (m, 2H, H-6, H-6'), 3.85-3.38 (m, 3H, H-7, H-7', H-8, H-8'), 2.88 (s, 2.5H, H-13'), 2.85 (s, 3.5H, H-13), 2.17-2.07 (m, 1H, H-8<sub>a</sub>, H-8'<sub>a</sub>), 1.88-1.71 (m, 1H, H-8<sub>b</sub>, H-8'<sub>b</sub>).</sub></sub></sub></sub></sub></sub></sub>

<sup>13</sup>C-NMR (126 MHz, dms<sub>o</sub>-d<sub>6</sub>, δ in ppm): 165.25 (C-5'), 165.17 (C-5), 154.60 (C-1), 154.51 (C-1'), 153.10 (C-12 or C-12'), 153.05 (C-12 or C-12'), 144.39 (C-2), 144.33 (C-2'), 135.49 (C-10'), 135.48 (C-10), 132.56 (C-11'), 132.39 (C-11), 131.02 (C-4'), 130.86 (C-4), 130.43 (C-3, C-3'), 124.25 (C-15'), 124.16 (C-15), 106.94 (C-14, C-14'), 54.23 (C-6'), 53.43 (C-6), 52.13 (C-7), 51.00 (C-7'), 47.03 (C-9'), 44.98 (C-9), 38.62 (C-13), 38.59 (C-13'), 31.73 (C-8'), 29.09 (C-8).

In NMR, two distinct rotamers in a ratio of 3:2 could be detected which appear on LC-MS as one species. The signals could not be assigned to the respective rotamers. For clarity we assigned the signals of the major rotamer to the first structure but it could be vice versa.

**(3-aminopyrazin-2-yl)(4-((5-(dimethylamino)pyridin-2-yl)amino)piperidin-1-yl)methanone (65)**

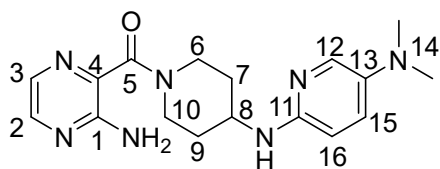


According to **standard procedure 3**, 1-(3-aminopyrazine-2-carbonyl)piperidin-4-one (**(18)**, 22.3 mg, 0.1 mmol, 1.0 eq) and N<sup>5</sup>,N<sup>5</sup>-dimethylpyridine-2,5-diamine (**(125)**, 14.0 mg, 0.1 mmol, 1.0 eq), dry. DCM (5.0 mL, [0.02M]), acetic acid (6 μL, 0.11 mmol, 1.1 eq) and BH(OAc)<sub>3</sub> (33 mg, 0.15 mmol, 1.5 eq) were used to gain 18.4 mg of a dark oil after workup.

The crude oil was solved in MeCN/H<sub>2</sub>O (1:1, 2 mL) and purified via prep. HPLC in three runs (5-50% MeCN in H<sub>2</sub>O in 30 min) to obtain 5.23 mg (0.015mmol, 15%) of the product as a yellow solid.

**LC-MS:** Column: Phenomenex Luna C18(2), gradient: MeCN/H<sub>2</sub>O + 0.05 % HCOOH, 5 % MeCN increase to 100% MeCN in 5.1 min, flow rate: 0.6 mL/min, t<sub>R</sub> = 1.73, m/z = 342.4 ([M+H]<sup>+</sup>).

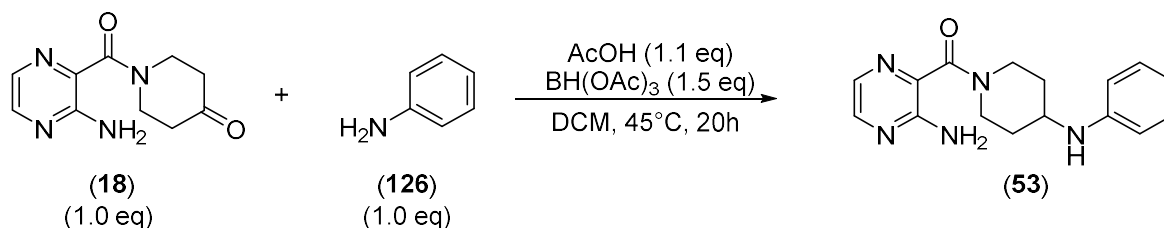
**HRMS:** m/z ([M+H]<sup>+</sup>), calculated: 342.2042, found: 342.2031



**<sup>1</sup>H-NMR** (500 MHz, dms<sub>o</sub>-d<sub>6</sub>, δ in ppm): 8.02 (d, <sup>3</sup>J<sub>2,3</sub> = 2.6 Hz, 1H, H-2), 7.76 (d, <sup>3</sup>J<sub>3,2</sub> = 2.6 Hz, 1H, H-3), 7.57 (d, <sup>4</sup>J<sub>12,15</sub> = 3.0 Hz, 1H, H-12), 7.09 (dd, <sup>3</sup>J<sub>15,16</sub> = 9.0 Hz, <sup>4</sup>J<sub>15,12</sub> = 3.0 Hz, 1H, H-15), 6.46-6.37 (m, 3H, H-16, ar-NH<sub>2</sub>), 5.86 (d, <sup>3</sup>J<sub>NH,8</sub> = 5.4 Hz, 1H, NH), 4.33 (d, <sup>2</sup>J = 13.1 Hz, 1H, H-6a), 3.95-3.80 (m, 1H, H-8), 3.62 (d, <sup>2</sup>J = 13.6 Hz, 1H, H-10a), 3.20-3.11 (m, 1H, H-10b), 3.09-3.00 (m, 1H, H6b), 2.69 (s, 6H, H-14), 2.00 (d, <sup>2</sup>J = 9.8 Hz, 1H, H-7a), 1.85 (d, <sup>2</sup>J = 10.2 Hz, 1H, H-9a), 1.48-1.32 (m, 2H, H-7b, H-9b).

**<sup>13</sup>C-NMR** (126 MHz, dms<sub>o</sub>-d<sub>6</sub>, δ in ppm): 164.99 (C-5), 153.26 (C-1), 151.70 (C-11), 143.29 (C-2), 139.13 (C-4), 133.53 (C-13), 133.04 (C-12), 130.68 (C-3), 125.81 (C-15), 108.88 (C-16), 47.36 (C-8), 45.28 (C-10), 41.75 (C-14), 40.42 (C-6), 32.50 (C-7), 31.60 (C-9).

### (3-aminopyrazin-2-yl)(4-(phenylamino)piperidin-1-yl)methanone (53)

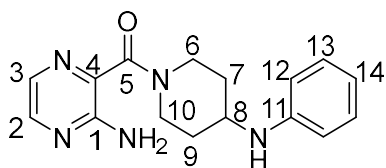


According to **standard procedure 3**, 1-(3-aminopyrazine-2-carbonyl)piperidin-4-one ((**18**), 26.0 mg, 0.12 mmol, 1.0 eq), Aniline ((**126**), 12  $\mu\text{L}$ , 0.13 mmol, 1.1 eq), dry. DCM (5mL), acetic acid (8  $\mu\text{L}$ , 0.13 mmol, 1.1 eq) and  $\text{BH(OAc)}_3$  (38.6 mg, 0.18 mmol, 1.50 eq) were used to gain 25.9 mg (0.09 mmol) of a slight pink, viscous oil after workup.

The crude was solved in MeCN/H<sub>2</sub>O/DMSO (1:1:1, 2 mL) and purified via prep. HPLC in 3 runs (5-50% MeCN in 30 min) to obtain 9.63 mg (0.032 mmol, 27%) of the product as a white solid.

**LC-MS:** Column: Phenomenex Luna C18(2), gradient: MeCN/H<sub>2</sub>O + 0.05 % HCOOH, 5 % MeCN increase to 100% MeCN in 5.1 min, flow rate: 0.6 mL/min,  $t_R = 2.07$ ,  $m/z = 298.4$  ( $[\text{M}+\text{H}]^+$ ).

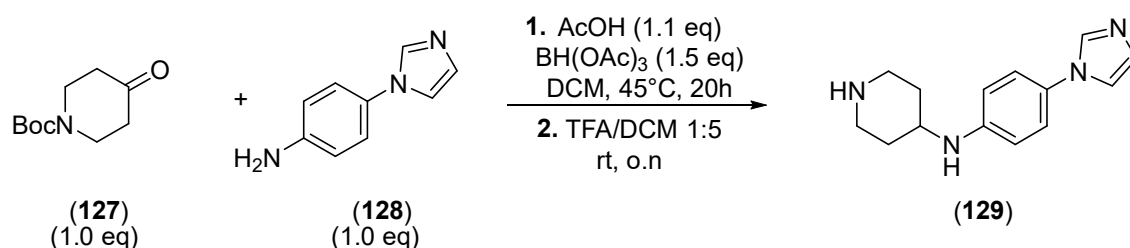
**HRMS:**  $m/z$  ( $[\text{M}+\text{H}]^+$ ), calculated: 298.1668, found: 298.1651



**<sup>1</sup>H-NMR** (500 MHz, dms<sub>o</sub>-d<sub>6</sub>,  $\delta$  in ppm): 8.02 (d,  $^3J_{2,3} = 2.6$  Hz, 1H, H-2), 7.76 (d,  $^3J_{3,2} = 2.5$  Hz, 1H, H-3), 7.05 (t,  $^3J_{13,12} = ^3J_{13,14} = 7.8$  Hz, 2H, H-13), 6.60 (d,  $^3J_{12,13} = 7.9$  Hz, 2H, H-12), 6.50 (t,  $^3J_{14,13} = 7.2$  Hz, 1H, H-14), 6.44 (br.s, 2H, Ar-NH<sub>2</sub>), 5.50 (d,  $^3J_{\text{NH},8} = 8.1$  Hz, 1H, NH), 4.35 (d,  $^2J = 13.2$  Hz, 1H, H-6a), 3.64 (d,  $^2J = 13.5$  Hz, 1H, H-10a), 3.57-3.46 (m, 1H, H-8), 3.18 (t,  $^2J = 11.5$  Hz, 1H, H-10b), 3.07 (t,  $^2J = 11.3$  Hz, 1H, H-6b), 2.01 (d,  $^2J = 11.3$  Hz, 1H, H-7a), 1.87 (d,  $^2J = 11.4$  Hz, 1H, H-9a), 1.45-1.29 (m, 2H, H-7b, H-9b).

**<sup>13</sup>C-NMR** (126 MHz, dms<sub>o</sub>-d<sub>6</sub>,  $\delta$  in ppm): 164.96 (C-5), 153.25 (C-1), 167.67 (C-11), 143.30 (C-2), 133.47 (C-4), 130.65 (C-3), 128.94 (C-13), 115.55 (C-14), 112.47 (C-12), 48.52 (C-8), 45.14 (C-10), 40.27 (C-6), 32.23 (C-7), 31.28 (C-9).

### N-(4-(1H-imidazol-1-yl)phenyl)piperidin-4-amine (129)

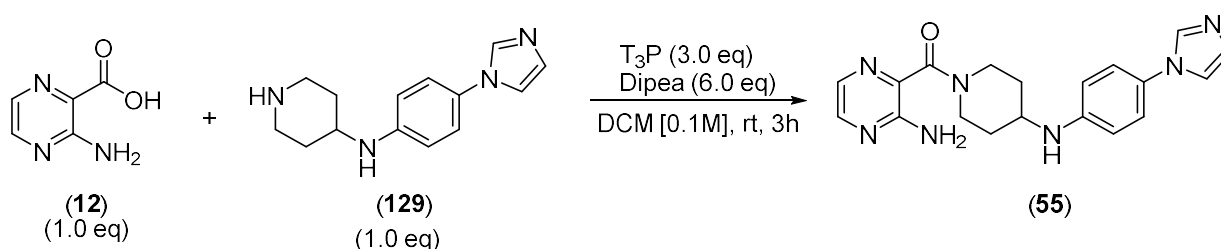


According to **standard procedure 3**, tert-butyl 4-oxopiperidine-1-carboxylate ((**127**), 100.1 mg, 0.50 mmol, 1.0 eq), 4-(1H-imidazol-1-yl)aniline ((**128**), 71.5 mg, 0.55 mmol, 1.1 eq), dry. DCM (5mL, [0.1M]), acetic acid (32  $\mu$ L, 0.55 mmol, 1.1 eq) and  $\text{BH}(\text{OAc})_3$  (159.5 mg, 0.75 mmol, 1.50 eq) were used to gain a yellow oil after workup.

Then the Boc group was cleaved according to **standard procedure 2** to gain the free amine which was solved in MeCN/H<sub>2</sub>O/DMSO (1:1:1, 2mL) and purified via flash. prep. HPLC in 1 run (5-50% MeCN in 30 min) to obtain 89.1 mg (0.37 mmol, 74%) of the product as a white solid.

**LC-MS:** Column: Phenomenex Luna C18(2), gradient: MeCN/H<sub>2</sub>O + 0.05 % HCOOH, 5 % MeCN increase to 100% MeCN in 5.1 min, flow rate: 0.6 mL/min,  $t_R = 0.69$ ,  $m/z = 243.2$  ( $[\text{M}+\text{H}]^+$ ).

**(4-((4-(1H-imidazol-1-yl)phenyl)amino)piperidin-1-yl)(3-aminopyrazin-2-yl)methanone**  
(**55**)

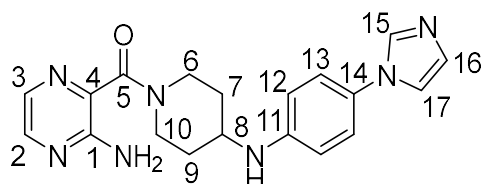


According to **standard procedure 1**, 3-aminopyrazine-2-carboxylic acid ((**12**), 52.1 mg, 0.37 mmol, 1.0 eq), N-(4-(1H-imidazol-1-yl)phenyl)piperidin-4-amine ((**129**), 89.1 mg, 0.37 mmol, 1.0 eq), dry. DCM (5 mL), Dipea (0.39 mL, 6.0 eq) and  $\text{T}_3\text{P}$  (50% in EtOAc, 0.71 mL, 3.0 eq) were used to gain 82.3 mg (90% pure) of a yellow oil after workup.

The crude oil was solved in MeCN/H<sub>2</sub>O/DMSO (1:1:1, 3 mL) and purified via prep. HPLC in two runs (5-50% MeCN in 30 min) to obtain 14.73 mg (0.04 mmol, 11%) of the product as an beige solid.

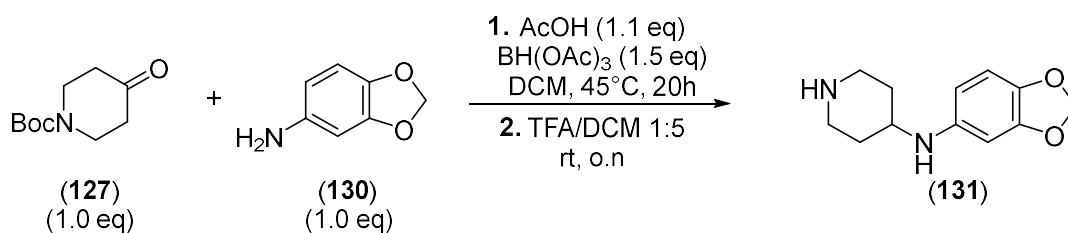
**LC-MS:** Column: Phenomenex Luna C18(2), gradient: MeCN/H<sub>2</sub>O + 0.05 % HCOOH, 5 % MeCN increase to 100% MeCN in 5.1 min, flow rate: 0.6 mL/min,  $t_R = 1.68$ ,  $m/z = 364.3$  ( $[\text{M}+\text{H}]^+$ ).

**HRMS:**  $m/z$  ( $[\text{M}+\text{H}]^+$ ), calculated: 364.1886, found: 364.1870



**<sup>1</sup>H-NMR** (500 MHz,  $\text{dms}\text{-d}_6$ ,  $\delta$  in ppm): 8.02 (d,  $^3J_{2,3} = 2.6\text{Hz}$ , 1H, H-2), 8.00 (s, 1H, H-17), 7.76 (d,  $^3J_{3,2} = 2.6\text{Hz}$ , 1H, H-3), 7.51 (s, 1H, H-16), 7.28 (d,  $^3J_{13,12} = 8.8\text{Hz}$ , 2H, H-13), 7.04 (s, 1H, H-15), 6.71 (d,  $^3J_{12,13} = 8.8\text{Hz}$ , 2H, H-12), 6.45 (s, 2H, Ar-NH<sub>2</sub>), 5.81 (br.s, 1H, NH), 4.36 (d,  $^2J = 13.2\text{Hz}$ , 1H, H-6a), 3.65 (d,  $^2J = 13.6\text{Hz}$ , 1H, H-10a), 3.62-3.53 (m, 1H, H-8), 3.20 (t,  $^2J = 11.2\text{Hz}$ , 1H, H-10b), 3.09 (t,  $^2J = 10.9\text{Hz}$ , H6b), 2.03 (d,  $^2J = 10.9\text{Hz}$ , 1H, H-7a), 1.90 (d,  $^2J = 10.9\text{Hz}$ , 1H, H-9a), 1.49-1.32 (m, 2H, H-7a, H-7<sub>b</sub>).

### N-(benzo[d][1,3]dioxol-5-yl)piperidin-4-amine (131)

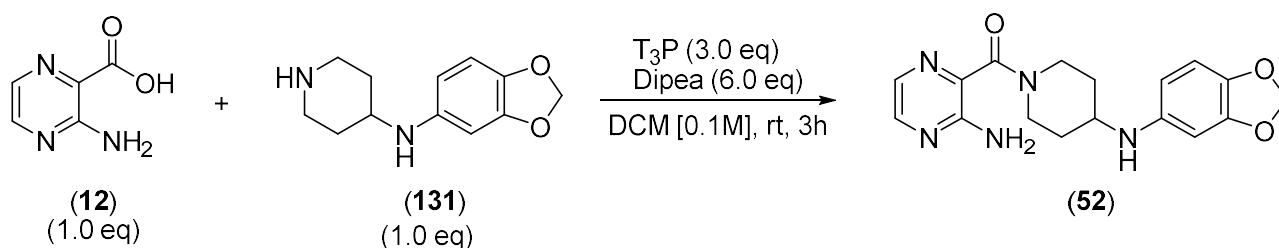


According to **standard procedure 3**, tert-butyl 4-oxopiperidine-1-carboxylate ((**127**), 200.4 mg, 1.00 mmol, 1.0 eq), benzo[d][1,3]dioxol-5-amine ((**130**), 156.4 mg, 1.10 mmol, 1.1 eq), dry. DCM (5mL, [0.2M]), acetic acid (65  $\mu$ L, 1.10 mmol, 1.1 eq) and BH(OAc)<sub>3</sub> (319.0 mg, 1.50mmol, 1.50 eq) were used to gain 303.8 mg of a brown viscous oil after workup.

Then the Boc group was cleaved according to **standard procedure 2** to gain the free amine which was solved in MeCN/H<sub>2</sub>O/DMSO (1:1:1, 2mL) and purified via flash. prep. HPLC in 1 run (0-20% MeCN in 20 min) to obtain 194.4 mg (0.88 mmol, 88%) of the product as a brown solid.

Column: Phenomenex Luna C18(2), gradient: MeCN/H<sub>2</sub>O + 0.05 % HCOOH, 5 % MeCN increase to 100% MeCN in 7 min, flow rate: 0.6 mL/min,  $t_R$  = 0.68,  $m/z$  = 221.2 ([M+H]<sup>+</sup>).

### (3-aminopyrazin-2-yl)(4-(benzo[d][1,3]dioxol-5-ylamino)piperidin-1-yl)methanone (52)

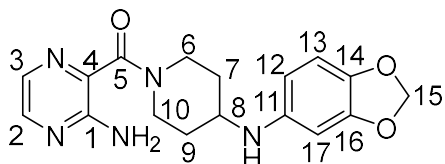


According to **standard procedure 1**, 3-aminopyrazine-2-carboxylic acid ((**12**), 122.4 mg, 0.88 mmol, 1.0 eq), N-(benzo[d][1,3]dioxol-5-yl)piperidin-4-amine ((**131**), 194.4 mg, 0.88 mmol, 1.0 eq), dry. DCM (10 mL), Dipea (0.92 mL, 6.0 eq) and T<sub>3</sub>P (50% in EtOAc, 1.70 mL, 3.0 eq) were used to gain 270.9 mg of a black oil after workup.

The crude oil was solved in MeCN/H<sub>2</sub>O/DMSO (1:1:1, 3 mL) and purified via prep. HPLC in 4 runs (5-50% MeCN in 30 min) to obtain 32.13 mg (0.09 mmol, 11%) of the product as a brown solid.

**LC-MS:** Column: Phenomenex Luna C18(2), gradient: MeCN/H<sub>2</sub>O + 0.05 % HCOOH, 5 % MeCN increase to 100% MeCN in 5.1 min, flow rate: 0.6 mL/min,  $t_R$  = 1.81,  $m/z$  = 342.2 ([M+H]<sup>+</sup>).

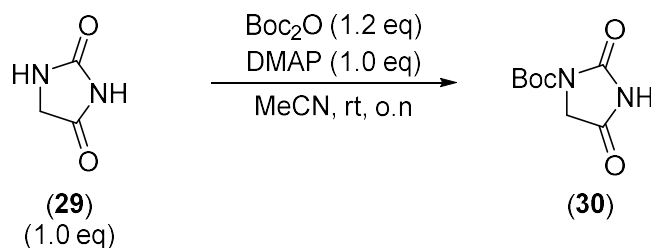
**HRMS:**  $m/z$  ([M+H]<sup>+</sup>), calculated: 342.1566, found: 342.1549



**<sup>1</sup>H-NMR** (500 MHz, dms<sub>o</sub>-d<sub>6</sub>, δ in ppm): 8.02 (d, <sup>3</sup>J<sub>2,3</sub> = 2.5 Hz, 1H, H-2), 7.75 (d, <sup>3</sup>J<sub>3,2</sub> = 2.5 Hz, 1H, H-3), 6.65 (d, <sup>3</sup>J<sub>13,12</sub> = 8.3 Hz, 1H, H-13), 6.43 (s, 2H, Ar-NH<sub>2</sub>), 6.34 (s, 1H, H-17), 6.06 (d, <sup>3</sup>J<sub>12,13</sub> = 7.5 Hz, 1H, H-12), 5.82 (s, 2H, H-15), 4.34 (d, <sup>2</sup>J = 13.1 Hz, 1H, H-6a), 3.63 (d, <sup>2</sup>J = 13.5 Hz, 1H, H-10a), 3.49-3.37 (m, 1H, H-8), 3.15 (t, <sup>2</sup>J = 11.4 Hz, 1H, H-10b), 3.03 (t, <sup>2</sup>J = 11.1 Hz, H6b), 1.99 (d, <sup>2</sup>J = 11.2 Hz, 1H, H-7a), 1.85 (d, <sup>2</sup>J = 11.4 Hz, 1H, H-9a), 1.41-1.25 (m, 2H, H-7a, H-7<sub>b</sub>).

**<sup>13</sup>C-NMR** (126 MHz, dms<sub>o</sub>-d<sub>6</sub>, δ in ppm): 164.95 (C-5), 153.25 (C-1), 147.85 (C-16), 143.30 (C-2), 138.10 (C-11), 133.46 (C-14), 130.66 (C-3), 108.56 (C-12), 104.34 (C-13), 100.00 (C-15), 95.79 (C-17), 49.57 (C-8), 45.14 (C-10), 40.27 (C-6), 32.20 (C-7), 31.26 (C-9).

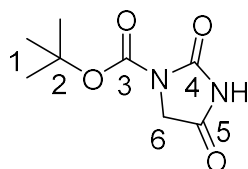
### Synthesis of tert-butyl 2,4-dioxoimidazolidine-1-carboxylate (**30**)



According to **general procedure 5**, Hydantoin (**(29)**, 999.7 mg, 9.99 mmol, 1.0 eq), DMAP (1211.6 mg, 9.92, 0.99 eq), Boc<sub>2</sub>O (2610 mg, 11.96 mmol, 1.20 eq) and 25 mL MeCN were used to gain 776.4 mg of a yellow oily residue after workup.

The crude oil was solved in DCM, absorbed on a minimum amount of Isolute and purified via Combiflash (24 g SiO<sub>2</sub>, PE/EtOAc 6:4, rf = 0.4, product staining anisaldehyde on TLC) to gain 294.1 mg (1.47 mmol, 15%) of a white solid as the product.

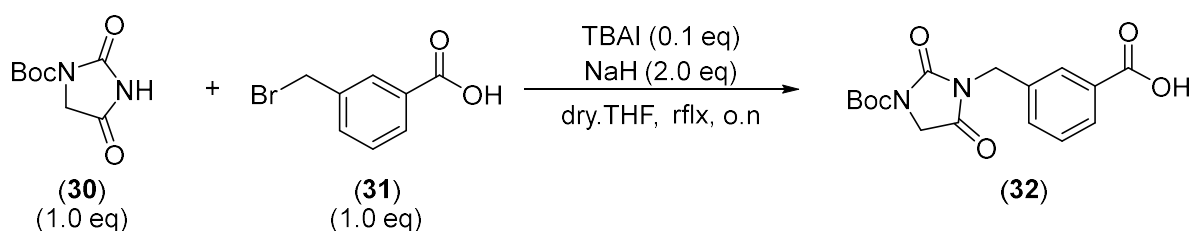
No LC-MS data, due to no UV-activity.



**<sup>1</sup>H-NMR** (500 MHz, CDCl<sub>3</sub>, δ in ppm): 4.28 (s, 2H, H-6), 1.55 (s, 9H, H-1).

**<sup>13</sup>C-NMR** (126 MHz, CDCl<sub>3</sub>, δ in ppm): 167.25 (C-5), 151.28 (C-4), 148.27 (C-3), 84.90 (C-2), 50.14 (C-6), 28.12 (C-1).

## Synthesis of 3-((3-(tert-butoxycarbonyl)-2,5-dioximidazolidin-1-yl)methyl)benzoic acid (32)

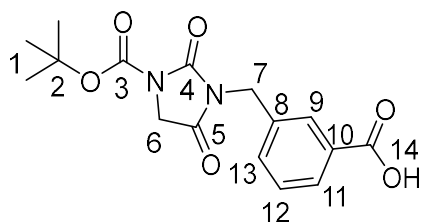


According to **general procedure 6**, Boc-Hydantoin (**(30)**, 604.6 mg, 3.02 mmol, 1.0 eq), 3-(bromomethyl)benzoic acid (**(31)**, 95% pure, 680.3 mg, 3.01 mmol, 1.0 eq), TBAI (110.6 mg, 0.30 mmol, 0.1 eq), NaH (60%, 248.7 mg, 6.22 mmol, 2.06 eq) and THF (40 mL) were used to gain 1260.5 mg of a yellow oil as the crude product.

The crude oil was solved in DCM, absorbed on a minimum amount of Isolute and purified via Combiflash (24 g SiO<sub>2</sub>, 0-100% EtOAc + 0.5 % AcOH) to gain 669.5 mg of an off-white solid, which contained 20% impurities according to NMR, but came as one peak in combi-flash.

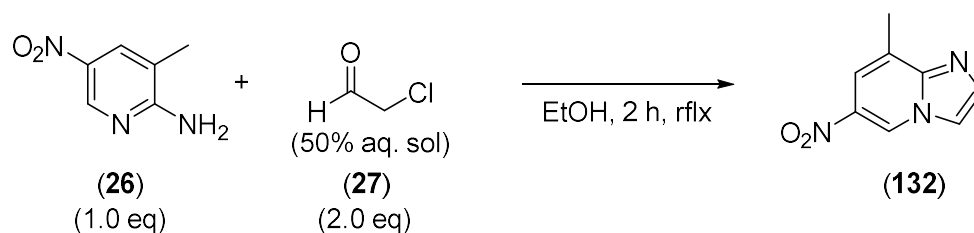
To further purify the product, it was solved in MeCN/H<sub>2</sub>O and purified via prep. Flash (reverse phase, 5-100% MeCN in H<sub>2</sub>O in 30 min, 3 runs) to gain 183 mg (0.55 mmol, 18%) of a white fluffy solid after drying on the Lyo overnight.

**LC-MS:** Column: Phenomenex Luna C18(2), gradient: MeCN/H<sub>2</sub>O + 0.05 % HCOOH, 5 % MeCN increase to 100% MeCN in 5.1 min, flow rate: 0.6 mL/min, t<sub>R</sub> = 2.90, m/z = 235.2 ([M-Boc]<sup>+</sup>).



**<sup>1</sup>H-NMR** (500 MHz, dms<sub>o</sub>-d<sub>6</sub>, δ in ppm): 13.05 (COOH), 7.89 (s, 1H, H-9), 7.86 (d, <sup>3</sup>J = 7.7 Hz, 1H, H-11), 7.56 (d, <sup>3</sup>J = 7.7 Hz, 1H, H-13), 7.47 (t, <sup>3</sup>J<sub>12,11</sub> = <sup>3</sup>J<sub>12,13</sub> = 7.7 Hz, 1H, H-12), 4.62 (s, 1H, H-7), 4.29 (s, 1H, H-6), 1.47 (s, 9H, H-1).

## Synthesis of 8-methyl-6-nitroimidazo[1,2-a]pyridine (132)

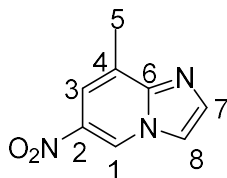


A 100 mL single neck flask, equipped with a reflux condenser was loaded with 3-methyl-5-nitropyridin-2-amine (**(26)**, 460.9 mg, 3.01 mmol, 1.0 eq), which was suspended in EtOH (100 mL). Then a 50 wt% aq. solution of (**(27)**), 1 mL, 500mg, 6.37 mmol, 2.12 eq) was added

dropwise. Subsequently the reaction mixture was heated to reflux, after which the suspension turned clear. After 2 h LC-MS reaction control confirmed full conversion.

The solvents were removed under reduced pressure, to obtain 740.3 mg of a brown solid, which still contained some EtOH and water but was used as such in the next reaction step without further drying or purification.

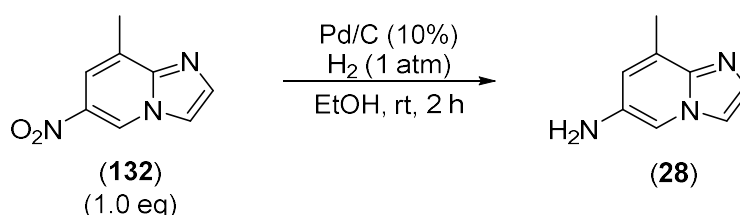
**LC-MS:** Column: Phenomenex Luna C18(2), gradient: MeCN/H<sub>2</sub>O + 0.05 % HCOOH, 5 % MeCN increase to 100% MeCN in 7 min, flow rate: 0.6 mL/min,  $t_R$  = 2.80,  $m/z$  = 178.18 ([M+H]<sup>+</sup>).



**<sup>1</sup>H-NMR** (500 MHz, dms<sub>o</sub>-d<sub>6</sub>,  $\delta$  in ppm): 9.94 (d,  $^4J_{1,3}$  = 1.2 Hz, 1H, H-1), 8.38 (d,  $^4J_{3,1}$  = 1.2 Hz, 1H, H-3), 8.23 (br.s, 1H, H-7 or H-8), 8.15 (br.s, 1H, H-7 or H-8), 2.65 (s, 3H, H-5).

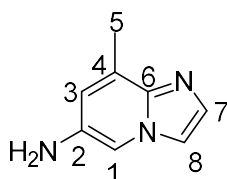
**<sup>13</sup>C-NMR** (126 MHz, dms<sub>o</sub>-d<sub>6</sub>,  $\delta$  in ppm): 138.25 (q.C), 131.60 (q.C), 126.73 (C-H), 125.21 (q.C), 117.54 (CH), 16.35 (C-5).

### Synthesis of 8-methylimidazo[1,2-a]pyridin-6-amine (28)



8-methyl-6-nitroimidazo[1,2-a]pyridine ((**132**), 3.0 mmol, 1.0 eq) was placed in a 100 mL single neck flask and was dissolved in EtOH (30 mL). The flask was closed by use of a septa, and the reaction mixture was degassed via Ar bubbling (10 min). Then an H<sub>2</sub> atmosphere (balloon, 1 atm) was applied and the mixture stirred for 2 h after which LC-MS confirmed full conversion. The crude mixture was filtered over Celite and washed with EtOH to gain 377.9 mg (2.57 mmol, 86%) of the desired product as a dark brown solid which was used without further purification, since NMR indicated high purity (>95 %)

**LC-MS:** Column: Phenomenex Luna C18(2), gradient: MeCN/H<sub>2</sub>O + 0.05 % HCOOH, 5 % MeCN increase to 100% MeCN in 7 min, flow rate: 0.6 mL/min,  $t_R$  = 0.53 min,  $m/z$  = 148.19 ([M+H]<sup>+</sup>).

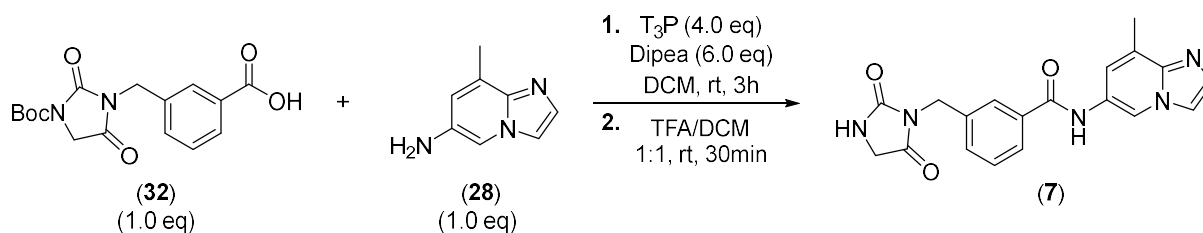




**<sup>1</sup>H-NMR** (500 MHz, dms<sub>o</sub>-d<sub>6</sub>, δ in ppm): 8.16 (d, <sup>3</sup>J<sub>7,8</sub> = 2.0 Hz, 1H, H-7 or H-8), 8.02 (d, <sup>3</sup>J<sub>7,8</sub> = 2.0 Hz, 1H, H-7 or H-8), 7.81 (d, <sup>4</sup>J<sub>1,3</sub> = 1.6 Hz, 1H, H-1), 7.22 (s, 1H, H-3), 5.65 (br.s, 2H, NH<sub>2</sub>), 2.48 (s, 3H, H-5).

**<sup>13</sup>C-NMR** (126 MHz, dms<sub>o</sub>-d<sub>6</sub>, δ in ppm): 140.15 (q.C), 134.34 (q.C), 125.58 (CH), 122.12 (CH), 122.10 (q.C), 114.83 (CH), 106.14 (CH), 15.98 (C-5).

### Synthesis of 3-((2,5-dioxoimidazolidin-1-yl)methyl)-N-(8-methylimidazo[1,2-a]pyridin-6-yl)benzamide (7)

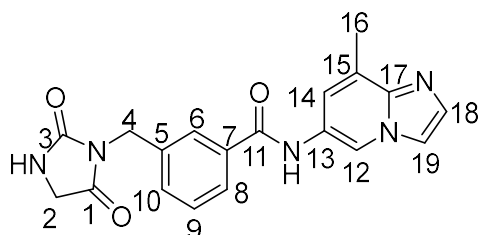


According to **standard procedure 1**, 8-methylimidazo[1,2-a]pyridin-6-amine (**(28)**, 49.1 mg, 0.33 mmol, 1.0 eq), 3-((3-(tert-butoxycarbonyl)-2,5-dioxoimidazolidin-1-yl)methyl)benzoic acid (**(32)**, 109.3 mg, 0.33 mmol, 1.0 eq), Dipea (340 μL, 2.0 mmol, 6.0 eq), T<sub>3</sub>P (50% in EtOAc, 820 μL, 1.3 mmol, 4.0 eq) and DCM (6 mL, [0.05M]) were used to gain 187.5 mg of a brown oil after 2 h reaction time and work-up.

According to **standard procedure 2**, DCM (7 mL) and TFA (3 mL) were used to gain the free amine in 90% purity on the LC-MS.

To further purify the product, it was solved in MeCN/H<sub>2</sub>O and purified via prep. HPLC (reverse phase, 5-50% MeCN in H<sub>2</sub>O in 30 min, 3 runs) to gain 12.6 mg (0,035 mmol, 11%) of an off-white fluffy solid after drying on the Lyo overnight.

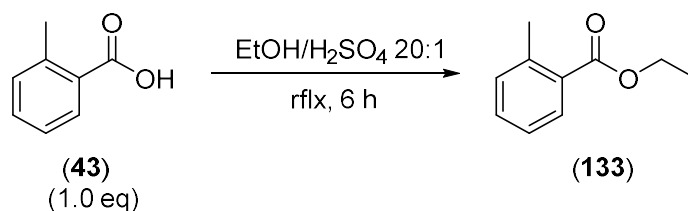
**LC-MS:** Column: Phenomenex Luna C18(2), gradient: MeCN/H<sub>2</sub>O + 0.05 % HCOOH, 5 % MeCN increase to 100% MeCN in 5.1 min, flow rate: 0.6 mL/min, t<sub>R</sub> = 1.81 min, m/z = 364.3 [[M+H]<sup>+</sup>]



**<sup>1</sup>H-NMR** (500 MHz, dms<sub>o</sub>-d<sub>6</sub>, δ in ppm): 10.47 (s, 1H, Amide-NH), 9.30 (s, 1H, H-12), 8.22-8.12 (m, 2H, H-18, H-19), 7.89 (d, <sup>3</sup>J = 7.7 Hz, 1H, H-8), 7.85 (s, 1H, H-6), 7.74 (s, 1H, Hydantoin-NH), 7.55-7.48 (m, 2H, H-9, H-10), 7.45 (1H, s, H-14), 4.62 (s, 1H, H-4), 4.01 (s, 1H, H-2), 2.53 (s, 3H, H-16).

**<sup>13</sup>C-NMR** (126 MHz, dms<sub>o</sub>-d<sub>6</sub>, δ in ppm): 172.03 (C-1), 165.62 (C-11), 157.33 (C-3), 141.02 (C-5), 137.30 (C-13), 134.44 (C-18), 130.86 (C-10), 129.60 (C-15), 128.71 (C-9), 127.14 (C-14), 126.85 (C-6), 126.61 (C-8), 124.91 (C-17), 121.99 (C-14), 115.98 (C-12), 115.17 (C-19), 46.08 (C-2), 40.86 (C-4), 16.45 (C-16).

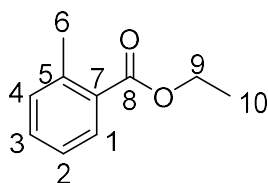
### Synthesis of ethyl 2-methylbenzoate (**133**)



In a 100 mL single neck flask, equipped with a reflux condenser, 2-methylbenzoic acid (**(43)**, 1362.3 mg, 10.0 mmol, 1.0 eq) was solved in EtOH (10 mL) and H<sub>2</sub>SO<sub>4</sub> (95% aq., 0.5 mL). The mixture was refluxed for 6 h, after which LC-MS confirmed full conversion. The EtOH was removed under reduced pressure. The remaining residue was extracted with water and EtOAc. After drying with anhydrous Na<sub>2</sub>SO<sub>4</sub> and removal of the solvent under reduced pressure, 1579 mg of a yellow liquid were received as the crude product.

The crude oil was solved in DCM, absorbed on a minimum amount of Isolute and purified via Combiflash (24 g SiO<sub>2</sub>, PE/EtOAc 95:5) to gain 1229.3 mg (7.49 mmol, 75%) of the pure product as an off white viscous liquid.

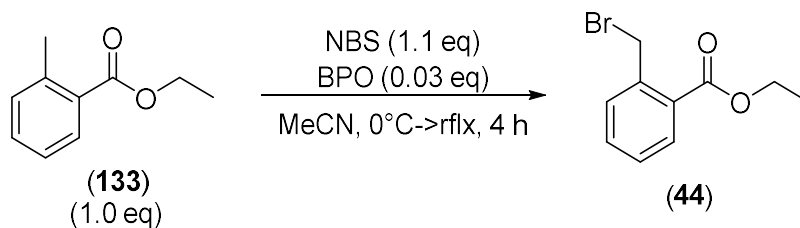
**LC-MS:** Column: Phenomenex Luna C18(2), gradient: MeCN/H<sub>2</sub>O + 0.05 % HCOOH, 5 % MeCN increase to 100% MeCN in 5.1 min, flow rate: 0.6 mL/min, t<sub>R</sub> = 3.64 min, m/z = 165.1 [[M+H]<sup>+</sup>]



**<sup>1</sup>H-NMR** (500 MHz, CDCl<sub>3</sub>, δ in ppm): 7.91 (dd, <sup>3</sup>J<sub>1,2</sub> = 7.8 Hz, <sup>4</sup>J<sub>1,2</sub> = 1.2 Hz, 1H, H-1), 7.89 (td, <sup>3</sup>J<sub>2,1</sub> = <sup>3</sup>J<sub>2,3</sub> = 7.6 Hz, <sup>4</sup>J<sub>2,4</sub> = 1.2 Hz, 1H, H-2), 7.27-7.21 (m, 2H, H-3, H-4), 4.36 (q, <sup>3</sup>J<sub>9,10</sub> = 7.1 Hz, 2H, H-9), 2.60 (s, 3H, H-6), 1.39 (t, <sup>3</sup>J<sub>10,9</sub> = 7.1 Hz, 3H, H-10).

**<sup>13</sup>C-NMR** (126 MHz, CDCl<sub>3</sub>, δ in ppm): 167.87 (C-8), 140.13 (C-5), 131.94 (C-1, C-3 or C-4), 131.77 (C-1, C-3 or C-4), 130.61 (C-1, C-3 or C-4), 130.11 (C-7), 125.80 (C-2), 60.83 (C-9), 21.84 (C-6), 14.48 (C-10).

### Synthesis of ethyl 2-(bromomethyl)benzoate (**44**)

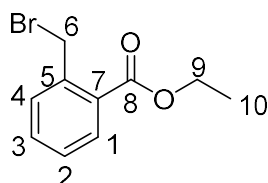


Ethyl 2-methylbenzoate (**(133)**, 7.5 mmol, 1.0 eq), NBS (1471.6 mg, 8.25 mmol, 1.1 eq) and BPO (36.3 mg, 0.15 mmol, 0.03 eq) were solved in MeCN (80 mL, [0.1 M]) in a 250 mL single

neck flask equipped with a reflux condenser. The mixture was refluxed for 4 h, after which LC-MS confirmed full conversion.

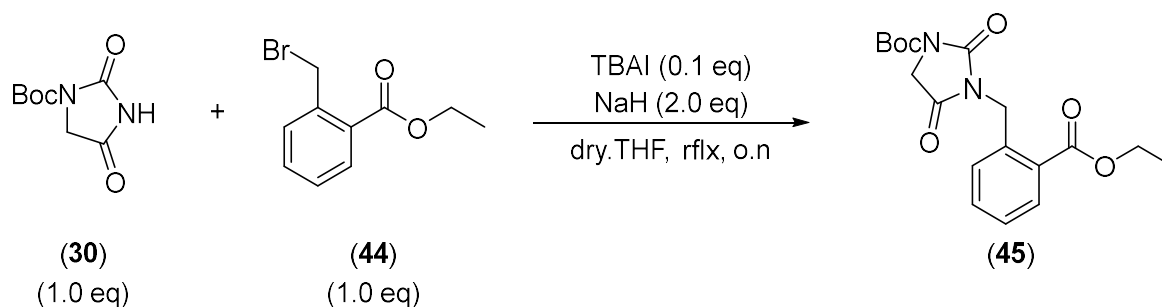
Then the acetonitrile was removed under reduced pressure and the crude was solved in a minimal amount of Et<sub>2</sub>O (30 mL). The solution was cooled to -78°C with an isopropanol/dry. Ice bath and the formed precipitate was filtrated off and discarded. After concentration of the filtrate in vacuo, 1069.7 mg (4.4 mmol, 59%, >90% pure) of an orange oil were gained as the desired product and used without further purification in the next step.

**LC-MS:** Column: Phenomenex Luna C18(2), gradient: MeCN/H<sub>2</sub>O + 0.05 % HCOOH, 5 % MeCN increase to 100% MeCN in 5.1 min, flow rate: 0.6 mL/min, t<sub>R</sub>= 3.69 min, m/z = 243.0/245.0 1:1 [[M+H]<sup>+</sup>]



**<sup>1</sup>H-NMR** (500 MHz, CDCl<sub>3</sub>, δ in ppm): 7.91 (d, <sup>3</sup>J<sub>1,2</sub> = 7.8 Hz, 1H, H-1), 7.52-7.43 (m, 2H, H-4, H-2), 7.37 (t, <sup>3</sup>J<sub>3,2</sub> = <sup>3</sup>J<sub>3,4</sub> = 7.0 Hz, 1H, H-3), 4.96 (s, 2H, H-6), 4.41 (q, <sup>3</sup>J<sub>9,10</sub> = 7.1 Hz, 2H, H-9), 1.43 (t, <sup>3</sup>J<sub>10,9</sub> = 7.1 Hz, 3H, H-10).

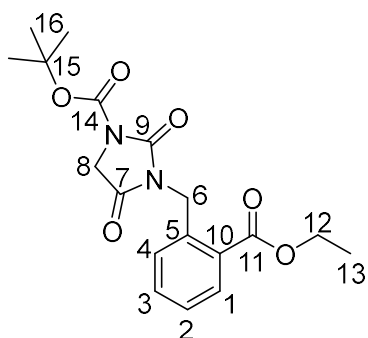
#### Synthesis of tert-butyl 3-(2-(ethoxycarbonyl)benzyl)-2,4-dioximidazolidine-1-carboxylate (**45**)



According to **standard procedure 6**, Boc-Hydantoin ((**30**), 212 mg, 1.06 mmol, 1.0 eq), ethyl 2-(bromomethyl)benzoate ((**44**), 90% pure, 271.1 mg, 1.06 mmol, 1.0 eq), TBAI (38.5 mg, 0.1 mmol, 0.1 eq), NaH (48 mg, 1.2 mmol, 1.13 eq) and dry. THF (10 mL) were used to gain, 413 mg of the crude product after work up.

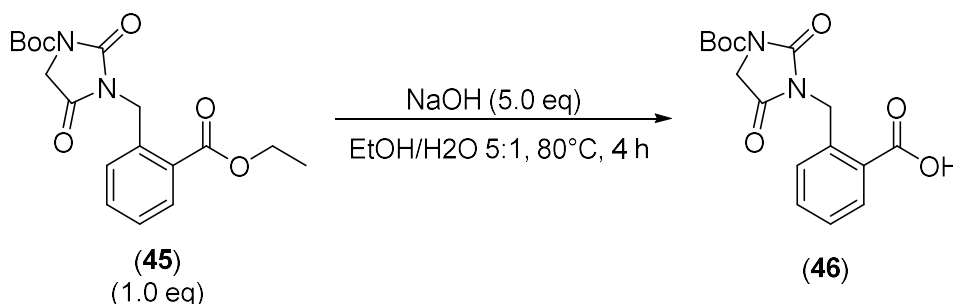
The crude oil was solved in DCM, absorbed on a minimum amount of Isolute and purified via Combiflash (24 g SiO<sub>2</sub>, Cy/EtOAc 8:2) to gain 189.9 mg (0.52 mmol, 52%) of the pure product as an white crystalline solid.

**LC-MS:** Column: Phenomenex Luna C18(2), gradient: MeCN/H<sub>2</sub>O + 0.05 % HCOOH, 5 % MeCN increase to 100% MeCN in 5.1 min, flow rate: 0.6 mL/min, t<sub>R</sub>= 3.56 min, m/z = 263.2 [[M-Boc+H]<sup>+</sup>]



**<sup>1</sup>H-NMR** (500 MHz, CDCl<sub>3</sub>, δ in ppm): 7.96 (dd, <sup>3</sup>J<sub>1,2</sub> = 7.8 Hz, <sup>4</sup>J<sub>1,2</sub> = 1.3 Hz, 1H, H-1), 7.46 (td, <sup>3</sup>J = 7.3 Hz, <sup>4</sup>J = 1.2 Hz, 1H, H-2 or H-3), 7.34 (t, <sup>3</sup>J = 7.5 Hz, 1H, H-2 or H-3), 7.21 (d, <sup>3</sup>J<sub>4,3</sub> = 7.8 Hz, 1H, H-4), 5.22 (s, 2H, H-6), 4.40 (q, <sup>3</sup>J<sub>12,13</sub> = 7.1 Hz, 2H, H-12), 4.29 (s, 2H, H-8), 1.56 (s, 9H, H-), 1.39 (t, <sup>3</sup>J<sub>13,12</sub> = 7.1 Hz, 3H, H-13).

### Synthesis of 2-((3-(tert-butoxycarbonyl)-2,5-dioxoimidazolidin-1-yl)methyl)benzoic acid (46)

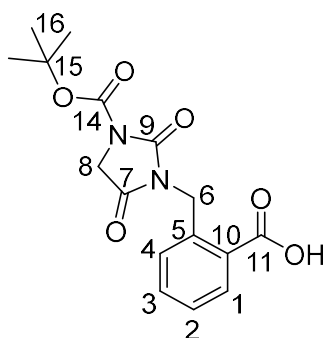


In a 50 mL single neck flask, tert-butyl 3-(2-(ethoxycarbonyl)benzyl)-2,4-dioxoimidazolidine-1-carboxylate ((**45**), 232.8 mg, 0.65 mmol, 1.0 eq) was suspended in EtOH. Subsequently NaOH (solved in 1 mL H<sub>2</sub>O, 129.4 mg, 3.2 mmol, 5.0 eq) was added, after which the reaction turned clear immediately. After stirring for 4 h at rt, LC-MS confirmed full conversion and formation of an unknown side product (30%).

After completed reaction, EtOH was removed under reduced pressure and the remaining aqueous layer was washed with EtOAc, which was discarded. The aqueous layer was acidified with 0.5 M aq. HCl solution to PH=5, but the corresponding free acid did not precipitate. Even after extraction with iPrOH/CHCl<sub>3</sub> 1:3 (3x), most of the product (90%) stayed in the aqueous phase, but the undesired side product was removed completely. The water was removed under reduced pressure.

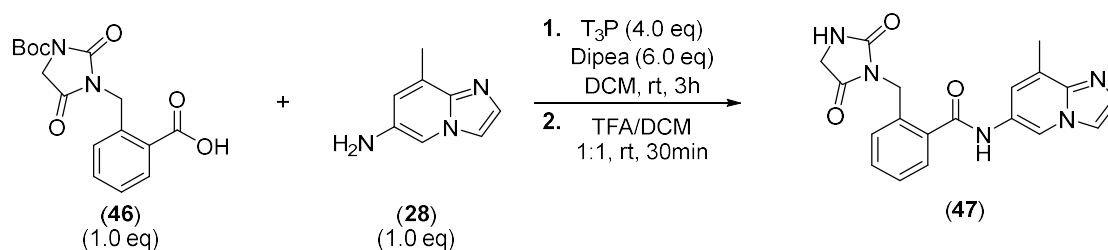
To further purify the product, it was solved in MeCN/H<sub>2</sub>O and purified via prep. Flash (reverse phase, 10-100% MeCN in H<sub>2</sub>O in 60 min, 2 runs) to gain 102.3 mg (0.31 mmol, 48%) of a white fluffy solid after drying on the Lyo overnight.

**LC-MS:** Column: Phenomenex Luna C18(2), gradient: MeCN/H<sub>2</sub>O + 0.05 % HCOOH, 5 % MeCN increase to 100% MeCN in 5.1 min, flow rate: 0.6 mL/min, t<sub>R</sub> = 1.80 min.



**<sup>1</sup>H-NMR** (500 MHz, dms<sub>o</sub>-d<sub>6</sub>, δ in ppm): 7.57 (d, <sup>3</sup>J<sub>1,2</sub> = 6.9 Hz, 1H, H-1), 7.21-7.07 (m, 3H, H-2, H-3, H-4), 4.37 (s, 2H, H-8), 3.29 (s, 2H, H-6), 2.54 (s, 9H, H-16).

### Synthesis of 2-((2,5-dioximidazolidin-1-yl)methyl)-N-(8-methylimidazo[1,2-a]pyridin-6-yl)benzamide (**47**)

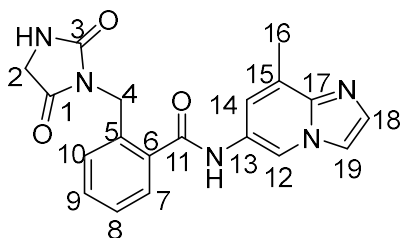


According to **standard procedure 1**, 8-methylimidazo[1,2-a]pyridin-6-amine (**28**), 44.3 mg, 0.30 mmol, 1.0 eq), 2-((3-(tert-butoxycarbonyl)-2,5-dioximidazolidin-1-yl)methyl)benzoic acid (**46**), 108.3 mg, 0.30 mmol, 1.0 eq), Dipea (320 μL, 1.80 mmol, 6.0 eq), T3P (50% in EtOAc, 300 μL, 0.47 mmol, 1.57 eq) and DCM (6 mL, [0.05M]) were used to gain 73.7 mg of a brown oil after 1 h reaction time at 0°C.

According to **standard procedure 2**, DCM (6 mL) and TFA (1 mL) were used to gain the free amine in 90% purity on the LC-MS

To further purify the product, it was solved in MeCN/H<sub>2</sub>O and purified via prep. HPLC (reverse phase, 5-50% MeCN in H<sub>2</sub>O in 30 min, 2 runs) to gain 5.5 mg (0,015 mmol, 5%) of a white fluffy solid after drying on the Lyo overnight.

**LC-MS:** Column: Phenomenex Luna C18(2), gradient: MeCN/H<sub>2</sub>O + 0.05 % HCOOH, 5 % MeCN increase to 100% MeCN in 5.1 min, flow rate: 0.6 mL/min, t<sub>R</sub> = 1.81 min, m/z = 364.2 [[M+H]<sup>+</sup>]

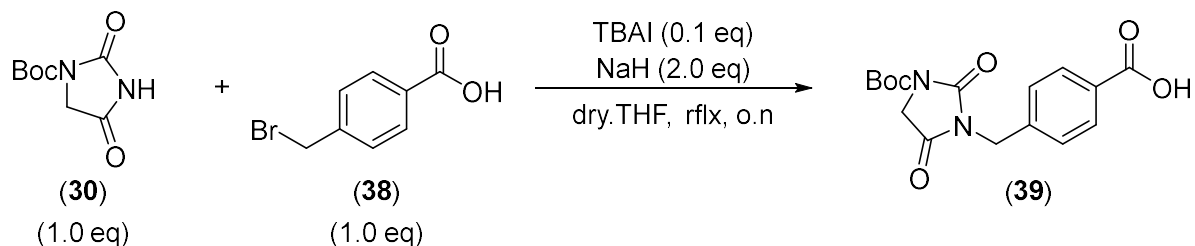


**<sup>1</sup>H-NMR** (500 MHz, dms<sub>o</sub>-d<sub>6</sub>, δ in ppm): 10.23 (s, 1H, Amide-NH), 9.23 (s, 1H, H-12), 8.23 (s, 1H, H-14), 8.91-7.82 (m, 2H, H-18, H-19), 7.45 (t, 3J = 7.7 Hz, 1H, H-8 or H-9), 7.45 (d, 3J =

7.5 Hz, 1H, H-7 or H-10), 7.35 (t, 3J = 7.5 Hz, 1H, H-8 or H-9), 7.31 (m, 1H, H-7 or H-10), 4.53 (d, 1H, H-4), 3.88 (d, 1H, H-2), 2.52 (s, 3H, H-16).

**<sup>13</sup>C-NMR** (126 MHz, dms<sub>o</sub>-d<sub>6</sub>, δ in ppm): 169.70 (C-1), 168.41 (C-11), 158.13(C-3), 141.91 (C-18), 134.82 (q.C), 132.01 (C-8 or C-9), 130.36 (C-19), 129.37 (C-7 or C-10), 128.58 (C-7 or C-10), 127.23 (q.C), 126.72 (q.C), 126.72 (C-8 or C-9), 124.37 (q.C), 122.86 (q.C), 115.59 (C-12), 114.91 (C-14), 43.52 (C-2), 41.70 (C-4), 16.25 (C-16).

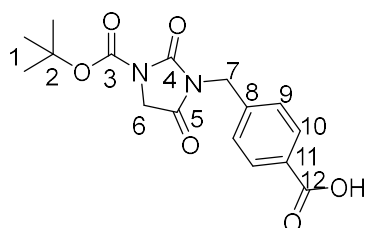
### Synthesis of 4-((3-(tert-butoxycarbonyl)-2,5-dioximidazolidin-1-yl)methyl)benzoic acid (39)



According to **general procedure 6**, Boc-Hydantoin ((30), 52.0 mg, 0.25 mmol, 1.0 eq), 4-(bromomethyl)benzoic acid ((38), 54.4 mg, 0.25 mmol, 1.0 eq), TBAI (10.0 mg, 0.025 mmol, 0.1 eq), NaH (60%, 20.2 mg, 0.5 mmol, 2.0 eq) and THF (4 mL) were used to gain 81.6 mg (0.24 mmol, quant.) of an off-white solid after 2.5 h at reflux and subsequent work-up.

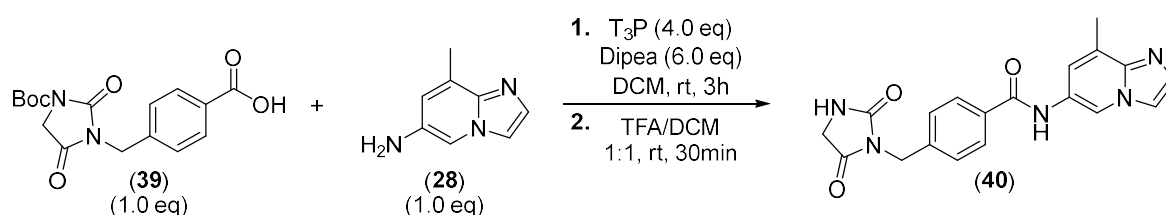
As NMR confirmed >90% purity, the crude was used in the next step, without further purification.

**LC-MS:** Column: Phenomenex Luna C18(2), gradient: MeCN/H<sub>2</sub>O + 0.05 % HCOOH, 5 % MeCN increase to 100% MeCN in 7 min, flow rate: 0.6 mL/min, t<sub>R</sub> = 3.56 min.



**<sup>1</sup>H-NMR** (500 MHz, dms<sub>o</sub>-d<sub>6</sub>, δ in ppm): 12.95 (s, 1H, COOH), 7.90 (d, <sup>3</sup>J<sub>10,9</sub> = 8.2 Hz, 1H, H-10), 7.42 (d, <sup>3</sup>J<sub>9,10</sub> = 8.2 Hz, 1H, H-9), 4.63 (s, 1H, H-7), 4.31 (s, 1H, H-6), 1.47 (s, 9H, H-1).

### Synthesis of 4-((2,5-dioximidazolidin-1-yl)methyl)-N-(8-methylimidazo[1,2-a]pyridin-6-yl)benzamide (40)

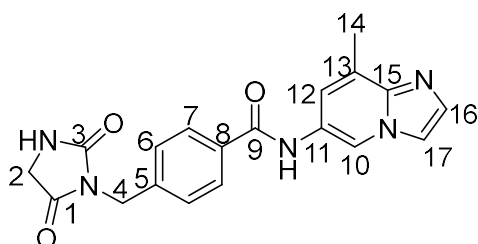


According to **standard procedure 1**, 8-methylimidazo[1,2-a]pyridin-6-amine ((**28**), 37.6 mg, 0.25 mmol, 1.0 eq), 4-((3-(tert-butoxycarbonyl)-2,5-dioxoimidazolidin-1-yl)methyl)benzoic acid ((**39**), 81.6 mg, 0.25 mmol, 1.0 eq), Dipea (260  $\mu$ L, 1.50 mmol, 6.0 eq), T3P (50% in EtOAc, 640  $\mu$ L, 1.00 mmol, 4.0 eq) and DCM (10 mL, [0.025M]) were used to gain 79 mg of a brown oil after 4 h reaction time at rt.

According to **standard procedure 2**, DCM (12 mL) and TFA (2 mL) were used to gain the free amine in 80% purity on the LC-MS

To further purify the product, it was solved in MeCN/H<sub>2</sub>O and purified via prep. HPLC (reverse phase, 10-50% MeCN in H<sub>2</sub>O in 50 min, 2 runs) to gain 6.93 mg (0,019 mmol, 8%) of a white fluffy solid after drying on the Lyo overnight.

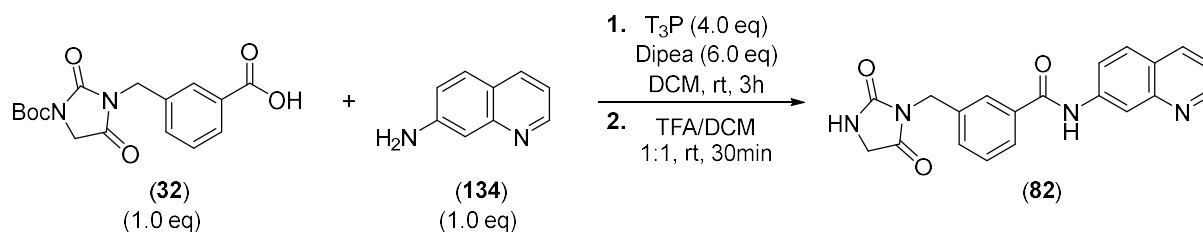
**LC-MS:** Column: Phenomenex Luna C18(2), gradient: MeCN/H<sub>2</sub>O + 0.05 % HCOOH, 5 % MeCN increase to 100% MeCN in 5.1 min, flow rate: 0.6 mL/min,  $t_R$  = 1.79 min,  $m/z$  = 364.2 [[M+H]<sup>+</sup>]



**<sup>1</sup>H-NMR** (500 MHz, dms<sub>o</sub>-d<sub>6</sub>,  $\delta$  in ppm): 10.68 (s, 1H, Amide-NH), 9.55 (s, 1H, H-10), 8.43 (s, 1H, H-16), 8.20 (s, 1H, H-17), 8.14 (br.s, 1H, Hydantoin-NH), 7.96 (d, <sup>3</sup>J<sub>7,6</sub> = 8.2 Hz, 1H, H-7), 7.82 (s, 1H, H-12), 7.45 (d, <sup>3</sup>J<sub>6,7</sub> = 8.1 Hz, 1H, H-6), 4.63 (s, 2H, H-4), 4.02 (s, 2H, H-2), 2.58 (s, 3H, H-14).

**<sup>13</sup>C-NMR** (126 MHz, dms<sub>o</sub>-d<sub>6</sub>,  $\delta$  in ppm): 170.05 (C-1), 165.78 (C-9), 157.31 (C-3), 141.06 (C-5), 137.62 (C-15), 132.84 (C-8), 129.70 (C-16), 128.04 (C-7), 127.50 (C-6), 126.41 (C-11), 124.05 (C-13), 122.92 (C-12), 116.41 (C-10 or C-17), 116.33 (C-10 or C-17), 46.12 (C-2), 40.78 (C-4), 16.10 (C-16).

### Synthesis of 3-((2,5-dioxoimidazolidin-1-yl)methyl)-N-(quinolin-7-yl)benzamide (**82**)

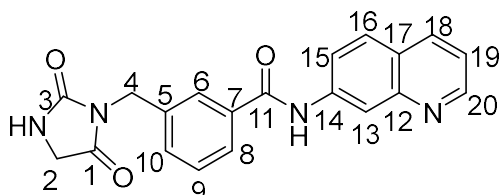


According to **standard procedure 1**, quinolin-7-amine ((**134**), 8.5 mg, 0.06 mmol, 1.18 eq), 3-((3-(tert-butoxycarbonyl)-2,5-dioxoimidazolidin-1-yl)methyl)benzoic acid ((**32**), 17.2 mg, 0.05 mmol, 1.0 eq), Dipea (50  $\mu$ L, 0.3 mmol, 6.0 eq), T3P (50% in EtOAc, 130  $\mu$ L, 1.3 mmol, 4.0 eq) and DCM (2 mL, [0.025M]) were used to gain 18.7 mg of an orange oil after 17 h reaction time and work-up.

According to **standard procedure 2**, DCM (3 mL) and TFA (0.5 mL) were used to gain the free amine in 95% purity on the LC-MS

To further purify the product, it was solved in MeCN/H<sub>2</sub>O and purified via prep. HPLC (reverse phase, 5-50% MeCN in H<sub>2</sub>O in 60 min, 2 runs) to gain 3.47 mg (0,01 mmol, 20%) of an off-white fluffy solid after drying on the Lyo overnight.

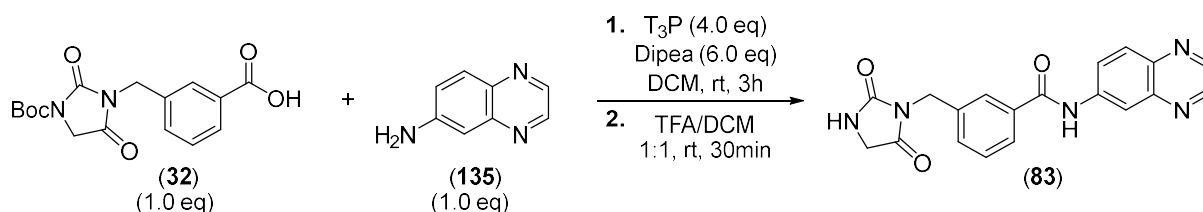
**LC-MS:** Column: Phenomenex Luna C18(2), gradient: MeCN/H<sub>2</sub>O + 0.05 % HCOOH, 5 % MeCN increase to 100% MeCN in 5.1 min, flow rate: 0.6 mL/min, t<sub>R</sub>= 1.94 min, m/z = 361.4 [[M+H]<sup>+</sup>).



**<sup>1</sup>H-NMR** (500 MHz, dms<sub>o</sub>-d<sub>6</sub>, δ in ppm): 10.68 (s, 1H, Amide-NH), 8.90 (d, <sup>3</sup>J<sub>20,19</sub> = 2.8 Hz, 1H, H-20), 8.61 (s, 1H, H-13), 8.38 (d, <sup>3</sup>J<sub>15,16</sub> = 8.0 Hz, 1H, H-16), 8.19 (s, 1H, Hydantoin-NH) 8.02-7.96 (m, 2H, H-8, H-18), 7.93 (d, <sup>3</sup>J<sub>16,15</sub> = 6.9 Hz, 1H, H-15), 7.88 (s, 1H, H-6), 7.57-7.46 (m, 3H, H-9, H-10, H-19), 4.65 (s, 1H, H-4), 4.02 (s, 1H, H-2).

**<sup>13</sup>C-NMR** (126 MHz, dms<sub>o</sub>-d<sub>6</sub>, δ in ppm): 172.05 (C-1), 165.98 (C-11), 157.36 (C-3), 150.46, 140.35 (C-5), 137.28, 135.05, 130.84 (C-10), 128.67 (C-9), 128.45, 127.0 (C-6 or C-8), 126.76 (C-6 or C-8), 124.74, 121.38, 120.27, 116.52, 46.09 (C-2), 40.87 (C-4).

### Synthesis of 3-((2,5-dioximidazolidin-1-yl)methyl)-N-(quinoxalin-6-yl)benzamide (**83**)



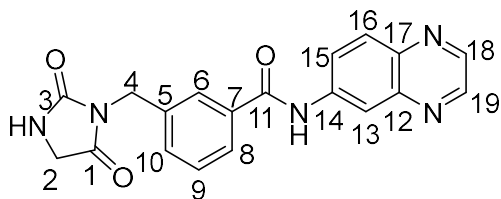
According to **standard procedure 1**, quinoxalin-6-amine ((**135**), 9.5 mg, 0.065 mmol, 1.3 eq), 3-((3-(tert-butoxycarbonyl)-2,5-dioximidazolidin-1-yl)methyl)benzoic acid ((**32**), 17.2 mg, 0.05 mmol, 1.0 eq), Dipea (50 μL, 0.3 mmol, 6.0 eq), T3P (50% in EtOAc, 130 μL, 1.3 mmol, 4.0 eq) and DCM (2 mL, [0.025M]) were used to gain 27.4 mg of a yellow solid after 18 h reaction at rt and work-up.

According to **standard procedure 2**, DCM (3 mL) and TFA (0.5 mL) were used to gain the free amine in 95% purity on the LC-MS

To further purify the product, it was solved in MeCN/H<sub>2</sub>O and purified via prep. HPLC (reverse phase, 5-50% MeCN in H<sub>2</sub>O in 60 min, 2 runs) to gain 5.02 mg (0,014 mmol, 28%) of a white fluffy solid after drying on the Lyo overnight.

**LC-MS:** Column: Phenomenex Luna C18(2), gradient: MeCN/H<sub>2</sub>O + 0.05 % HCOOH, 5 % MeCN increase to 100% MeCN in 5.1 min, flow rate: 0.6 mL/min, t<sub>R</sub>= 2.32 min, m/z = 362.2 [[M+H]<sup>+</sup>).

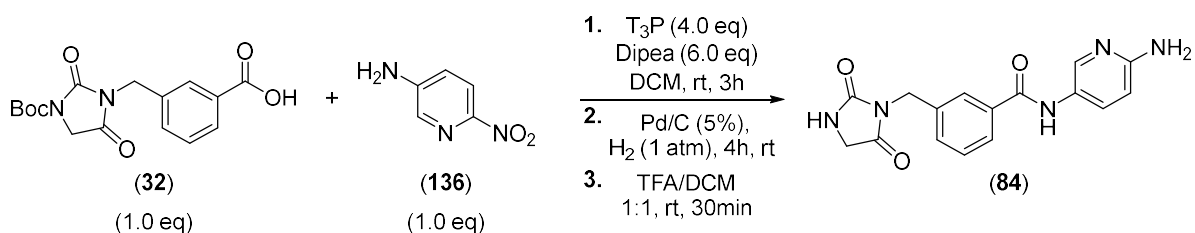




**<sup>1</sup>H-NMR** (500 MHz, dms<sub>o</sub>-d<sub>6</sub>, δ in ppm): 10.78 (s, 1H, Amide-NH), 8.90 (d, <sup>3</sup>J = 1.6 Hz, 1H, H-18 or H-19), 8.85 (d, <sup>3</sup>J = 1.7 Hz, 1H, H-18 or H-19), 8.67 (d, 4J=2.1 Hz, 1H, H-13), 8.19 (s, 1H, Hydantoin-NH), 8.18 (d, 3J = 2.2 Hz, 1H, H-15), 8.09 (d, 3J = 9.1 Hz, 1H, H-8), 7.94 (d, <sup>3</sup>J<sub>16,15</sub> = 6.9 Hz, 1H, H-15), 7.88 (s, 1H, H-6), 7.56-7.51 (m, 3H, H-9, H-10), 4.65 (s, 1H, H-4), 4.02 (s, 1H, H-2).

**<sup>13</sup>C-NMR** (126 MHz, dms<sub>o</sub>-d<sub>6</sub>, δ in ppm): 172.06 (C-1), 166.12 (C-11), 157.36 (C-3), 146.02, 144.24, 142.94, 140.42 (C-5), 139.39, 137.31, 134.90, 130.95 (C-10), 129.42, 128.71 (C-9), 127.02 (C-6 or C-8), 126.79 (C-6 or C-8), 124.67, 116.80, 46.10 (C-2), 40.87 (C-4).

### Synthesis of N-(6-aminopyridin-3-yl)-3-((2,5-dioxoimidazolidin-1-yl)methyl)benzamide (84)



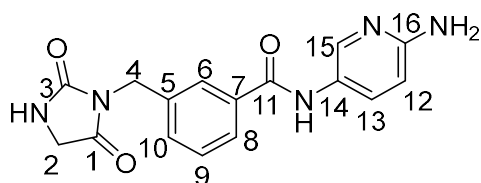
According to **standard procedure 1**, 6-nitropyridin-3-amine ((**136**), 8.5 mg, 0.06 mmol, 1.15 eq), 3-((3-(tert-butoxycarbonyl)-2,5-dioxoimidazolidin-1-yl)methyl)benzoic acid ((**32**), 16.6 mg, 0.05 mmol, 1.0 eq), Dipea (50 μL, 0.3 mmol, 6.0 eq), T3P (50% in EtOAc, 130 μL, 1.3 mmol, 4.0 eq) and DCM (2 mL, [0.025M]) were used to gain 23.6 mg of a yellow solid after 7 d reaction at rt (slow reaction, LC-MS control every 24 h) and work-up.

The crude product was solved in EtOH (3 mL), which was degassed using Ar (10 min, bubbling). Then Pd/C (5.4 mg, 0.0025 mmol, 0.1 eq) was added and a hydrogen atmosphere was applied by using a balloon (1 atm). After 3 h stirring at rt, LC-MS confirmed full conversion, after which the mixture was diluted with EtOH, filtered through a thick pad of Celite and washed with EtOH. Evaporation of the solvent gave 16.1 mg of the crude product as an orange solid.

According to **standard procedure 2**, DCM (5 mL) and TFA (1 mL) and the crude from the previous step were used to gain the free amine in 90% purity on the LC-MS

To further purify the product, it was solved in MeCN/H<sub>2</sub>O and purified via prep. HPLC (reverse phase, 5-50% MeCN in H<sub>2</sub>O in 30 min, 2 runs) to gain 3.27 mg (0.010 mmol, 20%) of a slight yellow solid after drying on the Lyo overnight.

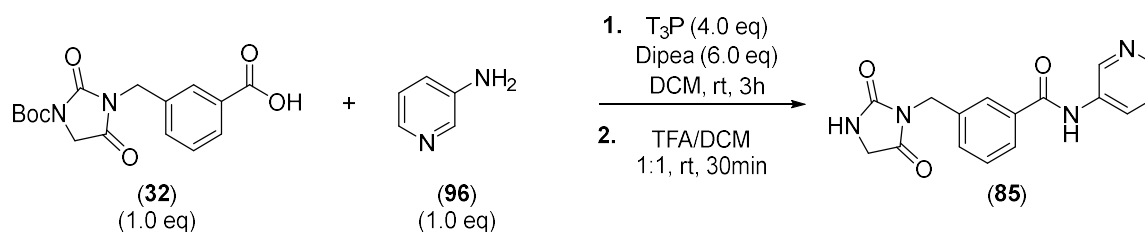
**LC-MS:** Column: Phenomenex Luna C18(2), gradient: MeCN/H<sub>2</sub>O + 0.05 % HCOOH, 5 % MeCN increase to 100% MeCN in 5.1 min, flow rate: 0.6 mL/min, t<sub>R</sub> = 1.66 min, m/z = 326.2 [[M+H]<sup>+</sup>]



**<sup>1</sup>H-NMR** (500 MHz, dms<sub>o</sub>-d<sub>6</sub>, δ in ppm): 10.46 (s, 1H, Amide-NH), 8.47 (s, 1H, H-15), 8.18 (s, 1H, Hydantoin-NH), 8.05 (d, <sup>3</sup>J<sub>13,12</sub> = 9.2 Hz, 1H, H-13), 7.86 (d, <sup>3</sup>J<sub>8,9</sub> = 6.4 Hz, 1H, H-8), 7.81 (s, 1H, H-6), 7.55-7.46 (m, 2H, H-9, H-10), 6.95 (d, <sup>3</sup>J<sub>12,13</sub> = 9.4 Hz, 1H, H-12), 4.61 (s, 1H, H-4), 4.00 (s, 1H, H-2).

**<sup>13</sup>C-NMR** (126 MHz, dms<sub>o</sub>-d<sub>6</sub>, δ in ppm): 172.06 (C-1), 165.44 (C-11), 157.35 (C-3), 152.27 (C-16), 137.50 (C-5), 137.35 (C-13), 134.20 (C-7), 131.00 (C-10), 128.76 (C-15, C-9), 126.82 (C-6), 126.55 (C-8), 125.77 (C-14), 112.77 (C-12), 46.10 (C-2), 40.87 (C-4).

### Synthesis of 3-((2,5-dioxoimidazolidin-1-yl)methyl)-N-(pyridin-3-yl)benzamide (**85**)

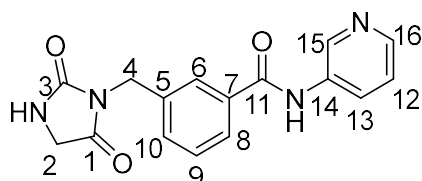


According to **standard procedure 1**, pyridin-3-amine (**96**), 5.3 mg, 0.05 mmol, 1.0 eq), 3-((3-(tert-butoxycarbonyl)-2,5-dioxoimidazolidin-1-yl)methyl)benzoic acid (**32**), 16.5 mg, 0.05 mmol, 1.0 eq), Dipea (50 μL, 0.3 mmol, 6.0 eq), T3P (50% in EtOAc, 130 μL, 1.3 mmol, 4.0 eq) and DCM (2 mL, [0.025M]) were used to gain 24.6 mg of an orange solid after 16 h reaction at rt and work-up.

According to **standard procedure 2**, DCM (3 mL) and TFA (0.5 mL) and the crude from the previous step were used to gain the free amine in 90% purity on the LC-MS

To further purify the product, it was solved in MeCN/H<sub>2</sub>O and purified via prep. HPLC (reverse phase, 5-50% MeCN in H<sub>2</sub>O in 30 min, 2 runs) to gain 7.21 mg (0,023 mmol, 46%) of a white fluffy solid after drying on the Lyo overnight.

**LC-MS:** Column: Phenomenex Luna C18(2), gradient: MeCN/H<sub>2</sub>O + 0.05 % HCOOH, 5 % MeCN increase to 100% MeCN in 5.1 min, flow rate: 0.6 mL/min, t<sub>R</sub> = 1.67 min, m/z = 311.2 [[M+H]<sup>+</sup>]

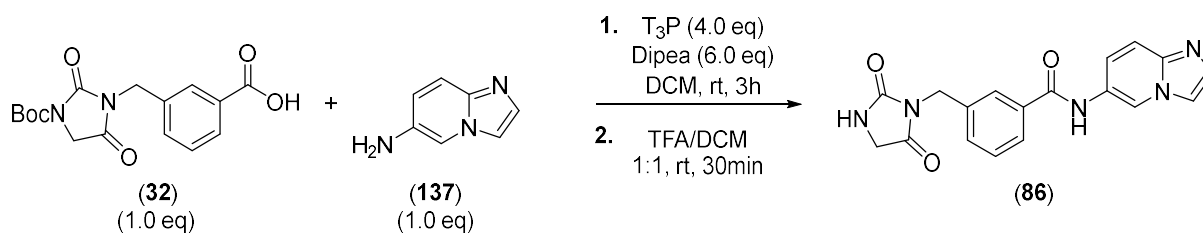


**<sup>1</sup>H-NMR** (500 MHz, dms<sub>o</sub>-d<sub>6</sub>, δ in ppm): 10.51 (s, 1H, Amide-NH), 8.93 (s, 1H, H-15), 8.33 (d, 3J = 2.9 Hz, 1H, H-16), 8.22-8.15 (m, 2H, Hydantoin-NH, H-13), 7.89 (d, <sup>3</sup>J<sub>8,9</sub> = 6.2 Hz, 1H, H-

8), 7.84 (s, 1H, H-6), 7.55-7.48 (m, 2H, H-9, H-10), 7.41 (dd,  $^3J = 8.2 \text{ Hz} = 4.6 \text{ Hz}$ , 1H, H-12), 4.63 (s, 1H, H-4), 4.01 (s, 1H, H-2).

$^{13}\text{C-NMR}$  (126 MHz, dms $\text{-d}_6$ ,  $\delta$  in ppm): 172.06 (C-1), 165.83 (C-11), 157.36 (C-3), 144.55 (C-13 or C-16), 141.93 (C-13 or C-16), 137.30 (C-5), 135.84 (C-7), 134.68 (C-12), 130.92 (C-10), 128.69 (C-9), 127.45 (c-15), 126.94 (C-6), 126.72 (C-8), 123.65 (C-14), 46.10 (C-2), 40.88 (C-4).

### Synthesis of 3-((2,5-dioxoimidazolidin-1-yl)methyl)-N-(imidazo[1,2-a]pyridin-6-yl)benzamide (86)

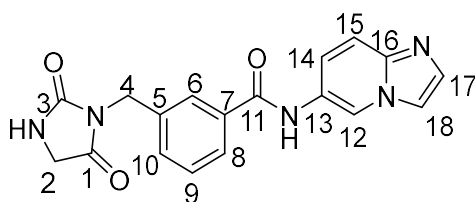


According to **standard procedure 1**, imidazo[1,2-a]pyridin-6-amine ((**137**), 7.7 mg, 0.058 mmol, 1.15 eq), 3-((3-(tert-butoxycarbonyl)-2,5-dioxoimidazolidin-1-yl)methyl)benzoic acid ((**32**), 16.7 mg, 0.05 mmol, 1.0 eq), DiPea (50  $\mu\text{L}$ , 0.3 mmol, 6.0 eq), T<sub>3</sub>P (50% in EtOAc, 130  $\mu\text{L}$ , 1.3 mmol, 4.0 eq) and DCM (2 mL, [0.025M]) were used to gain 24.9 mg of a brown solid after 16 h reaction at rt and work-up.

According to **standard procedure 2**, DCM (3 mL) and TFA (0.5 mL) and the crude from the previous step were used to gain the free amine.

To further purify the product, it was solved in MeCN/H<sub>2</sub>O/DMSO and purified via prep. HPLC (reverse phase, 5-50% MeCN in H<sub>2</sub>O in 30 min, 2 runs) to gain 3.05 mg (0,009 mmol, 18%) of a pale yellow solid after drying on the Lyo overnight.

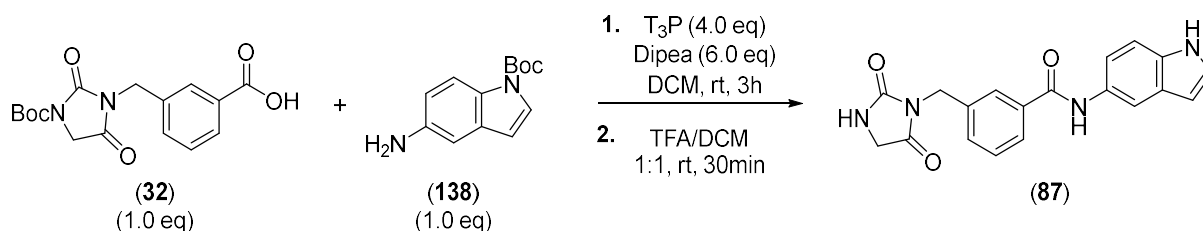
**LC-MS:** Column: Phenomenex Luna C18(2), gradient: MeCN/H<sub>2</sub>O + 0.05 % HCOOH, 5 % MeCN increase to 100% MeCN in 5.1 min, flow rate: 0.6 mL/min,  $t_{\text{R}} = 1.76 \text{ min}$ ,  $m/z = 350.2$  [[M+H]<sup>+</sup>)



$^1\text{H-NMR}$  (500 MHz, dms $\text{-d}_6$ ,  $\delta$  in ppm): 10.54 (s, 1H, Amide-NH), 9.44 (s, 1H, H-12), 8.19 (s, 1H, H-17 or H-18), 8.16 (s, 1H, H-17 or H-18), 7.90 (d,  $^3J = 6.8 \text{ Hz}$ , 1H, H-8), 7.85 (s, 1H, H-6), 7.74 (s, 2H, Hydantoin- NH, H-14 or H-15), 7.61 (d,  $^3J = 7.9 \text{ Hz}$ , 1H, H-14 or H-15), 7.56-7.47 (m, 2H, H-9, H-10), 4.64 (s, 1H, H-4), 4.01 (s, 1H, H-2).

$^{13}\text{C-NMR}$  (126 MHz, dms $\text{-d}_6$ ,  $\delta$  in ppm): 172.06 (C-1), 165.69 (C-11), 157.35 (C-3), 140.78 (C-5), 137.33 (C-13), 134.47, 130.89 (C-10), 130.50, 128.73 (C-9), 127.23, 126.87 (C-6), 126.64 (C-8), 123.23, 118.04, 115.44, 114.72, 46.09 (C-2), 40.86 (C-4).

### Synthesis of 3-((2,5-dioxoimidazolidin-1-yl)methyl)-N-(1H-indol-5-yl)benzamide (87)

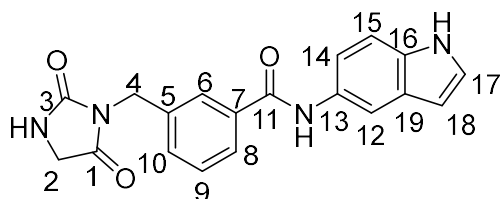


According to **standard procedure 1**, tert-butyl 5-amino-1H-indole-1-carboxylate ((**138**), 12.6 mg, 0.054 mmol, 1.15 eq), 3-((3-(tert-butoxycarbonyl)-2,5-dioxoimidazolidin-1-yl)methyl)benzoic acid ((**32**), 16.7 mg, 0.05 mmol, 1.0 eq), Dipea (50  $\mu$ L, 0.3 mmol, 6.0 eq), T3P (50% in EtOAc, 130  $\mu$ L, 1.3 mmol, 4.0 eq) and DCM (2 mL, [0.025M]) were used to gain 31.5 mg of a brown solid after 17 h reaction at rt and work-up.

According to **standard procedure 2**, DCM (3 mL) and TFA (0.5 mL) and the crude from the previous step were used to gain the free amine after 1h reaction time.

To further purify the product, it was solved in MeCN/H<sub>2</sub>O/DMSO and purified via prep. HPLC (reverse phase, 5-50% MeCN in H<sub>2</sub>O in 30 min, 2 runs) to gain 3.40 mg (0.01 mmol, 20%) of a pale red solid after drying on the Lyo overnight.

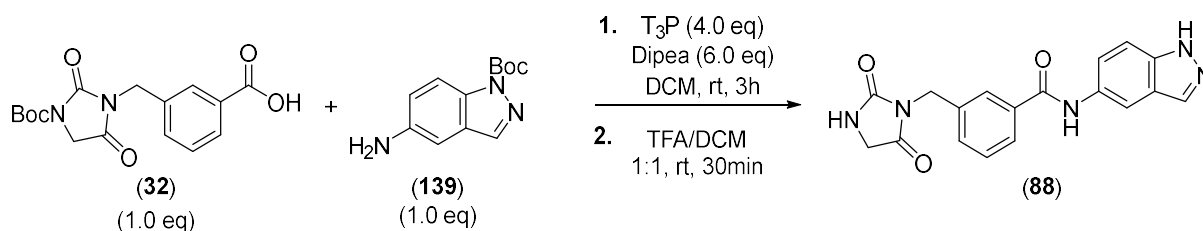
**LC-MS:** Column: Phenomenex Luna C18(2), gradient: MeCN/H<sub>2</sub>O + 0.05 % HCOOH, 5 % MeCN increase to 100% MeCN in 5.1 min, flow rate: 0.6 mL/min,  $t_R$  = 2.45 min,  $m/z$  = 349.2 [[M+H]<sup>+</sup>]



**<sup>1</sup>H-NMR** (500 MHz, dms<sub>o</sub>-d<sub>6</sub>,  $\delta$  in ppm): 11.00 (s, 1H, Indole-NH), 10.07 (s, 1H, Amide-NH), 8.14 (s, 1H, Hydantoin-NH), 7.93 (s, 1H, H-12), 7.83 (d, 3J = 7.2 Hz, 1H, H-8), 7.79 (s, 1H, H-6), 7.48-7.40 (m, 2H, H-9, H-10), 7.36-7.26 (m, 3H, H-14, H-15, H-17), 6.37 (m, 1H, H-18), 4.58 (s, 1H, H-4), 3.97 (s, 1H, H-2).

**<sup>13</sup>C-NMR** (126 MHz, dms<sub>o</sub>-d<sub>6</sub>,  $\delta$  in ppm): 172.05 (C-1), 164.98 (C-11), 157.38 (C-3), 137.07, 135.79, 133.04, 130.86 (C-10), 130.20, 128.50 (C-9), 127.41, 126.76 (C-6), 126.47 (C-8), 125.95, 116.12 (C-14), 112.27 (C-12 or C-15), 111.05 (C-12 or C-15), 101.18 (C-18), 46.08 (C-2), 40.92 (C-4).

### Synthesis of 3-((2,5-dioxoimidazolidin-1-yl)methyl)-N-(1H-indazol-5-yl)benzamide (88)

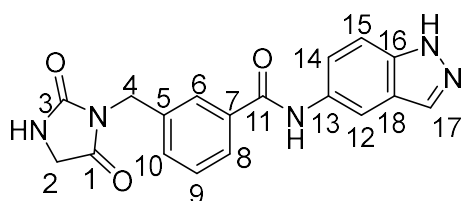


According to **standard procedure 1**, tert-butyl 5-amino-1H-indazole-1-carboxylate ((**139**), 12.5 mg, 0.054 mmol, 1.15 eq), 3-((3-(tert-butoxycarbonyl)-2,5-dioximidazolidin-1-yl)methyl)benzoic acid ((**32**), 16.8 mg, 0.05 mmol, 1.0 eq), Dipea (50  $\mu$ L, 0.3 mmol, 6.0 eq), T3P (50% in EtOAc, 130  $\mu$ L, 1.3 mmol, 4.0 eq) and DCM (2 mL, [0.025M]) were used to gain 28.5 mg of a yellow solid after 16 h reaction at rt and work-up.

According to **standard procedure 2**, DCM (3 mL) and TFA (0.5 mL) and the crude from the previous step were used to gain the free amine after 1h reaction time.

To further purify the product, it was solved in MeCN/H<sub>2</sub>O/DMSO and purified via prep. HPLC (reverse phase, 5-50% MeCN in H<sub>2</sub>O in 50 min, 2 runs) to gain 3.80 mg (0,011 mmol, 22%) of an off-white solid after drying on the Lyo overnight.

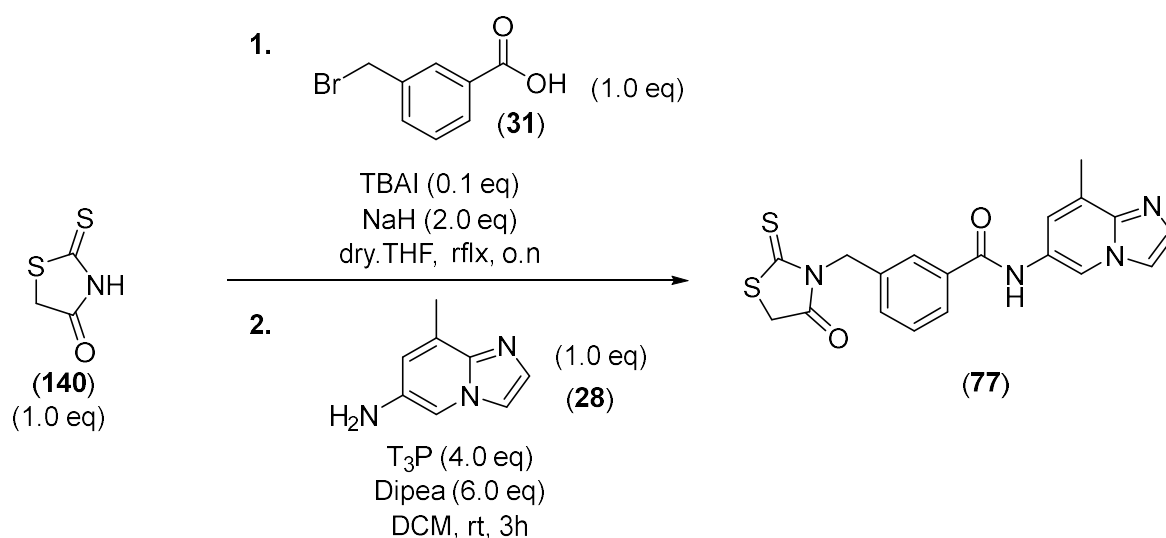
**LC-MS:** Column: Phenomenex Luna C18(2), gradient: MeCN/H<sub>2</sub>O + 0.05 % HCOOH, 5 % MeCN increase to 100% MeCN in 5.1 min, flow rate: 0.6 mL/min,  $t_R$  = 2.31 min,  $m/z$  = 350.2 [[M+H]<sup>+</sup>]



**<sup>1</sup>H-NMR** (500 MHz, dms<sub>o</sub>-d<sub>6</sub>,  $\delta$  in ppm): 12.95 (s, 1H, Indole-NH), 10.41 (s, 1H, Amide-NH), 8.26 (s, 1H, H-17), 8.19 (s, 1H, H-12), 8.00 (s, 1H, Hydantoin-NH), 7.88 (d, 3J = 7.0 Hz, 1H, H-8), 7.84 (s, 1H, H-6), 7.71 (d, 3J = 8.7 Hz, 1H, H-15), 7.55-7.45 (m, 2H, H-9, H-10), 7.37 (d, 3J = 8.6 Hz, 1H, H-14), 4.58 (s, 1H, H-4), 3.97 (s, 1H, H-2).

**<sup>13</sup>C-NMR** (126 MHz, dms<sub>o</sub>-d<sub>6</sub>,  $\delta$  in ppm): 172.05 (C-1), 165.73 (C-11), 157.36 (C-3), 140.30 (q.C), 137.31, 137.18, 135.42, 133.34 (q.C), 130.56 (C-10), 128.59 (C-9), 126.90 (C-6), 126.64 (C-8), 120.47 (C-14), 119.45 (q.C), 115.10 (C-15), 100.14 (C-12), 46.09 (C-2), 40.89 (C-4).

### Synthesis of N-(8-methylimidazo[1,2-a]pyridin-6-yl)-3-((4-oxo-2-thioxothiazolidin-3-yl)methyl)benzamide (**77**)



According to **general procedure 6**, Rhodanin ((**140**), 135.1 mg, 1.0 mmol, 1.0 eq), 3-(bromomethyl)benzoic acid ((**31**), 95% pure, 217.4 mg, 1.0mmol, 1.0 eq), TBAI (37.3 mg, 0.1 mmol, 0.1 eq), NaH (60%, 100.7 mg, 2.5 mmol, 2.5 eq) and THF (6 mL) were used to gain 296 mg of a red oil as the crude product.

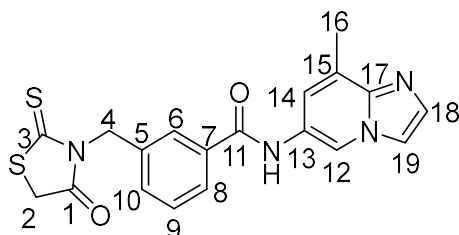
The crude was solved in MeCN/H<sub>2</sub>O and purified via prep. Flash (reverse phase, 5-100% MeCN in H<sub>2</sub>O in 30 min, 1 run) to gain 51.1 mg (0.19 mmol, 19%) 3-((4-oxo-2-thioxothiazolidin-3-yl)methyl)benzoic acid as a yellow solid after drying on the Lyo overnight.

The crude was hard to purify and degraded upon storage and purification and was used directly after prep in the next step.

According to **standard procedure 1**, 8-methylimidazo[1,2-a]pyridin-6-amine ((**28**), 28.7 mg, 0.19 mmol, 1.0 eq), 3-((4-oxo-2-thioxothiazolidin-3-yl)methyl)benzoic acid (51.1 mg, 0.19 mmol, 1.0 eq), Dipea (200  $\mu$ L, 1.14 mmol, 6.0 eq), T3P (50% in EtOAc, 360  $\mu$ L, 0.57 mmol, 3.0 eq) and DCM (5 mL, [0.05M]) were used to gain 49.5 mg of a brown solid after 21 h reaction at rt and work-up.

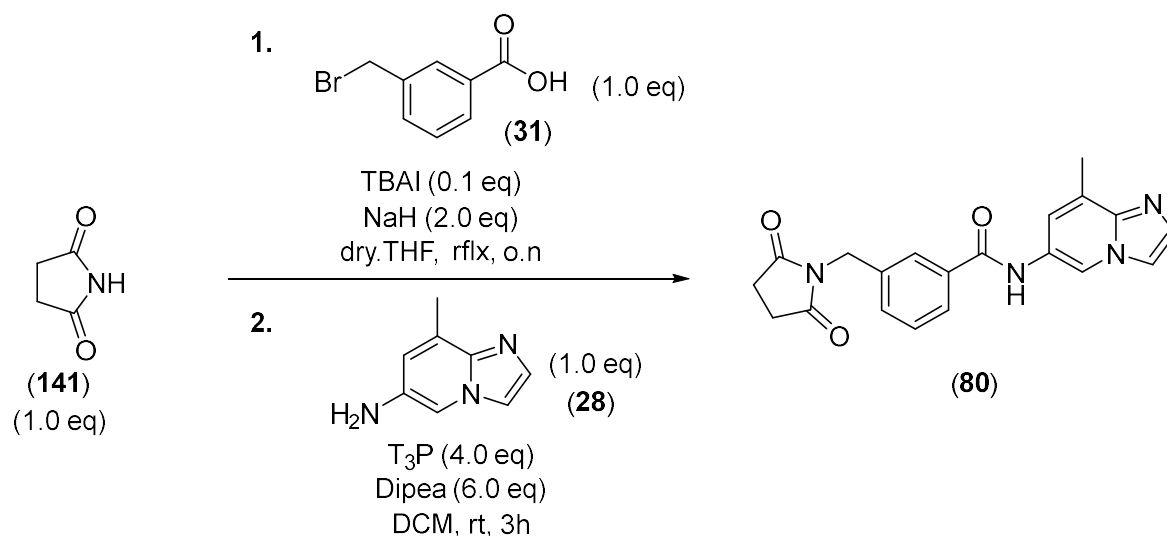
To further purify the product, it was solved in MeCN/H<sub>2</sub>O/DMSO and purified via prep. HPLC (reverse phase, 5-50% MeCN in H<sub>2</sub>O in 30 min, 2 runs) to gain 2.53 mg (0,006 mmol) of a pale yellow solid in 95% purity after drying on the Lyo overnight.

**LC-MS:** Column: Phenomenex Luna C18(2), gradient: MeCN/H<sub>2</sub>O + 0.05 % HCOOH, 5 % MeCN increase to 100% MeCN in 5.1 min, flow rate: 0.6 mL/min,  $t_R$  = 2.24 min,  $m/z$  = 397.0 [[M+H]<sup>+</sup>]



**<sup>1</sup>H-NMR** (500 MHz, dms<sub>o</sub>-d<sub>6</sub>,  $\delta$  in ppm): 10.45 (s, 1H, Amide-NH), 9.29 (s, 1H, H-12), 8.22-8.12 (m, 1H, H-18 or H-19), 8.04 (s, 1H, H-6), 7.90 (d, <sup>3</sup>J = 7.7 Hz, 1H, H-8), 7.75-7.67 (m, 2H, H-10, H-18 or H-19), 7.55 (t, 3J = 7.6 Hz, H-9), 7.45 (1H, s, H-14), 4.66 (s, 1H, H-4), 3.78 (s, 1H, H-2), 2.52 (s, 3H, H-16).

## Synthesis of 3-((2,5-dioxopyrrolidin-1-yl)methyl)-N-(8-methylimidazo[1,2-a]pyridin-6-yl)benzamide (80)

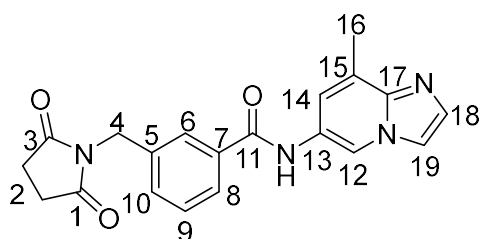


According to **general procedure 6**, pyrrolidine-2,5-dione ((**141**), 20.2 mg, 0.2 mmol, 1.0 eq), 3-(bromomethyl)benzoic acid ((**31**), 43.2 mg, 0.2 mmol, 1.0 eq), TBAI (8.2 mg, 0.02 mmol, 0.1 eq), NaH (60%, 18.9 mg, 0.44 mmol, 2.2 eq) and THF (3 mL) were used to gain 47.3 mg of a yellow oil as the crude product, which was used without purification in the next step.

According to **standard procedure 1**, 8-methylimidazo[1,2-a]pyridin-6-amine ((**28**), 29.4 mg, 0.2 mmol, 1.0 eq), the crude from the previous step (47.3 mg, 0.2 mmol, 1.0 eq), Dipea (210  $\mu$ L, 1.2 mmol, 6.0 eq), T<sub>3</sub>P (50% in EtOAc, 380  $\mu$ L, 0.6 mmol, 3.0 eq) and DCM (4 mL, [0.05M]) were used to gain 64.8 mg of a brown solid after 18 h reaction at rt and work-up in 80% purity.

To further purify the product, it was solved in MeCN/H<sub>2</sub>O/DMSO and purified via prep. HPLC (reverse phase, 5-50% MeCN in H<sub>2</sub>O in 30 min, 2 runs) to gain 5.57 mg (0.015 mmol, 8% over 2 steps) of a white solid, after drying on the Lyo overnight.

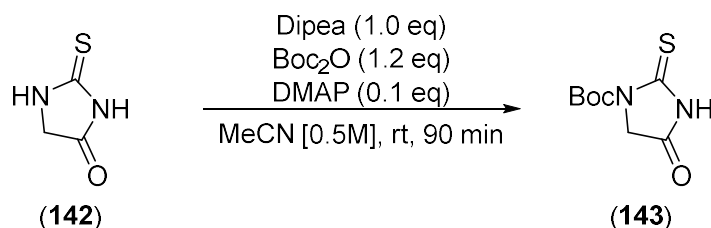
**LC-MS:** Column: Phenomenex Luna C18(2), gradient: MeCN/H<sub>2</sub>O + 0.05 % HCOOH, 5 % MeCN increase to 100% MeCN in 5.1 min, flow rate: 0.6 mL/min,  $t_R$  = 1.97 min,  $m/z$  = 363.2 [[M+H]<sup>+</sup>]



**<sup>1</sup>H-NMR** (500 MHz, dms<sub>o</sub>-d<sub>6</sub>,  $\delta$  in ppm): 10.32 (s, 1H, Amide-NH), 9.18 (s, 1H, H-12), 8.03 (s, 1H, H-18 or H-19), 7.87 (d, 3J = 7.0 Hz, 1H, H-8), 7.83 (s, 1H, H-6), 7.54 (s, 1H, H-18 or H-19), 7.52-7.45 (m, 2H, H-9, H-10), 7.27 (s, 1H, H-14), 4.64 (s, 2H, H-4), 2.72 (s, 4H, H-2), 2.50 (s, 3H, H-16).

<sup>13</sup>C-NMR (126 MHz, dms<sub>o</sub>-d<sub>6</sub>, δ in ppm): 177.76 (C-2), 165.57 (C-11), 142.66 (q.C), 136.78, 134.66 (q.C), 132.23 (q.C), 130.86 (C-10), 128.70 (C-9), 127.01 (C-6), 126.63 (C-8), 126.02, 125.89, 120.00 (q.C), 115.80, 114.70, 41.21 (C-4), 28.21 (C-2), 16.63 (C-16)

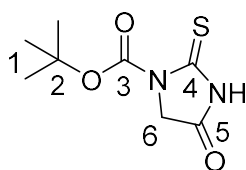
### Synthesis of tert-butyl 4-oxo-2-thioxoimidazolidine-1-carboxylate (**143**)



2-thioxoimidazolidin-4-one (**142**), 347.0 mg, 3 mmol, 1.0 eq) and DMAP (38.0 mg, 0.3 mmol, 0.1 eq) were placed in a 100 mL single neck flask and solved in MeCN (6mL, [0.5M]). Then Dipea (0.52 mL, 3.0 mmol, 1.0 eq) and subsequently Boc<sub>2</sub>O (784.4 mg, 3.6 mmol, 1.2 eq) were added at rt. The suspension turned clear after 30 min at room temperature. After 90 min, the acetonitrile was removed under reduced pressure and the residue was extracted with a 2% aq. Na<sub>2</sub>CO<sub>3</sub> solution and EtOAc to gain a yellow solid after drying with Na<sub>2</sub>SO<sub>4</sub> and removal of the solvents.

The crude was solved in DCM, absorbed on a minimum amount of Isolute and purified via Combiflash (24 g SiO<sub>2</sub>, PE/EtOAc 6:4, product UV-active) to gain 481.0 mg (2.22 mmol, 74%) of a yellow crystalline solid as the desired product.

**LC-MS:** Column: Phenomenex Luna C18(2), gradient: MeCN/H<sub>2</sub>O + 0.05 % HCOOH, 5 % MeCN increase to 100% MeCN in 7 min, flow rate: 0.6 mL/min, t<sub>R</sub> = 6.44, m/z = 117.13 ([M-Boc+H]<sup>+</sup>)

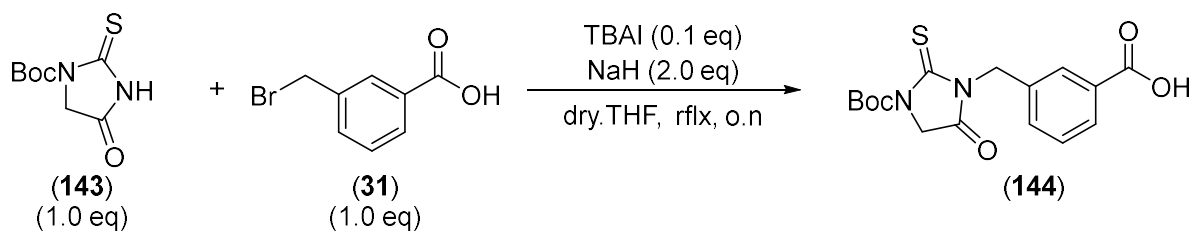


<sup>1</sup>H-NMR (500 MHz, CDCl<sub>3</sub>, δ in ppm): 4.41 (s, 2H, H-6), 1.57 (s, 9H, H-1)

<sup>13</sup>C-NMR (126 MHz, CDCl<sub>3</sub>, δ in ppm): 178.54 (C-4), 168.09 (C-5), 148.43 (C-3), 85.76 (C-2), 52.86 (C-6), 28.10 (C-1).



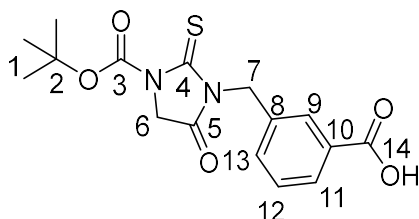
### Synthesis of 3-((3-(tert-butoxycarbonyl)-2-thioxoimidazolidin-1-yl)methyl)benzoic acid (144)



According to **general procedure 6**, tert-butyl 4-oxo-2-thioxoimidazolidine-1-carboxylate ((143), 215.3 mg, 1.0 mmol, 1.0 eq), 3-(bromomethyl)benzoic acid ((31), 215.4 mg, 3.01 mmol, 1.0 eq), TBAI (110.6 mg, 0.12 mmol, 0.12 eq), NaH (60%, 83.4 mg, 2.0 mmol, 2.0 eq) and THF (10 mL) were used to gain 367 mg of a yellow oil as the crude product.

The crude was solved in MeCN/H<sub>2</sub>O and purified via prep. Flash (reverse phase, 5-100% MeCN in H<sub>2</sub>O in 30 min, 1 run) to gain 60.3 mg (0.17 mmol, 17%) of a white fluffy solid after drying on the Lyo overnight as the pure fraction. A big mixt fraction of impure product was received but not further purified.

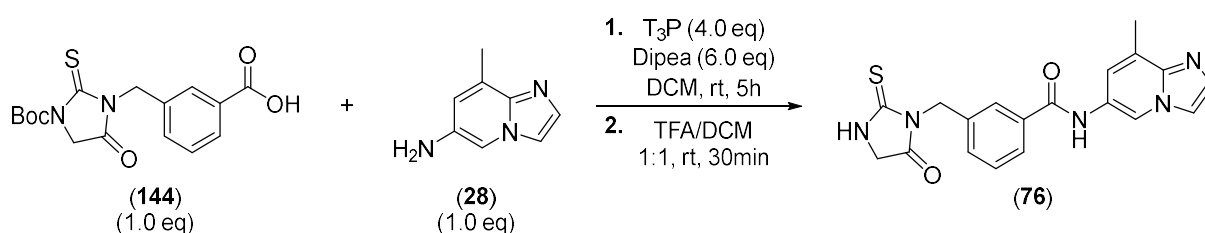
**LC-MS:** Column: Phenomenex Luna C18(2), gradient: MeCN/H<sub>2</sub>O + 0.05 % HCOOH, 5 % MeCN increase to 100% MeCN in 5.1 min, flow rate: 0.6 mL/min,  $t_R = 3.05$ ,  $m/z = 351.2$  ( $[M + H]^+$ ), 251.1 ( $[M - \text{Boc} + H]^+$ ).



**<sup>1</sup>H-NMR** (500 MHz, dms<sub>o</sub>-d<sub>6</sub>,  $\delta$  in ppm): 13.03 (s, 1H, COOH), 8.02 (s, 1H, H-9), 7.85 (d,  $^3J_{11,12} = 7.7$  Hz, 1H, H-11), 7.69 (d,  $^3J_{13,12} = 7.6$  Hz, 1H, H-13), 7.47 (t,  $^3J_{12,11} = ^3J_{12,13} = 7.7$  Hz, 1H, H-12), 4.46 (s, 2H, H-6), 4.30 (s, 2H, H-7), 1.46 (s, 9 H, H-1).

**<sup>13</sup>C-NMR** (126 MHz, dms<sub>o</sub>-d<sub>6</sub>,  $\delta$  in ppm): 183.41 (C-14), 182.24 (C-4), 167.07 (C-5), 148.03 (C-3), 137.27 (C-8), 133.69 (C-13), 131.10 (C-10), 129.99 (C-7 or C-11 or C-12), 128.81 (C-7 or C-11 or C-12), 128.28 (C-7 or C-11 or C-12), 84.29 (C-2), 52.90 (C-6), 35.73 (C-7), 27.51 (C-1).

### Synthesis of N-(8-methylimidazo[1,2-a]pyridin-6-yl)-3-((2-thioxoimidazolidin-1-yl)methyl)benzamide (76)

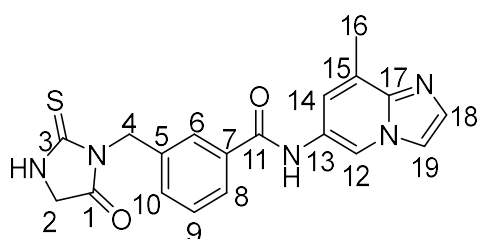


According to **standard procedure 1**, 8-methylimidazo[1,2-a]pyridin-6-amine ((**28**), 26.0 mg, 0.17 mmol, 1.0 eq), 3-((3-(tert-butoxycarbonyl)-2-thioxoimidazolidin-1-yl)methyl)benzoic acid ((**144**), crude, 60.3 mg, 0.17 mmol, 1.0 eq), Dipea (180  $\mu$ L, 1.02 mmol, 6.0 eq), T<sub>3</sub>P (50% in EtOAc, 330  $\mu$ L, 0.51 mmol, 3.0 eq) and DCM (2 mL, [0.1M]) were used to gain 63.0 mg of a brown oil after 5 h reaction time and work-up.

According to **standard procedure 2**, DCM (5 mL) and TFA (1 mL) were used to gain the free amine in 80% purity on the LC-MS after 40 min reaction time.

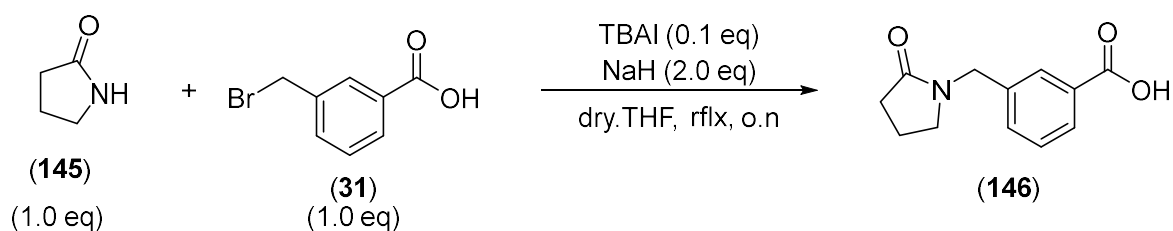
The crude was solved in MeCN/H<sub>2</sub>O (1:1) and purified via prep. HPLC (reverse phase, 5-50% MeCN in H<sub>2</sub>O in 30 min, 3 runs, elution after 18 min) to gain 6.34 mg (0,018 mmol, 11%) of an off-white solid after drying on the Lyo overnight.

**LC-MS:** Column: Phenomenex Luna C18(2), gradient: MeCN/H<sub>2</sub>O + 0.05 % HCOOH, 5 % MeCN increase to 100% MeCN in 5.1 min, flow rate: 0.6 mL/min, t<sub>R</sub> = 2.00 min, m/z = 380.1 [[M+H]<sup>+</sup>]



**<sup>1</sup>H-NMR** (500 MHz, dms<sub>o</sub>-d<sub>6</sub>,  $\delta$  in ppm): 10.66-10.31 (s, 1H, Amide-NH), 9.32 (s, 1H, H-12), 8.18 (s, 1H, H-18 or H-19), 8.04-7.34 (m, 8 H, Hydantoin-NH, H-18 or H-19, H-6, H-7, H-8, H-9, H-10, H-14), 4.29 (s, 2H, H-4), 3.85 (s, 2H, H-2), 2.53 (s, 3H, H-16).

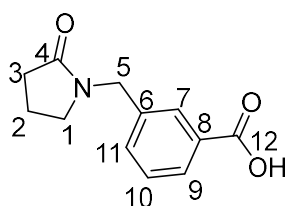
### Synthesis of 3-((2-oxopyrrolidin-1-yl)methyl)benzoic acid (**146**)



According to **general procedure 6**, pyrrolidin-2-one ((**145**), 43.4 mg, 0.5 mmol, 1.0 eq), 3-(bromomethyl)benzoic acid ((**31**), 109.9 mg, 0.5 mmol, 1.0 eq), TBAI (20.0 mg, 0.05 mmol, 0.1 eq), NaH (60%, 45.0 mg, 1.10 mmol, 2.2 eq) and THF (5 mL) were used to gain 120.4 mg of a yellow oil as the crude product after workup.

The crude was solved in MeCN/H<sub>2</sub>O and purified via prep. Flash (reverse phase, 10-100% MeCN in H<sub>2</sub>O in 60 min, 4 runs) to gain 35.92 mg (0.16 mmol, 133%) of the product as a white fluffy solid after drying on the Lyo overnight.

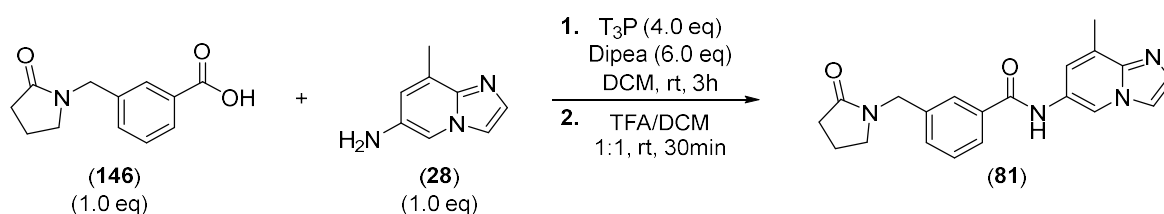
**LC-MS:** Column: Phenomenex Luna C18(2), gradient: MeCN/H<sub>2</sub>O + 0.05 % HCOOH, 5 % MeCN increase to 100% MeCN in 5.1 min, flow rate: 0.6 mL/min, t<sub>R</sub> = 2.14. m/z = 220.1 ([M+H]<sup>+</sup>).



**<sup>1</sup>H-NMR** (500 MHz, dms<sub>o</sub>-d<sub>6</sub>, δ in ppm): 13.00 (s, 1H, COOH), 7.88-7.82 (m, 1H, H-9), 7.80 (s, 1H, H-7), 7.51-7.44 (m, 2H, H-10, H-11), 4.43 (s, 2H, H-5), 3.23 (t, <sup>3</sup>J<sub>1,2</sub> = 7.0 Hz, 2H, H-1), 2.30 (t, <sup>3</sup>J<sub>3,2</sub> = 8.1 Hz, 2H, H-3), 1.99-1.87 (m, 2H, H-2).

**<sup>13</sup>C-NMR** (126 MHz, dms<sub>o</sub>-d<sub>6</sub>, δ in ppm): 174.10 (C-4), 167.18 (C-12), 137.70 (C-6), 132.13 (C-11), 131.09 (C-8), 128.92 (C-7 or C-9 or C-10), 128.49 (C-7 or C-9 or C-10), 128.23 (C-7 or C-9 or C-10), 46.14 (C-1 or C-5), 45.18 (C-1 or C-5), 30.19 (C-3), 17.38 (C-2).

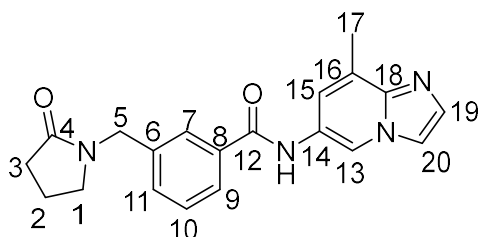
### Synthesis of N-(8-methylimidazo[1,2-a]pyridin-6-yl)-3-((2-oxopyrrolidin-1-yl)methyl)benzamide (81)



According to **standard procedure 1**, 8-methylimidazo[1,2-a]pyridin-6-amine ((**146**), 20.3 mg, 0.14 mmol, 1.0 eq), 3-((2-oxopyrrolidin-1-yl)methyl)benzoic acid ((**28**), 30.7 mg, 0.14 mmol, 1.0 eq), Dipea (150 μL, 0.84 mmol, 6.0 eq), T3P (50% in EtOAc, 260 μL, 0.42 mmol, 3.0 eq) and DCM (3 mL, [0.05M]) were used to gain 32.0 mg of a yellow oil after 21 h reaction time and work-up.

The crude was solved in MeCN/H<sub>2</sub>O (1:1) and purified via prep. HPLC (reverse phase, 5-50% MeCN in H<sub>2</sub>O in 30 min, 4 runs) to gain 6.34 mg (0,018 mmol, 13%) of an off-white solid after drying on the Lyo overnight.

**LC-MS:** Column: Phenomenex Luna C18(2), gradient: MeCN/H<sub>2</sub>O + 0.05 % HCOOH, 5 % MeCN increase to 100% MeCN in 7 min, flow rate: 0.6 mL/min, t<sub>R</sub> = 2.35 min, m/z = 349.3 [[M+H]<sup>+</sup>]



**<sup>1</sup>H-NMR** (500 MHz, dms<sub>o</sub>-d<sub>6</sub>, δ in ppm): 10.31 (s, 1H, Amide-NH), 9.16 (s, 1H, H-13), 8.01 (s, 1H, H-19 or H-20), 7.89 (d, <sup>3</sup>J<sub>9,10</sub> = 7.7 Hz, 1H, H-9), 7.81 (s, 1H, H-7), 7.52 (m, 2H, H-10, H-19 or H-20), 7.44 (d, <sup>3</sup>J<sub>11,10</sub> = 7.6 Hz, 1H, H-11), 7.25 (s, 1H, H-15), 2.49 (s, 1H, H-17), 4.47 (s,

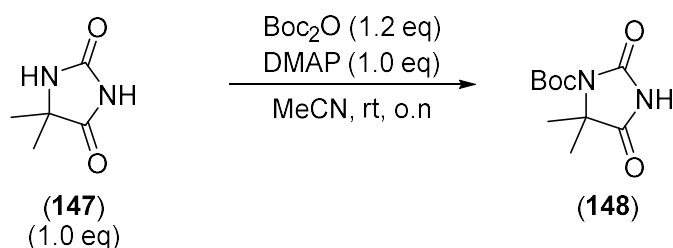
2H, H-5), 3.26 (t,  $^3J_{1,2} = 7.0$  Hz, 2H, H-1), 2.31 (t,  $^3J_{3,2} = 8.1$  Hz, 2H, H-3), 1.97-1.91 (m, 2H, H-2).

Spectra contains EtOAc (q at 4.03, s at 1.99, t at 1.17)

$^{13}\text{C-NMR}$  (126 MHz, dms $o$ -d $_6$ ,  $\delta$  in ppm): 174.16 (C-4), 165.53 (C-12), 142.91(C-6), 137.59 (C-14), 134.74 (C-19), 132.67 (C-11), 130.89 (C-16), 128.78 (C-10), 126.96 (C-15), 126.52 (C-7), 125.99 (C-9), 125.80 (C-18), 119.62 (C-15), 115.73 (C-13) 114.58 (C-20), 46.22 (C-1 or C-5), 45.34 (C-1 or C-5), 30.25 (C-3), 17.42 (C-2), 16.64 (C-17).

Spectra contains EtOAc (170.37, 59.78, 20.78, 14.10)

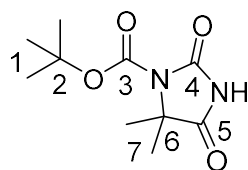
### Synthesis of tert-butyl 5,5-dimethyl-2,4-dioximidazolidine-1-carboxylate (148)



According to **general procedure 5**, 5,5-dimethylimidazolidine-2,4-dione ((147), 646 mg, 5.0 mmol, 1.0 eq), DMAP (619.5 mg, 5 mmol, 1.0 eq), Boc<sub>2</sub>O (1430 mg, 6.55 mmol, 1.3 eq) and 10 mL MeCN were used to gain 1383.9 mg of a white solid after workup.

The crude oil was solved in DCM, absorbed on a minimum amount of Isolute and purified via Combiflash (24 g SiO<sub>2</sub>, PE/EtOAc 6:4, product staining anisaldehyde on TLC) to gain 554.8 mg (2.43 mmol, 49%) of a white crystalline solid as the desired product.

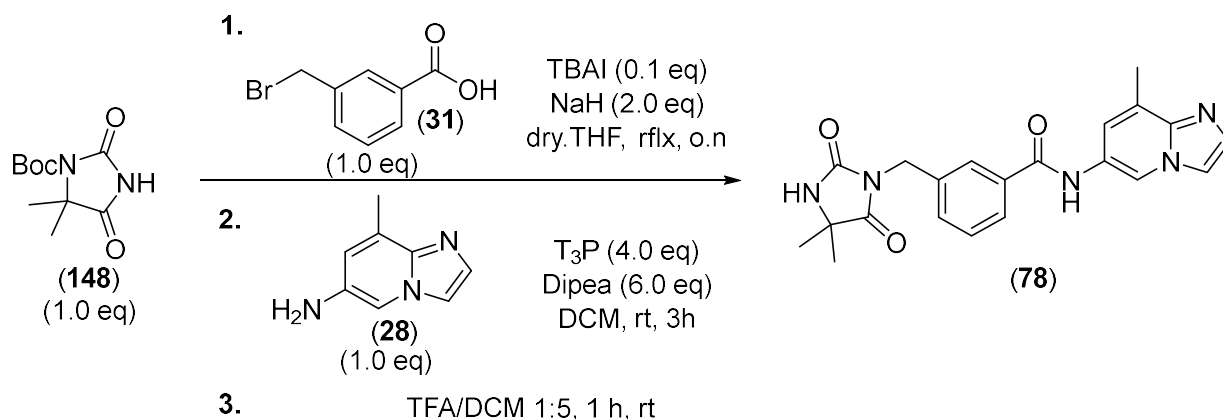
No LC-MS data, due to no UV-activity.



$^1\text{H-NMR}$  (500 MHz, CDCl<sub>3</sub>,  $\delta$  in ppm): 1.61 (s, 6H, H-7), 1.58 (s, 9H, H-1).

$^{13}\text{C-NMR}$  (126 MHz, CDCl<sub>3</sub>,  $\delta$  in ppm): 177.66 (C-5), 154.04 (C-4), 150.18 (C-3), 85.04 (C-2), 65.36 (c-6), 28.28 (c-2), 23.38 (C-7).

**Synthesis of 3-((4,4-dimethyl-2,5-dioximidazolidin-1-yl)methyl)-N-(8-methylimidazo[1,2-a]pyridin-6-yl)benzamide (78)**



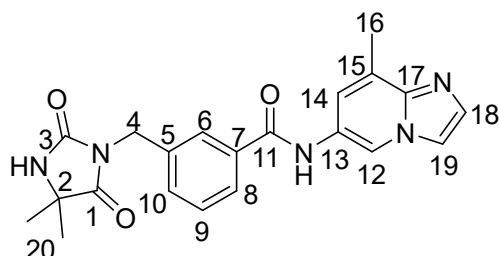
According to **general procedure 6**, tert-butyl 5,5-dimethyl-2,4-dioximidazolidine-1-carboxylate ((**148**), 177.2 mg, 0.5 mmol, 1.0 eq), 3-(bromomethyl)benzoic acid ((**31**), 126.2 mg, 0.5 mmol, 1.0 eq), TBAI (18.2 mg, 0.05 mmol, 0.1 eq), NaH (60%, 42.4 mg, 1.0 mmol, 2.0 eq) and THF (5 mL) were used to gain 202.6 mg of the crude 3-((3-(tert-butoxycarbonyl)-4,4-dimethyl-2,5-dioximidazolidin-1-yl)methyl)benzoic acid, as a yellow solid, which was used without purification in the next step.

According to **standard procedure 1**, 8-methylimidazo[1,2-a]pyridin-6-amine ((**28**), 73.5 mg, 0.5 mmol, 1.0 eq), 3-((3-(tert-butoxycarbonyl)-4,4-dimethyl-2,5-dioximidazolidin-1-yl)methyl)benzoic acid (crude from previous step, 202.6 mg, 0.5 mmol, 1.0 eq), Dipea (530  $\mu$ L, 3.0 mmol, 6.0 eq), T<sub>3</sub>P (50% in EtOAc, 960  $\mu$ L, 1.5 mmol, 3.0 eq) and DCM (5 mL, [0.1 M]) were used to gain 322.6 mg of a brown oil after 18 h reaction at rt and work-up.

According to **standard procedure 2**, the crude was solved in TFA (1 mL) and DCM (5 mL) to gain the free amine in 80% purity according to LC-MS.

To further purify the product, it was solved in MeCN/H<sub>2</sub>O/DMSO and purified via prep. HPLC (reverse phase, 5-50% MeCN in H<sub>2</sub>O in 30 min, 3 runs) to gain 8.46 mg (0,021 mmol, 4% over 2 steps) of a white solid after drying on the Lyo overnight.

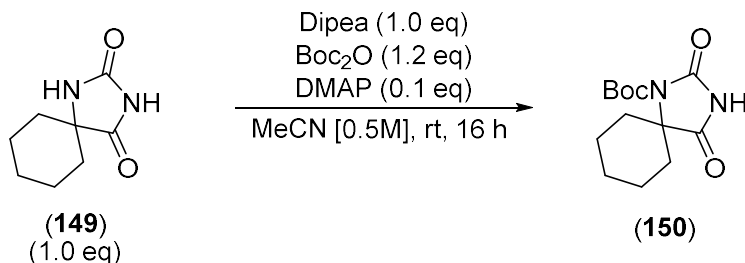
**LC-MS:** Column: Phenomenex Luna C18(2), gradient: MeCN/H<sub>2</sub>O + 0.05 % HCOOH, 5 % MeCN increase to 100% MeCN in 5.1 min, flow rate: 0.6 mL/min, t<sub>R</sub> = 2.24 min, m/z = 397.0 [[M+H]<sup>+</sup>]



**<sup>1</sup>H-NMR** (500 MHz, dms<sub>o</sub>-d<sub>6</sub>,  $\delta$  in ppm): 10.53 (s, 1H, Amide-NH), 9.36 (s, 1H, H-12), 8.48 (s, 1H, H-19 or H-18), 8.23 (s, 1H, H-19 or H-18), 7.92 (d, 3J = 7.7 Hz, 1H, H-8), 7.83 (s, 1H, Hydantoin-NH), 7.81 (s, 1H, H-6), 7.60-7.50 (m, 2H, H-9, H-14), 7.45 (d, 3J = 7.6 Hz, 1H, H-10), 4.64 (s, 1H, H-4), 2.54 (s, 3H, H-16), 1.34 (s, 6H, H-20).

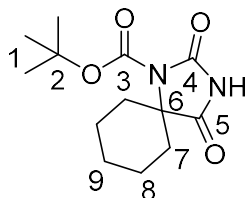
<sup>13</sup>C-NMR (126 MHz, dms<sub>o</sub>-d<sub>6</sub>, δ in ppm): 177.78 (C-1), 166.08 (C-11), 155.54 (C-3), 140.72 (C-5), 137.83, 134.82, 130.91 (C-10), 129.31 (C-9), 128.80 (q.C), 128.16 (q.C), 126.98 (C-6), 126.88 (C-8), 124.92, 123.40, 116.54, 115.90, 58.48 (C-2), 41.17(C-4), 25.12 (C-20), 16.83 (C-16).

### Synthesis of tert-butyl 2,4-dioxo-1,3-diazaspiro[4.5]decane-1-carboxylate (**150**)



1,3-diazaspiro[4,5]decane-2,4-dione (**149**), 504.8 mg, 3 mmol, 1.0 eq) and DMAP (35.4 mg, 0.3 mmol, 0.1 eq) were placed in a 100 mL single neck flask and solved in MeCN (8 mL, [0.5M]). Then Dipea (0.52 mL, 3.0 mmol, 1.0 eq) and subsequently Boc<sub>2</sub>O (785.7 mg, 3.6 mmol, 1.2 eq) were added at rt. The suspension turned clear after 5 h at room temperature. After 16 h, the acetonitrile was removed under reduced pressure and the residue was extracted with a 2% aq. Na<sub>2</sub>CO<sub>3</sub> solution and EtOAc to gain a yellow solid after drying with Na<sub>2</sub>SO<sub>4</sub> and removal of the solvents.

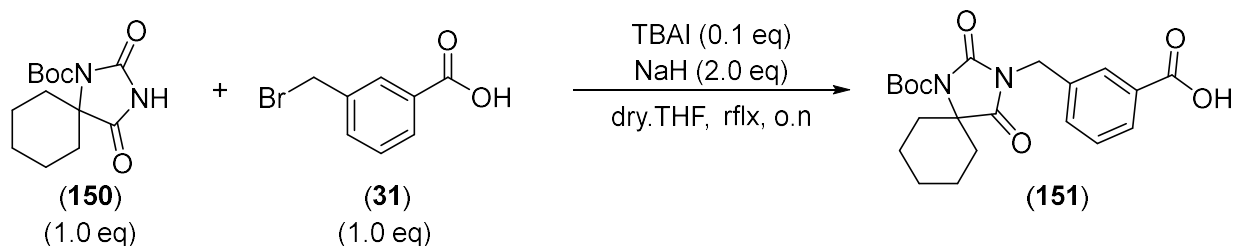
The crude was solved in DCM, absorbed on a minimum amount of Isolute and purified via Combiflash (24 g SiO<sub>2</sub>, PE/EtOAc 6:4, product UV-active) to gain 280.0 mg (1.42mmol, 47%) of a white crystalline solid as the desired product.



<sup>1</sup>H-NMR (500 MHz, CDCl<sub>3</sub>, δ in ppm): 1.93-1.79 (m, 4H, H-7), 1.73-1.60 (m, 4 H, H-8), 1.58 (s, 9H, H-1), 1.43-1.37 (m, 1H, H-9).

<sup>13</sup>C-NMR (126 MHz, CDCl<sub>3</sub>, δ in ppm): 173.19 (C-5), 152.39 (C-4), 146.42 (C-3), 85.70 (C-2), 61.19 (C-6), 33.75 (C-7), 27.96 (C-1), 24.52 (C-9), 21.62 (C-8).

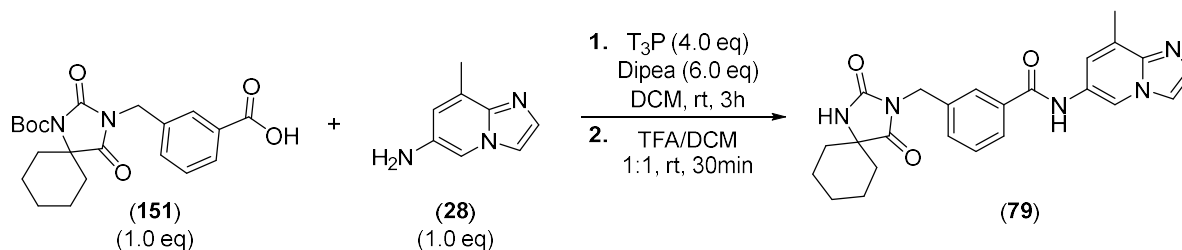
**Synthesis of 3-((1-(tert-butoxycarbonyl)-2,4-dioxo-1,3-diazaspiro[4.5]decan-3-yl)methyl)benzoic acid (151)**



According to **general procedure 6**, tert-butyl 2,4-dioxo-1,3-diazaspiro[4.5]decane-1-carboxylate (**(150)**, 79.1 mg, 0.3 mmol, 1.0 eq), 3-(bromomethyl)benzoic acid (**(31)**, 63.6 mg, 0.3 mmol, 1.0 eq), TBAI (11.1 mg, 0.03 mmol, 0.1 eq), NaH (60%, 25.7 mg, 0.63 mmol, 2.1 eq) and THF (3 mL) were used to gain 147.1 mg of a yellow oil as the crude product after 90 min reaction time.

The crude contained the desired product in 70% purity, among with 3 minor side products. The crude was used without further purification in the next reaction.

**Synthesis of 3-((2,4-dioxo-1,3-diazaspiro[4.5]decan-3-yl)methyl)-N-(8-methylimidazo[1,2-a]pyridin-6-yl)benzamide (79)**



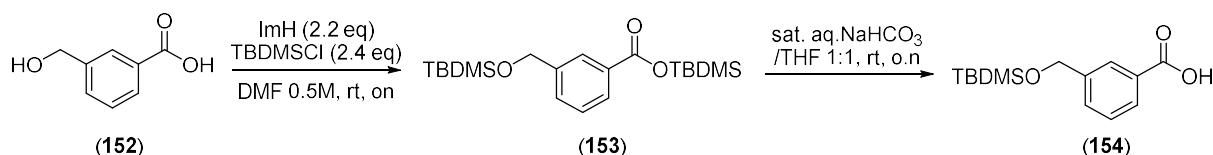
According to **standard procedure 1**, 8-methylimidazo[1,2-a]pyridin-6-amine (**(28)**, 44.0 mg, 0.3 mmol, 1.2 eq), 3-((1-(tert-butoxycarbonyl)-2,4-dioxo-1,3-diazaspiro[4.5]decan-3-yl)methyl)benzoic acid (**(151)**, crude, 147 mg, 0.3 mmol, 1.0 eq), Dipea (320  $\mu$ L, 1.8 mmol, 6.0 eq), T<sub>3</sub>P (50% in EtOAc, 580  $\mu$ L, 0.9 mmol, 3.0 eq) and DCM (4 mL, [0.1M]) were used to gain 157.1 mg of a brown oil after 3 h reaction time and work-up.

According to **standard procedure 2** the crude was solved in TFA (1 mL) and DCM (5 mL) to gain the crude amide in 60% purity (severe impurities).

The crude was solved in MeCN/H<sub>2</sub>O (1:1) and purified via prep. HPLC (reverse phase, 5-50% MeCN in H<sub>2</sub>O in 50 min, 2 runs) to gain 4.03 mg (0,0093 mmol, 3% over 2 steps) of an off-white solid after drying on the Lyo overnight.

**LC-MS:** Column: Phenomenex Luna C18(2), gradient: MeCN/H<sub>2</sub>O + 0.05 % HCOOH, 5 % MeCN increase to 100% MeCN in 5.1 min, flow rate: 0.6 mL/min, t<sub>R</sub> = 2.46 min, m/z = 432.6 [[M+H]<sup>+</sup>]

### Synthesis of 3-(((tert-butyldimethylsilyl)oxy)methyl)benzoic acid (**154**)

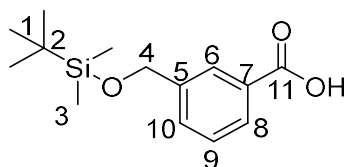


3-(hydroxymethyl)benzoic acid (**152**), 306.1 mg, 2.0 mmol, 1.0 eq) was placed in a 50 mL single neck flask and solved in dry. DMF (4 mL). Subsequently Imidazole (302.1 mg, 4.4 mmol, 2.2 eq) and TBDMSCl (726.2 mg, 4.8 mmol, 2.4 eq) were added and the mixture was stirred at rt for 19 h, after which LC-MS confirmed full conversion to the double protected intermediate (**153**). The reaction mixture was diluted with acetone and cooled to 0°C with an ice bath. The precipitate was filtered off and discarded. The DMF was removed under reduced pressure (azeotrope removal with toluene, 5x) to obtain a crude containing an 1:9 ratio of the mono to the bis TBDMS protected starting material.

The crude was dissolved with a 1:1 mixture of sat. aq. NaHCO<sub>3</sub> solution and THF, then it was stirred for 15 min, after which deprotection of the acid was complete. THF was removed under reduced pressure, the residue was acidified with an [0.25M] aq. HCl solution and extracted with E<sub>12</sub>O (3x). After washing with brine, drying over Na<sub>2</sub>SO<sub>4</sub> and removal of the solvents under reduced pressure 1.16 g of a wet crude were obtained.

The crude was solved in MeCN/H<sub>2</sub>O/DMSO (5:5:1) and purified via prep. Flash (reverse phase, 5-100% MeCN in H<sub>2</sub>O in 30 min, 1 runs) to gain 300.1 mg (1.12 mmol, 56%) of the desired product as an off-white solid after drying on the Lyo overnight.

**LC-MS:** Column: Phenomenex Luna C18(2), gradient: MeCN/H<sub>2</sub>O + 0.05 % HCOOH, 5 % MeCN increase to 100% MeCN in 7 min, flow rate: 0.6 mL/min, t<sub>R</sub> = 5.23 min.

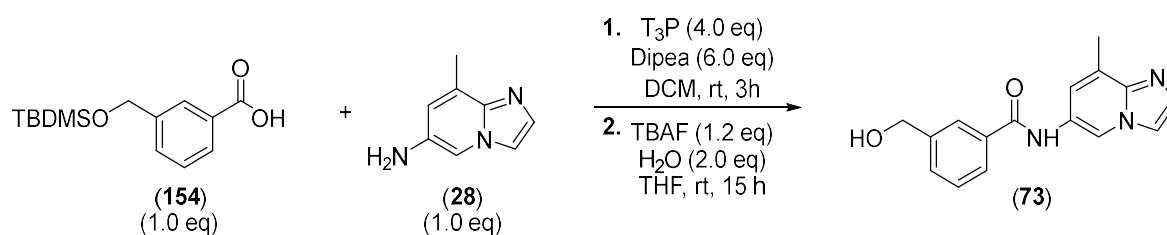


**<sup>1</sup>H-NMR** (500 MHz, CDCl<sub>3</sub>, δ in ppm): 8.07 (s, 1H, H-6), 8.01 (d, <sup>3</sup>J<sub>8,9</sub> = 7.7 Hz, 1H, H-8), 7.61 (d, <sup>3</sup>J<sub>10,9</sub> = 7.6 Hz, 1H, H-10), 7.45 (t, <sup>3</sup>J = 7.7 Hz, 1H, H-9), 4.80 (s, 2H, H-4), 0.96 (s, 9H, H-1), 0.12 (s, 6H, H-3).

**<sup>13</sup>C-NMR** (126 MHz, CDCl<sub>3</sub>, δ in ppm): 172.21 (C-11), 142.19 (C-5), 131.63, 129.33 (C-7), 128.96, 128.62, 127.88, 64.59 (C-4), 26.08 (C-1), 18.56 (C-2), -5.11 (C-3).



## Synthesis of 3-(hydroxymethyl)-N-(8-methylimidazo[1,2-a]pyridin-6-yl)benzamide (73)

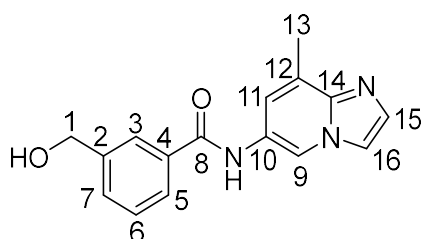


According to **standard procedure 1**, 8-methylimidazo[1,2-a]pyridin-6-amine ((**28**), 162.2 mg, 1.1 mmol, 1.0 eq), 3-(((tert-butyldimethylsilyloxy)methyl)benzoic acid ((**154**), crude, 297 mg, 1.1 mmol, 1.0 eq), Dipea (760  $\mu$ L, 4.4 mmol, 4.0 eq), T<sub>3</sub>P (50% in EtOAc, 2100  $\mu$ L, 3.3 mmol, 3.0 eq) and DCM (11 mL, [0.1M]) were used to gain 435.1 mg of a yellow solid after 3 h reaction time and work-up.

The crude was placed in a 100 mL single neck flask and solved in THF (10 mL), then TBAF ([1 M] in THF, 1320  $\mu$ L, 1.32 mmol, 1.2 eq) and water (40 $\mu$ L, 2.2 mmol, 2.0 eq) were added and the mixture was stirred for 15 h at rt, after which the solvents were removed under reduced pressure to receive the crude as a brown solid.

The crude was solved in MeCN/H<sub>2</sub>O (1:1) and purified via prep. HPLC (reverse phase, 5-100% MeCN in H<sub>2</sub>O in 30 min, 3 runs) to gain 56.0 mg (0,2 mmol, 18% over 2 steps) of a white solid after drying on the Lyo overnight.

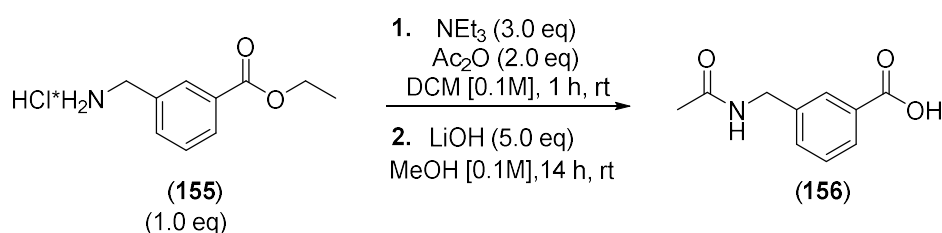
**LC-MS:** Column: Phenomenex Luna C18(2), gradient: MeCN/H<sub>2</sub>O + 0.05 % HCOOH, 5 % MeCN increase to 100% MeCN in 5.1 min, flow rate: 0.6 mL/min, t<sub>R</sub> = 1.95 min, m/z = 282.2 [[M+H]<sup>+</sup>)



**<sup>1</sup>H-NMR** (500 MHz, dms<sub>o</sub>-d<sub>6</sub>,  $\delta$  in ppm): 10.28 (s, 1H, amide-H), 9.19 (s, 1H, H-9), 8.02 (s, 1H, H-15 or H-16), 7.93 (s, 1H, H-3), 7.85 (d, 3J = 7.5 Hz, 1H, H-5), 7.60-7.40 (m, 3H, H-6, H-7, H-15 or H-16), 7.43 (s, 1H, H-11), 5.35 (s, 1H, OH), 4.60 (s, 2H, H-1), 2.49 (s, 3H, H-13).

**<sup>13</sup>C-NMR** (126 MHz, dms<sub>o</sub>-d<sub>6</sub>,  $\delta$  in ppm): 165.78 (C-8), 163.07, 142.96, 142.76, 134.21, 132.41, 129.70, 128.22, 125.99, 125.97, 125.88, 125.64, 199.72, 115.59, 114.58, 62.60 (C-1), 16.63 (C-13).

## Synthesis of 3-(acetamidomethyl)benzoic acid (156)



In a 100 mL single neck flask, ethyl 3-(aminomethyl)benzoate hydrochloride ((**155**), 404.9 mg, 2.0 mmol, 1.0 eq) was solved in DCM (20 mL, [0.1 M]). Then NEt<sub>3</sub> (840 μL, 6.0 mmol, 3.0 eq) and Ac<sub>2</sub>O (380 μL, 4.0 mmol, 2.0 eq) were added at 0°C. After 30 min, LC-MS confirmed full conversion and the volatiles were removed under reduced pressure.

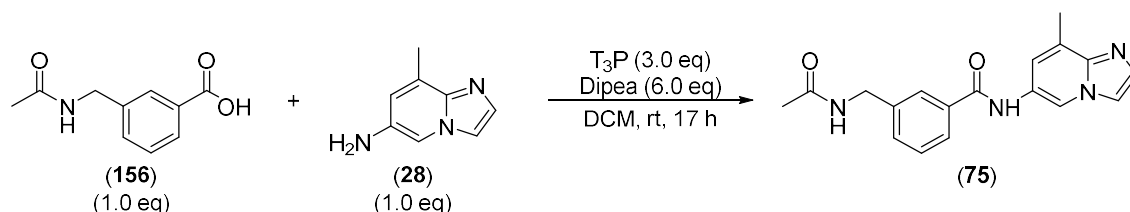
The remaining oil was solved in MeOH (20 mL, [0.1M]) and powdered LiOH (244.0 mg, 10.0 mmol, 5.0 eq) was added. The suspension was stirred for 14 h at rt.

Subsequently, the MeOH was removed under reduced pressure and desionized water (5 mL) was added. Acidification to PH = 3 with an aq. HCl [2 M] solution did not precipitate the acid. The acid was extracted with EtOAc, washed with brine and dried over Na<sub>2</sub>SO<sub>4</sub>. Removal of the solvent delivered the desired crude as a yellow oil.

The crude was solved in MeCN/H<sub>2</sub>O/DMSO (1:1:1) and purified via prep. Flash (reverse phase, 5-100% MeCN in H<sub>2</sub>O in 30 min, 2 runs, elution after 10 min) to gain the pure product as a white solid.

**LC-MS:** Column: Phenomenex Luna C18(2), gradient: MeCN/H<sub>2</sub>O + 0.05 % HCOOH, 5 % MeCN increase to 100% MeCN in 7 min, flow rate: 0.6 mL/min, t<sub>R</sub> = 2.01 min, m/z = 194.13 [[M+H]<sup>+</sup>).

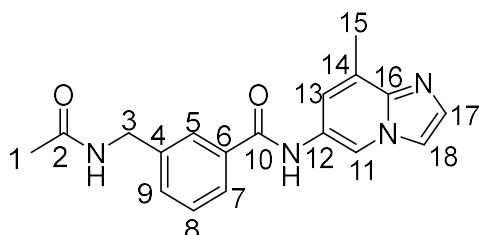
### Synthesis of 3-(acetamidomethyl)-N-(8-methylimidazo[1,2-a]pyridin-6-yl)benzamide (**75**)



According to **standard procedure 1**, 8-methylimidazo[1,2-a]pyridin-6-amine ((**28**), 30.4 mg, 0.2 mmol, 1.0 eq), 3-(acetamidomethyl)benzoic acid ((**156**), crude, 37.8 mg, 0.2 mmol, 1.0 eq), Dipea (210 μL, 1.2 mmol, 6.0 eq), T<sub>3</sub>P (50% in EtOAc, 380 μL, 0.6 mmol, 3.0 eq) and DCM (5 mL, [0.05 M]) were used to gain 37.4 mg of a yellow oil after 17 h reaction time and work-up.

The crude was solved in MeCN/H<sub>2</sub>O/DMSO (1:1:1) and purified via prep. HPLC (reverse phase, 5-50% MeCN in H<sub>2</sub>O in 30 min, 2 runs) to gain 5.76 mg (0,018 mmol, 9% over 2 steps) of a white solid after drying on the Lyo overnight.

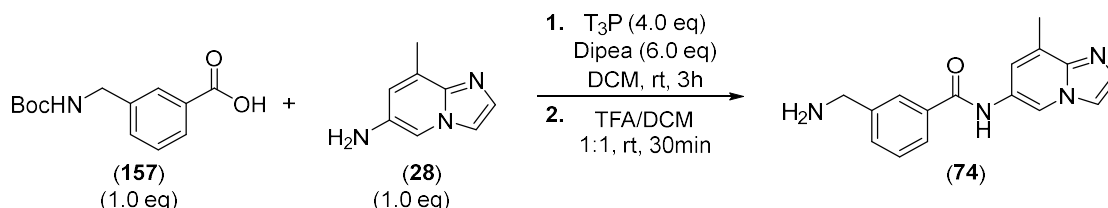
**LC-MS:** Column: Phenomenex Luna C18(2), gradient: MeCN/H<sub>2</sub>O + 0.05 % HCOOH, 5 % MeCN increase to 100% MeCN in 7 min, flow rate: 0.6 mL/min, t<sub>R</sub> = 1.73 min, m/z = 323.2 [[M+H]<sup>+</sup>).



**<sup>1</sup>H-NMR** (500 MHz, dms<sub>o</sub>-d<sub>6</sub>, δ in ppm): 10.29 (s, 1H, Amide-NH), 9.19 (s, 1H, 11-H), 4.35 (d, <sup>3</sup>J<sub>3,NH</sub> = 5.8 Hz, 1H, H-3), 8.44 (t, <sup>3</sup>J<sub>NH,3</sub> = 5.8 Hz, 1H, Acetylamine-NH), 8.03 (s, 1H, H-17 or H-18), 7.90-7.80 (m, 2H, H-5, H-7), 7.57-7.43 (m, 3H, H-8, H-9, H-17 or H-18), 7.27 (s, 1H, H-11), 2.50 (s, 3H, H-15), 1.90 (s, 3H, H-1).

**<sup>13</sup>C-NMR** (126 MHz, dms<sub>o</sub>-d<sub>6</sub>, δ in ppm): 169.26 (C-2), 165.65 (C-10), 142.81, 140.10, 134.41, 132.50, 130.58, 128.43, 126.61, 125.97, 125.94, 125.90, 119.65, 115.64, 114.58, 41.97 (C-3), 22.59 (C-1), 16.63 (C-15).

### Synthesis of 3-(aminomethyl)-N-(8-methylimidazo[1,2-a]pyridin-6-yl)benzamide (74)

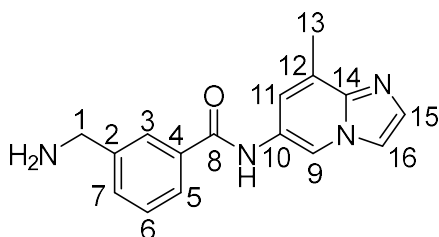


According to **standard procedure 1**, 8-methylimidazo[1,2-a]pyridin-6-amine ((**28**), 31.8 mg, 0.2 mmol, 1.0 eq), 3-(((tert-butoxycarbonyl)amino)methyl)benzoic acid ((**157**), 50.8 mg, 0.2 mmol, 1.0 eq), Dipea (210 μL, 1.2 mmol, 6.0 eq), T3P (50% in EtOAc, 380 μL, 0.6 mmol, 3.0 eq) and DCM (4 mL, [0.05M]) were used to gain 53 mg of a brown oil after 18 h reaction time and work-up.

According to **standard procedure 2** the crude was solved in TFA (1 mL) and DCM (5 mL) to gain the crude amide in 90% purity after 90 min reaction time.

The crude was solved in MeCN/H<sub>2</sub>O (1:9) and purified via prep. HPLC (reverse phase, 5 min 5% MeCN in H<sub>2</sub>O then 5-30% in 30 min, 2 runs) to gain 8.92 mg (0,032 mmol, 16%) of a pale yellow solid after drying on the Lyo overnight.

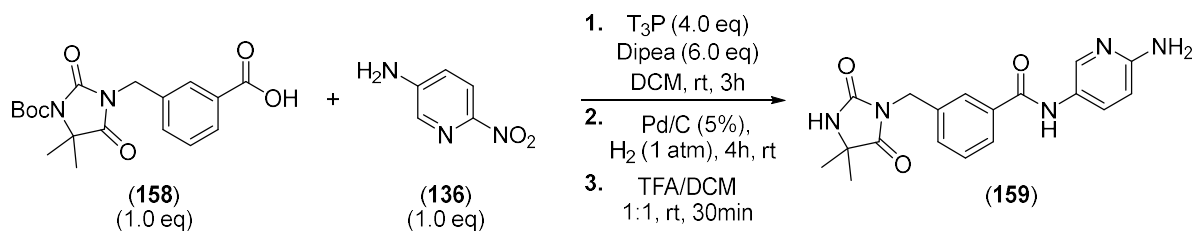
**LC-MS:** Column: Phenomenex Luna C18(2), gradient: MeCN/H<sub>2</sub>O + 0.05 % HCOOH, 5 % MeCN increase to 100% MeCN in 5.1 min, flow rate: 0.6 mL/min, t<sub>R</sub> = 1.18 min, m/z = 281.2 [[M+H]<sup>+</sup>]



**<sup>1</sup>H-NMR** (500 MHz, dms<sub>o</sub>-d<sub>6</sub>, δ in ppm): 10.82 (s, 1H, amide-H), 9.56 (s, 1H, H-9), 8.45 (s, 1H, H-15 or H-16), 8.39 (br.s, 2H, NH<sub>2</sub>), 8.13 (s, 1H, H-15 or H-16 or H-11), 8.12 (s, 1H, H-15 or H-16 or H-11), 8.04 (d, 3J = 7.8 Hz, 1H, H-5), 7.86 (s, 1H, H-3), 7.73 (d, 3J = 7.7 Hz, 1H, H-7), 7.64 (t, 3J = 7.7 Hz, 1H, H-6), 4.16 (s, 2H, H-1), 2.59 (s, 3H, H-13).

**<sup>13</sup>C-NMR** (126 MHz, dms<sub>o</sub>-d<sub>6</sub>, δ in ppm): 165.67 (C-8), 137.83 (q.C), 134.67, 134.09, 132.62 (q.C), 129.52 (q.C), 128.89, 128.65, 127.65, 126.07 (q.C), 124.38 (q.C), 123.09, 116.35, 116.32, 42.05(C-1), 16.11 (C-13).

### Synthesis of N-(6-aminopyridin-3-yl)-3-((4,4-dimethyl-2,5-dioximidazolidin-1-yl)methyl)benzamide (159)



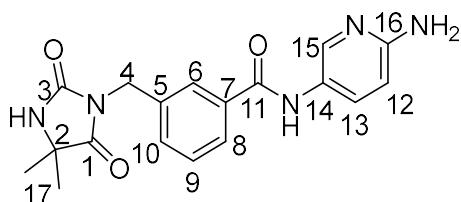
According to **standard procedure 1**, 6-nitropyridin-3-amine (**(136)**), 76.3 mg, 0.55 mmol, 1.0 eq), 3-((3-(tert-butoxycarbonyl)-4,4-dimethyl-2,5-dioximidazolidin-1-yl)methyl)benzoic acid (**(158)**), 194.6 mg, 0.55 mmol, 1.0 eq), Dipea (600  $\mu$ L, 3.3 mmol, 6.0 eq), T3P (50% in EtOAc, 1.4 mL, 2.2 mmol, 4.0 eq) and DMF (5 mL, [0.1M]) were used to gain 273.7 mg of a yellow oil after 16 h reaction at 60°C (slow reaction, performed at 60°C in DMF) and work-up.

The crude product was solved in EtOH (10 mL), which was degassed using Ar (10 min, bubbling). Then Pd/C (60.0 mg, 0.55 mmol, 0.1 eq) was added and a hydrogen atmosphere was applied by using a balloon (1 atm). After 3 h stirring at rt, LC-MS confirmed full conversion, after which the mixture was diluted with EtOH, filtered through a thick pad of Celite and washed with EtOH. Evaporation of the solvent gave 199.1mg of the crude product as a pale yellow oil.

According to **standard procedure 2**, DCM (10 mL) and TFA (2 mL) and the crude from the previous step were used to gain the free amine in 90% purity on the LC-MS after 30 min reaction time.

To purify the product, it was solved in MeCN/H<sub>2</sub>O and purified via prep. HPLC (reverse phase, 5-50% MeCN in H<sub>2</sub>O in 30 min, 3 runs) to gain 19.3 mg (0,055 mmol, 10% over 3 steps) of a slight yellow solid after drying on the Lyo overnight.

**LC-MS:** Column: Phenomenex Luna C18(2), gradient: MeCN/H<sub>2</sub>O + 0.05 % HCOOH, 5 % MeCN increase to 100% MeCN in 5.1 min, flow rate: 0.6 mL/min, t<sub>R</sub>= 1.88 min, m/z = 354.2 [[M+H]<sup>+</sup>]

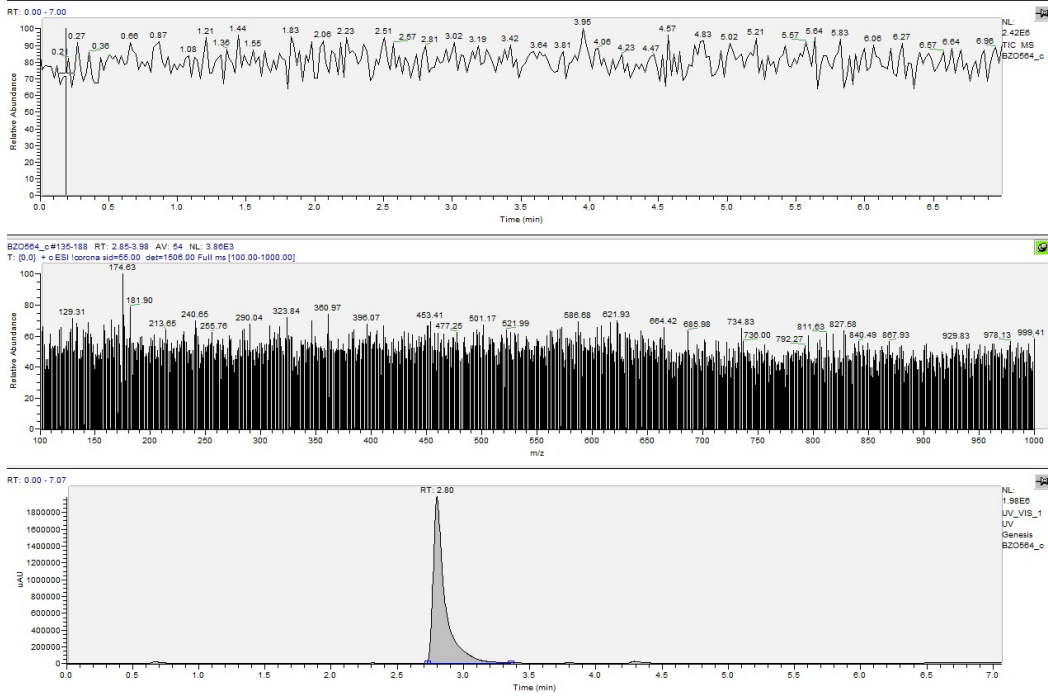


**<sup>1</sup>H-NMR** (500 MHz, dms<sub>o</sub>-d<sub>6</sub>,  $\delta$  in ppm): 10.31 (s, 1H, Amide-NH), 8.44 (s, 1H, Hydantoin-NH), 8.37 (d, <sup>4</sup>J<sub>15,13</sub> = 2.3 Hz, 1H H-15), 7.92 (dd, <sup>3</sup>J<sub>13,12</sub> = 9.2 Hz, <sup>4</sup>J<sub>13,15</sub> = 2.4 Hz, 1H, H-13), 7.86 (d, <sup>3</sup>J<sub>8,9</sub> = 7.7 Hz, 1H, H-8), 7.77 (s, 1H, H-6), 7.51 (t, <sup>3</sup>J<sub>9,10</sub> = <sup>3</sup>J<sub>9,8</sub> = 7.7 Hz, 1H, H-9), 7.43 (d, <sup>3</sup>J<sub>10,9</sub> = 7.7 Hz, 1H, H-10), 7.03 (br.s, 2H, NH<sub>2</sub>), 6.78 (d, <sup>3</sup>J<sub>12,13</sub> = 9.2 Hz, 1H, H-12), 4.61 (s, 1H, H-4), 1.32 (s, 6H, H-17).

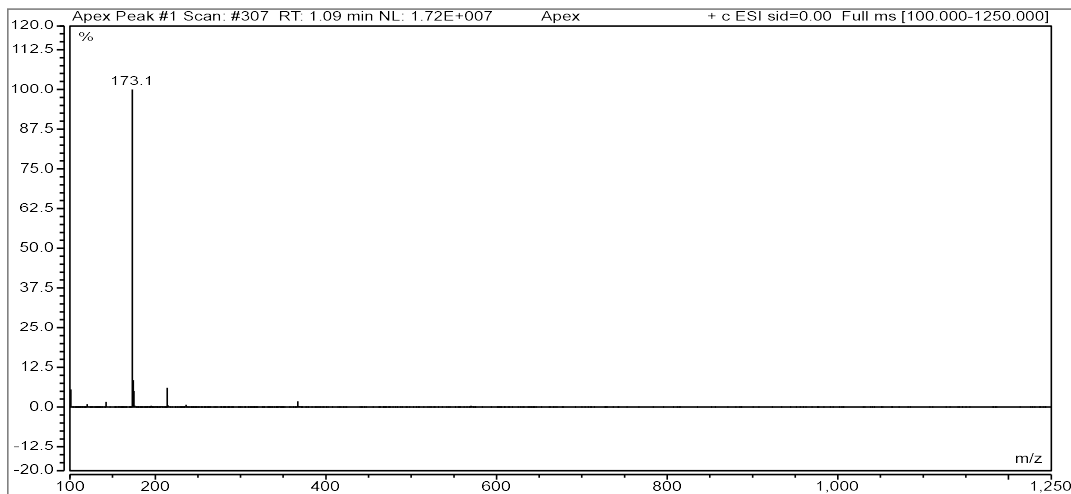
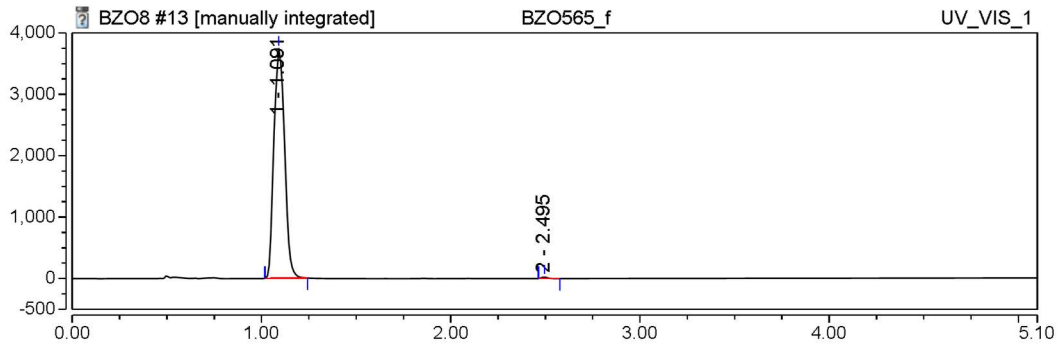
**<sup>13</sup>C-NMR** (126 MHz, dms<sub>o</sub>-d<sub>6</sub>,  $\delta$  in ppm): 177.30 (C-1), 165.17 (C-11), 155.08 (C-3), 153.74 (C-16), 137.27 (C-5), 135.42 (C-13), 134.47 (C-7), 132.86 (C-15), 130.27 (C-10), 128.78 (C-9), 126.38 (C-8 or C-6), 126.35 (C-8 or C-6), 125.58 (C-14), 110.91 (C-12), 58.00 (C-2), 40.73 (C-4), 24.65 (C-17).

# LC-MS Data

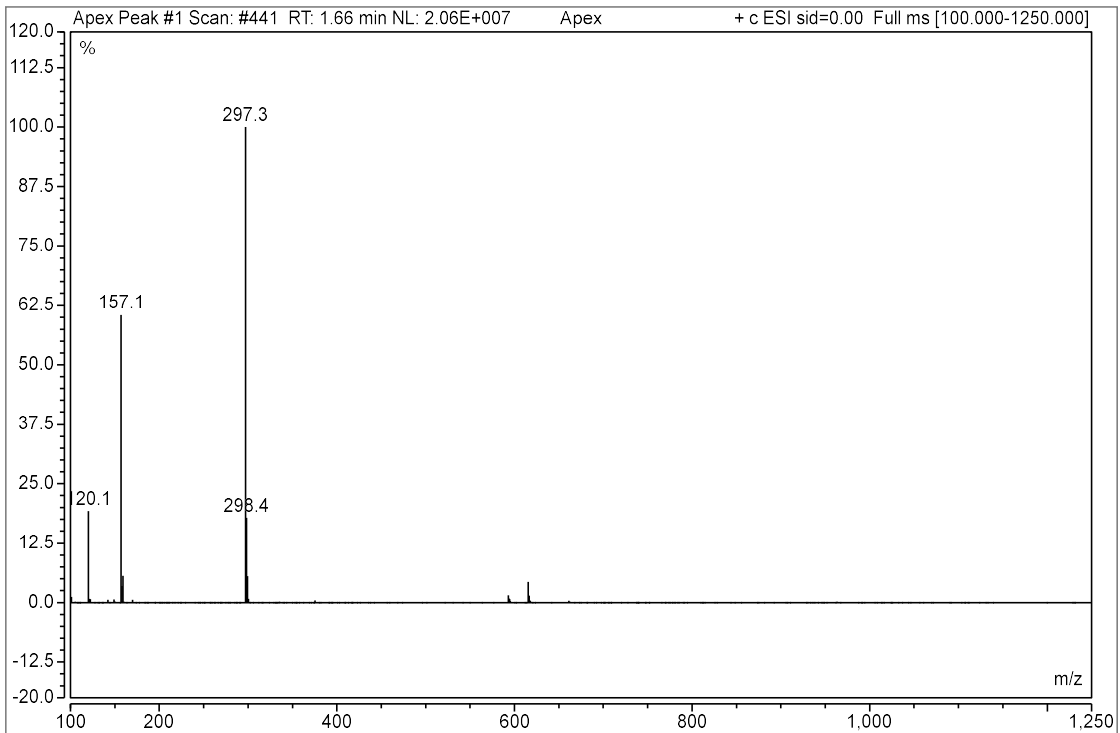
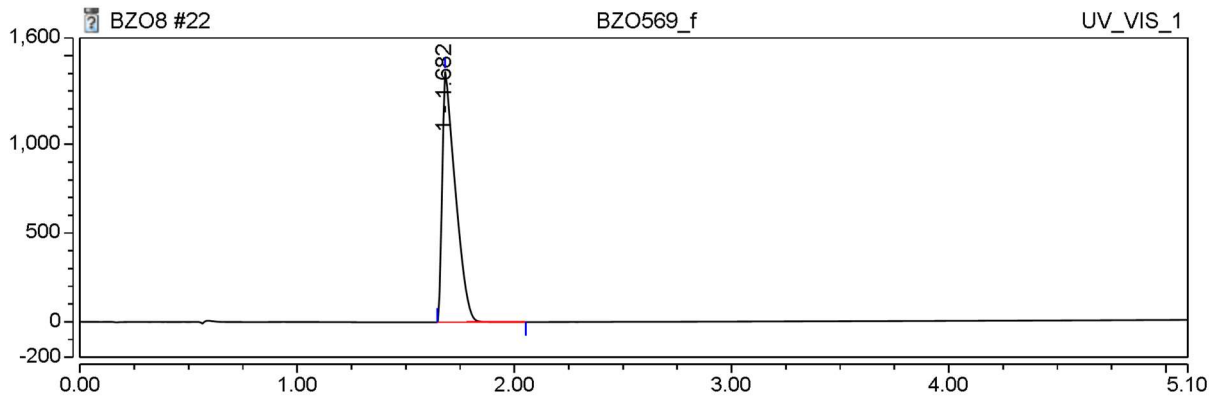
(10)



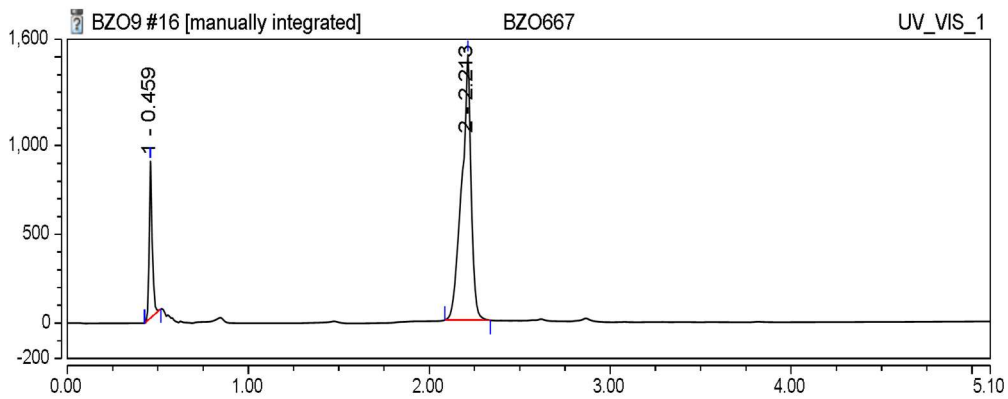
(11)

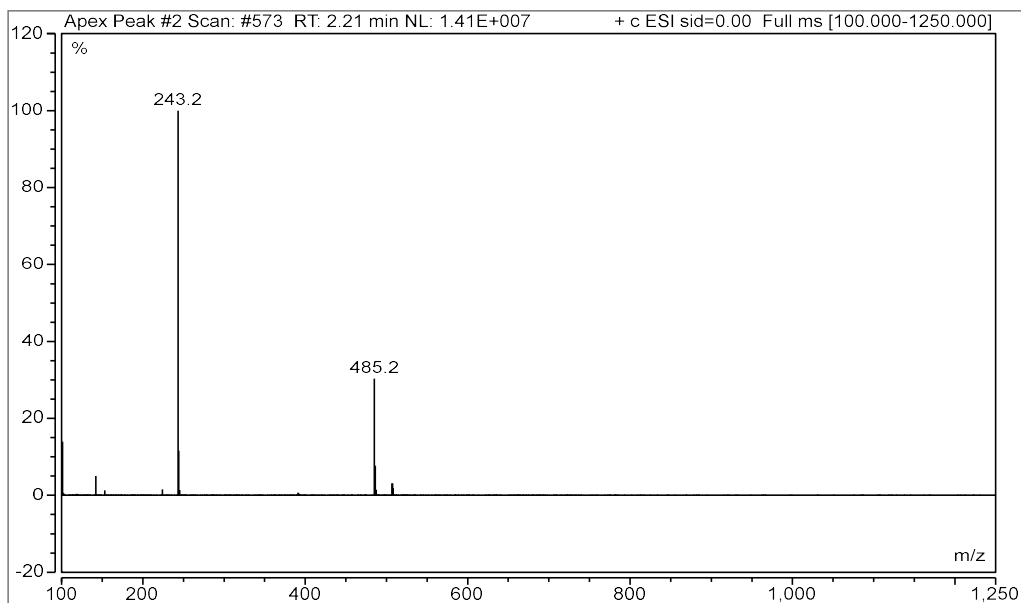


(1)

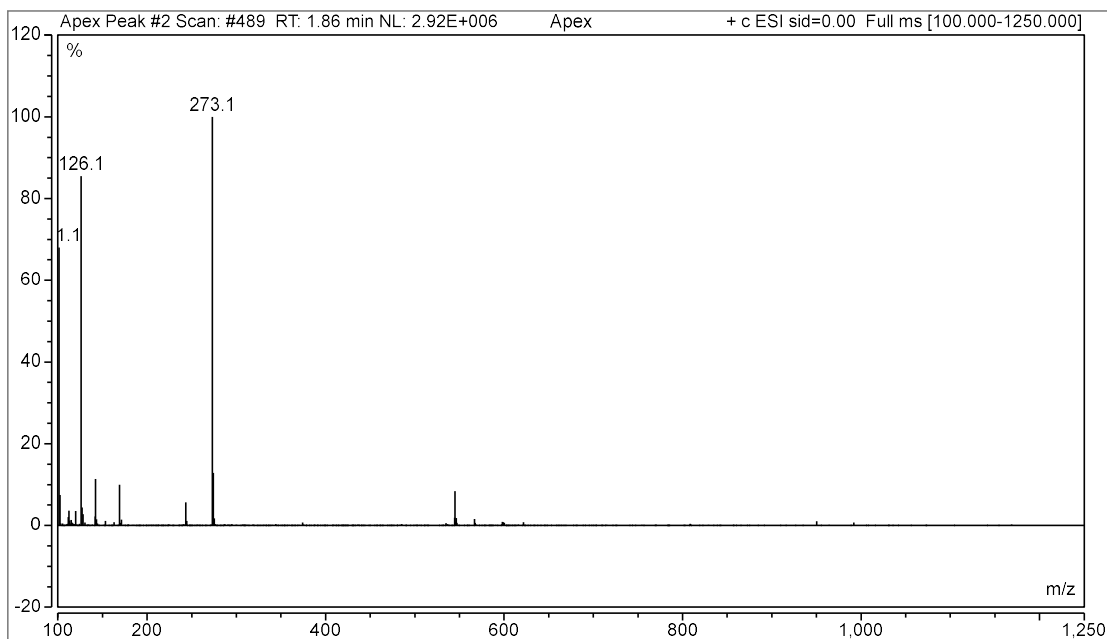
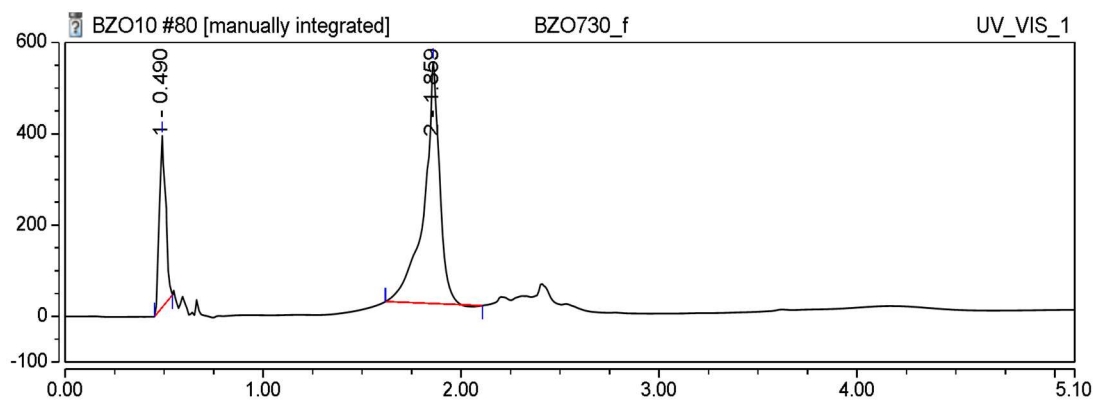


(22)

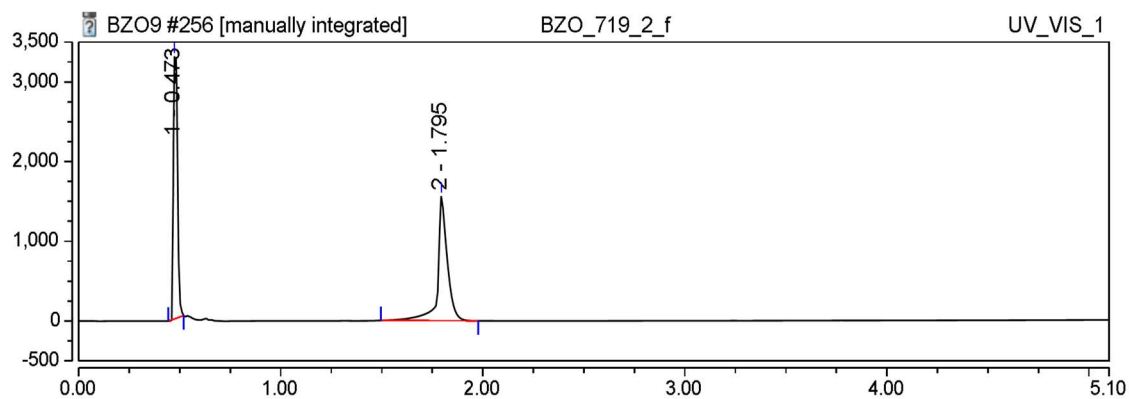




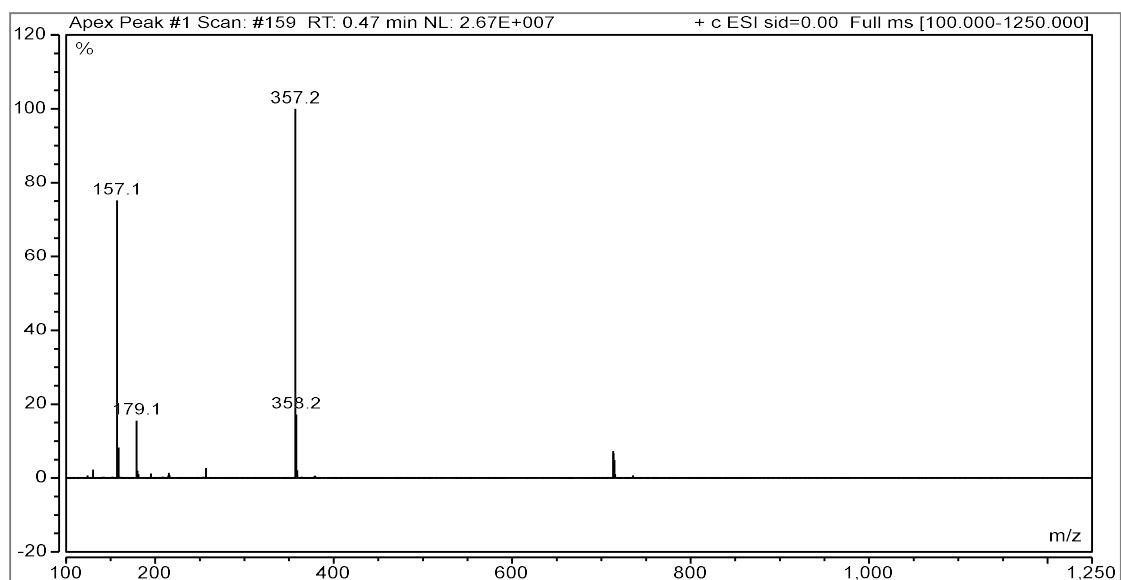
(23)



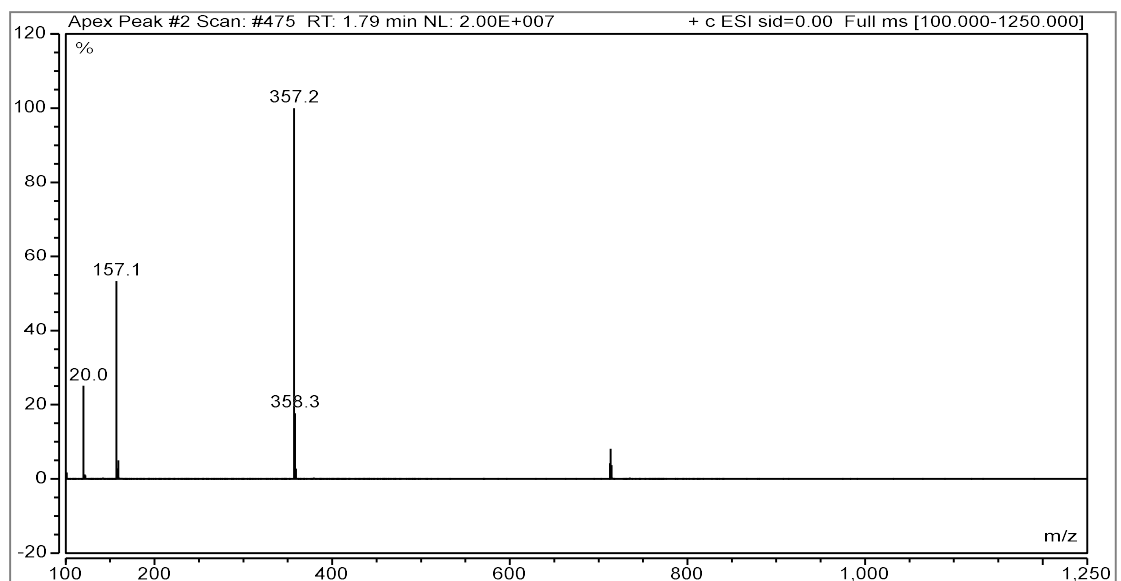
(3)



Peak1

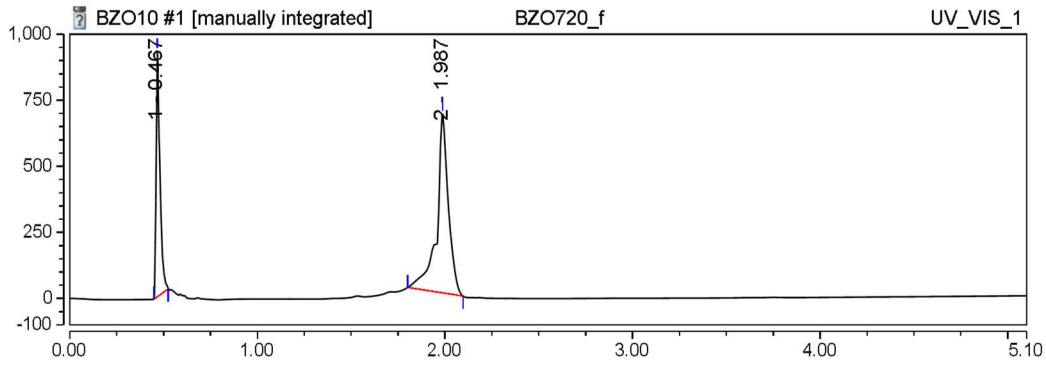


Peak2

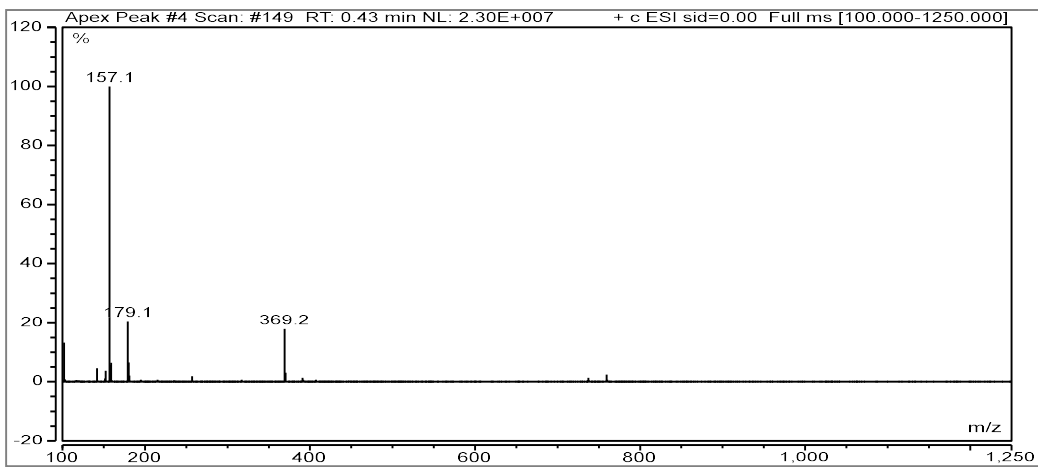




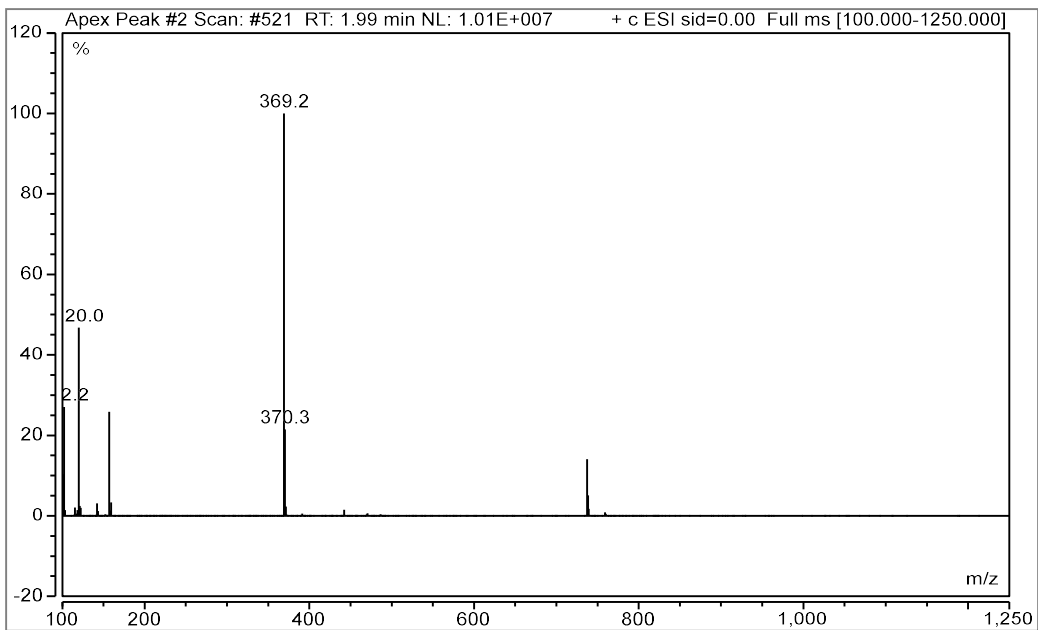
(4)



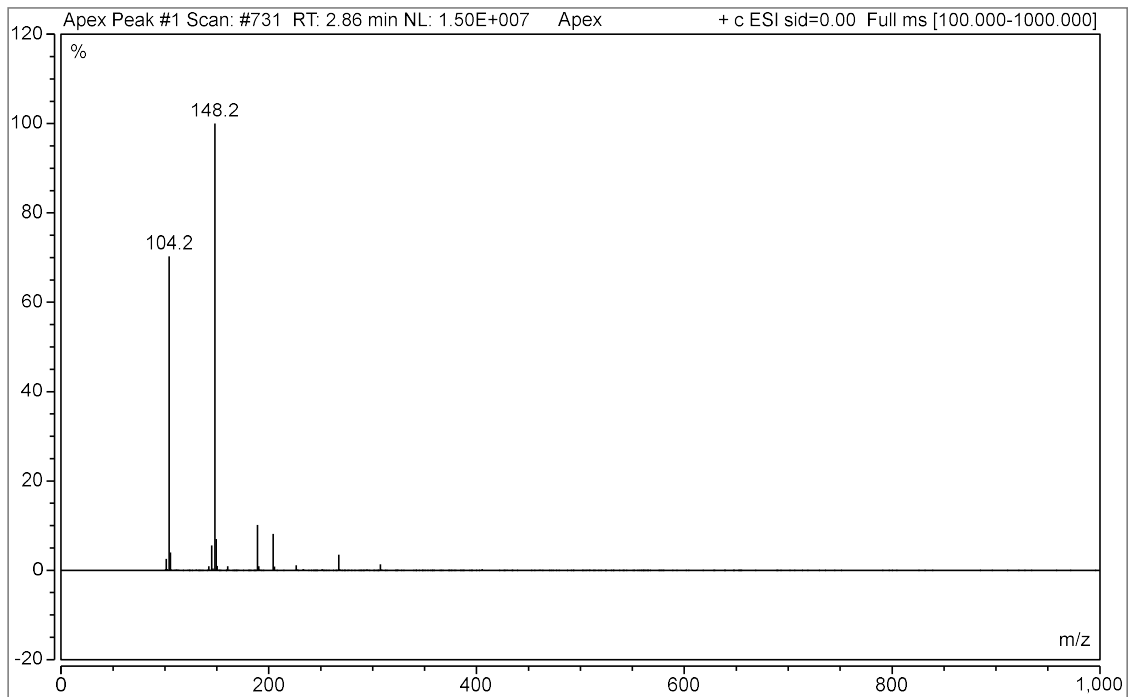
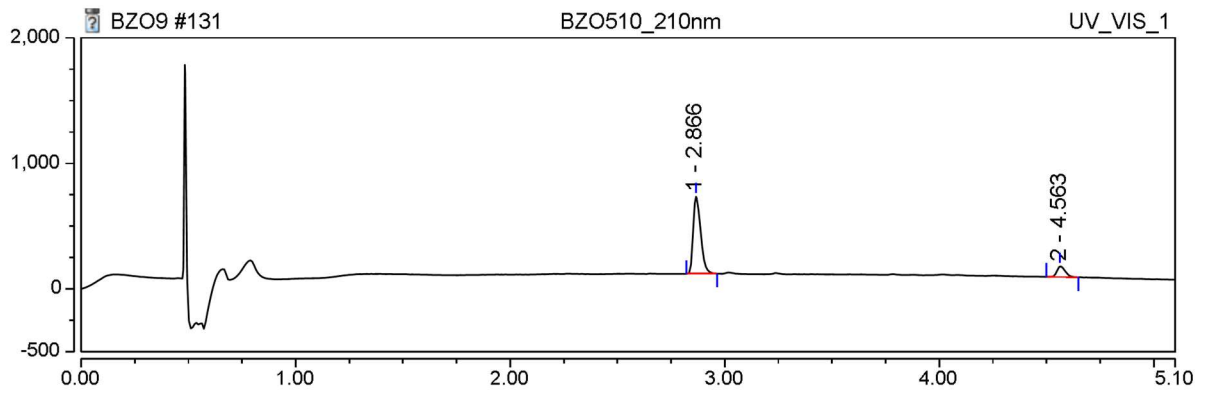
Peak1



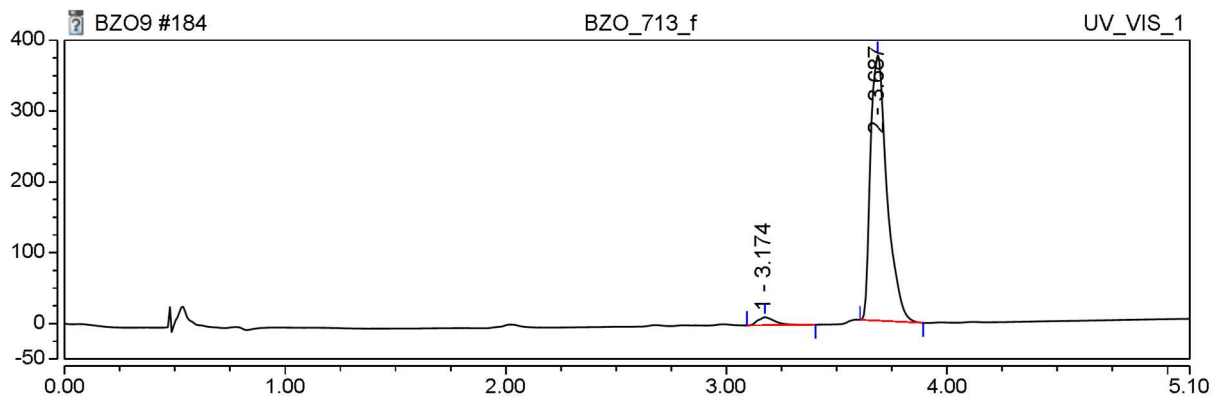
Peak2

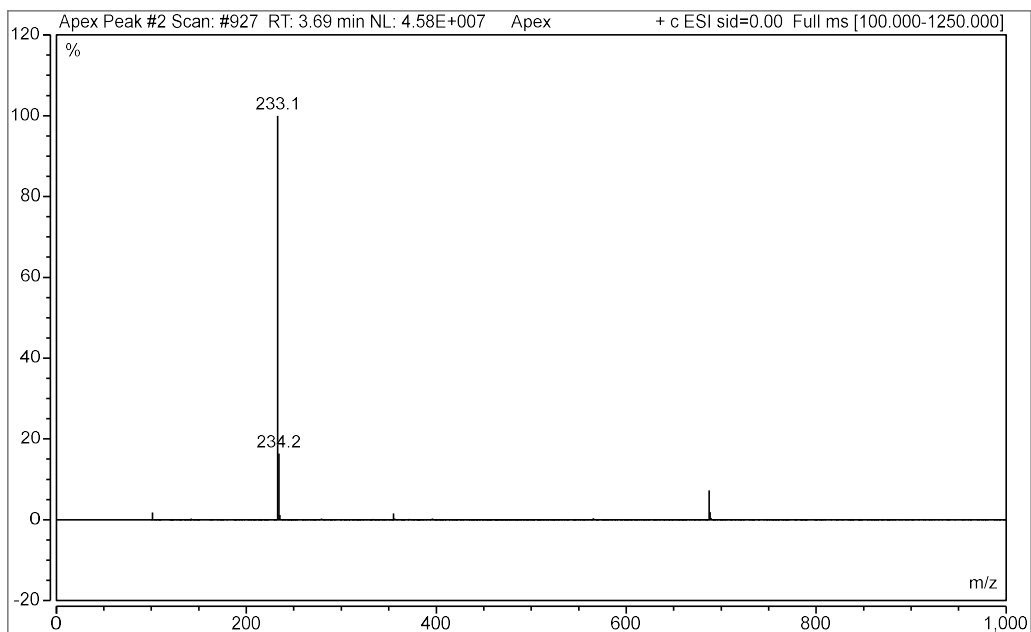


(92)

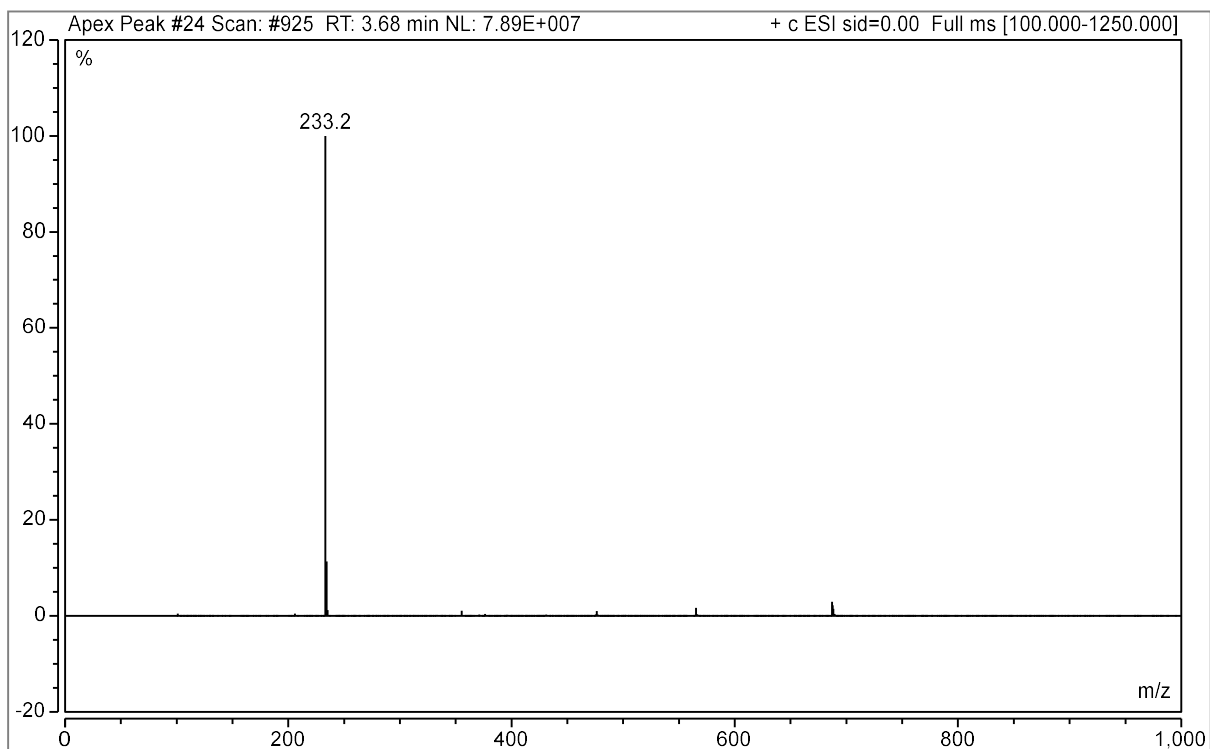
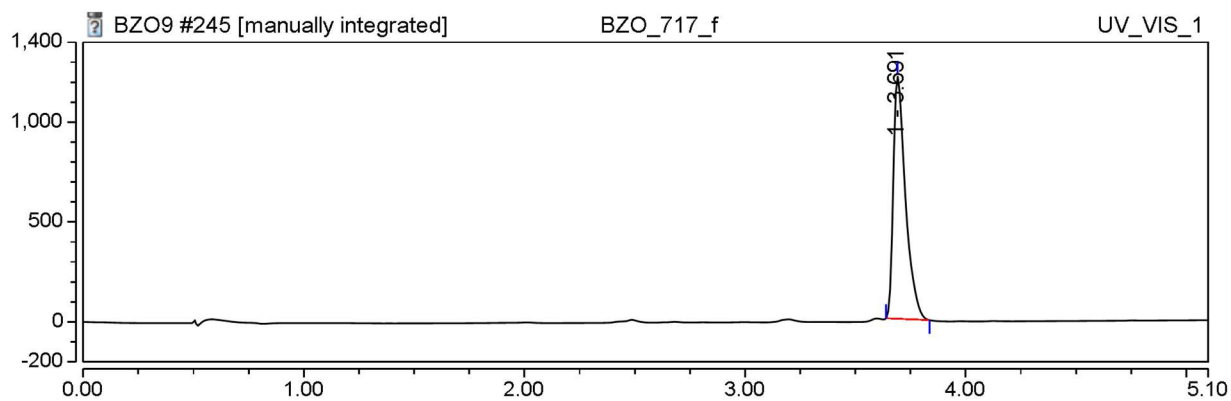


(93)



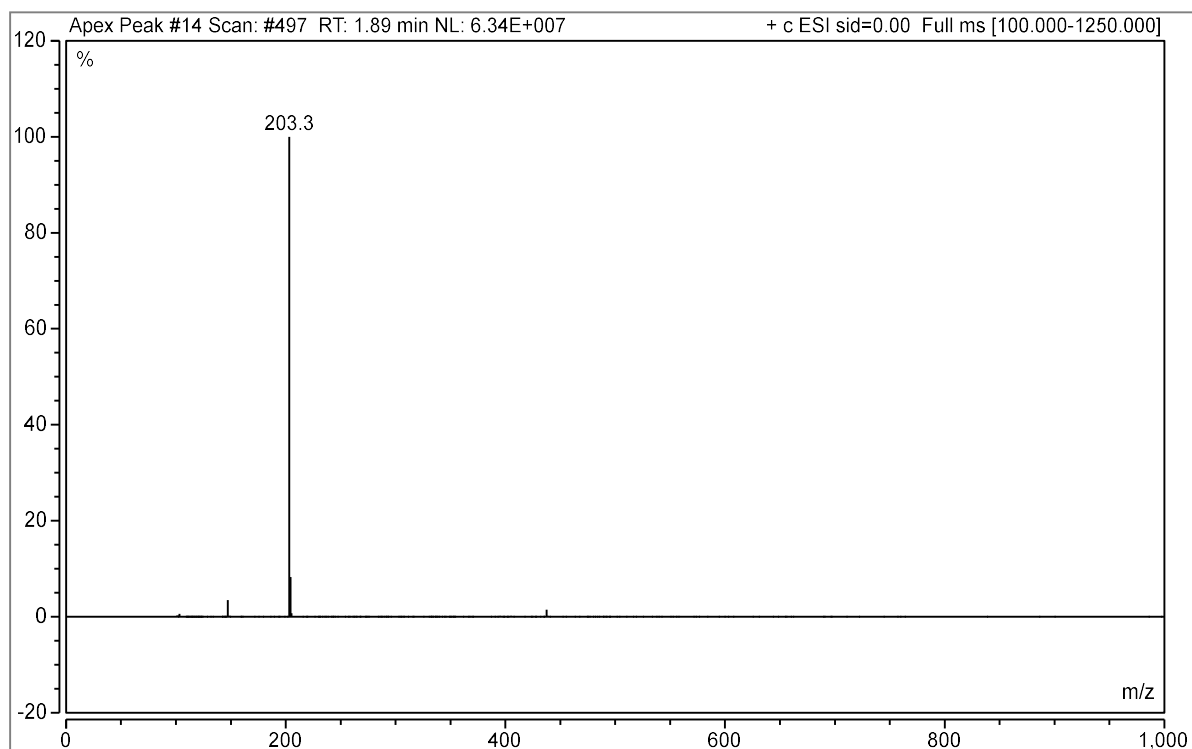


enantiomer of (93)

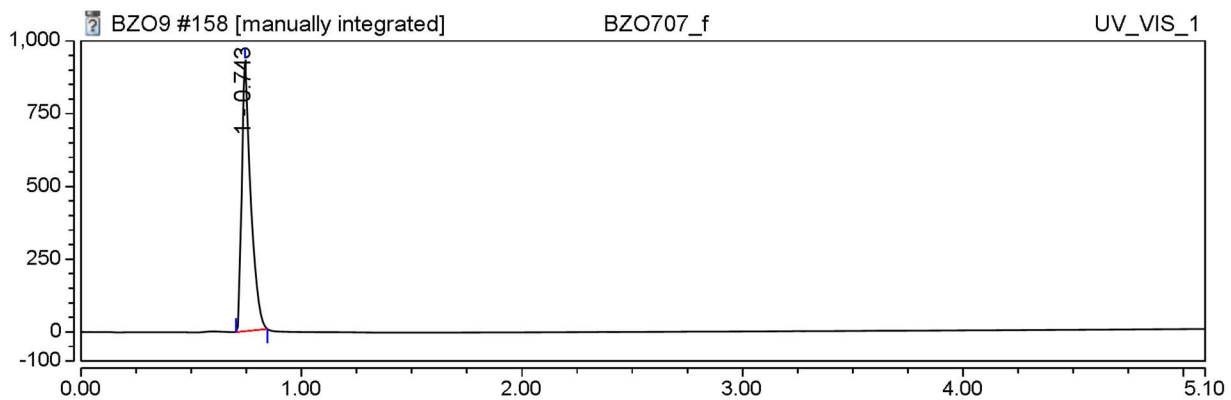


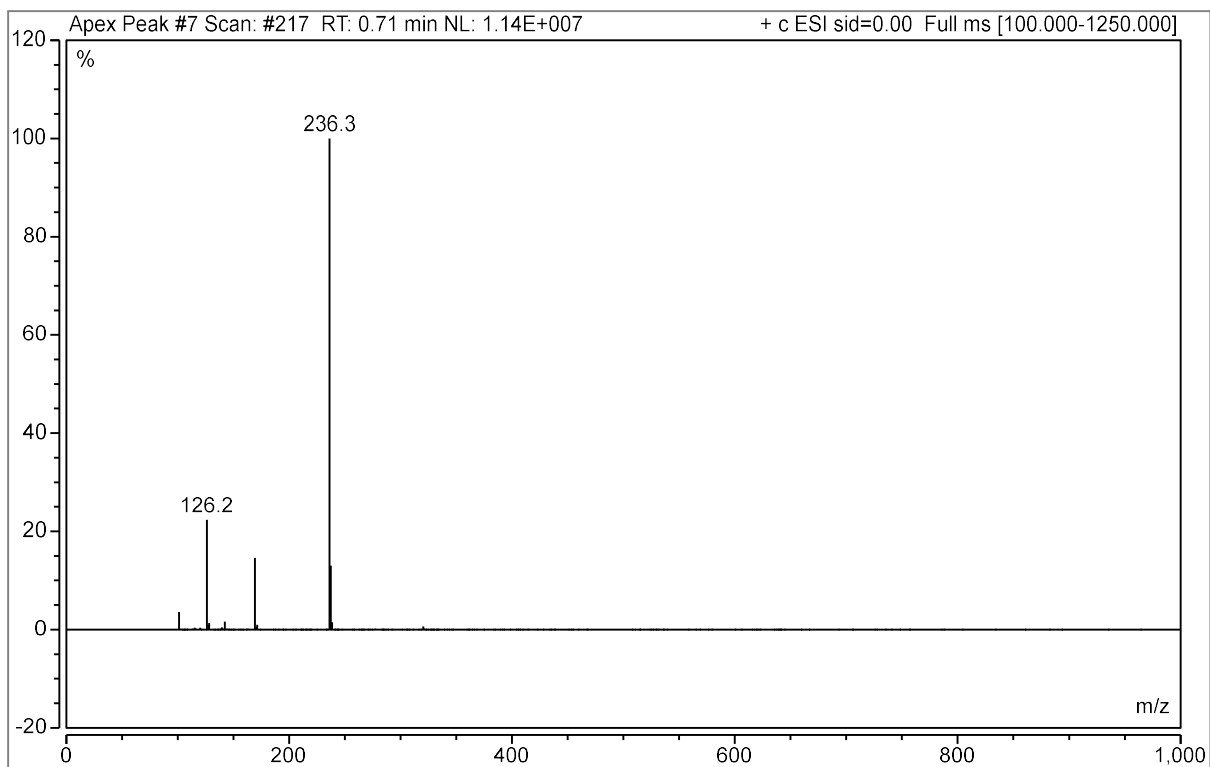
(20)

No UV at any wavelength, product at 1.886 min

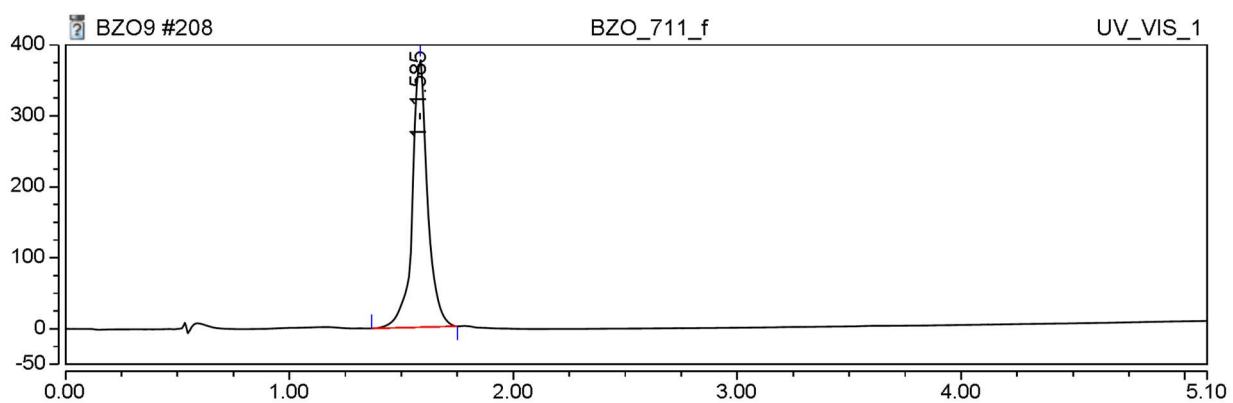


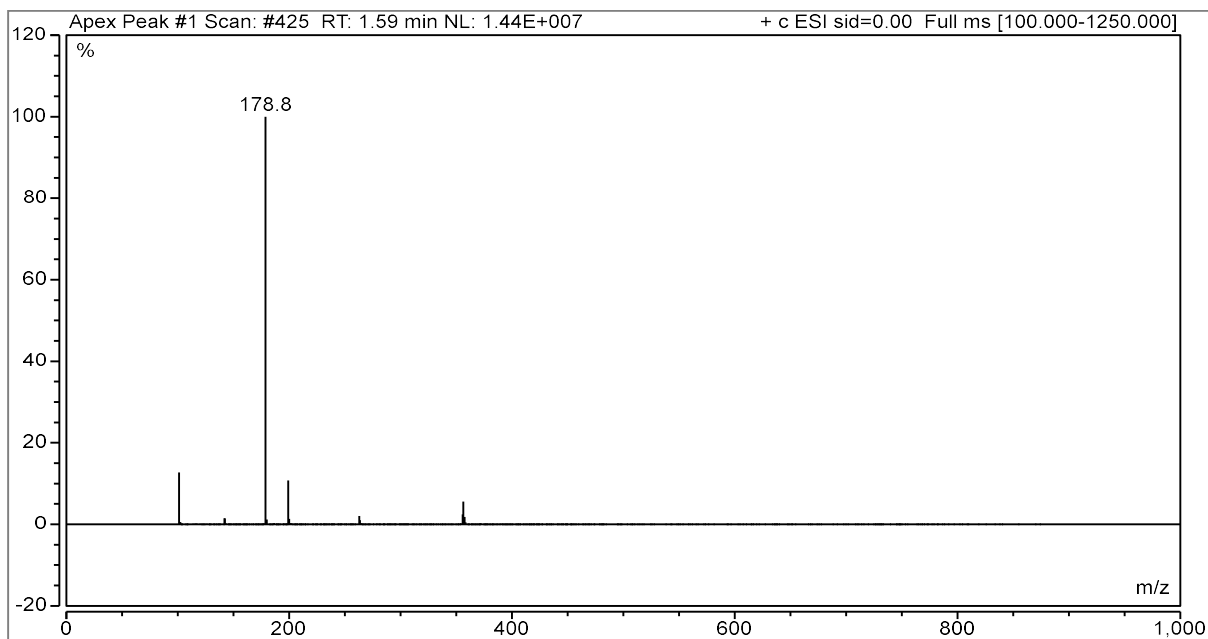
(14)



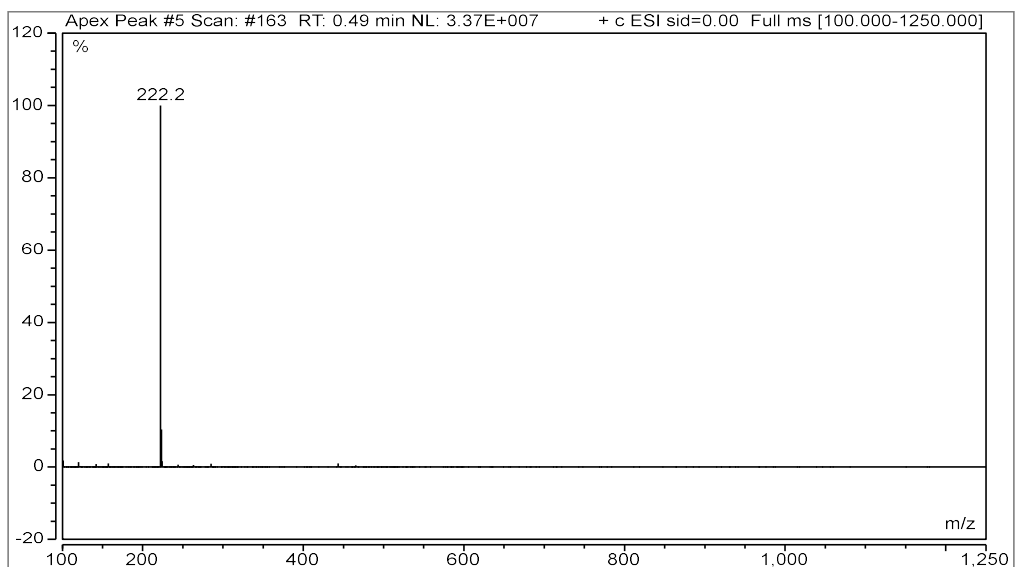
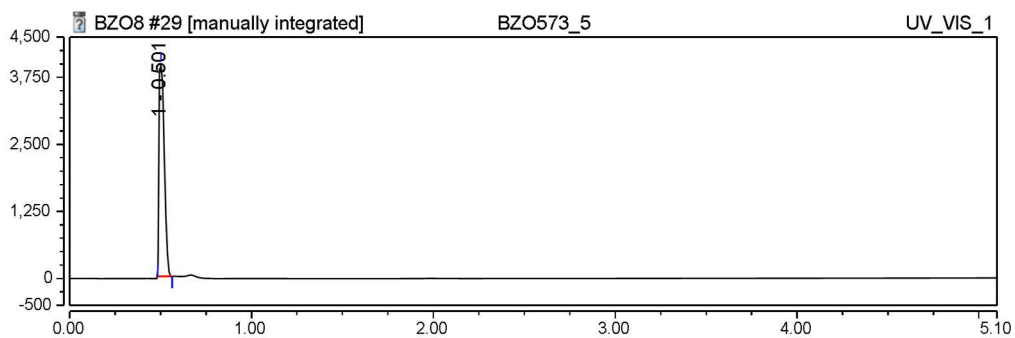


(2)

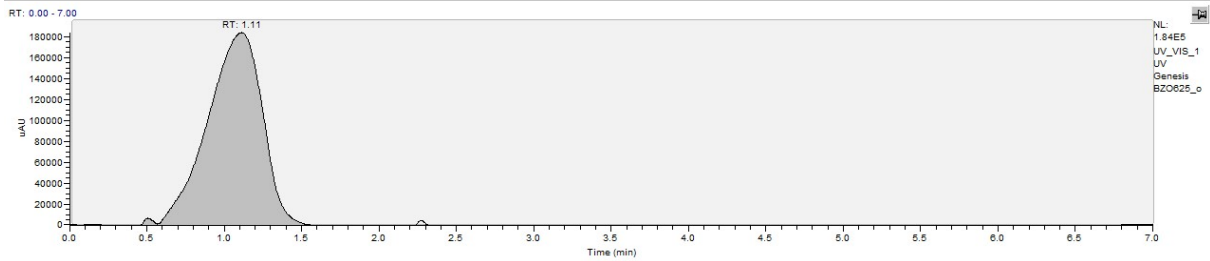
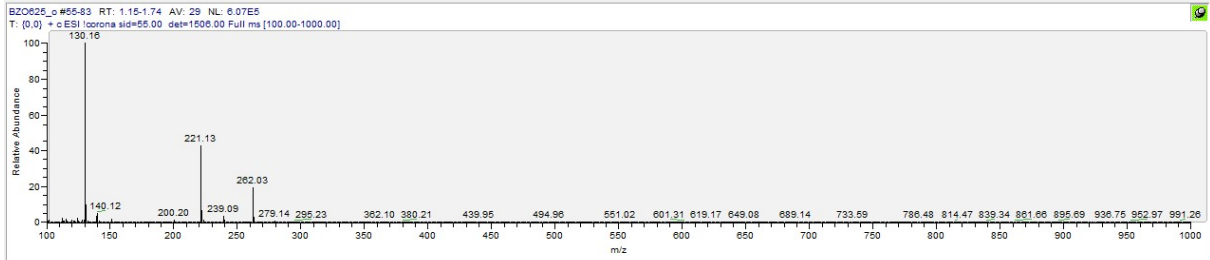
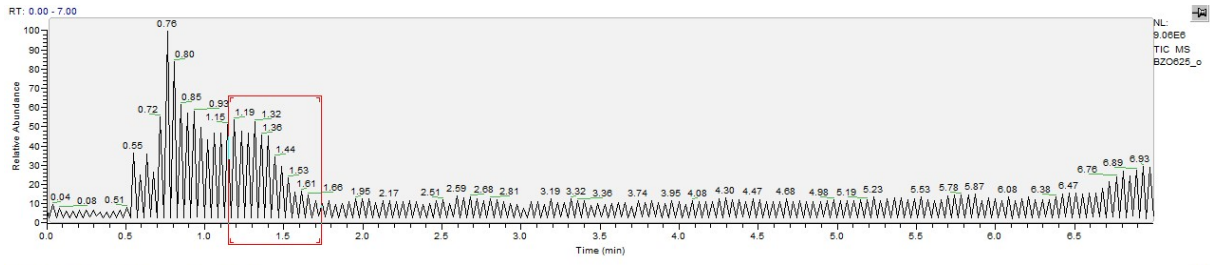




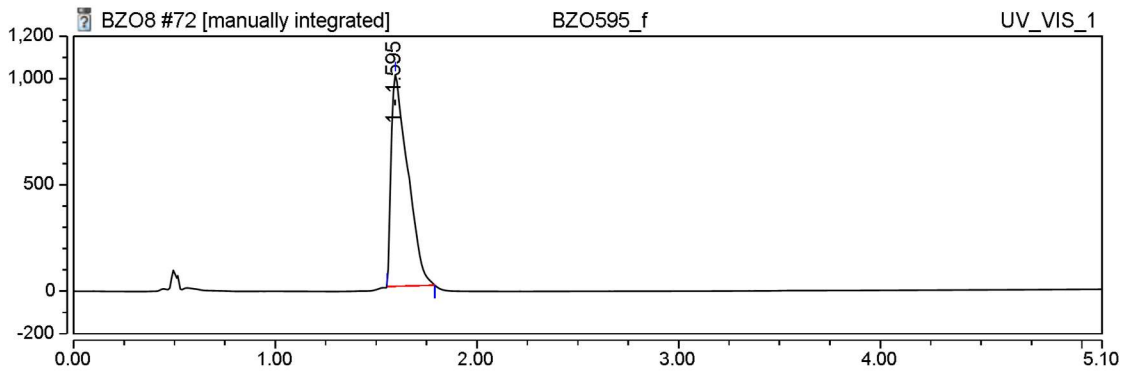
(16)

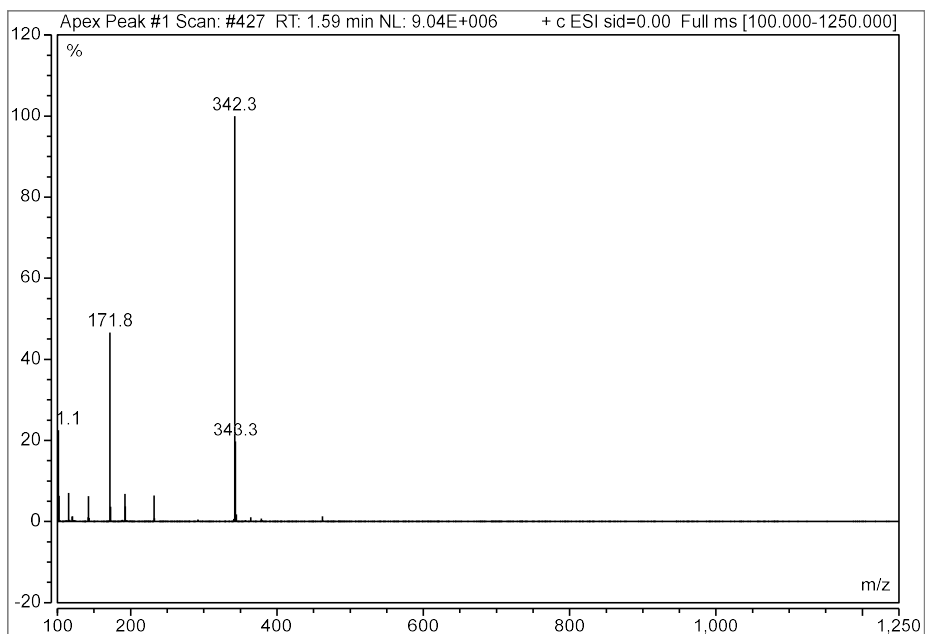


(18)

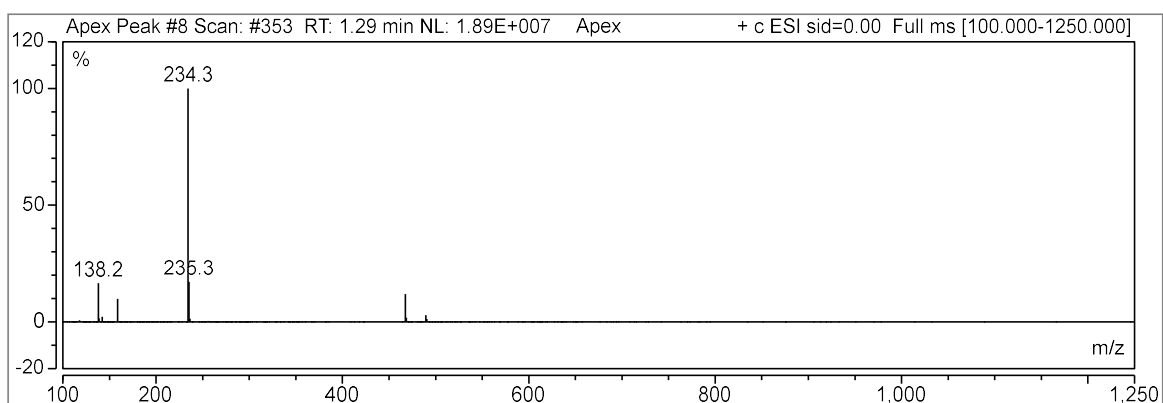
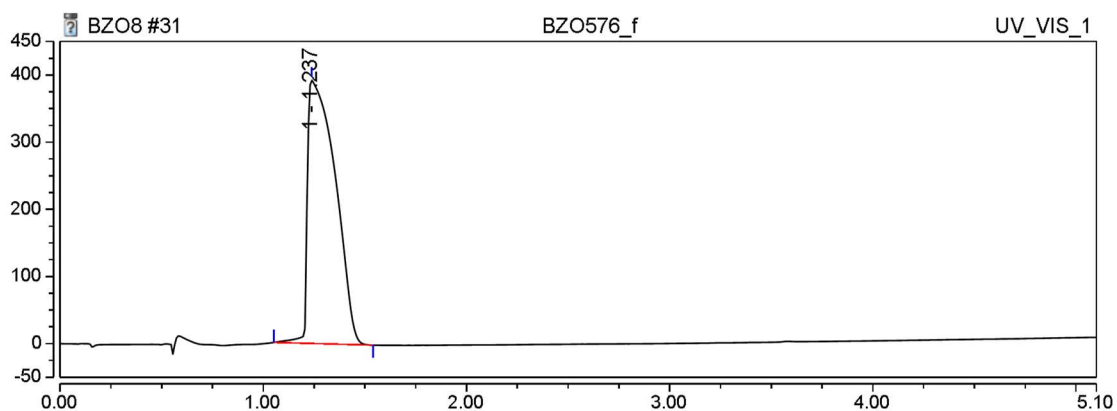


(6)



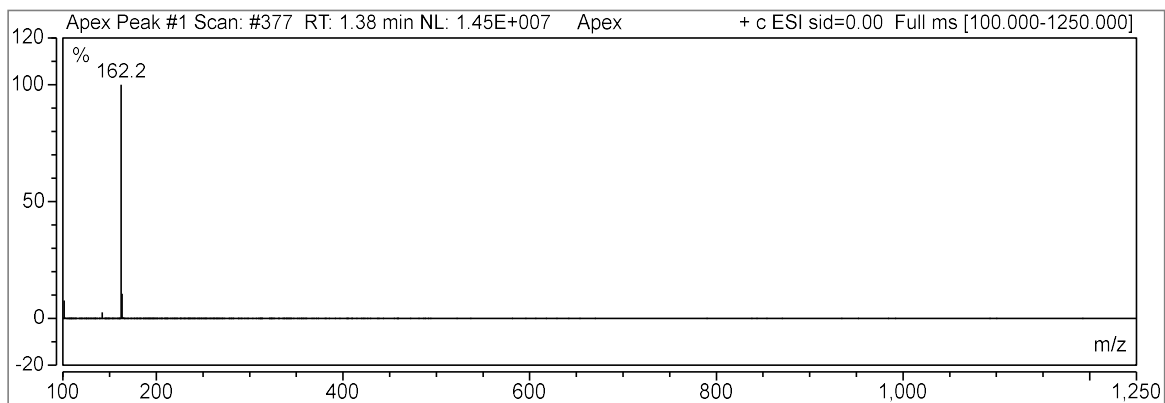
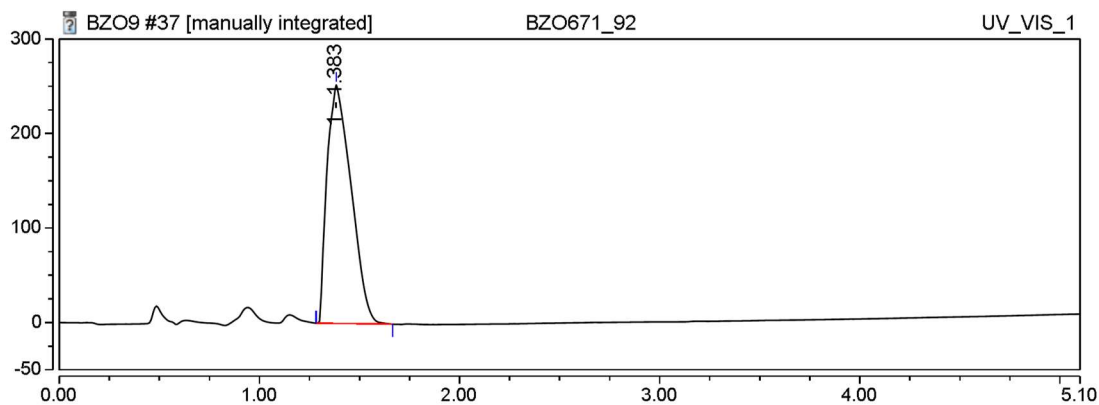


(4)

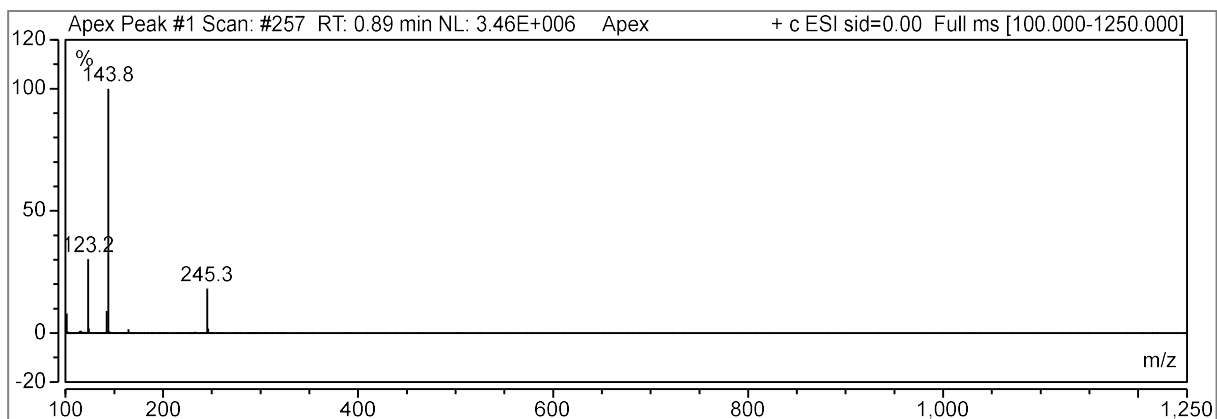
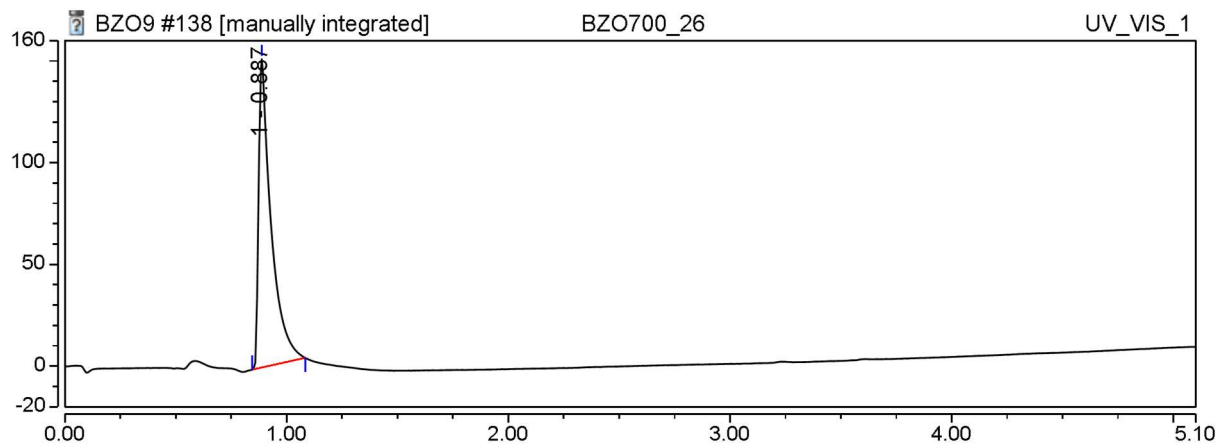




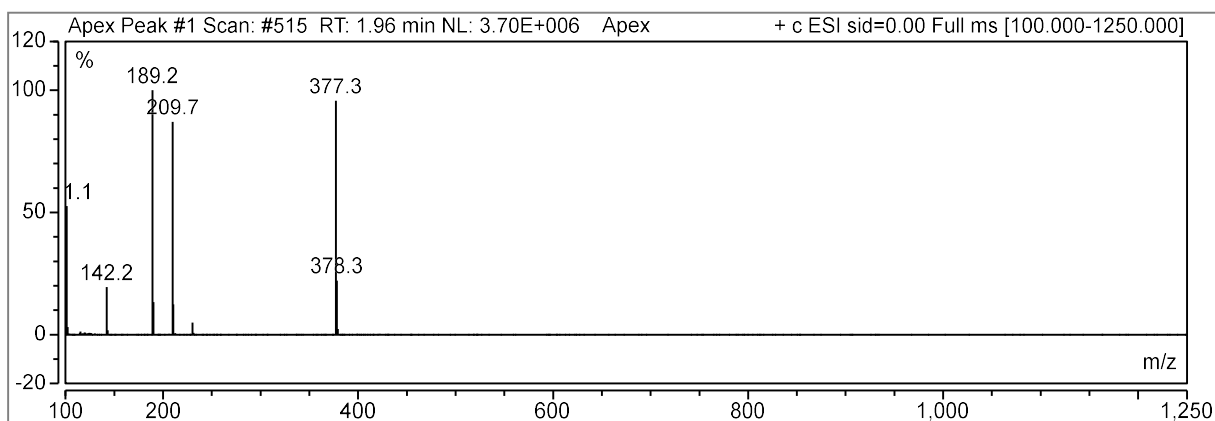
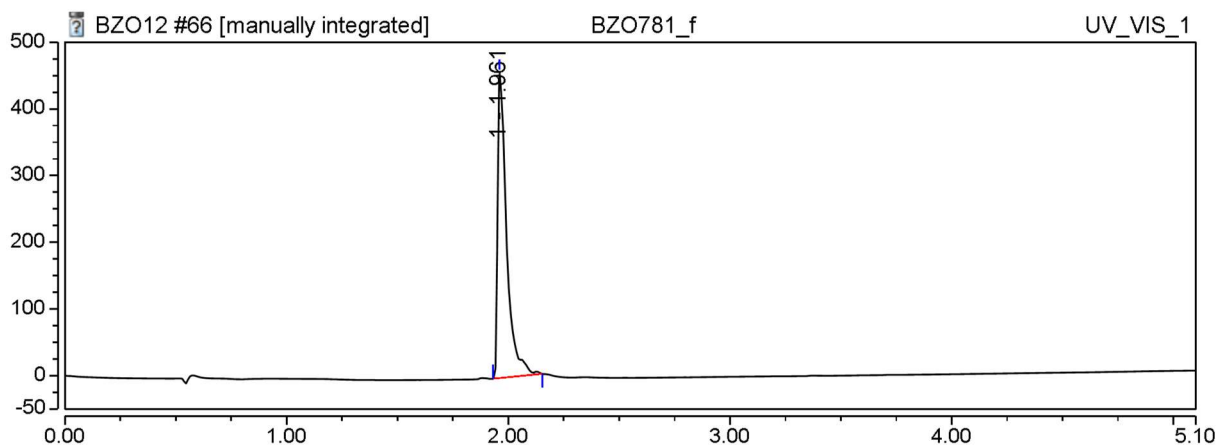
(35)



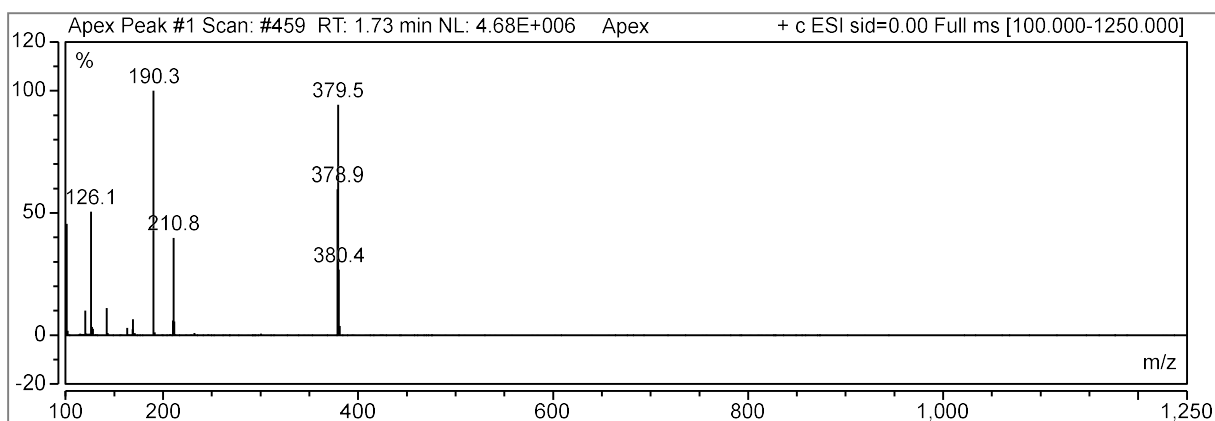
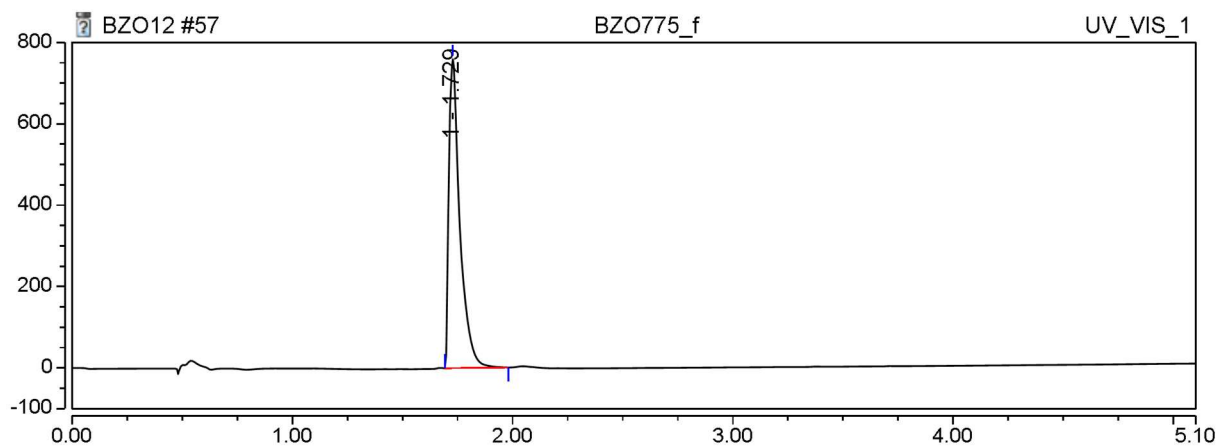
(36)



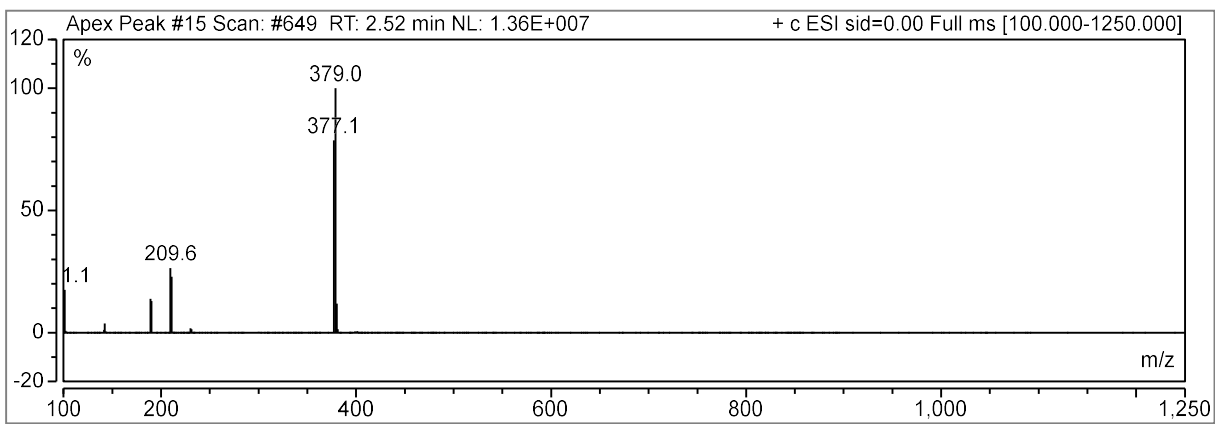
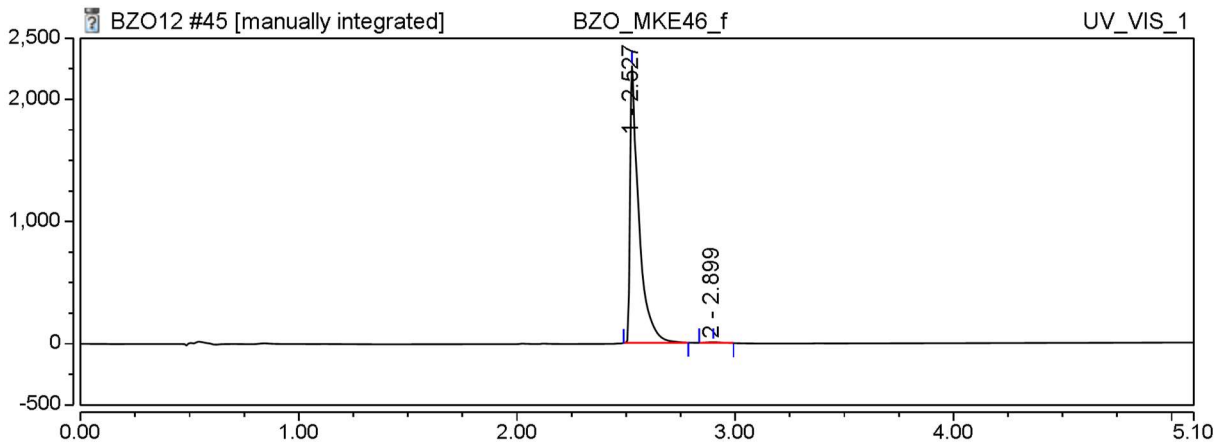
(71)



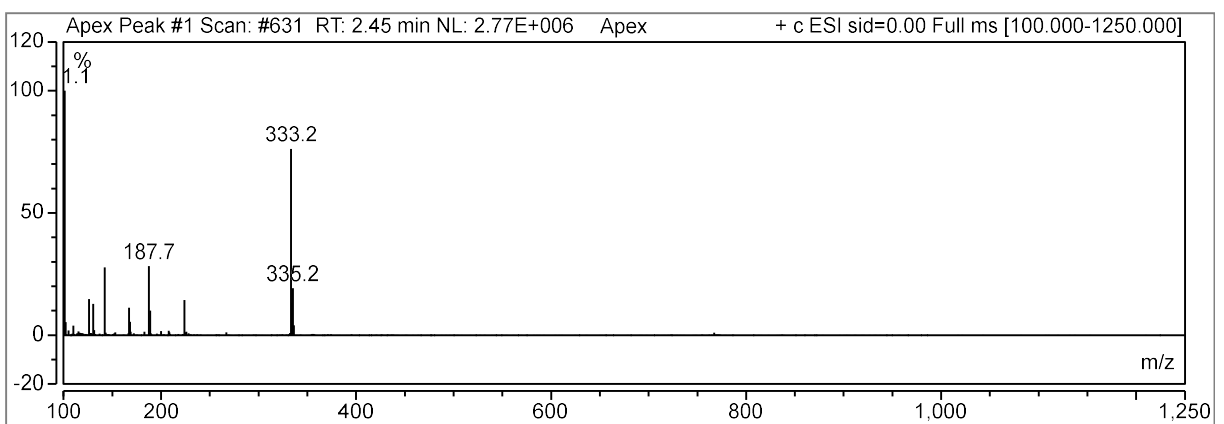
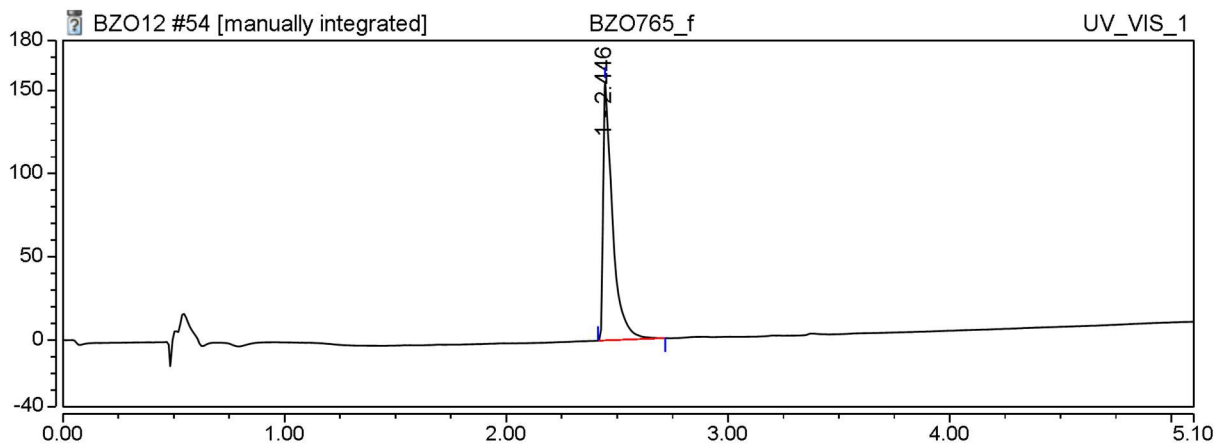
(72)



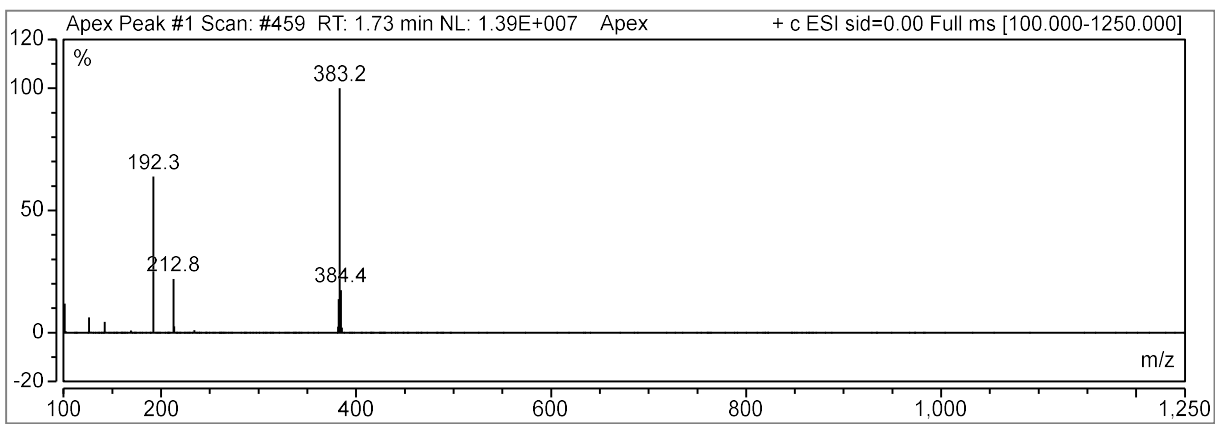
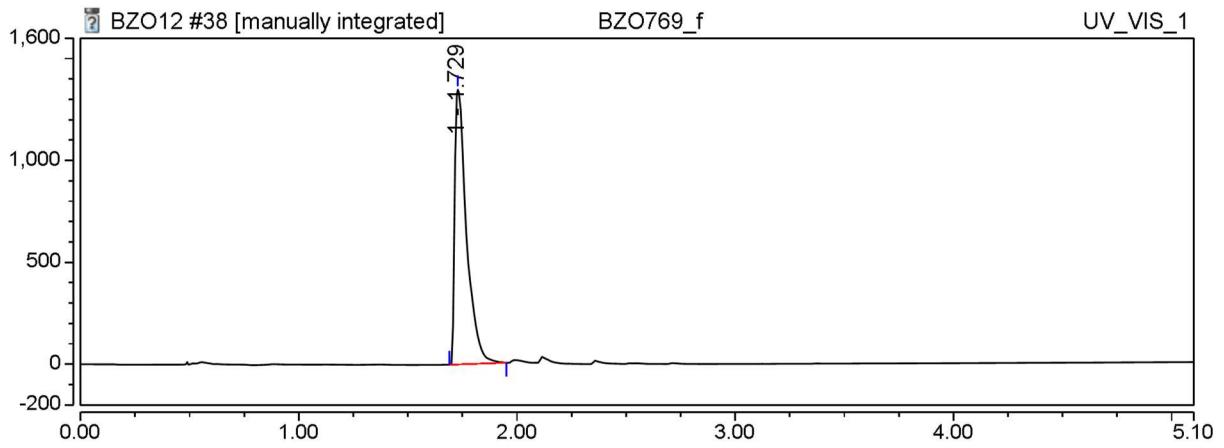
(59)



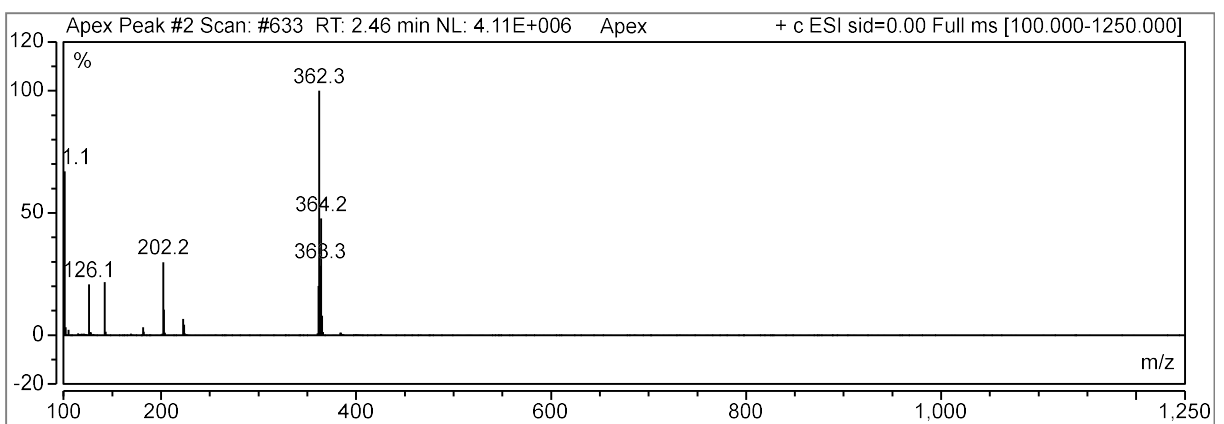
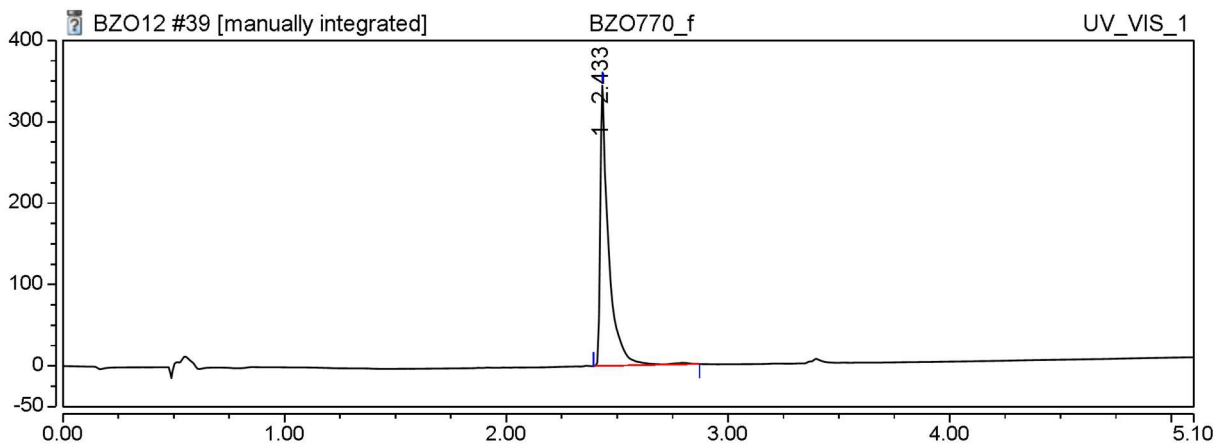
(56)



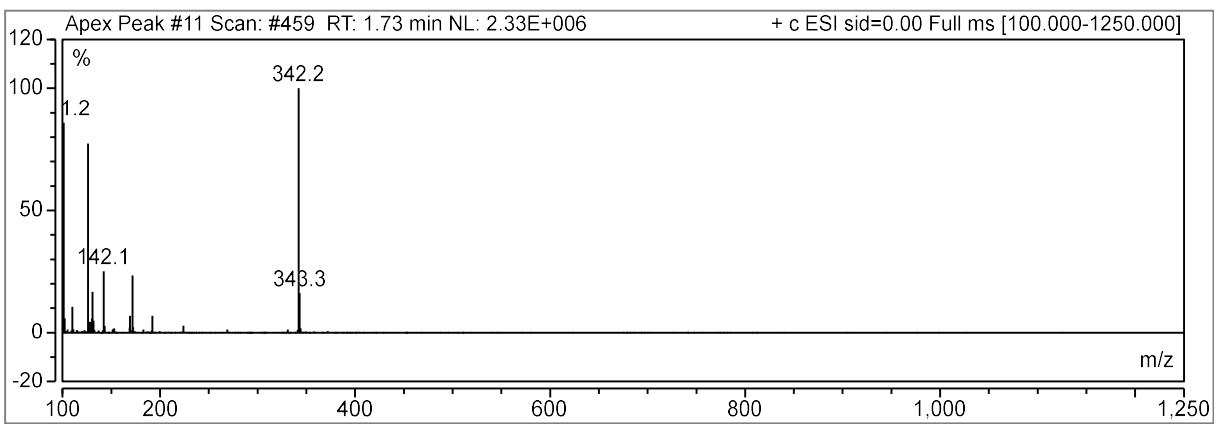
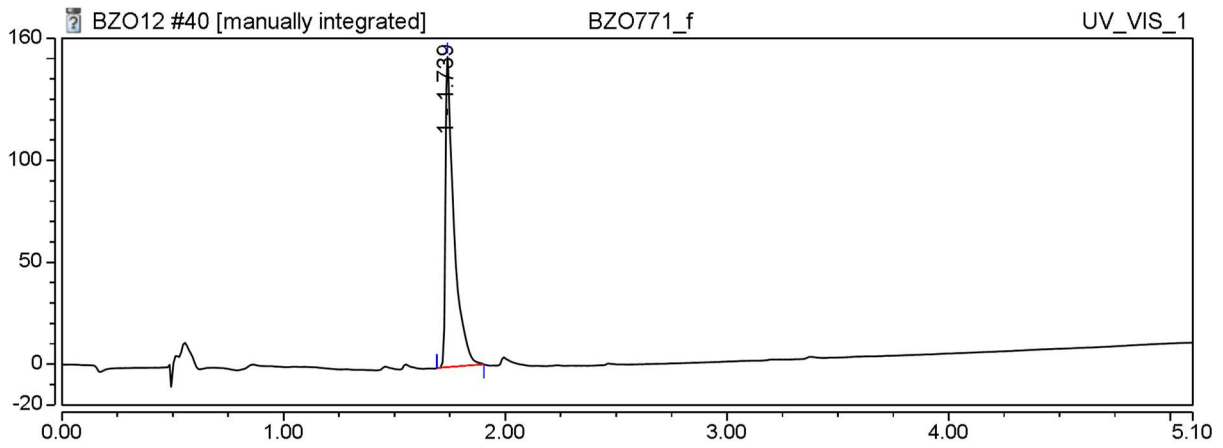
(58)



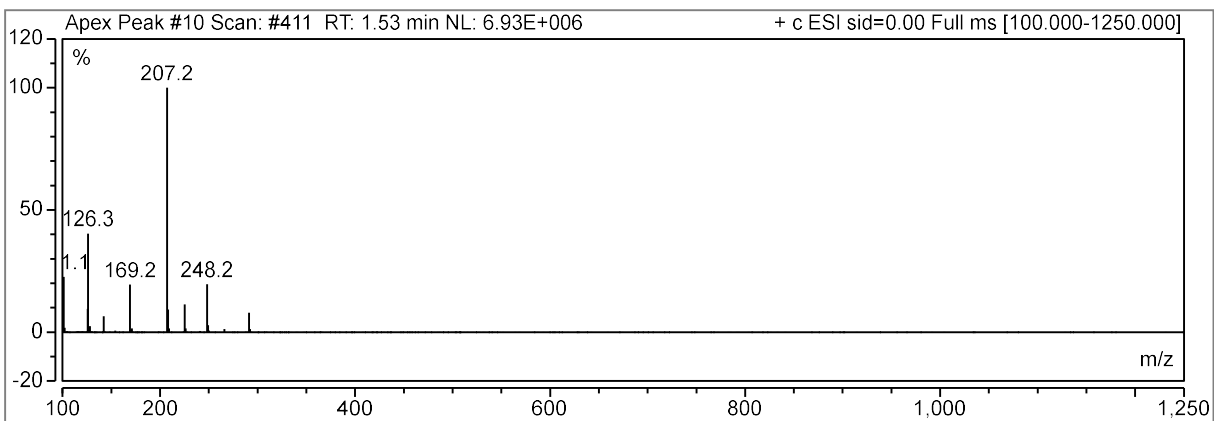
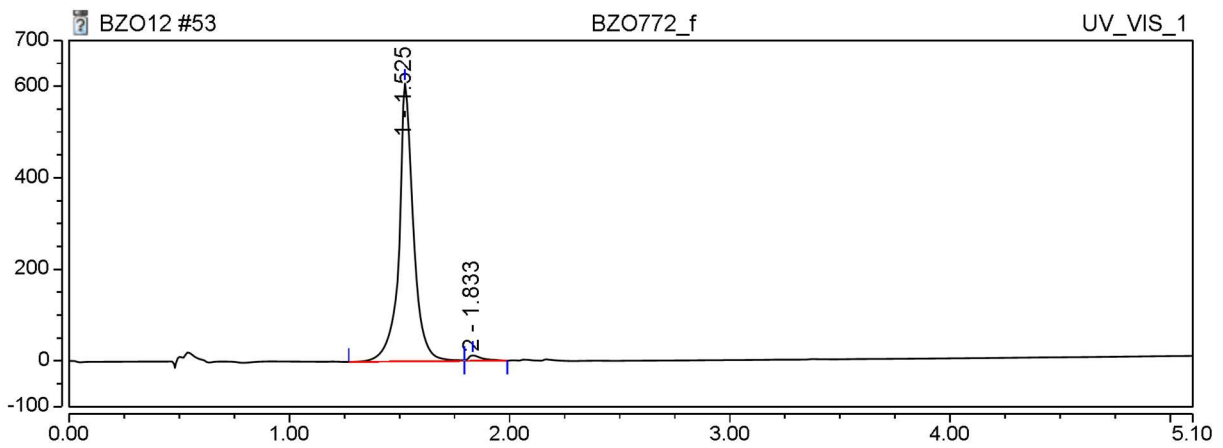
(57)



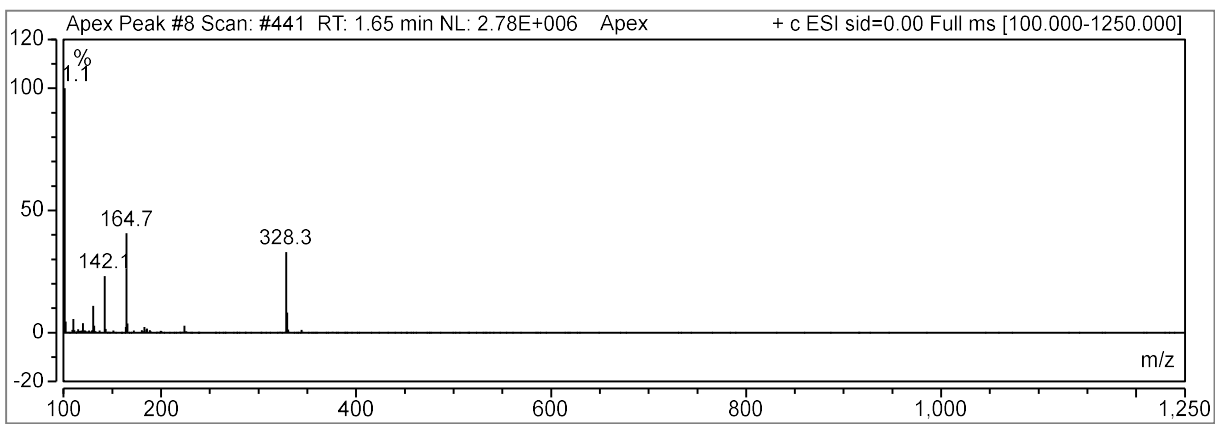
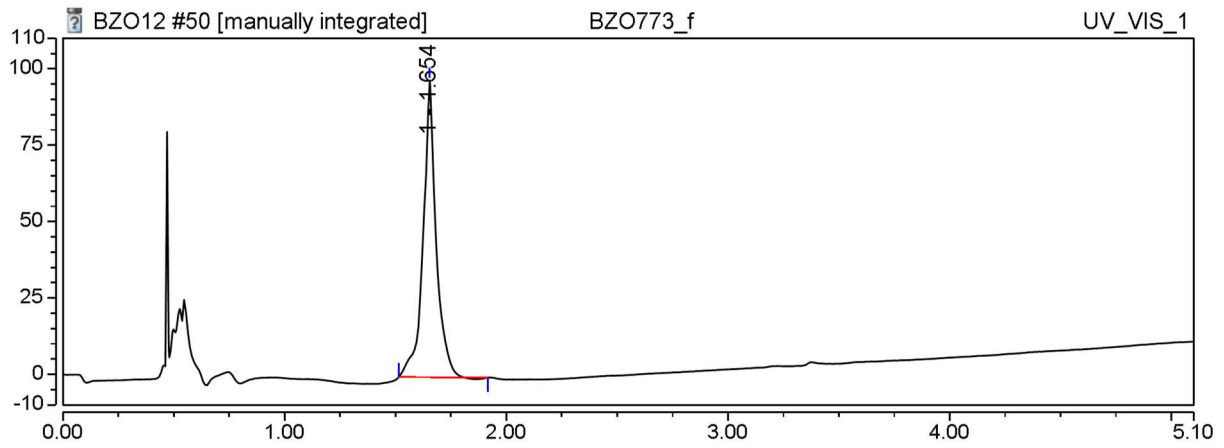
(65)



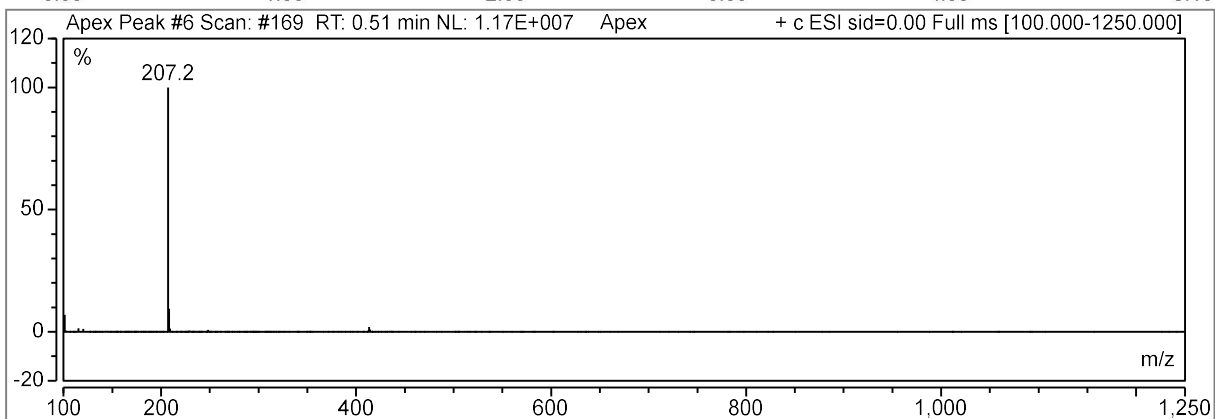
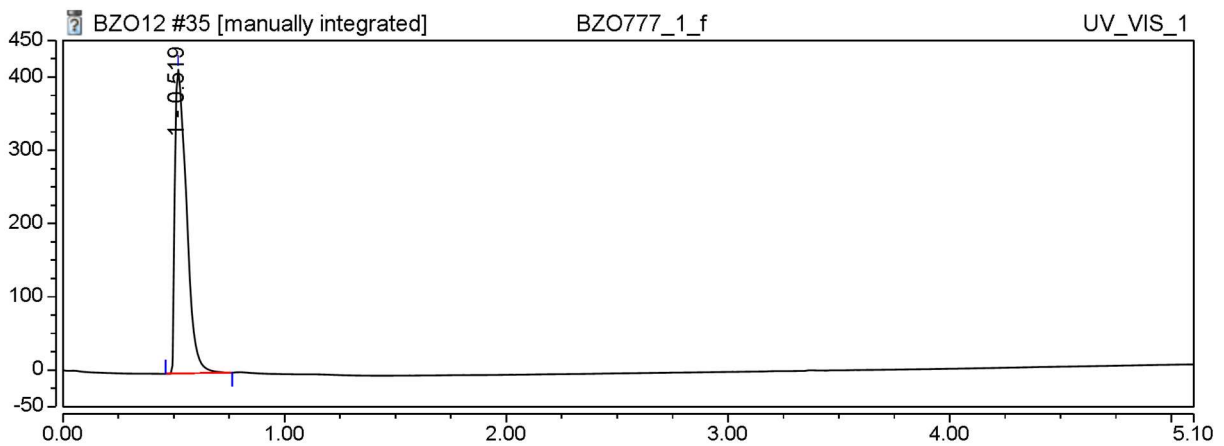
(124)



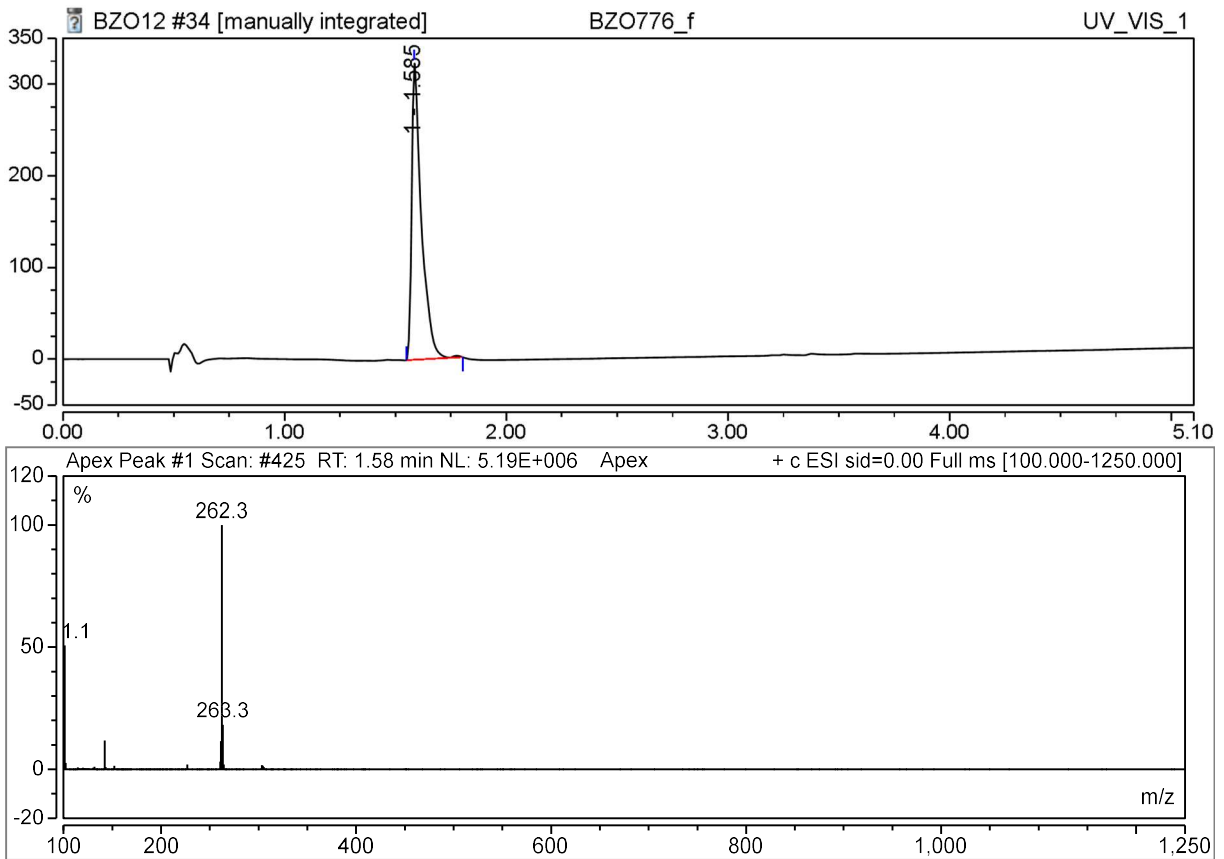
(48)



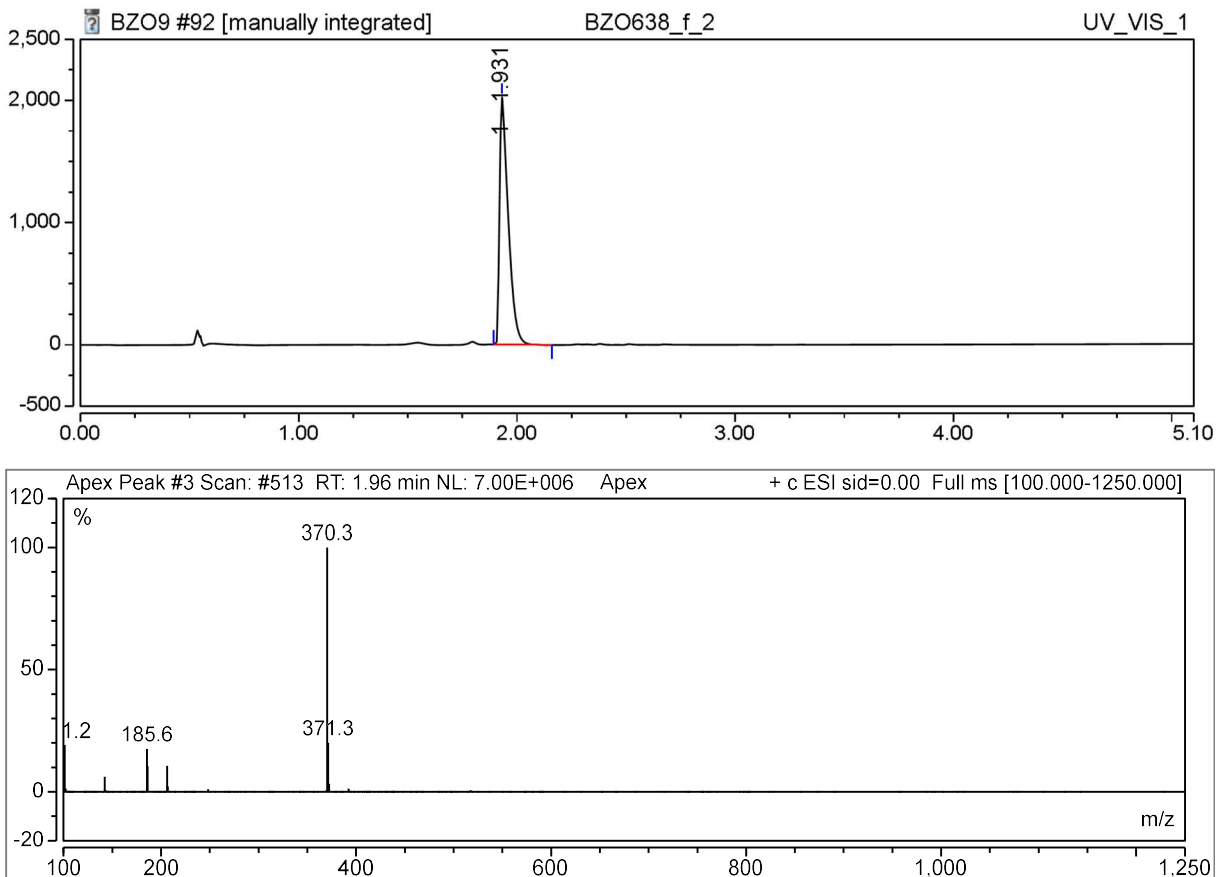
(99)



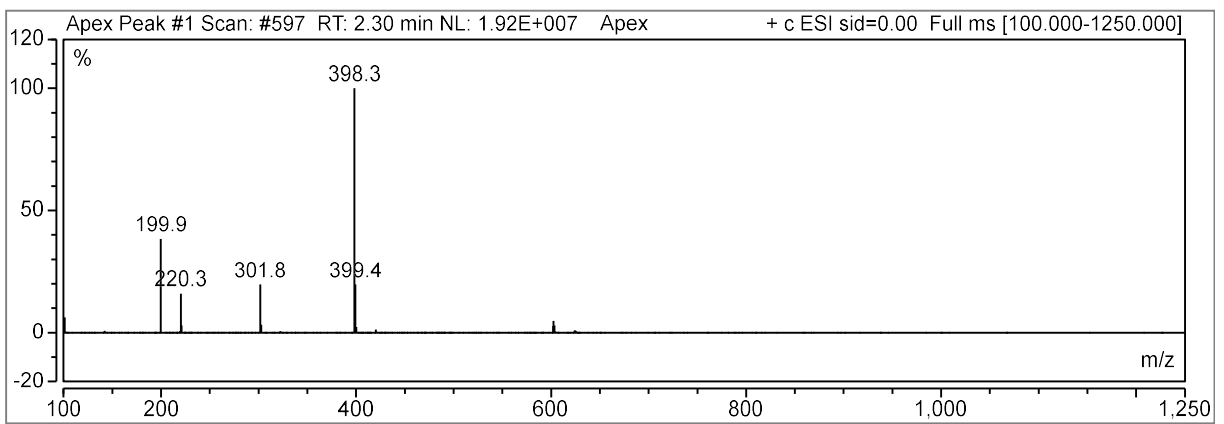
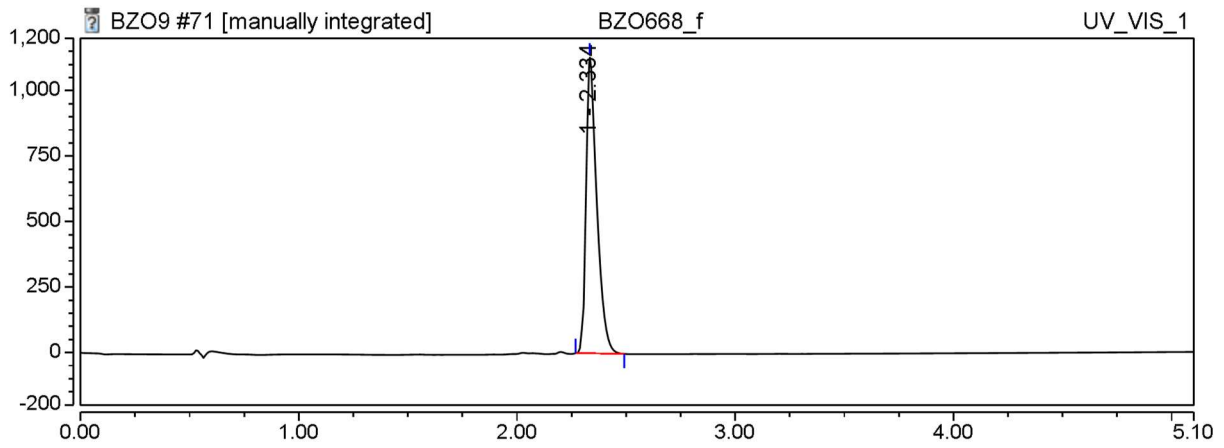
(49)



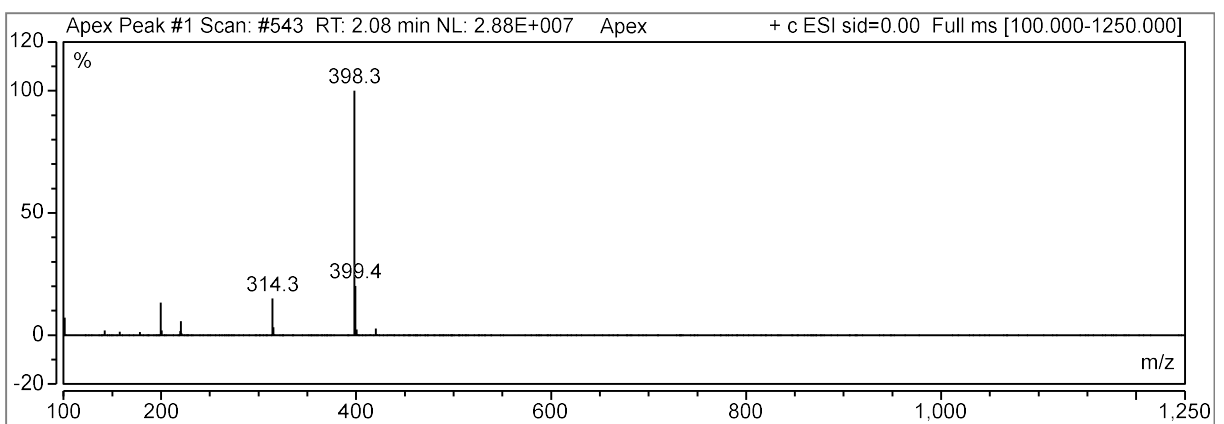
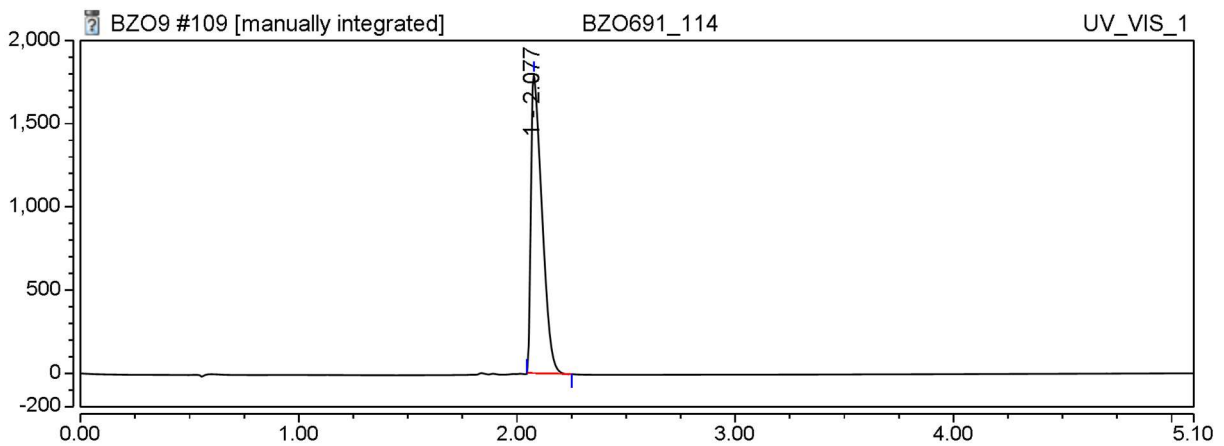
(68)



(69)

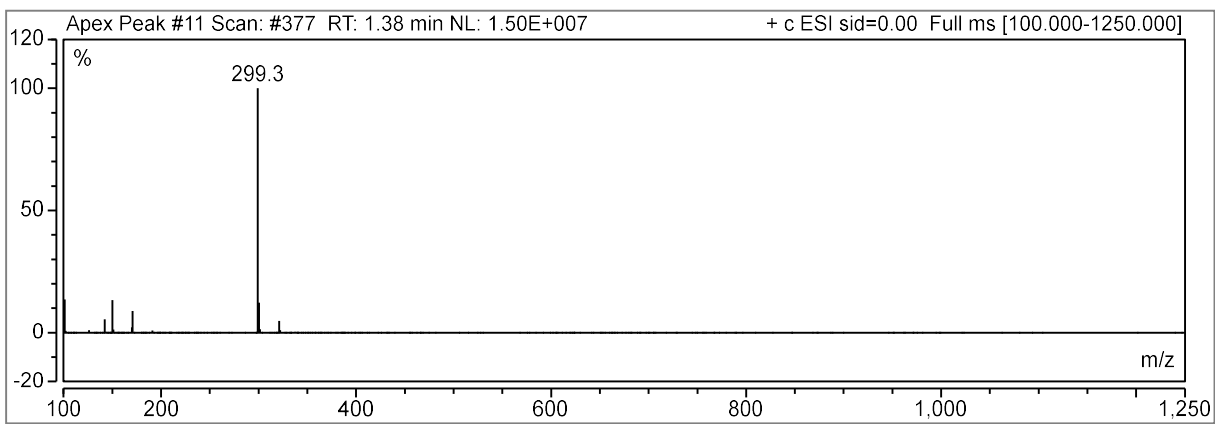
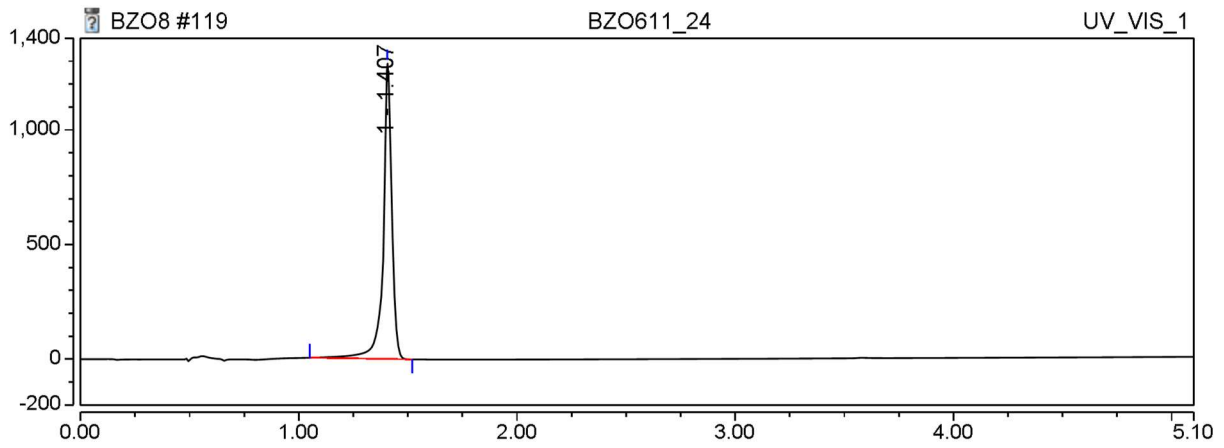


(61)

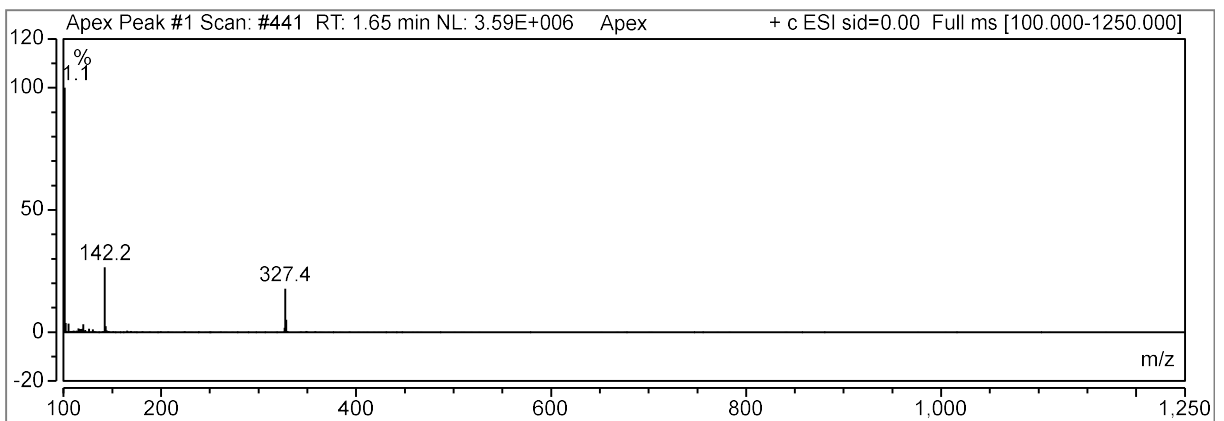
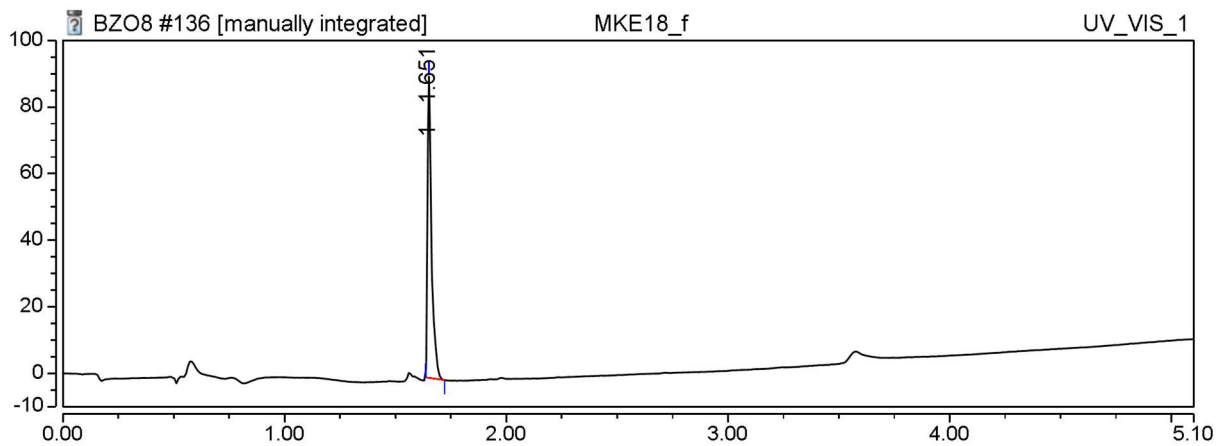




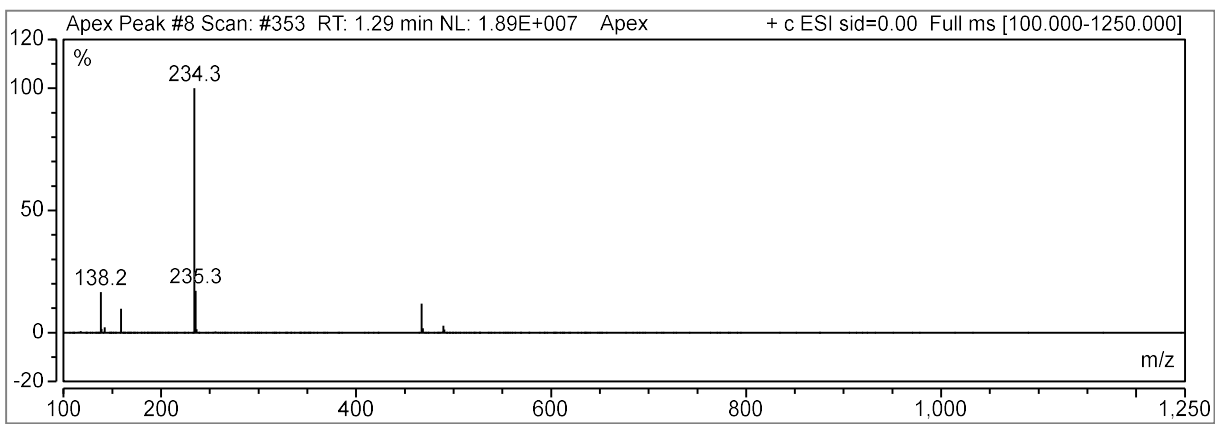
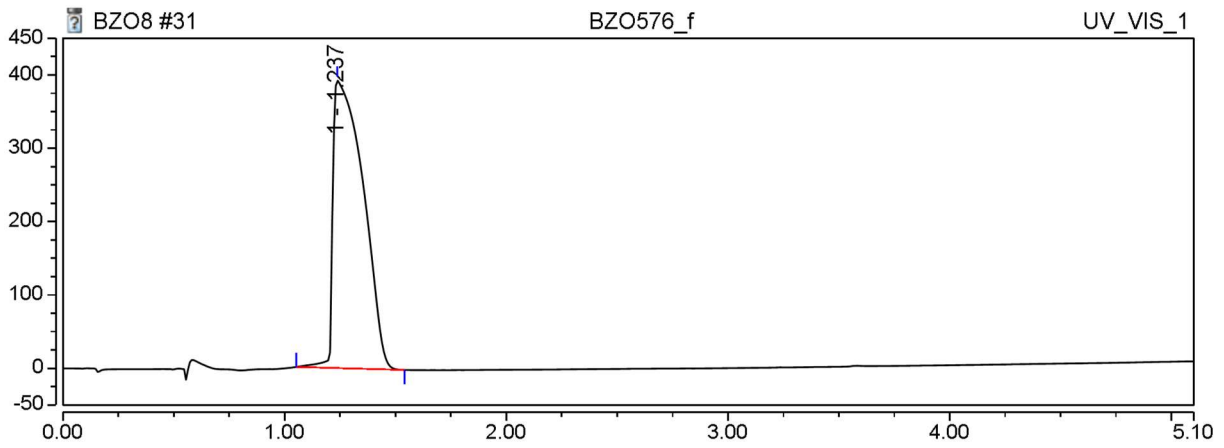
(70)



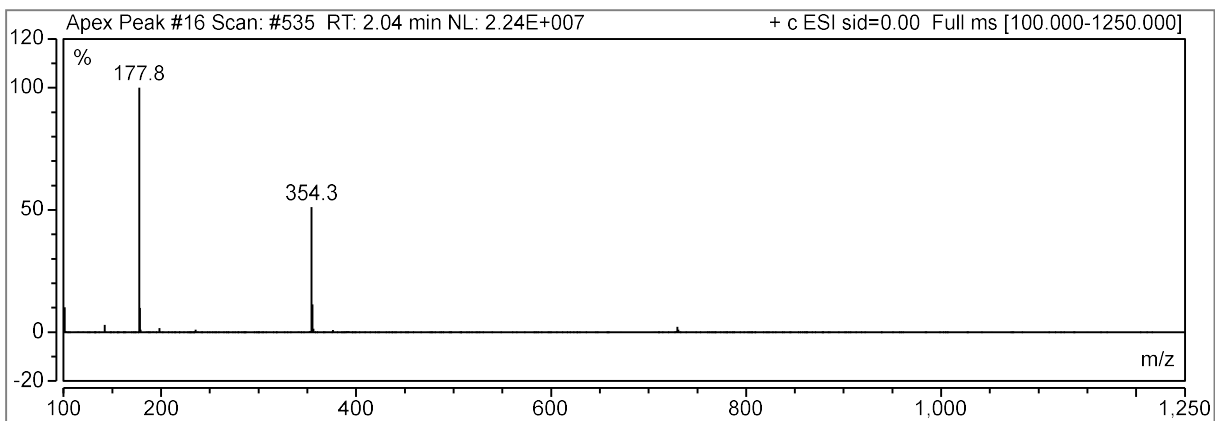
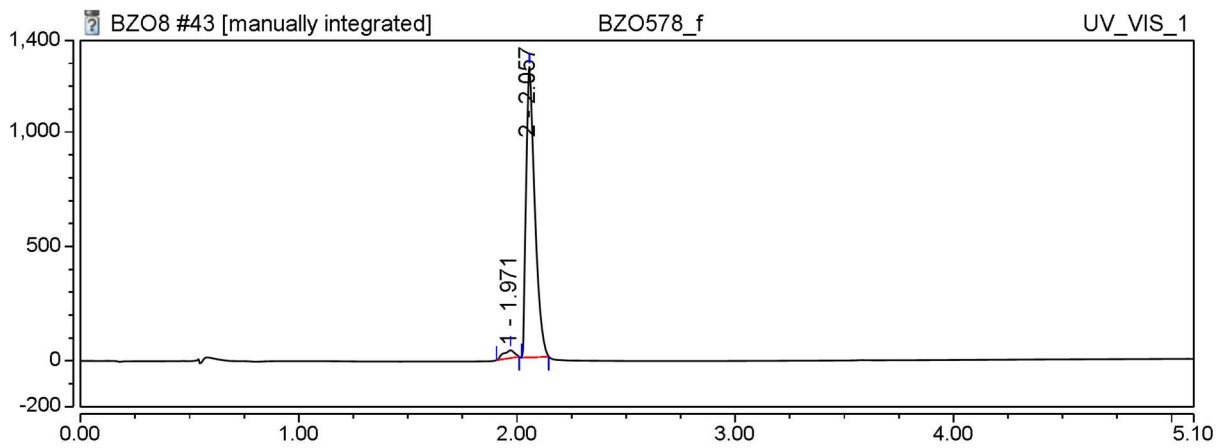
(50)



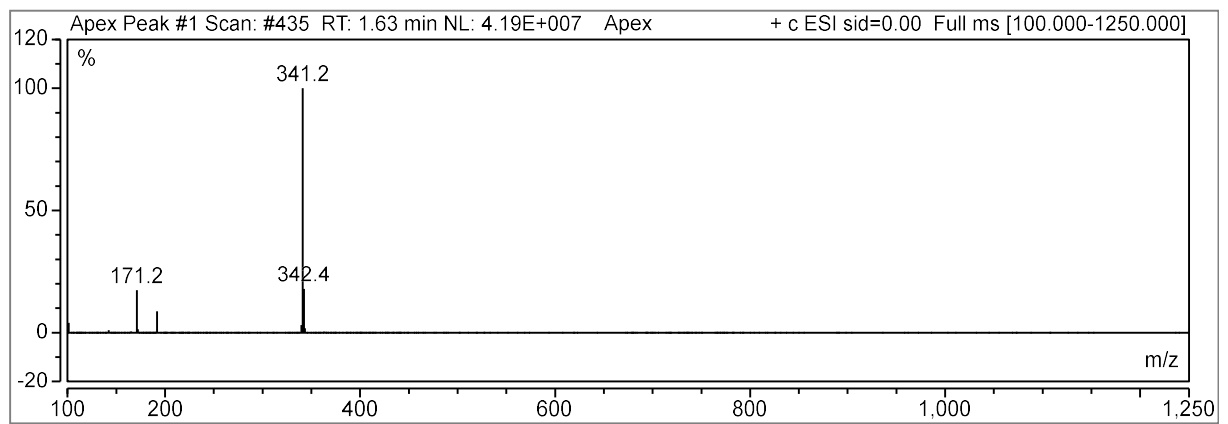
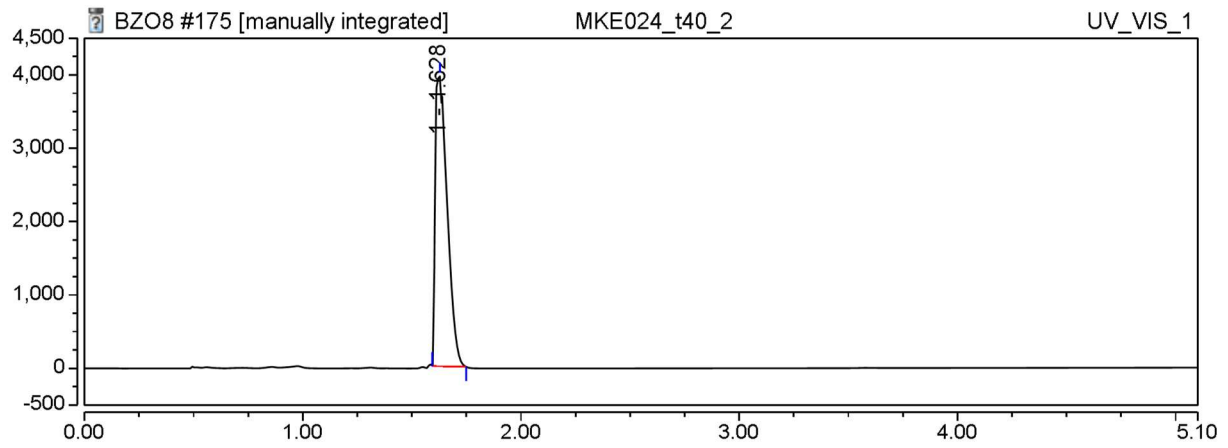
(14)



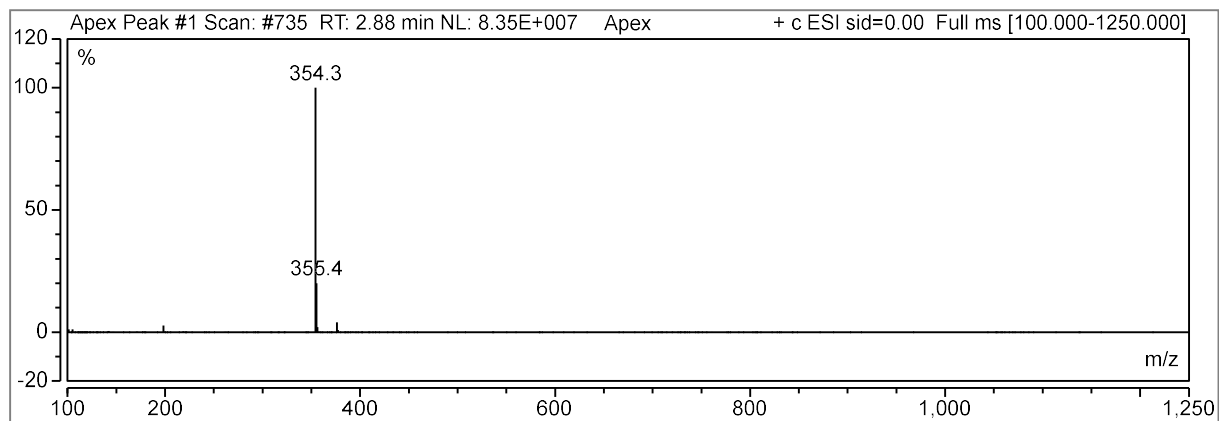
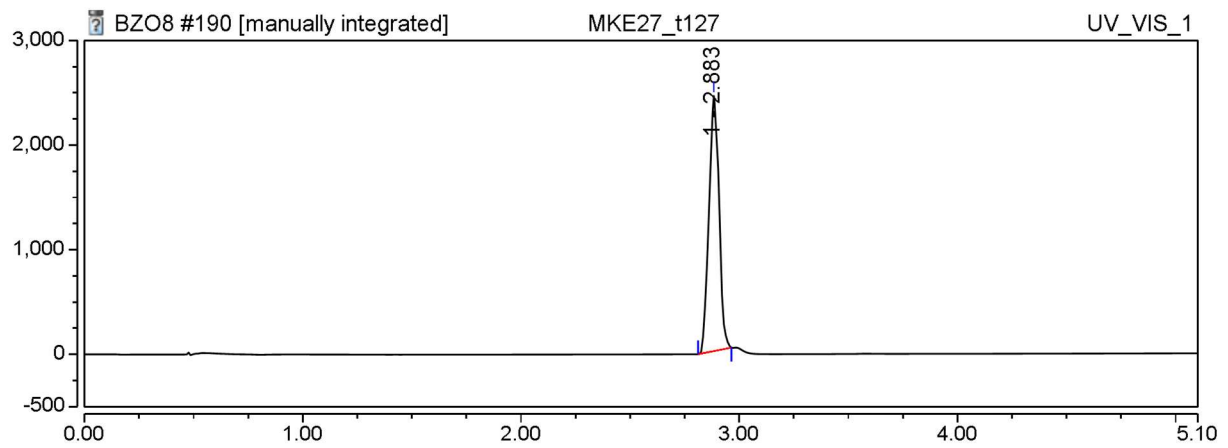
(51)



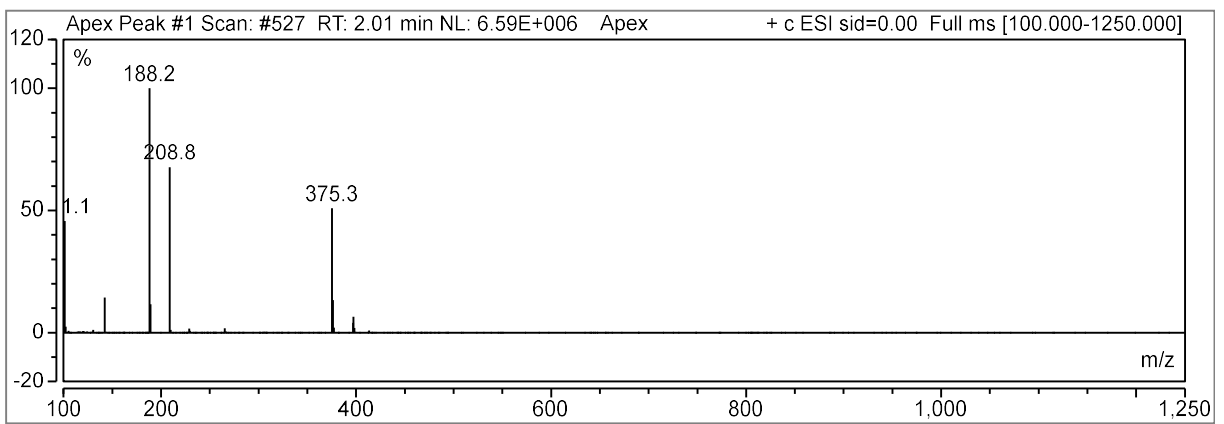
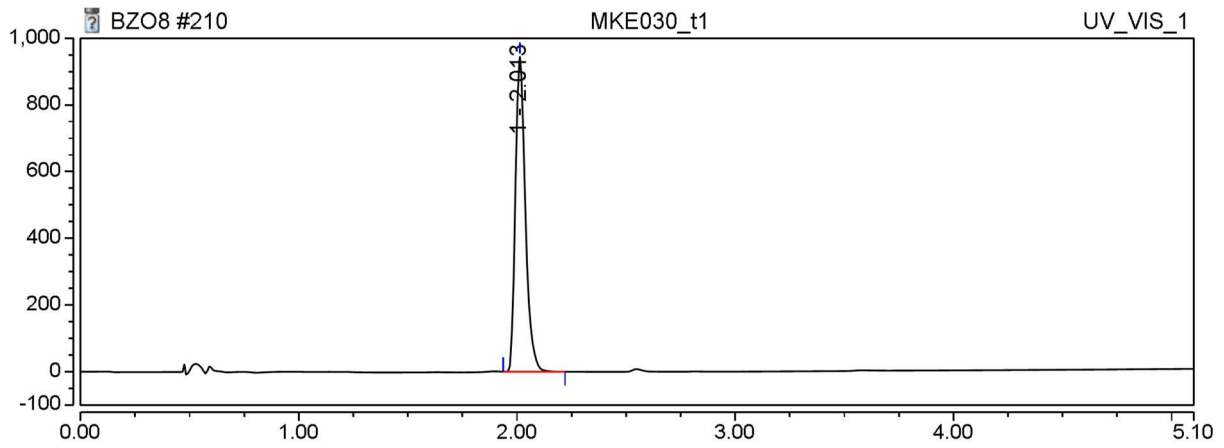
(54)



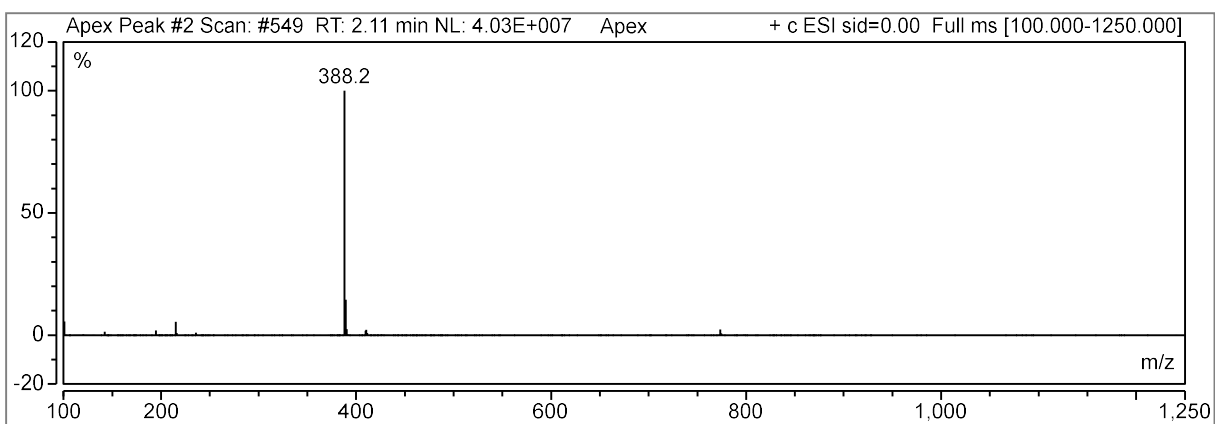
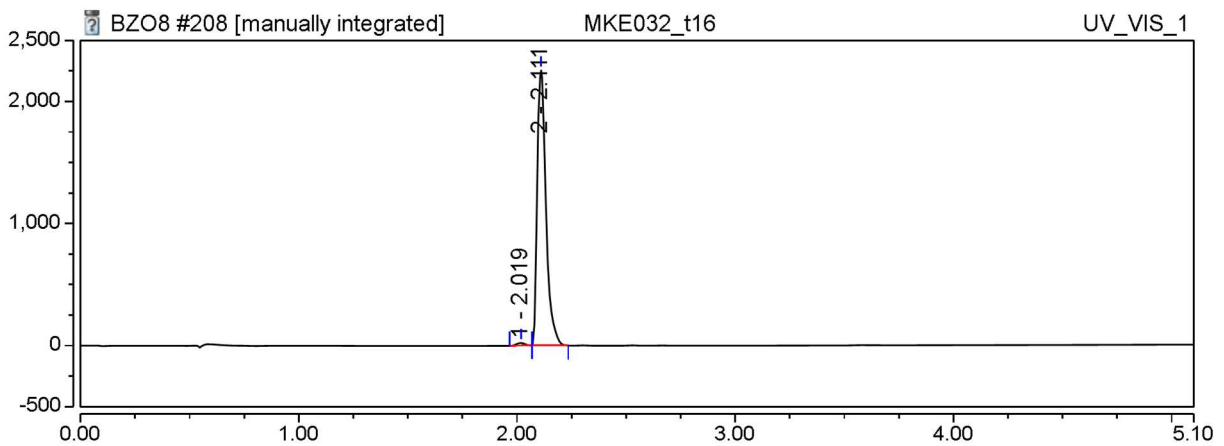
(62)



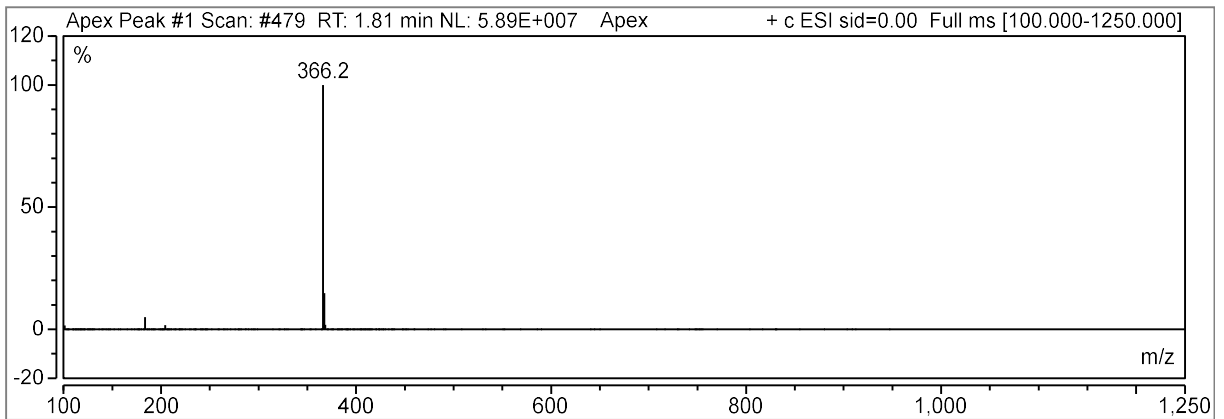
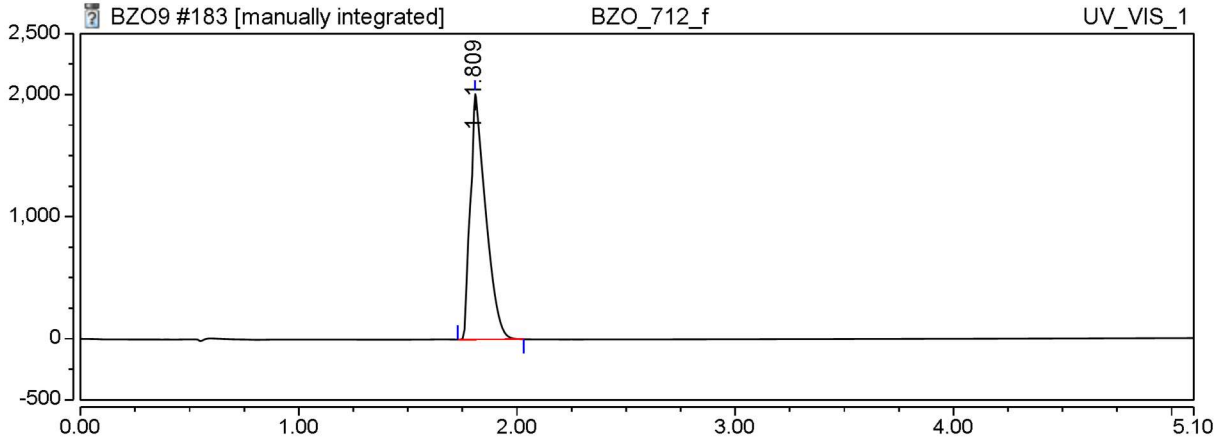
(66)



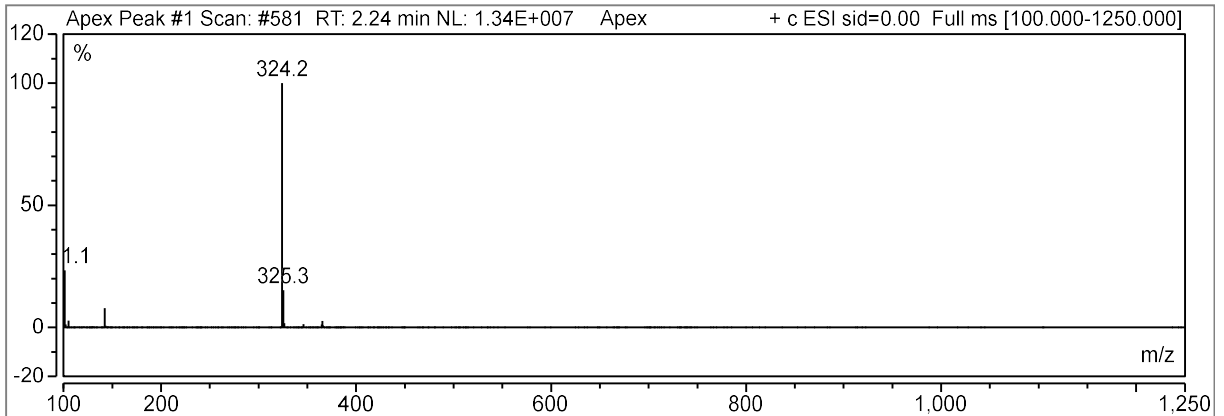
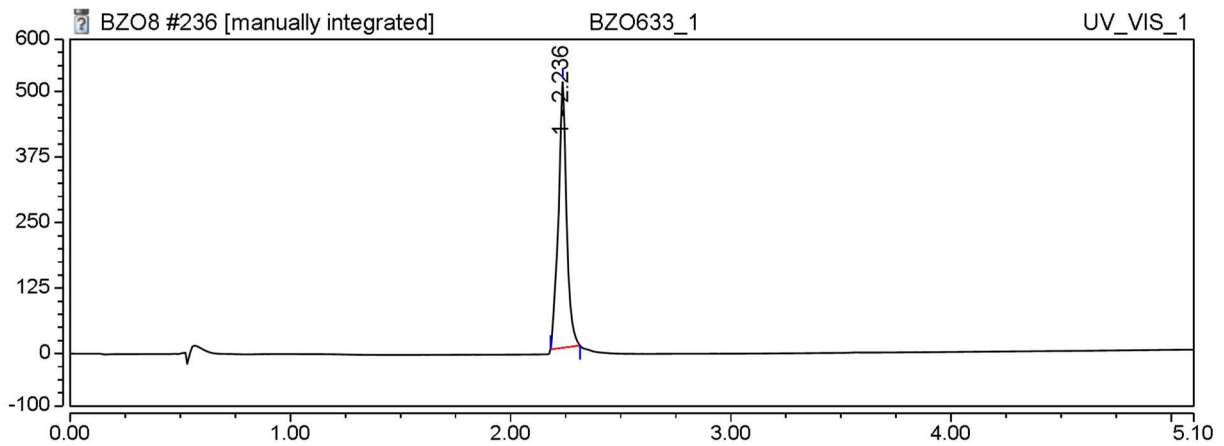
(64)



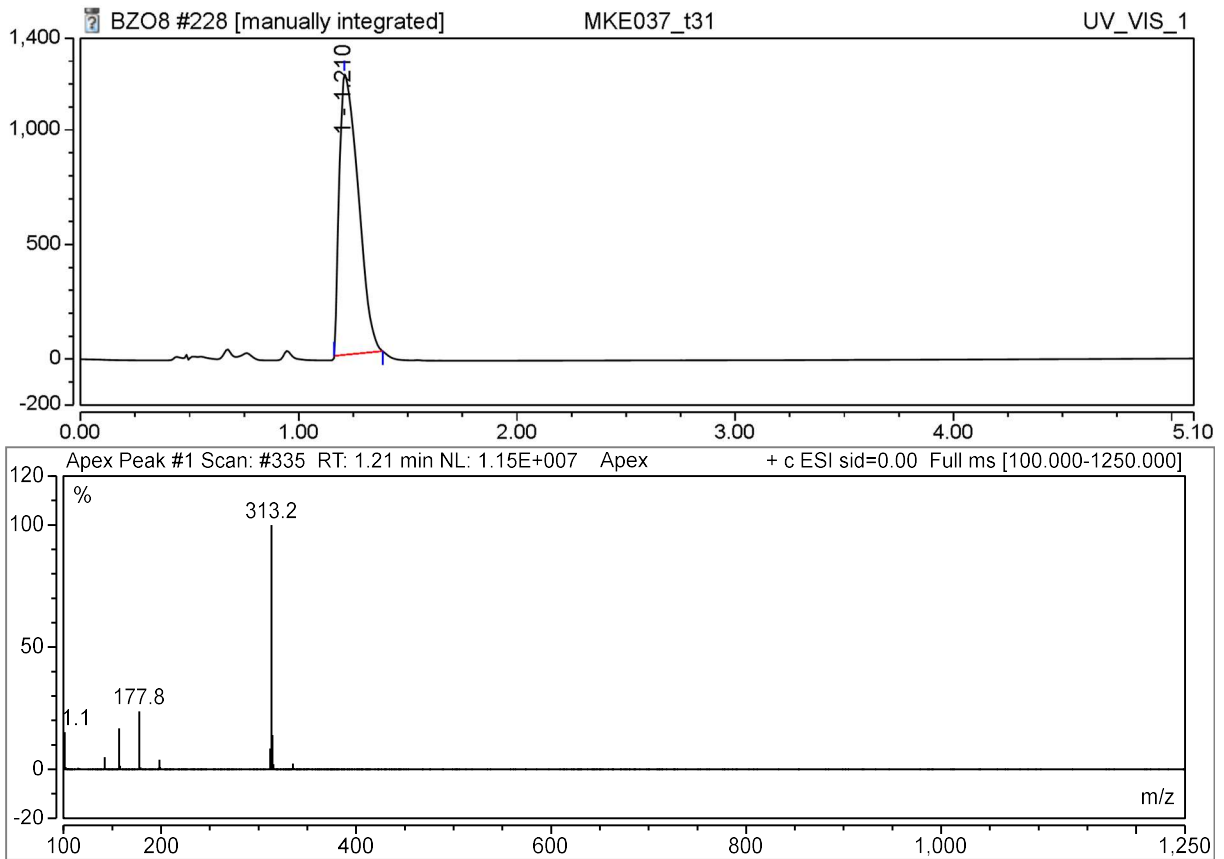
(37)



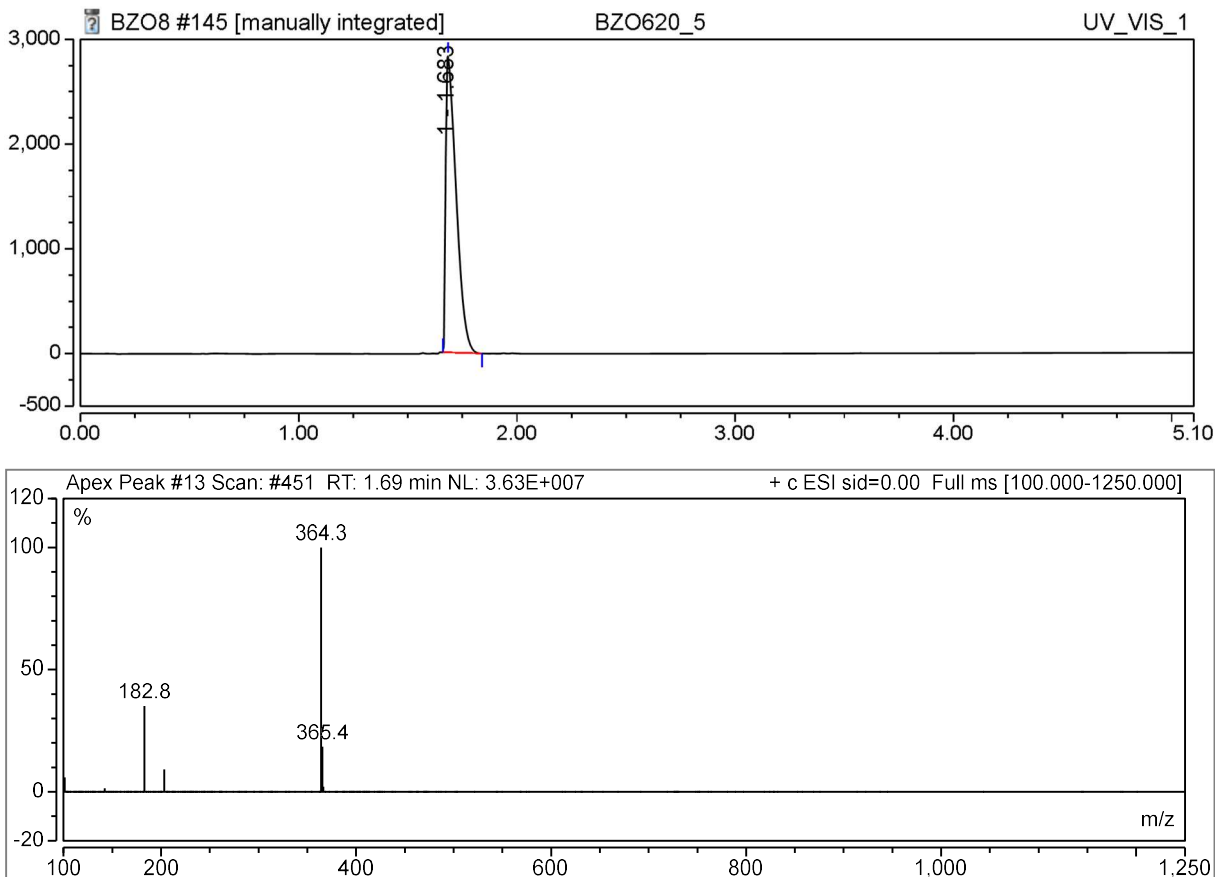
(33)



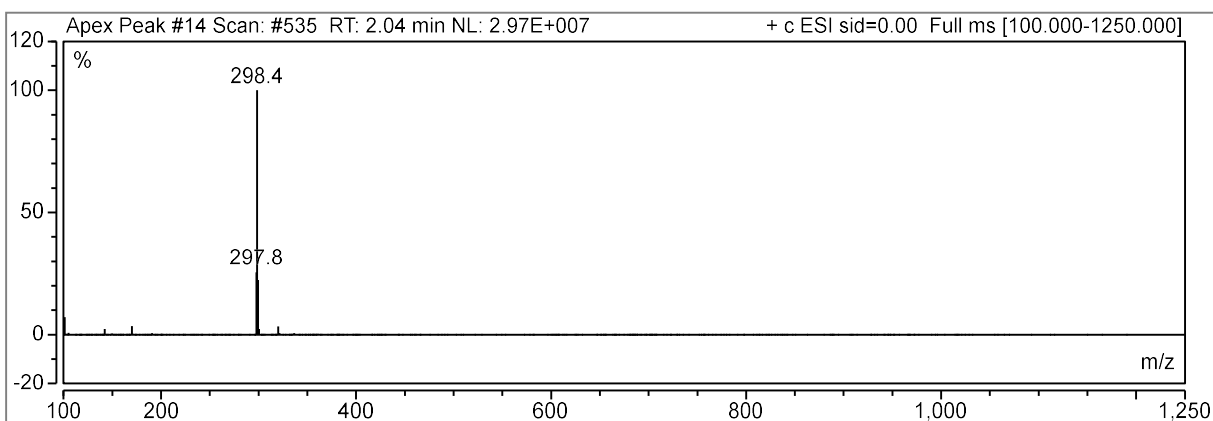
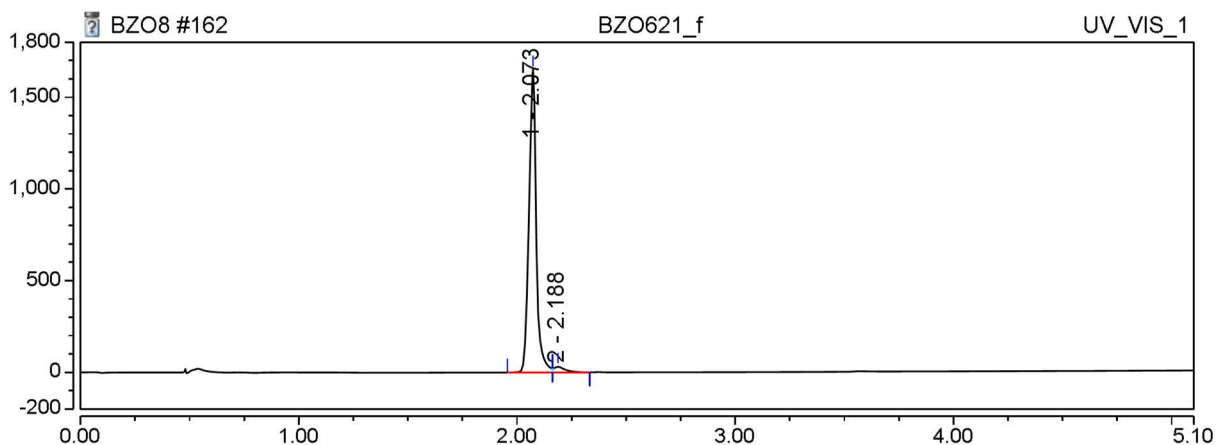
(63)



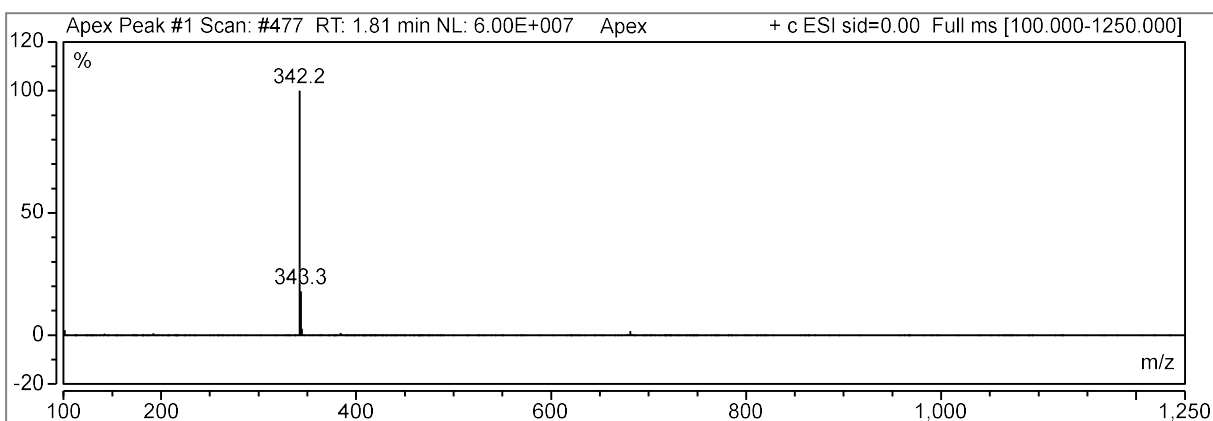
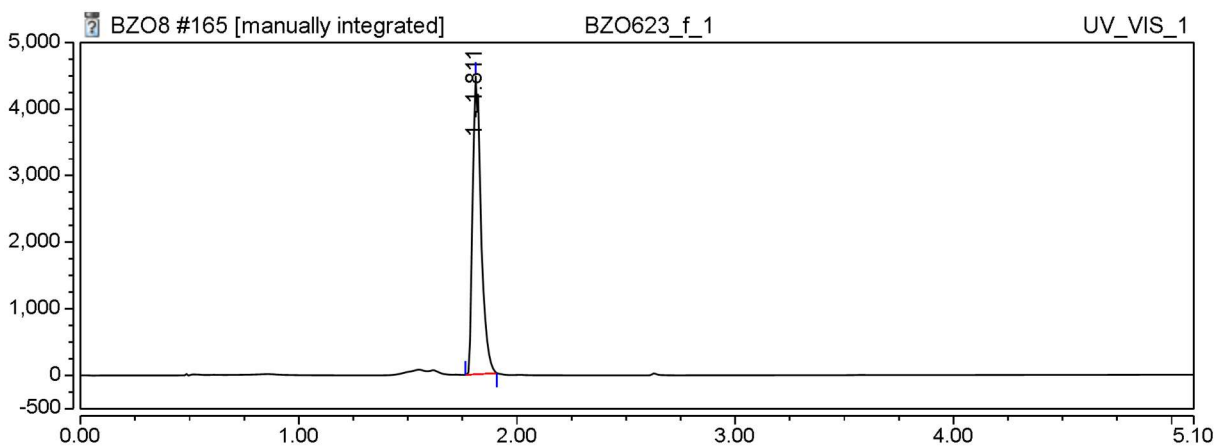
(55)



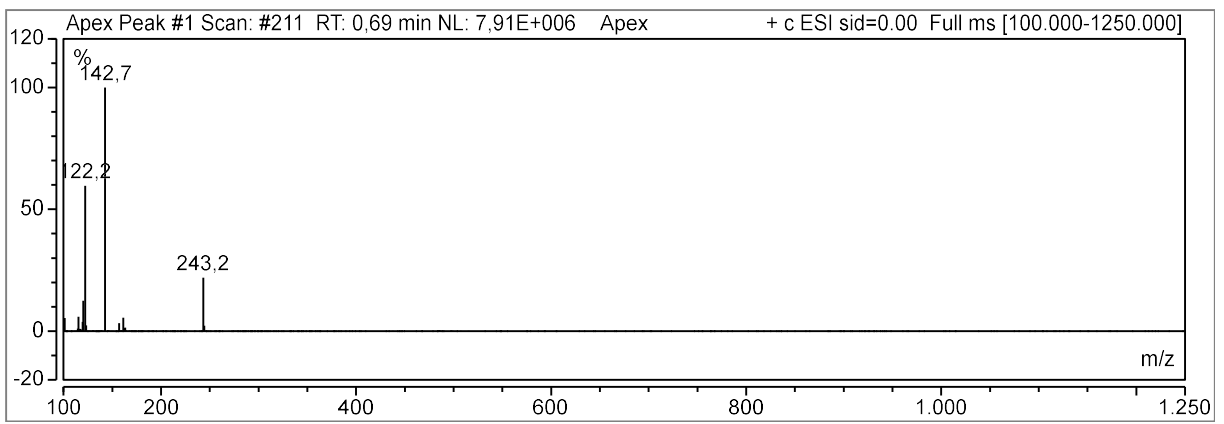
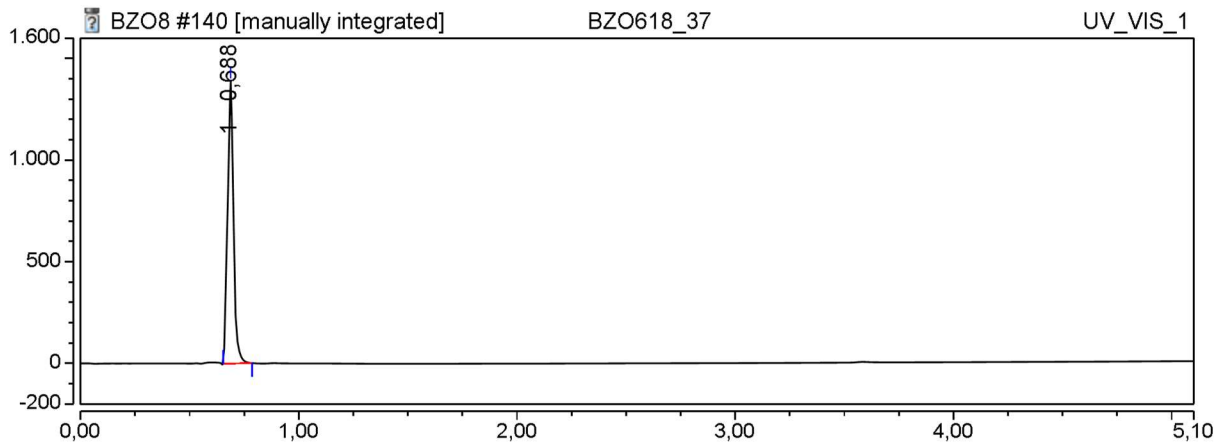
(53)



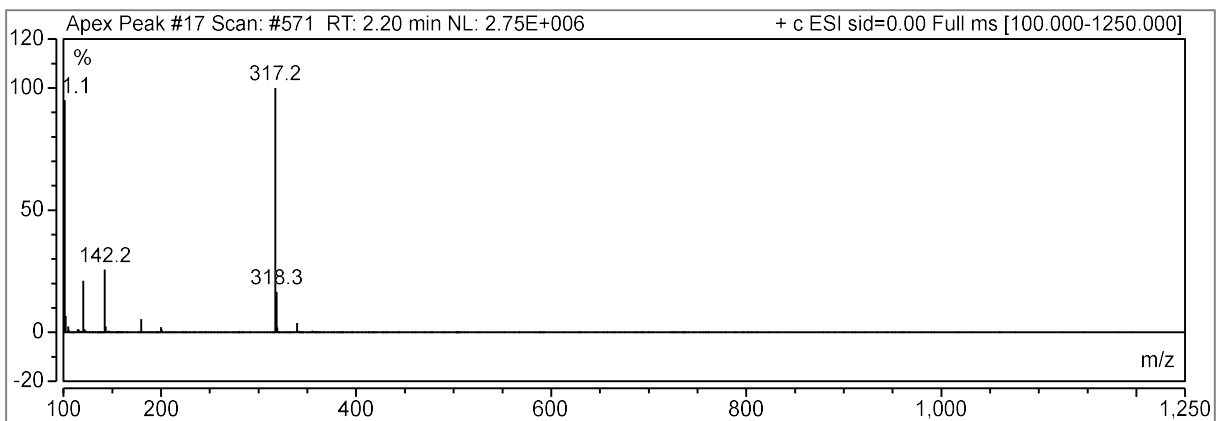
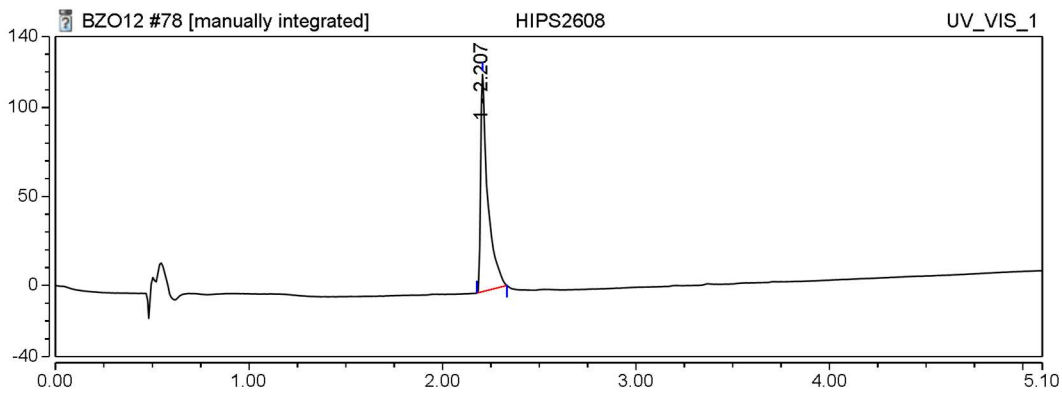
(52)



(129)

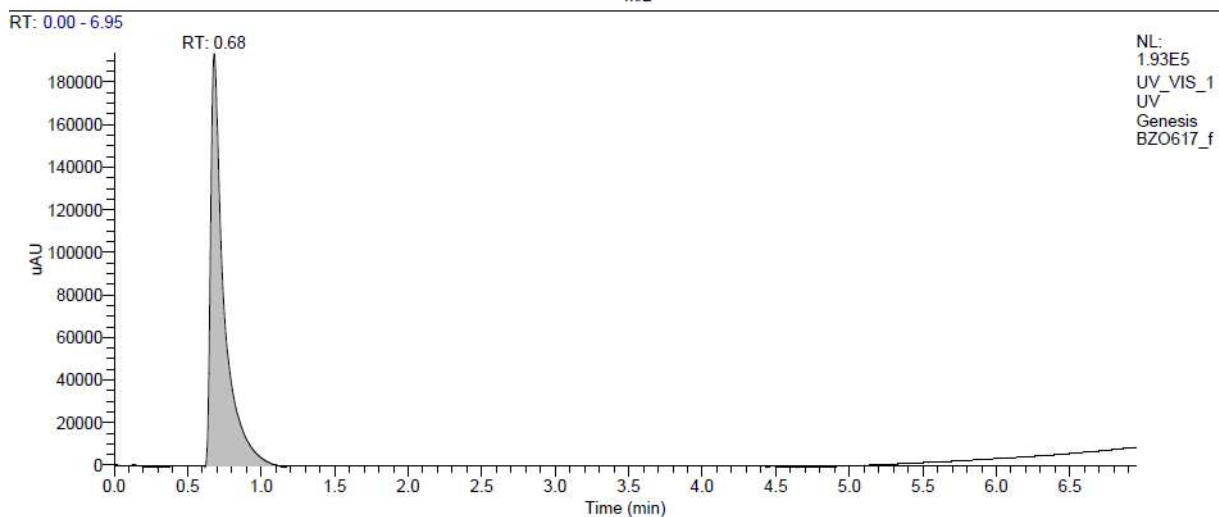
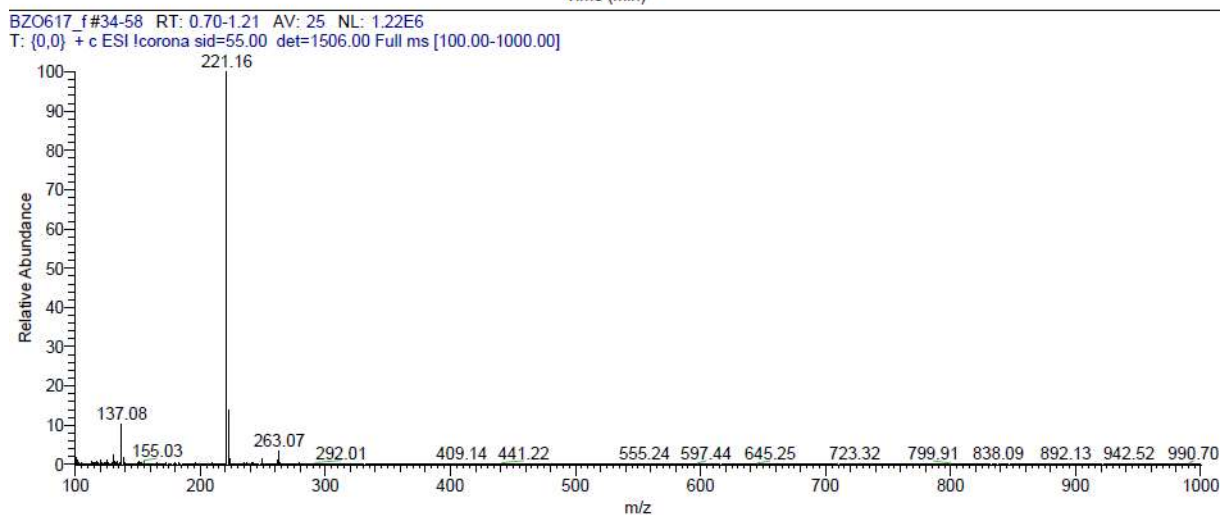
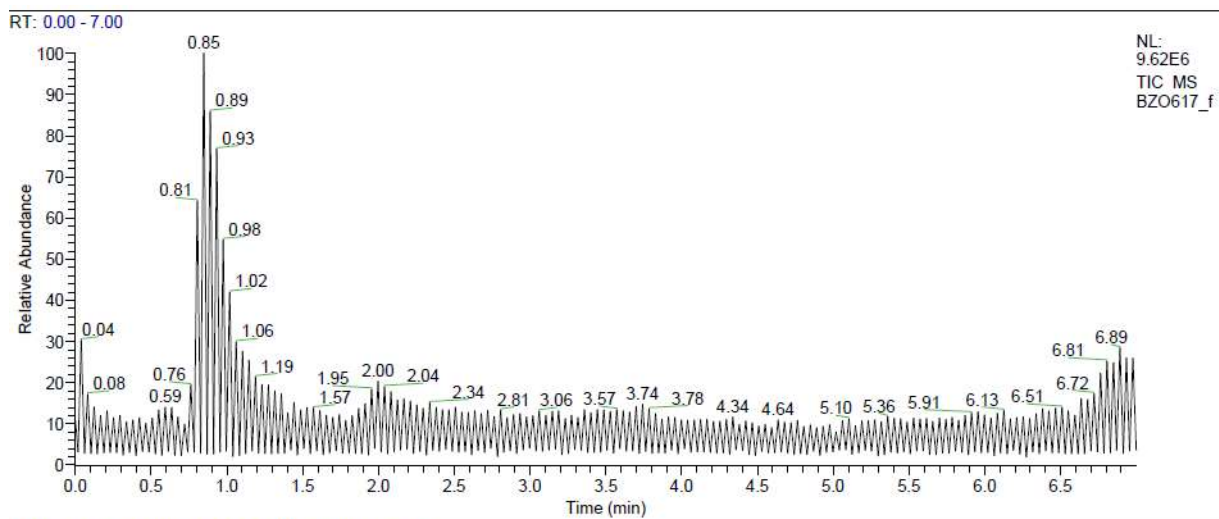


(67)

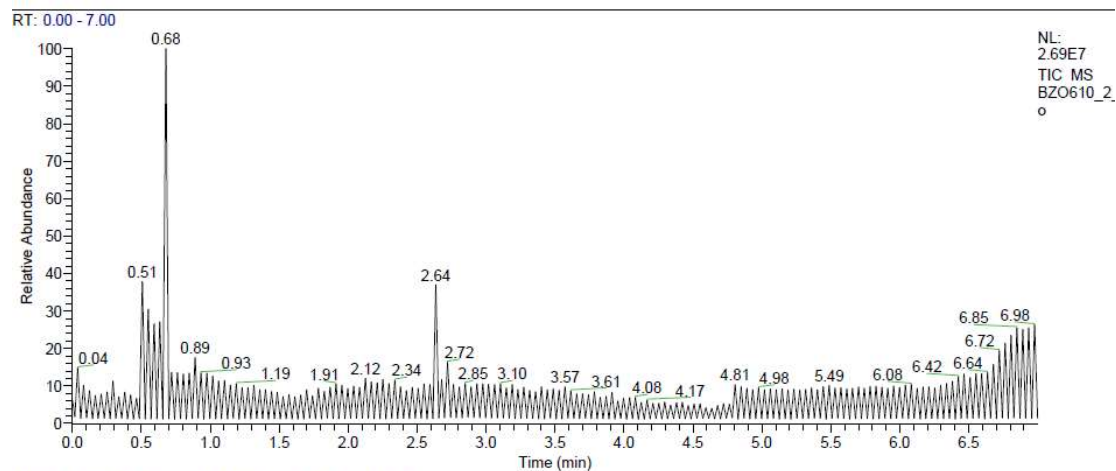




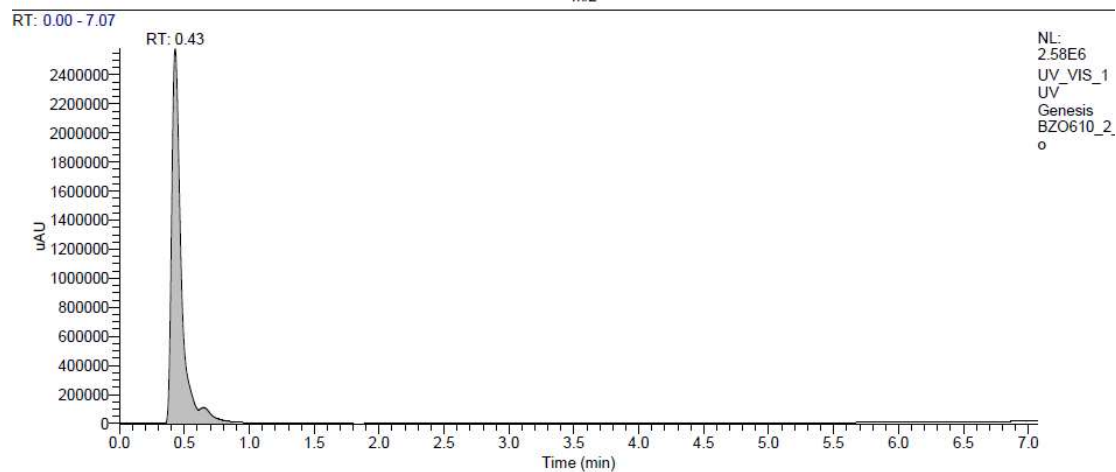
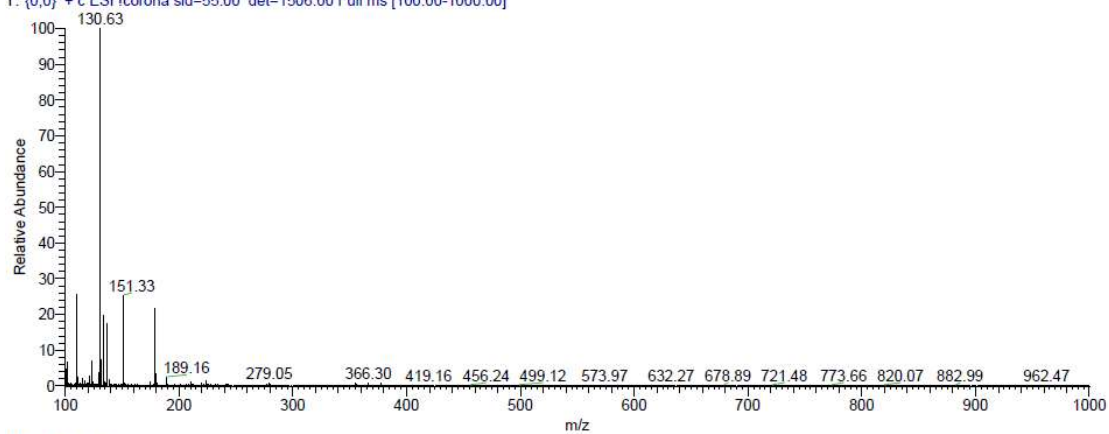
(131)



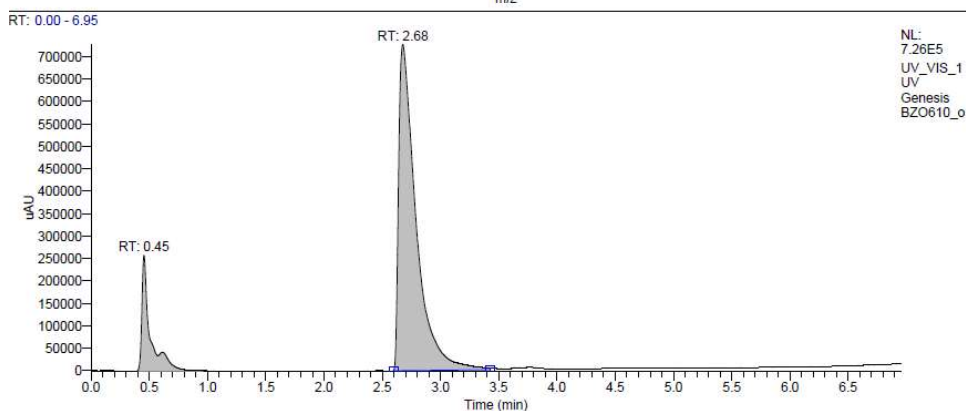
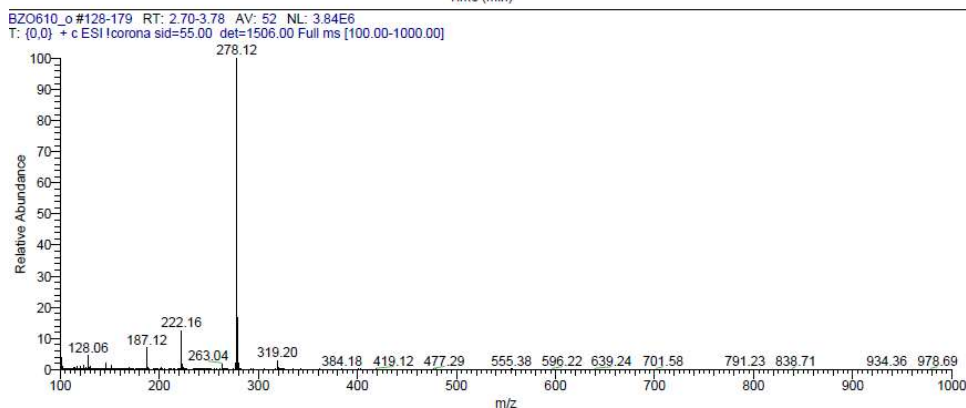
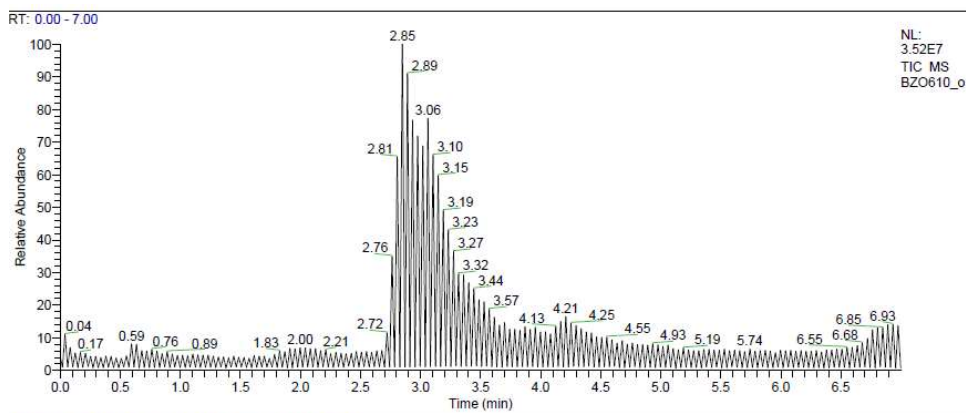
# Boc protected-(97)



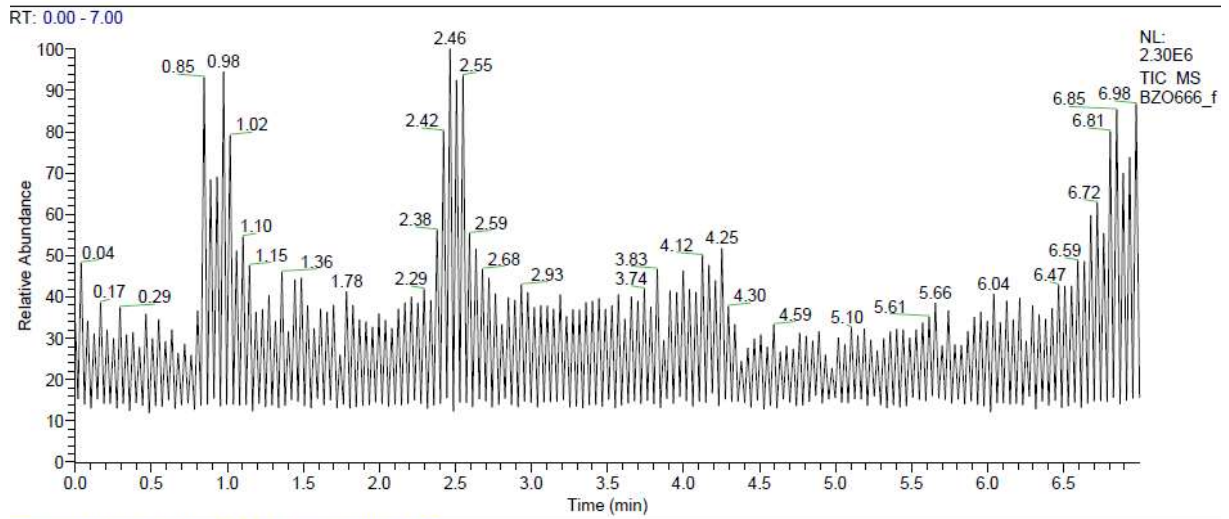
BZO610\_2\_o #20-40 RT: 0.40-0.83 AV: 21 NL: 1.15E6  
T: (0,0) + c ESI Icorona sid=55.00 det=1506.00 Full ms [100.00-1000.00]



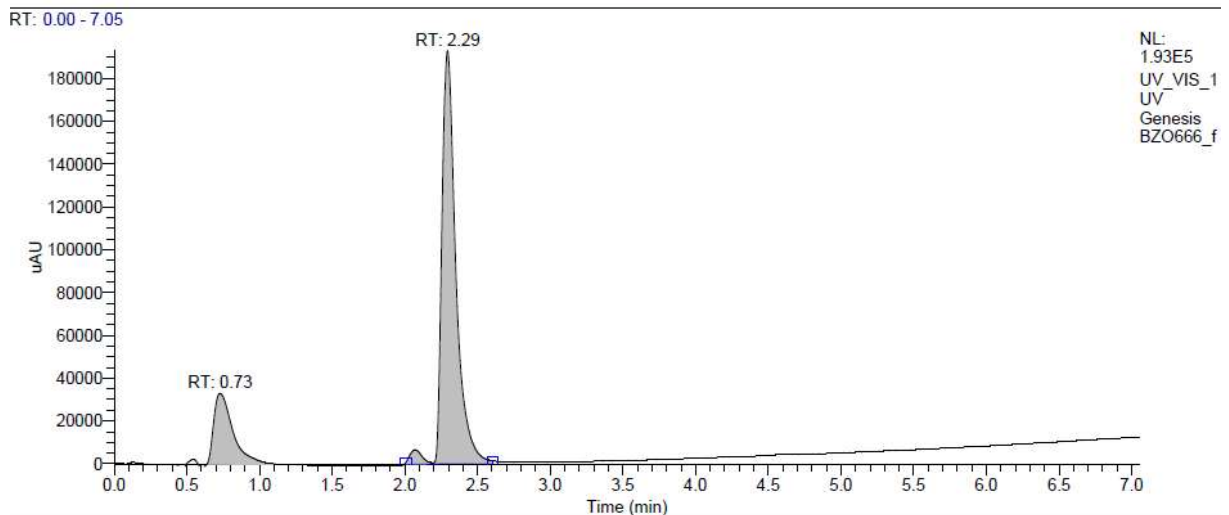
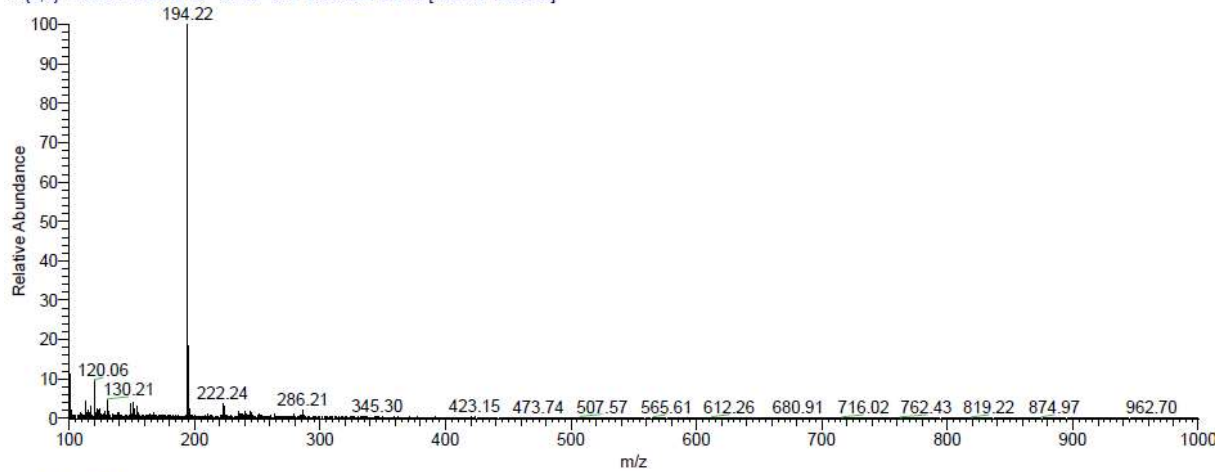
(97)



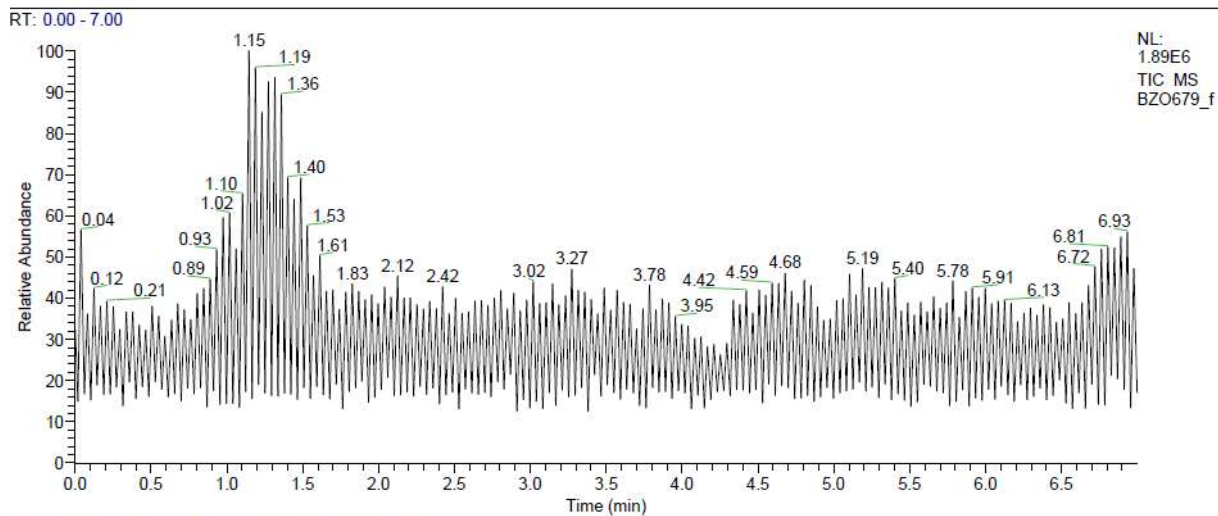
(118)



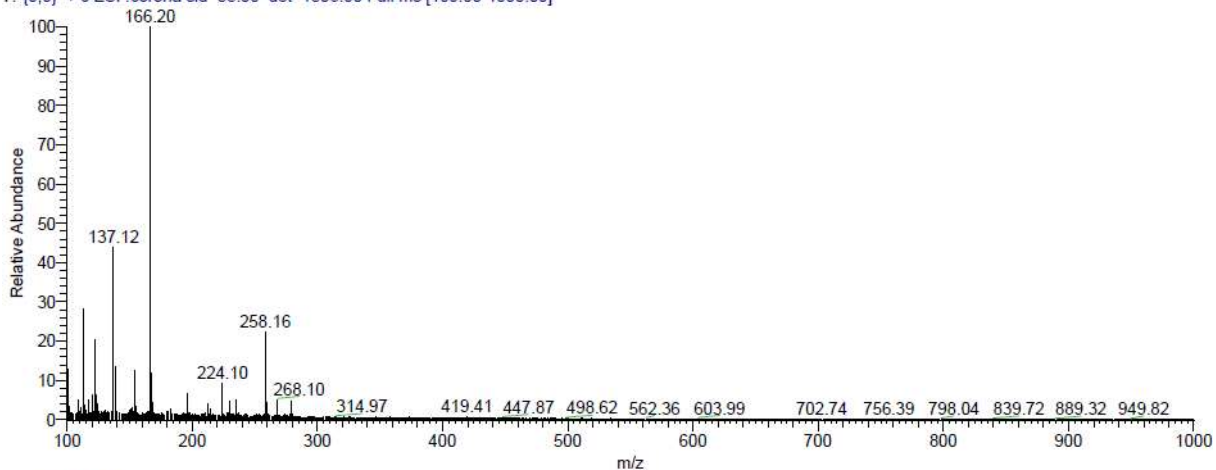
BZO666\_f#108-126 RT: 2.27-2.66 AV: 19 NL: 2.44E5  
T: (0,0) + c ESI Icorona sid=55.00 det=1506.00 Full ms [100.00-1000.00]



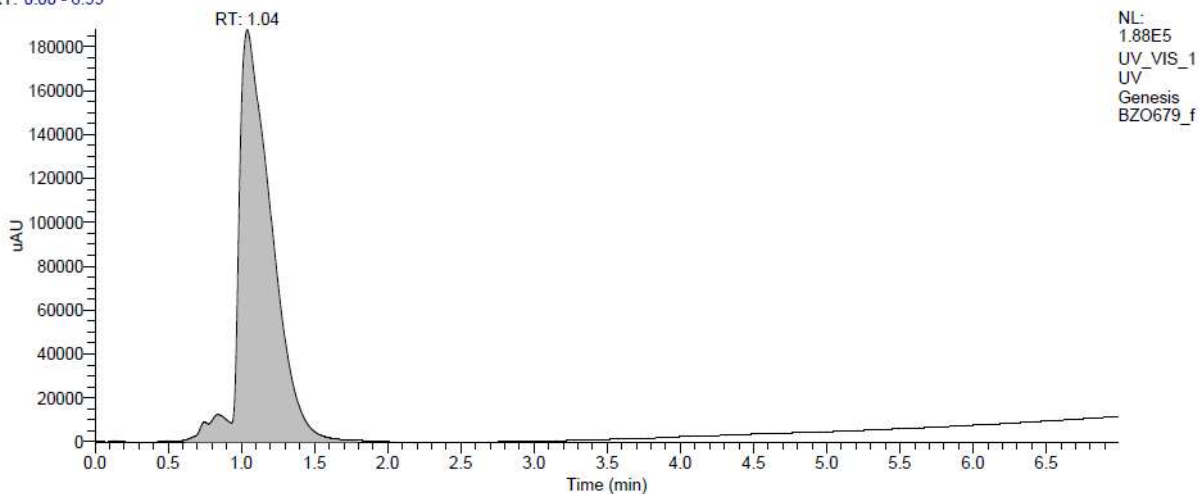
(116)



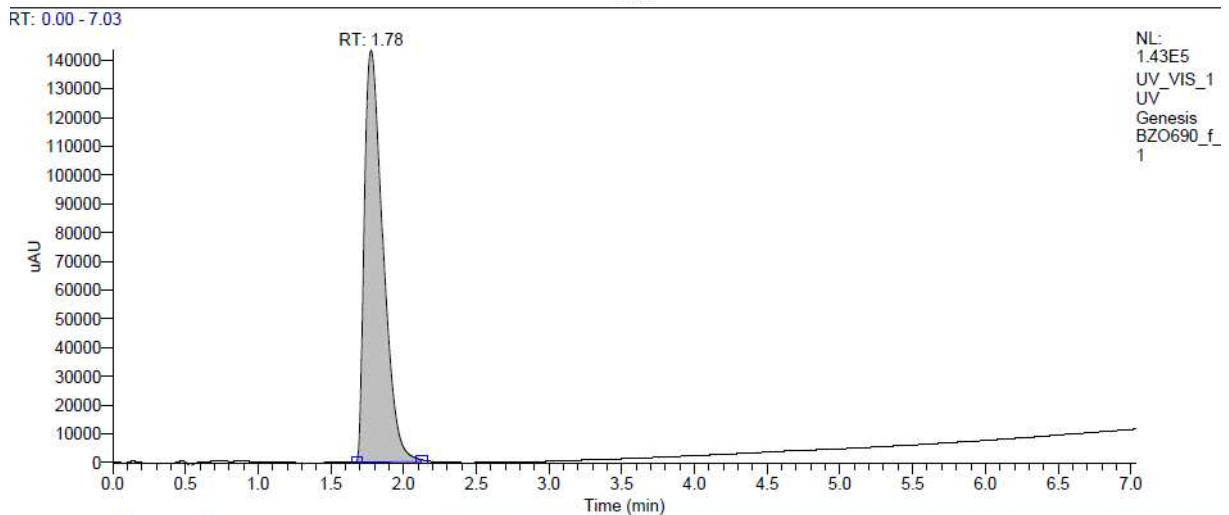
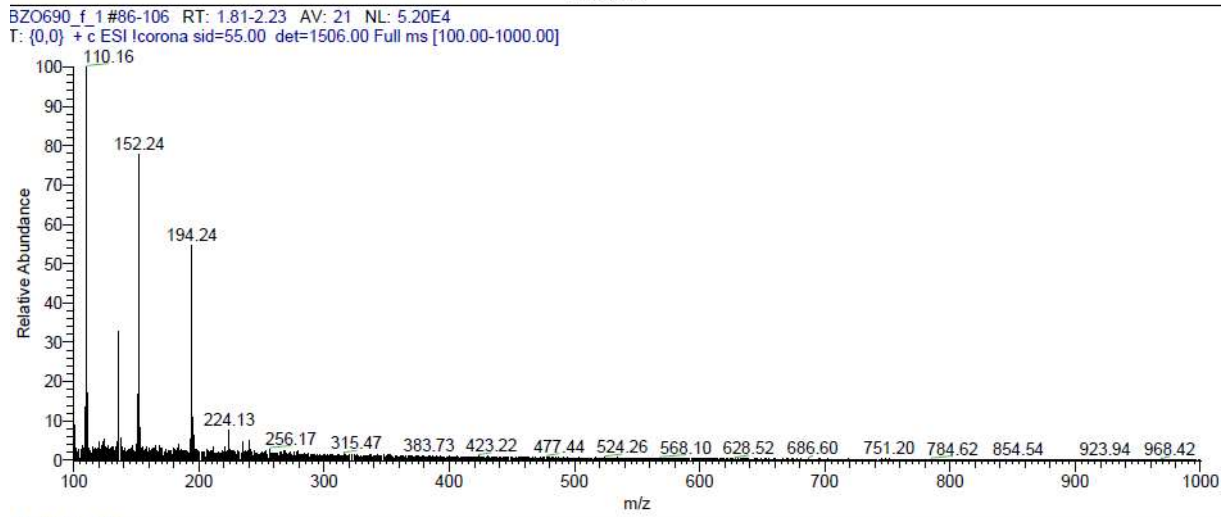
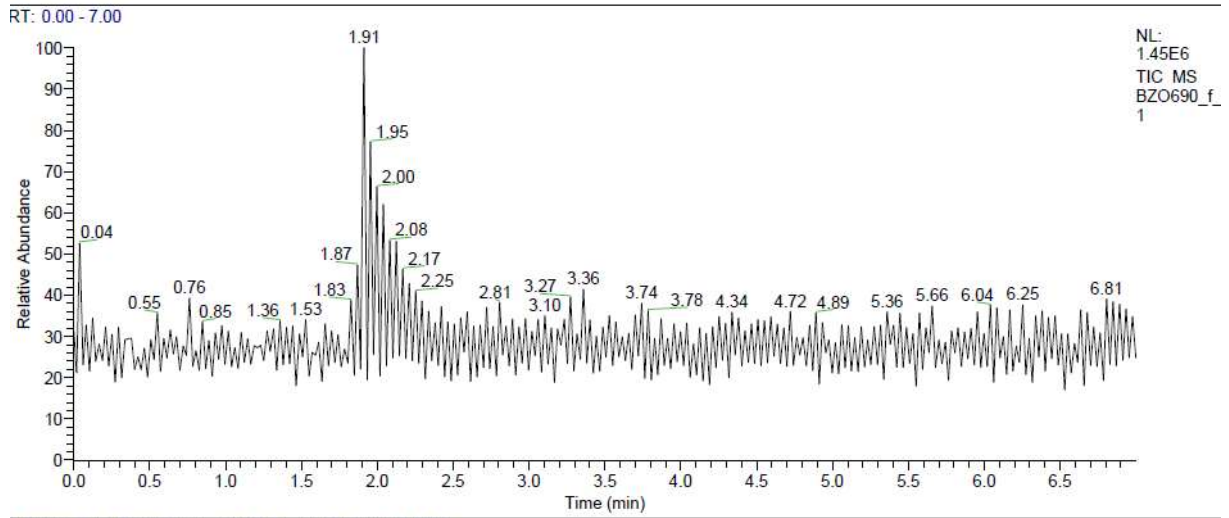
BZO679\_f#41-82 RT: 0.85-1.72 AV: 42 NL: 1.06E5  
T: {0,0} + c ESI Icorona sid=55.00 det=1506.00 Full ms [100.00-1000.00]



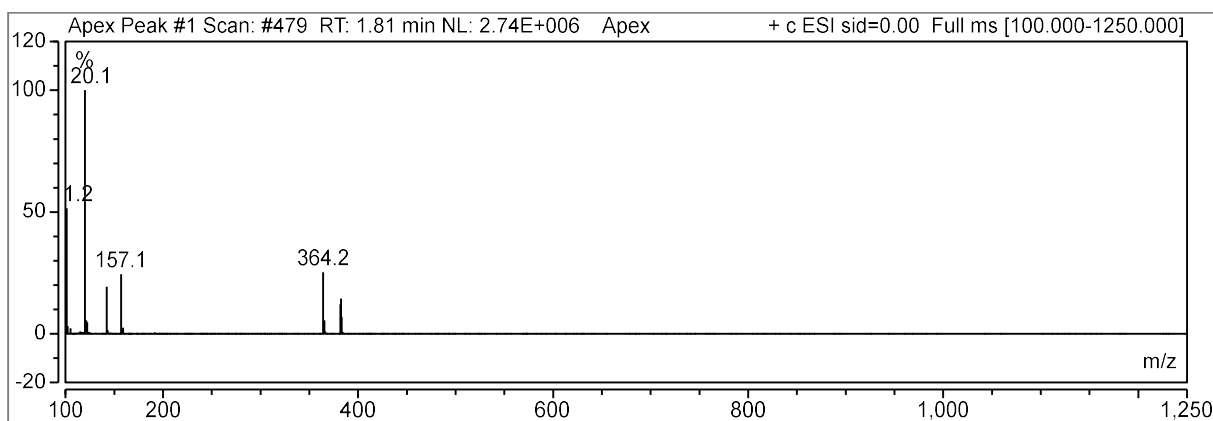
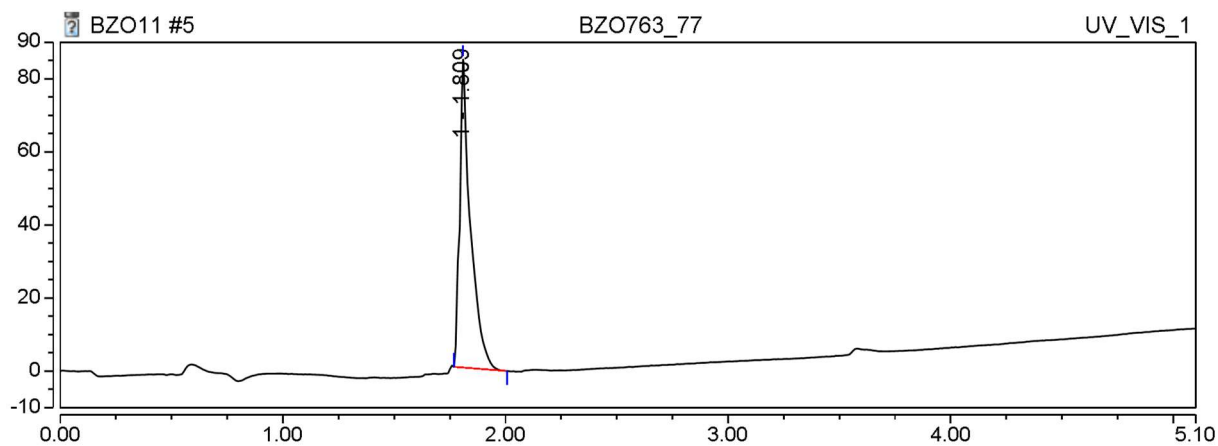
RT: 0.00 - 6.99



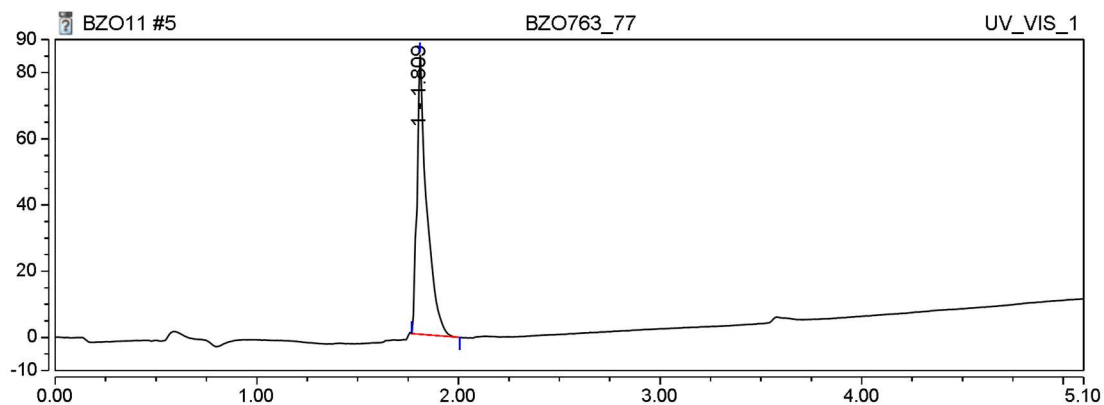
(120)

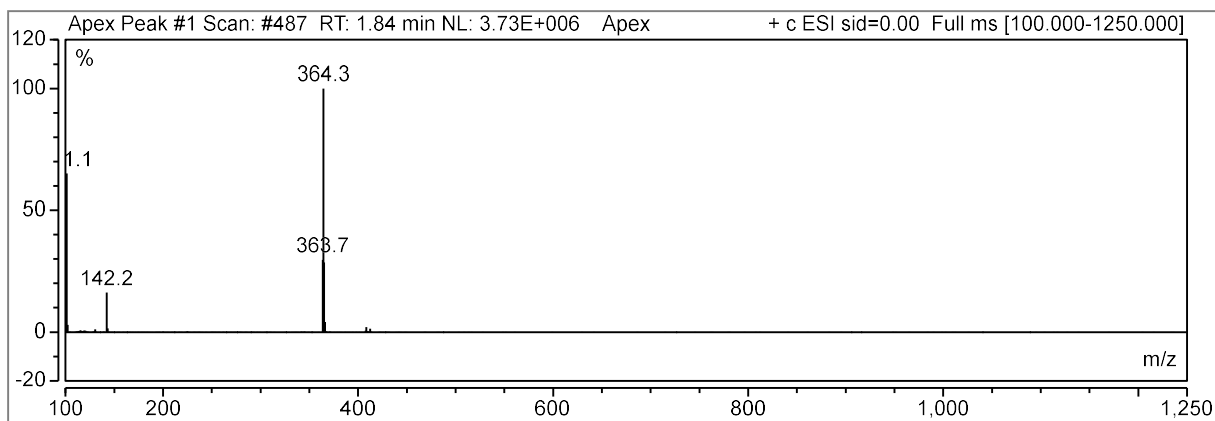


(47)

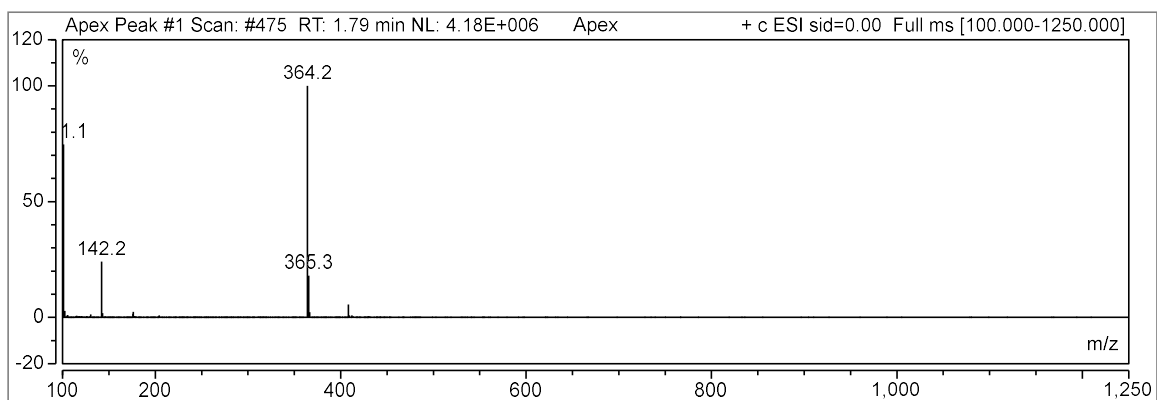
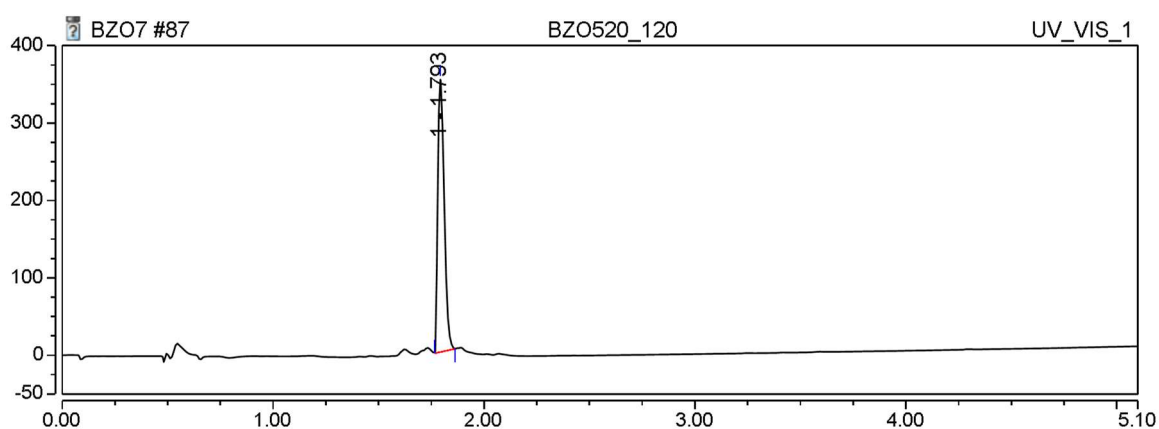


(7)

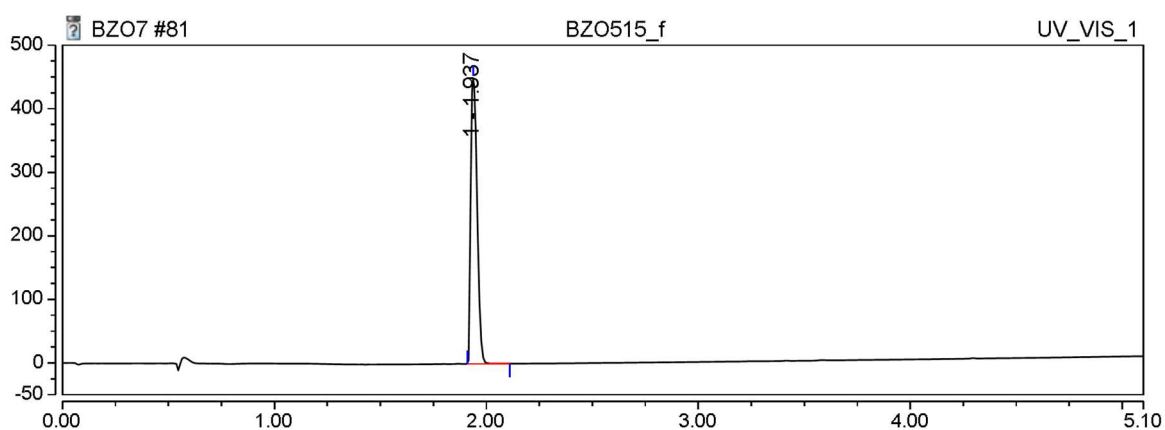




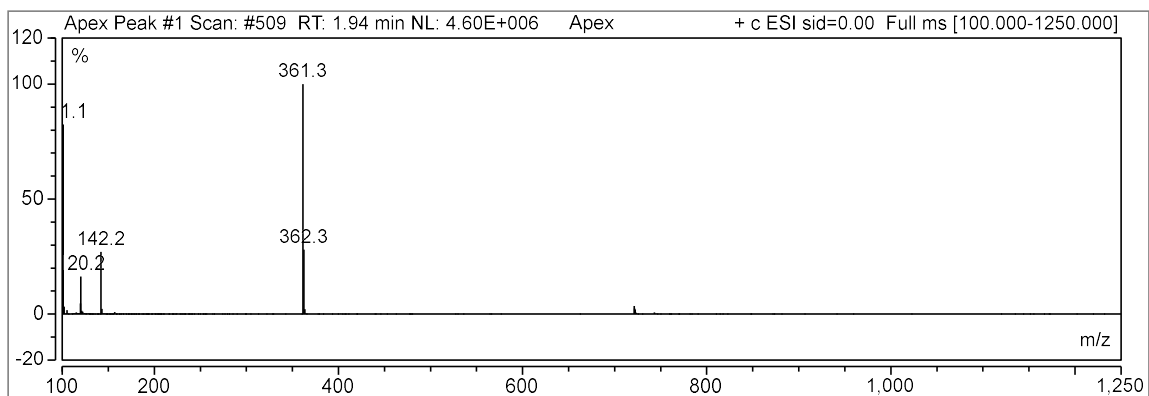
(40)



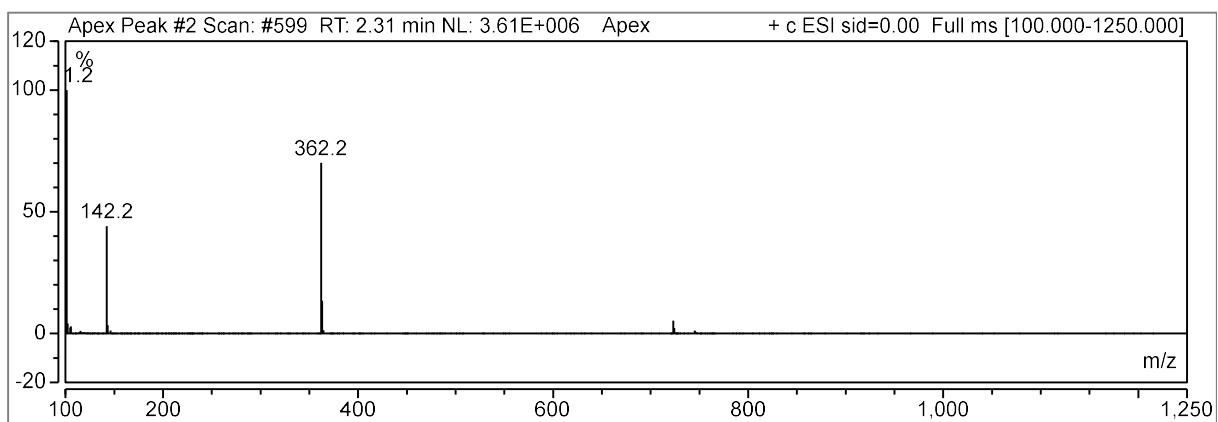
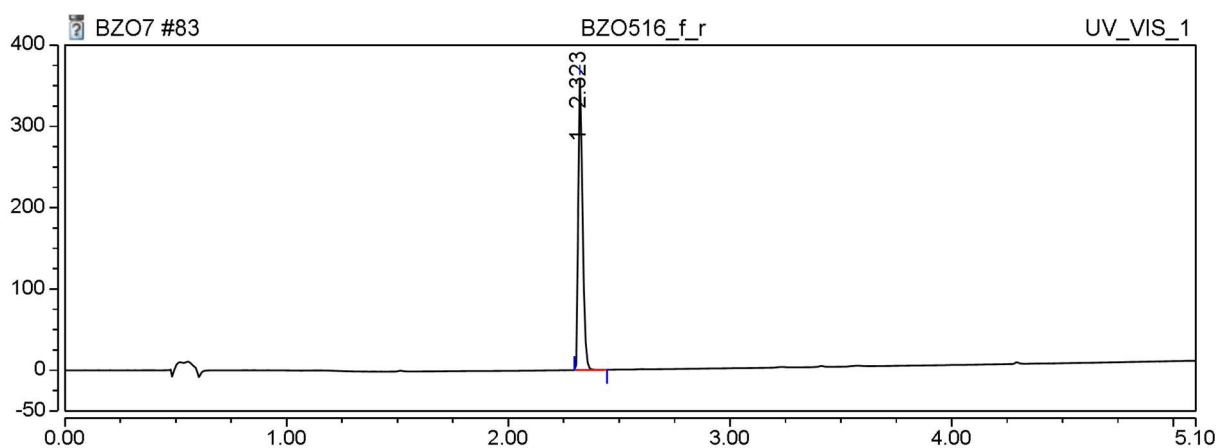
(82)



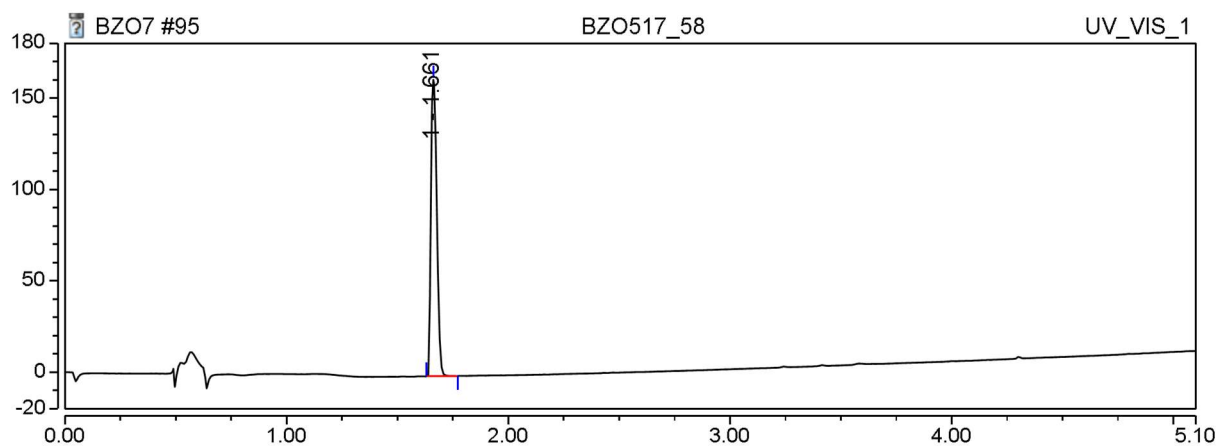


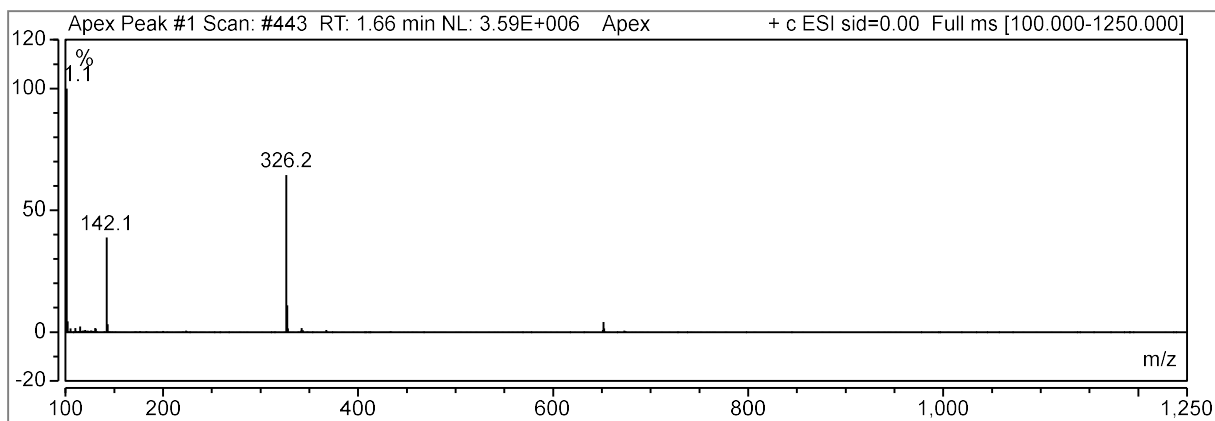


(83)

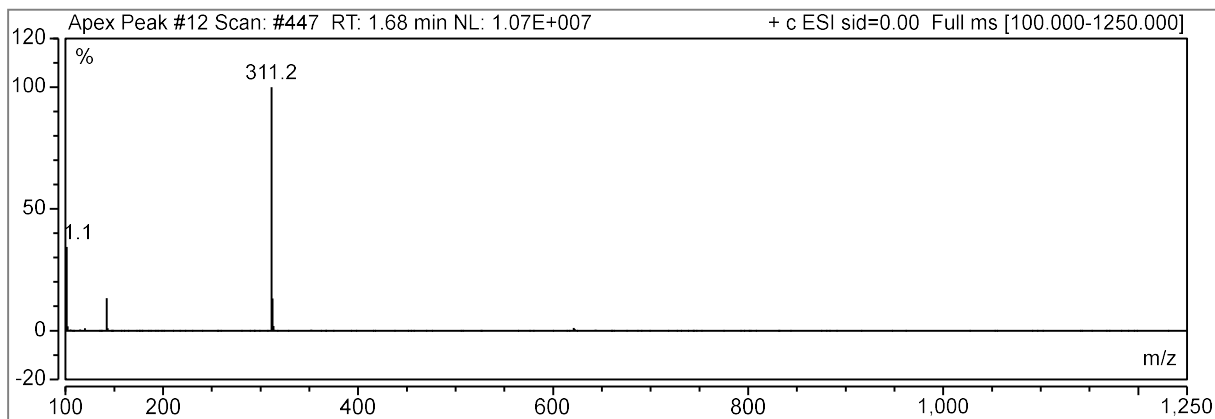
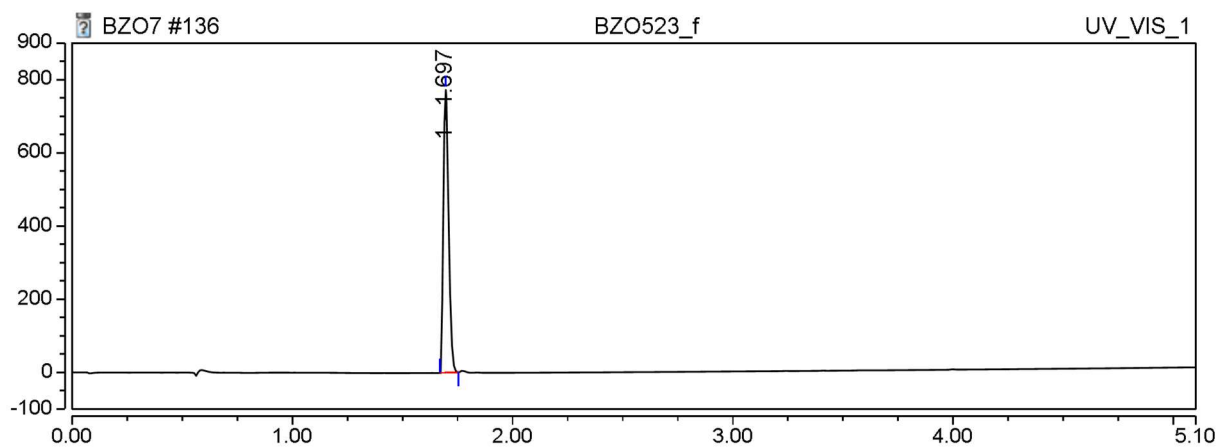


(84)

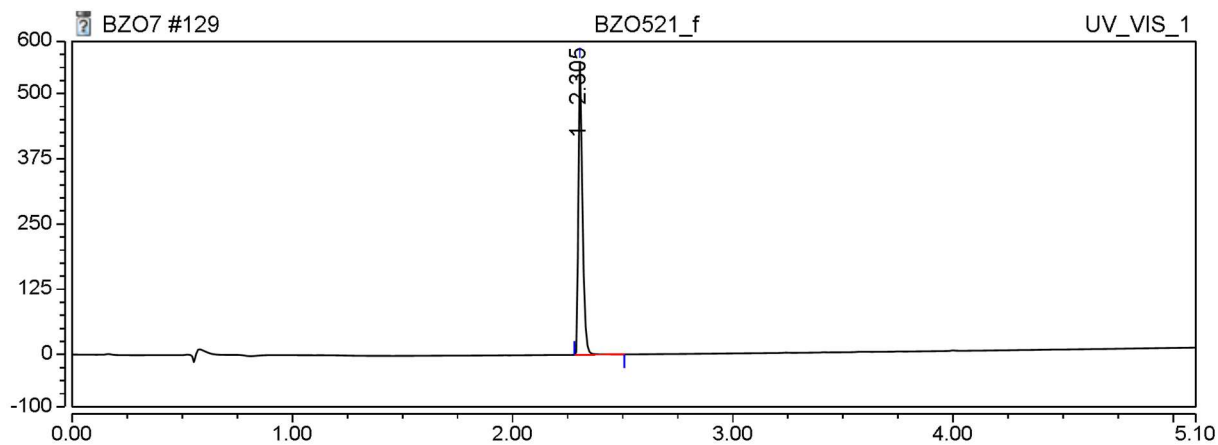


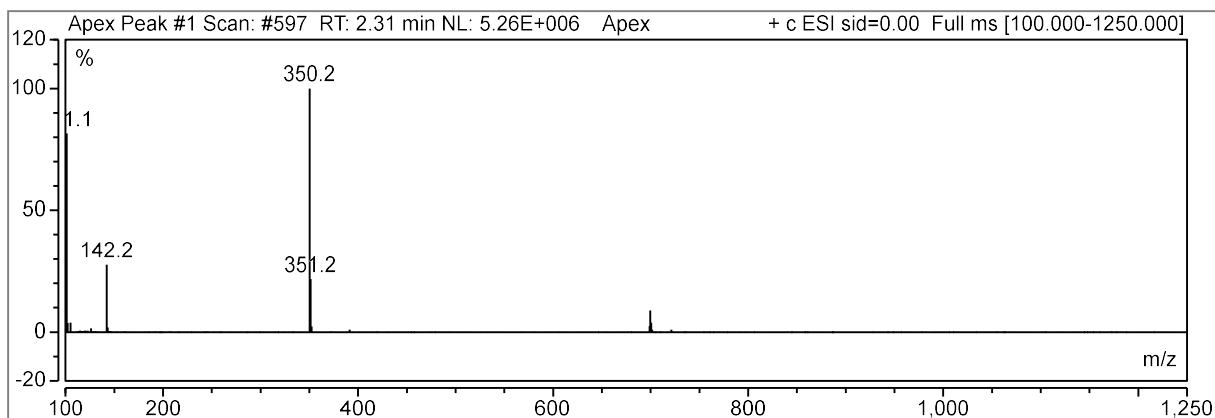


(85)

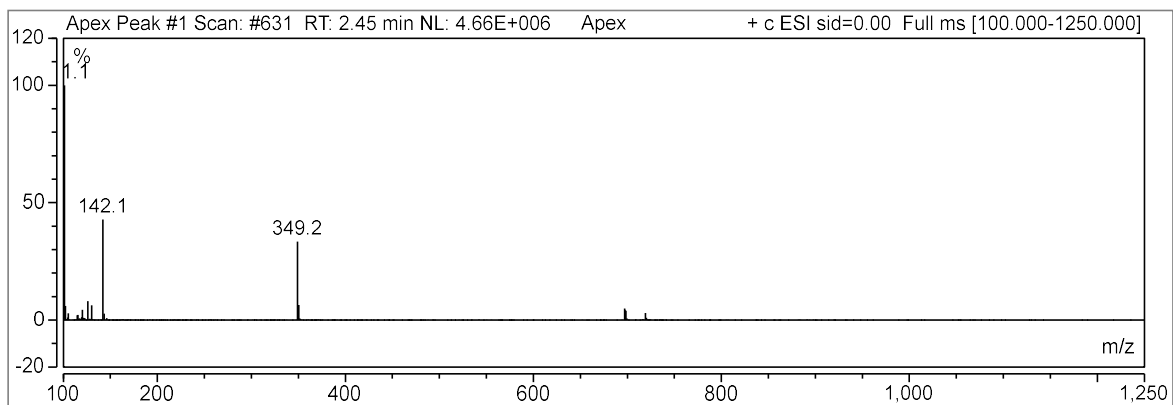
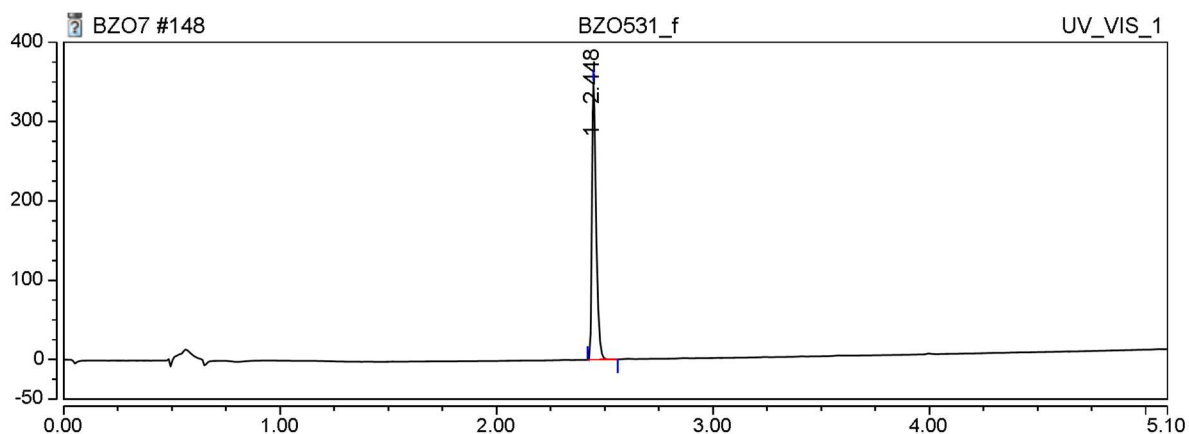


(88)

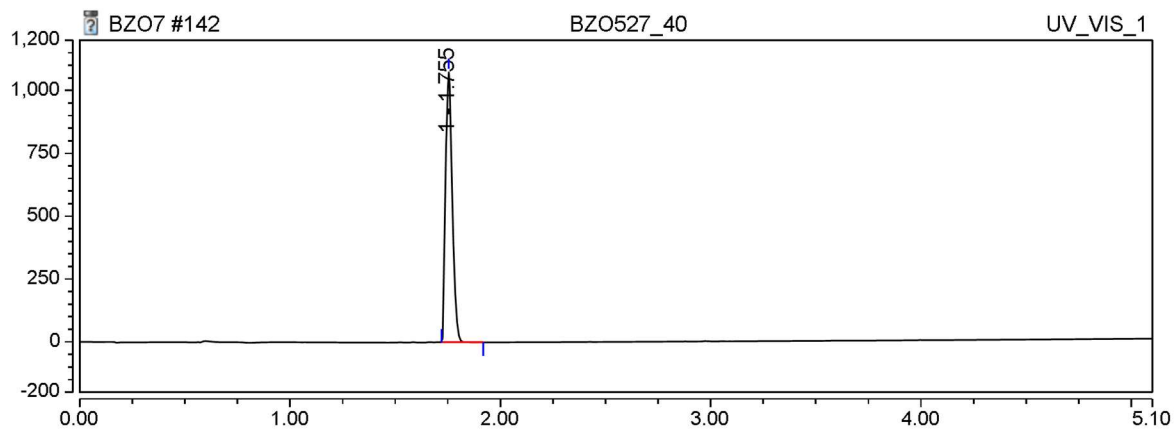


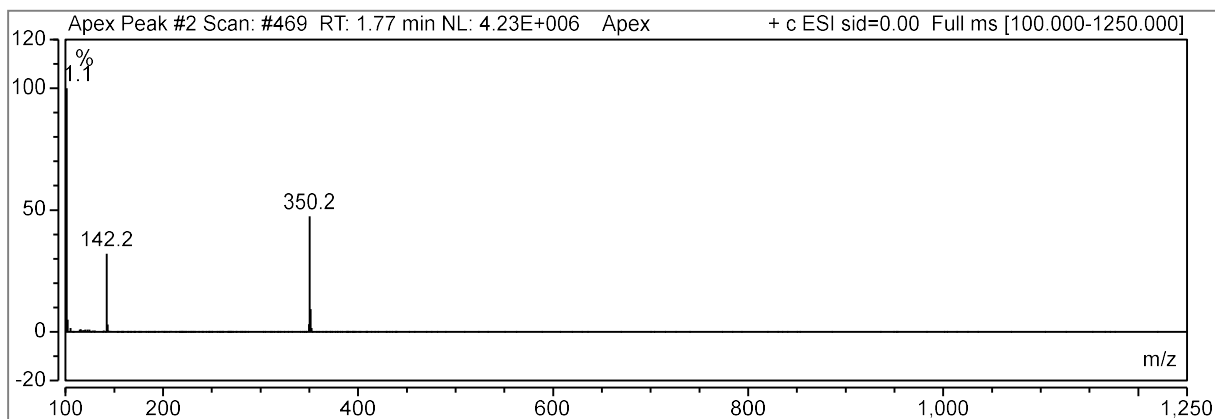


(87)

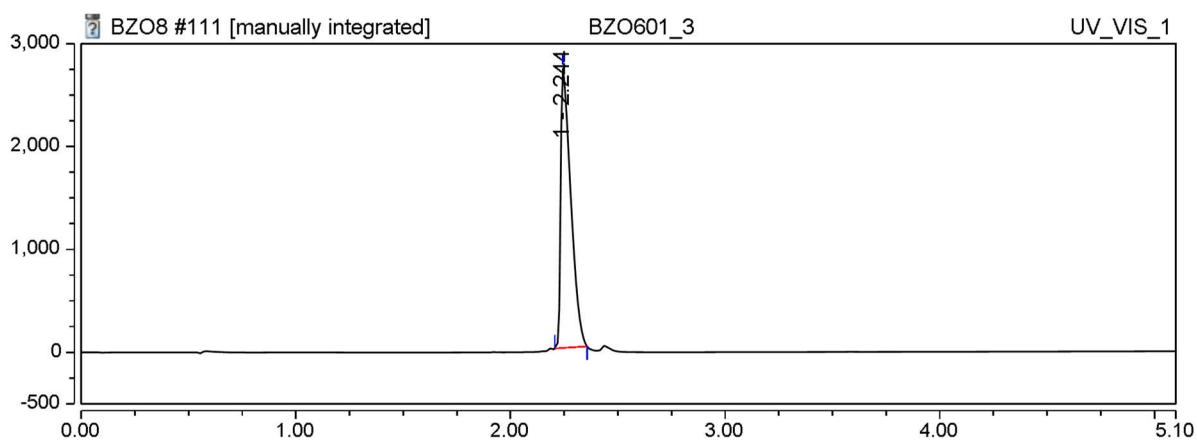


(86)

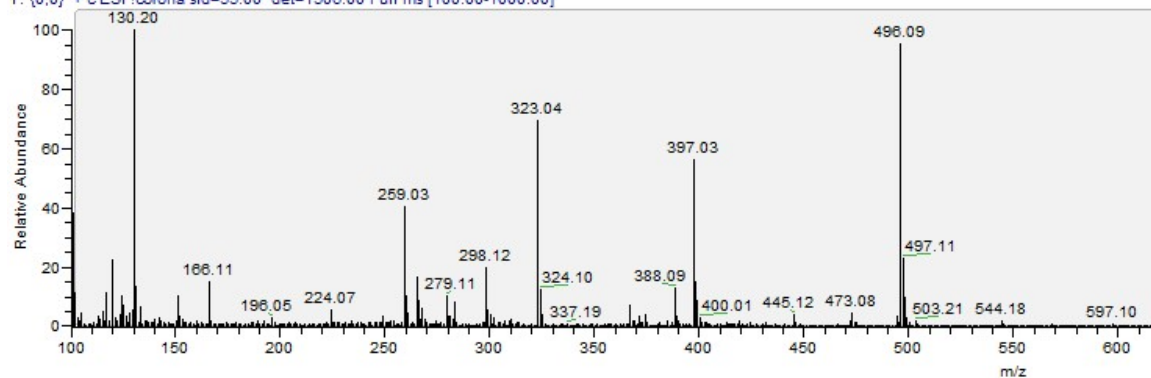




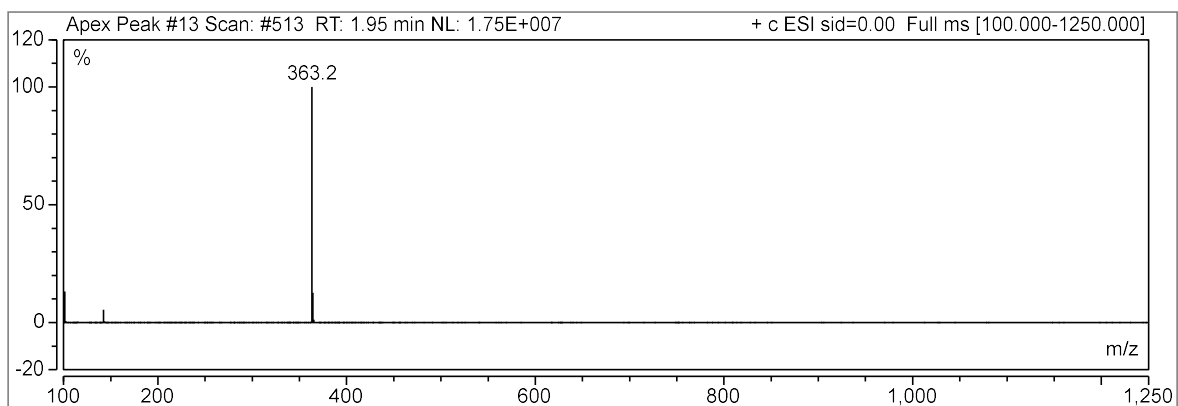
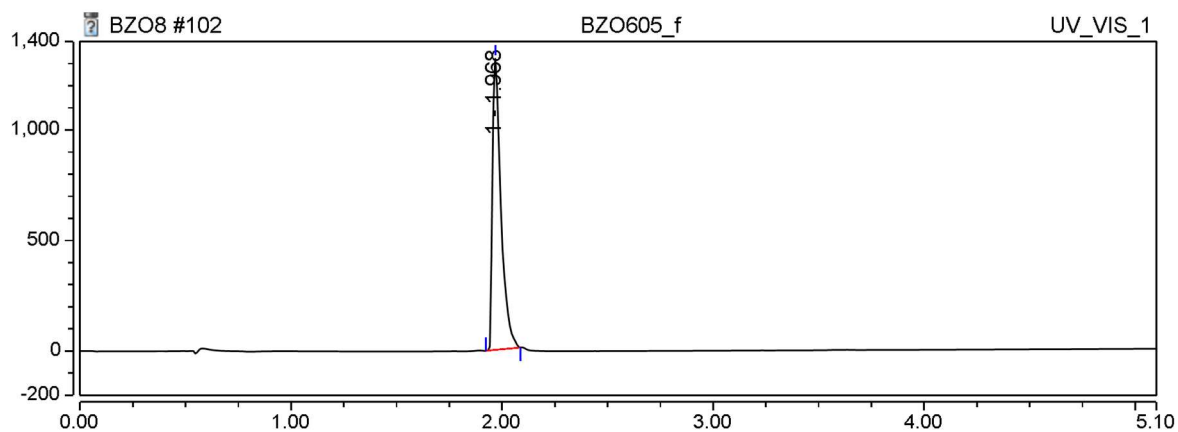
(77)



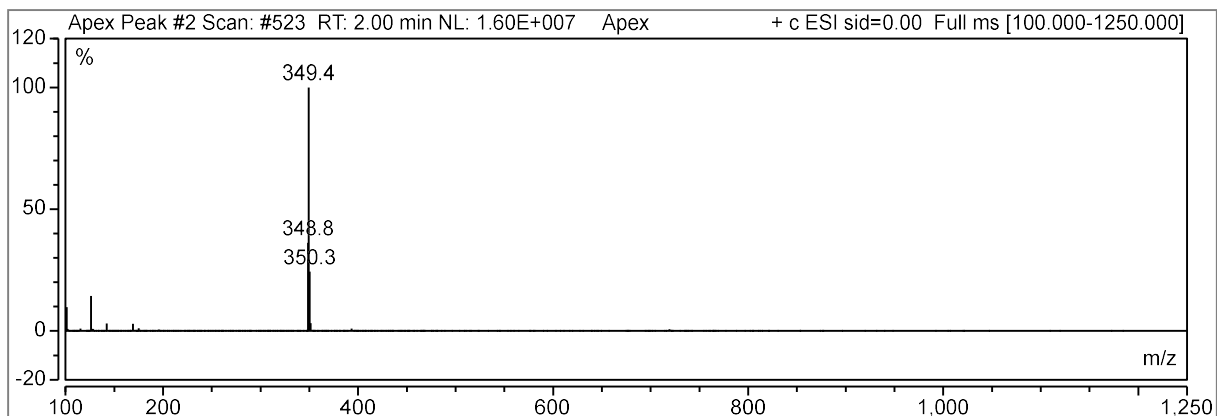
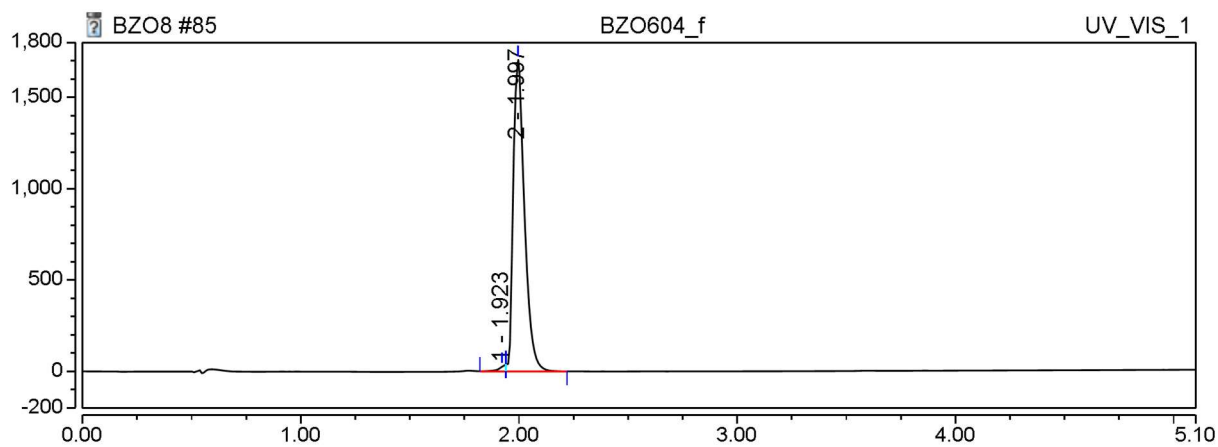
BZO601\_15h #135-142 RT: 2.85-3.00 AV: 8 NL: 3.70E5  
T: {0,0} + c ESI !corona sid=55.00 det=1506.00 Full ms [100.00-1000.00]



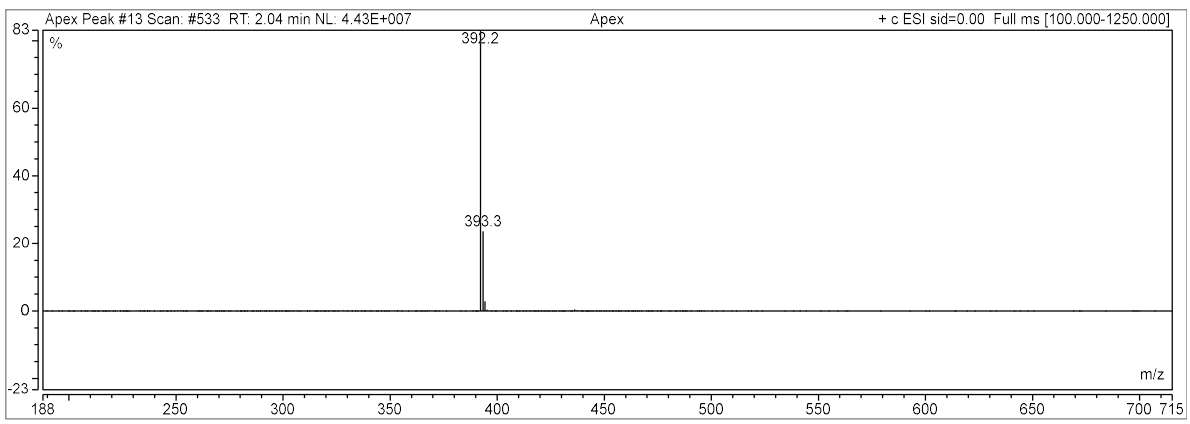
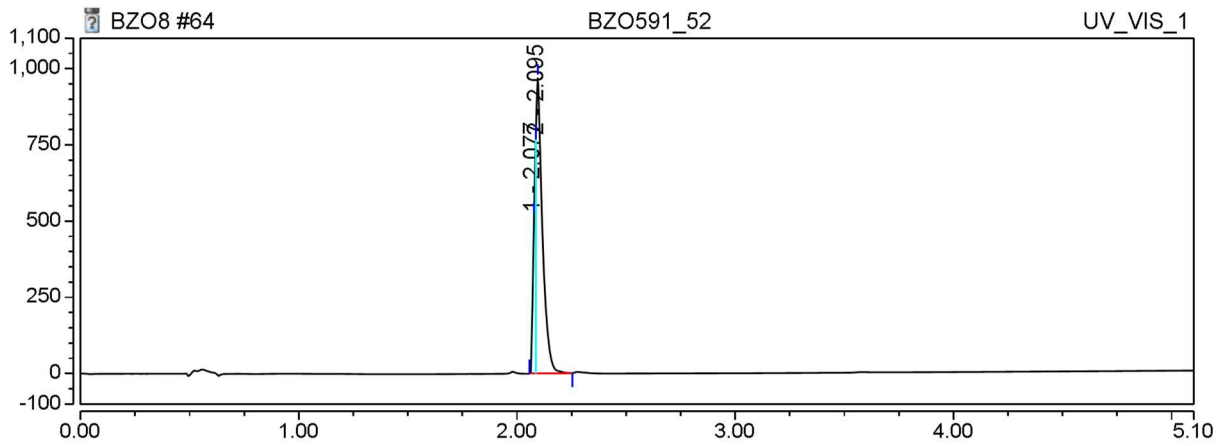
(80)



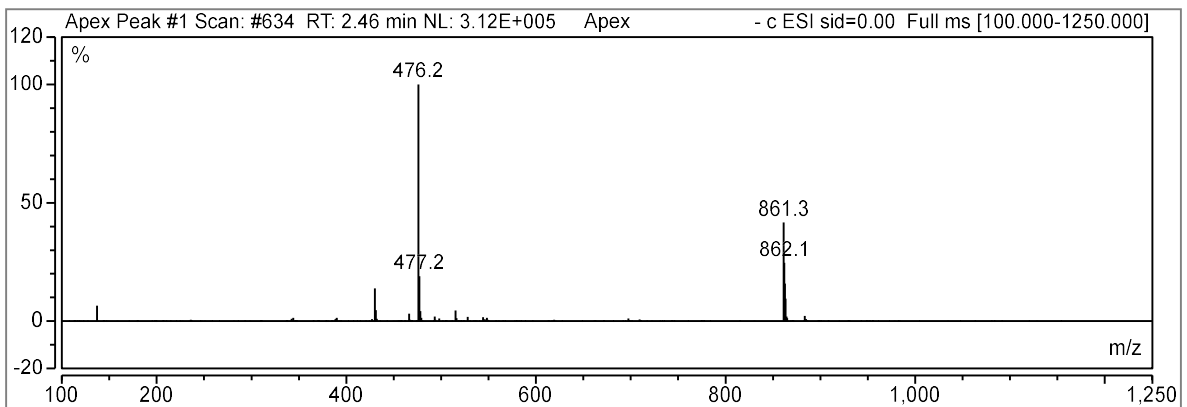
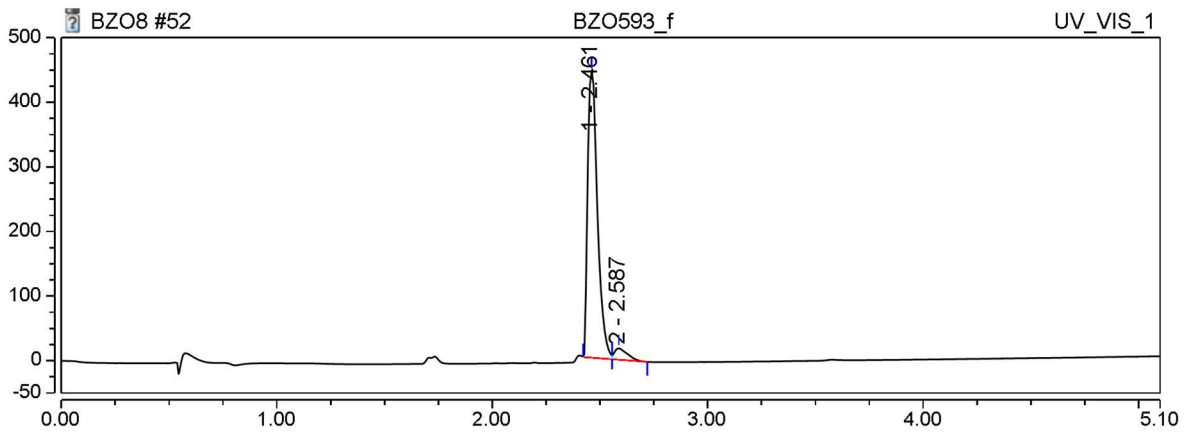
(81)



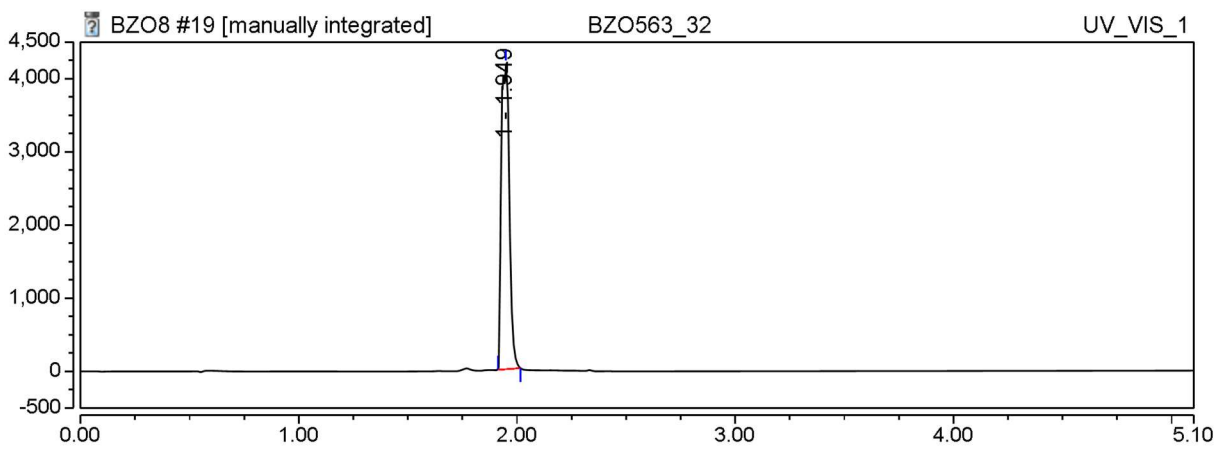
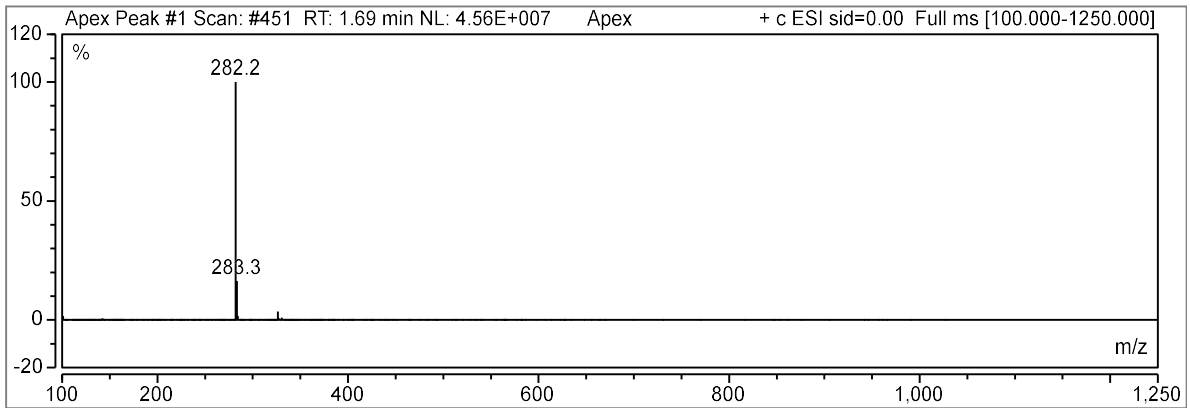
(78)



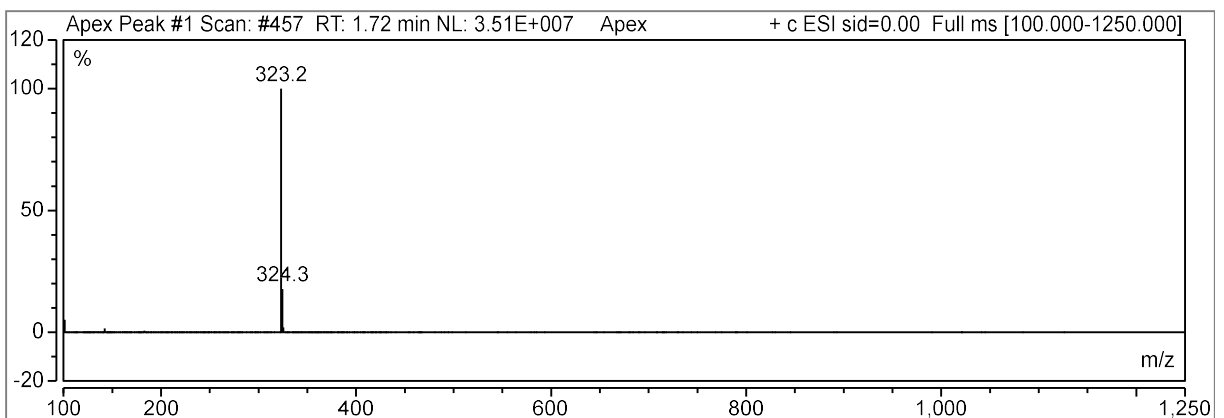
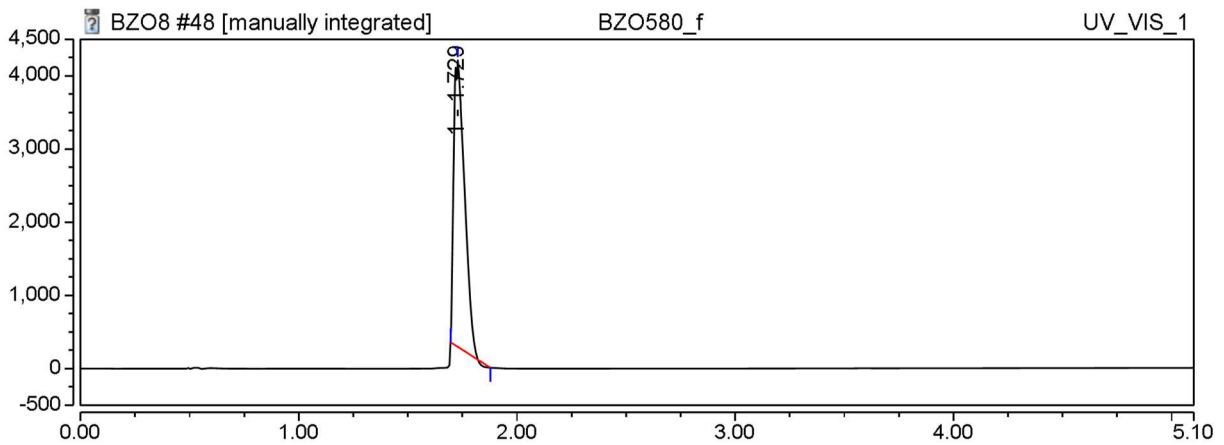
(79)



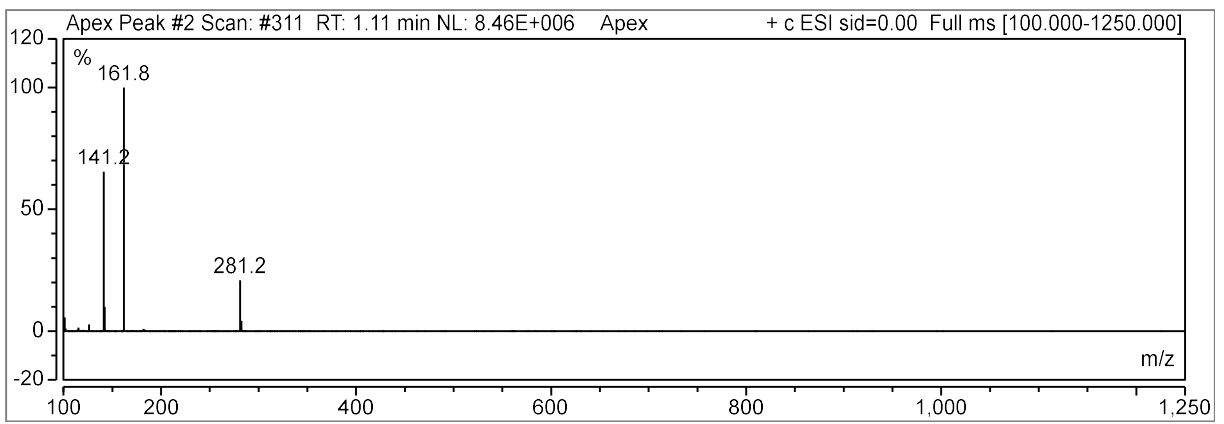
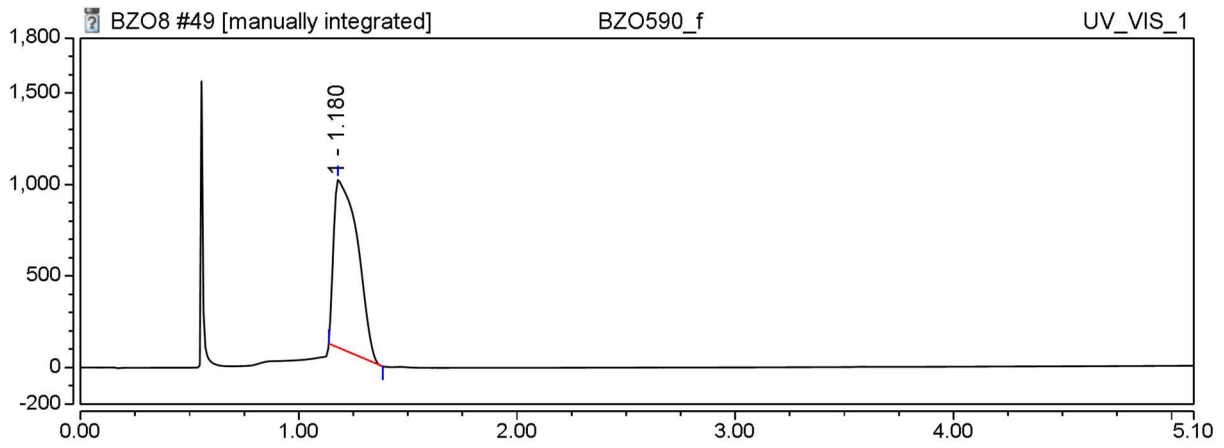
(73)



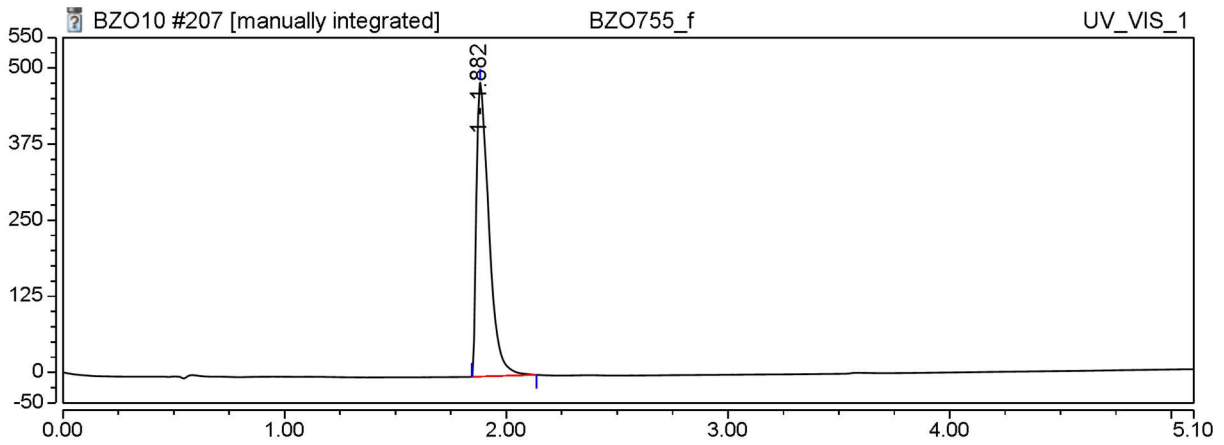
(75)



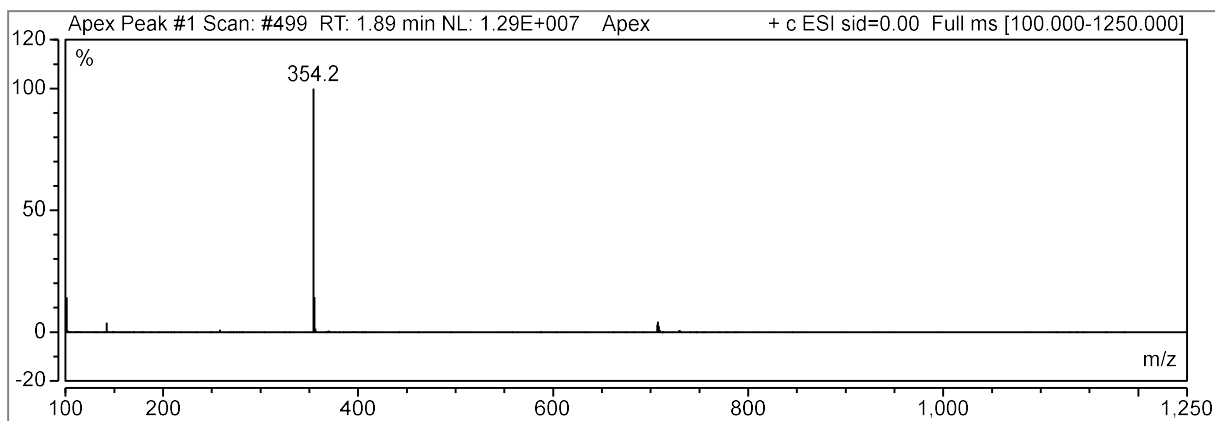
(74)



(159)

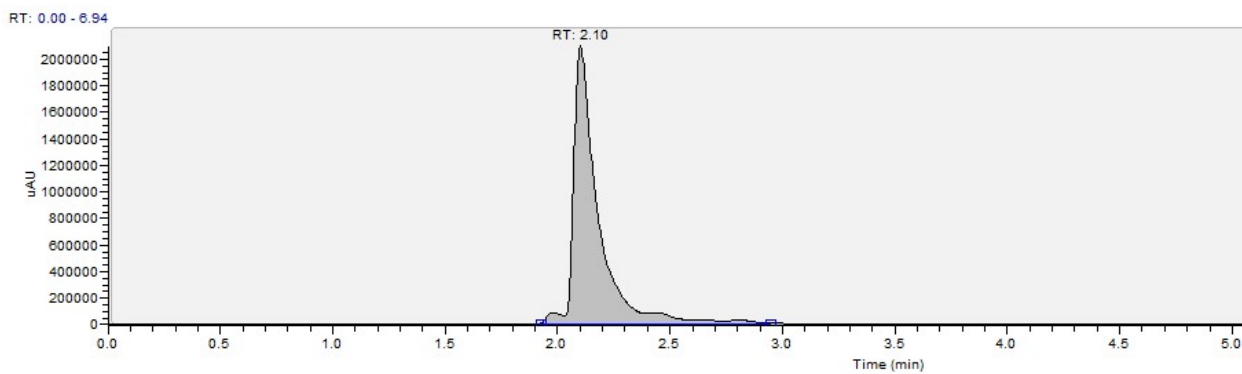
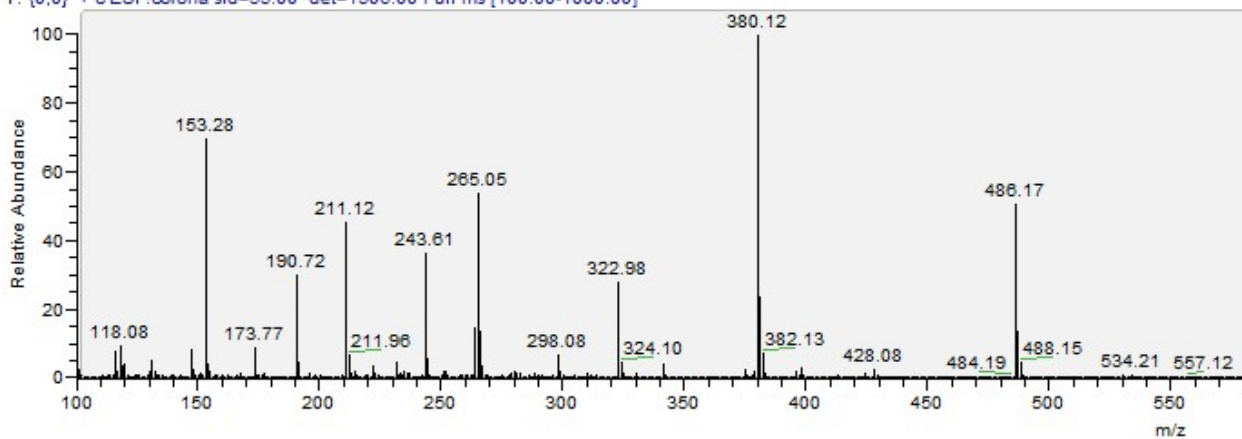




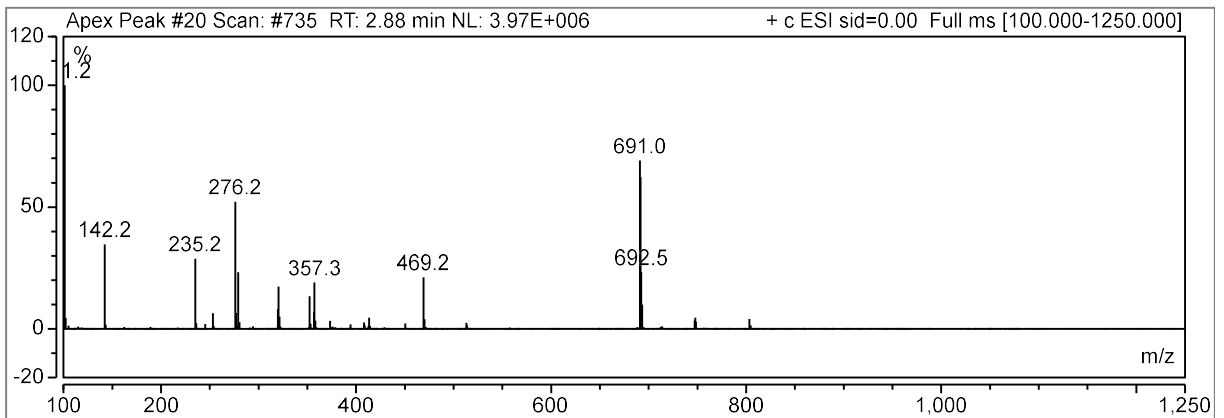
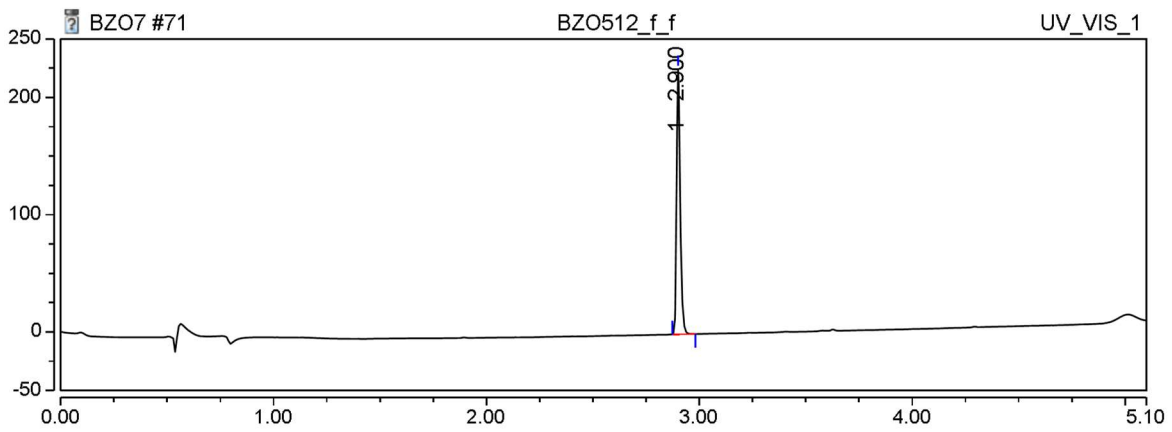


(76)

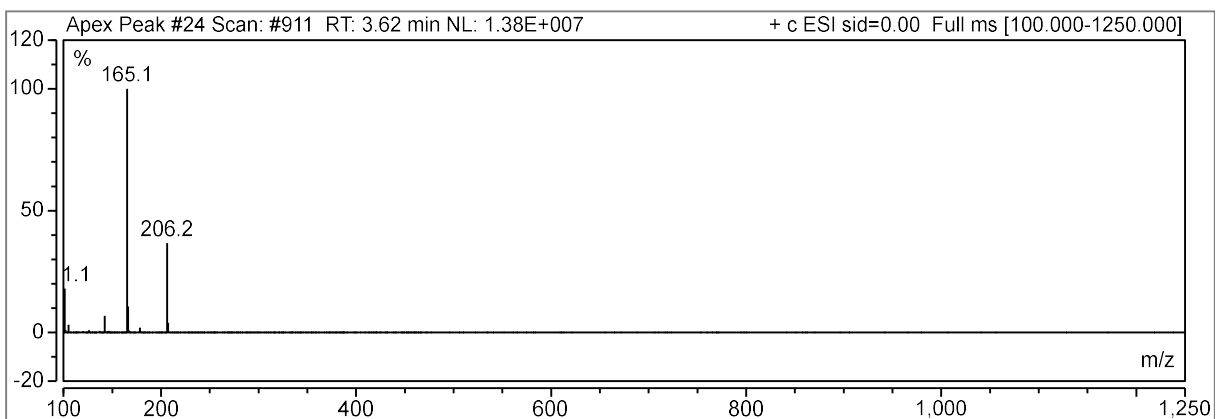
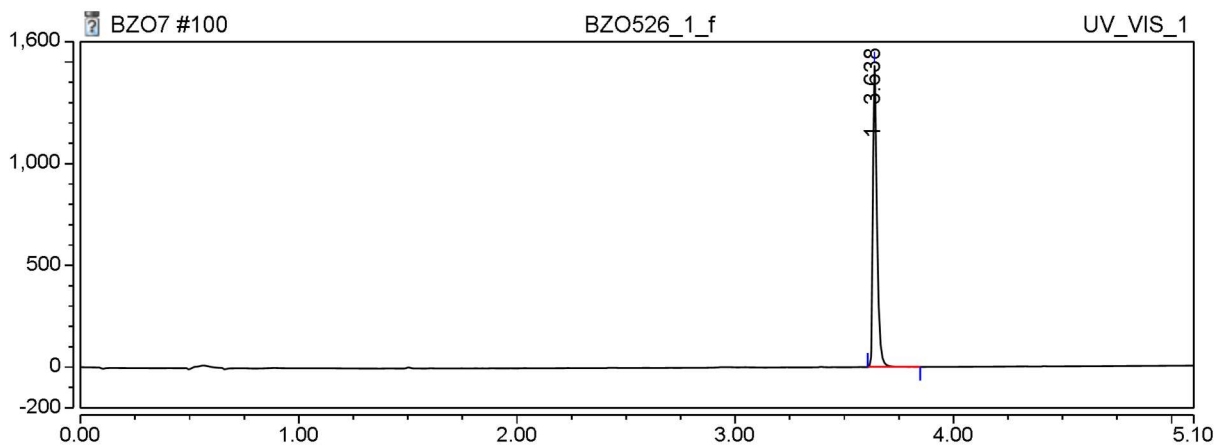
MKE023\_prept16 #96-132 RT: 2.02-2.78 AV: 37 NL: 4.51E5  
T: {0,0} + c ESI !corona sid=55.00 det=1506.00 Full ms [100.00-1000.00]



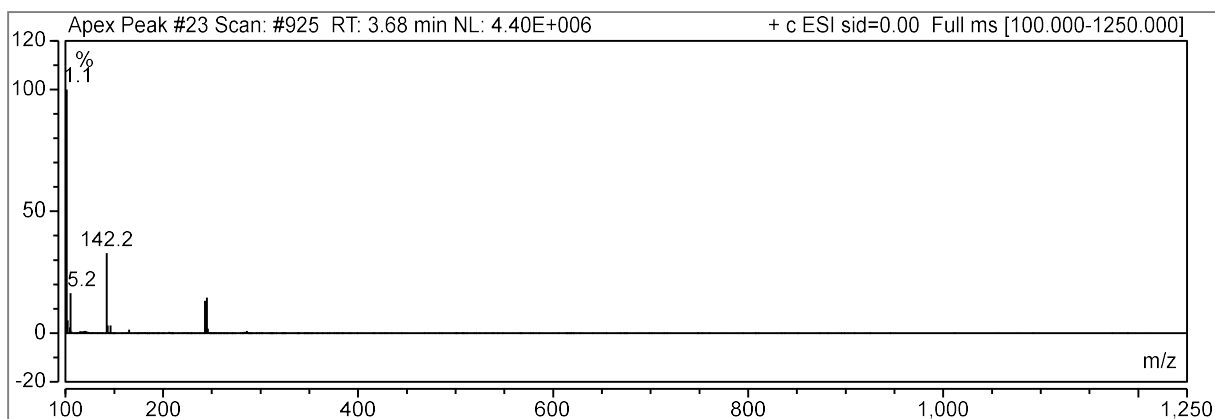
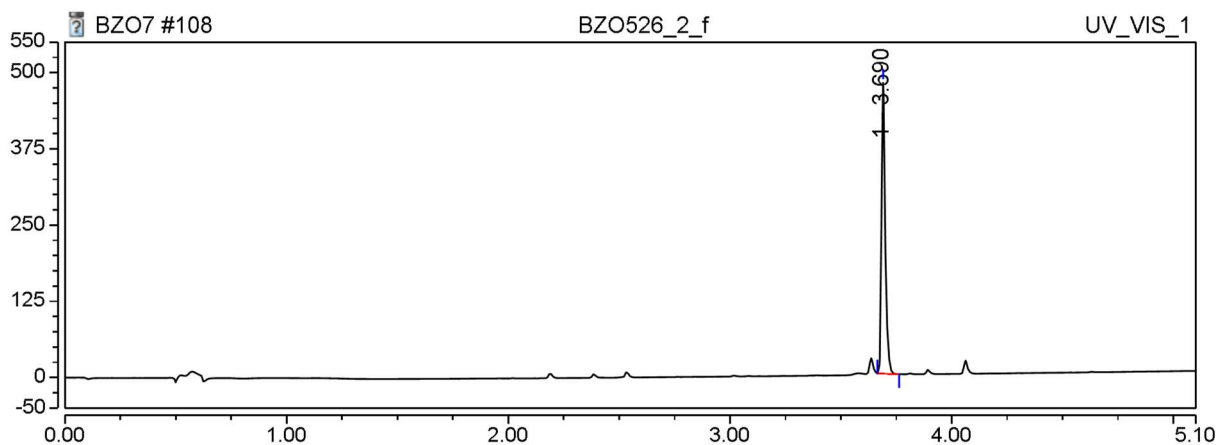
(32)



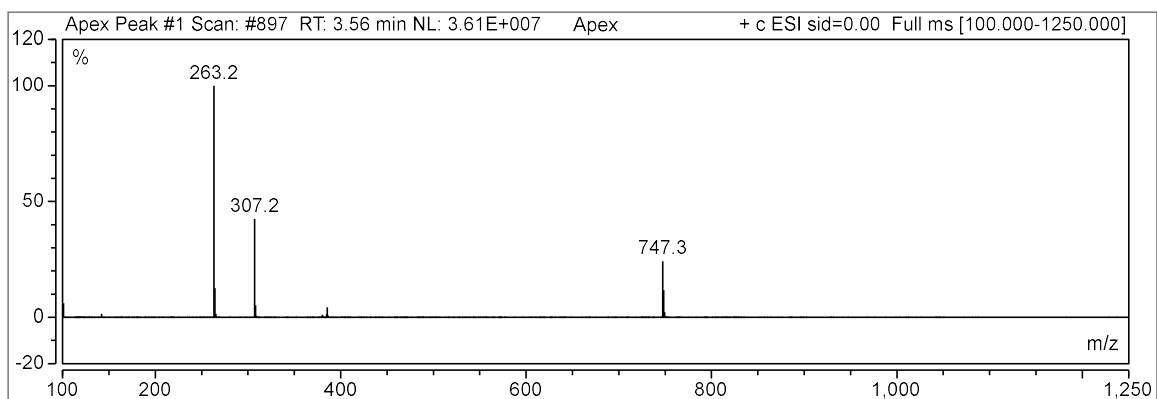
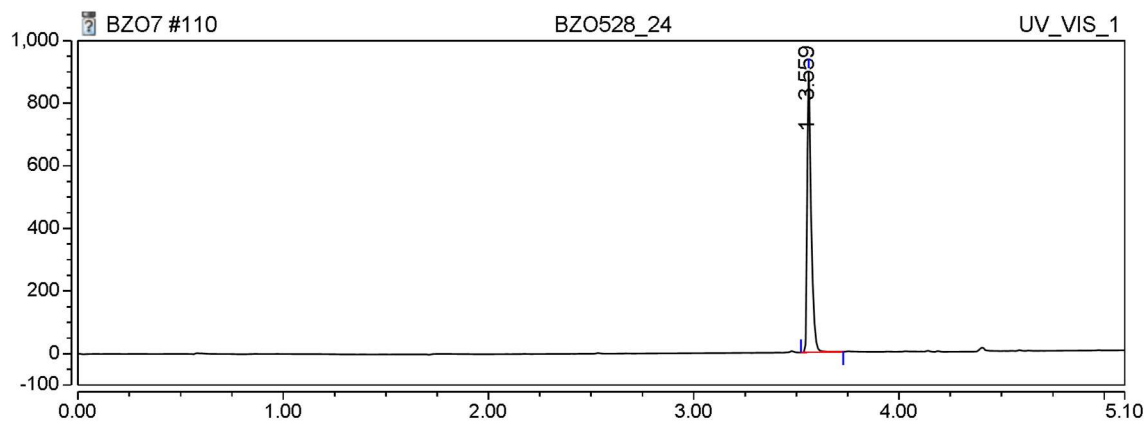
(133)



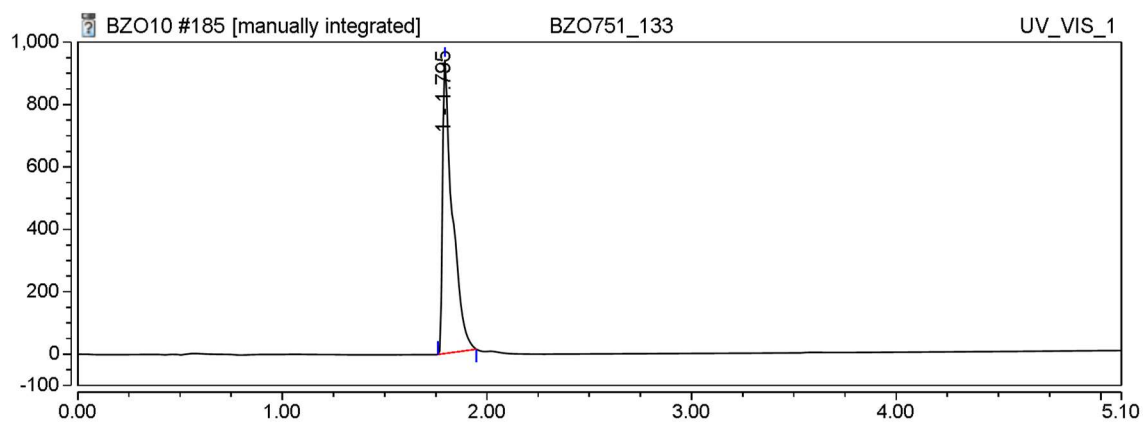
(44)



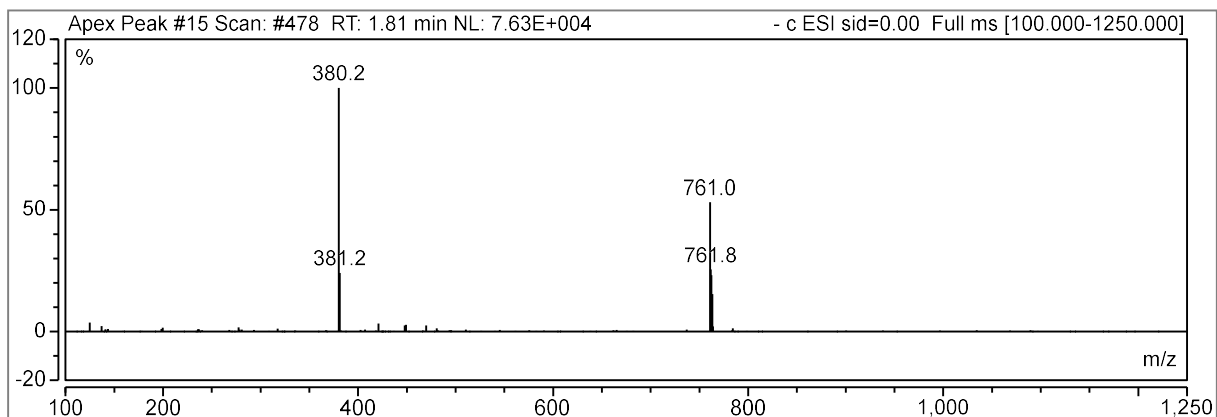
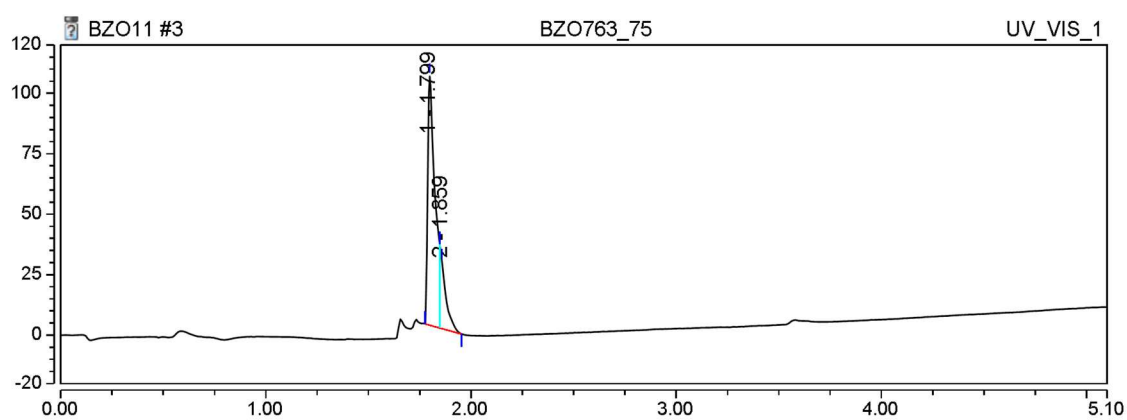
(45)



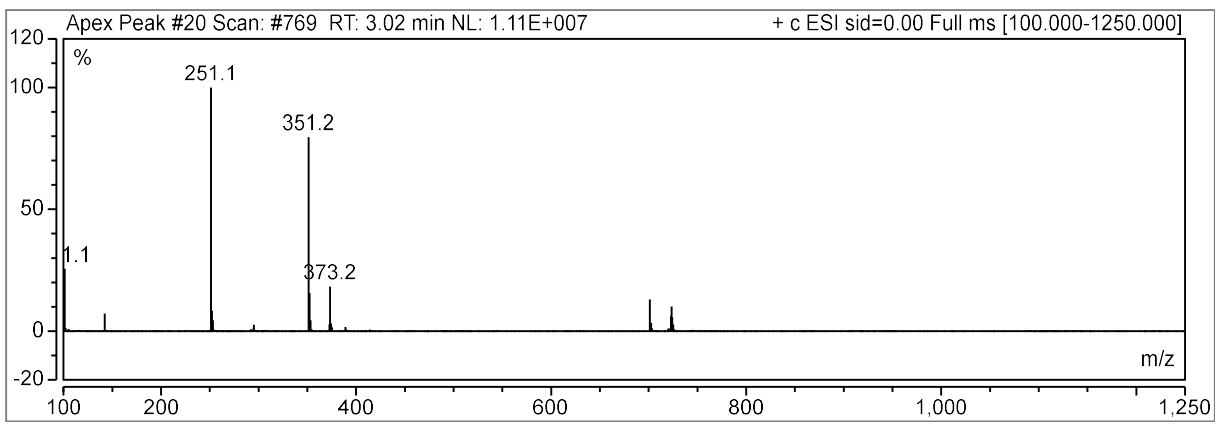
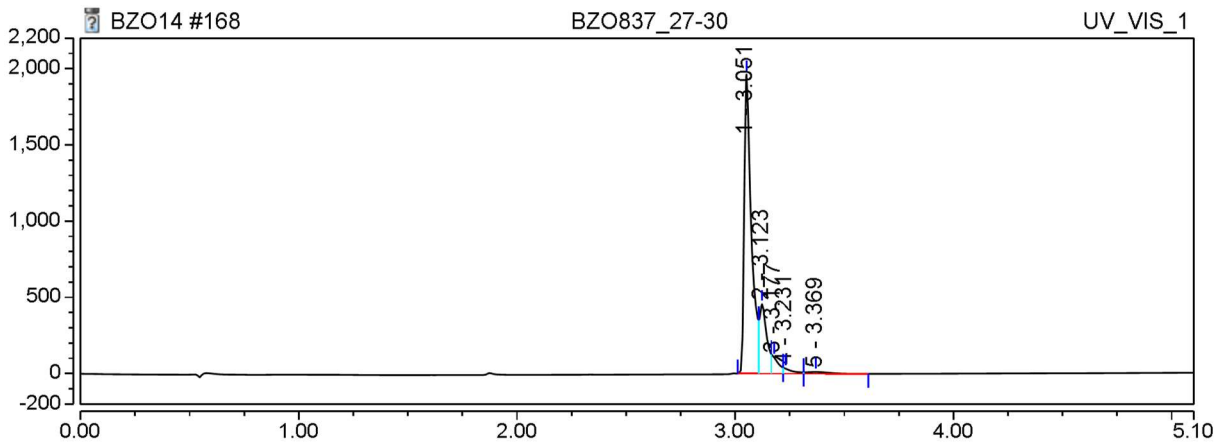
(46)



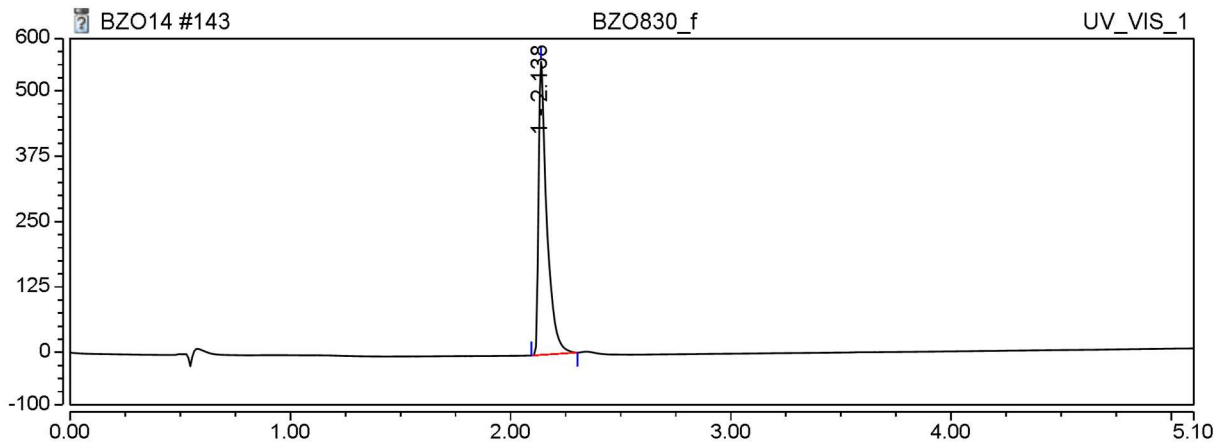
(47)

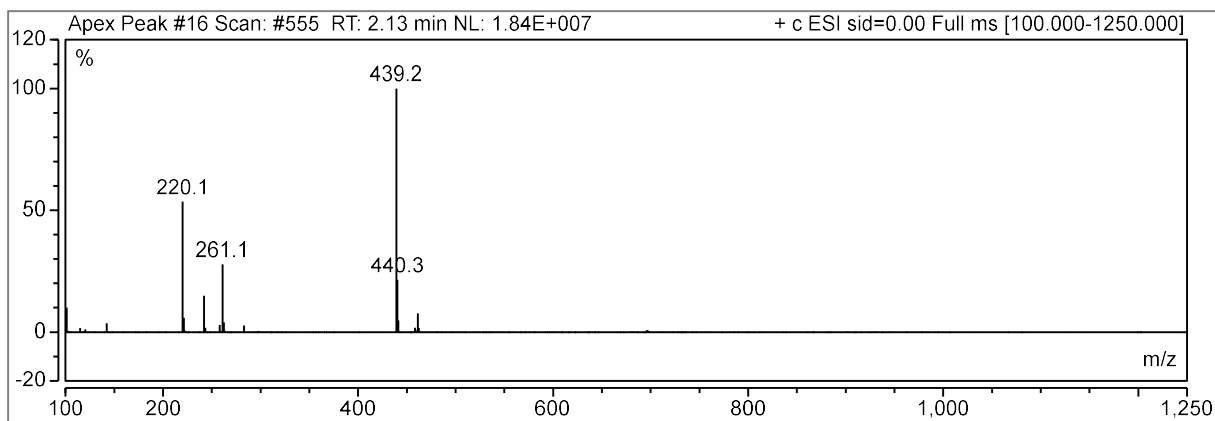


(144)

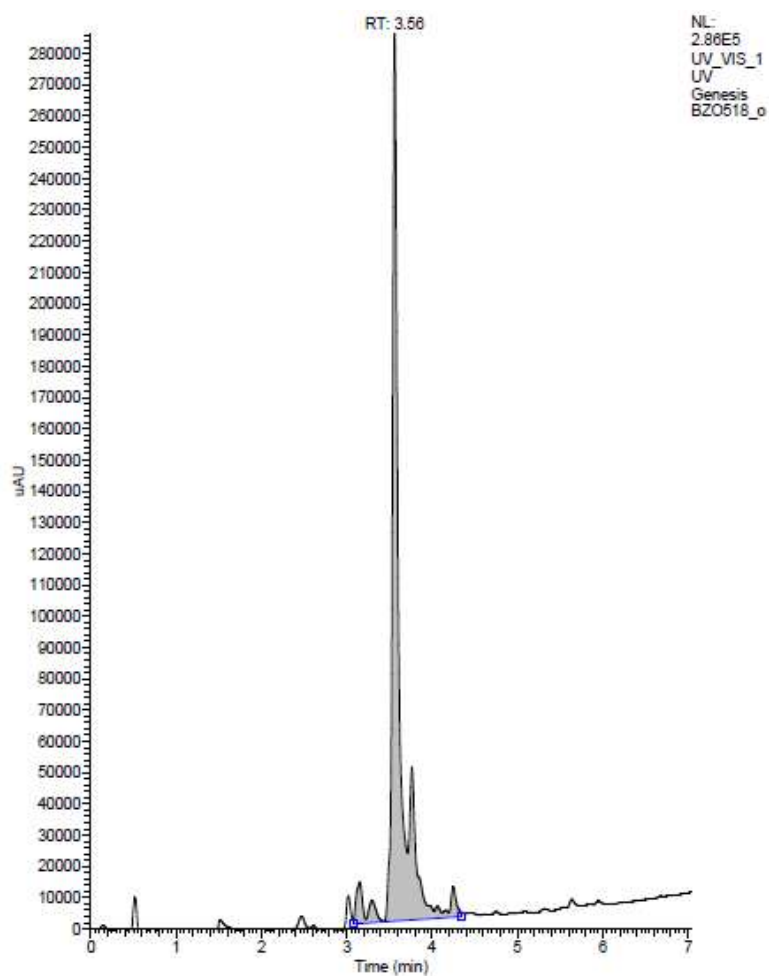


(146)

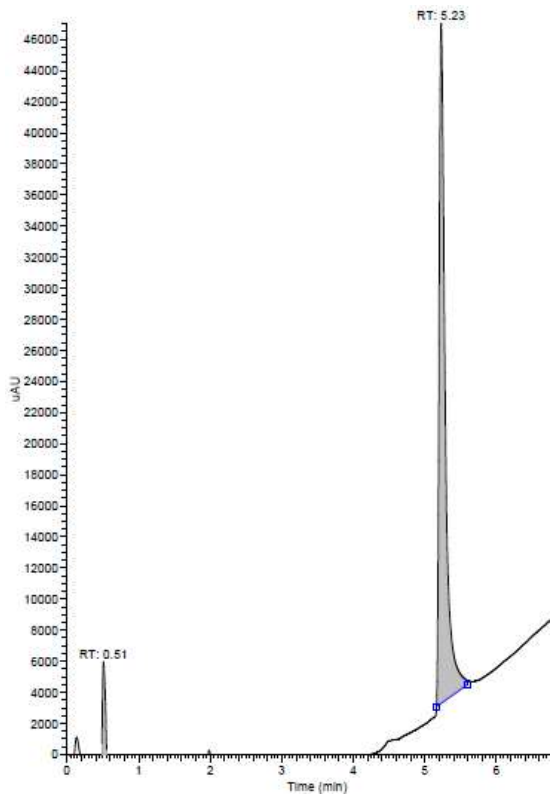




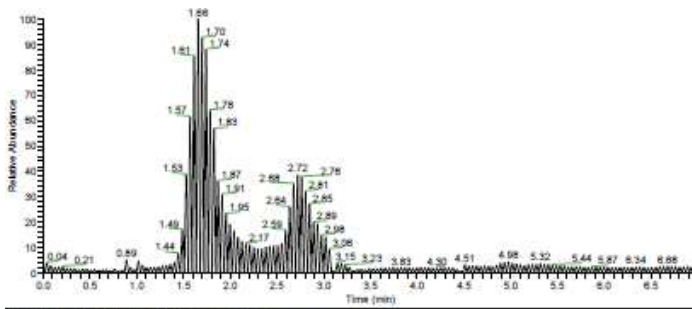
(39)



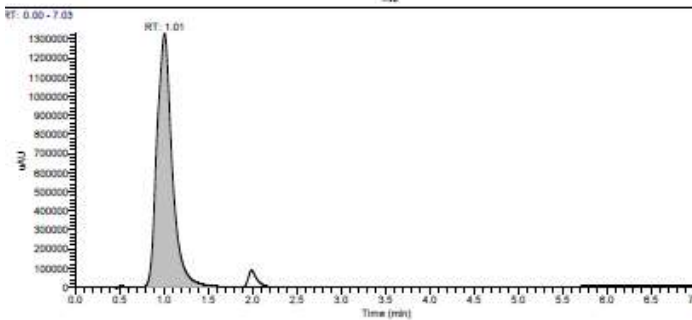
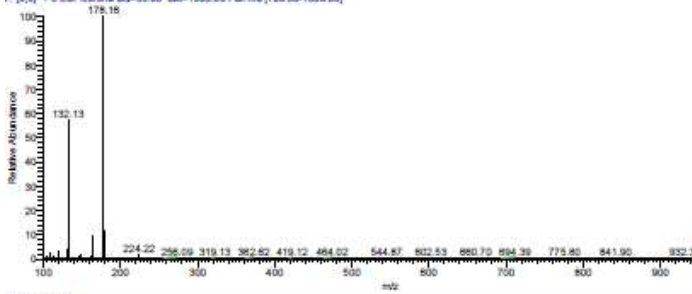
(154)



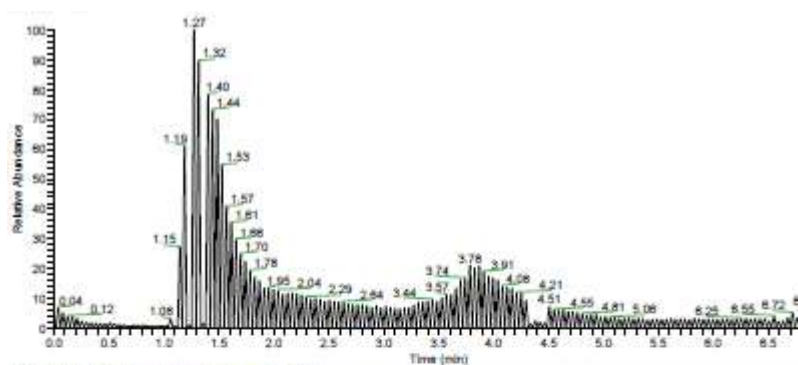
(132)



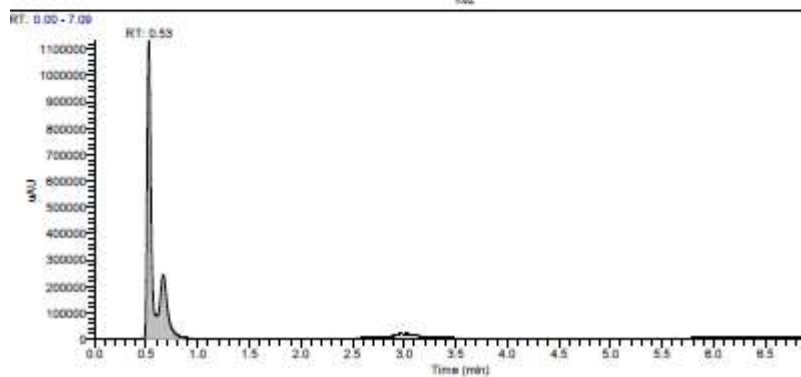
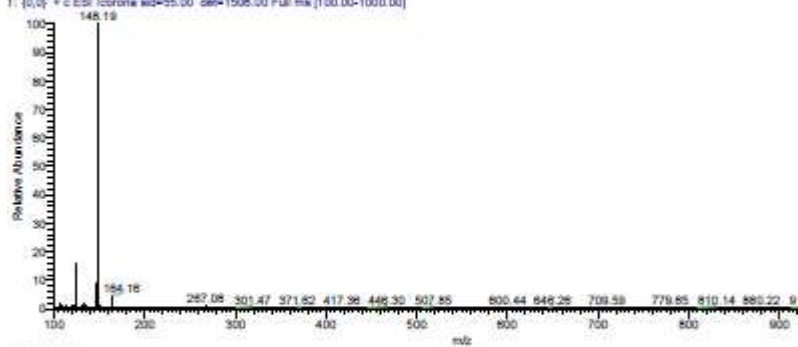
520491\_2n-#72-04 RT: 1.51-1.98 Av: 23 Nt: 8.08E8  
F: [0,0] = c ESI Ionora s04=85.00 det=1506.00 Full.ms [100.00-1000.00]



(28)

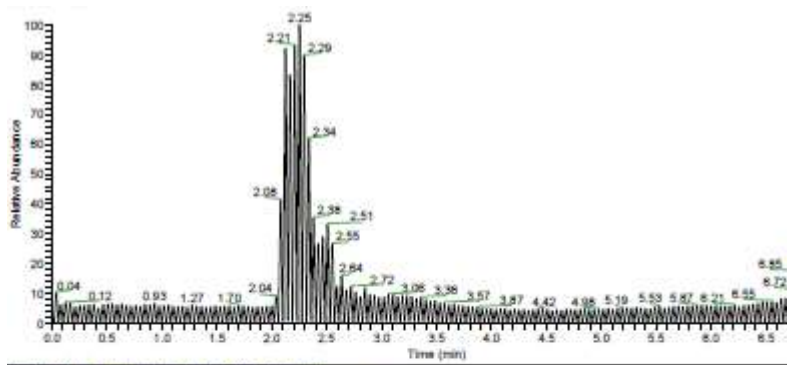


BZD490\_4h #52-80 RT: 1.08-1.89 AV: 39 NL: 6.19E5  
T: (0,0) + c ESI: icrona acid=55.00 det=1506.50 Full ms [100.00-1000.00]

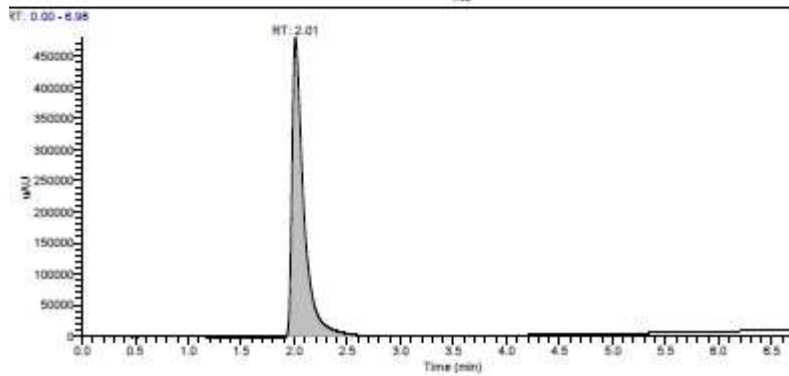
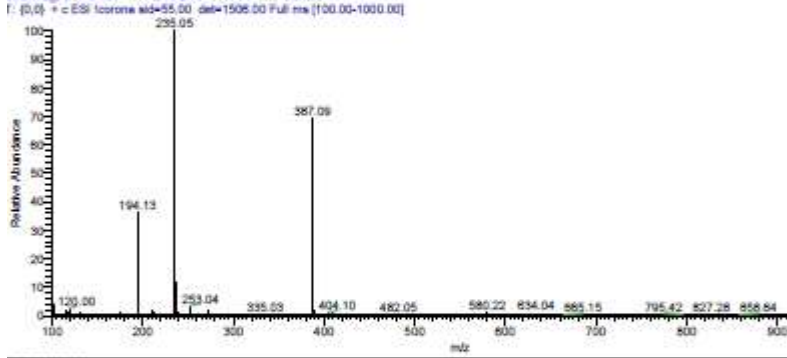




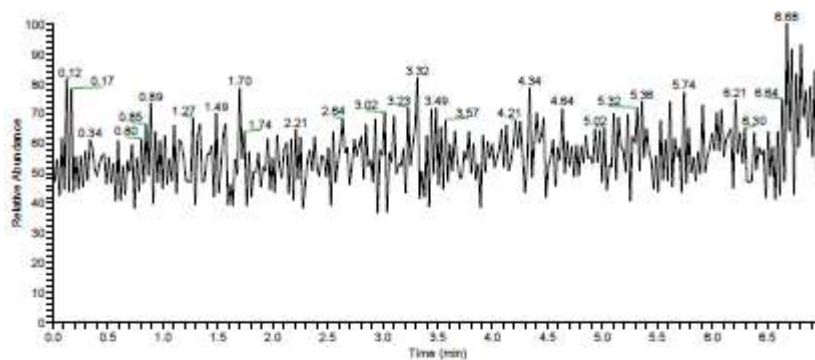
(156)



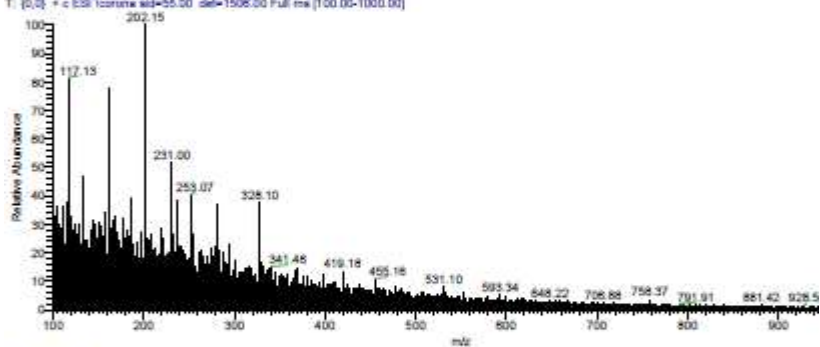
SZ0579\_02\_008-128 RT: 2.06-2.70 AV: 31 NL: 6.2068  
F: [0,0] \* c ESI Ionome sld=55.00 det=1505.00 Full ms [100.00-1000.00]



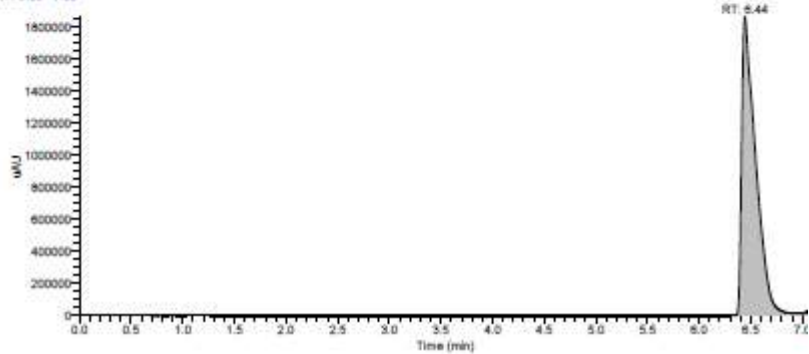
(143)



BZD630-#318-330 RT: 6.70-7.00 AV: 15 NL: 5.22E3  
T: (0.0) = c ESI (cone: sld=55.00 del=1500.00 Full res [100.00-1000.00])



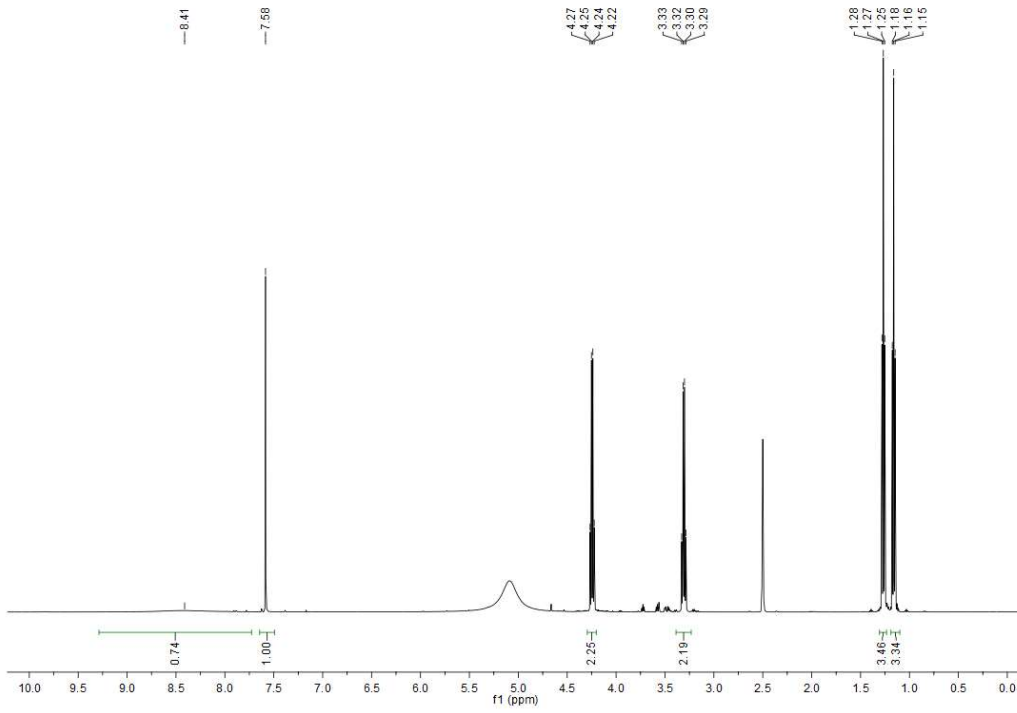
RT: 0.00 - 7.08



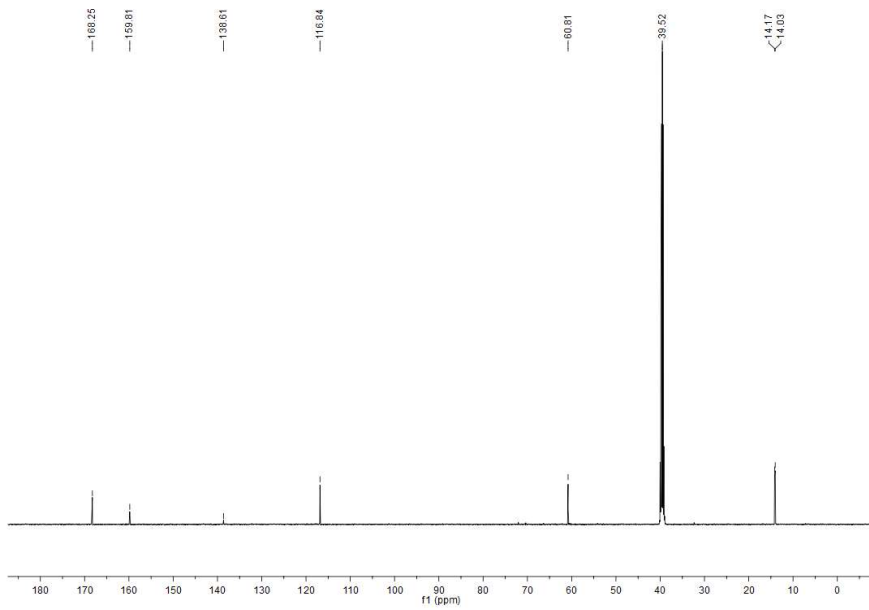
# NMR-Data

(10)

<sup>1</sup>H

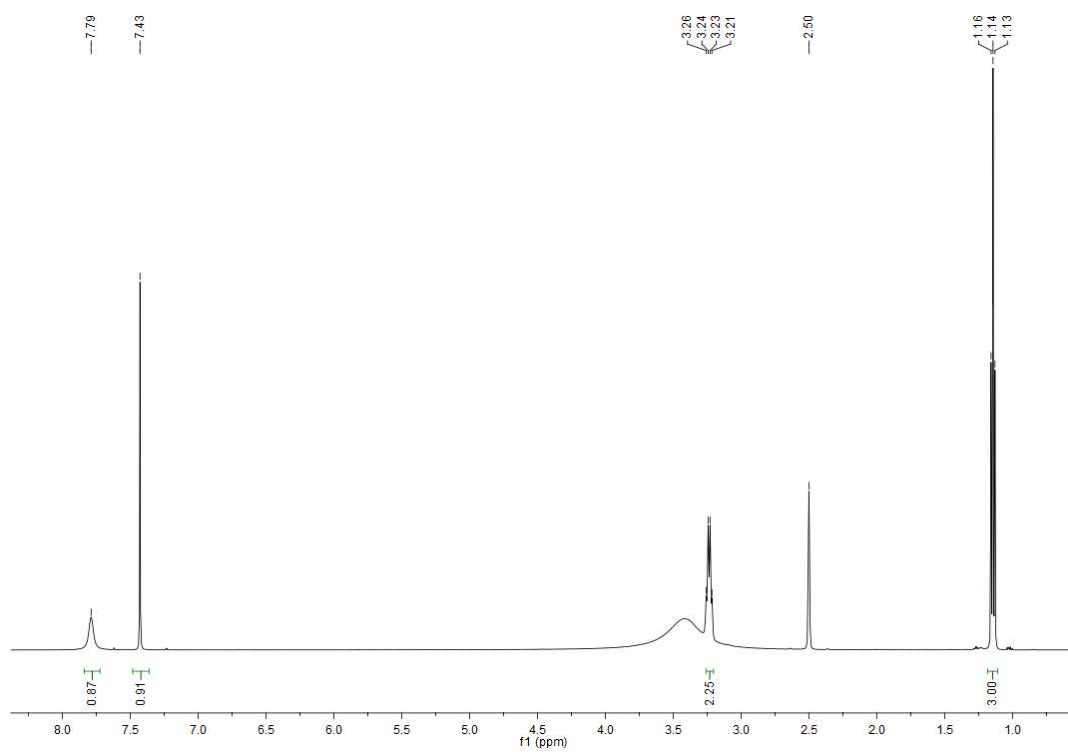


<sup>13</sup>C

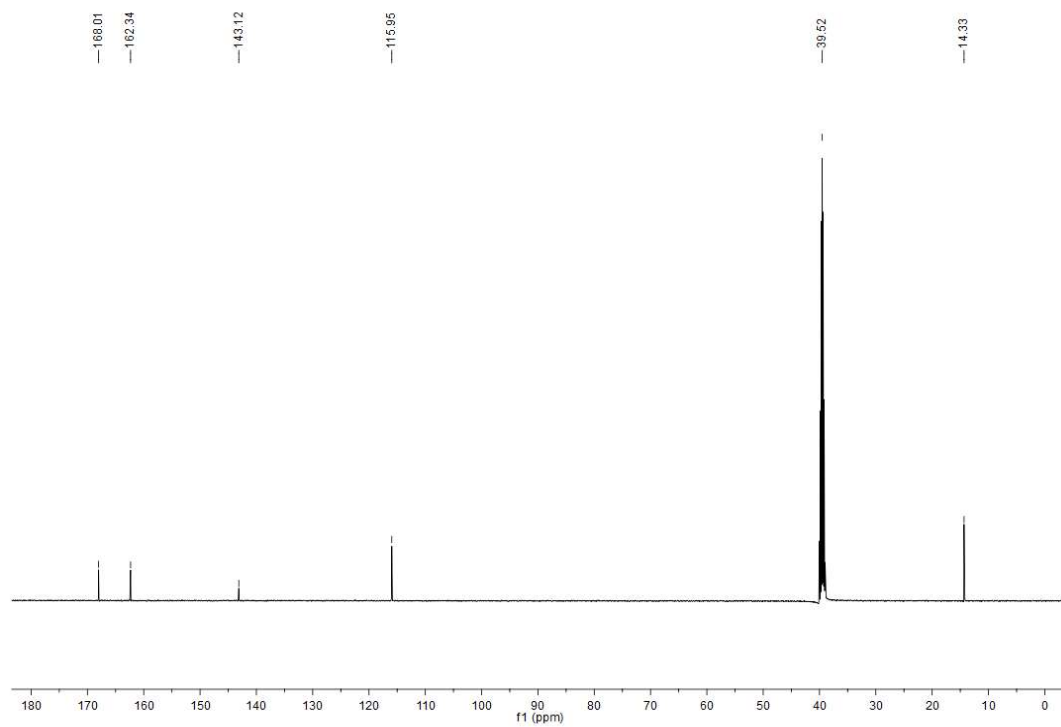


(11)

<sup>1</sup>H

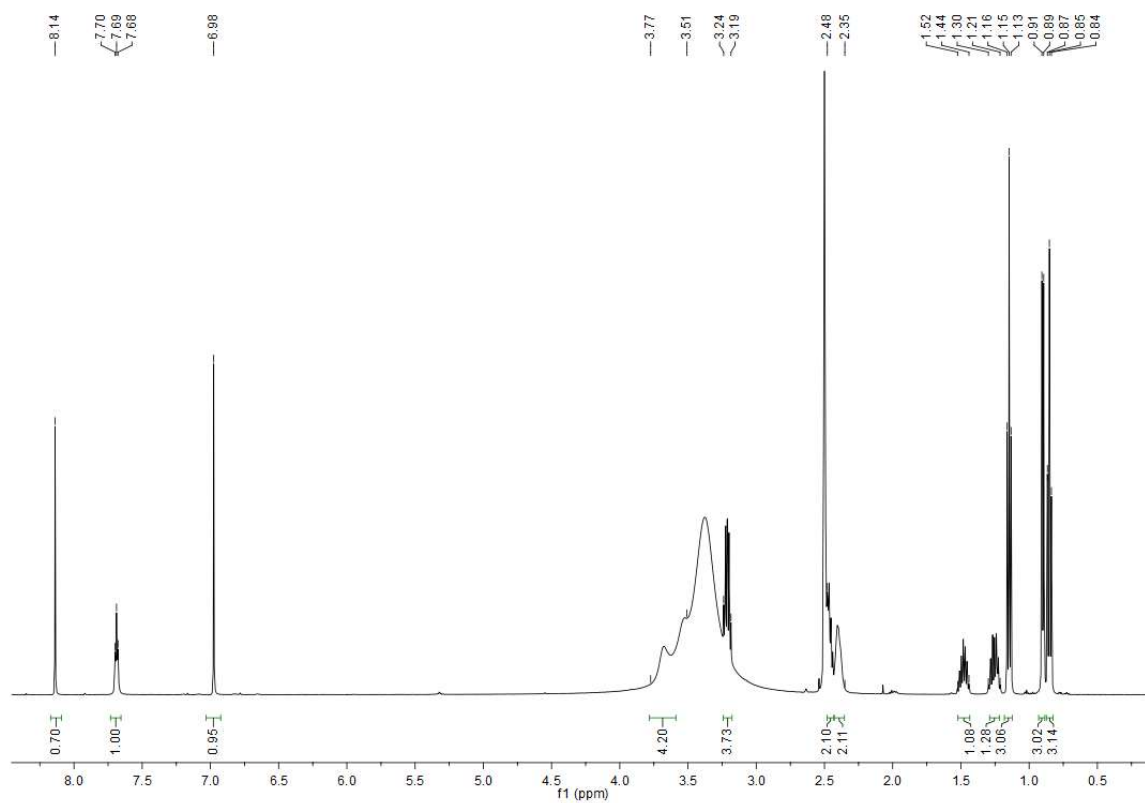


13C

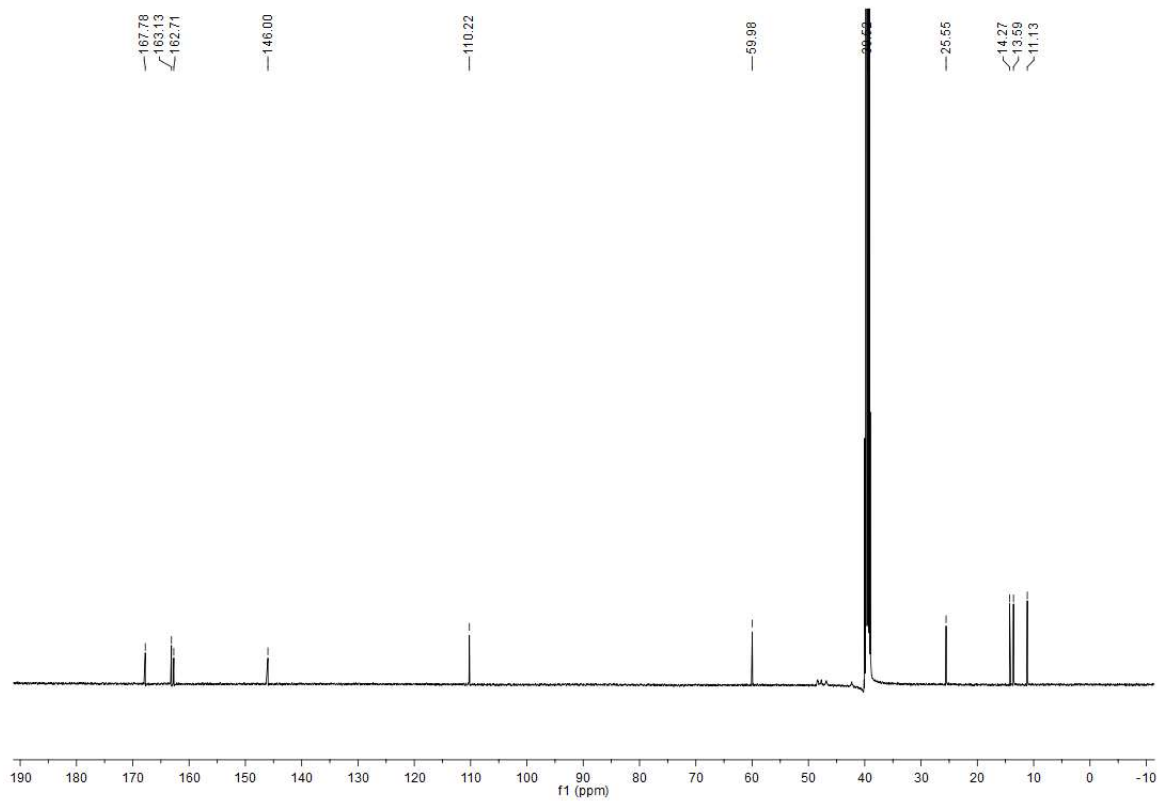


(1)

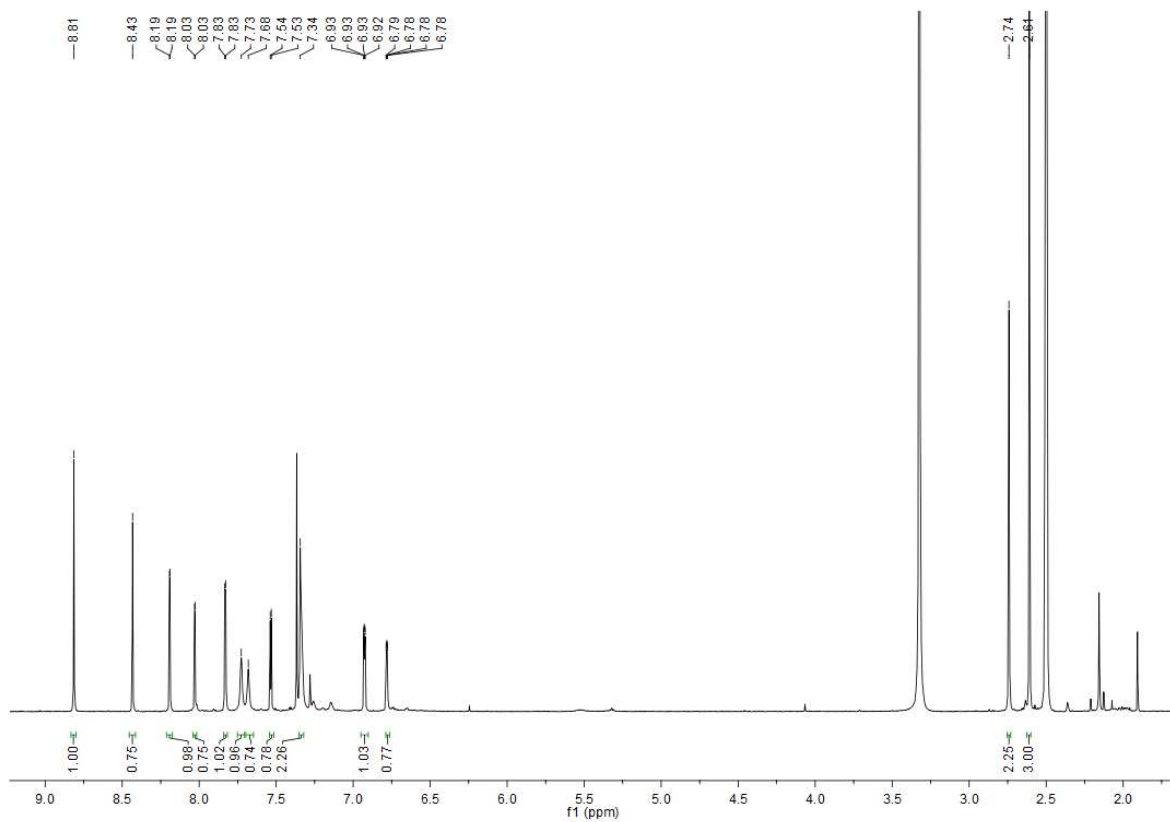
<sup>1</sup>H



<sup>13</sup>C

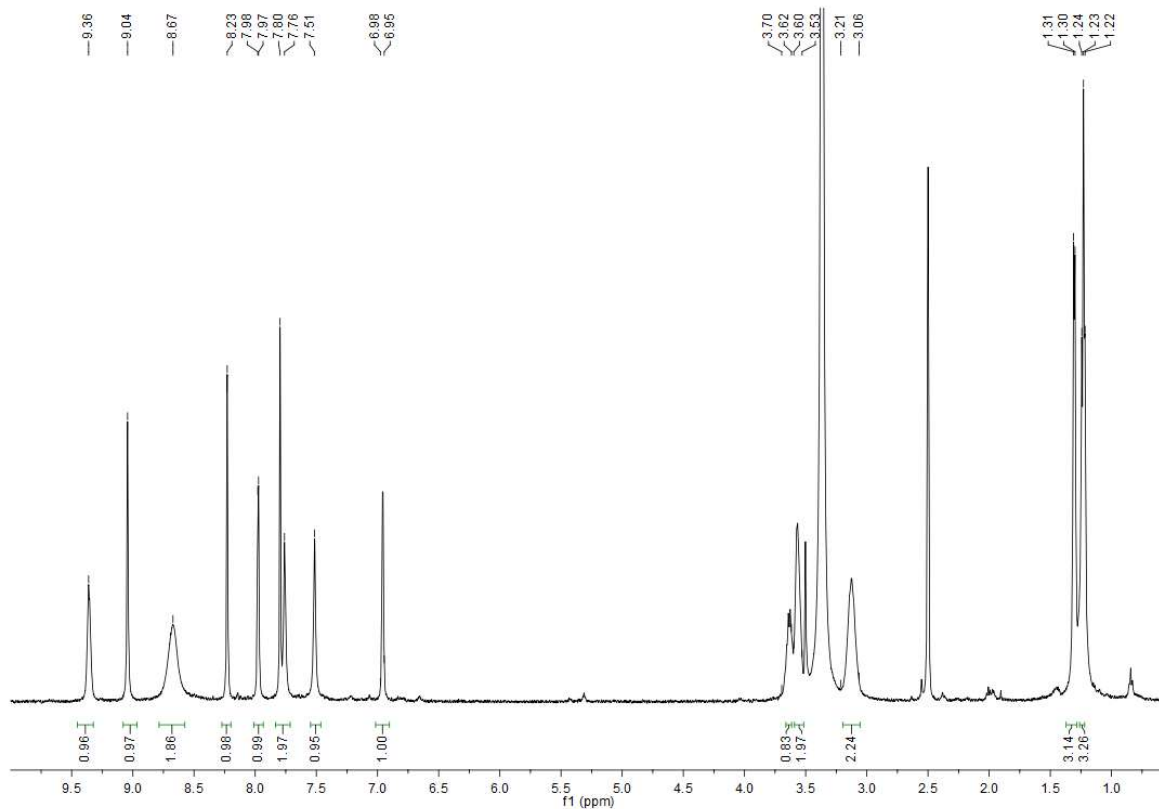


(22)

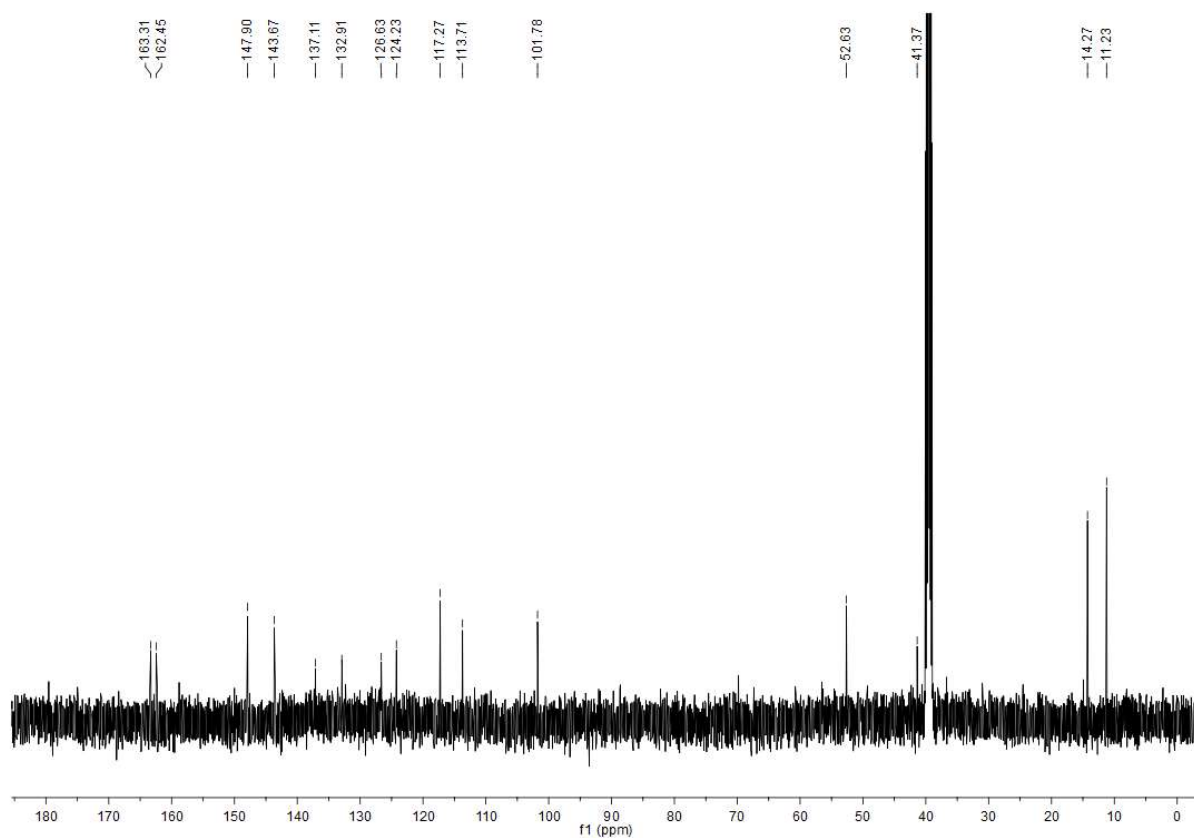


(3)

<sup>1</sup>H

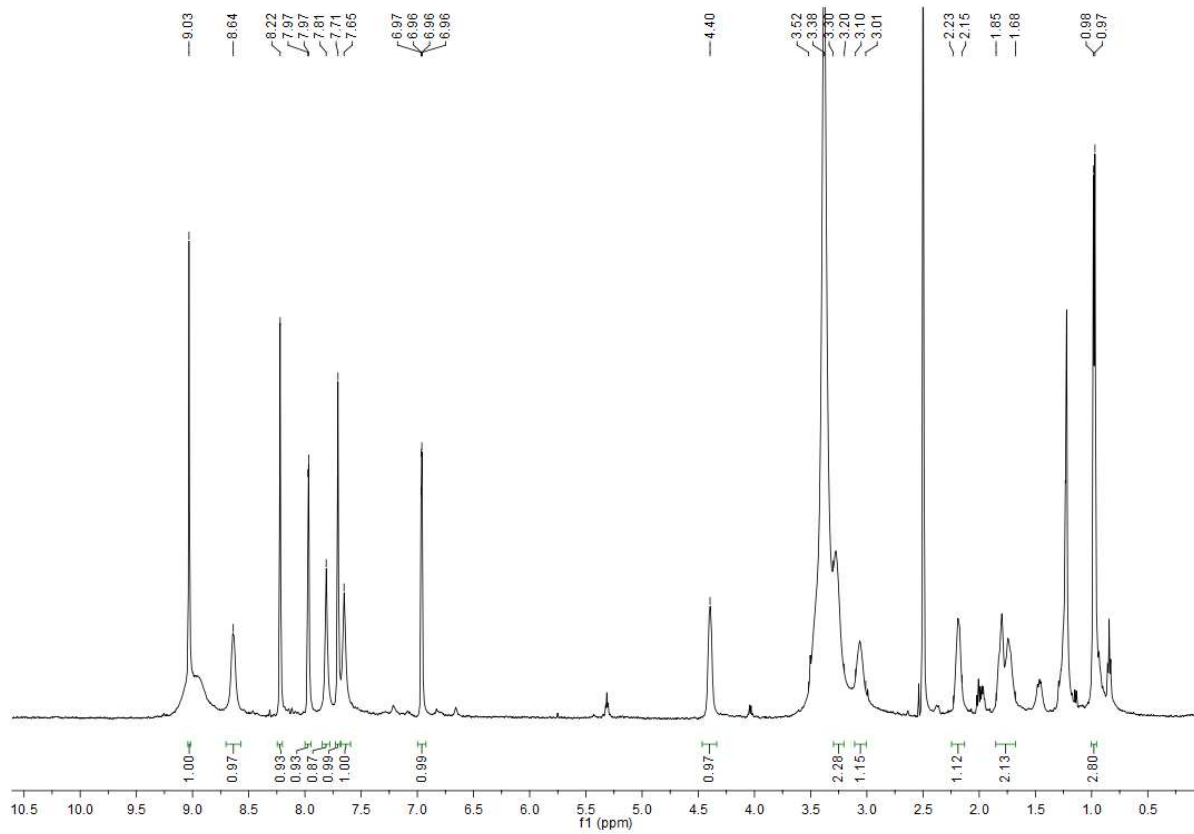


13C

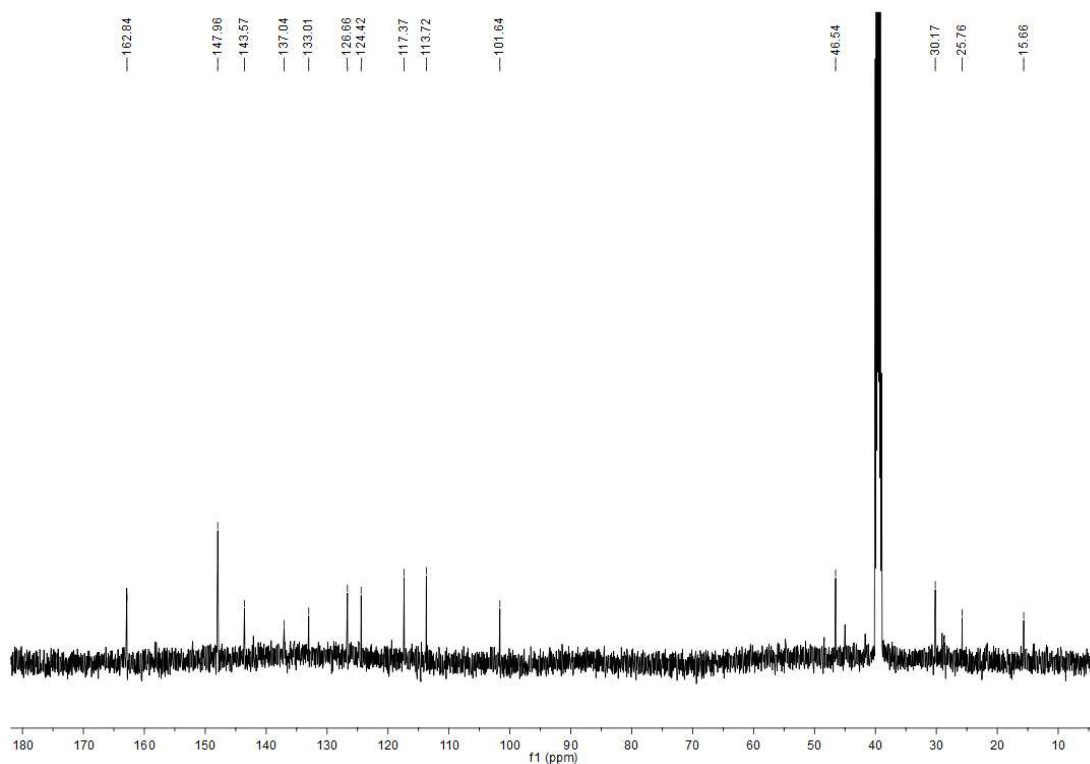


(4)

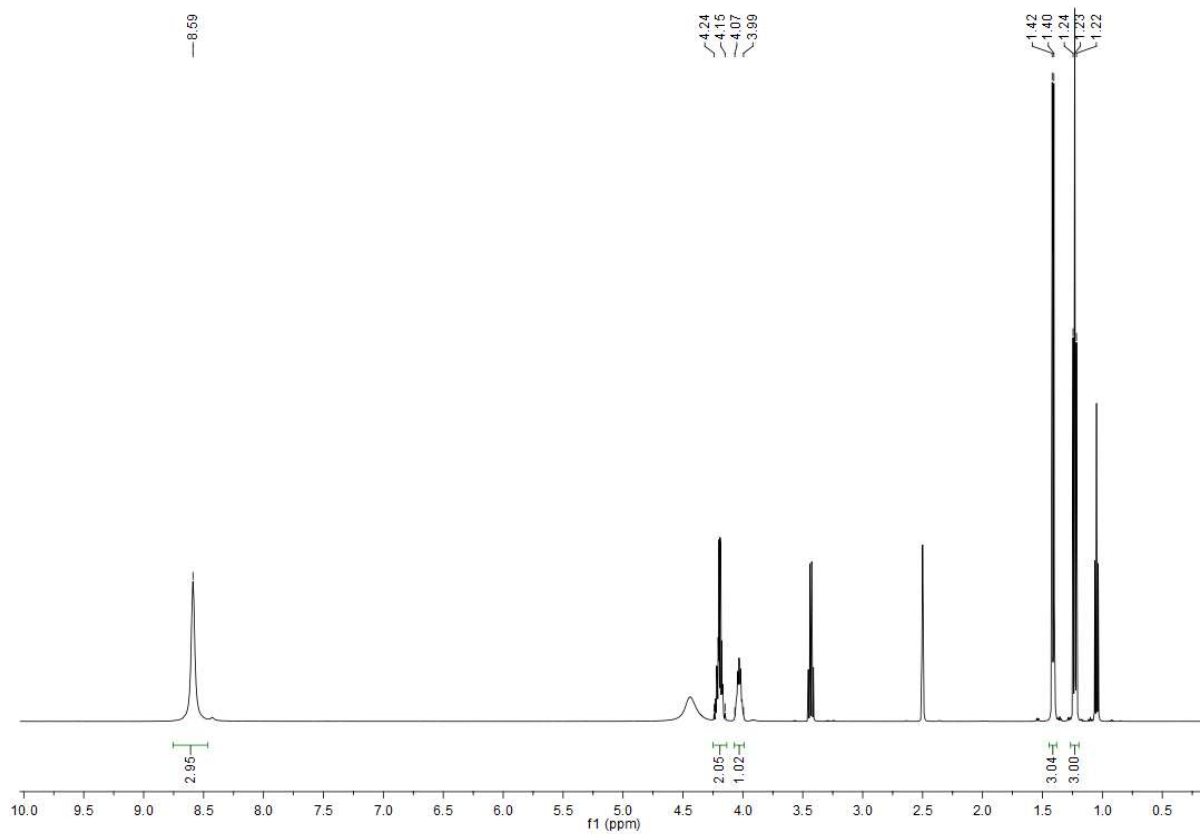
1H



13C



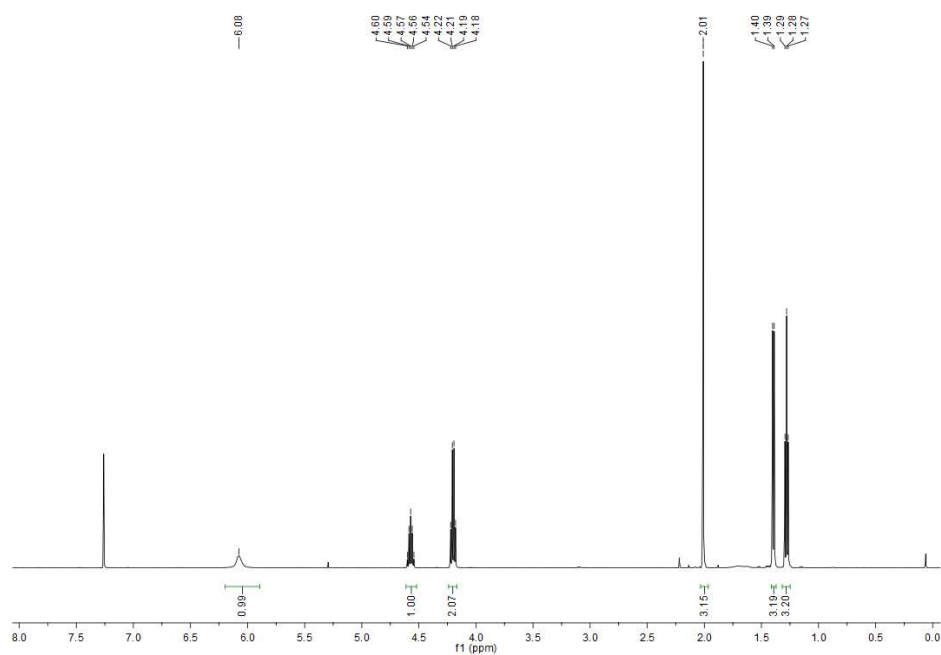
(89)



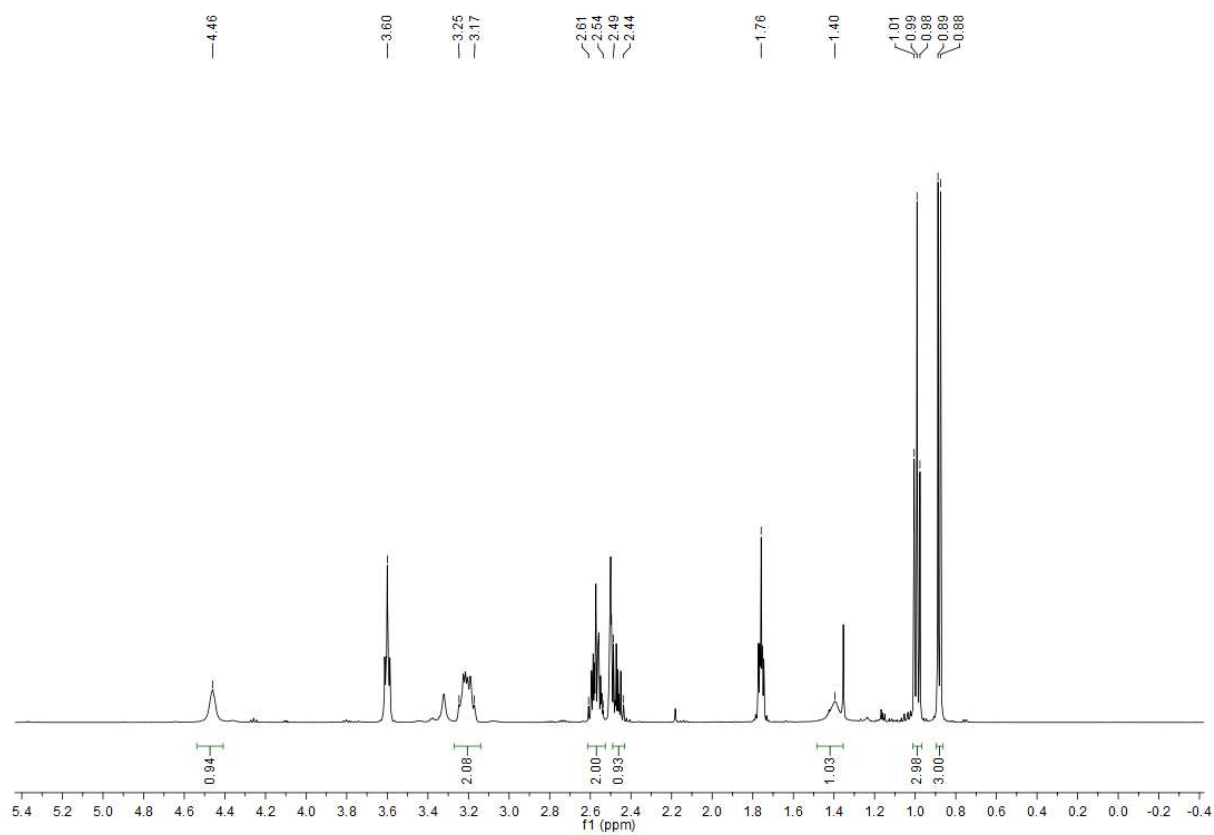
Contains EtOH at 4.44 (OH), 3.43 (q, 2H, CH<sub>2</sub>), 1.05 (t, 3H, CH<sub>3</sub>), not integrated



(90)



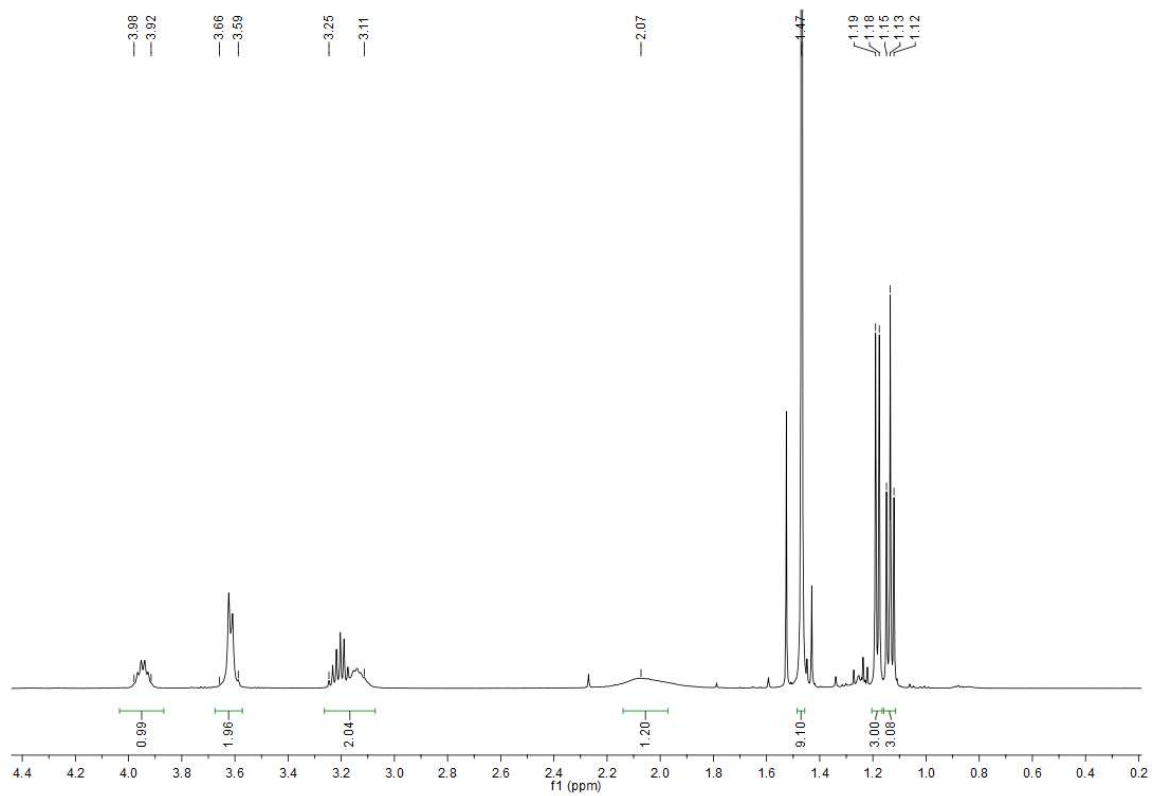
(91)



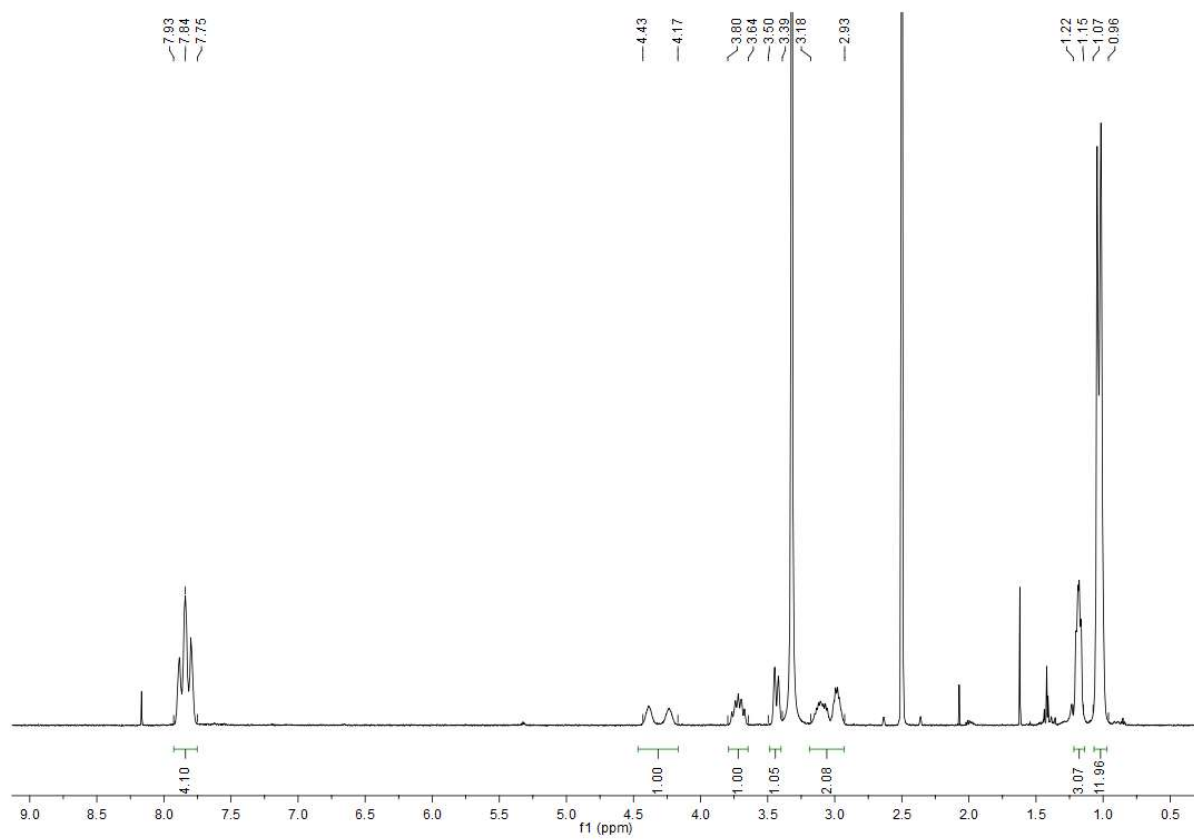
Contains THF 3.60 (m, 4H) and 1.76 (m, 4H)

(92)

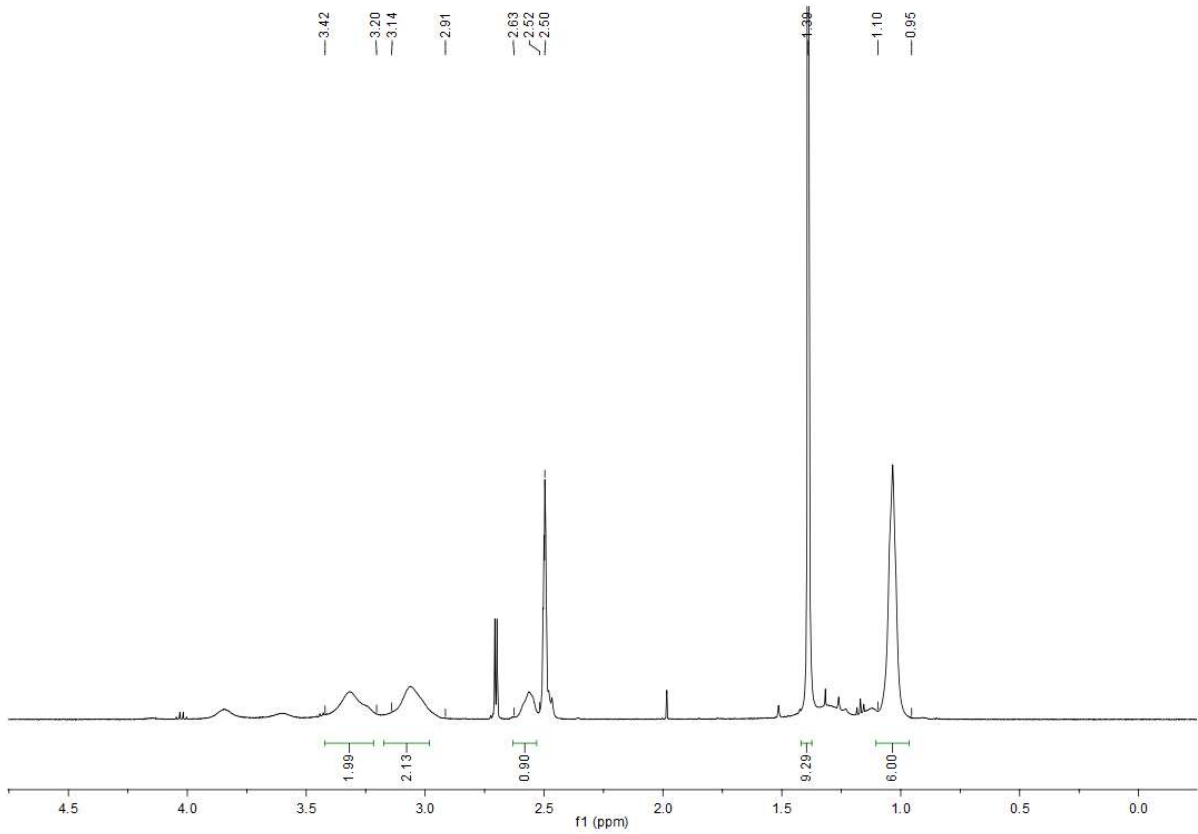
<sup>1</sup>H



(93)

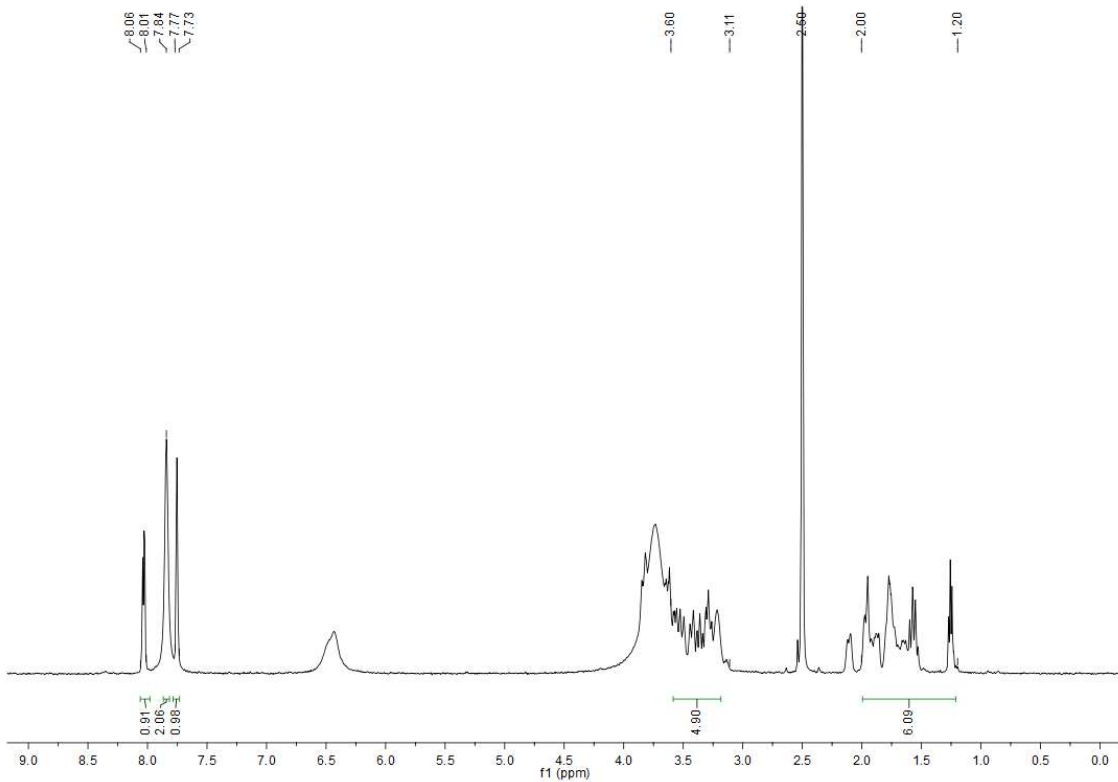


(20)



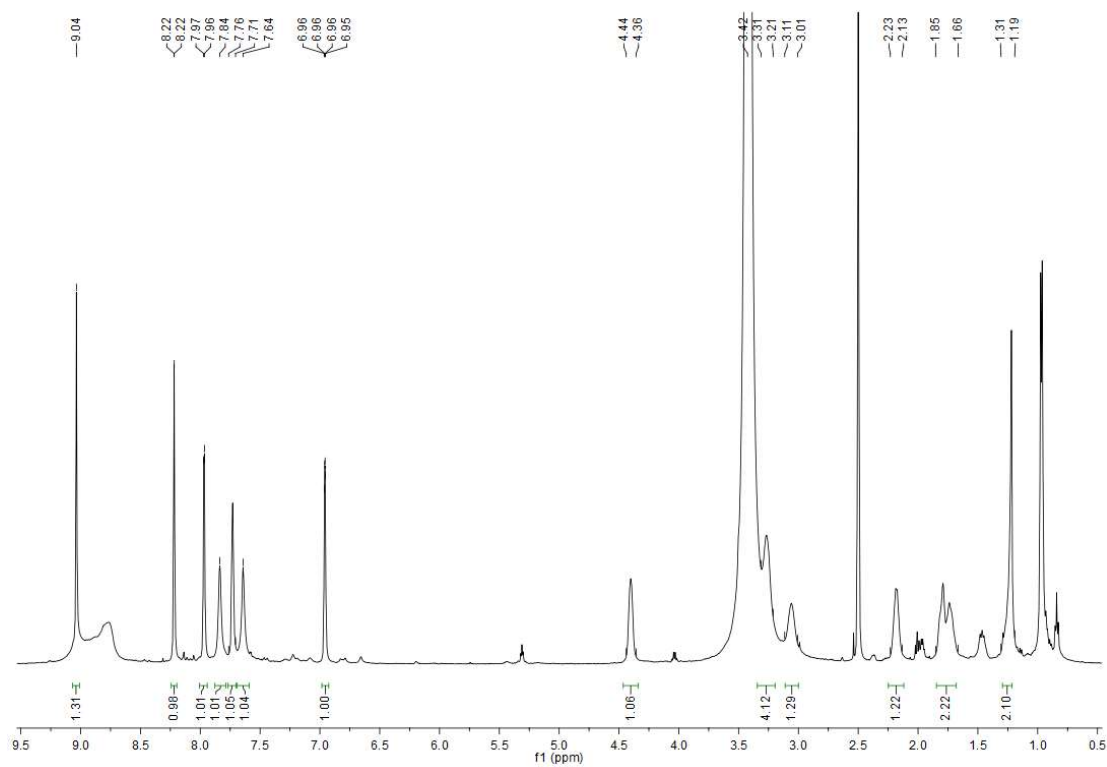
(14)

<sup>1</sup>H

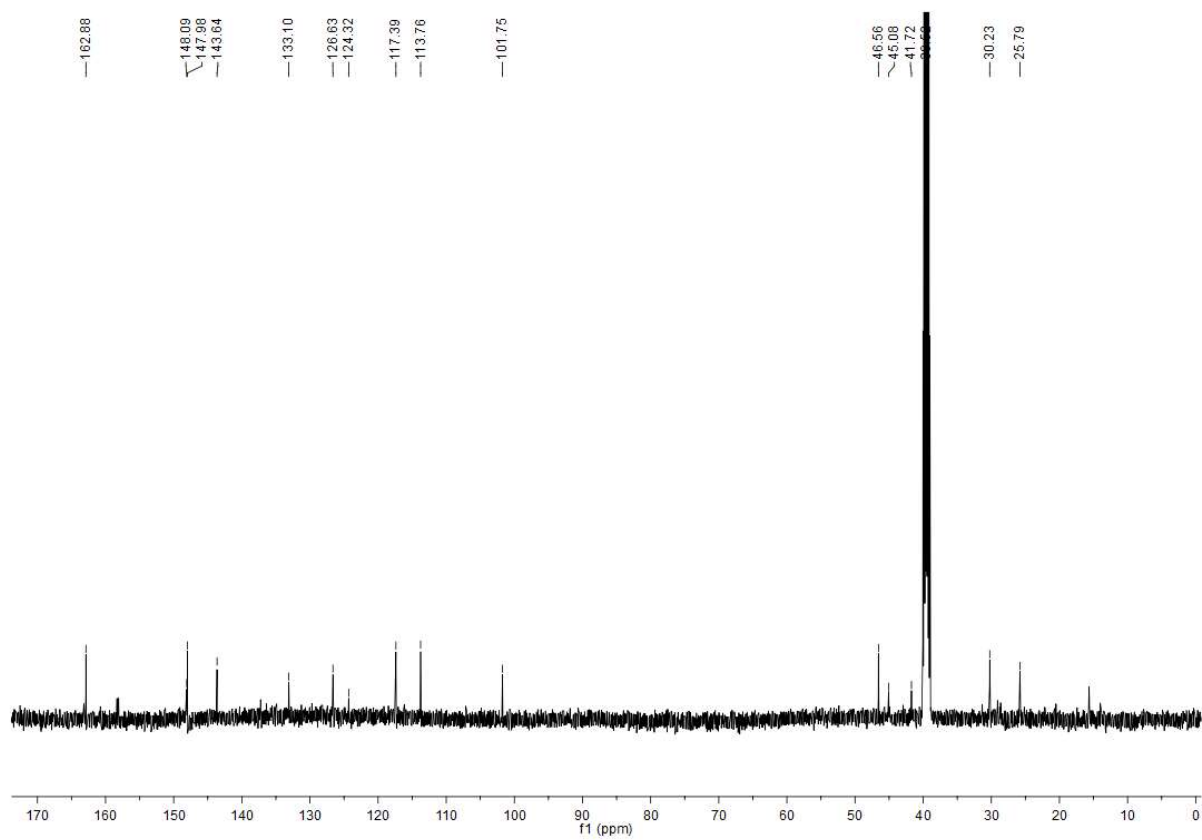


(2)

# 1H

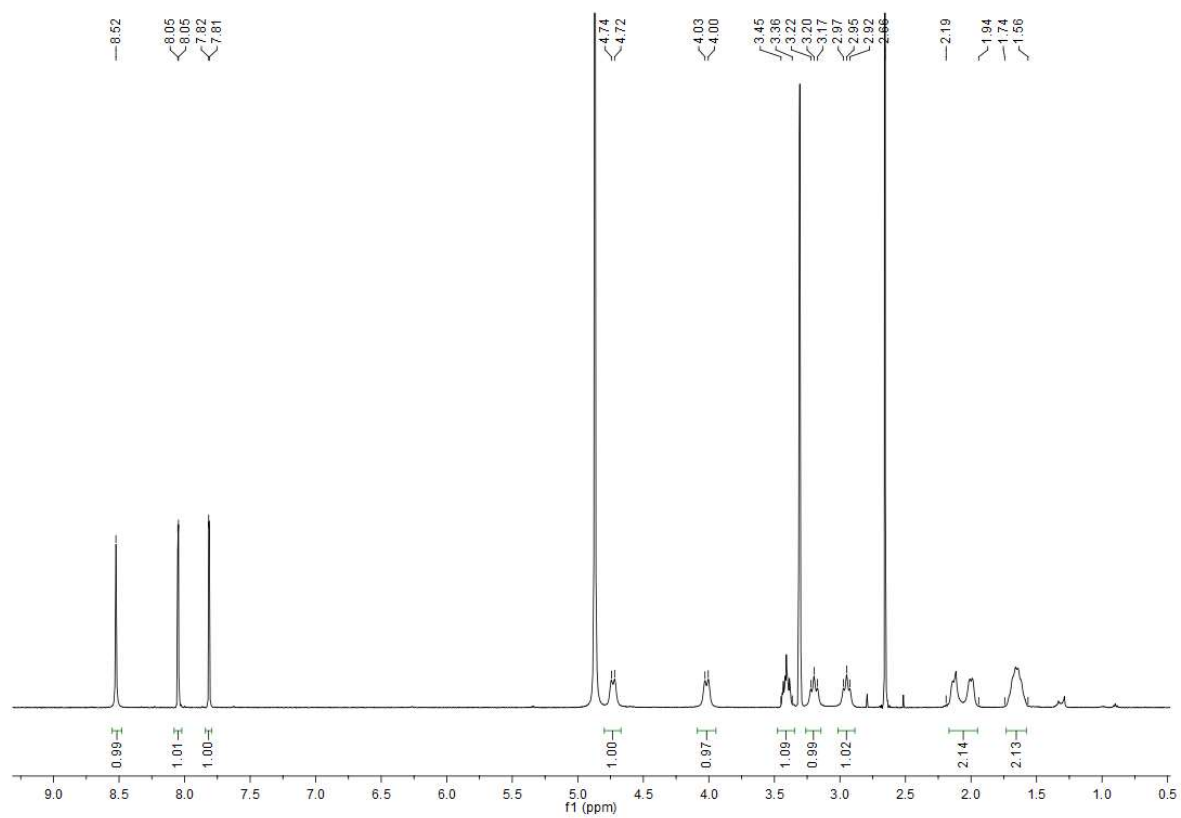


# 13C

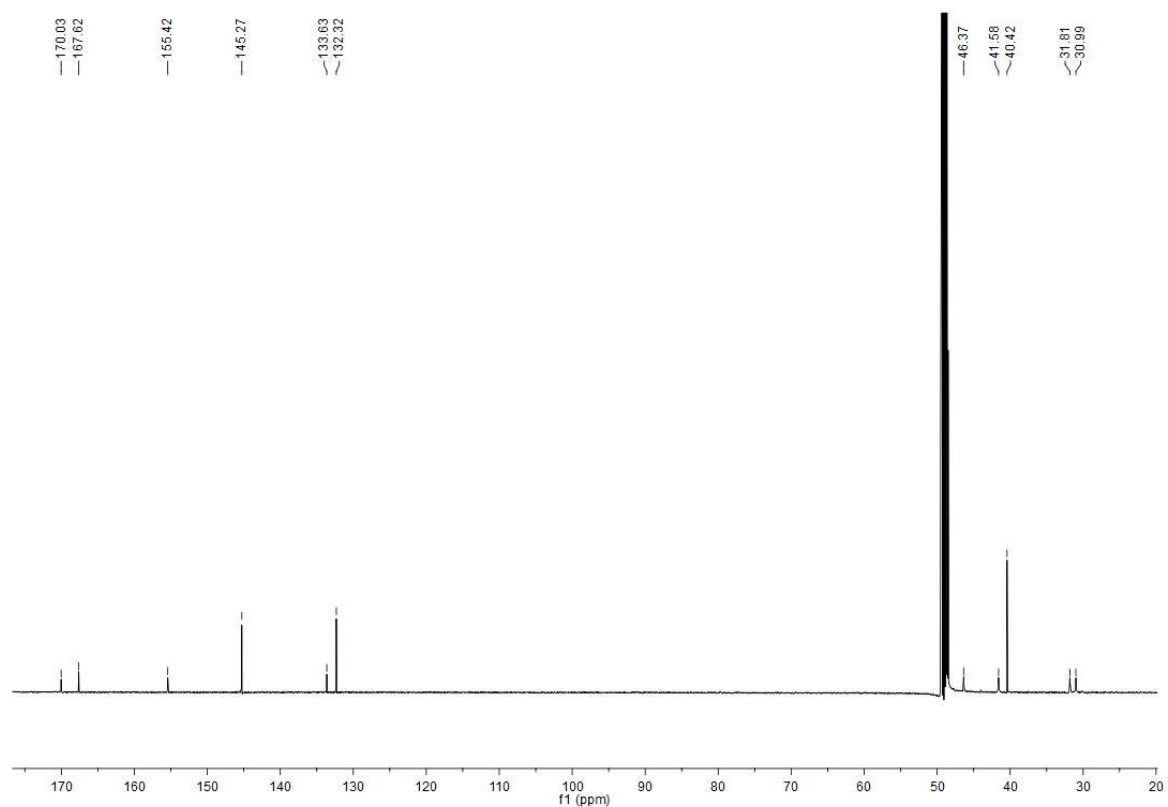


(16)

<sup>1</sup>H

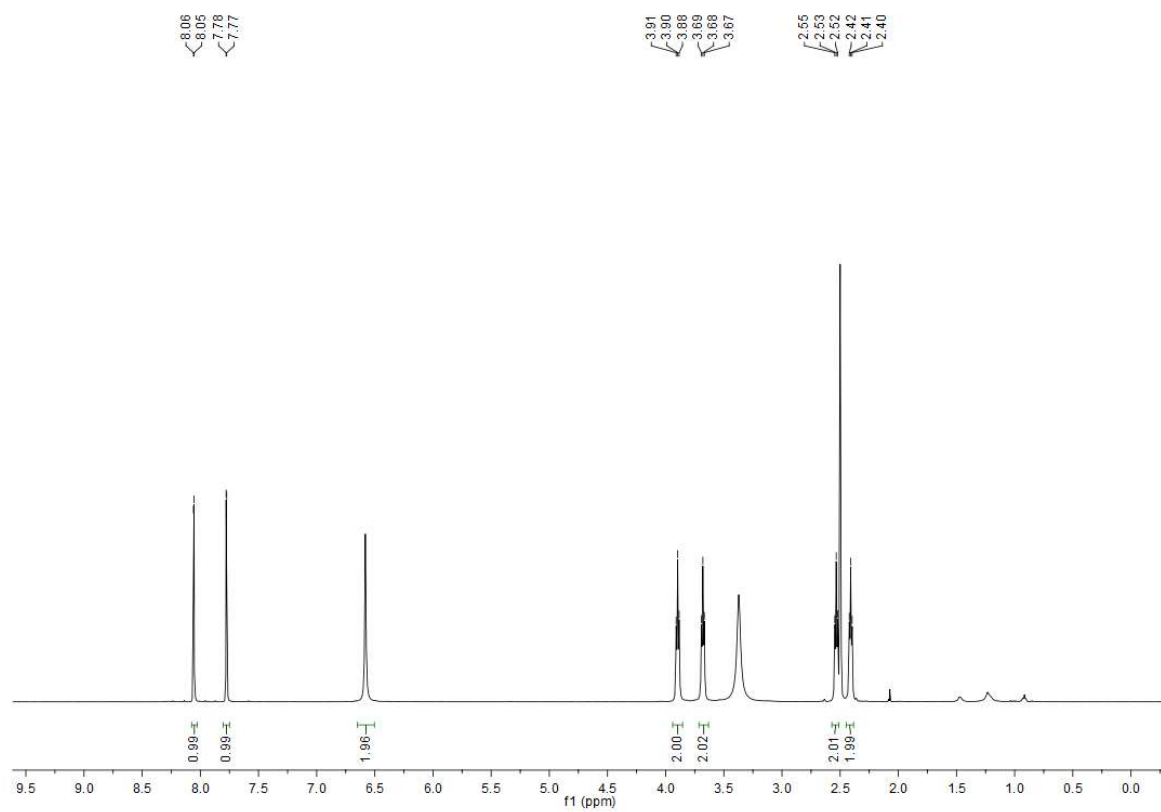


<sup>13</sup>C

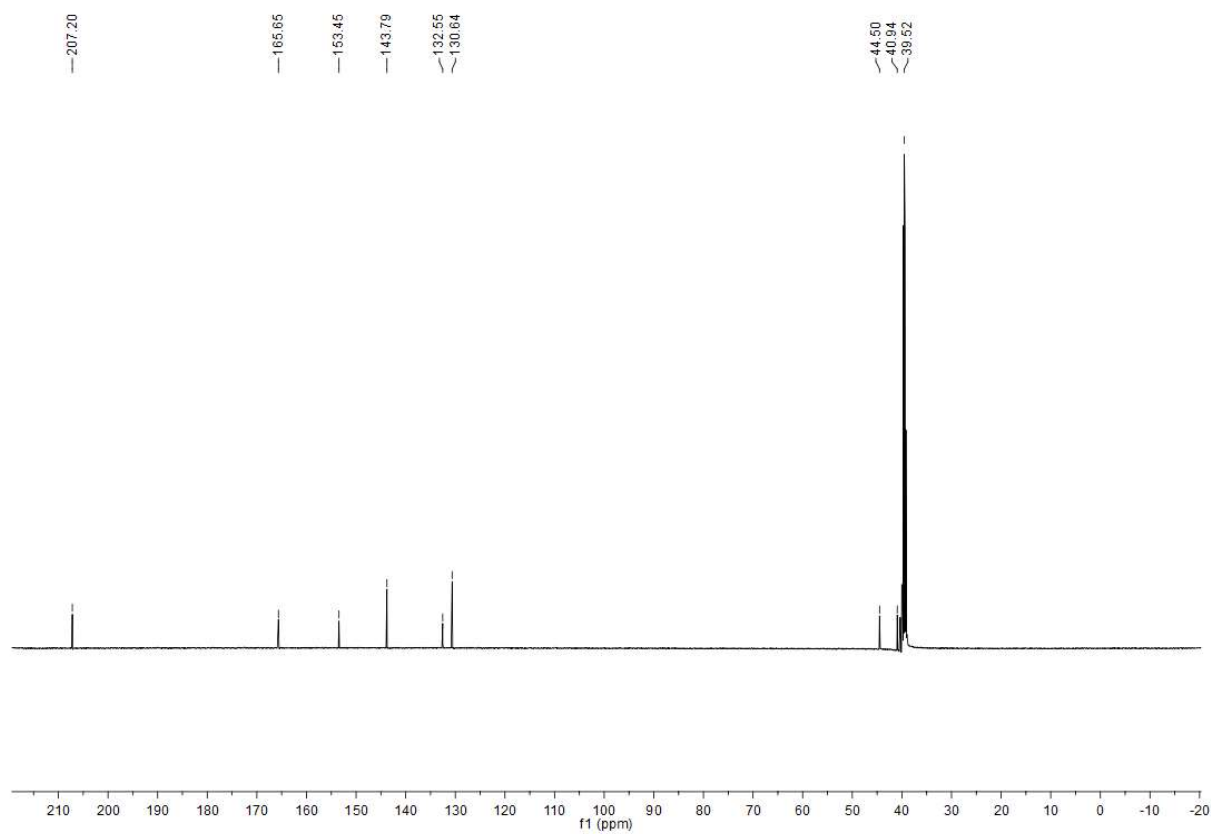


(18)

<sup>1</sup>H

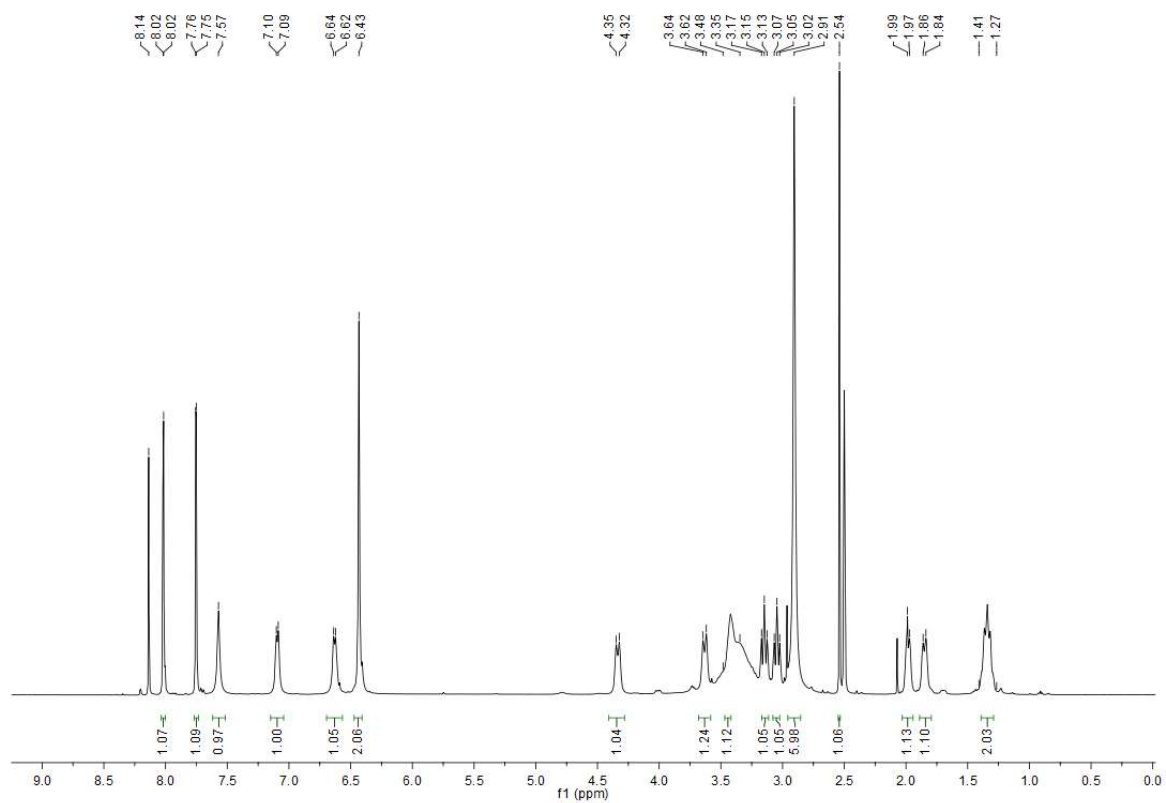


13C

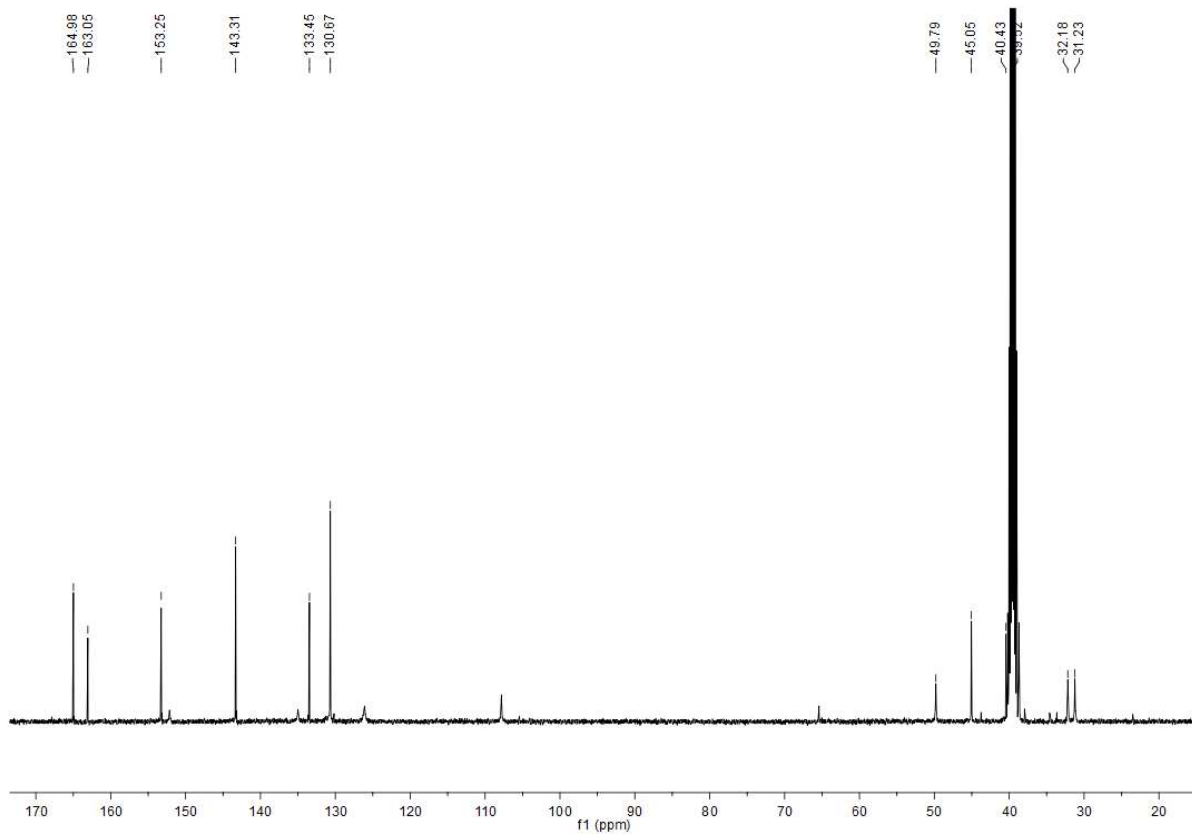


(6)

<sup>1</sup>H

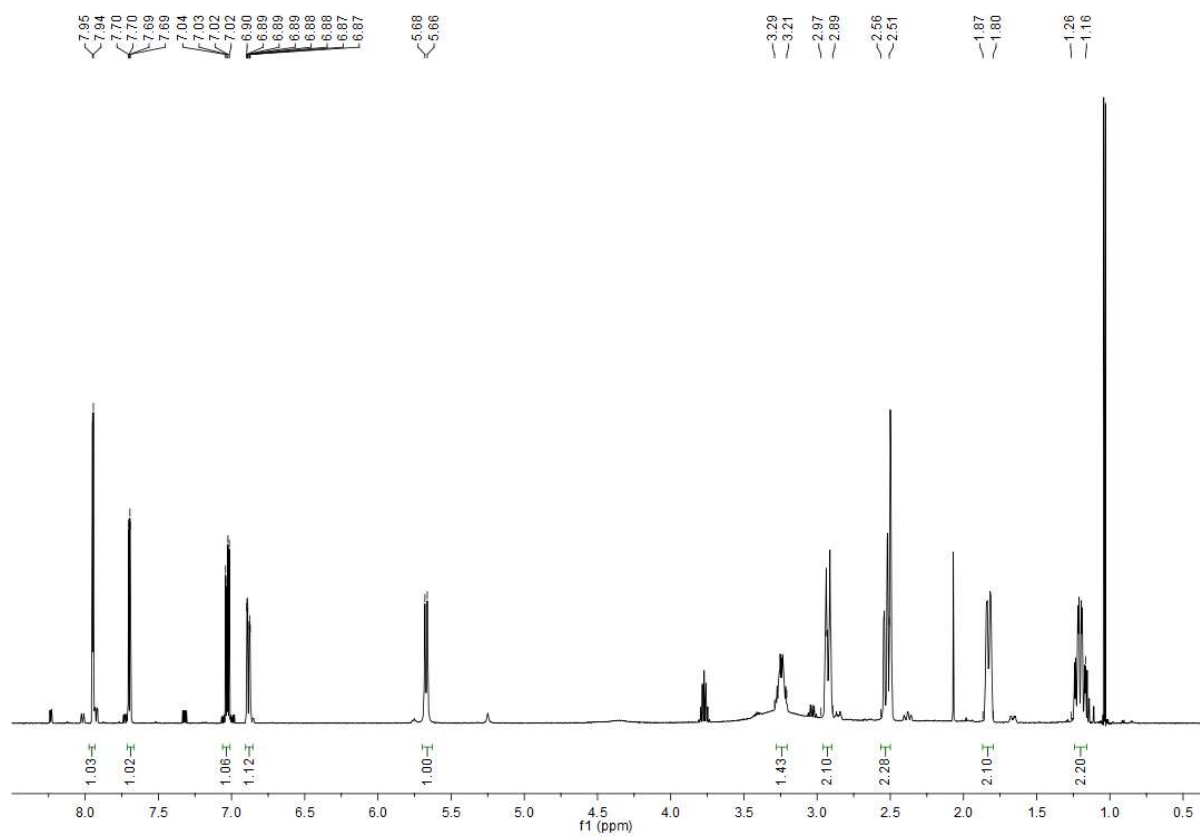


<sup>13</sup>C

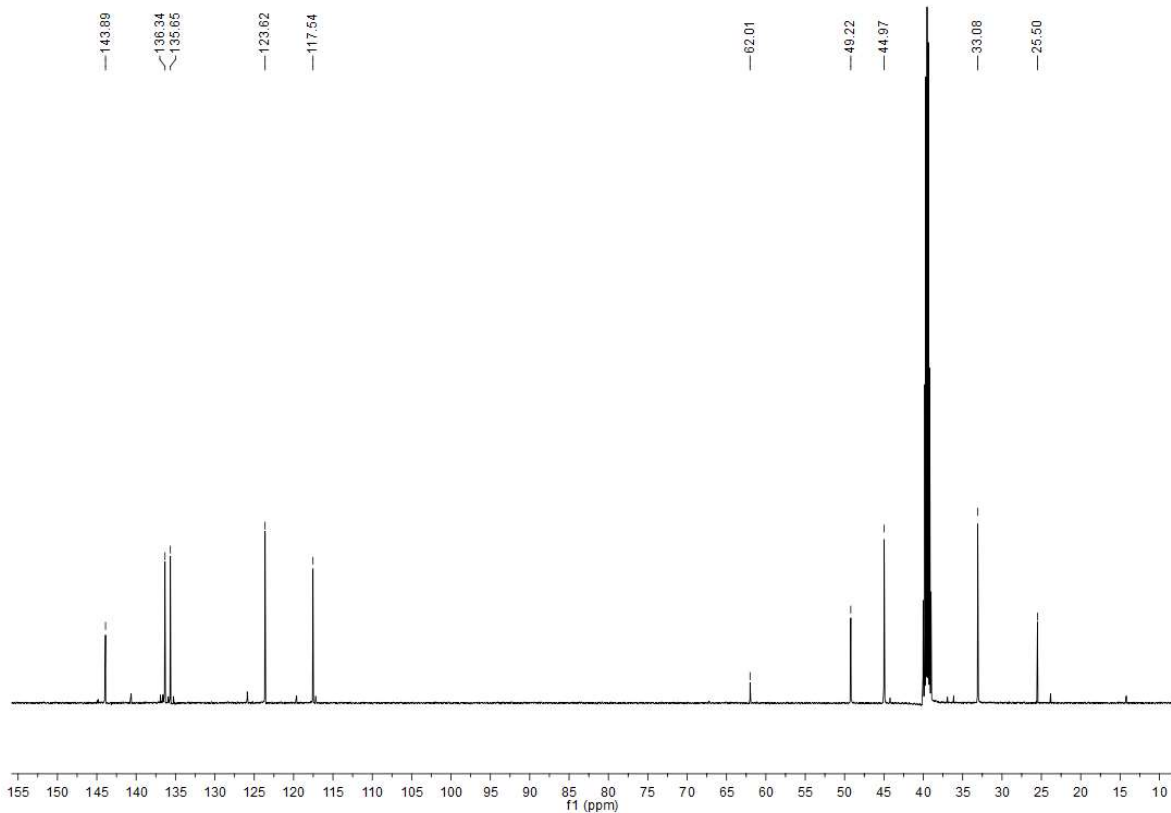


(97)

<sup>1</sup>H



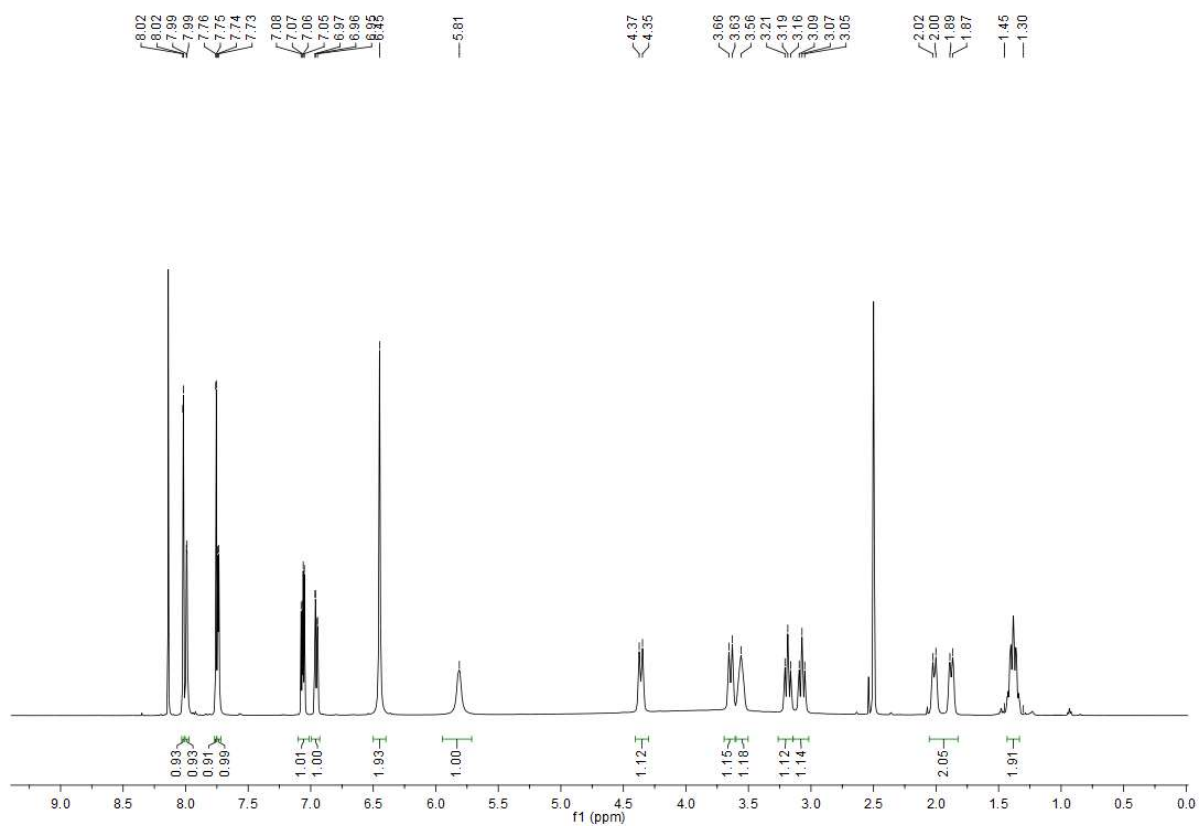
<sup>13</sup>C



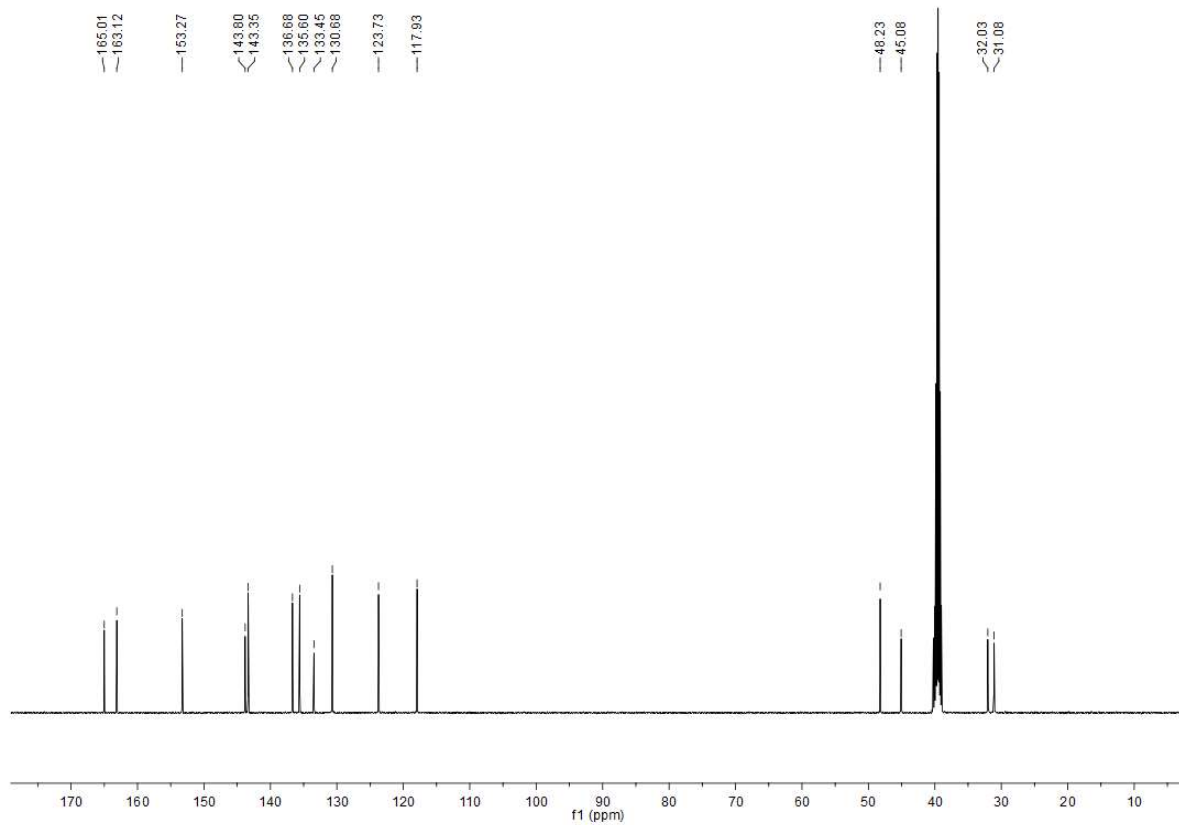


(70)

<sup>1</sup>H

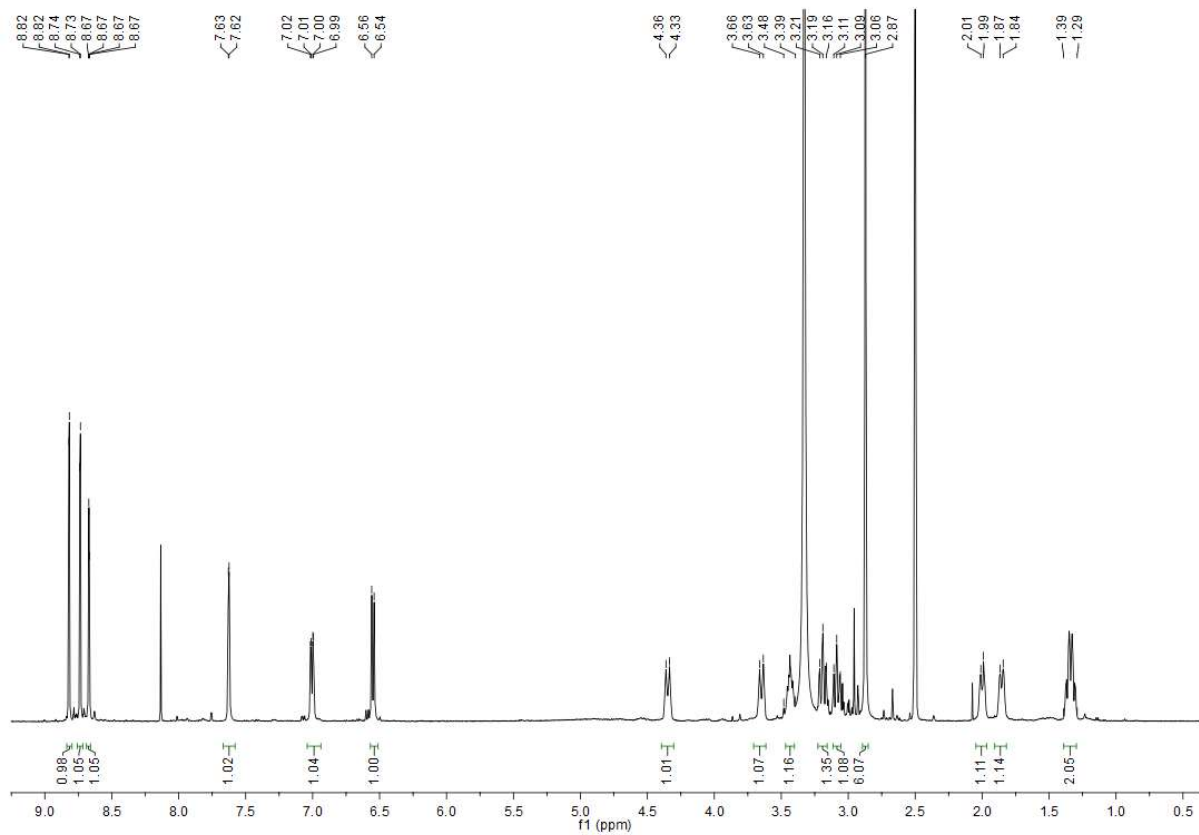


<sup>13</sup>C

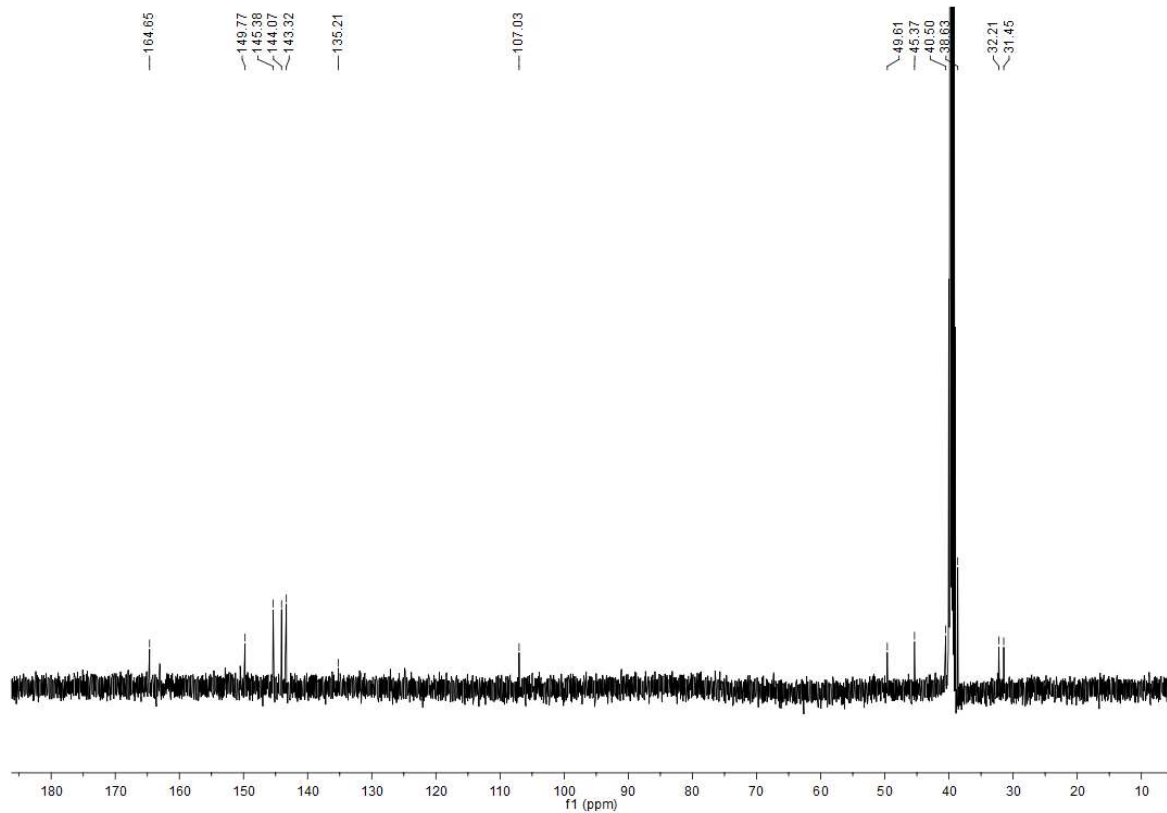


(50)

<sup>1</sup>H

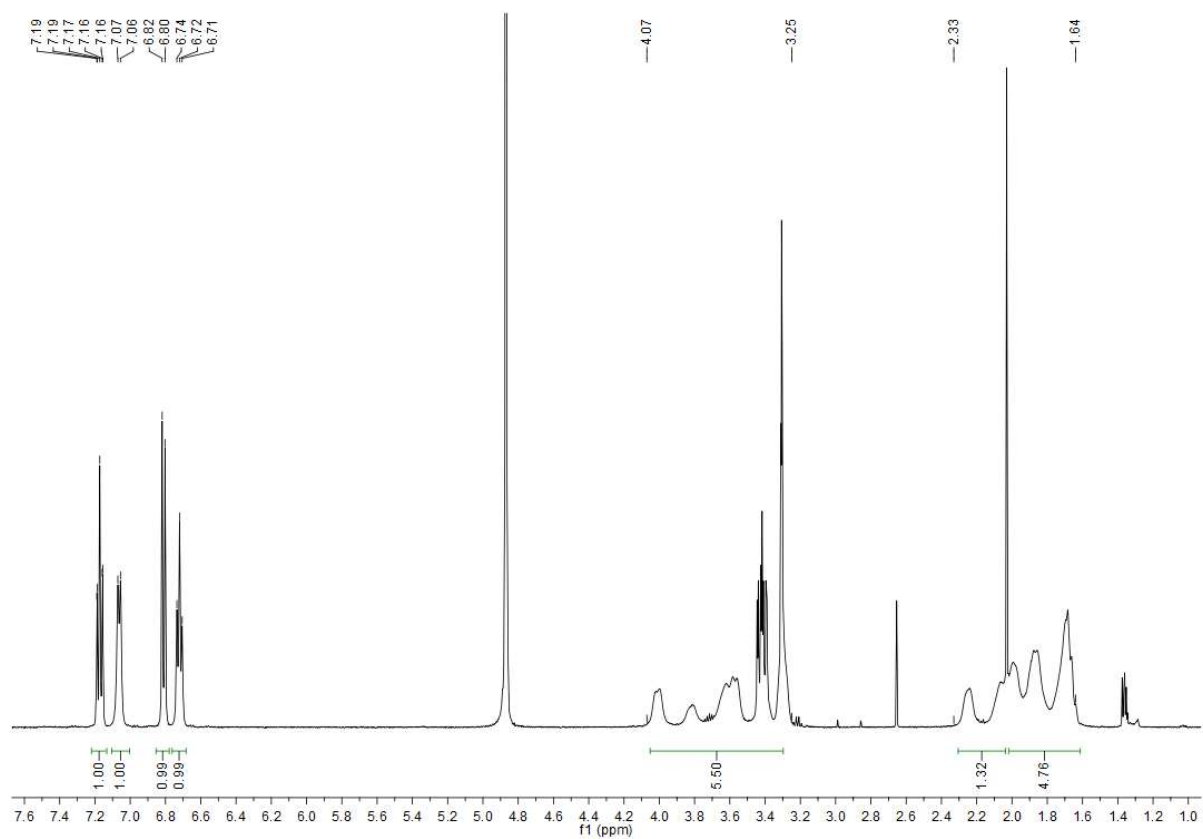


<sup>13</sup>C



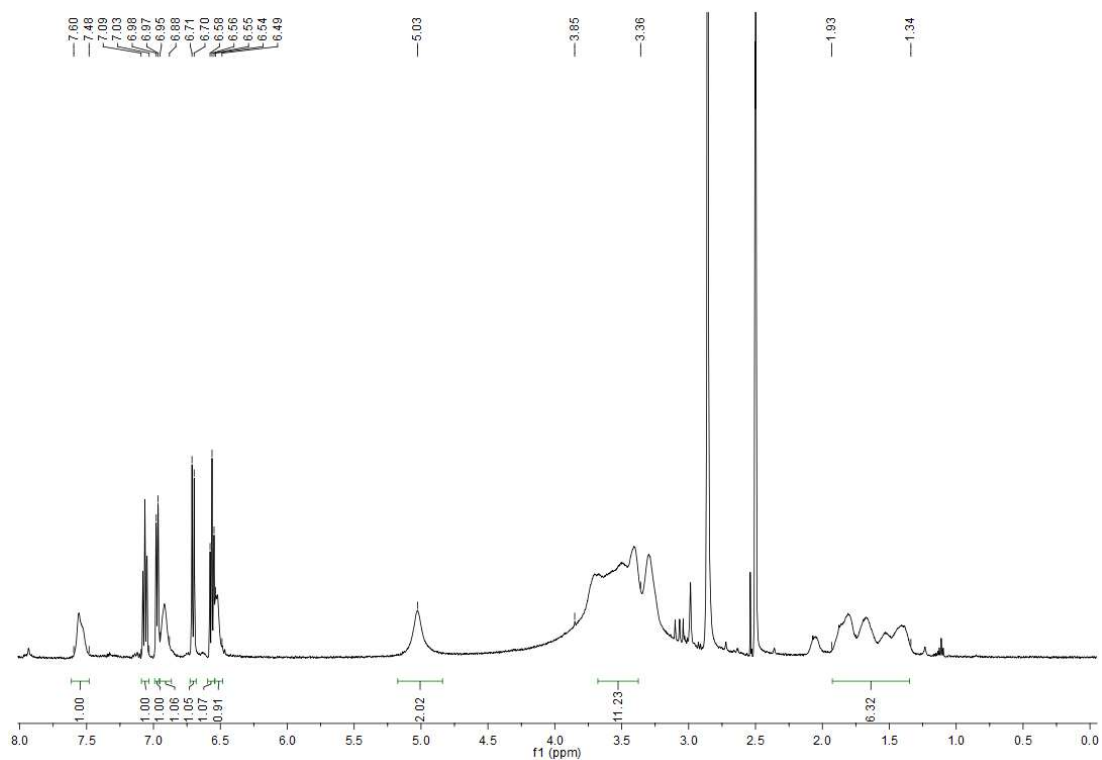
(14)

<sup>1</sup>H



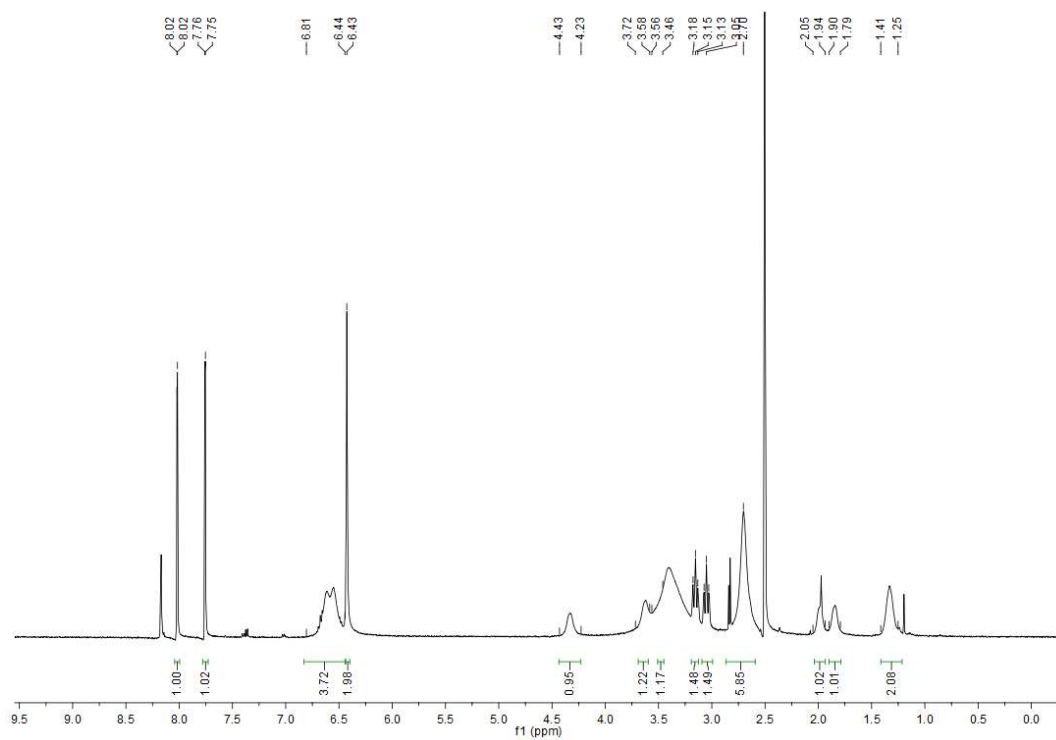
(51)

<sup>1</sup>H



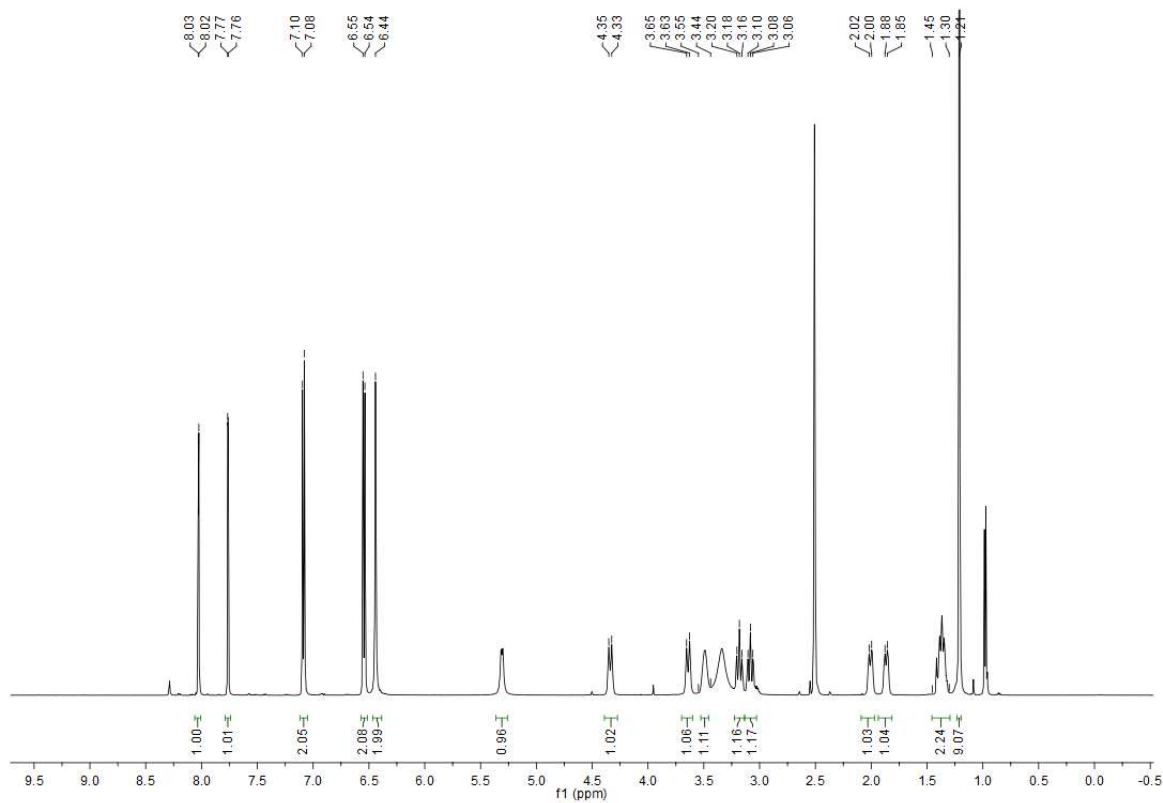
(54)

<sup>1</sup>H

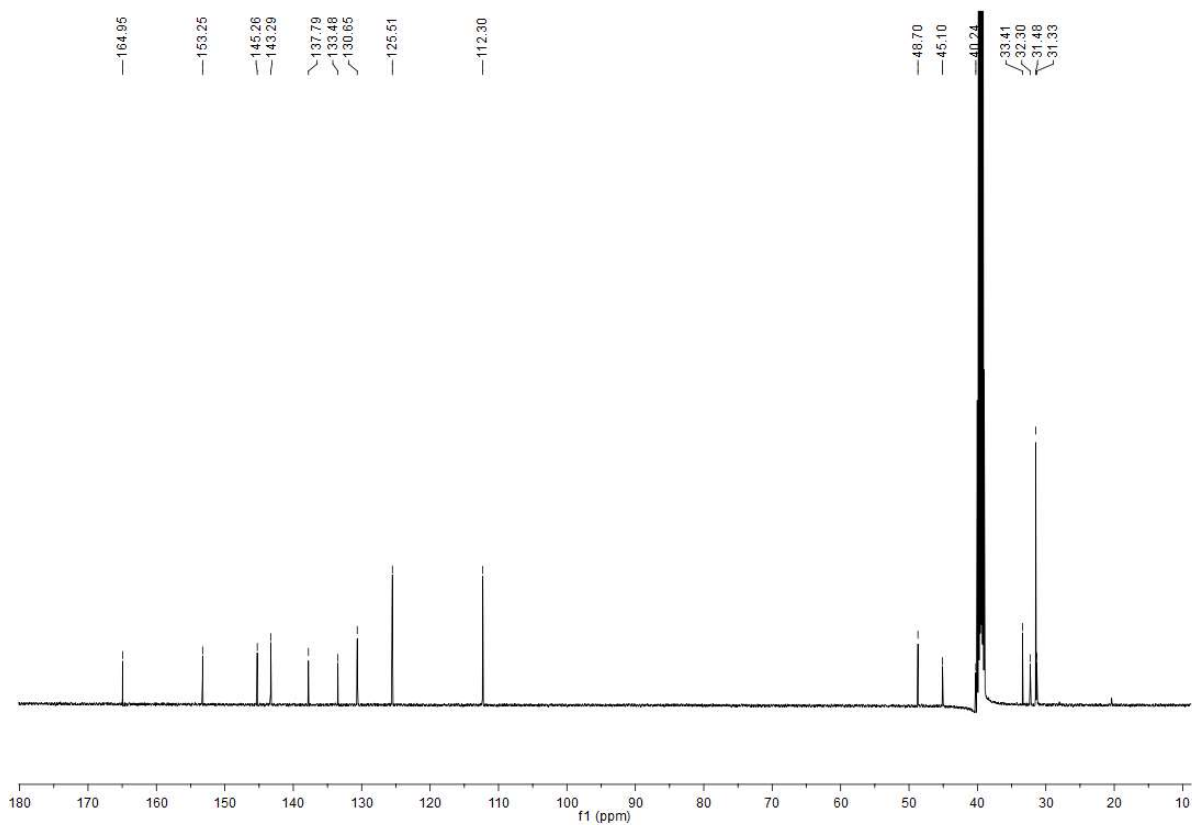


(62)

<sup>1</sup>H

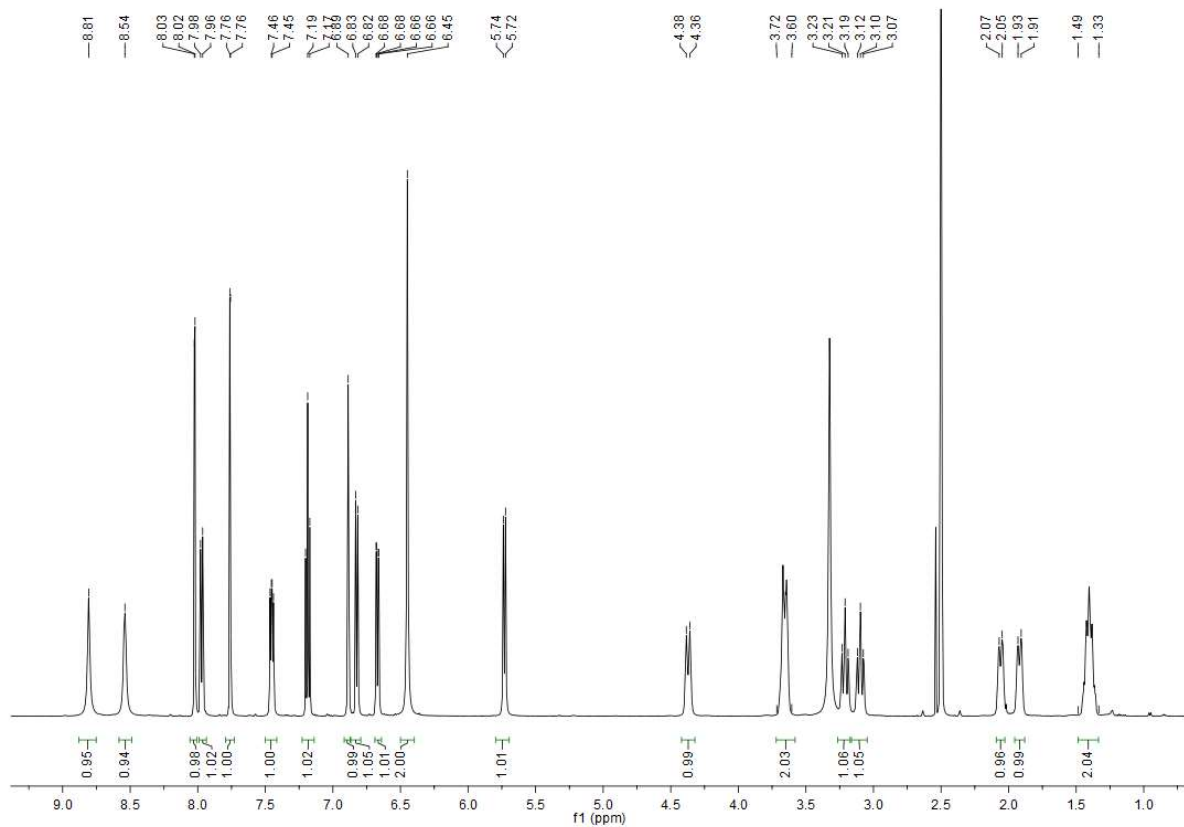


13C

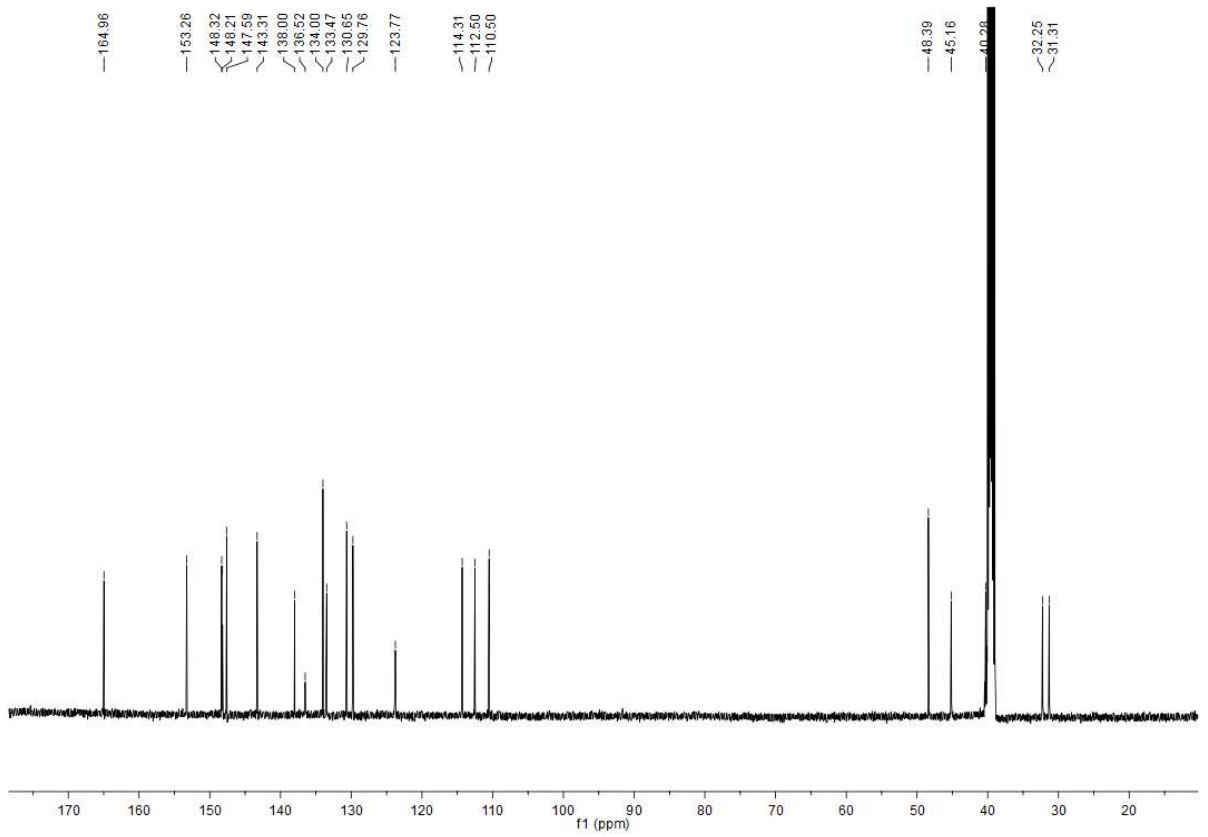


(66)

1H

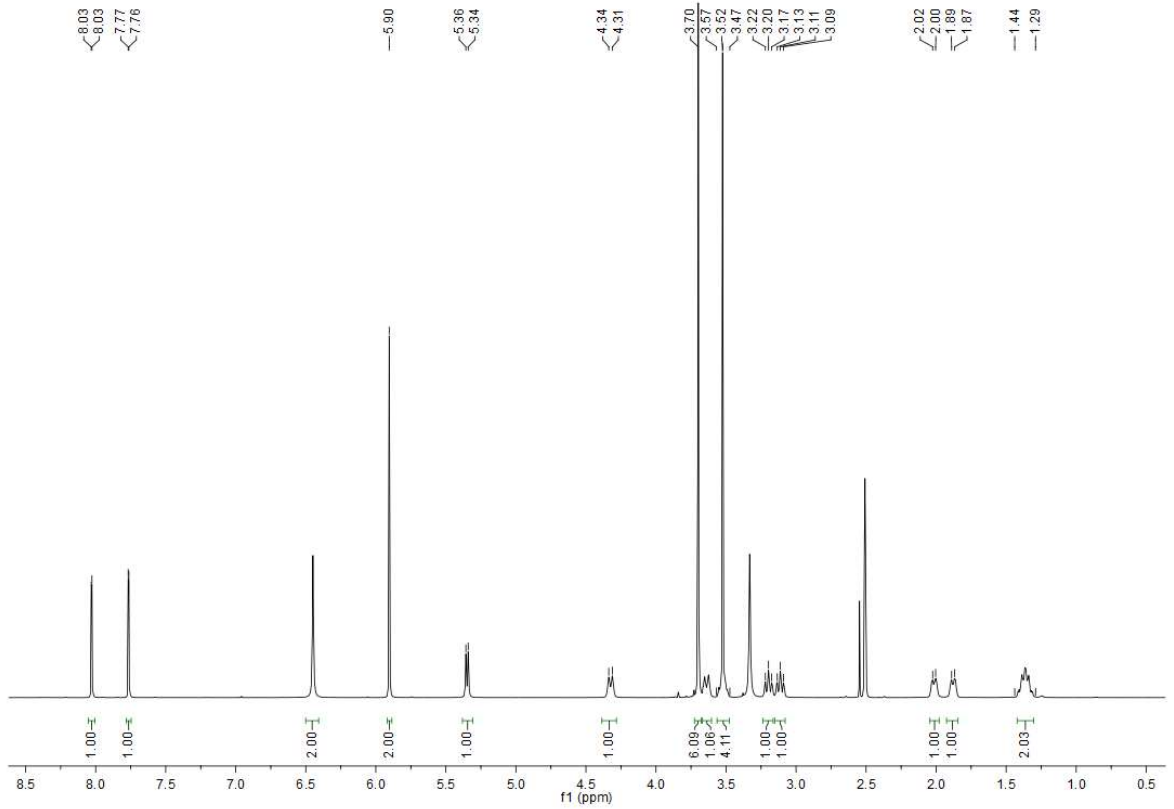


13C

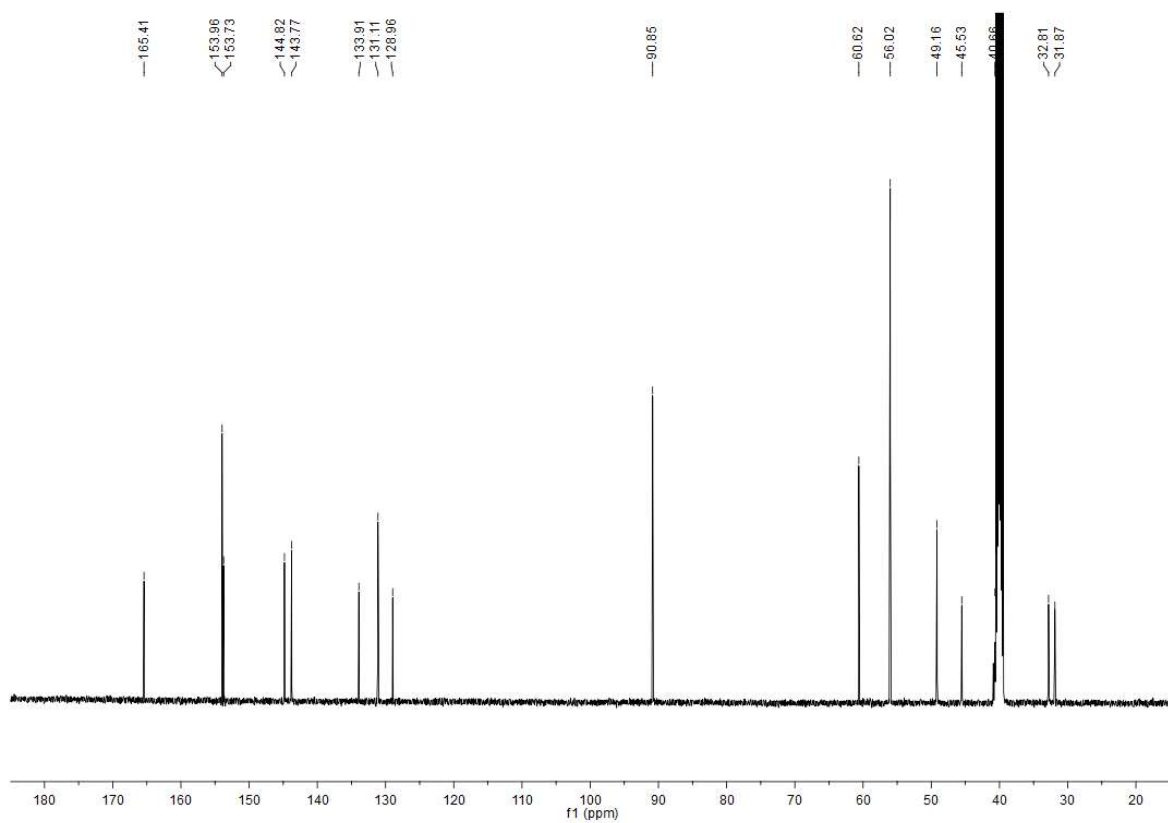


(63)

1H

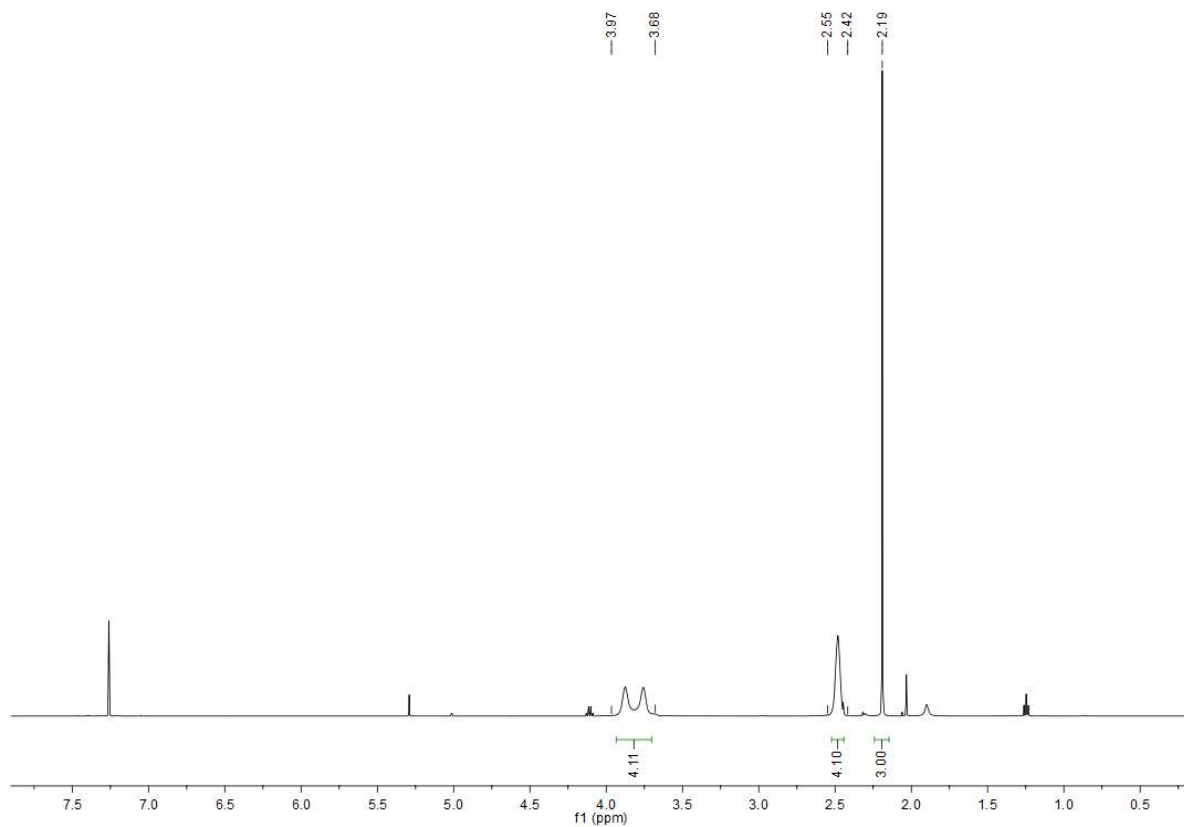


13C

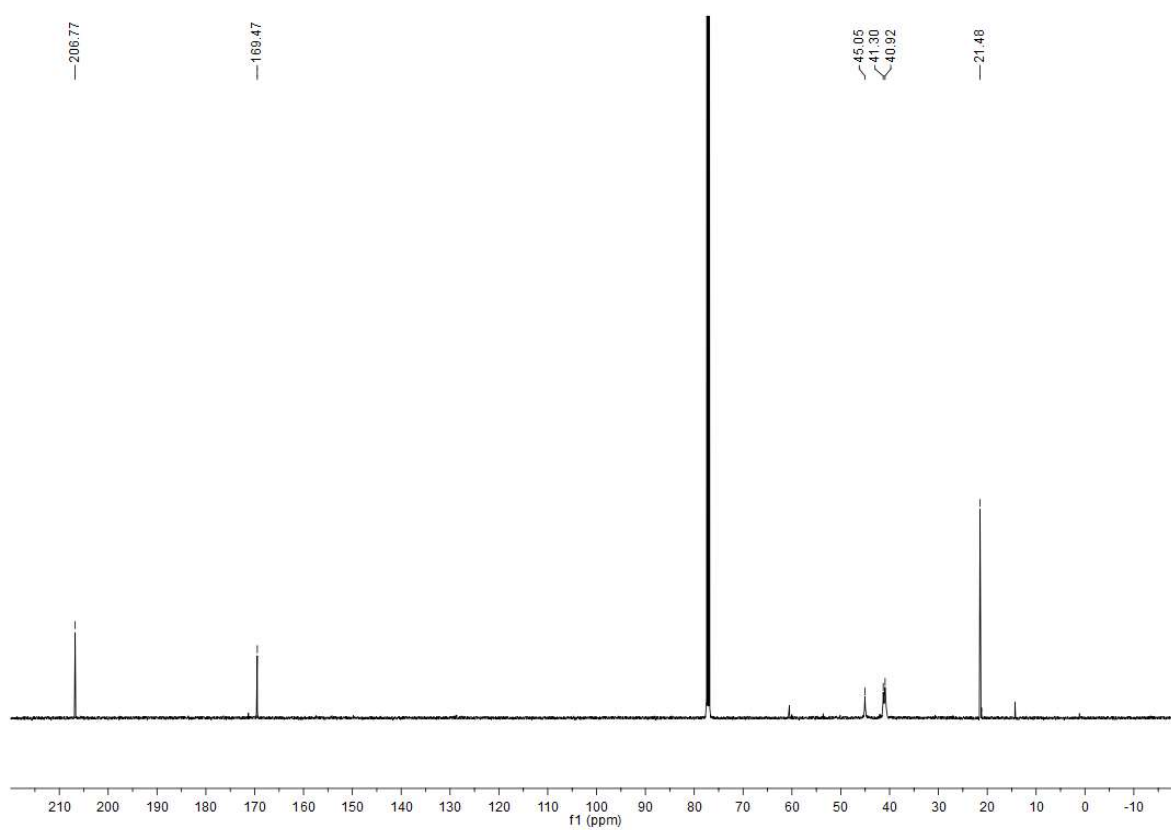


(106)

1H

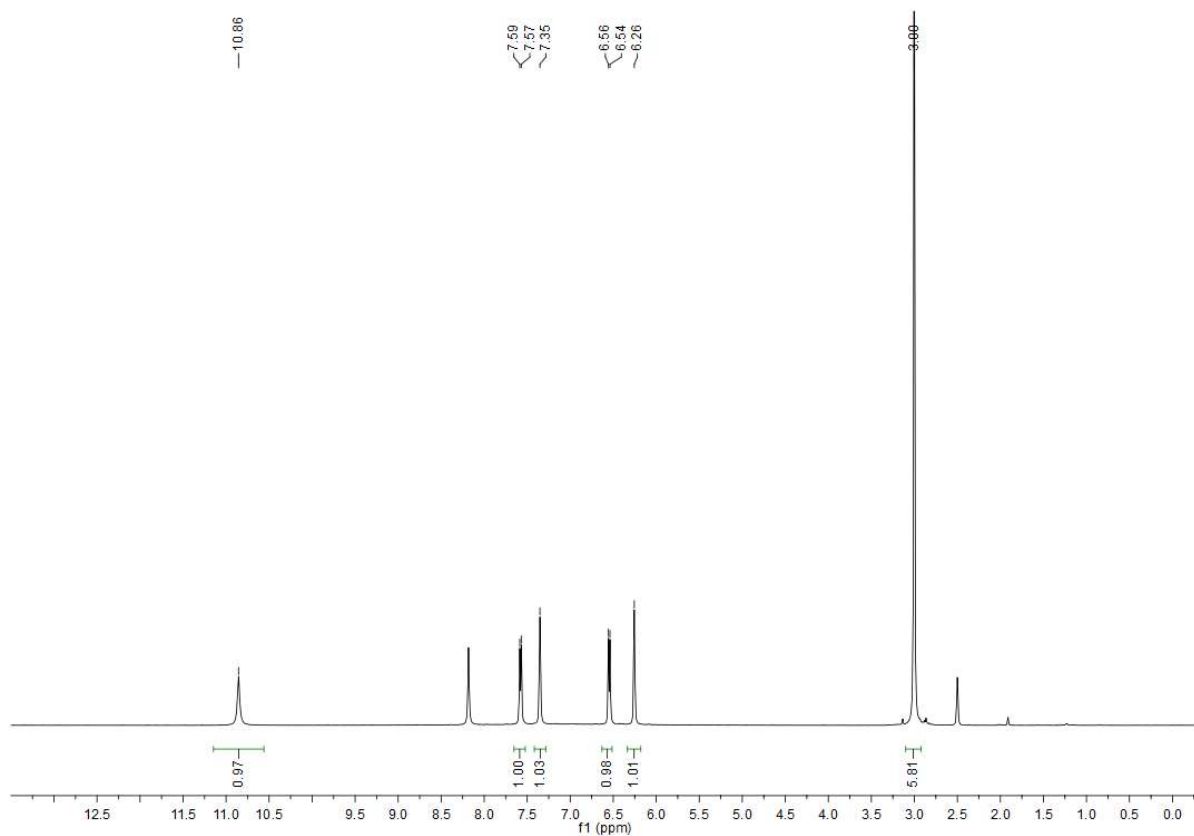


13C



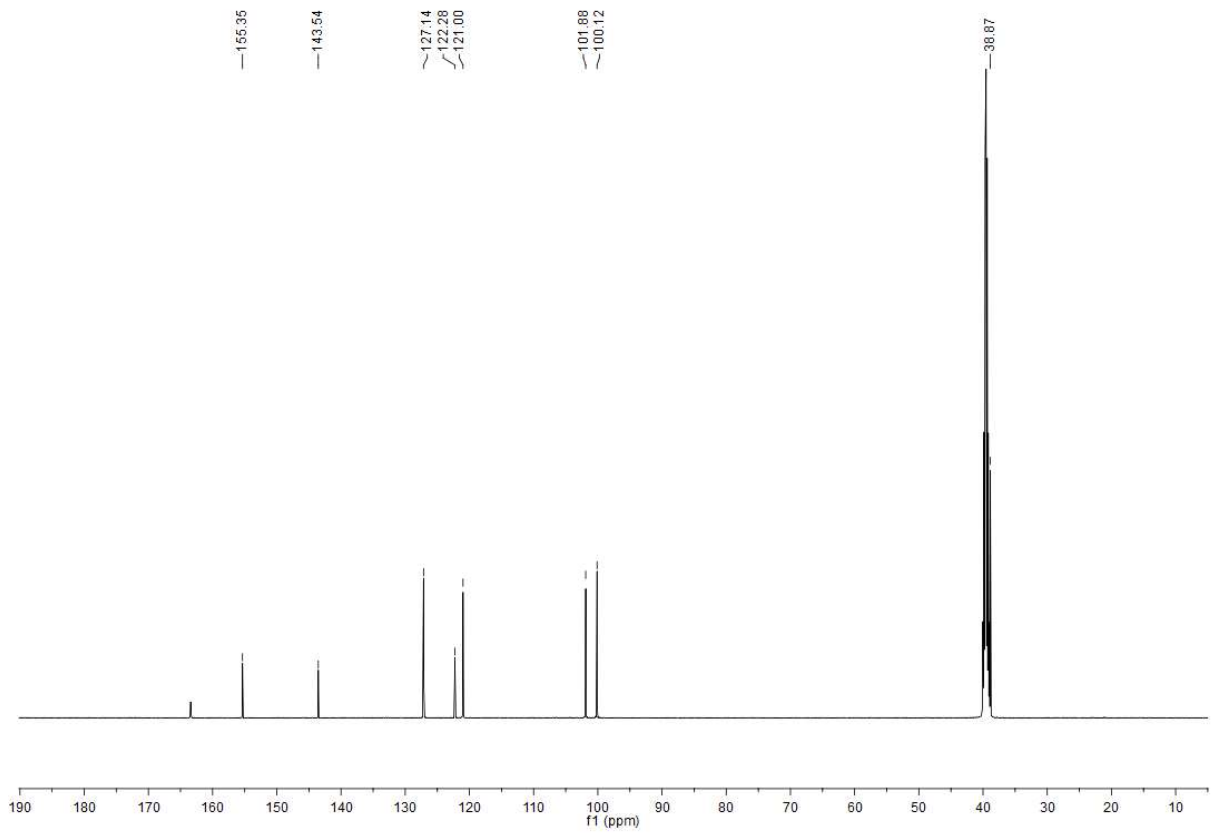
(35)

1H



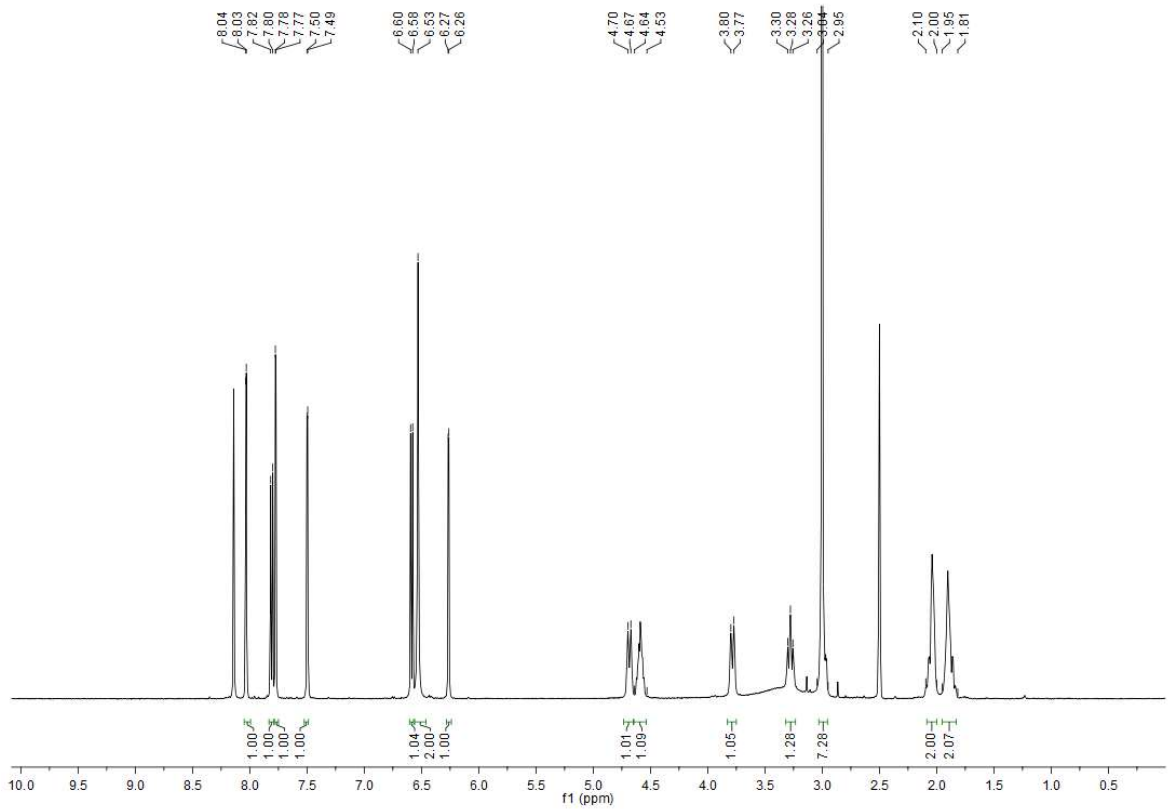


13C

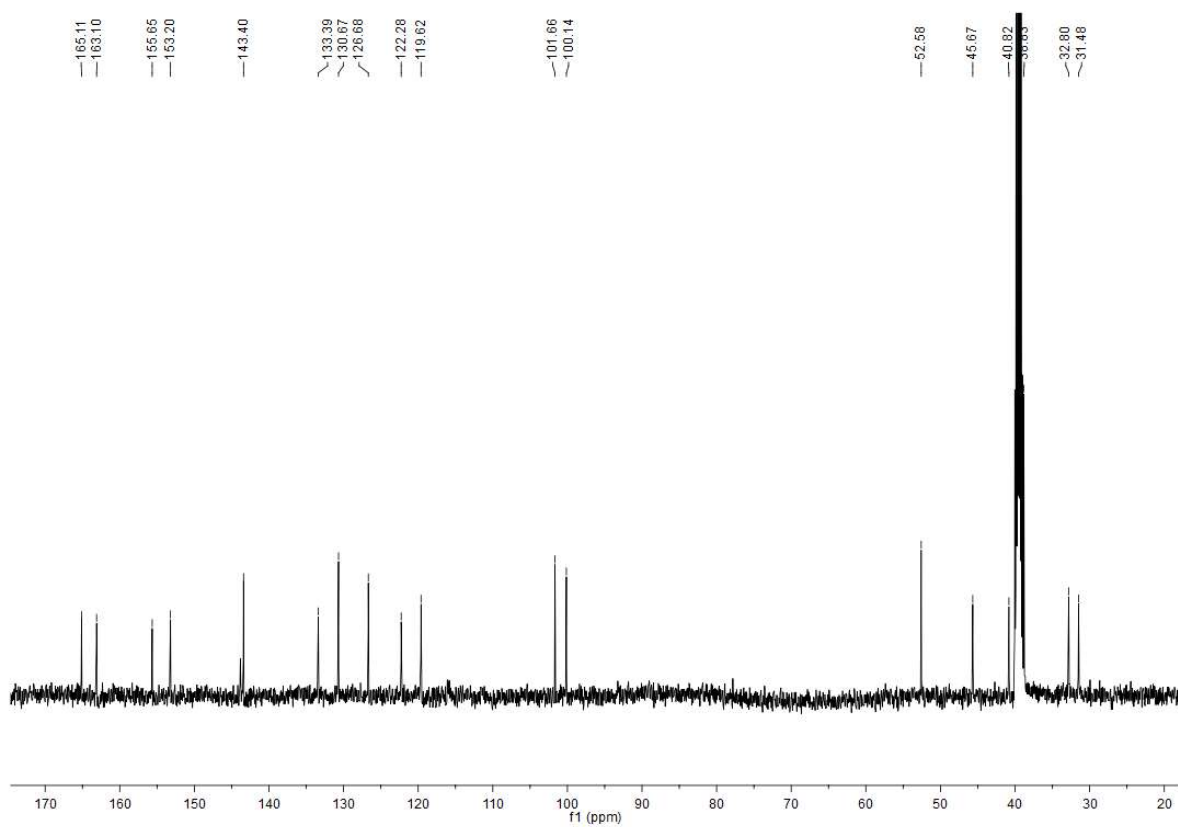


(37)

1H

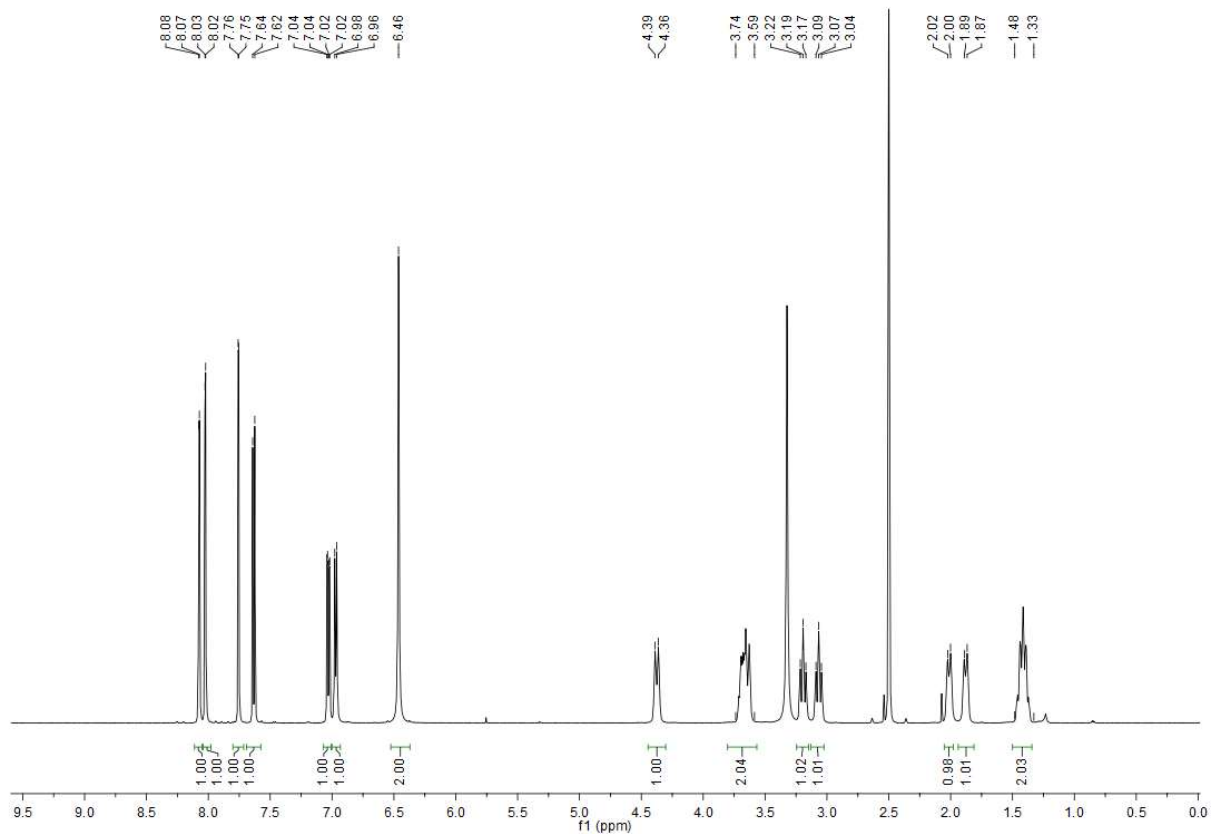


13C

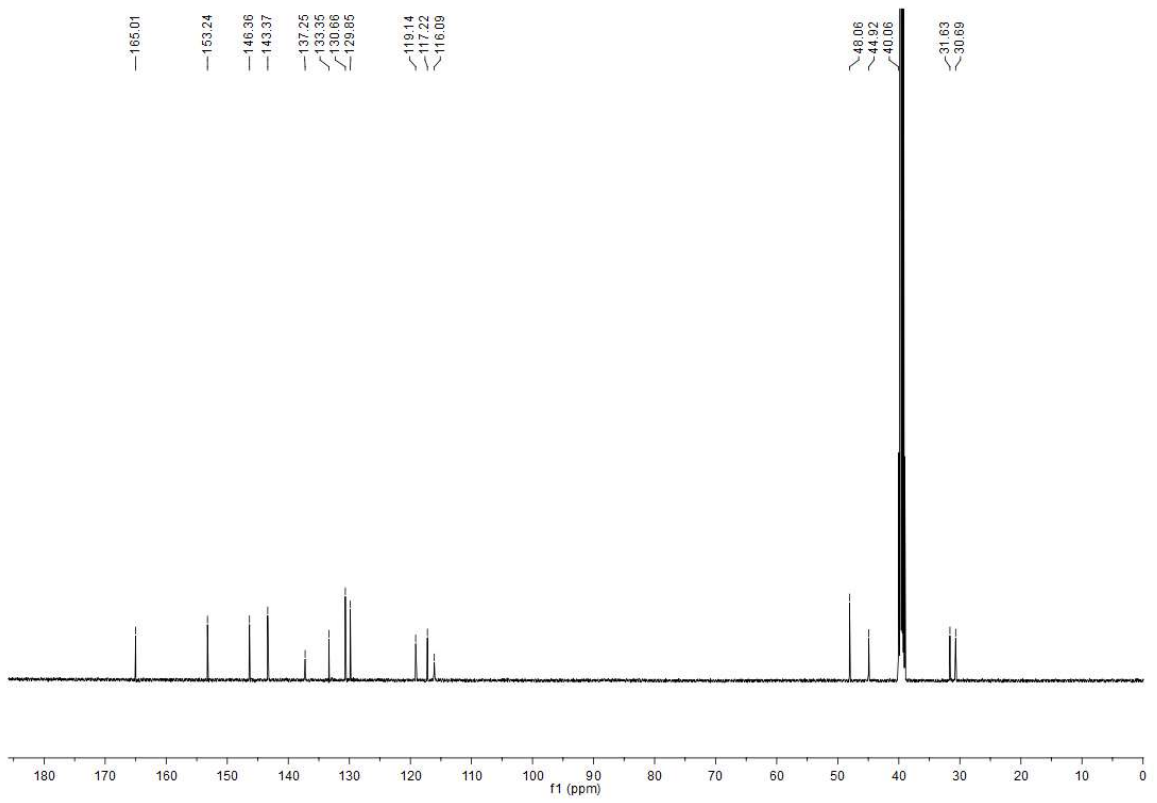


(33)

1H

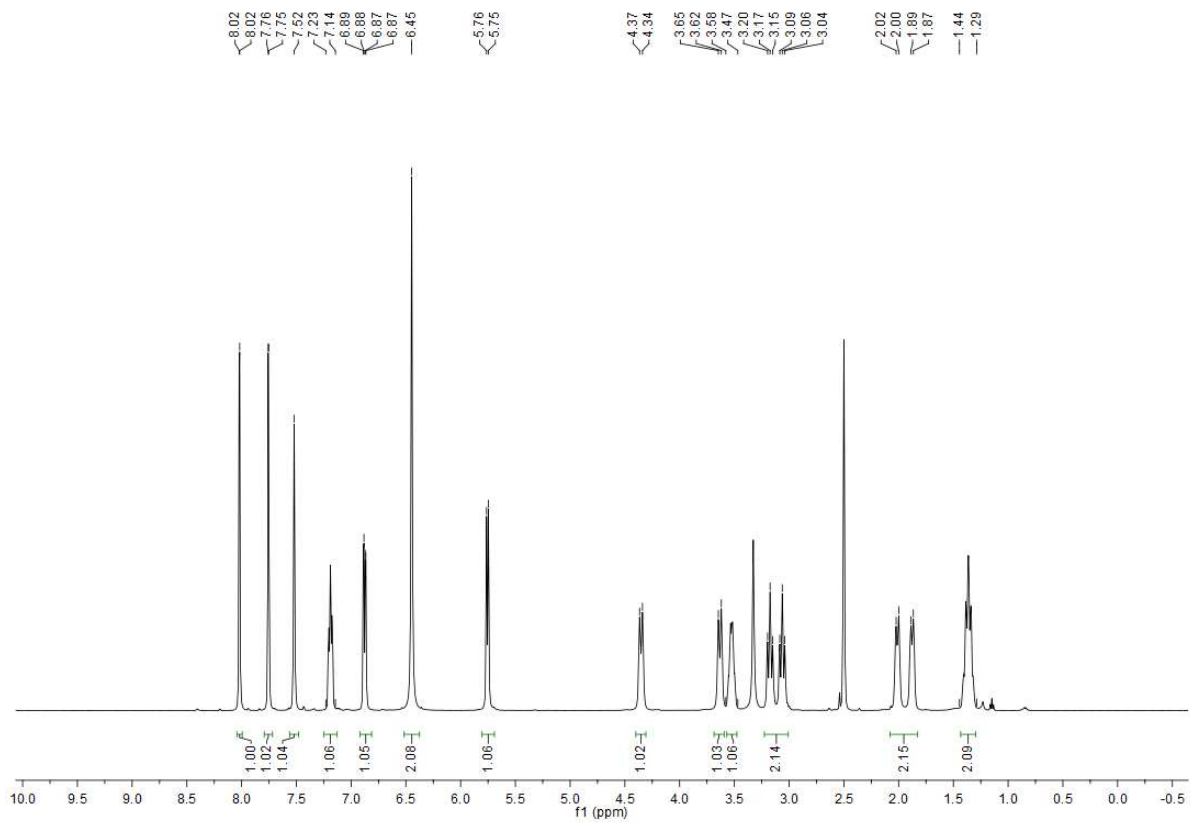


13C

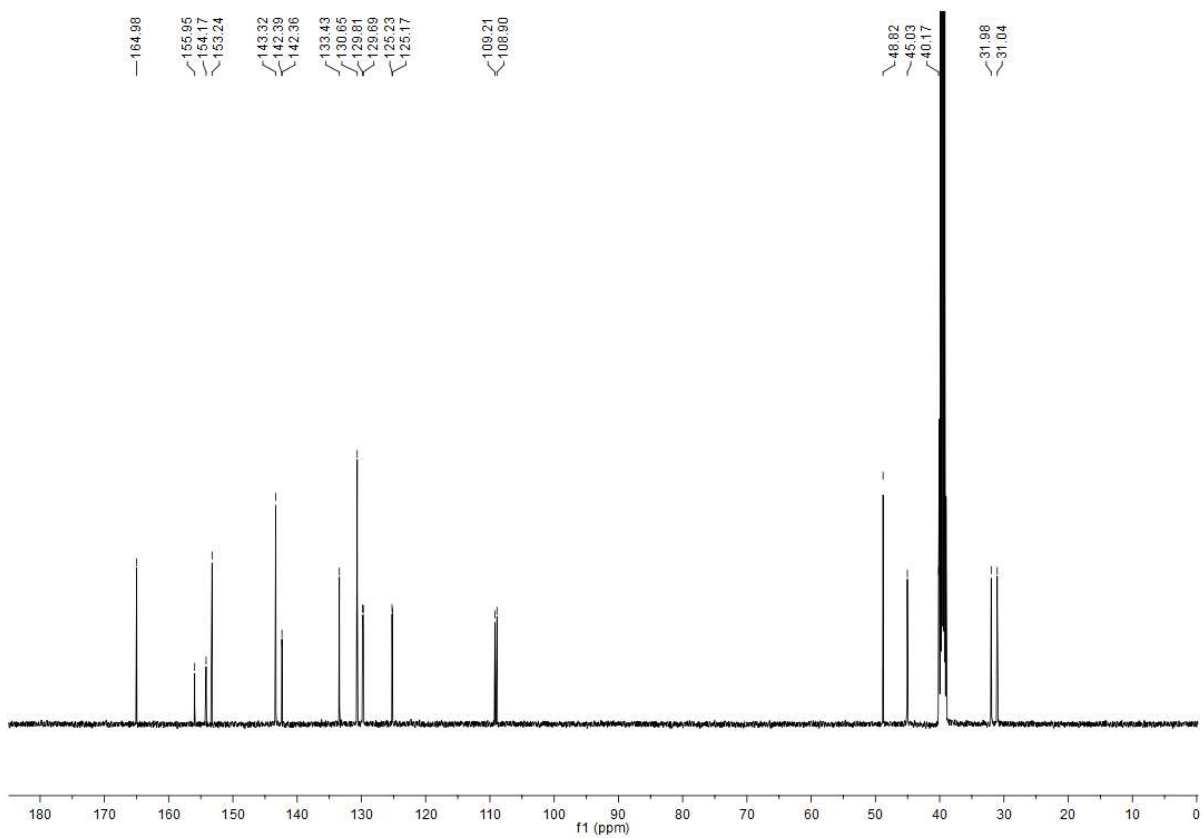


(67)

1H

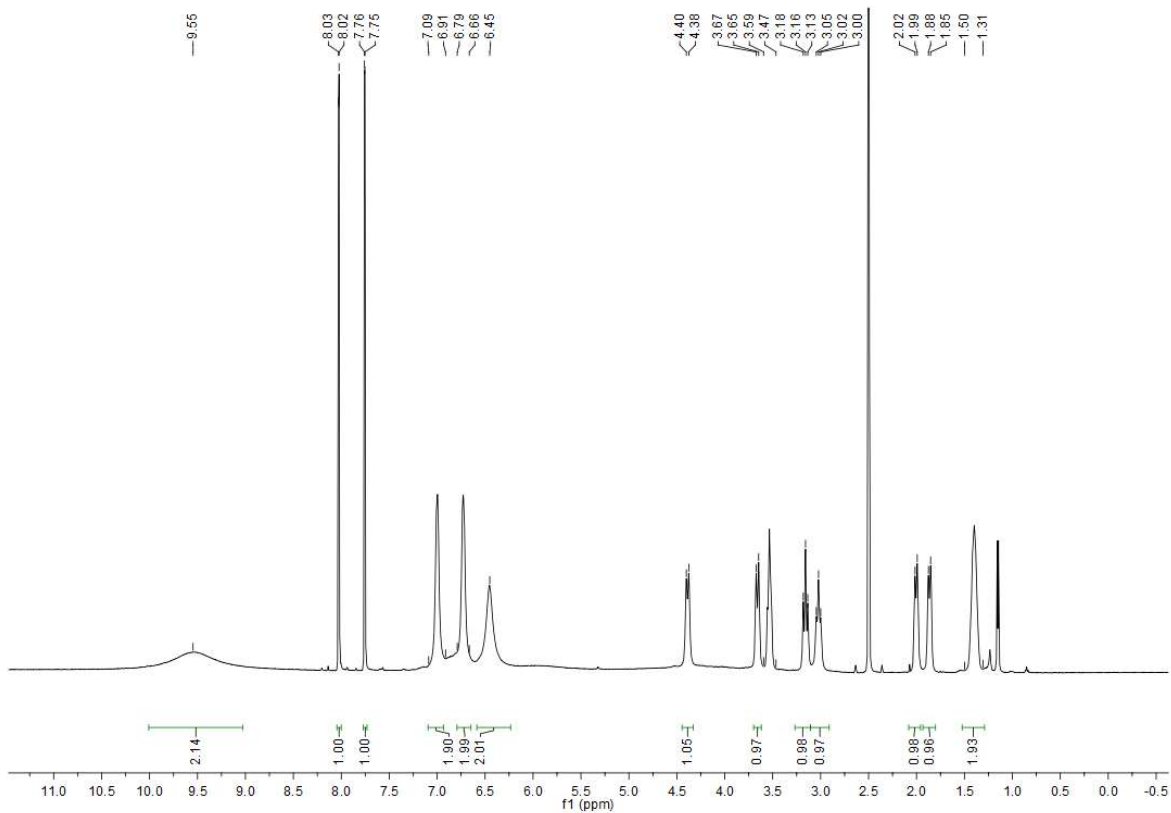


13C

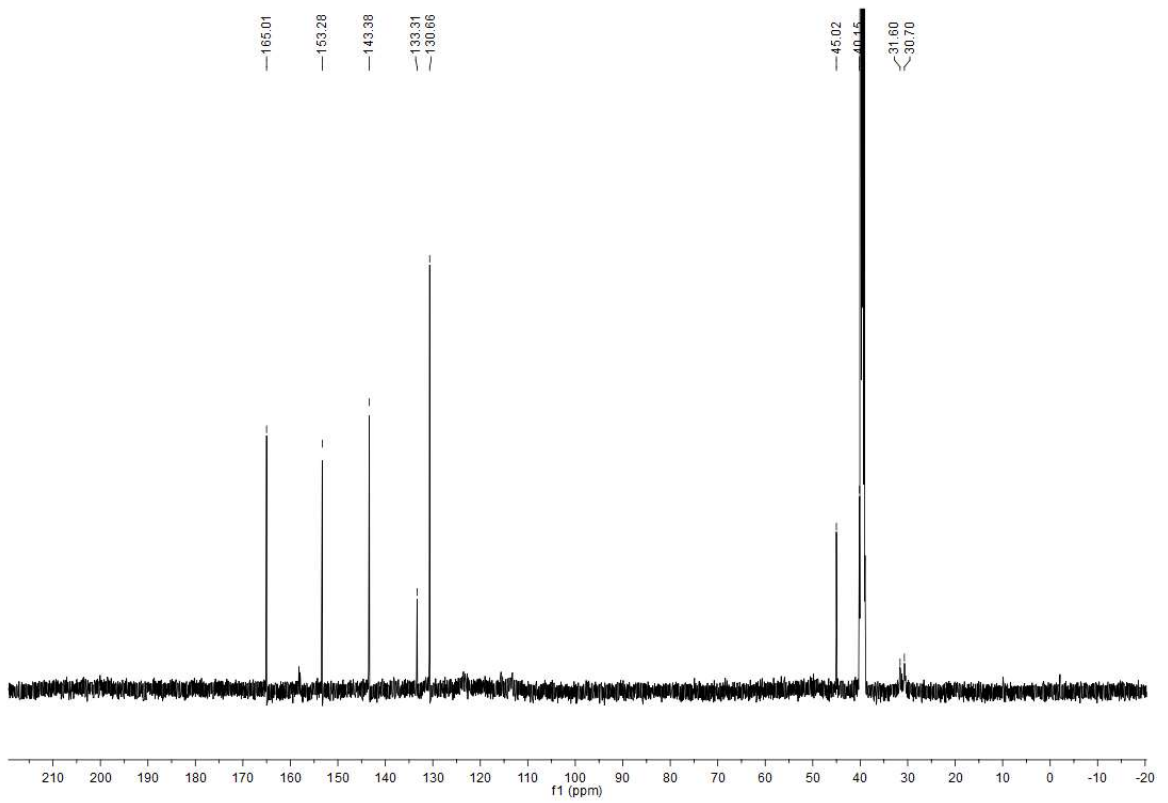


(63)

<sup>1</sup>H

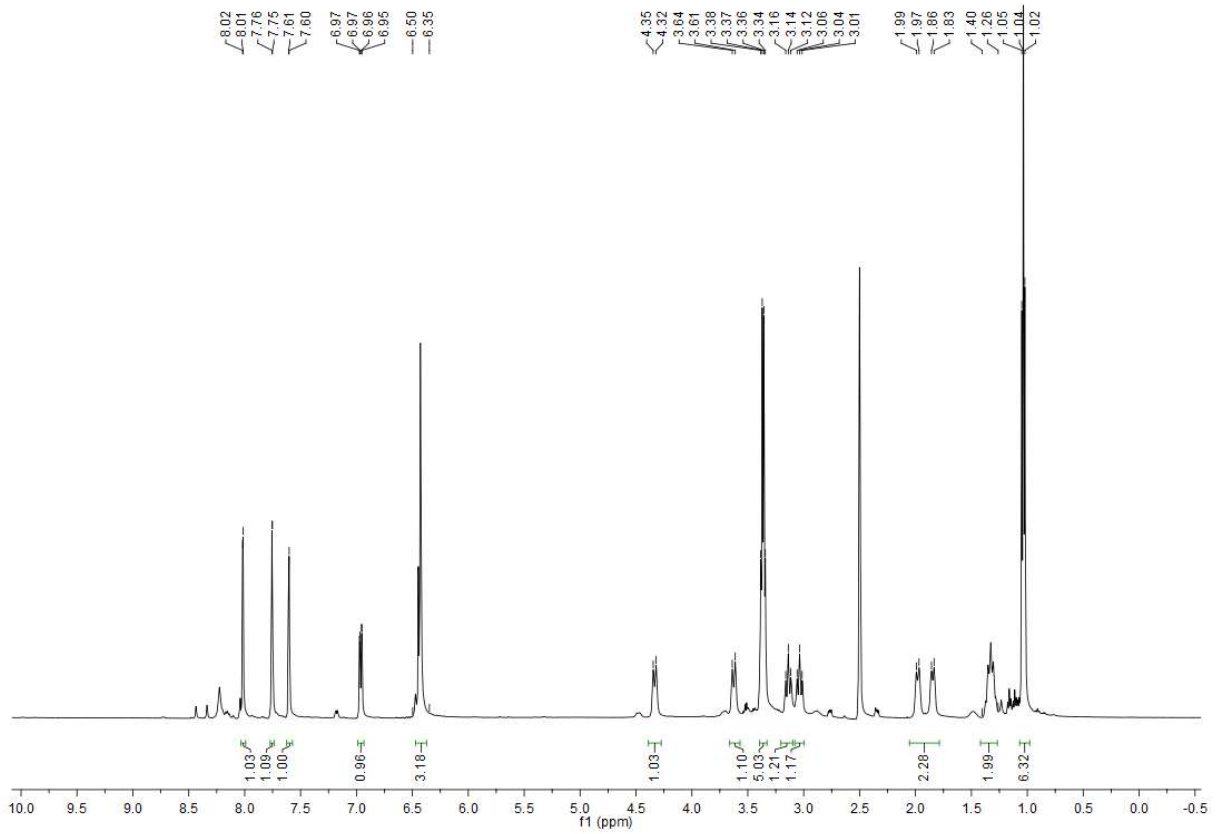


13C

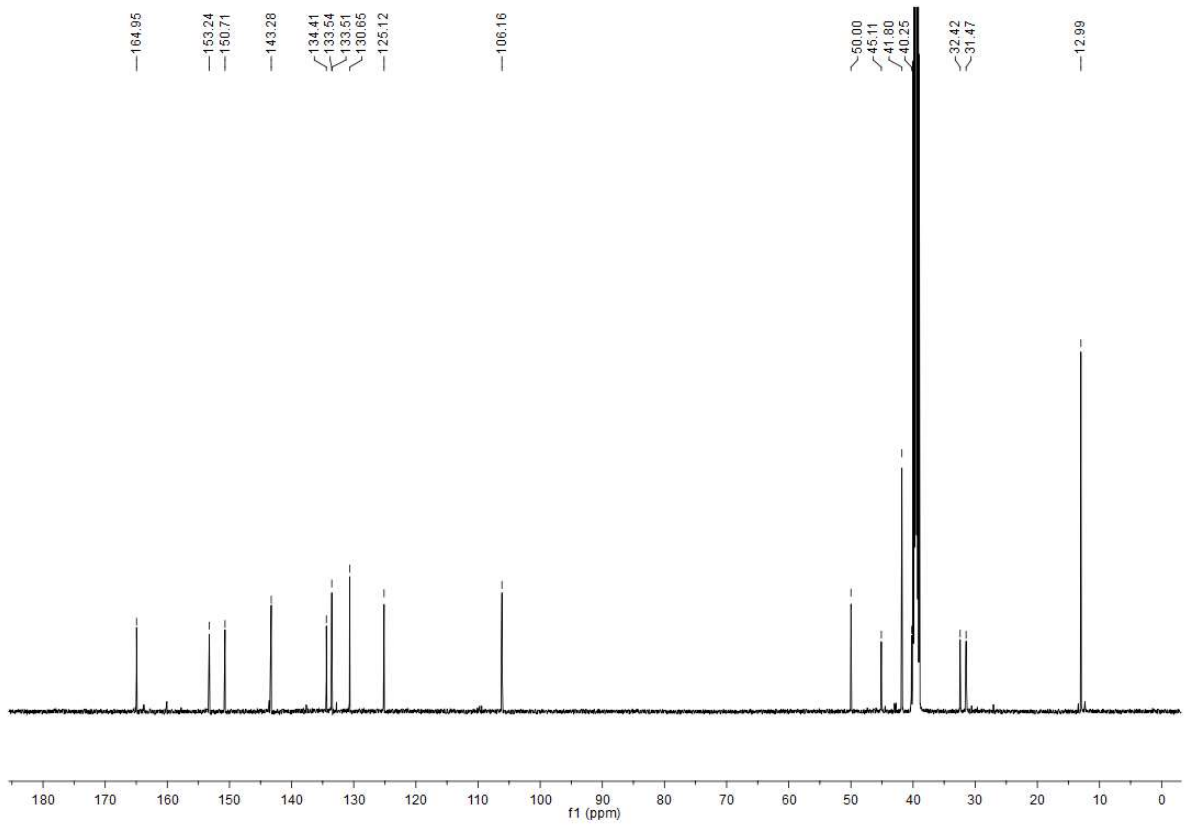


(68)

1H

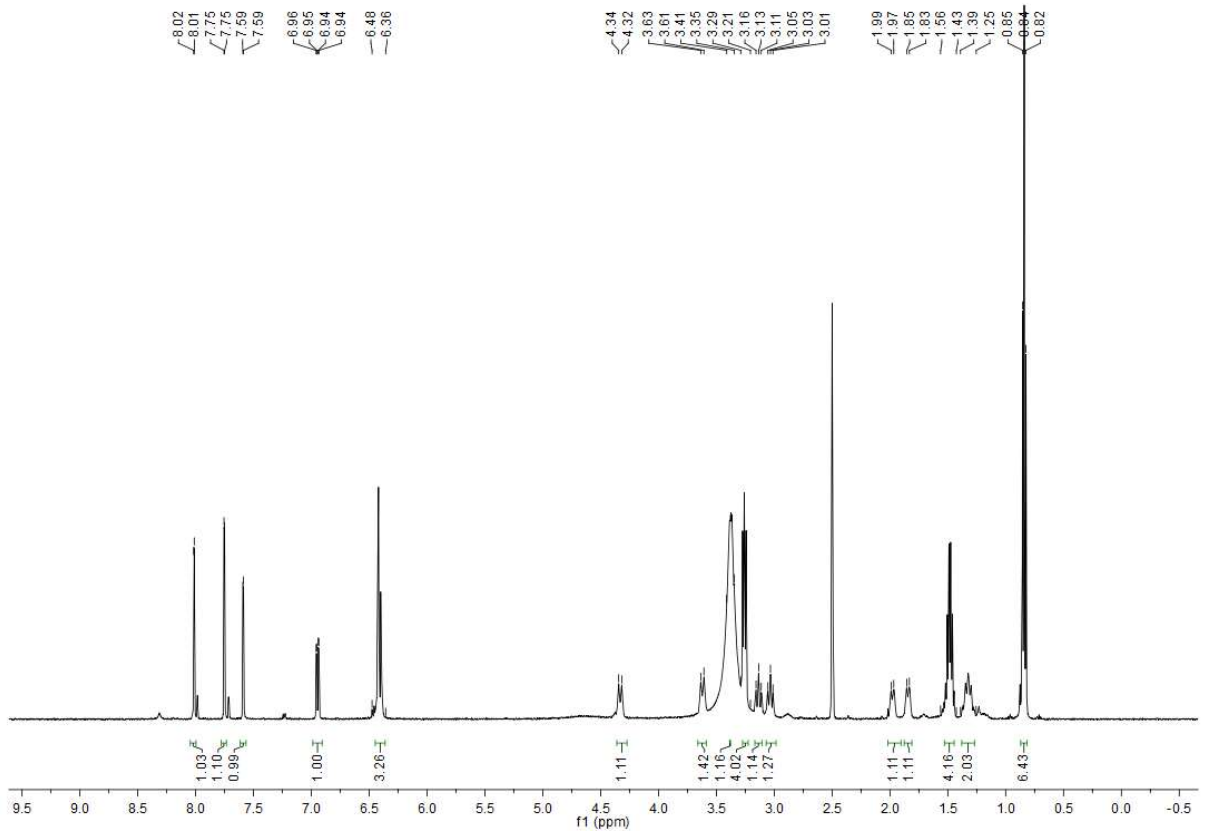


13C

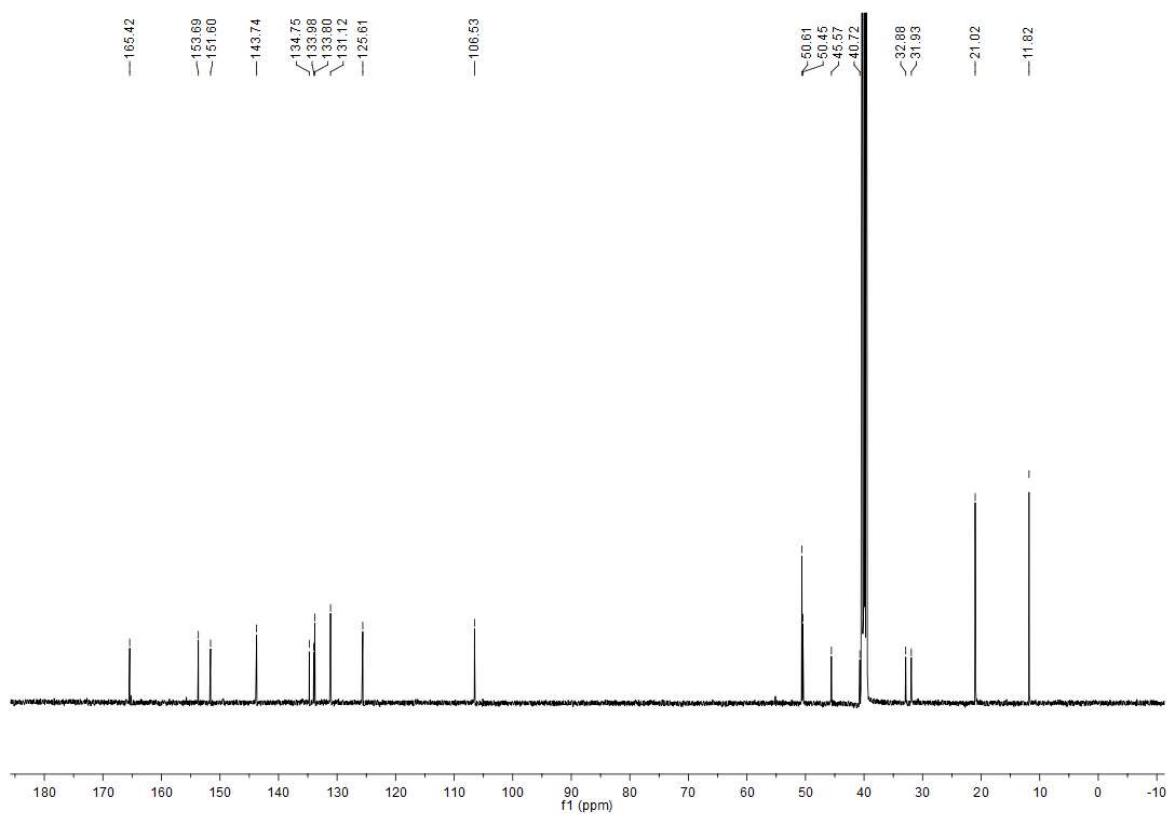


(69)

1H

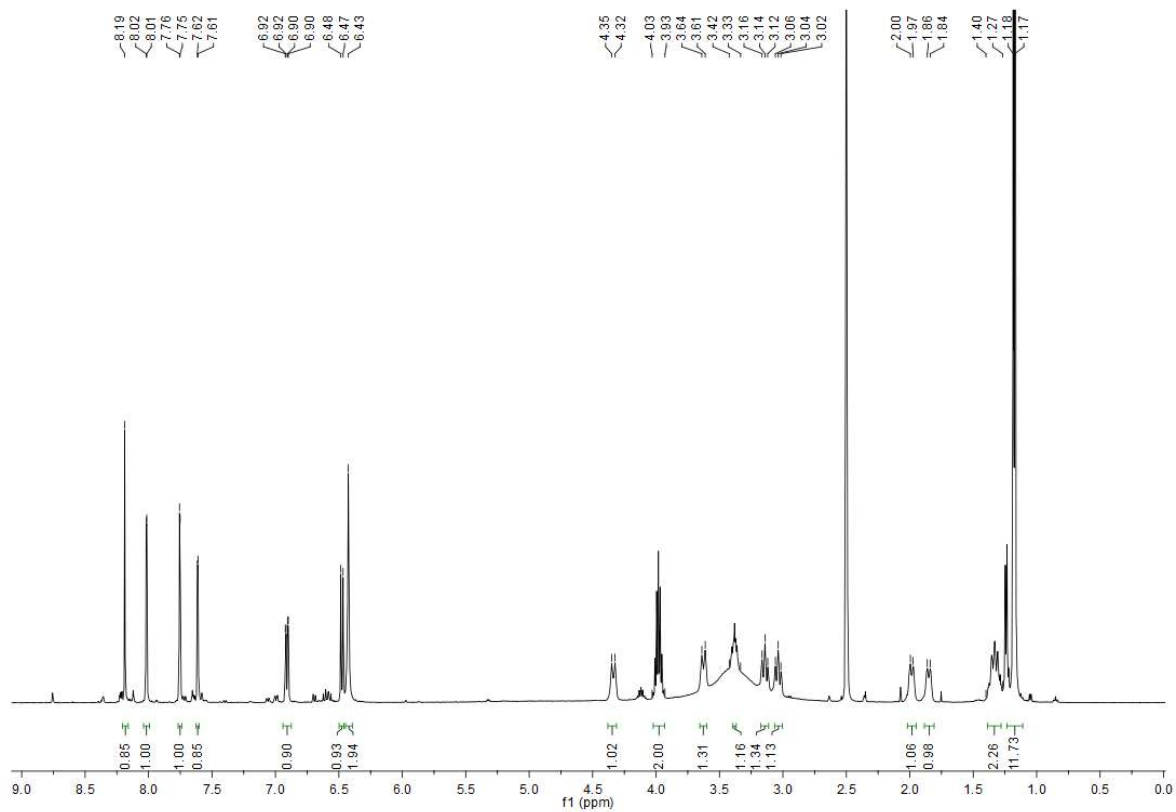


13C

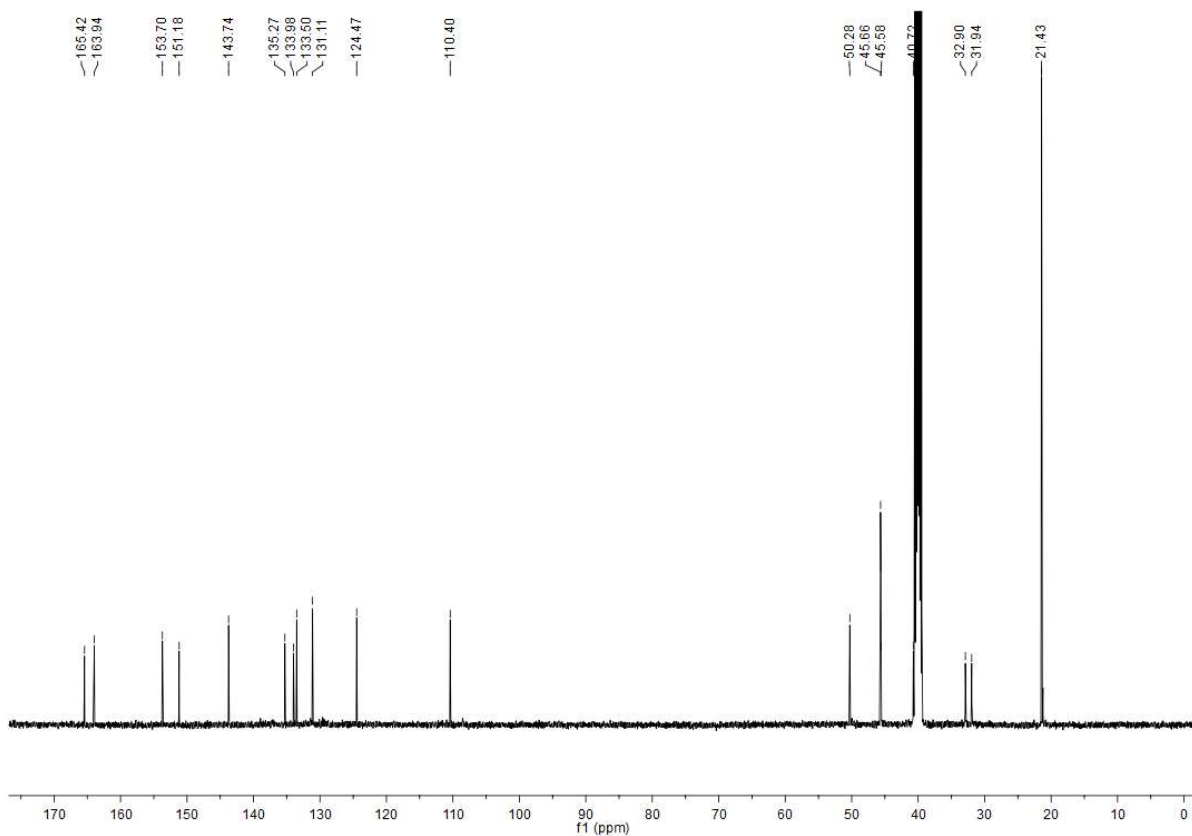


(61)

<sup>1</sup>H

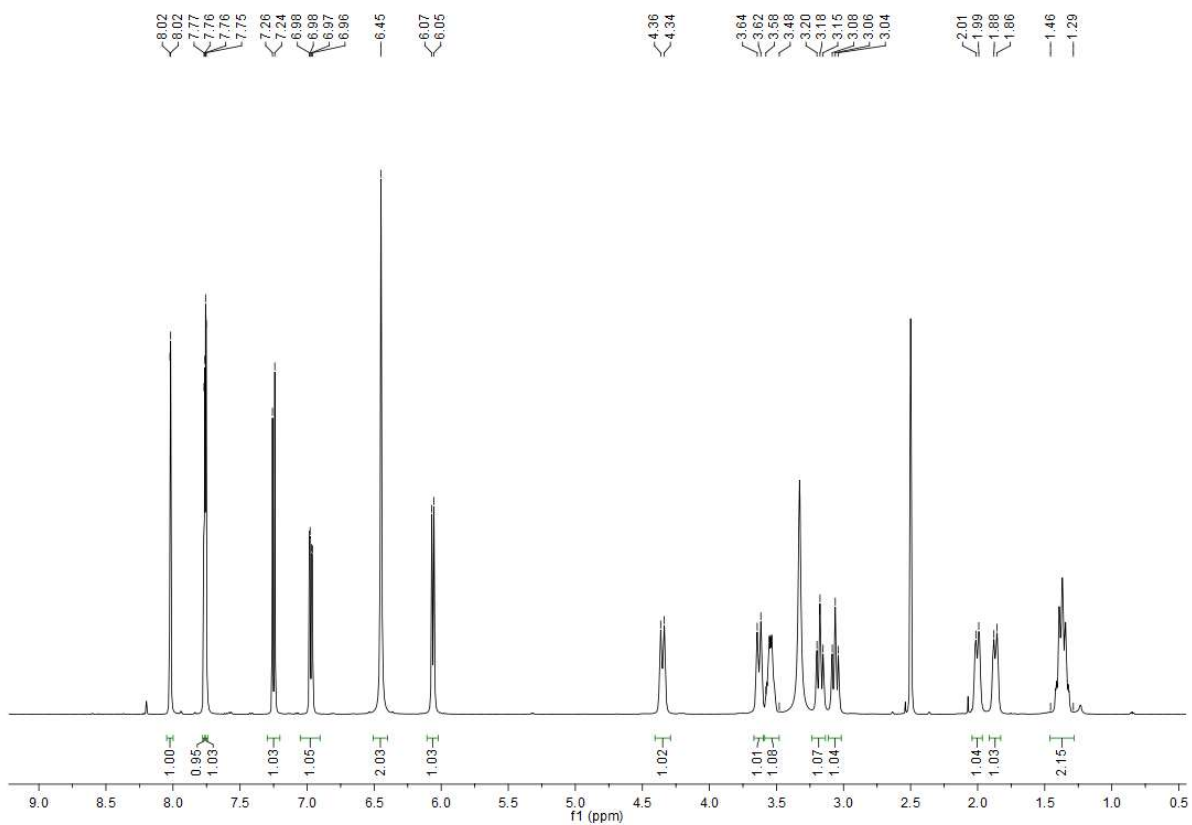


13C



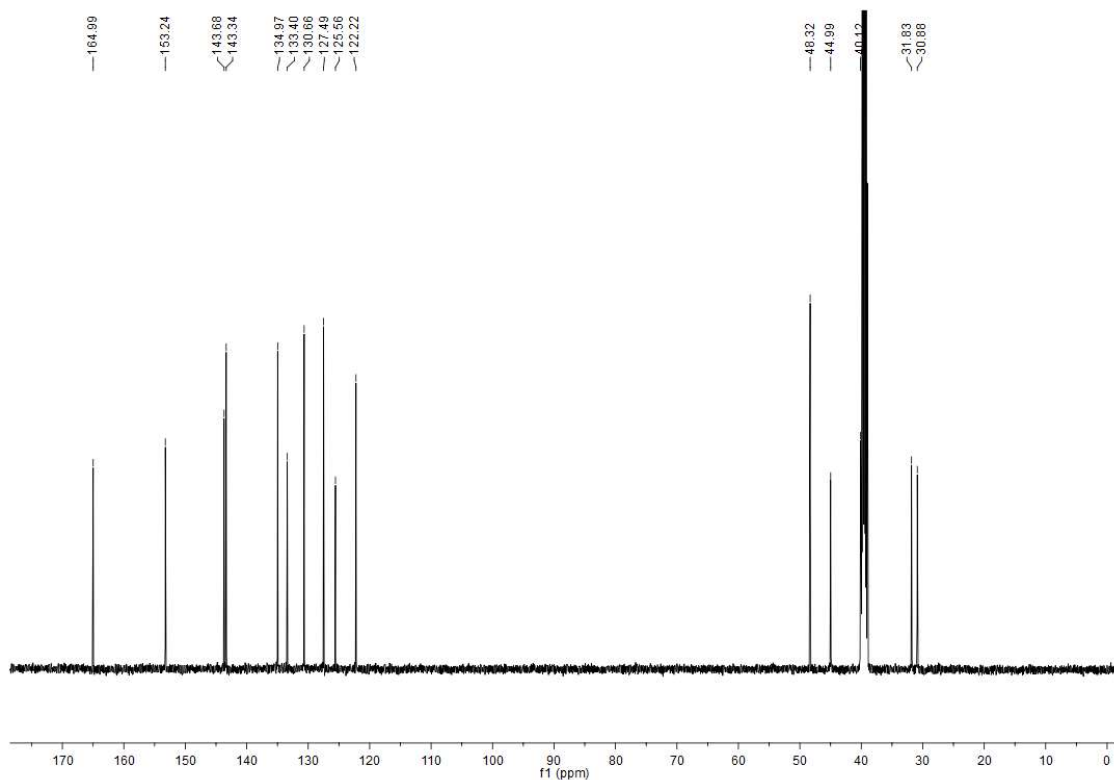
(59)

<sup>1</sup>H



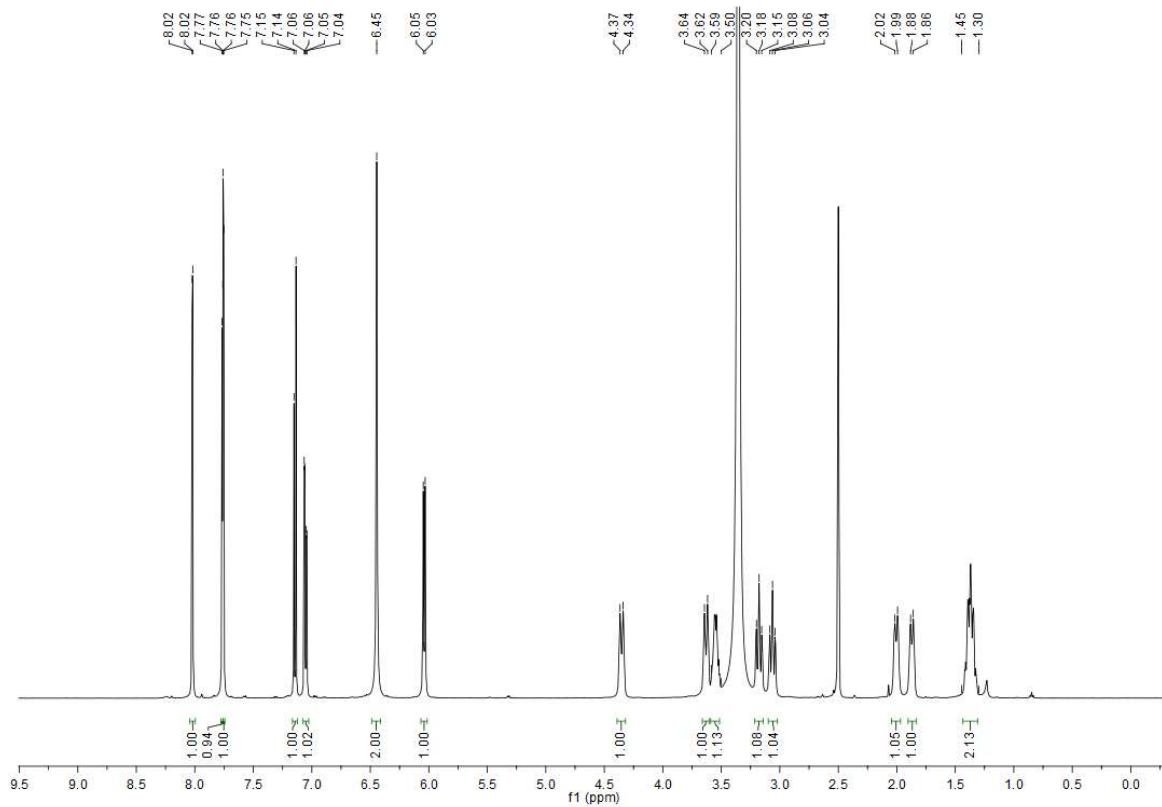


13C

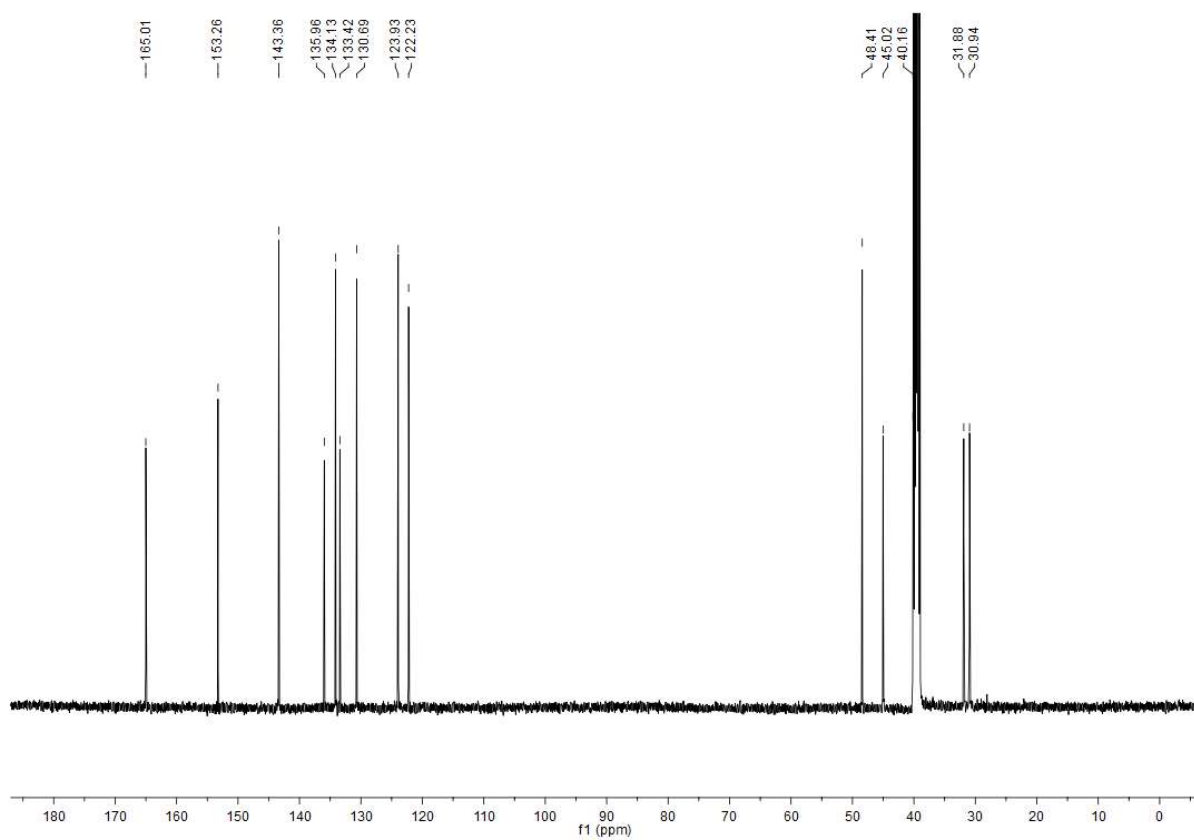


(56)

<sup>1</sup>H

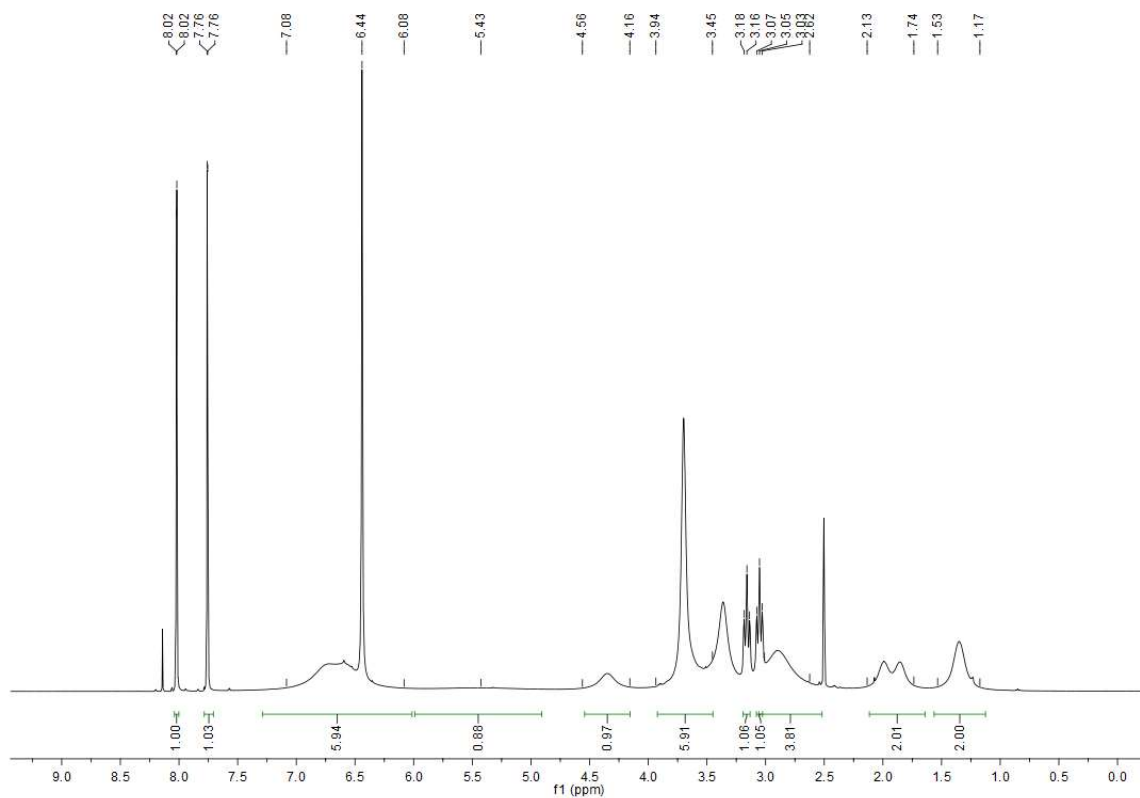


13C

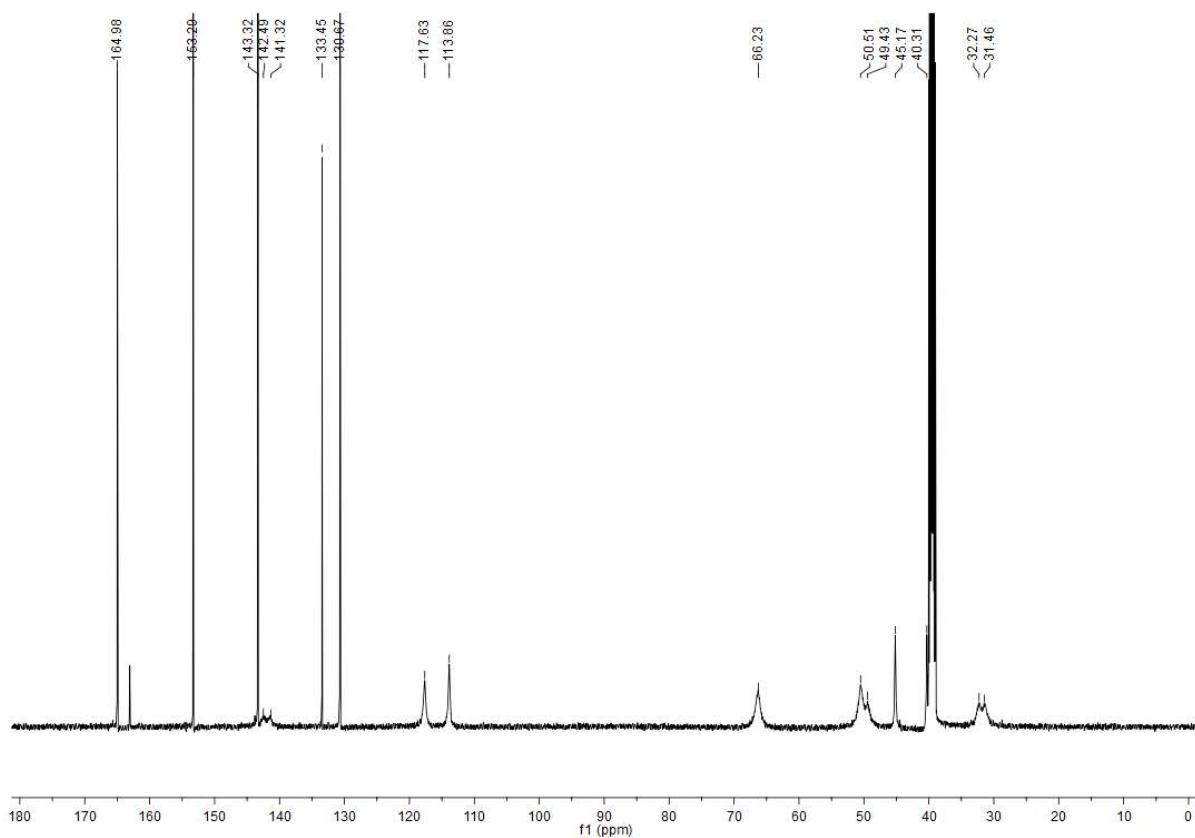


(58)

1H

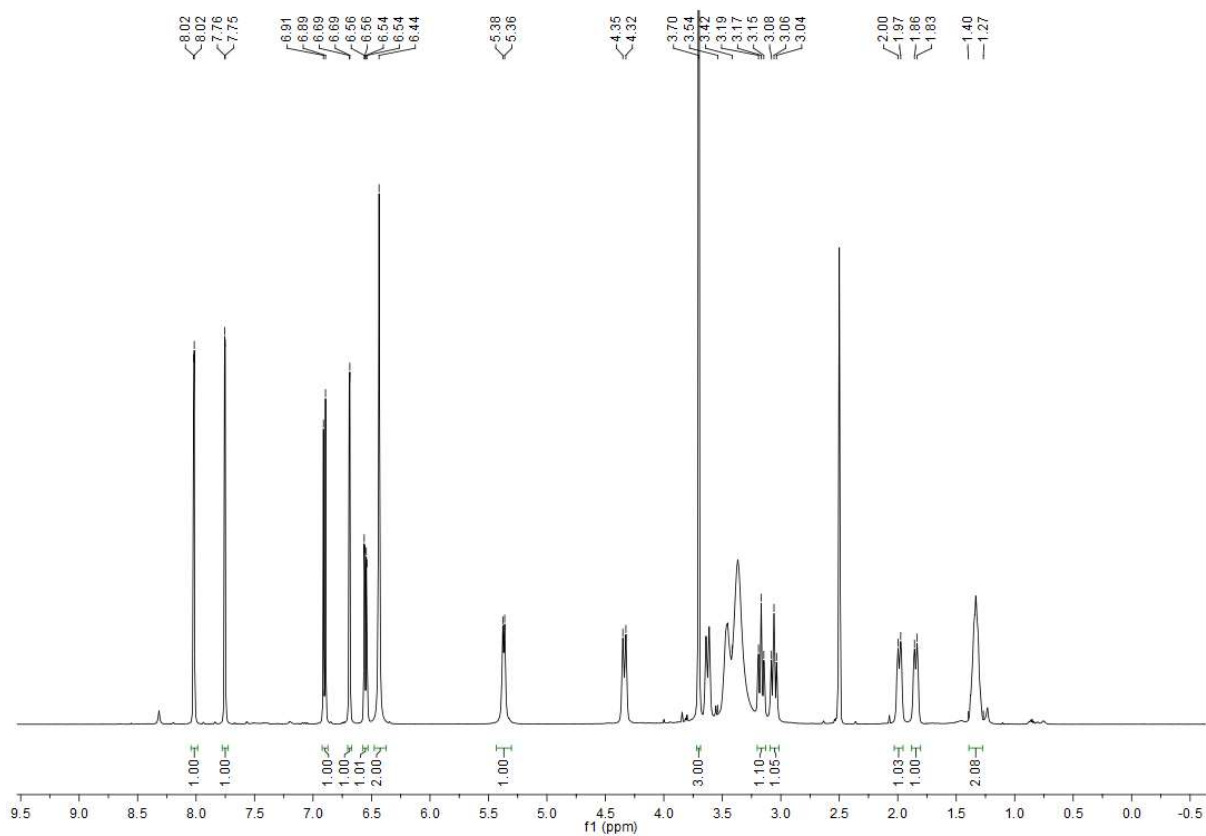


13C

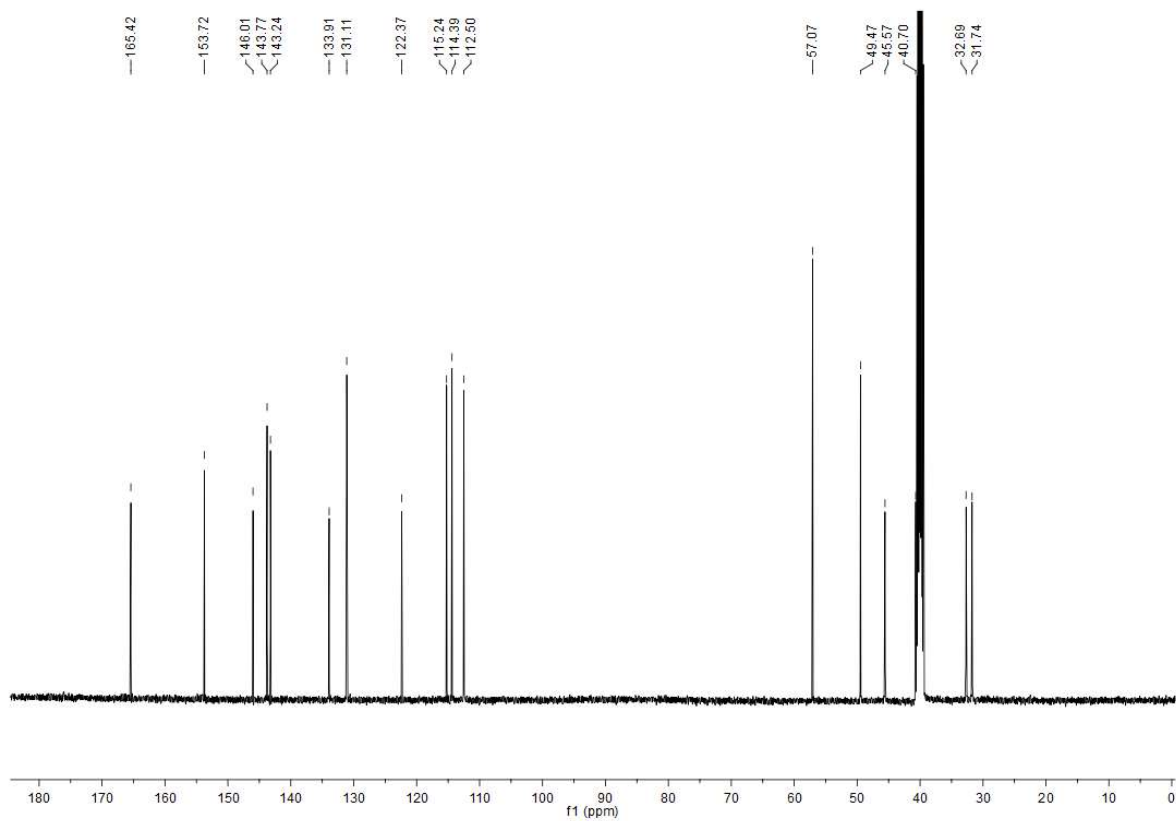


(57)

1H

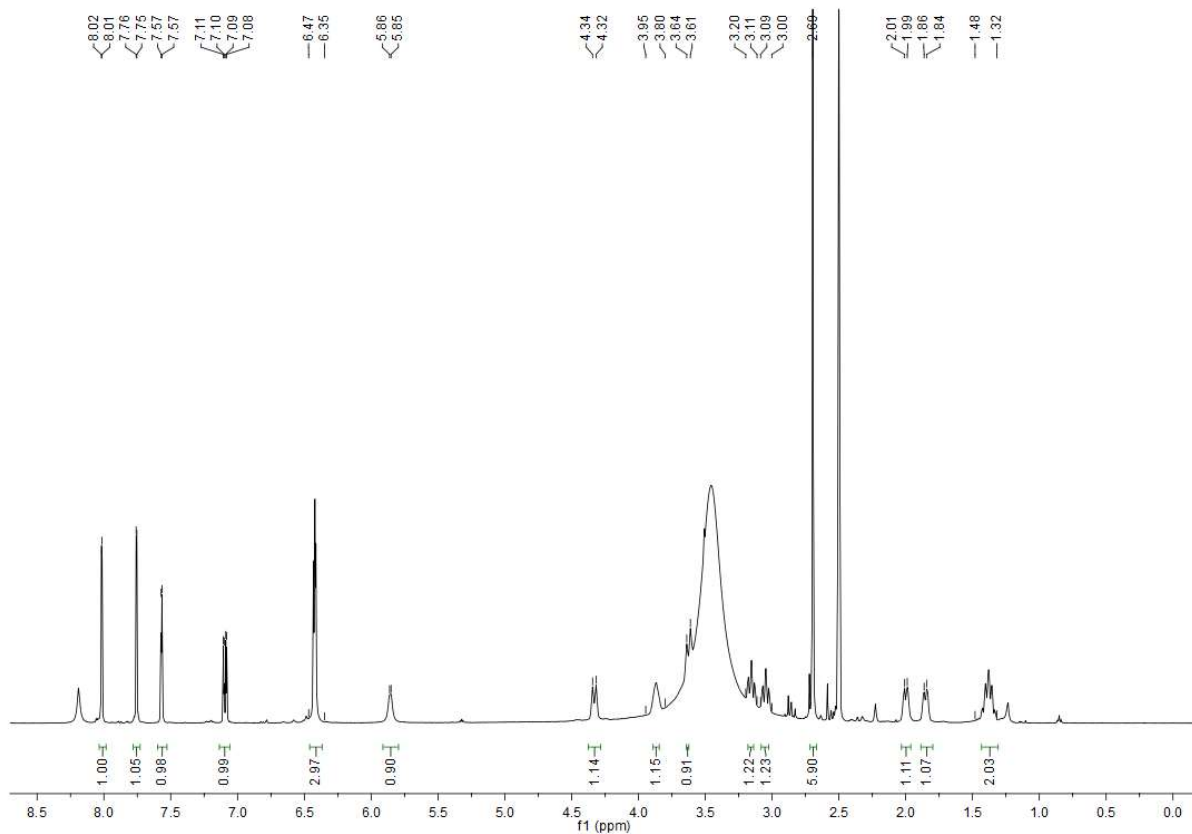


13C

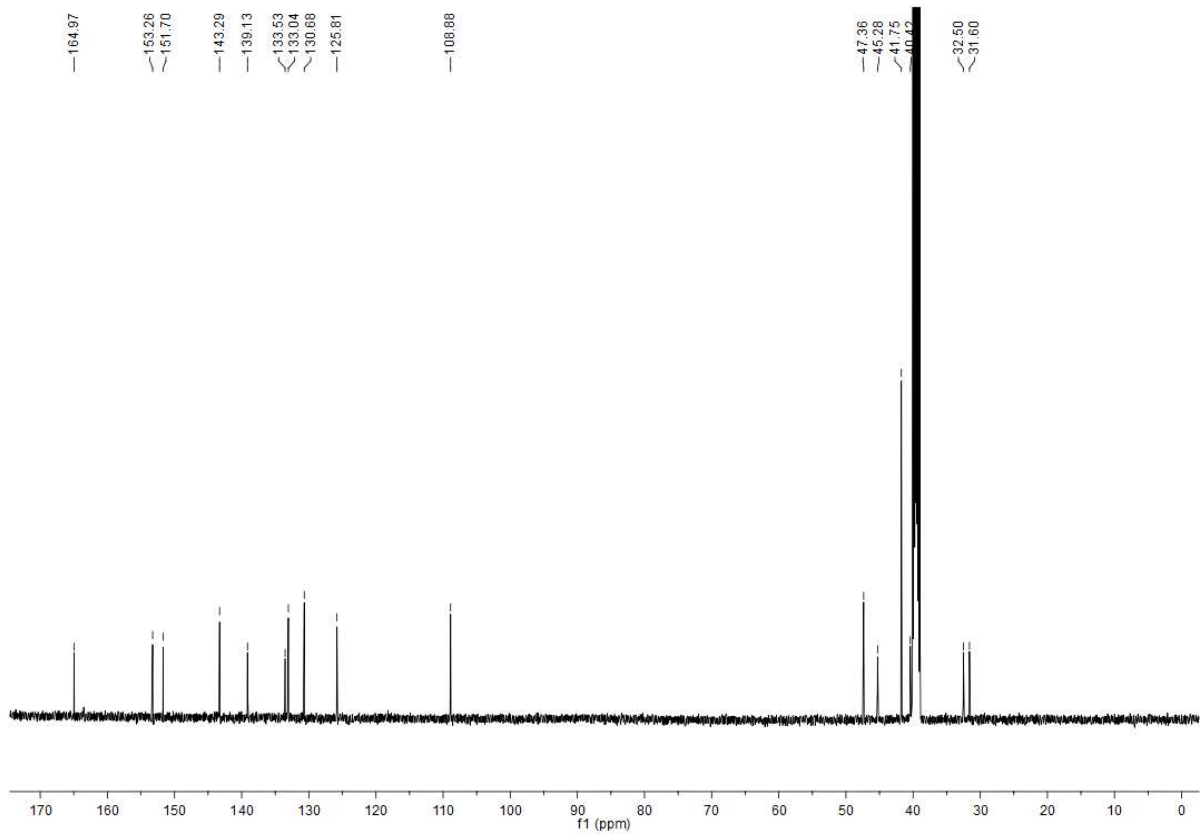


(65)

1H

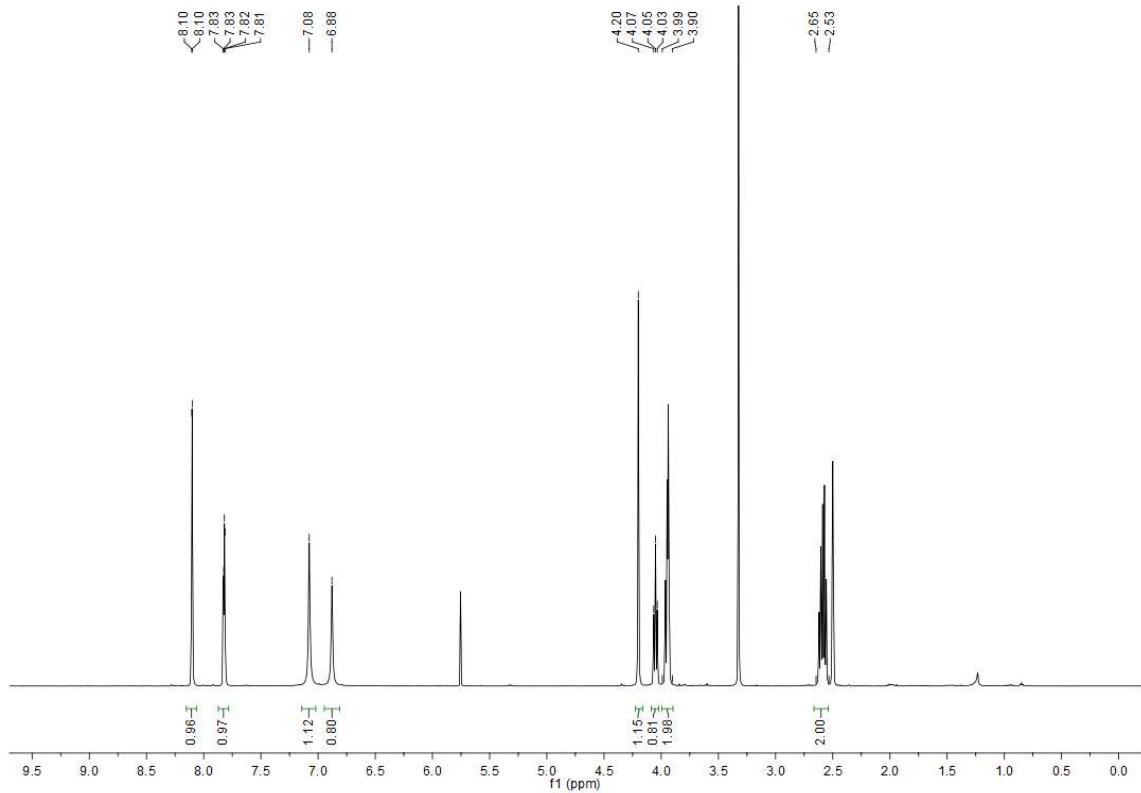


# 13C

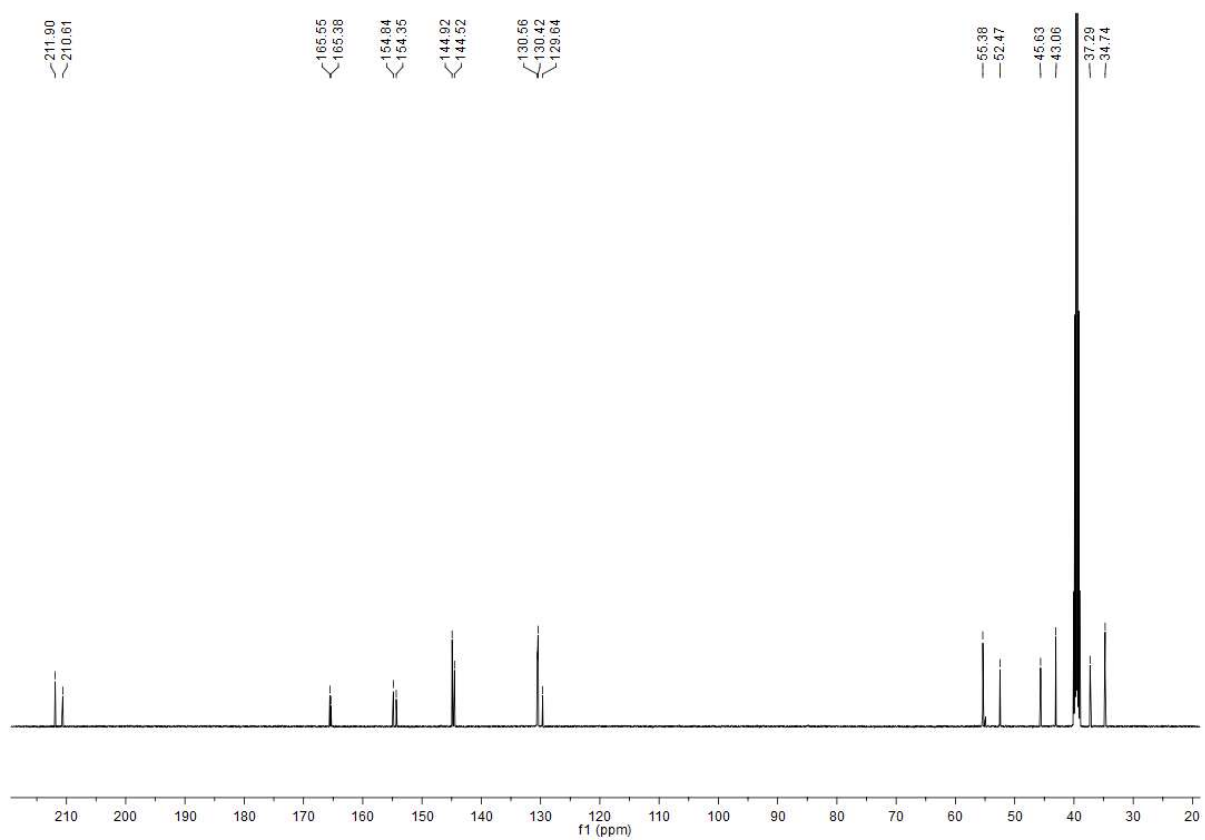


# (124)

# 1H

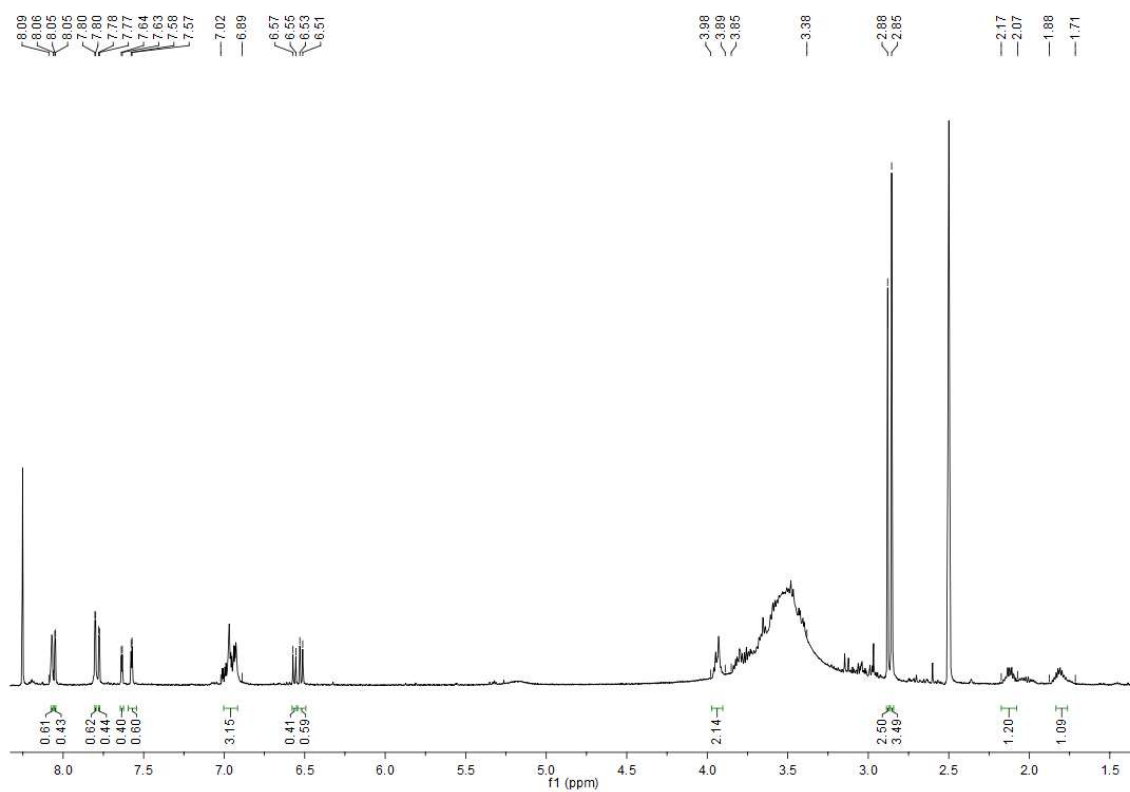


13C

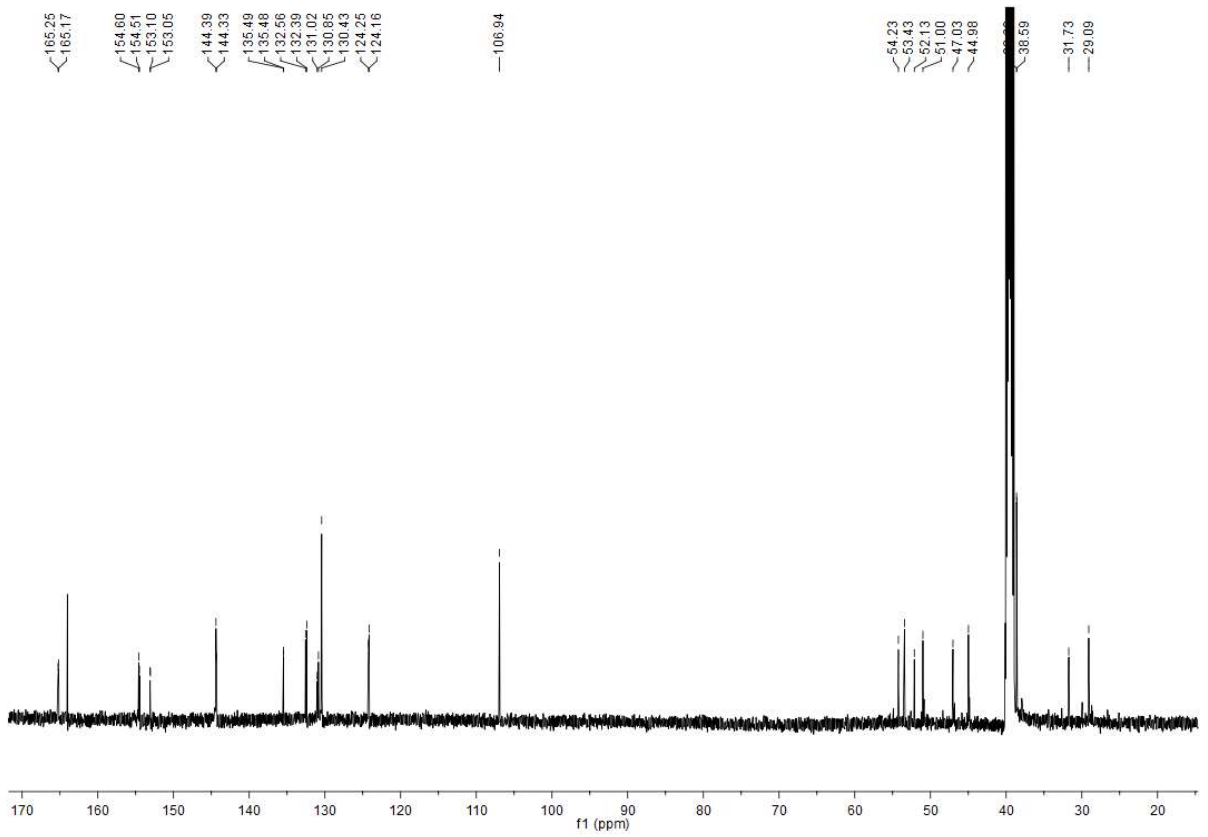


(48)

<sup>1</sup>H

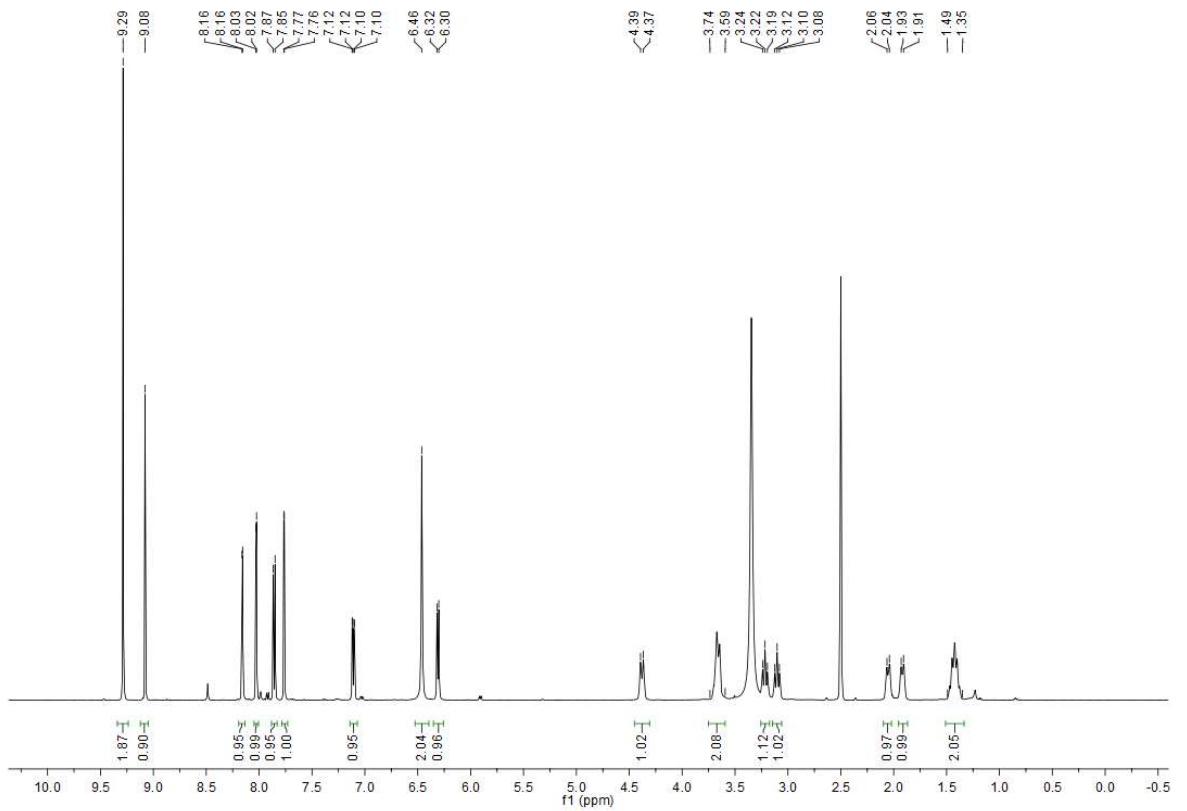


13C

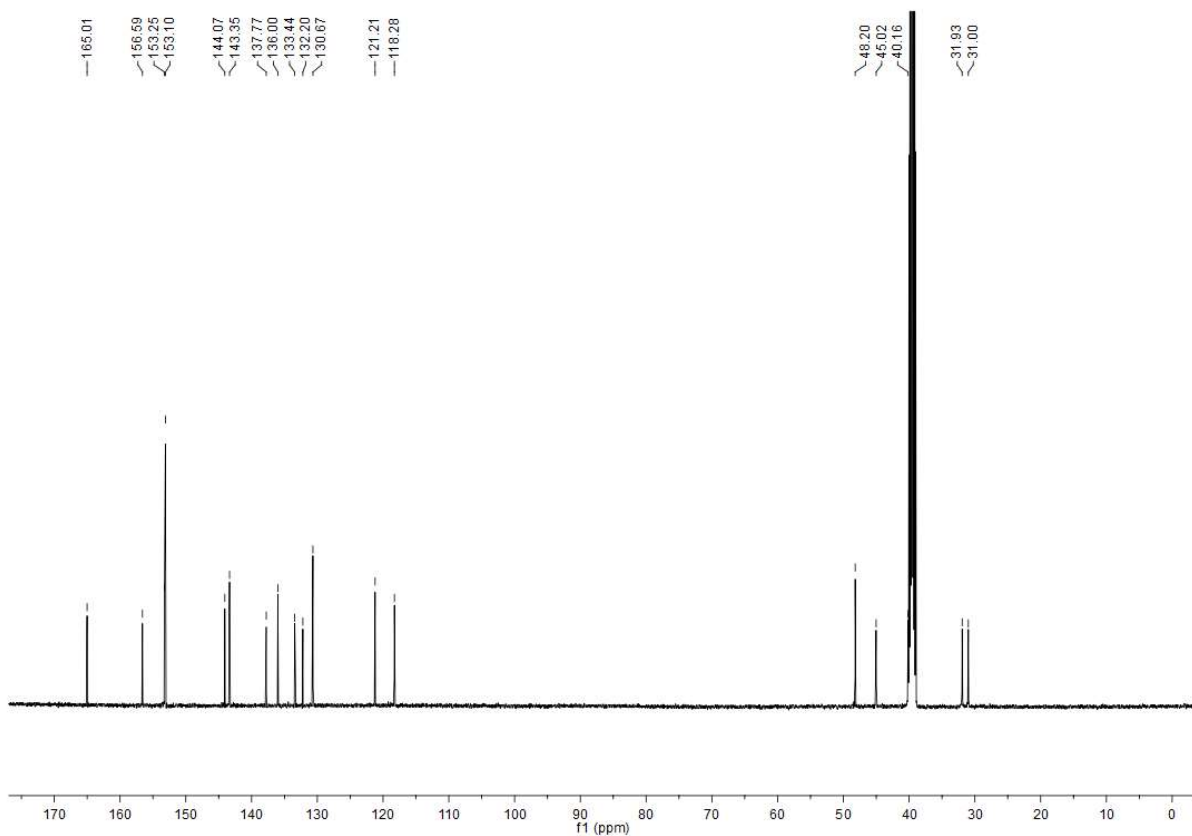


(71)

<sup>1</sup>H

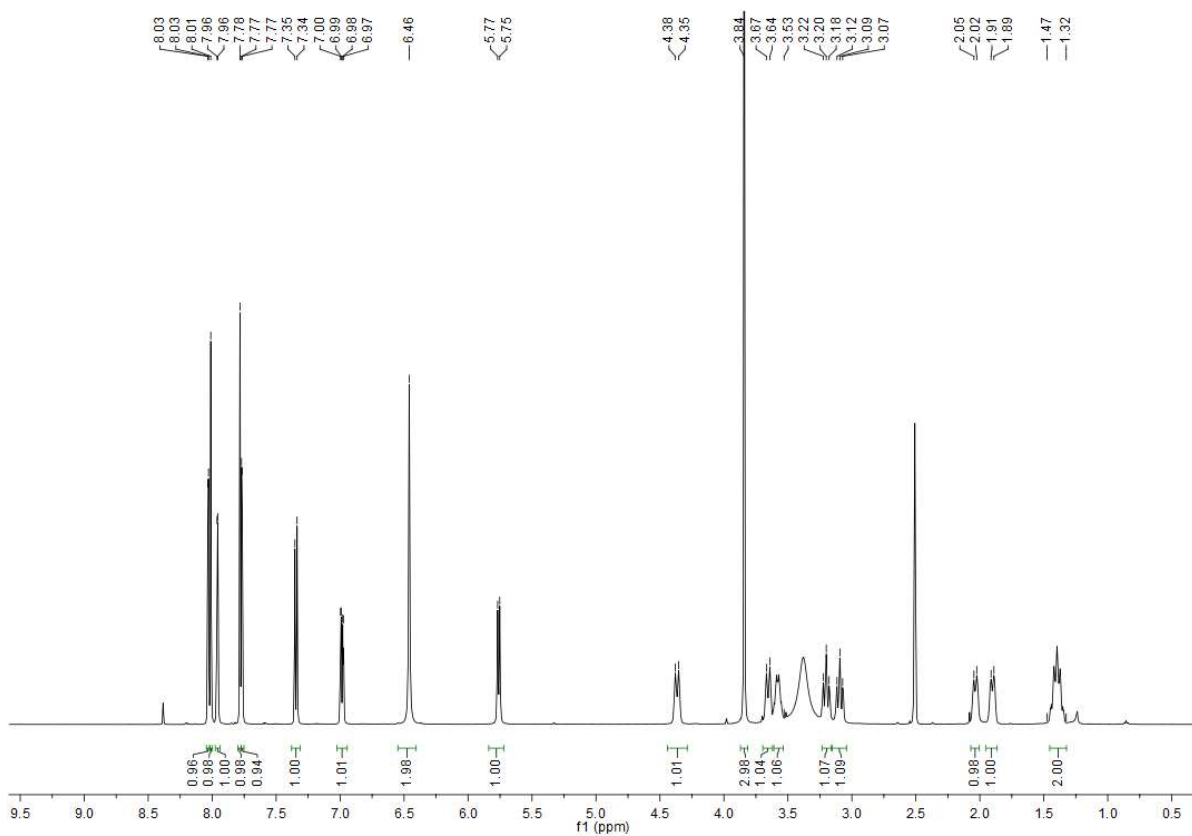


13C



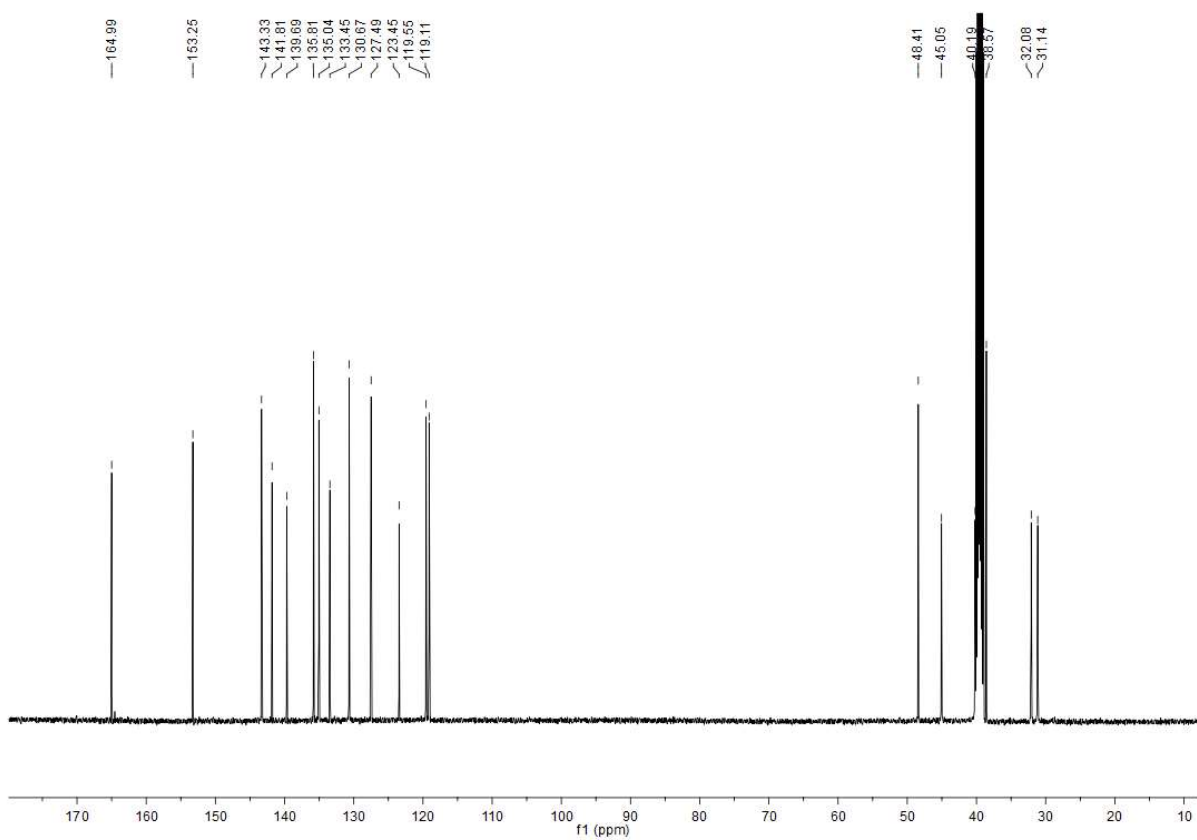
(72)

<sup>1</sup>H



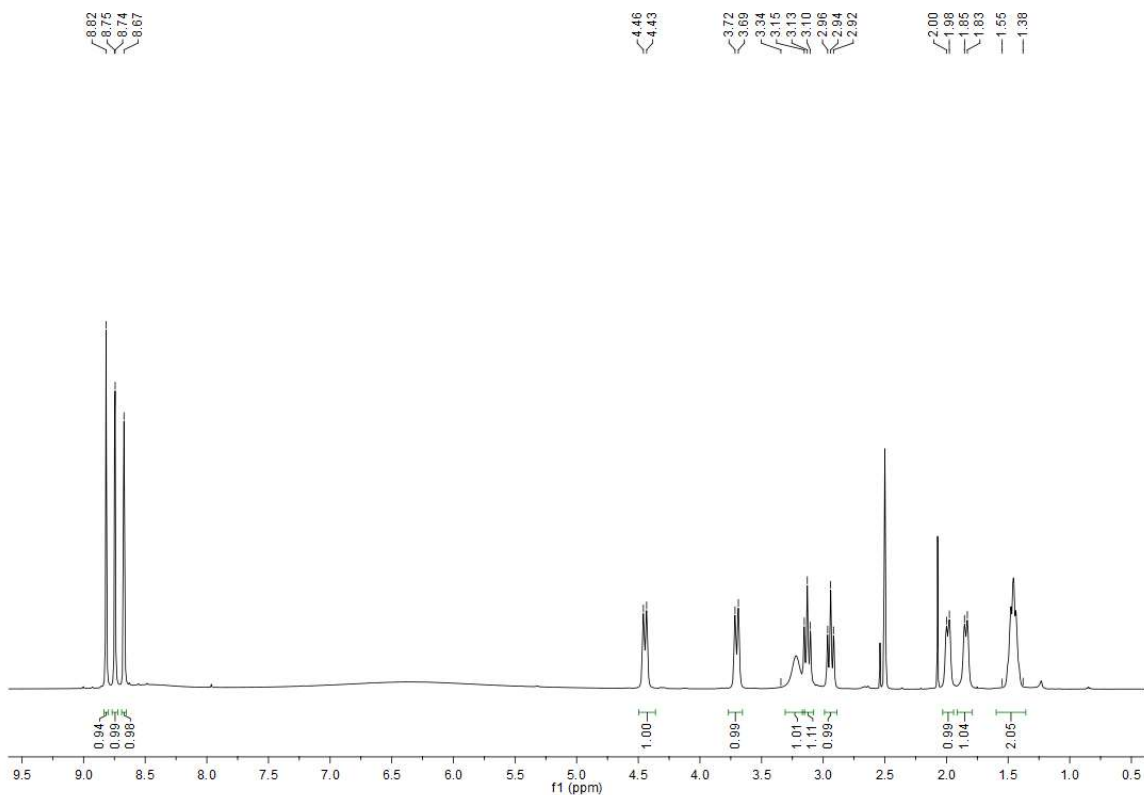


13C

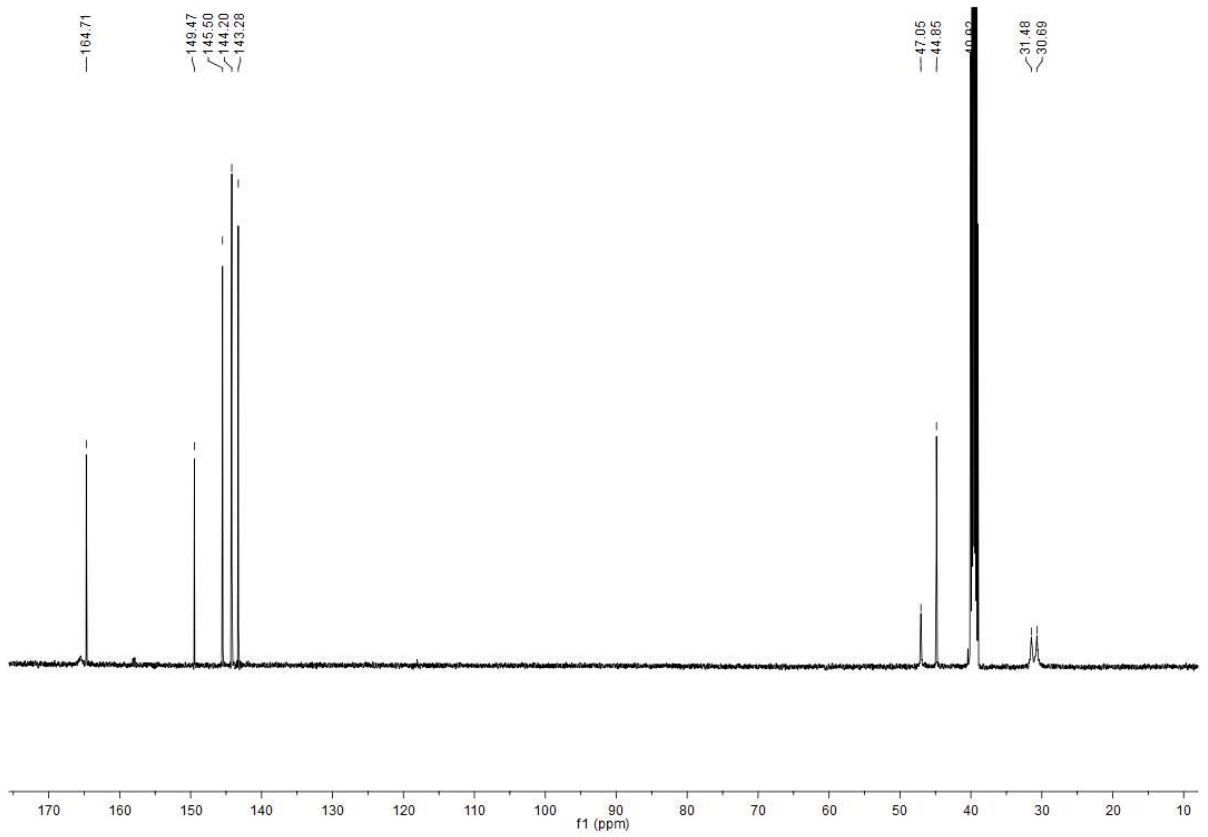


(99)

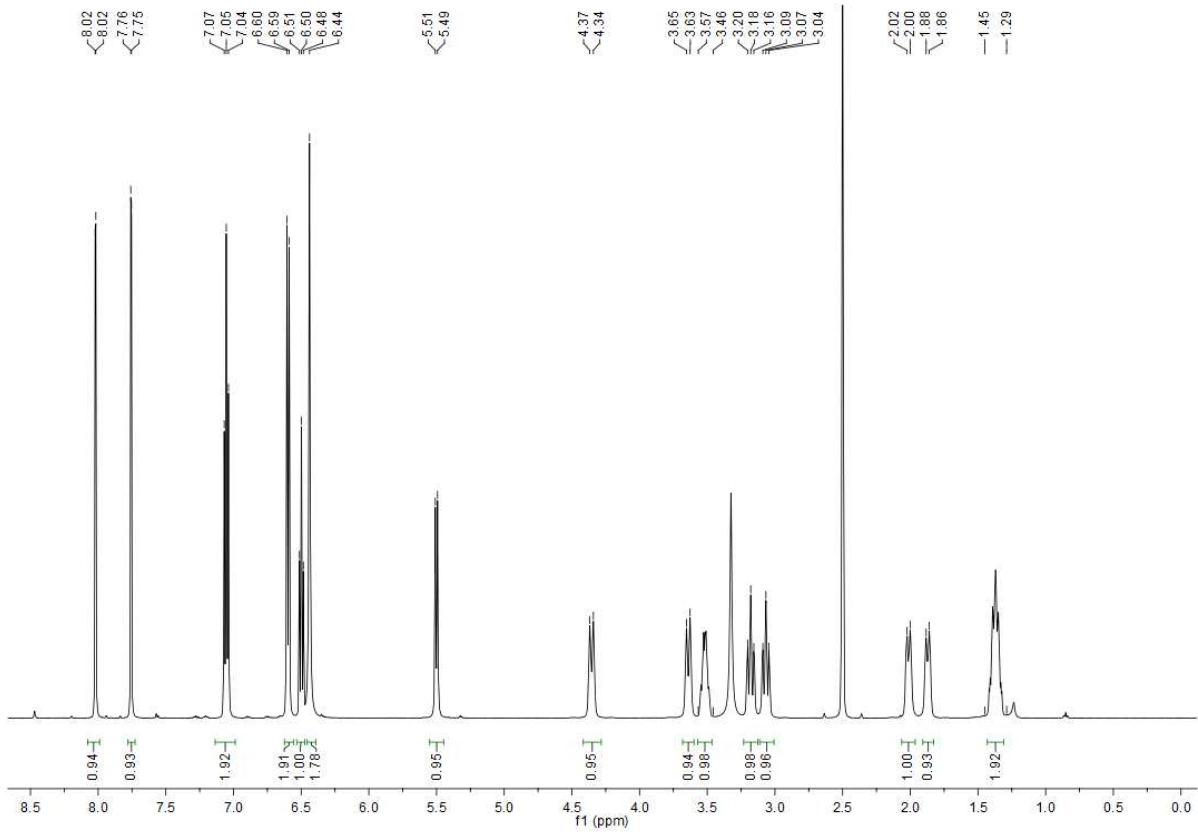
<sup>1</sup>H



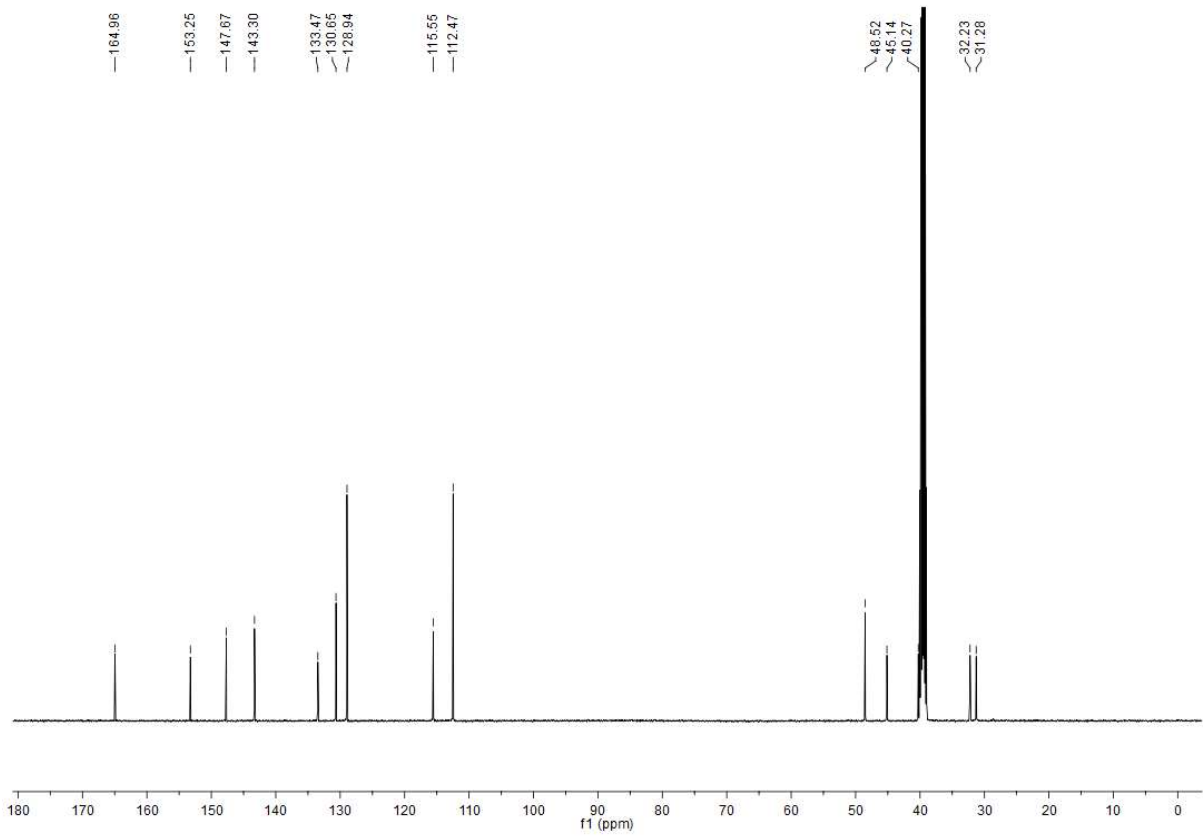
13C



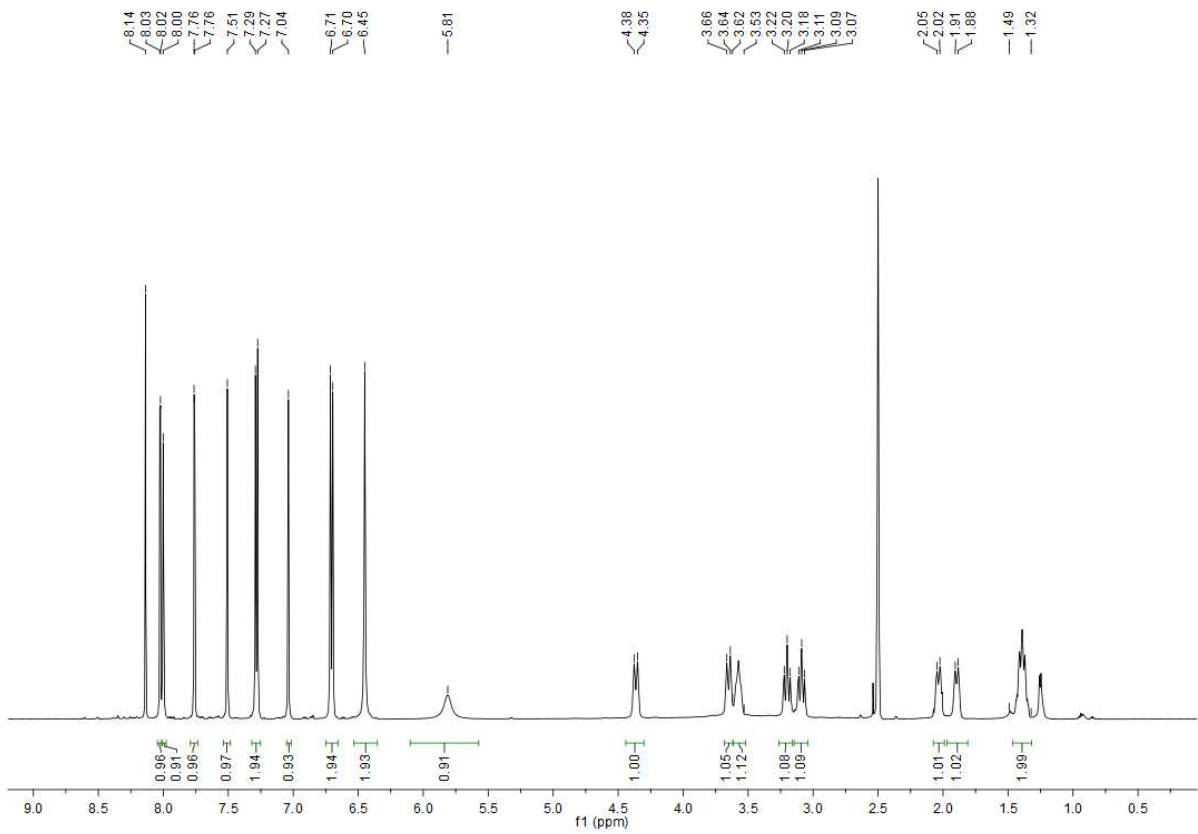
(53)



13C

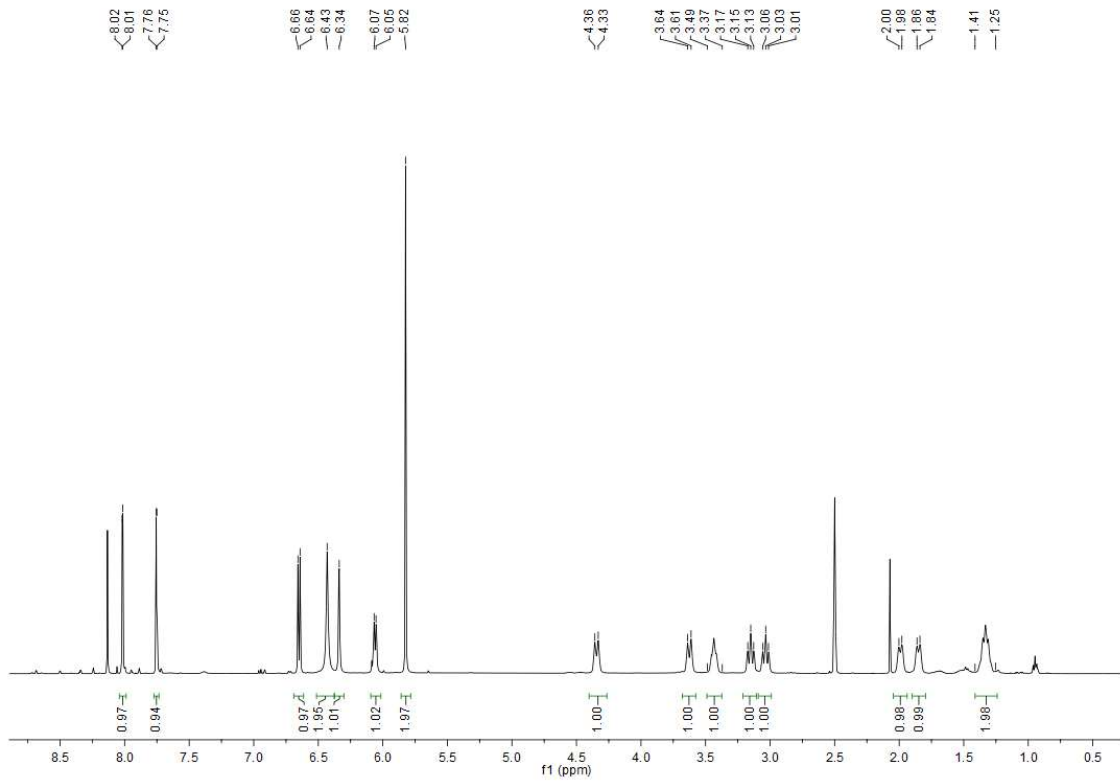


(55)

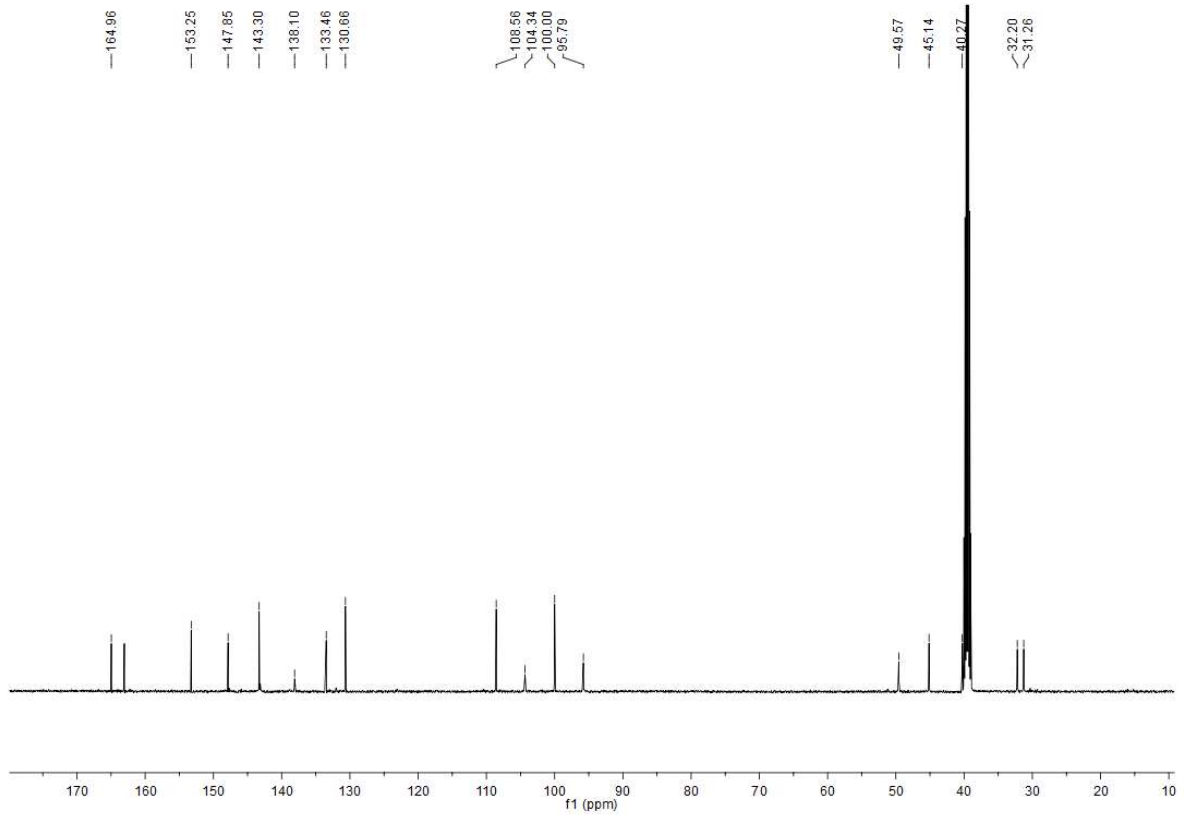


(52)

# 1H

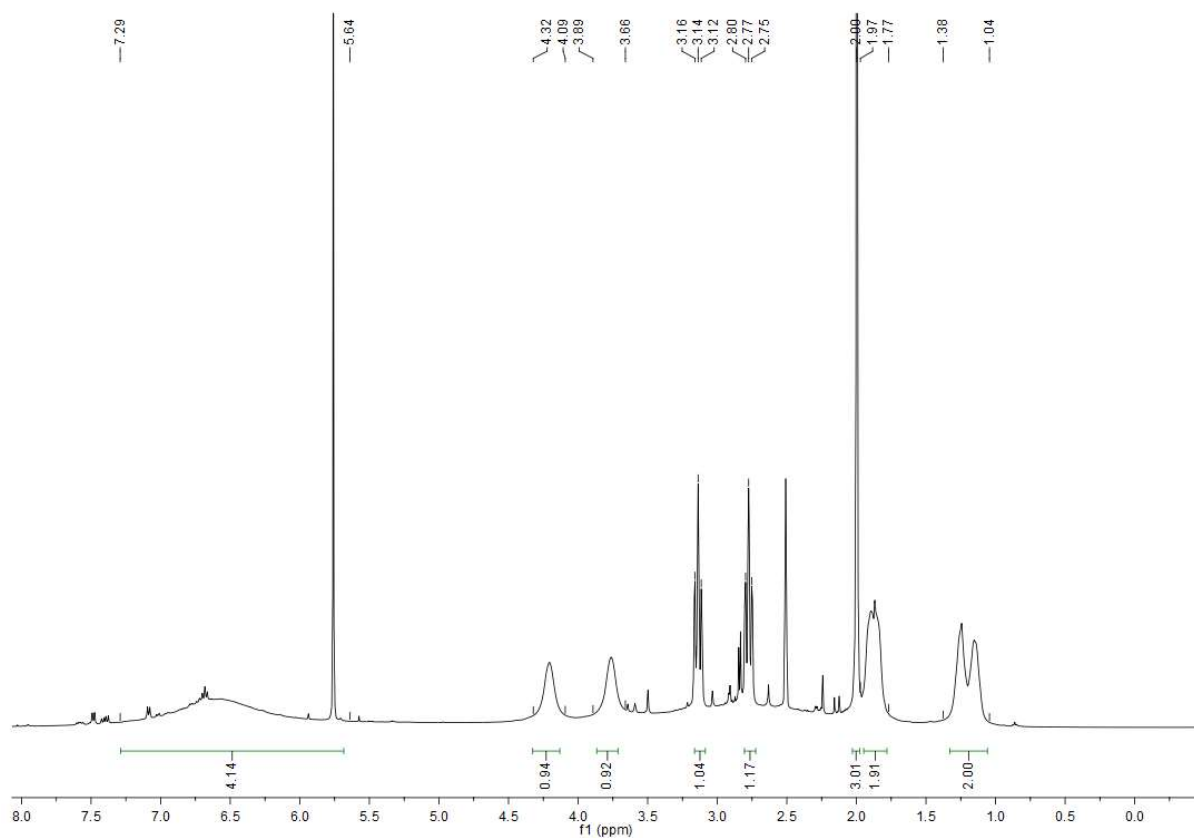


# 13C

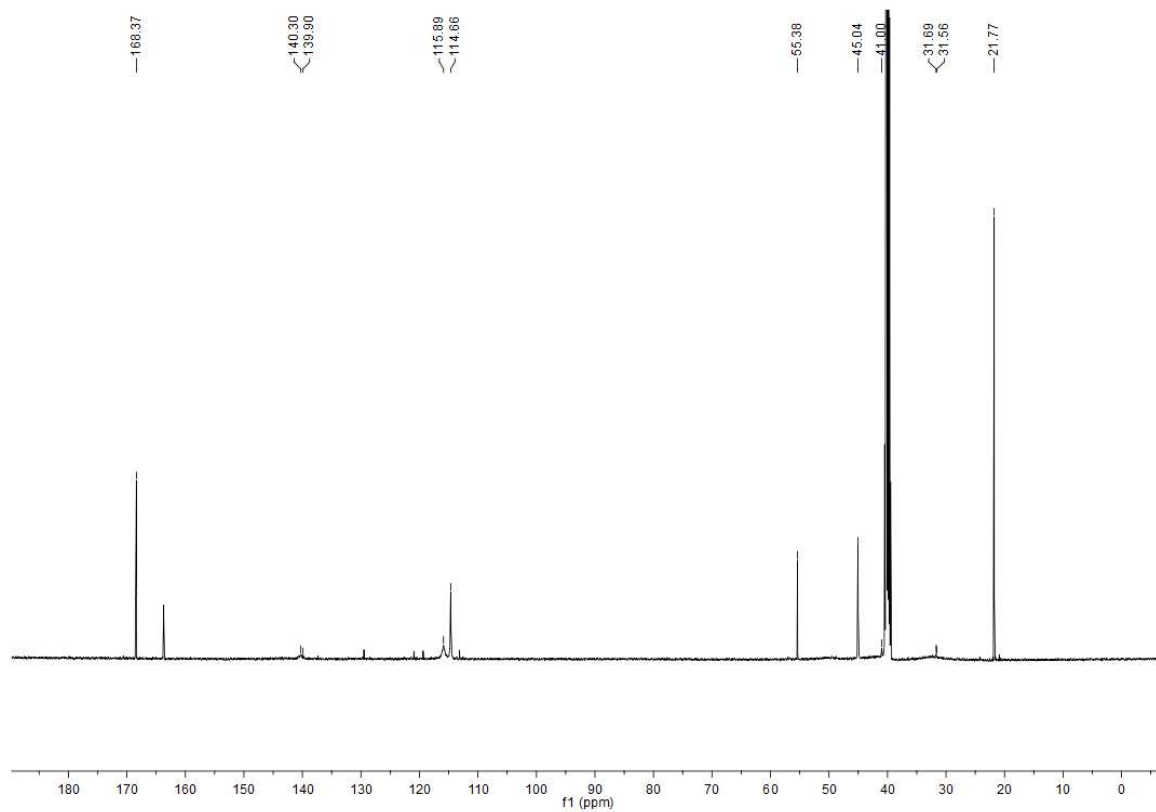


(106)

# 1H

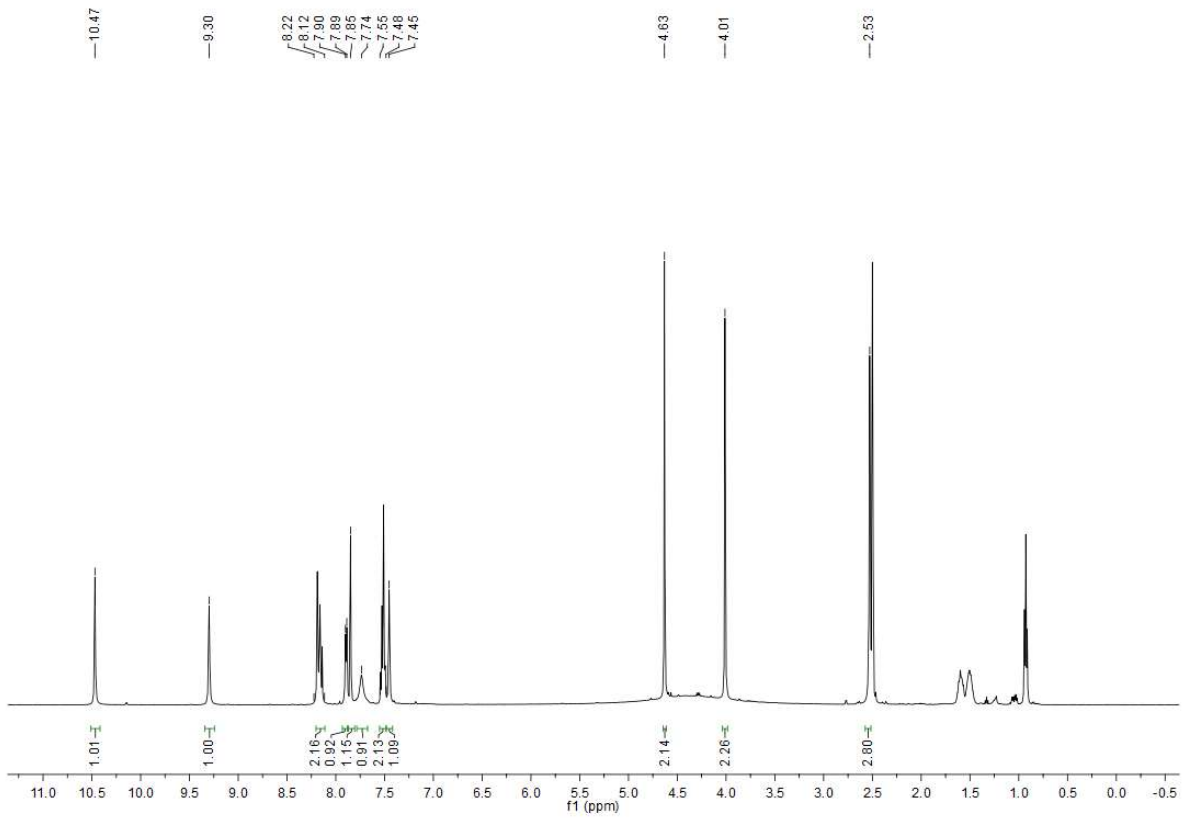


# 13C

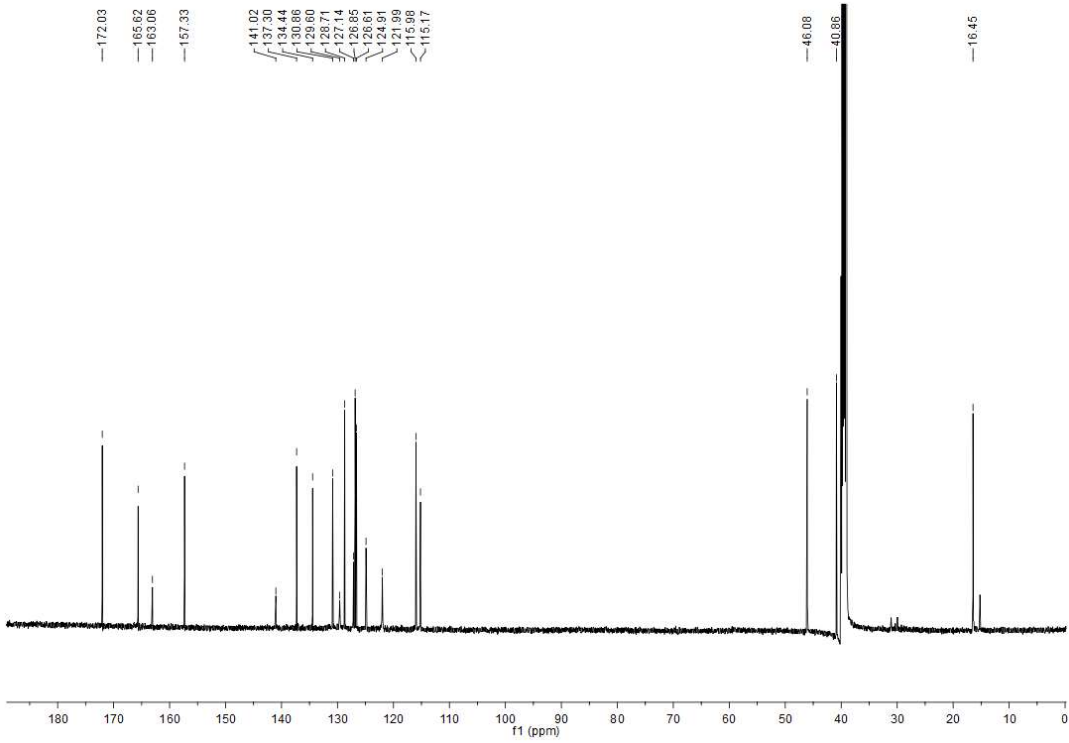


(7)

# 1H

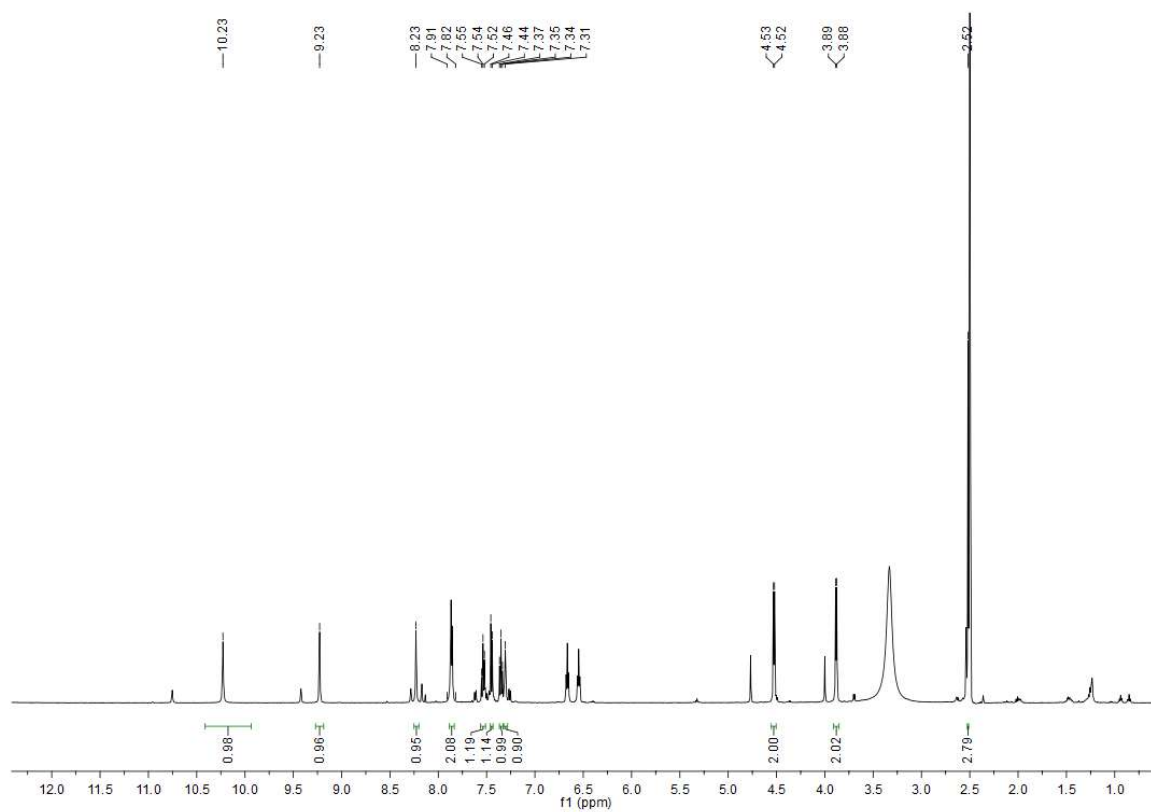


# 13C

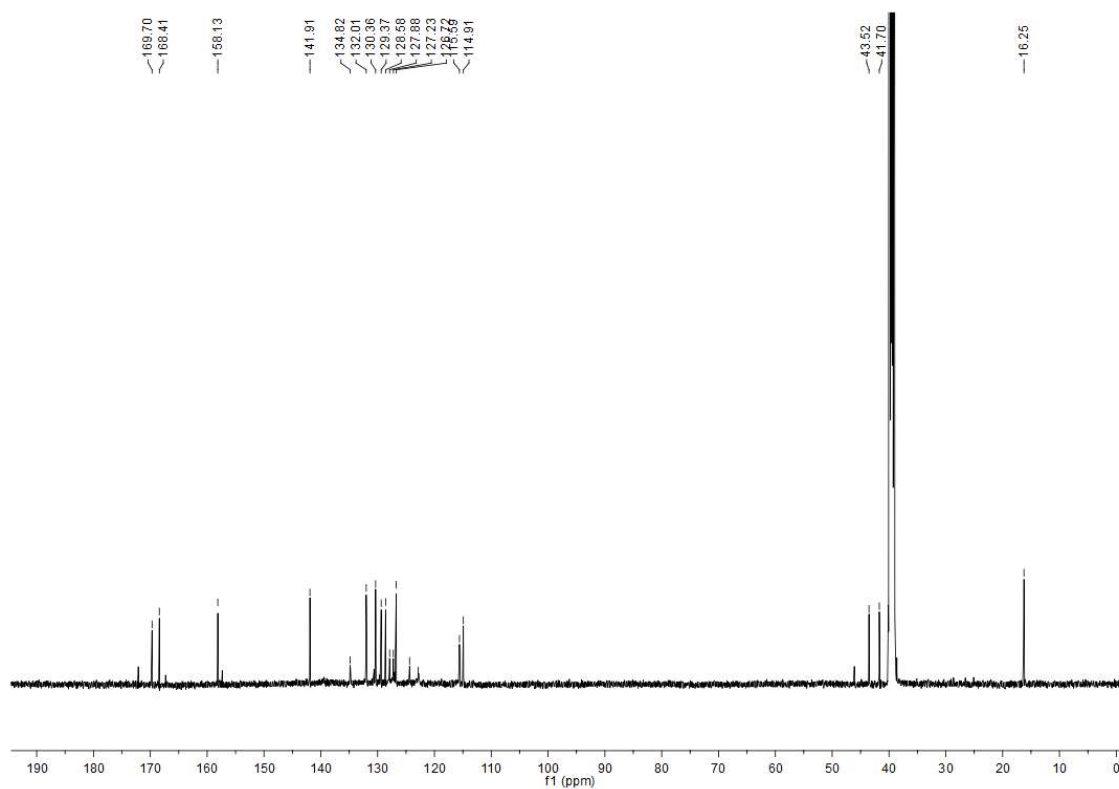


(47)

<sup>1</sup>H

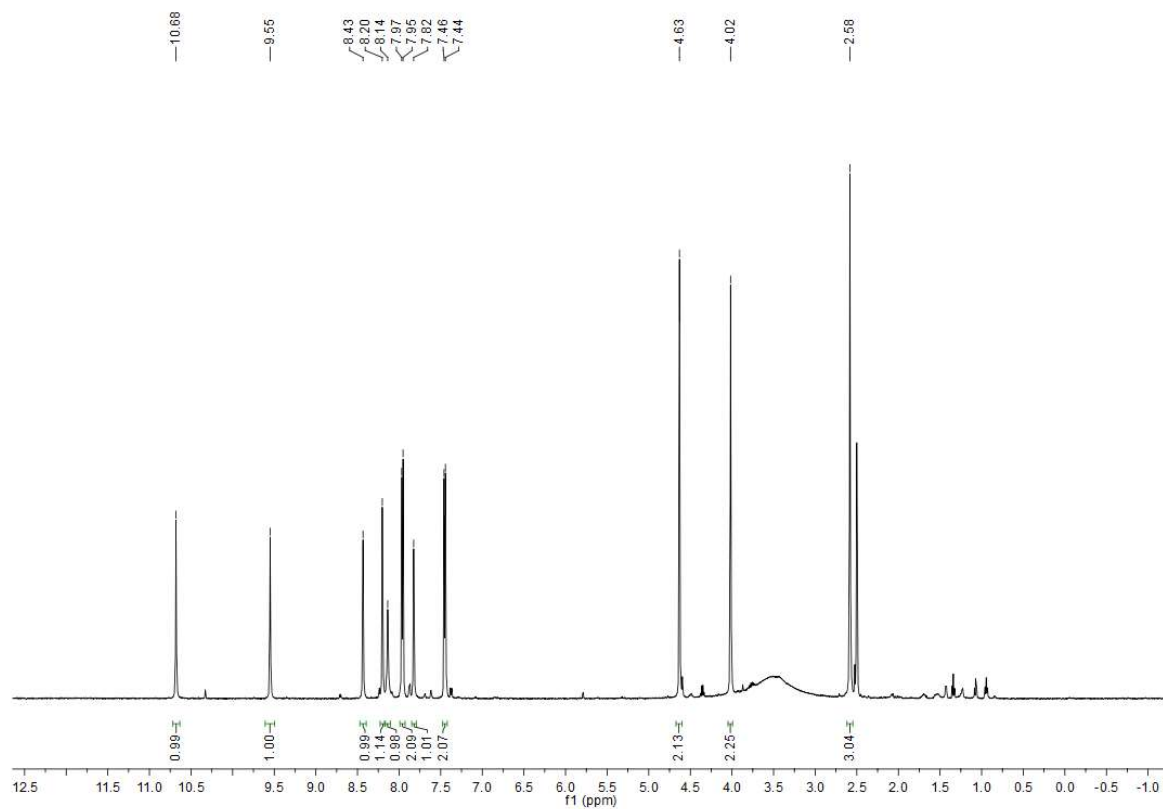


13C

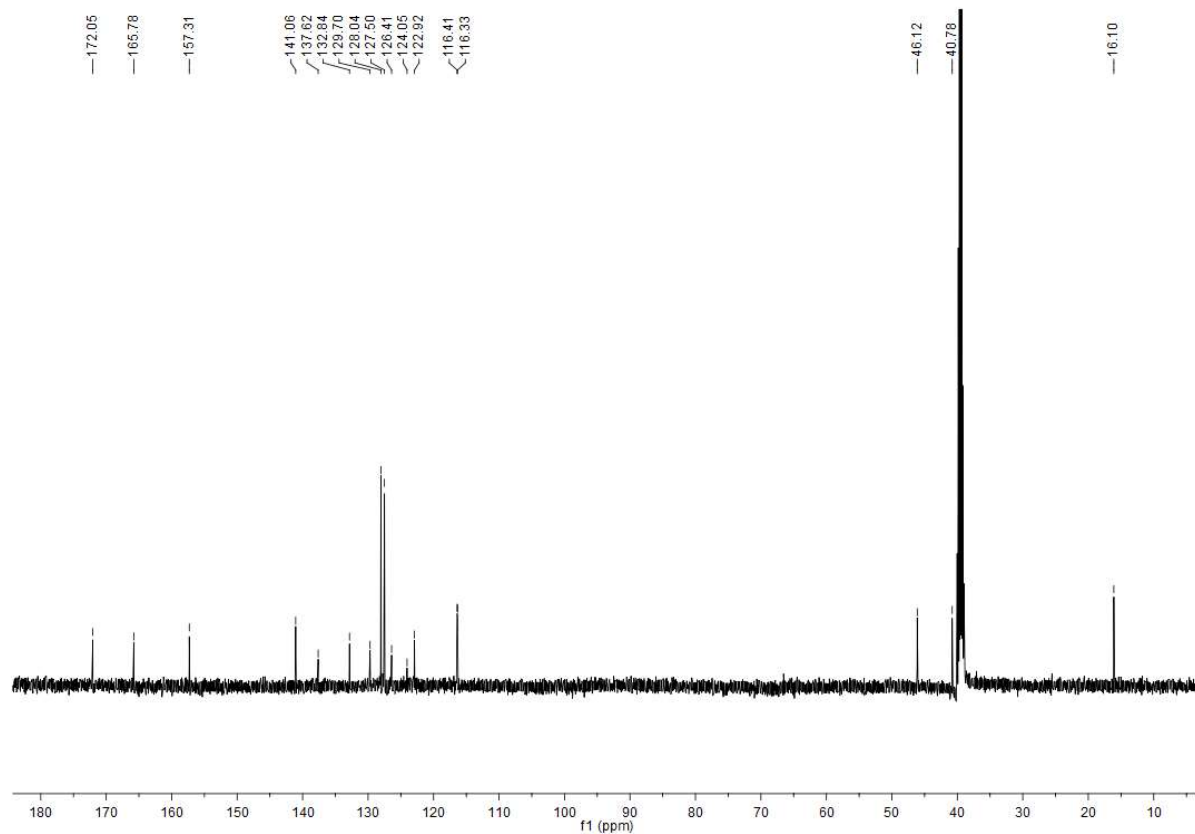


(40)

<sup>1</sup>H



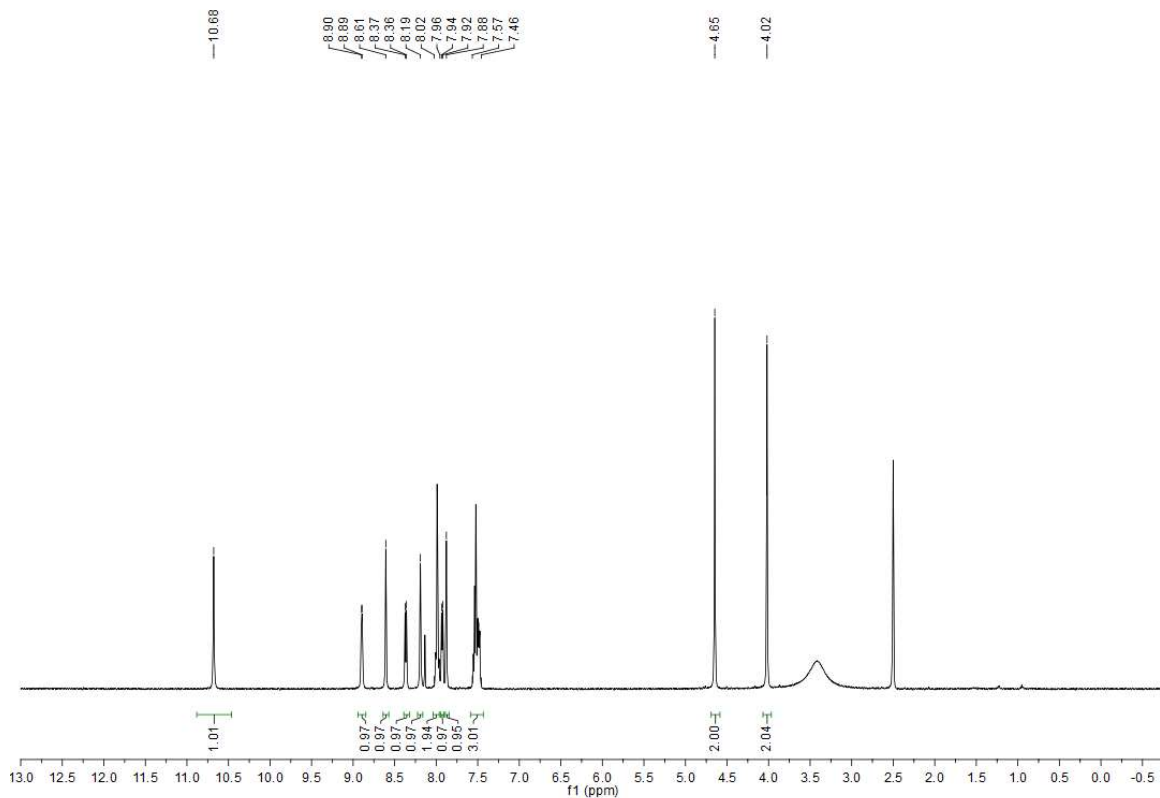
<sup>13</sup>C



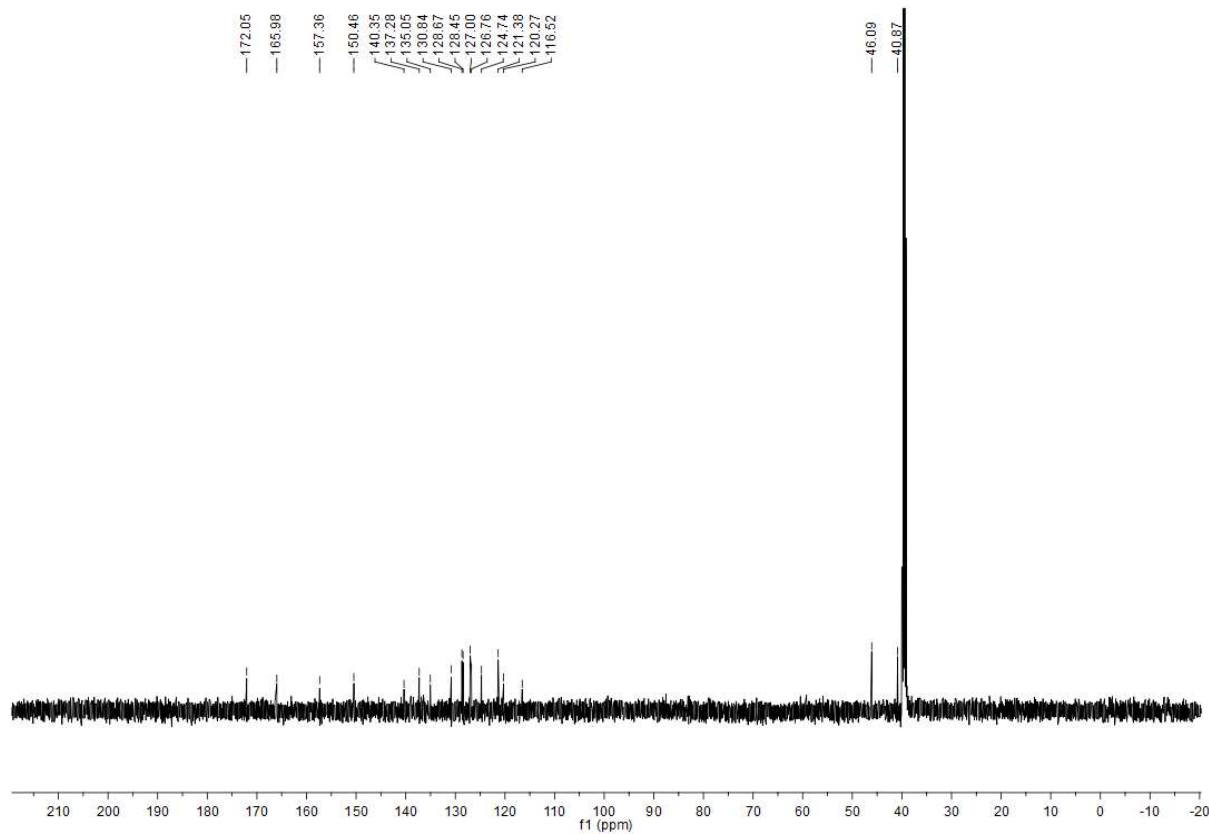


(82)

<sup>1</sup>H

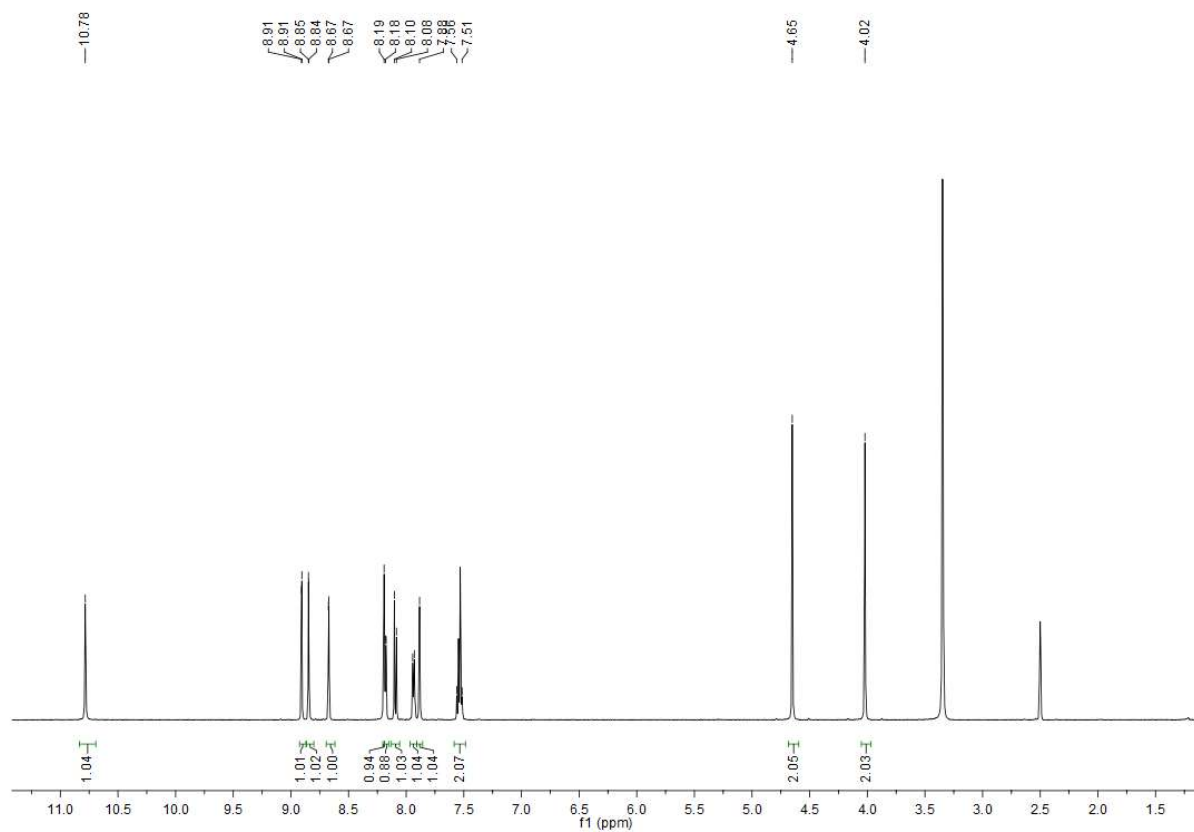


13C

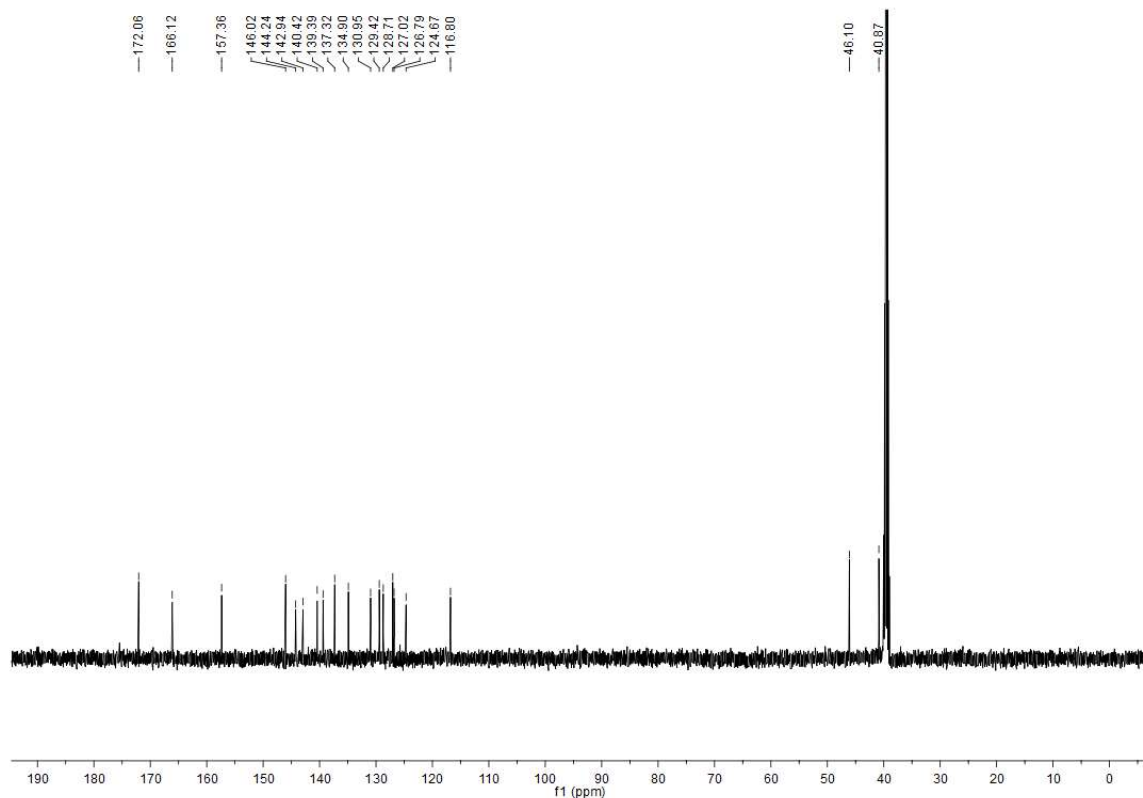


(83)

<sup>1</sup>H

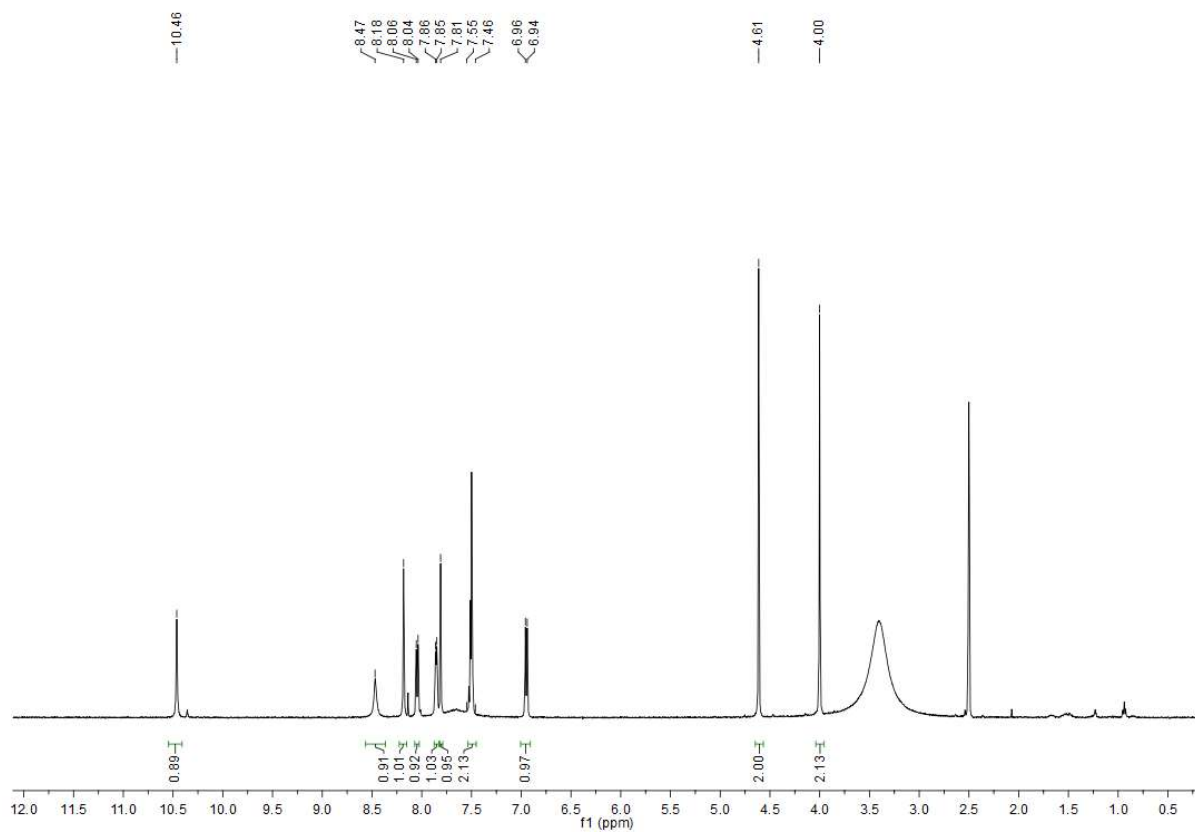


<sup>13</sup>C

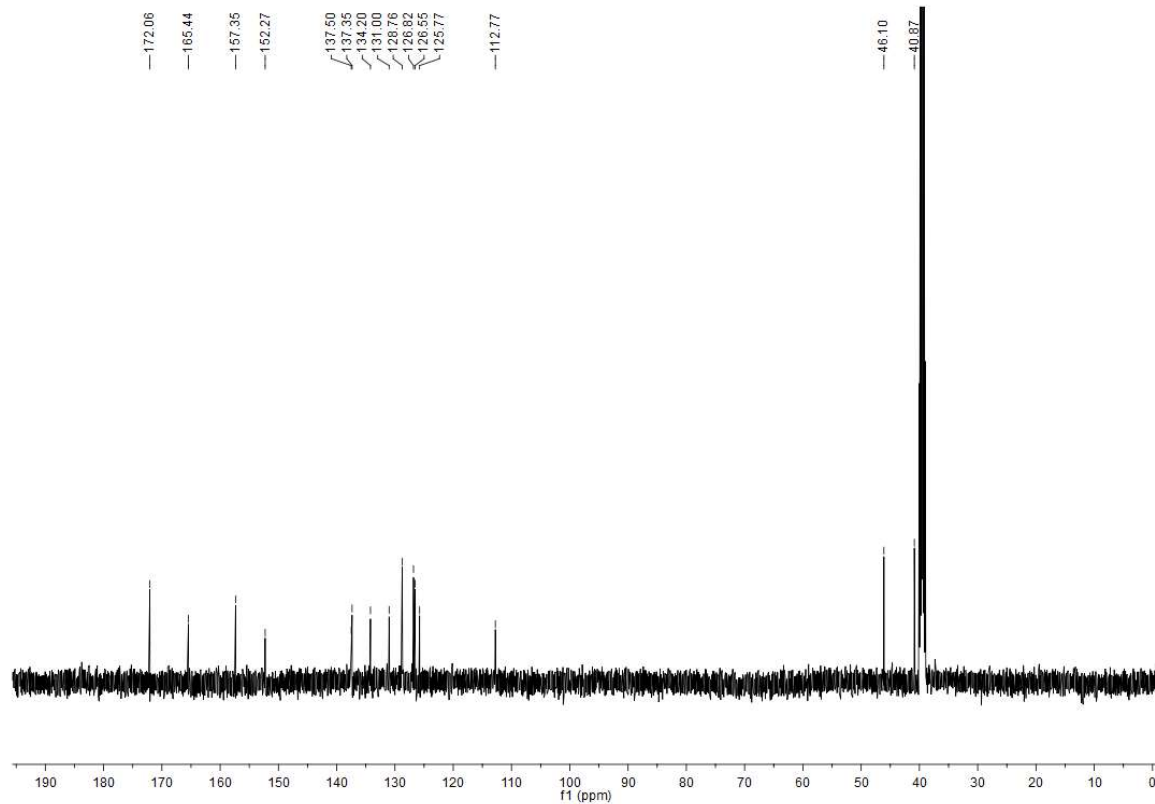


(84)

<sup>1</sup>H

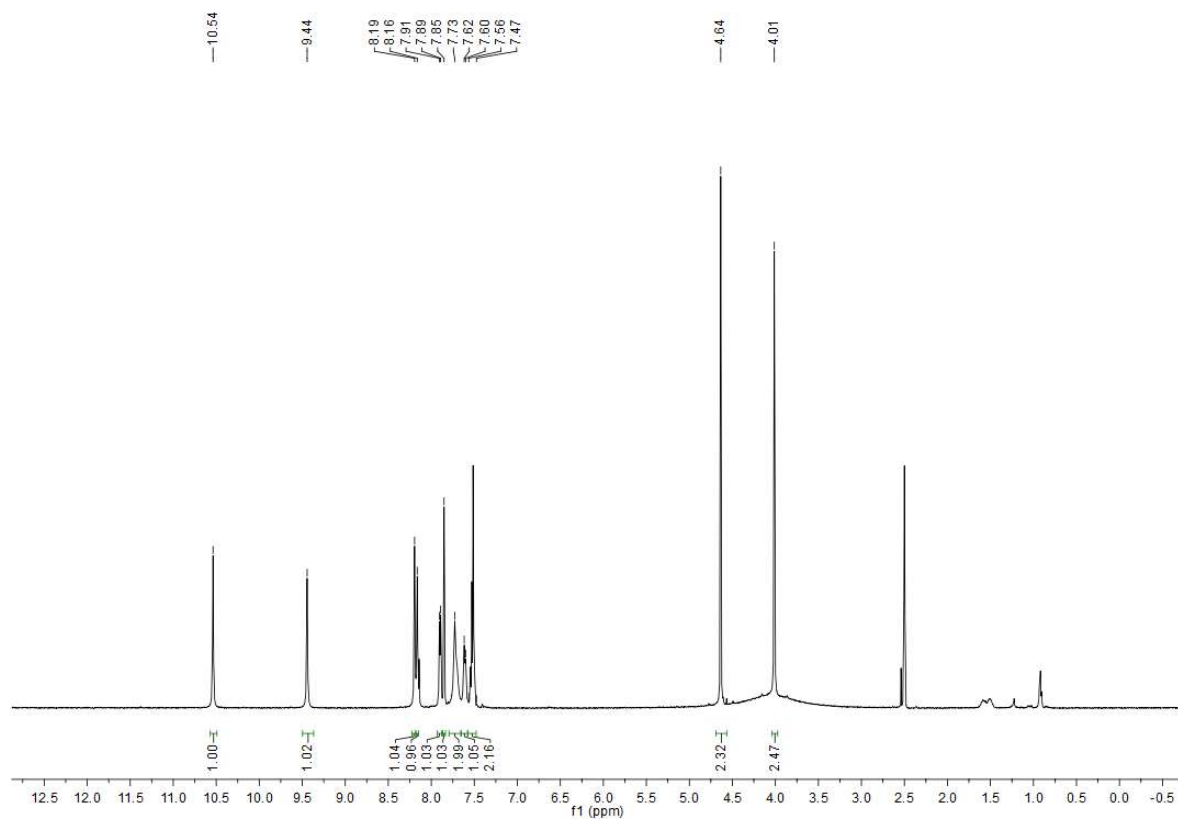


13C

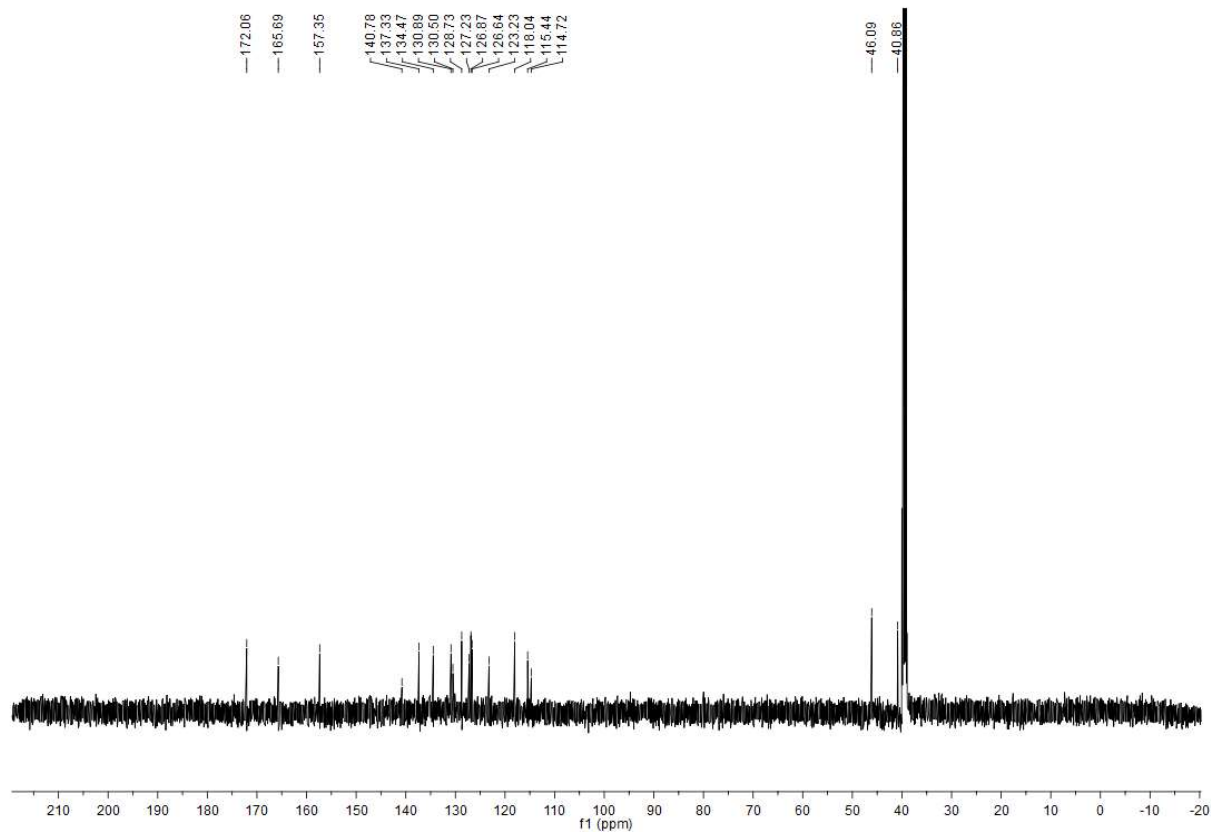


(86)

<sup>1</sup>H

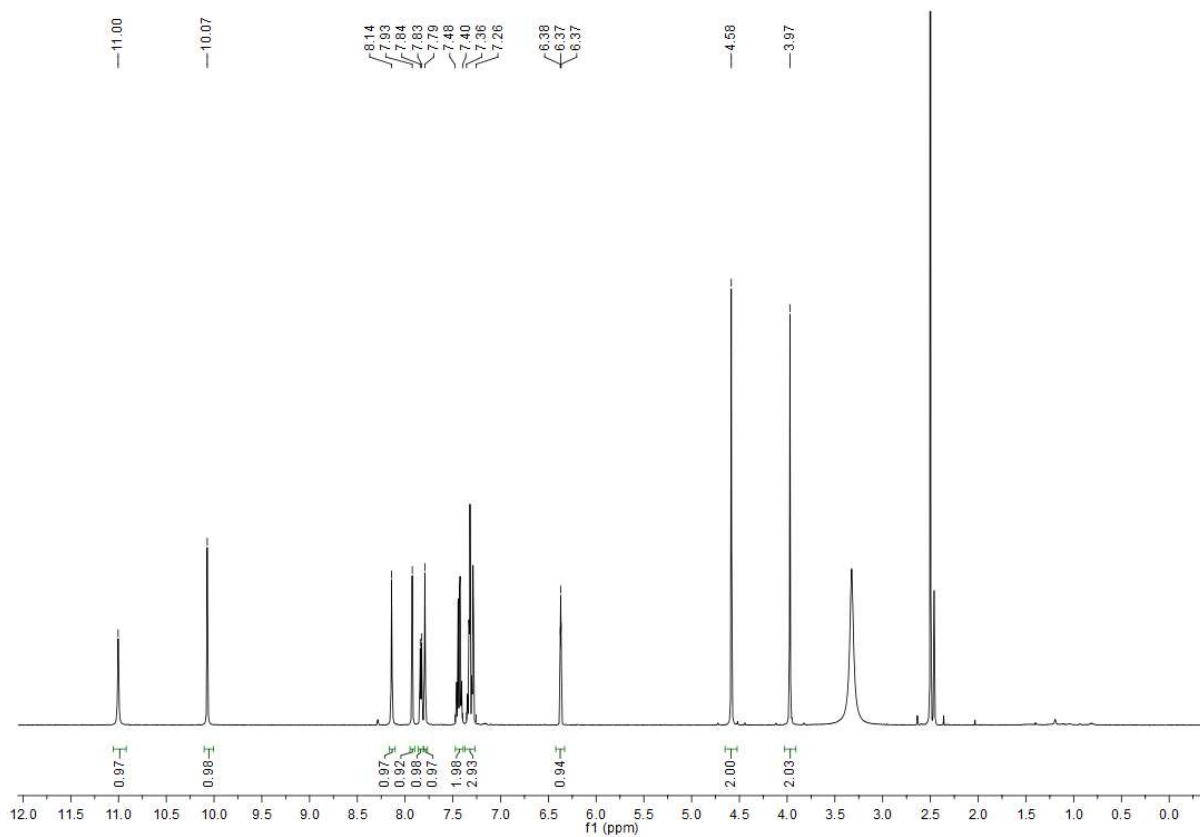


<sup>13</sup>C

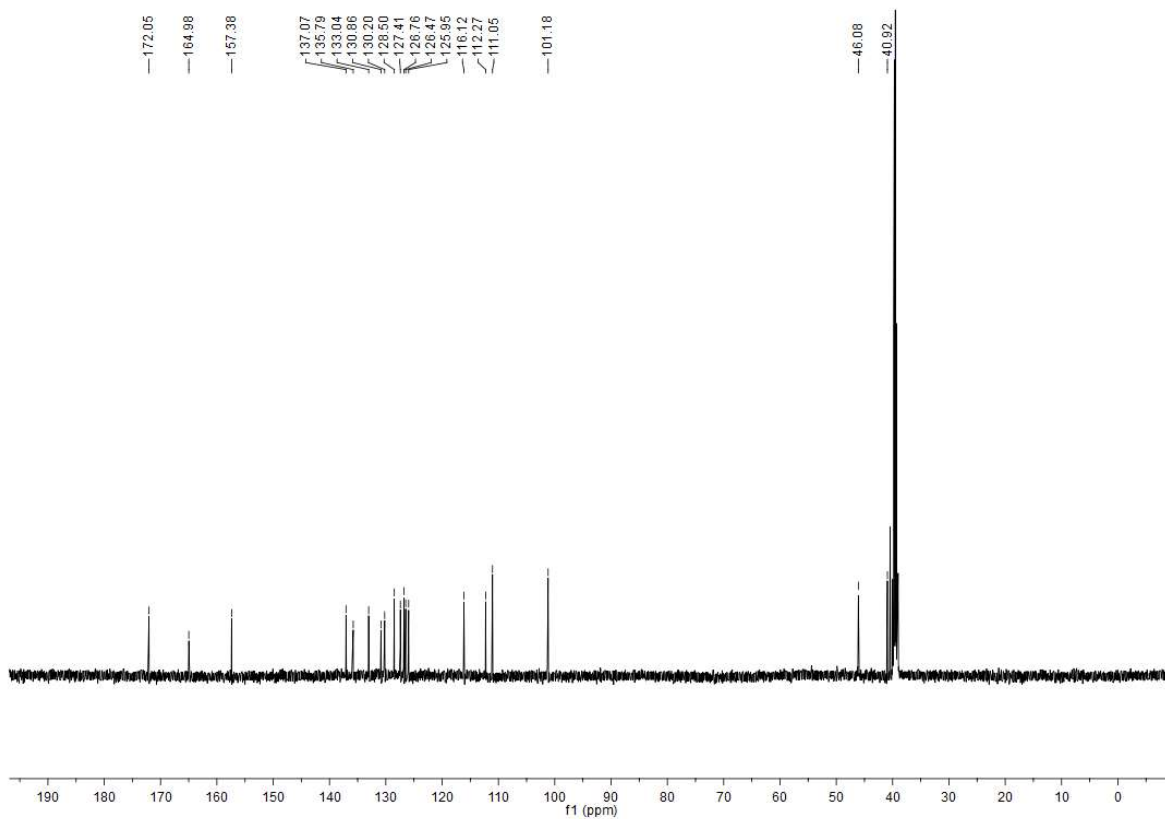


(87)

<sup>1</sup>H

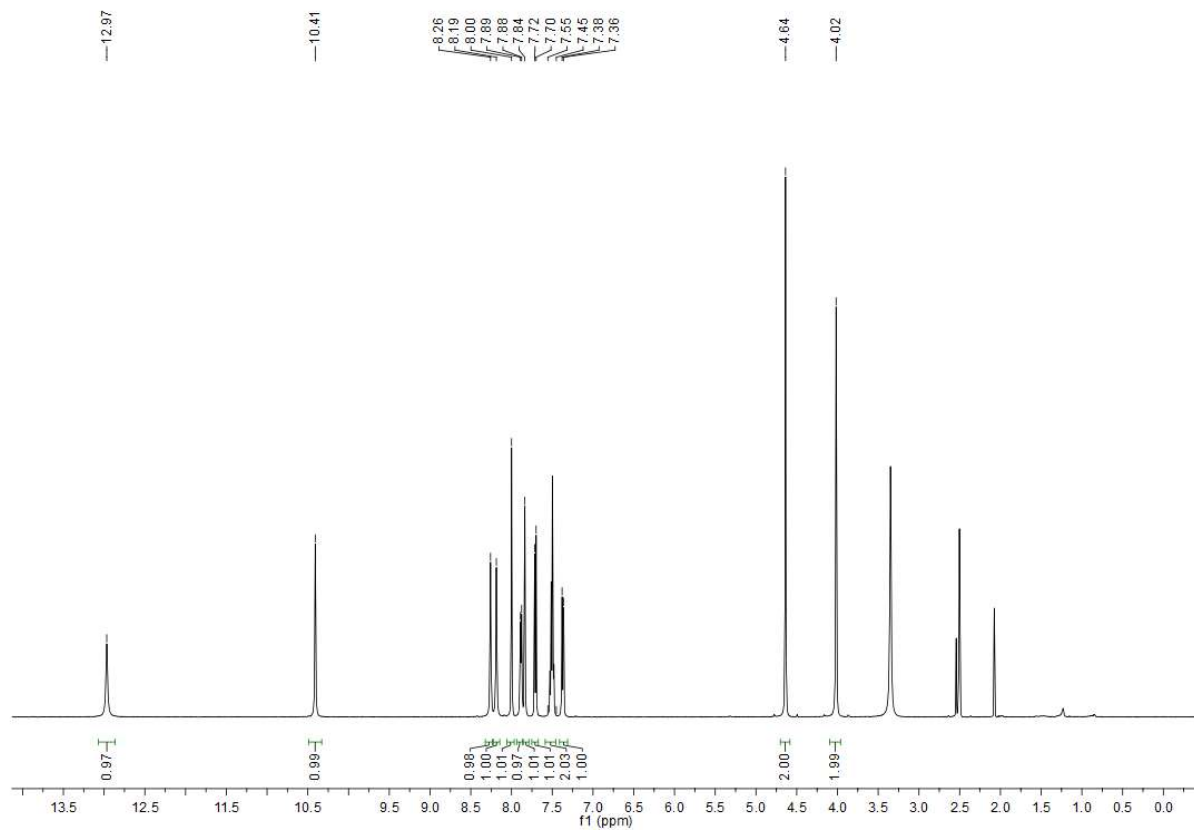


<sup>13</sup>C

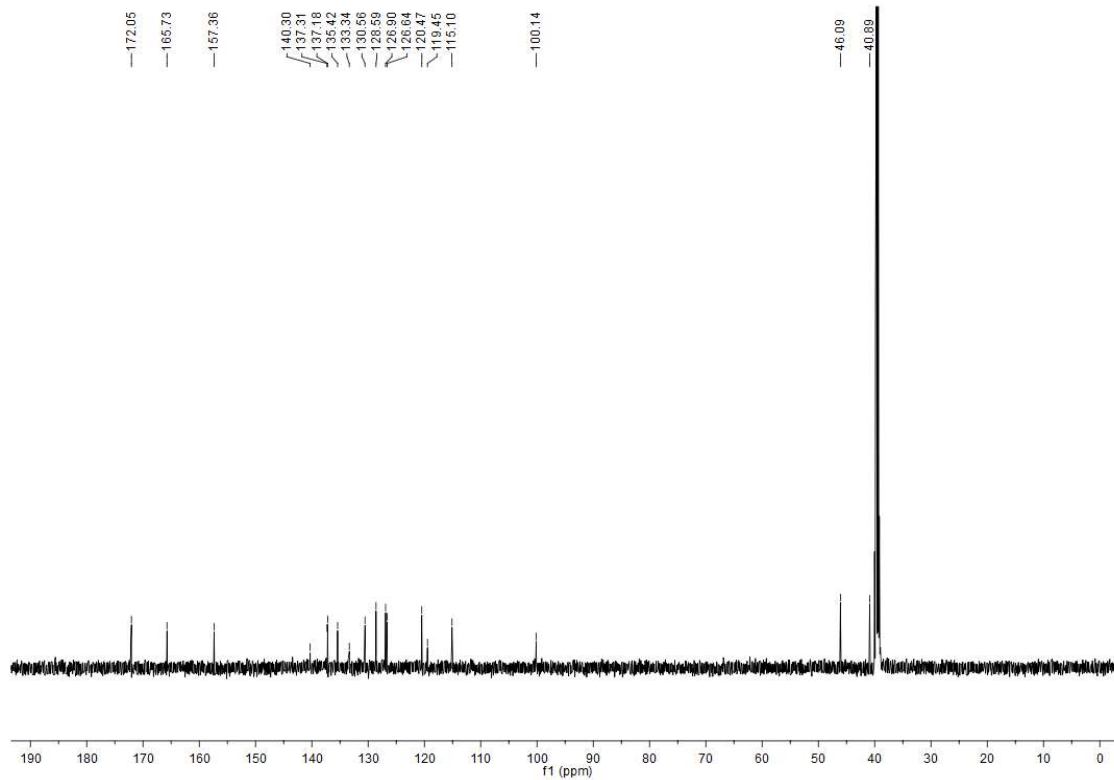


(88)

<sup>1</sup>H

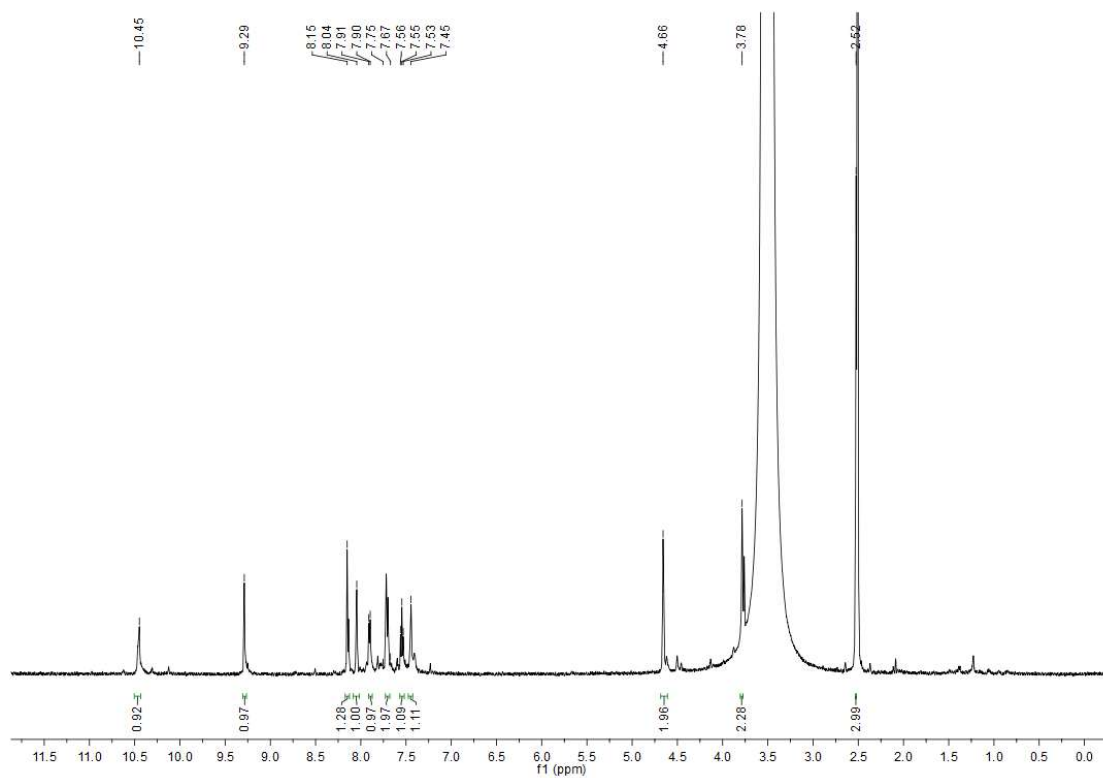


<sup>13</sup>C



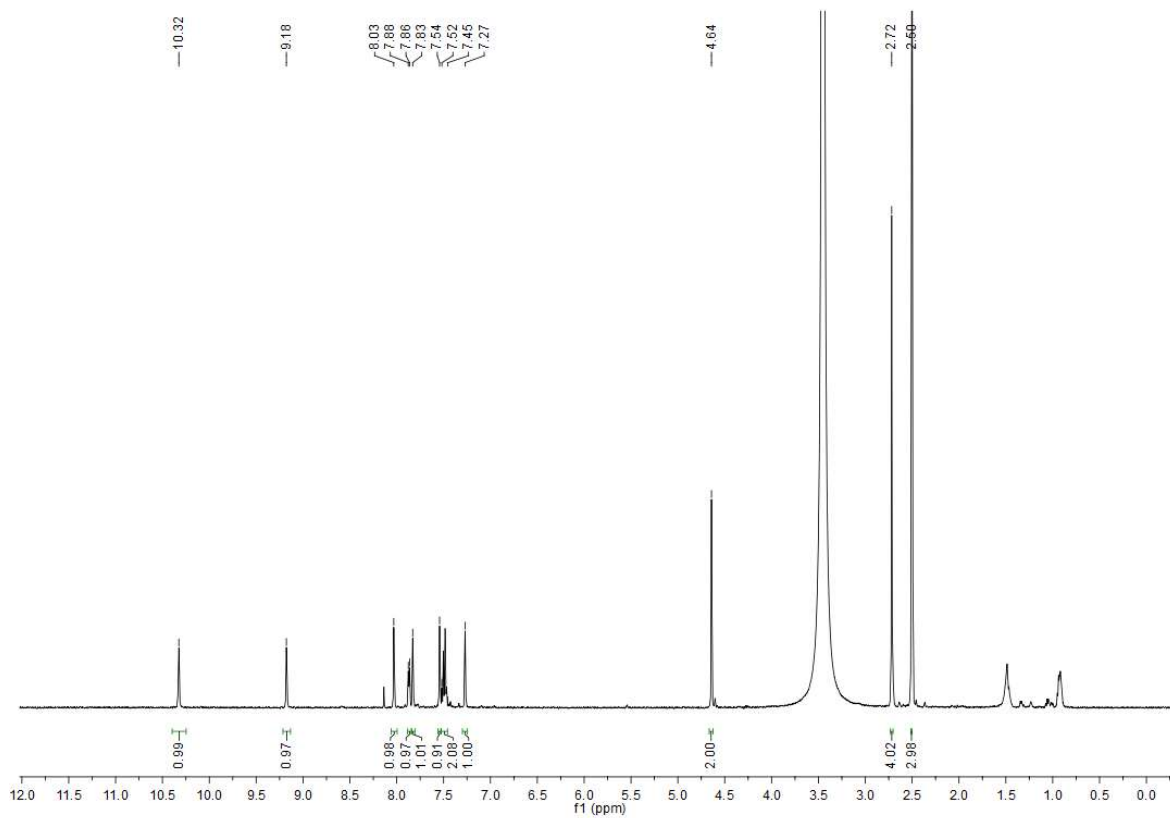
(77)

<sup>1</sup>H

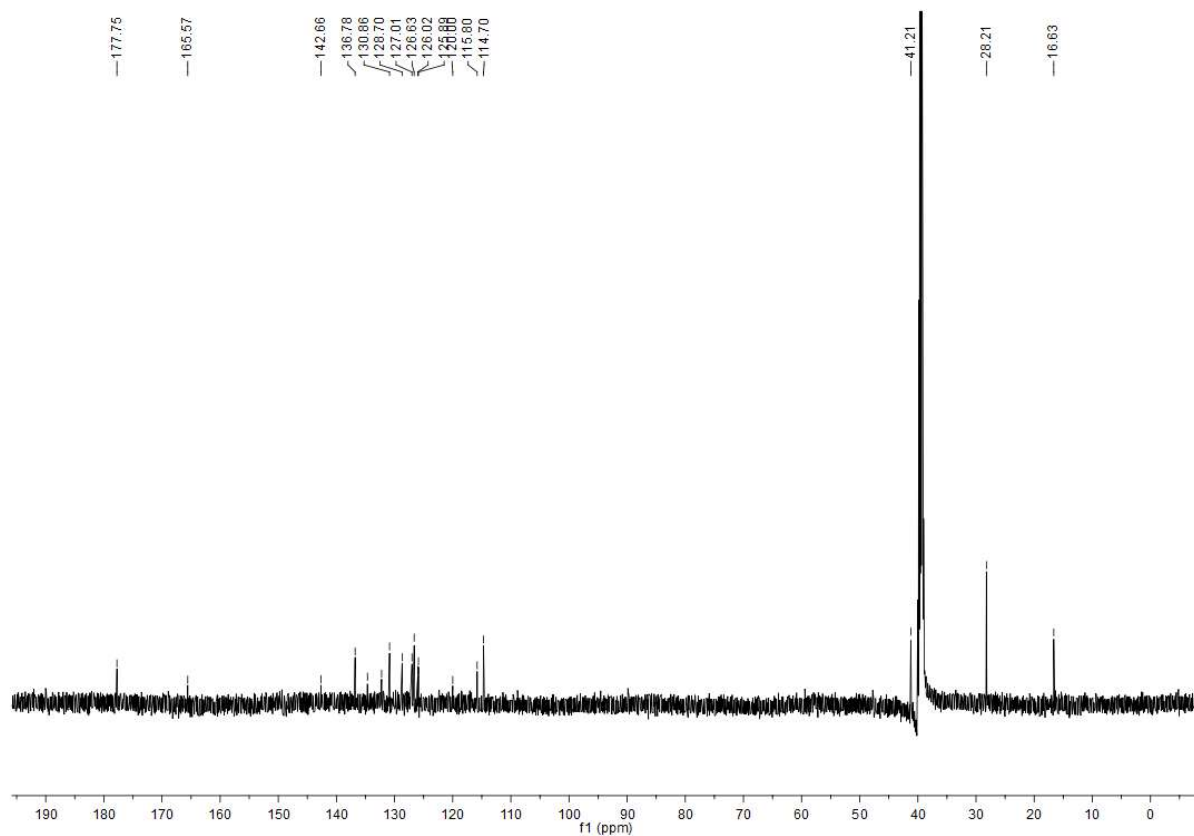


(80)

<sup>1</sup>H

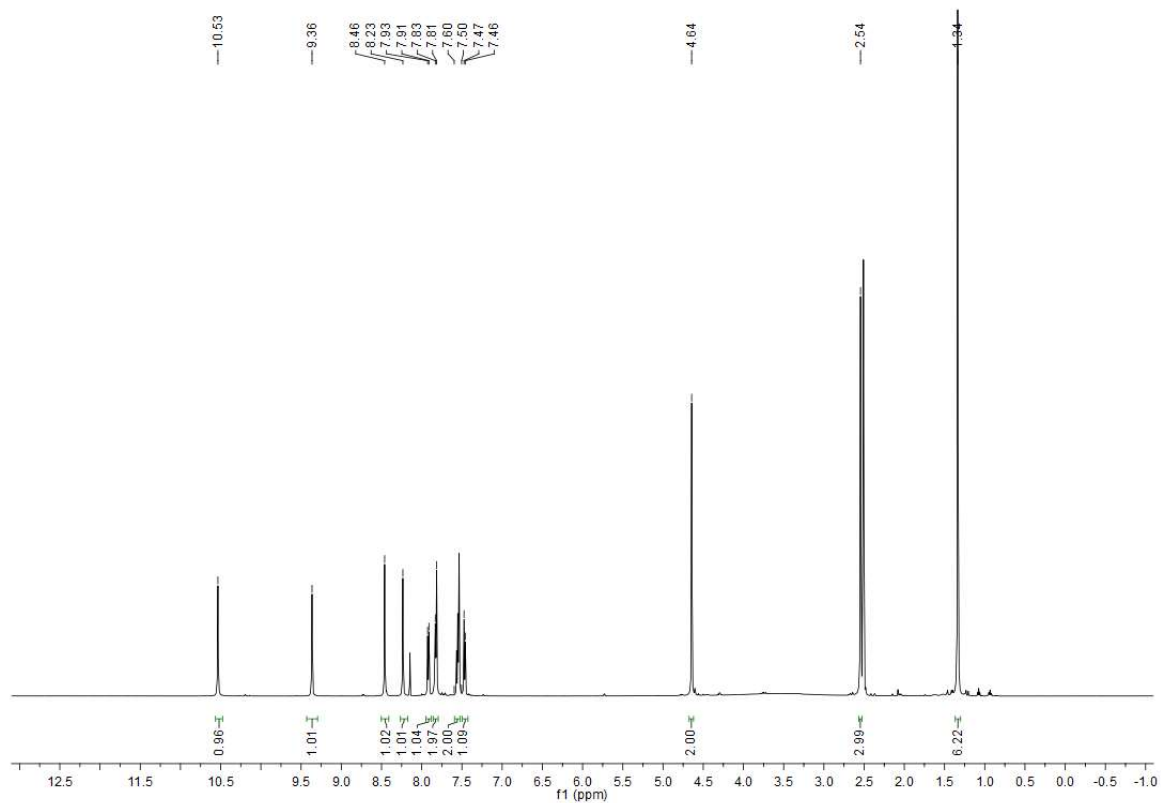


13C



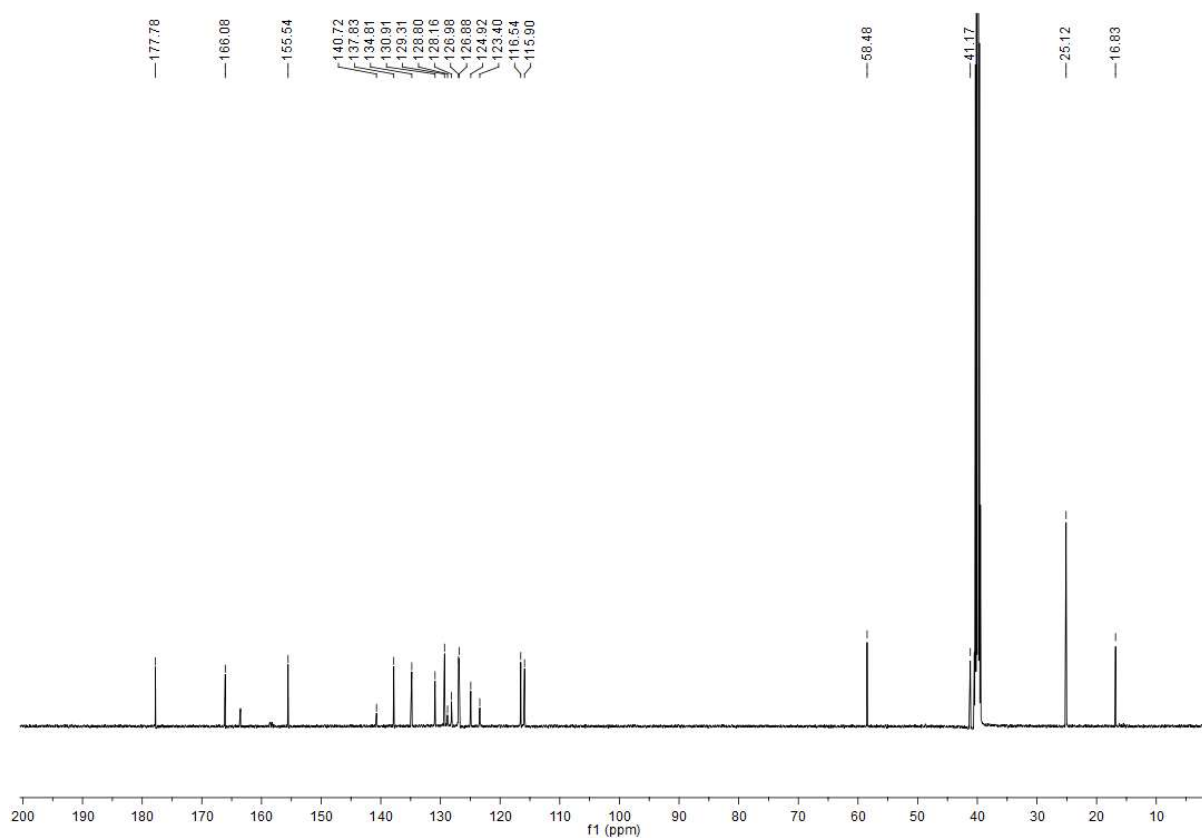
(78)

<sup>1</sup>H



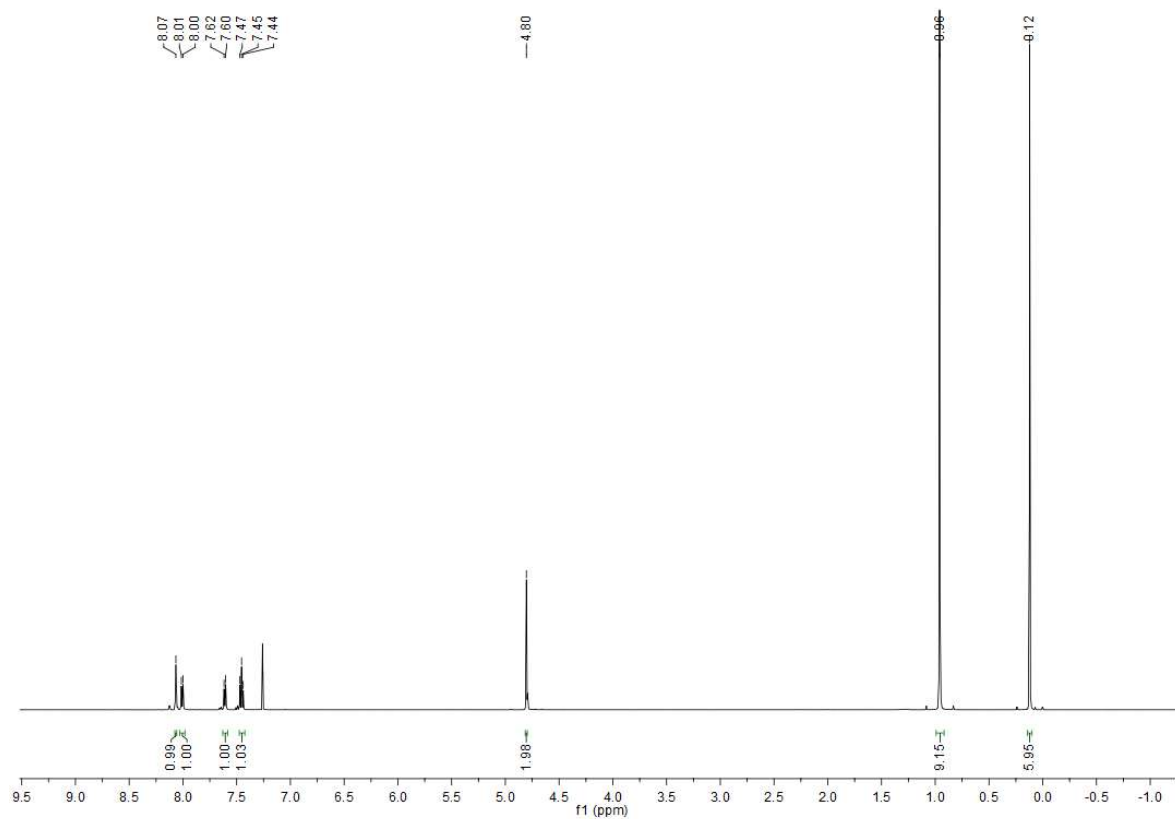


13C

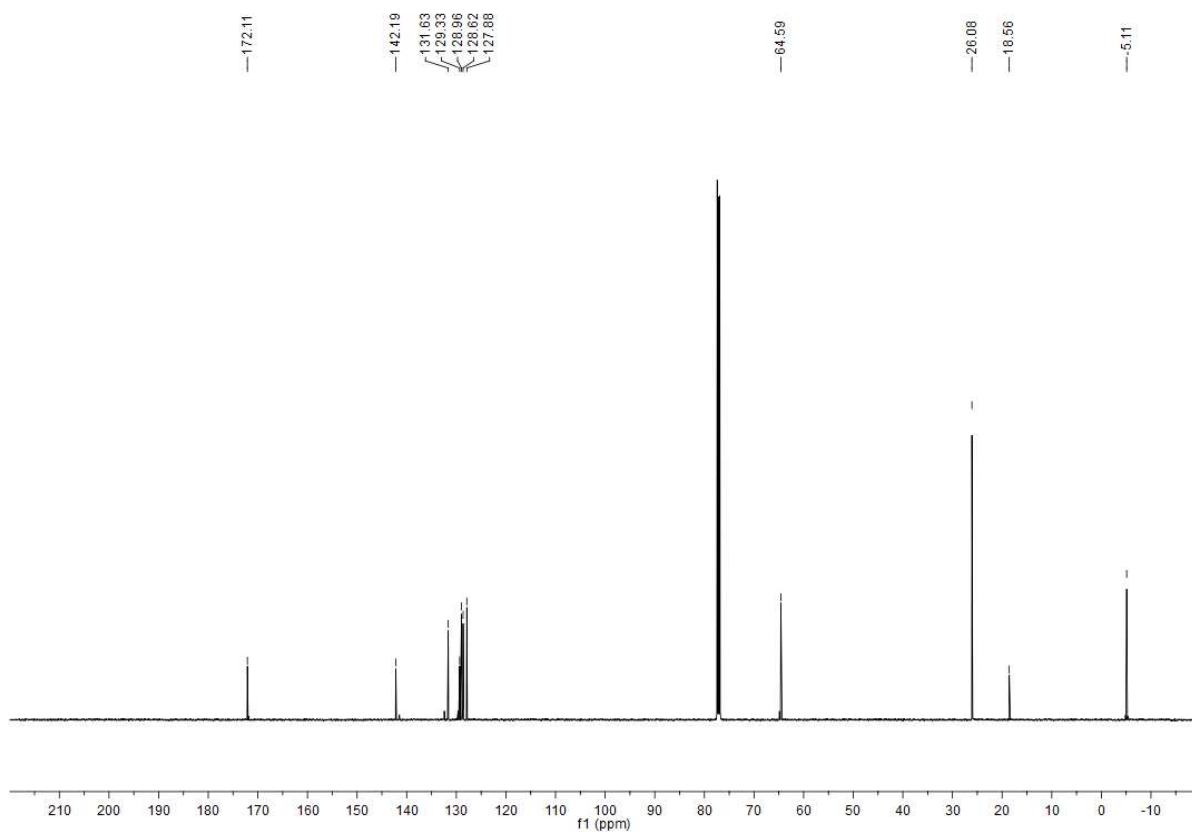


(154)

1H

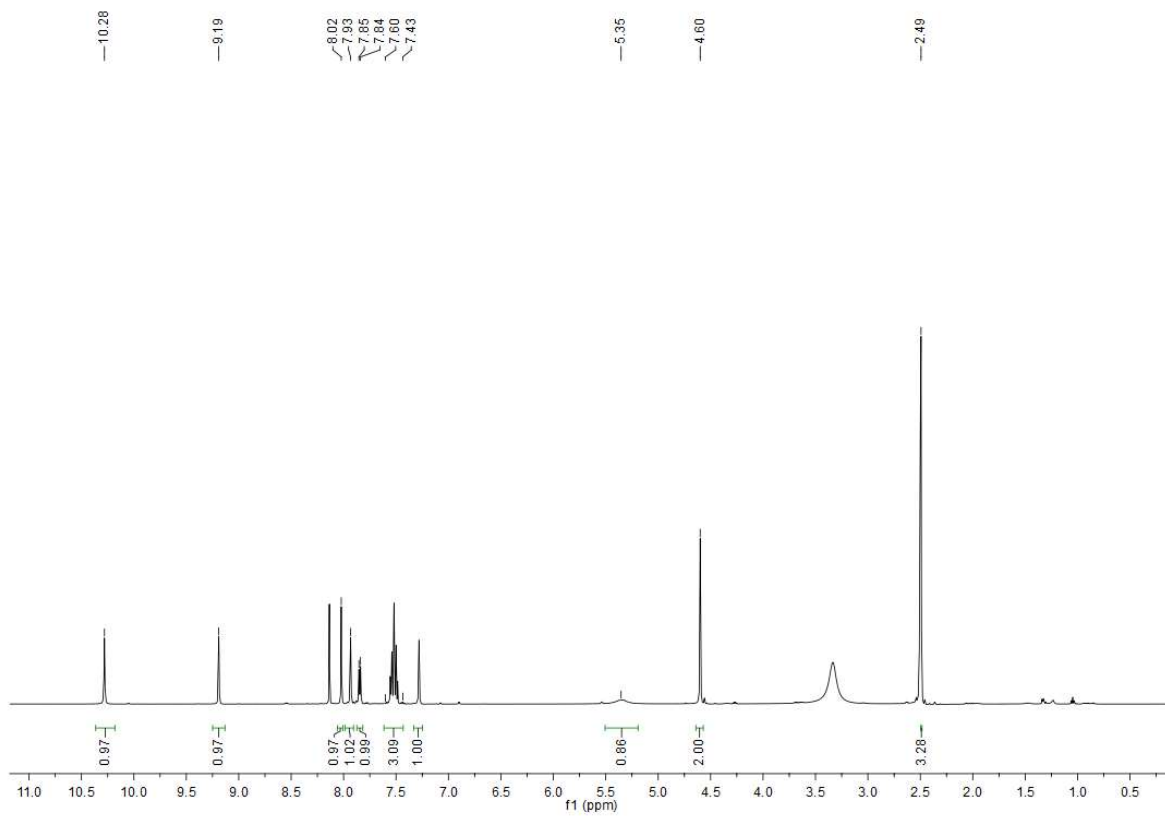


13C

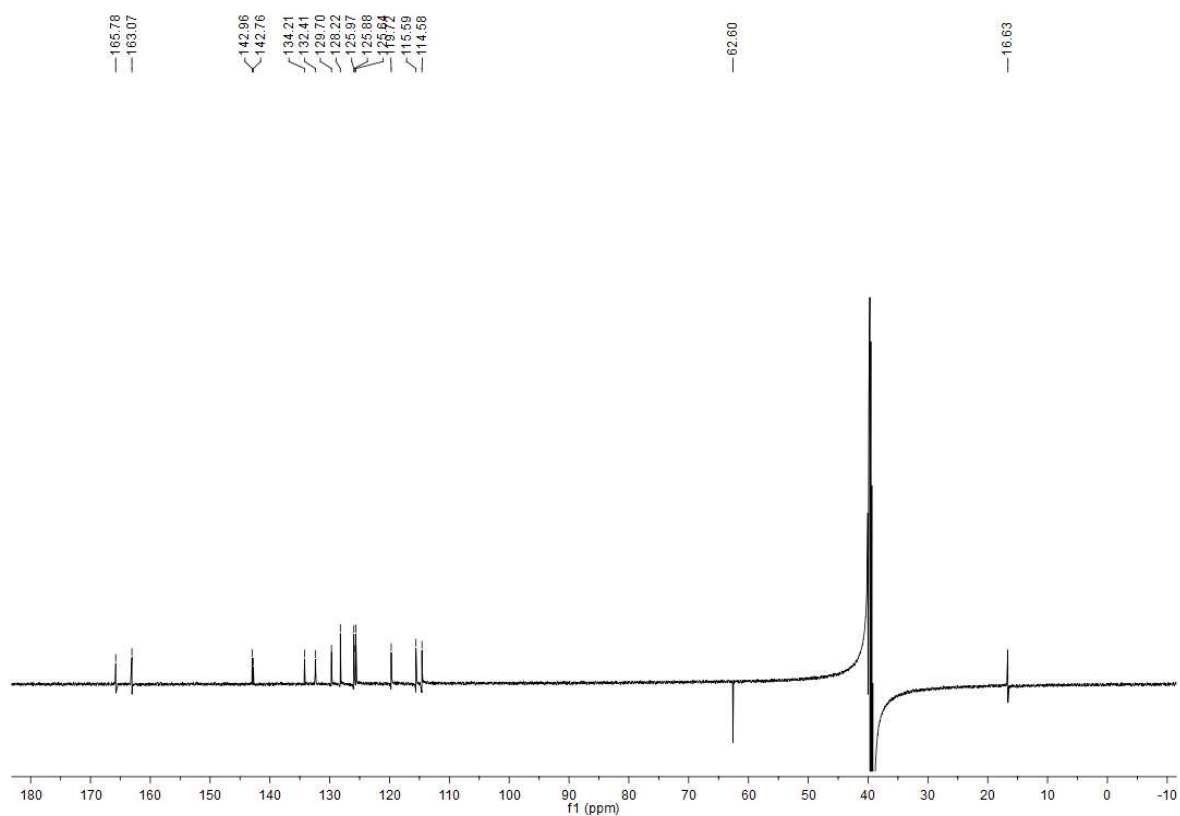


(73)

<sup>1</sup>H

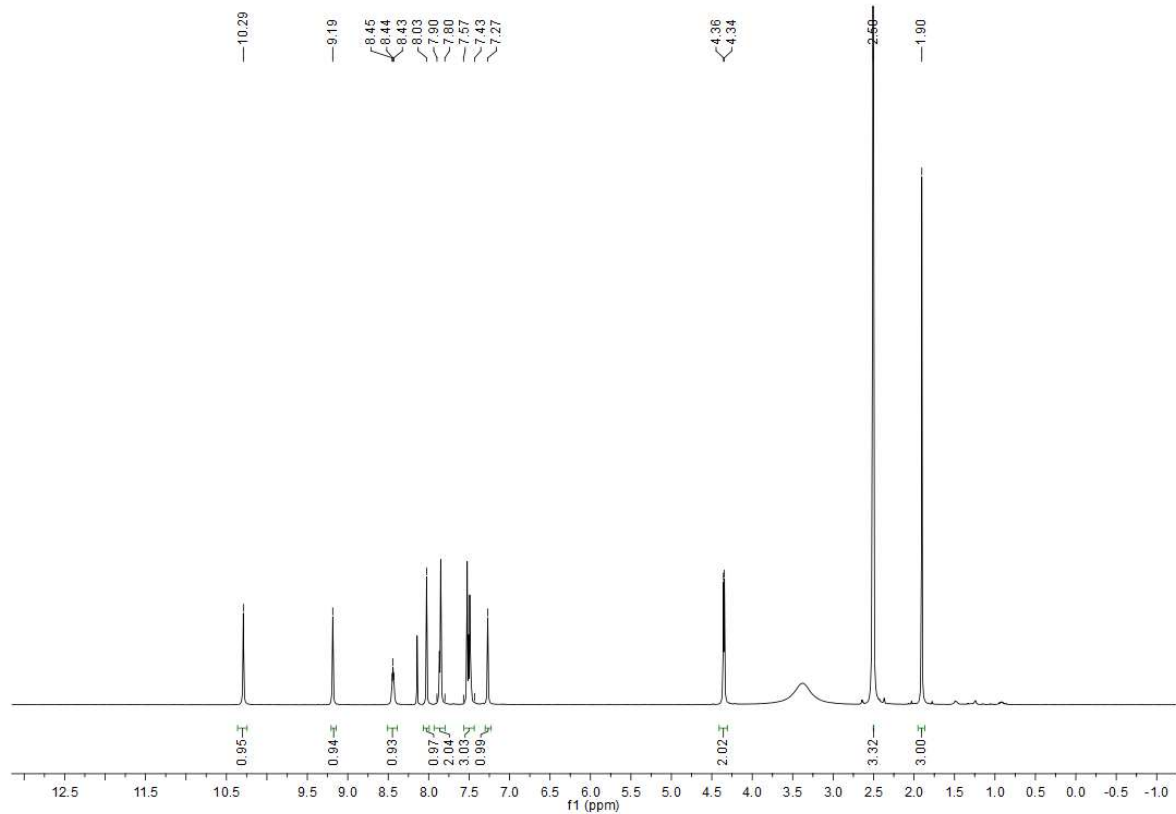


# 13C

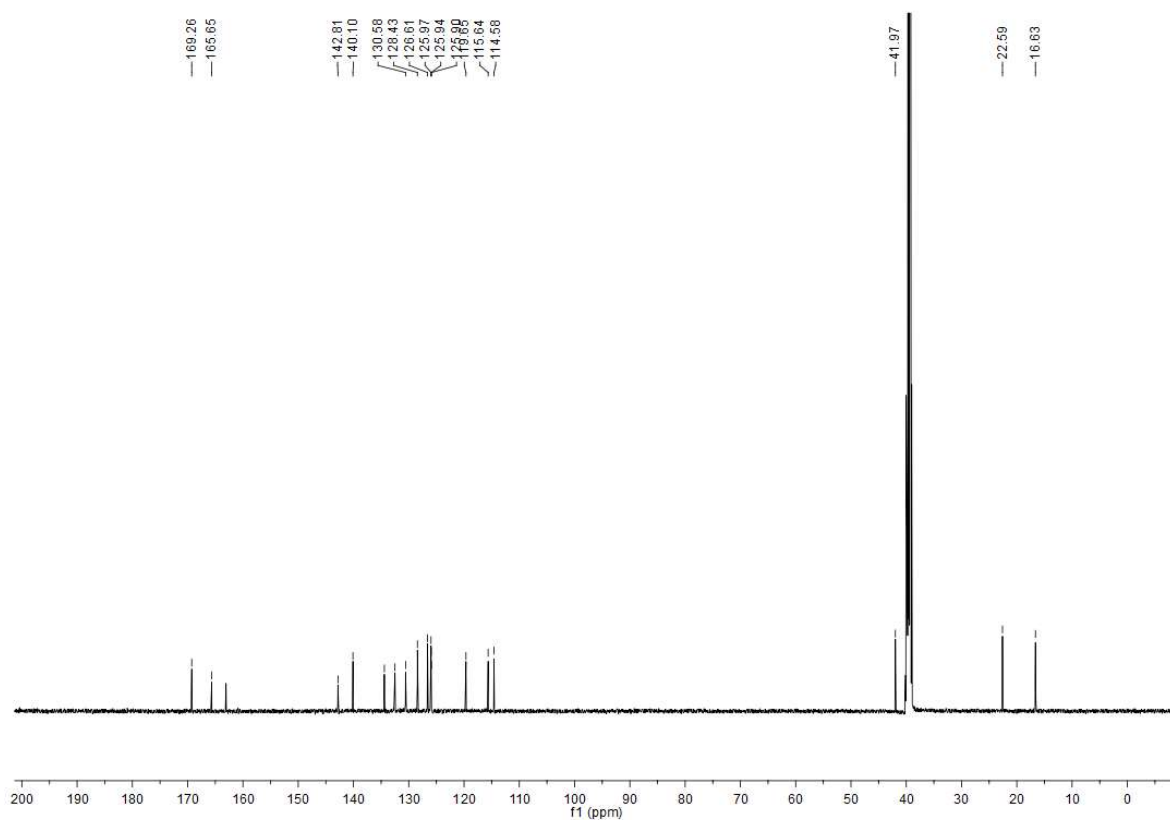


# (75)

# 1H

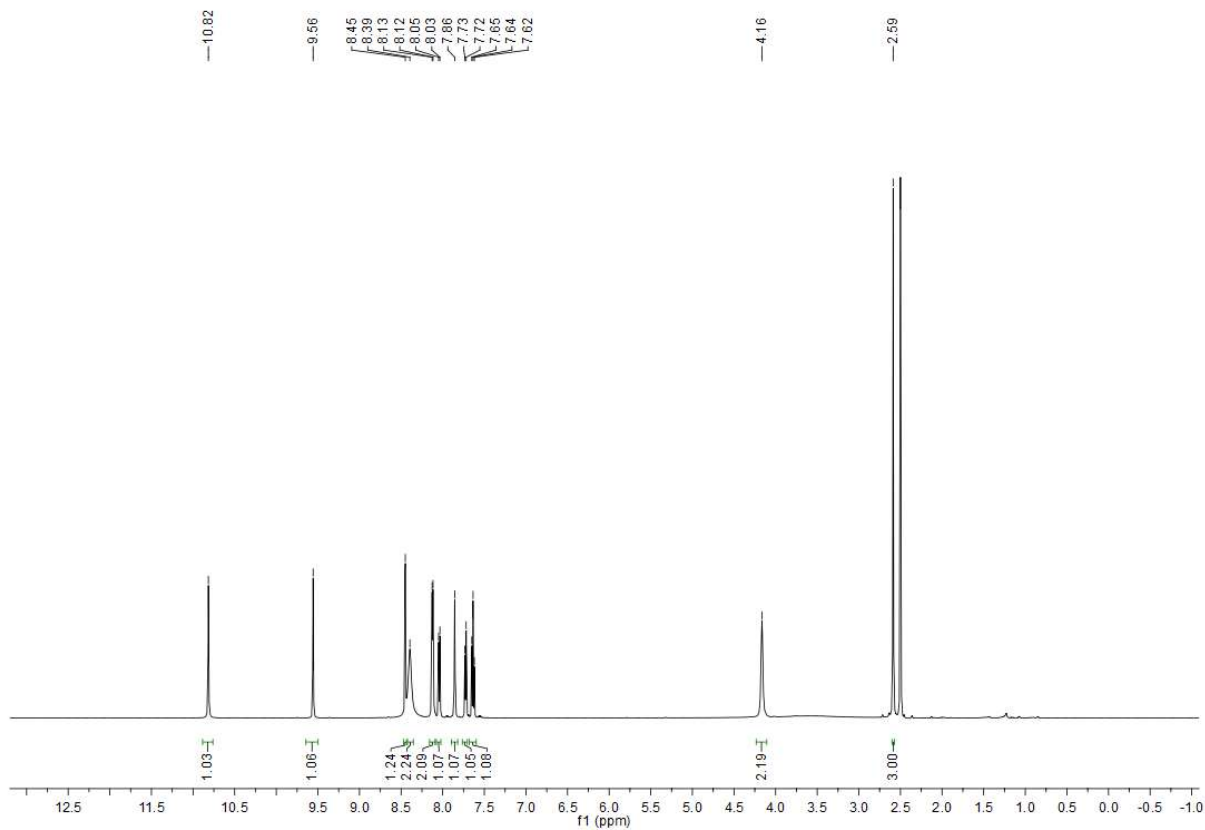


13C

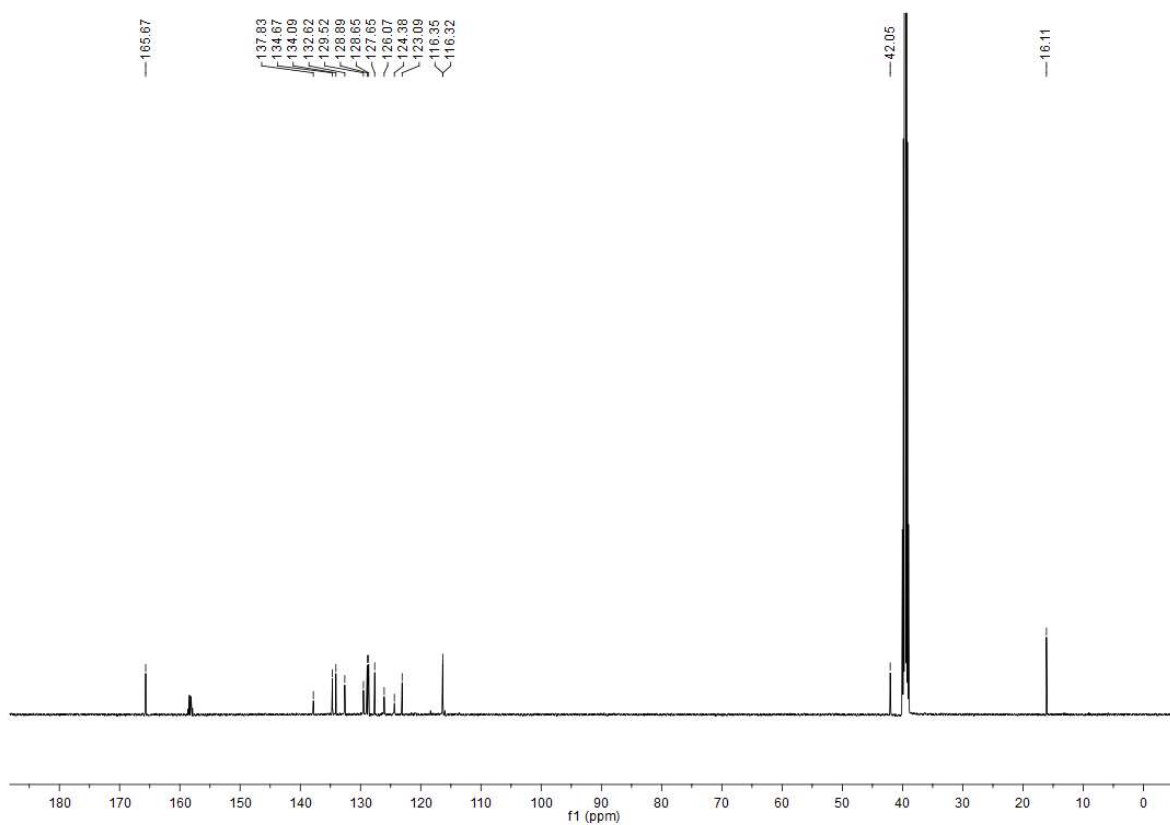


(74)

1H

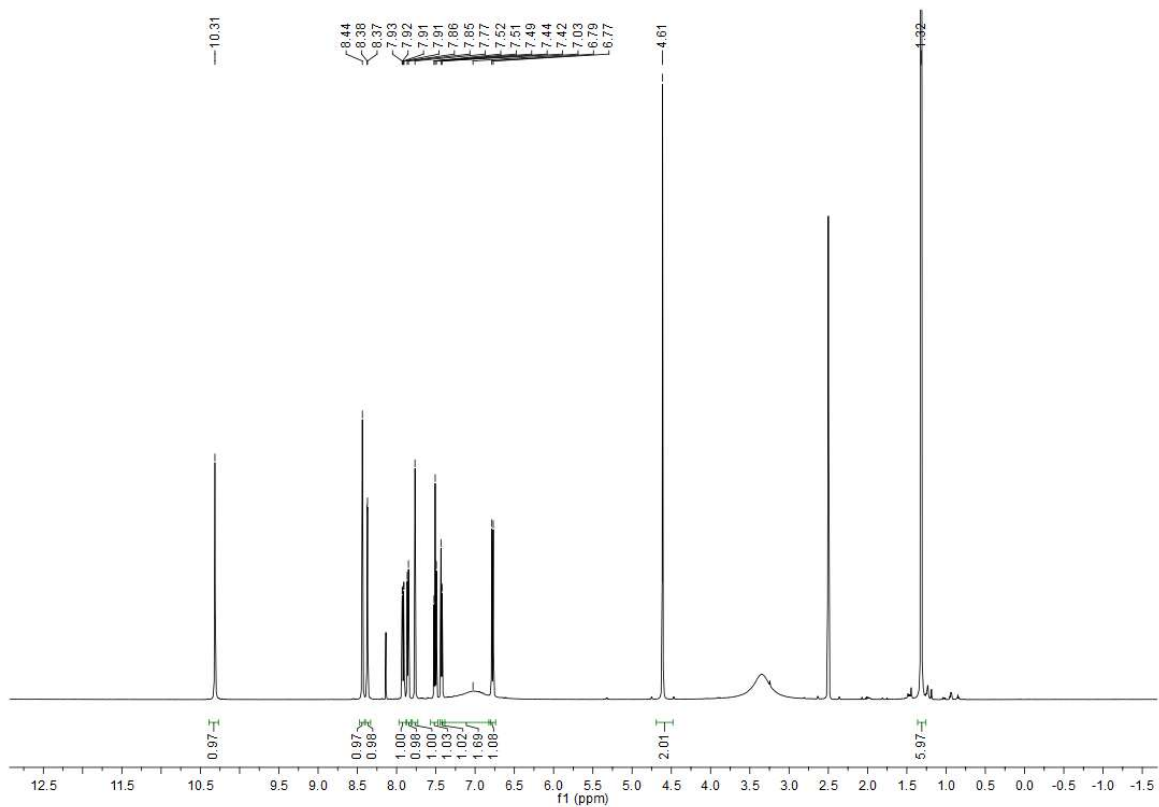


13C

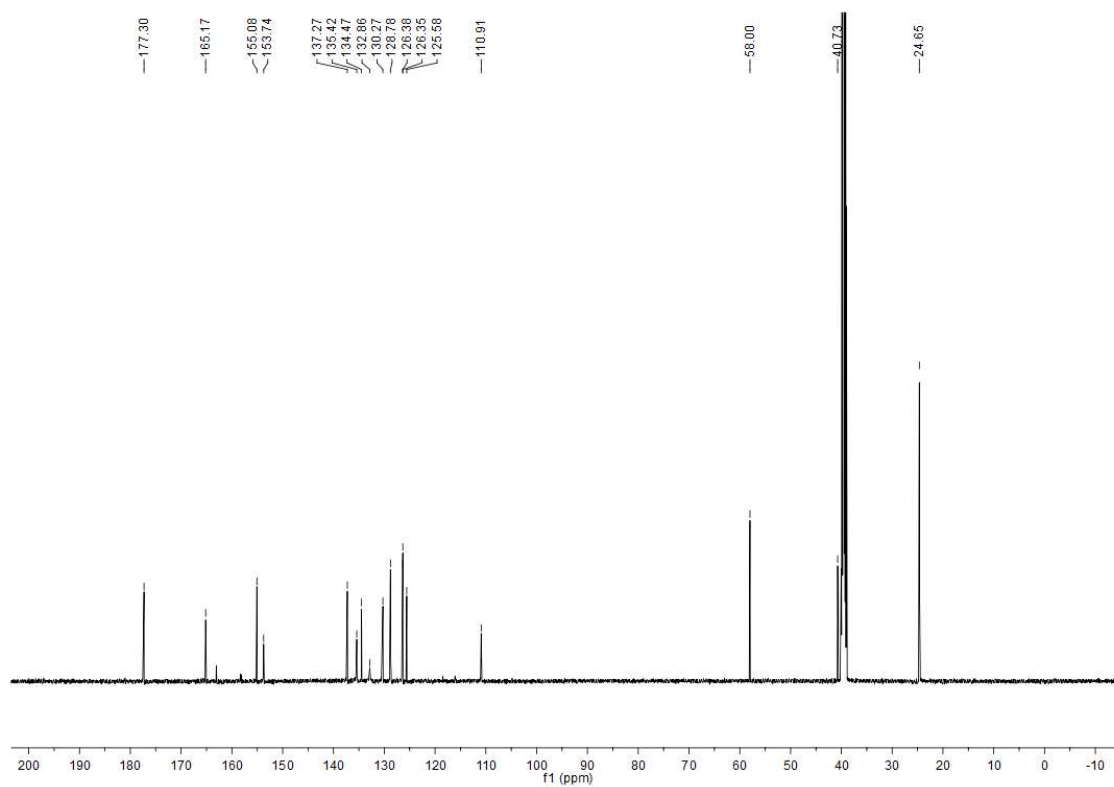


(159)

1H

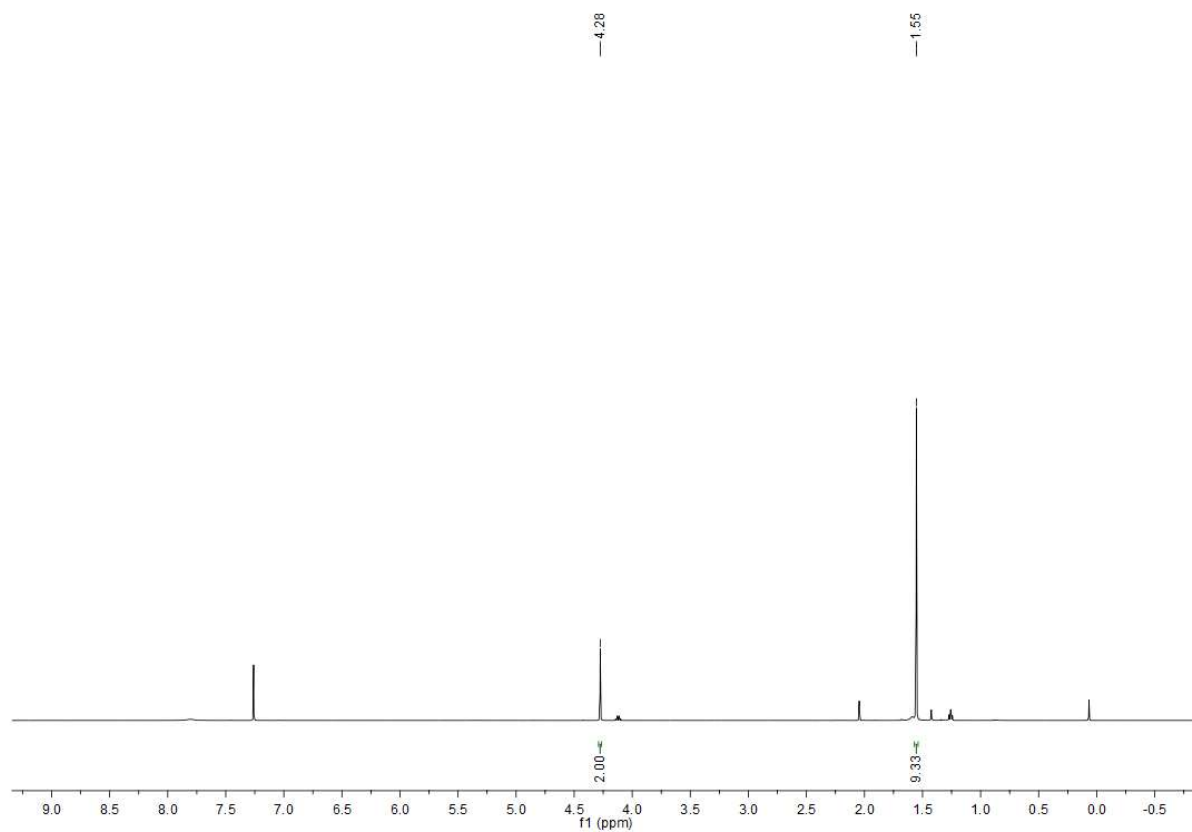


13C

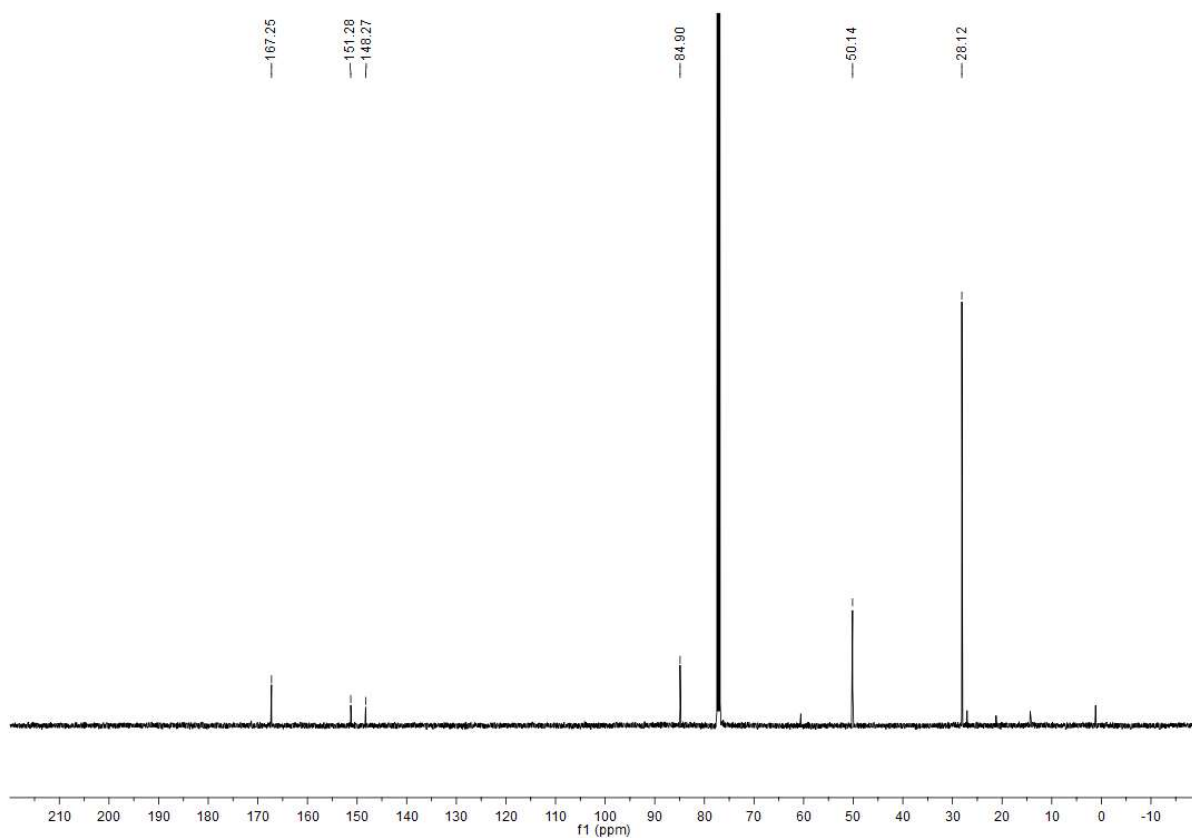


(30)

1H

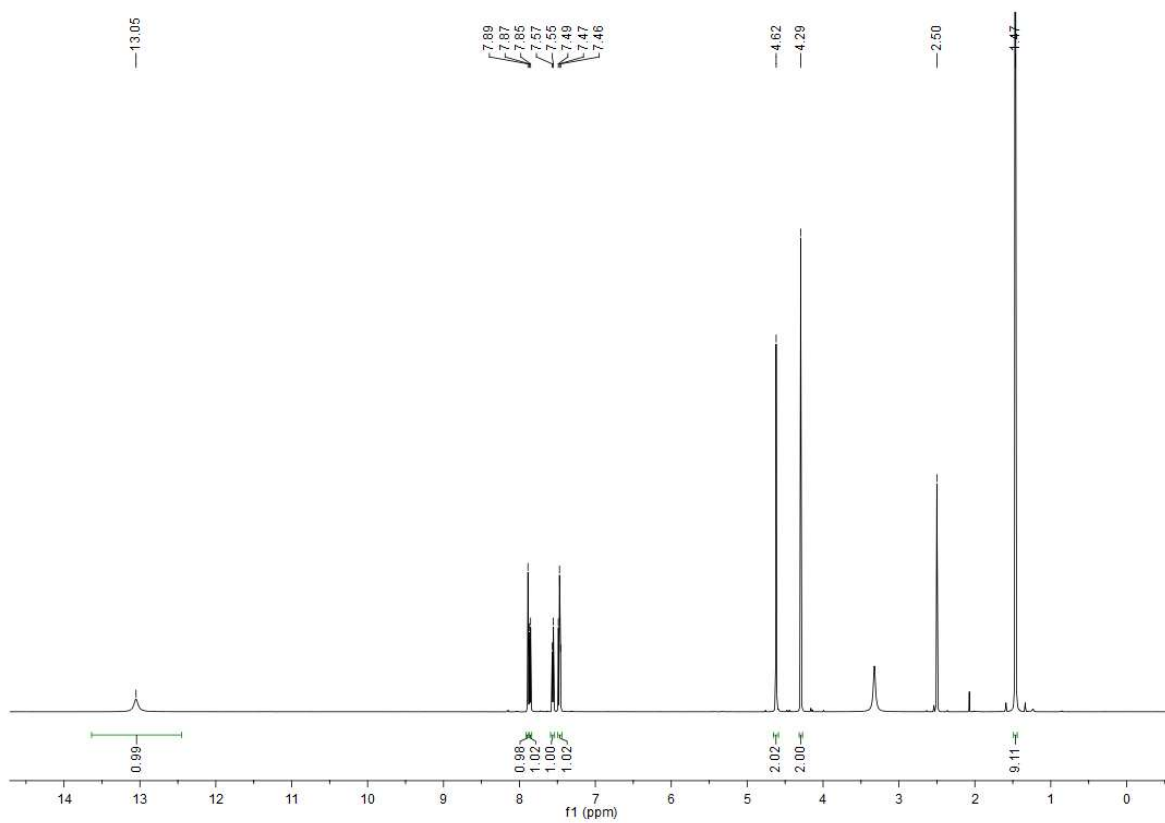


13C



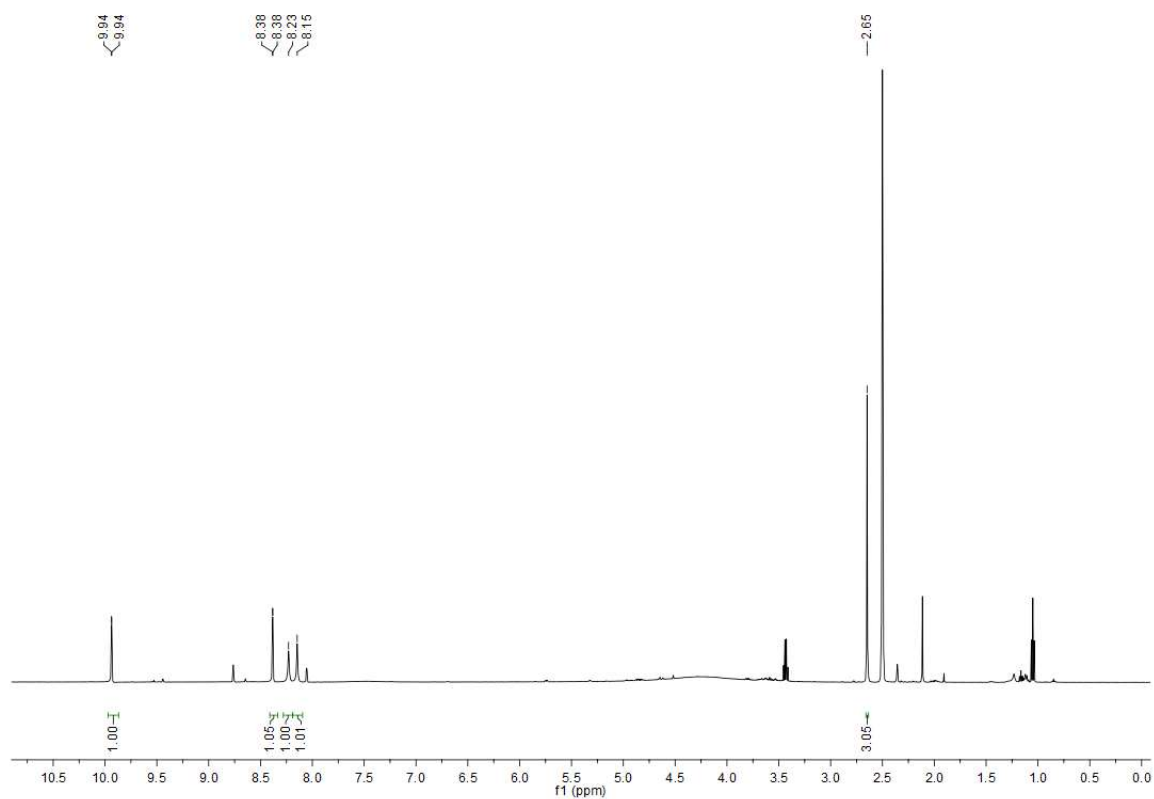
(32)

1H



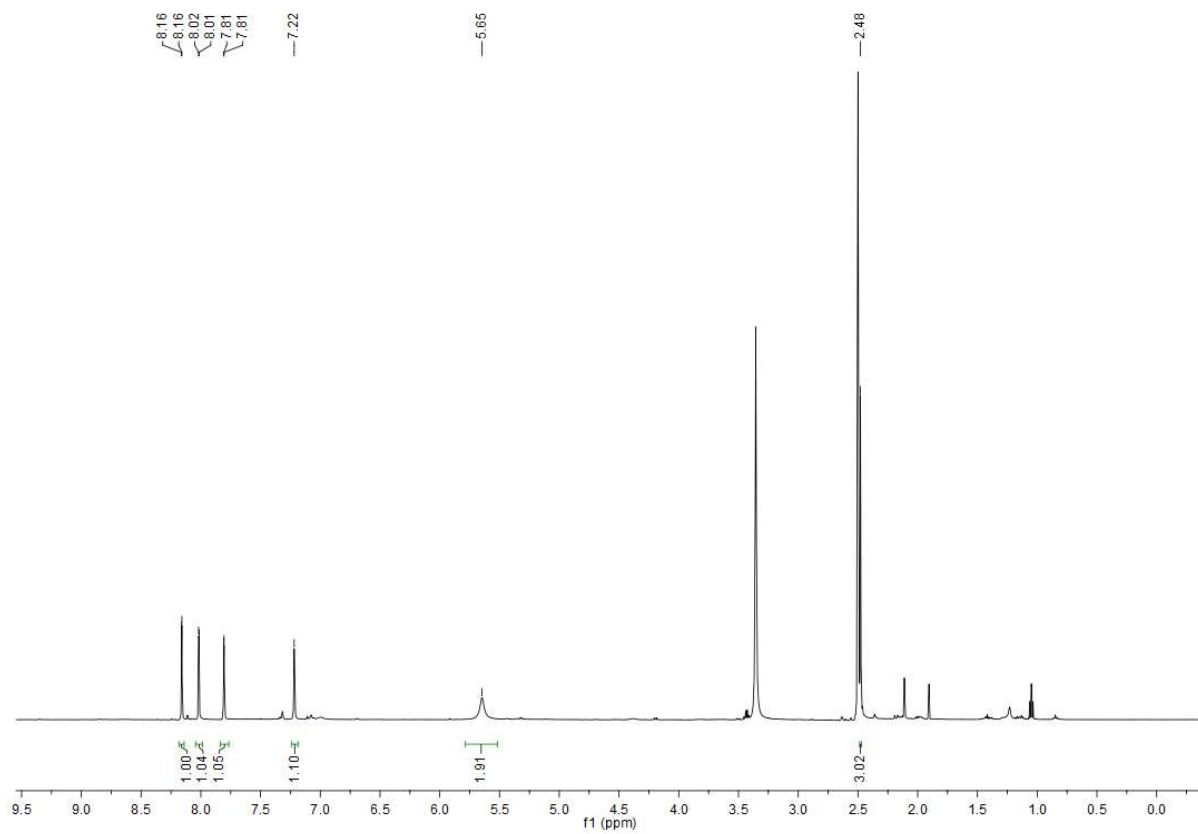
(132)

<sup>1</sup>H



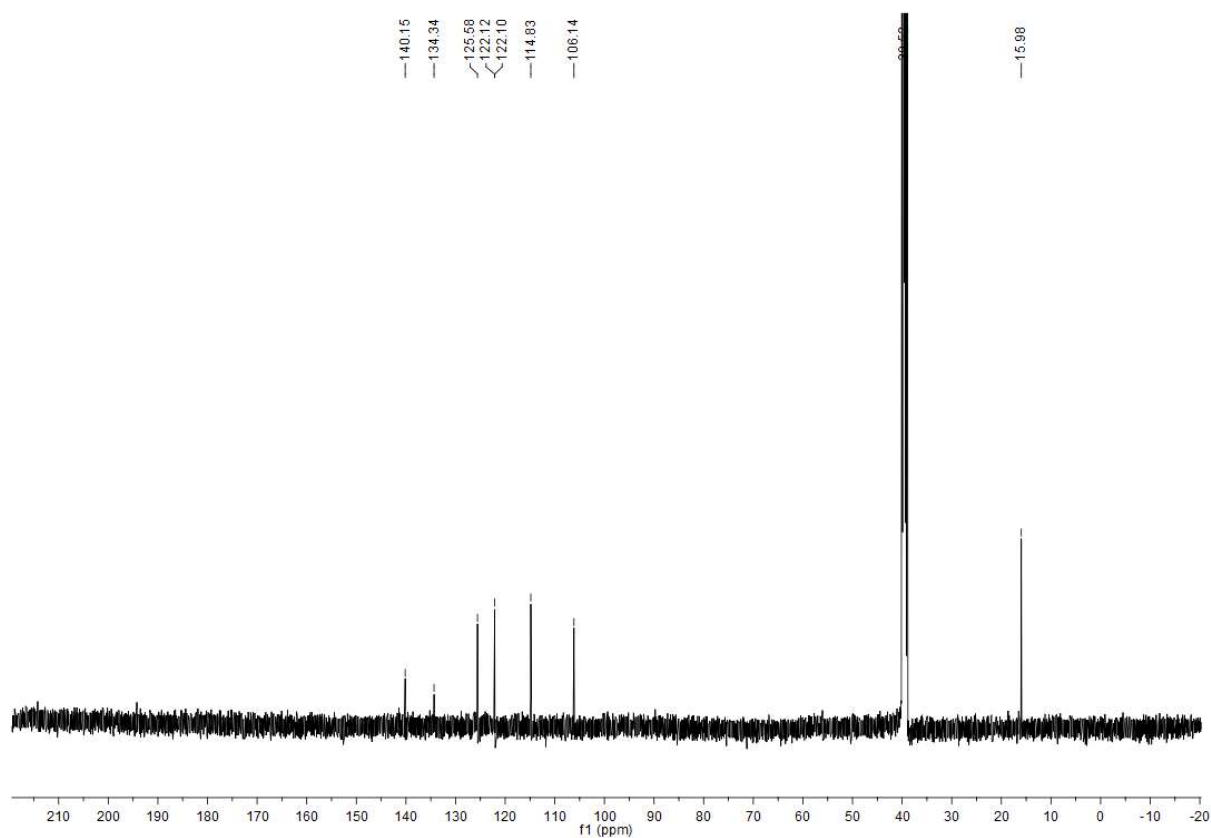
(28)

<sup>1</sup>H



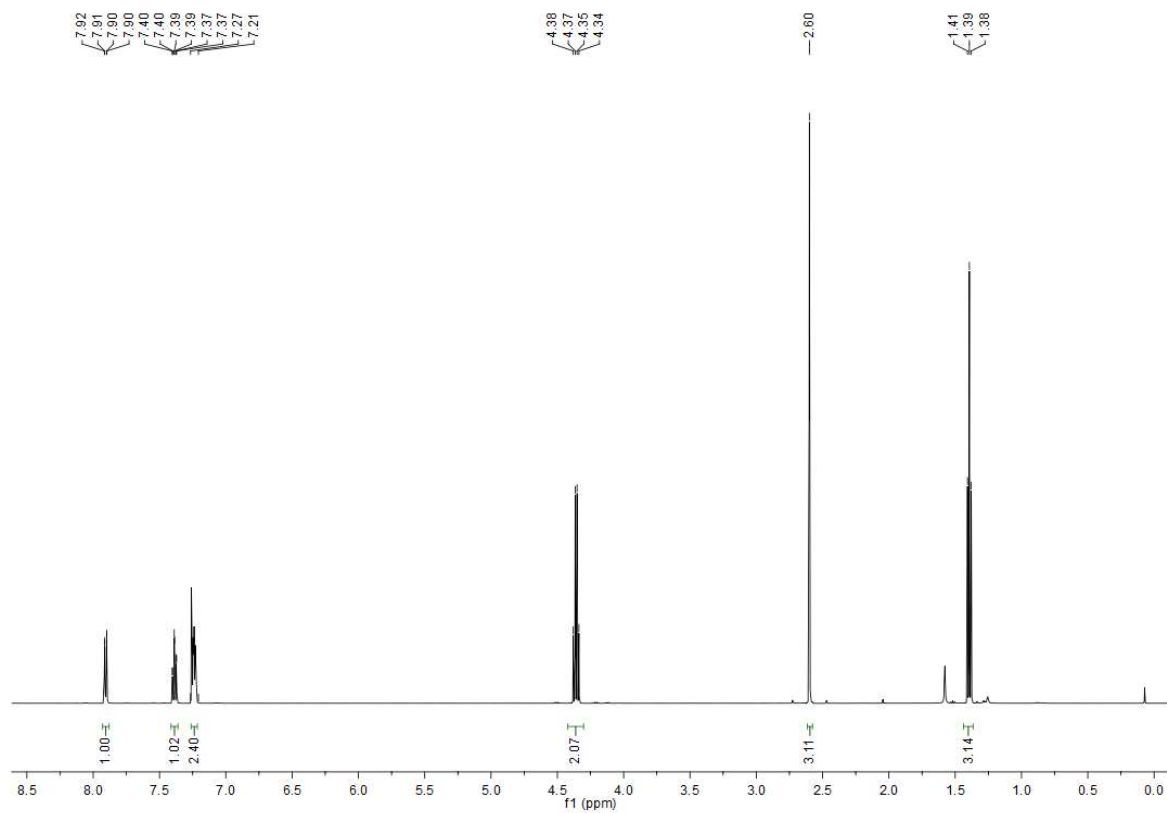


13C

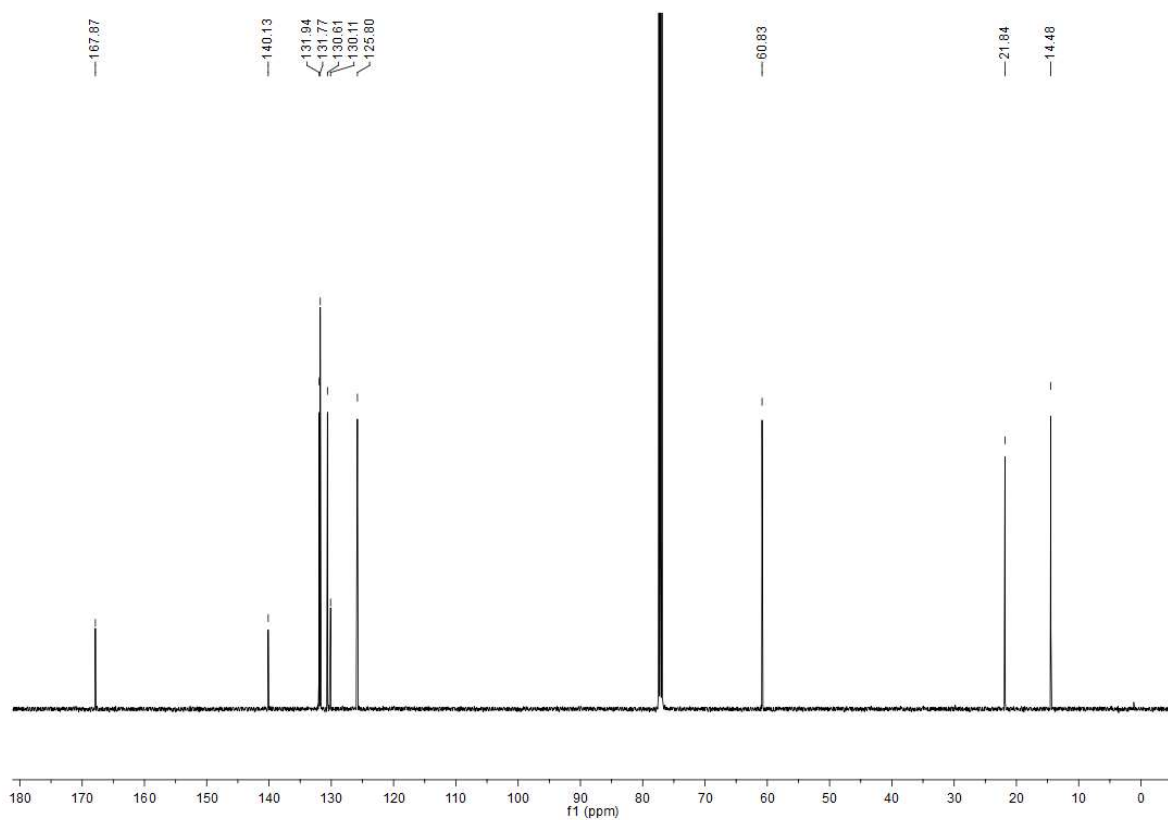


(133)

1H

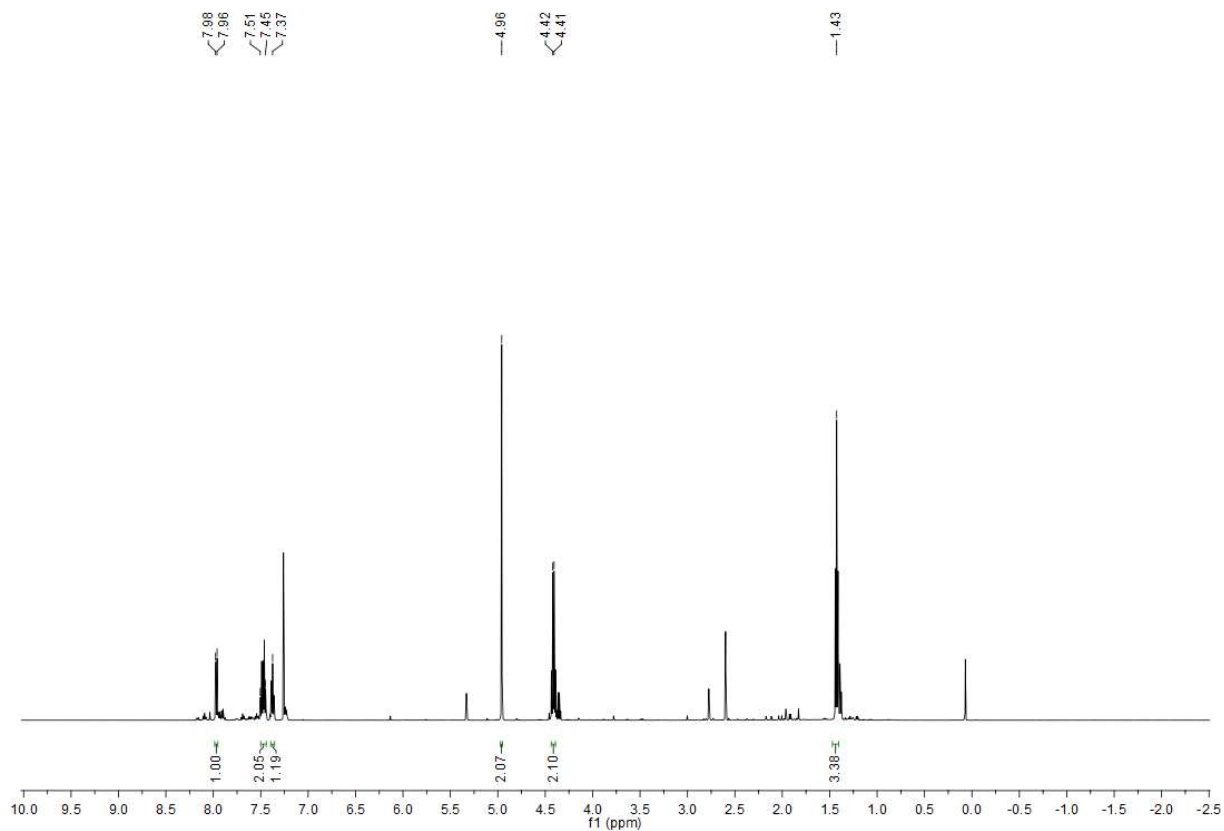


13C



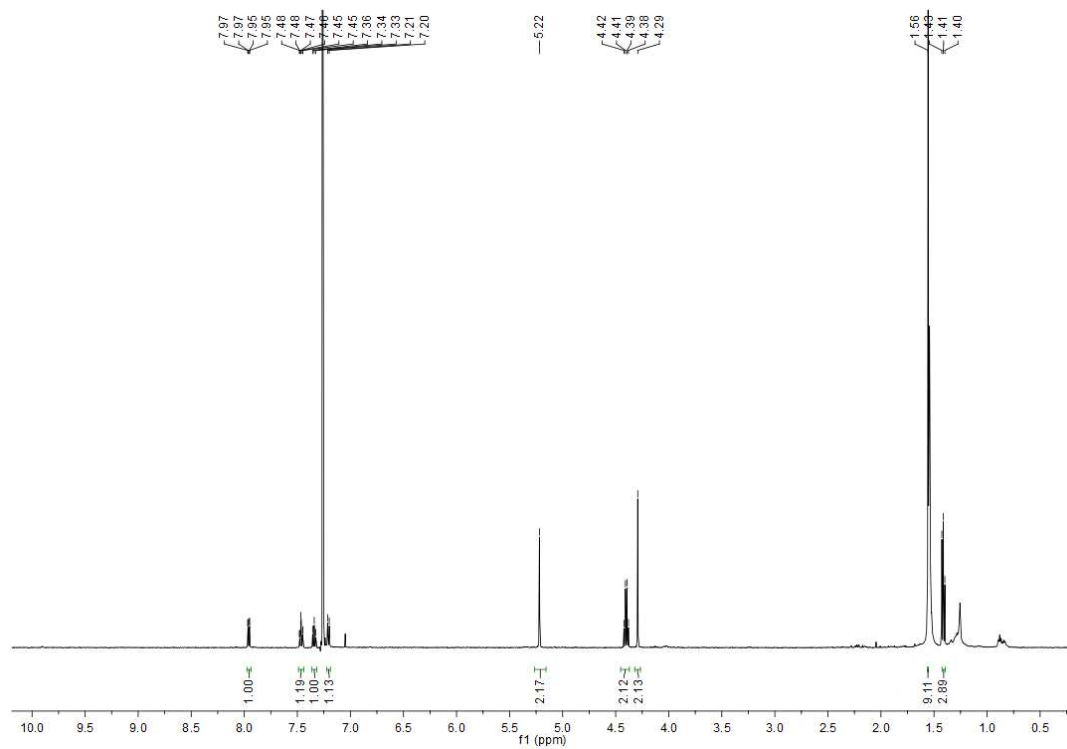
(44)

1H



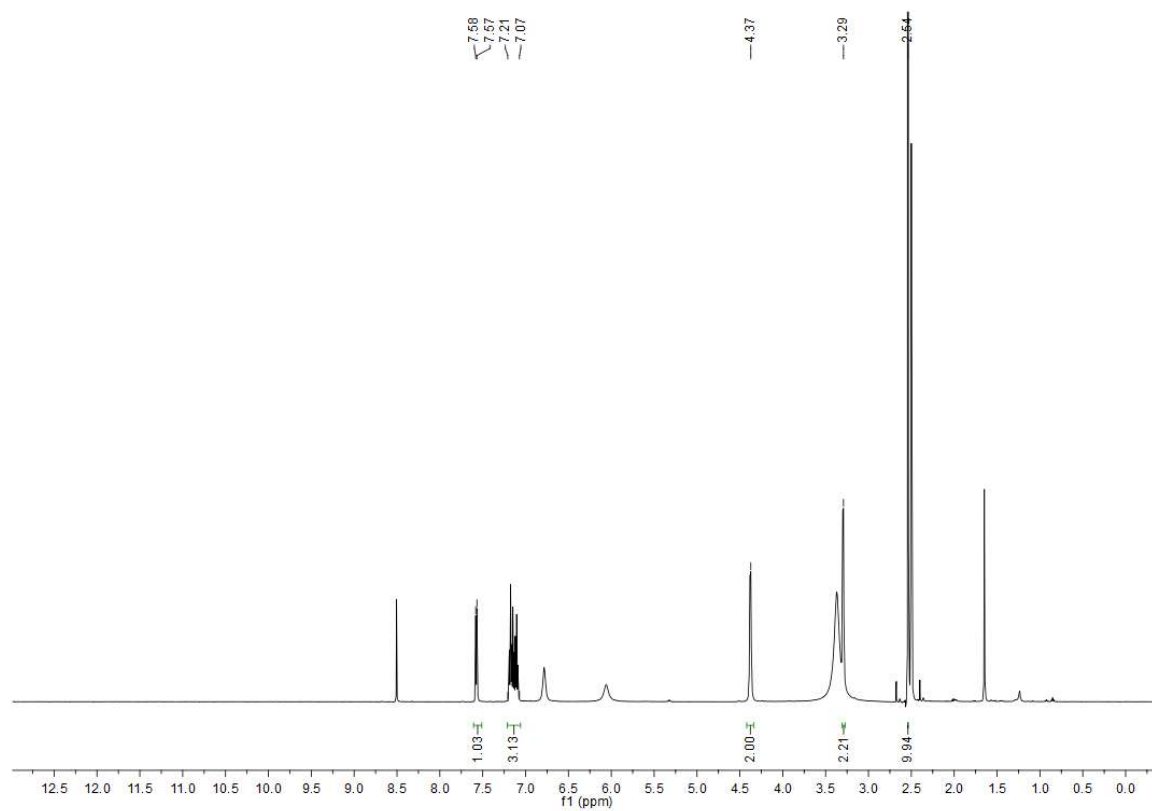
(45)

<sup>1</sup>H



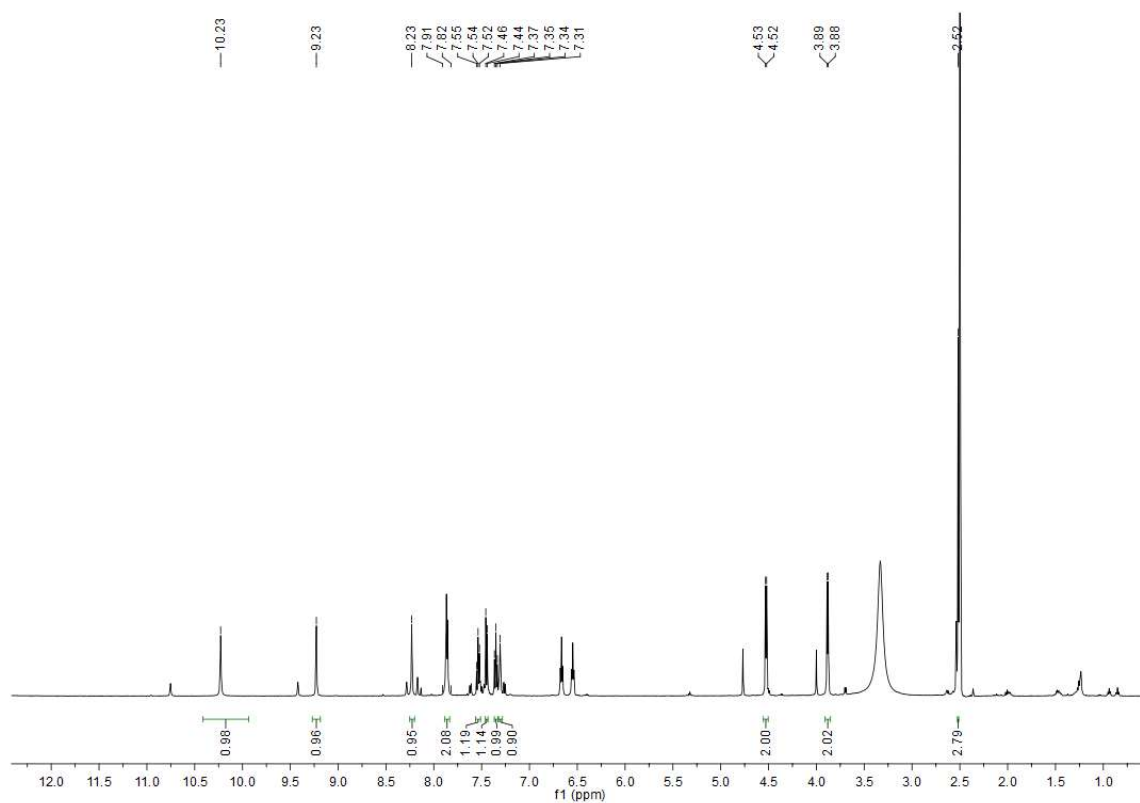
(46)

<sup>1</sup>H

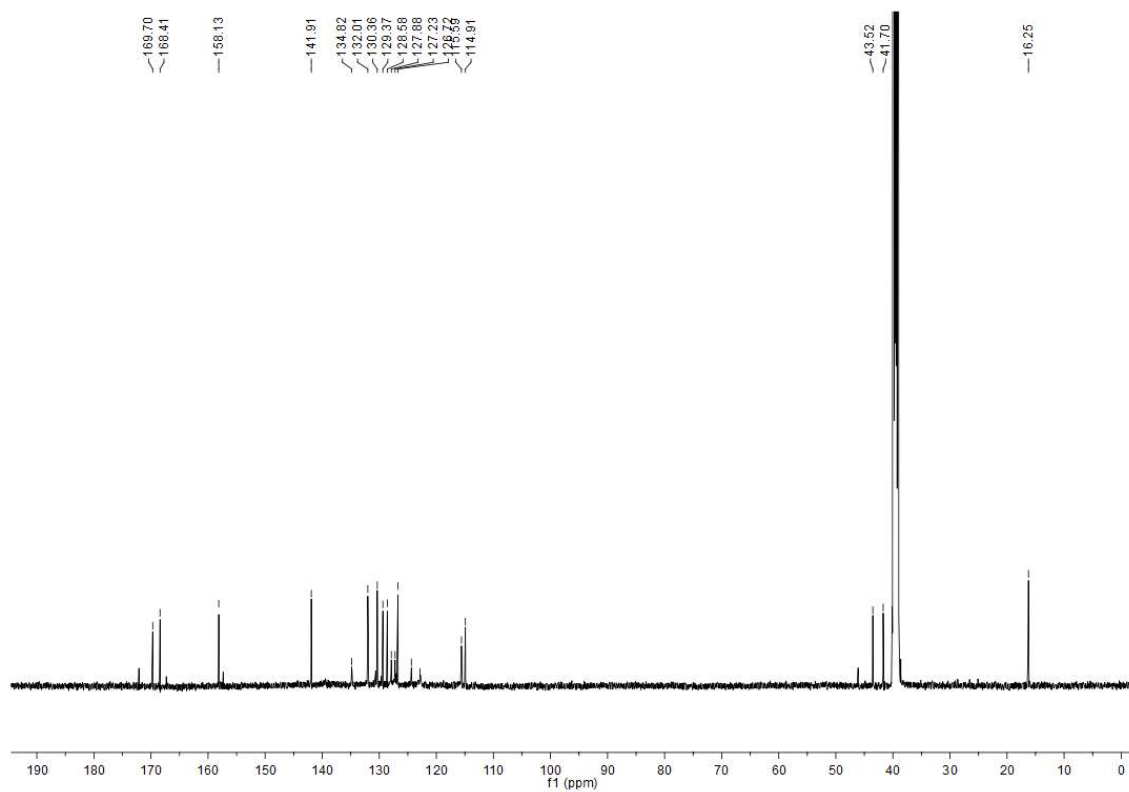


(47)

<sup>1</sup>H

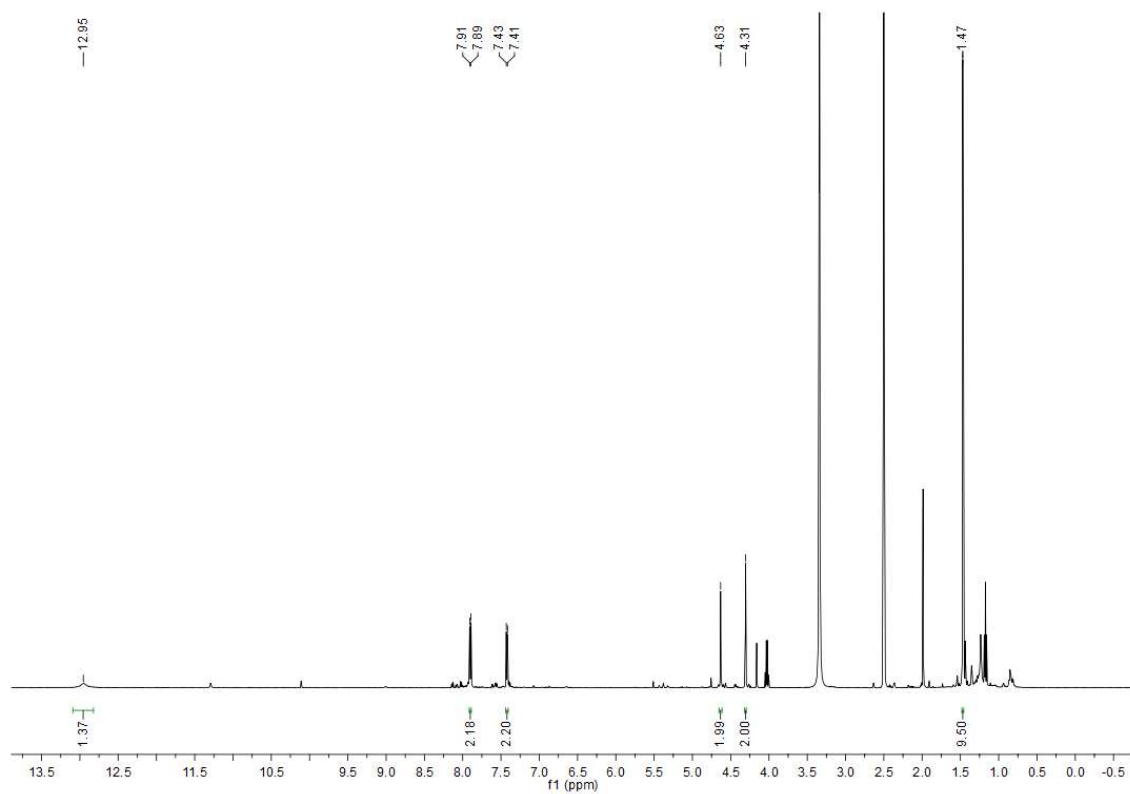


13C



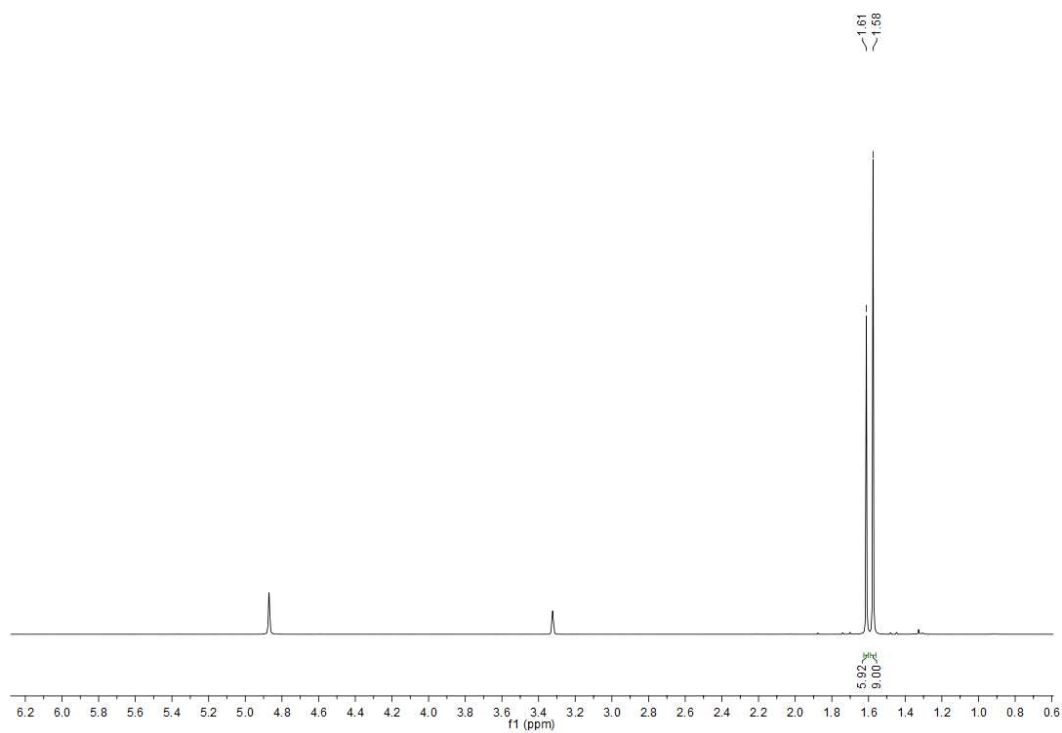
(39)

<sup>1</sup>H

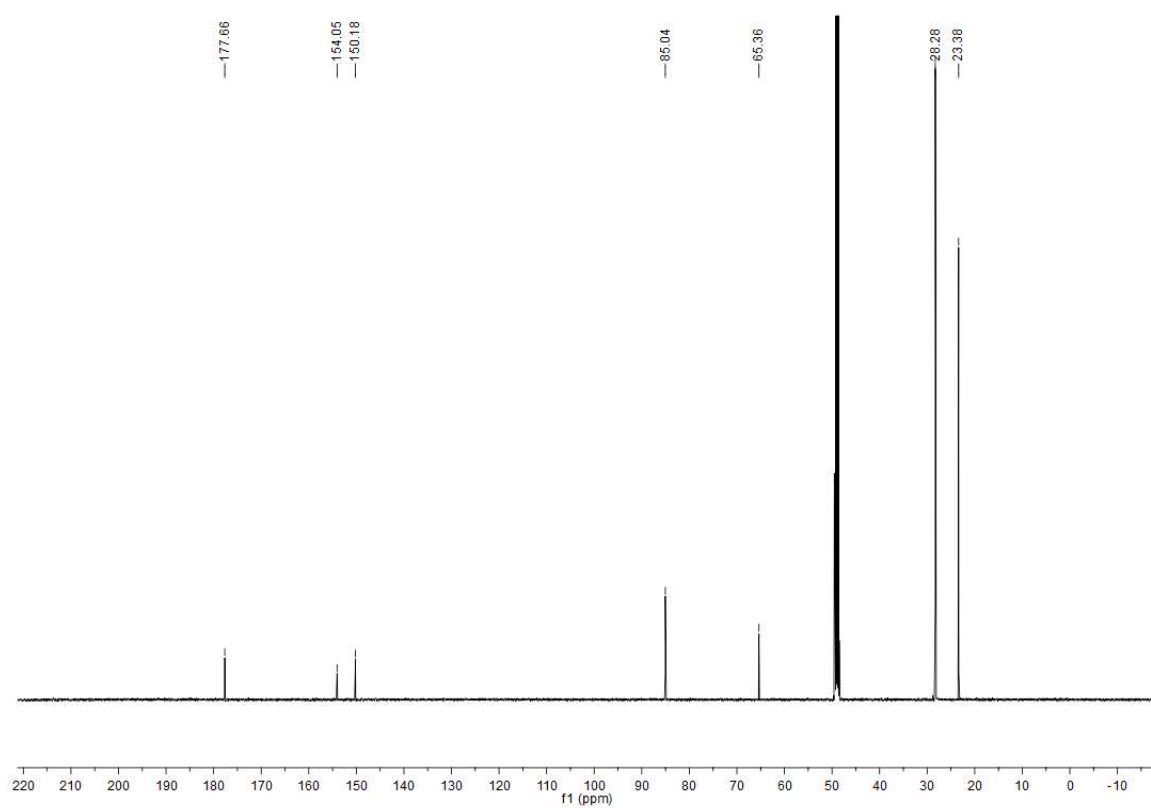


(148)

<sup>1</sup>H

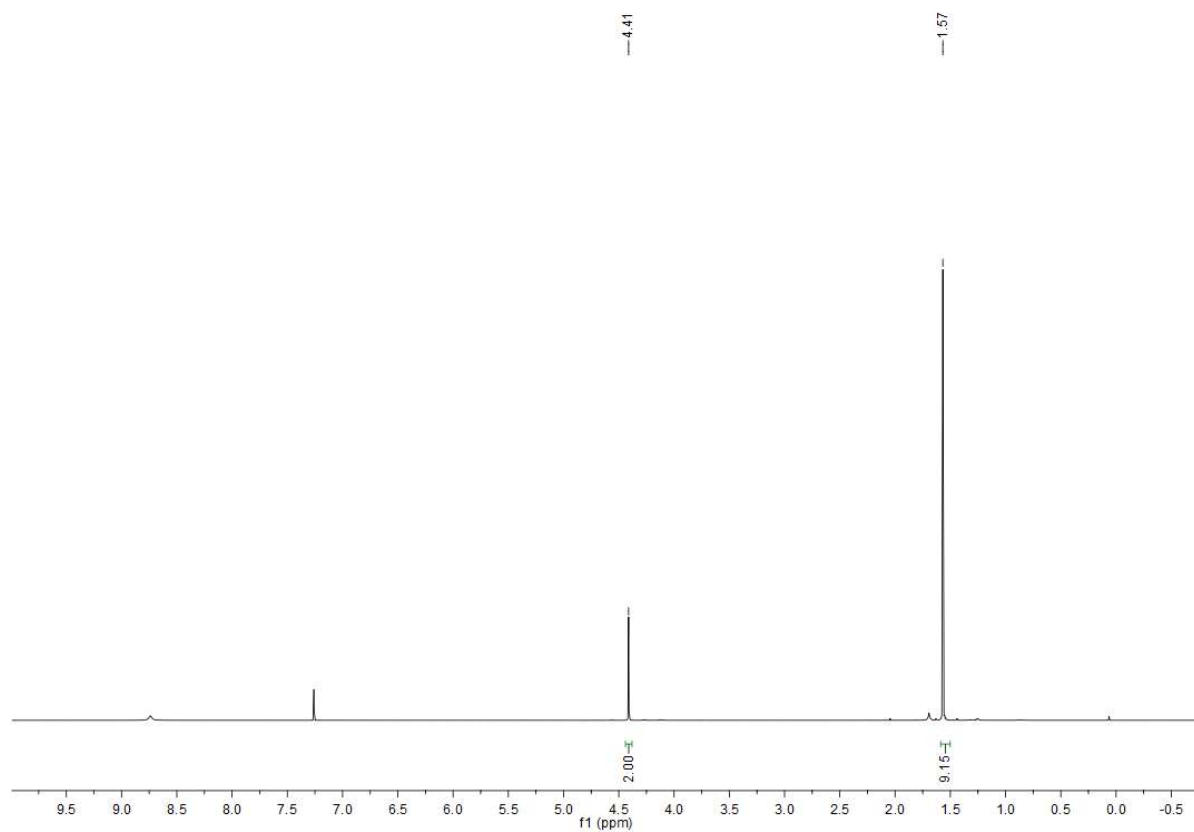


13C

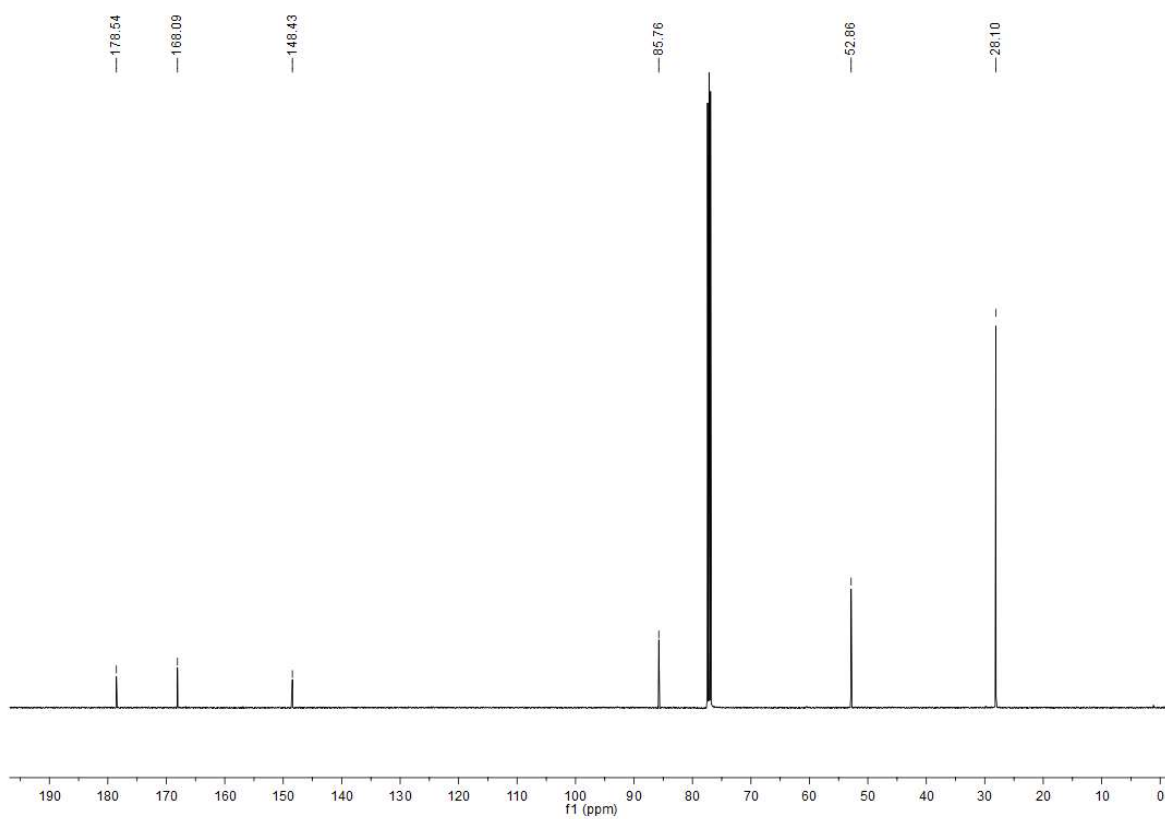


(143)

1H

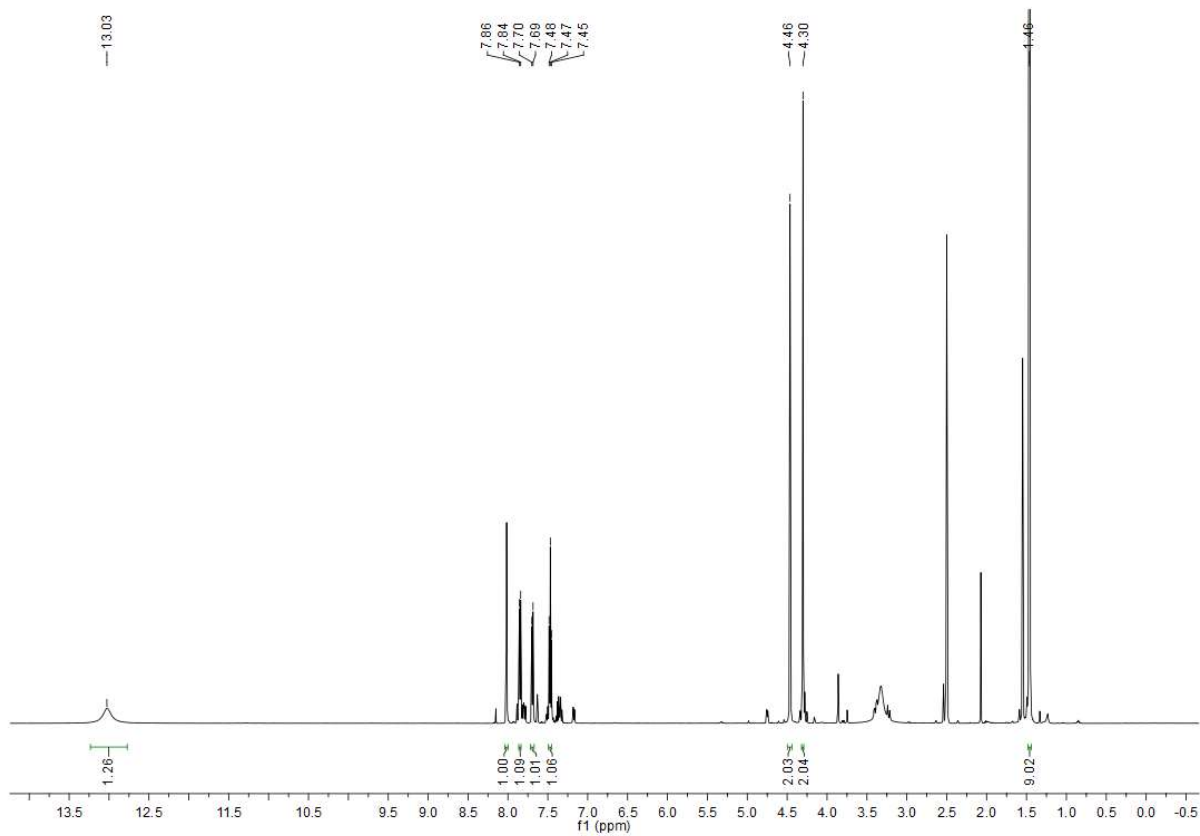


# 13C

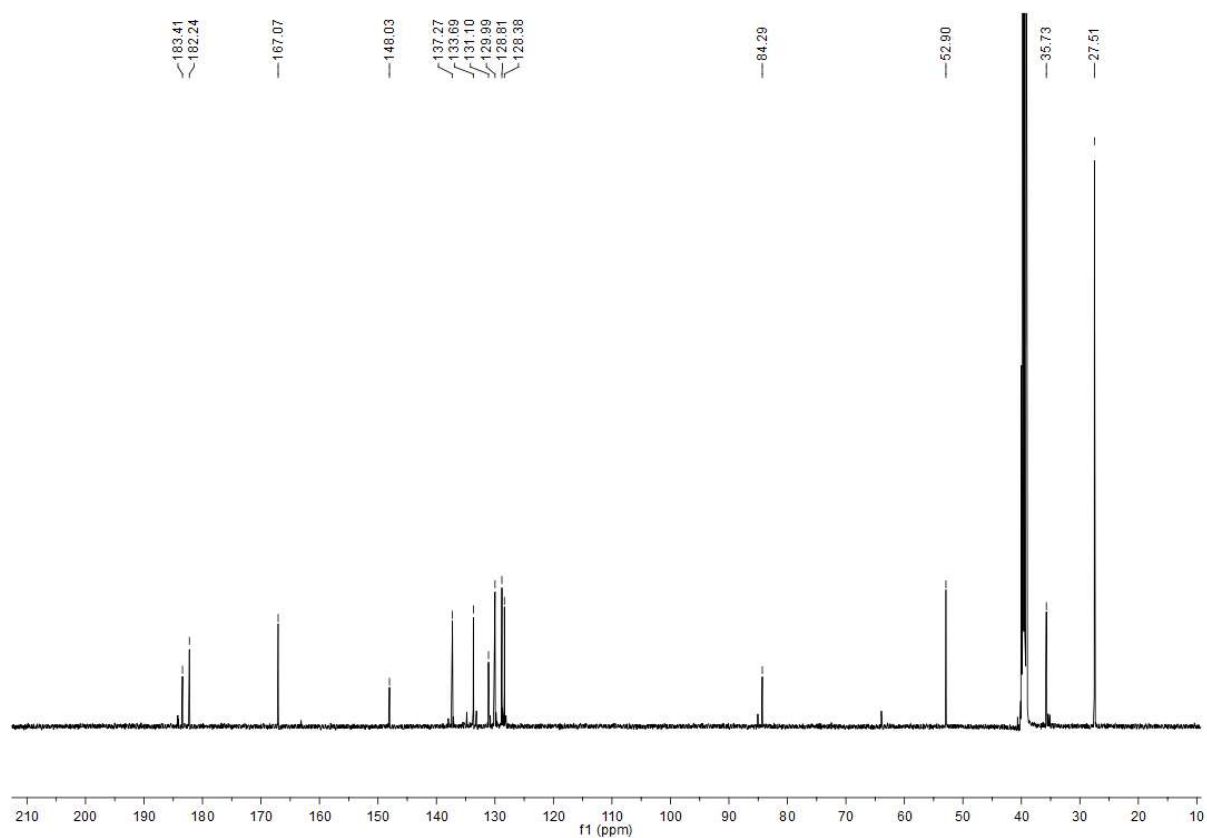


# (144)

## 1H

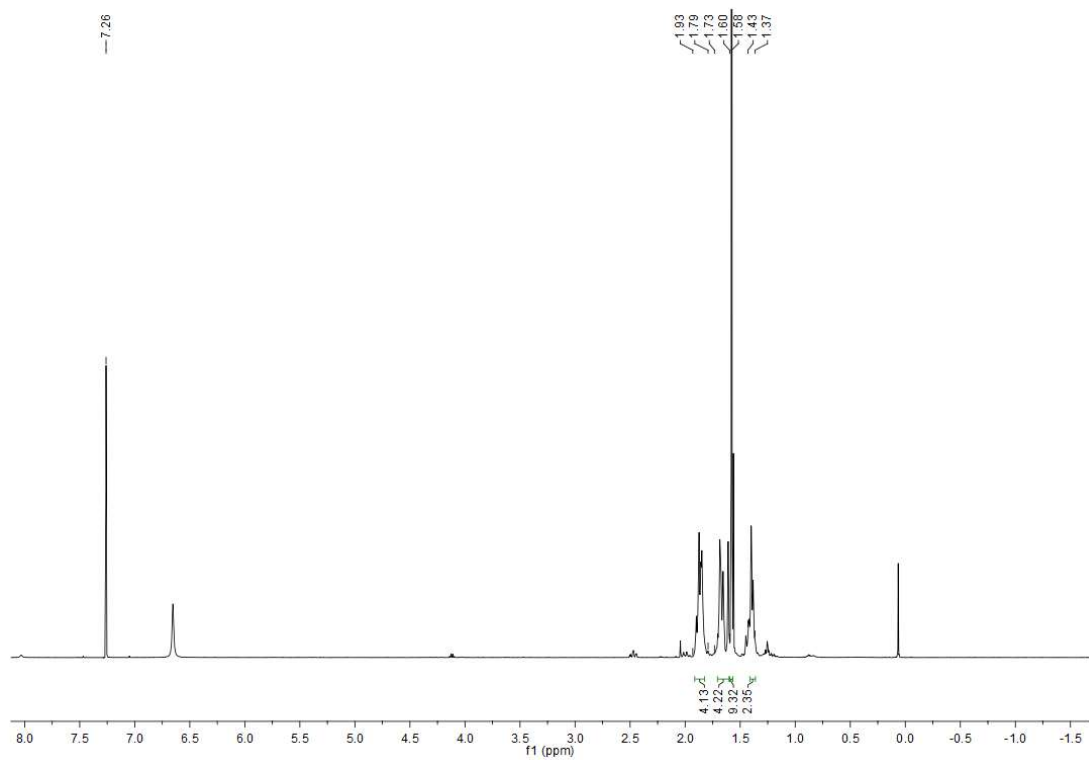


# 13C



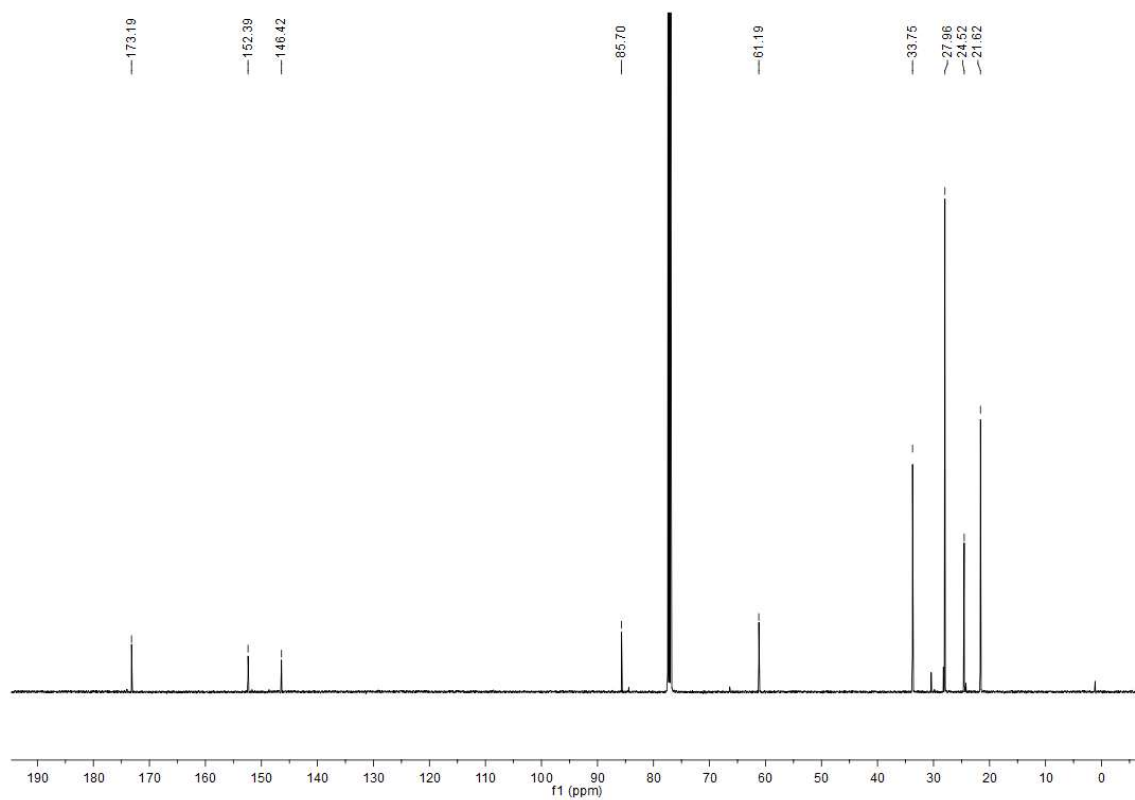
# (150)

# 1H



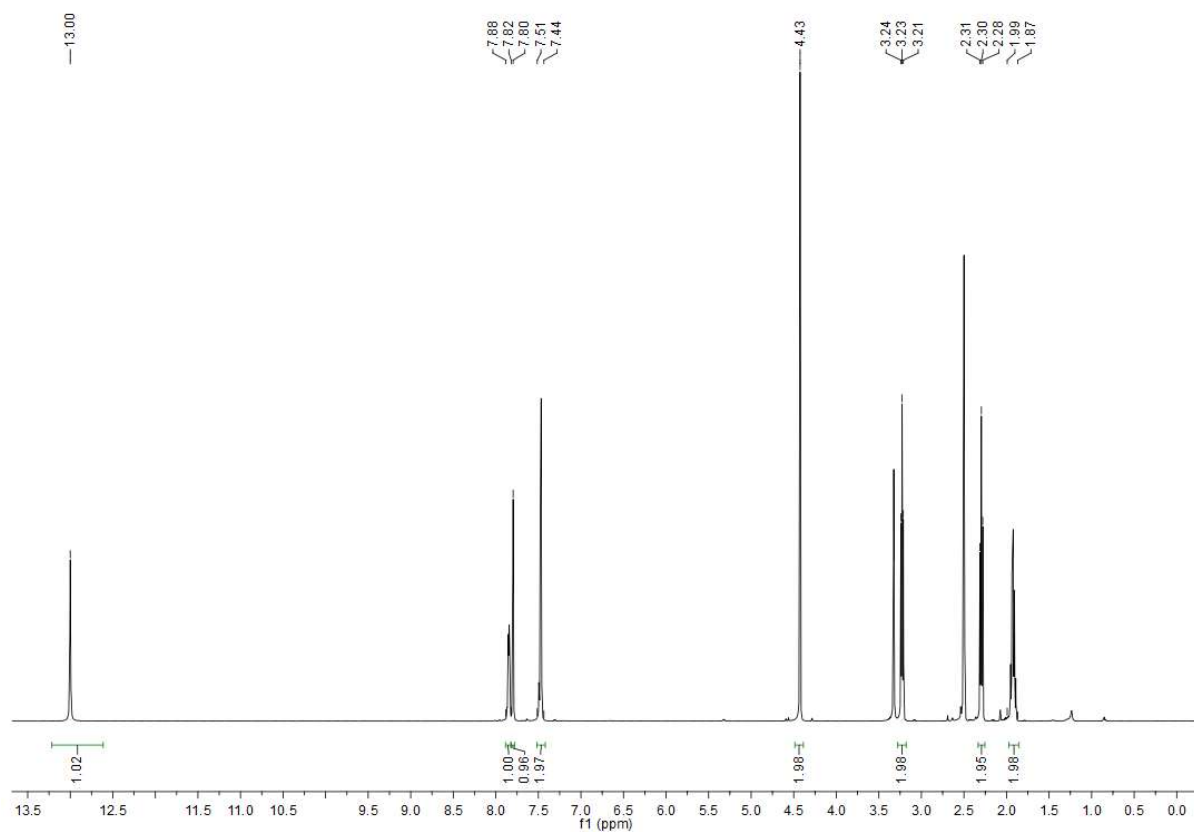


13C

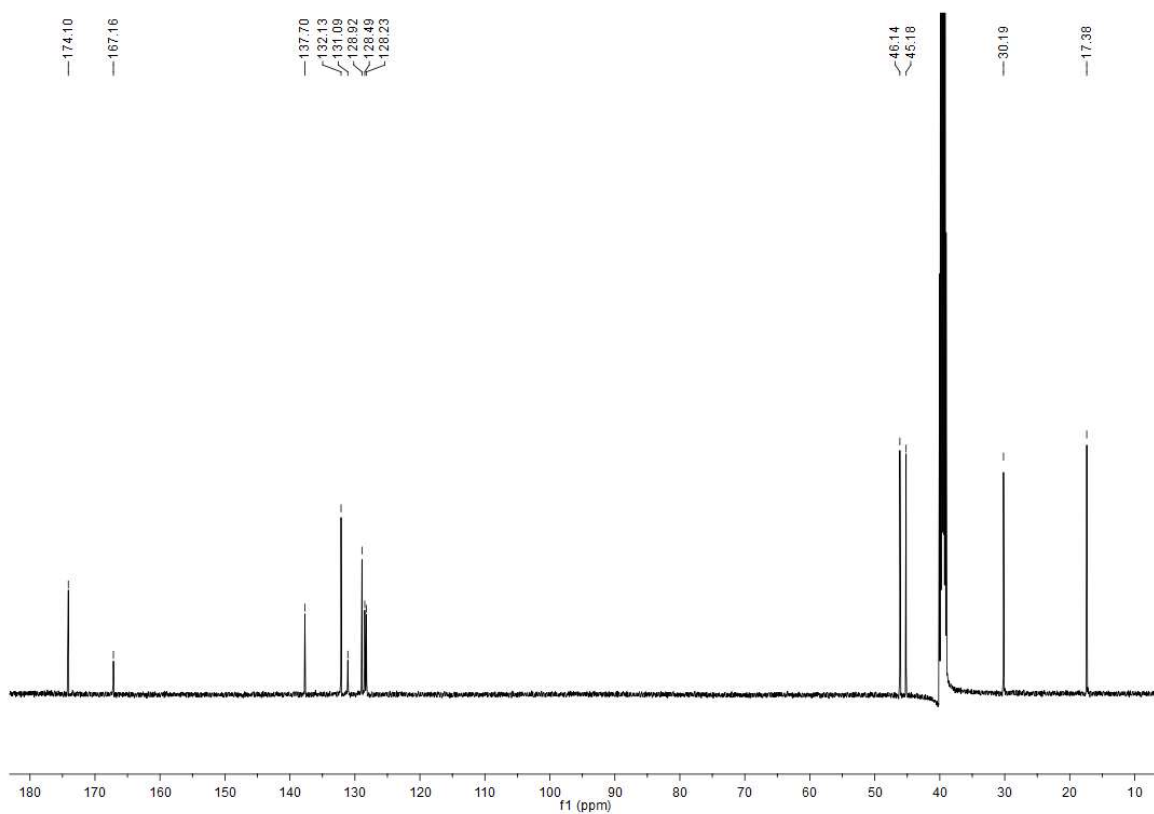


(146)

1H

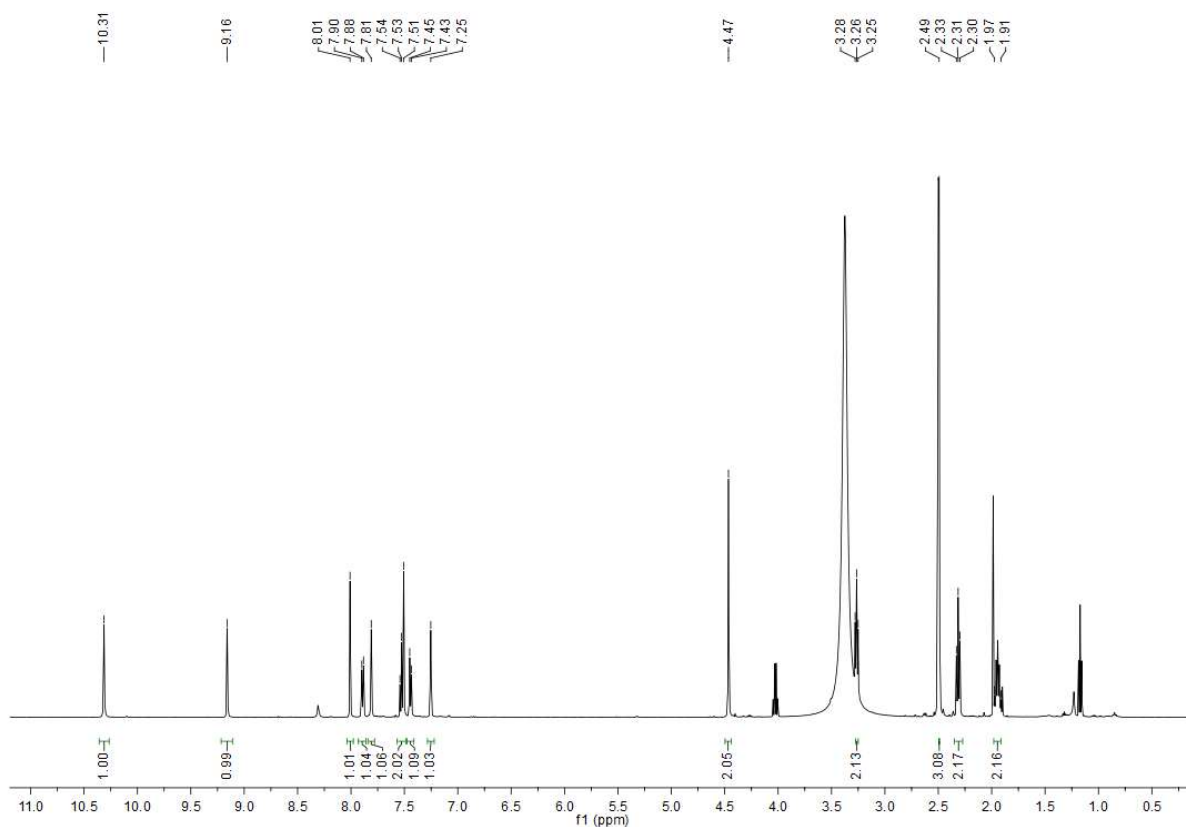


# 13C

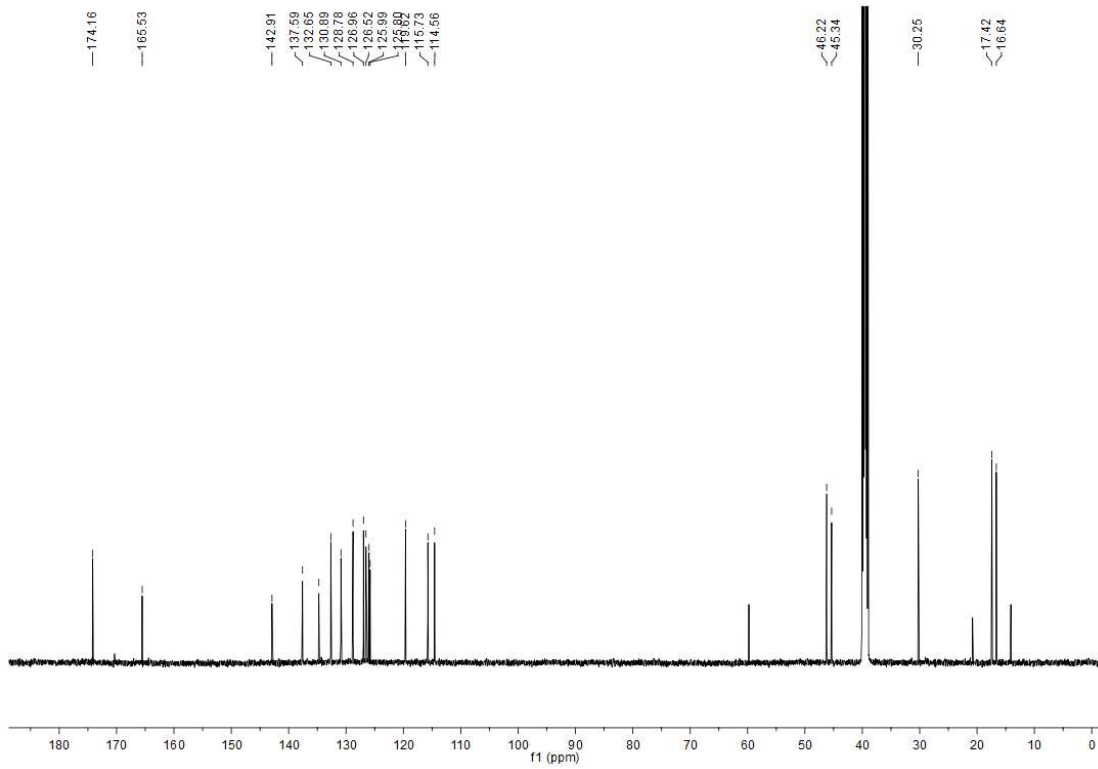


# (81)

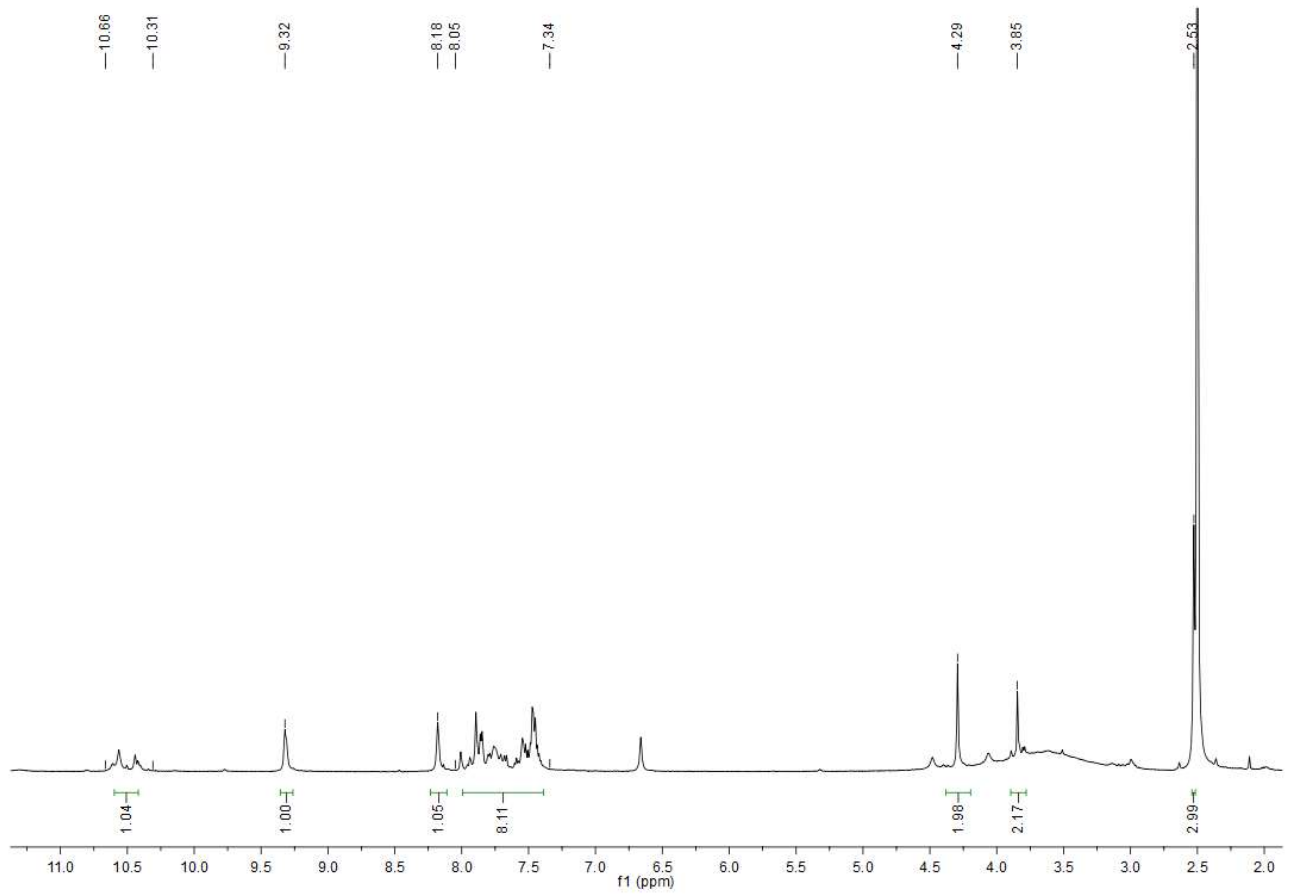
# 1H



13C



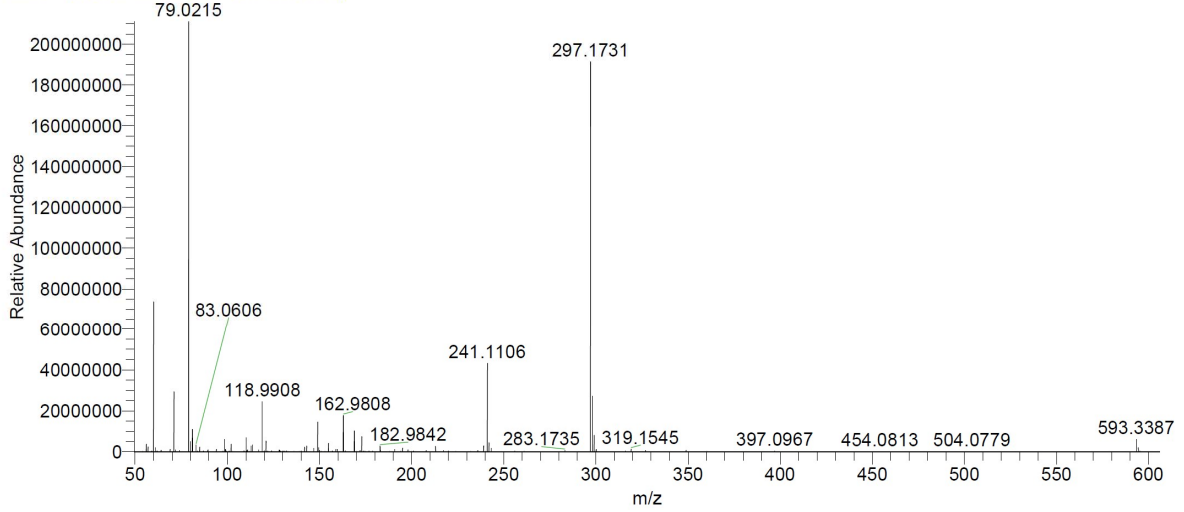
(76)



# HRMS-Data

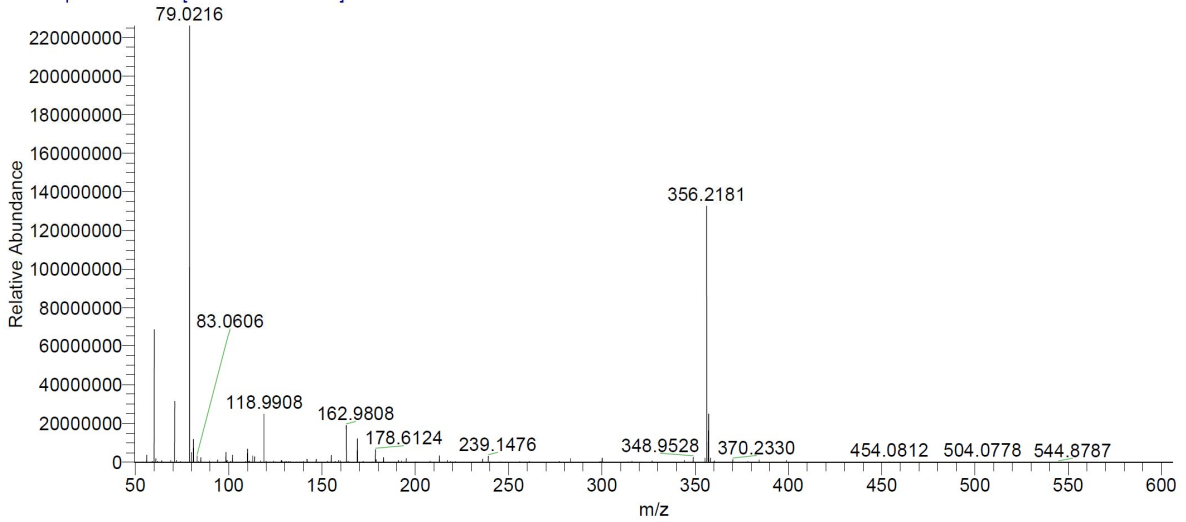
(1)

HIPS2501 #351-373 RT: 3.49-3.70 AV: 23 NL: 2.11E8  
T: FTMS + p ESI Full ms [50.0000-600.0000]



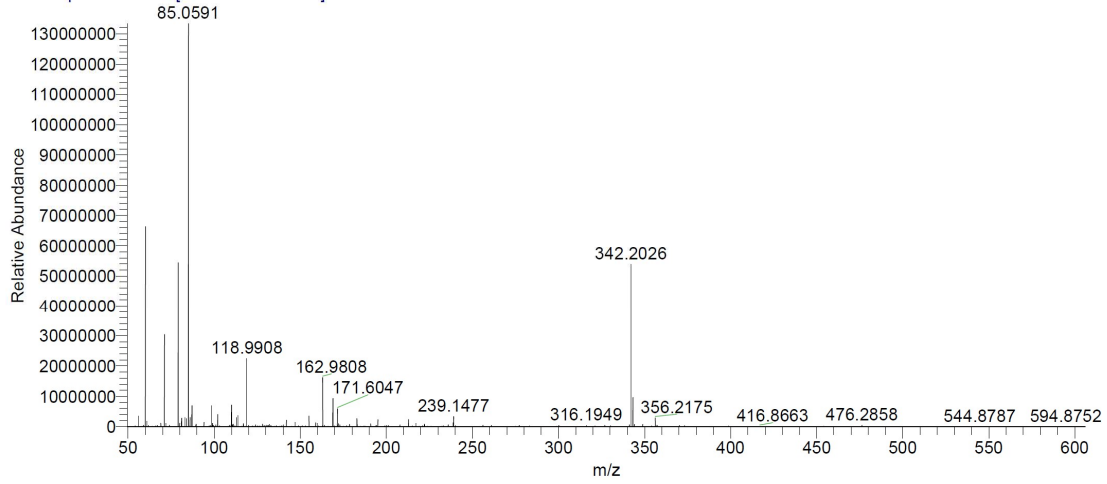
(2)

HIPS2513 #360-383 RT: 3.56-3.78 AV: 24 NL: 2.26E8  
T: FTMS - p ESI Full ms [50.0000-600.0000]



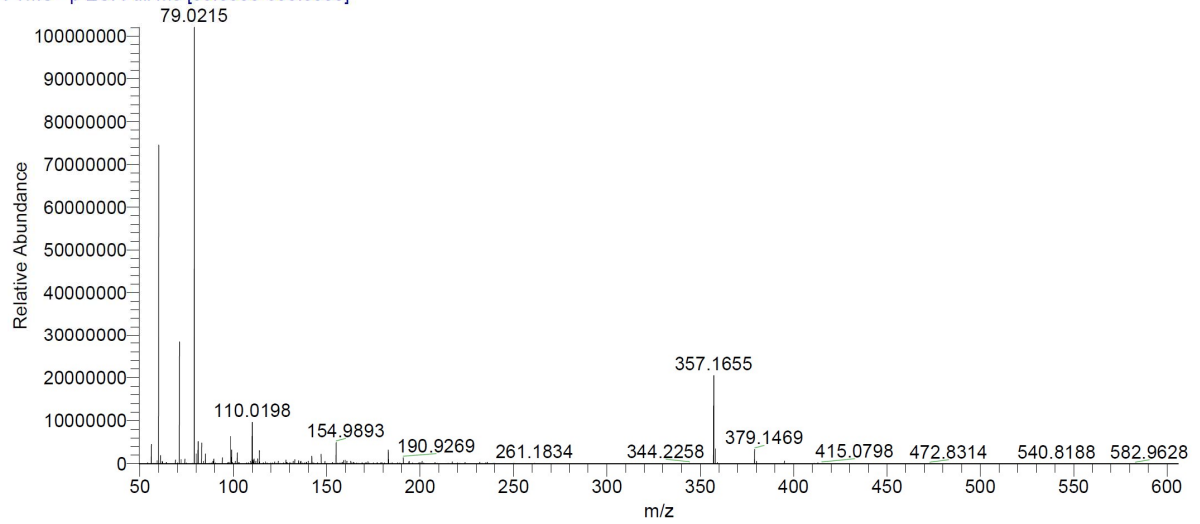
(6)

HIPS2536 #349-371 RT: 3.46-3.67 AV: 23 NL: 1.33E8  
T: FTMS + p ESI Full ms [50.0000-600.0000]



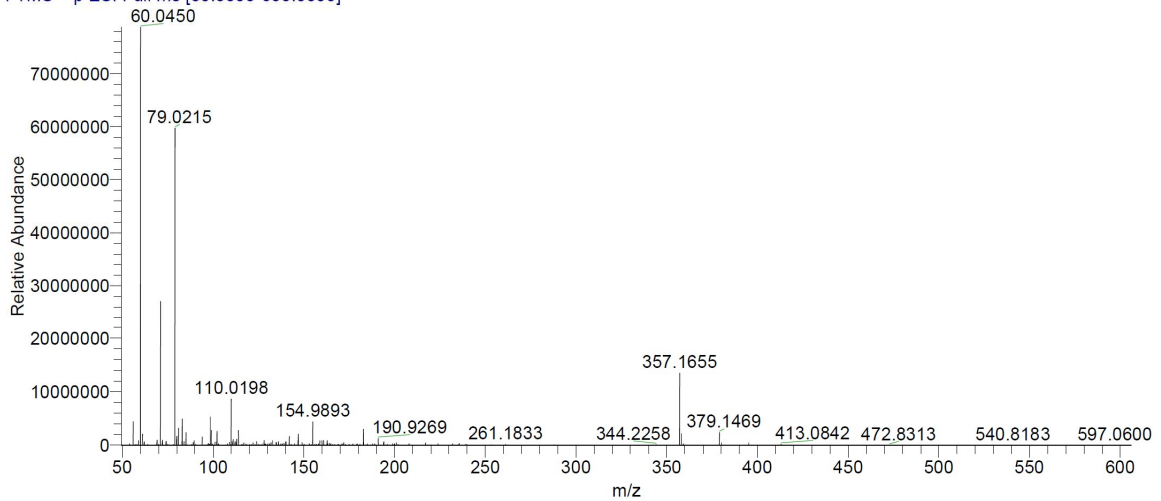
(3)

HIPS2629\_20230516095820 #358-387 RT: 3.61-3.90 AV: 30 NL: 1.02E8  
T: FTMS - p ESI Full ms [50.0000-600.0000]



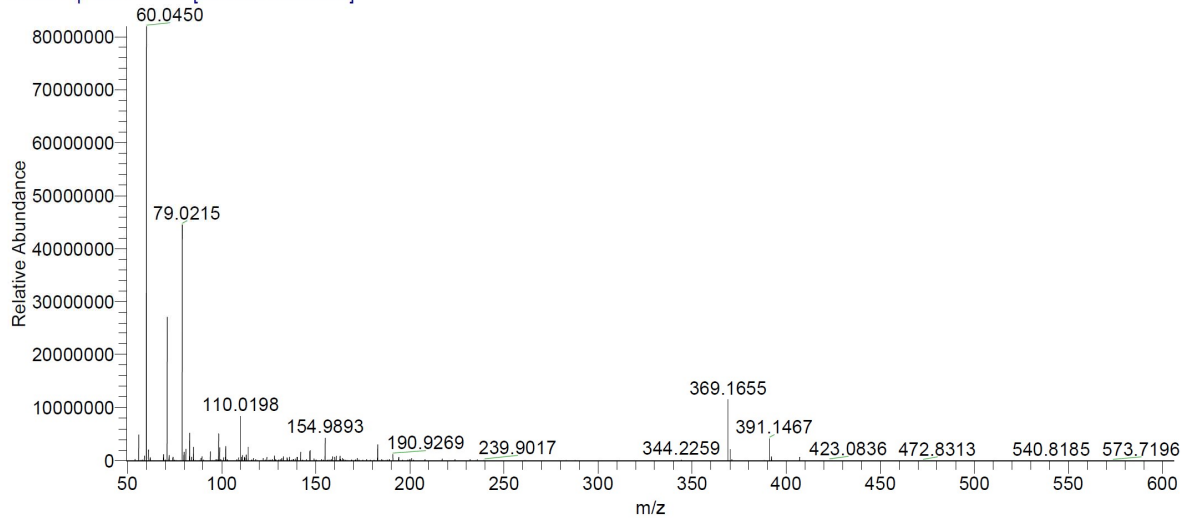
(5)

HIPS2630\_20230516101232 #357-396 RT: 3.60-3.99 AV: 40 NL: 7.87E7  
T: FTMS + p ESI Full ms [50.0000-600.0000]



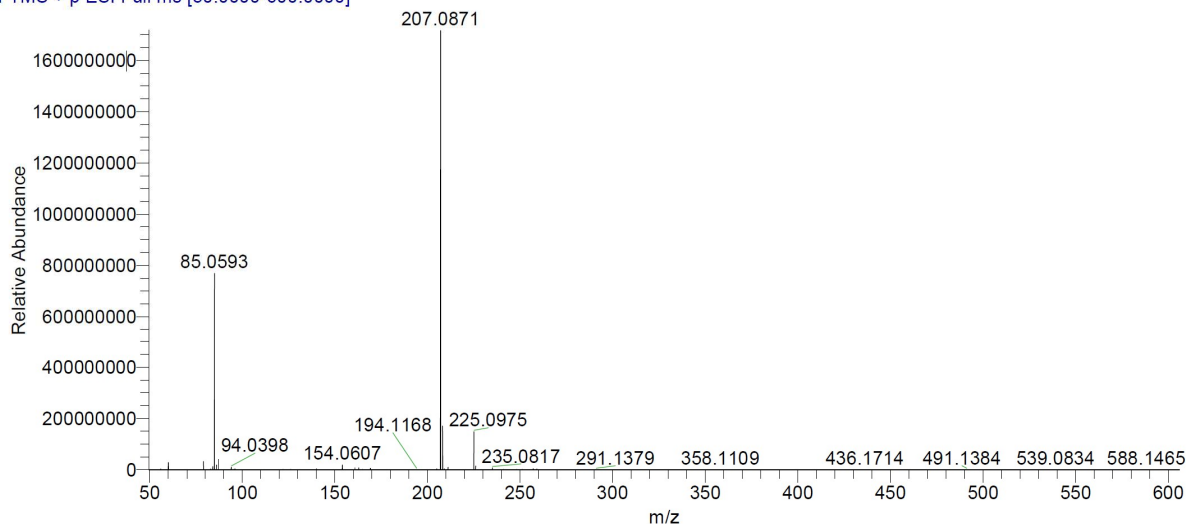
(4)

HIPS2631 #367-396 RT: 3.70-3.99 AV: 30 NL: 8.19E7  
T: FTMS + p ESI Full ms [50.0000-600.0000]



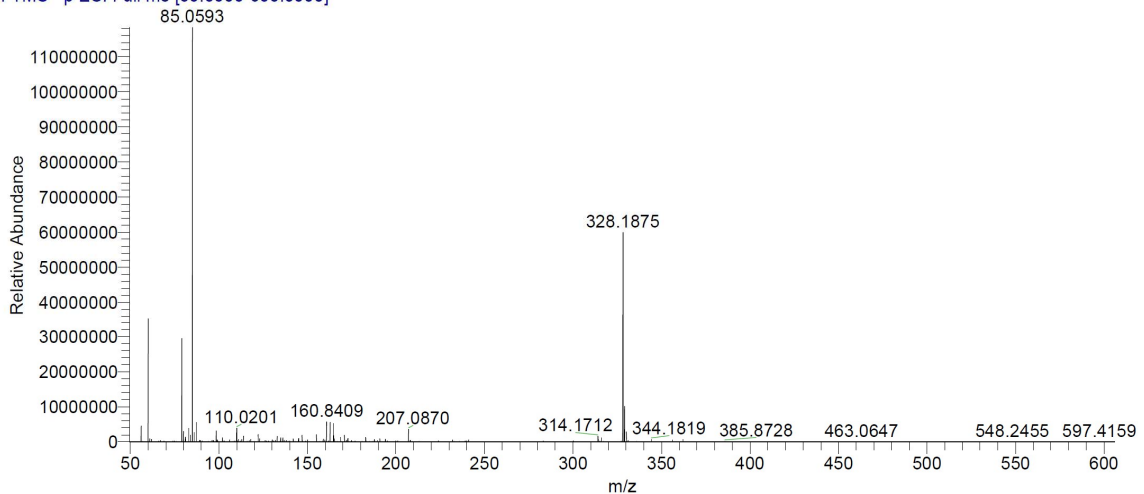
(124)

BZO772 #355-400 RT: 3.54-3.97 AV: 46 NL: 1.72E9  
T: FTMS + p ESI Full ms [50.0000-600.0000]



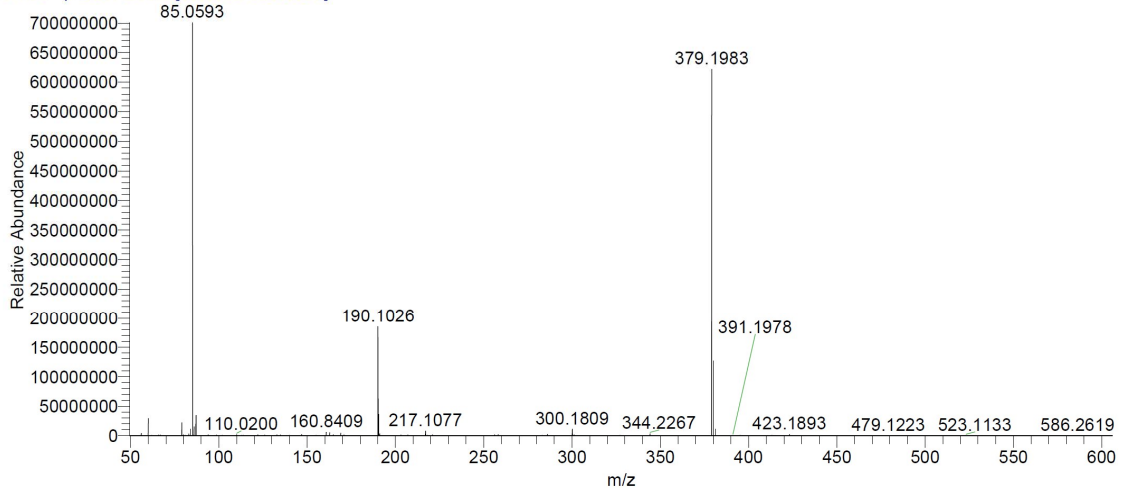
(48)

BZO773 #338-373 RT: 3.38-3.72 AV: 36 NL: 1.18E8  
T: FTMS - p ESI Full ms [50.0000-600.0000]



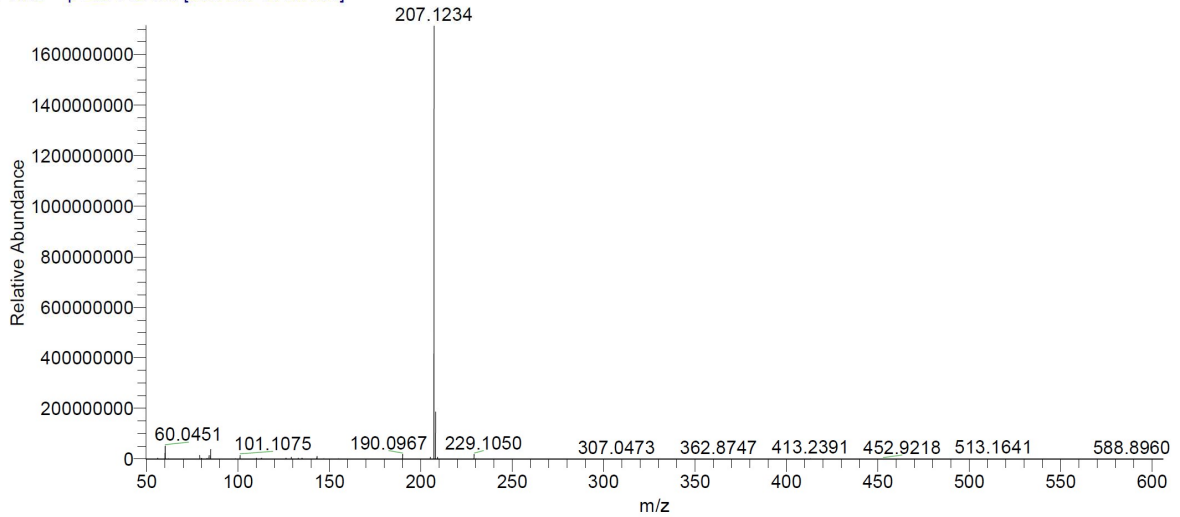
**(71)**

BZO775 #342-383 RT: 3.42-3.81 AV: 42 NL: 7.00E8  
T: FTMS - p ESI Full ms [50.0000-600.0000]



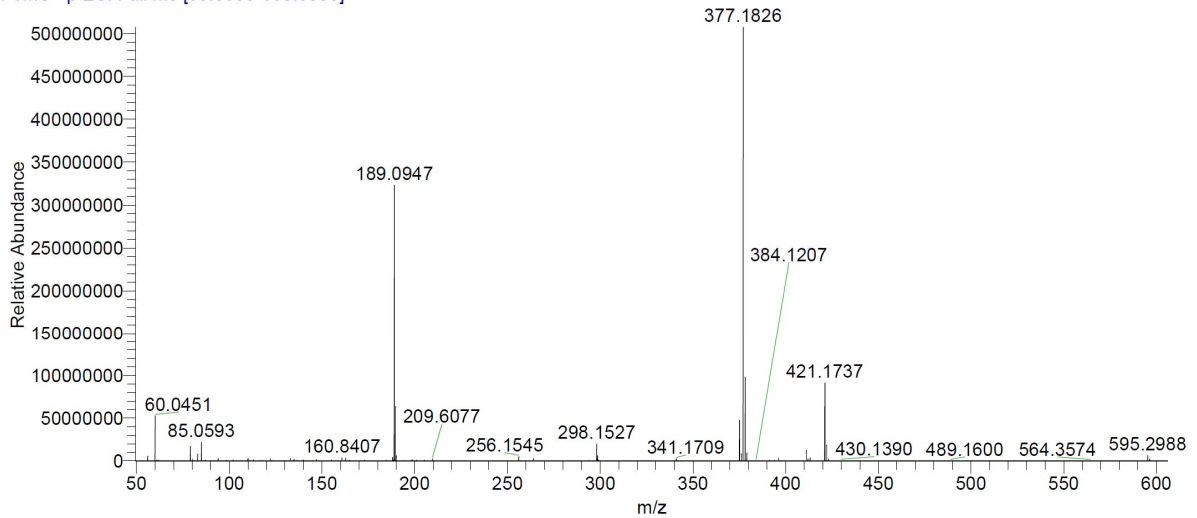
**(99)**

BZO777 #103-144 RT: 1.08-1.48 AV: 42 NL: 1.71E9  
T: FTMS + p ESI Full ms [50.0000-600.0000]



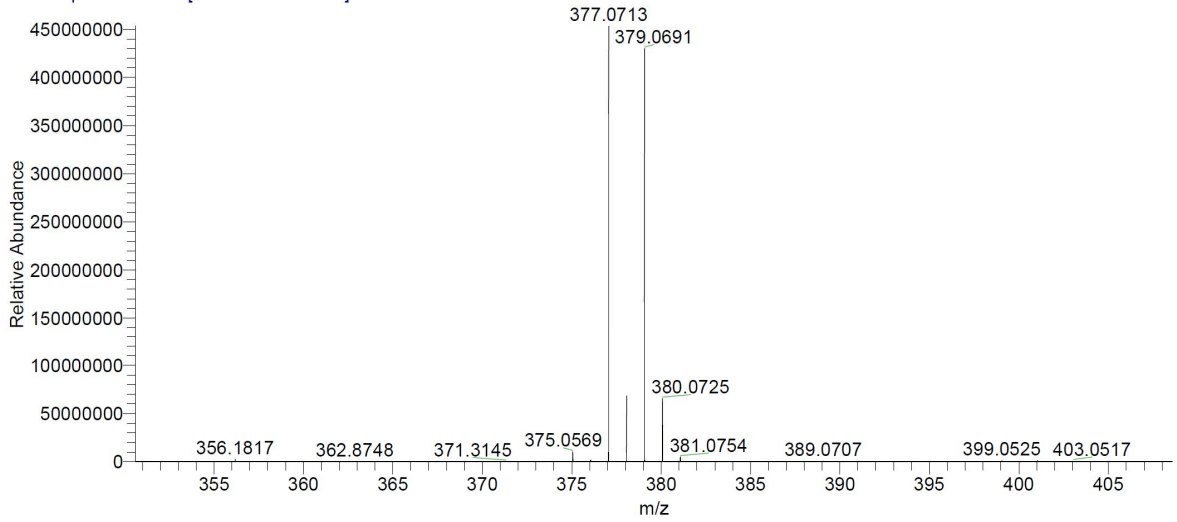
**(72)**

BZO781 #390-429 RT: 3.90-4.28 AV: 40 NL: 5.07E8  
T: FTMS - p ESI Full ms [50.0000-600.0000]



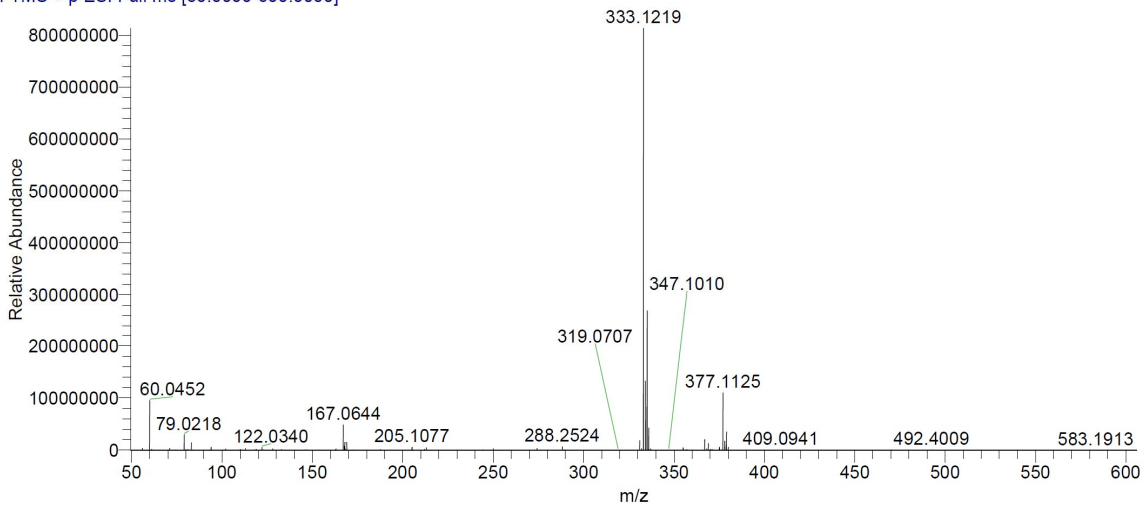
**(59)**

MKE46 #469-505 RT: 4.66-5.01 AV: 37 NL: 4.53E8  
T: FTMS + p ESI Full ms [50.0000-600.0000]



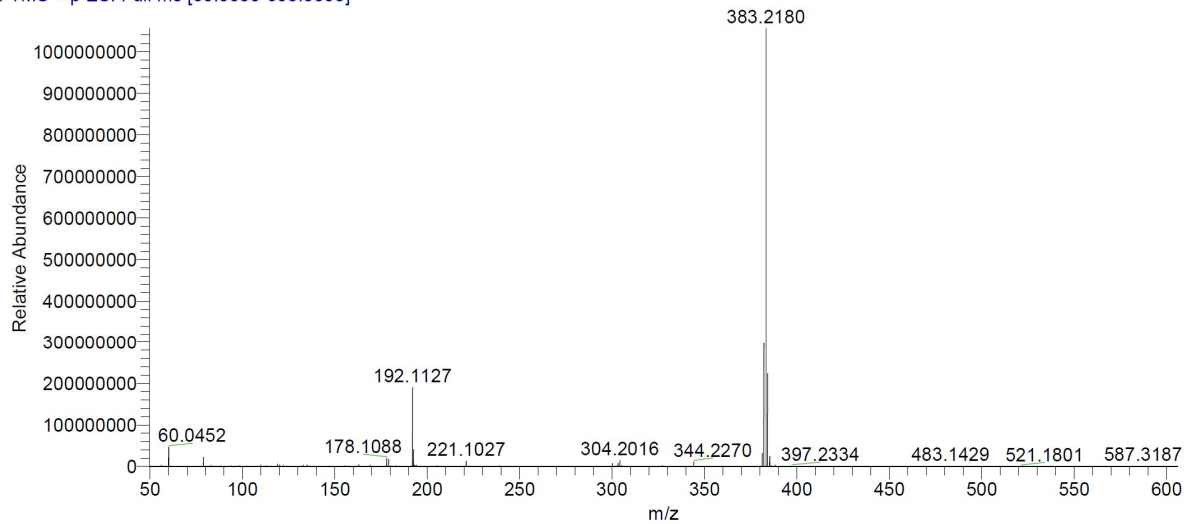
**(56)**

BZO765 #461-496 RT: 4.57-4.91 AV: 36 NL: 8.13E8  
T: FTMS + p ESI Full ms [50.0000-600.0000]



**(58)**

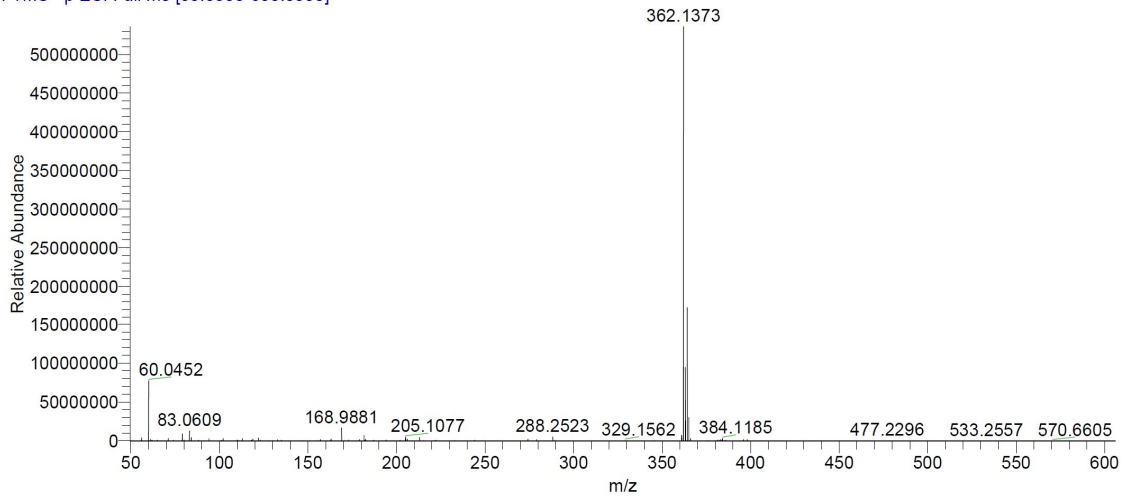
BZO769 #353-387 RT: 3.51-3.84 AV: 35 NL: 1.05E9  
T: FTMS + p ESI Full ms [50.0000-600.0000]





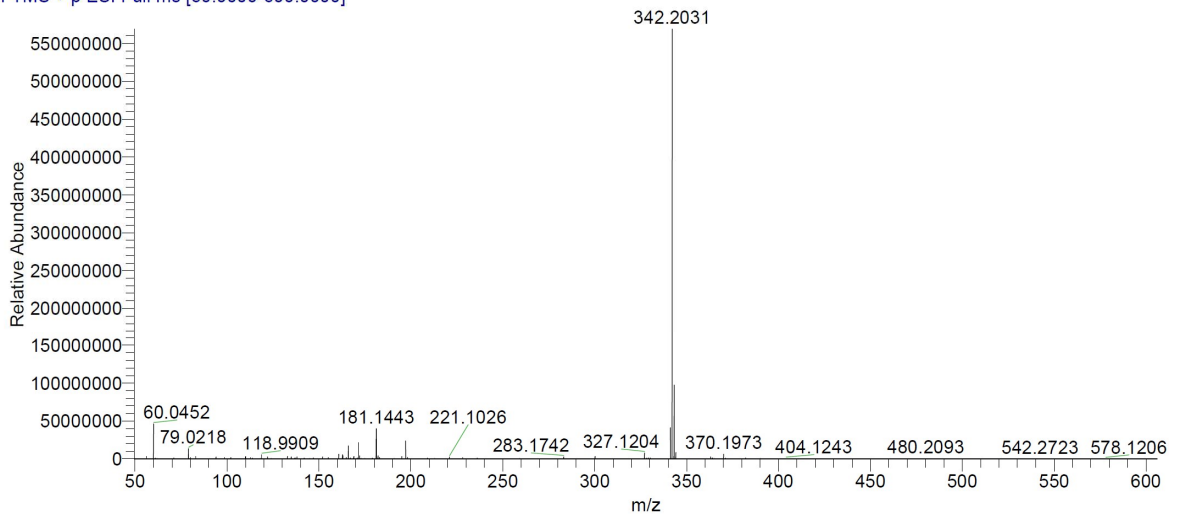
**(57)**

BZO770 #456-498 RT: 4.53-4.95 AV: 43 NL: 5.36E8  
T: FTMS - p ESI Full ms [50.0000-600.0000]



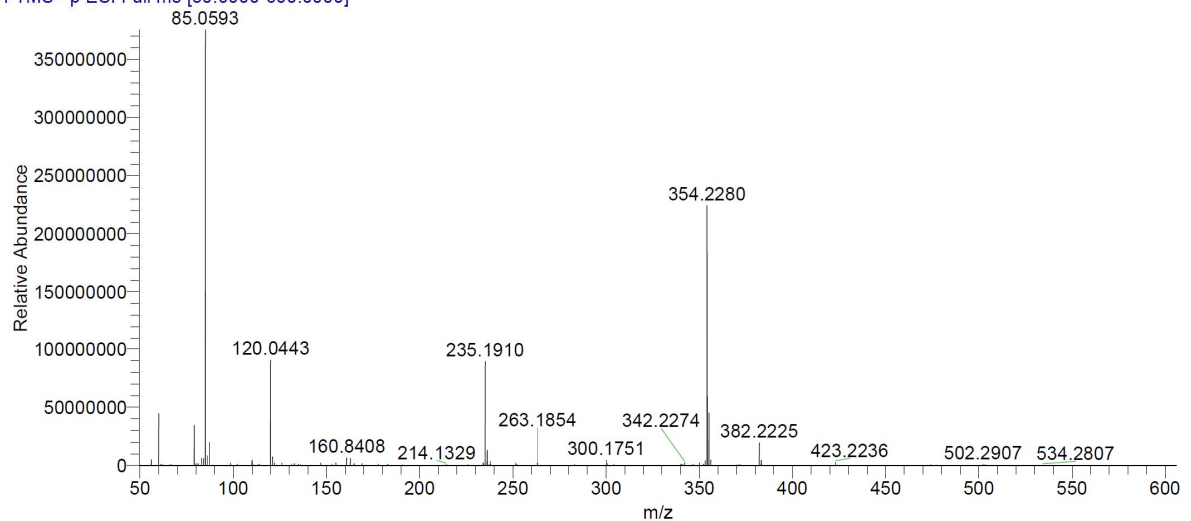
**(65)**

BZO771 #349-380 RT: 3.49-3.79 AV: 32 NL: 5.69E8  
T: FTMS + p ESI Full ms [50.0000-600.0000]



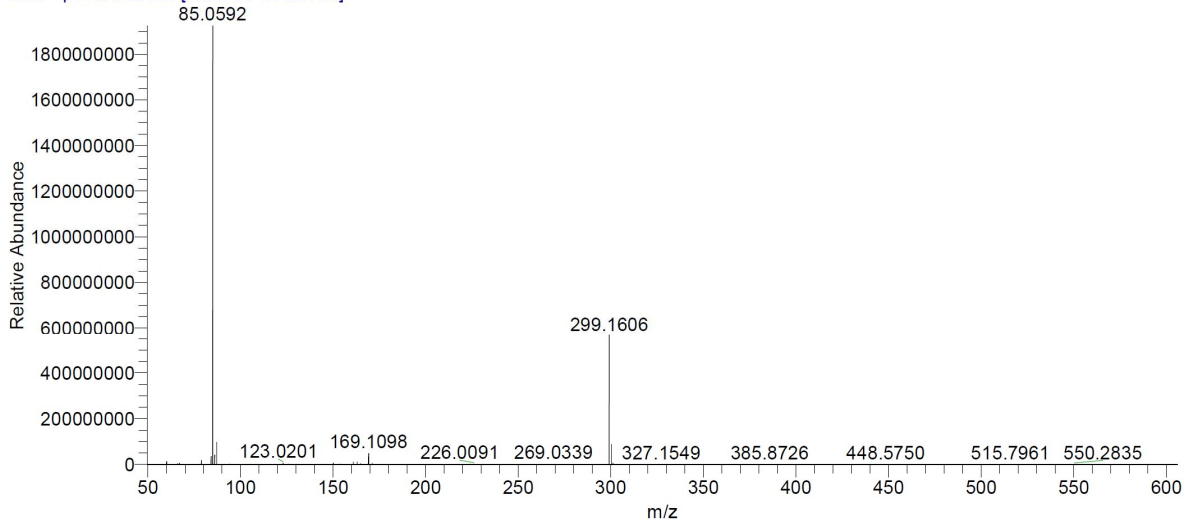
**(51)**

HIPS2537 #372-401 RT: 3.72-4.01 AV: 30 NL: 3.75E8  
T: FTMS - p ESI Full ms [50.0000-600.0000]



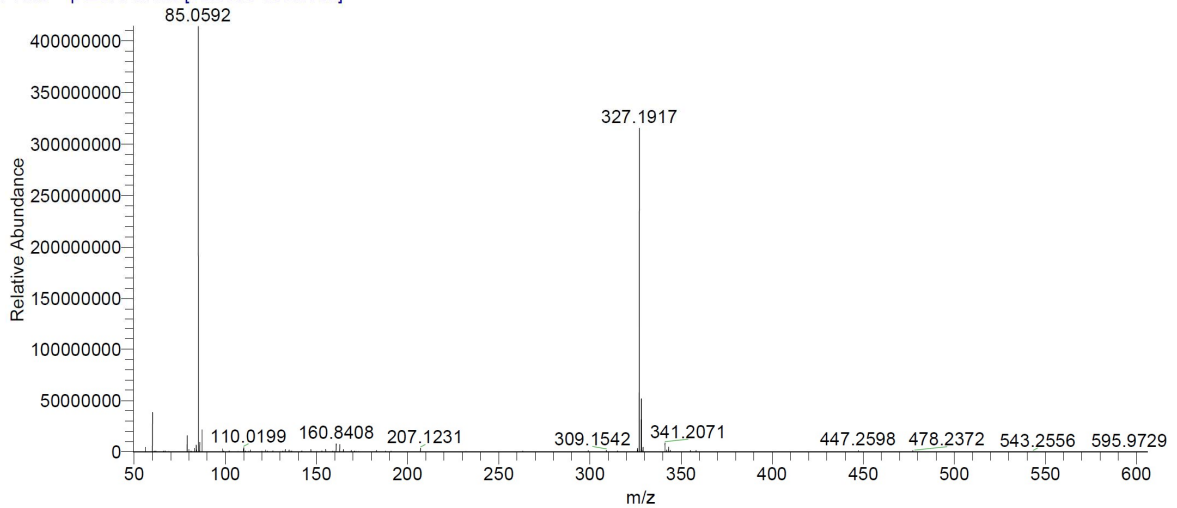
**(70)**

HIPS2558 #210-241 RT: 2.13-2.43 AV: 32 NL: 1.92E9  
T: FTMS - p ESI Full ms [50.0000-600.0000]



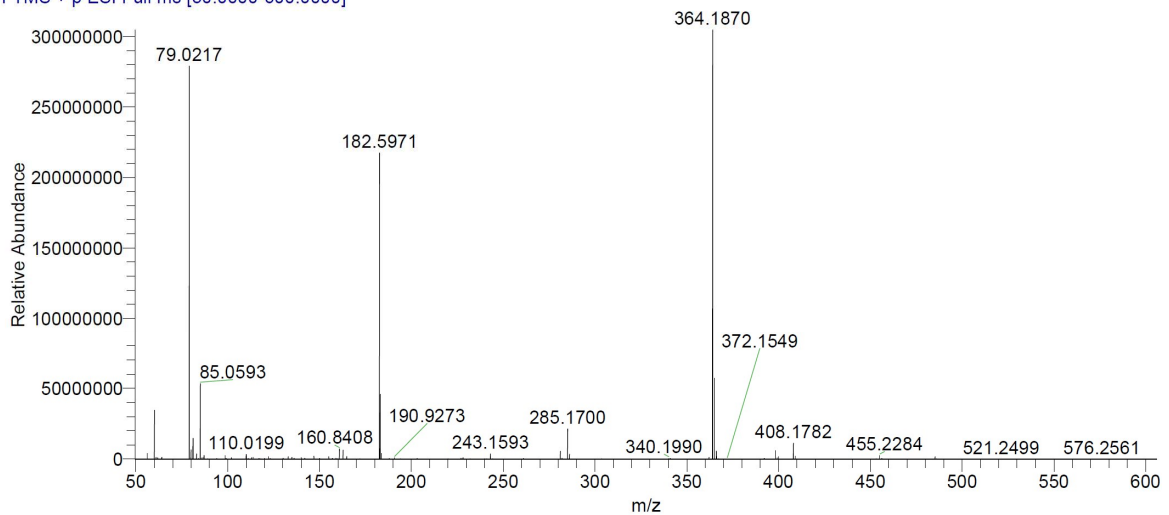
**(50)**

HIPS2563 #345-367 RT: 3.44-3.65 AV: 23 NL: 4.14E8  
T: FTMS + p ESI Full ms [50.0000-600.0000]



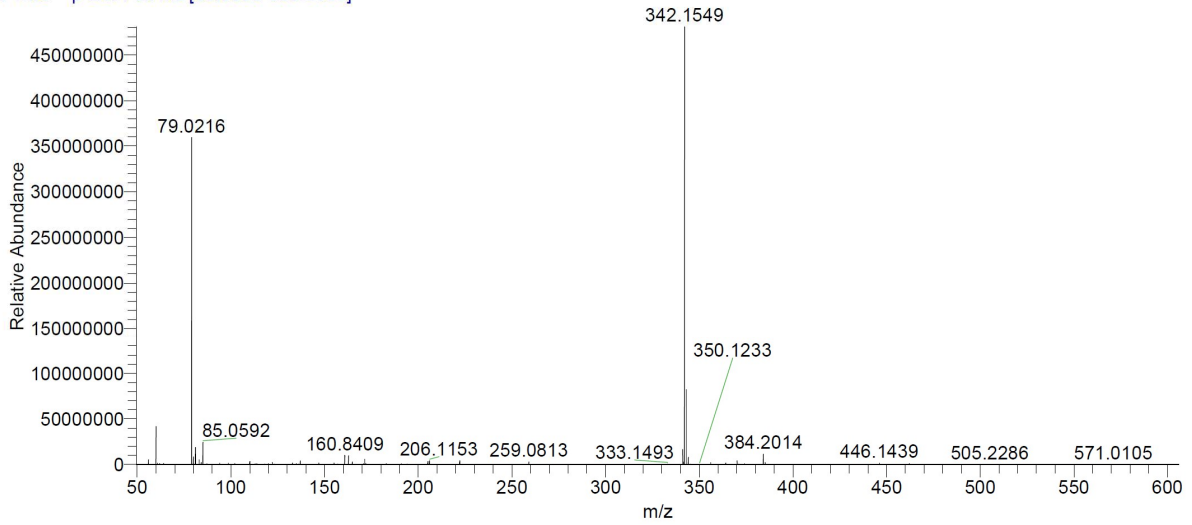
**(55)**

HIPS2565 #351-380 RT: 3.50-3.78 AV: 30 NL: 3.05E8  
T: FTMS + p ESI Full ms [50.0000-600.0000]



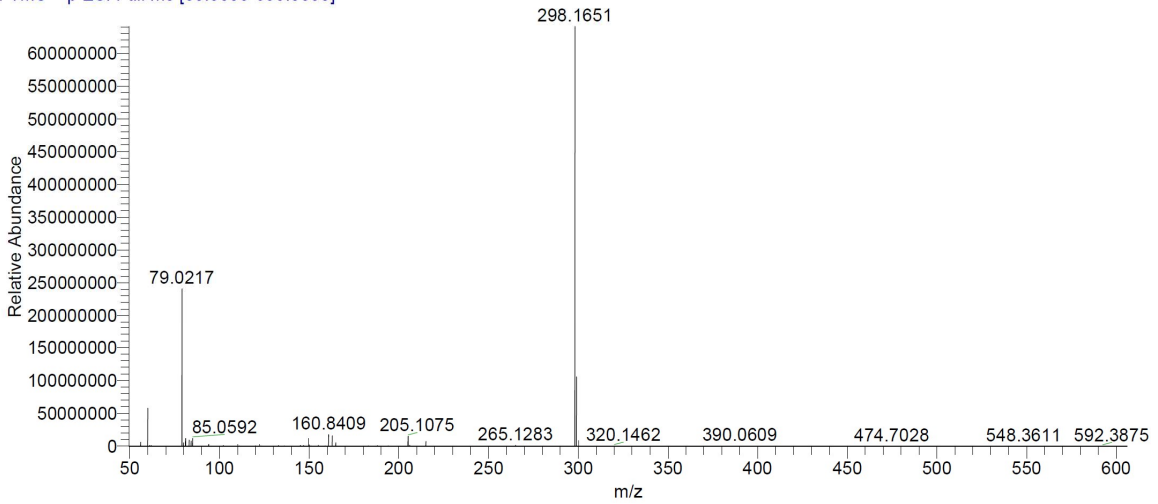
**(52)**

HIPS2566 #371-397 RT: 3.69-3.95 AV: 27 NL: 4.81E8  
T: FTMS + p ESI Full ms [50.0000-600.0000]



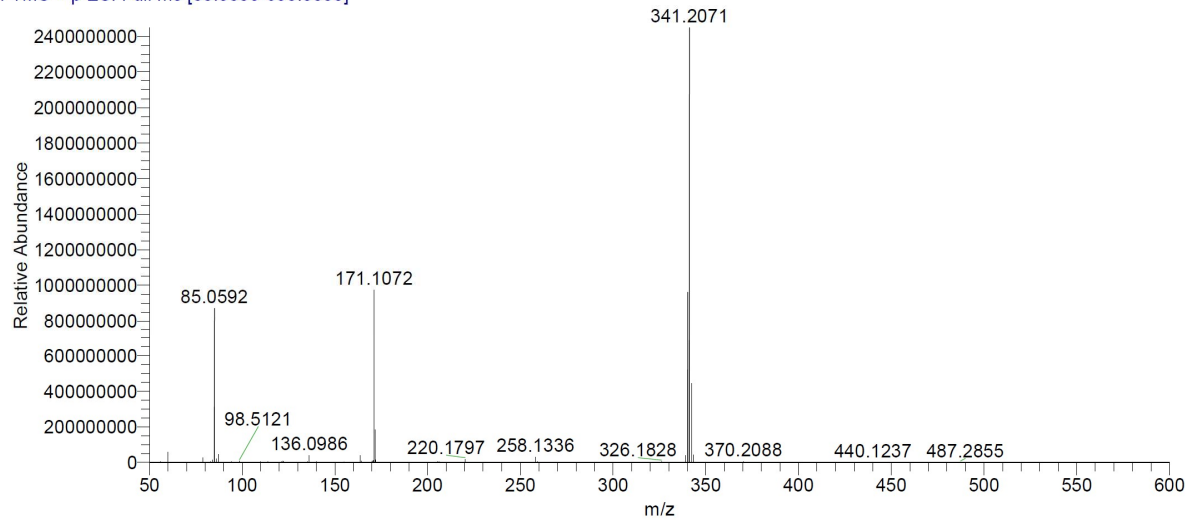
**(53)**

HIPS2567 #413-440 RT: 4.11-4.37 AV: 28 NL: 6.40E8  
T: FTMS + p ESI Full ms [50.0000-600.0000]



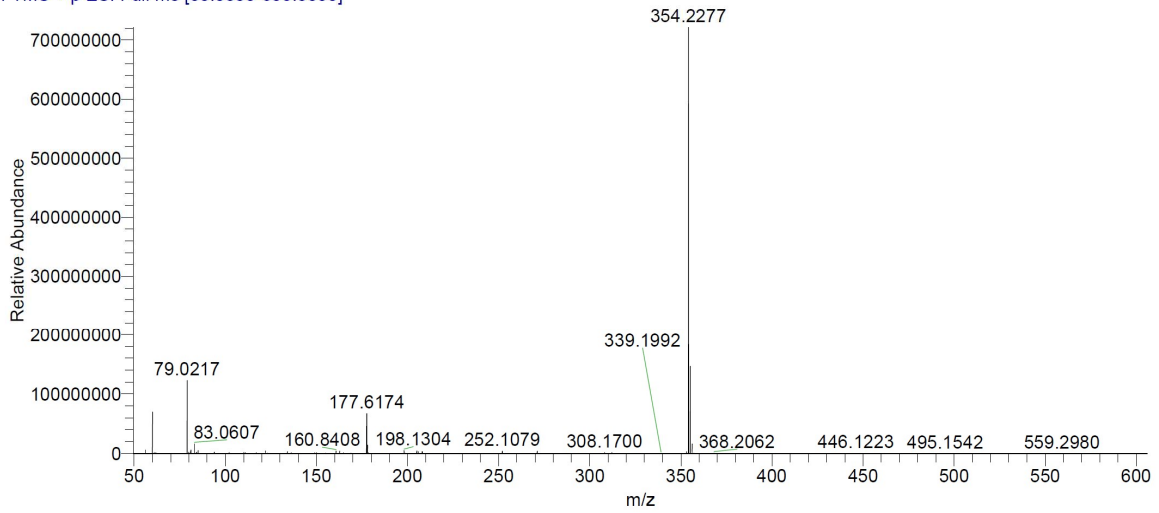
**(54)**

HIPS2569 #353 RT: 3.52 AV: 1 NL: 2.45E9  
T: FTMS + p ESI Full ms [50.0000-600.0000]



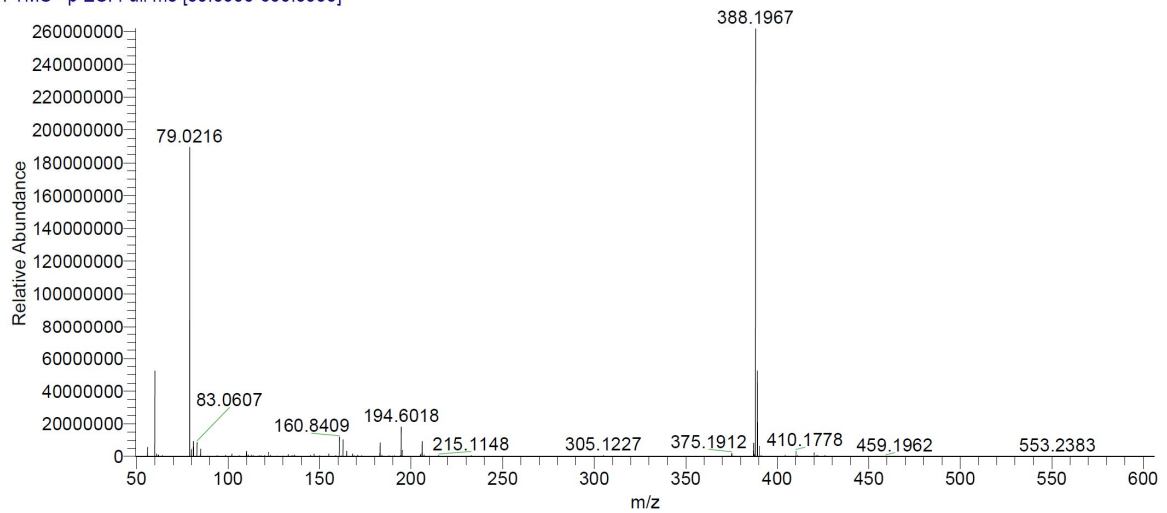
**(62)**

HIPS2572 #495-530 RT: 4.91-5.25 AV: 36 NL: 7.21E8  
T: FTMS - p ESI Full ms [50.0000-600.0000]



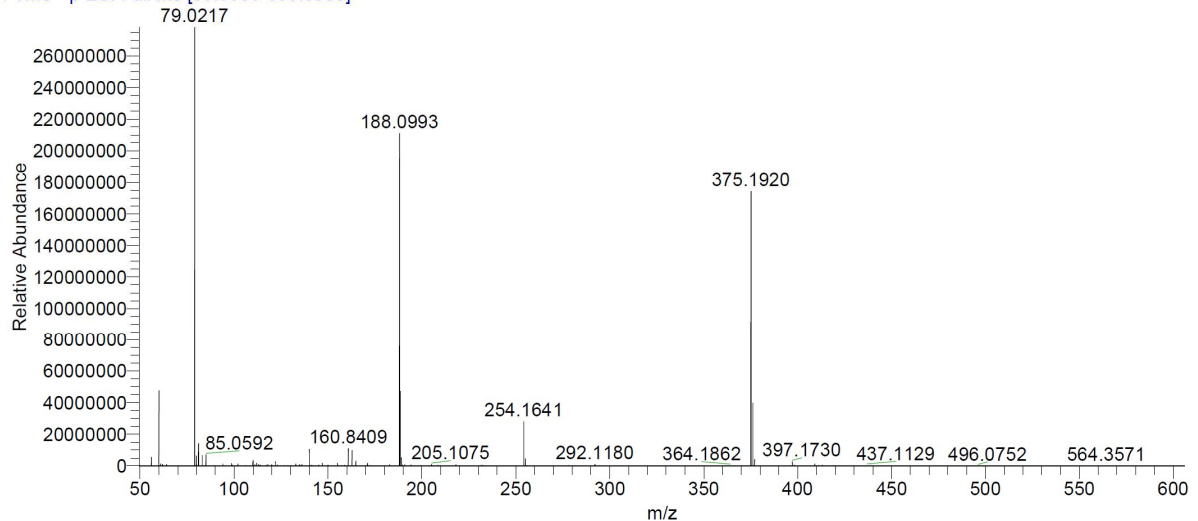
**(64)**

HIPS2582 #404-448 RT: 4.02-4.45 AV: 45 NL: 2.62E8  
T: FTMS - p ESI Full ms [50.0000-600.0000]



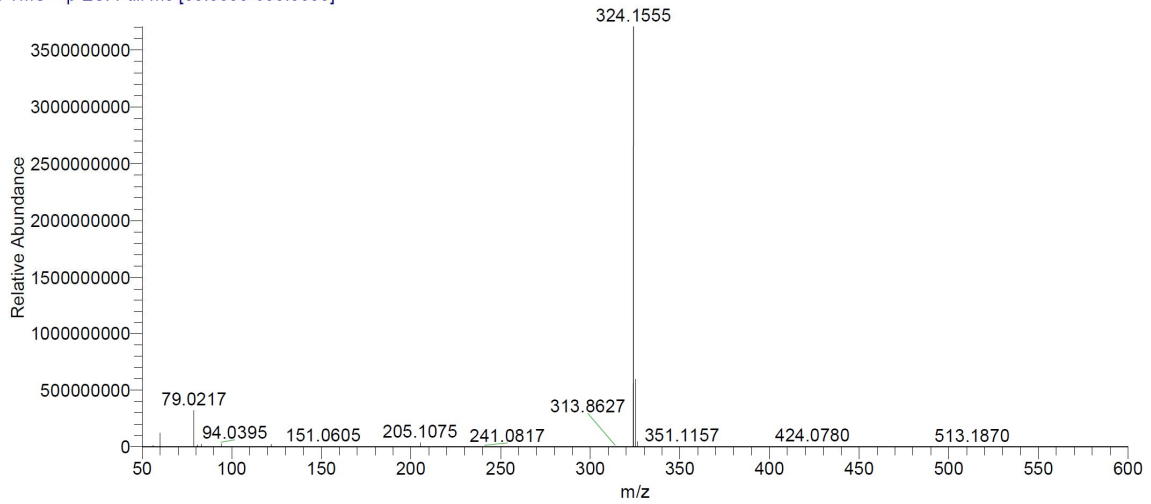
**(66)**

HIPS2593 #380-424 RT: 3.79-4.21 AV: 45 NL: 2.78E8  
T: FTMS - p ESI Full ms [50.0000-600.0000]



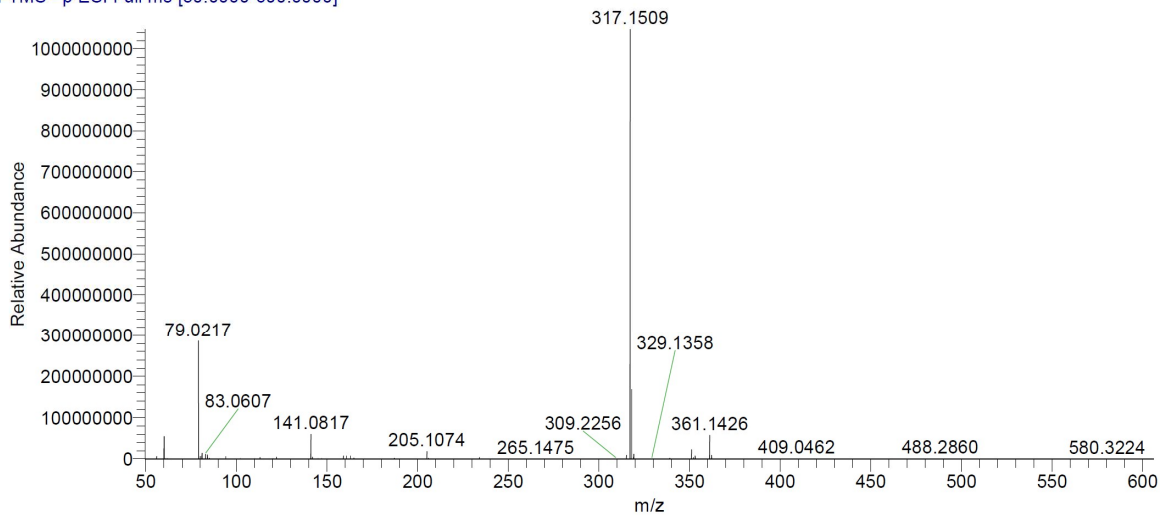
**(33)**

HIPS2601 #455 RT: 4.52 AV: 1 NL: 3.70E9  
T: FTMS + p ESI Full ms [50.0000-600.0000]



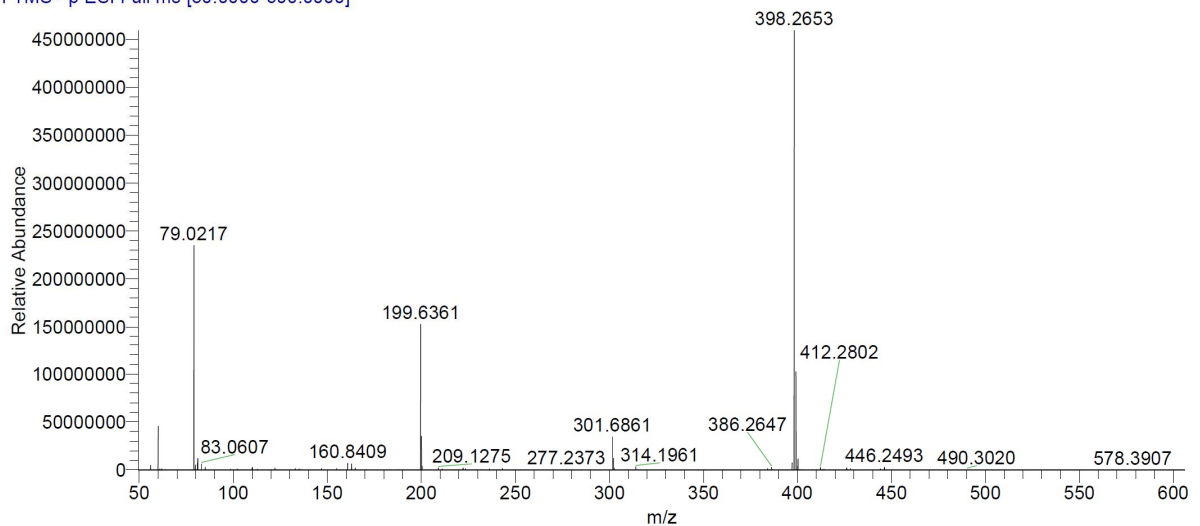
**(67)**

HIPS2608 #448-476 RT: 4.46-4.73 AV: 29 NL: 1.05E9  
T: FTMS - p ESI Full ms [50.0000-600.0000]



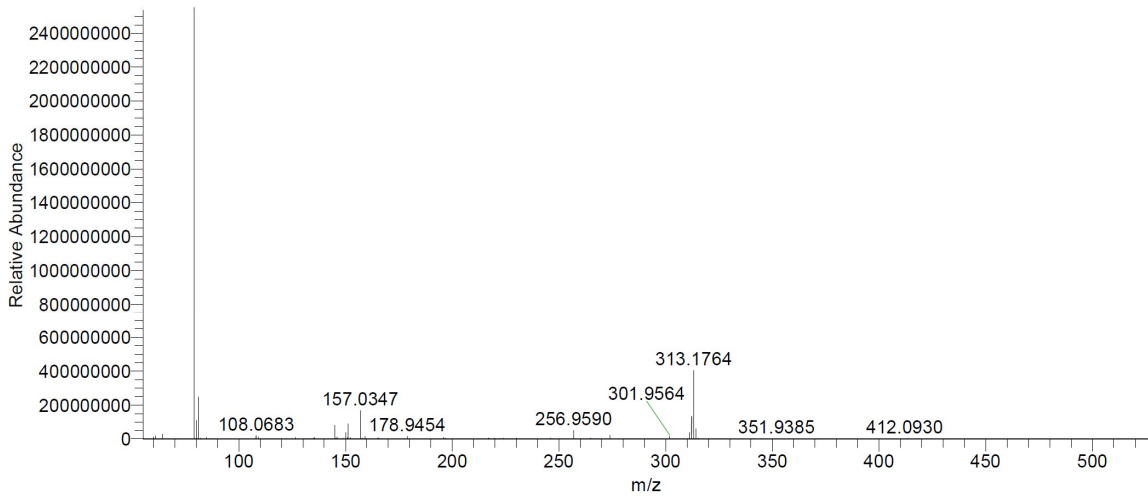
**(69)**

HIPS2609 #394-424 RT: 3.93-4.22 AV: 31 NL: 4.59E8  
T: FTMS - p ESI Full ms [50.0000-600.0000]



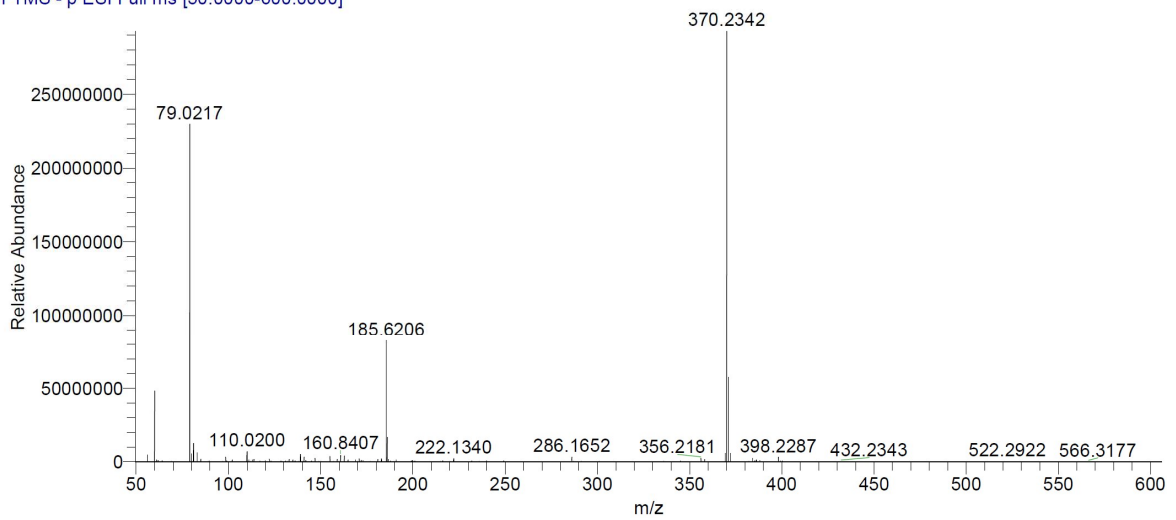
**(63)**

HIPS2619 #201 RT: 2.03 AV: 1 NL: 4.89E9  
T: FTMS + p ESI Full ms [50.0000-600.0000]



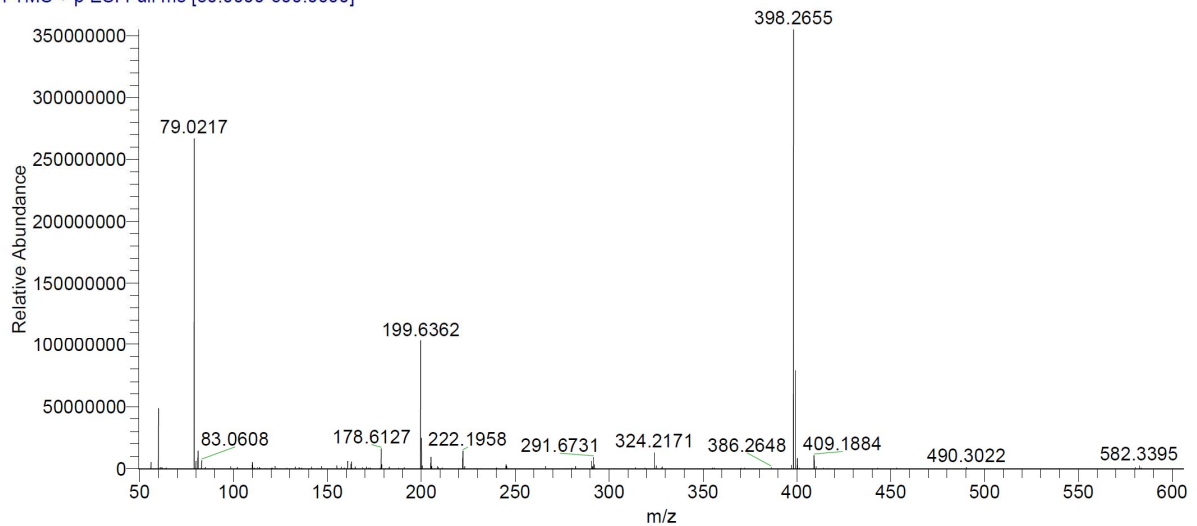
**(68)**

HIPS2620 #368-389 RT: 3.67-3.87 AV: 22 NL: 2.93E8  
T: FTMS - p ESI Full ms [50.0000-600.0000]



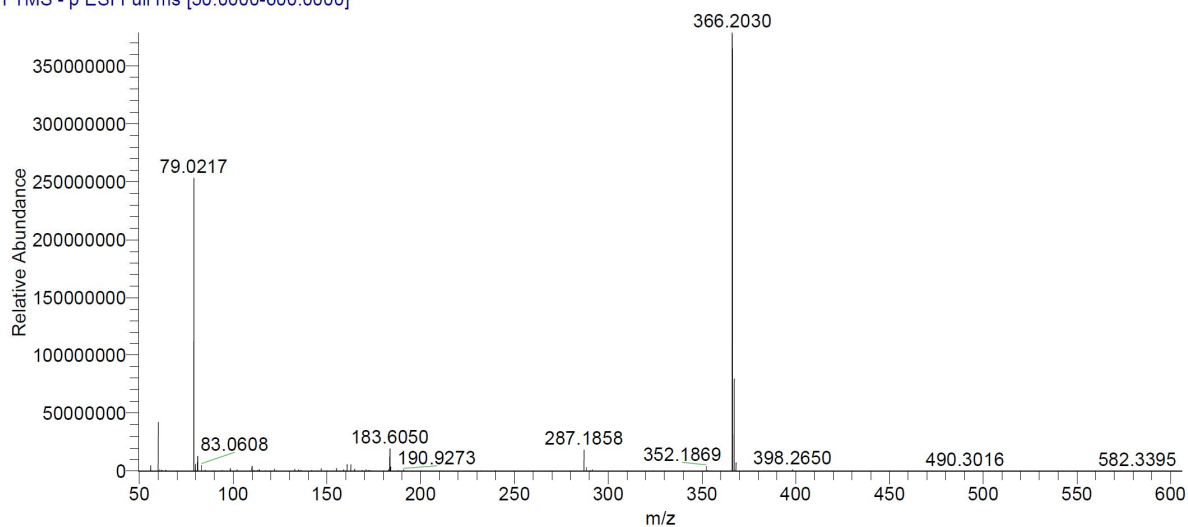
**(61)**

HIPS2621 #373-413 RT: 3.72-4.11 AV: 41 NL: 3.55E8  
T: FTMS + p ESI Full ms [50.0000-600.0000]



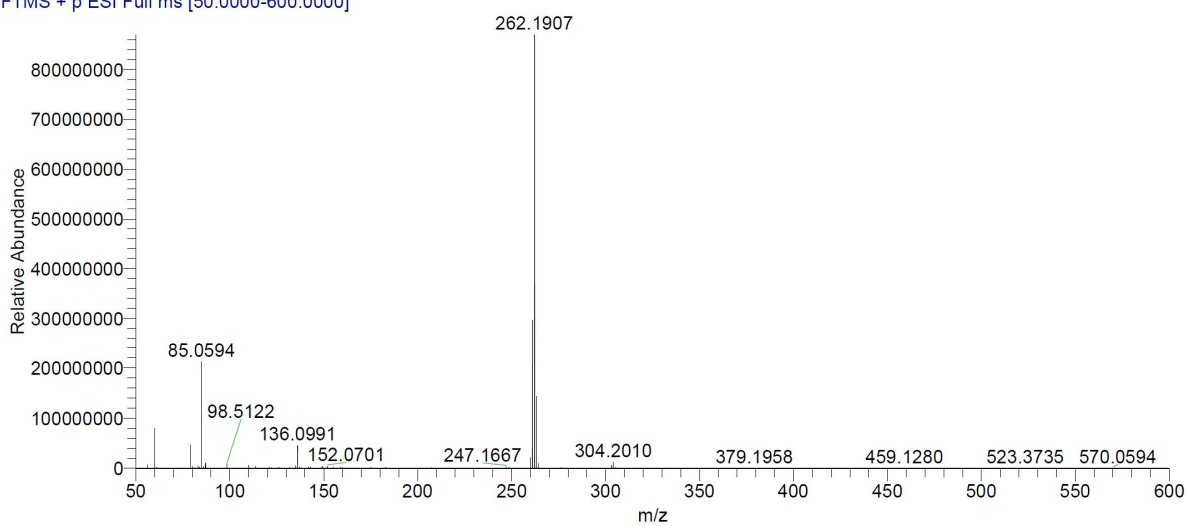
**(37)**

HIPS2627 #364-391 RT: 3.63-3.89 AV: 28 NL: 3.78E8  
T: FTMS - p ESI Full ms [50.0000-600.0000]

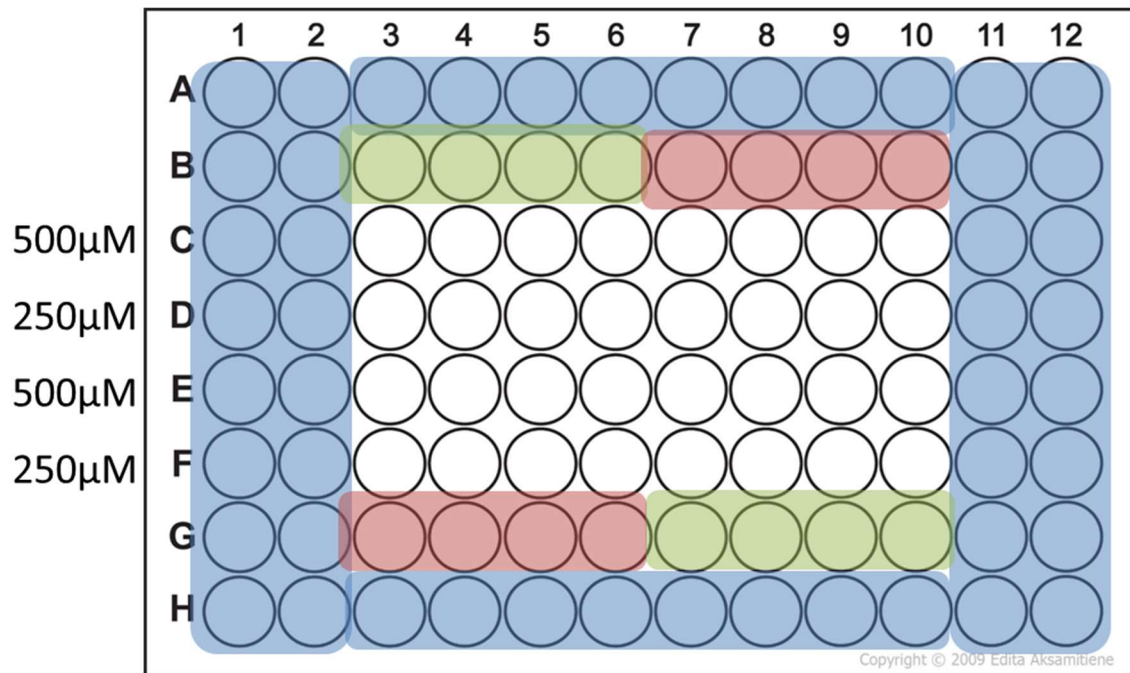


**(49)**

BZO776 #305 RT: 3.06 AV: 1 NL: 8.69E8  
T: FTMS + p ESI Full ms [50.0000-600.0000]



## Assay results



Microtiter plate scheme of the luciferase screening assay. Wells in blue represent water, wells in red represent the positive control with plasmid pNS6236 (cesT+) and 5% DMSO and wells in green represents the vehicle with 5% DMSO.



## 8.4 Small molecules inhibiting the IMP2-RNA interaction

### Supporting Information

#### The first small molecule inhibitors targeting the RNA binding protein IGF2BP2/IMP2 for cancer therapy

Charlotte Dahlem<sup>a,#</sup>, Ali Abuhaliema<sup>a,#</sup>, Sonja M. Kessler<sup>a,b,#</sup>, Tarek Kröhler<sup>a</sup>, Ben G. E. Zoller<sup>c</sup>, Shilpee Chanda<sup>a</sup>, Yingwen Wu<sup>c</sup>, Simon Both<sup>a</sup>, Fabian Müller<sup>d</sup>, Konstantin Lepikhov<sup>e</sup>, Susanne H. Kirsch<sup>f</sup>, Stephan Laggai<sup>a</sup>, Rolf Müller<sup>f,g</sup>, Martin Empting<sup>c,g</sup>, Alexandra K. Kiemer<sup>a,\*</sup>

<sup>a</sup> Department of Pharmacy, Pharmaceutical Biology, Saarland University, Saarbrücken, 66123, Germany

<sup>b</sup> Institute of Pharmacy, Experimental Pharmacology for Natural Sciences, Martin Luther University Halle-Wittenberg, Halle, 06108, Germany

<sup>c</sup> Department of Drug Design and Optimization, Helmholtz Institute for Pharmaceutical Research Saarland (HIPS), Helmholtz Centre for Infection Research (HZI), Saarland University, Saarbrücken, 66123, Germany <sup>d</sup> Center for Bioinformatics, Saarland University, Saarbrücken, 66123, Germany <sup>e</sup> Department of Genetics, Saarland University, 66123 Saarbrücken, 66123, Germany

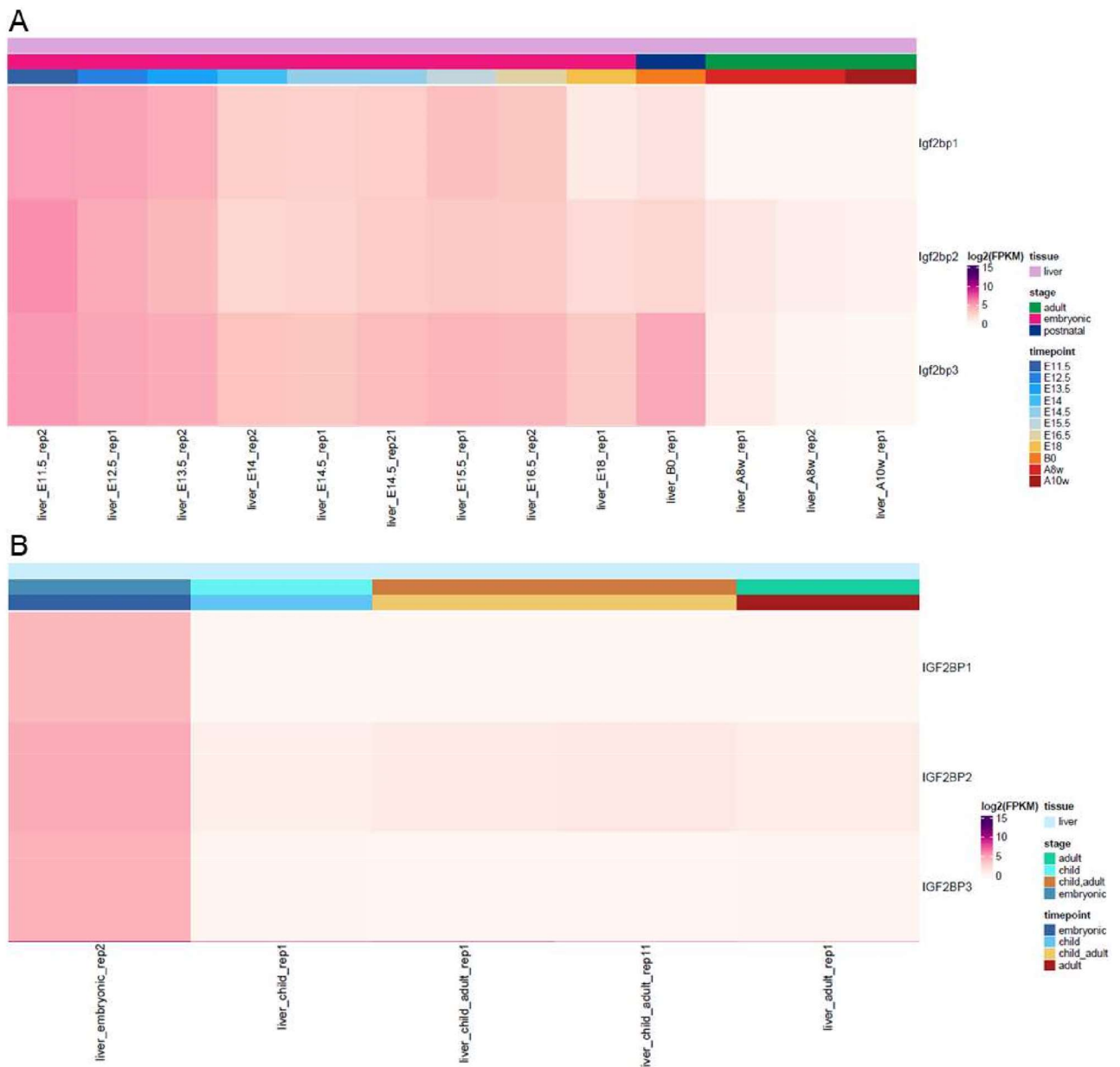
<sup>f</sup> Department of Microbial Natural Products, Helmholtz Institute for Pharmaceutical Research Saarland (HIPS), Helmholtz Centre for Infection Research, Saarland University Campus, 66123 Saarbrücken, Germany <sup>g</sup> Department of Pharmacy, Saarland University, Saarbrücken, 66123, Germany

# equal contribution

\* corresponding author

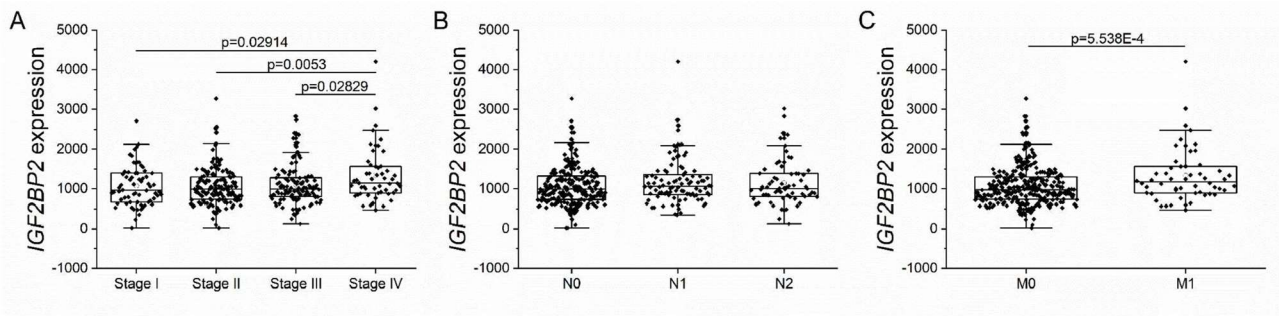
Alexandra K. Kiemer  
Saarland University  
Department of Pharmacy  
Pharmaceutical Biology  
Campus C2 3  
D-66123 Saarbrücken, Germany Fax:  
+49 681 3021 57302  
pharm.bio.kiemer@mx.uni-  
saarland.de

## Supplementary Figures



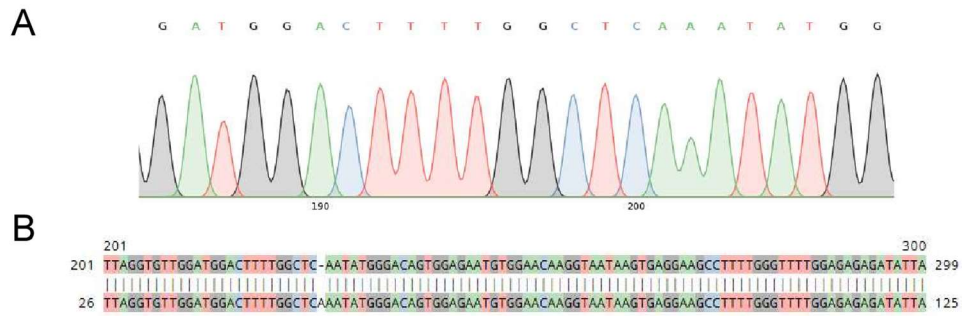
**Supplementary Figure S1. Comparison of IGF2BP2 expression with IGF2BP1 and IGF2BP3 in murine and human embryonic and adult livers**

Gene expression levels (log<sub>2</sub> FPKM) for IGF2BPs 1-3 in (A) mouse liver and (B) human liver in different developmental stages. Data originated from a mouse developmental atlas and the ENCODE project.



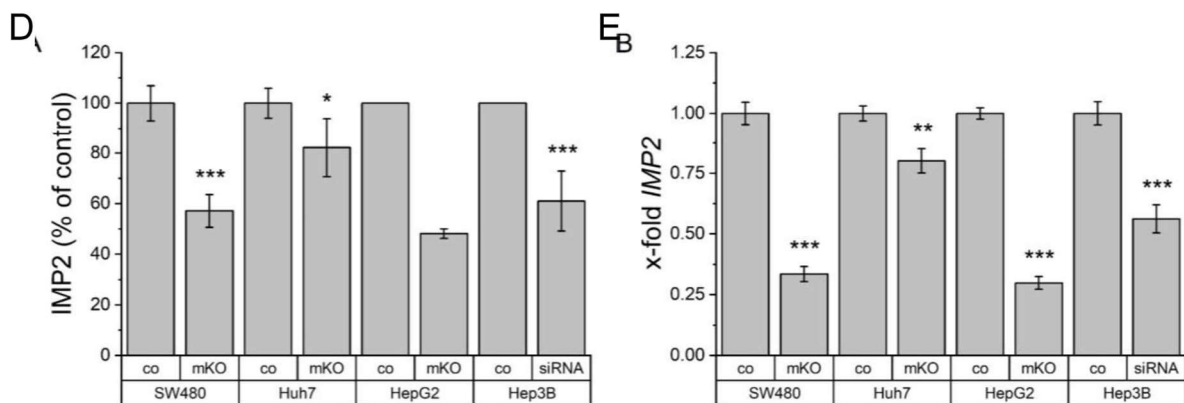
**Supplementary Figure S2. IGF2BP2 expression of COAD patients**

Analyses of the IGF2BP2 expression in the COAD dataset tumors characterized by (A) AJCC neoplasm disease stage and (B, C) pathology T/N/M stage.



**C**

„KO #1“ HCT116 clone 47-1	Biallelic A insertion
„KO #3“ HCT116 clone 47-2	Allele 1: A insertion Allele 2: 10 bp deletion
„KO #4“ HCT116 clone 47-6	Allele 1: 10 bp deletion Allele 2: G insertion
„KO #2“ HCT116 clone PE 12-1	Biallelic 2 bp deletion
Huh7 clone	Monoallelic A insertion
HepG2 clone	Monoallelic mutation: CGG instead of ATA



### Supplementary Figure S3. Sanger sequencing of IMP2 CRISPR clones

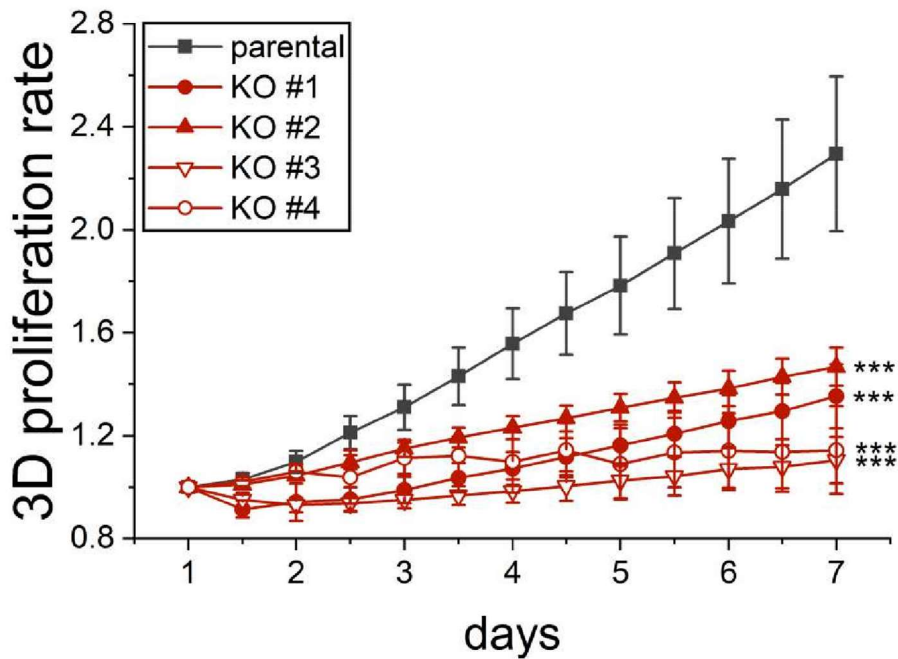
(A) Representative Sanger sequencing result of the IMP2 CRISPR HCT116 clone 47-1 that was used for target validation and compound testing (e.g., Figure 1 and Figure 5).

(B) Sequence alignment of IMP2 CRISPR HCT116 clone 47-1, demonstrating a bi-allelic A insertion.

(C) Table summarizing the editing of clones used in this study. HCT116 clone “KO #2” was generated using prime editing.

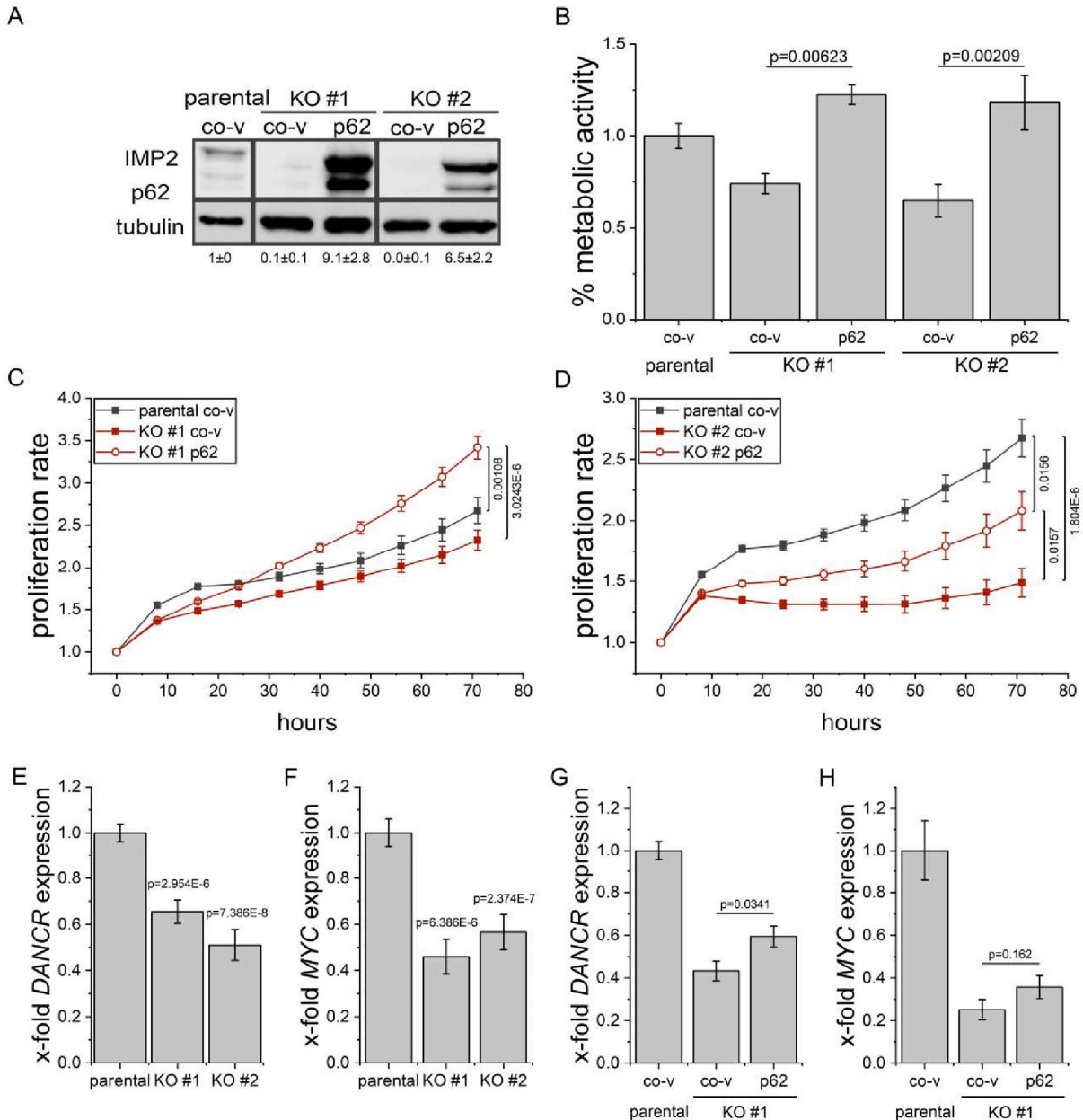
(D) Quantification of IMP2 protein levels in partial IMP2 knockdown cells compared to parental cells. Data are represented as means  $\pm$  SEM, n=2-6.

(E) Quantification of IMP2 gene levels in partial IMP2 knockdown cells compared to parental cells. Data are represented as means  $\pm$  SEM, n=3.



**Supplementary Figure S4. 3D growth comparison of HCT116 knockout clones**

The spheroid growth of different HCT116 IMP2 knockout clones showing different gene edits (see Supplementary Figure S2) was monitored by automated live-cell microscopy, starting after spheroid formation for 24 h. Spheroid area was analyzed using the IncuCyte® S3 system and was normalized to 1-day old spheroids. Data are represented as means  $\pm$  SEM, n=3 (quadruplicates). Statistical analysis was performed for the last acquired time point (7 days). Asterisks represent values for the comparisons between the growth of parental and respective knockout cells. p values comparing the growth of different clones were  $> 0.05$ .



### Supplementary Figure S5. Target specificity of IMP2 knockout in HCT116 cells

(A-D) HCT116 parental and IMP2 knockout HCT116 cells (CRISPR/Cas9 clone KO #1, prime editing clone KO #2) were transfected with p62/IMP2 or control vector (co-v).

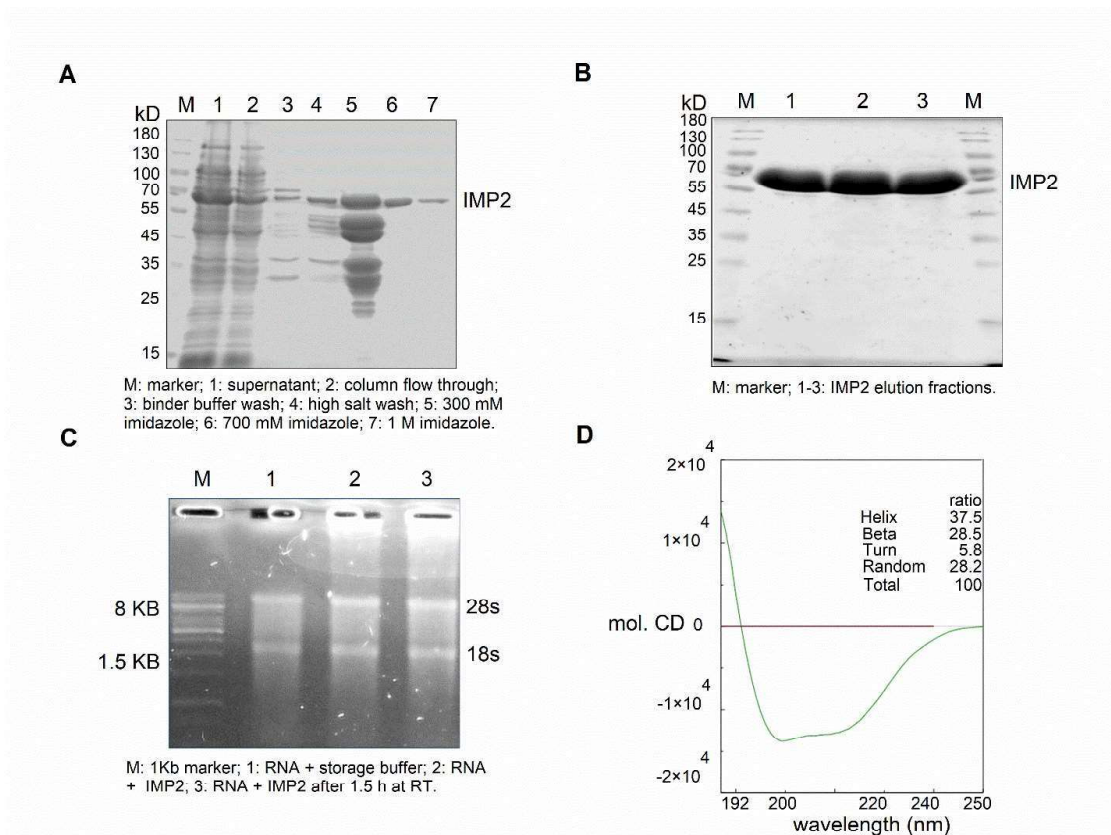
(A) Transfection efficiency and p62/IMP2 overexpression was controlled by Western blot 3 days post transfection.

(B) Metabolic activity was measured via MTT assay 3 days post transfection.

(C, D) Cell confluency was monitored using the IncuCyte® S3 system over 3 days. Confluency was normalized to the time point of transfection (0 h). Data are represented as means ± SEM, n=2 (quadruplicates).

(E, F) DANCR, and MYC gene expression was determined in HCT116 IMP2 knockout clones and (G, H) p62/IMP2 overexpressing parental and knockout cells by qPCR.

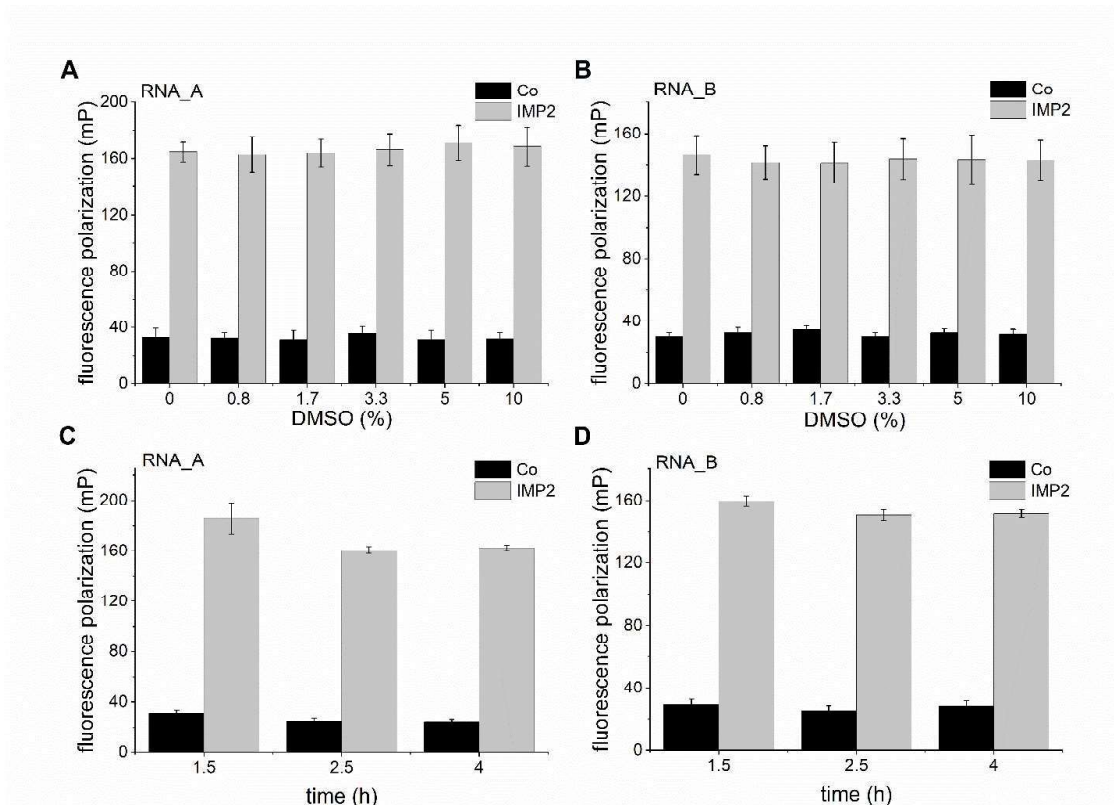
Values were normalized to the housekeeping gene RNA18S, n=3 (triplicates). Data are represented as means  $\pm$  SEM.



### Supplementary Figure S6. IMP2 isolation and characterization

Histidine-tagged IMP2 was overexpressed in *E. coli* and isolated via affinity chromatography using a HisTrap HP Nickel Sepharose column. Protein was eluted in an imidazole buffer with increasing imidazole concentrations.

- (A) Fractions were collected and run on an SDS-PAGE (lanes 5-7). A 10-180 kD protein ladder marker (M), the unpurified cell lysate (1), the column flow-through (2), and washing buffers (3-4) were also run on the gel. The gel was stained with Coomassie blue and revealed the pure IMP2 protein in the 300 mM and 700 mM imidazole fractions (lanes 6 and 7). IMP2 containing fractions were combined and concentrated.
- (B) The identity of the 67 kDa protein IMP2 was confirmed by Western blot analysis.
- (C) The absence of RNase activity was confirmed via RNA integrity measurement of MCF7 RNA in the presence of eluted protein, as visualized on an agarose gel. M: 1 kb marker, 1: RNA incubated with storage buffer for 1.5 h as a control, 2: RNA incubated with IMP2 for 1.5 h on ice, 3: RNA incubated with IMP2 for 1.5 h at room temperature (RT).
- (D) Circular dichroism (CD) spectroscopy was used to verify the correct protein folding of the purified protein.

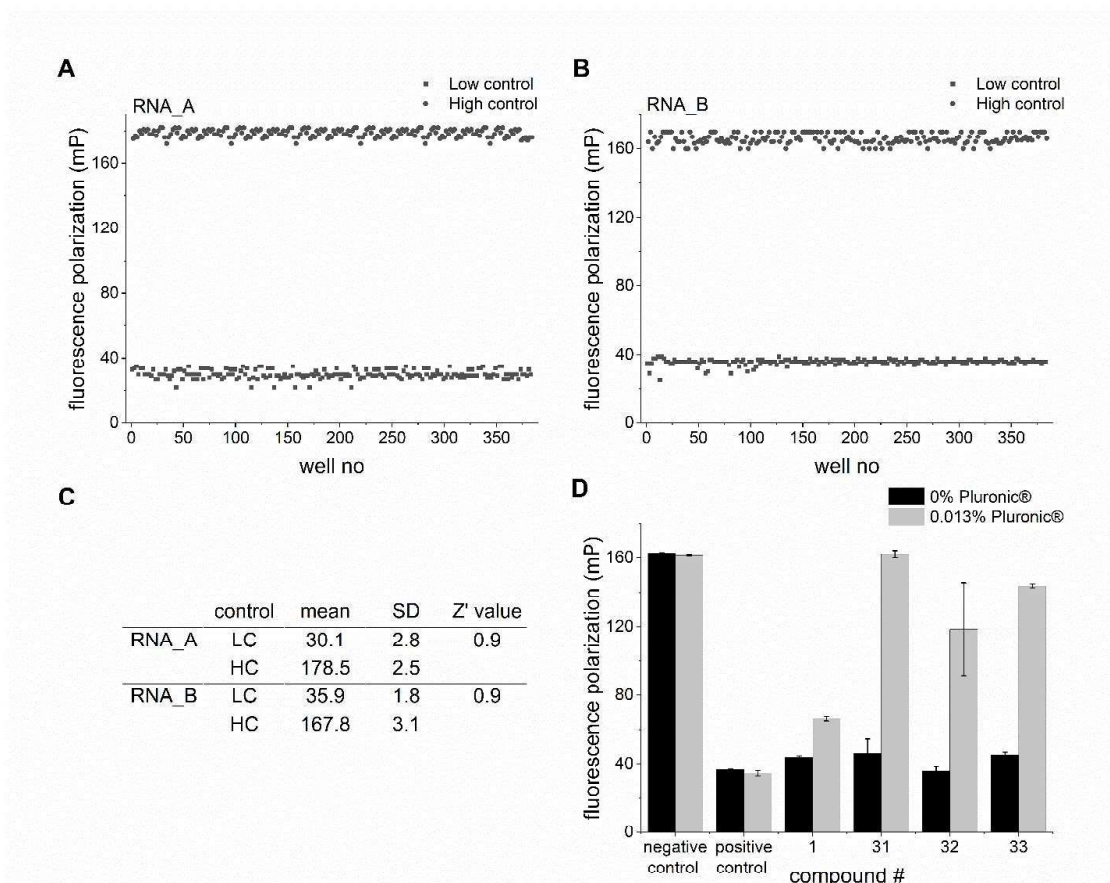


**Supplementary Figure S7. Fluorescence polarization assay development and validation**

(A, B) The DMSO tolerance of the FP assay was determined by using 1 nM of either the (A) RNA\_A or the (B) RNA\_B probe, IMP2 (120 nM for RNA\_A and 160 nM for RNA\_B), and varying concentrations of DMSO v/v. Unlabeled RNA was used as a control.

(C, D) The stability of the protein-RNA complex was assessed for 5% DMSO at different time points. Data are represented as means  $\pm$  SD, n=2 (triplicates).



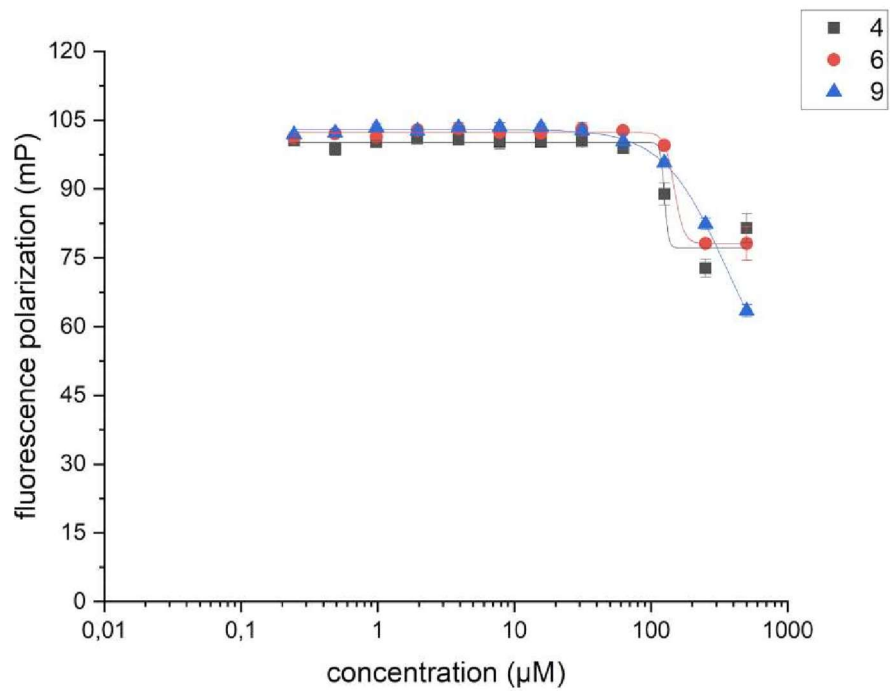


### Supplementary Figure S8. The robustness of the FP assay

(A, B) To determine the robustness of the FP assay, 192 samples of low controls (LC), containing 1 nM (A) RNA\_A or (B) RNA\_B without IMP2, and 192 samples of high controls (HC) containing additionally 120 nM and 160 nM IMP2 for RNA\_A and RNA\_B, respectively, were assessed at 5% DMSO in the FP assay after 1.5 h incubation.

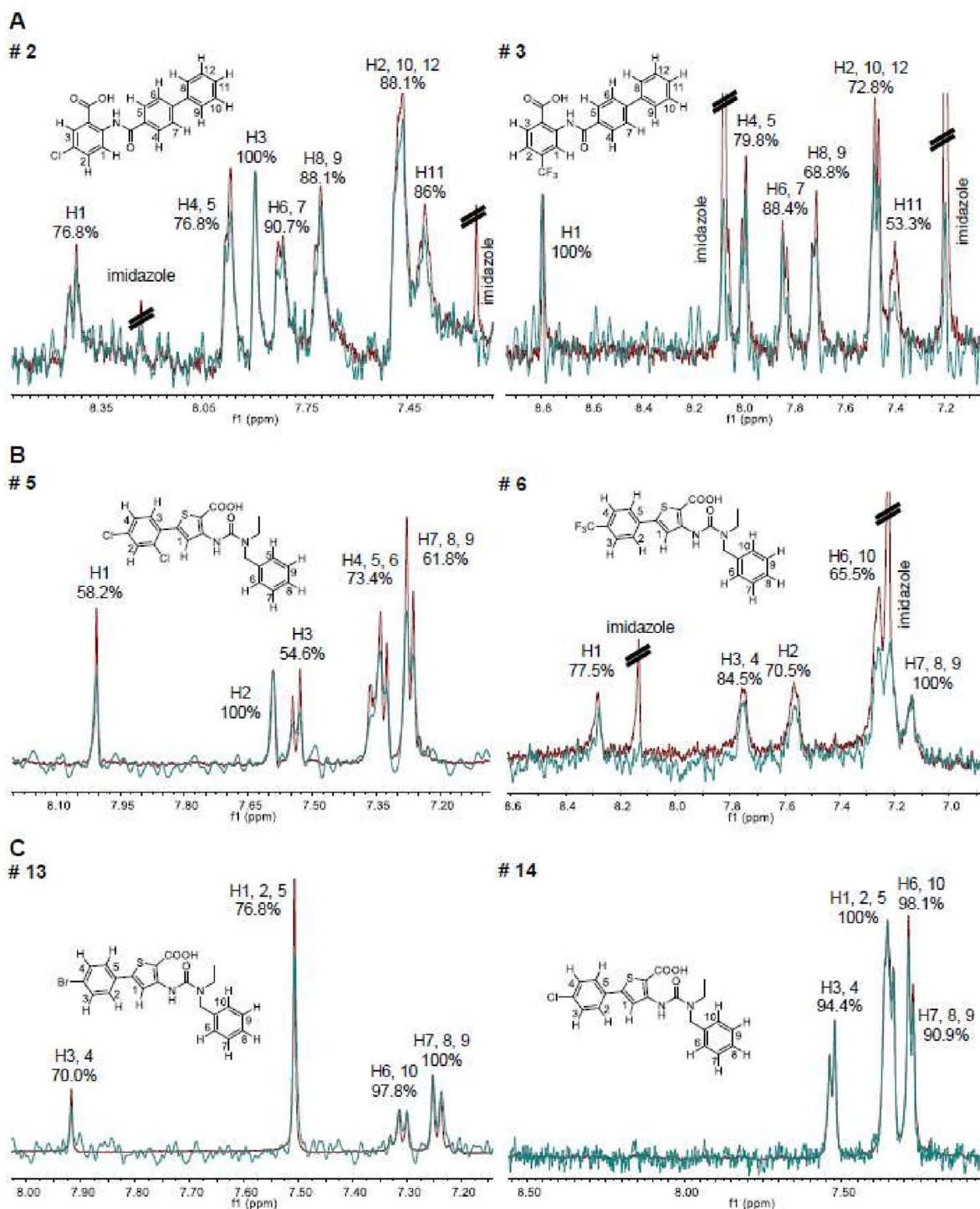
(C) Z'-factors were calculated based on the obtained data.

(D) To minimize unspecific aggregation and, therefore, false-positive results, 0.013% Pluronic® were added to FP buffer. The inhibitory effect of compounds 31 \_ 33 was lost after addition of Pluronic®, but not for compound 1. Data are represented as means  $\pm$  SD, n=1 (duplicates).



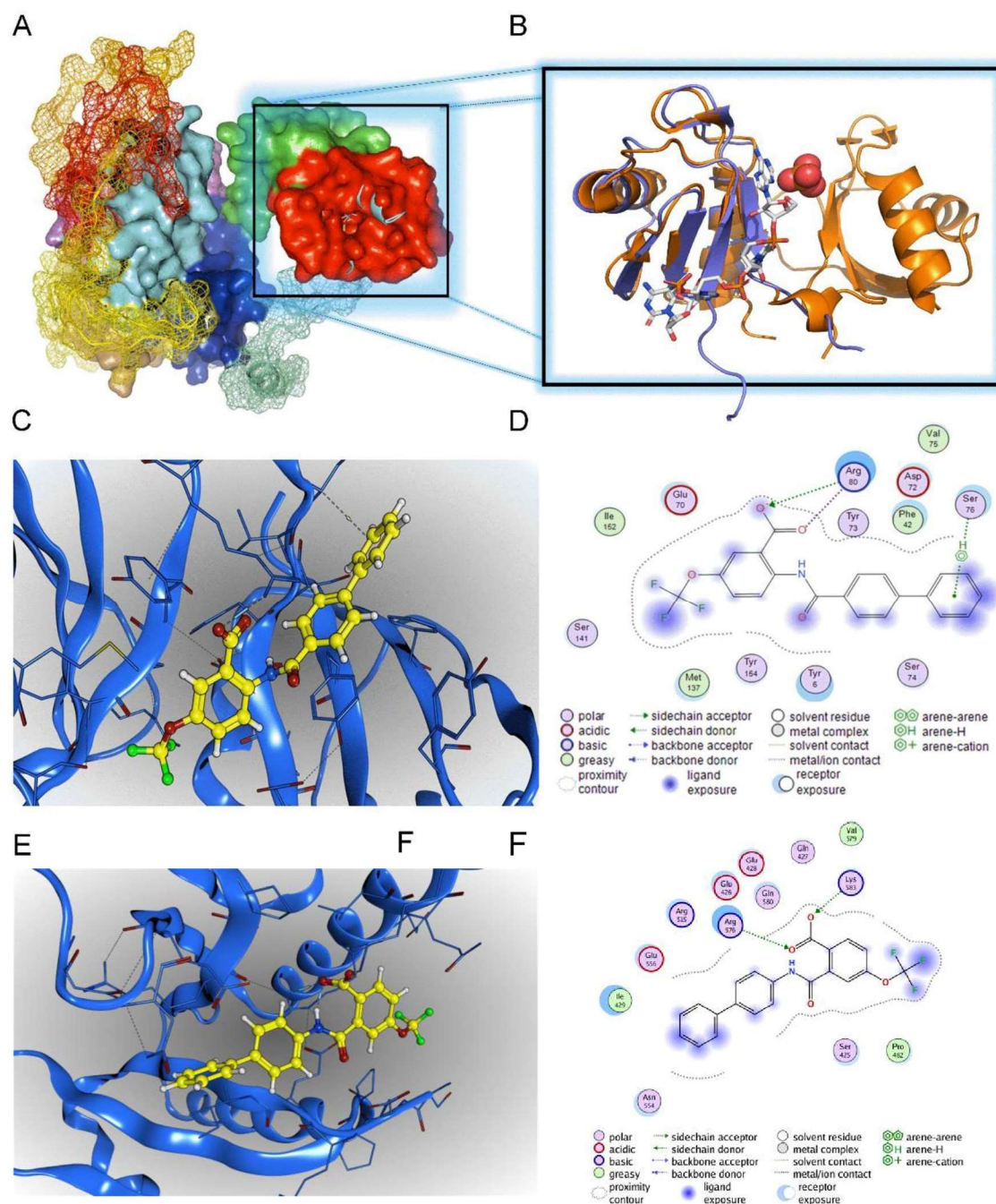
**Supplementary Figure S9. Hit compounds tested against the RBP CsrA**

Competition binding assays were performed by FP assay using CsrA from *Y. pseudotuberculosis* to test the specificity of IMP2:compound interactions. Hit compounds 4, 6 and 9 were used in concentrations up to 500 µM to compete with the fluorescence labelled target RNA (15 nM) for CsrA (400 nM) binding.



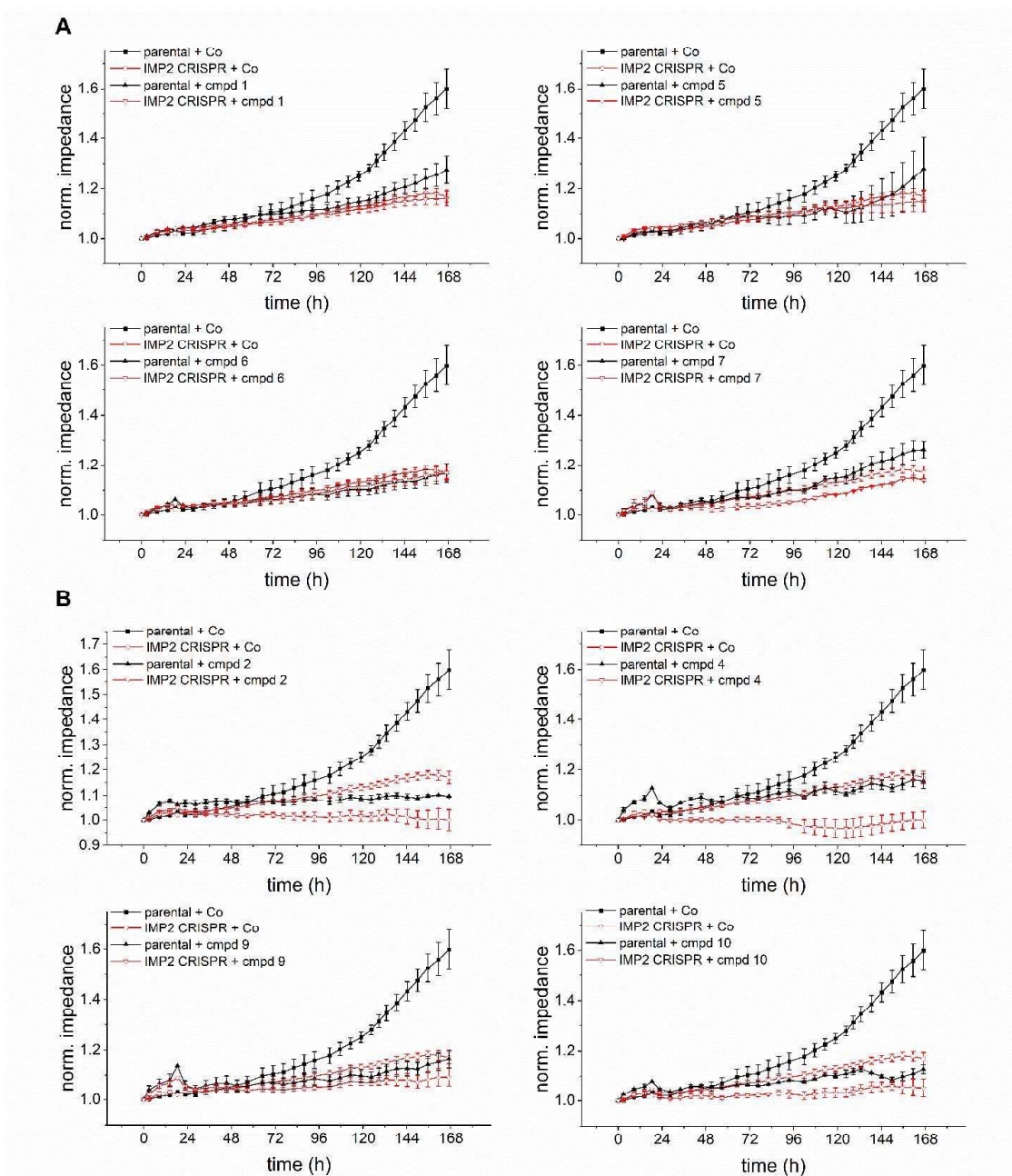
**Supplementary Figure S10. STD-NMR analysis**

STD-NMR experiments were performed at fixed concentrations of 2.5-5  $\mu\text{M}$  IMP2 and either 250  $\mu\text{M}$  for compound 2 and 3 or 500  $\mu\text{M}$  for compounds 5-6 and 13-14 based on the solubility limit in 10% DMSO  $\text{D}_6$  (molar ratio of protein to ligand was 1:100). Compounds 2 and 3 represent class A hit compounds (A), compounds 5 and 6 class B compounds (B), and compounds 13 and 14, selective RNA<sub>A</sub> inhibitors (C). The reference spectrum without protein is shown in red, and the STD difference spectrum of the IMP2/compound complexes is shown in green. Overlaid STD offresonance and STD effect spectra were normalized to the signal of the highest proton signal.



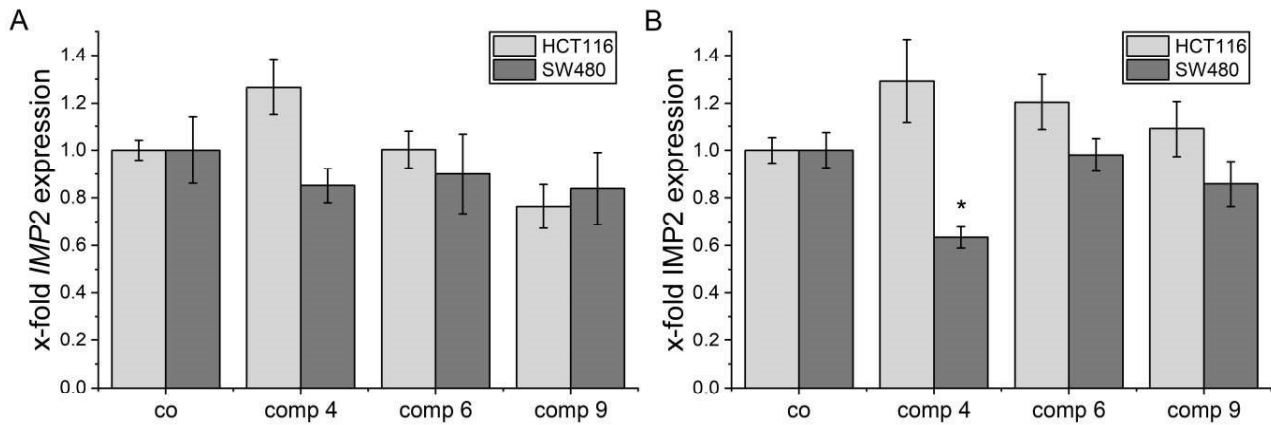
**Supplementary Figure S11. Molecular docking analysis of IMP complex**

- (A) IMP2 structure prediction based on IMP2 homology modeling.
- (B) Overlay of IMP2 RRM1 (blue), and IMP3 RRM12 (orange) crystals show 3D structure similarity. (C) 3D depiction of the docking-derived binding hypothesis for hit compound 4. RNA binding sites on the IMP2 RRM1 homology model were identified based on IMP3 RRM12-binding RNA coordinates and used as the docking site.
- (D) Ligand interaction scheme for the docking pose of compound 4 in complex with IMP2 RRM1. (E) 3D depiction of the docking-derived binding hypothesis for hit compound 4 to the IMP2 KH34 domain. RNA binding sites on the IMP2 KH34 domain are reported in the literature and were used as docking site (Biswas et al., 2019).
- (F) Ligand interaction scheme for the docking pose of compound 4 in complex with the IMP2 KH34 domain.



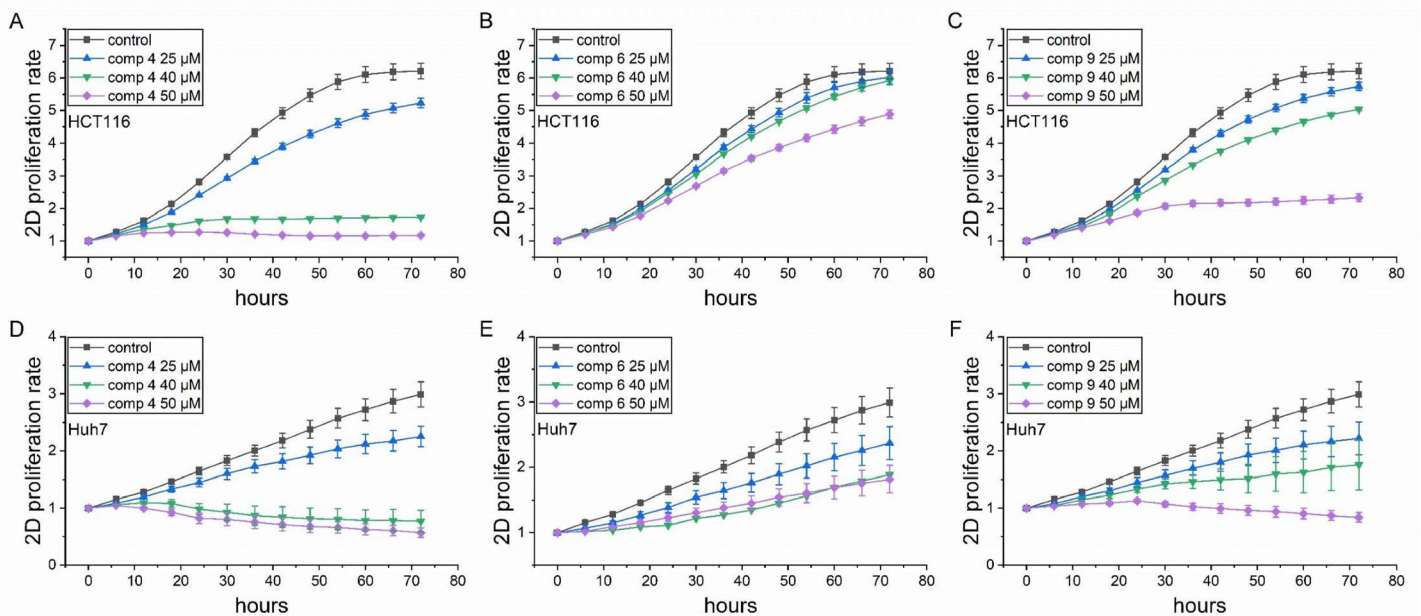
**Supplementary Figure S12. Action of hit compounds in the absence of the target on cell impedance changes**

Cell impedance was assessed as readout parameter for cell density and adhesion. HCT116 parental and IMP2 CRISPR/Cas9 knockout cells were seeded in equal numbers and treated with 25  $\mu\text{M}$  of the respective compound or DMSO solvent control (co). Hit compounds demonstrated effective anti-proliferative effects in HCT116 parental cells but (A) no or (B) lower effects in IMP2 CRISPR cells. Data are represented as means  $\pm$  SEM,  $n=2$  (triplicates).



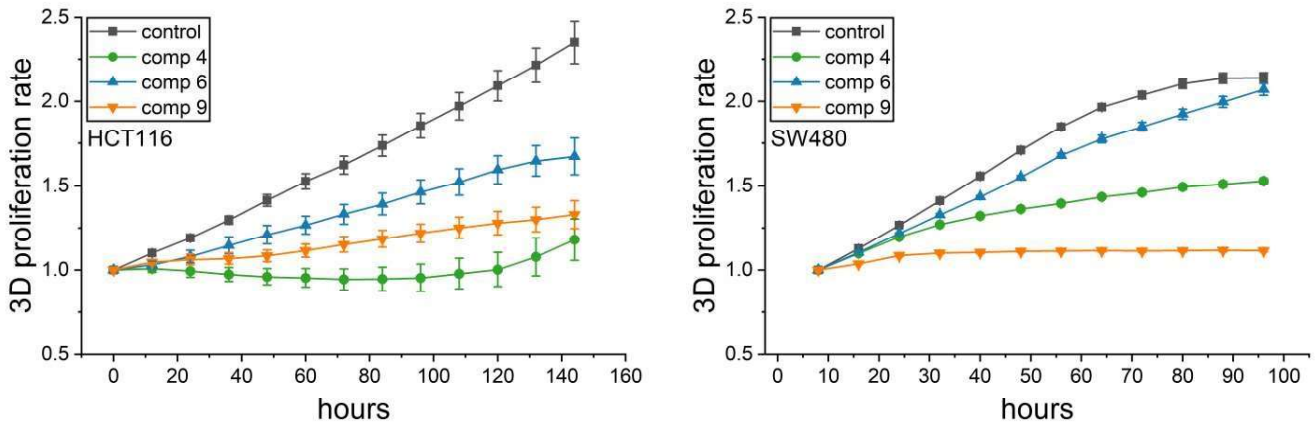
**Supplementary Figure S13. Expression of IMP2 upon compound treatment**

- (A) Quantification of IMP2 gene levels of HCT116 and SW480 cells, treated with compound 4 (40  $\mu$ M), 6 (50  $\mu$ M), or 9 (50  $\mu$ M) for 24 h. Data are normalized to RNA18S and are represented as means  $\pm$  SEM, n=3.
- (B) Quantification of IMP2 protein levels of HCT116 and SW480 cells, treated with compound 4 (40  $\mu$ M), 6 (50  $\mu$ M), or 9 (50  $\mu$ M) for 24 h. Data are normalized to tubulin and are represented as means  $\pm$  SEM, n=2.



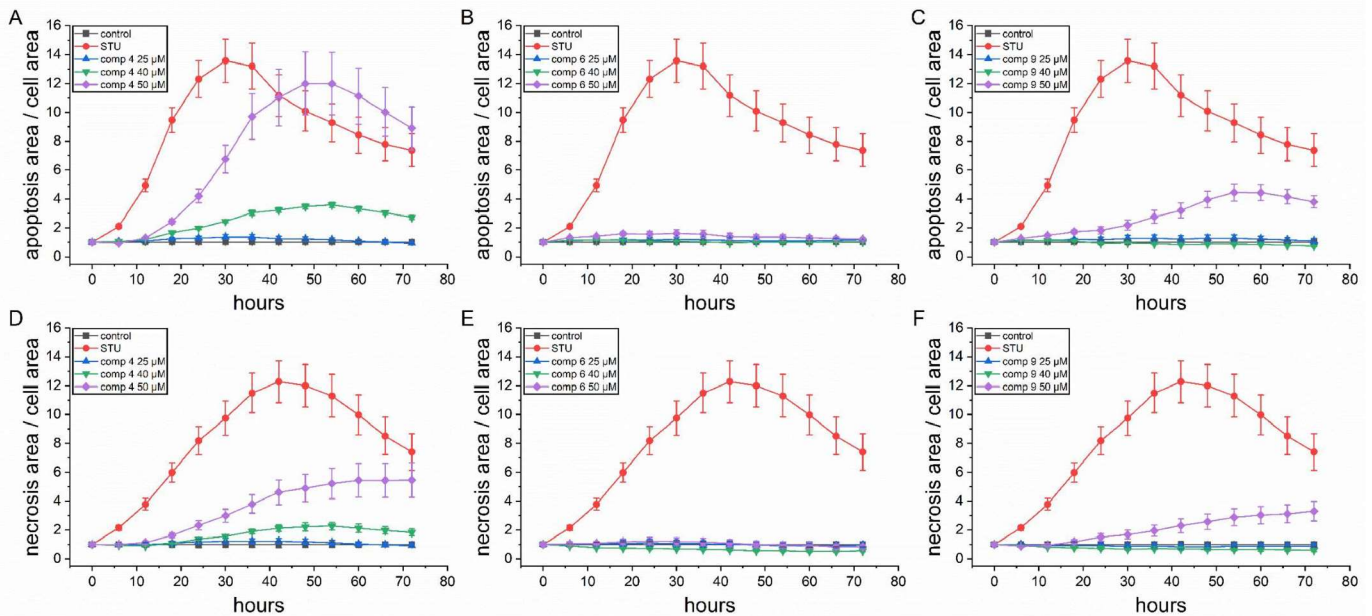
**Supplementary Figure S14. In vitro actions of compounds on 2D tumor cell proliferation**

Live-cell microscopy-based analysis of compound-induced anti-proliferative activity. Confluency of (A-C) HCT116 and (D-F) Huh7 cells was monitored in an IncuCyte<sup>®</sup> S3 system during compound (4, 6, 9) or control treatment over 72 h and normalized to the point of treatment (0 h). Data are represented as means  $\pm$  SEM, n=3 (quadruplicates).



**Supplementary Figure S15. In vitro actions of compounds on tumor cell proliferation**

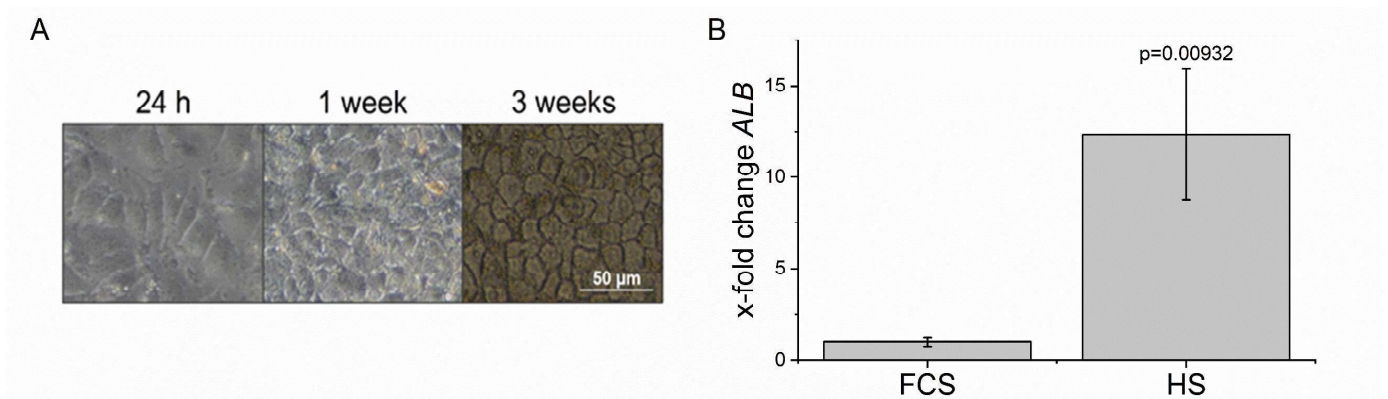
Live-cell microscopy-based analysis of compound-induced anti-proliferative activity. 3-day old HCT116 (left panel) and SW480 (right panel) spheroids were treated with 50  $\mu\text{M}$  of the respective compounds and the spheroid area was monitored by the IncuCyte<sup>®</sup> S3 system. The spheroid area was normalized to the first measuring point after treatment. Data are represented as means  $\pm$  SEM, n=3 (quadruplicates).



**Supplementary Figure S16. Evaluation of compound-induced cell death**

Live cell microscopy-based analysis of cell death upon compound treatment. HCT116 cells were stained for (A C) caspase 3/7 activity and (D-F) cell membrane permeability and monitored in an IncuCyte<sup>®</sup> S3 system during compound (4, 6, 9) or vehicle control

treatment over 72 h. The apoptosis inducer staurosporine (STU, 1  $\mu$ M) was used as positive control. Fluorescent signals from apoptotic (caspase 3/7 active) and necrotic (permeable membrane) cells were normalized to cell confluency and the time point of treatment (0h). Data are represented as means  $\pm$  SEM, n=3 (quadruplicates).



#### Supplementary Figure S17. Differentiation process of Huh7 in human serum

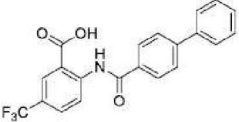
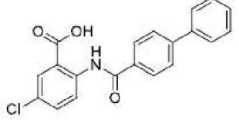
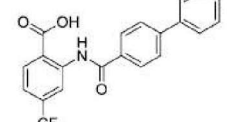
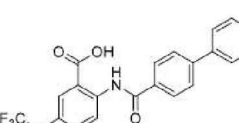
Huh7 cells were differentiated in media supplemented with 2% human serum (HS) for 3 weeks. (A) Cell morphology was monitored microscopically 24 h, 1 week, and 3 weeks after medium change.

(B) Gene expression of albumin (ALB) in differentiated and FCS-cultured cells. RNA was isolated 3 weeks after medium change and gene expression was assessed by qPCR. Values were normalized to the housekeeping gene RPS11. Data (x-fold of values for FCS-cultured cells) are represented as means  $\pm$  SEM, n=4 (triplicates).



### Supplementary Table 1. Descriptive data of class A compounds

Class A compounds: Molecular weights, chemical structures, and analytical data. Abbreviations: carbon-NMR ( $^{13}\text{C}$  NMR); coupling constant (J); deuterated dimethyl sulfoxide ( $\text{DMSO-}d_6$ ); doublet peak (d); liquid chromatography mass spectrometry (LC/MS); melting point (mp); multiplet peak (m); parts per million (ppm); proton NMR ( $^1\text{H}$  NMR); quartet peak (q); retention time ( $t_R$ ); singlet peak (s); triplet peak (t).

#	Reference	MW	Structure	Analytical Data
1	Hinsberger et al., 2014	385.34		$^1\text{H}$ NMR (500 MHz, $\text{DMSO-}d_6$ ) $\delta$ ppm 12.41 (s, 1H) 8.93 (d, $J = 8.8$ Hz, 1H) 8.28 (d, $J = 1.9$ Hz, 1H) 8.03 - 8.06 (m, 2H) 8.01 (dd, $J = 8.8, 1.9$ Hz, 1H) 7.87 - 7.92 (m, 2H) 7.73 - 7.78 (m, 2H) 7.47 - 7.54 (m, 2H) 7.40 - 7.46 (m, 1H). $^{13}\text{C}$ NMR (126 MHz, $\text{DMSO-}d_6$ ) $\delta$ ppm 168.90, 164.66, 144.27, 144.01, 138.75, 132.65, 130.85 (q, $J_{\text{CF}} = 3.7$ Hz) 129.06, 128.35, 127.94 (q, $J_{\text{CF}} = 3.7$ Hz), 127.84, 127.20, 126.95, 123.80 (q, $J_{\text{CF}} = 271.3$ Hz), 122.76 (q, $J_{\text{CF}} = 33.0$ Hz) 120.36, 116.81. LC/MS: $m/z = 386, 771$ ; $t_R = 14.60$ min; 99.76% pure (UV). White solid; mp. 264.8-266.0°C.
2	Hinsberger et al., 2014	351.78		$^1\text{H}$ NMR (500 MHz, $\text{DMSO-}d_6$ ) $\delta$ ppm 12.14 (s, 1H) 8.74 (d, $J = 9.1$ Hz, 1H) 8.02 - 8.05 (m, 2H) 8.00 (d, $J = 2.8$ Hz, 1H) 7.86 - 7.91 (m, 2H) 7.75 - 7.79 (m, 2H) 7.73 (dd, $J = 9.0, 2.7$ Hz, 1H) 7.48 - 7.54 (m, 2H) 7.41 - 7.47 (m, 1H). $^{13}\text{C}$ NMR (126 MHz, $\text{DMSO-}d_6$ ) $\delta$ ppm 168.77, 164.38, 143.80, 139.88, 138.82, 133.87, 132.92, 130.39, 129.08, 128.32, 127.75, 127.18, 126.96, 126.53, 121.81, 118.55. LC/MS: $m/z = 352, 354$ ; $t_R = 14.32$ min; 99.33% pure (UV). White solid; mp. 273.8-278.9°C.
3	Hinsberger et al., 2014	385.34		$^1\text{H}$ NMR (500 MHz, $\text{DMSO-}d_6$ ) $\delta$ ppm 12.35 (s, 1H) 9.10 (d, $J = 1.6$ Hz, 1H) 8.26 (d, $J = 8.2$ Hz, 1H) 8.04 - 8.08 (m, 2H) 7.89 - 7.95 (m, 2H) 7.75 - 7.81 (m, 2H) 7.57 (dd, $J = 8.2, 1.6$ Hz, 1H) 7.49 - 7.55 (m, 2H) 7.41 - 7.47 (m, 1H). $^{13}\text{C}$ NMR (126 MHz, $\text{DMSO-}d_6$ ) $\delta$ ppm 169.00, 164.78, 143.98, 141.41, 138.79, 133.38 (q, $J_{\text{CF}} = 32.0$ Hz), 132.67, 132.45, 129.08, 128.35, 127.80, 127.23, 126.97, 122.88 (q, $J_{\text{CF}} = 273.1$ Hz), 119.15 (q, $J_{\text{CF}} = 3.7$ Hz), 116.25 (q, $J_{\text{CF}} = 3.7$ Hz). LC/MS: $m/z = 386, 427, 771$ ; $t_R = 14.11$ min; 100.00% pure (UV). White solid; mp. 244.9-245.8°C.
4	Hinsberger et al., 2014	401.34		$^1\text{H}$ NMR (500 MHz, $\text{DMSO-}d_6$ ) $\delta$ ppm 12.17 (s, 1H) 8.81 (d, $J = 9.1$ Hz, 1H) 8.03 - 8.06 (m, 2H) 7.92 (dd, $J = 3.0, 0.8$ Hz, 1H) 7.88 - 7.91 (m, 2H) 7.74 - 7.78 (m, 2H) 7.68 - 7.74 (m, 1H) 7.49 - 7.53 (m, 2H) 7.41 - 7.46 (m, 1H). $^{13}\text{C}$ NMR (126 MHz, $\text{DMSO-}d_6$ ) $\delta$ ppm 168.61, 164.48, 143.86, 142.66 (q, $J_{\text{CF}} = 1.8$ Hz), 140.12, 138.82, 132.88, 129.08, 128.33, 127.80, 127.20, 127.04, 126.96, 123.31, 121.90, 118.55, 120.04 (q, $J_{\text{CF}} = 256.0$ Hz). LC/MS: $m/z = 402, 803$ ; $t_R = 14.58$ min; 100.00% pure (UV). White solid; mp. 244.6-245.9°C.

## Supplementary Table 2. Descriptive data of class B compounds

Class B compounds: Molecular weights, chemical structures, and analytical data. Abbreviations: carbon-NMR ( $^{13}\text{C}$  NMR); coupling constant (J); deuterated dimethyl sulfoxide (DMSO- $d_6$ ); doublet peak (d); liquid chromatography mass spectrometry (LC/MS); melting point (mp); multiplet peak (m); parts per million (ppm); proton NMR ( $^1\text{H}$  NMR); quartet peak (q); retention time ( $t_R$ ); singlet peak (s); triplet peak (t).

#	Reference	MW	Structure	Analytical Data
5	Sahner et al., 2013	449.35		$^1\text{H-NMR}$ (300 MHz, DMSO- $d_6$ ): $\delta$ ppm 1.15 (t, $J = 7.1$ , 3H), 3.39 (q, $J = 7.1$ , 2H), 4.58 (s, 2H), 7.23 – 7.37 (m, 5H), 7.53 (dd, $J = 8.5$ , 2.1, 1H), 7.68 (d, $J = 8.5$ , 1H), 7.79 (d, $J = 2.1$ , 1H), 8.27 (s, 1H), 10.04 (s, 1H), 13.51 (br. s., 1H). $^{13}\text{C}$ NMR (75 MHz, DMSO- $d_6$ ): $\delta$ ppm 13.1, 41.8, 49.3, 108.8, 122.1, 127.1, 128.1, 128.5, 130.1, 130.5, 132.1, 132.4, 134.3, 138.0, 142.3145.6, 153.0, 165.6. LC/MS: $m/z = [\text{M}+\text{H}^+]$ 448.55, $[2\text{M}+\text{H}^+]$ 896.57 $t_R = 15.14$ min, 99.3% pure (UV). mp: 212 – 214°C.
6	Sahner et al., 2013	448.46		$^1\text{H-NMR}$ (300 MHz, DMSO- $d_6$ ): $\delta$ ppm 1.16 (t, $J = 7.1$ , 3H), 3.40 (q, $J = 7.1$ , 2H), 4.59 (s, 2H), 7.24 – 7.38 (m, 5H), 7.79 (d, $J = 8.4$ , 2H), 7.91 (d, $J = 8.1$ , 2H), 8.41 (s, 1H), 10.05 (s, 1H), 13.47 (br. s., 1H). $^{13}\text{C}$ NMR (75 MHz, DMSO- $d_6$ ): $\delta$ ppm 13.1, 41.8, 49.3, 108.2, 124.0 (q, $^1J_{\text{CF}} = 272.0$ Hz), 126.2 (q, $^2J_{\text{CF}} = 3.7$ Hz), 126.4, 127.2, 128.4, 128.5, 129.3 (q, $^2J_{\text{CF}} = 32.0$ Hz) 136.5, 138.1, 145.3, 146.7, 153.0, 165.6. LC/MS: $m/z = [\text{M}+\text{H}^+]$ 448.68, $[2\text{M}+\text{H}^+]$ 896.93 $t_R = 14.59$ min, 98.02% pure (UV). mp: 193 – 194°C.
7	Sahner et al., 2013	510.96		$^1\text{H-NMR}$ (300 MHz, DMSO- $d_6$ ): $\delta$ ppm 0.88 (t, $J = 7.5$ , 3H), 1.25 – 1.37 (m, 2H), 1.52 – 1.63 (m, 2H), 3.32 (t, $J = 7.5$ , 2H), 4.59 (s, 2H), 7.23 – 7.38 (m, 5H), 7.77 – 7.80 (s, 1H), 7.98 – 8.00 (m, 2H), 8.38 (s, 1H), 10.08 (s, 1H), 13.56 (br. s., 1H). LC/MS: $m/z = [\text{M}+\text{H}^+]$ 510.85; $t_R = 16.16$ min, 100% pure (UV).
8	Sahner et al., 2013	511.42		$^1\text{H-NMR}$ (300 MHz, DMSO- $d_6$ ): $\delta$ ppm 4.64 (s, 4H), 7.26 – 7.38 (m, 10H), 7.65 – 7.71 (m, 2H), 7.94 (s, 1H), 8.35 (s, 1H), 10.08 (s, 1H), 12.66 (br. s., 1H). $^{13}\text{C}$ NMR (75 MHz, DMSO- $d_6$ ): $\delta$ ppm 49.9, 50.1, 118.8, 128.9, 127.1, 127.3, 127.3, 128.6, 128.6, 128.9, 130.0, 131.4, 131.6, 131.8, 132.1, 133.3, 137.2, 144.2, 146.2, 153.5, 165.4. LC/MS: $m/z = [\text{M}+\text{H}^+]$ 511.35; $t_R = 16.36$ min, 95.70% pure (UV). mp: 190 – 191°C.
9	Sahner et al., 2013	477.40		$^1\text{H-NMR}$ (300 MHz, DMSO- $d_6$ ): $\delta$ ppm 0.88 (t, $J = 7.4$ , 3H), 1.60 (q, $J = 7.4$ , 2H), 2.89 (t, $J = 7.4$ , 2H), 3.25 (t, $J = 7.4$ , 2H), 3.50, $J = 7.4$ , 2H), 7.19 – 7.32 (m, 5H), 7.65 – 7.71 (m, 2H), 7.93 (d, $J = \text{dd}$ , $J = 1.1$ , 1H), 8.33 (s, 1H), 10.03 (s, 1H), 13.56 (br. s., 1H). $^{13}\text{C}$ NMR (75 MHz, DMSO- $d_6$ ): $\delta$ ppm 11.0, 21.2, 34.1, 49.0, 49.1, 197.7, 118.7, 125.9, 126.2, 127.3, 128.4, 128.8, 131.4, 131.6, 132.1, 133.3, 138.7, 144.4, 146.7, 152.6, 165.8. LC/MS: $m/z = [\text{M}+\text{H}^+]$ 476.89, $[2\text{M}+\text{H}^+]$ 954.65 $t_R = 16.58$ min, 98.83% pure (UV). mp: 178 – 179°C.
10	Sahner et al., 2013	524.98		$^1\text{H-NMR}$ (300 MHz, DMSO- $d_6$ ): $\delta$ ppm 0.88 (t, $J = 7.3$ , 3H), 1.25 – 1.37 (m, 2H), 1.50 – 1.60 (m, 2H), 2.89 (t, $J = 7.8$ , 2H), 3.29 (t, $J = 8.1$ , 2H), 3.50 (t, $J = 8.2$ , 2H), 7.18 – 7.37 (m, 5H), 7.78 – 7.81 (m, 1H), 7.99 – 8.01 (m, 2H), 8.38 (s, 1H), 10.04 (s, 1H), 13.61 (br. s., 1H). LC/MS: $m/z = [\text{M}+\text{H}^+]$ 524.86 $t_R = 16.85$ min, 96.95% pure (UV).

**Supplementary Table 3. IC<sub>50</sub> values of hit compounds**

Metabolic activity was determined by MTT assay 96 h after treatment with hit compounds or DMSO solvent control. IC<sub>50</sub> values were calculated using non-linear regression analysis. n=2-5 (triplicates).

IC <sub>50</sub> values [μM]						
	MCF7	HCT116	SW480	HepG2	Huh7	Hep3B
1	43.6	48.1	35.1	30.7	34.7	54.7
2	46.7	29.9	22.5	29.1	40.9	45.5
3	> 80	53.2	78.5	75.0	34.5	58.0
4	48.1	31.0	18.2	29.6	33.3	35.5
5	> 80	62.6	61.2	> 80	> 80	> 80
6	55.1	46.9	49.0	42.9	45.4	52.6
7	> 80	44.7	27.1	35.0	38.8	47.7
8	50.3		37.1	33.6	43.5	
9	70.0	37.8	36.8	35.7	24.9	39.8
10	58.0	37.5	41.4	35.0	44.3	46.2

**Supplementary Table 4. Sequences of siRNA oligonucleotides used in IMP2 knockdown**

Individual sequences of the 4-oligo siRNA mixture purchased from Qiagen to knock down IMP2 and the random RNA oligo sequence.

Oligo RNA	Sequence (5'- 3')
oligo 1	CAGGGCGTTAAATTCACAGAT
oligo 2	TCCGCTAGCCAAGAACCTATA
oligo 3	CAGCGAAAGGATGGTCATCAT
oligo 4	CCCGGGTAGATATCCATAGAA
random	AACACGTCTATACGC